

# **New Liquid Biomaterials for Nanoemulsion-mediated Drug Delivery**

by  
Marshall Scott Padilla

A dissertation submitted in partial fulfillment of  
the requirements for the degree of

Doctor of Philosophy  
(Chemistry)

at the  
UNIVERSITY OF WISCONSIN-MADISON  
2021

Date of final oral examination: July 29<sup>th</sup>, 2021

The dissertation is approved by the following members of the Final Oral Committee:  
Sandro Mecozzi, Professor, Department of Chemistry and School of Pharmacy  
Helen Blackwell, Professor, Department of Chemistry  
Glen S. Kwon, Professor, School of Pharmacy  
Silvia Cavagnero, Professor, Department of Chemistry

# **New Liquid Biomaterials for Nanoemulsion-mediated Drug Delivery**

Marshall Scott Padilla

Under the supervision of Professor Sandro Mecozzi

At the University of Wisconsin-Madison

## **ABSTRACT**

Most potent therapeutics fail to reach clinical trials and FDA-approval due to their inability to reach their target in a safe and controlled manner. To overcome these barriers, nanotechnology can be employed to create vehicles that aid in the delivery of drugs. One promising class of drug delivery vehicles are nanoemulsions, which are nanometer-sized particles that contain a hydrophobic droplet that houses and protects the therapeutics. Nanoemulsions have seen success in the delivery of drugs as several nanoemulsion formulations have received FDA-approval. However, despite their success, one of their limiting factors is their lack of diverse hydrophobic components. Typically, the hydrophobic droplet is a lipid, and as a result, only drugs that are lipophilic can be dissolved. This means that hydrophilic small molecule and biological therapeutics cannot be formulated, significantly reducing the potential of this drug delivery vehicle

In this thesis, two unique strategies are employed to overcome the limitations of nanoemulsions. The majority of the chapters describe the synthesis, characterization, and application of hydrophobic ionic liquids (HILs), which are investigated as replacements for the traditional lipid droplet of nanoemulsions. HILs are a promising material as they can solubilize hydrophilic, hydrophobic, and even biological drugs due to their unique nanostructure. Chapter 2 describes the design and synthesis of several classes of novel HILs, whereas Chapter 3 discusses the physicochemical properties and toxicities of select HILs. In Chapter 4, certain HILs are explored as components for drug delivery formulations, especially as nanoemulsions.

The collective results highlight that diverse HILs can be rapidly produced, where they possess advantageous characteristics and low toxicity. Moreover, they can be successfully employed as a component for nanoemulsions with the capability of transporting various drug classes.

Chapter 5 represents a different approach to nanoemulsions, where instead of utilizing a new material to dissolve non-hydrophobic therapeutics, the hydrophilic drug of choice was tuned to become lipophilic. Here siRNA, a potent nucleic acid therapeutic, was chosen as the model drug and was noncovalently modified to become hydrophobic by complexing the nucleic acid with a cationic lipid. This allowed the drug to be formulated in a nanoemulsion composed of the FDA-approved oil, medium chain triglycerides, as the hydrophobic phase. The nanoemulsion is characterized and evaluated in a tumor murine model, where it facilitates significant gene knockdown with a good safety profile.

## ACKNOWLEDGMENTS

I would first like to thank my advisor Professor Sandro Mecozzi for his guidance and patience throughout my graduate experience. Obtaining a PhD requires an army of support and Sandro was the general through it all. His kindness and passion for science has taught me that being a scientist does not mean forgoing your humanity. Throughout the good results, great ideas, stupid ideas, and flooded labs, Sandro was there to encourage me on my down days and celebrate my successes, and so I am eternally grateful for his mentorship. Additionally, I want to thank my committee members, Professor Helen Blackwell, Professor Glen Kwon, and Professor Silvia Cavagnero for their willingness to be a part of my journey through graduate school as well as serving as my teachers, instructors, and motivational speakers.

To the current and former Mecozzi lab members, as well as our extended family, Lauren and Hye-Jin, thank you for your guidance and friendship. Your presence made for a fun working environment, and I appreciated the constant stream of delicious baked goods as well as your willingness to put up with my shenanigans. In particular, I would like to thank Dr. Mint, who, at a certain point, was my only labmate. You dealt my neediness and taught me important lessons about science. I admire your tail vein injection skills; thank you for all of the help with the *in vivo* experiments, especially on the bad days. I will always remember our time copying and shredding several thousand pieces of paper. Additionally, I am lucky to have worked on the 7<sup>th</sup> floor of Pharmacy, where I had the joy of interacting with fantastic and smart people. In particular, the members of the Tang lab were instrumental in their kindness as they allowed me to use their equipment and reagents, even at odd hours.

I would like to acknowledge the facilities, technicians, and other labs at the University of Wisconsin-Madison for making my life easier. Five years was not enough time for me to learn every instrument and procedure on my own, and so having these resources enabled me to learn a wide variety of cool scientific techniques. Professor Michael Taylor and his group introduced me to the unique world of zebrafish work, and while I still struggle with differentiating between male and female fish, I genuinely appreciated and enjoyed the work. Professor Charles Lauhon took me under his wing during my first year

and helped to refine my biochemical skills, which became invaluable later on in my research. The staff at the UW-Madison School of Pharmacy are experts in their fields and generous in their assistance. Since my thesis seems to be mostly NMR spectra, I need to thank Dr. Thomas Stringfellow of the Analytical Instrumentation Center for his friendship and willingness to teach me the power of NMR spectroscopy. Last, but certainly not least, a big shoutout to Gary Girdaukas who somehow manages to keep the equipment at the School of Pharmacy alive, despite our best attempts at destroying them.

During my time in the Mecozzi lab, I had the immense pleasure of working with some fantastic undergraduate students. To Nick, Colin, and Nicole, your company and friendship made lab a much more enjoyable place. I learned so much about myself through our mentoring relationships, and I had some of my most valuable experiences collaborating with each of you. Please know that your work was impactful and that you contributed to the results in this thesis.

Some of the most important tools I learned in graduate school were not related to my own research. UW-Madison, especially the Department of Chemistry, offered me endless opportunities to improve my teamwork and leadership skills. My experiences in Catalyst, the Graduate Student-Faculty Liaison Committee (GSFLC), and the Wellness and Professional Development Committee taught me the importance and the power of collaborating with like-minded people to achieve positive change. In particular, I would like to thank Dr. Matt Styles for being an awesome GSFLC cochair during our term, which started with a literal garbage fire and ended with a global pandemic. Furthermore, I want to give another big shoutout to the 2019 Climate Survey team. During graduate school, I struggled immensely with my own mental health, so it was an incredibly rewarding experience working to improve the mental health of the department. I would also like to thank Dr. Desiree Bates and Dr. Cheri Rossi for allowing me to be part of and contribute to the wonderful Catalyst community, as well as Professor Judith Burstyn who I had the pleasure of discussing all matters of life and lab with.

As early as my first year in graduate, teaching became a passion of mine. I was fortunate to collaborate with an array of wonderful instructors and co-TAs who provided me the tools and confidence to teach. In particular, I would like to thank Brian, Aubrey, and Ryan for believing in my teaching abilities

and allowing me to take on more responsibilities that served as excellent learning experiences. I would also like to shoutout the UW-Madison Delta program for giving me the knowledge and skills to further enhance my teaching. The Delta instructors, especially Devin, were instrumental in guiding me through the vast world of pedagogy, where I was able to construct my own ideas and philosophies on teaching. In a similar vein, the Delta program also enhanced my mentorship, particularly through the Research Mentoring Training course. In learning the value of mentorship, I eventually became a facilitator for Research Mentoring Training, where I, along with my awesome co-facilitator, Alissa, worked with a motivated group of graduate students and postdocs. The skills I learned through TAing and the Delta Program have given me the confidence to pursue my dreams of becoming a professor.

I am so grateful for the friends and family who motivated and supported me during my five years in graduate school. To Danny, Aaron, Marcell, Claire, Allison, and Ellen, your camaraderie always put a smile on my face, especially during the lonely periods of the pandemic. Who would have guessed that a bunch of awkward first-year students from Gooch Hall would still be close friends almost ten years later? To the frisbee community and my MUFA teams, especially Professor Randall Goldsmith and the Discertators, thank you for keeping me sane and in shape. I will throw a bad hammer in my next game to honor you all. To Adam, Big Steve, Lei, Keywan, and especially Tim, I am grateful I met a wonderful group of friends in Madison. I will always remember the movies at Marcus Theater, board game nights, our attempts at badminton and volleyball, and our championship scavenger hunt team – we made it! To other Adam, maybe one day you will beat me in Smash Bros. To my father and my sister Sophie, even though we were all far apart, we grew closer than ever. And to my brother Mickey and my sister-in-law Becky, you got your wish, I am finally moving back to Pennsylvania.

## TABLE OF CONTENTS

<b>ABSTRACT</b> .....	<b>i</b>
<b>ACKNOWLEDGEMENTS</b> .....	<b>iii</b>
<b>TABLE OF CONTENTS</b> .....	<b>vi</b>
<b>LIST OF FIGURES</b> .....	<b>xii</b>
<b>LIST OF TABLES</b> .....	<b>xiv</b>
<b>LIST OF SCHEMES</b> .....	<b>xvi</b>
<b>LIST OF ABBREVIATIONS</b> .....	<b>xviii</b>
<b>CHAPTER 1 – Introduction</b> .....	<b>1</b>
1.1 Ionic Liquids: Nomenclature, Structure, and Applications.....	2
<i>1.1.1 Ionic liquid, molten salt,, or something else?</i> .....	2
<i>1.1.2 Cation, anion, and IL synthesis</i> .....	3
<i>1.1.3 Nanostructure of ILs</i> .....	4
<i>1.1.4 IL properties and applications</i> .....	6
<i>1.1.5 The environmental reality of ILs</i> .....	7
1.2 Molecular Dynamics.....	9
<i>1.2.1 Choosing the phospholipid</i> .....	10
<i>1.2.2 Atomistic models</i> .....	11
<i>1.2.3 Coarse-grain models</i> .....	14
1.3 Biophysical Methods.....	17
<i>1.3.1 Development of artificial lipid membranes</i> .....	17
<i>1.3.2 Isothermal titration calorimetry</i> .....	18
<i>1.3.3 Differential scanning calorimetry</i> .....	19
<i>1.3.4 Quartz crystal microbalance with dissipation monitoring</i> .....	20
<i>1.3.5 Fluorescence spectroscopy</i> .....	21
<i>1.3.6 X-ray diffraction</i> .....	22

1.3.7 Neutron diffraction.....	24
1.3.8 Atomic force microscopy.....	25
1.3.9 Additional biophysical methods.....	27
1.4 Thesis Objectives and Overview.....	27
1.5 References.....	28
<b>CHAPTER 2 – Design and Synthesis of a New Generation of Hydrophobic Ionic Liquids.....</b>	<b>41</b>
Abstract.....	42
2.1 Introduction.....	43
2.2 Results and Discussion.....	45
2.2.1 Synthesis of cholinium-based cations.....	45
2.2.2 Synthesis of cholinium ILs containing fatty acid anions.....	47
2.2.3 Synthesis of morpholinium ILs containing fatty acid anions.....	51
2.2.4 Synthesis of dicholinium-based ILs containing fatty acid anions.....	54
2.2.5 Synthesis of ILs containing dichain fatty acids.....	56
2.2.6. Synthesis of ILs containing bis(trifluoromethanesulfonyl)azanide anions.....	60
2.2.7 Synthesis of second-generation dicholinium cations and corresponding ILs.....	63
2.2.8 Synthesis of dicholinium ILs containing artificial sweetener anions.....	65
2.2.9 Synthesis of first generation bis(sulfonyl)azanide anions.....	66
2.2.10 Synthesis of cholinium and dicholinium ILs containing first-generation bis(sulfonyl)azanides.....	68
2.2.11 Synthesis of second generation bis(sulfonyl)azanides and corresponding ionic liquids.....	73
2.2.12 Synthesis of second-generation bis(sulfonyl)azanide anions containing electron-withdrawing groups and corresponding ILs.....	76
2.2.13 Synthesis of third-generation bis(sulfonyl)azanide anions and corresponding ILs.....	81
2.3 Conclusion.....	83
2.4 Experimental.....	85

2.4.1 Materials and nuclear magnetic resonance methods.....	85
2.4.2 Synthesis of cholinium and alkyl-cholinium cations.....	86
2.4.3 Synthesis of alkyl morpholinium cations.....	88
2.4.4 Synthesis of dicholinium cations.....	90
2.4.5 Synthesis of cholinium ILs containing fatty acid anions.....	94
2.4.6 Synthesis of cholinium deep eutectic solvents.....	97
2.4.7 Synthesis of morpholinium-based ILs containing fatty acid anions.....	98
2.4.8 Synthesis of dicholinium ILs containing fatty acid anions.....	103
2.4.9 Synthesis of the DOP anion and corresponding ILs.....	107
2.4.10 Synthesis of second-generation dichain fatty acid anions and corresponding ILs.....	109
2.4.11 Synthesis of monocholinium, morpholinium, and dicholinium ILs containing [NTf <sub>2</sub> ] anions.....	118
2.4.12 Synthesis of dicholinium ILs containing octanoate and [NTf <sub>2</sub> ] anions.....	125
2.4.13 Synthesis of second-generation dicholinium cations.....	127
2.4.14 Synthesis of dicholinium ILs composed of artificial sugar anions.....	131
2.4.15 Synthesis of first-generation bis(sulfonyl)azanide anions.....	132
2.4.16 Synthesis of ILs containing first-generation bis(sulfonyl)azanide anions.....	141
2.4.17 Synthesis of second-generation bis(sulfonyl)azanide anions.....	155
2.4.18 Synthesis of third-generation bis(sulfonyl)azanide anions.....	172
2.4.19 Synthesis of cyclic monocholinium cations.....	175
2.4.20 Synthesis of ILs containing second-generation bis(sulfonyl)azanide anions.....	177
2.4.21 Synthesis of ILs containing third-generation bis(sulfonyl)azanide anions.....	189
2.5 References.....	193
<b>CHAPTER 3 – Physicochemical and Toxicological Analysis of Hydrophobic Ionic Liquids.....</b>	<b>196</b>
Abstract.....	197
3.1 Introduction.....	198

3.2 Results and Discussion.....	201
3.2.1 <i>Differential scanning calorimetry</i> .....	201
3.2.2 <i>Viscosity</i> .....	208
3.2.3 <i>Water solubility</i> .....	211
3.2.4 <i>Hygroscopicity</i> .....	219
3.2.5 <i>In vitro toxicity</i> .....	221
3.2.6 <i>Zebrafish developmental toxicity</i> .....	229
3.3 Conclusion.....	233
3.4 Experimental.....	235
3.4.1 <i>Materials</i> .....	235
3.4.2 <i>Differential scanning calorimetry</i> .....	236
3.4.3 <i>Viscosity</i> .....	236
3.4.4 <i>Quantitative NMR spectroscopy</i> .....	236
3.4.5 <i>Hygroscopicity</i> .....	238
3.4.6 <i>In vitro toxicity</i> .....	238
3.4.6 <i>Zebrafish developmental toxicity</i> .....	239
3.5 References.....	240
<b>CHAPTER 4 – Ionic Liquids as Components for Drug Delivery Vehicles.....</b>	<b>244</b>
Abstract.....	245
4.1 Introduction.....	246
4.2 Results and Discussion.....	248
4.2.1 <i>Poloxamer-based IL nanoparticles</i> .....	248
4.2.2 <i>Toxicity of poloxamer-based IL nanoparticles</i> .....	252
4.2.3 <i>Nanoemulsions incorporating [DC-5][2NTf<sub>2</sub>] and docusate</i> .....	254
4.2.4 <i>Nanoemulsions incorporating [DC-5][2NTf<sub>2</sub>] and DSG-PEG<sub>2000</sub></i> .....	255

4.2.5 Nanoemulsions incorporating monocholinium and [DC-ether] ILs.....	259
4.2.6 Nanoemulsions incorporating ILs containing first-generation bis(sulfonyl)azanide anions with alkyl-aryl substituents.....	261
4.2.7 Toxicity of IL nanoemulsions.....	263
4.3 Conclusion.....	264
4.4 Experimental.....	266
4.4.1 Materials.....	266
4.4.2 Formulation of poloxamer-based IL nanoparticles.....	266
4.4.3 Dynamic light scattering of poloxamer-based IL nanoparticles.....	266
4.4.4 Formulation of IL-containing nanoemulsions without microfluidization.....	267
4.4.5 Formulation of nanoparticles using microfluidization.....	267
4.4.6 Dynamic light scattering of IL-containing nanoemulsions.....	268
4.4.7 Evaluation of nanoparticle toxicity in mice.....	268
4.4.8 Zebrafish developmental toxicity.....	268
4.5 References.....	269
<b>CHAPTER 5 – MCT Nanoemulsions for the Efficient Delivery of siRNA.....</b>	<b>272</b>
Abstract.....	273
5.1 Introduction.....	274
5.2 Results.....	276
5.2.1 Hydrophobic ion pairing.....	276
5.2.2 Nanoemulsion preparation.....	277
5.2.3 Nanoemulsion characterization.....	277
5.2.4 Encapsulation efficiency and release.....	279
5.2.5 In vivo gene knockdown and histology.....	279
5.3 Discussion.....	280
5.4 Conclusion.....	282

5.5 Experimental.....	283
5.5.1 <i>Materials</i> .....	283
5.5.2 <i>Hydrophobic ion pairing</i> .....	283
5.5.3 <i>Pairing efficiency</i> .....	284
5.5.4 <i>Nanoemulsion preparation</i> .....	284
5.5.5 <i>siRNA integrity</i> .....	284
5.5.6 <i>Dynamic light scattering</i> .....	285
5.5.7 <i>Nanoparticle tracking analysis</i> .....	285
5.5.8 <i>Encapsulation efficiency</i> .....	285
5.5.9 <i>In vivo gene knockdown</i> .....	286
5.5.10 <i>Statistical analysis</i> .....	286
5.6 References.....	287
<b>CHAPTER 6 – Conclusions.....</b>	<b>289</b>
6.1 Primary Findings and Conclusions.....	290
6.1.1 <i>Synthesis and characterization of cholinium-based HILs</i> .....	291
6.1.2 <i>IL formulations</i> .....	292
6.1.3 <i>Delivery of hydrophobic siRNA using MCT-containing nanoemulsions</i> .....	293
6.2 Final Remarks.....	294
<b>APPENDIX.....</b>	<b>295</b>
A.1 Nuclear Magnetic Resonance Spectra for Synthesis.....	296
A.2 Differential Scanning Calorimetry Thermograms.....	484
A.3 Quantitative <sup>19</sup> F NMR Parameters and Spectra for Water Solubility Studies.....	502
A.4 Hygroscopicity of Dried Cholinium-based Ionic liquids containing [NTf <sub>2</sub> ] and first-generation bis(sulfonyl)azanide anions.....	526
A.5 Particle Size Analysis of NE <sub>scramble</sub> .....	527

## LIST OF FIGURES

<b>CHAPTER 1 – Introduction.....</b>	<b>1</b>
Figure 1.1 Structures and conventional abbreviations of commonly-used IL cations and anions.....	3
Figure 1.2 Snapshots of simulations of [C <sub>n</sub> mim][PF <sub>6</sub> ] with varying alkyl chains self-assembling.....	6
Figure 1.3 Active areas of research that involve ILs.....	6
Figure 1.4 Structures of lipids commonly employed in MD and biophysical experiments involving ILs.....	11
Figure 1.5 Penetration of imidazolium ILs into POPC lipid bilayers.....	13
Figure 1.6 Snapshots of the intercalation of 10 mol % [chol][phe] in POPC.....	14
Figure 1.7 Insertion of [C <sub>4</sub> mim] <sup>+</sup> into a POPC bilayer.....	15
Figure 1.8 Choline bicarbonate and CAGE insertion into model <i>E. coli</i> lipid membranes.....	16
Figure 1.9 QCM-D responses as DEPC vesicles form a SLBs and interact with [C <sub>8</sub> mim][Cl], [Li][NTf <sub>2</sub> ], and [BMP][NTf <sub>2</sub> ].....	21
Figure 1.10 SAXs patterns of cholesterol, egg PC, and egg PG LUVS exposed to different concentrations of [P <sub>1,8,8,8</sub> ][OAc].....	23
Figure 1.11 AFM images of MDA-MB-231 cells interacting with [C <sub>8</sub> mim][Cl].....	26
<b>CHAPTER 3 – Physicochemical and Toxicological Analysis of Hydrophobic Ionic Liquids.....</b>	<b>196</b>
Figure 3.1 DSC thermograms of [DC-4][2NTf <sub>2</sub> ], [DC-8][2NTf <sub>2</sub> ], and [DC-ether][2pBBSNTf].....	203
Figure 3.2 DSC thermograms of ILs containing the [NBNTs] anion and different cations.....	206
Figure 3.3 DSC thermograms of [DC-ether] ILs containing symmetric and asymmetric second generation bis(sulfonyl)azanide anions.....	207
Figure 3.4 <sup>19</sup> F NMR spectra of [DC-ether][2pBBSNTf] in acetone-d <sub>6</sub> and deuterium oxide.....	213
Figure 3.5 Images of zebrafish exposed to a variety of ILs and IL precursor salts.....	232
<b>CHAPTER 4 – Ionic Liquids as Components for Drug Delivery Vehicles.....</b>	<b>244</b>
Figure 4.1 Structure of poloxamers, [DC-ether][2TsNTf], and [DC-ether][2TBSNTf].....	248
Figure 4.2 Structures of sodium docusate, DSG-PEG <sub>2000</sub> , medium chain triglycerides, and the ILs used throughout the nanoemulsion studies.....	255
<b>CHAPTER 5 – MCT Nanoemulsions for the Efficient Delivery of siRNA.....</b>	<b>272</b>

Figure 5.1 Nanoemulsion DLS and NTA data, and siRNA integrity via urea-PAGE.....	278
Figure 5.2 Murine tumor model RT-qPCR statistics and histology images.....	280
<b>APPENDIX.....</b>	<b>295</b>
Figure A.1 NE <sub>scramble</sub> DLS and NTA data.....	527

## LIST OF TABLES

<b>CHAPTER 2 – Design and Synthesis of a New Generation of Hydrophobic Ionic Liquids.....</b>	<b>41</b>
Table 2.1 Cholinium ILs with carboxylate anions and their characteristics at room temperature.....	50
Table 2.2 Morpholinium ILs with fatty acid anions and their characteristics at room temperature.....	53
Table 2.3 Dicholinium IL containing fatty acid anions and their characteristics at room temperature.....	56
Table 2.4 Cholinium-based ILs containing second-generation dichain fatty acids and their characteristics at room temperature.....	59
Table 2.5 Cholinium and dicholinium-based ILs containing [NTf <sub>2</sub> ] anions and their characteristics at room temperature.....	61
Table 2.6 Dicholinium ILs containing first-generation bis(sulfonyl)azanide anions and their characteristics at room temperature.....	72
Table 2.7 Cholinium-based ILs containing third-generation bis(sulfonyl)azanide anions and their characteristics at room temperature.....	83
<b>CHAPTER 3 – Physicochemical and Toxicological Analysis of Hydrophobic Ionic Liquids.....</b>	<b>196</b>
Table 3.1 Physical transformation temperatures of monocholinium and dicholinium ILs paired with [NTf <sub>2</sub> ] anions and first-generation bis(sulfonyl)azanide anions.....	201
Table 3.2 Physical transformation temperatures of cholinium-based ILs with second- and third-generation bis(sulfonyl)azanide anions.....	204
Table 3.3 Viscosity values of monocholinium and dicholinium ILs with [NTf <sub>2</sub> ] anions and first-generation bis(sulfonyl)azanide anions.....	209
Table 3.4 Water solubility values of ILs containing [NTf <sub>2</sub> ] anions and first-generation bis(sulfonyl)azanide anions.....	211
Table 3.5 Water solubility of alkyl monocholinium ILs with first-generation bis(sulfonyl)azanide anions.....	215
Table 3.6 Water solubility values of second- and third-generation bis(sulfonyl)azanide anions and ILs with cholinium-based cations.....	216
Table 3.7 Hygroscopicity of cholinium and dicholinium ILs composed of [NTf <sub>2</sub> ] anions and first-generation bis(sulfonyl)azanide anions after being saturated with water and after drying.....	220
Table 3.8 LC50 values for alkyl cholinium, dicholinium, and first-generation bis(sulfonyl)azanide salt precursors and corresponding ILs in 4T1-Luc cells.....	222

Table 3.9 LC50 values for second- and third-generation IL salt precursors and ILs in 4T1 cells.....	226
Table 3.10 LC50 values for alkyl cholinium, dicholinium, and first-generation bis(sulfonyl)azanide salt precursors and corresponding ILs in zebrafish.....	230
<b>CHAPTER 4 – Ionic Liquids as Components for Drug Delivery Vehicles.....</b>	<b>244</b>
Table 4.1 List of components for each IL formulation containing P123.....	249
Table 4.2 List of components for each IL formulation containing L35, F68, or F127.....	250
Table 4.3 List of components for each IL formulation containing P123 and L35.....	252
Table 4.4 List of components for each IL formulation used in the zebrafish toxicity studies.....	254
Table 4.5 List of components for formulations containing [DC-5][2NTf <sub>2</sub> ] and DSG-PEG <sub>2000</sub> .....	256
Table 4.6 List of components for formulations containing monocholinium and [DC-ether] ILs as well as DSG-PEG <sub>2000</sub> .....	259
Table 4.7 List of components for formulations containing [DC-ether][2pOBSNTf].....	262
<b>APPENDIX.....</b>	<b>295</b>
Table A.1 Recycle delay ( $D_1$ ) parameters used for the inversion recovery experiments for each monocholinium and dicholinium IL composed of [NTf <sub>2</sub> ] and first-generation bis(sulfonyl)azanide anions, and corresponding $T_1$ values.....	502
Table A.2 Hygroscopicity of Dried Cholinium-based Ionic liquids containing [NTf <sub>2</sub> ] and first-generation bis(sulfonyl)azanide anions.....	526

## LIST OF SCHEMES

<b>CHAPTER 2 – Design and Synthesis of a New Generation of Hydrophobic Ionic Liquids.....</b>	<b>41</b>
Scheme 2.1 Synthesis of monocholinium, dicholinium, and morpholinium cations.....	46
Scheme 2.2 Synthesis of cholinium ILs with carboxylate anions.....	48
Scheme 2.3 Synthesis of morpholinium-based ILs with fatty acid anions.....	51
Scheme 2.4 Synthesis of dicholinium ILs with fatty acid anions.....	54
Scheme 2.5 Synthesis of the DOP anion and corresponding ILs.....	57
Scheme 2.6 Synthesis of second-generation dichain fatty acid anions and corresponding ILs.....	58
Scheme 2.7 Synthesis of cholinium- and morpholinium-based ILs with [NTf <sub>2</sub> ] anions.....	62
Scheme 2.8 Synthesis of dicholinium ILs containing both octanoate and [NTf <sub>2</sub> ] anions.....	63
Scheme 2.9 Synthesis of second-generation dicholinium cations and corresponding ILs containing [NTf <sub>2</sub> ] anions.....	64
Scheme 2.10 Synthesis of dicholinium ILs containing saccharine and acesulfame K anions.....	66
Scheme 2.11 Synthesis of first-generation bis(sulfonyl)azanide anions.....	67
Scheme 2.12 Synthesis of mono- and dicholinium ILs containing first-generation bis(sulfonyl)azanide anions.....	69
Scheme 2.13 Synthesis of second-generation bis(sulfonyl)azanide anions that incorporate phenyl, tosyl, and 4-methoxyphenyl groups.....	74
Scheme 2.14 Synthesis of cholinium and dicholinium ILs containing second-generation bis(sulfonyl)azanide anions that incorporate phenyl, tosyl, and 4-methoxyphenyl groups.....	75
Scheme 2.15 Synthesis of second-generation bis(sulfonyl)azanide anions containing aryl groups with electron-withdrawing moieties or tertbutyl groups.....	77
Scheme 2.16 Synthesis of cyclic monocholinium cations.....	78
Scheme 2.17 Synthesis of ILs with [DC-ether], [N <sub>1,1,4,2OH</sub> ], [N <sub>1,1,6,2OH</sub> ], and cyclic monocholinium cations paired with second-generation bis(sulfonyl)azanide anions that contain aryl groups with electron-withdrawing moieties and tertbutyl groups.....	79
Scheme 2.18 Synthesis of third-generation anions containing one aryl group and one alkyl group.....	81
Scheme 2.19 Synthesis of ILs containing [DC-ether] and cyclic monocholinium cations and third-generation anions.....	82

<b>CHAPTER 5 – MCT Nanoemulsions for the Efficient Delivery of siRNA.....</b>	<b>272</b>
Scheme 5.1 Hydrophobic ion pairing of DOTAP and siRNA.....	276
Scheme 5.2 Formulation methodology for MCT nanoemulsion.....	277

## LIST OF ABBREVIATIONS

[NTf <sub>2</sub> ]	Bis(trifluoromethanesulfonyl)azanide
4T1-Luc	Murine breast cancer cell line expressing luciferase
AFM	Atomic force microscopy
ANOVA	Analysis of variance
BGG	Bovine gamma globulin
BSA	Bovine serum albumin
CAGE	Choline and geranate
CLSM	Confocal laser scanning microscopy
D <sub>1</sub>	Recycle delay
DCM	Dichloromethane
DES	Deep eutectic solvent
DLS	Dynamic light scattering
DMEM	Dulbecco's modified eagle media
DMSO	Dimethyl sulfoxide
DOP	2-methyl-3(octanoyloxy)-2-((octanoyloxy)methyl)propanoic acid
DOTAP	Dioleoyl-3-trimethylammonium-propane
DSC	Differential scanning calorimetry
DSG-PEG <sub>2000</sub>	Distearoyl-rac-glycerol-PEG2K
EE	Encapsulation efficiency
EMT	Endothelial-to-mesenchymal transition
FDA	Food and Drug Administration
FF	Force field
HIL	Hydrophobic ionic liquid
HIP	Hydrophobic ion pairing
IACUC	Institutional Animal Care and Use Committee
IL	Ionic liquid
IL/w	Ionic-liquid-in-water
ITC	Isothermal titration calorimetry
LC50	Median lethal concentration
LUVs	Large unilamellar vesicles
MCT	Medium chain triglyceride(s)
MD	Molecular Dynamic
MILs	Magnetic ionic liquids
MLVs	Multilamellar vesicles
mRNA	Messenger ribonucleic acid
MWCO	Molecular weight cut off
NaTFA	Sodium trifluoroacetate
NE	Nanoemulsion
NMR	Nuclear magnetic resonance
NTA	Nanoparticle tracking analysis
o/w	Oil-in-water
PAGE	Polyacrylamide gel electrophoresis
PBS	Phosphate buffered saline

PC	Phosphatidylcholine
PE	Phosphatidylethanolamine
PEG	Polyethylene glycol
PEO	Polyethylene oxide
POPC	1-palmitoyl-2-oleoyl-sn-glycero-3-phosphocholine
POPE	1-palmitoyl-2-oleoyl-sn-glycero-3-phosphoethanolamine
PPO	Polypropylene oxide
PS	Phosphatidylserine
Psi	Pounds per square inch
PTX	Paclitaxel
QCM-D	Quartz crystal microbalance with dissipation monitoring
qNMR	Quantitative nuclear magnetic resonance
RNAi	RNA interference
ROS	Reactive oxygen species
RT-qPCR	Reverse transcriptase quantitative polymerase chain reaction
SANs	Small-angle neutron scattering
SAXs	Small-angle X-ray scattering
SEM	Standard error of measurement
siRNA	Small interfering ribonucleic acid
SLBs	Supported lipid bilayers
SLN	Solid lipid nanoparticle
SUVs	Small unilamellar vesicles
$T_1$	Spin-lattice relaxation time
WAXs	Wide-wangle X-ray scattering
XRR	X-ray reflectivity

# CHAPTER 1

## Introduction

---

**This chapter has been, in part, prepared as a review article with the tentative title: “Molecular Dynamic and Biophysical Methods to Probe the Interactions of Ionic Liquids and Lipid Bilayers” by Marshall S. Padilla and Sandro Mecozzi**

## 1.1 Ionic Liquids: Nomenclature, Structure, and Applications

### 1.1.1 Ionic liquid, molten salt,, or something else?

In the past two decades, an enormous effort has been put into discovering new materials that can be easily produced and widely-applied. In this time period, few other classes of compounds have been investigated as deeply as ionic liquids (ILs), despite their discovery over one-hundred years ago.<sup>1</sup> Although subject to some debate, ILs are loosely classified as materials composed entirely of anions and cations that have melting points below 100 °C.<sup>2</sup> This temperature cutoff is arbitrary as the properties of liquid salts are not significantly changed below this temperature. Still, 100 °C is used as a threshold to differentiate between molten salts and ILs.

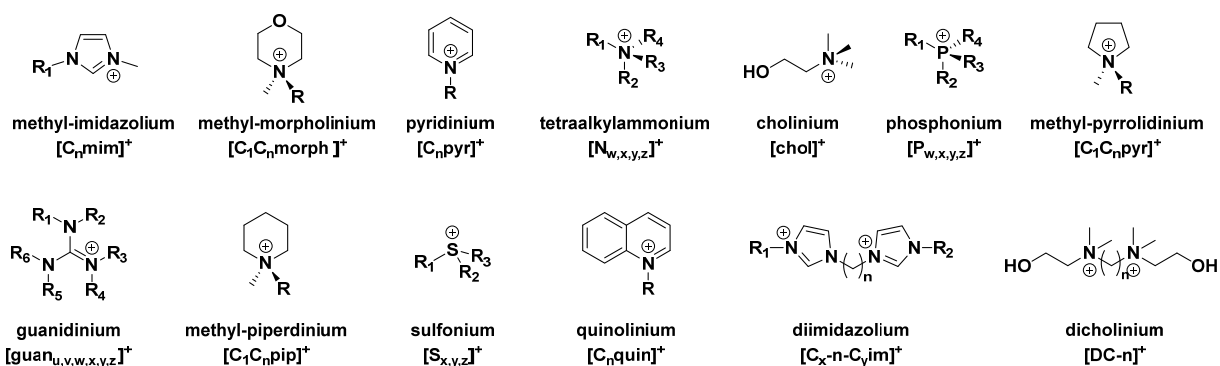
It is important to note that the term “ionic liquids” has not been used exclusively to define compounds of this category, as terms such as fused salts<sup>3</sup>, ionic glasses<sup>4</sup>, ionic fluids<sup>5</sup>, and others have been described in the literature. In some cases, the phrase “deep eutectic solvent (DES)”, which are mixtures of any compounds that have lower melting points than the parent molecules, is used in conjunction with ILs.<sup>6</sup> While all ILs are DESs, the latter does not need to be liquid below 100 °C nor composed of cations or ions. Due to the arbitrary designation of 100 °C as the cutoff, many compounds are erroneously classified as ILs, such as the commonly cited choline dihydrogen phosphate ([chol][DHP]), which has a melting point of 190 °C. Additionally, compounds like [chol][DHP] often are dissolved in water and called “ILs” as the solution contains IL-like ions and is a liquid.<sup>7</sup> Although these mixtures behave similarly to ILs, they are better described as “hydrated ILs”.<sup>8</sup>

The confusion in nomenclature stems from the fact that ILs are named based on a single attribute – melting temperature. More recently, ILs have been further defined based on their sub-class, which can be based on their properties, structure, and function. This includes room temperature ILs (RTIL; salts that are liquid below room temperature)<sup>9</sup>, hydrophobic ILs (HILs; ILs that are not appreciably solubilized by water)<sup>10</sup>, polymeric ILs (polymers composed of IL-like monomers)<sup>11</sup>, and magnetic ILs (MILs; ILs incorporating paramagnetic elements).<sup>12</sup>

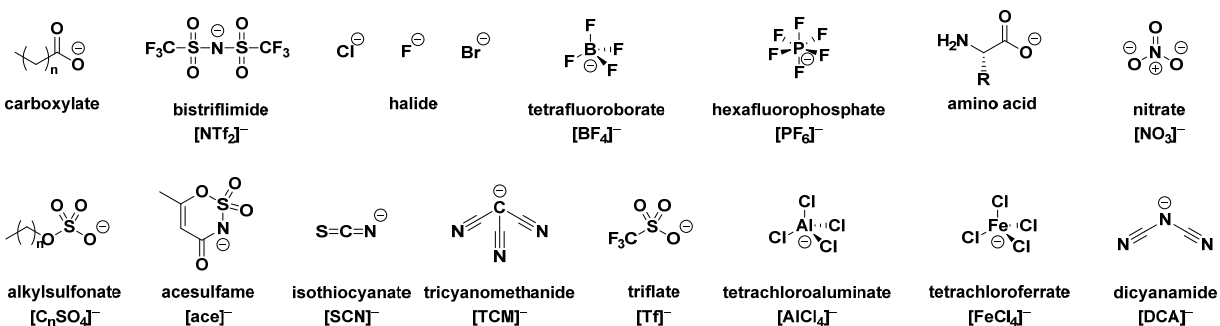
### 1.1.2 Cation, anion, and IL synthesis

ILs are typically composed of organic and inorganic ions; however, one of their key properties is their structural diversity. The cations often contain a quaternary amine, sulfonium, or phosphonium core, as these atoms can stabilize the lack of electron density as compared to carbocations and oxonium ions, which are not stable enough to form ILs. The most frequently used cations contain quaternary ammonium or N-heterocycle groups, the latter including imidazolium, morpholinium, pyridinium, and other heterocyclic compounds. The anions have greater structural range including simple halides ( $[\text{Br}]^-$ ,  $[\text{Cl}]^-$ ,  $[\text{I}]^-$ ) as well as complex non-coordinating species such as bis(trifluoromethanesulfonyl)amide ( $[\text{NTf}_2]^-$ ), hexafluorophosphate ( $[\text{PF}_6]^-$ ), and tetrafluoroborate ( $[\text{BF}_4]^-$ ). The greater structural diversity is due to the easier stabilization of negative charge. A list of commonly-used anions and cations can be found in **Figure 1.1**.

#### Cations



#### Anions



**Figure 1.1** Structures and conventional abbreviations of commonly-used IL cations and anions.

Large libraries of ILs can be readily synthesized using simple organic chemistry techniques as the starting materials are widely available through commercial vendors. Moreover, their popularity has resulted in companies producing and selling their own ILs. Although new ILs are synthesized every year, it is estimated that the total number of possible ILs exceeds  $10^{14}$  possible combinations of anions and cations.<sup>13</sup> The cations containing amine or phosphonium groups are usually synthesized by quaternization reactions, in which a tertiary amine or alkyl phosphine is reacted with an alkyl halogen. Since the reaction typically occurs in an organic solvent, the resulting salt will precipitate out, making purification easy and free from laborious chromatography steps. The anions are often purchased either in their ionic form or protonated form, the latter necessitating a deprotonation step.

The synthesis of the ILs themselves can require more optimization. For HILs, often, the components are mixed in water and the IL precipitates out through a metastasis reaction, requiring only washes with water to purify. Hydrophilic ILs can be prepared in this manner using solvents other than water, although the success of the reaction is strongly dependent on the solubility of the anion precursor salt, cation precursor salt, and resulting IL. A second strategy involves exchanging the anion component of the cation precursor salt with a hydroxide ion using Dowex® or other resins. Then, the cation-hydroxide salt undergoes a neutralization reaction with the protonated form of the anion. The resulting water can be removed during the reaction through a Dean-Stark trap, or afterwards via a vacuum oven or lyophilizer.

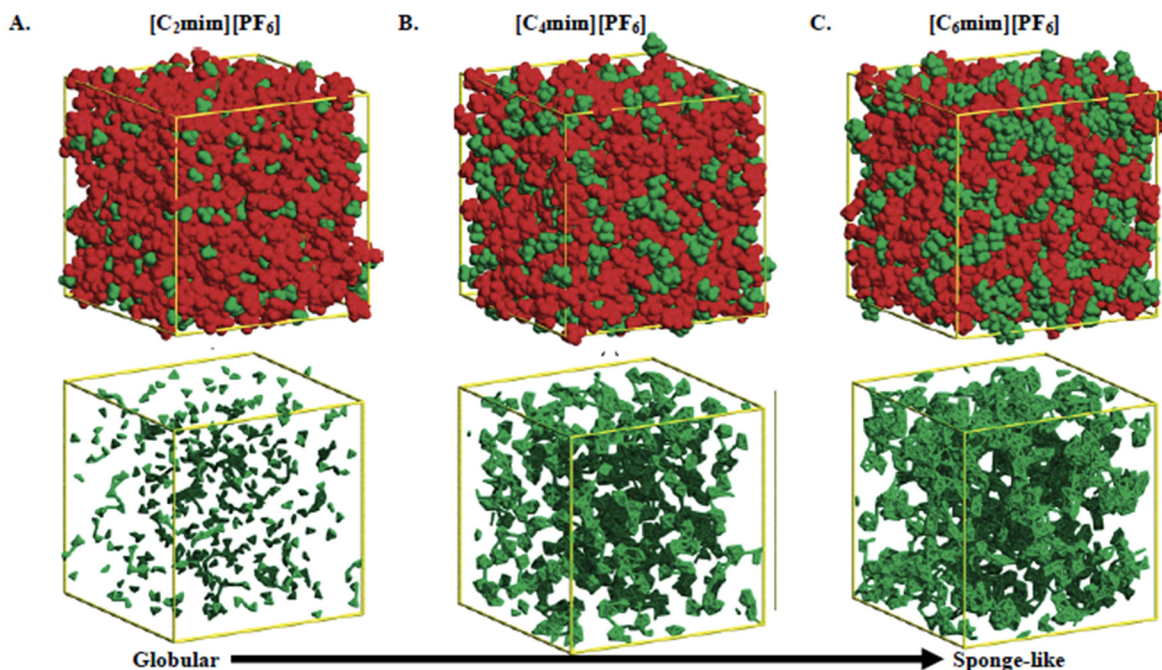
### *1.1.3 Nanostructure of ILs*

ILs have depressed melting temperatures compared to traditional salts due to the unique structure and bonding within the liquid materials. Salts, such as sodium chloride, have strong ionic bonds as a result of the wide disparity in electronegativity between the ions, and as a result, form crystal lattices. For ILs, the lattice energy is significantly decreased as the electron clouds of the cations and anions are more delocalized. This explains why the IL cations are large organic molecules and not smaller ions such as sodium and lithium cations. Functional groups such as imidazolium can delocalize electron density via  $\pi$ -conjugation, while tetraalkylammonium structures delocalize electron density through hyperconjugation.

HILs result from enhanced lipophilicity as well as the extreme electron delocalization of the ions, especially the anions, which is why HILs typically include  $[\text{NTf}_2]^-$ ,  $[\text{PF}_6]^-$ , and  $[\text{BF}_4]^-$ , as these molecules are unable to effectively engage in hydrogen bonding with water.

Depending on the IL molecular architecture, the ions can engage in a variety of intermolecular interactions other than ionic bonding, such as hydrogen bonding, Van der Waals forces,  $\pi$ -stacking, and ion-dipole forces. Although the Coulombic forces are typically the strongest intermolecular interactions in ILs, hydrogen bonding is essential in forming nanoscopic structures.<sup>14</sup> Protic ILs (PILs; ILs prepared via the neutralization of a Brønsted acid and Brønsted base)<sup>15</sup> have a complex hydrogen bonding network due to their electron deficient hydrogen atoms; however, aprotic ILs (AILs; ILs without an appreciably acidic protons)<sup>16</sup> also can form discrete hydrogen bonding systems.<sup>17</sup>

As a result of the numerous intermolecular interactions, homogenous and heterogenous structures form in the IL milieu. The simplest unit that is found in ILs is the ion pair between the cation and anion, which is not necessarily restricted to Coulombic interactions, as ions in ILs can also form pairs via hydrogen bond interactions.<sup>18</sup> This pair can act as a monomer that forms repeats, akin to a polymer, and as a result, large clusters and aggregates form that create unique three-dimensional structures due to the presence of non-Coulombic interactions, especially hydrogen bonding. Since these compounds are liquid, the structures are dynamic, meaning molecular arrangements can be transformed into new architectures through Brownian motion. Certain ILs can self-assemble into distinct structures, such as those with long alkyl chains that form lipophilic domains that separate from ionophilic domains (**Figure 1.2**).<sup>19</sup> Although earlier research suggested ILs formed micellar systems, newer studies have revealed that ILs may form larger and more complex mesoscopic structures.<sup>20</sup> Still, nanostructure is heavily dependent on the type of ILs, where ILs such as MILs can form unique magnetic interactions due to the presence of magnetic anions such as iron tetrachloride.



**Figure 1.2** Snapshots of the simulation boxes of the bulk structure of  $[C_nmim][PF_6]$  ILs at equilibrium for (A)  $[C_2mim][PF_6]$ , (B)  $[C_4mim][PF_6]$ , and (C)  $[C_6mim][PF_6]$ . Each box contains 700 ion pairs at equilibrium. The anion and the imidazolium ring of the cation are the polar domains and are depicted in red. The alkyl chains are depicted in green and represent the nonpolar domains. The bottom row (left to right) corresponds to the nonpolar domains of  $[C_2mim][PF_6]$ ,  $[C_4mim][PF_6]$ , and  $[C_6mim][PF_6]$ . The boxes fluctuate in size due to differences in ion size and box density. Figure adapted from reference 18 and prepared by Dr. Moira Esson<sup>21</sup>.

#### 1.1.4 IL properties and applications

ILs possess numerous physicochemical properties that are reflective of their unique nanostructure.<sup>22</sup> As a result of their ionic composition, ILs have negligible vapor pressure and excellent ionic conductivity. Additionally, ILs have thermal and chemical stability as well as low flammability, although these properties depend on the specific cations



**Figure 1.3** Active areas of research that involve ILs.

and anions of the IL. One of the most important properties of ILs is their ability to function as solvents. This is a direct result of their ability to engage in an array of intermolecular interactions, where ILs can dissolve a wide range of materials such as proteins<sup>23</sup>, cellulose<sup>24</sup>, Teflon<sup>25</sup>, and essential oils<sup>26</sup>. These characteristics have resulted in ILs being dubbed “designer solvents” and “green solvents” that could replace traditional organic solvents.<sup>27</sup> Along with being employed as solvents, IL have been utilized in other applications including catalysis<sup>28</sup>, battery development<sup>29</sup>, nuclear fuel extraction<sup>30</sup>, and liquid crystal displays<sup>31</sup> (**Figure 1.3**).

One area that has seen the promising applications of ILs is their use as drug formulation components. This is a result of their ability to solubilize a wide-range of pharmaceutical drugs, such as paclitaxel<sup>32</sup>, amphotericin B<sup>33</sup>, insulin<sup>34</sup>, and siRNA<sup>35</sup>. Often, ILs are added as cosolvents and emulsifiers to form drug formulations or even drug delivery vehicles, the latter mainly consisting of nanoemulsions<sup>36</sup> and microemulsions<sup>37</sup>. Additionally, therapeutics can be transformed into ILs by modulating their structure, forming IL-APIs (active pharmaceutical ingredients). Examples of IL-APIs include lidocaine<sup>38</sup>, naproxen<sup>39</sup>, and ibuprofen<sup>40</sup>. A list of formulations that utilize ILs as well as IL-APIs can be found in a review by Egorova *et al.*<sup>41</sup>

### 1.1.5 The environmental reality of ILs

Despite the promise of ILs as environmentally benign materials, the large investment in ILs has led to a startling realization – many of the so-called “green solvents” exhibit toxicity. Although this toxicity can be leveraged to design novel antibacterial<sup>42</sup>, antifungal<sup>43</sup>, and anticancer<sup>44</sup> ILs, many ILs show tremendous aquatic<sup>45</sup> and mammalian<sup>46</sup> toxicity. Still, the revelation of IL toxicity is understudied, despite reports from the early 2000s that detail the environmentally harmful nature of ILs.<sup>47</sup> A meta-analysis in 2016 uncovered that only 0.55% of the IL literature was devoted to studying toxicity.<sup>48</sup> Additionally, the study found that many ILs are more toxic than phthalates, bisphenols, and alcohol ethoxylates, and that those classes of compounds have a higher percentage of publications related to toxicity than ILs. Still, the past five years has seen a surge in studies on IL toxicity as the concept has become more mainstream. This

was demonstrated when the Journal of Analytical Chemistry's biennial review, *Water Analysis: Emerging Contaminants and Current Issues*, included ILs in its 2018 edition.<sup>49</sup> The focus on the environmental impacts of ILs is important now, more than ever, as several companies have begun producing ILs in metric ton scales.<sup>50</sup>

The quest to understand IL toxicity has been led primarily by academic research groups. Many studies focus on IL exposure to organisms such as zebrafish (*Danio rerio*)<sup>51-53</sup>, *Daphnia magna*<sup>54,55</sup>, *Vibrio fischeri*<sup>56-58</sup>, *Selenastrum capricornutum*<sup>59,60</sup>, *Scenedesmus quadricauda*<sup>61,62</sup>, *Scenedesmus obliquus*<sup>63,64</sup>, various cancer cell lines<sup>65-68</sup>, *Escherichia coli*<sup>69,70</sup>, yeast<sup>71,72</sup>, and Wistar rats<sup>73</sup>. Additionally, there have been several publications related to IL biodegradability, as summarized in a thorough review by Jordan and Gathergood.<sup>74</sup> One key outcome from the preliminary studies on IL toxicity is that ILs can diffuse into plasma membranes, distorting their structure and integrity, and even inducing apoptosis.<sup>75</sup> The degree to which ILs affect plasma membrane composition depends on the specific molecular architecture of the cations and anions, where features such as long alkyl chains and phosphonium cations are more likely to induce membrane dissociation.<sup>76</sup>

While organismal studies have been essential for establishing these trends, they do not reveal the underlying molecular interactions that cause toxicity. Instead, academic labs have employed advanced instrumentation and molecular dynamic (MD) simulations to provide mechanistic detail of IL and lipid membrane interactions. This has been made possible due to the technological advances in instrument resolution and computer power. The strength of these techniques can be partially attributed to the long history of artificial lipid bilayer development, either *in silico* or *in vitro*, which allows studies to utilize cell-like models when cells themselves are incompatible. The following sections, while not strictly related to the thesis work, provides an important summary of these methods, which have not been holistically reviewed in a single article.

## 1.2 Molecular Dynamics

MD approaches allow for the nanoscopic view of the interactions between individual and groups of molecules at a level often unobtainable by other methods. For studies on IL toxicity, MD simulations are employed to predict the effect of adding ILs to lipid bilayers. Although ILs have only recently reemerged as targets for computational studies, the first MD papers modeling biological membranes were in the 1980s, using simplistic molecules such as decanoate to represent cellular membranes.<sup>77</sup> Since then, there has been significant advances in modeling due to innovations in computer technology.<sup>78</sup> In the 1990s, a bilayer would only be composed of ~100 lipids and examined for a few picosecond, whereas current models can analyze ~10,000 lipids in microsecond timescales.<sup>79</sup> MD simulations rely on mathematical equations to predict the motion of particles. These equations factor in chemical parameters for inter- and intramolecular interactions, such as Van der Waals forces, electrostatic interactions, and hydrogen bonding. The amalgamation of these equations forms the force field (FF), which are the parameters used to calculate the potential energy of the particles, or in this case, the lipid bilayers.<sup>80</sup> The collection of the positional data over a period of time is known as the trajectory, which can subsequently be analyzed to quantitate membrane dynamics. Additionally, trajectory information can be visualized using software to produce realistic images of lipid bilayer interactions.

FFs can be classified by their level of resolution, meaning their level of detail. Resolutions range from all-atom models, in which every atom for each molecule is described, to implicit models, where individual components are reduced to bulk solvents. Typically, higher resolution models of lipid membranes are used to probe IL toxicity, where the most common are atomistic and coarse-grain models (described below).<sup>81</sup> Lower resolution models, such as implicit models, are seldom used, despite their importance for lipid membrane research, as they do not provide enough detail to accurately depict the influence of ILs on lipid membranes.<sup>82</sup> A full description of the FFs employed to model cellular membranes can be found in a comprehensive review by Marrink *et al.*<sup>83</sup>

The following sections provide a detailed overview of the methods that are used to probe the IL toxicity using MD. The first section describes the rationale for choosing a particular lipid or set of lipids to

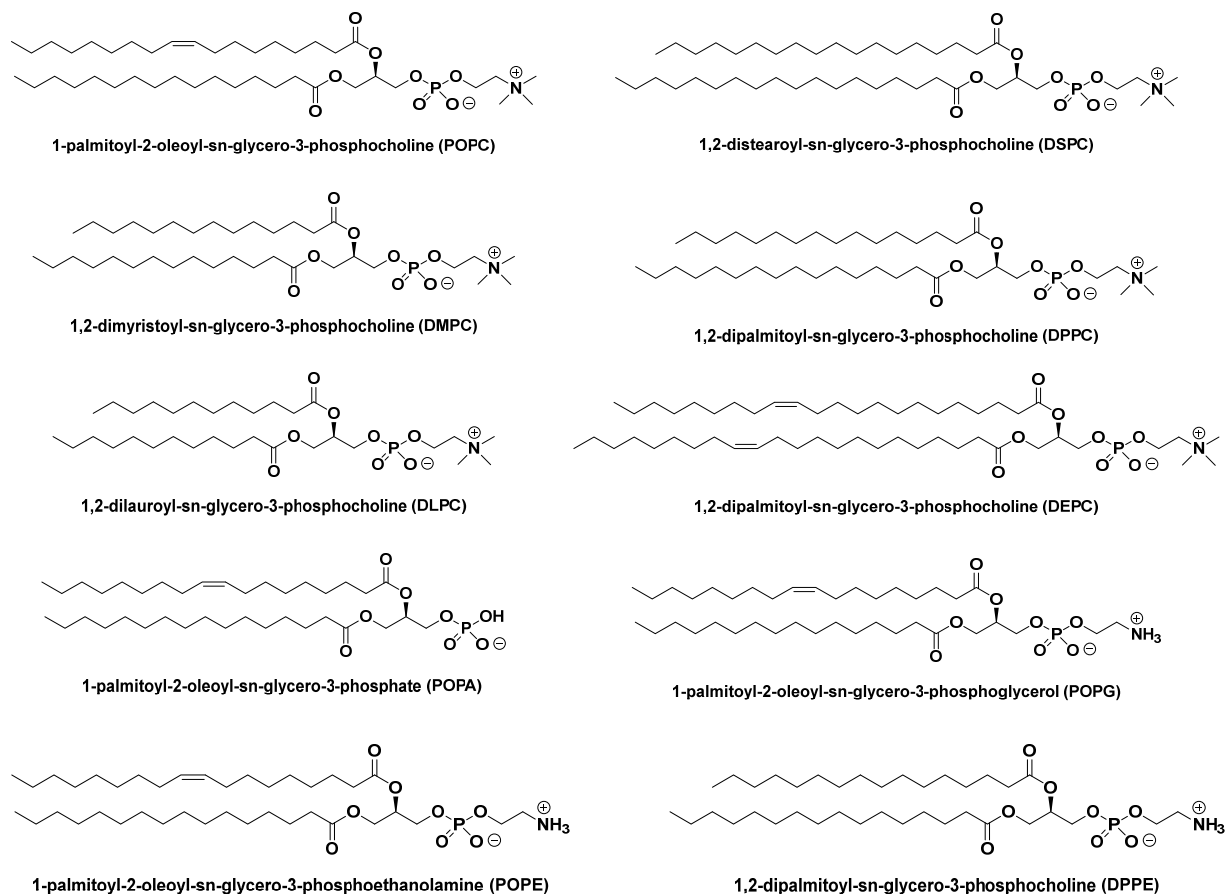
create a bilayer, while the subsequent sections discuss atomistic, coarse-grain, and other MD models used to predict the interactions between bilayers and ILs. In each section, the results of specific studies that utilize unique MD approaches are explored.

### 1.2.1 *Choosing the phospholipid*

The lipid composition of a cell strongly depends on the cell type and the organelle or feature of interest. For example, organelles such as the Golgi apparatus and mitochondria contain different distributions of lipids.<sup>84</sup> In MD simulations, the focus is on the plasma membrane as that is where ILs initially contact the cell. In general, the plasma membrane is small at around 5-6 nm wide, and is composed of roughly 34% cholesterol, 23% phosphatidylcholine (PC), 17% sphingomyelin, 11% phosphatidylethanolamine (PE), and 8% phosphatidylserine (PS), where the names of the lipids correspond to their head groups.<sup>85</sup> Within a certain class, lipids can vary in their alkyl chain length as well as their degree of saturation. Cholesterol is found ubiquitously in membranes as it adds structural support and forms lipid rafts with sphingolipids.<sup>86</sup> The plasma membrane is not an even distribution of lipids, and instead is heterogeneous and asymmetric, containing pockets composed of different classes of lipids.<sup>87</sup> The outer leaflet contains mostly PC and sphingolipids while the inner leaflet contains PE and PS. Proteins are also abundant among the plasma membrane, located on either the outer leaflet, inner leaflet, or both leaflets. The specific proteins in the bilayer depend on the type of cell.

Most MD simulations form bilayers using PC-related lipids as they compose the majority of the phospholipids in eukaryotes. The choice of PC lipid influences the overall structure of the lipid bilayer. For example, 1-palmitoyl-2-oleoyl-sn-glycero-3-phosphocholine (POPC) is cylindrical as a result of the *cis* alkene group and contributes to membrane fluidity.<sup>88</sup> Conversely, 1-palmitoyl-2-oleoyl-sn-glycero-3-phosphoethanolamine (POPE) is conical due to the small polar head that facilitates negative curvature stress on the membrane. A list of the common lipids employed in MD studies, as well as biophysical studies (see below), and their structures can be found in **Figure 1.4**. Most studies create lipid bilayers with one or two

lipids, as employing varying types of lipids significantly increases the complexity and computer power of the simulations.



**Figure 1.4** Structures of lipids commonly employed in MD and biophysical experiments involving ILs.

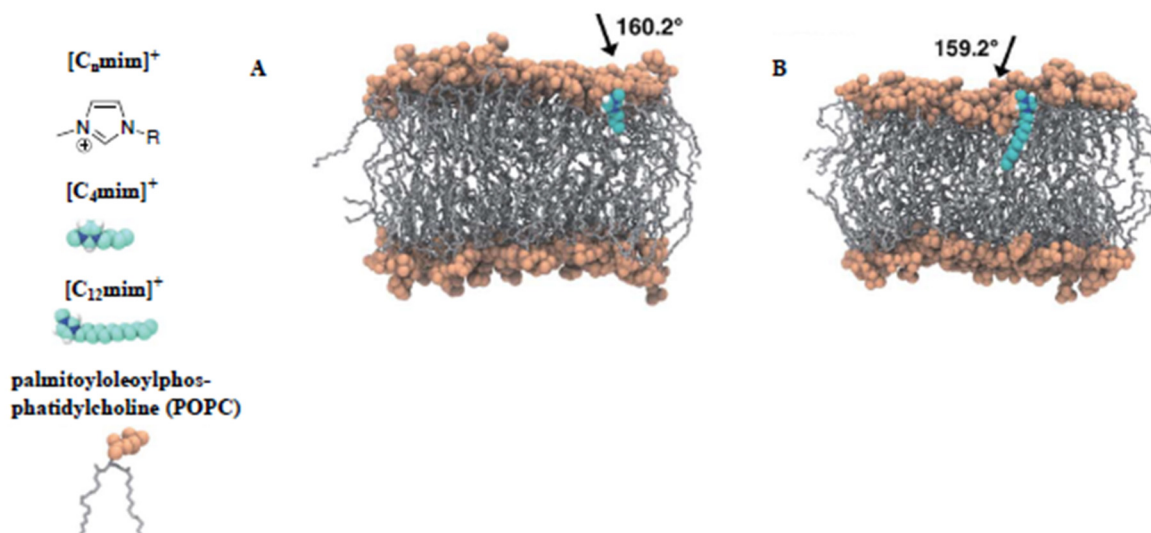
### 1.2.2 Atomistic models

Most MD studies involving ILs and lipid bilayers use atomistic models. In this framework, molecules are represented by a certain number of atomic sites joined by chemical bonds. The number of atoms may not represent the total number of atoms in a molecule but is enough to accurately represent its dynamics. For example, DPPC, which is composed of 134 atoms, is often represented by only 40–50 atoms, where the methylene and methyl groups are represented by a single atom.<sup>89</sup> This approach is needed for

modeling phospholipids, as calculations may examine hundreds to thousands of lipids, although all-atom simulations of lipid bilayers have been performed.<sup>90</sup> By reducing the total number of atoms, the computational power needed is drastically reduced. The most popular atomistic lipid bilayer FFs for IL studies are CHARMM<sup>91,92</sup> and AMBER<sup>93</sup>, although researchers have employed other FFs such as OPLS<sup>94,95</sup> and GROMOS<sup>96,97</sup>. The choice of FF is important as different models can yield distinct results.<sup>98</sup>

Lipid bilayers and ILs are often modeled using separate FFs, although it is important to ensure that the FFs are compatible. For example, in a study on POPC lipid bilayers and [C<sub>4</sub>mim][PF<sub>6</sub>] ILs, POPC was modeled using GROMOS and the ILs were modeled using a combined AMBER/OPLS FF; however some optimization was needed produce consistent results.<sup>97,99</sup> The modeling of ILs often employ distinct FFs due to their small size unique and nanostructure, the former meaning they are modeled in higher resolution, sometimes as an all-atom FF.<sup>100</sup> Specific FFs have been built for certain classes of ILs containing imidazolium<sup>100,101</sup> and pyridinium<sup>102</sup> cations as well as ILs containing [Tf]<sup>-</sup> and [NTf<sub>2</sub>]<sup>-</sup> anions<sup>103</sup>.

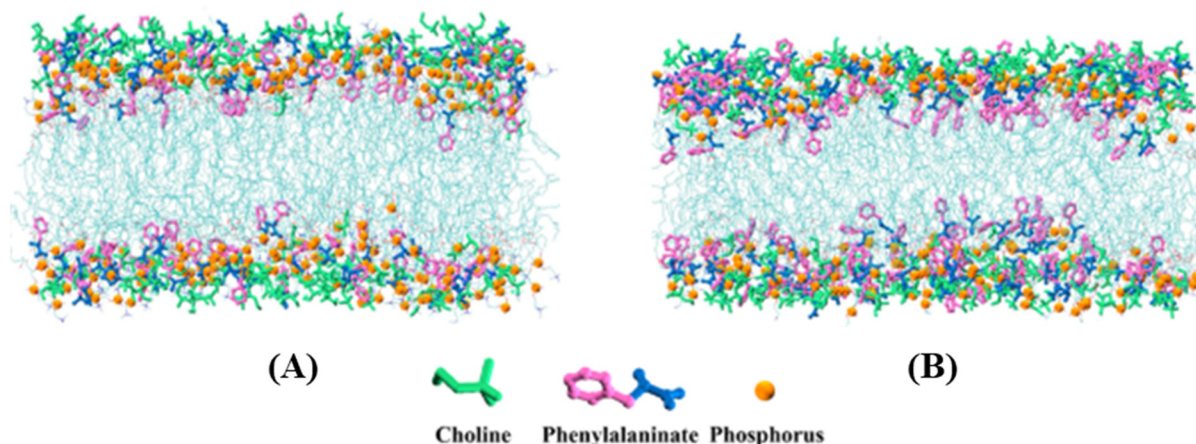
Owing to their broad use in many applications, a large number of studies focus on imidazolium ILs. In one study a from Yoo *et al*, imidazolium ILs with different alkyl chain lengths and different anions were examined in a POPC bilayer.<sup>104</sup> The POPC bilayer was constructed partially by the popular united-atom Berger model, which blends OPLS and GROMOS parameters.<sup>89</sup> The ILs employed united-atom models specific to imidazolium liquids.<sup>105,106</sup> The studies revealed that imidazolium-based ILs act as ionic surfactants, as the cation, regardless of the alkyl chain length, is energetically favorable to insert into the bilayer (**Figure 1.5**). Cation absorption results in the disturbance in the packing of the bilayer. Interestingly, out of the hydrophobic ions, [BF<sub>4</sub>]<sup>-</sup>, [PF<sub>6</sub>]<sup>-</sup>, and [NTf<sub>2</sub>]<sup>-</sup>, only [NTf<sub>2</sub>]<sup>-</sup> can fully insert into the bilayer and where it reassociates with the cationic component.



**Figure 1.5** Penetration of imidazolium ILs (A)  $[C_4mim][Cl]$  and (B)  $[C_{12}mim][Cl]$  into a POPC lipid bilayer. All other anions, cations and water molecules present in the system of the simulation are omitted for clarity. Figure adapted from reference 104 and prepared by Dr. Moira Esson<sup>21</sup>.

More recently, there has been a focus on modeling the interactions of biocompatible ILs such as choline- and amino acid-based ILs. In one study, cholinium glycinate ( $[chol][gly]$ ) was analyzed in homogeneous POPC and POPE layers.<sup>92</sup> Both the lipids and IL were modeled using CHARMM. The results indicated that POPC layers became compressed and more ordered when exposed to  $[chol][gly]$ , even at lower concentrations. On the other hand, POPE bilayers have a concentration-dependent affect, becoming compressed at higher concentrations, due to the strong inter- and intramolecular interactions between POPE lipids. Interestingly, these ions were not found in the hydrophobic sections of the bilayer, whereas heteroaromatic ions, such as imidazolium cations, can insert themselves. A recent study by Kumari *et al* revealed that amino acid anions with aromatic rings, such as phenylalaninate ( $[phe]^-$ ), can partially enter the alkyl chain section of the lipid bilayer as a result of the hydrophobic ring, where the anion can disturb the overall structure (**Figure 1.6**).<sup>107</sup> Intriguingly, the latter effect seems to be more pronounced in POPE layers rather than POPC layers. Other atomistic MD studies have examined ILs with more unique lipid

bilayers and environments, such as cholesterol bilayers<sup>108</sup>, bacterial membranes (POPE, POPG, and POPA)<sup>109</sup>, and pore formation in bilayers<sup>110</sup>.



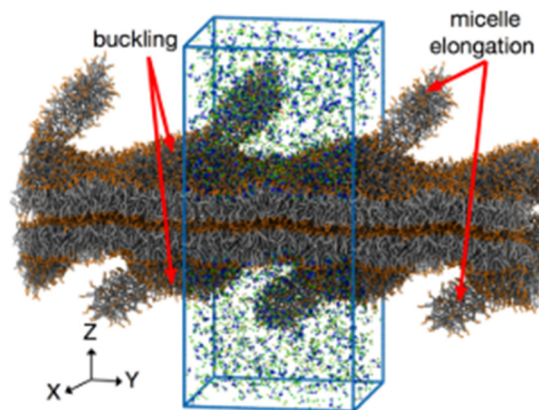
**Figure 1.6** Snapshots of the intercalation of 10 mol % [chol][phe] in (A) POPC and (B) POPE lipid bilayers. Lipid alkyl chains are displayed in cyan. IL ions outside of the interface and water molecules are not depicted. Figure adapted from reference 107.

### 1.2.3 Coarse-grain models

Although atomistic MD calculations are useful for examining specific inter- and intramolecular interactions of ILs with lipid bilayers, they are limited in the timeframe of the study, usually in the low nanosecond range. As a result, these studies only model the ILs entering the bilayer but not undergoing thermodynamic equilibrium within the membrane.<sup>111</sup> Much longer time scales can be gained by using coarse-grained MD simulations. In coarse-grained models, phospholipids and ILs are not represented by individual atoms, but rather, by groups of atoms dubbed “grains”.<sup>112</sup> By grouping atoms, the number of degrees of freedom is reduced, meaning MD calculations require less computational power, and thus allow for longer simulation times, albeit at lower resolution.<sup>113</sup> For example, in one study, POPC was represented by sixteen grains, where the grains were divided into eight characteristic groups, or beads.<sup>114</sup> The beads correspond to unique chemical groups, such as the positively-charged choline, negatively-charged phosphate, and methylene groups.

The field of coarse-grain MD simulations of IL and lipid bilayer interactions is relatively sparse compared to atomistic MD simulations, and thus there are no standard phospholipid FFs that have been established. Still, there are a plethora of coarse-grain FFs employed for other types of lipid bilayer studies, the most common include MARTINI<sup>115</sup>, SDK<sup>116</sup>, and SIRAH<sup>117</sup>. Similar to atomistic MD models, specific coarse-grain FFs have been developed for ILs, including imidazolium<sup>118–121</sup>, phosphonium<sup>122</sup> and tetraalkylammonium ILs<sup>123</sup>. These models are typically based on MARTINI FFs.

While there are several coarse-grain studies involving ILs and other materials, research on traditional lipid bilayers is limited to research by Maginn and co-workers.<sup>124,125</sup> In one study, imidazolium ILs were simulated distinct POPC lipid architectures, including bilayers, disks, double bilayers, and vesicles.<sup>125</sup> POPC was modeled using SDK, while the ILs employed FFs from a similar model.<sup>119,126</sup> Since a coarse-grain system was employed, a longer timescale of 200 ns was utilized that allowed the ILs to fully insert induce structural changes on the bilayers. The experiments revealed that asymmetric insertion of the imidazolium cations dramatically increases leaflet strain which can decrease the

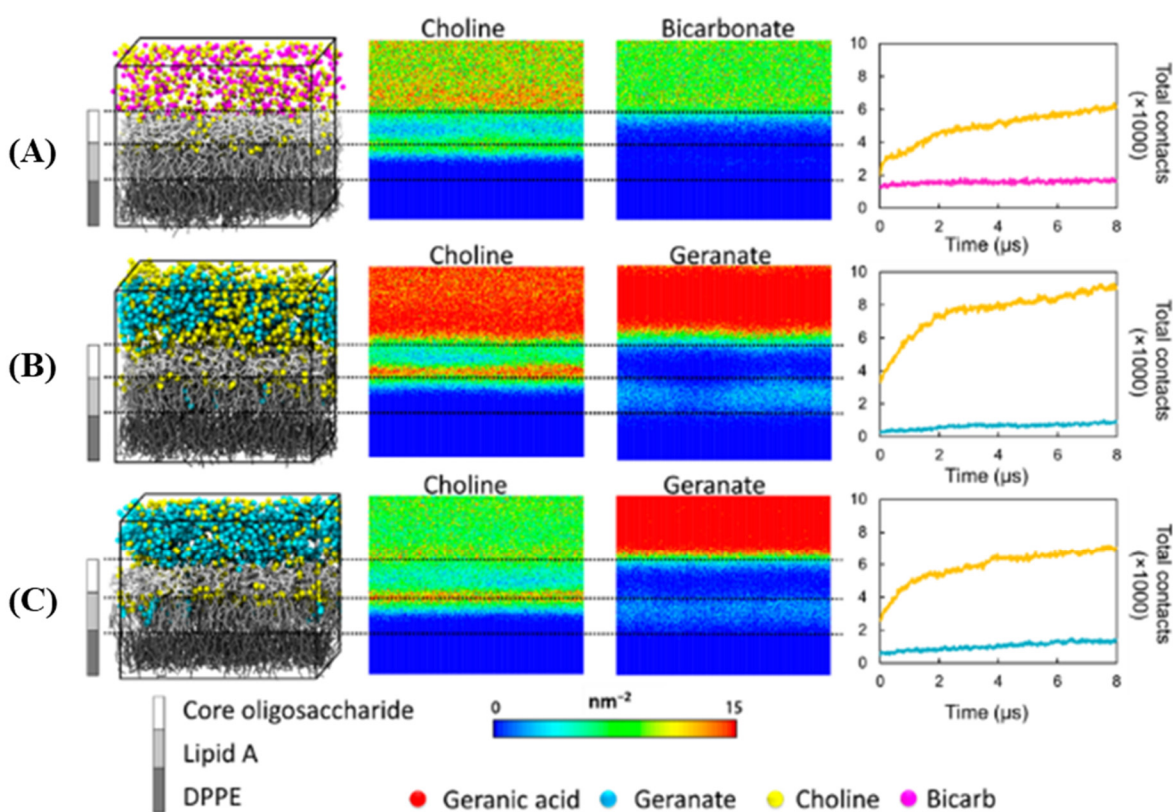


**Figure 1.7** Insertion of  $[C_4mim]^+$  into a POPC bilayer, which results in buckling and micelle nucleation. The image is a snapshot taken after 200 ns. Figure adapted from reference 125.

bending modulus by up to two orders of magnitude, leading to buckling (**Figure 1.7**). Additionally, stress-induced transitions were observed, where bilayer structures could fuse, due to IL aggregates, or form micelles.

Coarse-grain simulations have been used to probe other types of IL biological interactions, such as self-assembly of ILs<sup>127,128</sup>, solubilization of biomolecules by ILs<sup>129</sup>, and antibacterial activity of ILs<sup>42</sup>. In the latter example, choline and geranate (CAGE) ILs, at different ratios of cation and anion were simulated with bacterial membranes composed of LPC (lipid A and core oligosaccharides without O-antigen) and DPPE lipids. CAGE ILs were modeled using MARTINI and PyCGtool<sup>130</sup>, while the lipid membrane was

constructed using *insane.py*<sup>131</sup>. The results of the studies reveal that the small cholinium ion can easily penetrate the bilayer, where the cation becomes embedded in the negatively charged center of the oligosaccharide and lipid A molecules. Interestingly, the entrapped choline recruited the geranate anions that intercalated within the LPC (**Figure 1.8**). Higher ratios of geranate resulted in a significant increase in membrane presentation; however, in the absence of the cholinium cations, the penetration of geranic acid was severely restricted. Additionally, replacing cholinium with sodium also decreased the amount of geranate that entered the outer leaflet. The detailed interactions between CAGE and the bacterial membrane could be described due to the long 8 and 16  $\mu\text{s}$  simulation times made possible by the coarse-grain model, which could not be accomplished using current atomistic models.



**Figure 1.8** (A) Choline bicarbonate, (B) 2:1 CAGE, and (C) 1:1 CAGE insertion into a model *E. coli* lipid membrane. From left-to-right, the panels show the molecular simulation box, the number density of choline, the number density of the anions, and the number of contacts as a function of simulation time. Figure adapted from reference 42.

### 1.3 Biophysical methods

Biophysical methods allow for the interrogation of IL and membrane interactions at scales larger than molecular dynamic simulations. Still, these methods focus on interrogating how ILs influence lipid bilayers as a way to understand their toxicity. The size scale of these methods typically ranges from individual bilayers to giant vesicles and cells, meaning most biophysical techniques probe how ILs affect an entire cell-like system, rather than the local environment within a specific area of a lipid bilayer, as in the case of MD studies. Biophysical methods can fall under three categories: thermal, spectroscopic, and surface methods. Traditionally, artificial lipid bilayers are utilized in all three methods as a result of their simple and cheap production as well as their compatibility with the biophysical instruments. However, some non-invasive and non-toxic strategies such as fluorescence can measure the impact of ILs in live cells. In this section, the fabrication of artificial lipid membranes is discussed first as each of the methods utilize model membranes to some extent. Then, the common techniques use to evaluate IL interactions with artificial lipid membranes or cells are described. In each section of the sections describing a technique, one study is examined in detail to highlight how the corresponding method was used to understand IL toxicity. Additionally, the results of the studies are described.

#### *1.3.1 Development of artificial lipid membranes*

Experiments on model bilayers typically investigate vesicles, which are spherical shells that have inner and outer water sections separated by a lipid bilayer(s). Due to their similarity, vesicles can provide a realistic model to probe how ILs impact cells. Vesicles are classified based on their size and number individual bilayers within the vesicles, the latter classified as unilamellar or multilamellar. For example, small unilamellar and multilamellar vesicles have diameters below 100 nm, whereas large vesicles have sizes in between 100–1000 nm; giant vesicles have diameters greater than 1000 nm.<sup>132</sup> While many lipids naturally self-assemble into vesicles, the size and number of lipid bilayers can be modulated by the different vesicle preparation methods.

Most vesicles are prepared by extrusion, where lipid solutions are passed multiple times through polycarbonate filters with distinct pore sizes.<sup>133</sup> Smaller vesicles can be produced by using reduced pore dimensions and longer extrusion periods. Sonication<sup>134</sup> and solvent evaporation<sup>135</sup> are other common methods to construct vesicles. Many thermal and surface techniques require the lipid bilayers to be supported on a solid surface, which typically is glass, mica, and silicon oxide.<sup>136</sup> The conventional methods to prepare supported lipid bilayers (SLBs) are vesicle fusion<sup>137</sup> and Langmuir-Blodgett desposition<sup>138</sup>, although newer techniques such as solvent-assisted lipid bilayer (SALB) formation<sup>139</sup> and bicelles<sup>140</sup> have become popular. An excellent review of these latter techniques is described by Jackman and Cho.<sup>141</sup> The choice of the lipid(s) is an essential parameter. As compared to molecular dynamic simulations, the lipid bilayers need to be prepared, and thus commercial and equipment availability are important considerations. Still, the most common lipids employed are DMPC, DPPC, and other PC-related molecules due to their ubiquity in cell membranes. Additional lipids and molecules, such as cholesterol, can be added to create more biosimilar bilayers, although this can enhance the difficulty of synthesizing and characterizing the corresponding vesicles.<sup>142,143</sup>

### *1.3.2 Isothermal titration calorimetry*

Isothermal titration calorimetry (ITC) is a technique that measures the binding of small molecules to larger molecules, where the latter is normally biomolecules like proteins and nucleic acid. The ITC instrument is composed of two cells, a reference cell and a sample cell, which are kept at identical temperatures. The small molecule or ligand is loaded in a syringe device that injects aliquots of precise volume into the sample cell, which holds the larger molecule. If binding occurs, the temperature of the cell will change, which is then measured by the instrument. The amount of heat released or absorbed is proportional to the amount of binding, meaning measurements such as binding affinity, stoichiometry, and enthalpy can be determined. The elucidation of these parameters allows the entropy and Gibbs free energy to be calculated. ITC instruments are remarkably sensitive as the instrument can detect heat change of millionths of a degree.

Traditionally, ITC has been used to determine how ILs self-assemble, especially in aqueous media, which is important for understanding toxicity as dissolved ILs and IL particles interact with membranes in distinct fashions.<sup>144-146</sup> In a recent study, artificial POPC and POPG lipid membranes were fabricated in the sample cell to determine the thermodynamic properties of the IL cation  $[\text{C}_{12}\text{mim}]^+$  binding and inserting into the bilayers.<sup>147</sup> It was revealed that  $[\text{C}_{12}\text{mim}]^+$  has a lower binding constant with POPG than POPC, and in dilute IL solutions, 98% of the cation is bound to POPG membranes compared to 69% for POPC membranes. Other ITC studies have investigated the thermodynamic properties of IL and protein binding.<sup>148</sup> In one such analysis, it was discovered that the fluorinated IL  $[\text{C}_2\text{mim}][\text{C}_4\text{F}_9\text{SO}_3]$  could encapsulate bovine serum albumin.<sup>149</sup>

### 1.3.3 Differential scanning calorimetry

Similar to ITC, differential scanning calorimetry (DSC) utilizes temperature changes to analyze physical properties. However, instead of maintaining a constant temperature, the DSC instrument warms and cools to ascertain the amount of heat needed to change the temperature of a sample compared to a standard. As samples are heated and cooled, they may undergo phase transitions, meaning more or less heat is needed to maintain the same temperature as the standard. For endothermic processes like melting and molecular relaxations, the amount of heat needed increases, whereas for exothermic process, such as crystallization, less heat is required.

Although DSC is a common method to characterize ILs, DSC can be employed in the study of IL interactions with artificial membrane.<sup>150-153</sup> Here, the difference in membrane phase transition temperatures is measured before and after ILs are added to the solution. This phase transition, referred to as  $T_m$ , corresponds to the membranes transforming from an ordered gel phase into a fluidic phase. ILs can alter the ordering, or cooperativity, of the lipids, broadening and shifting the endothermic transition peak.<sup>57</sup> While many ILs have been found to decrease the phase temperature, some ILs increase  $T_m$ , such as  $[\text{M}(\text{OE})_2\text{mim}][\text{Cl}]$ , an alkoxyimidazolium compound, which increased the phase transition temperature of vesicles composed of DMPC and DMPG by almost 3 °C as described in a study by Gal *et al.*<sup>154</sup> It should

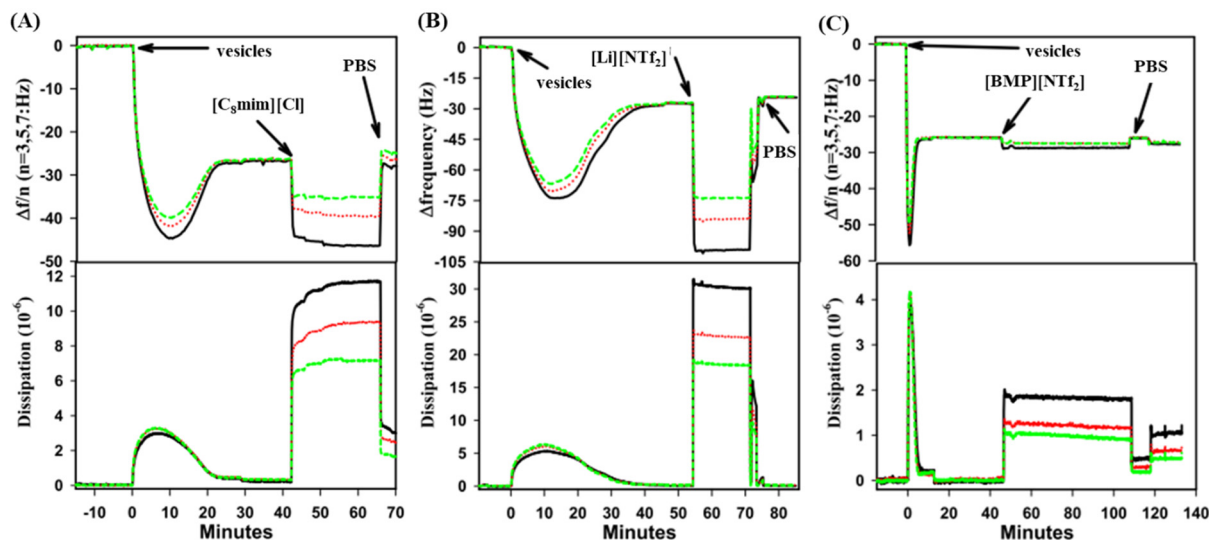
be noted that artificial membranes, especially those composed of a single lipid, are more ordered than cellular membranes, as the latter are composed of proteins, cholesterol, and a variety of saturated and unsaturated lipids. Therefore, while an IL may induce a significant change in  $T_m$  for a particular artificial membrane, the IL may not be toxic *in vivo*, as demonstrated in other studies.<sup>57</sup>

#### 1.3.4 Quartz crystal microbalance with dissipation monitoring

Unlike the previous two methods which rely on sensing heat and temperature change, quartz crystal microbalance with dissipation monitoring (QCM-D) takes advantage of the piezoelectric effect to measure adsorption on a surface. Piezoelectric materials oscillate in response to an electric current. This effect is reversible, meaning applying mechanical force to a piezoelectric material produces electric charge. When a compound is adsorbed or desorbed onto a quartz crystal surface, which is typically a silica coated quartz crystal, the resonance frequency changes. Additionally, when the electric generator is turned off, the energy dissipates, where the degree of dissipation is related to amount of material on the sensor. Therefore, QCM-D can sense a change in mass as well as determine the mechanical properties of the adsorbed layer, such as thickness and viscosity. Moreover, as many QCM instruments have sensitivities as low as  $0.5 \text{ ng/cm}^2$ , only a minute amount of sample is required.

When studying the interactions between artificial membranes and ILs, the sensor is washed with a solution of the artificial vesicles that adsorb onto a surface, typically silica, that is connected to the quartz sensor. Then, a solution containing the desired IL is washed over the supported vesicles. This method allows for the effects of the ILs on the vesicles to be monitored in real time.<sup>155,156</sup> In one study, QCD-M was used to discern the interactions between  $[\text{C}_8\text{mim}]^+$ ,  $[\text{NTf}_2]^-$ , and  $[\text{BMP}][\text{NTf}_2]$  (BMP: 1-butyl-1-methyl pyrrolidinium), and 1,2-dierucoyl-sn-glycero-3-phosphocholine (DEPC) small unilamellar vesicles (SUVs) adsorbed onto a silica surface of the sensor (**Figure 1.9**).<sup>157</sup> When the DEPC vesicles were incubated with  $[\text{C}_8\text{mim}]^+$ , a loss of mass was detected that indicated the cation ruptured the vesicles. However, upon incubating the adsorbed vesicles with  $[\text{NTf}_2]^-$ , only a small loss of mass was observed,

which was determined to be due to pores forming in the vesicles. Interestingly, adding [BMP][NTf<sub>2</sub>] resulted in an adsorbed layer of IL onto the vesicle, as determined by an increase in mass.



**Figure 1.9** QCM-D responses at 15 (black), 25 (red), and 35 (green) MHz as DEPC vesicles form a SLB and interact with (A) [C<sub>8</sub>mim][Cl], (B) [Li][NTf<sub>2</sub>], and (C) [BMP][NTf<sub>2</sub>] at 20 °C. Figure adapted from reference 157.

### 1.3.5 Fluorescence spectroscopy

When studying IL interactions with artificial membranes, fluorescence is the most common method due to its sensitivity and instrument accessibility. Although the traditional application of fluorescence examines the intensity of fluorescence emission, more specific experiments can be utilized that are better suited for analyzing the dynamic interactions of lipid membranes and ILs. Such experiments have included fluorescence anisotropy<sup>58,158</sup>, confocal laser scanning microscopy (CLSM)<sup>159</sup>, fluorescence correlation spectroscopy (FCS)<sup>160</sup>, fluorescence lifetime imaging microscopy (FLIM)<sup>161</sup>, and Förster resonance energy transfer (FRET)<sup>154</sup>. Since fluorescence is a non-invasive technique and the dyes are often biocompatible, experiments involving ILs can be performed with cells.<sup>71</sup>

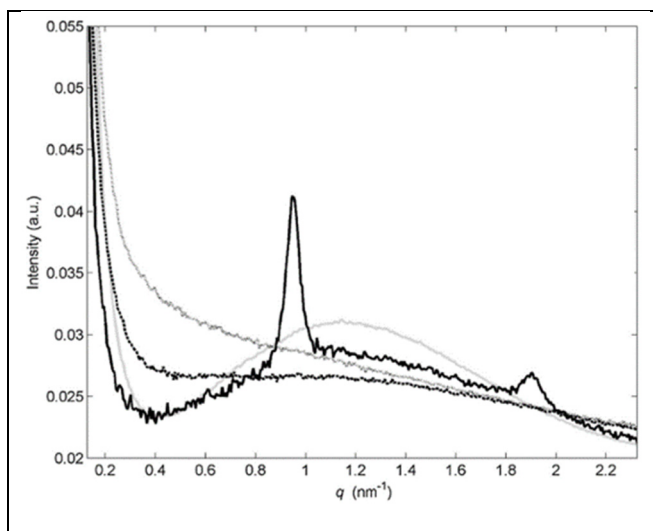
Many experiments investigate the influence of ILs on membrane permeability using fluorescence.<sup>152,162–165</sup> For studies involving artificial liposomes, the particles encapsulate a dye and

quencher, such as calcein and cobalt, so if an IL disturbs the membrane, the dye and quencher are separated causing an increase in fluorescence.<sup>166</sup> In one study, SLBs composed of PC and PC labeled with fluorescent lissamine rhodamine B were incubated with imidazolium cations with different alkyl lengths and analyzed by CLSM.<sup>159</sup> The experiments revealed that the SLBs swell when the ILs are inserted, where cations with longer alkyl chains induce more swelling, as deduced by a decrease in the fluorescence of the lipid bilayer. These results were further validated by adding R18, a self-quenching membrane fusion fluorescence probe, to the liposomes. The IL-induced swelling increased R18 fluorescence, indicating that the probe became diluted due to an increase in bilayer volume.

In cells, membrane permeability can be analyzed by adding a dye to a cell solution with or without ILs and measuring the fluorescence of the dye that accumulates in the membrane.<sup>63</sup> Since cells can be centrifuged, the residual dye can be removed easily, allowing for accurate measurements. In a unique approach to fluorescence, flow cytometry, which is a technique that allows individual cells to be analyzed, was employed to test the toxicity of [C<sub>4</sub>mim][Cl] in the microalga *Scenedesmus quadricauda* utilizing through measuring a series of distinct factors.<sup>61</sup> Here, [C<sub>4</sub>mim][Cl] was incubated with *S. quadricauda* and the toxicity indicators of chlorophyll concentration, membrane integrity, esterase activity, and reactive oxygen species (ROS) concentration were analyzed for each algal cell. While chlorophyll naturally fluoresces, the other parameters required the use of a separate dye. Propidium iodide was used to evaluate membrane integrity, while fluorescein diacetate and dichlorofluorescein diacetate were employed for monitoring esterase activity and ROS generation, respectively. A mechanistic toxicity profile of [C<sub>4</sub>mim][Cl] was obtained as a result of measuring different variables for each algal cell. The combined results reveal that [C<sub>4</sub>mim][Cl] rapidly inhibits esterases, but more slowly impairs chlorophyll and membrane integrity. Interestingly, ROS generation was not a significant factor in *S. quadricauda* toxicity.

### 1.3.6 X-ray diffraction

X-ray techniques have been used to probe IL structure and toxicity since the beginnings of the modern IL era. In fact, one of the first instances of reporting IL toxicity came in a seminal paper by Swatloski *et al* in 2003 that utilized single crystal X-ray diffraction to reveal that [C<sub>4</sub>mim][PF<sub>6</sub>] can hydrolyze to form hydrofluoric acid, an exceptionally deadly compound.<sup>167</sup> More recently, X-ray experiments have been employed to study the interactions of ILs and artificial lipid membranes using a variety of different techniques, including wide-angle X-ray scattering (WAXS)<sup>168</sup>, small-angle X-ray scattering (SAXS)<sup>153,159,169</sup>, grazing incidence X-ray diffraction (GIXD)<sup>170</sup>, and X-ray reflectivity (XRR)<sup>171-173</sup>. X-rays can provide impressive structural details as their small wavelengths. In general, the technique functions by shining X-rays on a sample, and while most of the X-rays will go through the surface, some X-rays will diffract off of electrons. Different diffraction patterns will result from the diverse electron densities in the sample. In XRR, a beam of X-rays is shined on a lipid surface, where a segment of the X-rays will reflect. The overall reflectometry patterns produced by the sample can be used to deduce the lipid bilayer density, thickness, and roughness before or after the bilayer interacts with ILs. In the scattering techniques, the X-rays will interact with the sample and scatter either at an angle smaller than the reflected angle (SAXS) or wider than the reflected angle (WAXS). For IL research, WAXS is useful for determining lipid bilayer crystallinity, while SAXS is utilized to analyze ordering and morphology within the lipid bilayer.<sup>152</sup>



**Figure 1.10** SAXS patterns of LUVs composed of egg PC, egg PG, and cholesterol exposed to [P<sub>1,8,8,8</sub>][OAc] at concentrations of 0.8 mM (black solid line), 8 mM (black dashed saline), and 17 mM (dark grey line). The light grey line corresponds to an LUV without IL. Figure adapted from reference 169.

In one study, SAXS was employed to study the interactions between phosphonium ILs and multilamellar vesicles (MLVs) and large unilamellar vesicles (LUVs) composed of PC, phosphatidylglycerol (PG), and cholesterol.<sup>169</sup> It was determined that increasing IL concentration,

regardless of alkyl chain length, shrunk the interlamellar distances in MLVs, indicating that the ILs can travel through the multi-layered vesicle structure. The presence of cholesterol provided a protective effect against [P<sub>1,8,8,8</sub>][OAc]-induced rupturing as LUVs without cholesterol ruptured at lower concentrations of the IL (**Figure 1.10**). Interestingly, when cholesterol-laden LUVs ruptured, they reformed into organized lamellae, which did not occur in cholesterol-free LUVs.

### 1.3.7 Neutron diffraction

Neutron diffraction has recently become a popular technique to analyze IL interactions with lipid bilayer. While X-rays diffract off of electrons, neutrons will diffract off of nuclei, which enables the technique to differentiate elements as well as isotopes. Neutron diffraction experiments are preferred over X-ray diffraction when examining sensitive samples, as X-ray exposure can damage materials. However, it should be noted that some materials may become radioactive when exposed to neutron beams. Additionally, neutron experiments can be more costly and often require dedicated facilities to produce the neutron beam. Similar to X-ray diffraction, neutron diffraction experiments fall under the categories of reflectometry and scattering. To probe the interactions of artificial lipid membranes and ILs, research groups have employed neutron scattering techniques such as small-angle neutron scattering (SANS)<sup>153</sup>, quasielastic neutron scattering (QENS)<sup>174,175</sup>, and neutron reflectometry<sup>176</sup>.

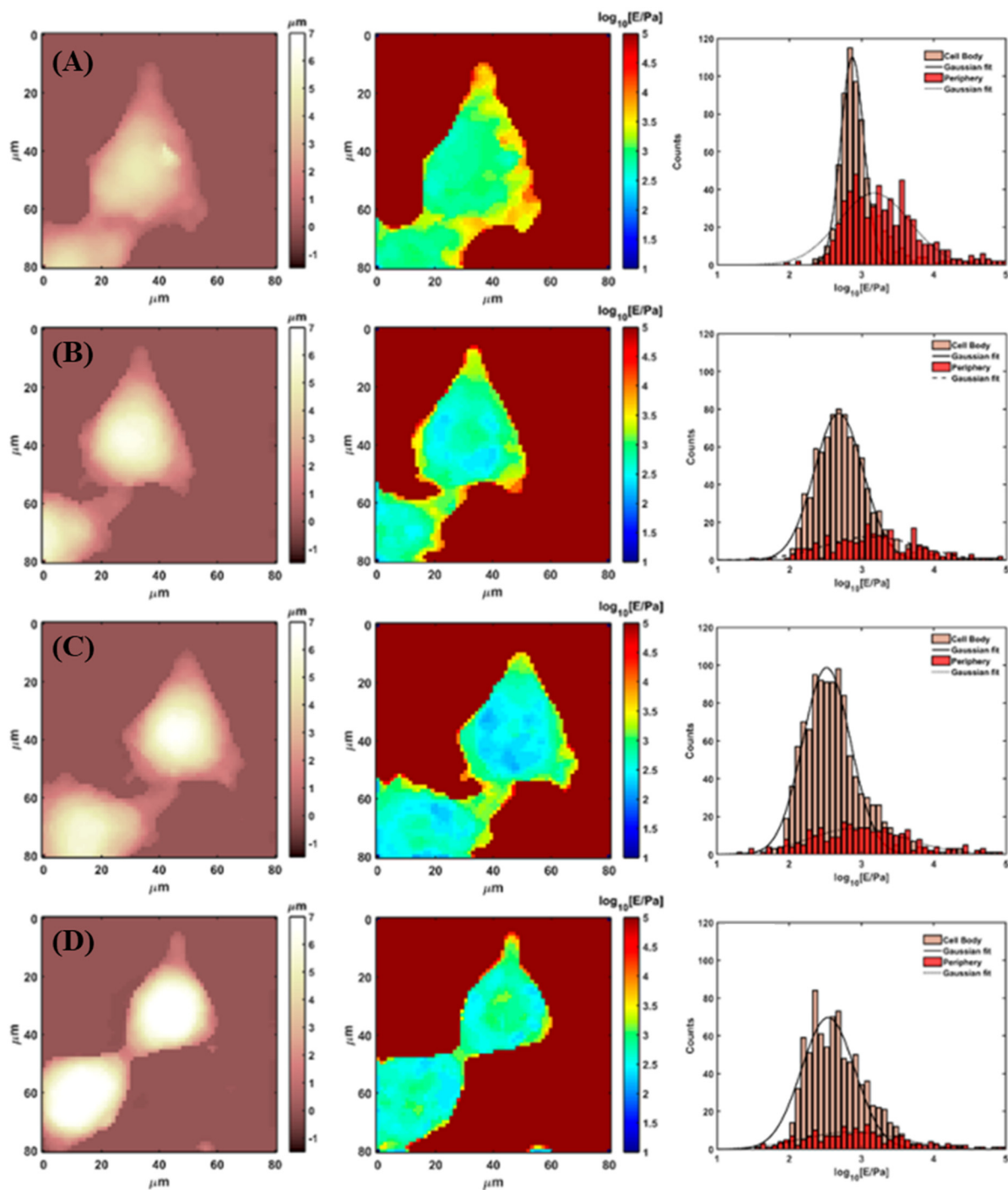
In a study by Kumari *et al*, a combination of SANS and neutron spin-echo (NSE) spectroscopy was applied to investigate the structural and elastic effects, respectively, of the IL [C<sub>4</sub>mim][Cl] on DMPC vesicles.<sup>177</sup> In NSE spectroscopy, the sample is emerged in deuterium oxide so that the hydrogen atoms of the sample exchange with the deuterium atoms of the solvent. As a result of the random exchange, distinct scattering patterns will emerge during the neutron experiments, even among identical molecules. The extraordinary energy resolution of spin echo spectrometers allows the technique to create snapshots of molecular arrangements at different time periods. By amalgamating the different arrangement, the overall motion of the sample at thermal equilibrium can be deduced. In this study, the SANS experiments revealed that DMPC vesicles incubated with 0.1 M [C<sub>4</sub>mim][Cl] resulted in an influx of cations [C<sub>4</sub>mim]<sup>+</sup>, where, after 1 h,

the bilayers were composed of a ~5:1 ratio of  $[C_4mim]^+$  and DMPC lipids. The NSE spectroscopy results further demonstrated that the incorporation of  $[C_4mim]^+$  increased the bending modulus of DMPC bilayers by 25% at 30 °C and 60% at 40 °C.

### 1.3.8 Atomic force microscopy

Atomic force microscopy (AFM) is a powerful scanning probe microscopy method that can measure forces, manipulate samples, and generate images of a surface at a sub-nanometer resolution. In AFM, a tip connected to a cantilever scans a sample by physically contacting the surface. A laser constantly reflects light off of the cantilever into a position-sensitive photodiode detector; therefore, as the tip height increases or decreases, depending on the surface topology, the position of the reflected laser light will change, allowing for the corresponding software to calculate and construct an image. In the field of ILs, AFM is used to characterize the physical structure of lipids bilayers, which can be accomplished in liquid solutions.<sup>159</sup> For example, AFM studies using tapping mode imaging on DEPC SLBs have revealed that  $[NTf_2]^-$  anions can form ~500 nm-wide defects in the bilayers.<sup>157</sup> Due to advances in AFM technologies, the scanning of cell surfaces is possible, which has been exploited to examine cell membrane architectures in response to ILs.<sup>178</sup>

In a study by Galluzzi *et al*, AFM was employed to characterize the morphology and rigidity of MDA-MB 231 cells, which are human breast cancer epithelial cells, in response to imidazolium ILs.<sup>179</sup> In general, low concentrations of ILs softened the cells as imidazolium cations inserted into the membranes. As the IL concentration increased, the cellular protrusions retracted, causing the overall cell morphology to become more round (**Figure 1.11**). At high concentrations, the morphology and rigidity depended on the IL alkyl chain length. The short-chain ILs  $[C_4mim][Cl]$  and  $[C_4mim][BF_4]$  increased the Young's modulus at high concentrations, whereas for  $[C_8mim][Cl]$ , a long chain IL, the cells continued to soften and quickly became apoptotic at high concentrations.



**Figure 1.11** AFM images of MDA-MB-231 cells interacting with  $[C_8mim][Cl]$  at concentrations of (A)  $0 \mu M$  (control), (B)  $1 \mu M$ , (C)  $10 \mu M$ , and (D)  $100 \mu M$ . From left-to-right, the columns correspond to the uncompressed topographic map, Young's modulus map, and the histograms of the Young's modulus values (cell body and periphery). Figure adapted from reference 179.

### 1.3.9 Additional biophysical methods

A variety of other biophysical techniques have been employed to understand the interactions of ILs and lipid membranes. These include solid-state nuclear magnetic resonance (ssNMR)<sup>147,164,180,181</sup>, nanoplasmonic sensing<sup>151</sup>, conductivity<sup>182</sup>, scanning electron microscopy<sup>183</sup>, and Fourier-transform infrared spectroscopy (FTIR)<sup>66,70,184</sup>. A few studies have employed analytical methods that are generally not considered in the realm of biophysics, such as desorption electrospray ionization mass spectrometry<sup>53</sup> and electrochemical studies including voltammetry and electrochemical impedance spectroscopy (EIS)<sup>185</sup>.

## 1.4 Thesis Objectives and Overview

The majority of this thesis research revolves around the development of ILs, particularly HILs, as potential media for drug delivery applications. Most studies employ ILs in solutions designed for transdermal delivery, and as such, there is a lack of intravenous (IV) formulations that incorporate ILs. IV delivery is the preferred route when administering certain drugs, such as anesthetics, anticancer agents, and contrast agents, and so there is an untapped area in which the unique drug solubilizing properties of ILs can be exploited. In particular, HILs have enormous potential as the hydrophobic component of formulations, and more specifically, drug delivery vehicles. To develop HILs that can be translated into medical fields, the ILs need to have favorable physicochemical properties such as low viscosity and high hydrophobicity as well as low toxicity. Since current HILs do not meet these criteria, Chapter 2 reports the design and synthesis of several new classes of HILs, where the cations are based on the low toxic choline moiety and the anions are either carboxylates or bis(sulfonyl)azanide analogues. In Chapter 3, select ILs are robustly characterized using techniques including DSC, viscometry, quantitative NMR, and Karl-Fisher titration. Additionally, the toxicity of some ILs and IL salt precursors are evaluated in an *in vitro* mammalian cell line as well as by a zebrafish teratology model.

The preliminary formulation experiments involving ILs are discussed in Chapter 4. Here, a few ILs are assessed for their compatibility in micellar systems with poloxamers and as the hydrophobic component in nanoemulsions. While these results are preliminary, certain trends are established that can aid in the

design of future IL-containing formulations. In particular, it is revealed that IL lipophilicity and the addition of cosolvents are important parameters for designing safe and stable drug delivery systems. In a related project, Chapter 5 investigates a strategy to deliver siRNA, a potent nucleic acid drug, using traditional nanoemulsions. Instead of exploiting the solubilization properties of ILs, the siRNA is modulated to become hydrophobic by pairing the therapeutic with cationic lipids. This allows the drug to be dissolved in high concentrations in medium chain triglycerides, an FDA-approved oil that is employed ubiquitously in formulations. The nanoemulsion system has high encapsulation efficiency, long-lasting stability, and demonstrates high efficacy in an *in vivo* model without showcasing signs of toxicity.

## 1.5 References

- (1) Gabriel, S. & Weiner, J. Ueber einige Abkömmlinge des Propylamins. *Berichte der Dtsch. Chem. Gesellschaft* **21**, 2669–2679 (1888).
- (2) Wilkes, J. S. A short history of ionic liquids - From molten salts to neoteric solvents. *Green Chem.* **4**, 73–80 (2002).
- (3) Pitzer, K. S. Electrolytes. From Dilute Solutions to Fused Salts. *J. Am. Chem. Soc.* **102**, 2902–2906 (1980).
- (4) Angell, C. A. Dynamic Processes in Ionic Glasses. *Chem. Rev.* **90**, 523–542 (1990).
- (5) Pitzer, K. S. Critical Phenomena in Ionic Fluids. *Acc. Chem. Res.* **23**, 333–338 (1990).
- (6) Banerjee, A. *et al.* Definitions of ionic liquids and deep eutectic solvents. *Proc. Natl. Acad. Sci. U. S. A.* **115**, E11000–E11001 (2018).
- (7) Weaver, K. D., Kim, H. J., Sun, J., MacFarlane, D. R. & Elliott, G. D. Cyto-toxicity and biocompatibility of a family of choline phosphate ionic liquids designed for pharmaceutical applications. *Green Chem.* **12**, 507–51 (2010).
- (8) Weaver, K. D. *et al.* Structure and function of proteins in hydrated choline dihydrogen phosphate ionic liquid. *Phys. Chem. Chem. Phys.* **14**, 790–801 (2012).
- (9) Kärnä, M., Lahtinen, M., Hakkarainen, P.-L. & Valkonen, J. Physicochemical Properties of New Dicationic Ether-Functionalized Low Melting Point Ammonium Salts. *Aust. J. Chem.* **63**, 1122–1137 (2010).
- (10) Van den Broeke, J. *et al.* Designing ionic liquids: 1-Butyl-3-methylimidazolium cations with substituted tetraphenylborate counterions. *Eur. J. Inorg. Chem.* 2798–2811 (2003)  
doi:10.1002/ejic.200300057.

- (11) Shaplov, A. S. *et al.* Design and synthesis of new anionic ‘polymeric ionic liquids’ with high charge delocalization. *Polym. Chem.* **2**, 2609–2618 (2011).
- (12) Clark, K. D. *et al.* Extraction of DNA by magnetic ionic liquids: Tunable solvents for rapid and selective DNA analysis. *Anal. Chem.* **87**, 1552–1559 (2015).
- (13) Chiappe, C. & Pieraccini, D. Ionic liquids: Solvent properties and organic reactivity. *J. Phys. Org. Chem.* **18**, 275–297 (2005).
- (14) Shi, B., Wang, Z. & Wen, H. Research on the strengths of electrostatic and van der Waals interactions in ionic liquids. *J. Mol. Liq.* **241**, 486–488 (2017).
- (15) Greaves, T. L. & Drummond, C. J. Protic ionic liquids: Properties and applications. *Chem. Rev.* **108**, 206–237 (2008).
- (16) Esperança, J. M. S. S. *et al.* Volatility of Aprotic Ionic Liquids-A Review. *J. Chem. Eng. Data* 3–12 (2010).
- (17) Fumino, K., Wulf, A. & Ludwig, R. The potential role of hydrogen bonding in aprotic and protic ionic liquids. *Phys. Chem. Chem. Phys.* **11**, 8790–8794 (2009).
- (18) Izgorodina, E. I. & MacFarlane, D. R. Nature of hydrogen bonding in charged hydrogen-bonded complexes and imidazolium-based ionic liquids. *J. Phys. Chem. B* **115**, 14659–14667 (2011).
- (19) Canongia Lopes, J. N. A. J. N. A. & Pádua, A. A. H. A. H. Nanostructural organization in ionic liquids. *J. Phys. Chem. B* **110**, 3330–3335 (2006).
- (20) Hayes, R., Warr, G. G. & Atkin, R. Structure and Nanostructure in Ionic Liquids. *Chem. Rev.* **115**, 6357–6426 (2015).
- (21) Esson, M. M. Design, synthesis, and characterization of dicholinium-based ionic liquids for drug delivery and materials science applications. (University of Wisconsin-Madison, 2019).
- (22) Zhang, S., Sun, N., He, X., Lu, X. & Zhang, X. Physical Properties of Ionic Liquids: Database and Evaluation. *J. Phys. Chem. Ref. Data* **35**, 1475–1517 (2006).
- (23) Sivapragasam, M., Moniruzzaman, M. & Goto, M. Recent advances in exploiting ionic liquids for biomolecules: Solubility, stability and applications. *Biotechnol. J.* **11**, 1000–1013 (2016).
- (24) Raut, D. G. *et al.* A morpholinium ionic liquid for cellulose dissolution. *Carbohydr. Polym.* **130**, 18–25 (2015).
- (25) Tsurumaki, A. & Ohno, H. Dissolution of oligo(tetrafluoroethylene) and preparation of poly(tetrafluoroethylene)-based composites by using fluorinated ionic liquids. *Chem. Commun.* **54**, 409–412 (2018).
- (26) Bica, K., Gaertner, P. & Rogers, R. D. Ionic liquids and fragrances – direct isolation of orange essential oil. *Green Chem.* **13**, 1997–1999 (2011).
- (27) Earle, M. J. & Seddon, K. R. Ionic liquids. Green solvents for the future. *Pure Appl. Chem.* **72**,

- 1391–1398 (2000).
- (28) Fang, D., Yang, J. & Jiao, C. Dicationic ionic liquids as environmentally benign catalysts for biodiesel synthesis. *ACS Catal.* **1**, 42–47 (2011).
- (29) Lewandowski, A. & Świdarska-Mocek, A. Ionic liquids as electrolytes for Li-ion batteries—An overview of electrochemical studies. *J. Power Sources* **194**, 601–609 (2009).
- (30) Nakashima, K., Kubota, F., Maruyama, T. & Goto, M. Ionic liquids as a novel solvent for lanthanide extraction. *Anal. Sci.* **19**, 1097–1098 (2003).
- (31) Lin, I. J. B. & Vasam, C. S. Metal-containing ionic liquids and ionic liquid crystals based on imidazolium moiety. *J. Organomet. Chem.* **690**, 3498–3512 (2005).
- (32) Chowdhury, M. R. *et al.* Ionic-Liquid-Based Paclitaxel Preparation: A New Potential Formulation for Cancer Treatment. *Mol. Pharm.* **15**, 2484–2488 (2018).
- (33) Esson, M. M. & Mecozzi, S. Preparation, Characterization, and Formulation Optimization of Ionic-Liquid-in-Water Nanoemulsions toward Systemic Delivery of Amphotericin B. *Mol. Pharm.* **17**, 2221–2226 (2020).
- (34) Vaidya, A. & Mitragotri, S. Ionic liquid-mediated delivery of insulin to buccal mucosa. *J. Control. Release* **327**, 26–34 (2020).
- (35) Zakrewsky, M. & Mitragotri, S. Therapeutic RNAi robed with ionic liquid moieties as a simple, scalable prodrug platform for treating skin disease. *J. Control. Release* **242**, 80–88 (2016).
- (36) Mahamat Nor, S. B., Woi, P. M. & Ng, S. H. Characterisation of ionic liquids nanoemulsion loaded with piroxicam for drug delivery system. *J. Mol. Liq.* **234**, 30–39 (2017).
- (37) Kandasamy, S., Moniruzzaman, M., Sivapragasam, M., Shamsuddin, M. R. & Mutalib, M. I. A. Formulation and characterization of acetate based ionic liquid in oil microemulsion as a carrier for acyclovir and methotrexate. *Sep. Purif. Technol.* **196**, 149–156 (2018).
- (38) Berton, P. *et al.* Transdermal Bioavailability in Rats of Lidocaine in the Forms of Ionic Liquids, Salts, and Deep Eutectic. *ACS Med. Chem. Lett.* **8**, 498–503 (2017).
- (39) Balk, A. *et al.* Transformation of acidic poorly water soluble drugs into ionic liquids. *Eur. J. Pharm. Biopharm.* **94**, 73–82 (2015).
- (40) Santos, M. M. *et al.* Ionic Liquids and Salts from Ibuprofen as Promising Innovative Formulations of an Old Drug. *ChemMedChem* **14**, 907–911 (2019).
- (41) Egorova, K. S., Gordeev, E. G. & Ananikov, V. P. Biological Activity of Ionic Liquids and Their Application in Pharmaceutics and Medicine. *Chem. Rev.* **117**, 7132–7189 (2017).
- (42) Ibsen, K. N. *et al.* Mechanism of Antibacterial Activity of Choline-Based Ionic Liquids (CAGE). *ACS Biomater. Sci. Eng.* **4**, 2370–2379 (2018).
- (43) Suchodolski, J., Feder-Kubis, J. & Krasowska, A. Antifungal activity of ionic liquids based on (–)-

- menthol: a mechanism study. *Microbiol. Res.* **197**, 56–64 (2017).
- (44) Dias, A. R., Costa-Rodrigues, J., Fernandes, M. H., Ferraz, R. & Prudêncio, C. The Anticancer Potential of Ionic Liquids. *ChemMedChem* **12**, 11–18 (2017).
- (45) Stolte, S. *et al.* Effects of different head groups and functionalised side chains on the aquatic toxicity of ionic liquids. *Green Chem.* **9**, 1170–1179 (2007).
- (46) Bailey, M. M. *et al.* A comparison of the effects of prenatal exposure of CD-1 mice to three imidazolium-based ionic liquids. *Birth Defects Res. Part B - Dev. Reprod. Toxicol.* **89**, 233–238 (2010).
- (47) Scammells, P. J., Scott, J. L. & Singer, R. D. Ionic liquids: The neglected issues. *Aust. J. Chem.* **58**, 155–169 (2005).
- (48) Heckenbach, M. E., Romero, F. N., Green, M. D. & Halden, R. U. Meta-analysis of ionic liquid literature and toxicology. *Chemosphere* **150**, 266–274 (2016).
- (49) Richardson, S. D. & Ternes, T. A. Water Analysis: Emerging Contaminants and Current Issues. *Anal. Chem.* **90**, 398–428 (2018).
- (50) Tullo, A. H. For ionic liquids, the time is now. *C&EN Glob. Enterp.* **98**, 24–27 (2020).
- (51) Pandey, A., Ekka, M. K., Ranjan, S., Maiti, S. & Sachidanandan, C. Teratogenic, cardiotoxic and hepatotoxic properties of related ionic liquids reveal the biological importance of anionic components. *RSC Adv.* **7**, 22927–22935 (2017).
- (52) Padilla, M., Bertz, C., Berdusco, N. & Mecozzi, S. Expanding the Structural Diversity of Hydrophobic Ionic Liquids: Physicochemical Properties and Toxicity of Novel Gemini Ionic Liquids. *Green Chem.* 4375–4385 (2021) doi:10.1039/d1gc00742d.
- (53) Perez, C. J., Tata, A., de Campos, M. L., Peng, C. & Ifa, D. R. Monitoring Toxic Ionic Liquids in Zebrafish (*Danio rerio*) with Desorption Electrospray Ionization Mass Spectrometry Imaging (DESI-MSI). *J. Am. Soc. Mass Spectrom.* **28**, 1136–1148 (2017).
- (54) Bernot, R. J., Brueseke, M. A., Evans-White, M. A. & Lamberti, G. A. Acute and chronic toxicity of imidazolium-based ionic liquids on *Daphnia magna*. *Environ. Toxicol. Chem.* **24**, 87–92 (2005).
- (55) Pretti, C. *et al.* Acute toxicity of ionic liquids for three freshwater organisms: *Pseudokirchneriella subcapitata*, *Daphnia magna* and *Danio rerio*. *Ecotoxicol. Environ. Saf.* **72**, 1170–1176 (2009).
- (56) Montalbán, M. G., Villora, G. & Licence, P. Ecotoxicity assessment of dicationic versus monocationic ionic liquids as a more environmentally friendly alternative. *Ecotoxicol. Environ. Saf.* **150**, 129–135 (2018).
- (57) Rantamäki, A. H. *et al.* Impact of surface-active guanidinium-, tetramethylguanidinium-, and cholinium-based ionic liquids on *Vibrio fischeri* cells and dipalmitoylphosphatidylcholine liposomes. *Sci. Rep.* **7**, 1–12 (2017).

- (58) Samori, C. *et al.* Introduction of oxygenated side chain into imidazolium ionic liquids: Evaluation of the effects at different biological organization levels. *Ecotoxicol. Environ. Saf.* **73**, 1456–1464 (2010).
- (59) Cho, C. W., Pham, T. P. T., Jeon, Y. C. & Yun, Y. S. Influence of anions on the toxic effects of ionic liquids to a phytoplankton *Selenastrum capricornutum*. *Green Chem.* **10**, 67–72 (2008).
- (60) Pham, T. P. T., Cho, C. W., Vijayaraghavan, K., Min, J. & Yun, Y. S. Effect of imidazolium-based ionic liquids on the photosynthetic activity and growth rate of *Selenastrum capricornutum*. *Environ. Toxicol. Chem.* **27**, 1583–1589 (2008).
- (61) Deng, Y. *et al.* Chronic effects of the ionic liquid [C4mim][Cl] towards the microalga *Scenedesmus quadricauda*. *Environ. Pollut.* **204**, 248–255 (2015).
- (62) Quraish, K. S. *et al.* Ionic liquids toxicity on fresh water microalgae, *Scenedesmus quadricauda*, *Chlorella vulgaris* & *Botryococcus braunii*; selection criterion for use in a two-phase partitioning bioreactor (TPPBR). *Chemosphere* **184**, 642–651 (2017).
- (63) Liu, D., Liu, H., Wang, S., Chen, J. & Xia, Y. The toxicity of ionic liquid 1-decylpyridinium bromide to the algae *Scenedesmus obliquus*: Growth inhibition, phototoxicity, and oxidative stress. *Sci. Total Environ.* **622–623**, 1572–1580 (2018).
- (64) Liu, H., Zhang, X., Chen, C., Du, S. & Dong, Y. Effects of imidazolium chloride ionic liquids and their toxicity to *Scenedesmus obliquus*. *Ecotoxicol. Environ. Saf.* **122**, 83–90 (2015).
- (65) Frade, R. F. M. *et al.* Toxicological evaluation on human colon carcinoma cell line (CaCo-2) of ionic liquids based on imidazolium, guanidinium, ammonium, phosphonium, pyridinium and pyrrolidinium cations. *Green Chem.* **11**, 1660–1665 (2009).
- (66) Hu, L. X. *et al.* New insight into the negative impact of imidazolium-based ionic liquid [C10mim]Cl on HeLa cells: From membrane damage to biochemical alterations. *Ecotoxicol. Environ. Saf.* **208**, 111629 (2021).
- (67) Wan, R. *et al.* Toxicity of imidazoles ionic liquid [C16mim]Cl to HepG2 cells. *Toxicol. Vitro.* **52**, 1–7 (2018).
- (68) Wang, P. *et al.* Cytotoxicity, genotoxicity, oxidative stress, and apoptosis in HepG2 cells induced by the imidazole ionic liquid 1-dodecyl-3-methylimidazolium chloride. *Environ. Toxicol.* **35**, 665–672 (2020).
- (69) Lee, S. M., Chang, W. J., Choi, A. R. & Koo, Y. M. Influence of ionic liquids on the growth of *Escherichia coli*. *Korean J. Chem. Eng.* **22**, 687–690 (2005).
- (70) Cornmell, R. J., Winder, C. L., Tiddy, G. J. T., Goodacre, R. & Stephens, G. Accumulation of ionic liquids in *Escherichia coli* cells. *Green Chem.* **10**, 836–84 (2008).
- (71) Cook, K. *et al.* Correlating lipid membrane permeabilities of imidazolium ionic liquids with their

- cytotoxicities on yeast, bacterial, and mammalian cells. *Biomolecules* **9**, 23–29 (2019).
- (72) Zhu, S. *et al.* Investigation of the toxicity of the ionic liquid 1-butyl-3-methylimidazolium chloride to *Saccharomyces cerevisiae* AY93161 for lignocellulosic ethanol production. *Polish J. Chem. Technol.* **15**, 94–98 (2013).
- (73) Jodynis-Liebert, J. *et al.* Cytotoxicity, acute and subchronic toxicity of ionic liquid, didecyldimethylammonium saccharinate, in rats. *Regul. Toxicol. Pharmacol.* **57**, 266–273 (2010).
- (74) Jordan, A. & Gathergood, N. Biodegradation of ionic liquids—a critical review. *Chem. Soc. Rev.* **44**, 8200–8237 (2015).
- (75) Hartmann, D. O. *et al.* Plasma membrane permeabilisation by ionic liquids: a matter of charge. *Green Chem.* **17**, 4587–4598 (2015).
- (76) Ventura, S. P. M. *et al.* Toxicity assessment of various ionic liquid families towards *Vibrio fischeri* marine bacteria. *Ecotoxicol. Environ. Saf.* **76**, 162–168 (2012).
- (77) Van Der Ploeg, P. & Berendsen, H. J. C. Molecular dynamics of a bilayer membrane. *Mol. Phys.* **49**, 233–248 (1983).
- (78) Feller, S. E. Molecular dynamics simulations of lipid bilayers. *Curr. Opin. Colloid Interface Sci.* **5**, 217–223 (2000).
- (79) Huggins, D. J. *et al.* Biomolecular simulations: From dynamics and mechanisms to computational assays of biological activity. *Wiley Interdiscip. Rev. Comput. Mol. Sci.* **9**, 1–23 (2019).
- (80) Mackerell, A. D. Empirical force fields for biological macromolecules: Overview and issues. *J. Comput. Chem.* **25**, 1584–1604 (2004).
- (81) Benedetto, A. & Ballone, P. An overview of neutron scattering and molecular dynamics simulation studies of phospholipid bilayers in room-temperature ionic liquid/water solutions. *Phys. B Condens. Matter* **551**, 227–231 (2018).
- (82) Kleinjung, J. & Fraternali, F. Design and application of implicit solvent models in biomolecular simulations. *Curr. Opin. Struct. Biol.* **25**, 126–134 (2014).
- (83) Marrink, S. J. *et al.* Computational Modeling of Realistic Cell Membranes. *Chem. Rev.* **119**, 6184–6226 (2019).
- (84) Zambrano, F., Fleischer, S. & Fleischer, B. Lipid composition of the golgi apparatus of rat kidney and liver in comparison with other subcellular organelles. *Biochim. Biophys. Acta (BBA)/Lipids Lipid Metab.* **380**, 357–369 (1975).
- (85) Casares, D., Escribá, P. V. & Rosselló, C. A. Membrane lipid composition: Effect on membrane and organelle structure, function and compartmentalization and therapeutic avenues. *Int. J. Mol. Sci.* **20**, (2019).
- (86) Silvius, J. R. Role of cholesterol in lipid raft formation: Lessons from lipid model systems. *Biochim.*

- Biophys. Acta - Biomembr.* **1610**, 174–183 (2003).
- (87) Ingólfsson, H. I. *et al.* Lipid organization of the plasma membrane. *J. Am. Chem. Soc.* **136**, 14554–14559 (2014).
- (88) Beaven, A. H., Arnarez, C., Lyman, E., Bennett, W. F. D. & Sodt, A. J. Curvature energetics determined by alchemical simulation on four topologically distinct lipid phases. *J. Phys. Chem. B* **125**, 1815–1824 (2021).
- (89) Berger, O., Edholm, O. & Jähnig, F. Molecular dynamics simulations of a fluid bilayer of dipalmitoylphosphatidylcholine at full hydration, constant pressure, and constant temperature. *Biophys. J.* **72**, 2002–2013 (1997).
- (90) Shahane, G., Ding, W., Palaiokostas, M. & Orsi, M. Physical properties of model biological lipid bilayers: insights from all-atom molecular dynamics simulations. *J. Mol. Model.* **25**, 1–13 (2019).
- (91) Brooks, B. R. *et al.* CHARMM: The biomolecular simulation program. *J. Comput. Chem.* **30**, 1545–1614 (2009).
- (92) Kumari, P. & Kashyap, H. K. Sensitivity and Resilience of Phosphatidylcholine and Phosphatidylethanolamine Lipid Membranes against Cholinium Glycinate Biocompatible Ionic Liquid. *J. Phys. Chem. B* **123**, 4550–4561 (2019).
- (93) Weiner, P. K. & Kollman, P. A. AMBER: Assisted model building with energy refinement. A general program for modeling molecules and their interactions. *J. Comput. Chem.* **2**, 287–303 (1981).
- (94) Jorgensen, W. L., Maxwell, D. S. & Tirado-Rives, J. Development and testing of the OPLS all-atom force field on conformational energetics and properties of organic liquids. *J. Am. Chem. Soc.* **118**, 11225–11236 (1996).
- (95) Wang, D. *et al.* Imidazolium-Based Lipid Analogues and Their Interaction with Phosphatidylcholine Membranes. *Langmuir* **32**, 12579–12592 (2016).
- (96) Oostenbrink, C., Villa, A., Mark, A. E. & Van Gunsteren, W. F. A biomolecular force field based on the free enthalpy of hydration and solvation: The GROMOS force-field parameter sets 53A5 and 53A6. *J. Comput. Chem.* **25**, 1656–1676 (2004).
- (97) Bingham, R. J. & Ballone, P. Computational study of room-temperature ionic liquids interacting with a POPC phospholipid bilayer. *J. Phys. Chem. B* **116**, 11205–11216 (2012).
- (98) Pluhackova, K. *et al.* A Critical Comparison of Biomembrane Force Fields: Structure and Dynamics of Model DMPC, POPC, and POPE Bilayers. *J. Phys. Chem. B* **120**, 3888–3903 (2016).
- (99) Benedetto, A., Bingham, R. J. & Ballone, P. Structure and dynamics of POPC bilayers in water solutions of room temperature ionic liquids. *J. Chem. Phys.* **142**, 124706 (2015).
- (100) Canongia Lopes, J. N., Deschamps, J. & Pádua, A. A. H. Modeling Ionic Liquids Using a Systematic

- All-Atom Force Field. *J. Phys. Chem. B* **108**, 2038–2047 (2004).
- (101) McDaniel, J. G., Choi, E., Son, C. Y., Schmidt, J. R. & Yethiraj, A. Ab Initio Force Fields for Imidazolium-Based Ionic Liquids. *J. Phys. Chem. B* **120**, 7024–7036 (2016).
- (102) Voroshylova, I. V. & Chaban, V. V. Atomistic force field for pyridinium-based ionic liquids: Reliable transport properties. *J. Phys. Chem. B* **118**, 10716–10724 (2014).
- (103) Lopes, J. N. C. & Pádua, A. A. H. Molecular force field for ionic liquids composed of triflate or bistriflylimide anions. *J. Phys. Chem. B* **108**, 16893–16898 (2004).
- (104) Yoo, B., Shah, J. K., Zhu, Y. & Maginn, E. J. Amphiphilic interactions of ionic liquids with lipid biomembranes: A molecular simulation study. *Soft Matter* **10**, 8641–8651 (2014).
- (105) Zhong, X., Liu, Z. & Cao, D. Improved classical united-atom force field for imidazolium-based ionic liquids: Tetrafluoroborate, hexafluorophosphate, methylsulfate, trifluoromethylsulfonate, acetate, trifluoroacetate, and bis(trifluoromethylsulfonyl)amide. *J. Phys. Chem. B* **115**, 10027–10040 (2011).
- (106) Liu, Z., Wu, X. & Wang, W. A novel united-atom force field for imidazolium-based ionic liquids. *Phys. Chem. Chem. Phys.* **8**, 1096–1104 (2006).
- (107) Kumari, M., Gupta, A., Shobhna & Kashyap, H. K. Molecular Dynamics Evaluation of the Effect of Cholinium Phenylalaninate Biocompatible Ionic Liquid on Biomimetic Membranes. *J. Phys. Chem. B* **124**, 6748–6762 (2020).
- (108) Cromie, S. R. T., Del Pópolo, M. G. & Ballone, P. Interaction of room temperature ionic liquid solutions with a cholesterol bilayer. *J. Phys. Chem. B* **113**, 11642–11648 (2009).
- (109) Lim, G. S., Zidar, J., Cheong, D. W., Jaenicke, S. & Klahn, M. Impact of ionic liquids in aqueous solution on bacterial plasma membranes studied with molecular dynamics simulations. *J. Phys. Chem. B* **118**, 10444–10459 (2014).
- (110) Gurtovenko, A. A. & Vattulainen, I. Pore formation coupled to ion transport through lipid membranes as induced by transmembrane ionic charge imbalance: Atomistic molecular dynamics study. *J. Am. Chem. Soc.* **127**, 17570–17571 (2005).
- (111) Orsi, M., Michel, J. & Essex, J. W. Coarse-grain modelling of DMPC and DOPC lipid bilayers. *J. Phys. Condens. Matter* **22**, (2010).
- (112) Ingólfsson, H. I. *et al.* *The power of coarse graining in biomolecular simulations.* Wiley *Interdisciplinary Reviews: Computational Molecular Science* vol. 4 225–248 (Blackwell Publishing Inc., 2014).
- (113) Orsi, M., Haubertin, D. Y., Sanderson, W. E. & Essex, J. W. A quantitative coarse-grain model for lipid bilayers. *J. Phys. Chem. B* **112**, 802–815 (2008).
- (114) Wang, Z. J. & Deserno, M. A systematically coarse-grained solvent-free model for quantitative phospholipid bilayer simulations. *J. Phys. Chem. B* **114**, 11207–11220 (2010).

- (115) Souza, P. C. T. *et al.* Martini 3: a general purpose force field for coarse-grained molecular dynamics. *Nat. Methods* **18**, 382–388 (2021).
- (116) Shinoda, W., Devane, R. & Klein, M. L. Zwitterionic lipid assemblies: Molecular dynamics studies of monolayers, bilayers, and vesicles using a new coarse grain force field. *J. Phys. Chem. B* **114**, 6836–6849 (2010).
- (117) Machado, M. R. *et al.* The SIRAH 2.0 Force Field: Altius, Fortius, Citius. *J. Chem. Theory Comput.* **15**, 2719–2733 (2019).
- (118) Fajardo, O. Y., DI Lecce, S. & Bresme, F. Molecular dynamics simulation of imidazolium C:nMIM-BF<sub>4</sub> ionic liquids using a coarse grained force-field. *Phys. Chem. Chem. Phys.* **22**, 1682–1692 (2020).
- (119) Bhargava, B. L., Devane, R., Klein, M. L. & Balasubramanian, S. Nanoscale organization in room temperature ionic liquids: A coarse grained molecular dynamics simulation study. *Soft Matter* **3**, 1395–1400 (2007).
- (120) Wang, Y., Izvekov, S., Yan, T. & Voth, G. A. Multiscale coarse-graining of ionic liquids. *J. Phys. Chem. B* **110**, 3564–3575 (2006).
- (121) Moradzadeh, A., Motevaselian, M. H., Mashayak, S. Y. & Aluru, N. R. Coarse-Grained Force Field for Imidazolium-Based Ionic Liquids. *J. Chem. Theory Comput.* **14**, 3252–3261 (2018).
- (122) Schaeffer, N. *et al.* Mechanisms of phase separation in temperature-responsive acidic aqueous biphasic systems. *Phys. Chem. Chem. Phys.* **21**, 7462–7473 (2019).
- (123) Pérez-Sánchez, G., Gomes, J. R. B. & Jorge, M. Modeling self-assembly of silica/surfactant mesostructures in the templated synthesis of nanoporous solids. *Langmuir* **29**, 2387–2396 (2013).
- (124) Yoo, B. *et al.* Molecular mechanisms of ionic liquid cytotoxicity probed by an integrated experimental and computational approach. *Sci. Rep.* **6**, 2–8 (2016).
- (125) Yoo, B., Zhu, Y. & Maginn, E. J. Molecular Mechanism of Ionic-Liquid-Induced Membrane Disruption: Morphological Changes to Bilayers, Multilayers, and Vesicles. *Langmuir* **32**, 5403–5411 (2016).
- (126) Bhargava, B. L. & Klein, M. L. Formation of micelles in aqueous solutions of a room temperature ionic liquid: A study using coarse grained molecular dynamics. *Mol. Phys.* **107**, 393–401 (2009).
- (127) Liu, X., Zhou, G., Huo, F., Wang, J. & Zhang, S. Unilamellar Vesicle Formation and Microscopic Structure of Ionic Liquids in Aqueous Solutions. *J. Phys. Chem. C* **120**, 659–667 (2016).
- (128) Ghaed-Sharaf, T., Yang, D. S., Baldelli, S. & Ghatee, M. H. From Micelles to Vesicle and Membrane Structures of Double-Strand Ionic Liquids in Water: Molecular Dynamics Simulation. *Langmuir* **35**, 2780–2791 (2019).
- (129) Jaeger, V. W. & Pfaendtner, J. Destabilization of human serum albumin by ionic liquids studied

- using enhanced molecular dynamics simulations. *J. Phys. Chem. B* **120**, 12079–12087 (2016).
- (130) Graham, J. A., Essex, J. W. & Khalid, S. PyCGTOOL: Automated Generation of Coarse-Grained Molecular Dynamics Models from Atomistic Trajectories. *J. Chem. Inf. Model.* **57**, 650–656 (2017).
- (131) Wassenaar, T. A., Ingólfsson, H. I., Böckmann, R. A., Tieleman, D. P. & Marrink, S. J. Computational lipidomics with insane: A versatile tool for generating custom membranes for molecular simulations. *J. Chem. Theory Comput.* **11**, 2144–2155 (2015).
- (132) Lin, C. M., Li, C. S., Sheng, Y. J., Wu, D. T. & Tsao, H. K. Size-dependent properties of small unilamellar vesicles formed by model lipids. *Langmuir* **28**, 689–700 (2012).
- (133) MacDonald, R. C. *et al.* Small-volume extrusion apparatus for preparation of large, unilamellar vesicles. *BBA - Biomembr.* **1061**, 297–303 (1991).
- (134) Maulucci, G. *et al.* Particle distribution in DMPC vesicles solutions undergoing different sonication times. *Biophys. J.* **88**, 3545–3550 (2005).
- (135) Moscho, A., Orwar, O. W. E., Chiu, D. T., Modi, B. P. & Zare, R. N. Rapid preparation of GUVs. *Proc. Natl. Acad. Sci. USA* **93**, 11443–11447 (1996).
- (136) Castellana, E. T. & Cremer, P. S. Solid supported lipid bilayers: From biophysical studies to sensor design. *Surf. Sci. Rep.* **61**, 429–444 (2006).
- (137) Hardy, G. J., Nayak, R. & Zauscher, S. Model cell membranes: Techniques to form complex biomimetic supported lipid bilayers via vesicle fusion. *Curr. Opin. Colloid Interface Sci.* **18**, 448–458 (2013).
- (138) Kalb, E., Frey, S. & Tamm, L. K. Formation of supported planar bilayers by fusion of vesicles to supported phospholipid monolayers. *BBA - Biomembr.* **1103**, 307–316 (1992).
- (139) Tabaei, S. R., Choi, J. H., Haw Zan, G., Zhdanov, V. P. & Cho, N. J. Solvent-assisted lipid bilayer formation on silicon dioxide and gold. *Langmuir* **30**, 10363–10373 (2014).
- (140) Sut, T. N., Park, S., Choe, Y. & Cho, N. J. Characterizing the Supported Lipid Membrane Formation from Cholesterol-Rich Bicelles. *Langmuir* **35**, 15063–15070 (2019).
- (141) Jackman, J. A. & Cho, N. J. Supported Lipid Bilayer Formation: Beyond Vesicle Fusion. *Langmuir* **36**, 1387–1400 (2020).
- (142) Siontorou, C. G., Nikoleli, G. P., Nikolelis, D. P. & Karapetis, S. K. Artificial lipid membranes: Past, present, and future. *Membranes (Basel)*. **7**, 1–24 (2017).
- (143) Lin, Q. & London, E. Preparation of artificial plasma membrane mimicking vesicles with lipid asymmetry. *PLoS One* **9**, (2014).
- (144) Łuczak, J., Jungnickel, C., Joskowska, M., Thöming, J. & Hupka, J. Thermodynamics of micellization of imidazolium ionic liquids in aqueous solutions. *J. Colloid Interface Sci.* **336**, 111–116 (2009).

- (145) Pereira, A. B. *et al.* Aggregation behavior and total miscibility of fluorinated ionic liquids in water. *Langmuir* **31**, 1283–1295 (2015).
- (146) Geng, F. *et al.* Micelle formation of long-chain imidazolium ionic liquids in aqueous solution measured by isothermal titration microcalorimetry. *J. Chem. Eng. Data* **55**, 147–151 (2010).
- (147) Kumar, S. *et al.* Amphiphilic Ionic Liquid-Induced Membrane Permeabilization: Binding is Not Enough. *J. Phys. Chem. B* **122**, 6763–6770 (2018).
- (148) Bharmoria, P. & Kumar, A. Thermodynamic investigations of protein's behaviour with ionic liquids in aqueous medium studied by isothermal titration calorimetry. *Biochim. Biophys. Acta - Gen. Subj.* **1860**, 1017–1025 (2016).
- (149) Alves, M. M. S., Araújo, J. M. M., Martins, I. C., Pereira, A. B. & Archer, M. Insights into the interaction of Bovine Serum Albumin with Surface-Active Ionic Liquids in aqueous solution. *J. Mol. Liq.* **322**, (2021).
- (150) Weaver, K. D., Van Vorst, M. P., Vijayaraghavan, R., MacFarlane, D. R. & Elliott, G. D. Interaction of choline salts with artificial biological membranes: DSC studies elucidating cellular interactions. *Biochimica et Biophysica Acta - Biomembranes* vol. 1828 1856–1862 (2013).
- (151) Russo, G., Witos, J., Rantamäki, A. H. & Wiedmer, S. K. Cholesterol affects the interaction between an ionic liquid and phospholipid vesicles. A study by differential scanning calorimetry and nanoplasmonic sensing. *Biochim. Biophys. Acta - Biomembr.* **1859**, 2361–2372 (2017).
- (152) Guo, H. Y. *et al.* Effect of Imidazolium-Based Ionic Liquids on the Structure and Phase Behavior of Palmitoyl-oleoyl-phosphatidylethanolamine. *J. Phys. Chem. B* **123**, 5474–5482 (2019).
- (153) Bryant, S. J., Wood, K., Atkin, R. & Warr, G. G. Effect of protic ionic liquid nanostructure on phospholipid vesicle formation. *Soft Matter* **13**, 1364–1370 (2017).
- (154) Gal, N. *et al.* Membrane interactions of ionic liquids: Possible determinants for biological activity and toxicity. *Biochim. Biophys. Acta - Biomembr.* **1818**, 2967–2974 (2012).
- (155) Duša, F., Ruokonen, S. K., Petrovaj, J., Viitala, T. & Wiedmer, S. K. Ionic liquids affect the adsorption of liposomes onto cationic polyelectrolyte coated silica evidenced by quartz crystal microbalance. *Colloids Surfaces B Biointerfaces* **136**, 496–505 (2015).
- (156) Losada-Pérez, P., Khorshid, M. & Renner, F. U. Interactions of aqueous imidazolium-based ionic liquid mixtures with solid-supported phospholipid vesicles. *PLoS One* **11**, 1–15 (2016).
- (157) Evans, K. O. Supported phospholipid bilayer interaction with components found in typical room-temperature ionic liquids - a QCM-D and AFM study. *Int. J. Mol. Sci.* **9**, 498–511 (2008).
- (158) Rantamäki, A. H. *et al.* Interactions of Ionic Liquids and Spirocyclic Compounds with Liposome Model Membranes. A Steady-State Fluorescence Anisotropy Study. *Sci. Rep.* **9**, 1–11 (2019).
- (159) Jing, B., Lan, N., Qiu, J. & Zhu, Y. Interaction of Ionic Liquids with a Lipid Bilayer: A Biophysical

- Study of Ionic Liquid Cytotoxicity. *J. Phys. Chem. B* **120**, 2781–2789 (2016).
- (160) Oulego, P. *et al.* Relationships between the physical properties and biodegradability and bacteria toxicity of fatty acid-based ionic liquids. *J. Mol. Liq.* **292**, (2019).
- (161) Kundu, N., Roy, S., Mukherjee, D., Maiti, T. K. & Sarkar, N. Unveiling the Interaction between Fatty-Acid-Modified Membrane and Hydrophilic Imidazolium-Based Ionic Liquid: Understanding the Mechanism of Ionic Liquid Cytotoxicity. *J. Phys. Chem. B* **121**, 8162–8170 (2017).
- (162) Bai, Z., Zhao, B. & Lodge, T. P. Bilayer membrane permeability of ionic liquid-filled block copolymer vesicles in aqueous solution. *J. Phys. Chem. B* **116**, 8282–8289 (2012).
- (163) El Khoury, E. D. & Patra, D. Ionic liquid expedites partition of curcumin into solid gel phase but discourages partition into liquid crystalline phase of 1,2-dimyristoyl-sn- glycerol-3-phosphocholine liposomes. *J. Phys. Chem. B* **117**, 9699–9708 (2013).
- (164) Kumar, S., Kaur, N. & Mithu, V. S. Amphiphilic ionic liquid induced fusion of phospholipid liposomes. *Phys. Chem. Chem. Phys.* **22**, 25255–25263 (2020).
- (165) Kumari, P., Kaur, S., Sharma, S. & Kashyap, H. K. Impact of amphiphilic molecules on the structure and stability of homogeneous sphingomyelin bilayer: Insights from atomistic simulations. *J. Chem. Phys.* **148**, 165102 (2018).
- (166) Evans, K. O. Room-temperature ionic liquid cations act as short-chain surfactants and disintegrate a phospholipid bilayer. *Colloids Surfaces A Physicochem. Eng. Asp.* **274**, 11–17 (2006).
- (167) Swatloski, R. P., Holbrey, J. D. & Rogers, R. D. Ionic liquids are not always green: Hydrolysis of 1-butyl-3-methylimidazolium hexafluorophosphate. *Green Chem.* **5**, 361–363 (2003).
- (168) Dvir, T., Fink, L., Schilt, Y. & Raviv, U. Charging and softening, collapse, and crystallization of dipolar phospholipid membranes by aqueous ionic liquid solutions. *Langmuir* **30**, 14725–14733 (2014).
- (169) Kontro, I. *et al.* Effects of phosphonium-based ionic liquids on phospholipid membranes studied by small-angle X-ray scattering. *Chem. Phys. Lipids* **201**, 59–66 (2016).
- (170) Gupta, R., Singh, A., Srihari, V. & Ghosh, S. K. Ionic Liquid-Induced Phase-Separated Domains in Lipid Multilayers Probed by X-ray Scattering Studies. *ACS Omega* **6**, 4977–4987 (2021).
- (171) Bhattacharya, G. *et al.* Structural changes in cellular membranes induced by ionic liquids: From model to bacterial membranes. *Chemistry and Physics of Lipids* vol. 215 1–10 (2018).
- (172) Bhattacharya, G. *et al.* X-ray Reflectivity Study of the Interaction of an Imidazolium-Based Ionic Liquid with a Soft Supported Lipid Membrane. *Langmuir* **33**, 1295–1304 (2017).
- (173) Mitra, S. *et al.* Surface Activities of a Lipid Analogue Room-Temperature Ionic Liquid and Its Effects on Phospholipid Membrane. *Langmuir* **36**, 328–339 (2020).
- (174) Sharma, V. K., Ghosh, S. K., García Sakai, V. & Mukhopadhyay, R. Enhanced Microscopic

- Dynamics of a Liver Lipid Membrane in the Presence of an Ionic Liquid. *Front. Chem.* **8**, 1–10 (2020).
- (175) Sharma, V. K. *et al.* Effects of ionic liquids on the nanoscopic dynamics and phase behaviour of a phosphatidylcholine membrane. *Soft Matter* **13**, 8969–8979 (2017).
- (176) Benedetto, A. *et al.* Structure and stability of phospholipid bilayers hydrated by a room-temperature ionic liquid/water solution: A neutron reflectometry study. *J. Phys. Chem. B* **118**, 12192–12206 (2014).
- (177) Kumari, P., Faraone, A., Kelley, E. G. & Benedetto, A. Stiffening Effect of the [Bmim][Cl] Ionic Liquid on the Bending Dynamics of DMPC Lipid Vesicles. *J. Phys. Chem. B* (2021) doi:10.1021/acs.jpcc.1c01347.
- (178) Kumari, P., Pillai, V. V. S., Rodriguez, B. J., Prencipe, M. & Benedetto, A. Sub-toxic concentrations of ionic liquids enhance cell migration by reducing the elasticity of the cellular lipid membrane. *J. Phys. Chem. Lett.* **11**, 7327–7333 (2020).
- (179) Galluzzi, M., Schulte, C., Milani, P. & Podestà, A. Imidazolium-Based Ionic Liquids Affect Morphology and Rigidity of Living Cells: An Atomic Force Microscopy Study. *Langmuir* **34**, 12452–12462 (2018).
- (180) Kumar, S. *et al.* Effect of the Alkyl Chain Length of Amphiphilic Ionic Liquids on the Structure and Dynamics of Model Lipid Membranes. *Langmuir* **35**, 12215–12223 (2019).
- (181) Kaur, N. *et al.* Role of cationic head-group in cytotoxicity of ionic liquids: Probing changes in bilayer architecture using solid-state NMR spectroscopy. *J. Colloid Interface Sci.* **581**, 954–963 (2021).
- (182) Rengstl, D., Kraus, B., Van Vorst, M., Elliott, G. D. & Kunz, W. Effect of choline carboxylate ionic liquids on biological membranes. *Colloids Surfaces B Biointerfaces* **123**, 575–581 (2014).
- (183) Jeong, S. *et al.* Elucidation of molecular interactions between lipid membranes and ionic liquids using model cell membranes. *Soft Matter* **8**, 5501–5506 (2012).
- (184) Mester, P. *et al.* FTIR Spectroscopy Suggests a Revised Mode of Action for the Cationic Side-Chain Effect of Ionic Liquids. *ACS Comb. Sci.* **21**, 90–97 (2019).
- (185) Galluzzi, M. *et al.* Interaction of imidazolium-based room-temperature ionic liquids with DOPC phospholipid monolayers: Electrochemical study. *Langmuir* **29**, 6573–6581 (2013).

## CHAPTER 2

# Design and Synthesis of a New Generation of Hydrophobic Ionic Liquids

---

**Contributions:** Nick Ruark, Colin Bertz, and Nicole Berdusco assisted in synthesizing monocholinium and dicholinium ILs composed of bis(trifluoromethanesulfonyl)azanide and first-generation bis(sulfonyl)azanide anions.

**This chapter has been published, in part, as a manuscript – Reference:** Padilla, M., Bertz, C., Berdusco, N. & Mecozzi, S. Expanding the Structural Diversity of Hydrophobic Ionic Liquids: Physicochemical Properties and Toxicity of Novel Gemini Ionic Liquids. *Green Chem.* 4375–4385 (2021) doi:10.1039/d1gc00742d.

## Abstract

Among the many unique properties of ionic liquids (ILs) that allow them to be employed in a variety of applications, perhaps the most important is their structural diversity. Unlike solvents and other materials, ILs can be tuned to have specific characteristics. Libraries of ILs with distinct architectures can be rapidly synthesized using relatively simple organic chemistry techniques. Still, the structural diversity of hydrophobic ILs (HILs) is lacking compared to hydrophilic ILs due to the limited architectures that can increase hydrophobicity. Additionally, the same groups that reduce water solubility also facilitate toxicity, meaning HILs are often more environmentally unfriendly than hydrophilic ILs.

In this chapter, novel cations and anions were developed with the goal of forming unique HILs with lower toxicity. Choline, an environmentally benign nutrient, was employed as the core of the cations, where several monocholinium and dicholinium molecules were synthesized. These cations were first paired with fatty acid-based anions to form the corresponding ILs. Unfortunately, these ILs were typically water soluble and solid at room temperature. Then, bis(trifluoromethanesulfonyl)azanide ( $[\text{NTf}_2]$ ) was used as the anion and was paired with the cholinium-based cations. The resulting ILs were hydrophobic and liquid at room temperature. However, owing to the toxicity inherent in  $\text{NTf}_2$ , three distinct libraries of new bis(sulfonyl)azanide anions were developed. Instead of incorporating two trifluoromethane moieties, the anions had one or both moieties replaced with alkyl or aryl groups. For the aryl compounds, a wide range of electron-withdrawing and electron-donating functionalities were employed. The bis(sulfonyl)azanide anions were paired with the cholinium-based cations to form many unique ILs with wide-ranging characteristics and properties.

## 2.1 Introduction

Technological advances are fueled by the discovery and application of new materials; however, there is a growing demand that these new materials be environmentally friendly. In the past two decades, ILs have surfaced as a potential answer to this challenge.<sup>1</sup> ILs are broadly classified as salts that are liquid below 100 °C, but they can be further classified into separate subcategories that are representative of their structure, function, and physical characteristics. Examples include room temperature ILs (RTILs; ILs that are liquid at or below room temperature)<sup>2</sup>, HILs, polymeric ILs (PILs; polyelectrolytes composed of IL monomers)<sup>3</sup>, and task specific ILs (TSILs; functionalized ILs for specific applications)<sup>4</sup>. ILs are unique in their tunability as the anions and cations can have a wide range of inorganic and organic architectures. Additionally, ILs have favorable physical properties such as negligible vapor pressure, low flammability, and chemical inertness. Their ionic composition allows them to be excellent solvents, capable of dissolving a diverse array of substances, including cellulose<sup>5</sup>, DNA<sup>6</sup>, and lathanides<sup>7</sup>. Due to these properties, ILs have been labelled “green” materials that could replace traditional organic solvents, toxic electrolytes, and other environmentally harmful substances. As such, ILs have been explored as materials in tribology<sup>8</sup>, batteries<sup>9</sup>, pharmaceutical sciences<sup>10</sup>, catalysts<sup>11</sup>, liquid crystal displays<sup>12</sup>, and CO<sub>2</sub> capture<sup>13</sup>.

While initially designated as “environmentally friendly”, the wealth of research on ILs has revealed that many are toxic.<sup>14</sup> Among the different classes of ILs, HILs typically are more toxic than hydrophilic ILs, as the former utilize long alkyl chains on the cations to increase hydrophobicity. The lipophilic cations act as surfactants which can severely damage lipid membranes.<sup>15</sup> Additionally, HILs often employ a limited variety of toxic weakly-coordinating anions, such as bis(trifluoromethanesulfonyl)amide ([NTf<sub>2</sub>]), hexafluorophosphate ([PF<sub>6</sub>]), and tetrafluoroborate ([BF<sub>4</sub>]). More information on IL toxicity can be found in Chapter 1 and Chapter 3.

One promising subclass of ILs that has gained recent attention is Gemini ILs (GILs). The prototypical GIL has an alkyl chain tethered between two identical cationic head groups and is paired with the same two anions. Alternative GILs exist where the tether is connected to different cationic head groups<sup>16</sup> or the dication is paired with two different anions<sup>16</sup>. GILs have a niche in separations technology<sup>17</sup> and

catalysis<sup>18</sup> as their thermal stability is higher than traditional monocationic ILs<sup>19</sup>. Due to their use in these applications, the majority of GILs are hydrophobic. Toxicological analysis has revealed that the tethered alkyl chains are less able to penetrate lipid bilayers due to the bulky and charged headgroups, meaning GILs have reduced toxicity compared to their monocationic counterparts, while still maintaining their hydrophobicity.<sup>20</sup>

Although toxicity is a crucial factor, other characteristics are important when designing new HILs. This includes facile IL synthesis as each additional step increases the cost and lowers the yield. Also, HILs need to be pure to have their desired properties. As chromatography cannot be easily employed due to the ionic nature of the compounds, other strategies are necessary to remove impurities and excess starting materials. Moreover, the HILs should possess favorable physicochemical properties, such as low viscosity to facilitate easier handling, melting points below room temperatures which allows HILs to be employed in more applications, and high hydrophobicity as many HILs have high water solubilities. These traits are important for translating HILs into materials that can be applied to different research fields.

Recently, the Mecozzi group developed a novel room temperature hydrophobic GIL that uses a dicholinium cation in a formulation for the delivery of amphotericin B.<sup>21</sup> While most GILs use imidazolium headgroups, this IL incorporated a cholinium-based moiety, which are known to be less toxic than the commonly used tetraalkylammonium and aromatic heterocycle cations, as choline is an essential nutrient in most organisms.<sup>22</sup> Although the dicholinium cation was paired with a [NTf<sub>2</sub>] anion, the GIL showed a favorable toxicity profile in zebrafish.

Building on the previous work, the aim of this chapter is to continue to expand the structural diversity of HILs by investigating cholinium-based cations as well probing new anion architectures. In the first part, a small library of monocholinium and dicholinium cations was synthesized and paired with fatty acid anions to make the corresponding ILs. However, due to the tendencies of these ILs to be solid at room temperature and water soluble, the cations were then paired with [NTf<sub>2</sub>] anions. While the resulting ILs were hydrophobic and liquid at room temperature, the toxicity profiles, especially for aquatic species, were undesirable (see Chapter 3). Next, a series of novel symmetric and asymmetric bis(sulfonyl)azanide anions

were synthesized. The first-generation utilized an asymmetric structure in which one side incorporated a trifluoromethane group, while the other side incorporated either an alkyl chain, aryl group, or alkyl-aryl moiety. The second-generation compounds were composed of both symmetric and asymmetric anions that had aryl moieties on each side of the bis(sulfonyl)azanide core. Lastly, the third-generation anions were asymmetric and incorporated an aryl group on one end and an alkyl chain or alkyl-like chain on the other end. The three generations of bis(sulfonyl)azanide anions were paired with monocholinium and dicholinium cations to create a large library of ILs. The syntheses and characteristics of the cations, anions, and ILs are described below, whereas the physicochemical and toxicological properties of these compounds are described in Chapter 3.

## 2.2 Results and Discussion

### 2.2.1 Synthesis of cholinium-based cations

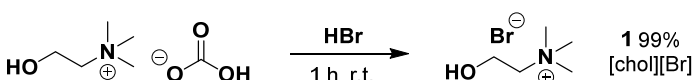
As previously mentioned, the low toxicity of choline, coupled with previous research on the synthesis and applications of hydrophilic cholinium-based ILs, offers a promising architecture to design new HILs.<sup>8,22,23</sup> As choline is water soluble, the molecule must be made more hydrophobic, which can be accomplished by adding alkyl chains. Derivatized cholinium species can be readily synthesized via quaternization reactions, in which dimethylaminoethanol is reacted with various alkyl halide reagents. Therefore, several cholinium, cholinium-based, and dicholinium cations were developed with a range of alkyl chain lengths, to probe how the size of the alkyl chain affects the properties of the resulting ILs.

As a control cation, choline bromide (**1**) was synthesized by neutralizing choline bicarbonate with hydrobromic acid (**Scheme 2.1A**). The alkyl monocholinium derivatives (**2a–2d**) were formed via quaternization reactions using dimethylaminoethanol with various alkyl bromide reagents (**Scheme 2.1B**). Alkyl lengths of butyl, pentyl, hexyl, and octyl were chosen as larger lengths can induce severe toxicity, while shorter chains are not significantly hydrophobic.<sup>24</sup> Additionally, owing to their structural similarity to cholinium cations, a small series of morpholinium cations were synthesized (**3a–3c**). Morpholinium cations have been employed to generate a variety of ILs that are less toxic than the prototypical

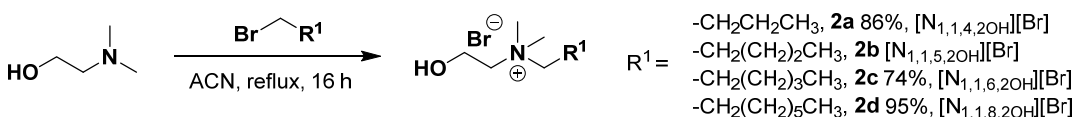
imidazolium-based ILs.<sup>5,25</sup> Here, *N*-methylmorpholine underwent quaternization reactions with bromoethane, 1-bromoethan-2-ol, and 1-bromopropane (**Scheme 2.1C**).

Lastly, the dicholinium species (**4a–4i**) were synthesized by reacting two equivalents of dimethylaminoethanol with different terminal alkyl dibromides (**Scheme 2.1D**). Due to the novelty of these dications, a wider range of linker lengths were employed for the dicholinium species, including ethyl, propyl, butyl, pentyl, hexyl, heptyl, octyl, nonyl, and dodecyl. Recent studies have shown that installing an alkoxy linker instead of an alkyl linker can reduce viscosity of the corresponding IL.<sup>26</sup> As such, a dicholinium cation with an octyl alkoxy linker was developed to probe this phenomenon (**4j**, **Scheme 2.1E**). Each of the monocholinium, morpholinium, and dicholinium compounds were synthesized in high purity, and most of the compounds were synthesized in high yields. During the reaction, many of the products precipitated in the reaction flasks as cationic species are often not soluble in organic solvents. As result, simply washing these compounds with fresh solvent removed the impurities and starting materials. Other products were purified by removing the solvent used in the reaction and washing with different solvents.

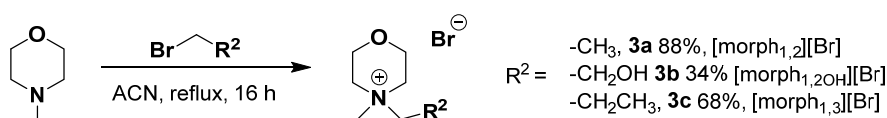
#### A. Synthesis of [chol][Br]



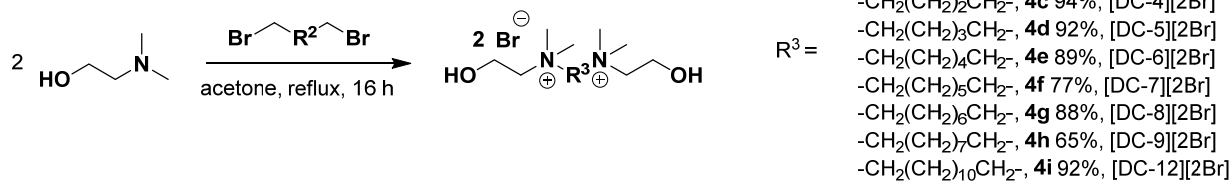
#### B. Synthesis of [N<sub>1,1,X,2OH</sub>][Br] salts



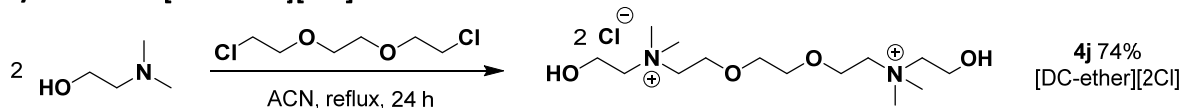
#### C. Synthesis of [morph<sub>1,x</sub>][Br] salts



### D. Synthesis of [DC-X][2Br] salts



### E. Synthesis of [DC-ether][2Cl]



**Scheme 2.1** Synthesis of monocholinium, dicholinium, and morpholinium cations

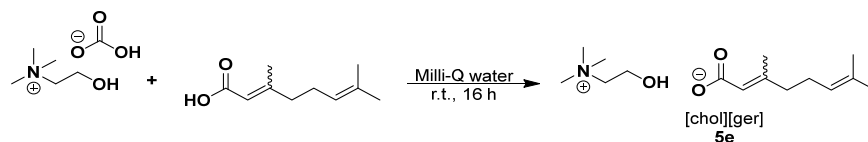
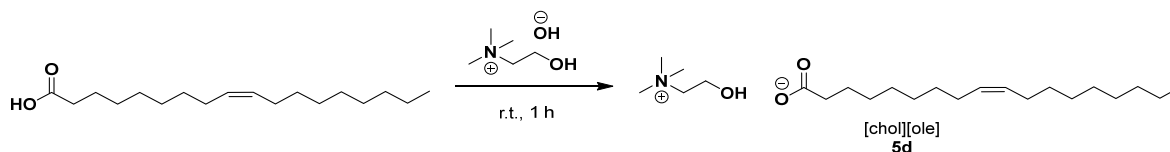
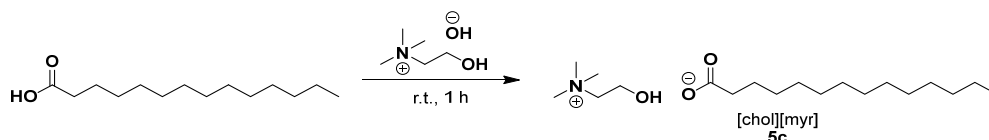
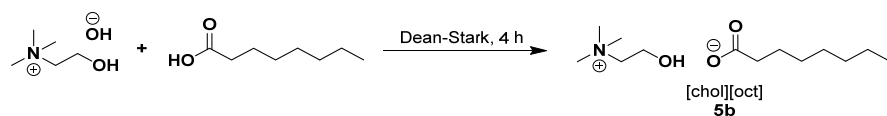
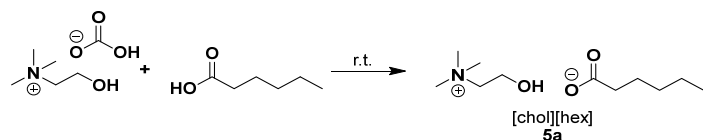
#### 2.2.2 Synthesis of cholinium ILs containing fatty acid anions

Although long alkyl chains can increase toxicity, one strategy to produce hydrophobic anions is to use biobased fatty acids. Biological systems utilize fatty acids as energy storage and building blocks, and thus these classes of molecules are relatively non-toxic.<sup>27</sup> As such, these anions were deemed an ideal starting place to pair with the cholinium-based cations to produce ILs.

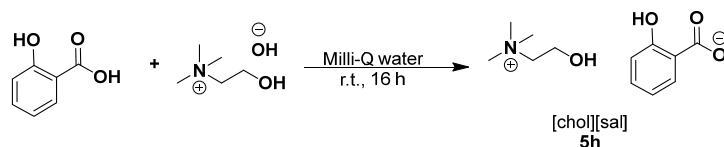
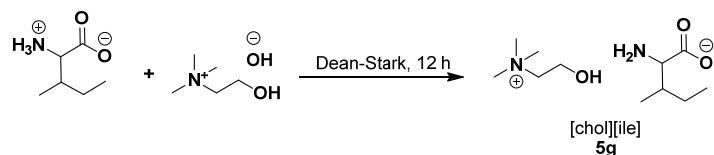
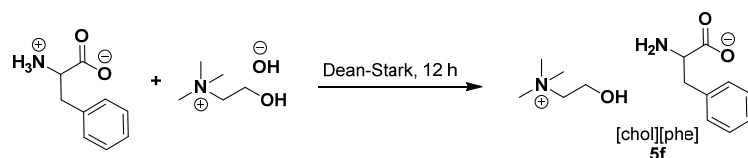
As a control, cholinium was used as the cation for the first set of ILs. Cholinium bicarbonate or cholinium hydroxide was reacted with a series of fatty acids via neutralization reactions (**Scheme 2.2A**). Cholinium hydroxide was initially used; however, the reagent is corrosive and tends to degrade rapidly. Cholinium bicarbonate was found to be a superior reagent due to its increased stability as well as its transformation into carbon dioxide when reacted with acid molecules, the latter allowing for neutralization reactions to be tracked by installing a bubbler to the reaction flask. Hexanoic, octanoic, myristic, and oleic, were used as representative fatty acids as they possess a wide range of alkyl chain length and saturation. Although less well-known, geranic acid, a pheromone, was also employed as an IL anion. Geranate has seen promising utility in so-called choline and geranate (CAGE) ILs.<sup>28</sup> These ILs have low toxicity and can be used as excipients in formulations for the delivery of biomolecules, such as insulin.<sup>29</sup> Despite the different architectures, the fatty acid ILs with the cholinium cations (**5a–5e**) were all water soluble, with

many being solid at room temperature. This is unsurprising as cholinium is extremely hydrophilic, and when paired with long chain fatty acids, can produce surfactant-like ILs. A full list of the cholinium-based ILs with fatty acid anions and their characteristics can be found in **Table 2.1**.

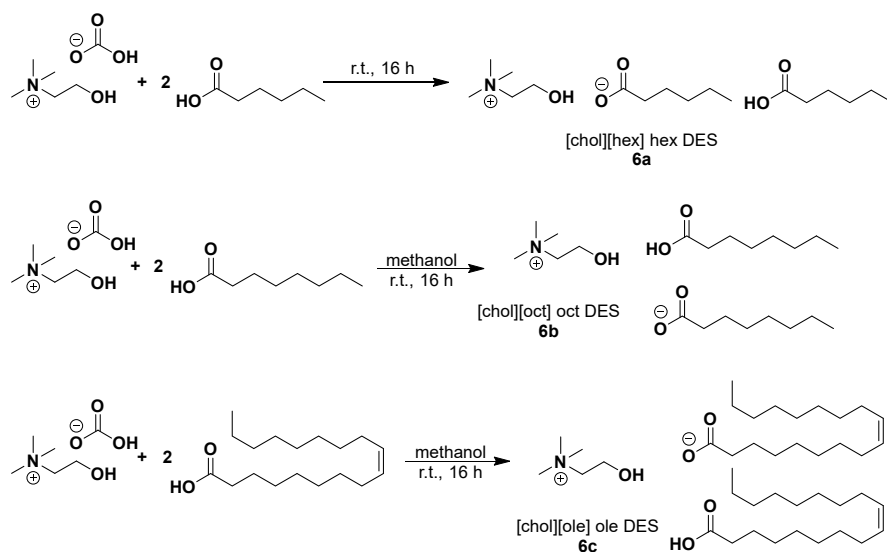
#### A. Synthesis of cholinium fatty acid ILs



#### B. Synthesis of cholinium amino acid and salicylic acid ILs



### C. Synthesis of cholinium DESs



**Scheme 2.2** Synthesis of cholinium ILs with carboxylate anions

Other carboxylate molecules were pair with cholinium, including the hydrophobic amino acids phenylalanine and isoleucine, as well as salicylic acid (**5f–5h**; **Scheme 2.2B**). ILs containing amino acids, especially cholinium amino acid ILs, are used ubiquitously as environmentally-friendly ILs.<sup>30–32</sup> Salicylic acid-based ILs belong to a class of active pharmaceutical ingredient (API) ILs, in which a drug is transformed into an ionic liquid by pairing a charged version of the drug with an appropriate counterion.<sup>33</sup> Despite containing hydrophobic moieties, the three corresponding cholinium ILs were water soluble.

To boost the hydrophobicity of cholinium-based liquids, deep eutectic solvents (DESs) were tried. Similar to ILs, DESs are composed of two or more components, typically ionic compounds, that form a mixture that has a melting point much lower than the original components.<sup>34</sup> Since the components do not need to be ionic, neutral hydrophobic compounds can be utilized. Here, the DESs were created by forming a ternary system composed of cholinium, a carboxylate anion, and the corresponding parent carboxylic acid. Here, cholinium bicarbonate was reacted with two equivalents of hexanoic acid, octanoic acid, or oleic acid (**6a–6c**; **Scheme 2.2C**). Unfortunately, the resulting compounds were solid, likely due to the large

abundance of long alkyl chains. No further DESs were produced in this study as they did not fit the scope of the research.

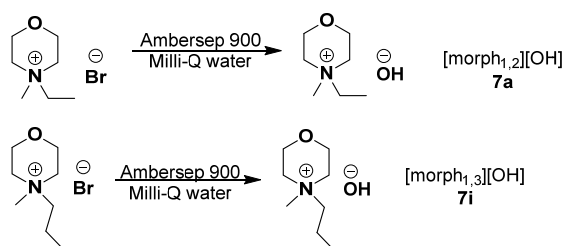
Regardless of the fatty and or carboxylate molecule, the resulting ILs, when paired with cholinium, are water soluble. Even with very hydrophobic fatty acids, such as myristic acid, the corresponding ILs became a surfactant-like compound that is quasi-water soluble. To form a HIL, both ions need to have some form of hydrophobicity.

<b>Table 2.1</b> Cholinium ILs with carboxylate anions and their characteristics at room temperature.			
#	Compound	Structure	Form
5a	[chol][hex]		Water soluble
5b	[chol][oct]		Solid
5c	[chol][myr]		Solid
5d	[chol][ole]		Solid
5e	[chol][ger]		Solid
5f	[chol][phe]		Water soluble
5g	[chol][ile]		Water soluble
5h	[chol][sal]		Water soluble
6a	[chol][hex] hex DES		Solid
6b	[chol][oct] oct DES		Solid
6c	[chol][ole] ole DES		Solid

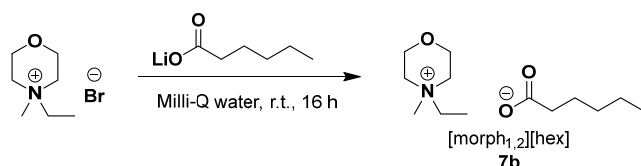
### 2.2.3 Synthesis of morpholinium ILs containing fatty acid anions

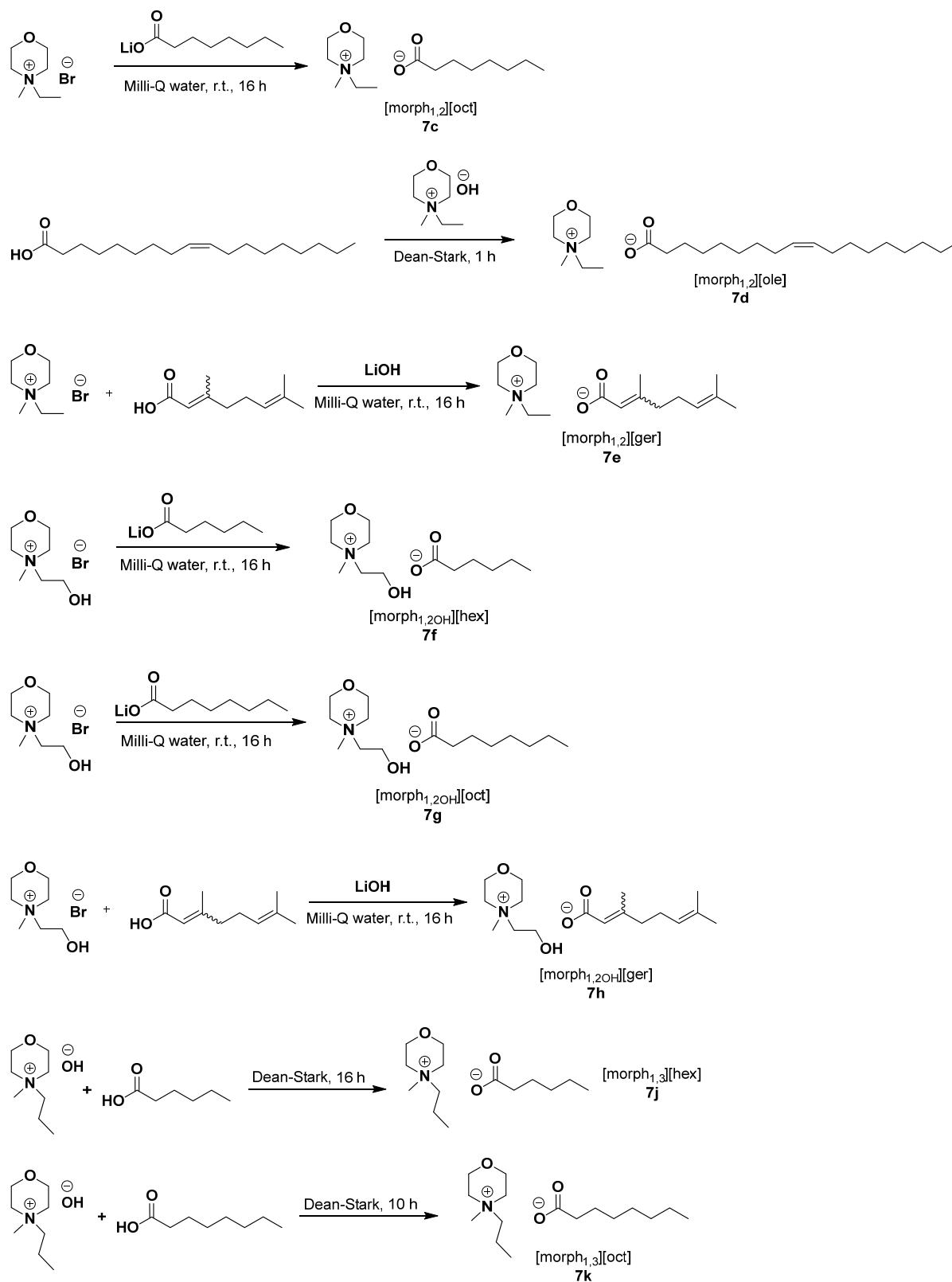
Since the cholinium cations did not form room temperature HILs with the fatty acid anions, the more hydrophobic morpholinium cations were paired. The initial ILs were formed by neutralizing the corresponding morpholinium hydroxide salts with fatty acids, as demonstrated in section 2.2.2. Since the morpholinium hydroxide compounds are not commercially available, the morpholinium bromide salts underwent an anionic exchange reaction using an Ambersep resin system that exchanges a bromide for a hydroxide anion (**Scheme 2.3A**). Similar to cholinium hydroxide, the morpholinium hydroxide compounds (**7a,7i**) were corrosive and tended to degrade rapidly, and thus were used sparingly. Therefore, a new strategy was developed that involved a direct ion metathesis reaction between the cation salt and anion salt. Here, the alkylated morpholinium bromide salts stirred in an aqueous solution containing the lithium salt of the corresponding fatty acid. If a second layer formed, the product was worked up; however, if no second layer formed, the product was deemed water soluble, and no further workup was performed. Various combinations of morpholinium cations and fatty acid anions were tried (**7b–7h, 7j, 7k; Scheme 2.3B**). Unfortunately, the morpholinium-based ILs were water soluble or formed surfactants-like solutions. A full list of these ILs and their characteristics can be found in **Table 2.2**.

#### A. Anion exchange of morpholinium salts

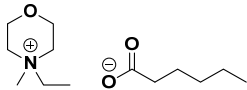
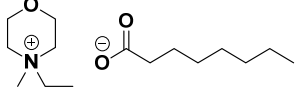
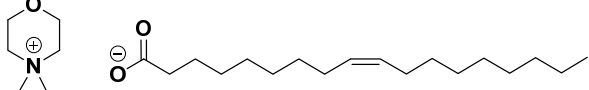
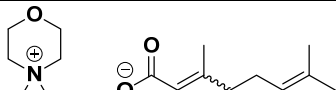
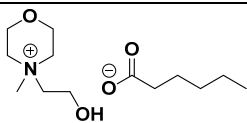
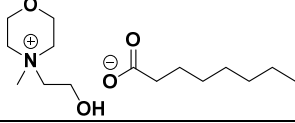
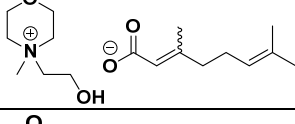
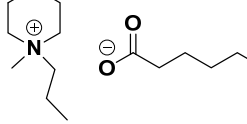
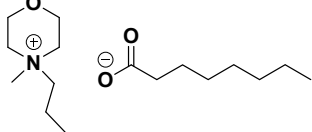


#### B. Synthesis of morpholinium ILs with fatty acids





**Scheme 2.3** Synthesis of morpholinium-based ILs with fatty acid anions

#	Compound	Structure	Form
7b	[morph <sub>1,2</sub> ][hex]		Water soluble
7c	[morph <sub>1,2</sub> ][oct]		Water soluble
7d	[morph <sub>1,2</sub> ][ole]		Solid
7e	[morph <sub>1,2</sub> ][ger]		Water soluble
7f	[morph <sub>1,2OH</sub> ][hex]		Water soluble
7g	[morph <sub>1,2OH</sub> ][oct]		Water soluble
7h	[morph <sub>1,2OH</sub> ][ger]		Water soluble
7j	[morph <sub>1,3</sub> ][hex]		Water soluble
7k	[morph <sub>1,3</sub> ][oct]		Water soluble

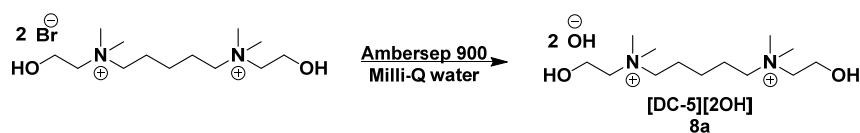
Despite containing a slightly more hydrophobic cation, the morpholinium cations are unable to form HILs when paired with these fatty acids. It is likely that the morpholinium cations are still too polar, as they are small cations that lack sufficiently long alkyl chains. Heterocyclic cations are found ubiquitously in the IL literature, although most are heteroaromatic. Morpholinium cations can be advantageous as they offer the same cyclic architecture but are not aromatic, and thus less toxic.<sup>35</sup> Since the morpholinium structure is advantageous, future studies could involve adding on longer alkyl chains to increase the

hydrophobicity; although, it would be important that the chains would not be so long as to disrupt lipid bilayers.

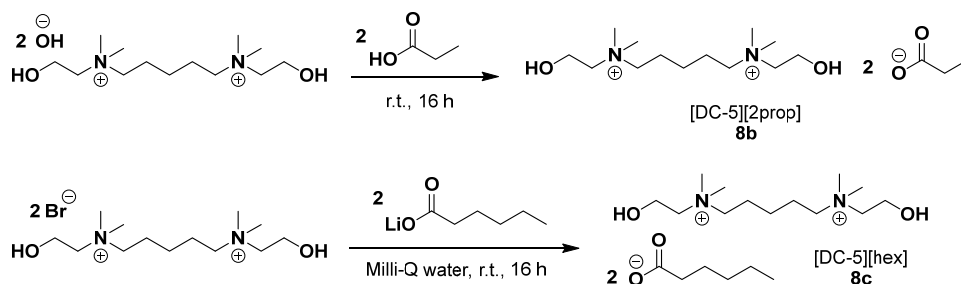
#### 2.2.4 Synthesis of dicholinium-based ILs containing fatty acid anions

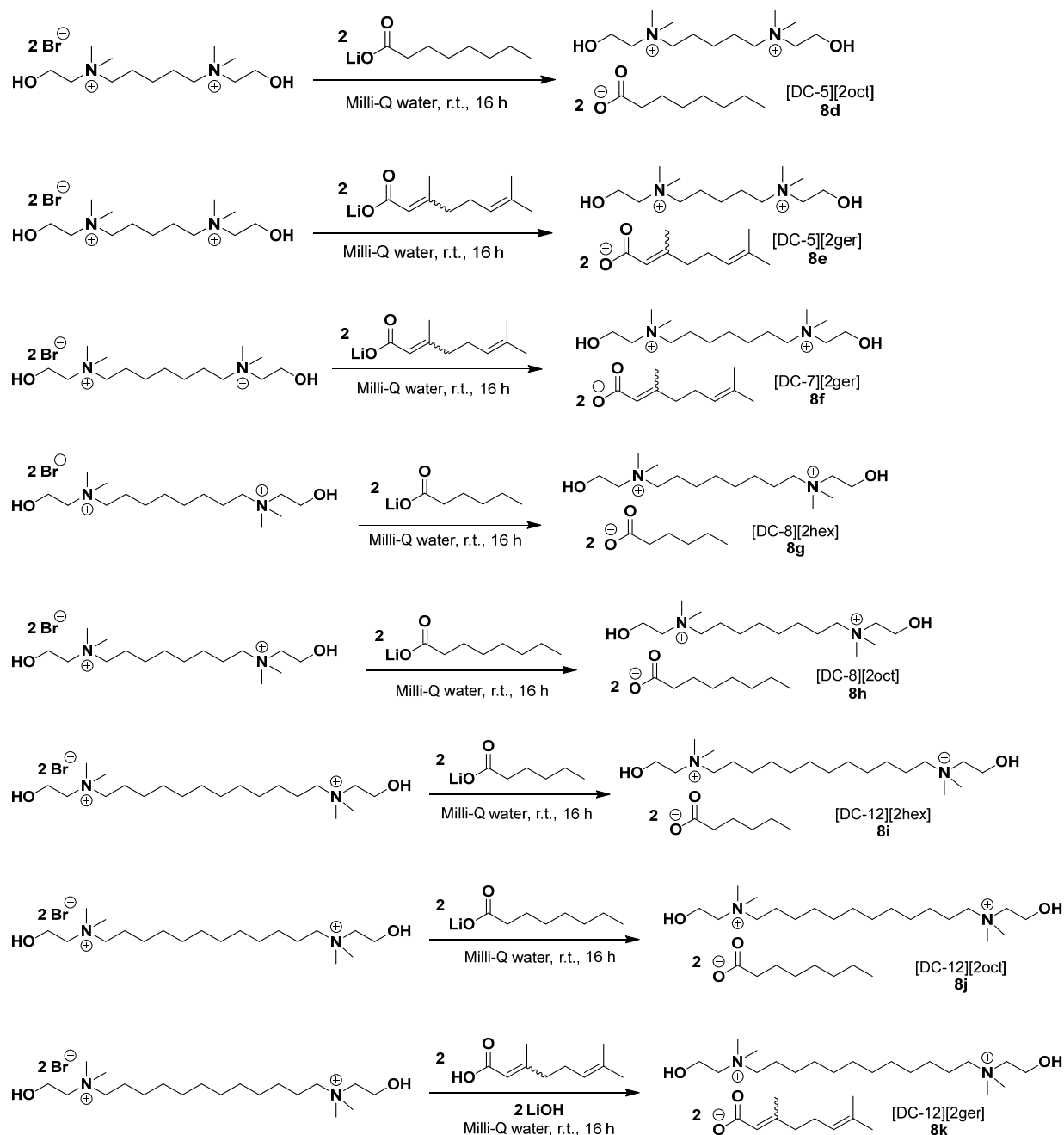
Using Gemini ILs can be advantageous for forming HILs as the dication must be paired with two anions. Since the anions are often more hydrophobic than the dication, the ILs are more likely to be hydrophobic. Additionally, the dicholinium architecture utilizes an alkyl chain linker, which can add hydrophobicity to the resulting IL. Akin to the morpholinium reactions, an anion exchange resin was utilized to form dicholinium hydroxide species. Only [DC-5][2Br] (**4d**) could be exchanged, producing [DC-5][2OH] (**8a**; Scheme 2.4A). Unfortunately, the compound degraded rapidly and thus was used for only a few reactions. Additional dicholinium cations were unsuccessfully exchanged, likely due to the inability of the dication to interact with the resin beads. While [DC-5][2OH] (**8a**) was used in a neutralization reaction to synthesize some dicholinium ILs, a direct metastasis reaction, as described in section 2.2.3, was utilized in all other cases.

##### A. Anion exchange of dicholinium salts



##### B. Synthesis of dicholinium ILs with fatty acids

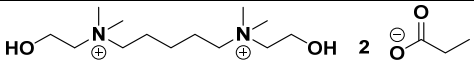
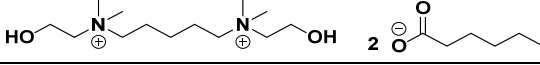
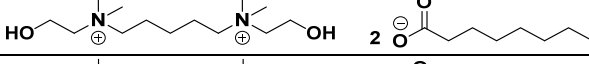
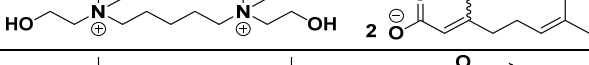
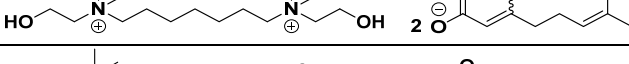
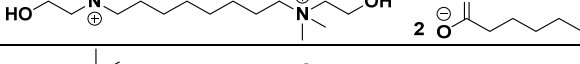
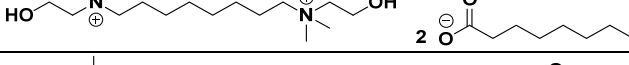
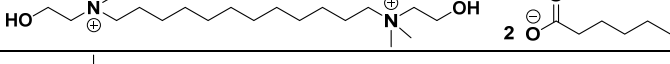
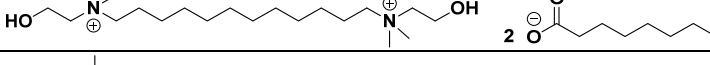
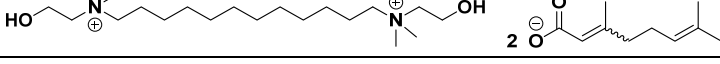




**Scheme 2.4** Synthesis of dicholinium ILs with fatty acid anions

Four dicholinium cations, [DC-5][2Br] (**4d**), [DC-7][2Br] (**4f**), [DC-8][2Br] (**4g**), and [DC-12][2Br] (**4i**), reacted with various fatty acids, including propionic, hexanoic, octanoic, and geranic acid (**Scheme 2.4B**). The longer fatty acids, such as myristic and oleic acid, were not employed as they tended to form solids due to their long alkyl tails, as shown in sections 2.2.2 and 2.2.3. Interestingly, regardless of

the dicholinium linker length and fatty acid chain length, the corresponding products (**8b–8k**) were all water soluble, and some were solid at room temperature. See **Table 2.3** for a full list of reactions and IL characteristics.

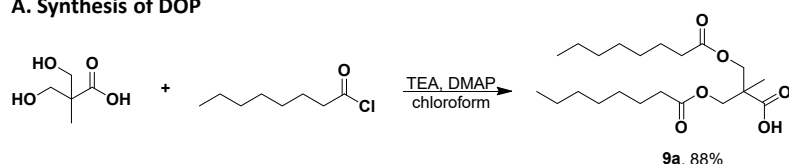
<b>Table 2.3</b> Dicholinium ILs containing fatty acid anions and their characteristics at room temperature.			
#	Compound	Structure	Form
<b>8b</b>	[DC-5][2prop]		Water soluble
<b>8c</b>	[DC-5][2hex]		Water soluble
<b>8d</b>	[DC-5][2oct]		Solid
<b>8e</b>	[DC-5][2ger]		Water soluble
<b>8f</b>	[DC-7][2ger]		Water soluble
<b>8g</b>	[DC-8][2hex]		Water soluble
<b>8h</b>	[DC-8][2oct]		Solid
<b>8i</b>	[DC-12][2hex]		Water soluble
<b>8j</b>	[DC-12][2oct]		Water soluble
<b>8k</b>	[DC-12][2ger]		Water soluble

### 2.2.5 Synthesis of ILs containing dichain fatty acids

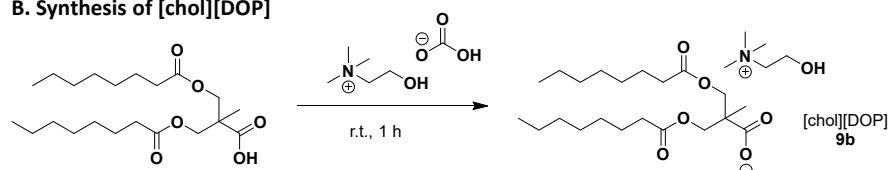
The inability of the cholinium- and morpholinium-based cations to form HILs with fatty acids prompted the development of non-natural fatty acids. Here, the fatty acids contained two alkyl chains, which was hypothesized to greatly increase the hydrophobicity of the resulting IL. While these anions required additional synthetic steps, they could be readily produced using relatively simple reactions. The first dichain fatty acid was synthesized by reacting 3-hydroxy-2-(hydroxymethyl)-2-methylpropanoic acid with two equivalents of octanoyl chloride (**Scheme 2.5A**). Since acyl chlorides are selective to alcohols over carboxylic acids, no protecting steps were needed. The resulting fatty acid (DOP, **9a**) was produced in

high yield and in one step. As a control, DOP underwent a neutralization reaction with cholinium bicarbonate (**Scheme 2.5B**). As with the other reactions with cholinium, the product ([chol][DOP], **9b**) is water soluble.

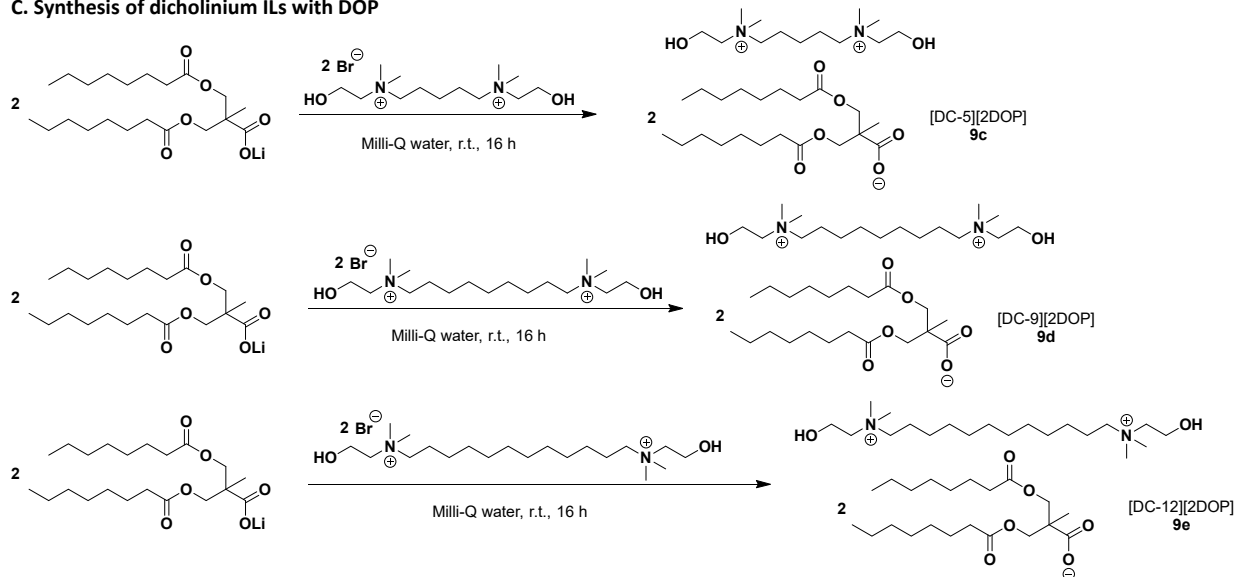
### A. Synthesis of DOP



### B. Synthesis of [chol][DOP]



### C. Synthesis of dicholinium ILs with DOP



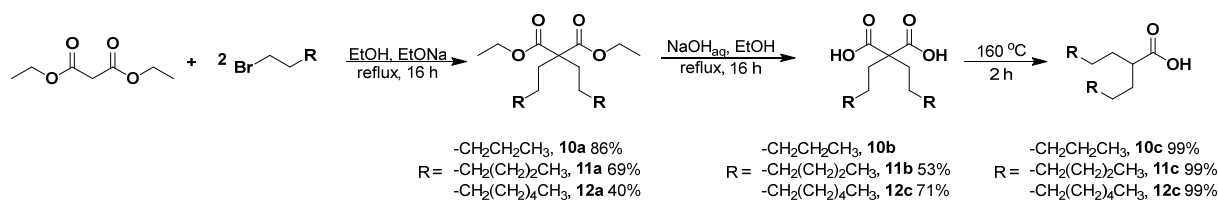
### Scheme 2.5 Synthesis of the DOP anion and corresponding ILs

Next, the lithium salt of DOP ([Li][DOP]) underwent metathesis reactions with [DC-5][2Br] (**4d**), [DC-9][2Br] (**4h**), and [DC-12][2Br] (**4i**) (**Scheme 2.5C**). Interestingly, upon dissolving [Li][DOP] in water, the solution immediately became cloudy, likely due to the inherent surfactant-like properties of DOP. Upon adding the corresponding dicholinium salt, the solution became slightly less cloudy, although no

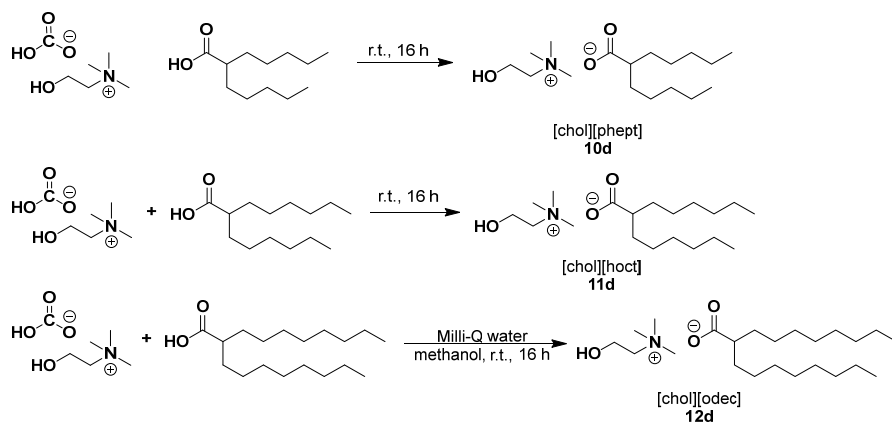
second layer formed. A product could not be isolated, as attempting to extract the aqueous solution with organic solvents resulted in the formation of an emulsion that could not be easily phase separated. Since no obvious hydrophobic layer formed the reactions with DOP (**9a**) were abandoned.

A new strategy was developed that involved the synthesis of dichain fatty acid molecules without ester groups. These new fatty acids have shorter chain lengths, so they were hypothesized to be less likely to form surfactants. A malonic ester synthesis strategy was employed to construct these compounds (**Scheme 2.6A**). In a series of separate reactions, diethyl malonate was reacted with excess alkyl bromides, including bromopentane, bromohexane, and bromooctane (**10a**, **11a**, **12a**). The resulting malonic acid species underwent saponification with sodium hydroxide in ethanol to form the corresponding malonic acids (**10b**, **11b**, **12b**). Finally, decarboxylation was accomplished by heating the neat compounds to form the dichain carboxylic acids (**10c**, **11c**, **12c**).

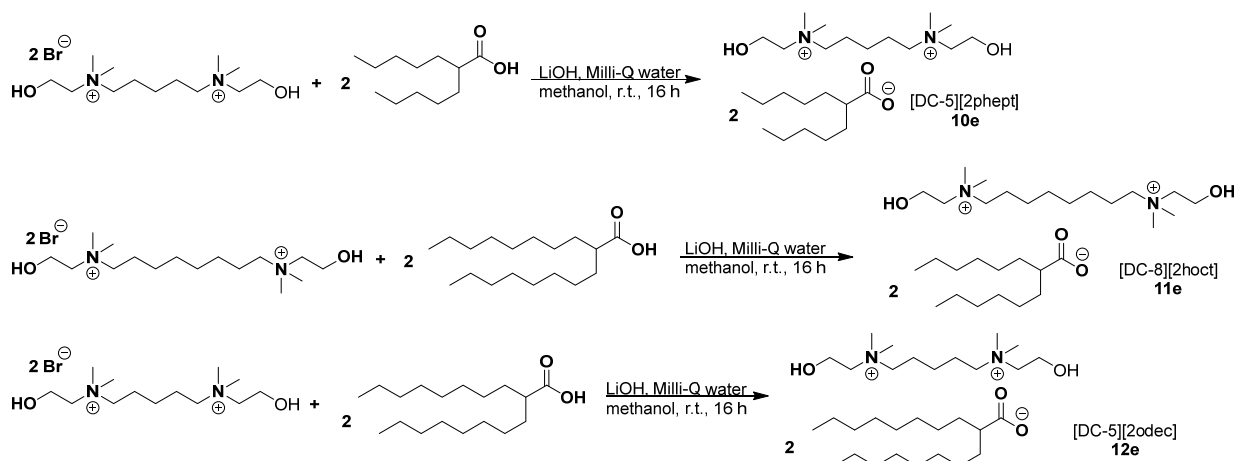
#### A. Malonic ester synthesis



#### B. Synthesis of cholinium ILs with 2<sup>nd</sup> generation dichain fatty acids



### C. Synthesis of dicholinium ILs with 2<sup>nd</sup> generation dichain fatty acids

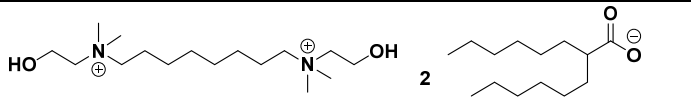


**Scheme 2.6** Synthesis of second-generation dichain fatty acid anions and corresponding ILs

The three new dichain carboxylic acids first underwent neutralization reactions with cholinium bicarbonate, which formed water soluble ILs (**10d**, **11d**, **12d**; **Scheme 2.6B**). However, when the lithium salts of the new carboxylic acids underwent metastasis reactions with different dicholinium bromide salts, the resulting compounds (**10e**, **11e**, **12e**) were hydrophobic (**Scheme 2.6C**). Unfortunately, these latter compounds were all solid at room temperature. A full list of ILs and their characteristics can be found in

**Table 2.4.**

<b>Table 2.4</b> Cholinium-based ILs containing second-generation dichain fatty acids and their characteristics at room temperature.			
#	Compound	Structure	Form
<b>10d</b>	[chol][phept]		Water Soluble
<b>10e</b>	[DC-5][2phept]		Water Soluble
<b>11d</b>	[chol][2hocht]		Water Soluble
<b>11e</b>	[DC-8][2hocht]		Hydrophobic Solid

<b>12d</b>	[chol][odec]		Water Soluble
<b>12e</b>	[DC-5][2odec]		Hydrophobic Solid

Despite several attempts to form room temperature HILs using cholinium, morpholinium, and dicholinium cations with fatty acids, none were formed. There are a variety of factors that explain these results. First, the cations are very hydrophilic. Although some of the dicholinium compounds contain long alkyl tethers, the two positive charges on the molecule distort the hydrophobicity, creating areas of hydrophobicity and hydrophilicity. While the fatty acid molecules are largely hydrophobic due to the long alkyl tails, the negative charge is localized only on the carboxylate. Computational and experimental studies on HILs reveal that weakly coordinated anions with widely delocalized negative charge are fundamental to forming HILs, especially for forming room temperature HILs.<sup>36–38</sup> It is likely that the current fatty acid strategy has a very small window in which hydrophobic room temperature ionic liquids can be formed. If the tail lengths are too short, the IL will be water soluble, but if the tail lengths are too long, the IL will become solid at room temperature. Additionally, many of the synthesized ILs showcased properties resembling surfactants, which can be unfavourable properties depending on the intended application.

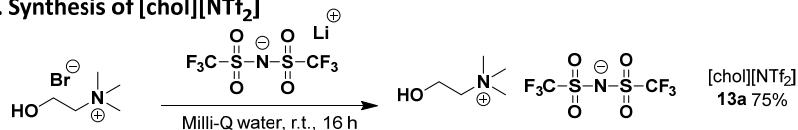
#### 2.2.6. Synthesis of ILs containing bis(trifluoromethanesulfonyl)azanide anions

With the limited success of the fatty acid ILs, a new strategy was tried that involved more delocalized and weakly coordinated anions. As previously mentioned, [PF<sub>6</sub>], [BF<sub>4</sub>], and [NTf<sub>2</sub>] are commonly used to create HILs. Due to the ability of [PF<sub>6</sub>] and [BF<sub>4</sub>] to hydrolyze and form hydrofluoric acid as well as studies that determined ILs with [NTf<sub>2</sub>] are more hydrophobic and less viscous than ILs with [PF<sub>6</sub>] and [BF<sub>4</sub>], [NTf<sub>2</sub>] was chosen as the anion.<sup>35,37,39,40</sup> The cholinium, morpholinium, and dicholinium cations were paired with [NTf<sub>2</sub>] via salt metathesis reactions, as described in section 2.2.3 (**Scheme 2.7**). Fortunately, most of the products (**13a–13p**) were hydrophobic and liquid at room temperature. See **Table**

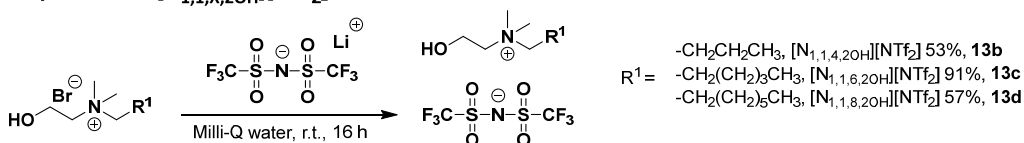
2.5 for the full list of ILs and their characteristics. These results are in stark contrast to the ILs containing fatty acid anions, which rarely formed HILs, despite many containing long lipophilic alkyl chains.

<b>Table 2.5</b> Cholinium and dicholinium-based ILs containing [NTf <sub>2</sub> ] anions and their characteristics at room temperature.			
#	Compound	Structure	Form
13a	[chol][NTf <sub>2</sub> ]		Hydrophobic Liquid
13b	[N <sub>1,1,4,2OH</sub> ][NTf <sub>2</sub> ]		Hydrophobic Liquid
13c	[N <sub>1,1,6,2OH</sub> ][NTf <sub>2</sub> ]		Hydrophobic Liquid
13d	[N <sub>1,1,8,2OH</sub> ][NTf <sub>2</sub> ]		Hydrophobic Liquid
13e	[morph <sub>1,2OH</sub> ][NTf <sub>2</sub> ]		Water Soluble
13f	[morph <sub>1,3</sub> ][NTf <sub>2</sub> ]		Hydrophobic Gel
13g	[DC-2][2NTf <sub>2</sub> ]		Hydrophobic Liquid
13h	[DC-3][2NTf <sub>2</sub> ]		Hydrophobic Solid
13i	[DC-4][2NTf <sub>2</sub> ]		Hydrophobic Solid
13j	[DC-5][2NTf <sub>2</sub> ]		Hydrophobic Liquid
13k	[DC-6][2NTf <sub>2</sub> ]		Hydrophobic Liquid
13l	[DC-7][2NTf <sub>2</sub> ]		Hydrophobic Liquid
13m	[DC-8][2NTf <sub>2</sub> ]		Hydrophobic Liquid
13n	[DC-9][2NTf <sub>2</sub> ]		Hydrophobic Liquid
13o	[DC-12][2NTf <sub>2</sub> ]		Hydrophobic Liquid
13p	[DC-ether][2NTf <sub>2</sub> ]		Hydrophobic Liquid

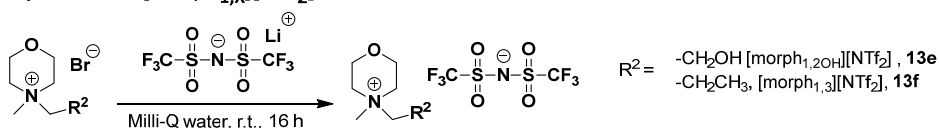
### A. Synthesis of [chol][NTf<sub>2</sub>]



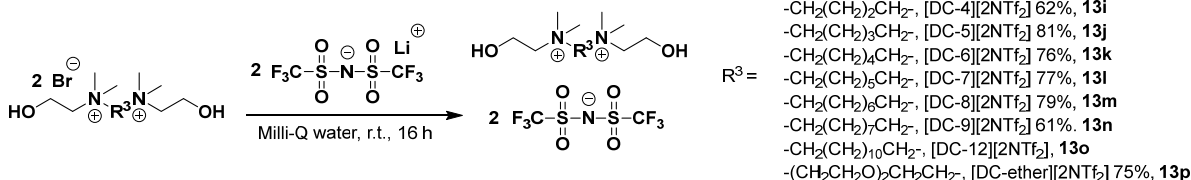
### B. Synthesis of [N<sub>1,1,X,2OH</sub>][NTf<sub>2</sub>] ILs



### C. Synthesis of [morph<sub>1,x</sub>][NTf<sub>2</sub>] ILs



### D. Synthesis of [DC-X][2NTf<sub>2</sub>] ILs

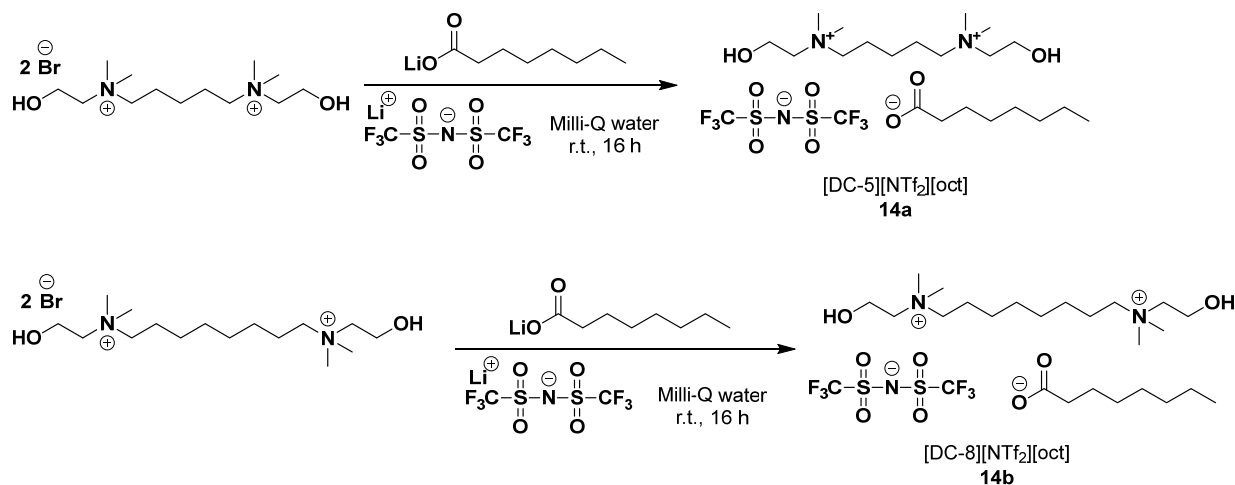


**Scheme 2.7** Synthesis of cholinium- and morpholinium-based ILs with [NTf<sub>2</sub>] anions

Out of the sixteen ILs synthesized in this group, only [morph<sub>1,2OH</sub>][NTf<sub>2</sub>] (**13e**) is water-soluble; although, it is possible that the IL is hydrophobic, albeit at a very high concentration. Similarly, [chol][NTf<sub>2</sub>] (**13a**) has high water solubility and is on the border of hydrophilic-hydrophobic. The presence of only one [NTf<sub>2</sub>] anion coupled with the small hydrophilic cation does not create enough hydrophobic domains to resist water solubility. Interestingly, [morph<sub>1,3</sub>][NTf<sub>2</sub>] (**13f**) is a gel and more hydrophobic than [morph<sub>1,2OH</sub>][NTf<sub>2</sub>] (**13e**), likely due to the lack of the additional polar hydroxyl group. Specific water solubility compounds for select ILs can be found in section 3.2.3.

While the pair of the [NTf<sub>2</sub>] anion produced many HILs, a new strategy was tried that involved using the dicholinium cations with two different anions, at 1:1:1 molar equivalence. In this case, the cations [DC-5] and [DC-8] were paired with both [NTf<sub>2</sub>] and [oct] to produce HILs that also contained lipophilicity

(**14a**, **14b**; **Scheme 2.8**). In both trials, upon mixing the three salt precursors, hydrophobic layers formed; however, upon further analysis, the layers were composed of only [DC-5][NTf<sub>2</sub>] or [DC-8][2NTf<sub>2</sub>], whereas the octanoate anion was found in the aqueous layers. These results demonstrate that certain intermolecular interactions are incompatible for forming a cohesive IL. It is possible that the hydrophobic tail of octanoate cannot interact as strongly as the intermolecular bonding between the dicholinium cations and [NTf<sub>2</sub>] anions.



**Scheme 2.8** Synthesis of dicholinium ILs containing both octanoate and [NTf<sub>2</sub>] anions

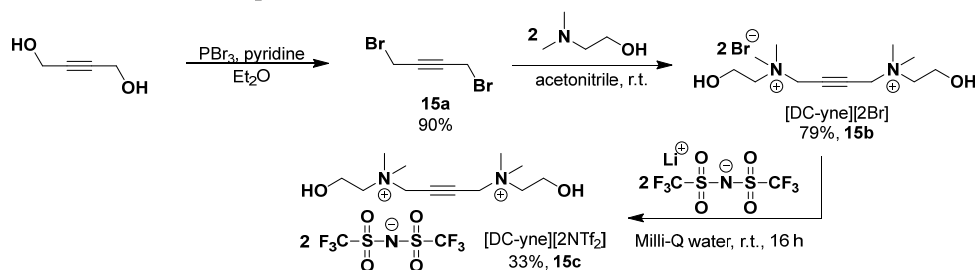
### 2.2.7 Synthesis of second-generation dicholinium cations and corresponding ILs

Since the alkyl and alkoxy dicholinium cations demonstrated immense promise in forming room temperature HILs, a new class of dicholinium compounds was developed. These cations utilized the same dicholinium moieties but incorporated unique tethers that could engage in more complex intermolecular interactions. The synthetic strategy involved creating linkers with terminal leaving groups, and then subjecting the linkers to two equivalents of dimethylaminoethanol, in a similar strategy that was used to produce the previous dicholinium compounds (see section 2.2.1). Lastly, the new dicationic precursors were mixed with lithium bis(trifluoromethanesulfonyl)amide to form second generation [DC-X][2NTf<sub>2</sub>] ILs. The first new dication incorporated an alkyne group (**Scheme 2.9A**). Here, but-2-yne-1,4-diol was reacted with

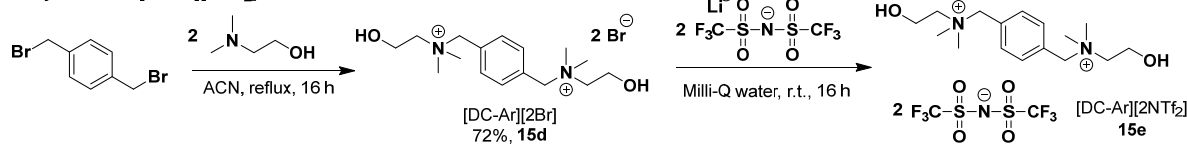
phosphorous tribromide to install terminal bromine leaving groups, producing 1,4-dibromobut-2-yne (**15a**). Next, the compound was subjected to a solution of dimethylaminoethanol to undergo a dual quaternization reaction, spontaneously forming the cation salt ([DC-yne][Br]; **15b**) when the starting materials were added. Finally, the salt underwent a metathesis reaction with lithium bis(trifluoromethanesulfonyl)amide to produce the IL, [DC-yne][2NTf<sub>2</sub>] (**15c**).

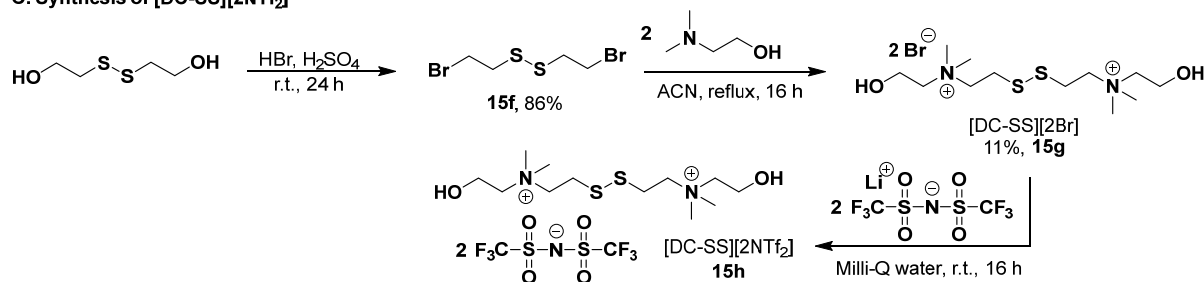
The second new cation contained an internal benzene ring (**Scheme 2.9B**). 1,4-bis(bromomethyl)benzene was commercially available and was reacted with two equivalents of dimethylaminoethanol to produce [DC-Ar][2Br] (**15d**). The cation underwent anion metathesis with lithium bis(trifluoromethanesulfonyl)amide to form [DC-Ar][2NTf<sub>2</sub>] (**15e**). The final new dicholinium species utilized a disulfide bond, which was hypothesized to create a responsive IL that could dissociate upon the presence of reducing conditions (**Scheme 2.9C**).<sup>41</sup> The cation was synthesized by first stirring 2,2'-disulfanediybis(ethan-1-ol) in a mixture of hydrobromic acid and sulfuric acid to form 1,2-bis(2-bromoethyl)disulfane (**15f**). The terminal dibromide compound then underwent the dual quaternization reaction with two equivalents of dimethylaminoethanol to form the corresponding cation salt ([DC-SS][2Br], **15g**). Finally, an IL was created by mixing [DC-SS][2Br] with lithium bis(trifluoromethanesulfonyl)amide, producing [DC-SS][2NTf<sub>2</sub>] (**15h**).

#### A. Synthesis of [DC-yne][2NTf<sub>2</sub>]



#### B. Synthesis of [DC-Ar][2NTf<sub>2</sub>]



C. Synthesis of [DC-SS][2NTf<sub>2</sub>]

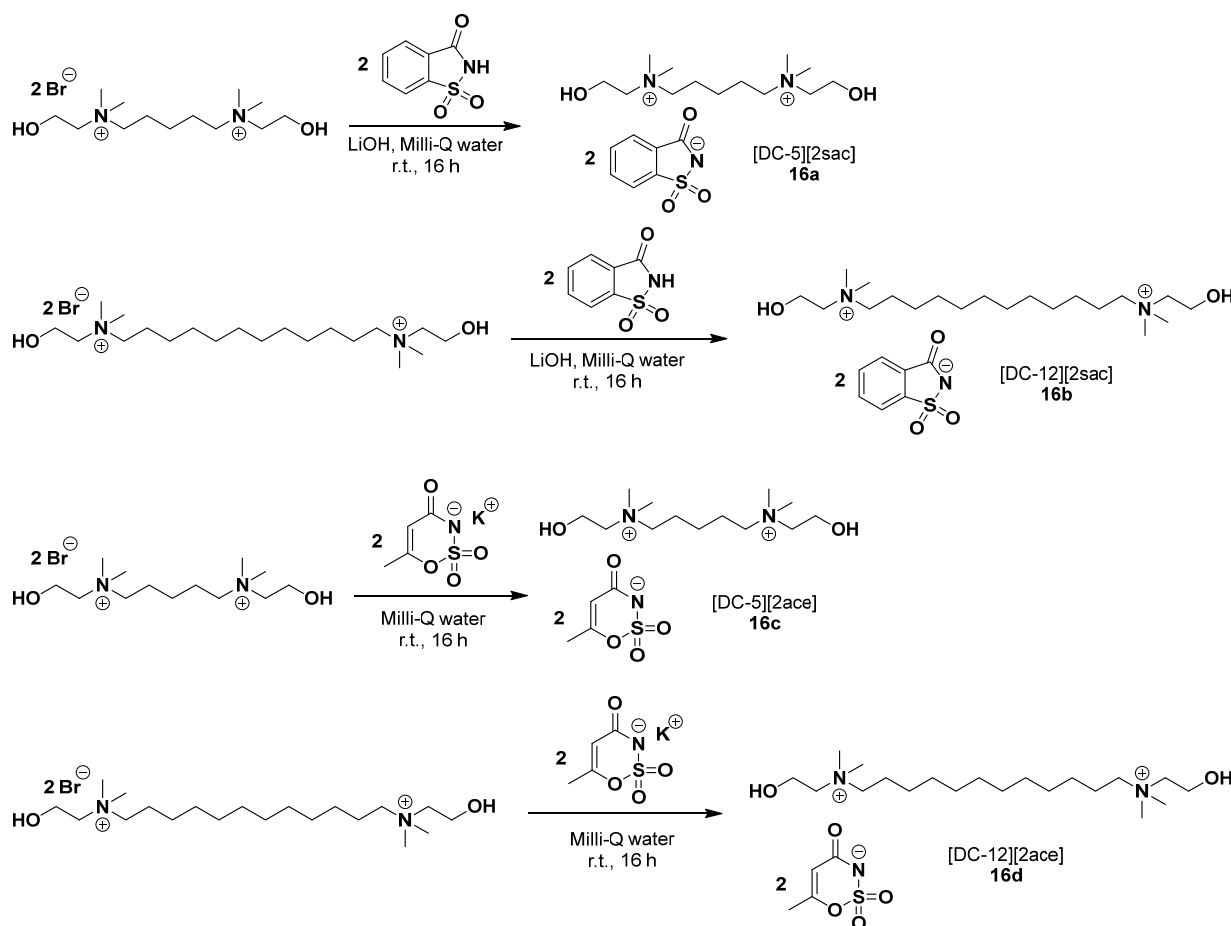
**Scheme 2.9** Synthesis of second-generation dicholinium cations and corresponding ILs containing [NTf<sub>2</sub>] anions

While the syntheses of the new cations were relatively simple, the resulting ILs were all solid at room temperature. For [DC-yne][2NTf<sub>2</sub>] (**15c**) and [DC-Ar][2NTf<sub>2</sub>] (**15e**), this is likely due to stronger intermolecular interactions that are now possible due to the addition of the  $\pi$ -bonds, especially [DC-Ar][2NTf<sub>2</sub>] (**15e**), which can engage in  $\pi$ -stacking interactions. For [DC-SS][2NTf<sub>2</sub>] (**15h**), it is possible that the addition of the two sulfur atoms allows for dipole-dipole interactions, although this hypothesis would need to be validated with further testing. Since RTILs are formed via weak interactions between the cations and anions, introducing molecules that can engage in stronger intermolecular interactions will increase the melting point. The first generation of dicholinium cations, apart from [DC-ether], contain only methylene groups, which associate via very weak Van der Waals interactions. Due to the complexity of these new cations, no further work was performed and no new dicholinium cations were synthesized.

### 2.2.8 Synthesis of dicholinium ILs containing artificial sweetener anions

When tested in toxicological models, compounds containing [NTf<sub>2</sub>] exhibited toxicity in both cells and zebrafish (see sections 3.2.5 and 3.2.6). These outcomes underscore the need for more biofriendly anions. As a result, two artificial sweeteners, saccharin and acesulfame K, were evaluated as replacements for the [NTf<sub>2</sub>] anion. These compounds contain a similar sulfonamide core as [NTf<sub>2</sub>] and have been previously used to create non-toxic ILs.<sup>42</sup> Here, the two anions were coupled with [DC-5][2Br] (**4d**) and the more hydrophobic [DC-12][2Br] (**4i**) using the standard anion metathesis reaction (**Scheme 2.10**). Unfortunately, none of the four ILs (**16a–16d**) synthesized were hydrophobic. It is likely that the extended

$\pi$ -conjugation system of the artificial sweetener anions does not sufficiently delocalize the anion in a similar capacity as  $[\text{NTf}_2]$ , as the latter has trifluoromethane groups that provide substantial electron delocalization through inductive effects.



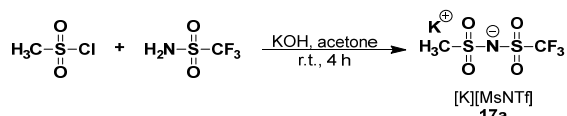
**Scheme 2.10** Synthesis of dicholinium ILs containing saccharine and acesulfame K anions

### 2.2.9 Synthesis of first-generation bis(sulfonyl)azanide anions

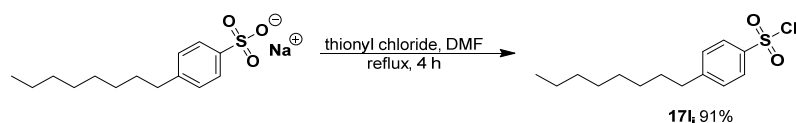
The results from the ILs containing artificial sweeteners revealed that at least one strongly electron-withdrawing trifluoromethane group may be necessary to create sufficient electron delocalization to form a HIL, especially with the hydrophilic dicholinium cations. As such, a small library of anions was synthesized that contained a trifluoromethane group on one end of the azanide and a different moiety on the other end.

Initially, the reaction conditions involved subjecting trifluoromethanesulfonamide in a solution of potassium hydroxide, and then adding an appropriate sulfonyl chloride reagent. This strategy (**Scheme 2.11A**) was used to create a mesyl-triflate asymmetric anion ( $[K][MsNTf]$ , **17a**). Due to the difficult workup and low yield, the base was replaced with sodium carbonate, which can be used as the azanide has a sufficiently low pKa to be deprotonated by the weaker base. Additionally, due to the formation of CO<sub>2</sub> during the reaction, the yields greatly increased.

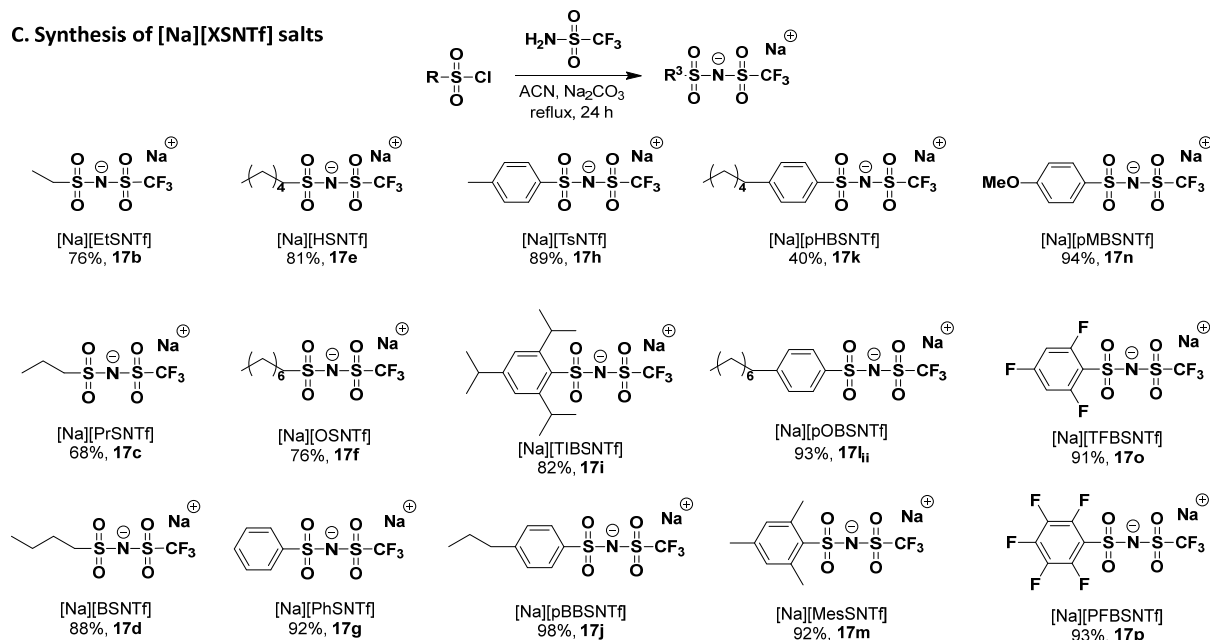
### A. Synthesis of $[K][MsNTf]$



### B. Synthesis of 4-octylbenzenesulfonyl chloride



### C. Synthesis of $[Na][XSNTf]$ salts



**Scheme 2.11** Synthesis of first-generation bis(sulfonyl)azanide anions

Since a wide variety of sulfonyl chloride reagents are commercially available, several distinct structures were chosen, including alkyl chains, aryl groups, and alkyl-aryl moieties (**17b–17p**). Various chain lengths were used for the alkyl-derived azanide anions, while butyl, hexyl, and octyl chains were utilized for the alkyl-aryl anions. Only one of the sulfonyl chloride reagents, octylbenzenesulfonyl chloride, was not available. Therefore, the compound was synthesized by heating sodium 4-octylbenzenesulfonate in a solution of thionyl chloride and dimethylformamide to form **17i** (**Scheme 2.11B**). Traditional chromatography cannot be employed to purify the anions, so a stepwise workup was performed that selectively removed each starting material. After refluxing, the solution was filtered to remove residual sodium carbonate and solid impurities. The filtrate was then concentrated and dissolved in cold acetone to precipitate the trifluoromethanesulfonamide starting material, which was filtered out. Lastly, the crude product was washed in toluene, as the solvent solubilized the sulfonyl chloride and other sulfonyl derivative impurities, without dissolving the product. Yields for the anion syntheses were typically 80–90% and showcased good purity.

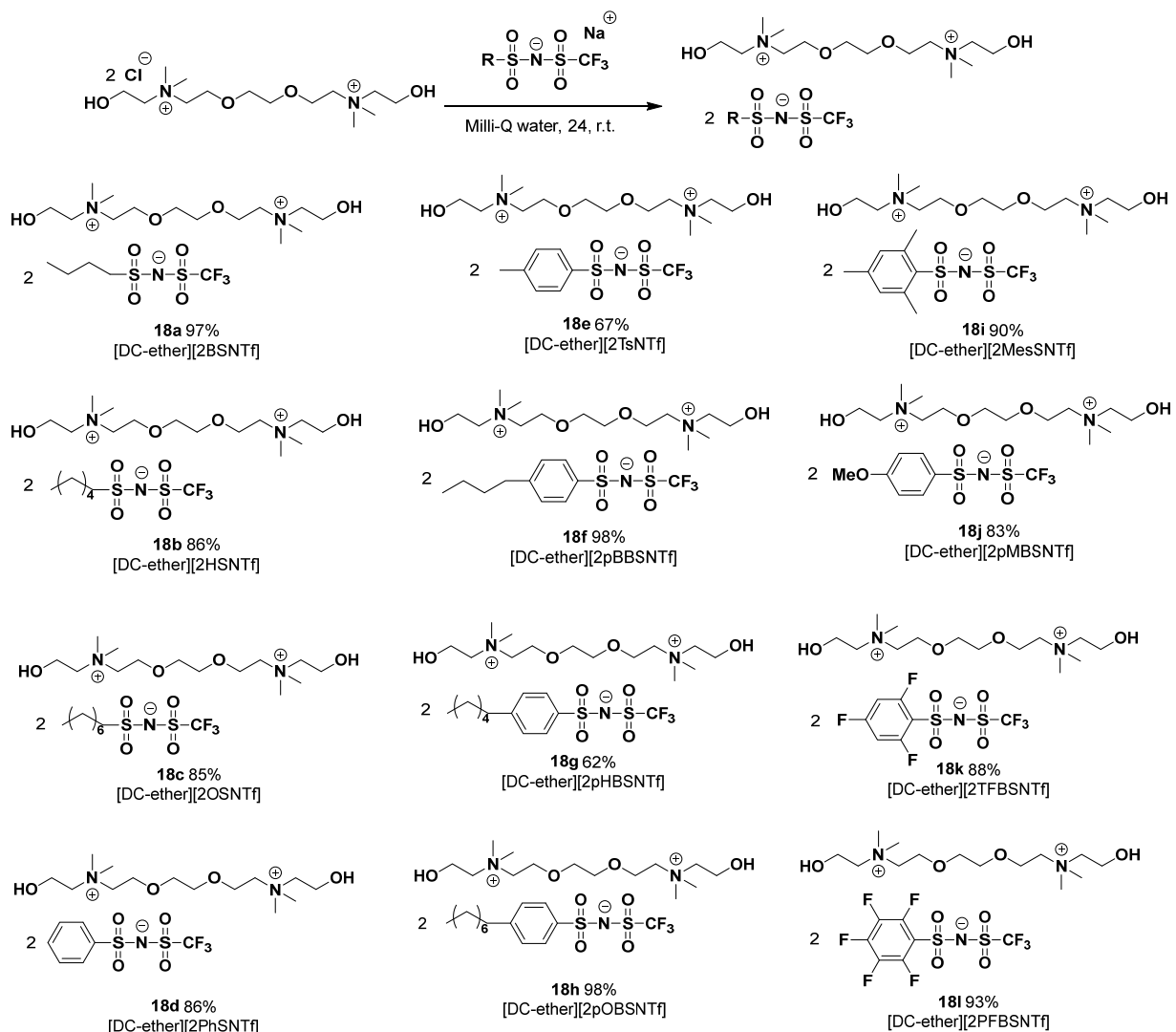
#### 2.2.10 Synthesis of cholinium and dicholinium ILs containing first-generation bis(sulfonyl)azanides

The asymmetric anions containing a trifluoromethane group were paired with the alkyl cholinium and dicholinium cations. In the first set of ILs, [DC-ether][2Cl] (**4j**) was paired with each of the asymmetric anions except for [Na][MsNTf] (**17a**), [Na][EtSNTf] (**17b**), [Na][PrSNTf] (**17c**), and [Na][TIBSNTf] (**17i**) (**Scheme 2.12A**). The excluded anions were not chosen to their high hydrophilicity or tendency to form solids (see below). [DC-ether][2Cl] (**4j**) was chosen as the cation because other dicholinium species formed more viscous ILs (data not shown). The resulting ILs (**18a–18l**) are all liquid at room temperature and all but [DC-ether][2BSNTf] (**18a**) are hydrophobic.

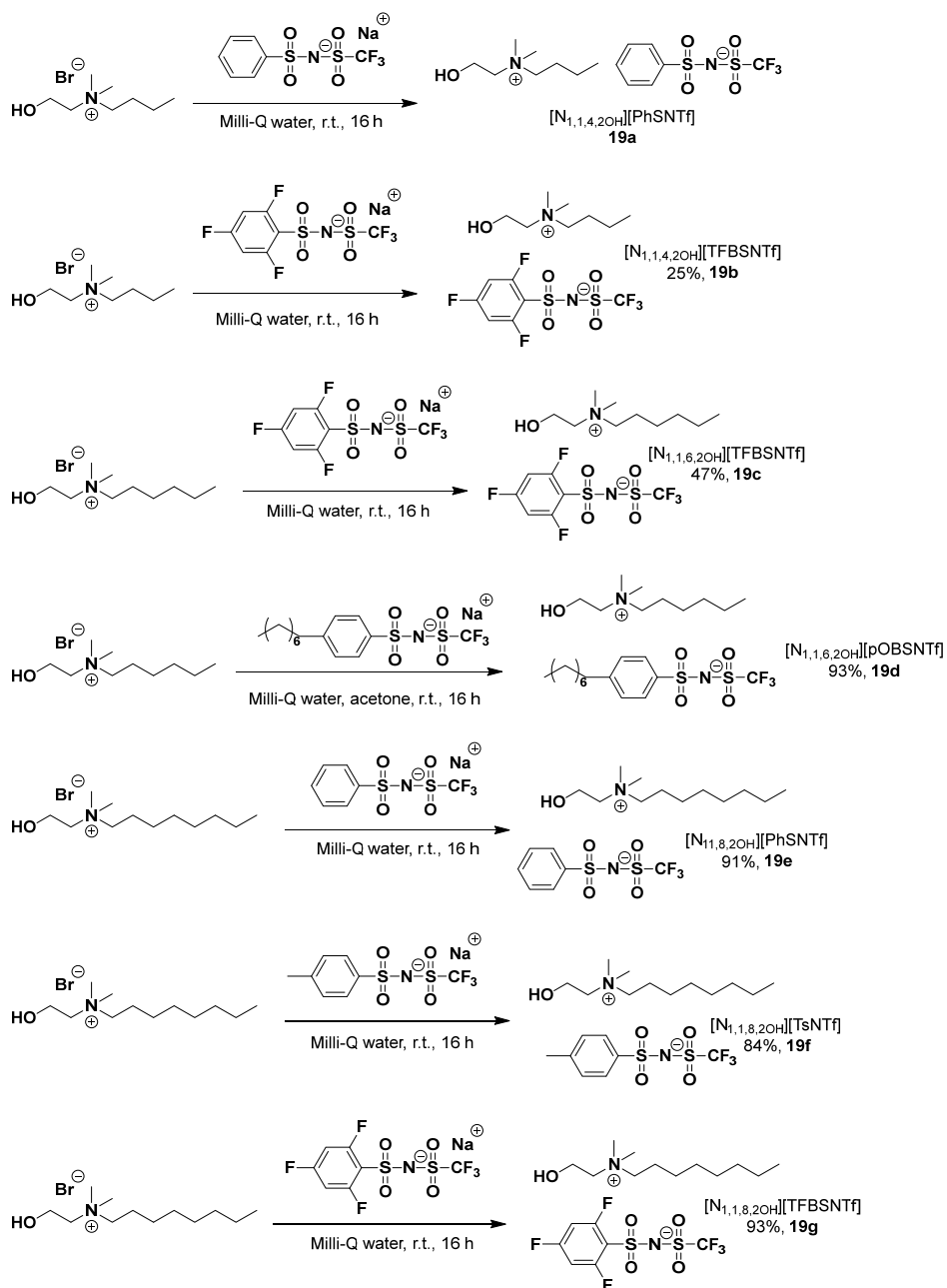
Next, the alkyl cholinium cations [N<sub>1,1,4,2OH</sub>][Br] (**2a**), [N<sub>1,1,6,2OH</sub>][Br] (**2c**), and [N<sub>1,1,8,2OH</sub>][Br] (**2d**) were paired with select asymmetric anions to probe how non-Gemini ILs compared (**Scheme 2.12B**). The ILs (**19a–19g**) were all liquid at room temperature and all but [N<sub>1,1,4,2OH</sub>][PhSNTf] (**19a**) were hydrophobic. The water solubility of the latter IL is unsurprising as both ions are relatively hydrophilic (this is further

discussed in section 3.2.3). Interestingly, although Gemini ILs are known to be more viscous than monocationic ILs, these ILs had similar viscosity (data not shown). It is likely that the aromatic groups facilitate  $\pi$ -stacking interactions that greatly increase the number of strong intermolecular interactions. In future studies, this could be assessed by pairing the monocholinium cations with bis(sulfonyl)azanide anions that only have alkyl groups.

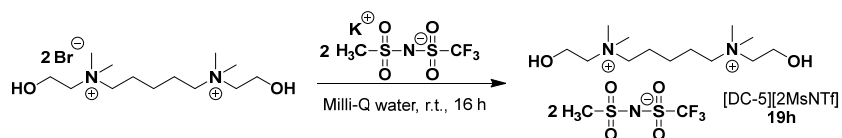
#### A. Synthesis of [DC-ether] ILs containing asymmetric bis(sulfonyl)azanide anions



## B. Synthesis of monocholinium ILs containing asymmetric bis(sulfonyl)azanide anions

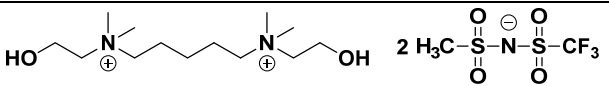
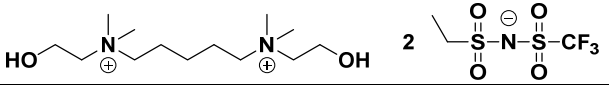
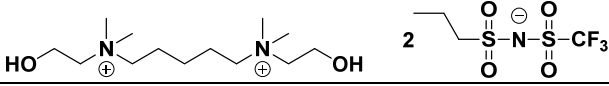
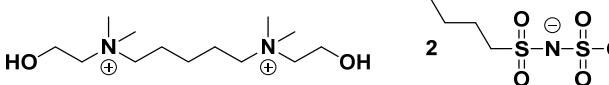
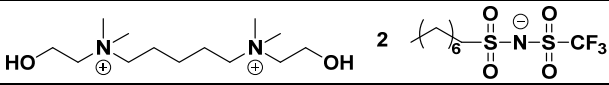
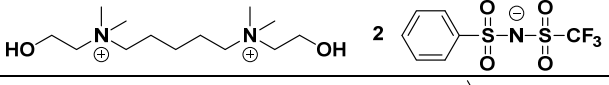
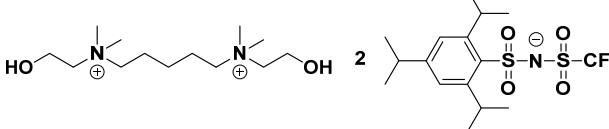


## C. Synthesis of alkyl dicholinium ILs containing asymmetric bis(sulfonyl)azanide anions





The final series of ILs utilized dicholinium cations, not including [DC-ether][2Cl] (**4j**), that were paired with a diverse array of first-generation bis(sulfonyl)azanide anions (**Scheme 2.12C**). Interestingly, these ILs (**19h–19p**) showed a wide-range of melting temperatures and hydrophobicities (see sections 3.2.1 and 3.2.3). The cations paired with [Na][MsNTf] (**17a**), [Na][EtSNTf] (**17b**), [Na][PrSNTf] (**17c**), and [Na][BSNTf] (**17d**) are hydrophilic, likely due to the small alkyl chains that do not provide sufficient lipophilicity to form an HIL, as is the case for [DC-ether][2BSNTf] (**18a**). The alkyl dicholinium cations paired with anions containing long alkyl chains and aromatic groups are hydrophobic solids, apart from [DC-5][2PhSNTf] (**19m**), which is an extremely viscous hydrophobic liquid. The difference between the latter set of ILs and the ILs formed with [DC-ether] is a result of the tether architecture. For [DC-ether], the oxygen atoms disrupt Van der Waals interactions that would otherwise occur between molecules with long alkyl tethers. This leads to decreased melting temperature and viscosity. Information regarding this latter series of ILs (**19h–19p**) is summarized in **Table 2.6**.

<b>Table 2.6</b> Dicholinium ILs containing first-generation bis(sulfonyl)azanide anions and their characteristics at room temperature.			
#	Compound	Structure	Form
<b>19h</b>	[DC-5][2MsNTf]		Hydrophobic Solid
<b>19i</b>	[DC-5][2EtSNTf]		Water Soluble
<b>19j</b>	[DC-5][2PrSNTf]		Water Soluble
<b>19k</b>	[DC-5][2BSNTf]		Water Soluble
<b>19l</b>	[DC-5][2OSNTf]		Water Soluble
<b>19m</b>	[DC-5][2PhSNTf]		Hydrophobic Liquid
<b>19n</b>	[DC-5][2TIBSNTf]		Hydrophobic Solid

<b>19o</b>	[DC-6][2PhSNTf]		Hydrophobic Solid
<b>19p</b>	[DC-9][2PhSNTf]		Hydrophobic Solid

### 2.2.11 Synthesis of second generation bis(sulfonyl)azanides and corresponding ionic liquids

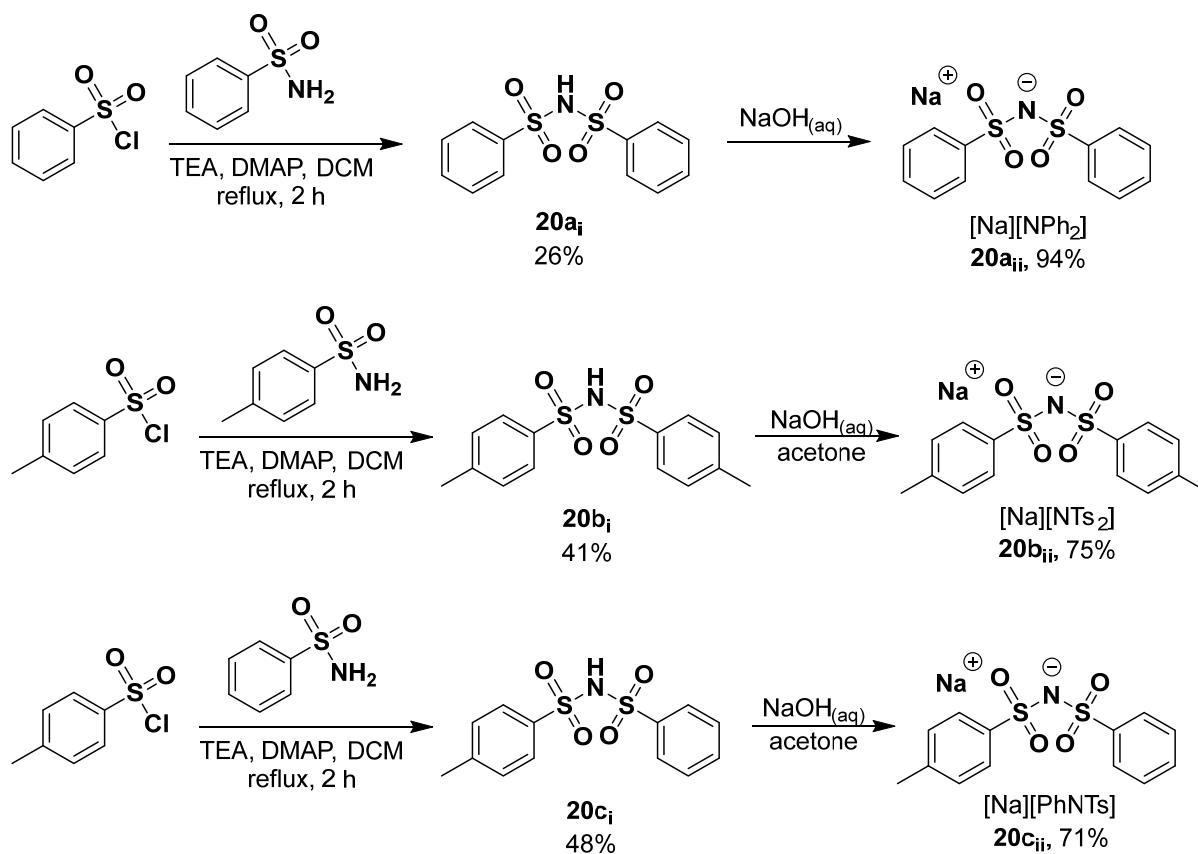
First-generation bis(sulfonyl)azanide anions, where one end contained a trifluoromethane group, facilitated the creation of a unique group of HILs. However, some of the properties were not ideal, including the necessity to use the [DC-ether][2Cl] (**4j**) cation, the high viscosity, and the wide-range of toxicity (see sections 3.2.5 and 3.2.6 for information on toxicity). As a result, a new class of anions were synthesized that eliminated the trifluoromethane group entirely. The first subclass of these second-generation anions incorporated symmetric or asymmetric aryl groups on either side of the azanide. Aryl groups, as described above, can delocalize the excess electron density, creating a more hydrophobic anion.

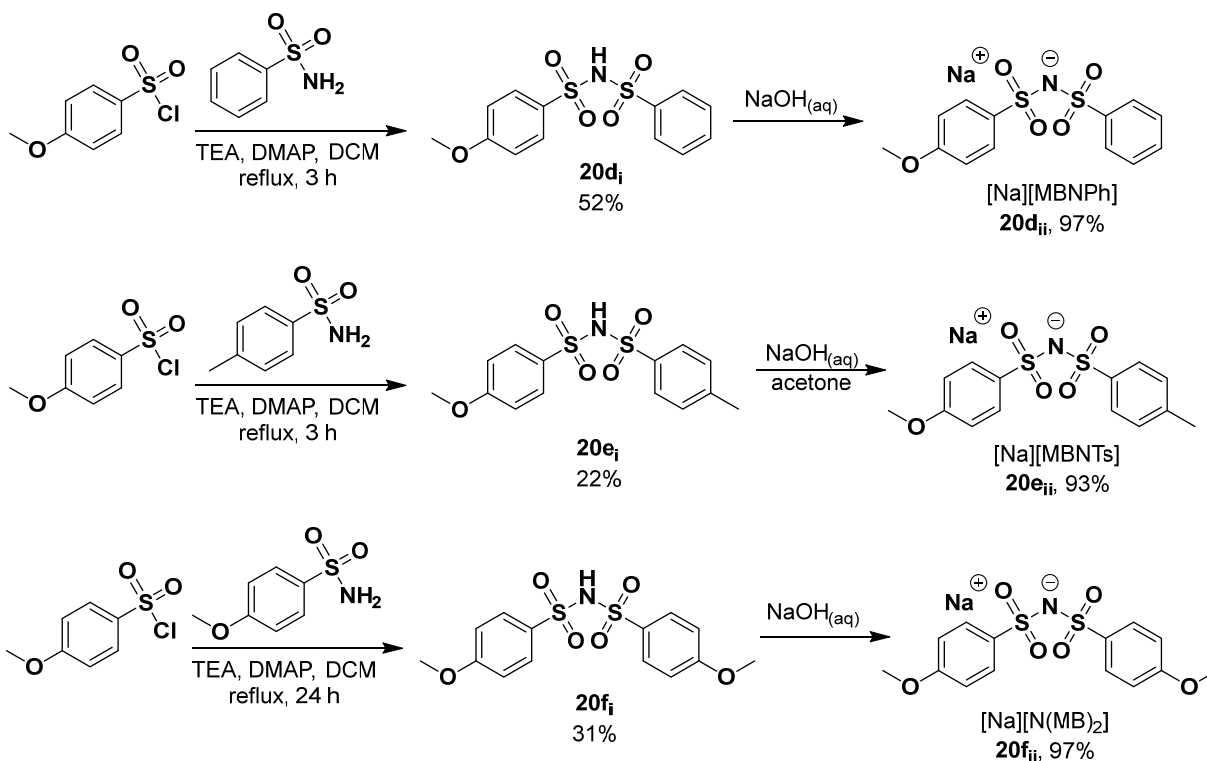
The previous synthetic scheme was attempted, where a sulfonyl chloride and sulfonamide reacted in a solution of sodium carbonate; however, this did not work for these anions. The previous reactions used acetonitrile as the organic solvent, which many of the arylsulfonamide compounds are less soluble in. Additionally, the corresponding acid is less acidic, likely due to the absence of the trifluoromethane moiety, meaning sodium carbonate was not basic enough to deprotonate the anion. Instead, a two-step scheme was employed. In the first step, the sulfonyl chloride and sulfonamide reacted in a dichloromethane (DCM) solution containing triethylamine and 4-dimethylaminopyridine, serving as the base and catalyst, respectively. The protonated anion (acid) was isolated by first washing the DCM mixture with HCl and then washing the crude product with a solution of chloroform and hexanes.

In the second step, the acid was neutralized by stirring in an aqueous sodium hydroxide solution. Small quantities of acetone were added for the compounds that were insoluble in water. Residual starting material was removed by washing the aqueous phase with ethyl acetate. To ensure that excess sodium hydroxide was not in the products, a 1.125:1 molar ratio of the acid and sodium hydroxide was used for the starting materials. The yields from the first step were low, usually below 50%, perhaps due to the bulkiness

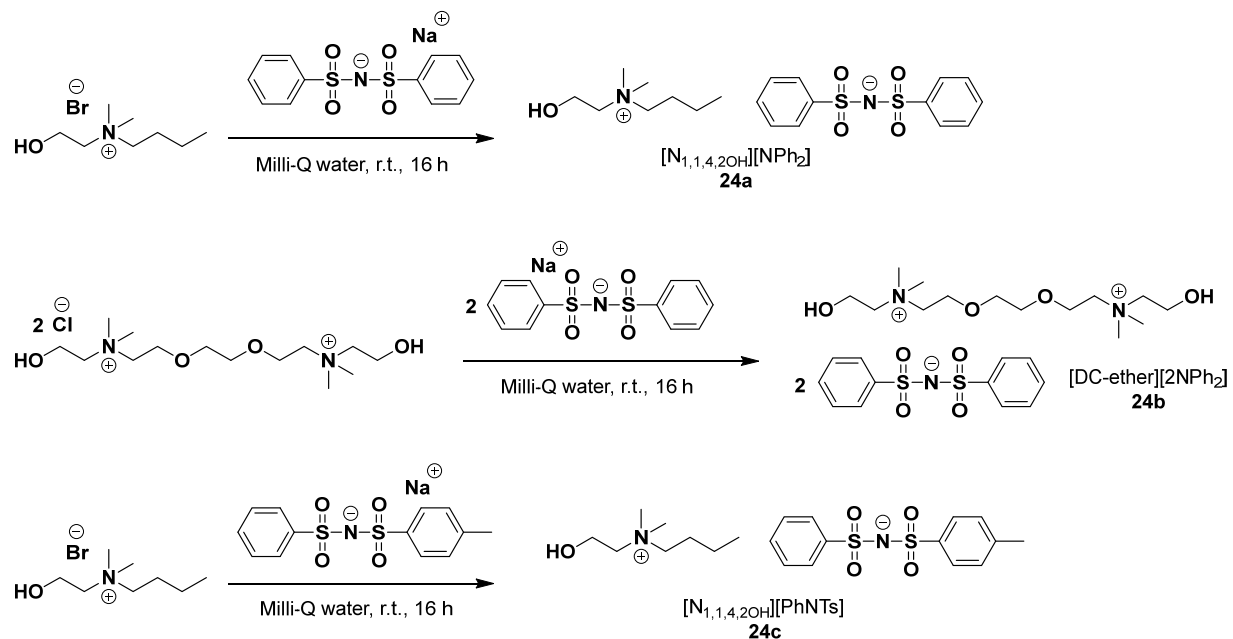
of the aryl reagents. However, the yields for the second step were typically greater than 80%, as the acid is sufficiently acidic to be deprotonated by sodium hydroxide.

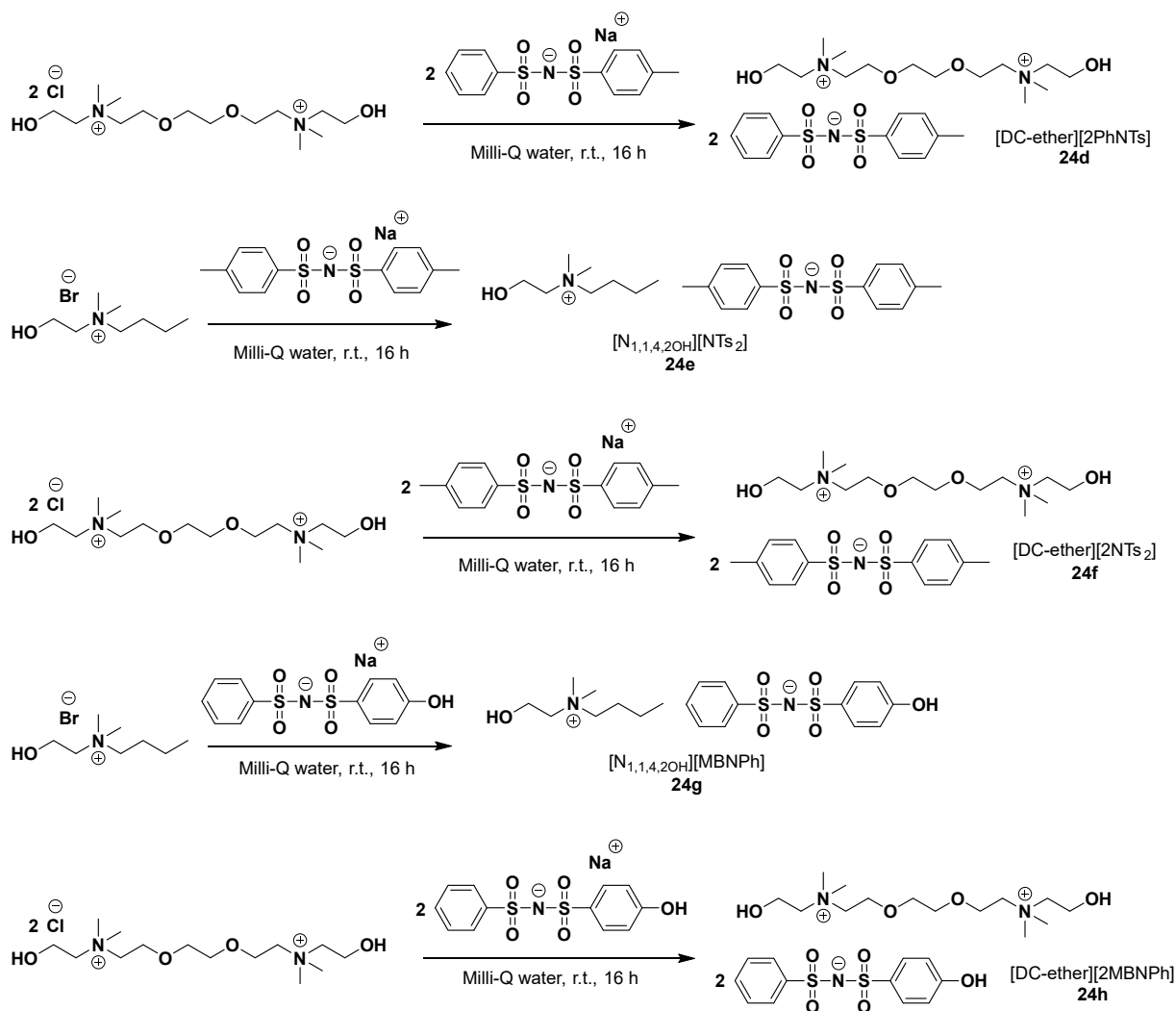
The first set of second-generation bis(arylsulfonyl)azanide anions utilized the same aryl groups as before – phenyl, 4-tosyl, and 4-methoxyphenyl, but in different combinations (**20a–20f**; **Scheme 2.13**). The anions were paired with  $[N_{1,1,4,2OH}][Br]$  (**2a**) and  $[DC\text{-ether}][2Cl]$  (**4j**) to produce ILs (**24a–24h**; **Scheme 2.14**). Unfortunately, every IL, regardless of the combination of cation and anion, is hydrophilic. It is likely that the aryl groups do not sufficiently delocalize the charge to produce HILs. Additionally, the 4-methoxyphenyl group possesses a hydrophilic methoxy group, which is electron-donating and inhibits the ability of the aromatic ring to delocalize negative charge. The anions with tosyl groups, when mixed with the cations in water, formed cloudy solutions; however, the hydrophobicity of these ILs were so low that they could not be measured and were deemed hydrophilic.





**Scheme 2.13** Synthesis of second-generation bis(sulfonyl)azanide anions that incorporate phenyl, tosyl, and 4-methoxyphenyl groups



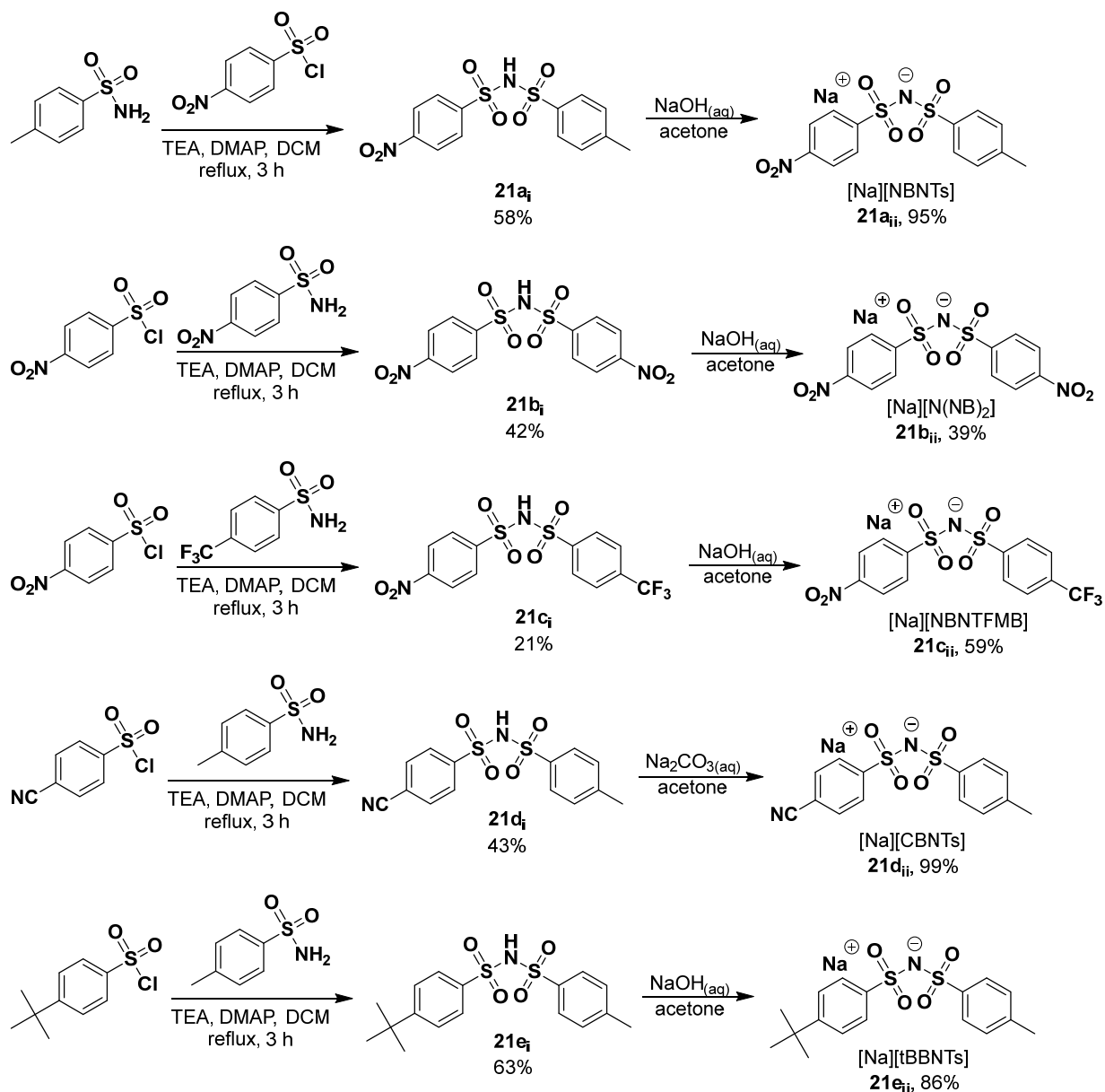


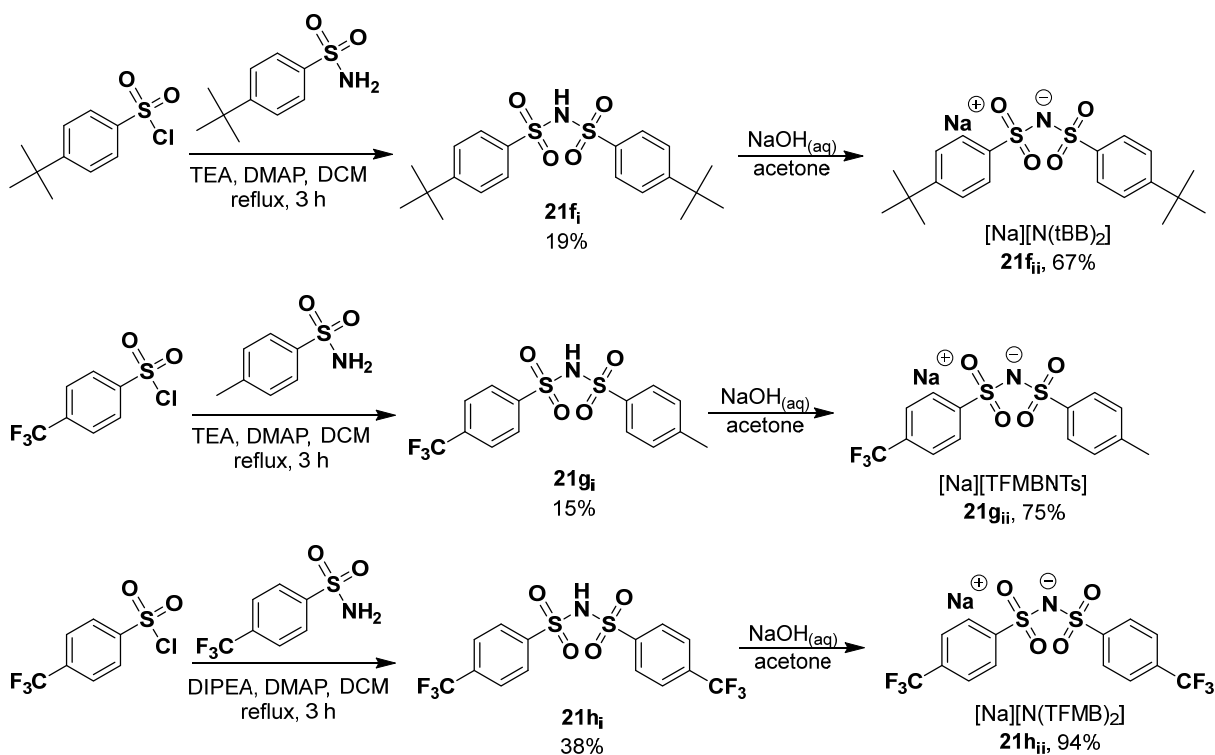
**Scheme 2.14** Synthesis of cholinium and dicholinium ILs containing second-generation bis(sulfonyl)azanide anions that incorporate phenyl, tosyl, and 4-methoxyphenyl groups

### 2.2.12 Synthesis of second-generation bis(sulfonyl)azanide anions containing electron-withdrawing groups and corresponding ILs

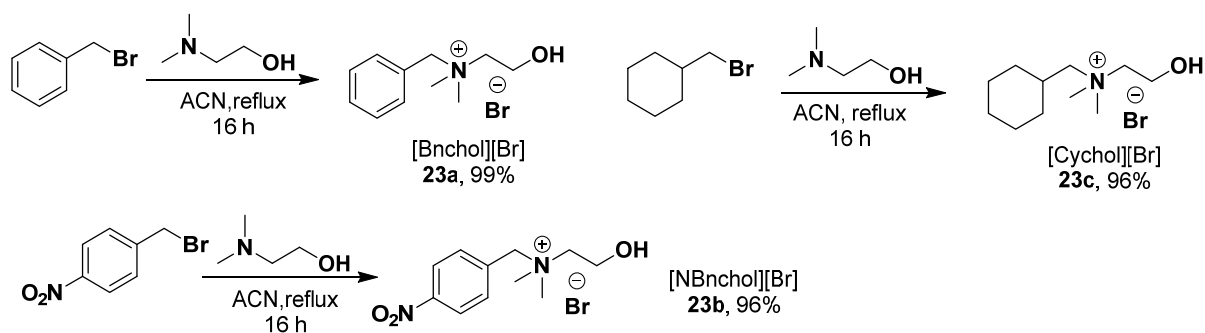
The anions previous set of second-generation bis(sulfonyl)azanide anions were too hydrophilic to produce HILs, so aryl moieties containing electron-withdrawing groups, including 4-nitrobenzene, 4-cyanobenzene, and 4-(trifluoromethyl)benzene, were employed. Additionally, 4-(tertbutyl)benzene was also used to investigate how a bulky alkane group affects hydrophobicity. These anions (**21a–21h**) were synthesized in the same manner as described in section 2.2.11 (**Scheme 2.15**). The one exception was  $[\text{Na}][\text{CBNTs}]$  (**21d<sub>ii</sub>**), which required sodium carbonate instead of sodium hydroxide for the second step,

as the latter reacted with the cyano group. Due to concerns about hydrophilicity, new monocholinium cations were also synthesized. These new cations were redesigns of the  $[N_{1,1,6,20H}][Br]$  (**2c**) cation, where instead of a linear chain, cyclic architectures were used. This included benzyl, 4-nitrobenzyl, and cyclohexyl structures. The cations (**23a–23c**) were synthesized using a similar one-step quaternization reaction described in section 2.2.1 (**Scheme 2.16**). Gratifyingly, the three cations were synthesized in high yields and high purities.





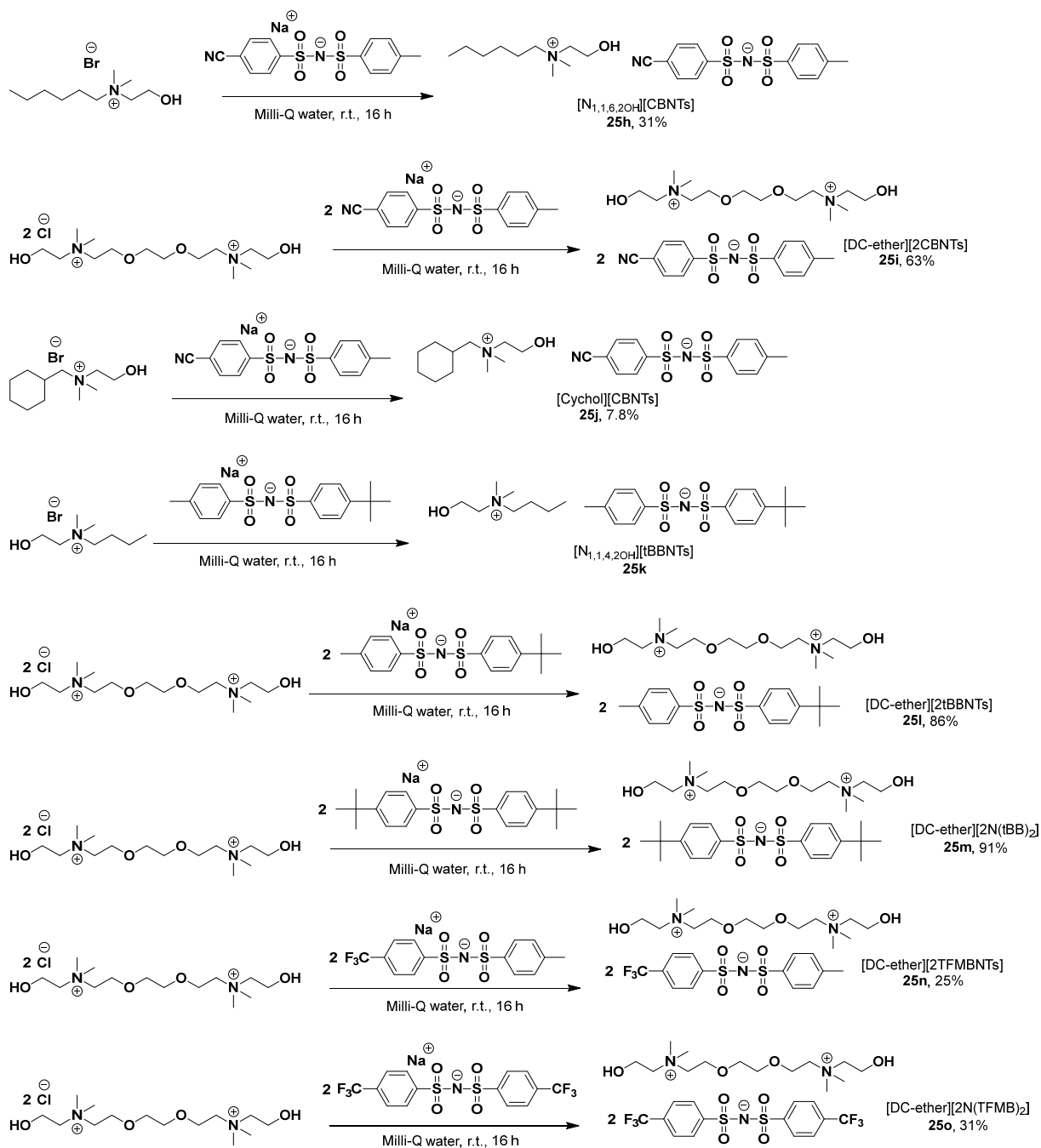
**Scheme 2.15** Synthesis of second-generation bis(sulfonyl)azanide anions containing aryl groups with electron-withdrawing moieties or tertbutyl groups



**Scheme 2.16** Synthesis of cyclic monocholinium cations

The new anions were paired with the three new cations as well as [DC-ether][2Cl] (**4j**), [N<sub>1,1,4,2OH</sub>][Br] (**2a**), and [N<sub>1,1,6,2OH</sub>][Br] (**2c**) (**Scheme 2.17**). The resulting ILs (**25a–25o**) are all hydrophobic except for [N<sub>1,1,4,2OH</sub>][tBBNTs] (**25k**), which is water soluble due to the short butyl chain on the cation. While the hydrophobicity was substantially improved, all the ILs are solid at room temperature,



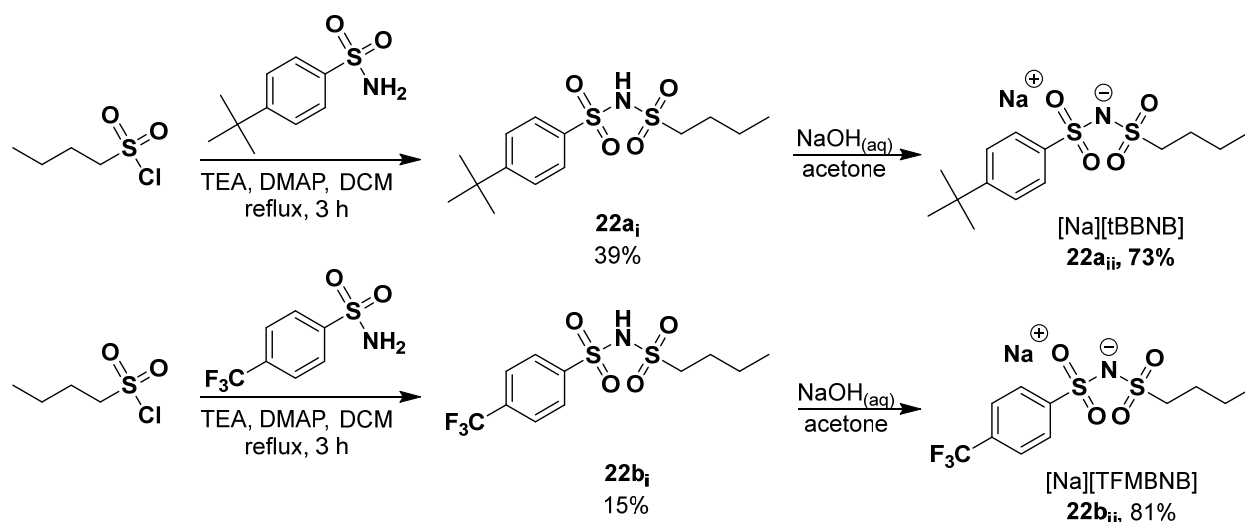


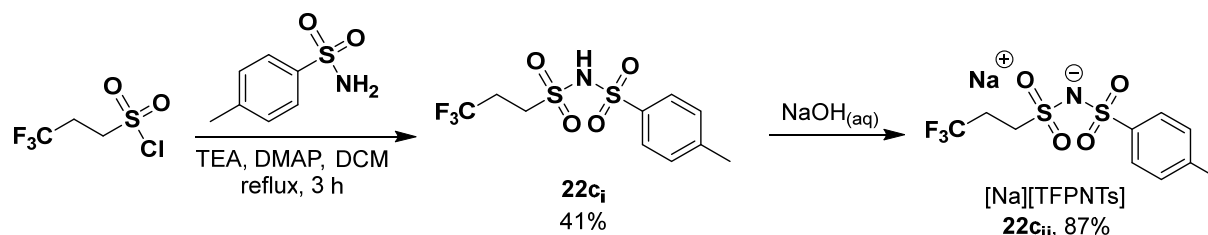
**Scheme 2.17** Synthesis of ILs with [DC-ether], [N<sub>1,1,4,2OH</sub>], [N<sub>1,1,6,2OH</sub>], and cyclic monocholinium cations paired with second-generation bis(sulfonyl)azanide anions that contain aryl groups with electron-withdrawing moieties and tertbutyl groups

### 2.2.13 Synthesis of third-generation bis(sulfonyl)azanide anions and corresponding ILs

Through the synthesis of several new bis(arylsulfonyl) anions, it was revealed that  $\pi$ -stacking interactions between anions, and possibly cations, greatly increase viscosity and melting temperature of ILs, despite potentially increasing hydrophobicity. As a result, a third generation of anions was synthesized that incorporated one aryl group and one alkyl chain. This class of anions is different from the first-generation anions, which utilized one aryl or alkyl group and a trifluoromethane moiety. These compounds were constructed to probe whether the high viscosity and melting temperature of an aryl group can be diminished by incorporating a short alkyl chain. As will be discussed in section 3.2.1, butyl alkyl chains interrupt more polar intermolecular interactions without contributing significant Van der Waals interactions themselves.

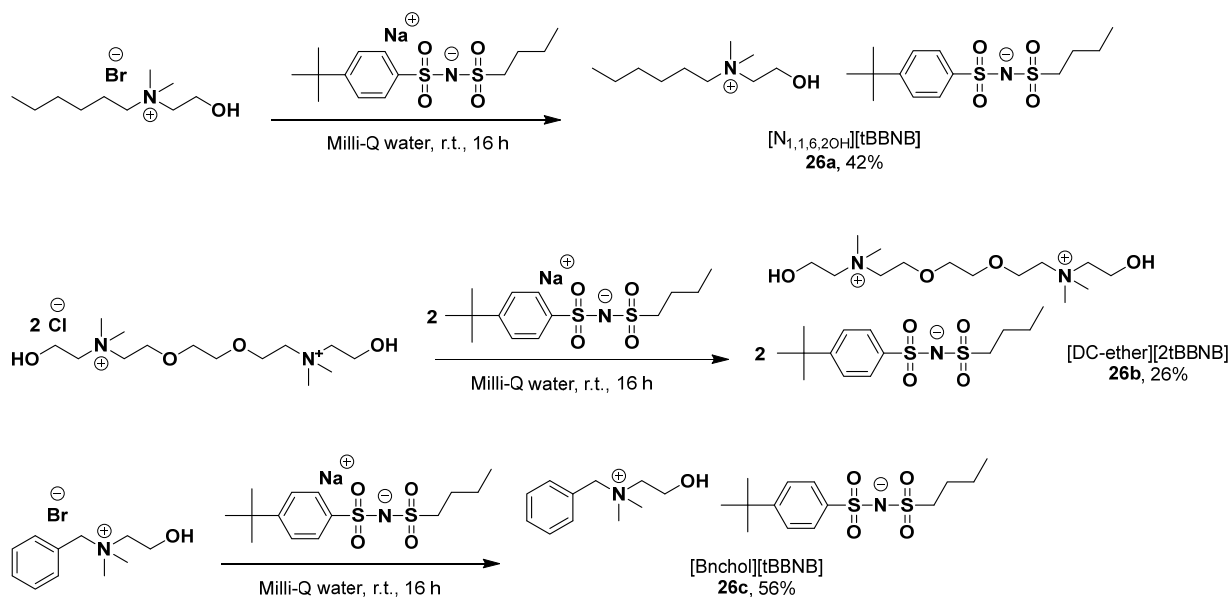
As such, two anions were constructed where a butyl chain was added to one end, while the other end incorporated a 4-(tertbutyl)benzene or 4-(trifluoromethane)benzene group. An additional anion was synthesized that utilized a tosyl group on one end and a 3,3,3-trifluoropentyl group on the other end. This latter anion was hypothesized to be more hydrophobic due to the presence of the trifluoromethane group and still offer an intermolecular-disrupting chain. The anions (**22a–22c**) were synthesized (**Scheme 2.18**) using the two-step process described in section 2.2.11.

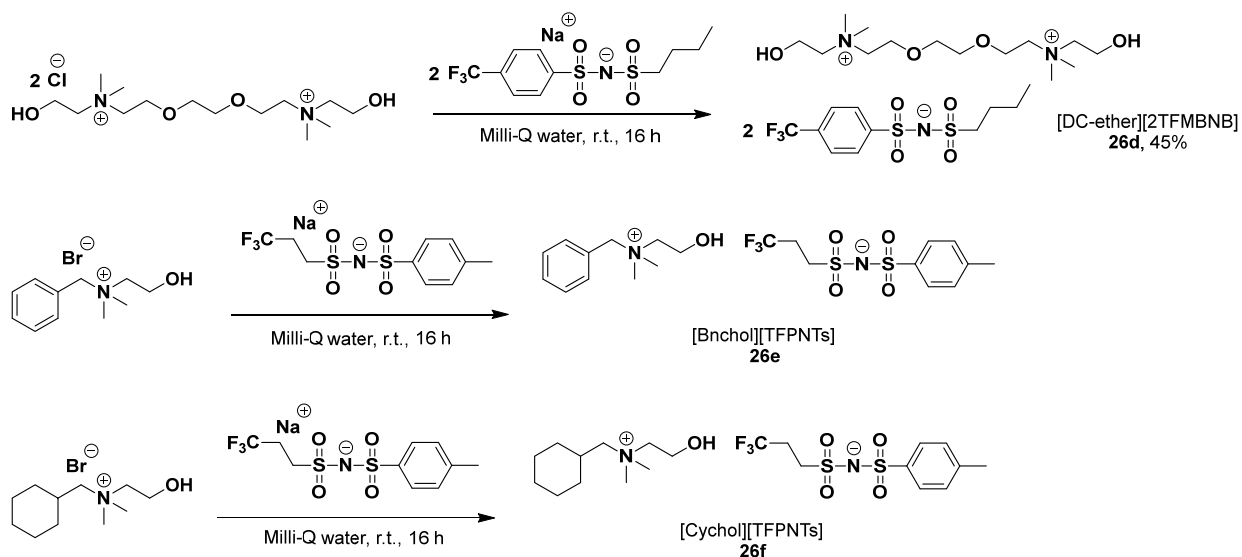




**Scheme 2.18** Synthesis of third-generation anions containing one aryl group and one alkyl group

The third-generation anions were paired with different cholinium-based cations to form ILs (**Scheme 2.19**). These ILs (**26a–26f**) were liquid at room temperature, but extremely viscous. It is likely that the butyl chain lowers the melting point, but not the viscosity. It appears that to form low viscous ILs, aromatic groups on the anion need to be avoided. Another interesting observation is that the ILs with the 3,3,3-trifluoropentyl group were water soluble, while the others were hydrophobic. It appears that the inductive effects of a trifluoromethane moiety are severely limited when extended by two methylene units. A list of these ILs and their characteristic can be found in **Table 2.7**. These results are in stark contrast to ILs such as [DC-ether][2TsNTf] (**18e**), which contain both tosyl and trifluoromethane groups and are hydrophobic.





**Scheme 2.19** Synthesis of ILs containing [DC-ether] and cyclic monocholinium cations and third-generation anions

#	Compound	Structure	Form
26a	[N <sub>1,1,6,2OH</sub> ][tBBNB]		Hydrophobic Liquid
26b	[DC-ether][2tBBNB]		Hydrophobic Liquid
26c	[Bnchol][tBBNB]		Hydrophobic Liquid
26d	[DC-ether][2TFMBNB]		Hydrophobic Liquid
26e	[Bnchol][TFPNTs]		Water Soluble
26f	[Cychol][TFPNTs]		Water Soluble

### 2.3 Conclusion

This chapter explored unique structural motifs that can be used to construct HILs. In the first section, sets of monocations and dicationic were synthesized using choline, a biologically essential nutrient, as the core structure. IL cations typically are restricted to nitrogen-containing molecules as few other atoms

are stable with a positive charge. While most HILs incorporate long chain tetraalkylammonium or imidazolium cations, the cholinium compounds, especially the dicholinium species, displayed improved toxicity (the physicochemical properties and toxicity of the HILs can be found in Chapter 3).

For IL anions, a wider structural diversity is available as negative charges can be tolerated by many atoms. Here, the cholinium-based cations were paired with fatty acid anions initially; although, this produced water soluble and solid ILs. Through these preliminary studies, it was revealed that enhancing electron delocalization is essential for forming ILs that are both hydrophobic and liquid at room temperature. Additionally, the presence of long alkyl chains, while increasing hydrophobicity, significantly increases melting temperature due to the substantial number of Van der Waals interactions. Therefore, the  $[\text{NTf}_2]$  anion became the focal point as the molecule has extreme electron delocalization through a combination of inductive effects and  $\pi$ -conjugation. When paired with  $[\text{NTf}_2]$ , most of the cholinium-based cations formed room temperature HILs.

Despite the success of the ILs containing  $[\text{NTf}_2]$ , the anion causes several morphological deformations and induces mortality at sub-millimolar concentrations (see sections 3.2.5 and 3.2.6). As a result, new anions based on the bis(sulfonyl)azanide core were developed. The first-generation anions were asymmetric – incorporating a trifluoromethane group and an alkyl, aryl, or alkyl-aryl moiety. When paired with monocholinium and dicholinium cations, the corresponding ILs had low melting temperatures, but also had high viscosities and a broad range of hydrophobicities and LC50 values (see Chapter 3).

To further probe the effects of modulating the bis(sulfonyl)azanide core, a library of second-generation anions was synthesized that featured two identical or different aryl groups. The first set of bis(arylsulfonyl)azanide anions used aryl groups with electron-donating functionalities, whereas the second set utilized electron-withdrawing moieties. The latter set of anions were significantly more hydrophobic, likely due to enhanced electron delocalization. Unfortunately, when paired with the cholinium-based cations, the resulting ILs were almost exclusively solid at room temperature. A third generation of bis(sulfonyl)azanide anions are currently being developed. The initial anions contain an aromatic group and a small alkyl or alkyl-like chain on either end of the azanide core. The lack of a second aryl group

substantially reduced the melting temperature; however, the small alkyl chains provided minimal hydrophobicity, resulting in ILs with high water solubility values.

The cumulative results from the anion syntheses reveal that aromatic groups, despite their potential to increase hydrophobicity, may not be ideal as they dramatically increase the melting temperature as well as the viscosity of the corresponding ILs. However, the bis(sulfonyl)azanide structure represents a promising scaffold to produce anions that have sufficient electron delocalization. Additionally, the cholinium-based cations offer an approach that can lower the toxicity of the resulting ILs. There are several directions that can be explored to develop new HILs with more preferred properties. This could include developing novel azanide structures, such as modulating the artificial sugar anions to become more hydrophobic, including inductively electron withdrawing moieties other than trifluoromethane, and adding lipophilicity without increasing toxicity and melting temperature. Furthermore, new cholinium cations should be investigated to further probe the relationship between IL structure and properties. Overall, this chapter describes an approach for rationally designing new HILs that can be used as a starting place for others interested in constructing novel HILs.

## **2.4 Experimental**

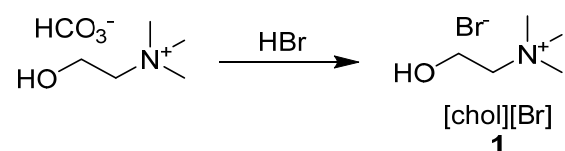
### *2.4.1 Materials and nuclear magnetic resonance methods*

4-n-butylbenzenesulfonyl chloride, 1,8-dibromooctane, sodium ethoxide, and 1-bromohexane were purchased from Alfa Aesar (Ward Hill, MA). Lithium bis(trifluoromethanesulfonyl)imide, trifluoromethanesulfonamide, 1,3-dibromopropane, 1,5-dibromopentane, acesulfame K, and 2-mesitylenesulfonyl chloride were purchased from TCI (Portland, OR). 4-nitrobenzenesulfonyl chloride and 4-dimethylaminopyridine were purchased from Chem-Impex International (Bensenville, IL). 4-nitrobenzenesulfonamide was purchased from Ambeed (Arlington Heights, IL). 1,2-bis(2-chloroethoxy)ethane was purchased from Frontier Scientific (Logan, UT). Sodium hydroxide was purchased from DOT Scientific (Burton, Michigan). Sodium carbonate, 1-butanesulfonyl chloride, sodium and 4-n-octylbenzenesulfonate, were purchased from Thermo Fisher Scientific (Waltham, MA). Silver

nitrate and benzyl bromide was purchased from BeanTown Chemical (Hudson, NH). Bromoethane, benzenesulfonamide ethanesulfonyl chloride and diethyl malonate were purchased from Acros Organics (Fair Lawn, NJ). 4-tert-butylbenzenesulfonyl chloride, 4-methoxybenzenesulfonamide, 4-(trifluoromethyl)benzenesulfonyl chloride, and 4-(trifluoromethyl)benzenesulfonamide were purchased from Matrix Scientific (Columbia, SC). Solvents and all other reagents were purchased from Sigma-Aldrich (Milwaukee, WI).

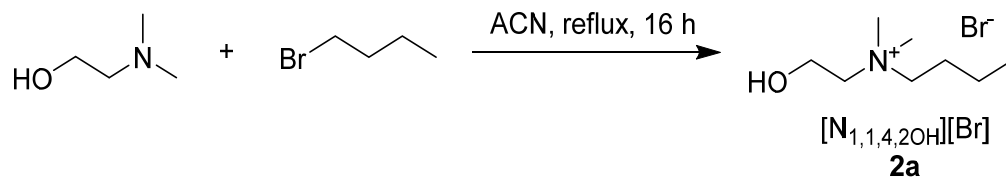
$^1\text{H}$  NMR,  $^{13}\text{C}$  NMR,  $^{19}\text{F}$  NMR, and HSQC spectra were obtained using a Bruker Avance III HD 400 MHz spectrometer (Billerica, MA) and a Varian UI 500 MHz spectrometer (Palo Alto, CA). Compounds were prepared in deuterium oxide, chloroform-d, methanol-d<sub>4</sub>, acetone-d<sub>6</sub>, or DMSO-d<sub>6</sub>.

#### 2.4.2 Synthesis of cholinium and alkyl-cholinium cations

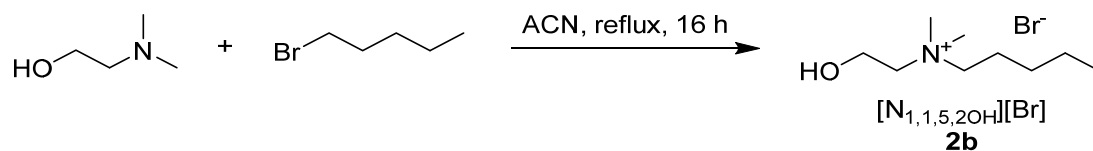


**2-hydroxy-N,N,N-trimethylethan-1-aminium bromide (1):** A 50 mL round bottom flask was attached to a bubbler and placed on ice. To the flask was added hydrobromic acid (48% in water; 2.67 mL, 23.8 mmol, 1.0 equiv.). Then, choline bicarbonate (80% in water; 4.20 mL, 23.8 mmol, 1.0 equiv.) was added to the flask dropwise with stirring. The reaction was stopped after bubbling ceased. Water was removed via lyophilization to produce the product (**1**) as a white solid in 99% yield.  $^1\text{H}$  NMR (400 MHz, Deuterium Oxide)  $\delta$  4.03 – 3.96 (m, 2H), 3.49 – 3.42 (m, 2H), 3.14 (s, 9H);  $^{13}\text{C}\{^1\text{H}\}$  NMR (101 MHz, Deuterium Oxide)  $\delta$  67.63, 67.22 (m), 55.61, 54.00 – 53.74 (m).

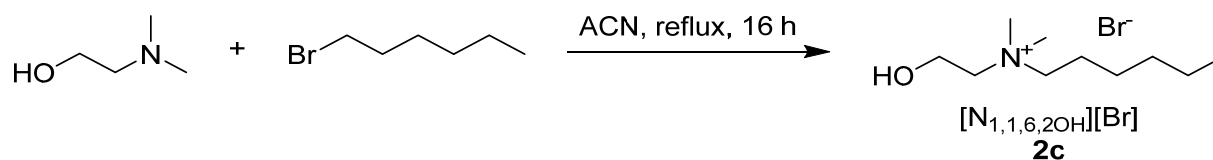
**General Procedure “A”: Alkyl Cholinium Bromide ( $[\text{N}_{1,1,x,2\text{OH}}][\text{Br}]$ ) Synthesis:** To a 100 mL round bottom was added dimethylaminoethanol, the corresponding bromoalkane, and anhydrous acetonitrile (25 mL). The reaction stirred at 80 °C for 16 h. The acetonitrile was removed *in vacuo* and the crude product was redissolved in diethyl ether, which caused a solid to precipitate out. The solid was filtered, washed with diethyl ether (3x5 mL), collected, and excess solvent was removed *in vacuo*.



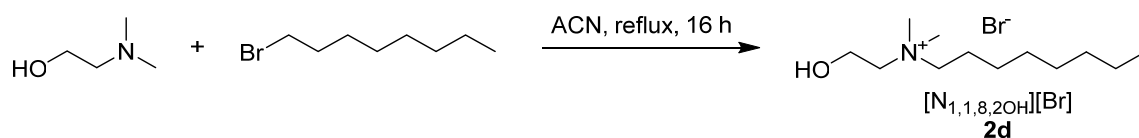
**N-(2-hydroxyethyl)-N,N-dimethylbutan-1-aminium bromide (2a):** The general procedure “A” was applied to dimethylaminoethanol (2.82 mL, 28.0 mmol, 1.0 equiv.) and 1-bromobutane (3.00 mL, 28.0 mmol, 1.0 equiv.). The product (**2a**) was isolated as a white solid in 85.5% yield. <sup>1</sup>H NMR (400 MHz, Deuterium Oxide) δ 4.02 (tt, *J* = 5.0, 2.4 Hz, 4H), 3.52 – 3.44 (m, 4H), 3.41 – 3.33 (m, 4H), 3.12 (s, 12H), 1.82 – 1.68 (m, 4H), 1.36 (h, *J* = 7.4 Hz, 4H), 0.93 (t, *J* = 7.4 Hz, 6H); <sup>13</sup>C {<sup>1</sup>H} NMR (101 MHz, Deuterium Oxide) δ 65.54 – 65.26 (m), 65.01 – 64.80 (m), 55.47, 51.67 – 51.35 (m), 24.05, 19.18, 13.02; HSQC (Deuterium Oxide) δ {0.92, 12.93}, {1.35, 19.05}, {1.73, 24.05}, {3.10, 51.46}, {4.01, 55.33}, {3.46, 64.84}, {3.34, 65.33}.



**N-(2-hydroxyethyl)-N,N-dimethylpentan-1-aminium bromide (2b):** The general procedure “A” was applied to dimethylaminoethanol (2.25 mL, 22.4 mmol, 1.0 equiv.) and 1-bromopentane (3.34 mL, 26.9 mmol, 1.2 equiv.). The product (**2b**) was isolated as a white solid in 74.0% yield. <sup>1</sup>H NMR (400 MHz, Deuterium Oxide) δ 3.98 (tt, *J* = 5.1, 2.5 Hz, 2H), 3.46 – 3.39 (m, 2H), 3.35 – 3.27 (m, 2H), 3.07 (s, 6H), 1.73 (dq, *J* = 14.2, 7.2 Hz, 2H), 1.30 (pd, *J* = 8.1, 7.5, 4.0 Hz, 4H), 0.84 (t, *J* = 6.9 Hz, 3H); <sup>13</sup>C NMR (101 MHz, Deuterium Oxide) δ 65.51 (t, *J* = 2.5 Hz), 64.82 (t, *J* = 2.9 Hz), 55.38, 51.54 – 51.25 (m), 27.64, 13.08.



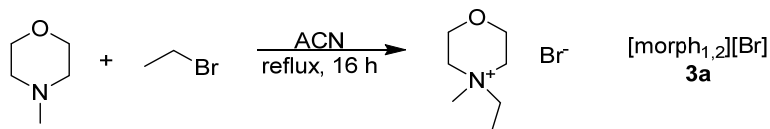
***N*-(2-hydroxyethyl)-*N,N*-dimethylhexan-1-aminium bromide (2c):** The general procedure “A” was applied to dimethylaminoethanol (2.82 mL, 28.0 mmol, 1.0 equiv.) and 1-bromohexane (3.93 mL, 28.0 mmol, 1.0 equiv.). The product (2c) was isolated as a white solid in 74.0% yield.  $^1\text{H}$  NMR (400 MHz, Deuterium Oxide)  $\delta$  3.98 (dq,  $J = 7.5, 2.2$  Hz, 2H), 3.46 – 3.40 (m, 2H), 3.35 – 3.27 (m, H), 3.07 (s, 6H), 1.80 – 1.66 (m, 2H), 1.36 – 1.22 (m, 6H), 0.86 – 0.78 (m, 3H);  $^{13}\text{C}\{^1\text{H}\}$  NMR (101 MHz, Deuterium Oxide)  $\delta$  65.51 (d,  $J = 3.0$  Hz), 64.81 (t,  $J = 2.9$  Hz), 55.37, 51.35 (t,  $J = 3.8$  Hz), 30.40, 25.12, 21.86, 21.70, 13.22. HSQC (Deuterium Oxide)  $\delta$  {0.81, 13.25}, {1.27, 21.63}, {1.71, 21.79}, {1.29, 25.02}, {1.28, 30.34}, {3.06, 51.30}, {3.97, 55.33}, {3.42, 64.84}, {3.31, 65.39}.



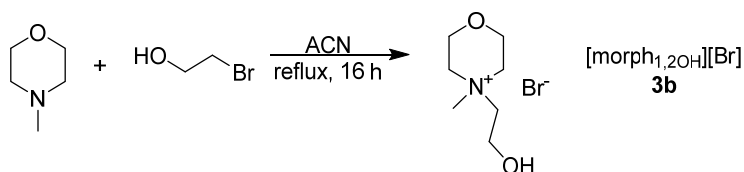
***N*-(2-hydroxyethyl)-*N,N*-dimethyloctan-1-aminium bromide (2d):** The general procedure “A” was applied to dimethylaminoethanol (2.82 mL, 28.0 mmol, 1.0 equiv.) and 1-bromooctane (4.84 mL, 28.0 mmol, 1.0 equiv.). The product (2d) was isolated as a white solid in 94.5% yield.  $^1\text{H}$  NMR (400 MHz, Deuterium Oxide)  $\delta$  4.03 – 3.96 (m, 2H), 3.48 – 3.41 (m, 2H), 3.38 – 3.29 (m, 2H), 3.09 (s, 6H), 1.80 – 1.68 (m, 2H), 1.31 (q,  $J = 3.2, 2.6$  Hz, 4H), 1.31 – 1.19 (m, 6H), 0.87 – 0.79 (m, 3H);  $^{13}\text{C}\{^1\text{H}\}$  NMR (101 MHz, Deuterium Oxide)  $\delta$  68.05, 67.42, 57.96, 53.99 (t,  $J = 3.5$  Hz), 33.66, 30.86, 30.82, 28.13, 24.67, 24.56, 16.12; HSQC (Deuterium Oxide)  $\delta$  {0.80, 13.41}, {1.70, 21.79}, {1.16, 21.84}, {1.28, 25.34}, {1.28, 28.08}, {1.21, 30.98}, {3.05, 51.30}, {3.96, 55.33}, {3.41, 64.84}, {3.29, 65.49}.

#### 2.4.3 Synthesis of alkyl morpholinium cations

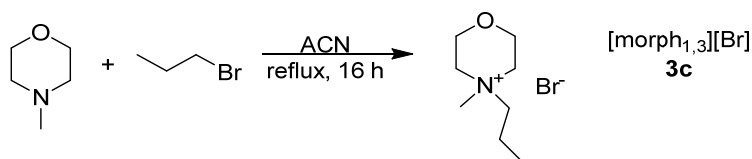
**General Procedure “B”: Methylmorpholinium Bromide ([morph]<sub>1,x</sub>)[Br] Synthesis:** To 250 mL round bottom flask equipped with a reflux condenser was added *N*-methylmorpholine, the corresponding bromoalkane, and anhydrous acetonitrile. The reaction stirred at 80 °C for 16 h, in which a white solid precipitated. The solid was filtered off, washed with acetone (3x30 mL), and collected. Residual solvent was removed *in vacuo*.



**4-ethyl-4-methylmorpholin-4-ium bromide (3a):** The general procedure “B” was applied to *N*-methylmorpholine (10.0 mL, 91.0 mmol, 1.0 equiv.), bromoethane (6.75 mL, 91.0 mmol, 1.0 equiv.), and anhydrous acetonitrile (50 mL). The product (**3a**) was isolated as a white solid in 88.0% yield. <sup>1</sup>H NMR (400 MHz, Deuterium Oxide) δ 3.99 (dp, *J* = 6.2, 1.9 Hz, 4H), 3.54 – 3.34 (m, 6H), 3.10 (d, *J* = 2.0 Hz, 3H), 1.32 (tt, *J* = 7.4, 2.0 Hz, 2.0 Hz, 3H); <sup>13</sup>C{<sup>1</sup>H} NMR (101 MHz, Deuterium Oxide) δ 60.82, 60.40, 59.09, 59.06, 59.03, 46.04, 6.53.



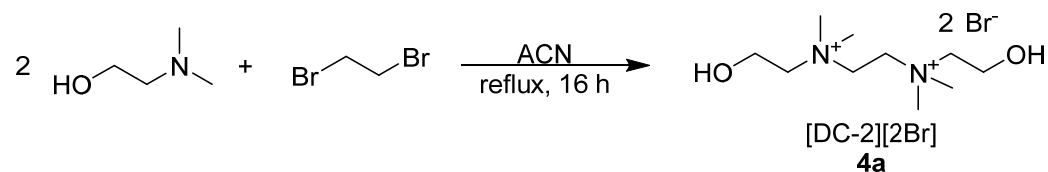
**4-(2-hydroxyethyl)-4-methylmorpholin-4-ium bromide (3b):** The general procedure “B” was applied to *N*-methylmorpholine (1.18 mL, 16.0 mmol, 1.0 equiv.), 2-bromoethanol (1.13 mL, 16.0 mmol, 1.0 equiv.), and anhydrous acetonitrile (25 mL). The product (**3b**) was isolated as a white solid in 33.7% yield. <sup>1</sup>H NMR (400 MHz, Deuterium Oxide) δ 4.03 (dtd, *J* = 14.0, 4.7, 2.4 Hz, 6H), 3.67 – 3.54 (m, 4H), 3.48 (dt, *J* = 12.5, 4.0 Hz, 2H), 3.44 (s, 2H), 3.24 (s, 3H); <sup>13</sup>C{<sup>1</sup>H} NMR (101 MHz, Deuterium Oxide) δ 65.66, 60.54, 60.51, 60.48, 60.40, 54.89, 48.07.



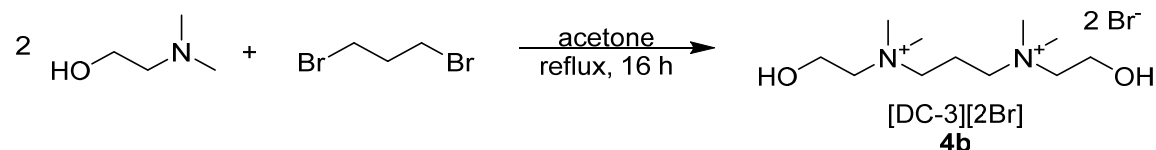
**4-methyl-4-propylmorpholin-4-ium bromide (3c):** The general procedure “B” was applied to *N*-methylmorpholine (9.2 mL, 98.9 mmol, 1.0 equiv.), 3-bromopentane (11.2 mL, 122 mmol, 1.2 equiv.), and anhydrous acetonitrile (50 mL). The product (**3c**) was isolated as a white solid in 67.9% yield.

#### 2.4.4 Synthesis of dicholinium cations

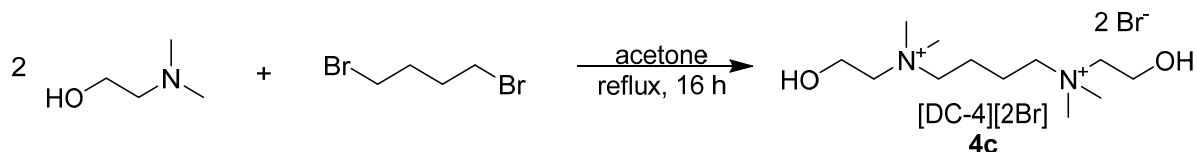
**General Procedure “C”: Dicholinium Bromide ([DC-X][2Br]) Synthesis:** To a 100 mL round bottom flask equipped with a reflux condenser was added 2-dimethylaminoethanol, the corresponding terminal dibromoalkane, and anhydrous acetone or anhydrous acetonitrile. The reaction stirred at 70 °C for 16 h, in which a white solid precipitated. The solid was filtered off, washed with acetone (3x30 mL), and collected. Residual solvent was removed *in vacuo*.



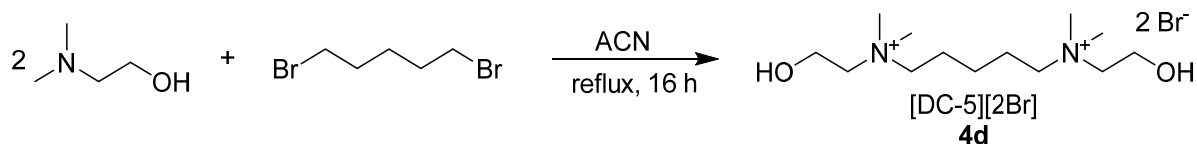
***N*<sup>1</sup>,*N*<sup>2</sup>-bis(2-hydroxyethyl)-*N*<sup>1</sup>,*N*<sup>1</sup>,*N*<sup>2</sup>,*N*<sup>2</sup>-tetramethylethane-1,2-diaminium bromide (4a):** The general procedure “C” was applied to dimethylaminoethanol (2.26 mL, 22.4 mmol, 2.0 equiv.), 1,2-dibromoethane (0.967 mL, 11.2 mmol, 1.0 equiv.), and anhydrous acetonitrile (35 mL). The product (4a) was isolated as a white solid in 27.9% yield. <sup>1</sup>H NMR (400 MHz, Deuterium Oxide) δ 4.00 (dq, *J* = 5.3, 2.6 Hz, 4H), 3.90 – 3.68 (m, 8H), 3.54 – 3.47 (m, 4H), 3.15 (s, 12H); <sup>13</sup>C NMR (101 MHz, Deuterium Oxide) δ 65.21 (dt, *J* = 80.1, 2.7 Hz), 55.29, 51.70 – 51.50 (m), 20.75.



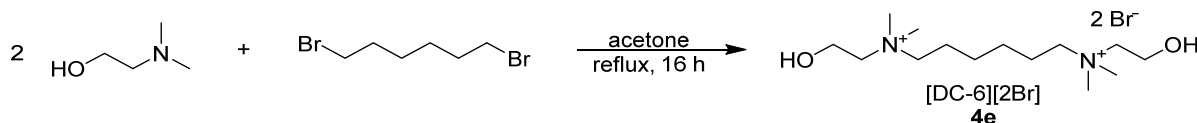
***N*<sup>1</sup>,*N*<sup>3</sup>-bis(2-hydroxyethyl)-*N*<sup>1</sup>,*N*<sup>1</sup>,*N*<sup>3</sup>,*N*<sup>3</sup>-tetramethylpropane-1,3-diaminium bromide (4b):** The general procedure “C” was applied to dimethylaminoethanol (3.12 mL, 31.0 mmol, 2.0 equiv.), 1,3-dibromopropane (1.58 mL, 15.5 mmol, 1.0 equiv.), and anhydrous acetonitrile (50 mL). The product (4b) was isolated as a white solid in 79.4% yield. <sup>1</sup>H NMR (400 MHz, Deuterium Oxide) δ 4.02 (dq, *J* = 4.9, 2.5 Hz, 4H), 3.57 – 3.50 (m, 4H), 3.48 – 3.39 (m, 4H), 3.17 (s, 12H), 2.40 – 2.28 (m, 2H); <sup>13</sup>C NMR (101 MHz, Deuterium Oxide) δ 65.48 (t, *J* = 2.7 Hz), 61.13, 55.35, 52.01 – 51.71 (m), 17.03.



***N*<sup>1</sup>,*N*<sup>4</sup>-bis(2-hydroxyethyl)-*N*<sup>1</sup>,*N*<sup>1</sup>,*N*<sup>4</sup>,*N*<sup>4</sup>-tetramethylbutane-1,4-diaminium bromide (4c):** The general procedure “C” was applied to dimethylaminoethanol (5.44 mL, 54.4 mmol, 2.0 equiv.), 1,4-dibromobutane (3.24 mL, 27.2 mmol, 1.0 equiv.), and anhydrous acetone (50 mL). The product (**4c**) was isolated as a white solid in 94.4% yield. <sup>1</sup>H NMR (400 MHz, Deuterium Oxide) δ 4.05 – 3.97 (m, 4H), 3.52 – 3.46 (m, 4H), 3.44 (dd, *J* = 9.9, 5.6 Hz, 4H), 3.12 (s, 12H), 1.85 (dt, *J* = 8.3, 3.6 Hz, 4H); <sup>13</sup>C{<sup>1</sup>H} NMR (101 MHz, Deuterium Oxide) δ 65.26 – 65.03 (m), 64.29 – 64.10 (m), 55.41, 51.73 – 51.38 (m), 19.43 – 19.20 (m); HSQC (Deuterium Oxide) δ {1.87, 19.32}, {3.14, 51.56}, {4.03, 55.41}, {3.50, 64.84}, {3.50, 65.16}.

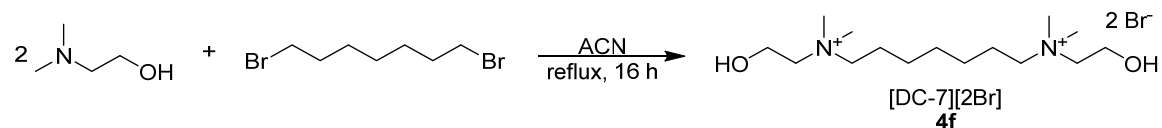


***N*<sup>1</sup>,*N*<sup>5</sup>-bis(2-hydroxyethyl)-*N*<sup>1</sup>,*N*<sup>1</sup>,*N*<sup>5</sup>,*N*<sup>5</sup>-tetramethylpentane-1,5-diaminium bromide (4d):** The general procedure “C” was applied to dimethylaminoethanol (9.02 mL, 87.0 mmol, 2.0 equiv.), 1,5-dibromopentane (5.92 mL, 43.5 mmol, 1.0 equiv.), and anhydrous acetonitrile (75 mL). The product (**4d**) was isolated as a white solid in 92.4% yield. <sup>1</sup>H NMR (400 MHz, Deuterium Oxide) δ 4.04 (dq, *J* = 7.6, 2.5 Hz, 4H), 3.54 – 3.47 (m, 4H), 3.46 – 3.37 (m, 4H), 3.15 (s, 12H), 1.88 (dq, *J* = 12.0, 8.0 Hz, 4H), 1.44 (p, *J* = 7.6 Hz, 2H). <sup>13</sup>C{<sup>1</sup>H} NMR (101 MHz, Deuterium Oxide) δ 65.10, 65.07, 65.04, 64.97, 64.94, 64.92, 55.49, 51.64, 51.60, 51.56, 22.54, 21.81.

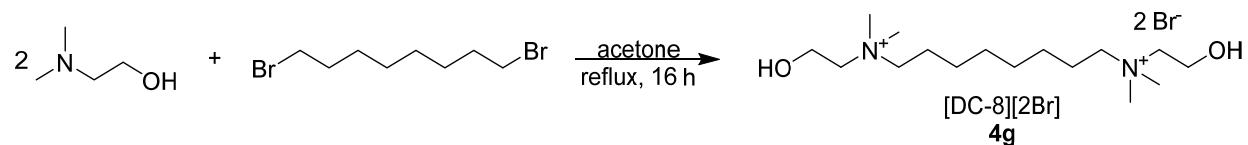


***N*<sup>1</sup>,*N*<sup>6</sup>-bis(2-hydroxyethyl)-*N*<sup>1</sup>,*N*<sup>1</sup>,*N*<sup>6</sup>,*N*<sup>6</sup>-tetramethylhexane-1,6-diaminium bromide (4e):** The general procedure “C” was applied to dimethylaminoethanol (5.44 mL, 54.4 mmol, 2.0 equiv.), 1,6-dibromohexane

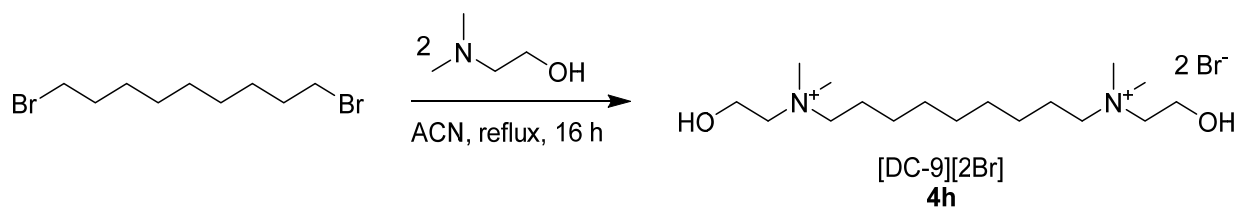
(4.18 mL, 27.2 mmol, 1.0 equiv.), and anhydrous acetone (50 mL). The product (**4e**) was isolated as a white solid in 88.6% yield.  $^1\text{H}$  NMR (400 MHz, Deuterium Oxide)  $\delta$  3.99 (dq,  $J = 5.0, 2.5$  Hz, 4H), 3.47 – 3.40 (m, 4H), 3.37 – 3.29 (m, 4H), 3.08 (s, 12H), 1.76 (qd,  $J = 7.9, 5.4, 4.1$  Hz, 4H), 1.42 – 1.34 (m, 4H);  $^{13}\text{C}$   $\{^1\text{H}\}$  NMR (101 MHz, Deuterium Oxide)  $\delta$  65.16, 64.90 (t,  $J = 2.9$  Hz), 55.38, 51.39 (t,  $J = 3.8$  Hz), 25.07, 21.87; HSQC (Deuterium Oxide)  $\delta$  {1.79, 21.95}, {1.41, 25.02}, {3.11, 51.46}, {4.01, 55.49}, {3.47, 64.99}, {3.37, 65.17}.



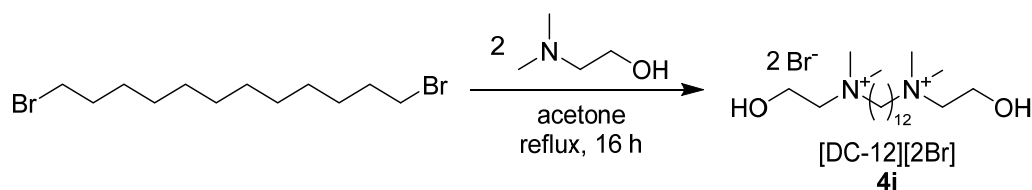
***N*<sup>1</sup>,*N*<sup>7</sup>-bis(2-hydroxyethyl)-*N*<sup>1</sup>,*N*<sup>1</sup>,*N*<sup>7</sup>,*N*<sup>7</sup>-tetramethylheptane-1,7-diaminium bromide (**4f**):** The general procedure “C” was applied to dimethylaminoethanol (4.67 mL, 46.7 mmol, 2.0 equiv.), 1,7-dibromoheptane (3.99 mL, 23.3 mmol, 1.0 equiv.), and anhydrous acetone (50 mL). The product (**4f**) was isolated as a white solid in 77.1% yield.  $^1\text{H}$  NMR (400 MHz, Deuterium Oxide)  $\delta$  3.97 (dq,  $J = 7.3, 2.2$  Hz, 4H), 3.46 – 3.38 (m, 4H), 3.35 – 3.26 (m, 4H), 3.06 (s, 12H), 1.73 (dd,  $J = 10.4, 6.0$  Hz, 4H), 1.42 – 1.26 (m, 6H);  $^{13}\text{C}$  NMR (101 MHz, Deuterium Oxide)  $\delta$  65.32, 64.84, 55.35, 51.38, 51.34, 27.67, 25.23, 21.83.



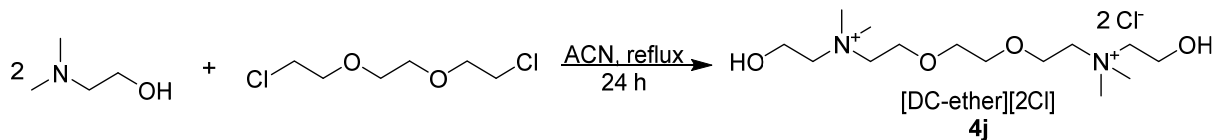
***N*<sup>1</sup>,*N*<sup>8</sup>-bis(2-hydroxyethyl)-*N*<sup>1</sup>,*N*<sup>1</sup>,*N*<sup>8</sup>,*N*<sup>8</sup>-tetramethyloctane-1,8-diaminium bromide (**4g**):** The general procedure “C” was applied to dimethylaminoethanol (5.44 mL, 54.4 mmol, 2.0 equiv.), 1,8-dibromooctane (5.00 mL, 27.2 mmol, 1.0 equiv.), and anhydrous acetone (50 mL). The product (**4g**) was isolated as a white solid in 88.6% yield.  $^1\text{H}$  NMR (400 MHz, Deuterium Oxide)  $\delta$  3.98 (dq,  $J = 5.0, 2.5$  Hz, 4H), 3.46 – 3.39 (m, 4H), 3.35 – 3.26 (m, 4H), 3.07 (s, 12H), 1.71 (p,  $J = 5.5$  Hz, 4H), 1.34 – 1.26 (m, 8H);  $^{13}\text{C}$   $\{^1\text{H}\}$  NMR (101 MHz, Deuterium Oxide)  $\delta$  65.43, 64.83, 55.36, 51.35, 27.89, 25.31, 21.89; HSQC (Deuterium Oxide)  $\delta$  {1.77, 21.94}, {1.36, 25.34}, {1.36, 27.85}, {3.12, 51.44}, {4.02, 55.40}, {3.47, 64.85}, {3.36, 65.46}.



***N*<sup>1</sup>,*N*<sup>9</sup>-bis(2-hydroxyethyl)-*N*<sup>1</sup>,*N*<sup>1</sup>,*N*<sup>9</sup>,*N*<sup>9</sup>-tetramethylnonane-1,9-diaminium bromide (4h):** The general procedure “C” was applied to dimethylaminoethanol (8.97 mL, 86.6 mmol, 2.0 equiv.), 1,9-dibromononane (8.80 mL, 43.3 mmol, 1.0 equiv.), and anhydrous acetonitrile (50 mL). The product (**4h**) was isolated as a white solid in 64.9% yield. <sup>1</sup>H NMR (400 MHz, Deuterium Oxide) δ 4.01 – 3.94 (m, 4H), 3.46 – 3.39 (m, 4H), 3.35 – 3.26 (m, 4H), 3.07 (s, 12H), 1.72 (tt, *J* = 10.8, 6.3 Hz, 4H), 1.30 (s, 10H); <sup>13</sup>C NMR (101 MHz, Deuterium Oxide) δ 65.48, 64.82, 55.37, 51.40, 51.36, 51.32, 28.13, 27.99, 25.40, 21.91.

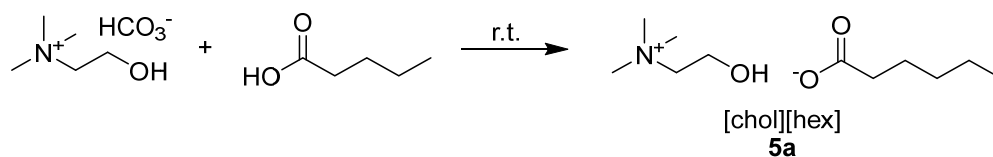


***N*<sup>1</sup>,*N*<sup>12</sup>-bis(2-hydroxyethyl)-*N*<sup>1</sup>,*N*<sup>1</sup>,*N*<sup>12</sup>,*N*<sup>12</sup>-tetramethyldodecane-1,12-diaminium bromide (4i):** The general procedure “C” was applied to dimethylaminoethanol (3.62 mL, 29.2 mmol, 2.0 equiv.), 1,12-dibromododecane (4.81 g, 14.6 mmol, 1.0 equiv.), and anhydrous acetone (50 mL). The product (**4i**) was isolated as a white solid in 91.6% yield. <sup>1</sup>H NMR (400 MHz, Deuterium Oxide) δ 4.05 – 3.91 (m, 4H), 3.46 – 3.37 (m, 4H), 3.34 – 3.25 (m, 4H), 3.06 (s, 12H), 1.72 (dq, *J* = 11.6, 5.4, 5.0 Hz, 4H), 1.37 – 1.16 (m, 16H); <sup>13</sup>C NMR (101 MHz, Deuterium Oxide) δ 65.49, 64.79, 55.35, 51.33, 28.53, 28.41, 28.12, 25.43, 21.88.

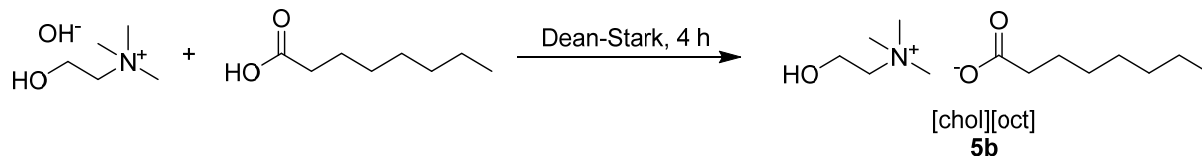


**2,2'-(ethane-1,2-diylbis(oxy))bis(N-(2-hydroxyethyl)-N,N-dimethylethan-1-aminium) chloride (4j):** A 250 mL round bottom flask wrapped in aluminum foil and equipped with a reflux condenser was purged with argon. To the flask was added anhydrous acetonitrile (30 mL), 1,2-bis(2-chloroethoxy)ethane (10.0 mL, 64.0 mmol, 1.0 equiv.), and dimethylaminoethanol (19.3 mL, 192 mmol, 3.0 equiv.). The reaction stirred at 80 °C for 24 h, in which a white solid precipitated out. The white solid was filtered, washed with acetone (3x20 mL), and collected. Residual solvent was removed *in vacuo*. The product (**4j**) was isolated as a white solid in 74.5% yield. <sup>1</sup>H NMR (400 MHz, Deuterium Oxide) δ 4.02 – 3.96 (m, 4H), 3.92 (dq, J = 5.2, 2.5 Hz, 4H), 3.67 (s, 4H), 3.64 – 3.57 (m, 4H), 3.55 – 3.48 (m, 4H), 3.14 (s, 12H); <sup>13</sup>C {<sup>1</sup>H} NMR (101 MHz, Deuterium Oxide) δ 69.61, 66.69 – 65.76 (m), 64.16 (d, J = 3.4 Hz), 55.37, 52.53 – 51.70 (m); HSQC (Deuterium Oxide) δ {3.18, 52.11}, {4.02, 55.33}, {3.64, 64.19}, {3.96, 64.20}, {3.49, 67.57}, {3.70, 69.68}.

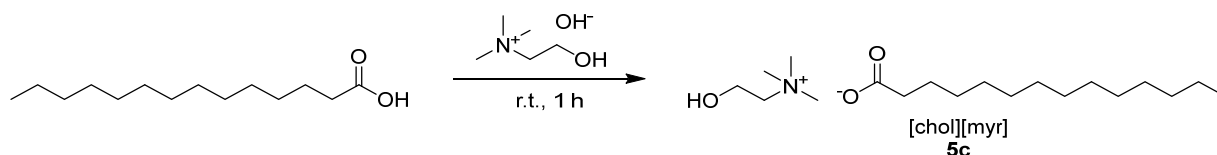
#### 2.4.5 Synthesis of cholinium ILs containing fatty acid anions



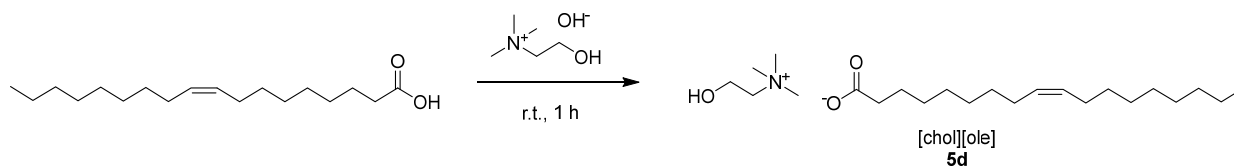
**2-hydroxy-N,N,N-trimethylethan-1-aminium hexanoate (5a):** To a 50 mL round bottom flask equipped with a bubbler was added hexanoic acid (4.85 mL, 38.7 mmol, 1.0 equiv.). Then, choline bicarbonate (80% in water; 6.84 mL, 38.7 mmol, 1.0 equiv.) was added to the flask dropwise with stirring. The reaction stopped after bubbling ceased. Water was removed *in vacuo* to produce the product (**5a**) as a yellow liquid in 99% yield. <sup>1</sup>H NMR (400 MHz, Deuterium Oxide) δ 3.99 – 3.90 (m, 2H), 3.44 – 3.37 (m, 2H), 3.09 (d, J = 0.9 Hz, 9H), 2.07 (t, J = 7.5 Hz, 2H), 1.44 (p, J = 7.4 Hz, 2H), 1.27 – 1.10 (m, 4H), 0.77 (t, J = 7.0 Hz, 3H); <sup>13</sup>C NMR (101 MHz, Deuterium Oxide) δ 183.54, 67.41, 67.38, 67.35, 55.55, 53.87, 53.83, 53.79, 37.27, 30.98, 25.44, 21.78, 13.31.



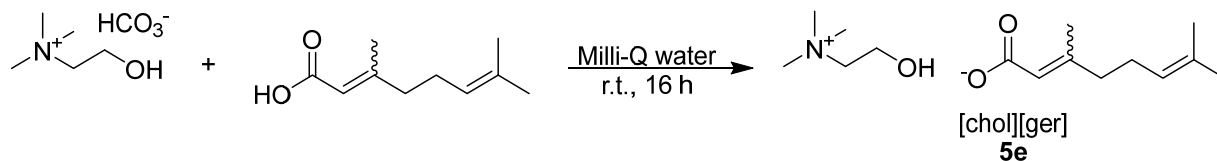
**2-hydroxy-*N,N,N*-trimethylethan-1-aminium octanoate (5b):** To a 100 mL round bottom flask on ice was added octanoic acid (7 mL, 44.2 mmol, 1.0 equiv.). Then, choline hydroxide (46% in water; 10.8 mL, 44.2 mmol, 1.0 equiv.) was slowly added to the flask dropwise with stirring. After all the choline hydroxide was added, a Dean-Stark trap was attached. The reaction stirred at 120 °C for 4 h to remove the water. The product (**5b**) was isolated as a solid. No further workup was performed.



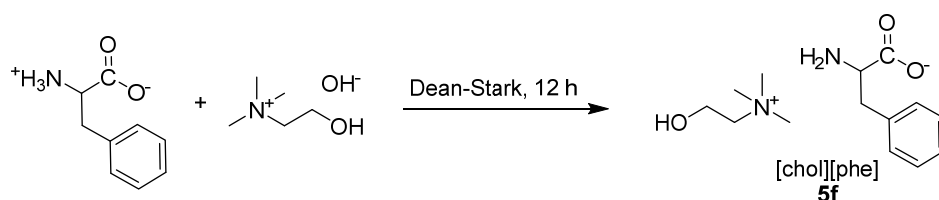
**2-hydroxy-*N,N,N*-trimethylethan-1-aminium tetradecanoate (5c):** To a 50 mL round bottom flask on ice was added myristic acid (566 mg, 2.48 mmol, 1.0 equiv.). Then, choline hydroxide (46% in water; 0.625 mL, 2.48 mmol, 1.0 equiv.) was slowly added to the flask dropwise with stirring. The product (**5c**) formed as a solid immediately. No further workup was performed.



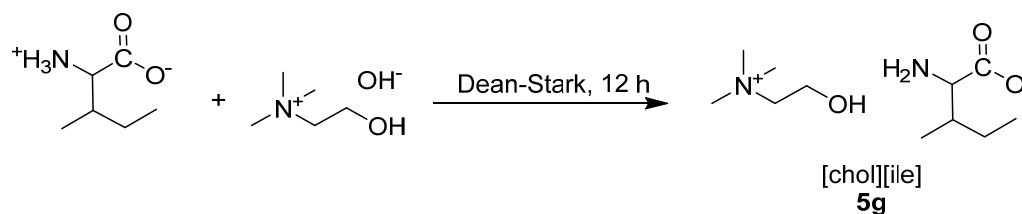
**2-hydroxy-*N,N,N*-trimethylethan-1-aminium oleate (5d):** To a 100 mL round bottom flask on ice was added oleic acid (1.61 mL, 5.00 mmol, 1.0 equiv.). Then, choline hydroxide (46% in water; 1.25 mL, 5.00 mmol, 1.0 equiv.) was slowly added to the flask dropwise with stirring. The product (**5d**) immediately formed as a solid. No further workup was performed.



**2-hydroxy-*N,N,N*-trimethylethan-1-aminium 3,7-dimethylocta-2,6-dienoate (5e):** To a 25 mL round bottom flask equipped with a bubbler was added geranic acid (1.0 mL, 5.76 mmol, 1.0 equiv.). Then, choline bicarbonate (80% in water; 1.02 mL, 5.76 mmol, 1.0 equiv.) was added to the flask dropwise with stirring. The reaction stopped after bubbling ceased. The reaction then stirred for 16 h. A second layer did not form so no further workup was performed.

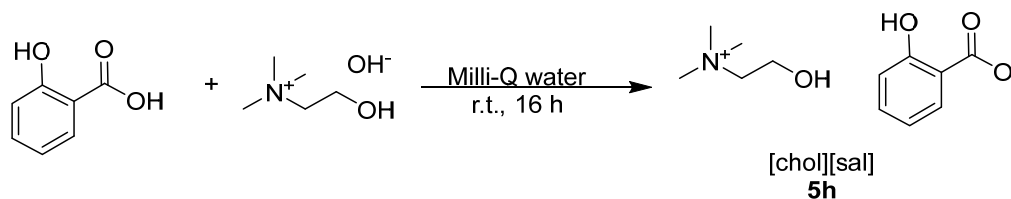


**2-hydroxy-*N,N,N*-trimethylethan-1-aminium phenylalaninate (5f):** To a 50 mL round bottom flask on ice was added phenylalanine (1.00 g, 6.00 mmol, 1.0 equiv.). Then, choline hydroxide (46% in water; 1.54 mL, 6.00 mmol, 1.0 equiv.) was slowly added to the flask dropwise with stirring. After all the choline hydroxide was added, a Dean-Stark trap was attached. The reaction stirred at 120 °C for 12 h to remove the water. The product (**5f**) was isolated as a red viscous liquid in 99% yield. Since the product was water soluble, no characterization was performed.



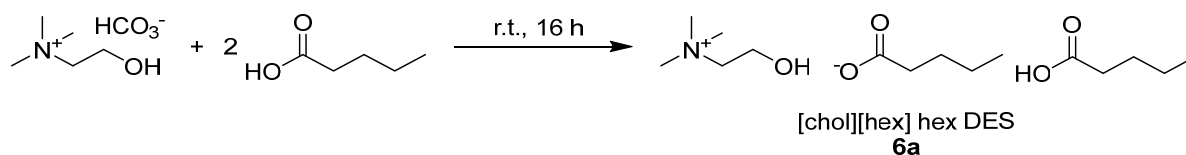
**2-hydroxy-*N,N,N*-trimethylethan-1-aminium 2-amino-3-methylpentanoate (5g):** To a 50 mL round bottom flask on ice was added isoleucine (0.803 g, 6.10 mmol, 1.0 equiv.). Then, choline hydroxide (46% in water; 1.55 mL, 6.10 mmol, 1.0 equiv.) was slowly added to the flask dropwise with stirring. After all

the choline hydroxide was added, a Dean-Stark trap was attached. The reaction stirred at 130 °C for 12 h to remove the water. The product (**5g**) was isolated as a viscous liquid in 99% yield. Since the product was water soluble, no characterization was performed.

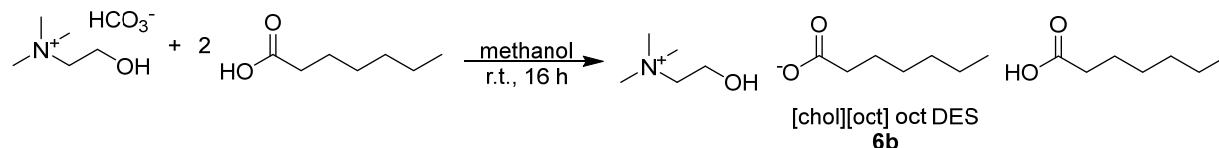


**2-hydroxy-*N,N,N*-trimethylethan-1-aminium 2-hydroxybenzoate (5h):** To a 100 mL round bottom flask on ice was added salicylic acid (1.38 g, 10.0 mmol, 1.0 equiv.). Then, choline hydroxide (46% in water; 2.46 mL, 10.0 mmol, 1.0 equiv.) was slowly added to the flask dropwise with stirring. After the choline hydroxide was added, the reaction continued to stir for 16 h at room temperature. Since no second layer formed, the reaction was not worked up further.

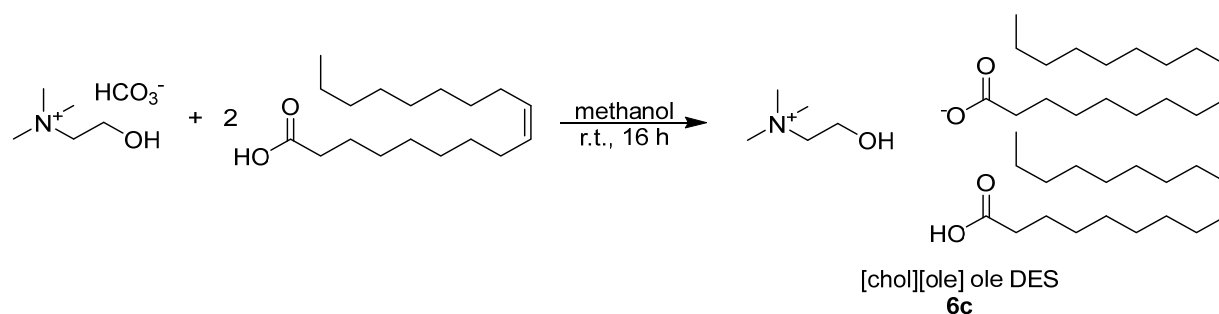
#### 2.4.6 Synthesis of cholinium deep eutectic solvents



**2-hydroxy-*N,N,N*-trimethylethan-1-aminium hexanoate hexanoic acid (6a):** To a 100 mL round bottom flask was added hexanoic acid (4.86 mL, 38.8 mmol, 2.0 equiv.) and choline bicarbonate (80% in water; 3.42 mL, 19.4 mmol, 1.0 equiv.). The reaction then stirred for 16 h at room temperature. Residual water was removed *in vacuo* to reveal the product (**6a**) as a water-soluble liquid at 99% yield. <sup>1</sup>H NMR (400 MHz, Deuterium Oxide) δ 3.98 – 3.90 (m, 2H), 3.44 – 3.37 (m, 2H), 3.09 (s, 9H), 2.08 (t, *J* = 7.5 Hz, 4H), 1.44 (p, *J* = 7.4 Hz, 4H), 1.18 (tdt, *J* = 10.3, 6.9, 4.2 Hz, 8H), 0.76 (t, *J* = 6.9 Hz, 6H); <sup>13</sup>C NMR (101 MHz, Deuterium Oxide) δ 183.20, 67.41, 67.38, 67.35, 55.55, 53.88, 53.84, 53.80, 37.05, 31.32, 30.96, 25.36, 21.78, 13.32.

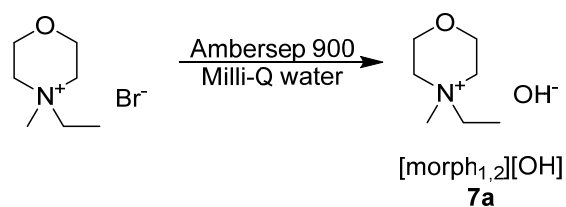


**2-hydroxy-*N,N,N*-trimethylethan-1-aminium octanoate octanoic acid (6b):** To a 250 mL round bottom flask was added octanoic acid (6.13 mL, 38.8 mmol, 2.0 equiv.), choline bicarbonate (80% in water; 3.42 mL, 19.4 mmol, 1.0 equiv.), and methanol (10 mL). The reaction then stirred for 16 h at room temperature. Residual water was removed *in vacuo* to reveal the product (**6b**) as a solid at 99% yield. Since the product was a solid, no further workup nor analysis was performed.

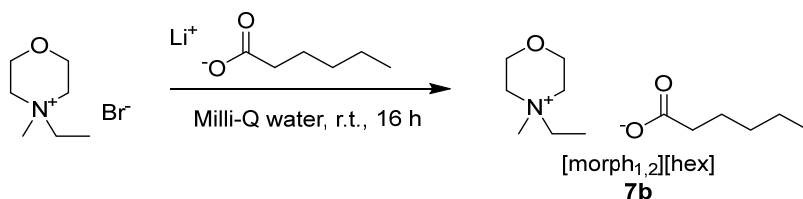


**2-hydroxy-*N,N,N*-trimethylethan-1-aminium oleate oleic acid (6c):** To a 100 mL round bottom flask was added oleic acid (6.12 mL, 19.4 mmol, 2.0 equiv.), choline bicarbonate (80% in water; 1.71 mL, 9.7 mmol, 1.0 equiv.), and methanol (10 mL). The reaction then stirred for 16 h at room temperature. Residual water was removed *in vacuo* to reveal the product (**6c**) as a solid at 99% yield. Since the product was a solid, no further workup nor analysis was performed.

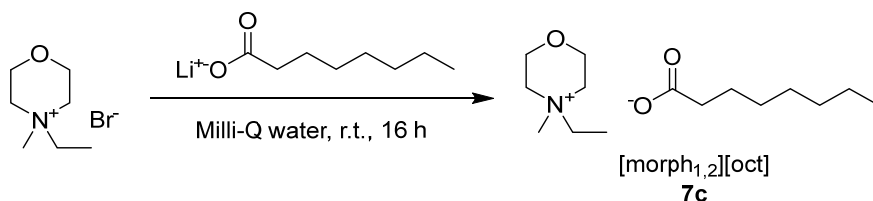
#### 2.4.7 Synthesis of morpholinium-based ILs containing fatty acid anions



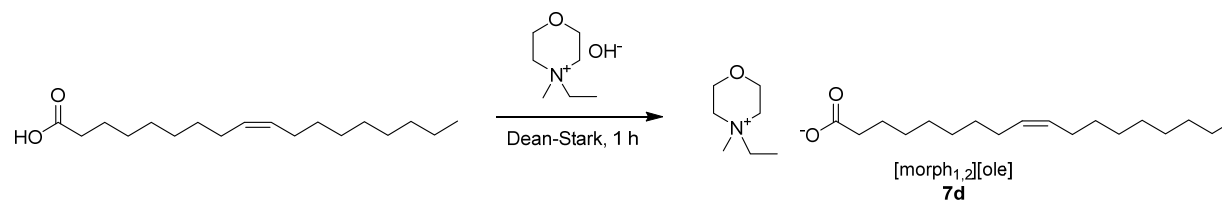
**4-ethyl-4-methylmorpholin-4-ium hydroxide (7a):** To a 100 mL round bottom flask was added **3a** ([morph<sub>1,2</sub>][Br]; 6.54 g, 31.1 mmol), Ambersep 900 (7.00 g), and Milli-Q water (26.1 mL). The solution stirred at room temperature. After every 12–16 h, the Ambersep 900 beads were filtered out and washed with fresh Milli-Q water (3x15 mL). The reaction was deemed complete when there was no yellow precipitant upon adding silver nitrate. To prevent degradation, the product (**7a**) was kept as an aqueous solution and assumed to be 100% yield. No characterization was performed.



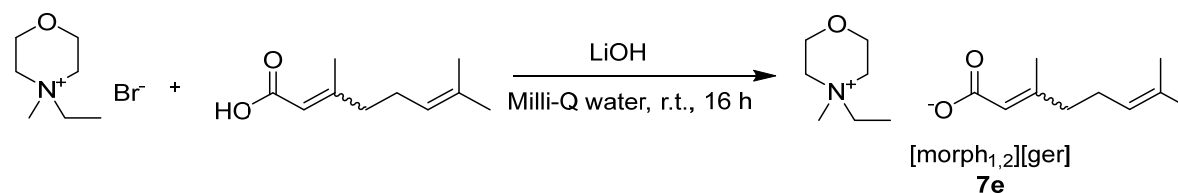
**4-ethyl-4-methylmorpholin-4-ium hexanoate (7b):** To a 4 mL glass vial was added **3a** ([morph<sub>1,2</sub>][Br]; 233 mg, 1.11 mmol, 1.0 equiv.), lithium hexanoate (135 mg, 1.11 mmol, 1.0 equiv.), and Milli-Q water (3 mL). The reaction stirred at room temperature for 16 h. Since no second layer precipitated, the reaction was not worked up nor characterized.



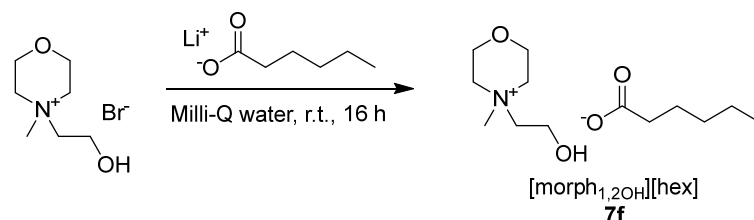
**4-ethyl-4-methylmorpholin-4-ium octanoate (7c):** To a 4 mL glass vial was added **3a** ([morph<sub>1,2</sub>][Br]; 592 mg, 2.81 mmol, 1.0 equiv.), lithium hexanoate (423 mg, 2.81 mmol, 1.0 equiv.), and Milli-Q water (3 mL). The reaction stirred at room temperature for 16 h. Since no second layer precipitated, the reaction was not worked up nor characterized further.



**4-ethyl-4-methylmorpholin-4-ium oleate (7d):** To a 50 mL round bottom flask on ice was added **3a** ([morph<sub>1,2</sub>][Br]). Then, choline hydroxide (46% in water;) was slowly added to the flask dropwise with stirring. After all the choline hydroxide was added, a Dean-Stark trap was attached. The reaction stirred at 130 °C for 11 h to remove the water, to reveal the product (**7d**) as a gel. Since the compound was a gel, it was not worked up nor analyzed further.

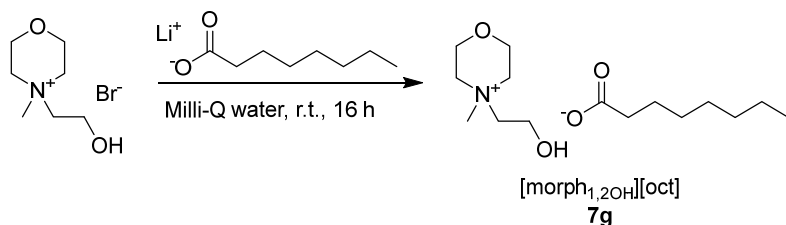


**4-ethyl-4-methylmorpholin-4-ium 3,7-dimethylocta-2,6-dienoate (7e):** To a 25 mL round bottom flask was added geranic acid (0.488 mL, 2.82 mmol, 1.0 equiv.), lithium hydroxide (67.5 mg, 2.82 mmol, 1.0 equiv.), and Milli-Q water (5 mL). The reaction stirred until the compounds dissolved. Then, **3a** ([morph<sub>1,2</sub>][Br]; 592 mg, 2.82 mmol, 1.0 equiv.) was added. The reaction stirred at room temperature for 16 h. Since no second layer precipitated, the reaction was not worked up nor characterized further.

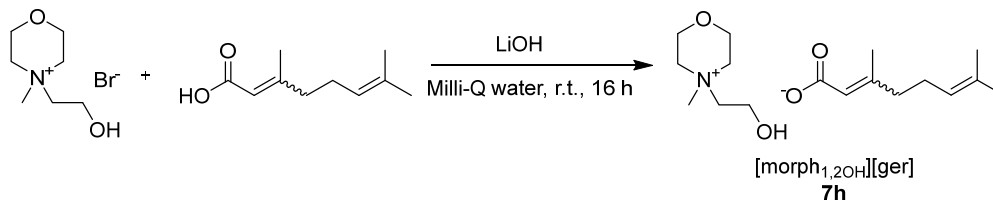


**4-(2-hydroxyethyl)-4-methylmorpholin-4-ium hexanoate (7f):** To a 3 mL glass vial was added **3b** ([morph<sub>1,2OH</sub>][Br]; 250 mg, 1.11 mmol, 1.0 equiv.), lithium hexanoate (135 mg, 1.11 mmol, 1.0 equiv.), and

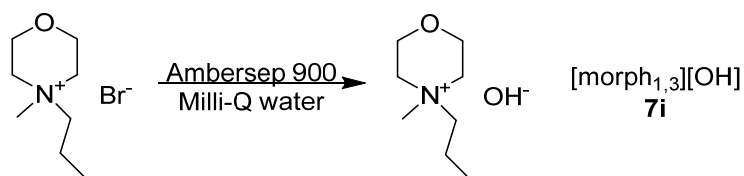
Milli-Q water (3 mL). The reaction stirred at room temperature for 16 h. Since no second layer precipitated, the reaction was not worked up nor characterized further.



**4-(2-hydroxyethyl)-4-methylmorpholin-4-ium octanoate (7g):** To a 3 mL glass vial was added **3b** ([morph<sub>1,2OH</sub>][Br]; 250 mg, 1.11 mmol, 1.0 equiv.), lithium octanoate (165 mg, 1.11 mmol, 1.0 equiv.), and Milli-Q water (3 mL). The reaction stirred at room temperature for 16 h. Since no second layer precipitated, the reaction was not worked up nor characterized further.

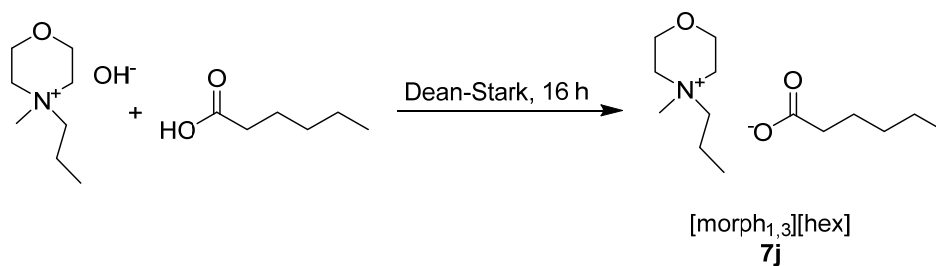


**4-(2-hydroxyethyl)-4-methylmorpholin-4-ium 3,7-dimethylocta-2,6-dienoate (7h):** To a 3 mL glass vial was added geranic acid (0.191 mL, 1.11 mmol, 1.0 equiv.), lithium hydroxide (26.4 mg, 1.11 mmol, 1.0 equiv.), and Milli-Q water (3 mL). The reaction stirred until the compounds dissolved. Then, **3b** ([morph<sub>1,2OH</sub>][Br]; 250 mg, 1.11 mmol, 1.0 equiv.) was added. The reaction stirred at room temperature for 16 h. Since no second layer precipitated, the reaction was not worked up nor characterized.

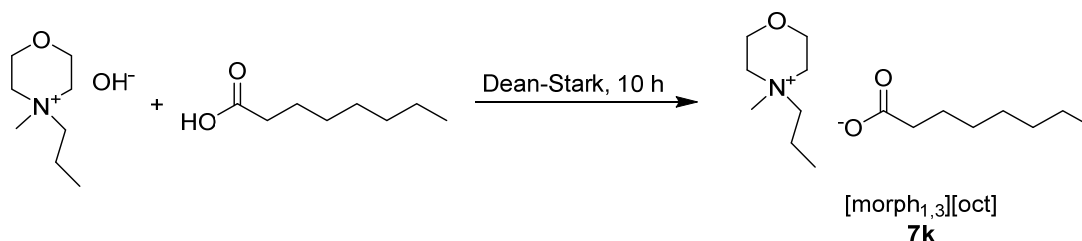


**4-methyl-4-propylmorpholin-4-ium hydroxide (7i):** To a 100 mL round bottom flask was added **3c** ([morph<sub>1,3</sub>][Br]; 10.0 g, 44.6 mmol), Ambersep 900 (10.0 g), and Milli-Q water (40 mL). The solution

stirred at room temperature. After every 12–16 h, the Ambersep 900 beads were filtered out and washed with fresh Milli-Q water (3x15 mL). The reaction progress deemed complete when there was no yellow precipitant upon adding silver nitrate. To prevent degradation, the product (**7i**) was kept as an aqueous solution and assumed to be 100% yield. No characterization was performed.

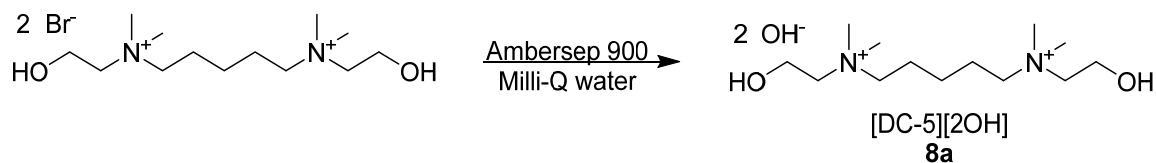


**4-methyl-4-propylmorpholin-4-ium hexanoate (7j):** To a 100 mL round bottom flask was added **3c** ([morph<sub>1,3</sub>][OH]; 7.50 mL, 47.8 mmol, 1.0 equiv.). Then, hexanoic acid (6.00 mL, 47.8 mmol, 1.0 equiv.) was slowly added to the flask dropwise with stirring. After all the hexanoic acid was added, a Dean-Stark trap was attached. The reaction stirred at 110 °C for 13 h to remove the water, to reveal the product (**7j**) as a yellow liquid. Since the product was water soluble, no characterization was performed.

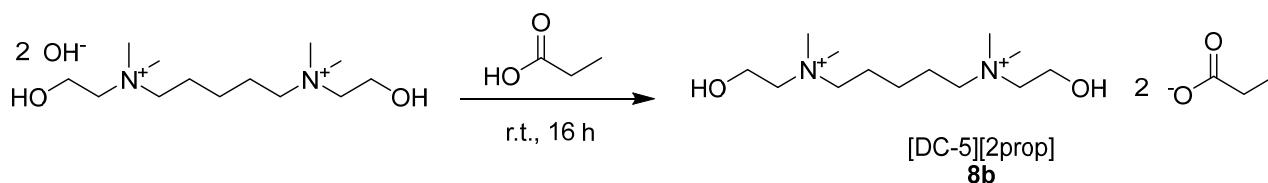


**4-methyl-4-propylmorpholin-4-ium octanoate (7k):** To a 100 mL round bottom flask was added **3c** ([morph<sub>1,3</sub>][OH]; 7.50 mL, 47.8 mmol, 1.0 equiv.). Then, octanoic acid (7.56 mL, 47.8 mmol, 1.0 equiv.) was slowly added to the flask dropwise with stirring. After all the octanoic acid was added, a Dean-Stark trap was attached. The reaction stirred at 120 °C for 10 h to remove the water, to reveal the product (**7k**) as a solid. Since the product was water soluble, no characterization was performed.

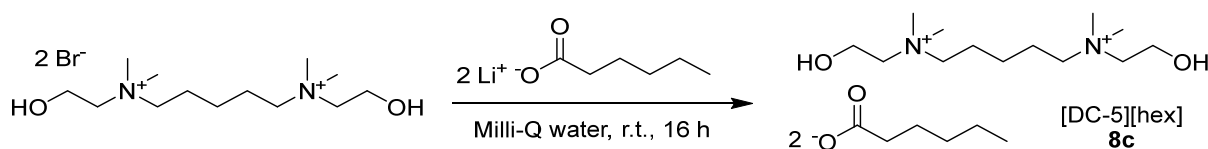
### 2.4.8 Synthesis of dicholinium ILs containing fatty acid anions



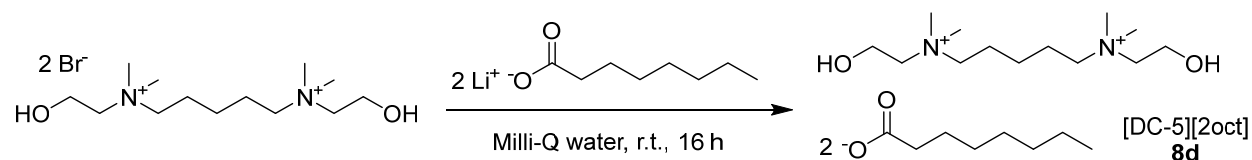
***N*<sup>1</sup>,*N*<sup>5</sup>-bis(2-hydroxyethyl)-*N*<sup>1</sup>*N*<sup>1</sup>,*N*<sup>5</sup>,*N*<sup>5</sup>-tetramethylpentane-1,5-diaminium hydroxide (8a):** To a 100 mL round bottom flask was added **4d** ([DC-5][Br]; 2.00 g, 49.0 mmol), Ambersep 900 (6.00 g), and Milli-Q water (50 mL). The solution stirred at room temperature. After every 12–16 h, the Ambersep 900 beads were filtered out and washed with fresh Milli-Q water (3x15 mL). The reaction was deemed complete when there was no yellow precipitant upon adding silver nitrate. The water was removed *in vacuo* to produce the product (**8a**) as a viscous yellow liquid in 93.0% yield. <sup>1</sup>H NMR (400 MHz, Deuterium Oxide) δ 3.97 (dq, *J* = 5.1, 2.5 Hz, 4H), 3.46 – 3.39 (m, 4H), 3.38 – 3.30 (m, 4H), 3.08 (s, 12H), 1.81 (qd, *J* = 10.1, 8.3, 6.3 Hz, 4H), 1.36 (p, *J* = 7.7 Hz, 2H); <sup>13</sup>C NMR (101 MHz, Deuterium Oxide) δ 65.18 – 64.94 (m), 64.90 – 64.68 (m), 55.37, 51.48 – 51.27 (m), 22.45, 21.69.



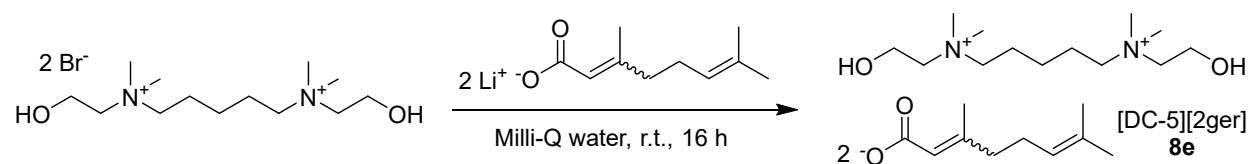
***N*<sup>1</sup>,*N*<sup>5</sup>-bis(2-hydroxyethyl)-*N*<sup>1</sup>*N*<sup>1</sup>,*N*<sup>5</sup>,*N*<sup>5</sup>-tetramethylpentane-1,5-diaminium propionate (8b):** To a 25 mL round bottom flask was added **4d** ([DC-5][2Br]; 415 mg, 1.47 mmol, 1.0 equiv.) and propionic acid (0.220 mL, 2.94 mmol, 2.0 equiv.). The reaction stirred for 16 h at room temperature. The water was removed *in vacuo* to reveal the product (**8b**) as a water soluble solid in 50.4% yield. Since the product was water soluble, no characterization was performed.



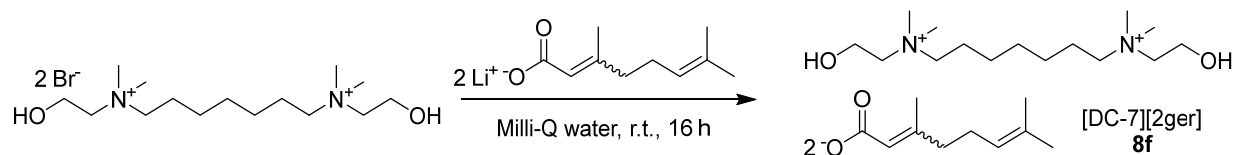
***N*<sup>1</sup>,*N*<sup>5</sup>-bis(2-hydroxyethyl)-*N*<sup>1</sup>*N*<sup>1</sup>,*N*<sup>5</sup>,*N*<sup>5</sup>-tetramethylpentane-1,5-diaminium hexanoate (8c):** To a 250 mL round bottom flask was added **4d** ([DC-5][2Br]; 3.35 g, 8.19 mmol, 1.0 equiv.), lithium hexanoate (water; 8.38 mL, 0.239 g/mL, 16.4 mmol, 2.0 equiv.), and Milli-Q water (10 mL). The reaction stirred for 16 h at room temperature. Since no second layer formed, the reaction was not worked up nor analyzed.



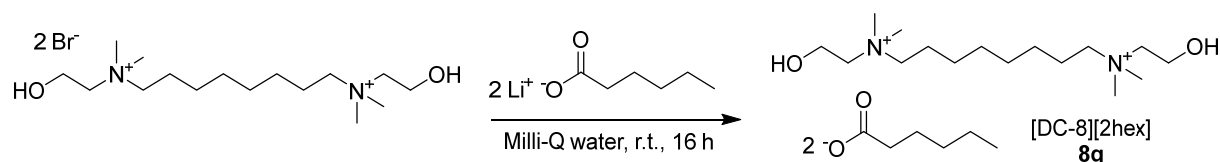
***N*<sup>1</sup>,*N*<sup>5</sup>-bis(2-hydroxyethyl)-*N*<sup>1</sup>*N*<sup>1</sup>,*N*<sup>5</sup>,*N*<sup>5</sup>-tetramethylpentane-1,5-diaminium octanoate (8d):** To a 250 mL round bottom flask was added **4d** ([DC-5][2Br]; 3.34 g, 8.19 mmol, 1.0 equiv.), lithium octanoate (2.46 g, 16.4 mmol, 2.0 equiv.), and Milli-Q water (10 mL). The reaction stirred for 16 h at room temperature. A solid precipitated. The solid was filtered out and was revealed to be mainly **4d** ([DC-5][2Br]). No further workup nor characterization was performed. <sup>1</sup>H NMR (400 MHz, Deuterium Oxide) δ 4.02 (dq, *J* = 7.5, 2.5 Hz, 4H), 3.52 – 3.45 (m, 4H), 3.43 – 3.35 (m, 4H), 3.13 (s, 12H), 2.12 (t, *J* = 7.5 Hz, 0H), 1.85 (ddd, *J* = 12.0, 10.1, 6.3 Hz, 4H), 1.51 (q, *J* = 7.2 Hz, 0H), 1.41 (p, *J* = 7.7 Hz, 2H), 1.24 (q, *J* = 5.3 Hz, 1H), 0.87 – 0.80 (m, 0H); <sup>13</sup>C NMR (101 MHz, Deuterium Oxide) δ 184.01, 65.07, 65.05, 65.02, 64.94, 64.92, 64.89, 55.46, 51.59, 51.55, 51.51, 37.78, 31.13, 28.82, 28.35, 26.03, 22.52, 22.10, 21.78, 13.60.



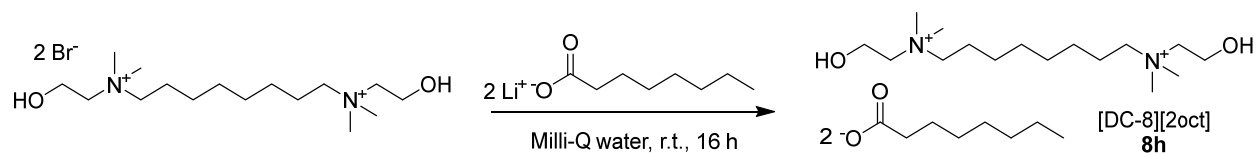
***N*<sup>1</sup>,*N*<sup>5</sup>-bis(2-hydroxyethyl)-*N*<sup>1</sup>*N*<sup>1</sup>,*N*<sup>5</sup>,*N*<sup>5</sup>-tetramethylpentane-1,5-diaminium 3,7-dimethylocta-2,6-dienoate (8e):** To a 250 mL round bottom flask was added **4d** ([DC-5][2Br]; 1.17 g, 2.88 mmol, 1.0 equiv.), lithium geranate (1.00 g, 5.77 mmol, 2.0 equiv.), and Milli-Q water (30 mL). The reaction stirred for 16 h at room temperature. Since no second layer formed, the reaction was not worked nor characterized.



***N*<sup>1</sup>,*N*<sup>7</sup>-bis(2-hydroxyethyl)-*N*<sup>1</sup>*N*<sup>1</sup>,*N*<sup>7</sup>,*N*<sup>7</sup>-tetramethylheptane-1,7-diaminium 3,7-dimethylocta-2,6-dienoate (**8f**):** To a 250 mL round bottom flask was added **4f** ([DC-7][2Br]; 1.26 g, 2.88 mmol, 1.0 equiv.), lithium geranate (1.00 g, 5.77 mmol, 2.0 equiv.), and Milli-Q water (25 mL). The reaction stirred for 16 h at room temperature. Since no second layer formed, the reaction was not workup nor characterized.

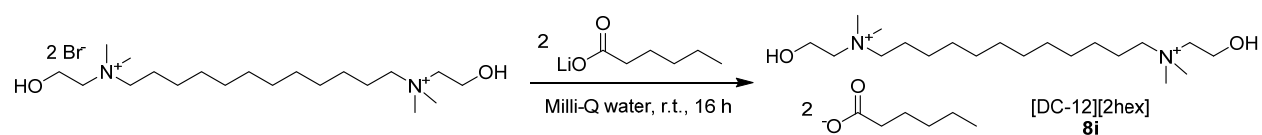


***N*<sup>1</sup>,*N*<sup>8</sup>-bis(2-hydroxyethyl)-*N*<sup>1</sup>*N*<sup>1</sup>,*N*<sup>8</sup>,*N*<sup>8</sup>-tetramethyloctane-1,8-diaminium hexanoate (**8g**):** To a 250 mL round bottom flask was added **4g** ([DC-8][2Br]; 3.69 g, 8.19 mmol, 1.0 equiv.), lithium hexanoate (water; 8.38 mL, 0.239 g/mL, 16.4 mmol, 2.0 equiv.), and Milli-Q water (10 mL). The reaction stirred for 16 h at room temperature. Since no second layer formed, the reaction was not worked up nor characterized.

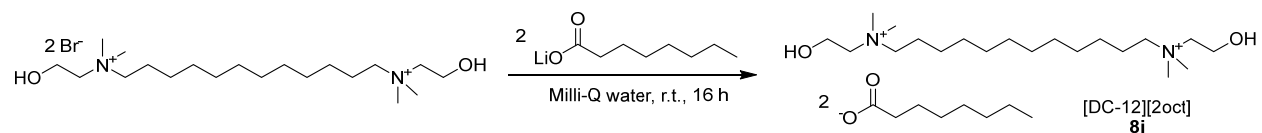


***N*<sup>1</sup>,*N*<sup>8</sup>-bis(2-hydroxyethyl)-*N*<sup>1</sup>*N*<sup>1</sup>,*N*<sup>8</sup>,*N*<sup>8</sup>-tetramethyloctane-1,8-diaminium octanoate (**8h**):** To a 250 mL round bottom flask was added **4g** ([DC-8][2Br]; 3.69 g, 8.19 mmol, 1.0 equiv.), lithium octanoate (2.46 g, 16.4 mmol, 2.0 equiv.), and Milli-Q water (10 mL). The reaction stirred for 16 h at room temperature. A solid precipitated. The solid was filtered out and was revealed to be mainly octanoic acid. The filtrate was concentrated *in vacuo* and revealed to be mainly **4g** ([DC-8][2Br]). No further workup nor characterization was performed. Precipitant: <sup>1</sup>H NMR (400 MHz, Deuterium Oxide) δ 3.98 – 3.91 (m, 0H), 3.43 – 3.36 (m, 0H), 3.32 – 3.23 (m, 0H), 3.04 (s, 1H), 2.08 (t, *J* = 7.5 Hz, 2H), 1.69 (t, *J* = 6.6 Hz, 0H), 1.45 (p, *J* = 7.3 Hz, 2H), 1.29 (d, *J* = 2.7 Hz, 1H), 1.19 (q, *J* = 5.5 Hz, 9H), 0.81 – 0.73 (m, 3H); <sup>13</sup>C NMR (101 MHz,

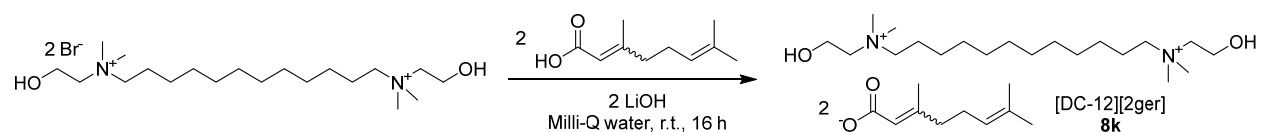
Deuterium Oxide)  $\delta$  184.26, 65.40, 64.81, 55.32, 51.32, 37.66, 31.05, 28.72, 28.26, 27.97, 25.91, 25.36, 22.00, 21.92, 13.41. Filtrate:  $^1\text{H}$  NMR (400 MHz, Deuterium Oxide)  $\delta$  3.99 (t,  $J = 4.9$  Hz, 4H), 3.48 – 3.41 (m, 4H), 3.37 – 3.29 (m, 4H), 3.09 (s, 12H), 2.11 (t,  $J = 7.5$  Hz, 1H), 1.80 – 1.68 (m, 4H), 1.49 (p,  $J = 7.3$  Hz, 1H), 1.33 (d,  $J = 2.7$  Hz, 9H), 1.23 (q,  $J = 5.0$  Hz, 3H), 0.92 – 0.72 (m, 1H);  $^{13}\text{C}$  NMR (101 MHz, Deuterium Oxide)  $\delta$  183.83, 65.47, 64.87, 55.43, 51.47, 51.44, 51.40, 37.64, 31.14, 28.81, 28.35, 27.91, 25.96, 25.35, 22.09, 21.94, 13.56.



**$N^1,N^{12}$ -bis(2-hydroxyethyl)- $N^1N^1,N^{12},N^{12}$ -tetramethyldodecane-1,12-diaminium hexanoate (8i):** To a 25 mL round bottom flask was added **4i** ([DC-12][2Br]; 400 mg, 0.790 mmol, 1.0 equiv.), lithium hexanoate (193 mg, 1.58 mmol, 2.0 equiv.), and Milli-Q water (5 mL). The reaction stirred for 16 h at room temperature. Since no second layer formed, the reaction was not worked up nor characterized.



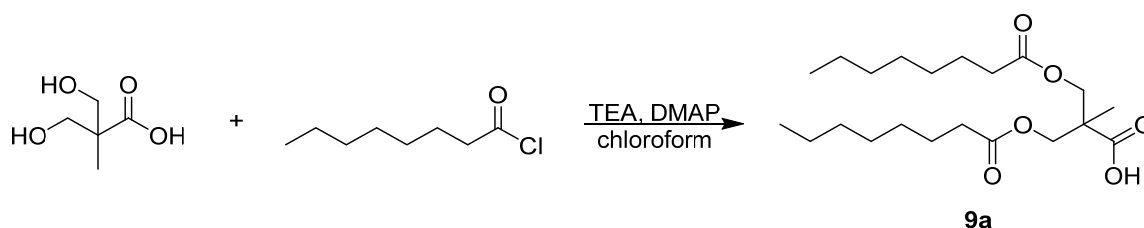
**$N^1,N^{12}$ -bis(2-hydroxyethyl)- $N^1N^1,N^{12},N^{12}$ -tetramethyldodecane-1,12-diaminium octanoate (8j):** To a 25 mL round bottom flask was added **4i** ([DC-12][2Br]; 400 mg, 0.790 mmol, 1.0 equiv.), lithium octanoate (237 mg, 1.58 mmol, 2.0 equiv.), and Milli-Q water (5 mL). The reaction stirred for 16 h at room temperature. Since no second layer formed, the reaction was not worked up nor characterized.



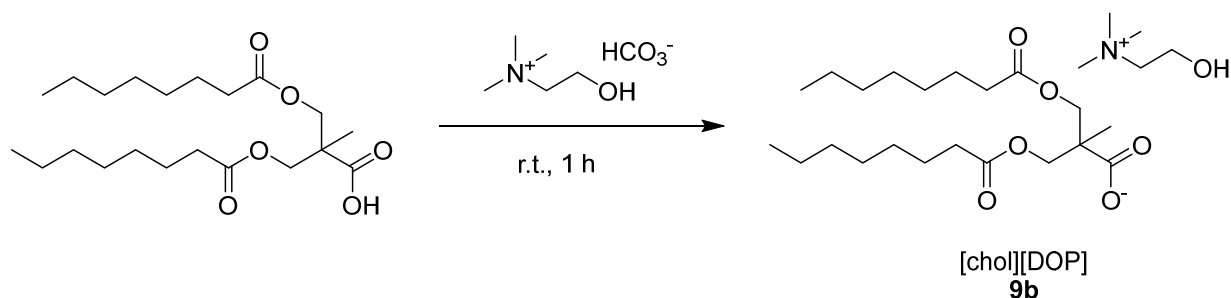
**$N^1,N^{12}$ -bis(2-hydroxyethyl)- $N^1N^1,N^{12},N^{12}$ -tetramethyldodecane-1,12-diaminium 3,7-dimethylocta-2,6-dienoate (8k):** To a 25 mL round bottom flask was added geranic acid (266 mg, 1.58 mmol, 2.0 equiv.), lithium hydroxide (37.8 mg, 1.58 mmol, 2.0 equiv.), and Milli-Q water (5 mL). The mixture stirred until

the components dissolved. Then, **4i** ([DC-12][2Br]; 400 mg, 0.790 mmol, 1.0 equiv.) was added. The reaction stirred for 16 h at room temperature. Since no second layer formed, the reaction was not worked up nor characterized.

#### 2.4.9 Synthesis of the DOP anion and corresponding ILs

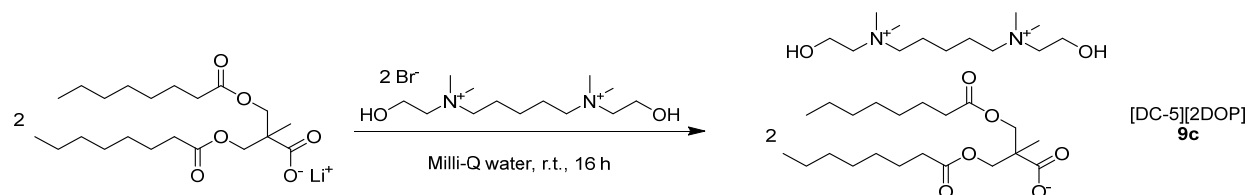


**2-methyl-3-(octanoyloxy)-2-((octanoyloxy)methyl)propanoic acid (9a):** To a 250 mL round bottom flask equipped with a reflux condenser was added octanoyl chloride (4.72 mL, 27.7 mmol, 3.73 equiv.), 2,2-bis(hydroxymethyl)propionic acid (1.00 g, 7.40 mmol, 1.0 equiv.), and chloroform (35 mL). The reaction vessel was purged with argon. The mixture stirred until all was dissolved. Triethylamine (3.42 mL, 24.5 mmol, 3.3 equiv.) and 4-dimethylaminopyridine (2.28 grams, 3.7 mmol, 0.5 equiv.) were then added and the resulting mixture was heated at reflux under argon for 16 hours. The reaction was then cooled to room temperature and quenched with 200 mL of water. The solution was acidified to pH 3 with concentrated aqueous hydrochloric acid and extracted three times with methylene chloride (3x25 mL). The combined methylene chloride layers were washed with 1% aqueous hydrochloric acid (1x25 mL) and saturated aqueous sodium chloride (1x25 mL). The organic layer was then dried over anhydrous magnesium sulfate, filtered, and the solvents removed *in vacuo* to obtain a yellow oil. The crude product was then purified using flash chromatography eluting with hexanes, ethyl acetate, and acetic acid (95:4:1). The product (**9a**) was obtained as a yellow oil in 87.5% yield.  $^1\text{H}$  NMR (400 MHz, Chloroform-*d*)  $\delta$  11.24 (s, 1H), 4.31 – 4.19 (m, 2H), 2.41 – 2.24 (m, 4H), 1.71 – 1.52 (m, 4H), 1.38 – 1.21 (m, 19H), 0.92 – 0.84 (m, 6H).  $^{13}\text{C}$  NMR (101 MHz, Chloroform-*d*)  $\delta$  178.94, 173.35, 64.99, 46.11, 34.09, 31.64, 31.62, 31.61, 29.07, 29.02, 29.00, 28.90, 28.87, 24.84, 22.57, 17.74, 14.20, 14.01.



**2-hydroxy-*N,N,N*-trimethylethan-1-aminium 2-methyl-3-(octanoyloxy)-2-((octanoyloxy)methyl)**

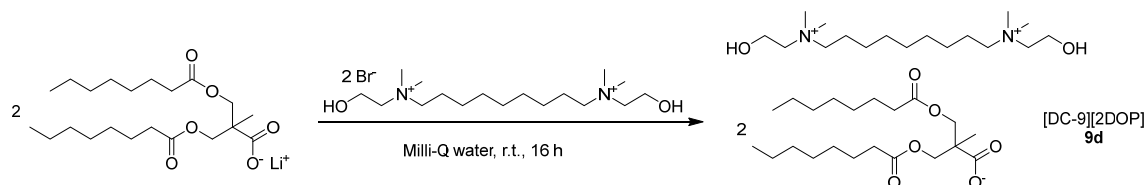
**propanoate (9b):** To a 2 mL glass vial was added **9a** (0.500 g, 1.29 mmol, 1.0 equiv.) and choline bicarbonate (0.227 mL, 1.29 mmol, 1.0 equiv.). The reaction stirred at room temperature for 1 h. Afterwards, the water was removed *in vacuo* to reveal the product (**9b**) as a viscous liquid.  $^1\text{H}$  NMR (400 MHz, Deuterium Oxide)  $\delta$  4.12 (dd,  $J = 79.5, 10.8$  Hz, 3H), 4.00 – 3.94 (m, 2H), 3.48 – 3.41 (m, 2H), 3.13 (s, 8H), 2.17 (dt,  $J = 65.4, 7.4$  Hz, 4H), 1.57 – 1.41 (m, 5H), 1.26 – 1.18 (m, 20H), 0.79 (h,  $J = 5.0$  Hz, 6H);  $^{13}\text{C}$  NMR (101 MHz, Deuterium Oxide)  $\delta$  184.16, 174.53, 67.44, 67.41, 67.38, 66.39, 55.58, 53.89, 53.85, 53.81, 46.50, 37.56, 33.96, 31.67, 31.04, 28.94, 28.70, 28.25, 25.87, 24.79, 22.50, 21.99, 18.20, 13.73, 13.37.



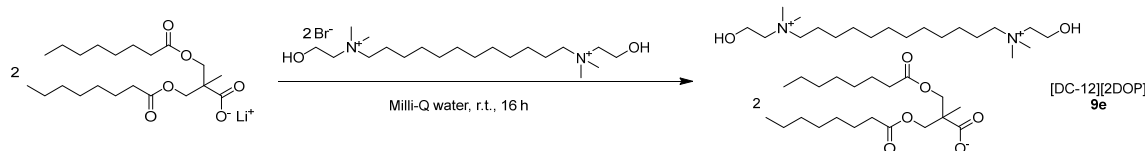
***N*<sup>1</sup>,*N*<sup>5</sup>-bis(2-hydroxyethyl)-*N*<sup>1</sup>*N*<sup>1</sup>,*N*<sup>5</sup>,*N*<sup>5</sup>-tetramethylpentane-1,5-diaminium 2-methyl-3-**

**(octanoyloxy)-2-((octanoyloxy)methyl) propanoate (9c):** To a 10 mL round bottom flask was added **4d** ([DC-5][2Br]; 260 mg, 0.635 mmol, 1.0 equiv.) and lithium 2-methyl-3-(octanoyloxy)-2-((octanoyloxy)methyl) propanoate (3.00 mL, 0.167 g/mL, 1.27 mmol, 2.0 equiv.). The reaction stirred at room temperature for 16 h. The mixture was extracted with DCM (3x10 mL). The organic layer was then concentrated *in vacuo* to reveal a viscous liquid that was mainly 2-methyl-3-(octanoyloxy)-2-((octanoyloxy)methyl) propanoate.  $^1\text{H}$  NMR (400 MHz, Chloroform-*d*)  $\delta$  4.25 (d,  $J = 11.0$  Hz, 2H), 4.04

(d,  $J = 10.9$  Hz, 2H), 2.20 (t,  $J = 7.7$  Hz, 3H), 1.50 (p,  $J = 7.1$  Hz, 4H), 1.28 – 1.16 (m, 18H), 1.02 (s, 2H), 0.80 (t,  $J = 6.8$  Hz, 6H);  $^{13}\text{C}$  NMR (101 MHz, Chloroform- $d$ )  $\delta$  178.87, 173.12, 76.37, 76.05, 75.73, 65.43, 45.69, 33.27, 30.72, 28.23, 28.18, 28.02, 23.93, 21.68, 21.62, 17.53, 13.03.

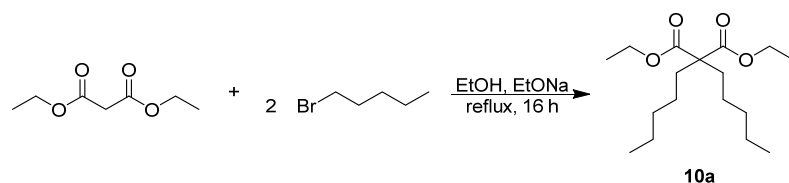


**$N^1, N^9$ -bis(2-hydroxyethyl)- $N^1 N^1, N^9, N^9$ -tetramethylnonane-1,9-diaminium 2-methyl-3-(octanoyloxy)-2-((octanoyloxy)methyl) propanoate (9d):** To a 50 mL round bottom flask was added **4h** ([DC-9][2Br]; 464 mg, 1.00 mmol, 1.0 equiv.), lithium 2-methyl-3-(octanoyloxy)-2-((octanoyloxy)methyl) propanoate (800 mg, 2.00 mmol, 2.0 equiv.), and Milli-Q water (15 mL). The solution stirred at room temperature for 16 h. A second layer did not form so no workup nor characterization was performed.

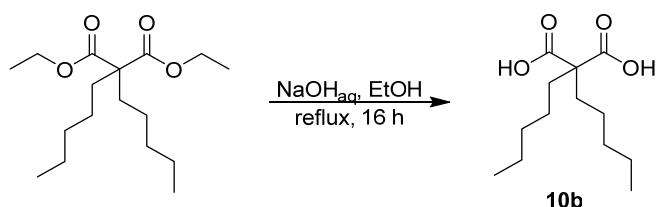


**$N^1, N^{12}$ -bis(2-hydroxyethyl)- $N^1 N^1, N^{12}, N^{12}$ -tetramethyldodecane-1,12-diaminium 2-methyl-3-(octanoyloxy)-2-((octanoyloxy)methyl) propanoate (9e):** To a 50 mL round bottom flask was added **4i** ([DC-12][2Br]; 506 mg, 1.00 mmol, 1.0 equiv.), lithium 2-methyl-3-(octanoyloxy)-2-((octanoyloxy)methyl) propanoate (800 mg, 2.00 mmol, 2.0 equiv.), and Milli-Q water (15 mL). The solution stirred at room temperature for 16 h. A second layer did not form so no workup nor characterization was performed.

#### 2.4.10 Synthesis of second-generation dichain fatty acid anions and corresponding ILs

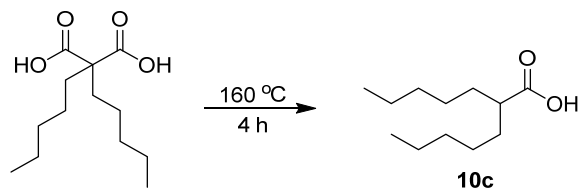


**diethyl 2,2-dipentylmalonate (10a):** To a 250 mL round bottom flask was added sodium ethoxide (6.81 g, 100 mmol, 2.5 equiv.) and ethanol (100 mL). The mixture stirred until the salt dissolved. To the solution was then added diethyl malonate (6.07 mL, 40.0 mmol, 1.0 equiv.) and 1-bromopentane (12.4 mL, 100 mmol, 2.5 equiv.). The solution stirred at 90 °C for 16 h. The ethanol was removed *in vacuo*. To the resulting cream-colored oil was added water (104 mL). The mixture was stirred until the solid dissolved. Ethyl acetate (3x75 mL) was used to extract the aqueous phase. The organic layers were combined, washed with brine (1x150 mL), dried with MgSO<sub>4</sub>, and concentrated *in vacuo*. The resulting yellow/orange oil/solid was purified with flash chromatography using 97:3 hexanes and ethyl acetate as the mobile phase. The product (**10a**) was isolated as yellow oil in 58.5% yield. <sup>1</sup>H NMR (400 MHz, Chloroform-d) δ 4.24 – 4.12 (m, 0H), 4.17 (q, *J* = 7.1 Hz, 4H), 1.92 – 1.82 (m, 4H), 1.38 (s, 13H), 1.39 – 1.17 (m, 14H), 1.22 – 1.09 (m, 4H), 0.87 (t, *J* = 6.9 Hz, 6H); <sup>13</sup>C NMR (101 MHz, Chloroform-d) δ 171.79, 77.42, 77.10, 76.78, 60.68, 57.39, 31.97, 31.91, 28.57, 23.45, 22.23, 13.92, 13.76.

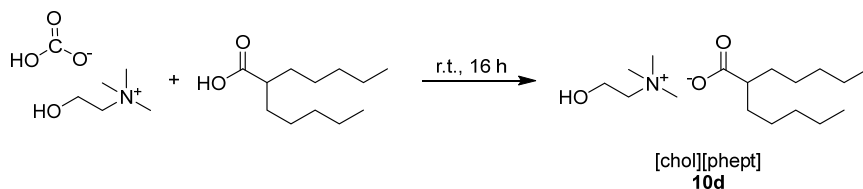


**2,2-dipentylmalonic acid (10b):** To a 125 mL Erlenmeyer flask was added sodium hydroxide (9.35 g, 234 mmol, 10 equiv.) and water (22 mL). The solution stirred until the sodium hydroxide pellets dissolved. This solution was transferred to a 250 mL round bottom containing **10a** (diethyl-2,2-dipentylmalonate; 7.02 g, 23.4 mmol, 1.0 equiv.) and ethanol (22 mL). The reaction stirred at 80 °C for 16 h. The ethanol was removed *in vacuo* leaving a sticky brown solid. The solid was resuspended in water (100 mL) and extracted with ethyl acetate (3x50 mL) and diethyl ether (1x50 mL). The aqueous layer was then separated and acidified to pH 1 using HCl (6 M). The aqueous layer was then extracted with ethyl acetate (2x50 mL). The organic fractions were combined, washed with brine (1x100 mL), dried with magnesium sulfate, and concentrated *in vacuo*, to reveal the product (**10b**) as a yellow/orange solid. <sup>1</sup>H NMR (400 MHz,

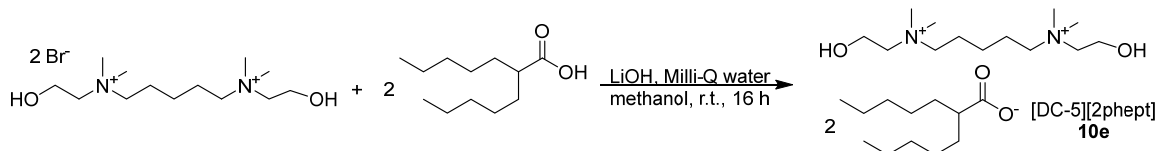
Chloroform-d)  $\delta$  11.88 (s, 2H), 2.00 – 1.84 (m, 4H), 1.40 – 1.17 (m, 12H), 0.96 – 0.79 (m, 6H);  $^{13}\text{C}$  NMR (101 MHz, Chloroform-d)  $\delta$  178.04, 77.34, 77.02, 76.70, 57.94, 34.49, 31.82, 24.18, 22.29, 13.92.



**2-pentylheptanoic acid (10c):** To a 50 mL round bottom flask was added **10b** (dipentylmalonic acid). A needle connected to a bubbler was attached and the reaction flask was placed in a silicone oil bath and heated to 160 °C for 4 h with stirring. The resulting compound was a dark brown liquid. The liquid was purified using flash chromatography with a 9:1 hexanes and ethyl acetate mobile phase. The product (**10c**) was isolated as a light brown liquid;  $^1\text{H}$  NMR (400 MHz,  $\text{CDCl}_3$ )  $\delta$  12.11 (s, 1H), 2.34 (td,  $J = 8.8, 4.5$  Hz, 1H), 1.62 (ddd,  $J = 14.2, 8.8, 5.7$  Hz, 2H), 1.46 (ddd,  $J = 13.3, 8.0, 5.4$  Hz, 2H), 1.31 (dt,  $J = 15.1, 5.8$  Hz, 12H), 1.07 – 0.67 (m, 6H).

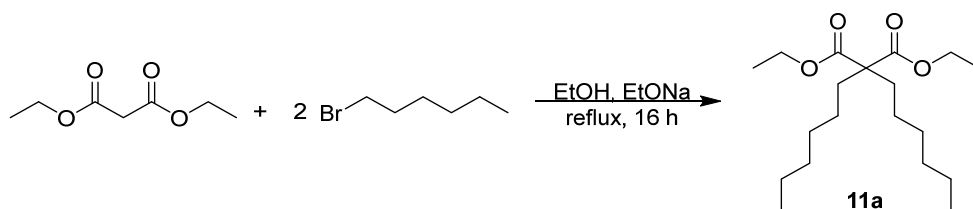


**2-hydroxy-*N,N,N*-trimethylethan-1-aminium 2-pentylheptanoate (10d):** To a 25 mL round bottom flask was added **10c** (2-pentylheptanoic acid; 657 mg, 3.28 mmol, 1.0 equiv.). A bubbler was connected to the flask and choline bicarbonate (80% in water; 0.868 mL, 4.92 mmol, 1.5 equiv.) was added slowly. After all the choline bicarbonate was added, the reaction stirred at room temperature for 16 h. Since no second layer was observed, the reaction was not worked up nor analyzed further.

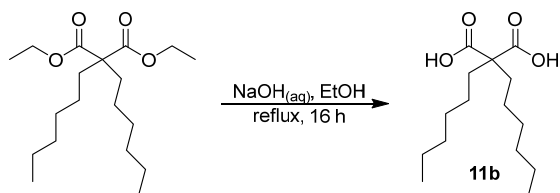


***N*<sup>1</sup>,*N*<sup>5</sup>-bis(2-hydroxyethyl)-*N*<sup>1</sup>*N*<sup>1</sup>,*N*<sup>5</sup>,*N*<sup>5</sup>-tetramethylpentane-1,5-diaminium 2-pentylheptanoate (10e):**

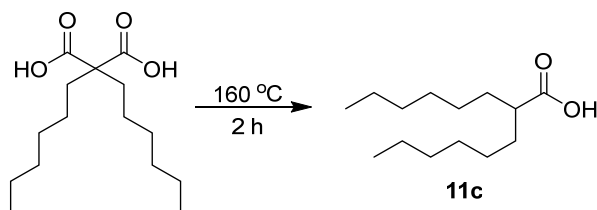
To a 100 mL round bottom flask was added **10c** (2-pentylheptanoic acid; 0.689 g, 3.44 mmol, 1.5 equiv.), lithium hydroxide (0.082 g, 3.44 mmol, 1.5 equiv.), and Milli-Q water (10 mL). The mixture stirred until the components dissolved. Then, **4d** ([DC-5][2Br]; 0.936 g, 2.29 mmol, 1.0 equiv.) and methanol were added. The reaction stirred at room temperature for 16 h. The solvent was removed *in vacuo* revealing a water soluble solid. Since the compound is solid and water soluble, no further workup nor analysis was performed.



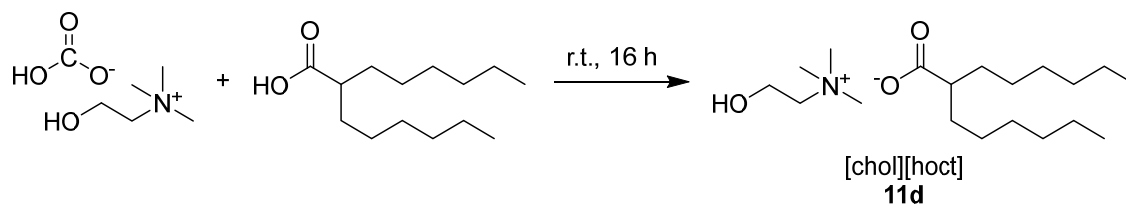
**diethyl 2,2-dihexylmalonate (11a):** To a 250 mL round bottom flask was added sodium ethoxide (8.305 g, 122 mmol, 3 equiv.) and ethanol (140 mL). The solution stirred until all the sodium ethoxide dissolved. Then, diethyl malonate (6.07 mL, 40 mmol, 1.0 equiv.) and 1-bromohexane (20.212 mL, 144 mmol, 3.5 equiv.) was added. The reaction stirred at 80 °C for 16 h. The ethanol was removed *in vacuo*. To the resulting cream-colored oil was added water (140 mL), where the mixture was stirred until all the solid was dissolved. Ethyl acetate (3x50 mL) was used to extract the aqueous phase. The organic layers were combined, dried with MgSO<sub>4</sub>, and concentrated *in vacuo*. The resulting yellow/orange oil/solid was purified with flash chromatography using 4:1 hexanes and ethyl acetate as the mobile phase. The product (**11a**) was isolated as a yellow oil in 69.3% yield. <sup>1</sup>H NMR (400 MHz, Chloroform-d) δ 4.16 (q, *J* = 7.2 Hz, 5H), 1.94 – 1.81 (m, 4H), 1.27 (ddd, *J* = 17.3, 13.1, 7.6 Hz, 18H), 1.16 (ddt, *J* = 15.9, 11.7, 4.9 Hz, 4H), 0.94 (d, *J* = 7.4 Hz, 0H), 0.94 – 0.84 (m, 6H); <sup>13</sup>C NMR (101 MHz, Chloroform-d) δ 171.62, 60.56, 57.31, 31.98, 31.36, 29.36, 23.69, 22.37, 13.87, 13.77.



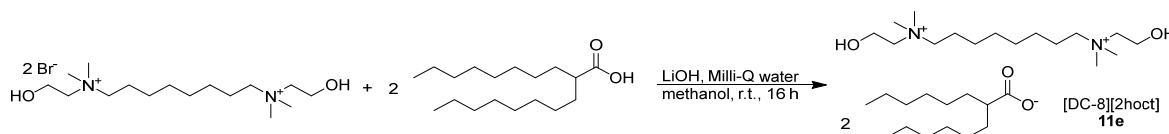
**2,2-dihexylmalonic acid (11b):** To a 125 mL Erlenmeyer flask was added sodium hydroxide (5.48 g, 137 mmol, 10 equiv.) and water (20 mL). The mixture stirred until all the sodium hydroxide dissolved. The aqueous solution was transferred to a 100 mL round bottom flask containing **11a** (diethyl-2,2-dihexylmalonate; 4.50 g, 13.7 mmol, 1.0 equiv.) and ethanol (17 mL). The solution stirred at 80 °C for 16 h. The solvent was removed *in vacuo* and a solid remained. The solid was acidified using HCl (50 mL, 6 M). The aqueous layer was extracted with ethyl acetate (2x50 mL). The organic layers were combined, washed with brine (1x100 mL), dried with magnesium sulfate, and concentrated *in vacuo*. The product (**11b**) was isolated in 52.7% yield. <sup>1</sup>H NMR (400 MHz, Chloroform-d) δ 10.77 (s, 2H), 1.99 – 1.89 (m, 4H), 1.44 – 1.17 (m, 16H), 0.92 – 0.84 (m, 6H); <sup>13</sup>C NMR (101 MHz, Chloroform-d) δ 177.71, 175.06, 77.34, 77.02, 76.70, 57.89, 51.51, 34.68, 31.44, 31.43, 29.33, 28.81, 27.20, 24.52, 22.54, 22.53, 14.01.



**2-hexyloctanoic acid (11c):** To a 25 mL round bottom was added **11b** (2,2-dihexylmalonic acid; 2.253 g, 8.27 mmol). The round bottom was submerged in an oil bath set to 160 °C. A bubbler was connected to the round bottom flask and the reaction stopped after no carbon dioxide bubbles appeared (~2 h). The product (**11c**) was observed as a viscous oil in 99% yield. <sup>1</sup>H NMR (400 MHz, Chloroform-d) δ 12.02 (s, 1H), 2.34 (qt, *J* = 8.6, 3.7 Hz, 1H), 1.62 (qd, *J* = 8.5, 7.9, 3.7 Hz, 2H), 1.53 – 1.41 (m, 2H), 1.37 – 1.21 (m, 12H), 0.92 – 0.84 (m, 6H); <sup>13</sup>C NMR (101 MHz, Chloroform-d) δ 183.50, 77.32, 77.01, 76.69, 45.67, 32.20, 31.67, 29.23, 27.33, 22.60, 14.02.

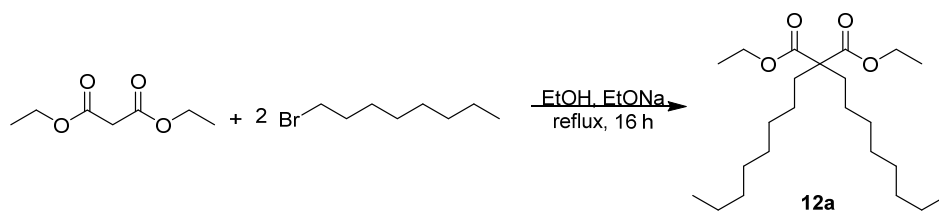


**2-hydroxy-*N,N,N*-trimethylethan-1-aminium 2-hexyloctanoate (11d):** To a 25 mL round bottom flask was added **11c** (2-hexyloctanoic acid; 750 mg, 3.28 mmol, 1.0 equiv.). A bubbler was connected to the flask and choline bicarbonate (80% in water; 2.0 mL, 11.33 mmol, 3.5 equiv.) was added slowly. After all the choline bicarbonate was added, the reaction stirred at room temperature for 16 h. Then, to the flask was added acetone (5 mL) and Milli-Q water (5 mL), which resulted in the formation of a clear bottom layer and a yellow top layer. The top layer was isolated and concentrated *in vacuo* to reveal the product (**11d**) as a water-soluble liquid.  $^1\text{H}$  NMR (400 MHz, Chloroform-*d*)  $\delta$  4.01 (dq,  $J = 7.5, 2.5$  Hz, 2H), 3.62 – 3.52 (m, 2H), 3.25 (s, 9H), 2.06 (ddd,  $J = 13.9, 7.9, 5.7$  Hz, 1H), 1.52 – 1.28 (m, 4H), 1.25 (d,  $J = 8.1$  Hz, 18H), 0.87 (t,  $J = 6.8$  Hz, 6H);  $^{13}\text{C}$  NMR (101 MHz, Chloroform-*d*)  $\delta$  183.24, 77.44, 77.12, 76.80, 68.00, 55.80, 54.27, 54.23, 54.20, 49.07, 33.05, 31.83, 29.57, 27.89, 22.64, 14.04.

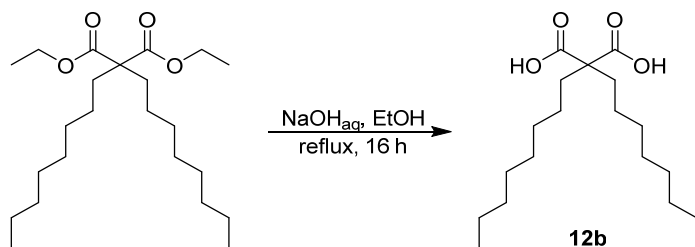


***N*<sup>1</sup>,*N*<sup>8</sup>-bis(2-hydroxyethyl)-*N*<sup>1</sup>*N*<sup>1</sup>,*N*<sup>8</sup>,*N*<sup>8</sup>-tetramethyloctane-1,8-diaminium 2-hexyloctanoate (11e):** To a 50 mL round bottom flask was added **11c** (2-hexyloctanoic acid; 0.785 g, 3.44 mmol, 2.0 equiv.), lithium hydroxide (100 mg, 4.17 mmol, 2.4 equiv.), and methanol (25 mL). The reaction stirred for 30 min at room temperature. Then, to the solution was added **4g** ([DC-8][2Br]; 0.797 g, 1.77 mmol, 1.0 equiv.). The reaction stirred at room temperature for 16 h. After, the solvent was removed *in vacuo* to reveal a solid. The solid was washed with Milli-Q water (3x10 mL). Residual water was removed *in vacuo*. Since the solid had little [DC-8], the compound was not worked up nor analyzed further.  $^1\text{H}$  NMR (400 MHz, Chloroform-*d*)  $\delta$  4.18 – 4.02 (m, 1H), 3.69 – 3.57 (m, 1H), 3.50 – 3.33 (m, 1H), 3.27 (s, 2H), 2.31 – 2.16 (m, 1H), 1.82 (s,

1H), 1.61 – 1.50 (m, 3H), 1.42 (s, 3H), 1.27 (h,  $J = 6.8$  Hz, 18H), 0.87 (t,  $J = 6.7$  Hz, 6H);  $^{13}\text{C}$  NMR (101 MHz, Chloroform-d)  $\delta$  77.34, 77.02, 76.70, 46.64, 32.53, 31.80, 29.44, 27.54, 22.69, 14.10.

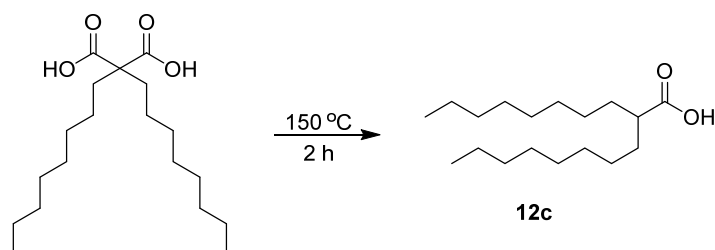


**diethyl 2,2-dioctylmalonate (12a):** To a 250 mL round bottom flask was added sodium ethoxide (68.1 g, 100 mmol, 2.5 equiv.) and ethanol (100 mL). The mixture stirred until the salt dissolved. To the solution was then added diethyl malonate (6.07 mL, 40.0 mmol, 1.0 equiv.) and 1-bromooctane (17.3 mL, 100 mmol, 2.5 equiv.). The solution stirred at 90° C for 16 h. The ethanol was removed *in vacuo*. To the resulting cream-colored oil was added water (104 mL), where the mixture was stirred until all the solid was dissolved. Ethyl acetate (3x75 mL) was used to extract the aqueous phase. The organic layers were combined, washed with brine (1x150 mL), dried with  $\text{MgSO}_4$ , and concentrated *in vacuo*. The resulting yellow/orange oil/solid was purified with flash chromatography using 4:1 hexanes and ethyl acetate as the mobile phase. The product (12a) was isolated as a yellow oil in 40.0% yield.  $^1\text{H}$  NMR (400 MHz, Chloroform-d)  $\delta$  4.17 (q,  $J = 7.1$  Hz, 4H), 1.92 – 1.82 (m, 4H), 1.60 (s, 0H), 1.45 – 1.07 (m, 33H), 0.88 (t,  $J = 6.8$  Hz, 6H);  $^{13}\text{C}$  NMR (101 MHz,  $\text{CDCl}_3$ )  $\delta$  171.86, 77.37, 77.05, 76.74, 70.71, 65.94, 60.73, 57.44, 32.03, 31.78, 29.78, 29.43, 29.22, 29.13, 26.18, 23.81, 22.58, 15.13, 14.00, 13.96.



**2,2-dioctylmalonic acid (12b):** To a 125 mL Erlenmeyer flask was added sodium hydroxide (5.27 g, 132 mmol, 10 equiv.) and water (17 mL). The mixture stirred until all the sodium hydroxide dissolved. To a 100 mL round bottom flask was added 12a (diethyl-2,2-dioctylmalonate; 5.07 g, 13.2 mmol, 1.0 equiv.),

ethanol (17 mL), and the aqueous sodium hydroxide solution. The solution stirred at 80 °C overnight. The ethanol was removed *in vacuo* and a white solid precipitated out of solution. The white solid was filtered, washed with diethyl ether, and then placed in a round bottom flask. The solid was acidified using HCl (50 mL, 1.5 M). The aqueous layer was extracted with diethyl ether (2x50 mL). The organic layers were combined, washed with brine (1x100 mL), dried with magnesium sulfate, and concentrated *in vacuo*. The resulting oil was left at room temperature for 48 h where white solid precipitated out.. The solid was filtered and washed with ethyl acetate. The compound was then acidified using HCl (50 mL, 6 M), extracted with ethyl acetate (2x50 mL), dried with magnesium sulfate, and concentrated *in vacuo*. The product (**12b**) was isolated as an oil in 71.0% yield. <sup>1</sup>H NMR (400 MHz, Chloroform-d) δ 10.81 (s, 2H), 1.98 – 1.90 (m, 4H), 1.33 – 1.20 (m, 24H), 0.87 (t, *J* = 6.8 Hz, 6H); <sup>13</sup>C NMR (101 MHz, CDCl<sub>3</sub>) δ 177.50, 77.34, 77.02, 76.70, 57.84, 35.06, 31.81, 29.64, 29.22, 29.18, 24.66, 22.64, 14.09.

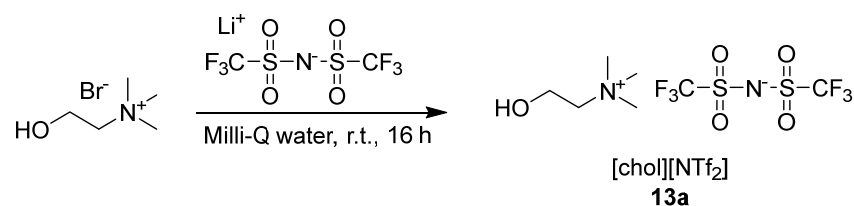


**2-octyldecanoic acid (12c):** To a 50 mL round bottom flask was added **12c** (2,2-dioctylmalonic acid; 3.076 g, 9.36 mmol, 1.0 equiv.). The reaction was attached to a bubbler and placed into a silicone oil bath. The bath was heated to 150 °C and the reaction stirred for 2 h. The flask was then put on high vacuum for 2 h, to reveal the product (**12c**) as a yellow oil in 99% yield. <sup>1</sup>H NMR (400 MHz, Chloroform-d) δ 11.66 (s, 1H), 2.34 (tt, *J* = 8.6, 5.2 Hz, 1H), 1.70 – 1.40 (m, 4H), 1.38 – 1.15 (m, 24H), 1.07 – 0.67 (m, 6H); <sup>13</sup>C NMR (101 MHz, CDCl<sub>3</sub>) δ 183.00, 77.33, 77.02, 76.70, 45.56, 32.18, 31.87, 29.57, 29.43, 29.27, 29.08, 27.37, 22.67, 14.10.

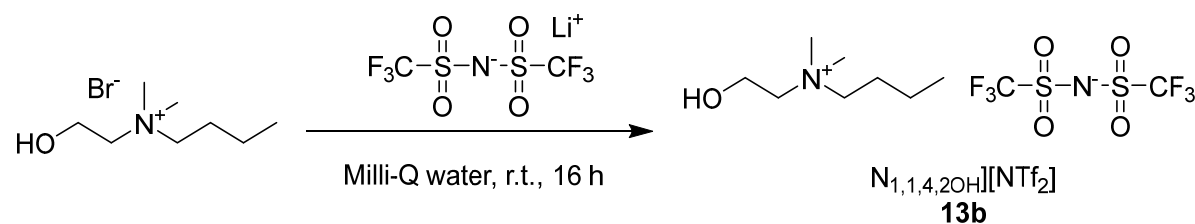


### 2.4.11 Synthesis of monocholinium, morpholinium, and dicholinium ILs containing [NTf<sub>2</sub>] anions

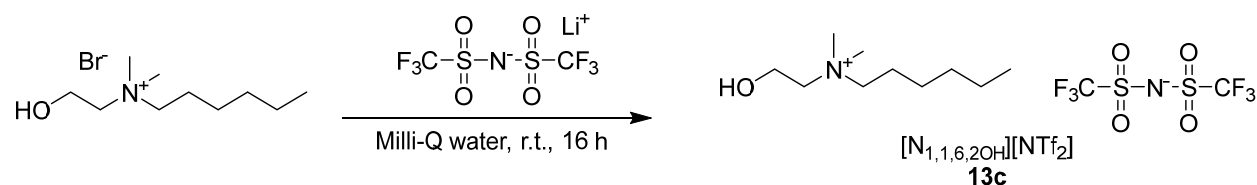
**General Procedure “D”:** Alky Cholinium Bis(triflate) ([N<sub>1,1,x,2OH</sub>][NTf<sub>2</sub>]) **Synthesis:** To a 50 mL round bottom flask was added the corresponding alkyl cholinium bromide, lithium bis(trifluoromethanesulfonyl)imide, and Millipore Milli-Q water (15 mL). The reaction stirred at room temperature for 16 h, in which a second layer formed. Water was removed *in vacuo*. The crude product was dissolved in acetone, in which excess alkyl cholinium bromide precipitated. The solid was filtered, washed with acetone (3x5 mL), and the filtrate was collected and concentrated *in vacuo*. The resulting ionic liquid was mixed with DCM (10 mL). The DCM and ionic liquid mixture was washed with Millipore Milli-Q water until the water wash showed no precipitant upon addition of silver nitrate. DCM and residual water were removed via a rotary evaporator followed by a vacuum oven set to 80 °C.



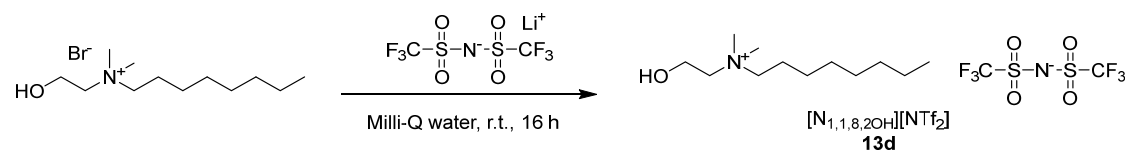
**2-hydroxy-*N,N,N*-trimethylethan-1-aminium bis((trifluoromethyl)sulfonyl)azanide (13a):** The general procedure “C” was applied to **1** ([chol][Br]; 4.90 g, 26.6 mmol, 1.5 equiv.) and lithium bis(trifluoromethanesulfonyl)imide (5.09 g, 17.7 mmol, 1.0 equiv.). The product (**13a**) was isolated as a clear liquid in 74.8% yield. <sup>1</sup>H NMR (400 MHz, Acetone-d<sub>6</sub>) δ 4.54 (t, J = 4.7 Hz, 1H), 4.20 – 4.12 (m, 2H), 3.73 – 3.66 (m, 2H), 3.40 (d, J = 1.0 Hz, 9H); <sup>13</sup>C{<sup>1</sup>H} NMR (101 MHz, Acetone-d<sub>6</sub>) δ 120.07 (q, J = 321.2 Hz), 68.50 – 67.05 (m), 56.12, 53.90 – 52.77 (m); <sup>19</sup>F NMR (376 MHz, Acetone-d<sub>6</sub>) δ -79.91.



***N*-(2-hydroxyethyl)-*N,N*-dimethylbutan-1-aminium bis((trifluoromethyl)sulfonyl)azanide (13b):** The general procedure “D” was applied to **2a** ( $[N_{1,1,4,2OH}][Br]$ ; 4.00 g, 17.7 mmol, 1.3 equiv.) and lithium bis(trifluoromethanesulfonyl)imide (3.91 g, 13.6 mmol, 1.0 equiv.). The product (**13b**) was isolated as a clear liquid in 53.2% yield.  $^1H$  NMR (400 MHz, Methanol- $d_4$ )  $\delta$  3.99 (dq,  $J = 7.7, 2.6$  Hz, 2H), 3.49 – 3.44 (m, 2H), 3.43 – 3.37 (m, 2H), 3.15 (s, 6H), 1.85 – 1.73 (m, 2H), 1.42 (h,  $J = 7.4$  Hz, 2H), 1.02 (t,  $J = 7.4$  Hz, 3H);  $^{13}C\{^1H\}$  NMR (101 MHz, Methanol- $d_4$ )  $\delta$  119.82 (q,  $J = 320.4$  Hz), 65.43 – 65.29 (m), 65.18 – 65.06 (m), 55.51, 51.20 – 50.60 (m), 24.14, 19.46 – 18.92 (m), 12.44;  $^{19}F$  NMR (376 MHz, Methanol- $d_4$ )  $\delta$  -80.53.

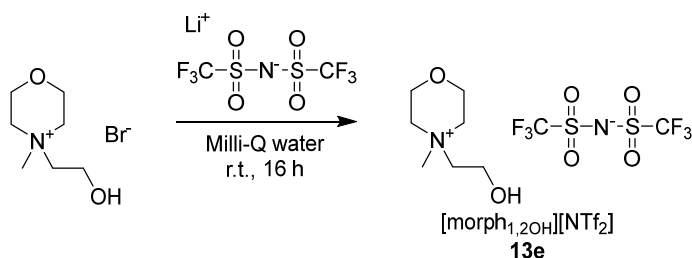


***N*-(2-hydroxyethyl)-*N,N*-dimethylhexan-1-aminium bis((trifluoromethyl)sulfonyl)azanide (13c):** The general procedure “D” was applied to **2c** ( $[N_{1,1,6,2OH}][Br]$ ; 4.30 g, 16.9 mmol, 1.3 equiv.) and lithium bis(trifluoromethanesulfonyl)imide (3.74 g, 13.0 mmol, 1.0 equiv.). The product (**13c**) was isolated as a clear liquid in 91.2% yield.  $^1H$  NMR (400 MHz, Methanol- $d_4$ )  $\delta$  4.58 (s, 1H), 3.99 (dq,  $J = 7.4, 2.4$  Hz, 2H), 3.50 – 3.42 (m, 2H), 3.41 – 3.34 (m, 2H), 3.14 (s, 6H), 1.85 – 1.73 (m, 2H), 1.42 – 1.32 (m, 6H), 0.97 – 0.88 (m, 3H);  $^{13}C\{^1H\}$  NMR (101 MHz, Methanol- $d_4$ )  $\delta$  119.81 (q,  $J = 320.5$  Hz), 65.63 (t,  $J = 2.5$  Hz), 65.08 (t,  $J = 2.7$  Hz), 55.56, 50.86 (t,  $J = 3.8$  Hz), 30.83, 25.51, 22.14, 22.03, 12.90;  $^{19}F$  NMR (376 MHz, Methanol- $d_4$ )  $\delta$  -80.32.

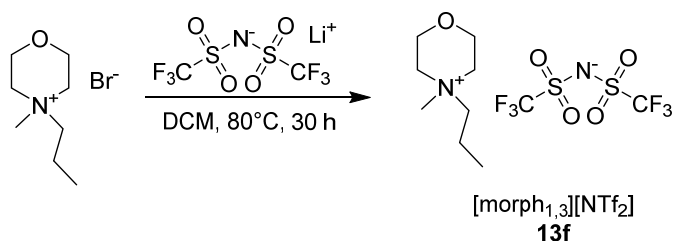


***N*-(2-hydroxyethyl)-*N,N*-dimethylhexan-1-aminium bis((trifluoromethyl)sulfonyl)azanide (13d):** The general procedure “D” was applied to **2d** ( $[N_{1,1,8,2OH}][Br]$ ; 4.60 g, 16.3 mmol, 1.3 equiv.) and lithium

bis(trifluoromethanesulfonyl)imide (3.60 g, 12.5 mmol, 1.0 equiv.). The product (**13d**) was isolated as a clear liquid in 57.4% yield.  $^1\text{H}$  NMR (400 MHz, Methanol- $d_4$ )  $\delta$  3.99 (dq,  $J = 5.1, 2.5$  Hz, 2H), 3.50 – 3.43 (m, 2H), 3.43 – 3.35 (m, 2H), 3.15 (s, 6H), 1.87 – 1.73 (m, 2H), 1.46 – 1.28 (m, 10H), 0.97 – 0.87 (m, 3H);  $^{13}\text{C}\{^1\text{H}\}$  NMR (101 MHz, Methanol- $d_4$ )  $\delta$  119.82 (q,  $J = 320.5$  Hz), 65.58 (t,  $J = 2.5$  Hz), 65.08 (t,  $J = 2.7$  Hz), 55.53, 51.00 – 50.53 (m), 31.43, 28.76, 28.68, 25.89, 22.24, 22.20, 13.06;  $^{19}\text{F}$  NMR (376 MHz, Methanol- $d_4$ )  $\delta$  -80.43.



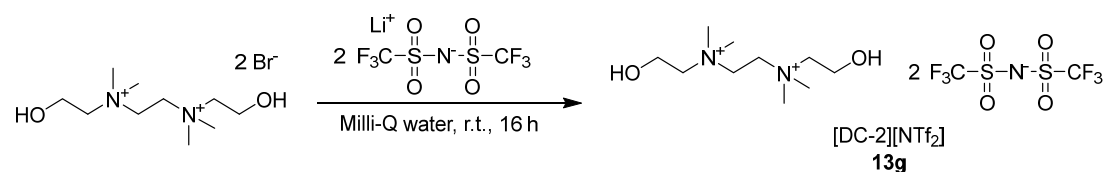
**4-(2-hydroxyethyl)-4-methylmorpholin-4-ium bis((trifluoromethyl)sulfonyl)azanide (13e):** To a 3 mL glass vial was added **3b** ([morph<sub>1,2OH</sub>][Br<sup>-</sup>]; 250 mg, 1.11 mmol, 1 equiv.), lithium bis(trifluoromethylsulfonyl)imide (317 mg, 1.11 mmol, 1 equiv.), and Milli-Q water (3 mL). The reaction stirred at room temperature for 16 h. Since a second layer did not form, the reaction was not worked up nor analyzed further.



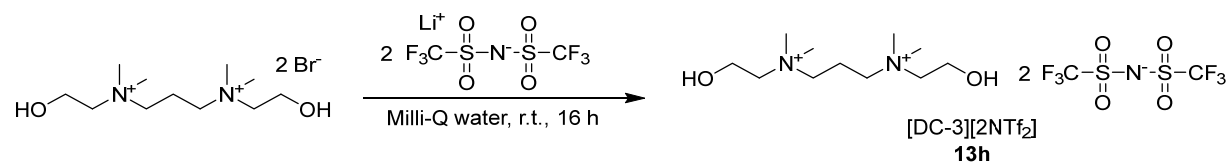
**4-methyl-4-propylmorpholin-4-ium bis((trifluoromethyl)sulfonyl)azanide (13f):** To a 250 mL round bottom flask equipped with a reflux condenser was added **3c** ([morph<sub>1,3</sub>][Br<sup>-</sup>]; 2.73 g, 12.2 mmol, 1.0 equiv.), lithium bis(trifluoromethylsulfonyl)imide, and DCM (50 mL). The reaction stirred at 80 °C for 30 h. The reaction was then filtered and then stirred in activated charcoal at room temperature for 12 h. The charcoal

was filtered off and the filtrate was concentrated *in vacuo*. The product (**13f**) was isolated as a gel, and as such, no further workup nor analysis was performed.

**General Procedure “E”: Dicholinium Bis(triflate) ([DC-X][2NTf<sub>2</sub>]) Synthesis:** To a 100 mL round bottom flask was added the corresponding dicholinium bromide, lithium bis(trifluoromethanesulfonyl)imide, and Millipore Milli-Q water (15 mL). The solution stirred at room temperature for 16 h, in which a second layer formed. The upper water layer was removed, and the ionic liquid layer was washed with Millipore Milli-Q water until the water wash showed no precipitant upon addition of silver nitrate. Residual water was removed by a vacuum oven set to 80 °C.

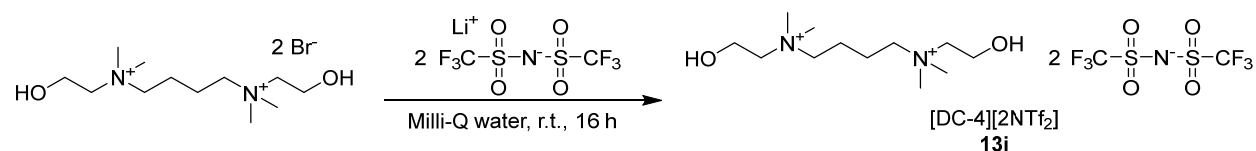


**N<sup>1</sup>,N<sup>2</sup>-bis(2-hydroxyethyl)-N<sup>1</sup>,N<sup>1</sup>,N<sup>2</sup>,N<sup>2</sup>-tetramethylethane-1,2-diaminium bis((trifluoromethyl)sulfonyl)azanide (**13g**):** The general procedure “E” was applied to **4a** ([DC-2][2Br<sup>-</sup>]; 1.00 g, 2.72 mmol, 1.0 equiv.) and lithium bis(trifluoromethanesulfonyl)imide (1.58 g, 5.49 mmol, 2.0 equiv.). The product (**13g**) was isolated as a clear liquid in 14.7% yield. <sup>1</sup>H NMR (400 MHz, Methanol-d<sub>4</sub>) δ 4.01 (dq, *J* = 7.6, 2.6 Hz, 4H), 3.90 – 3.73 (m, 8H), 3.56 – 3.48 (m, 4H), 3.21 (s, 12H); <sup>13</sup>C NMR (101 MHz, Methanol-d<sub>4</sub>) δ 119.75 (q, *J* = 320.3 Hz), 65.32 (dt, *J* = 66.8, 2.5 Hz), 55.51, 51.30 (t, *J* = 3.6 Hz); <sup>19</sup>F NMR (376 MHz, Methanol-d<sub>4</sub>) δ -80.24.

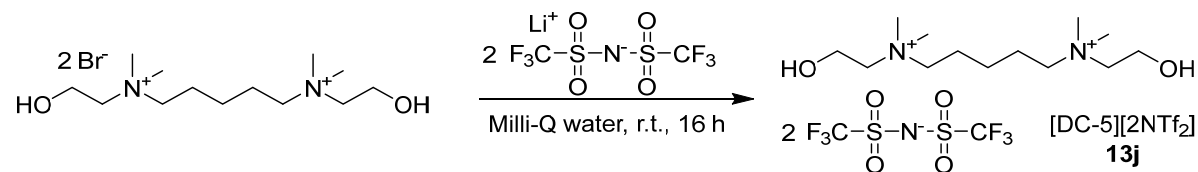


**N<sup>1</sup>,N<sup>3</sup>-bis(2-hydroxyethyl)-N<sup>1</sup>,N<sup>1</sup>,N<sup>3</sup>,N<sup>3</sup>-tetramethylpropane-1,3-diaminium bis((trifluoromethyl)sulfonyl)azanide (**13h**):** The general procedure “E” was applied to **4b** ([DC-3][2Br<sup>-</sup>]; 1.00 g, 2.63 mmol, 1.0 equiv.) and lithium bis(trifluoromethanesulfonyl)imide (1.51 g, 5.26 mmol, 2.0 equiv.). The product

(**13h**) was isolated as a clear solid in 36.6% yield.  $^1\text{H}$  NMR (400 MHz, Methanol- $d_4$ )  $\delta$  3.91 (dq,  $J = 5.2$ , 2.5 Hz, 4H), 3.49 – 3.42 (m, 4H), 3.41 – 3.31 (m, 4H), 3.12 (s, 12H), 2.27 (td,  $J = 10.4$ , 9.2, 6.4 Hz, 2H);  $^{13}\text{C}$  NMR (101 MHz, Methanol- $d_4$ )  $\delta$  119.79 (d,  $J = 320.1$  Hz), 65.57, 61.22, 55.41, 51.25, 16.99;  $^{19}\text{F}$  NMR (376 MHz, Methanol- $d_4$ )  $\delta$  -80.64.

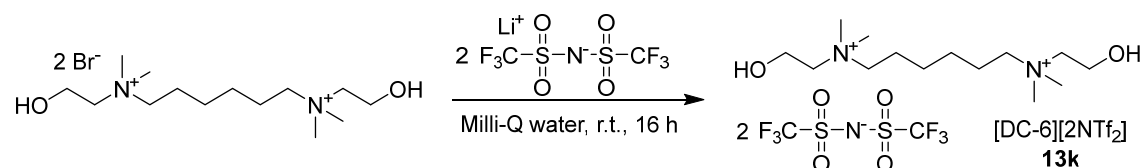


**$N^1,N^4$ -bis(2-hydroxyethyl)- $N^1,N^1,N^4,N^4$ -tetramethylbutane-1,4-diaminium bis((trifluoromethyl)sulfonyl)azanide (**13i**):** The general procedure “E” was applied to **4c** ([DC-4][2Br]; 6.00 g, 15.2 mmol, 1.0 equiv.) and lithium bis(trifluoromethanesulfonyl)imide (4.37 g, 15.2 mmol, 1.0 equiv.). The product (**13i**) was isolated as a clear solid in 62.4% yield.  $^1\text{H}$  NMR (400 MHz, Acetone- $d_6$ )  $\delta$  4.56 (t,  $J = 4.6$  Hz, 2H), 4.16 (ddt,  $J = 7.4$ , 5.1, 2.6 Hz, 4H), 3.77 – 3.67 (m, 8H), 3.37 (s, 12H), 2.20 – 2.09 (m, 4H);  $^{13}\text{C}$  { $^1\text{H}$ } NMR (101 MHz, Acetone- $d_6$ )  $\delta$  120.07 (q,  $J = 321.2$  Hz), 65.93 – 65.55 (m), 64.70 – 64.18 (m), 55.90, 51.73 – 51.27 (m), 19.81 – 19.30 (m);  $^{19}\text{F}$  NMR (376 MHz, Acetone- $d_6$ )  $\delta$  -79.86.

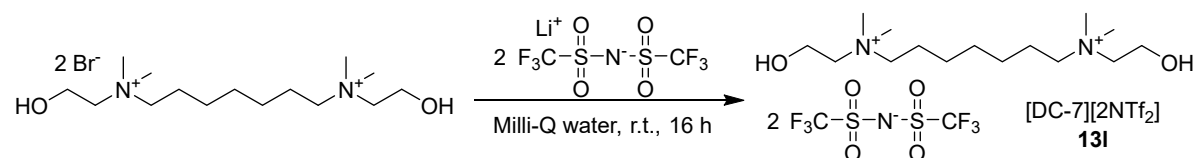


**$N^1,N^5$ -bis(2-hydroxyethyl)- $N^1,N^1,N^5,N^5$ -tetramethylpentane-1,5-diaminium bis((trifluoromethyl)sulfonyl)azanide (**13j**):** The general procedure “E” was applied to **4d** ([DC-5][2Br]; 6.33 g, 15.6 mmol, 1.0 equiv.) and lithium bis(trifluoromethanesulfonyl)imide (8.95 g, 31.2 mmol, 2.0 equiv.). The product (**13j**) was isolated as a clear liquid in 80.5% yield.  $^1\text{H}$  NMR (400 MHz, Acetone- $d_6$ )  $\delta$  4.52 (t,  $J = 4.6$  Hz, 2H), 4.14 (ddt,  $J = 7.4$ , 5.0, 2.5 Hz, 4H), 3.70 – 3.63 (m, 4H), 3.67 – 3.58 (m, 4H), 3.33 (s, 12H), 2.13 – 2.01 (m, 3H), 1.56 (q,  $J = 7.7$  Hz, 2H);  $^{13}\text{C}$  NMR (101 MHz, Acetone- $d_6$ )  $\delta$  120.04 (q,  $J = 321.2$  Hz), 65.55,

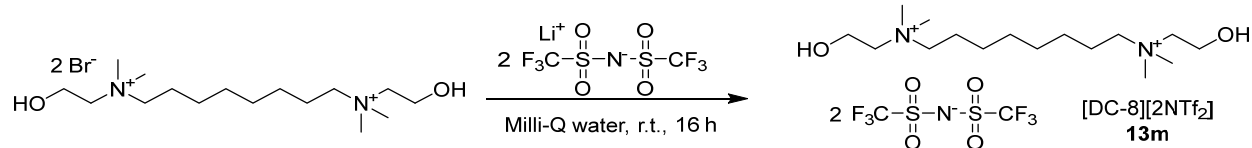
65.52, 65.49, 65.08, 65.05, 65.02, 55.90, 51.43, 51.39, 51.35, 22.84, 21.91;  $^{19}\text{F}$  NMR (376 MHz, Acetone- $d_6$ )  $\delta$  -79.85.



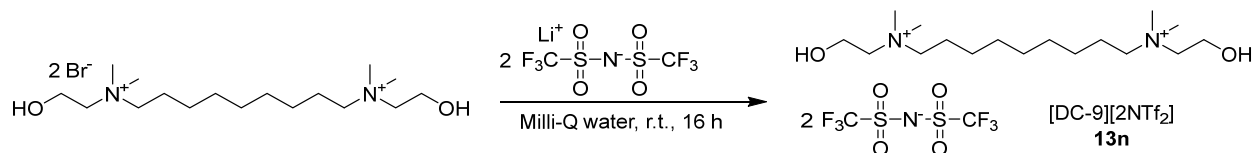
***N*<sup>1</sup>,*N*<sup>6</sup>-bis(2-hydroxyethyl)-*N*<sup>1</sup>,*N*<sup>1</sup>,*N*<sup>6</sup>,*N*<sup>6</sup>-tetramethylhexane-1,6-diaminium bis((trifluoromethyl)sulfonyl)azanide (13k):** The general procedure “E” was applied to **4e** ([DC-6][2NTf<sub>2</sub>]; 6.00 g, 14.2 mmol, 1.0 equiv.) and lithium bis(trifluoromethanesulfonyl)imide (4.08 g, 14.2 mmol, 1.0 equiv.). The product (**13k**) was isolated as a clear liquid in 76.2% yield.  $^1\text{H}$  NMR (400 MHz, Methanol- $d_4$ )  $\delta$  4.07 – 3.95 (m, 6H), 3.44 (dd,  $J$  = 6.4, 3.5 Hz, 4H), 3.39 – 3.31 (m, 4H), 3.12 (s, 12H), 1.81 (qd,  $J$  = 8.8, 5.4, 4.7 Hz, 4H), 1.45 (d,  $J$  = 6.4 Hz, 4H);  $^{13}\text{C}\{^1\text{H}\}$  NMR (101 MHz, Methanol- $d_4$ )  $\delta$  119.77 (q,  $J$  = 320.3 Hz), 65.26 (d,  $J$  = 20.8 Hz), 55.63 (d,  $J$  = 11.7 Hz), 50.99, 24.90, 21.69;  $^{19}\text{F}$  NMR (376 MHz, Methanol- $d_4$ )  $\delta$  -80.10.



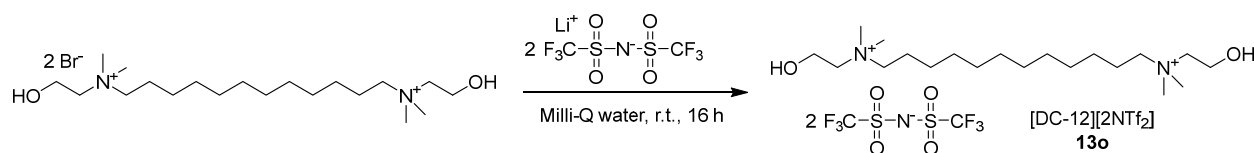
***N*<sup>1</sup>,*N*<sup>7</sup>-bis(2-hydroxyethyl)-*N*<sup>1</sup>,*N*<sup>1</sup>,*N*<sup>7</sup>,*N*<sup>7</sup>-tetramethylheptane-1,7-diaminium bis((trifluoromethyl)sulfonyl)azanide (13l):** The general procedure “E” was applied to **4f** ([DC-7][2NTf<sub>2</sub>]; 3.74 g, 8.58 mmol, 1.0 equiv.) and lithium bis(trifluoromethanesulfonyl)imide (4.08 g, 14.2 mmol, 1.66 equiv.). The product (**13l**) was isolated as a clear liquid in 76.8% yield.  $^1\text{H}$  NMR (400 MHz, Acetone- $d_6$ )  $\delta$  4.54 (t,  $J$  = 4.7 Hz, 2H), 4.15 (qt,  $J$  = 5.0, 2.6 Hz, 4H), 3.72 – 3.64 (m, 4H), 3.64 – 3.54 (m, 4H), 3.33 (s, 12H), 2.01 – 1.89 (m, 4H), 1.59 – 1.45 (m, 4H), 1.48 – 1.39 (m, 2H);  $^{13}\text{C}$  NMR (101 MHz, Acetone- $d_6$ )  $\delta$  205.59, 120.08 (q,  $J$  = 321.3 Hz), 65.72 – 65.24 (m), 55.91, 51.44 – 51.20 (m), 28.26, 25.78, 22.21;  $^{19}\text{F}$  NMR (376 MHz, Acetone- $d_6$ )  $\delta$  -79.86.



***N*<sup>1</sup>,*N*<sup>8</sup>-bis(2-hydroxyethyl)-*N*<sup>1</sup>,*N*<sup>1</sup>,*N*<sup>8</sup>,*N*<sup>8</sup>-tetramethyloctane-1,8-diaminium bis((trifluoromethyl)sulfonyl)azanide (**13m**):** The general procedure “E” was applied to **4g** ([DC-8][2Br<sup>-</sup>]; 3.00 g, 6.46 mmol, 1.0 equiv.) and lithium bis(trifluoromethanesulfonyl)imide (3.71 g, 12.9 mmol, 2.0 equiv.). The product (**13m**) was isolated as a clear liquid in 78.6% yield. <sup>1</sup>H NMR (400 MHz, Acetone-d<sub>6</sub>) δ 4.49 (t, *J* = 4.7 Hz, 2H), 4.14 (qt, *J* = 5.0, 2.5 Hz, 4H), 3.69 – 3.62 (m, 4H), 3.61 – 3.52 (m, 4H), 3.32 (s, 12H), 1.92 (dq, *J* = 13.8, 7.1 Hz, 4H), 1.42 (d, *J* = 7.3 Hz, 8H); <sup>13</sup>C{<sup>1</sup>H} NMR (101 MHz, Acetone-d<sub>6</sub>) δ 120.07 (q, *J* = 321.2 Hz), 65.48 (dt, *J* = 7.6, 2.7 Hz), 55.92, 51.53 – 51.05 (m), 28.54, 25.87, 22.27; <sup>19</sup>F NMR (376 MHz, Acetone-d<sub>6</sub>) δ -79.83.

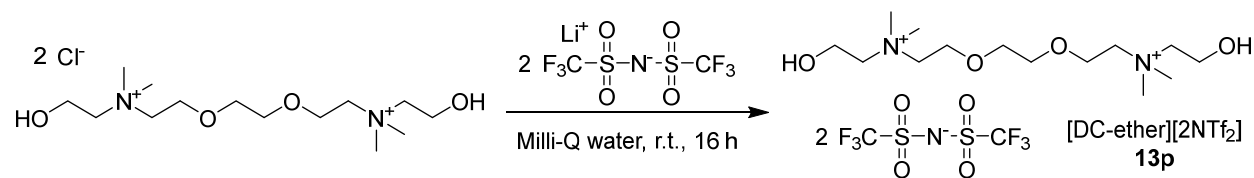


***N*<sup>1</sup>,*N*<sup>9</sup>-bis(2-hydroxyethyl)-*N*<sup>1</sup>,*N*<sup>1</sup>,*N*<sup>9</sup>,*N*<sup>9</sup>-tetramethylnonane-1,9-diaminium bis((trifluoromethyl)sulfonyl)azanide (**13n**):** The general procedure “E” was applied to **4h** ([DC-9][2Br<sup>-</sup>]; 3.03 g, 6.53 mmol, 1.0 equiv.) and lithium bis(trifluoromethanesulfonyl)imide (3.75 g, 13.1 mmol, 2.0 equiv.). The product (**13n**) was isolated as a clear liquid in 61.4% yield. <sup>1</sup>H NMR (400 MHz, Acetone-d<sub>6</sub>) δ 4.53 (t, *J* = 4.7 Hz, 2H), 4.13 (qt, *J* = 5.0, 2.4 Hz, 4H), 3.68 – 3.61 (m, 4H), 3.60 – 3.52 (m, 4H), 3.32 (s, 12H), 1.92 (tt, *J* = 10.4, 6.1 Hz, 4H), 1.44 – 1.37 (m, 10H); <sup>13</sup>C NMR (101 MHz, Acetone-d<sub>6</sub>) δ 120.07 (q, *J* = 321.3 Hz), 65.49 (dt, *J* = 11.0, 2.8 Hz), 55.91, 51.61 – 51.01 (m), 28.86, 28.67, 25.97, 22.30; <sup>19</sup>F NMR (376 MHz, Acetone-d<sub>6</sub>) δ -79.84.



*N*<sup>1</sup>,*N*<sup>12</sup>-bis(2-hydroxyethyl)-*N*<sup>1</sup>,*N*<sup>1</sup>,*N*<sup>12</sup>,*N*<sup>12</sup>-tetramethyldodecane-1,12-diaminium

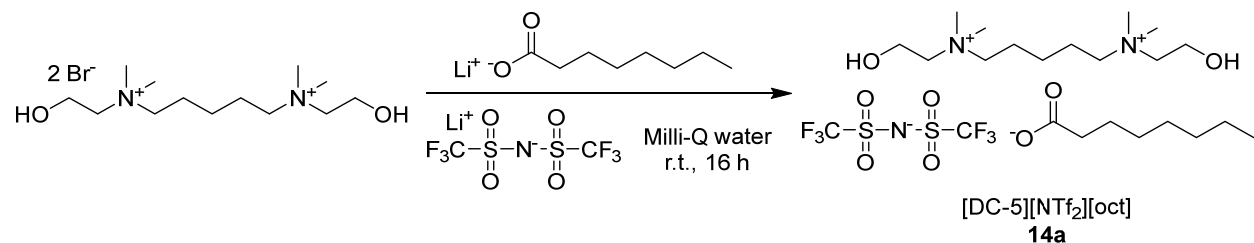
**bis((trifluoromethyl) sulfonyl)azanide (13o):** The general procedure “E” was applied to **4i** ([DC-12][2Br]; 400 mg, 0.790 mmol, 1.0 equiv.) and lithium bis(trifluoromethanesulfonyl)imide (454 mg, 1.58 mmol, 2.0 equiv.). The product (**13o**) was isolated as a clear liquid. <sup>1</sup>H NMR (400 MHz, Acetone-d<sub>6</sub>) δ 4.42 – 4.34 (m, 2H), 4.19 – 4.02 (m, 4H), 3.63 – 3.55 (m, 4H), 3.54 – 3.45 (m, 4H), 3.26 (s, 12H), 1.86 (dq, *J* = 14.1, 6.3, 5.3 Hz, 4H), 1.47 – 1.20 (m, 16H); <sup>13</sup>C NMR (101 MHz, Acetone) δ 119.98 (q, *J* = 321.1 Hz), 65.59, 65.29 (d, *J* = 2.8 Hz), 55.91, 51.23 (t, *J* = 3.6 Hz), 29.06, 29.00, 28.72, 25.93, 22.25; <sup>19</sup>F NMR (376 MHz, Acetone) δ -79.75.



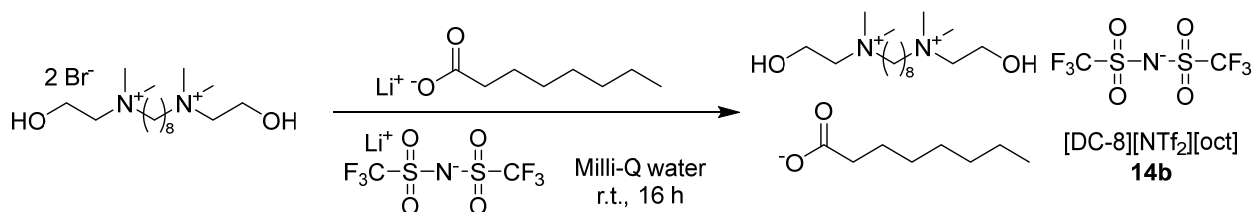
**2,2'-(ethane-1,2-diylbis(oxy))bis(N-(2-hydroxyethyl)-*N,N*-dimethylethan-1-aminium)**

**bis((trifluoromethyl)sulfonyl)azanide (13p):** The general procedure “E” was applied to **4j** ([DC-ether][2Cl]; 4.17 g, 11.4 mmol, 1.0 equiv.), lithium bis(trifluoromethanesulfonyl)imide (6.00 g, 20.9 mmol, 1.8 equiv.), and Millipore Milli-Q water (15 mL). The product (**13p**) was isolated as a clear liquid in 73.6% yield. <sup>1</sup>H NMR (400 MHz, Acetone-d<sub>6</sub>) δ 4.54 (qd, *J* = 6.3, 5.4, 3.2 Hz, 2H), 4.18 (tq, *J* = 4.9, 2.6 Hz, 4H), 4.12 (qt, *J* = 5.0, 2.5 Hz, 4H), 3.93 – 3.86 (m, 4H), 3.82 – 3.75 (m, 8H), 3.42 (s, 12H); <sup>13</sup>C {<sup>1</sup>H} NMR (101 MHz, Acetone-d<sub>6</sub>) δ 120.08 (q, *J* = 321.2 Hz), 69.94, 66.84 – 66.71 (m), 64.82 – 64.68 (m), 64.54, 55.97, 52.37 – 52.15 (m); <sup>19</sup>F NMR (376 MHz, Acetone-d<sub>6</sub>) δ -79.89.

*2.4.12 Synthesis of dicholinium ILS containing octanoate and [NTf<sub>2</sub>] anions*

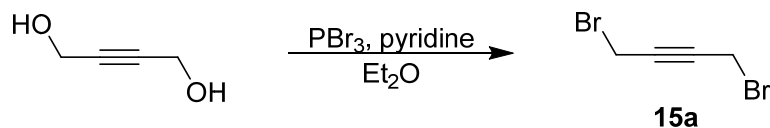


***N*<sup>1</sup>,*N*<sup>5</sup>-bis(2-hydroxyethyl)-*N*<sup>1</sup>,*N*<sup>1</sup>,*N*<sup>5</sup>,*N*<sup>5</sup>-tetramethylpentane-1,5-diaminium octanoate bis((trifluoromethyl)sulfonyl)azanide (14a):** To a 50 mL round bottom flask was added **4d** ([DC-5][2Br]; 250 mg, 0.612 mmol, 1.0 equiv.), lithium octanoate (92 mg, 0.612 mmol, 1.0 equiv.), lithium bis(trifluoromethylsulfonyl)imide (176 mg, 0.612 mmol, 1.0 equiv.), and Milli-Q water (25 mL). The mixture stirred at room temperature for 16 h. A second layer emerged below the water layer. The water was removed, and the ionic liquid layer was washed with Milli-Q water (3x5 mL). The ionic liquid was then dried *in vacuo*. <sup>1</sup>H NMR (400 MHz, Acetone-d<sub>6</sub>) δ 4.63 (s, 2H), 4.15 (dq, *J* = 5.2, 2.6 Hz, 4H), 3.72 – 3.61 (m, 8H), 3.36 (s, 12H), 2.16 – 2.05 (m, 4H), 1.57 (p, *J* = 7.6 Hz, 2H); <sup>13</sup>C NMR (101 MHz, Acetone-d<sub>6</sub>) δ 120.08 (q, *J* = 321.3 Hz), 65.86 – 65.38 (m), 65.31 – 64.77 (m), 55.87, 51.59 – 51.18 (m), 22.90, 21.95; <sup>19</sup>F NMR (376 MHz, Acetone-d<sub>6</sub>) δ -79.88.

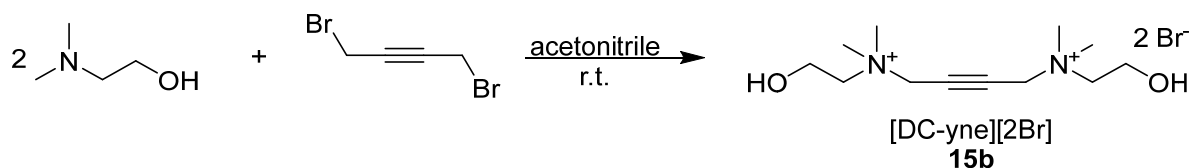


***N*<sup>8</sup>,*N*<sup>8</sup>-bis(2-hydroxyethyl)-*N*<sup>1</sup>,*N*<sup>1</sup>,*N*<sup>8</sup>,*N*<sup>8</sup>-tetramethyloctane-1,8-diaminium octanoate bis((trifluoromethyl)sulfonyl)azanide (14b):** To a 50 mL round bottom flask was added **4g** ([DC-8][2Br]; 276 mg, 0.612 mmol, 1.0 equiv.), lithium octanoate (92 mg, 0.612 mmol, 1.0 equiv.), lithium bis(trifluoromethylsulfonyl)imide (176 mg, 0.612 mmol, 1.0 equiv.), and Milli-Q water (25 mL). The mixture stirred at room temperature for 16 h. A second layer emerged below the water layer. The water was removed, and the ionic liquid layer was washed with Milli-Q water (3x5 mL). The ionic liquid was then dried *in vacuo*. <sup>1</sup>H NMR (400 MHz, Acetone-d<sub>6</sub>) δ 4.61 (s, 2H), 4.13 (dq, *J* = 7.6, 2.5 Hz, 4H), 3.69 – 3.62 (m, 4H), 3.61 – 3.53 (m, 4H), 3.32 (s, 12H), 1.93 (ddt, *J* = 14.5, 10.8, 5.5 Hz, 4H), 1.43 (d, *J* = 6.8 Hz, 8H); <sup>13</sup>C NMR (101 MHz, Acetone-d<sub>6</sub>) δ 120.07 (q, *J* = 321.3 Hz), 65.47 (q, *J* = 2.8 Hz), 55.88, 53.00 – 50.34 (m), 25.88, 22.27; <sup>19</sup>F NMR (376 MHz, Acetone-d<sub>6</sub>) δ -79.85.

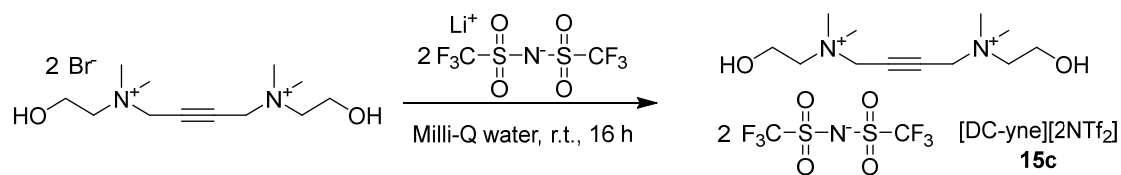
### 2.4.13 Synthesis of second-generation dicholinium cations



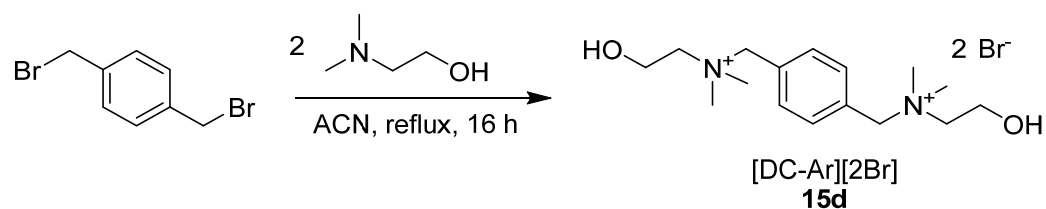
**1,4-dibromobut-2-yne (15a):** To a 250 mL round bottom was added 1,4-dihydroxybut-2-yne (5.64 g, 58.1 mmol, 5.64 equiv.), anhydrous diethyl ether (75 mL), and pyridine (0.830 mL, 10.3 mmol, 1.0 equiv.). The reaction vessel was purged with acetone and cooled to 0° C. Phosphorous tribromide (4.38 mL, 46.5 mmol, 4.5 equiv.) was added dropwise to the reaction. The solution stirred at 0° C for 30 min, then at reflux for 4 h. The solution was then left stirring at room temperature for 2 days. Water (30 mL) was added to quench the reaction. The aqueous layer was then separated and extracted with diethyl ether (50 mL). The organic layers were combined, washed with saturated sodium bicarbonate solution (1x100 mL) and brine (1x100 mL), dried with MgSO<sub>4</sub>, filtered, and concentrated *in vacuo*. The product (**15a**) was isolated in 90.3% yield. <sup>1</sup>H NMR (400 MHz, CDCl<sub>3</sub>) δ 4.00 (s, 4H); <sup>13</sup>C NMR (101 MHz, CDCl<sub>3</sub>) δ 81.78, 14.50.



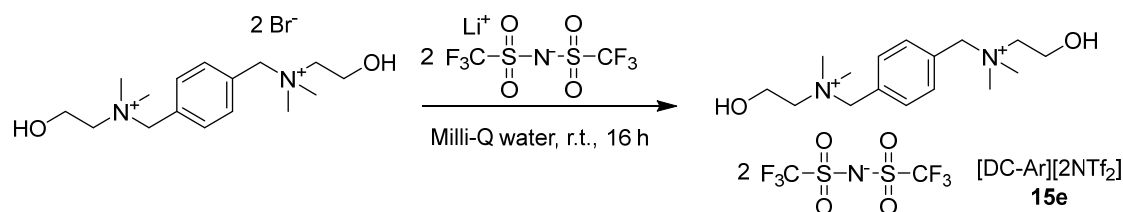
**N<sup>1</sup>,N<sup>4</sup>-bis(2-hydroxyethyl)-N<sup>1</sup>,N<sup>1</sup>,N<sup>4</sup>,N<sup>4</sup>-tetramethylbut-2-yne-1,4-diaminium bromide (15b):** To a 250 mL round bottom flask was added anhydrous acetonitrile (40 mL), dimethylaminoethanol (2.84 mL, 28.4 mmol, 2.0 equiv.), and **15a** (1,4-dibromobut-4-yne; 3 g, 14.2 mmol, 1.0 equiv.). Upon addition of **15a**, a solid immediately precipitated. The solution was filtered and the solid was washed with acetone (3x20 mL). Residual solvent was removed *in vacuo*. The product (**15b**) was isolated as a brown and white solid in 79.3% yield. <sup>1</sup>H NMR (400 MHz, Deuterium Oxide) δ 4.53 (s, 4H), 4.08 – 4.01 (m, 4H), 3.65 – 3.58 (m, 4H), 3.25 (s, 12H); <sup>13</sup>C NMR (101 MHz, Deuterium Oxide) δ 80.10, 65.55, 55.51, 55.43, 51.71; HSQC (Deuterium Oxide) δ {3.25, 51.62}, {4.53, 55.33}, {4.05, 55.49}, {3.62, 65.48}.



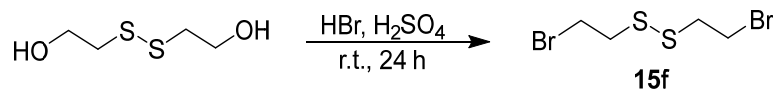
***N*<sup>1</sup>,*N*<sup>4</sup>-bis(2-hydroxyethyl)-*N*<sup>1</sup>,*N*<sup>1</sup>,*N*<sup>4</sup>,*N*<sup>4</sup>-tetramethylbut-2-yne-1,4-diaminium bis((trifluoromethyl)sulfonyl)azanide (15c):** To a 50 mL round bottom flask was added **15b** ([DC-yne][2Br]) (2.00 g, 5.13 mmol, 1.0 equiv.), bis(trifluoromethylsulfonyl)imide (3.39 g, 11.8 mmol, 2.3 equiv.), and Milli-Q water (15 mL). The reaction stirred overnight at room temperature. The water layer was removed, and the ionic liquid was washed with Milli-Q water (2x20 mL). A test with silver nitrate resulted in no precipitant, confirming the absence of the **15b** starting material. The residual water was removed *in vacuo*. The product (**15c**) was isolated as a solid in 33.3% yield. <sup>1</sup>H NMR (400 MHz, Methanol-d<sub>4</sub>) δ 4.59 (s, 4H), 4.08 – 4.01 (m, 4H), 3.66 – 3.59 (m, 4H), 3.30 (s, 12H); <sup>13</sup>C NMR (101 MHz, Methanol-d<sub>4</sub>) δ 119.77 (q, *J* = 320.3 Hz), 80.18, 65.69, 55.55, 55.10, 51.04; <sup>19</sup>F NMR (376 MHz, Methanol-d<sub>4</sub>) δ -80.55.



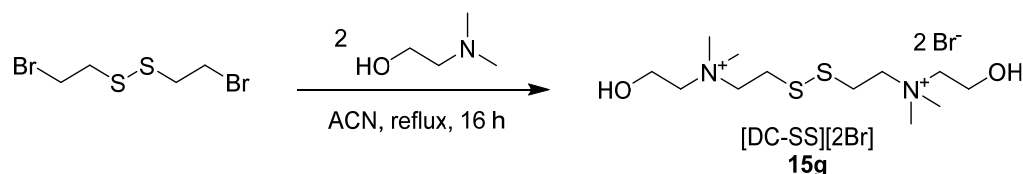
***N*<sup>1</sup>,*N*<sup>1</sup>-(1,4-phenylenebis(methylene))bis(2-hydroxy-*N*,*N*-dimethylethan-1-aminium) bromide (15d):** To a 250 mL round bottom flask was added 1,4-bis(bromomethyl)benzene (2.5 g, 9.74 mmol, 1.0 equiv.), dimethylaminoethanol (1.90 mL, 18.9 mmol, 2.0 equiv.), and anhydrous acetonitrile (50 mL). The reaction stirred at 80 °C for 16 h. A solid precipitated. The solid was then filtered and washed with acetone (3x25 mL). Residual solvent was removed *in vacuo*. The product (**15d**) was isolated as a solid in 71.6% yield. <sup>1</sup>H NMR (400 MHz, Deuterium Oxide) δ 7.67 (s, 4H), 4.60 (s, 4H), 4.08 (dq, *J* = 7.4, 2.4 Hz, 4H), 3.54 – 3.47 (m, 4H), 3.09 (s, 12H); <sup>13</sup>C NMR (101 MHz, Deuterium Oxide) δ 133.76, 129.63, 68.39, 65.52, 55.40, 50.61 – 50.31 (m).s



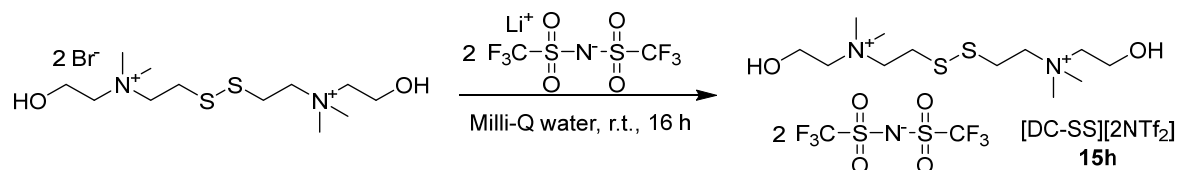
***N,N'*-(1,4-phenylenebis(methylene))bis(2-hydroxy-*N,N*-dimethylethan-1-aminium) bis((trifluoromethyl)sulfonyl)azanide (**15e**):** To a 50 mL round bottom flask was added **15d** ([DC-Ar][Br]; 3 g, 3.56 mmol, 1.0 equiv.), bis(trifluoromethylsulfonyl) imide (2.04 g, 7.12 mmol, 2.0 equiv.), and Milli-Q water (8 mL). The reaction stirred overnight at room temperature. The white solid precipitated, which was filtered off and washed with Milli-Q water (3x5 mL). Excess water was removed *in vacuo*. The product (**15e**) was isolated as a white solid. <sup>1</sup>H NMR (400 MHz, Acetone-d<sub>6</sub>) δ 7.93 (s, 4H), 4.94 (s, 2H), 4.84 (t, *J* = 4.5 Hz, 2H), 4.25 (tp, *J* = 4.9, 2.3 Hz, 4H), 3.77 – 3.70 (m, 4H), 3.35 (s, 12H); <sup>13</sup>C NMR (101 MHz, Acetone-d<sub>6</sub>) δ 133.99, 130.36, 120.08 (q, *J* = 321.2 Hz), 68.22, 65.89, 55.92, 50.52 (t, *J* = 3.8 Hz); <sup>19</sup>F NMR (376 MHz, Acetone-d<sub>6</sub>) δ -79.89.



**1,2-bis(2-bromoethyl)disulfane (**15f**):** To a 250 mL round bottom flask was added HBr (48% in water; 14 mL). The vessel was cooled to 0 °C and purged with argon. Then, hydrosulfuric acid (concentrated; 10 mL) and bis(2-hydroxyethyl)disulfide (0.790 mL, 6.48 mmol, 1.0 equiv.) were added dropwise to the reaction mixture. The solution stirred for 1 h at 0 °C, and then room temperature overnight. The solution turned a yellow-orange color. The product was extracted with diethyl ether (2x35 mL). The organic layers were collected, washed with brine (1x50 mL), washed with saturated sodium bicarbonate (1x50 mL), dried with magnesium sulfate, filtered, and concentrated *in vacuo*. The product (**15f**) was isolated as a yellow liquid in 86.3% yield. <sup>1</sup>H NMR (400 MHz, Chloroform-d) δ 3.66 – 3.58 (m, 4H), 3.15 – 3.06 (m, 4H); <sup>13</sup>C NMR (101 MHz, Chloroform-d) δ 40.56, 29.91.



**2,2'-disulfanediyldis(*N*-(2-hydroxyethyl)-*N,N*-dimethylethan-1-aminium) bromide (15g):** To a 250 mL round bottom flask was added dimethylaminoethanol (1.16 mL, 11.8 mmol, 2.0 equiv.), **15f** (1,2-bis(2-bromoethyl)disulfane; 1.56 g, 5.59 mmol, 1.0 equiv.), and anhydrous acetonitrile (25 mL). The reaction stirred at 80 °C for 16 h. A white solid precipitated which was filtered and washed with acetonitrile (3x15 mL). Residual solvent was removed *in vacuo*. The product (**15g**) was isolated as a white solid in 11.1%. <sup>1</sup>H NMR (400 MHz, Methanol-d<sub>4</sub>) δ 4.06 (dq, *J* = 7.6, 2.7 Hz, 4H), 3.90 – 3.82 (m, 4H), 3.67 – 3.60 (m, 4H), 3.36 – 3.32 (m, 4H), 3.30 (s, 12H); <sup>13</sup>C NMR (101 MHz, Methanol-d<sub>4</sub>) δ 65.68 – 65.39 (m), 64.27 (d, *J* = 2.3 Hz), 55.60, 51.40 – 51.16 (m), 30.28.

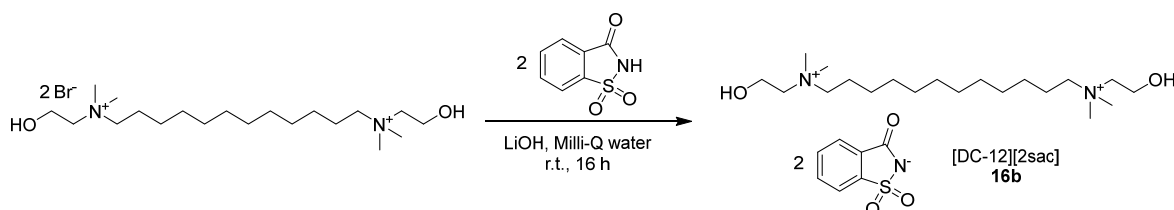


**2,2'-disulfanediyldis(*N*-(2-hydroxyethyl)-*N,N*-dimethylethan-1-aminium) bis((trifluoromethyl)sulfonyl)azanide (15h):** To a 100 mL round bottom flask was added **15g** ([DC-SS][2Br]; 370 mg, 0.807 mmol, 1.0 equiv.), bis(trifluoromethylsulfonyl)imide (463 mg, 1.61 mmol, 2.0 equiv.), and Milli-Q water (8 mL). The reaction stirred at room temperature overnight. A brown liquid layer precipitated out which was isolated and washed with Milli-Q water (2x10 mL). Residual water was removed *in vacuo* to reveal the product (**15h**) as a solid. <sup>1</sup>H NMR (400 MHz, Acetone-d<sub>6</sub>) δ 4.49 (t, *J* = 4.5 Hz, 2H), 4.05 (tt, *J* = 4.8, 2.4 Hz, 4H), 3.88 – 3.78 (m, 4H), 3.63 – 3.55 (m, 4H), 3.28 (d, *J* = 14.2 Hz, 16H); <sup>13</sup>C NMR (101 MHz, Acetone-d<sub>6</sub>) δ 120.03 (q, *J* = 321.2 Hz), 66.01 – 65.78 (m), 64.50 – 64.25 (m), 55.97 (d, *J* = 2.2 Hz), 51.72 – 51.46 (m), 30.02; <sup>19</sup>F NMR (376 MHz, Acetone-d<sub>6</sub>) δ -79.79.

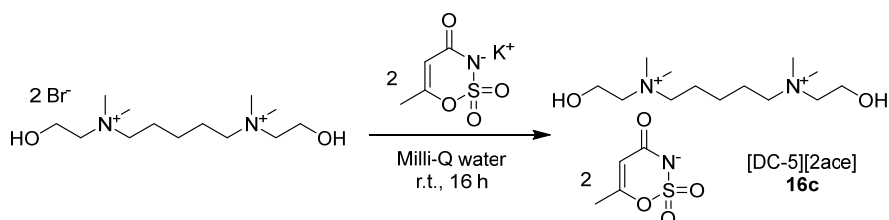
#### 2.4.14 Synthesis of dicholinium ILs composed of artificial sugar anions



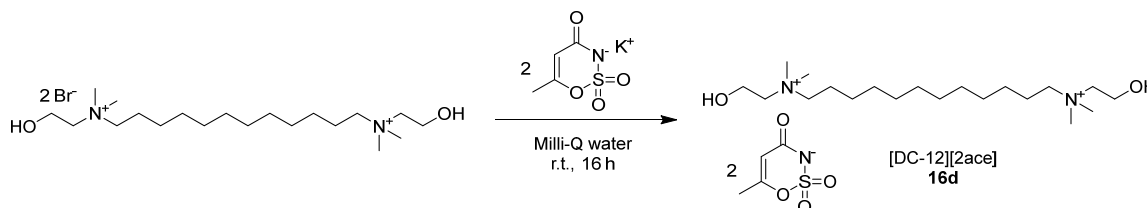
***N*<sup>1</sup>,*N*<sup>5</sup>-bis(2-hydroxyethyl)-*N*<sup>1</sup>,*N*<sup>1</sup>,*N*<sup>5</sup>,*N*<sup>5</sup>-tetramethylpentane-1,5-diaminium 3-oxo-3H-benzo[d]isothiazol-2-ide 1,1-dioxide (16a):** To a 100 mL round flask was added saccharin (447 mg, 2.44 mmol, 2.0 equiv.), lithium hydroxide (72.0 mg, 3.00 mmol, 2.46 equiv.), and Milli-Q water (50 mL). The reactions stirred at room temperature until the components dissolved. Then, **4d** ([DC-5][2Br]; 500 mg, 1.22 mmol, 1.0 equiv.) was added. The solution stirred at room temperature for 16 h. Since no second layer was observed, the reaction was not worked up nor characterized.



***N*<sup>1</sup>,*N*<sup>12</sup>-bis(2-hydroxyethyl)-*N*<sup>1</sup>,*N*<sup>1</sup>,*N*<sup>12</sup>,*N*<sup>12</sup>-tetramethyldodecane-1,12-diaminium 3-oxo-3H-benzo[d]isothiazol-2-ide 1,1-dioxide (16b):** To a 100 mL round flask was added saccharin (447 mg, 2.44 mmol, 2.0 equiv.), lithium hydroxide (72.0 mg, 3.00 mmol, 2.46 equiv.), and Milli-Q water (50 mL). The reactions stirred at room temperature until the components dissolved. Then, **4i** ([DC-12][2Br]; 618 mg, 1.22 mmol, 1.0 equiv.) was added. The solution stirred at room temperature for 16 h. Since no second layer was observed, the reaction was not worked up nor characterized.

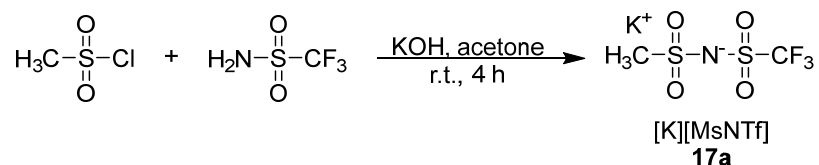


***N*<sup>1</sup>,*N*<sup>5</sup>-bis(2-hydroxyethyl)-*N*<sup>1</sup>,*N*<sup>1</sup>,*N*<sup>5</sup>,*N*<sup>5</sup>-tetramethylpentane-1,5-diaminium 6-methyl-4-oxo-4*H*-1,2,3-oxathiazin-3-ide 2,2-dioxide (16c)**: To a 50 mL round flask was added acesulfame K (491 mg, 2.44 mmol, 2.0 equiv.), **4d** ([DC-5][2Br]; 500 mg, 1.22 mmol, 1.0 equiv.), and Milli-Q water (50 mL). The solution stirred at room temperature for 16 h. Since no second layer was observed, the reaction was not worked up nor characterized.



***N*<sup>1</sup>,*N*<sup>12</sup>-bis(2-hydroxyethyl)-*N*<sup>1</sup>,*N*<sup>1</sup>,*N*<sup>12</sup>,*N*<sup>12</sup>-tetramethyldodecane-1,12-diaminium 6-methyl-4-oxo-4*H*-1,2,3-oxathiazin-3-ide 2,2-dioxide (16d)**: To a 100 mL round flask was added acesulfame K (491 mg, 2.44 mmol, 2.0 equiv.), **4i** ([DC-12][2Br]; 618 mg, 1.22 mmol, 1.0 equiv.), and Milli-Q water (25 mL). The solution stirred at room temperature for 16 h. Since no second layer was observed, the reaction was not worked up nor characterized.

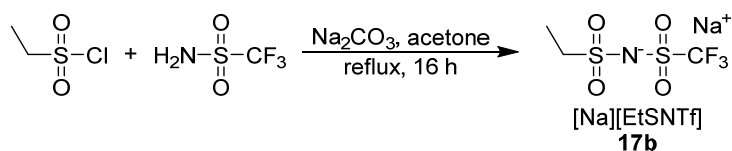
#### 2.4.15 Synthesis of first-generation bis(sulfonyl)azanide anions



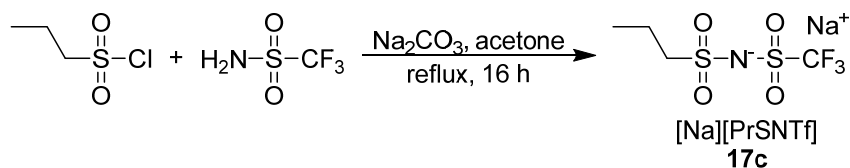
**potassium (methylsulfonyl)((trifluoromethyl)sulfonyl)azanide (17a)**: To a 50 mL round bottom flask was added trifluoromethanesulfonamide (1.00 g, 6.70 mmol, 1.0 equiv.), potassium hydroxide (0.752 g, 13.4 mmol, 2.0 equiv.), and acetone (20 mL). The mixture stirred at room temperature until the components dissolved. Then, mesyl chloride (0.519 mL, 6.7 mmol, 1.0 equiv.) was added to the flask. The reaction stirred at room temperature for 4 h. A solid precipitated, which was filtered, collected, and dried *in vacuo*. The crude solid was then stirred in ethyl acetate (40 mL) at room temperature for 1 h. An off-white solid precipitated, which was filtered, washed with ethyl acetate (3x20 mL), and residual solvent was removed

*in vacuo*. The product (**17a**) was isolated as an off-white solid in 36.2% yield.  $^1\text{H}$  NMR (400 MHz, Deuterium Oxide)  $\delta$  3.12 (s, 3H);  $^{13}\text{C}$  NMR (101 MHz, Deuterium Oxide)  $\delta$  121.26, 118.06, 114.88, 42.99;  $^{13}\text{C}$  NMR (101 MHz, Deuterium Oxide)  $\delta$  121.26, 118.06, 114.88, 42.99.

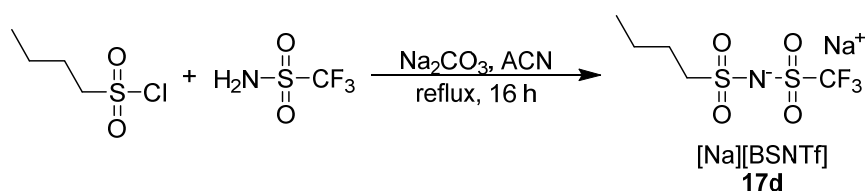
**General Procedure “F”: Sodium Asymmetric Bis(sulfonyl)azanide ([Na][XSNTf]) Synthesis:** A 100 mL round bottom flask equipped with a reflux condenser and attached to a bubbler was purged with argon. To the flask was added sodium carbonate, trifluoromethanesulfonamide, the corresponding sulfonyl chloride, and anhydrous acetonitrile or acetone (25 mL). The reaction stirred for 16 h at 80 °C. Afterwards, the white solid was filtered out, and the filtrate was collected and concentrated *in vacuo* to form a white solid. The white solid was resuspended in acetone (5 mL) and cooled to  $-20^\circ\text{C}$ , resulting in the precipitation of starting material. The solution was filtered, and the filtrate was collected and concentrated *in vacuo* to produce a white solid. Finally, the product stirred in toluene (50 mL) for 4 h. The solid was filtered, washed with toluene (3x5 mL), collected, and residual solvent was removed *in vacuo*.



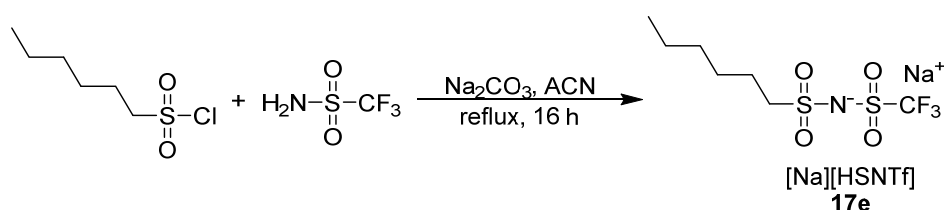
**sodium (ethylsulfonyl)((trifluoromethyl)sulfonyl)azanide (**17b**):** The general procedure “F” was applied to trifluoromethanesulfonamide (0.500 g, 3.35 mmol, 1.0 equiv.), sodium carbonate (0.745 g, 7.00 mmol, 2.1 equiv.), and 1-ethanesulfonyl chloride (0.317 mL, 3.35 mmol, 1.0 equiv.). The product (**17b**) was isolated as a white solid in 76.2% yield.  $^1\text{H}$  NMR (400 MHz, Deuterium Oxide)  $\delta$  3.19 (qd,  $J = 7.4, 0.8$  Hz, 2H), 1.30 (td,  $J = 7.4, 0.8$  Hz, 3H);  $^{13}\text{C}$  NMR (101 MHz, Deuterium Oxide)  $\delta$  121.25 (q), 50.01, 7.63;  $^{19}\text{F}$  NMR (376 MHz,  $\text{D}_2\text{O}$ )  $\delta$  -78.57.



**sodium (propylsulfonyl)((trifluoromethyl)sulfonyl)azanide (17c):** The general procedure “F” was applied to trifluoromethanesulfonamide (1.00 g, 6.70 mmol, 1.0 equiv.), sodium carbonate (1.49 g, 14.1 mmol, 2.1 equiv.), and 1-propanesulfonyl chloride (0.754 mL, 6.7 mmol, 1.0 equiv.). The product (17c) was isolated as a white solid in 68.2% yield.  $^1\text{H}$  NMR (400 MHz, Deuterium Oxide)  $\delta$  3.21 – 3.12 (m, 2H), 1.84 – 1.70 (m, 2H), 0.97 (t,  $J = 7.5$  Hz, 3H);  $^{13}\text{C}$  NMR (101 MHz, Deuterium Oxide)  $\delta$  57.05, 17.11, 12.01;  $^{19}\text{F}$  NMR (376 MHz, Deuterium Oxide)  $\delta$  -78.59.

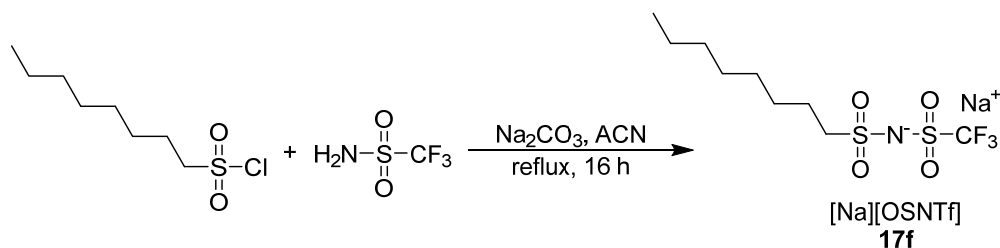


**sodium (butylsulfonyl)((trifluoromethyl)sulfonyl)azanide (17d):** The general procedure “F” was applied to trifluoromethanesulfonamide (2.38 g, 16.0 mmol, 1.0 equiv.), sodium carbonate (2.54 g, 24.0 mmol, 1.5 equiv.), and 1-butan sulfonyl chloride (2.07 mL, 16.0 mmol, 1.0 equiv.). The product (17d) was isolated as a white solid in 87.9% yield.  $^1\text{H}$  NMR (400 MHz, Deuterium Oxide)  $\delta$  3.29 – 3.13 (m, 1H), 1.82 – 1.67 (m, 1H), 1.42 (h,  $J = 7.4$  Hz, 1H), 0.88 (t,  $J = 7.4$  Hz, 1H);  $^{13}\text{C}\{^1\text{H}\}$  NMR (101 MHz, Deuterium Oxide)  $\delta$  119.67 (q,  $J = 320.9$  Hz), 55.08, 25.29, 20.75, 12.79;  $^{19}\text{F}$  NMR (376 MHz, Deuterium Oxide)  $\delta$  -78.53.

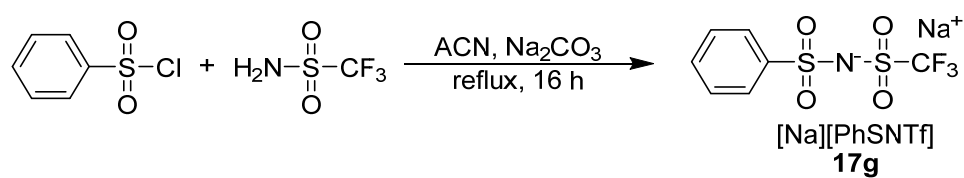


**sodium (hexylsulfonyl)((trifluoromethyl)sulfonyl)azanide (17e):** The general procedure “F” was applied to trifluoromethanesulfonamide (2.02 g, 13.5 mmol, 1.0 equiv.), sodium carbonate (2.15 g, 20.3 mmol, 1.5 equiv.), and 1-hexanesulfonyl chloride (2.20 mL, 13.5 mmol, 1.0 equiv.). The product (17e) was isolated as a white solid in 80.7 % yield.  $^1\text{H}$  NMR (400 MHz, Deuterium Oxide)  $\delta$  3.25 – 3.16 (m, 2H), 1.77 (p, 2H), 1.41 (p,  $J = 7.5$  Hz, 2H), 1.27 (h,  $J = 3.7$  Hz, 4H), 0.87 – 0.79 (m, 3H);  $^{13}\text{C}\{^1\text{H}\}$  NMR (101 MHz,

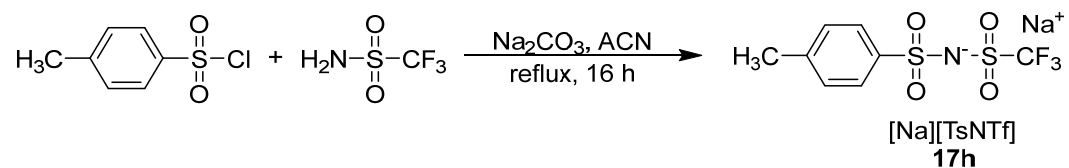
Deuterium Oxide)  $\delta$  119.68 (q,  $J = 321.0$  Hz), 55.30, 30.42, 26.94, 23.14, 21.69, 13.27;  $^{19}\text{F}$  NMR (376 MHz, Deuterium Oxide)  $\delta$  -78.52. HSQC (Deuterium Oxide)  $\delta$  {0.86, 13.25}, {1.30, 21.79}, {1.79, 23.24}, {1.43, 27.11}, {1.30, 30.50}, {3.21, 55.33}.



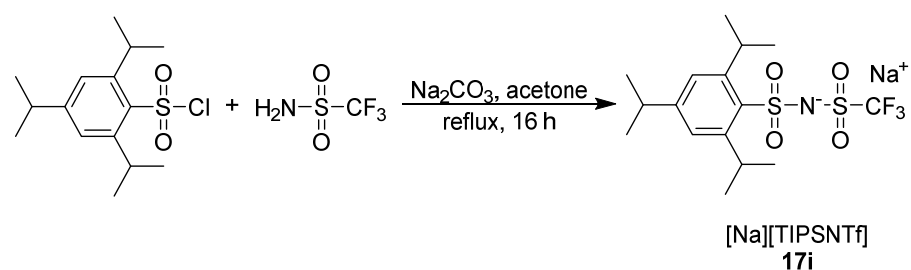
**sodium (octylsulfonyl)((trifluoromethyl)sulfonyl)azanide (17f):** The general procedure “F” was applied to trifluoromethanesulfonamide (2.38 g, 16.0 mmol, 1.0 equiv.), sodium carbonate (2.54 g, 24 mmol, 1.5 equiv.), and 1-octanesulfonyl chloride (3.13 mL, 16.0 mmol, 1.0 equiv.). The product (**17f**) was isolated as a white solid in 76.1% yield.  $^1\text{H}$  NMR (400 MHz, DMSO- $d_6$ )  $\delta$  2.98 – 2.90 (m, 1H), 1.65 (tt,  $J = 7.9, 6.2$  Hz, 1H), 1.40 – 1.30 (m, 1H), 1.33 – 1.23 (m, 4H), 0.91 – 0.83 (m, 1H);  $^{13}\text{C}\{^1\text{H}\}$  NMR (101 MHz, DMSO- $d_6$ )  $\delta$  120.62 (q,  $J = 324.5$  Hz), 54.96, 31.66, 29.07, 28.91, 28.17, 24.10, 22.54, 14.38;  $^{19}\text{F}$  NMR (376 MHz, DMSO- $d_6$ )  $\delta$  -77.57. HSQC (DMSO- $d_6$ )  $\delta$  {0.87, 13.84}, {1.26, 21.90}, {1.66, 23.51}, {1.34, 28.24}, {1.26, 29.05}, {1.25, 31.63}, {2.94, 54.47}.



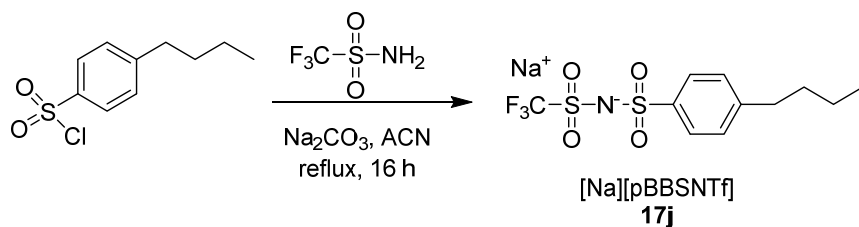
**sodium (phenylsulfonyl)((trifluoromethyl)sulfonyl)azanide (17g):** The general procedure “F” was applied to trifluoromethanesulfonamide (2.50 g, 16.8 mmol, 1.0 equiv.), sodium carbonate (2.67 g, 25.2 mmol, 1.5 equiv.), and benzenesulfonyl chloride (2.14 mL, 16.8 mmol, 1.0 equiv.). The product (**17g**) was isolated as a white solid in 92.1% yield.  $^1\text{H}$  NMR (400 MHz, Deuterium Oxide)  $\delta$  7.90 – 7.83 (m, 2H), 7.67 – 7.45 (m, 3H);  $^{13}\text{C}\{^1\text{H}\}$  NMR (101 MHz, Deuterium Oxide)  $\delta$  141.79, 133.15, 129.23, 126.03, 119.55 (q,  $J = 321.1$  Hz);  $^{19}\text{F}$  NMR (376 MHz, Deuterium Oxide)  $\delta$  -78.53.



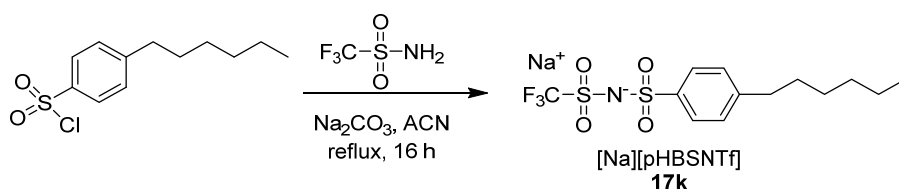
**sodium tosyl((trifluoromethyl)sulfonyl)azanide (17h):** The general procedure “F” was applied to trifluoromethanesulfonamide (2.50 g, 16.8 mmol, 1.0 equiv.), sodium carbonate (2.67 g, 25.2 mmol, 1.5 equiv.), and 4-toluenesulfonyl chloride (3.20 g, 16.8 mmol, 1.0 equiv.). The product (**17h**) was isolated as a white solid in 89.5% yield.  $^1\text{H}$  NMR (400 MHz, Deuterium Oxide)  $\delta$  7.74 – 7.67 (m, 2H), 7.26 – 7.18 (m, 2H), 2.23 (s, 3H);  $^{13}\text{C}\{^1\text{H}\}$  NMR (101 MHz, Deuterium Oxide)  $\delta$  144.31, 138.84, 129.63, 126.07, 119.65 (q,  $J = 321.3$  Hz), 20.62;  $^{19}\text{F}$  NMR (376 MHz, Deuterium Oxide)  $\delta$  -78.41.



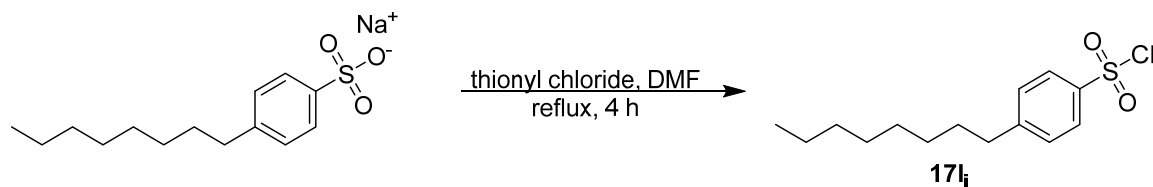
**sodium ((trifluoromethyl)sulfonyl)((2,4,6-triisopropylphenyl)sulfonyl)amide (17i):** The general procedure “F” was applied to trifluoromethanesulfonamide (0.500 g, 3.35 mmol, 1.0 equiv.), sodium carbonate (0.745 g, 7.00 mmol, 2.1 equiv.), and 2,4,6-triisopropylbenzenesulfonyl chloride (1.01 g, 3.35 mmol, 1.0 equiv.). The product (**17i**) was isolated as a white solid in 82.2% yield.  $^1\text{H}$  NMR (400 MHz, Deuterium Oxide)  $\delta$  7.03 (s, 2H), 4.08 (hept,  $J = 6.8$  Hz, 2H), 2.69 (h,  $J = 6.9$  Hz, 1H), 1.08 (d,  $J = 4.2$  Hz, 0H), 1.04 (dd,  $J = 9.7, 6.8$  Hz, 18H);  $^{13}\text{C}$  NMR (101 MHz, Deuterium Oxide)  $\delta$  152.14, 149.72, 135.95, 123.23, 119.75 (d,  $J = 322.3$  Hz), 33.80, 29.12, 23.98, 23.15;  $^{19}\text{F}$  NMR (376 MHz, Deuterium Oxide)  $\delta$  -78.30.



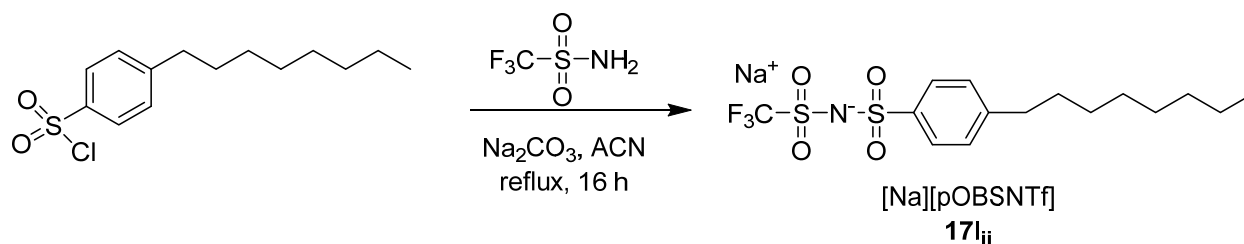
**sodium ((4-butylphenyl)sulfonyl)((trifluoromethyl)sulfonyl)azanide (17j):** The general procedure “F” was applied to trifluoromethanesulfonamide (1.92 g, 12.9 mmol, 1.2 equiv.), sodium carbonate (1.71 g, 16.1 mmol, 1.5 equiv.), and 4-butylbenzenesulfonyl chloride (2.50 g, 10.7 mmol, 1.0 equiv.). The product (**17j**) was isolated as a white solid in 97.9% yield.  $^1\text{H}$  NMR (400 MHz, Acetone- $d_6$ )  $\delta$  7.85 – 7.78 (m, 2H), 7.33 – 7.26 (m, 2H), 2.72 – 2.64 (m, 2H), 1.68 – 1.56 (m, 2H), 1.37 (dq,  $J = 14.7, 7.4$  Hz, 2H), 0.93 (t,  $J = 7.4$  Hz, 3H);  $^{13}\text{C}\{^1\text{H}\}$  NMR (101 MHz, Acetone- $d_6$ )  $\delta$  146.03, 143.29, 127.97, 126.44, 120.54 (q,  $J = 323.1$  Hz), 35.05, 33.33, 22.02, 13.24;  $^{19}\text{F}$  NMR (376 MHz, Acetone- $d_6$ )  $\delta$  -79.23.



**sodium ((4-hexylphenyl)sulfonyl)((trifluoromethyl)sulfonyl)azanide (17k):** The general procedure “E” was applied to trifluoromethanesulfonamide (0.685 g, 4.60 mmol, 1.2 equiv.), sodium carbonate (0.610 g, 5.76 mmol, 1.5 equiv.), and 4-hexylbenzenesulfonyl chloride (1.00 g, 3.83 mmol, 1.0 equiv.). The product (**17k**) was isolated as a white solid in 40.1% yield.  $^1\text{H}$  NMR (400 MHz, Deuterium Oxide)  $\delta$  7.79 – 7.53 (m, 2H), 7.17 – 7.01 (m, 2H), 2.41 (dd,  $J = 8.8, 6.7$  Hz, 2H), 1.51 – 1.27 (m, 2H), 1.12 (d,  $J = 4.7$  Hz, 6H), 0.82 – 0.62 (m, 3H);  $^{13}\text{C}\{^1\text{H}\}$  NMR (101 MHz, Deuterium Oxide)  $\delta$  147.98, 139.18, 128.57, 126.41, 119.63 (q,  $J = 321.7$  Hz), 35.29, 31.34, 30.61, 28.56, 22.26, 13.58;  $^{19}\text{F}$  NMR (376 MHz, Deuterium Oxide)  $\delta$  -78.49; HSQC (Deuterium Oxide)  $\delta$  {0.74, 13.57}, {1.13, 22.28}, {1.12, 28.57}, {1.38, 30.66}, {1.12, 31.31}, {7.67, 126.43}, {7.08, 128.53}.

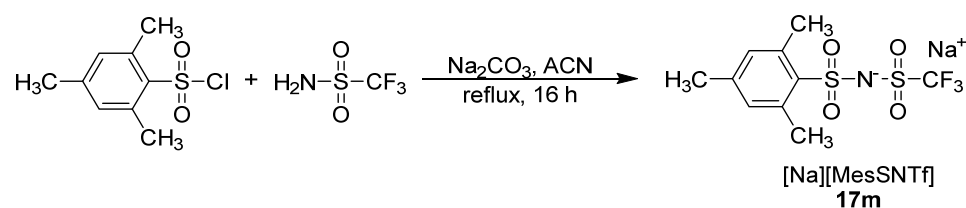


**4-octylbenzenesulfonyl chloride (17I<sub>i</sub>):** A 50 mL round bottom flask equipped with a reflux condenser was purged with argon. To the flask was added sodium 4-octylbenzenesulfonate (3.40 g, 11.6 mmol, 1.0 equiv.). Then, thionyl chloride (3.56 mL, 49.1 mmol, 4.25 equiv.) followed by dimethylformamide (1.25 mL, 16.2 mmol, 1.4 equiv.) were slowly added. The solution stirred at 80 °C for 4 h. The crude mixture was then added to a beaker of crushed ice water (100 mL). Once the ice melted, the organic and water layers were separated. The water layer was extracted with DCM (3x50 mL). The organic fractions were combined and washed with water (3x50 mL) followed by brine (1x50 mL). The organic layer was dried with magnesium sulfate, filtered, and concentrated *in vacuo* to produce an orange oil. The crude product was purified by flash chromatography using 9:1 hexanes and ethyl acetate as the mobile phase. Finally, the resulting pale orange liquid was further purified by stirring in a mixture of DCM and activated charcoal. After 4 h, the charcoal was filtered out and the solution was concentrated *in vacuo* to produce the product (**17I<sub>i</sub>**) as a yellow oil in 91.4% yield. <sup>1</sup>H NMR (400 MHz, Chloroform-d) δ 7.97 – 7.89 (m, 2H), 7.49 – 7.38 (m, 2H), 2.73 (dd, J = 8.7, 6.9 Hz, 2H), 1.71 – 1.59 (m, 2H), 1.39 – 1.24 (m, 10H), 0.92 – 0.84 (m, 3H); <sup>13</sup>C{<sup>1</sup>H} NMR (101 MHz, Chloroform-d) δ 151.77, 141.77, 129.64, 127.07, 36.07, 31.85, 30.95, 29.37, 29.21, 29.19, 22.66, 14.11.

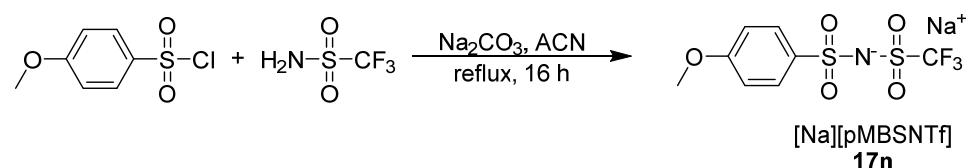


**sodium ((4-octylphenyl)sulfonyl)((trifluoromethyl)sulfonyl)azanide (17I<sub>ii</sub>):** The general procedure “F” was applied to trifluoromethanesulfonamide (1.89 g, 12.7 mmol, 1.2 equiv.), sodium carbonate (1.68 g,

15.8 mmol, 1.5 equiv.), and **17i** (3.05 g, 10.6 mmol, 1.0 equiv.). The product (**17i**) was isolated as a white solid in 93.1% yield.  $^1\text{H}$  NMR (400 MHz, DMSO- $d_6$ )  $\delta$  7.68 (d,  $J$  = 8.1 Hz, 2H), 7.29 (d,  $J$  = 8.1 Hz, 2H), 2.62 (t,  $J$  = 7.6 Hz, 2H), 1.58 (t,  $J$  = 7.4 Hz, 2H), 1.27 (dt,  $J$  = 15.4, 4.0 Hz, 11H), 0.86 (t,  $J$  = 6.7 Hz, 3H);  $^{13}\text{C}\{^1\text{H}\}$  NMR (101 MHz, DMSO- $d_6$ )  $\delta$  146.18, 143.13, 128.54, 126.60, 120.51 (q,  $J$  = 324.5 Hz), 35.35, 31.73, 31.16, 29.27, 29.12, 29.06, 22.55, 14.39;  $^{19}\text{F}$  NMR (376 MHz, DMSO- $d_6$ )  $\delta$  -77.82; HSQC (DMOS- $d_6$ )  $\delta$  {0.86, 14.38}, {1.25, 22.44}, {1.28, 29.21}, {1.58, 31.13}, {1.24, 31.79}, {7.67, 126.59}, {7.30, 128.53}.

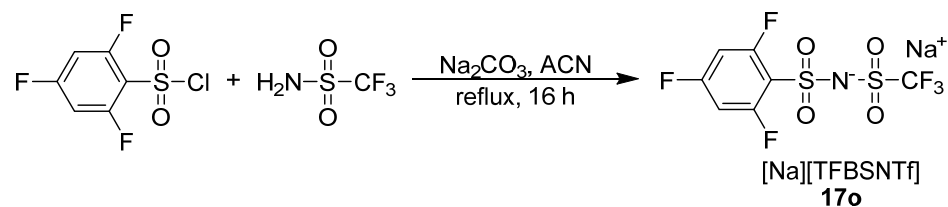


**sodium (mesitylsulfonyl)((trifluoromethyl)sulfonyl)azanide (17m):** The general procedure “F” was applied to trifluoromethanesulfonamide (2.50 g, 16.8 mmol, 1.0 equiv.), sodium carbonate (2.84 g, 26.8 mmol, 1.6 equiv.), and 2-mesitylenesulfonyl chloride (3.67 g, 16.8 mmol, 1.0 equiv.). The product (**17m**) was isolated as a white solid in 92.0% yield.  $^1\text{H}$  NMR (400 MHz, Deuterium Oxide)  $\delta$  6.93 (s, 2H), 2.52 (s, 6H), 2.14 (s, 3H);  $^{13}\text{C}\{^1\text{H}\}$  NMR (101 MHz, Deuterium Oxide)  $\delta$  143.11, 138.42, 136.09, 131.50, 119.58 (q,  $J$  = 319.8 Hz), 21.79, 19.97;  $^{19}\text{F}$  NMR (376 MHz, Deuterium Oxide)  $\delta$  -78.57.

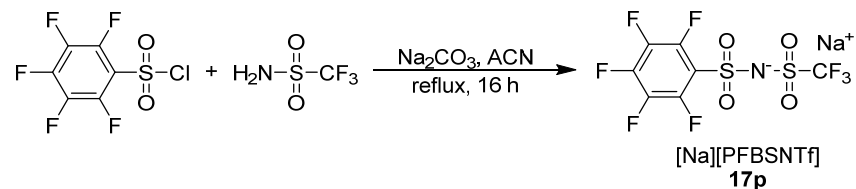


**sodium ((4-methoxyphenyl)sulfonyl)((trifluoromethyl)sulfonyl)azanide (17n):** The general procedure “F” was applied to trifluoromethanesulfonamide (2.50 g, 16.8 mmol, 1.0 equiv.), sodium carbonate (2.67 g, 25.2 mmol, 1.5 equiv.), and 4-methoxybenzenesulfonyl chloride (3.47 g, 16.8 mmol, 1.0 equiv.). The product (**17n**) was isolated as a white solid in 94.3% yield.  $^1\text{H}$  NMR (400 MHz, Deuterium Oxide)  $\delta$  7.82

- 7.73 (m, 2H), 7.05 – 6.97 (m, 2H), 3.79 (s, 3H);  $^{13}\text{C}\{^1\text{H}\}$  NMR (101 MHz, Deuterium Oxide)  $\delta$  162.47, 133.86, 128.34, 119.56 (q,  $J = 321.3$  Hz), 114.32, 55.65;  $^{19}\text{F}$  NMR (376 MHz, Deuterium Oxide)  $\delta$  -78.53.



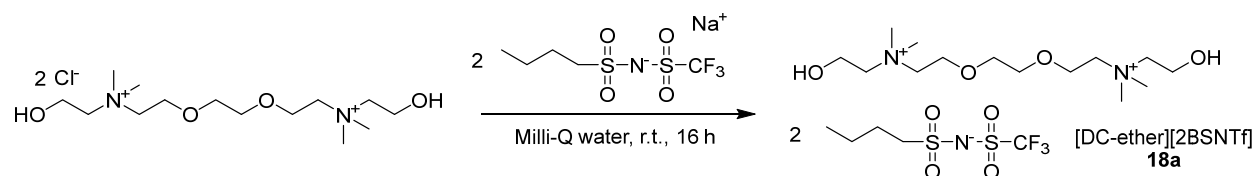
**sodium ((trifluoromethyl)sulfonyl)((2,4,6-trifluorophenyl)sulfonyl)azanide (17o):** The general procedure “F” was applied to trifluoromethanesulfonamide (1.57 g, 10.5 mmol, 1.0 equiv.), sodium carbonate (1.67 g, 15.8 mmol, 1.5 equiv.), and 2,4,6-trifluorobenzenesulfonyl chloride (1.53 mL, 10.9 mmol, 1.04 equiv.). The product (**17o**) was isolated as a white solid in 91.4% yield.  $^1\text{H}$  NMR (400 MHz, Deuterium Oxide)  $\delta$  7.01 – 6.93 (m, 2H);  $^{13}\text{C}\{^1\text{H}\}$  NMR (101 MHz, Deuterium Oxide)  $\delta$  165.28 (dt,  $J = 255.6, 16.3$  Hz), 159.81 (ddd,  $J = 257.3, 15.9, 6.5$  Hz), 119.39 (q,  $J = 320.9$  Hz), 116.53 – 115.75 (m), 102.16 (ddd,  $J = 27.9, 26.4, 4.0$  Hz);  $^{19}\text{F}$  NMR (376 MHz, Deuterium Oxide)  $\delta$  -78.75, -99.28 (t,  $J = 11.6$  Hz), -105.36 (d,  $J = 11.5$  Hz).



**sodium ((perfluorophenyl)sulfonyl)((trifluoromethyl)sulfonyl)azanide (17p):** The general procedure “E” was applied to trifluoromethanesulfonamide (1.40 g, 9.38 mmol, 1.0 equiv.), sodium carbonate (1.49 g, 14.1 mmol, 1.5 equiv.), and 2,3,4,5,6-pentafluorobenzenesulfonyl chloride (1.39 mL, 9.38 mmol, 1.0 equiv.). The product (**17p**) was isolated as a white solid in 93.0% yield.  $^{13}\text{C}\{^1\text{H}\}$  NMR (101 MHz, Deuterium Oxide)  $\delta$  145.81 – 142.45 (m), 139.55 – 136.23 (m), 119.37 (q,  $J = 320.8$  Hz), 117.56 – 117.11 (m).;  $^{19}\text{F}$  NMR (376 MHz, Deuterium Oxide)  $\delta$  -78.83, -138.41 – -138.63 (m), -146.97 (tt,  $J = 21.0, 7.1$  Hz), -160.16 – -160.41 (m).

#### 2.4.16 Synthesis of ILs containing first-generation bis(sulfonyl)azanide anions

**General Procedure “G”: Dicholinium Bis(sulfonyl)azanide ([DC-ether][XSNTf]) Synthesis:** To a 50 mL round bottom flask was added **4j** ([DC-ether][2Cl]), the corresponding sodium bis(sulfonyl)azanide, and Millipore Milli-Q water or Millipore Milli-Q water and acetone. The reaction stirred at room temperature for 16 h. The solvent was removed *in vacuo*. The crude product was dissolved in acetone (15 mL), in which residual starting material precipitated. The solid was filtered, washed with acetone (3x5 mL), and the filtrate was collected and concentrated *in vacuo*. The resulting liquid was mixed with DCM (10 mL), and the DCM and ionic liquid mixture was washed with Millipore Milli-Q water until the water wash showed no precipitant upon addition of silver nitrate. DCM and residual water were removed via a rotary evaporator followed by a vacuum oven set to 80 °C.



#### 2,2'-(ethane-1,2-diylbis(oxy))bis(N-(2-hydroxyethyl)-N,N-dimethylethan-1-aminium) (butylsulfonyl)

**((trifluoromethyl)sulfonyl)azanide (18a):** The general procedure “G” was applied to **4j** ([DC-ether][2Cl];

3.17 g, 8.67 mmol, 1.0 equiv.), **17d** ([Na][BSNTf]; 2.53 g, 8.67 mmol, 1.0 equiv.), and Millipore Milli-Q

water (15 mL). The product (**18a**) was isolated as a clear liquid in 97.0% yield. <sup>1</sup>H NMR (500 MHz,

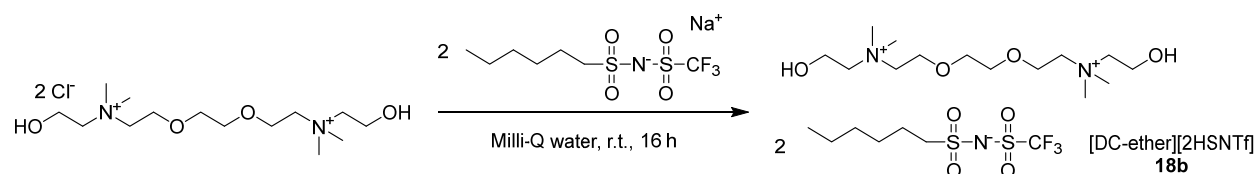
Methanol-d<sub>4</sub>) δ 4.85 (s, 2H), 4.11 – 4.05 (m, 4H), 4.05 – 4.00 (m, 4H), 3.77 (s, 4H), 3.76 (dd, J = 4.3, 2.4

Hz, 4H), 3.67 – 3.61 (m, 4H), 3.30 (s, 12H), 3.22 – 3.16 (m, 4H), 1.91 – 1.81 (m, 4H), 1.53 (h, J = 7.4 Hz,

4H), 1.02 (t, J = 7.4 Hz, 6H); <sup>13</sup>C {<sup>1</sup>H} NMR (126 MHz, Methanol-d<sub>4</sub>) δ 121.64 (q, J = 322.1 Hz), 71.26,

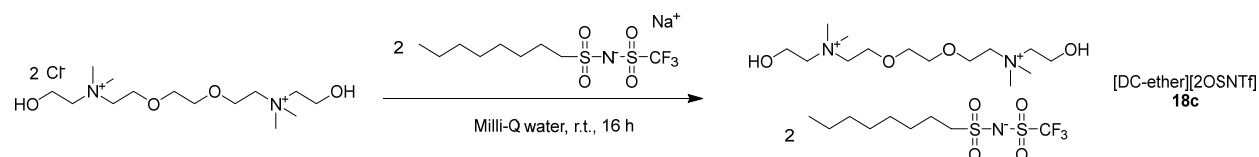
68.01 – 67.77 (m), 66.07 – 65.79 (m), 65.77, 56.96, 56.04, 53.44 – 52.86 (m), 27.17, 22.54, 14.02; <sup>19</sup>F NMR

(470 MHz, Methanol-d<sub>4</sub>) δ -79.53.



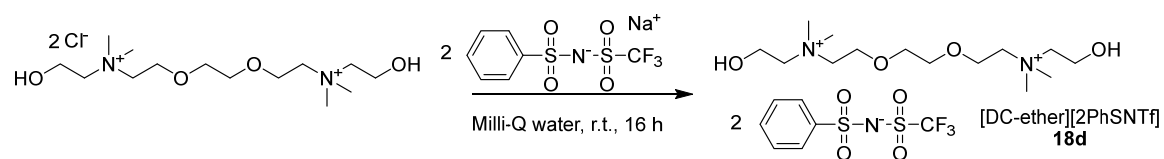
**2,2'-(ethane-1,2-diylbis(oxy))bis(N-(2-hydroxyethyl)-N,N-dimethylethan-1-aminium) (hexylsulfonyl)**

**((trifluoromethyl)sulfonyl)azanide (18b):** The general procedure “G” was applied to **4j** ([DC-ether][2Cl]; 2.10 g, 5.74 mmol, 1.0 equiv.), **17e** ([Na][HSNTf]; 2.75 g, 8.61 mmol, 1.5 equiv.), and Millipore Milli-Q water (10 mL). The product (**18b**) was isolated as a clear liquid in 86.0% yield. <sup>1</sup>H NMR (400 MHz, Acetone-d<sub>6</sub>) δ 4.47 (s, 2H), 4.19 – 4.04 (m, 8H), 3.90 – 3.83 (m, 4H), 3.81 – 3.72 (m, 8H), 3.39 (s, 12H), 3.14 – 3.01 (m, 4H), 1.85 – 1.75 (m, 4H), 1.48 – 1.38 (m, 4H), 1.33 (tdd, J = 7.9, 4.9, 3.4 Hz, 8H), 0.94 – 0.87 (m, 6H); <sup>13</sup>C{<sup>1</sup>H} NMR (101 MHz, Acetone-d<sub>6</sub>) δ 120.65 (q, J = 323.4 Hz), 69.98, 66.79 – 66.52 (m), 64.75 – 64.63 (m), 64.62, 56.01, 54.76, 52.30 – 52.11 (m), 31.31, 27.94, 23.99, 22.24, 13.42; <sup>19</sup>F NMR (376 MHz, Acetone-d<sub>6</sub>) δ -78.74.



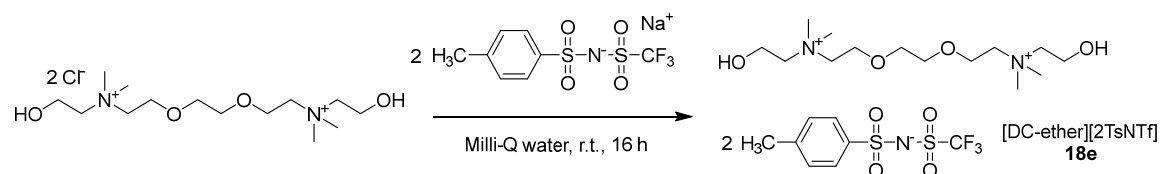
**2,2'-(ethane-1,2-diylbis(oxy))bis(N-(2-hydroxyethyl)-N,N-dimethylethan-1-aminium) (octyl**

**sulfonyl)((trifluoromethyl)sulfonyl)azanide (18c):** The general procedure “G” was applied to **4j** ([DC-ether][2Cl]; 2.45 g, 6.71 mmol, 1.0 equiv.), **17f** ([Na][OSNTf]; 3.50 g, 10.1 mmol, 1.5 equiv.), Millipore Milli-Q water (15 mL), and acetone (15 mL). The product (**18c**) was isolated as a clear liquid in 85.4% yield. <sup>1</sup>H NMR (400 MHz, Methanol-d<sub>4</sub>) δ 4.03 (dq, J = 7.6, 2.6 Hz, 4H), 3.98 (dt, J = 4.9, 2.4 Hz, 4H), 3.72 (d, J = 4.3 Hz, 8H), 3.63 – 3.56 (m, 4H), 3.26 (s, 12H), 3.19 – 3.10 (m, 4H), 1.89 – 1.77 (m, 4H), 1.45 (t, J = 7.4 Hz, 4H), 1.34 (dq, J = 11.6, 4.7, 4.2 Hz, 16H), 0.98 – 0.89 (m, 6H); <sup>13</sup>C{<sup>1</sup>H} NMR (101 MHz, Methanol-d<sub>4</sub>) δ 120.28 (q, J = 322.1 Hz), 69.91, 66.52 (t, J = 2.7 Hz), 64.69 – 64.50 (m), 64.43, 55.64, 54.95, 51.99 – 51.72 (m), 31.56, 28.92, 28.80, 28.04, 23.75, 22.33, 13.15; <sup>19</sup>F NMR (376 MHz, Methanol-d<sub>4</sub>) δ -79.45.



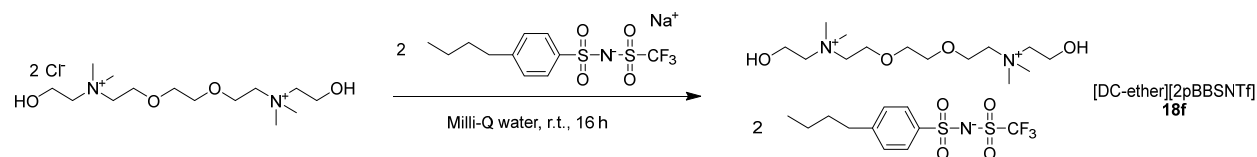
**2,2'-(ethane-1,2-diylbis(oxy))bis(N-(2-hydroxyethyl)-N,N-dimethylethan-1-aminium) (phenyl**

**sulfonyl)((trifluoromethyl)sulfonyl)azanide (18d):** The general procedure “G” was applied to **4j** ([DC-ether][2Cl]; 3.54 g, 9.69 mmol, 1.0 equiv.), **17g** ([Na][PhSNTf]; 2.30 g, 7.39 mmol, 1.3 equiv.), and Millipore Milli-Q water (15 mL). The product (**18d**) was isolated as a clear liquid in 85.7% yield.  $^1\text{H}$  NMR (400 MHz, Acetone- $d_6$ )  $\delta$  7.98 – 7.87 (m, 4H), 7.58 – 7.45 (m, 6H), 4.59 (t,  $J = 4.9$  Hz, 2H), 4.10 (qt,  $J = 5.1, 2.7$  Hz, 4H), 4.04 (dq,  $J = 7.5, 2.6$  Hz, 5H), 3.84 – 3.78 (m, 4H), 3.75 – 3.68 (m, 8H), 3.35 (s, 12H);  $^{13}\text{C}\{^1\text{H}\}$  NMR (101 MHz, Acetone- $d_6$ )  $\delta$  145.61, 131.12, 128.27, 126.52, 120.53 (q,  $J = 323.5$  Hz), 69.94, 66.80 – 66.51 (m), 64.72 – 64.61 (m), 64.55, 55.98, 52.41 – 51.99 (m);  $^{19}\text{F}$  NMR (376 MHz, Acetone- $d_6$ )  $\delta$  -78.87.



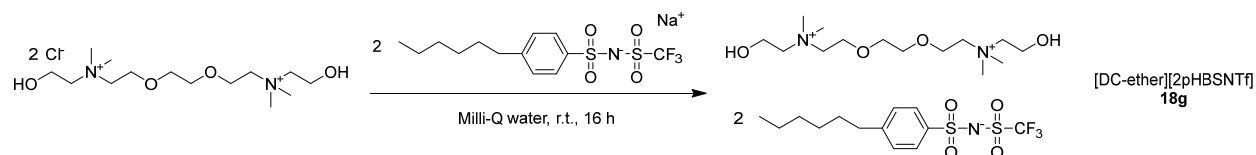
**2,2'-(ethane-1,2-diylbis(oxy))bis(N-(2-hydroxyethyl)-N,N-dimethylethan-1-aminium) tosyl((trifluoro**

**methyl)sulfonyl)azanide (18e):** The general procedure “G” was applied to **4j** ([DC-ether][2Cl]; 3.00 g, 8.21 mmol, 1.0 equiv.), **17h** ([Na][TsNTf]; 4.00 g, 12.3 mmol, 1.5 equiv.), and Millipore Milli-Q water (15 mL). The product (**18e**) was isolated as a clear liquid in 66.9% yield.  $^1\text{H}$  NMR (400 MHz, Methanol- $d_4$ )  $\delta$  7.84 – 7.76 (m, 4H), 7.37 – 7.29 (m, 4H), 4.00 (dq,  $J = 5.2, 2.6$  Hz, 4H), 3.97 – 3.90 (m, 4H), 3.71 – 3.64 (m, 8H), 3.59 – 3.52 (m, 4H), 3.21 (s, 12H), 2.41 (s, 6H);  $^{13}\text{C}\{^1\text{H}\}$  NMR (101 MHz, Methanol- $d_4$ )  $\delta$  142.34, 141.54, 128.76, 126.30, 120.20 (q,  $J = 322.4$  Hz), 69.88, 66.74 – 66.32 (m), 64.69 – 64.53 (m), 64.37, 55.59, 52.32 – 51.48 (m), 20.07;  $^{19}\text{F}$  NMR (376 MHz, Methanol- $d_4$ )  $\delta$  -79.65.



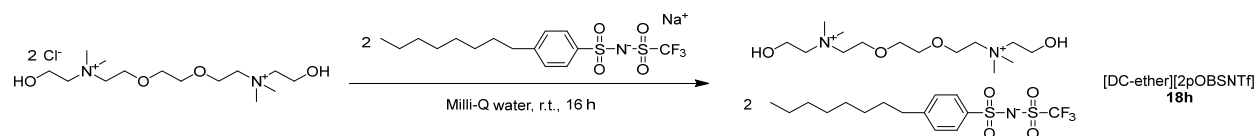
**2,2'-(ethane-1,2-diylbis(oxy))bis(N-(2-hydroxyethyl)-N,N-dimethylethan-1-aminium) ((4-butyl phenyl)sulfonyl)((trifluoromethyl)sulfonyl)azanide (18f):** The general procedure “G” was applied to **4j**

([DC-ether][2Cl]; 2.11 g, 5.78 mmol, 1.0 equiv.), **17j** ([Na][pBBSNTf]; 3.19 g, 8.68 mmol, 1.5 equiv.), Millipore Milli-Q water (15 mL), and acetone (15 mL). The product (**18f**) was isolated as a clear liquid in 98.2% yield.  $^1\text{H}$  NMR (400 MHz, Acetone- $d_6$ )  $\delta$  7.92 – 7.74 (m, 4H), 7.41 – 7.26 (m, 4H), 4.46 (t,  $J$  = 4.5 Hz, 2H), 4.13 (dq,  $J$  = 5.7, 2.8 Hz, 4H), 4.07 (tt,  $J$  = 4.9, 2.6 Hz, 4H), 3.90 – 3.82 (m, 4H), 3.79 – 3.71 (m, 8H), 3.38 (s, 12H), 2.76 – 2.58 (m, 4H), 1.72 – 1.52 (m, 4H), 1.36 (dq,  $J$  = 14.7, 7.4 Hz, 4H), 0.93 (t,  $J$  = 7.4 Hz, 6H);  $^{13}\text{C}\{^1\text{H}\}$  NMR (101 MHz, Acetone- $d_6$ )  $\delta$  146.14, 143.22, 128.07, 126.62, 120.59 (q,  $J$  = 323.7 Hz), 69.98, 66.75 – 66.48 (m), 64.79 – 64.65 (m), 64.60, 56.04, 52.53 – 51.81 (m), 35.07, 33.33, 22.05, 13.29;  $^{19}\text{F}$  NMR (376 MHz, Acetone- $d_6$ )  $\delta$  -78.88.

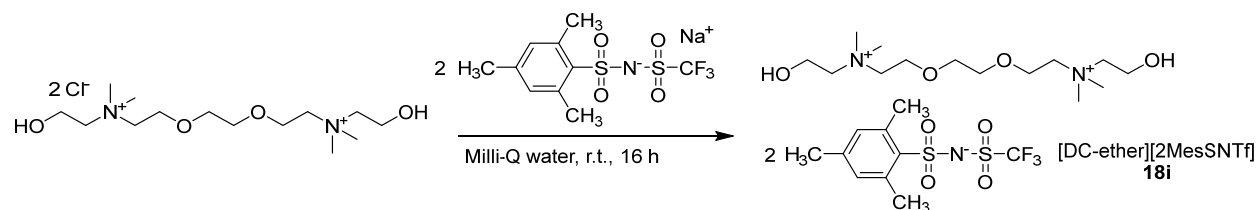


**2,2'-(ethane-1,2-diylbis(oxy))bis(N-(2-hydroxyethyl)-N,N-dimethylethan-1-aminium) ((4-hexyl phenyl)sulfonyl)((trifluoromethyl)sulfonyl)azanide (18g):** The general procedure “G” was applied to **4j**

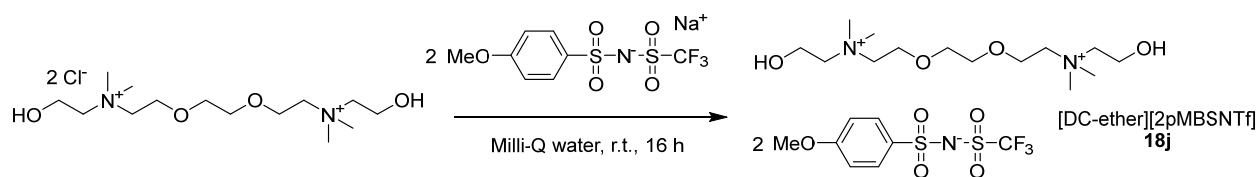
([DC-ether][2Cl]; 0.823 g, 2.26 mmol, 1.0 equiv.), **17k** ([Na][pHBSNTf]; 1.00 g, 3.39 mmol, 1.5 equiv.), Millipore Milli-Q water (5 mL), and acetone (5 mL). The product (**18g**) was isolated as a clear liquid in 62.3% yield.  $^1\text{H}$  NMR (400 MHz, Acetone- $d_6$ )  $\delta$  7.87 – 7.79 (m, 4H), 7.35 – 7.28 (m, 4H), 4.52 (s, 2H), 4.13 (dq,  $J$  = 5.3, 2.6 Hz, 4H), 4.08 (dq,  $J$  = 7.5, 2.6 Hz, 5H), 3.89 – 3.82 (m, 4H), 3.79 – 3.72 (m, 8H), 3.39 (s, 12H), 2.72 – 2.64 (m, 4H), 1.70 – 1.58 (m, 4H), 1.41 – 1.27 (m, 12H), 0.95 – 0.84 (m, 6H);  $^{13}\text{C}\{^1\text{H}\}$  NMR (101 MHz, Acetone- $d_6$ )  $\delta$  146.14, 143.24, 128.04, 126.63, 120.59 (q,  $J$  = 323.7 Hz), 69.99, 66.81 – 66.42 (m), 64.86 – 64.61 (m), 64.61, 56.02, 52.44 – 52.06 (m), 35.38, 31.50, 31.16, 28.75, 22.37, 13.47;  $^{19}\text{F}$  NMR (376 MHz, Acetone- $d_6$ )  $\delta$  -78.89.



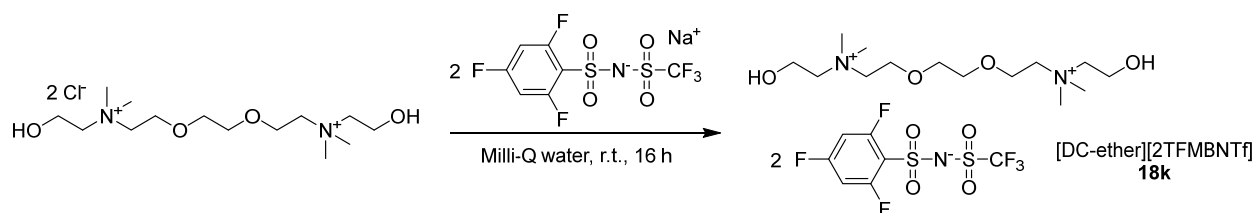
**2,2'-(ethane-1,2-diylbis(oxy))bis(N-(2-hydroxyethyl)-N,N-dimethylethan-1-aminium) ((4-octylphenyl)sulfonyl)((trifluoromethyl)sulfonyl)azanide (18h):** The general procedure “G” was applied to **4j** ([DC-ether][2Cl]; 1.44 g, 3.94 mmol, 1.0 equiv.), **17li** ([Na][pOBSNTf]; 2.50 g, 5.90 mmol, 1.5 equiv.), Millipore Milli-Q water (15 mL), and acetone (15 mL). The product (**18h**) was isolated as a yellow liquid in 97.9% yield.  $^1\text{H}$  NMR (400 MHz, Acetone- $d_6$ )  $\delta$  7.86 – 7.78 (m, 4H), 7.35 – 7.25 (m, 4H), 4.55 (s, 2H), 4.16 – 4.11 (m, 4H), 4.08 (dq,  $J = 5.1, 2.5$  Hz, 4H), 3.89 – 3.84 (m, 4H), 3.78 – 3.73 (m, 8H), 3.39 (s, 12H), 2.72 – 2.63 (m, 4H), 1.70 – 1.59 (m, 4H), 1.41 – 1.23 (m, 20H), 0.93 – 0.85 (m, 6H);  $^{13}\text{C}\{^1\text{H}\}$  NMR (101 MHz, Acetone- $d_6$ )  $\delta$  146.11, 143.26, 128.02, 126.64, 120.59 (q,  $J = 323.7$  Hz), 69.99, 66.75 – 66.65 (m), 64.79 – 64.67 (m), 64.61, 56.01, 52.64 – 51.49 (m), 35.39, 31.71, 31.21, 29.26, 29.10, 29.10, 22.42, 13.48;  $^{19}\text{F}$  NMR (376 MHz, Acetone- $d_6$ )  $\delta$  -78.90.



**2,2'-(ethane-1,2-diylbis(oxy))bis(N-(2-hydroxyethyl)-N,N-dimethylethan-1-aminium) (mesitylsulfonyl)((trifluoromethyl)sulfonyl)azanide (18i):** The general procedure “G” was applied to **4j** ([DC-ether][2Cl]; 3.45 g, 9.43 mmol, 1.0 equiv.), **17m** ([Na][MesSNTf]; 5.00 g, 14.2 mmol, 1.5 equiv.), and Millipore Milli-Q water (25 mL). The product (**18i**) was isolated as a clear liquid in 90.2% yield.  $^1\text{H}$  NMR (400 MHz, Acetone- $d_6$ )  $\delta$  6.91 (s, 4H), 4.49 (t,  $J = 4.9$  Hz, 2H), 4.14 (tq,  $J = 5.0, 2.6$  Hz, 4H), 4.08 (dq,  $J = 5.2, 2.5$  Hz, 4H), 3.88 – 3.83 (m, 4H), 3.78 – 3.73 (m, 8H), 3.38 (s, 12H), 2.68 (s, 12H), 2.25 (s, 6H);  $^{13}\text{C}\{^1\text{H}\}$  (101 MHz, Acetone- $d_6$ )  $\delta$  139.91, 139.89, 138.23, 130.81, 120.60 (q,  $J = 324.0$  Hz), 69.99, 67.08 – 66.16 (m), 64.80 – 64.67 (m), 64.60, 56.01, 52.41 – 52.03 (m), 22.26, 19.96;  $^{19}\text{F}$  NMR (376 MHz, Acetone- $d_6$ )  $\delta$  -78.91.

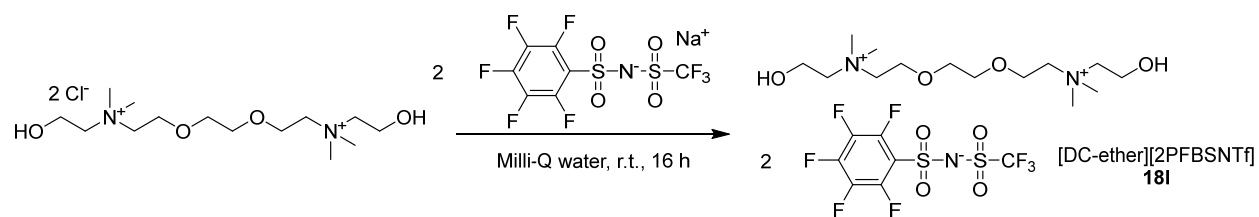


**2,2'-(ethane-1,2-diylbis(oxy))bis(N-(2-hydroxyethyl)-N,N-dimethylethan-1-aminium) ((4-methoxyphenyl)sulfonyl)((trifluoromethyl)sulfonyl)azanide (**18j**):** The general procedure “F” was applied to **4j** ([DC-ether][2Cl]; 2.68 g, 7.33 mmol, 1.0 equiv.), **17n** ([Na][pMBSNTf]; 3.75 g, 11.0 mmol, 1.5 equiv.), and Millipore Milli-Q water (20 mL). The product (**18j**) was isolated as a clear liquid in 83.3% yield.  $^1\text{H}$  NMR (400 MHz, Methanol- $d_4$ )  $\delta$  7.89 – 7.81 (m, 4H), 7.07 – 6.98 (m, 4H), 4.04 – 3.98 (m, 4H), 3.95 (ddd,  $J = 7.4, 4.9, 2.6$  Hz, 4H), 3.87 (s, 6H), 3.71 – 3.67 (m, 8H), 3.61 – 3.54 (m, 4H), 3.23 (s, 12H);  $^{13}\text{C}\{^1\text{H}\}$  NMR (101 MHz, Methanol- $d_4$ )  $\delta$  162.38, 136.18, 128.33, 120.19 (q,  $J = 322.4$  Hz), 113.26, 69.88, 66.51 (t,  $J = 2.7$  Hz), 64.66 – 64.53 (m), 64.38, 55.57, 54.74, 51.90 – 51.71 (m);  $^{19}\text{F}$  NMR (376 MHz, Methanol- $d_4$ )  $\delta$  -79.73.

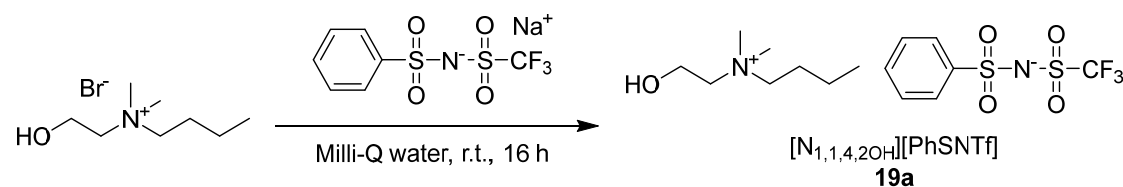


**2,2'-(ethane-1,2-diylbis(oxy))bis(N-(2-hydroxyethyl)-N,N-dimethylethan-1-aminium) ((trifluoromethyl)sulfonyl)((2,4,6-trifluorophenyl)sulfonyl)azanide (**18k**):** The general procedure “F” was applied to **4j** ([DC-ether][2Cl]; 2.00 g, 5.47 mmol, 1.0 equiv.), **17o** ([Na][TFBSNTf]; 3.00 g, 8.21 mmol, 1.5 equiv.), and Millipore Milli-Q water (15 mL). The product (**18k**) was isolated as a yellow liquid in 87.7% yield.  $^1\text{H}$  NMR (400 MHz, Acetone- $d_6$ )  $\delta$  7.04 – 6.93 (m, 4H), 4.53 (t,  $J = 4.7$  Hz, 2H), 4.16 (dp,  $J = 7.2, 2.4$  Hz, 4H), 4.12 (dq,  $J = 7.5, 2.7$  Hz, 4H), 3.92 – 3.85 (m, 4H), 3.82 – 3.75 (m, 8H), 3.42 (s, 12H);  $^{13}\text{C}\{^1\text{H}\}$  NMR (101 MHz, Acetone- $d_6$ )  $\delta$  163.96 (dt,  $J = 251.7, 15.6$  Hz), 160.46 (ddd,  $J = 257.5, 15.5, 7.4$  Hz), 120.36 (q,  $J = 322.9$  Hz), 119.79 (td,  $J = 17.2, 5.2$  Hz), 101.06 (ddd,  $J = 28.5, 25.7, 4.0$  Hz), 69.98, 66.98 –

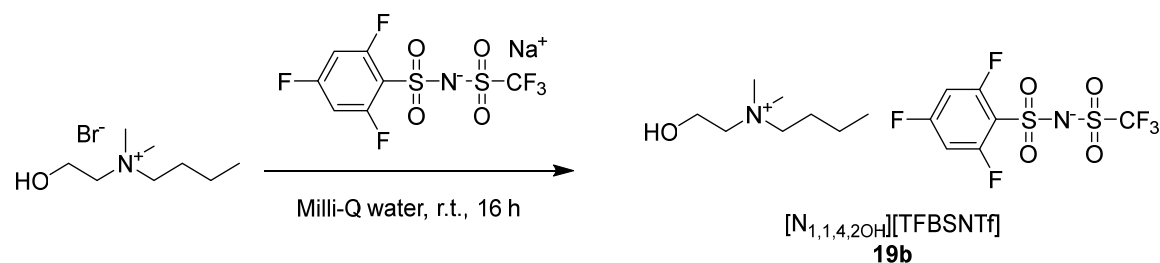
66.54 (m), 64.83 – 64.70 (m), 64.60, 56.00, 52.38 – 52.07 (m);  $^{19}\text{F}$  NMR (376 MHz, Acetone- $d_6$ )  $\delta$  -79.16, -103.69 (d,  $J$  = 10.0 Hz), -105.12 (t,  $J$  = 10.1 Hz).



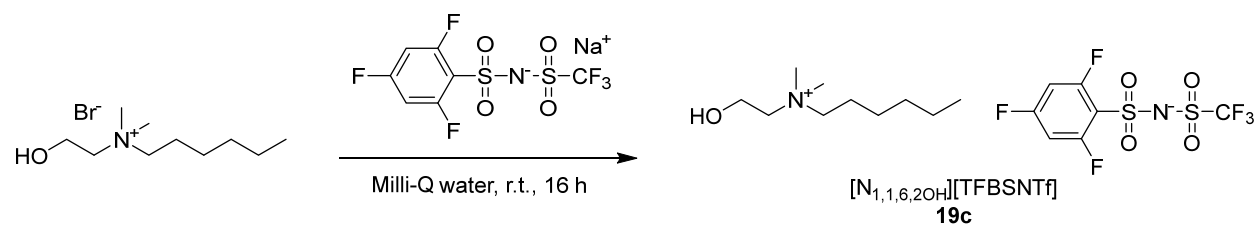
**2,2'-(ethane-1,2-diylbis(oxy))bis(*N*-(2-hydroxyethyl)-*N,N*-dimethylethan-1-aminium) ((perfluorophenyl)sulfonyl)((trifluoromethyl)sulfonyl)azanide (**181**):** The general procedure “G” was applied to **4j** ([DC-ether][2Cl]; 2.19 g, 5.98 mmol, 1.0 equiv.), **17p** ([Na][PFBSNTf]; 3.00 g, 7.48 mmol, 1.25 equiv.), and Millipore Milli-Q water (15 mL). The product (**181**) was isolated as a yellow liquid in 92.9% yield.  $^1\text{H}$  NMR (400 MHz, Acetone- $d_6$ )  $\delta$  4.52 (s, 2H), 4.20 – 4.07 (m, 8H), 3.92 – 3.85 (m, 4H), 3.81 – 3.73 (m, 8H), 3.42 (s, 12H);  $^{13}\text{C}\{^1\text{H}\}$  NMR (101 MHz, Acetone- $d_6$ )  $\delta$  145.93 – 142.95 (m), 142.76 (dtt,  $J$  = 255.5, 13.6, 4.8 Hz), 139.31 – 135.88 (m), 121.11 – 120.29 (m), 120.19 (q,  $J$  = 322.4 Hz), 69.98, 66.94 – 66.55 (m), 64.90 – 64.67 (m), 64.59, 55.99, 52.45 – 52.12 (m);  $^{19}\text{F}$  NMR (376 MHz, Acetone- $d_6$ )  $\delta$  -79.32, -138.06 (dp,  $J$  = 16.5, 5.6 Hz), -152.76 (tt,  $J$  = 20.5, 5.3 Hz), -163.71 – -164.22 (m).



***N*-(2-hydroxyethyl)-*N,N*-dimethylbutan-1-aminium ((phenylsulfonyl)((trifluoromethyl)sulfonyl)azanide (**19a**):** To a 50 mL round bottom flask was added **2a** ([ $\text{N}_{1,1,4,2\text{OH}}$ ][Br]; 0.100 g, 0.442 mmol, 1.0 equiv.), **17g** ([Na][PhSNTf]; 0.138 g, 0.442 mmol, 1.0 equiv.), and Milli-Q water (5 mL). The reaction stirred at room temperature for 16 h. Since second layer precipitated, no further workup nor characterization was performed.

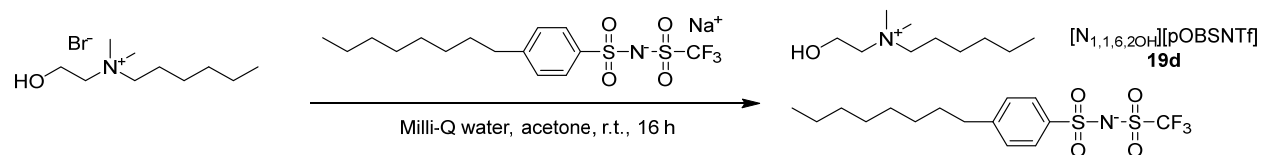


***N*-(2-hydroxyethyl)-*N,N*-dimethylbutan-1-aminium ((trifluoromethyl)sulfonyl)((2,4,6-trifluorophenyl)sulfonyl)azanide (19b):** To a 25 mL round bottom flask was added **2a** ( $[N_{1,1,4,2OH}][Br]$ ; 0.100 g, 0.442 mmol, 1.0 equiv.), **17o** ( $[Na][TFBSNTf]$ ; 0.161 g, 0.442 mmol, 1.0 equiv.), and Milli-Q water (5 mL). The reaction stirred at room temperature for 16 h. The solvent was removed *in vacuo*. The crude product was dissolved in acetone (10 mL), where a white solid precipitated. The mixture was filtered, washed with acetone (2x5 mL), and the filtrate was concentrated *in vacuo*. The product (**19b**) was isolated as a yellow liquid in 24.6% yield.  $^1H$  NMR (400 MHz, Acetone- $d_6$ )  $\delta$  6.88 – 6.77 (m, 2H), 4.35 (s, 1H), 4.01 (dt,  $J = 7.4, 3.0$  Hz, 2H), 3.58 – 3.51 (m, 2H), 3.50 – 3.41 (m, 2H), 3.21 (s, 6H), 1.83 – 1.70 (m, 2H), 1.29 (h,  $J = 7.4$  Hz, 2H), 0.84 (t,  $J = 7.4$  Hz, 3H);  $^{19}F$  NMR (376 MHz, Acetone- $d_6$ )  $\delta$  -79.12, -103.59 (d,  $J = 10.0$  Hz), -105.44 (t,  $J = 10.1$  Hz).



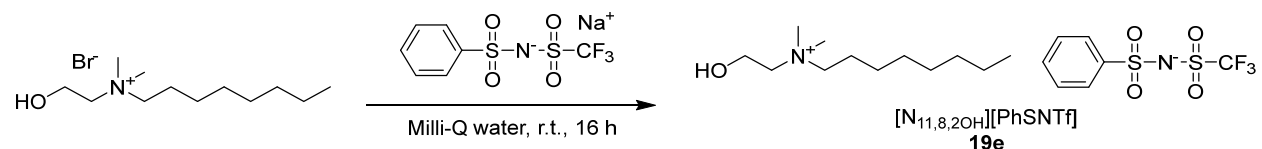
***N*-(2-hydroxyethyl)-*N,N*-dimethylhexan-1-aminium ((trifluoromethyl)sulfonyl)((2,4,6-trifluorophenyl)sulfonyl)azanide (19c):** To a 10 mL round bottom flask was added **2c** ( $[N_{1,1,6,2OH}][Br]$ ; 0.050 g, 0.197 mmol, 1.0 equiv.), **17o** ( $[Na][TFBSNTf]$ ; 71.9 mg, 0.197 mmol, 1.0 equiv.), and Milli-Q water (5 mL). The reaction stirred at room temperature for 16 h. The solvent was removed *in vacuo*. The crude product was dissolved in acetone (10 mL), where a white solid precipitated. The mixture was filtered, washed with acetone (2x5 mL), and the filtrate was concentrated *in vacuo*. The product (**19c**) was isolated

as a yellow liquid in 47.3% yield.  $^1\text{H}$  NMR (400 MHz, Acetone- $d_6$ )  $\delta$  6.88 – 6.76 (m, 2H), 4.36 (t,  $J$  = 4.8 Hz, 1H), 4.01 (qt,  $J$  = 5.0, 2.6 Hz, 2H), 3.59 – 3.52 (m, 2H), 3.50 – 3.42 (m, 2H), 3.22 (s, 6H), 1.79 (dq,  $J$  = 11.6, 7.6 Hz, 2H), 1.36 – 1.09 (m, 6H), 0.88 – 0.62 (m, 3H);  $^{19}\text{F}$  NMR (376 MHz, Acetone- $d_6$ )  $\delta$  -79.12, -103.55 (d,  $J$  = 9.8 Hz), -105.56 (t,  $J$  = 10.1 Hz).



***N*-(2-hydroxyethyl)-*N,N*-dimethylhexan-1-aminium ((4-octylphenyl)sulfonyl)((trifluoromethyl)**

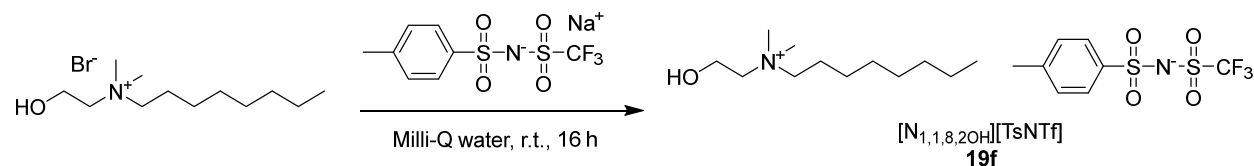
**sulfonyl)azanide (19d):** To a 10 mL round bottom flask was added **2c** ( $[\text{N}_{1,1,6,2\text{OH}}][\text{Br}]$ ; 0.050 g, 0.197 mmol, 1.0 equiv.), **17Iii** ( $[\text{Na}][\text{pOBSNTf}]$ ; 91.3 mg, 0.216 mmol, 1.1 equiv.), acetone (5 mL), and Milli-Q water (5 mL). The reaction stirred at room temperature for 16 h. The solvent was removed *in vacuo*. The crude product was dissolved in acetone (10 mL), where a white solid precipitated. The mixture was filtered, washed with acetone (2x5 mL), and the filtrate was concentrated *in vacuo*. The product (**19d**) was isolated as a viscous liquid in 93.1% yield.  $^1\text{H}$  NMR (400 MHz, Acetone- $d_6$ )  $\delta$  7.72 – 7.64 (m, 2H), 7.18 – 7.11 (m, 2H), 4.38 (t,  $J$  = 4.9 Hz, 1H), 3.99 (ddt,  $J$  = 7.4, 5.0, 2.5 Hz, 2H), 3.57 – 3.50 (m, 2H), 3.48 – 3.39 (m, 2H), 3.19 (s, 6H), 2.53 (dd,  $J$  = 8.7, 6.7 Hz, 2H), 1.82 – 1.70 (m, 2H), 1.54 – 1.46 (m, 2H), 1.19 (dq,  $J$  = 20.7, 7.8, 6.8, 3.7 Hz, 14H), 0.75 (tt,  $J$  = 7.1, 2.0 Hz, 6H);  $^{19}\text{F}$  NMR (376 MHz, Acetone- $d_6$ )  $\delta$  -78.93.



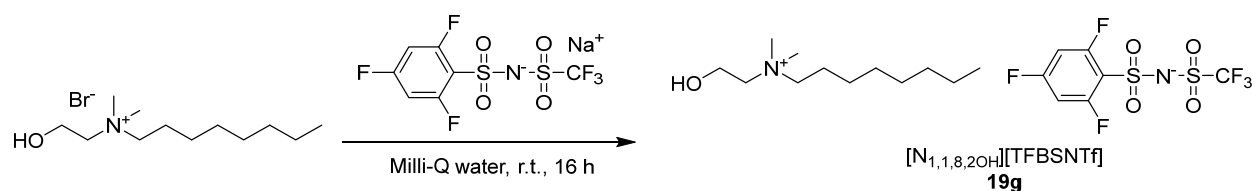
***N*-(2-hydroxyethyl)-*N,N*-dimethyloctan-1-aminium (phenylsulfonyl)((trifluoromethyl)sulfonyl)**

**azanide (19e):** To a 10 mL round bottom flask was added **2d** ( $[\text{N}_{1,1,8,2\text{OH}}][\text{Br}]$ ; 500 mg, 1.77 mmol, 1.0 equiv.), **17g** ( $[\text{Na}][\text{PhSNTf}]$ ; 556 mg, 1.77 mmol, 1.1 equiv.), acetone (5 mL), and Milli-Q water (5 mL). The reaction stirred at room temperature for 16 h. The solvent was removed *in vacuo*. The crude product was dissolved in acetone (10 mL), where a white solid precipitated. The mixture was filtered, washed with

acetone (2x5 mL), and the filtrate was concentrated *in vacuo*. The product (**19e**) was isolated as a viscous liquid in 91.4% yield.  $^1\text{H}$  NMR (400 MHz, Acetone- $d_6$ )  $\delta$  7.98 – 7.90 (m, 2H), 7.64 – 7.35 (m, 3H), 4.46 (t,  $J = 5.0$  Hz, 1H), 4.10 (ddt,  $J = 7.5, 5.1, 2.5$  Hz, 2H), 3.67 – 3.60 (m, 2H), 3.58 – 3.49 (m, 2H), 3.28 (s, 6H), 1.93 – 1.81 (m, 2H), 1.47 – 1.19 (m, 10H), 0.92 – 0.85 (m, 3H);  $^{19}\text{F}$  NMR (376 MHz, Acetone- $d_6$ )  $\delta$  -78.87.



**N-(2-hydroxyethyl)-N,N-dimethyloctan-1-aminium tosyl((trifluoromethyl)sulfonyl)azanide (19f):** To a 25 mL round bottom flask was added **2d** ( $[\text{N}_{1,1,8,2\text{OH}}][\text{Br}]$ ; 0.868 g, 3.07 mmol, 1.0 equiv.), **17h** ( $[\text{Na}][\text{TsNTf}]$ ; 1.00 g, 3.07 mmol, 1.0 equiv.), and Milli-Q water (10 mL). The reaction stirred at room temperature for 16 h. The solvent was removed *in vacuo*. The crude product was dissolved in acetone and a white solid precipitated. The mixture was filtered, washed with acetone (3x5 mL), and the filtrate was concentrated *in vacuo*. To the flask was added methylene chloride (10 mL) and the mixture was washed with Milli-Q water (4x25 mL). A test with silver nitrate confirmed the absence of starting material. The solvent was removed *in vacuo*, including in a vacuum oven set to 80 °C. The product (**19f**) was isolated as a yellow liquid in 83.6% yield.  $^1\text{H}$  NMR (400 MHz, Acetone- $d_6$ )  $\delta$  7.85 – 7.77 (m, 2H), 7.32 (s, 0H), 7.33 – 7.25 (m, 2H), 4.44 (t,  $J = 4.9$  Hz, 1H), 4.10 (qt,  $J = 4.9, 2.3$  Hz, 2H), 3.67 – 3.60 (m, 2H), 3.58 – 3.49 (m, 2H), 3.29 (s, 6H), 2.38 (s, 3H), 1.93 – 1.81 (m, 2H), 1.40 – 1.23 (m, 10H), 0.94 – 0.85 (m, 3H);  $^{13}\text{C}$  NMR (101 MHz, Acetone- $d_6$ )  $\delta$  143.20, 141.18, 128.65, 126.59, 120.61 (q,  $J = 323.6$  Hz), 65.40 (dt,  $J = 13.6, 2.9$  Hz), 56.00, 51.44 – 50.99 (m), 31.57, 28.92, 28.86, 26.08 (d,  $J = 1.7$  Hz), 22.37 (d,  $J = 3.8$  Hz), 20.52, 13.52;  $^{19}\text{F}$  NMR (376 MHz, Acetone- $d_6$ )  $\delta$  -78.85.



***N*-(2-hydroxyethyl)-*N,N*-dimethyloctan-1-aminium ((trifluoromethyl)sulfonyl)((2,4,6-trifluoro**

**phenyl)sulfonyl)azanide (19g):** To a 25 mL round bottom flask was added **2d** ( $[N_{1,1,8,2OH}][Br]$ ; 0.773 g,

2.74 mmol, 1.0 equiv.), **17o** ( $[Na][TFBSNTf]$ ; 1.00 g, 2.74 mmol, 1.0 equiv.), and Milli-Q water (10 mL).

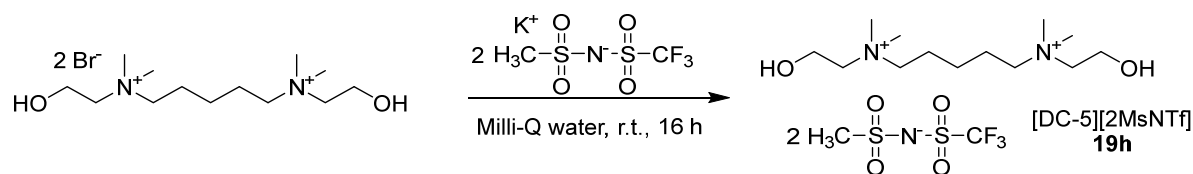
The reaction stirred at room temperature for 16 h. The solvent was removed *in vacuo*. The crude product was dissolved in acetone and a white solid precipitated. The mixture was filtered, washed with acetone (3x5 mL), and the filtrate was concentrated *in vacuo*. To the flask was added methylene chloride (10 mL) and the mixture was washed with Milli-Q water (4x25 mL). A test with silver nitrate confirmed the absence of

starting material. The solvent was removed *in vacuo*, including in a vacuum oven set to 80 °C. The product (**19g**) was isolated as a yellow liquid in 93.4% yield.  $^1H$  NMR (400 MHz, Acetone- $d_6$ )  $\delta$  7.03 – 6.92 (m,

2H), 4.44 (t,  $J = 4.8$  Hz, 1H), 4.14 (qt,  $J = 5.0, 2.5$  Hz, 2H), 3.71 – 3.64 (m, 2H), 3.62 – 3.53 (m, 2H), 3.33 (s, 6H), 3.32 (s, 0H), 1.98 – 1.85 (m, 2H), 1.45 – 1.23 (m, 10H), 0.92 – 0.83 (m, 3H);  $^{13}C$  NMR (101 MHz,

Acetone- $d_6$ )  $\delta$  163.95 (dt,  $J = 251.7, 15.5$  Hz), 160.45 (ddd,  $J = 257.6, 15.5, 7.4$  Hz), 120.37 (q,  $J = 323.1$  Hz), 119.84 (td,  $J = 17.2, 5.3$  Hz), 101.07 (ddd,  $J = 28.6, 25.7, 4.0$  Hz), 65.45 (dt,  $J = 13.4, 2.8$  Hz), 55.99,

51.46 – 51.23 (m), 31.54, 28.87, 28.83, 26.05 (t,  $J = 1.5$  Hz), 22.35, 13.46;  $^{19}F$  NMR (376 MHz, Acetone- $d_6$ )  $\delta$  -79.08, -103.62 (d,  $J = 10.1$  Hz), -104.99 (t,  $J = 10.2$  Hz).

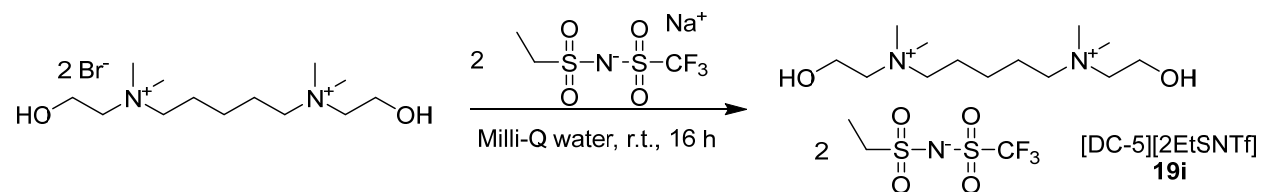


***N*<sup>1</sup>,*N*<sup>5</sup>-bis(2-hydroxyethyl)-*N*<sup>1</sup>,*N*<sup>1</sup>,*N*<sup>5</sup>,*N*<sup>5</sup>-tetramethylpentane-1,5-diaminium (methylsulfonyl)**

**((trifluoromethyl)sulfonyl)azanide (19h):** To a 50 mL round bottom flask was added **4d** ( $[DC-5][2Br]$ ;

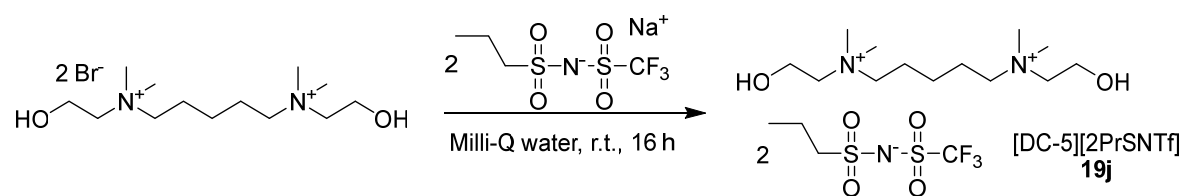
800 mg, 1.96 mmol, 1.00 equiv.), **17a** ( $[K][MsNTf]$ ; 800 mg, 3.02 mmol, 1.54 equiv.), and Milli-Q water

(20 mL). The reaction stirred at room temperature for 16 h. Since no second layer precipitated, no further workup nor analysis was performed.



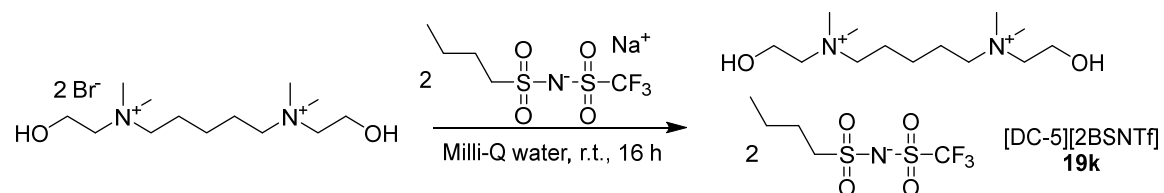
***N*<sup>1</sup>,*N*<sup>5</sup>-bis(2-hydroxyethyl)-*N*<sup>1</sup>,*N*<sup>1</sup>,*N*<sup>5</sup>,*N*<sup>5</sup>-tetramethylpentane-1,5-diaminium (ethylsulfonyl)**

**((trifluoromethyl)sulfonyl)azanide (19i):** To a 50 mL round bottom flask was added **4d** ([DC-5][2Br]; 700 mg, 1.71 mmol, 1.00 equiv.), **17b** ([Na][EtSNTf]; 672 mg, 2.55 mmol, 1.49 equiv.), and Milli-Q water (10 mL). The reaction stirred at room temperature for 16 h. Since no second layer precipitated, no workup nor analysis was performed.



***N*<sup>1</sup>,*N*<sup>5</sup>-bis(2-hydroxyethyl)-*N*<sup>1</sup>,*N*<sup>1</sup>,*N*<sup>5</sup>,*N*<sup>5</sup>-tetramethylpentane-1,5-diaminium (propylsulfonyl)**

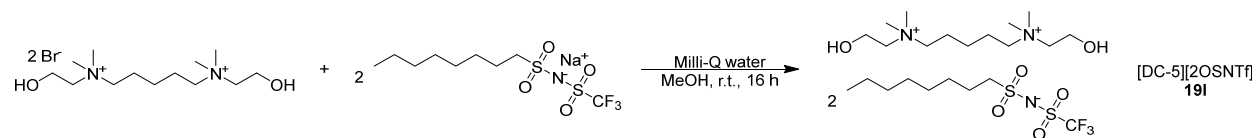
**((trifluoromethyl)sulfonyl)azanide (19j):** To a 50 mL round bottom flask was added **4d** ([DC-5][2Br]; 800 mg, 1.96 mmol, 1.0 equiv.), **17c** ([Na][PrSNTf]; 633 mg, 2.16 mmol, 1.1 equiv.), and Milli-Q water (10 mL). The reaction stirred at room temperature for 16 h. Since no second layer precipitated, no workup nor analysis was performed.



***N*<sup>1</sup>,*N*<sup>5</sup>-bis(2-hydroxyethyl)-*N*<sup>1</sup>,*N*<sup>1</sup>,*N*<sup>5</sup>,*N*<sup>5</sup>-tetramethylpentane-1,5-diaminium (butylsulfonyl)**

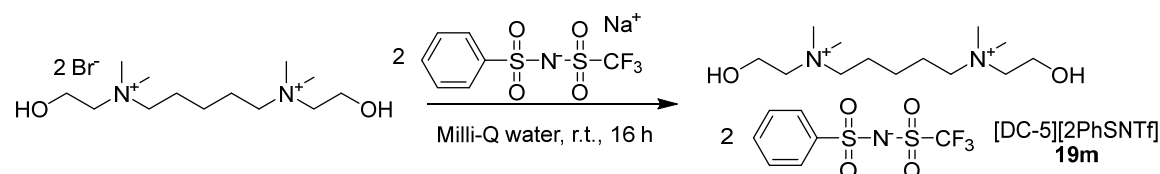
**((trifluoromethyl)sulfonyl)azanide (19k):** To a 50 mL round bottom flask was added **4d** ([DC-5][2Br];

569 mg, 1.39 mmol, 1.0 equiv.), **17d** ([Na][BSNTf]; 609 mg, 2.10 mmol, 1.5 equiv.), and Milli-Q water (10 mL). The reaction stirred at room temperature for 16 h. Since no second layer precipitated, no workup nor analysis was performed.



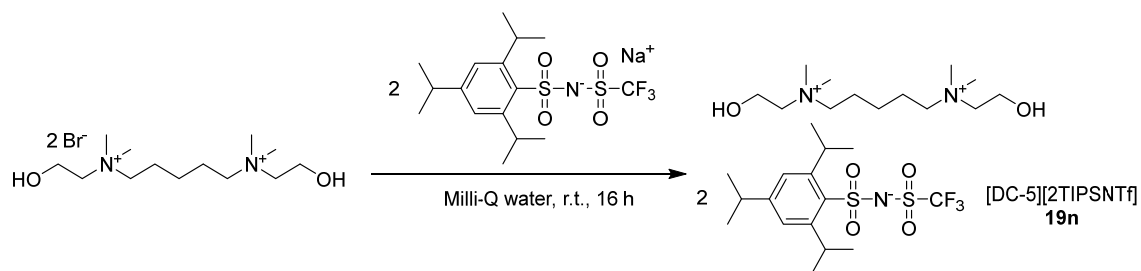
***N*<sup>1</sup>,*N*<sup>5</sup>-bis(2-hydroxyethyl)-*N*<sup>1</sup>,*N*<sup>1</sup>,*N*<sup>5</sup>,*N*<sup>5</sup>-tetramethylpentane-1,5-diaminium (octylsulfonyl)**

**((trifluoromethyl)sulfonyl)azanide (19l):** To a 50 mL round bottom flask was added **4d** ([DC-5][2Br]; 1.08 g, 2.64 mmol, 1.24 equiv.), **17f** ([Na][OSNTf]; 0.567 g, 2.12 mmol, 1.0 equiv.), Milli-Q water (5 mL), and methanol (5 mL). The reaction stirred at room temperature for 16 h. The methanol was removed *in vacuo* and a solid precipitated out. Since the compound was a solid, no further workup nor analysis was performed.

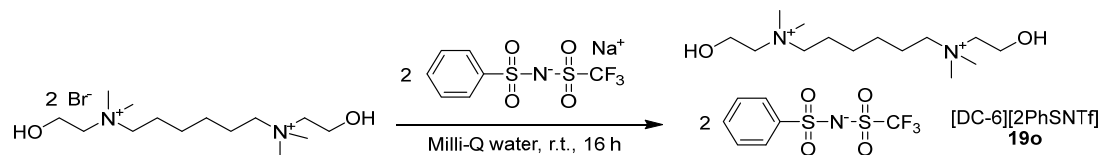


***N*<sup>1</sup>,*N*<sup>5</sup>-bis(2-hydroxyethyl)-*N*<sup>1</sup>,*N*<sup>1</sup>,*N*<sup>5</sup>,*N*<sup>5</sup>-tetramethylpentane-1,5-diaminium (phenylsulfonyl)**

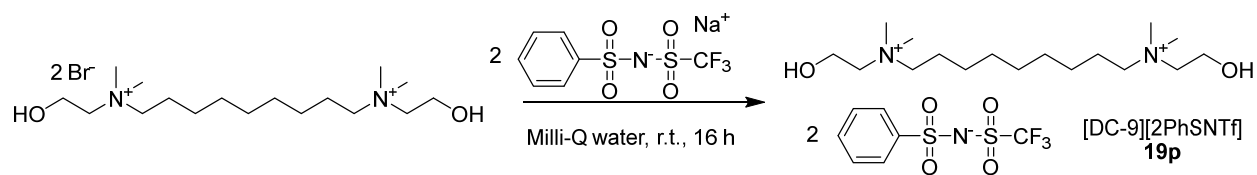
**((trifluoromethyl)sulfonyl)azanide (19m):** To a 50 mL round bottom flask was added **4d** ([DC-5][2Br]; 612 mg, 1.50 mmol, 1.0 equiv.), **17g** ([Na][PhSNTf]; 700 mg, 2.25 mmol, 1.4 equiv.), and Milli-Q water (10 mL). The reaction stirred at room temperature for 16 h. The solvent was removed *in vacuo*. The resulting white solid was washed with acetone (3x20 mL), filtered, and the filtrate was concentrated *in vacuo*. The product (**19m**) was isolated as a clear viscous liquid. <sup>1</sup>H NMR (400 MHz, Acetone-d<sub>6</sub>) δ 8.00 – 7.92 (m, 4H), 7.60 – 7.48 (m, 6H), 4.10 – 4.03 (m, 4H), 3.62 – 3.56 (m, 4H), 3.56 – 3.47 (m, 4H), 3.23 (s, 12H), 2.00 – 1.87 (m, 4H), 1.42 (p, *J* = 7.5 Hz, 2H); <sup>13</sup>C NMR (101 MHz, Acetone-d<sub>6</sub>) δ 145.23, 131.46, 128.50, 126.45, 120.49 (q, *J* = 323.2 Hz), 65.27, 64.92, 55.92, 51.33 (t, *J* = 3.7 Hz), 21.72; <sup>19</sup>F NMR (376 MHz, Acetone-d<sub>6</sub>) δ -78.80.



***N*<sup>1</sup>,*N*<sup>5</sup>-bis(2-hydroxyethyl)-*N*<sup>1</sup>,*N*<sup>1</sup>,*N*<sup>5</sup>,*N*<sup>5</sup>-tetramethylpentane-1,5-diaminium ((trifluoromethyl)sulfonyl)((2,4,6-triisopropylphenyl)sulfonyl)amide (**19n**):** To a 100 mL round bottom flask was added **4d** ([DC-5][2Br]; 700 mg, 1.71 mmol, 1.0 equiv.), **17i** ([Na][TIPSNTf]; 746 mg, 2.40 mmol, 1.4 equiv.), and Milli-Q water (25 mL). The reaction stirred at room temperature for 16 h. A white solid precipitated. The solvent was removed *in vacuo*, and the white solid was washed with water (3x20 mL), filtered, the collected, and residual water was removed *in vacuo*. The product (**19n**) was isolated as a white solid. <sup>1</sup>H NMR (400 MHz, Chloroform-d) δ 7.08 (s, 4H), 4.31 (hept, *J* = 6.7 Hz, 2H), 4.01 (dt, *J* = 11.4, 5.4 Hz, 6H), 3.57 – 3.48 (m, 8H), 3.15 (s, 12H), 2.86 (p, *J* = 6.9 Hz, 2H), 2.03 – 1.90 (m, 4H), 1.55 (p, *J* = 7.2 Hz, 2H), 1.21 (t, *J* = 6.0 Hz, 36H); <sup>13</sup>C NMR (101 MHz, Chloroform-d) δ 151.53, 149.11, 137.09, 123.21, 121.89 (q), 65.20 (d, *J* = 13.0 Hz), 56.32, 51.98, 34.05, 29.19, 24.71, 23.66, 21.60; <sup>19</sup>F NMR (376 MHz, Chloroform-d) δ -78.16.



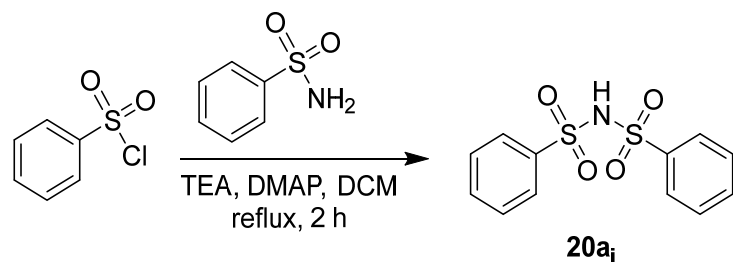
***N*<sup>1</sup>,*N*<sup>6</sup>-bis(2-hydroxyethyl)-*N*<sup>1</sup>,*N*<sup>1</sup>,*N*<sup>6</sup>,*N*<sup>6</sup>-tetramethylhexane-1,6-diaminium (phenylsulfonyl)((trifluoromethyl)sulfonyl)azanide (**19o**):** To a 50 mL round bottom flask was added **4e** ([DC-6][2Br]; 500 mg, 1.18 mmol, 1.0 equiv.), **17g** ([Na][PhSNTf]; 551 mg, 1.77 mmol, 1.4 equiv.), and Milli-Q water (5 mL). The reaction stirred at room temperature for 16 h. The solvent was removed *in vacuo*. The resulting white solid was washed with acetone (3x20 mL), filtered, and the filtrate was concentrated *in vacuo*. The product (**19o**) was isolated as a white solid. Since the product was a solid, no analysis was performed.



***N*<sup>1</sup>,*N*<sup>9</sup>-bis(2-hydroxyethyl)-*N*<sup>1</sup>,*N*<sup>1</sup>,*N*<sup>9</sup>,*N*<sup>9</sup>-tetramethylnonane-1,9-diaminium (phenylsulfonyl)**

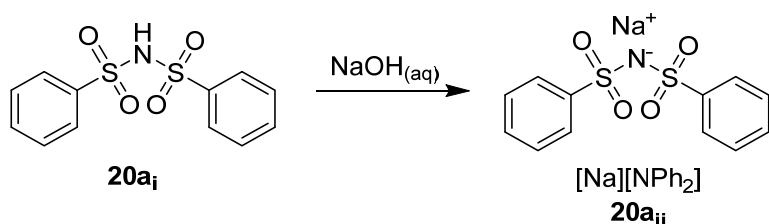
**((trifluoromethyl)sulfonyl)azanide (19p):** To a 50 mL round bottom flask was added **4h** ([DC-9][2Br]); 696 mg, 1.50 mmol, 1.0 equiv.), **17g** ([Na][PhSNTf]; 700 mg, 2.25 mmol, 1.0 equiv.), and Milli-Q water (10 mL). The reaction stirred at room temperature for 16 h. The solvent was removed *in vacuo*. The resulting white solid was washed with acetone (3x20 mL), filtered, and the filtrate was concentrated *in vacuo*. The product (**19p**) was isolated as a clear solid. <sup>1</sup>H NMR (400 MHz, Acetone-d<sub>6</sub>) δ 7.99 – 7.89 (m, 4H), 7.60 – 7.48 (m, 6H), 4.10 – 4.03 (m, 4H), 3.65 – 3.58 (m, 4H), 3.55 – 3.47 (m, 4H), 3.26 (s, 12H), 1.82 (tt, *J* = 10.5, 6.3 Hz, 4H), 1.45 – 1.20 (m, 10H); <sup>13</sup>C NMR (101 MHz, Acetone-d<sub>6</sub>) δ 145.45, 131.38, 128.48, 126.45, 120.53 (q, *J* = 323.5 Hz), 65.38, 65.19, 55.82, 51.30, 30.05, 28.51, 25.84, 22.25; <sup>19</sup>F NMR (376 MHz, Acetone-d<sub>6</sub>) δ -78.71.

*2.4.17 Synthesis of second-generation bis(sulfonyl)azanide anions*

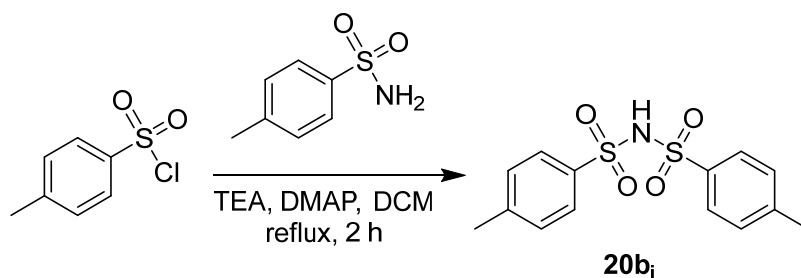


***N*-(phenylsulfonyl)benzenesulfonamide (20a<sub>i</sub>):** To a 100 mL round bottom flask was added triethylamine (6.65 mL, 47.7 mmol, 3.0 equiv.), dichloromethane (25 mL), benzenesulfonamide (2.81 g, 15.9 mmol, 1.0 equiv.), benzenesulfonyl chloride (2.03 mL, 15.9 mmol, 1.0 equiv.), and 4-dimethylaminopyridine (0.388 g, 3.18 mmol, 0.2 equiv.). The reaction stirred for 2 h at 40 °C. Then, to the flask was added HCl (50 mL, 3 N). The solution stirred at room temperature for 15 min. Afterwards, the aqueous and organic layers were separated, and the aqueous layer was extracted with dichloromethane

(1x50 mL). The organic fractions were combined, washed with HCl (3 N; 3x50 mL), dried with magnesium sulfate, filtered, and concentrated *in vacuo*. The crude product was then resuspended in a 3:1 chloroform and hexanes mixture and stirred at room temperature for 1 h, where a white solid precipitated. The white solid was filtered, washed with 3:1 chloroform and hexanes (3x10 mL), and residual solvent was removed *in vacuo*. The product (**20a<sub>i</sub>**) was isolated as a white solid in 27.8% yield. <sup>1</sup>H NMR (400 MHz, Acetone-d<sub>6</sub>) δ 10.35 (s, 1H), 7.97 – 7.90 (m, 4H), 7.77 – 7.68 (m, 2H), 7.66 – 7.57 (m, 4H).



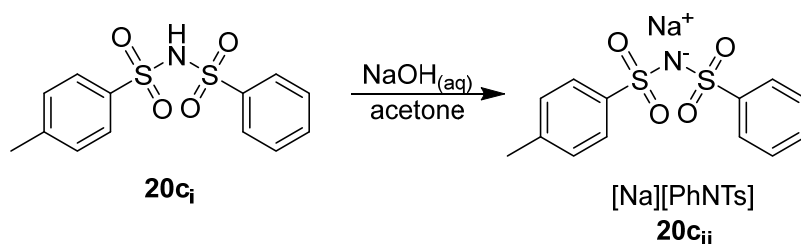
**sodium bis(phenylsulfonamoyl)azanide (20a<sub>ii</sub>):** To a 250 mL round bottom flask was added **20a<sub>i</sub>** (1.22 g, 4.10 mmol, 1.21 equiv.), NaOH (136 mg, 3.39 mmol, 1.00 equiv.), and Milli-Q water (100 mL). The mixture stirred until the components dissolved. Then, the aqueous solution was washed with ethyl acetate (3x75 mL). The water layer was then removed *in vacuo*. The product (**20a<sub>ii</sub>**) was isolated as a white powder in 93.8% yield. <sup>1</sup>H NMR (400 MHz, Deuterium Oxide) δ 7.54 – 7.47 (m, 4H), 7.45 – 7.36 (m, 2H), 7.32 – 7.22 (m, 4H); <sup>13</sup>C NMR (101 MHz, Deuterium Oxide) δ 140.82, 132.32, 128.86, 128.81, 126.11.



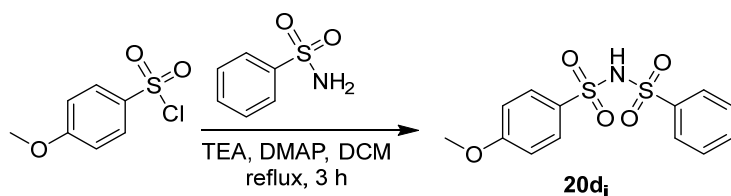
**4-methyl-N-tosylbenzenesulfonamide (20b<sub>i</sub>):** To a 100 mL round bottom flask was added triethylamine (6.65 mL, 47.7 mmol, 3.0 equiv.), dichloromethane (25 mL), 4-toluenesulfonamide (2.72 g, 15.9 mmol, 1.0 equiv.), tosyl chloride (3.03 mL, 15.9 mmol, 1.0 equiv.), and 4-dimethylaminopyridine (0.388 g, 3.18 mmol, 0.2 equiv.). The reaction stirred for 2 h at 40 °C. Then, to the flask was added HCl



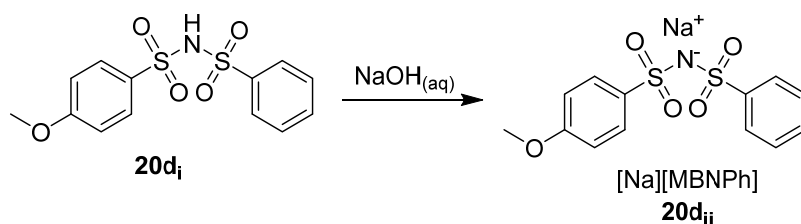
**4-methyl-*N*-(phenylsulfonyl)benzenesulfonamide (20c<sub>i</sub>):** To a 100 mL round bottom flask was added triethylamine (6.65 mL, 47.7 mmol, 3.0 equiv.), dichloromethane (25 mL), benzenesulfonamide (2.50 g, 15.9 mmol, 1.0 equiv.), tosyl chloride (3.03 g, 15.9 mmol, 1.0 equiv.), and 4-dimethylaminopyridine (0.388 g, 3.18 mmol, 0.2 equiv.). The reaction stirred for 2 h at 40 °C. Then, to the flask was added HCl (50 mL, 3 N). The solution stirred at room temperature for 15 min. Afterwards, the aqueous and organic layers were separated, and the aqueous layer was extracted with dichloromethane (1x50 mL). The organic fractions were combined, washed with HCl (3 N; 3x50 mL), dried with magnesium sulfate, filtered, and concentrated *in vacuo*. The crude product was then resuspended in a 3:1 chloroform and hexanes mixture and stirred at room temperature for 1 h, where a white solid precipitated. The white solid was filtered, washed with 3:1 chloroform and hexanes (3x10 mL), and residual solvent was removed *in vacuo*. The product (**20c<sub>i</sub>**) was isolated as a white solid in 47.9% yield. <sup>1</sup>H NMR (400 MHz, Acetone-d<sub>6</sub>) δ 7.95 – 7.87 (m, 2H), 7.83 – 7.75 (m, 2H), 7.78 – 7.68 (m, 1H), 7.77 – 7.68 (m, 0H), 7.65 – 7.56 (m, 2H), 7.65 – 7.56 (m, 0H), 7.44 – 7.36 (m, 2H), 2.45 (s, 3H); <sup>13</sup>C NMR (101 MHz, Acetone-d<sub>6</sub>) δ 144.82, 140.48, 137.50, 133.61, 129.64, 129.14, 127.52, 127.41, 20.63.



**sodium (phenylsulfonyl)(tosyl)azanide (20c<sub>ii</sub>):** To a 100 mL round bottom flask was added **20c<sub>i</sub>** (2.37 g, 7.61 mmol, 1.125 equiv.), NaOH (271 mg, 6.76 mmol, 1.000 equiv.), acetone (15 mL), and Milli-Q water (100 mL). The mixture stirred until the components dissolved. Then, the aqueous solution was washed with ethyl acetate (3x50 mL). The water layer was then removed *in vacuo*. The product (**20c<sub>ii</sub>**) was isolated as a white solid in 70.9% yield. <sup>1</sup>H NMR (400 MHz, DMSO-d<sub>6</sub>) δ 7.69 – 7.62 (m, 2H), 7.54 (d, *J* = 7.8 Hz, 2H), 7.39 (dq, *J* = 14.1, 6.9 Hz, 3H), 7.16 (d, *J* = 7.9 Hz, 2H), 2.32 (s, 3H); <sup>13</sup>C NMR (101 MHz, DMSO-d<sub>6</sub>) δ 146.93, 144.17, 140.12, 130.36, 128.70, 128.25, 126.60, 126.55, 21.33.

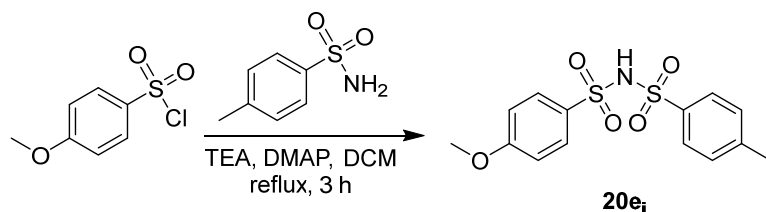


**4-methoxy-*N*-(phenylsulfonyl)benzenesulfonamide (20<sub>di</sub>):** To a 100 mL round bottom flask was added triethylamine (6.65 mL, 47.7 mmol, 3.0 equiv.), dichloromethane (25 mL), benzenesulfonamide (2.50 g, 15.9 mmol, 1.0 equiv.), 4-methoxybenzenesulfonyl chloride (3.29 g, 15.9 mmol, 1.0 equiv.), and 4-dimethylaminopyridine (0.388 g, 3.18 mmol, 0.2 equiv.). The reaction stirred for 3 h at 40 °C. Then, to the flask was added HCl (50 mL, 3 N). The solution stirred at room temperature for 15 min. Afterwards, the aqueous and organic layers were separated, and the aqueous layer was extracted with dichloromethane (1x50 mL). The organic fractions were combined, washed with HCl (3 N; 3x50 mL), dried with magnesium sulfate, filtered, and concentrated *in vacuo*. The crude product was then resuspended in a 3:1 chloroform and hexanes mixture and stirred at room temperature for 1 h, where a white solid precipitated. The white solid was filtered, washed with 3:1 chloroform and hexanes (3x10 mL), and residual solvent was removed *in vacuo*. The product (**20<sub>di</sub>**) was isolated as a white solid in 52.1% yield. <sup>1</sup>H NMR (400 MHz, Acetone-*d*<sub>6</sub>) δ 7.95 – 7.88 (m, 2H), 7.92 – 7.79 (m, 2H), 7.76 – 7.67 (m, 1H), 7.60 (ddt, *J* = 8.0, 6.8, 1.3 Hz, 2H), 7.13 – 7.04 (m, 2H), 3.93 (s, 3H); <sup>13</sup>C NMR (101 MHz, Acetone-*d*<sub>6</sub>) δ 205.43, 163.86, 140.51, 133.58, 131.73, 129.84, 129.14, 127.40, 114.25, 55.41.

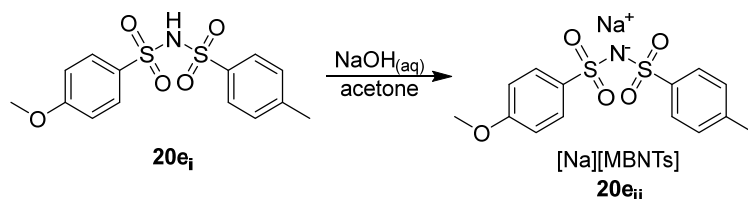


**sodium ((4-methoxyphenyl)sulfonyl)(phenylsulfonyl)azanide (20<sub>dii</sub>):** To a 100 mL round bottom flask was added **20<sub>di</sub>** (2.37 g, 7.61 mmol, 1.125 equiv.), NaOH (271 mg, 6.76 mmol, 1.000 equiv.), and Milli-Q water (100 mL). The mixture stirred until the components dissolved. Then, the aqueous solution was

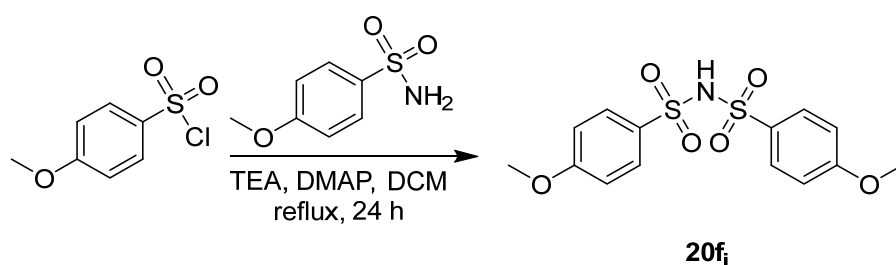
washed with ethyl acetate (3x50 mL). The water layer was then removed *in vacuo*. The product (**20d<sub>ii</sub>**) was isolated as a white solid in 97.3% yield. <sup>1</sup>H NMR (400 MHz, Acetone-d<sub>6</sub>) δ 7.72 – 7.64 (m, 2H), 7.64 – 7.56 (m, 2H), 7.39 – 7.30 (m, 1H), 7.29 – 7.20 (m, 2H), 6.77 – 6.69 (m, 2H), 3.79 (s, 3H); <sup>13</sup>C NMR (101 MHz, Acetone-d<sub>6</sub>) δ 205.52, 161.29, 144.78, 136.76, 130.10, 128.40, 127.76, 126.54, 112.88, 54.93.



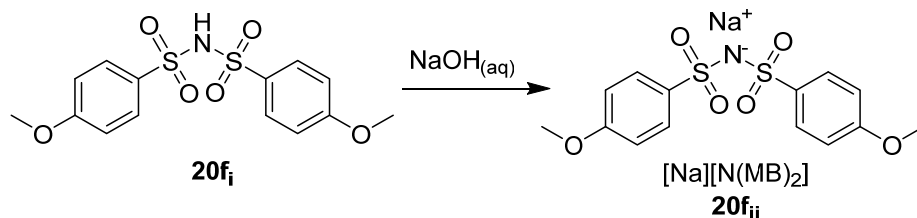
**4-methoxy-N-tosylbenzenesulfonamide (20e<sub>i</sub>):** To a 100 mL round bottom flask was added triethylamine (3.32 mL, 23.9 mmol, 3.080 equiv.), dichloromethane (25 mL), 4-toluenesulfonamide (2.72 g, 15.9 mmol, 2.050 equiv.), 4-methoxybenzenesulfonyl chloride (1.60 g, 7.74 mmol, 1.000 equiv.), and 4-dimethylaminopyridine (0.388 g, 3.18 mmol, 0.411 equiv.). The reaction stirred for 3 h at 40 °C. Then, to the flask was added HCl (50 mL, 3 N). The solution stirred at room temperature for 15 min. Afterwards, the aqueous and organic layers were separated, and the aqueous layer was extracted with dichloromethane (1x50 mL). The organic fractions were combined, washed with HCl (3 N; 3x50 mL), dried with magnesium sulfate, filtered, and concentrated *in vacuo*. The crude product was then resuspended in a 3:1 chloroform and hexanes mixture and stirred at room temperature for 1 h, where a white solid precipitated. The white solid was filtered, washed with 3:1 chloroform and hexanes (3x10 mL), and residual solvent was removed *in vacuo*. The product (**20e<sub>i</sub>**) was isolated as a white solid in 21.7% yield. <sup>1</sup>H NMR (400 MHz, Methanol-d<sub>4</sub>) δ 7.75 – 7.69 (m, 2H), 7.68 – 7.64 (m, 2H), 7.29 (dt, *J* = 8.0, 0.7 Hz, 2H), 7.00 – 6.93 (m, 2H), 3.87 (s, 3H), 2.42 (s, 3H).



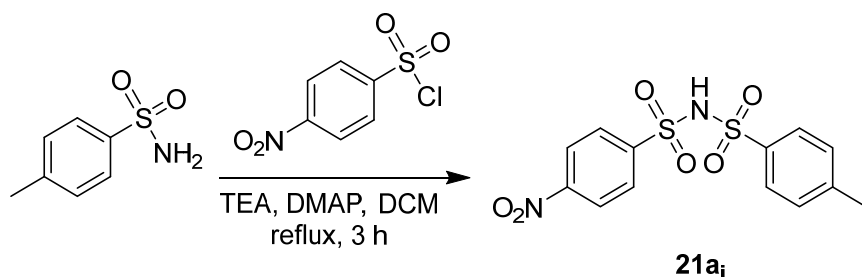
**sodium ((4-methoxyphenyl)sulfonyl)(tosyl)azanide (20e<sub>ii</sub>):** To a 100 mL round bottom flask was added **20e<sub>i</sub>** (0.550 g, 7.61 mmol, 1.125 equiv.), NaOH (59.7 mg, 1.49 mmol, 1.000 equiv.), acetone (25 mL), and Milli-Q water (50 mL). The mixture stirred until the components dissolved. Then, the aqueous solution was washed with ethyl acetate (3x50 mL). The water layer was then removed *in vacuo*. The product (**20e<sub>ii</sub>**) was isolated as a white solid in 93.1% yield. <sup>1</sup>H NMR (400 MHz, Methanol-d<sub>4</sub>) δ 7.59 – 7.47 (m, 4H), 7.12 – 7.05 (m, 2H), 6.81 – 6.73 (m, 2H), 3.81 (s, 3H), 2.34 (s, 3H); <sup>13</sup>C NMR (101 MHz, Methanol-d<sub>4</sub>) δ 161.86, 141.28, 140.63, 135.33, 128.30, 126.41, 112.85, 54.63, 19.98.



**4-hydroxy-N-((4-methoxyphenyl)sulfonyl)benzenesulfonamide (20f<sub>i</sub>):** To a 100 mL round bottom flask was added triethylamine (5.58 mL, 40.1 mmol, 3.0 equiv.), dichloromethane (25 mL), 4-methoxybenzenesulfonamide (2.50 g, 13.4 mmol, 2.0 equiv.), 4-methoxybenzenesulfonyl chloride (2.76 g, 13.4 mmol, 1.0 equiv.), and 4-dimethylaminopyridine (0.326 g, 2.67 mmol, 0.2 equiv.). The reaction stirred for 24 h at 50 °C. Then, to the flask was added HCl (50 mL, 3 N). The solution stirred at room temperature for 15 min. Afterwards, the aqueous and organic layers were separated, and the aqueous layer was extracted with dichloromethane (1x50 mL). The organic fractions were combined, washed with HCl (3 N; 3x50 mL), dried with magnesium sulfate, filtered, and concentrated *in vacuo*. The crude product was then resuspended in a 3:1 chloroform and hexanes mixture and stirred at room temperature for 1 h, where a white solid precipitated. The white solid was filtered, washed with 1:2 chloroform and hexanes (3x10 mL), and residual solvent was removed *in vacuo*. The product (**20f<sub>i</sub>**) was isolated as a white solid in 31.3% yield. <sup>1</sup>H NMR (400 MHz, Methanol-d<sub>4</sub>) δ 7.73 – 7.65 (m, 2H), 7.00 – 6.91 (m, 2H), 3.87 (s, 3H).

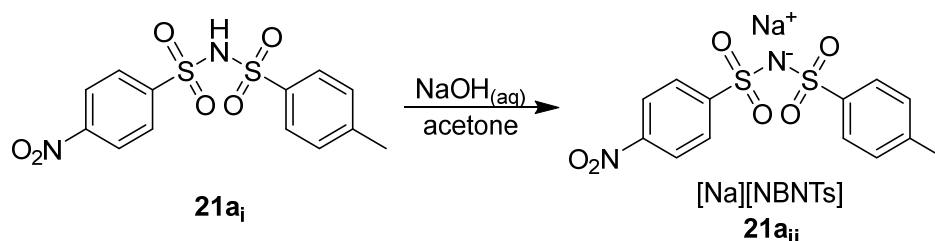


**sodium bis((4-hydroxyphenyl)sulfonyl)azanide (20f<sub>ii</sub>):** To a 100 mL round bottom flask was added **20f<sub>i</sub>** (1.38 g, 4.18 mmol, 1.125 equiv.), NaOH (149 mg, 3.71 mmol, 1.000 equiv.), and Milli-Q water (50 mL). The mixture stirred until the components dissolved. Then, the aqueous solution was washed with ethyl acetate (3x50 mL). The water layer was then removed *in vacuo*. The product (**20f<sub>ii</sub>**) was isolated as a white solid in 97.3% yield. <sup>1</sup>H NMR (400 MHz, Methanol-d<sub>4</sub>) δ 7.58 – 7.50 (m, 4H), 6.82 – 6.74 (m, 4H), 3.81 (s, 6H); <sup>13</sup>C NMR (101 MHz, Methanol-d<sub>4</sub>) δ 161.80, 135.35, 128.30, 112.86, 54.57.

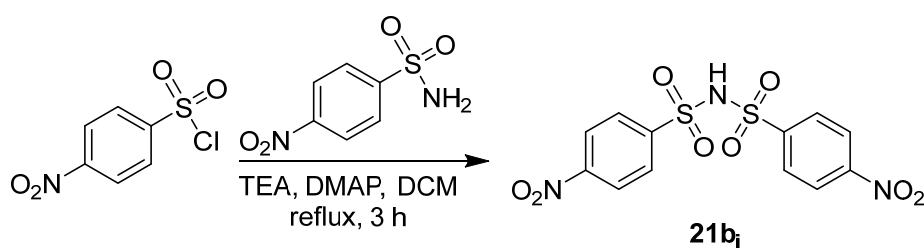


**4-methyl-N-((4-nitrophenyl)sulfonyl)benzenesulfonamide (21a<sub>i</sub>):** To a 100 mL round bottom flask was added triethylamine (6.11 mL, 43.8 mmol, 3.0 equiv.), dichloromethane (25 mL), 4-nitrobenzenesulfonyl chloride (3.24 g, 14.6 mmol, 1.0 equiv.), 4-toluenesulfonamide (3.00 g, 17.5 mmol, 1.2 equiv.), and 4-dimethylaminopyridine (0.357 g, 2.92 mmol, 0.2 equiv.). The reaction stirred for 3 h at 50 °C. To the solution was added HCl (50 mL, 3 N), and the solution stirred at room temperature for 2 h. The layers were separated, and the organic layer was washed with more HCl (3x50 mL, 3 N). During this, a white solid precipitated, which was filtered and dried. From the organic layer, the DCM was dried using magnesium sulfate, filtered, and the filtrate was concentrated *in vacuo*. The crude compound was dissolved with chloroform and precipitated using small volumes of hexanes. The solid was filtered off and residual solvent was removed *in vacuo*. The two fractions were combined to give the product (**21a<sub>i</sub>**) as a white solid in

57.5% yield.  $^1\text{H}$  NMR (400 MHz, Methanol- $d_4$ )  $\delta$  8.39 – 8.30 (m, 2H), 8.33 (d,  $J$  = 17.6 Hz, 0H), 8.10 – 8.01 (m, 0H), 8.09 – 8.01 (m, 2H), 7.75 – 7.68 (m, 2H), 7.36 – 7.28 (m, 2H), 2.42 (s, 3H);  $^{13}\text{C}$  NMR (101 MHz, Methanol- $d_4$ )  $\delta$  150.34, 146.05, 144.70, 137.38, 129.27, 128.59, 127.23, 123.82, 20.11.

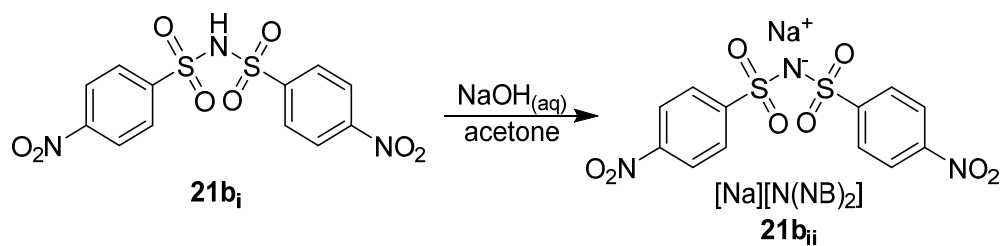


**sodium ((4-nitrophenyl)sulfonyl)(tosyl)azanide (21a<sub>ii</sub>):** To a 100 mL round bottom flask was added **21a<sub>i</sub>** (2.99 g, 8.40 mmol, 1.125 equiv.), NaOH (299 mg, 7.46 mmol, 1.0 equiv.), acetone (75 mL), and Milli-Q water (75 mL). The mixture was sonicated and then stirred until dissolved. After, the solution was concentrated *in vacuo*. The crude product was then stirred in DCM (25 mL) at room temperature for 1 h. The white solid was filtered out, collected, residual solvent was removed *in vacuo*. The product (**21a<sub>ii</sub>**) was isolated as a white solid in 95.1% yield.  $^1\text{H}$  NMR (400 MHz, Methanol- $d_4$ )  $\delta$  8.17 – 8.09 (m, 2H), 7.89 – 7.81 (m, 2H), 7.58 – 7.50 (m, 2H), 7.13 – 7.07 (m, 2H), 2.32 (s, 3H);  $^{13}\text{C}$  NMR (101 MHz, Methanol- $d_4$ )  $\delta$  149.54, 148.94, 141.78, 140.48, 128.37, 127.80, 126.48, 122.98, 19.89.

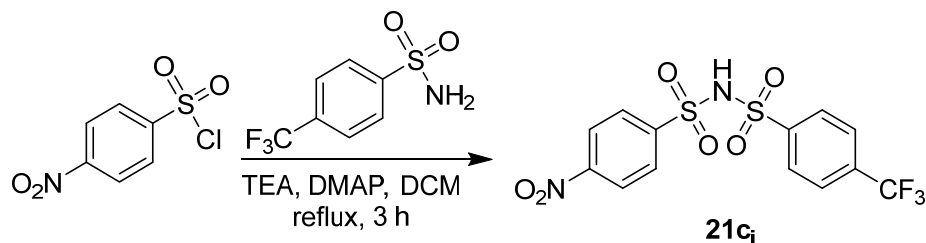


**4-nitro-N-((4-nitrophenyl)sulfonyl)benzenesulfonamide (21b<sub>i</sub>):** To a 100 mL round bottom flask was added triethylamine (5.17 mL, 37.1 mmol, 3.000 equiv.), dichloromethane (25 mL), 4-nitrobenzenesulfonamide (2.50 g, 12.4 mmol, 1.000 equiv.), 4-nitrobenzenesulfonyl chloride (2.74 g, 12.4 mmol, 1.000 equiv.), and 4-dimethylaminopyridine (0.388 g, 3.18 mmol, 0.257 equiv.). The reaction stirred for 3 h at 50 °C. A white solid precipitated out, which was filtered, and residual solvent removed *in vacuo*.

The solid was then mixed in a solution of DCM (25 mL) and Milli-Q water (25 mL) which stirred at room temperature for 16 h. The solid was recollected and stirred in 2:1 hexanes and chloroform (25 mL) at room temperature for 1 h. Finally, the solid was filtered and excess solvent was removed *in vacuo*. The product (**21b<sub>i</sub>**) was isolated as a white solid in 42.2% yield. <sup>1</sup>H NMR (400 MHz, DMSO-d<sub>6</sub>) δ 8.25 (s, 2H), 7.92 (s, 2H).

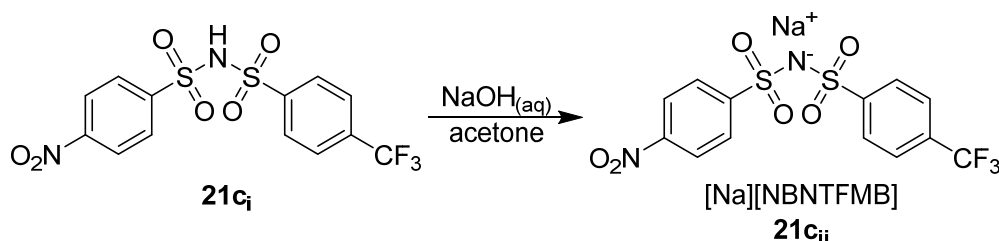


**sodium bis((4-nitrophenyl)sulfonyl)azanide (21b<sub>ii</sub>):** To a 250 mL round bottom flask was added **21b<sub>i</sub>** (2.02 g, 5.22 mmol, 1.125 equiv.), NaOH (186 mg, 4.64 mmol, 1.0 equiv.), acetone (50mL), and Milli-Q water (100 mL). The mixture was sonicated and then stirred until dissolved. The solution turned yellow. The solvent was removed *in vacuo* resulting in a multi-colored solid. The solid was dissolved in DCM (15 mL) and stirred at room temperature for 1 h, resulting in some of the crude product dissolving. The mixture was filtered, washed with Milli-Q water (3x15 mL), and residual solvent was removed *in vacuo*. The resulting product (**21b<sub>ii</sub>**) was isolated as a yellow compound in 38.6% yield. <sup>1</sup>H NMR (400 MHz, DMSO-d<sub>6</sub>) δ 8.24 (s, 2H), 7.92 (s, 2H); <sup>13</sup>C NMR (101 MHz, DMSO-d<sub>6</sub>) δ 151.74, 148.77, 128.25, 123.98.

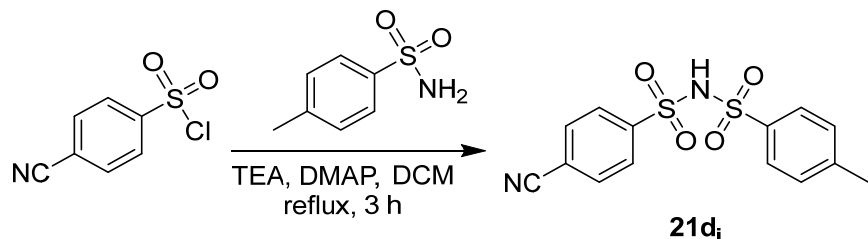


**4-nitro-N-((4-(trifluoromethyl)phenyl)sulfonyl)benzenesulfonamide (21c<sub>i</sub>):** To a 100 mL round bottom flask was added triethylamine (4.64 mL, 33.3 mmol, 3.0 equiv.), dichloromethane (25 mL), 4-trifluoromethanebenzenesulfonamide (2.50 g, 11.1 mmol, 1.0 equiv.), 4-

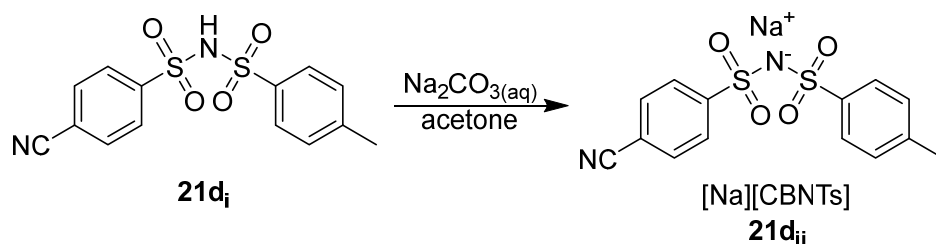
nitrobenzenesulfonylchloride (2.46 g, 11.1 mmol, 1.0 equiv.), and 4-dimethylaminopyridine (0.271 g, 2.22 mmol, 0.2 equiv.). The reaction stirred for 3 h at 50 °C. To the solution was added HCl (50 mL, 2 N). The solution stirred for at room temperature for 1 h. The phases were separated and the HCl phase was extracted with DCM (1x50 mL). The organic fractions were combined and were washed with HCl (2x50 mL, 2 N), dried with magnesium sulfate, filtered, and concentrated *in vacuo*. The crude product was then stirred in chloroform (100 mL) at room temperature for 1 h, forming a white solid. The white solid was filtered out, washed with chloroform (3x15 mL), and dried *in vacuo*. The product (**21c<sub>i</sub>**) was isolated as a white solid in 20.6% yield. <sup>1</sup>H NMR (400 MHz, Methanol-d<sub>4</sub>) δ 8.37 – 8.29 (m, 2H), 8.30 (s, 2H), 8.13 – 8.01 (m, 4H), 7.82 (d, *J* = 8.3 Hz, 2H); <sup>13</sup>C NMR (101 MHz, Methanol-d<sub>4</sub>) δ 150.08, 147.22, 145.37, 134.13 – 133.21 (m), 128.43, 127.81, 125.68 (q, *J* = 3.9 Hz), 123.68, 125.39 – 121.18 (m); <sup>19</sup>F NMR (376 MHz, Methanol-d<sub>4</sub>) δ -64.59.



**sodium ((4-nitrophenyl)sulfonyl)((4-(trifluoromethyl)phenyl)sulfonyl)azanide (**21c<sub>ii</sub>**):** To a 100 mL round bottom flask was added **21c<sub>i</sub>** (0.936 g, 2.28 mmol, 1.125 equiv.), NaOH (81.1 mg, 2.03 mmol, 1.000 equiv.), acetone (25 mL), and Milli-Q water (25mL). The mixture was sonicated and then stirred until dissolved. Afterwards, the aqueous solution was removed *in vacuo*. To the crude product was added DCM (10 mL) and Milli-Q water (10 mL). The solution stirred at room temperature for 1 h. Then, the DCM was removed *in vacuo* resulting in the precipitation of a solid. The solid was filtered out of the water phase and residual solvent was removed *in vacuo*. The product (**21c<sub>ii</sub>**) was isolated as a white solid in 58.9% yield. <sup>1</sup>H NMR (400 MHz, Methanol-d<sub>4</sub>) δ 8.23 – 8.15 (m, 2H), 7.98 – 7.88 (m, 4H), 7.70 – 7.63 (m, 2H); <sup>13</sup>C NMR (101 MHz, Methanol-d<sub>4</sub>) δ 149.78, 149.09, 147.66, 133.06 – 131.57 (m), 127.81, 127.24, 125.00 (q, *J* = 3.9 Hz), 123.07, 122.33; <sup>19</sup>F NMR (376 MHz, Methanol-d<sub>4</sub>) δ -64.42.

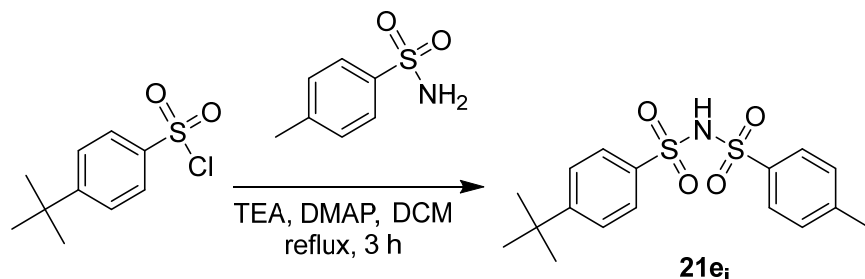


**4-cyano-*N*-tosylbenzenesulfonamide (21d<sub>i</sub>):** To a 100 mL round bottom flask was added triethylamine (5.19 mL, 37.2 mmol, 2.670 equiv.), dichloromethane (25 mL), 4-cyanobenzenesulfonyl chloride (2.80 g, 13.9 mmol, 1.000 equiv.), 4-toluenesulfonamide (2.55 g, 14.9 mmol, 1.200 equiv.), and 4-dimethylaminopyridine (0.303 g, 2.48 mmol, 0.179 equiv.). The reaction stirred for 3 h at 50 °C. To the solution was added HCl (50 mL, 3 N). The mixture stirred at room temperature for 2 h. The layers were separated and the HCl layer was extracted with DCM (1x50 mL). The organic layers combined and washed with HCl (4x75 mL, 3 N). The organic layer was then dried with magnesium sulfate, filtered, and concentrated *in vacuo*. The crude layer was then stirred in chloroform (50 mL) at room temperature for 1 h. The white solid was filtered out and residual solvent was dried *in vacuo*. The product (**21d<sub>i</sub>**) was isolated as a white solid in 42.6% yield. <sup>1</sup>H NMR (400 MHz, Methanol-d<sub>4</sub>) δ 8.02 – 7.94 (m, 2H), 7.92 – 7.83 (m, 2H), 7.78 – 7.68 (m, 2H), 7.37 – 7.29 (m, 2H), 2.45 (s, 3H); <sup>13</sup>C NMR (101 MHz, Methanol-d<sub>4</sub>) δ 144.75, 144.59, 137.30, 132.70, 129.31, 127.87, 127.23, 116.97, 116.40, 20.16.

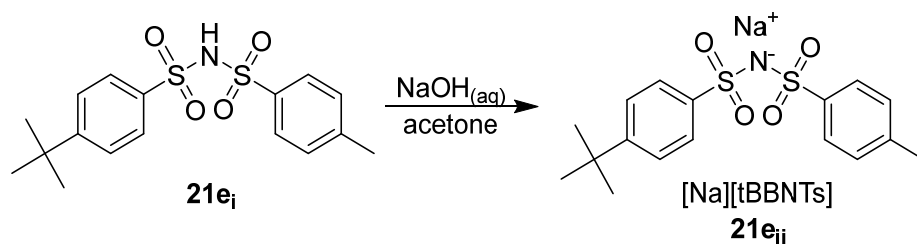


**sodium ((4-cyanophenyl)sulfonyl)(tosyl)azanide (21d<sub>ii</sub>):** To a 100 mL round bottom flask was added **21d<sub>i</sub>** (1.78 g, 5.28 mmol, 1.125 equiv.), sodium carbonate (497 mg, 4.69 mmol, 1.000 equiv.), and Milli-Q water (50 mL), and acetone (35 mL). The mixture was stirred until dissolved. The acetone was then removed *in vacuo*. The water layer was then washed with ethyl acetate (3x50 mL) and concentrated *in vacuo*, revealing

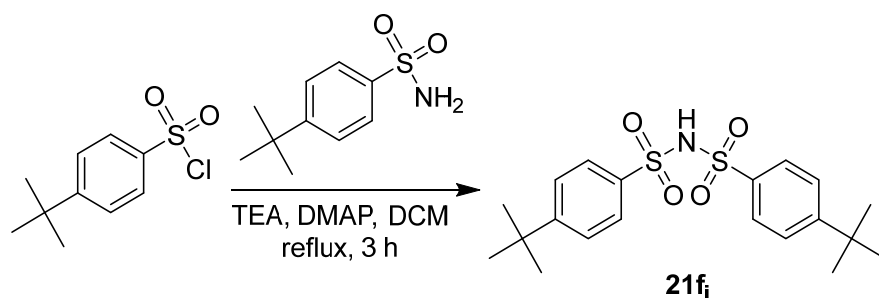
the product (**21d<sub>ii</sub>**) in 99% yield. <sup>1</sup>H NMR (400 MHz, Methanol-d<sub>4</sub>) δ 7.84 – 7.76 (m, 2H), 7.70 – 7.63 (m, 2H), 7.58 – 7.51 (m, 2H), 7.16 – 7.09 (m, 2H), 2.37 (s, 3H); <sup>13</sup>C NMR (101 MHz, Methanol-d<sub>4</sub>) δ 148.13, 141.71, 140.55, 131.85, 128.40, 127.27, 126.44, 117.53, 113.89, 19.96.



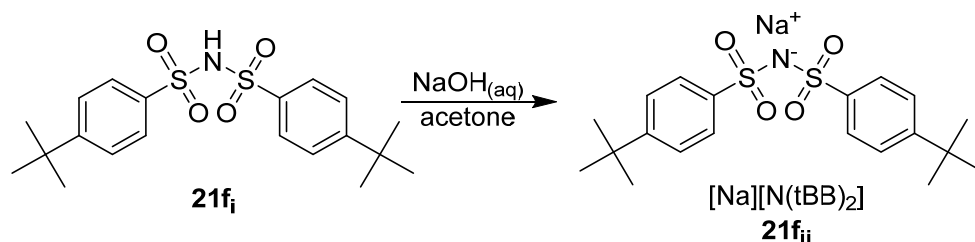
**4-(tert-butyl)-N-tosylbenzenesulfonamide (21e<sub>i</sub>):** To a 100 mL round bottom flask was added triethylamine (4.90 mL, 35.2 mmol, 3.0 equiv.), dichloromethane (25 mL), 4-toluenesulfonamide (2.01 g, 11.7 mmol, 1.0 equiv.), 4-tertbutylbenzenesulfonyl chloride (2.73 g, 11.7 mmol, 1.0 equiv.), and 4-dimethylaminopyridine (0.286 g, 2.34 mmol, 0.2 equiv.). The reaction stirred for 3 h at 50 °C. To the solution was added HCl (50 mL, 2 N). The solution stirred at room temperature for 10 min. Afterwards, the layers were separated, and the organic layer was washed with HCl (3x50 mL, 2 N), dried with magnesium sulfate, and concentrated *in vacuo*. The crude product was purified by stirring in 2:1 hexanes and chloroform (75 mL) at room temperature for 3 h. The mixture was filtered, and residual solvent from the solid was removed *in vacuo*. The product (**21e<sub>i</sub>**) was purified as a white solid in 62.6% yield. <sup>1</sup>H NMR (400 MHz, Acetone-d<sub>6</sub>) δ 9.75 (s, 1H), 7.84 – 7.78 (m, 2H), 7.78 – 7.72 (m, 2H), 7.65 – 7.57 (m, 2H), 7.40 (s, 0H), 7.37 (d, *J* = 8.2 Hz, 2H), 2.43 (s, 3H), 1.37 (s, 9H).



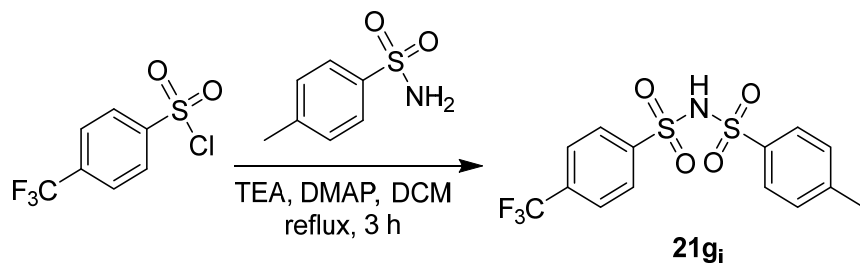
**sodium ((4-(tert-butyl)phenyl)sulfonyl)(tosyl)azanide (**21e<sub>ii</sub>**):** To a 250 mL round bottom flask was added **21e<sub>i</sub>** (2.70 g, 7.34 mmol, 1.125 equiv.), NaOH (261 mg, 6.53 mmol, 1.000 equiv.), acetone (40 mL), and Milli-Q water (175 mL). The mixture stirred and was sonicated until clear. Afterwards, the solution was washed with ethyl acetate (3x75 mL). The water layer was then removed *in vacuo* to product the product (**21e<sub>ii</sub>**) as a white solid in 86.0% yield. <sup>1</sup>H NMR (400 MHz, Methanol-d<sub>4</sub>) δ 7.58 – 7.52 (m, 2H), 7.52 – 7.46 (m, 2H), 7.33 – 7.25 (m, 2H), 7.05 (d, *J* = 8.0 Hz, 2H), 2.32 (s, 3H), 1.31 (s, 9H); <sup>13</sup>C NMR (101 MHz, Methanol-d<sub>4</sub>) δ 154.27, 141.09, 140.63, 140.47, 128.22, 126.38, 126.19, 124.60, 34.29, 30.23, 20.07.



**4-(tert-butyl)-N-((4-(tert-butyl)phenyl)sulfonyl)benzenesulfonamide (**21f<sub>i</sub>**):** To a 100 mL round bottom flask was added diisopropylethylamine (6.13 mL, 35.2 mmol, 3.0 equiv.), dichloromethane (25 mL), 4-tertbutylbenzenesulfonamide (2.50 g, 11.7 mmol, 1.0 equiv.), 4-tertbutylbenzenesulfonyl chloride (2.73 g, 11.7 mmol, 1.0 equiv.), and 4-dimethylaminopyridine (0.286 g, 2.34 mmol, 0.2 equiv.). The reaction stirred for 3 h at 50 °C. To the solution was added HCl (50 mL, 1 M). The mixture stirred at room temperature for 1 h. The layers were separated, and the aqueous layer was extracted with DCM (1x50 mL). The organic layers were combined, washed with HCl (4x50 mL, 2 M), dried with magnesium sulfate, and concentrated *in vacuo*. Then, the crude yellow/white solid was stirred in a 3:1 chloroform and hexanes solution (100 mL) at room temperature for 1 h. Finally, the solid was filtered and residual solvent was removed *in vacuo*. The product (**21f<sub>i</sub>**) was isolated as a white solid in 18.7% yield. <sup>1</sup>H NMR (400 MHz, Methanol-d<sub>4</sub>) δ 7.81 – 7.73 (m, 2H), 7.63 – 7.54 (m, 2H), 1.38 (s, 9H).

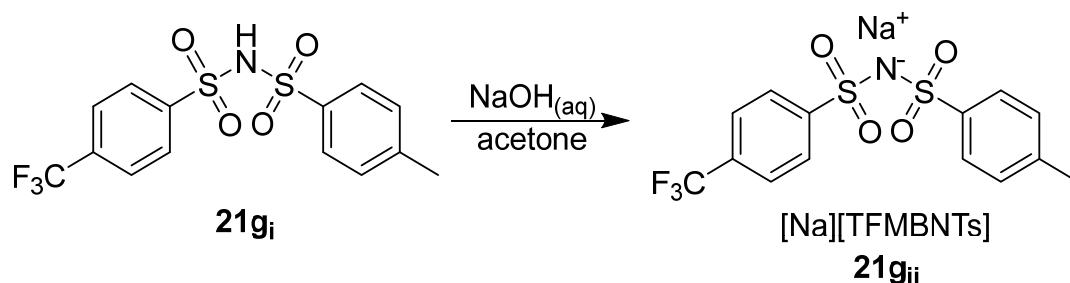


**sodium bis((4-(tert-butyl)phenyl)sulfonyl)azanide (21f<sub>ii</sub>):** To a 250 mL round bottom flask was added **21f<sub>i</sub>** (0.898 g, 2.19 mmol, 1.125 equiv.), NaOH (78.0 mg, 1.95 mmol, 1.0 equiv.), acetone (33 mL), and Milli-Q water (100 mL). The mixture stirred until the components dissolved. The solvent was removed *in vacuo* to produce the product (**21f<sub>ii</sub>**) in 66.7% yield. <sup>1</sup>H NMR (400 MHz, Methanol-d<sub>4</sub>) δ 7.65 – 7.58 (m, 4H), 7.39 – 7.32 (m, 4H), 1.32 (s, 18H); <sup>13</sup>C NMR (101 MHz, Methanol-d<sub>4</sub>) δ 154.30, 141.11, 126.15, 124.66, 34.35, 30.26.

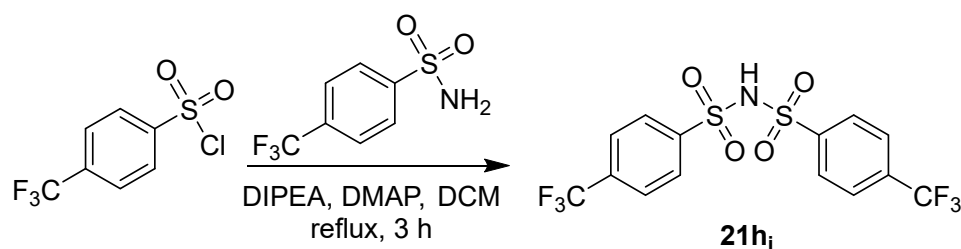


**4-methyl-N-((4-(trifluoromethyl)phenyl)sulfonyl)benzenesulfonamide (21g<sub>i</sub>):** To a 100 mL round bottom flask was added triethylamine (4.64 mL, 33.3 mmol, 3.0 equiv.), dichloromethane (25 mL), 4-toluenesulfonamide (1.90 g, 11.1 mmol, 1.0 equiv.), 4-(trifluoromethyl)benzenesulfonyl chloride (2.72 g, 11.1 mmol, 1.0 equiv.), and 4-dimethylaminopyridine (0.271 g, 2.22 mmol, 0.2 equiv.). The reaction stirred for 3 h at 50 °C. To the solution was added HCl (50 mL, 2 N). The solution stirred at room temperature for 10 min. The mixture was transferred to a separatory funnel and the aqueously layer was removed. The organic layer was then washed with HCl (3x50 mL, 2 N). Then, the organic layer was dried with magnesium sulfate and concentration *in vacuo*. The crude product was washed with 1:1 chloroform and hexanes (50 mL) at room temperature for 1 h. The product was then filtered, and residual solvent was removed *in vacuo*. The product (**21g<sub>i</sub>**) was isolated as a white solid in 15.2% yield. <sup>1</sup>H NMR (400 MHz, Methanol-d<sub>4</sub>) δ 8.01

–7.94 (m, 2H), 7.84 – 7.76 (m, 2H), 7.71 – 7.64 (m, 2H), 7.32 – 7.24 (m, 2H), 2.41 (s, 3H);  $^{13}\text{C}$  NMR (101 MHz, Methanol-d<sub>4</sub>)  $\delta$  144.63, 144.06 (d,  $J = 1.6$  Hz), 137.13, 134.14 (q,  $J = 32.8$  Hz), 129.24, 127.91, 127.18, 125.81 (q,  $J = 3.8$  Hz), 123.41 (d,  $J = 271.9$  Hz), 20.08;  $^{19}\text{F}$  NMR (376 MHz, Methanol-d<sub>4</sub>)  $\delta$  -64.57.

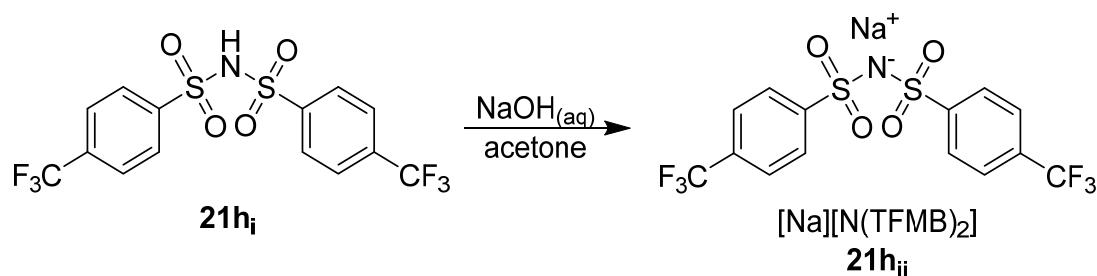


**sodium tosyl((4-(trifluoromethyl)phenyl)sulfonyl)azanide (21g<sub>ii</sub>):** To a 250 mL round bottom flask was added **21g<sub>i</sub>** (0.638 g, 1.68 mmol, 1.125 equiv.), NaOH (59.8 mg, 1.50 mmol, 1.000 equiv.), acetone (20 mL), and Milli-Q water (50 mL). The mixture stirred until the components dissolved. Afterwards, the solution was washed with ethyl acetate (3x75 mL). Finally, the water layer was removed *in vacuo*. The product (**21g<sub>ii</sub>**) was isolated as a white solid in 75.2% yield.  $^1\text{H}$  NMR (400 MHz, Methanol-d<sub>4</sub>)  $\delta$  7.82 – 7.75 (m, 2H), 7.56 (d,  $J = 8.2$  Hz, 2H), 7.53 – 7.46 (m, 2H), 7.09 – 7.02 (m, 2H), 2.32 (s, 3H);  $^{13}\text{C}$  NMR (101 MHz, Methanol-d<sub>4</sub>)  $\delta$  147.24, 141.59, 140.28, 131.98 (q,  $J = 32.4$  Hz), 128.32, 127.16, 126.41, 125.13 (q), 124.81 (q,  $J = 3.9$  Hz), 19.86;  $^{19}\text{F}$  NMR (376 MHz, Methanol-d<sub>4</sub>)  $\delta$  -64.28.



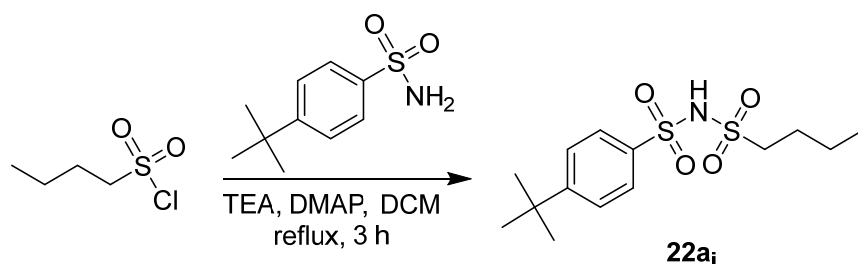
**4-(trifluoromethyl)-N-((4-(trifluoromethyl)phenyl)sulfonyl)benzenesulfonamide (21h<sub>i</sub>):** To a 100 mL round bottom flask was added diisopropylethylamine (5.80 mL, 33.3 mmol, 3.0 equiv.), dichloromethane (25 mL), 4-(trifluoromethyl)benzenesulfonamide (2.50 g, 11.1 mmol, 1.0 equiv.), 4-

(trifluoromethyl)benzenesulfonyl chloride (2.72 g, 11.1 mmol, 1.0 equiv.), and 4-dimethylaminopyridine (0.271 g, 2.22 mmol, 0.2 equiv.). The reaction stirred for 3 h at 50 °C. To the solution was added HCl (50 mL, 1 M), and the mixture stirred at room temperature for 1 h. The layers were separated, and the aqueous layer was extracted with DCM (1x50 mL). The organic layers were combined, washed with HCl (4x50 mL, 2 M), dried with magnesium sulfate, and concentrated *in vacuo*. The crude yellow/white solid was washed with a 3:1 chloroform and hexanes solution (100 mL) at room temperature for 1 h. A white solid precipitated and was filtered out, collected, and residual solvent was removed *in vacuo*. The product (**21h<sub>i</sub>**) was isolated as a white solid in 37.9% yield. <sup>1</sup>H NMR (500 MHz, Methanol-d<sub>4</sub>) δ 7.93 (d, *J* = 8.2 Hz, 9H), 7.71 (d, *J* = 8.3 Hz, 9H).

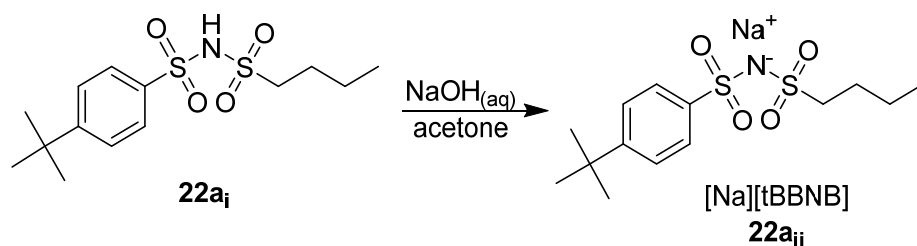


**sodium bis((4-(trifluoromethyl)phenyl)sulfonyl)azanide (21h<sub>ii</sub>):** To a 250 mL round bottom flask was added **21h<sub>i</sub>** (1.82 g, 4.21 mmol, 1.125 equiv.), NaOH (150 mg, 3.74 mmol, 1.0 equiv.), acetone (25 mL), and Milli-Q water (100 mL). The mixture was sonicated and stirred until dissolved. Afterwards, the solution was washed with ethyl acetate (3x75 mL). The water layer was then removed *in vacuo*. Separately, the organic layer was concentrated *in vacuo*, and the resulting crude solid was washed in DCM (25 mL) at room temperature for 1 h. The white solid was filtered, and residual solvent was removed *in vacuo*. The two fractions were combined as the product (**21h<sub>ii</sub>**) as a white solid in 94.0% yield. <sup>1</sup>H NMR (400 MHz, Methanol-d<sub>4</sub>) δ 7.85 (d, *J* = 8.2 Hz, 4H), 7.62 (d, *J* = 8.1 Hz, 4H); <sup>13</sup>C NMR (101 MHz, Methanol-d<sub>4</sub>) δ 147.42, 132.30 (q, *J* = 32.7 Hz), 127.14, 128.15 – 119.51 (m), 124.94 (dd, *J* = 4.9, 2.9 Hz); <sup>19</sup>F NMR (376 MHz, Methanol-d<sub>4</sub>) δ -64.45.

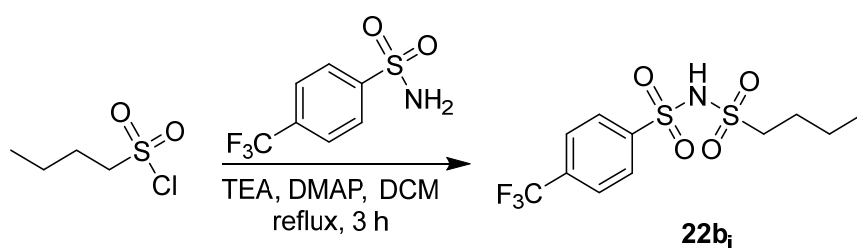
## 2.4.18 Synthesis of third-generation bis(sulfonyl)azanide anions



**4-(tert-butyl)-N-(butylsulfonyl)benzenesulfonamide (22a<sub>i</sub>):** To a 100 mL round bottom flask was added triethylamine (6.67 mL, 47.9 mmol, 3.0 equiv.), dichloromethane (25 mL), 4-(tertbutyl)benzenesulfonamide (3.40 g, 16.0 mmol, 1.0 equiv.), n-butanoyl chloride (2.07 mL, 16.0 mmol, 1.0 equiv.), and 4-dimethylaminopyridine (0.390 g, 3.19 mmol, 0.2 equiv.). The reaction stirred for 3 h at 50 °C. To the solution was added HCl (50 mL, 3 N). The solution stirred for at least an hour. The phases were separated and the HCl phase was extracted with DCM (1x50 mL). The organic fractions were combined and were washed with HCl (3x50 mL, 3 N), dried with magnesium sulfate, filtered, and concentrated *in vacuo*. The crude product was redissolved in DCM (25 mL) and was washed with sat. sodium bicarbonate (2x25 mL). The organic layer wash chilled to 0 °C, which resulted in the precipitation of a white solid. The solid was filtered, collected, and residual solvent was removed *in vacuo*. The product (**22a<sub>i</sub>**) was isolated as a white solid in 39.1% yield. <sup>1</sup>H NMR (400 MHz, Methanol-d<sub>4</sub>) δ 7.90 – 7.82 (m, 2H), 7.62 – 7.42 (m, 2H), 3.03 – 2.94 (m, 2H), 1.72 (dddd, *J* = 8.9, 7.9, 6.7, 5.7 Hz, 2H), 1.43 – 1.29 (m, 2H), 1.36 (s, 9H), 0.91 (t, *J* = 7.4 Hz, 3H); <sup>13</sup>C NMR (101 MHz, Methanol-d<sub>4</sub>) δ 154.56, 141.96, 126.21, 124.94, 53.97, 34.42, 30.22, 25.77, 21.27, 12.67.

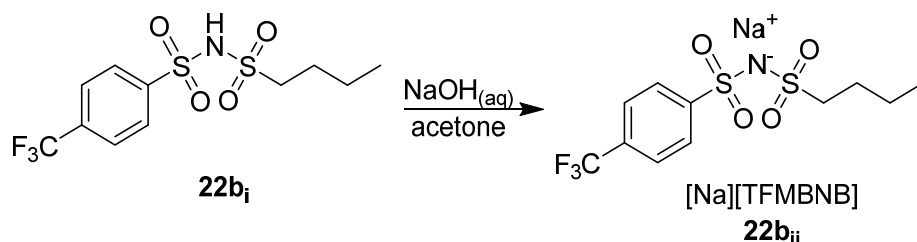


**sodium ((4-(tert-butyl)phenyl)sulfonyl)(butylsulfonyl)azanide (22a<sub>ii</sub>):** To a 100 mL flask was added **22a<sub>i</sub>** (2.082 g, 6.24 mmol, 1.125 equiv.), NaOH (222 mg, 5.55 mmol, 1.0 equiv.), Milli-Q water (50 mL), and acetone (35 mL). The mixture stirred until all components dissolved. The acetone was removed *in vacuo*, and the water layer was washed with ethyl acetate (3x25 mL). Then, the water layer was removed *in vacuo* revealing the product (**22a<sub>ii</sub>**) as a white solid in 72.9% yield. <sup>1</sup>H NMR (400 MHz, Methanol-d<sub>4</sub>) δ 7.92 – 7.84 (m, 2H), 7.57 – 7.49 (m, 2H), 2.97 – 2.88 (m, 2H), 1.77 – 1.62 (m, 2H), 1.35 (s, 9H), 1.30 (p, *J* = 7.4 Hz, 2H), 0.87 (t, *J* = 7.4 Hz, 3H); <sup>13</sup>C NMR (101 MHz, Methanol-d<sub>4</sub>) δ 179.20, 154.70, 141.69, 126.28, 125.03, 53.79, 34.46, 30.29, 25.73, 22.99, 21.26, 12.73.

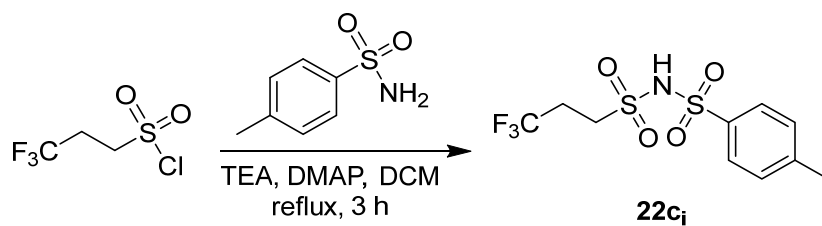


**N-(butylsulfonyl)-4-(trifluoromethyl)benzenesulfonamide (22b<sub>i</sub>):** To a 100 mL round bottom flask was added triethylamine (6.67 mL, 47.9 mmol, 3.0 equiv.), dichloromethane (25 mL), 4-(trifluoromethyl)benzenesulfonamide (3.59 g, 16.0 mmol, 1.0 equiv.), n-butanesulfonyl chloride (2.07 mL, 16.0 mmol, 1.0 equiv.), and 4-dimethylaminopyridine (0.390 g, 3.19 mmol, 0.2 equiv.). The reaction stirred for 3 h at 50 °C. To the solution was added HCl (50 mL, 3 N). The solution stirred for at room temperature for 1 h. The phases were separated and the HCl phase was extracted with DCM (1x50 mL). The organic fractions were combined, washed with HCl (3x50 mL, 3 N), dried with magnesium sulfate, filtered, and concentrated *in vacuo*. Then, the compound was redissolved in DCM (25 mL) was washed with sat. sodium bicarbonate (3x25 mL), which resulted in the precipitation of a white solid. The solid was filtered out and dried *in vacuo*. The product (**22b<sub>i</sub>**) was isolated as a white solid in 14.9% yield. <sup>1</sup>H NMR (400 MHz, Methanol-d<sub>4</sub>) δ 8.14 – 8.07 (m, 2H), 7.82 – 7.75 (m, 2H), 3.17 – 3.08 (m, 2H), 1.85 – 1.73 (m, 2H), 1.45 (h, *J* = 7.4 Hz, 2H), 0.95 (t, *J* = 7.4 Hz, 3H); <sup>13</sup>C NMR (101 MHz, Methanol-d<sub>4</sub>) δ 149.08, 133.49 – 131.08

(m), 127.18, 125.00 (q,  $J = 3.9$  Hz), 123.84 (d,  $J = 271.7$  Hz), 54.31, 25.79, 21.27, 12.62;  $^{19}\text{F}$  NMR (376 MHz, Methanol- $d_4$ )  $\delta$  -64.34.

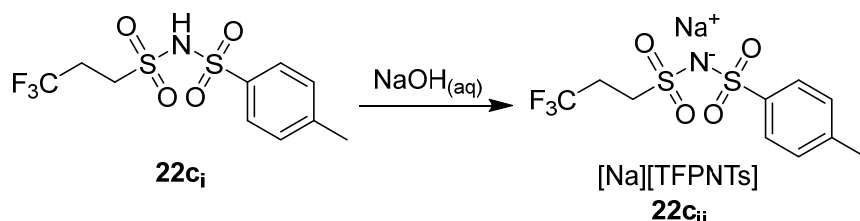


**sodium (butylsulfonyl)((4-(trifluoromethyl)phenyl)sulfonyl)azanide (22b<sub>ii</sub>):** To a 100 mL round bottom flask was added **22b<sub>i</sub>** (0.819 g, 2.37 mmol, 1.125 equiv.), NaOH (84.3 mg, 2.11 mmol, 1.0 equiv.), Milli-Q water (50 mL), and acetone (35 mL). The reaction stirred until all components dissolved. Then, the acetone was removed *in vacuo*. The water layer was washed with ethyl acetate (3x25 mL) and concentrated *in vacuo* to reveal the product (**22b<sub>ii</sub>**) as a white solid in 81.1% yield.  $^1\text{H}$  NMR (400 MHz, Methanol- $d_4$ )  $\delta$  8.14 – 8.06 (m, 2H), 7.83 – 7.75 (m, 2H), 3.17 – 3.08 (m, 2H), 1.85 – 1.73 (m, 2H), 1.45 (h,  $J = 7.4$  Hz, 2H), 0.96 (t,  $J = 7.4$  Hz, 3H);  $^{13}\text{C}$  NMR (101 MHz, Methanol- $d_4$ )  $\delta$  149.11, 132.04, 127.18, 124.99 (q,  $J = 3.9$  Hz), 122.49, 54.31, 25.79, 21.27, 12.61;  $^{19}\text{F}$  NMR (376 MHz, Methanol- $d_4$ )  $\delta$  -64.35.



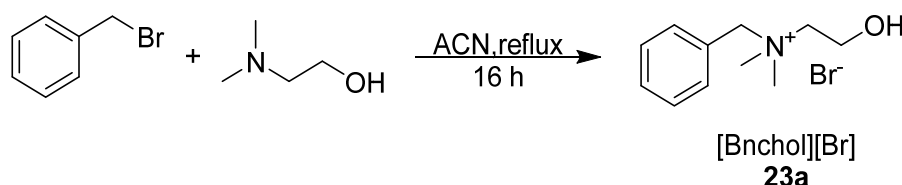
**4-methyl-N-((3,3,3-trifluoropropyl)sulfonyl)benzenesulfonamide (22c<sub>i</sub>):** To a 100 mL round bottom flask was added 3,3,3-trifluoropropanesulfonyl chloride (1.51 mL, 10.2 mmol, 1.0 equiv.), 4-toluenesulfonamide (2.09 g, 12.2 mmol, 1.2 equiv.), 4-dimethylaminopyridine (248 mg, 2.03 mmol, 0.2 equiv.), DCM (25 mL), and TEA (4.25 mL, 30.5 mmol, 3.0 equiv.). The compound stirred for 3 h at 50°C. To the reaction solution was added HCl (50 mL, 3 N). The mixture stirred at room temperature for 1 h. The organic layer was separated and then washed with HCl (4x75 mL, 3 N). The organic layer was dried with

magnesium sulfate, filtered, and then concentrated *in vacuo*. The compound (**22c<sub>i</sub>**) was carried over to the next step without further purification. <sup>1</sup>H NMR (400 MHz, Methanol-d<sub>4</sub>) δ 7.85 (d, *J* = 8.4 Hz, 2H), 7.43 – 7.36 (m, 2H), 3.69 – 3.60 (m, 2H), 2.84 – 2.67 (m, 2H), 2.43 (s, 3H); <sup>19</sup>F NMR (376 MHz, Methanol-d<sub>4</sub>) δ -67.42.



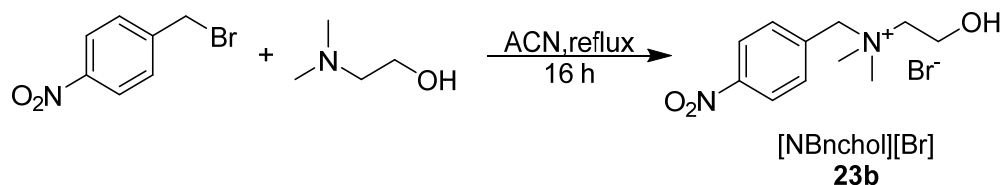
**sodium tosyl((3,3,3-trifluoropropyl)sulfonyl)azanide (22c<sub>ii</sub>):** To a 100 mL round bottom flask was added **22c<sub>i</sub>** (1.38 g, 4.15 mmol, 1.125 equiv.), NaOH (148 mg, 3.69 mmol, 1.000 equiv.), and Milli-Q water (50mL). The mixture was sonicated and then stirred at room temperature until dissolved. The water layer was washed with ethyl acetate (3x50 mL) and then concentrated *in vacuo* to produce the product (**22c<sub>ii</sub>**) as a white solid in 87.0% yield. <sup>1</sup>H NMR (400 MHz, Methanol-d<sub>4</sub>) δ 7.85 – 7.77 (m, 2H), 7.34 – 7.26 (m, 2H), 3.30 – 3.21 (m, 2H), 2.73 – 2.57 (m, 2H), 2.41 (s, 3H); <sup>13</sup>C NMR (101 MHz, Methanol-d<sub>4</sub>) δ 141.77 (d, *J* = 2.2 Hz), 128.54, 126.37, 126.33 (q, *J* = 275.4 Hz), 46.87 (q, *J* = 3.0 Hz), 29.14 (q, *J* = 30.4 Hz), 19.99; <sup>19</sup>F NMR (376 MHz, Methanol-d<sub>4</sub>) δ -67.72.

#### 2.4.19 Synthesis of cyclic monocholinium cations

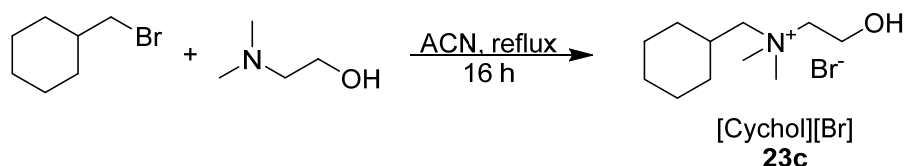


**N-benzyl-2-hydroxy-N,N-dimethylethan-1-aminium bromide (23a):** To a 250 mL round bottom flask was added anhydrous acetonitrile (35 mL). A reflux condenser was attached, and the reaction vessel was purged with argon for 15 min. Then, to the reaction flask was added benzyl bromide (7.62 mL, 64.0 mmol, 1.0 equiv.) and dimethylaminoethanol (6.44 mL, 64.0 mmol, 1.0 equiv.). The reaction stirred at 80 °C for

24 h, in which a white solid precipitated out. The white solid was filtered, crushed, and washed with acetone (3x20 mL). The solid was collected, and residual solvent was removed *in vacuo*. The product (**23a**) was isolated as a white solid in 99.0% yield.  $^1\text{H}$  NMR (400 MHz, Deuterium Oxide)  $\delta$  7.65 – 7.30 (m, 5H), 4.49 (s, 2H), 4.09 – 4.01 (m, 2H), 3.48 – 3.41 (m, 2H), 3.03 (s, 6H);  $^{13}\text{C}$  NMR (101 MHz, Deuterium Oxide)  $\delta$  133.07, 130.81, 129.16, 127.04, 69.70 – 68.88 (m), 65.81 – 65.00 (m), 55.38, 51.13 – 49.49 (m).



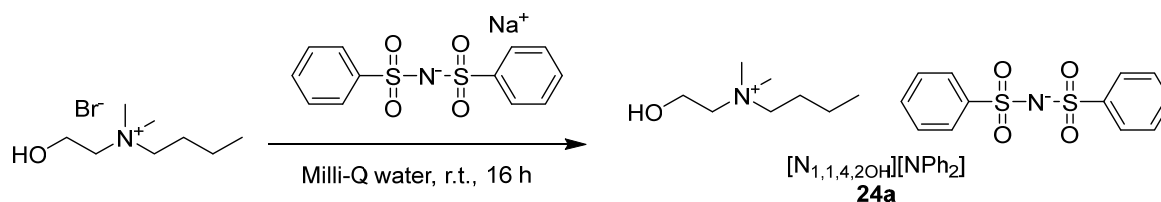
**2-hydroxy-*N,N*-dimethyl-*N*-(4-nitrobenzyl)ethan-1-aminium bromide (23b):** To a 100 mL round bottom flask was added anhydrous acetonitrile (20 mL). A reflux condenser was attached, and the reaction vessel was purged with argon. Then, to the reaction flask was added 4-nitrobenzyl bromide (6.91 g, 32.0 mmol, 1.0 equiv.) and dimethylaminoethanol (3.22 mL, 32.0 mmol, 1.0 equiv.). The reaction stirred at 80 °C for 24 h, in which the solution turned orange. The orange solution was then concentrated *in vacuo*, and the solid was stirred in acetone (25 mL) at room temperature for 2 h. The solid was then filtered, washed with acetone (3x20 mL), collected, and residual solvent was removed *in vacuo*. The product (**23b**) was isolated as a solid in 95.8% yield.  $^1\text{H}$  NMR (400 MHz, Deuterium Oxide)  $\delta$  8.33 – 8.25 (m, 2H), 7.76 (d,  $J$  = 18.4 Hz, 0H), 7.80 – 7.72 (m, 2H), 4.66 (s, 2H), 4.08 (dq,  $J$  = 7.2, 2.2 Hz, 2H), 3.55 – 3.48 (m, 2H), 3.10 (s, 6H);  $^{13}\text{C}$  NMR (101 MHz, Deuterium Oxide)  $\delta$  148.97, 134.35, 133.99, 124.09, 67.74, 65.79, 55.38, 50.62.



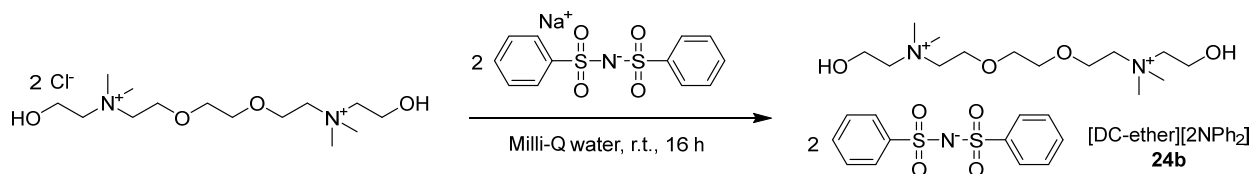
***N*-(cyclohexylmethyl)-2-hydroxy-*N,N*-dimethylethan-1-aminium bromide (23c):** To a 100 mL round bottom flask was added anhydrous acetonitrile (25 mL). A reflux condenser was attached. Then, to the

reaction vessel was added (bromomethyl)cyclohexane (3.94 mL, 28.2 mmol, 1.0 equiv.) and dimethylaminoethanol (2.84 mL, 28.2 mmol, 1.0 equiv.). The reaction stirred at 80 °C for 24 h. The solvent was removed *in vacuo*, producing a white solid. The white solid was crushed and stirred in diethyl ether (25 mL) at room temperature for 1 h hour. The white solid was then filtered off and residual solvent was removed *in vacuo*. The product (**23c**) was isolated as a white solid in 96.0% yield. <sup>1</sup>H NMR (400 MHz, Deuterium Oxide) δ 4.06 – 3.94 (m, 2H), 3.54 – 3.40 (m, 2H), 3.21 (d, *J* = 4.5 Hz, 2H), 3.10 (s, 6H), 2.07 – 0.97 (m, 11H); <sup>13</sup>C NMR (101 MHz, Deuterium Oxide) δ 72.52 – 72.32 (m), 65.61 (t, *J* = 3.0 Hz), 55.41, 51.89 – 51.19 (m), 32.84, 31.97, 25.37, 25.07.

#### 2.4.20 Synthesis of ILs containing second-generation bis(sulfonyl)azanide anions

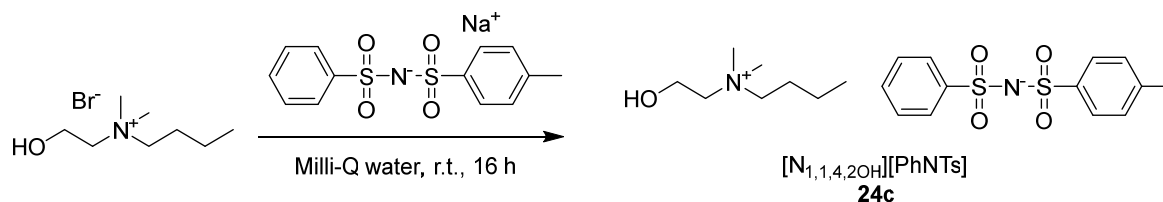


***N*-(2-hydroxyethyl)-*N,N*-dimethylbutan-1-aminium bis(phenylsulfonyl)azanide (24a):** To a 25 mL round bottom flask was added **2a** ([N<sub>1,1,4,2OH</sub>][Br]); 0.305 g, 1.35 mmol, 1.0 equiv.), **20a<sub>ii</sub>** ([Na][NPh<sub>2</sub>]); 0.400 g, 1.35 mmol, 1.0 equiv.), and Milli-Q water (15 mL). The reaction stirred at room temperature for 24 h. No ionic liquid phase separated so the product was deemed water soluble, and thus, no workup nor characterization was performed.

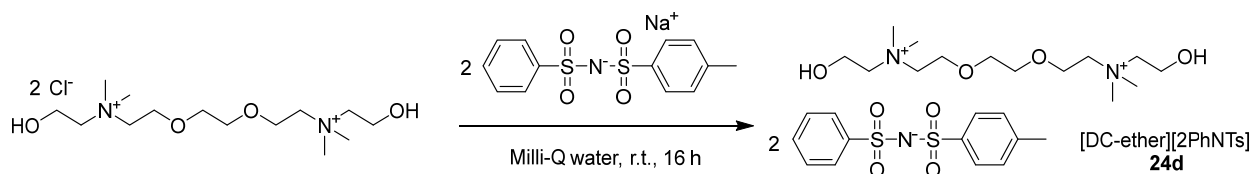


**2,2'-(ethane-1,2-diylbis(oxy))bis(*N*-(2-hydroxyethyl)-*N,N*-dimethylethan-1-aminium) bis(phenylsulfonyl)azanide (24b):** To a 25 mL round bottom was added **4j** ([DC-ether][2Cl]); 0.305 g, 0.835 mmol, 1.0 equiv.), **20a<sub>ii</sub>** ([Na][NPh<sub>2</sub>]); 0.400 g, 1.25 mmol, 1.5 equiv.), and Milli-Q water (15 mL). The reaction

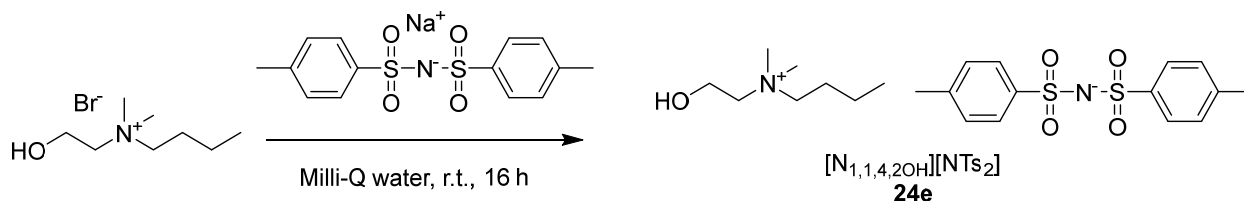
stirred overnight at room temperature. No ionic liquid phase separated so the product was deemed water soluble, and thus, no workup nor characterization was performed.



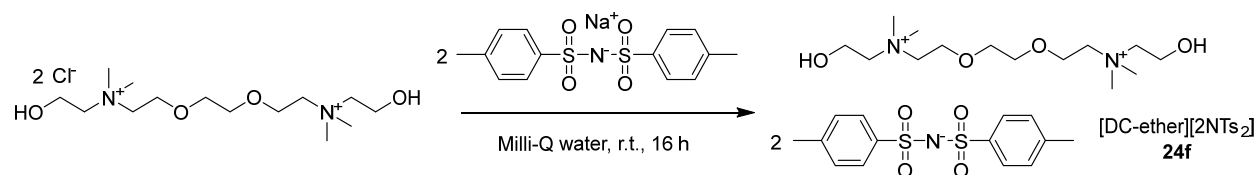
***N*-(2-hydroxyethyl)-*N,N*-dimethylbutan-1-aminium (phenylsulfonyl)(tosyl)azanide (24c):** To a 25 mL round bottom flask was added **2a** ([N<sub>1,1,4,2OH</sub>][Br]; 0.271 g, 1.20 mmol, 1.0 equiv.), **20c<sub>ii</sub>** ([Na][PhNTs]; 0.400 g, 1.20 mmol, 1.0 equiv.), and Milli-Q water (15 mL). The reaction stirred at room temperature for 24 h. The ionic liquid was mainly water soluble, although there was some cloudiness; however, since no second layer formed, the product was deemed water soluble, and no further workup nor characterization was performed.



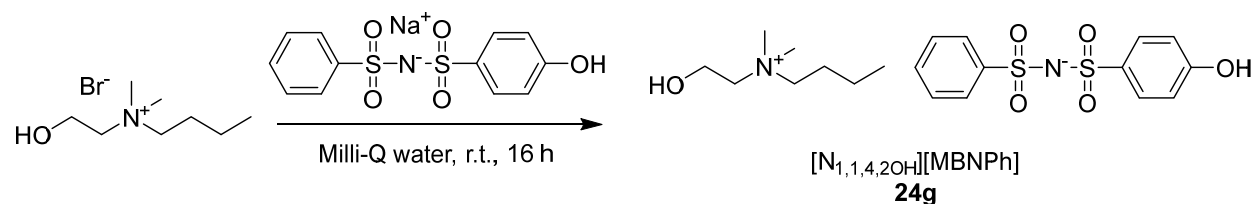
**2,2'-(ethane-1,2-diylbis(oxy))bis(*N*-(2-hydroxyethyl)-*N,N*-dimethylethan-1-aminium (phenylsulfonyl)(tosyl)azanide (24d):** To a 25 mL round bottom was added **4j** ([DC-ether][2Cl]; 0.292 g, 0.800 mmol, 1.0 equiv.), **20c<sub>ii</sub>** ([Na][PhNTs]; 0.400 g, 1.20 mmol, 1.5 equiv.), and Milli-Q water (15 mL). The reaction stirred for 24 h at room temperature. The ionic liquid was mainly water soluble, although there was some cloudiness; however, since no second layer formed, the product was deemed water soluble, and no workup nor characterization was performed.



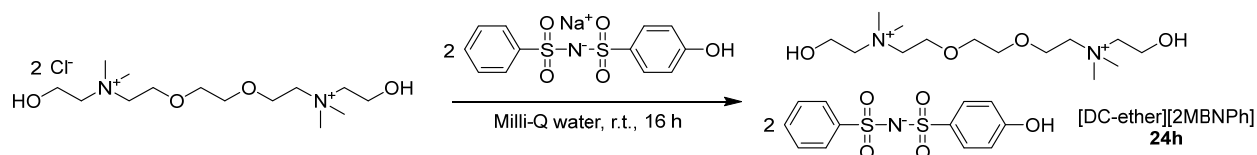
***N*-(2-hydroxyethyl)-*N,N*-dimethylbutan-1-aminium ditosylazanide (24e):** To a 25 mL round bottom flask was added **2a** ( $[N_{1,1,4,2OH}][Br]$ ; 0.260 g, 1.15 mmol, 1.0 equiv.), **20b<sub>ii</sub>** ( $[Na][NTs_2]$ ; 0.400 g, 1.15 mmol, 1.0 equiv.), and Milli-Q water (15 mL). The reaction stirred at room temperature for 24 h. The ionic liquid was mainly water soluble, although there was some cloudiness; however, since no second layer formed, the product was deemed water soluble, and thus, no workup nor characterization was performed.



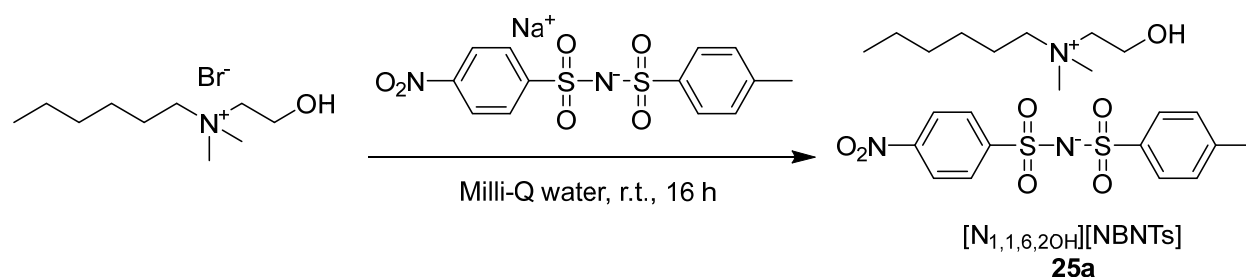
**2,2'-(ethane-1,2-diylbis(oxy))bis(*N*-(2-hydroxyethyl)-*N,N*-dimethylethan-1-aminium) ditosylazanide (24f):** To a 25 mL round bottom flask was added **4j** ( $[DC\text{-ether}][2Cl]$ ; 0.280 g, 0.768 mmol, 1.0 equiv.), **20b<sub>ii</sub>** ( $[Na][NTs_2]$ ; 0.400 g, 1.15 mmol, 1.5 equiv.), and Milli-Q water (15 mL). The reaction stirred at room temperature for 24 h. The ionic liquid was mainly water soluble, although there was some cloudiness; however, since no second layer formed, the product was deemed water soluble, and thus, no workup nor characterization was performed.



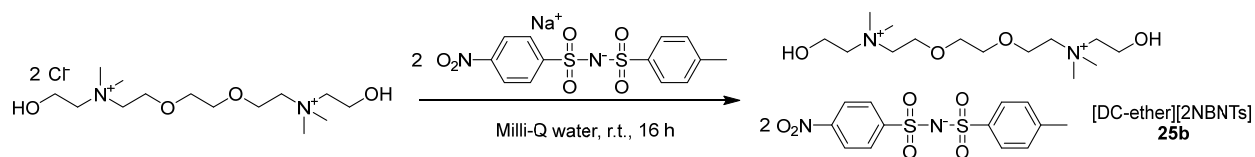
***N*-(2-hydroxyethyl)-*N,N*-dimethylbutan-1-aminium ((4-hydroxyphenyl)sulfonyl)(phenylsulfonyl)azanide (24g):** To a 25 mL round bottom flask was added **2a** ( $[N_{1,1,4,2OH}][Br]$ ; 0.270 g, 1.19 mmol, 1.0 equiv.), **20d<sub>ii</sub>** ( $[Na][MBNPh]$ ; 0.400 g, 1.19 mmol, 1.0 equiv.), and Milli-Q water (15 mL). The reaction stirred at room temperature for 24 h. No ionic liquid phase separated so the product was deemed water soluble, and thus, no workup nor characterization was performed.



**2,2'-(ethane-1,2-diylbis(oxy))bis(*N*-(2-hydroxyethyl)-*N,N*-dimethylethan-1-aminium) ((4-hydroxyphenyl)sulfonyl)(phenylsulfonyl)azanide (**24h**):** To a 25 mL round bottom flask was added **4j** ([DC-ether][2Cl]); 0.291 g, 0.795 mmol, 1.0 equiv.), **20d<sub>ii</sub>** ([Na][MBNPh]; 0.400 g, 1.19 mmol, 1.5 equiv.), and Milli-Q water (15 mL). The reaction stirred at room temperature for 24 h. No ionic liquid phase separated so the product was deemed water soluble, and thus, no workup nor characterization was performed.



***N*-(2-hydroxyethyl)-*N,N*-dimethylhexan-1-aminium ((4-nitrophenyl)sulfonyl)(tosyl)azanide (**25a**):** To a 25 mL round bottom flask was added **2c** ([N<sub>1,1,6,20H</sub>][Br]) (322 mg, 1.27 mmol, 1.2 equiv.), **21a<sub>ii</sub>** ([Na][NBNTs]; 0.400 g, 1.06 mmol, 1.0 equiv.), acetone (15 mL), and Milli-Q water (15 mL). The reaction stirred at room temperature for 24 h. The acetone was removed *in vacuo*. A white solid precipitated in the water, so the solid was filtered out, washed with Milli-Q water (2x10 mL), and residual water was removed using lyophilization. The product (**25a**) was isolated as a white solid in 58.1% yield. <sup>1</sup>H NMR (400 MHz, Acetone-d<sub>6</sub>) δ 8.22 – 8.15 (m, 2H), 8.02 – 7.94 (m, 2H), 7.69 – 7.61 (m, 2H), 7.18 – 7.11 (m, 2H), 4.63 (t, *J* = 5.1 Hz, 1H), 4.12 (tp, *J* = 5.0, 2.4 Hz, 2H), 3.72 – 3.65 (m, 2H), 3.60 – 3.51 (m, 2H), 3.31 (s, 6H), 2.33 (s, 3H), 1.92 – 1.80 (m, 2H), 1.39 – 1.25 (m, 6H), 0.91 – 0.82 (m, 3H); <sup>13</sup>C NMR (101 MHz, Acetone-d<sub>6</sub>) δ 152.39, 148.49, 143.27, 140.44, 128.33, 128.06, 126.72, 123.05, 65.39 (t, *J* = 2.7 Hz), 56.03, 51.60 – 50.99 (m), 31.09, 25.79, 22.33, 22.22, 20.41, 13.37.



**2,2'-(ethane-1,2-diylbis(oxy))bis(*N*-(2-hydroxyethyl)-*N,N*-dimethylethan-1-aminium) ((4-nitro**

**phenyl)sulfonyl)(tosyl)azanide (25b):** To a 25 mL round bottom was added **4j** ([DC-ether][2Cl<sup>-</sup>]; 0.257 g,

0.705 mmol, 1.0 equiv.), **21a<sub>ii</sub>** ([Na][NBNTs]; 0.400 g, 1.06 mmol, 1.5 equiv.), and Milli-Q water (15 mL).

The reaction stirred at room temperature for 24 h. The solvent was removed *in vacuo*. The crude product

was dissolved in acetone (15 mL), in which a white precipitant was observed. The mixture was filtered, and

the filtrate was collected and concentrated *in vacuo*. To the product was added DCM (10 mL), in which one

layer formed. This layer was washed with Milli-Q water (1x20 mL). The final water wash was checked for

residual chloride using silver nitrate and no precipitant appeared. The DCM and residual water were

removed *in vacuo*. The product (**25b**) was isolated as a white solid in 85.0% yield. <sup>1</sup>H NMR (400 MHz,

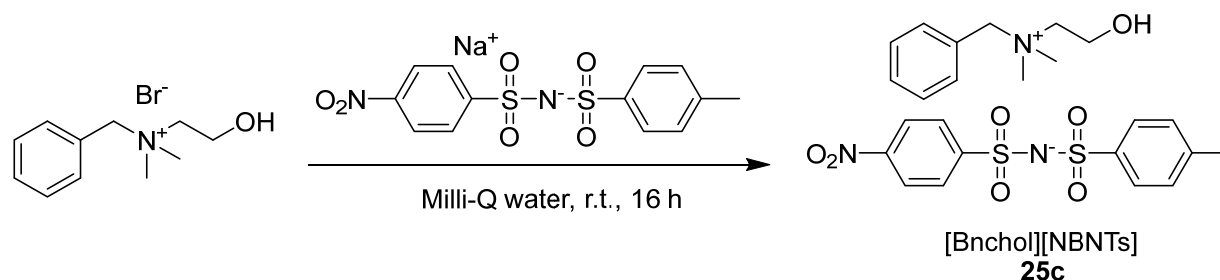
Methanol-*d*<sub>4</sub>) δ 8.17 – 8.09 (m, 4H), 7.88 – 7.80 (m, 4H), 7.57 – 7.49 (m, 4H), 7.15 – 7.07 (m, 4H), 4.02

(dq, *J* = 7.7, 2.7 Hz, 4H), 3.96 (dq, *J* = 5.1, 2.5 Hz, 4H), 3.74 (d, *J* = 1.6 Hz, 0H), 3.71 (d, *J* = 9.9 Hz, 8H),

3.63 – 3.56 (m, 4H), 3.25 (s, 12H), 2.32 (s, 6H); <sup>13</sup>C NMR (101 MHz, Methanol-*d*<sub>4</sub>) δ 149.73, 148.94,

141.80, 140.69, 128.46, 127.78, 126.47, 123.07, 69.89, 66.80 – 66.15 (m), 64.76 – 64.50 (m), 64.43, 55.62,

52.06 – 51.50 (m), 19.92.

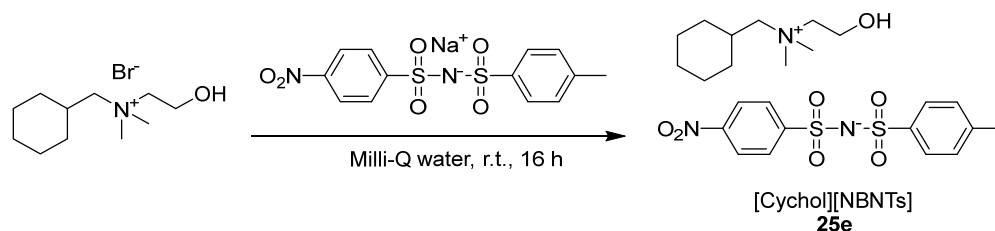


***N*-benzyl-2-hydroxy-*N,N*-dimethylethan-1-aminium ((4-nitrophenyl)sulfonyl)(tosyl)azanide (25c):**

To a 25 mL round bottom flask was added **23a** ([Bnchol][Br]; 330 mg, 1.27 mmol, 1.2 equiv.), **21a<sub>ii</sub>**

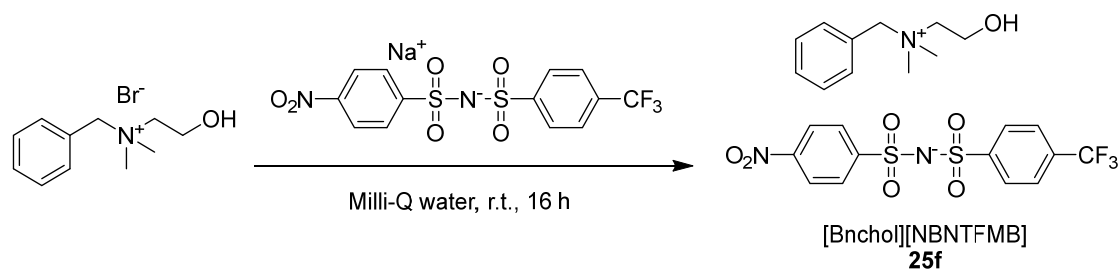
([Na][NBNTs]; 0.400 g, 1.06 mmol, 1.0 equiv.), acetone (15 mL), and Milli-Q water (15 mL). The reaction





***N*-(cyclohexylmethyl)-2-hydroxy-*N,N*-dimethylethan-1-aminium ((4-nitrophenyl)sulfonyl)(tosyl)azanide (25e):**

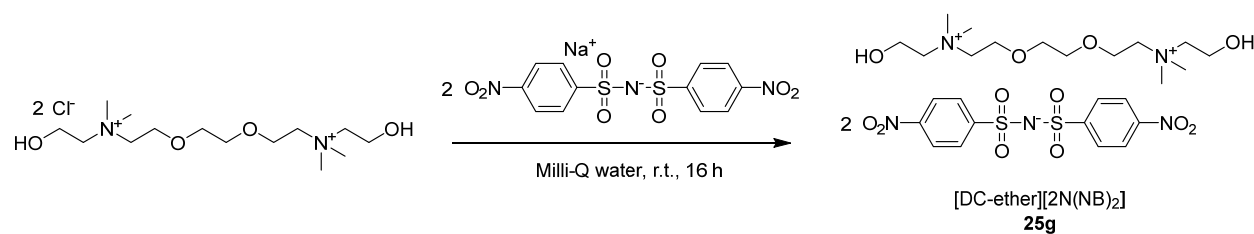
To a 25 mL round bottom flask was added **23c** ([Cychol][Br]; 338 mg, 1.27 mmol, 1.2 equiv.), **21a<sub>ii</sub>** ([Na][NBNTs]; 0.400 g, 1.06 mmol, 1.0 equiv.), acetone (15 mL), and Milli-Q water (15 mL). The reaction stirred at room temperature for 24 h. The acetone was removed *in vacuo*, which resulted in the precipitation of the white solid. The solid was filtered out and washed with Milli-Q water (3x10 mL). The residual solvent from the solid was removed *in vacuo*. The product (**25e**) was isolated as a white solid in 63.9%. <sup>1</sup>H NMR (400 MHz, Acetone-*d*<sub>6</sub>) δ 8.22 – 8.14 (m, 2H), 8.02 – 7.94 (m, 2H), 7.69 – 7.61 (m, 2H), 7.17 – 7.10 (m, 2H), 4.64 (t, *J* = 5.1 Hz, 1H), 4.14 (ddt, *J* = 7.9, 5.2, 2.6 Hz, 2H), 3.77 – 3.70 (m, 2H), 3.45 (d, *J* = 4.4 Hz, 2H), 3.36 (s, 6H), 2.33 (s, 3H), 2.22 – 1.06 (m, 11H); <sup>13</sup>C NMR (101 MHz, Acetone-*d*<sub>6</sub>) δ 152.75, 148.42, 143.60, 140.19, 128.19, 128.05, 126.74, 122.93, 72.40, 66.10, 56.03, 55.91, 51.50 – 51.29 (m), 33.11, 32.06, 25.57, 25.33, 20.36.



***N*-benzyl-2-hydroxy-*N,N*-dimethylethan-1-aminium ((4-nitrophenyl)sulfonyl)((4-(trifluoromethyl)phenyl)sulfonyl)azanide (25f):**

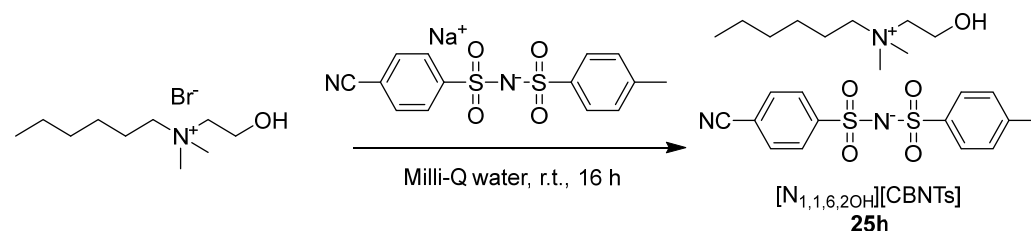
To a 50 mL round bottom flask was added **23a** ([Bnchol][Br]; 289 mg, 1.11 mmol, 1.2 equiv.), **21c<sub>ii</sub>** ([Na][NBNTFMB]; 0.400 g, 0.925 mmol, 1.0 equiv.), acetone (15 mL), and Milli-Q water (15 mL). The reaction stirred at room temperature for 24 h. The acetone was removed *in vacuo*, which resulted in the precipitation of the white solid. The solid was filtered out and washed with

Milli-Q water (3x10 mL). The residual solvent from the solid was removed *in vacuo*. The product (**25f**) was isolated as a white solid in 66.1%.  $^1\text{H}$  NMR (400 MHz, Acetone- $d_6$ )  $\delta$  8.23 – 8.15 (m, 2H), 8.05 – 7.96 (m, 4H), 7.75 – 7.66 (m, 4H), 7.61 – 7.50 (m, 2H), 7.51 (d,  $J$  = 6.8 Hz, 1H), 4.84 (s, 2H), 4.72 – 4.65 (m, 1H), 4.25 (tp,  $J$  = 5.1, 2.6 Hz, 2H), 3.78 – 3.71 (m, 2H), 3.31 (s, 6H);  $^{13}\text{C}$  NMR (101 MHz, Acetone- $d_6$ )  $\delta$  152.13, 149.95 (d,  $J$  = 1.5 Hz), 148.62, 133.37, 131.21 (q,  $J$  = 32.2 Hz), 130.51, 129.03, 128.07, 128.02, 127.52, 124.98 (q,  $J$  = 3.8 Hz), 123.12, 127.30 – 119.76 (m), 68.92, 66.04 – 65.26 (m), 56.04, 50.66 – 49.90 (m);  $^{19}\text{F}$  NMR (376 MHz, Acetone- $d_6$ )  $\delta$  -63.17.



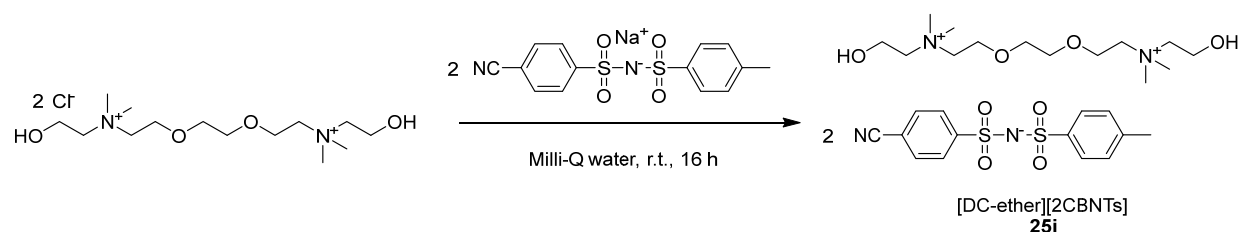
**2,2'-(ethane-1,2-diylbis(oxy))bis(*N*-(2-hydroxyethyl)-*N,N*-dimethylethan-1-aminium)) bis((4-nitrophenyl)sulfonyl)azanide (**25g**):**

To a 25 mL round bottom was added **4j** ([DC-ether][2Cl]); 0.298 g, 0.814 mmol, 1.0 equiv.), **21bii** ([Na][N(NB) $_2$ ]; 0.500 g, 1.22 mmol, 1.5 equiv.), and Milli-Q water (100 mL). The reaction stirred at room temperature for 16 h. The solution was concentrated *in vacuo*. Upon removing the solvent, the solution was dissolved in methanol (25 mL) revealing a white precipitant. The mixture was filtered, and the solid was washed with Milli-Q water (3x15 mL) and lyophilized. The product (**25g**) was isolated as a white solid in 42.5% yield.  $^1\text{H}$  NMR (400 MHz, Deuterium Oxide)  $\delta$  8.11 (d,  $J$  = 8.4 Hz, 8H), 7.73 (d,  $J$  = 8.5 Hz, 8H), 3.98 (s, 4H), 3.91 (s, 4H), 3.66 (s, 4H), 3.59 (s, 4H), 3.51 (d,  $J$  = 5.5 Hz, 4H), 3.13 (s, 12H).



***N*-(2-hydroxyethyl)-*N,N*-dimethylhexan-1-aminium ((4-cyanophenyl)sulfonyl)(tosyl)azanide (25h):**

To a 25 mL round bottom flask was added **2c** ( $[N_{1,1,6,2OH}][Br]$ ; 340 mg, 1.34 mmol, 1.2 equiv.), **21d<sub>ii</sub>** ( $[Na][CBNTs]$ ; 0.400 g, 1.12 mmol, 1.0 equiv.), and Milli-Q water (30 mL). The reaction stirred at room temperature for 1 h. A solid precipitated that was filtered off and washed with Milli-Q water (3x5 mL). The solid was then lyophilized, to produce the product (**25h**) as a white solid in 31.28% yield;  $^1H$  NMR (400 MHz, Acetone- $d_6$ )  $\delta$  7.95 – 7.88 (m, 2H), 7.77 – 7.70 (m, 2H), 7.69 – 7.61 (m, 2H), 7.14 (d,  $J = 7.9$  Hz, 2H), 4.67 (s, 1H), 4.12 (dq,  $J = 7.8, 2.6$  Hz, 2H), 3.73 – 3.66 (m, 2H), 3.62 – 3.53 (m, 2H), 3.33 (s, 6H), 2.35 (s, 3H), 1.88 (td,  $J = 11.6, 9.6, 5.8$  Hz, 2H), 1.35 (q,  $J = 5.5$  Hz, 6H), 0.93 – 0.85 (m, 3H);  $^{13}C$  NMR (101 MHz, Acetone- $d_6$ )  $\delta$  131.72, 128.22, 127.55, 126.70, 65.41 (d,  $J = 3.0$  Hz), 55.96, 51.78 – 50.82 (m), 31.07, 25.78, 22.32, 22.20, 20.41, 13.34.



**2,2'-(ethane-1,2-diylbis(oxy))bis(*N*-(2-hydroxyethyl)-*N,N*-dimethylethan-1-aminium) ((4-cyano**

**phenyl)sulfonyl)(tosyl)azanide (25i):** To a 25 mL round bottom was added **4j** ( $[DC\text{-ether}][2Cl]$ ; 0.272 g,

0.744 mmol, 1.0 equiv.), **21d<sub>ii</sub>** ( $[Na][CBNTs]$  (0.400 g, 1.12 mmol, 1.5 equiv.), acetone (25 mL), and Milli-

Q water (25 mL). The reaction stirred room temperature for 16 h. The acetone was removed *in vacuo*,

revealing a quasi-liquid. To the IL-water mixture was added DCM (10 mL). The mixture was mixed well,

and the water layer was removed. The DCM-IL layer was then washed with Milli-Q water (1x10 mL). The

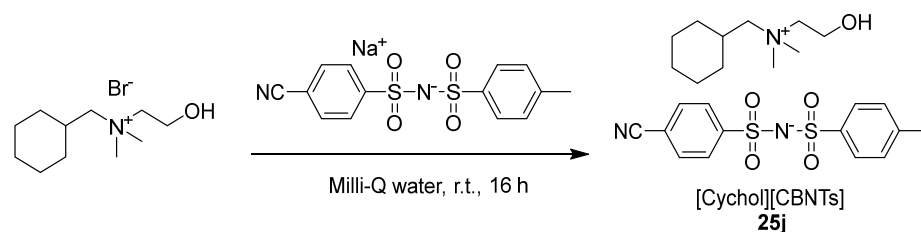
DCM and residual water were removed *in vacuo*. The product (**25i**) was isolated as a viscous liquid in

63.3% yield.  $^1H$  NMR (400 MHz, Acetone- $d_6$ )  $\delta$  7.91 – 7.84 (m, 4H), 7.75 – 7.68 (m, 4H), 7.64 – 7.57 (m,

4H), 7.14 (d,  $J = 8.1$  Hz, 4H), 4.73 (s, 2H), 4.15 – 4.08 (m, 4H), 4.04 (tt,  $J = 5.1, 2.4$  Hz, 4H), 3.88 – 3.81

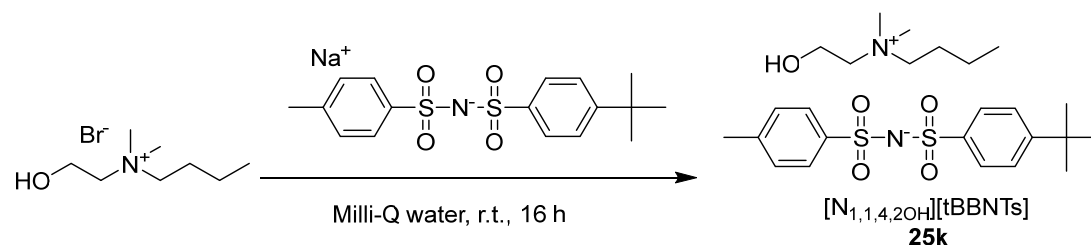
(m, 4H), 3.80 – 3.73 (m, 4H), 3.36 (s, 12H), 2.33 (s, 6H);  $^{13}C$  NMR (101 MHz, Acetone- $d_6$ )  $\delta$  150.04,

142.68, 140.67, 131.97, 128.49, 127.54, 126.71, 118.08, 113.27, 69.97, 66.62, 64.65, 56.04, 52.25 (t,  $J = 3.6$  Hz), 20.47.



***N*-(cyclohexylmethyl)-2-hydroxy-*N,N*-dimethylethan-1-aminium ((4-cyanophenyl)sulfonyl)(tosyl)**

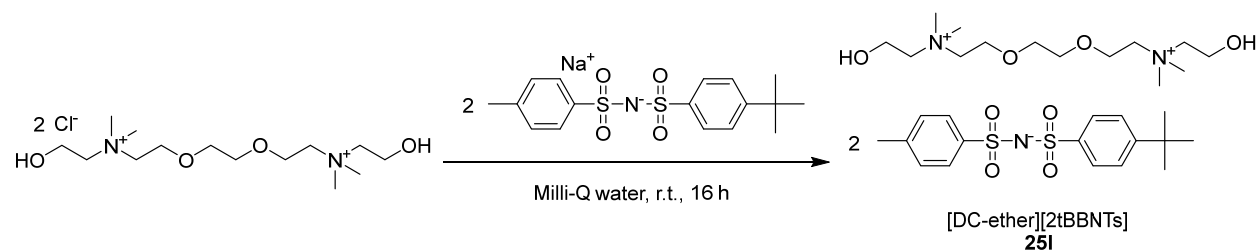
**azanide (25j):** To a 25 mL round bottom flask was added **25c** ([Cychol][Br]; 356 mg, 1.34 mmol, 1.2 equiv.), **21d<sub>ii</sub>** ([Na][CBNTs]; 0.400 g, 1.12 mmol, 1.0 equiv.), and Milli-Q water (30 mL). The reaction stirred at room temperature for 1 h. The water was removed *in vacuo*. To the flask was then added acetone (25 mL). The acetone mixture was then sonicated for an hour and filtered. The filtrate was collected and washed with Milli-Q water (1x10 mL) for one hour and then filtered. The solid was collected and lyophilized, revealing the product (**25j**) as a white solid in 7.79%. <sup>1</sup>H NMR (400 MHz, Acetone-*d*<sub>6</sub>)  $\delta$  7.96 – 7.88 (m, 4H), 7.77 – 7.69 (m, 4H), 7.69 – 7.62 (m, 4H), 7.17 – 7.11 (m, 4H), 4.70 – 4.63 (m, 1H), 4.18 – 4.09 (m, 4H), 3.77 – 3.71 (m, 4H), 3.47 (d,  $J = 4.4$  Hz, 4H), 3.37 (s, 12H), 2.35 (s, 6H), 2.25 – 0.97 (m, 22H); <sup>13</sup>C NMR (101 MHz, Acetone-*d*<sub>6</sub>)  $\delta$  151.32, 143.91, 139.98, 131.63, 128.12, 127.57, 126.72, 118.14, 112.93, 72.43 (d,  $J = 2.6$  Hz), 66.13, 56.00, 55.88, 52.37 – 50.64 (m), 33.12, 32.07, 25.58, 25.32, 20.38.



***N*-(2-hydroxyethyl)-*N,N*-dimethylbutan-1-aminium ((4-(tert-butyl)phenyl)sulfonyl)(tosyl)azanide**

**(25k):** To a 25 mL round bottom flask was added **2a** ([N<sub>1,1,4,2OH</sub>][Br]; 290 g, 1.28 mmol, 1.0 equiv.), **21e<sub>ii</sub>** ([Na][tBBNTs]; 0.500 g, 1.28 mmol, 1.0 equiv.), and Milli-Q water (15 mL). The reaction stirred at room

temperature for 16 h. No ionic liquid phase separated so the product was deemed water soluble, and thus, no workup nor characterization was performed.



**2,2'-(ethane-1,2-diylbis(oxy))bis(*N*-(2-hydroxyethyl)-*N,N*-dimethylethan-1-aminium) bis((4-(tert-**

**butyl)phenyl)sulfonyl)(tosyl)azanide (**25i**):** To a 25 mL round bottom was added **4j** ([DC-ether][2Cl];

0.313 g, 0.856 mmol, 1.0 equiv.), **21e<sub>ii</sub>** ([Na][tBBNTs]; 0.500 g, 1.28 mmol, 1.5 equiv.), and Milli-Q water

(25 mL). The reaction stirred at room temperature for 16 h. The water was removed *in vacuo*, and the crude

compound was dissolved in acetone (15 mL) and stirred at room temperature for 1 h. The mixture was

filtered, and the filtrate was concentrated *in vacuo*. The product (**25i**) was isolated as a white solid in 85.8%

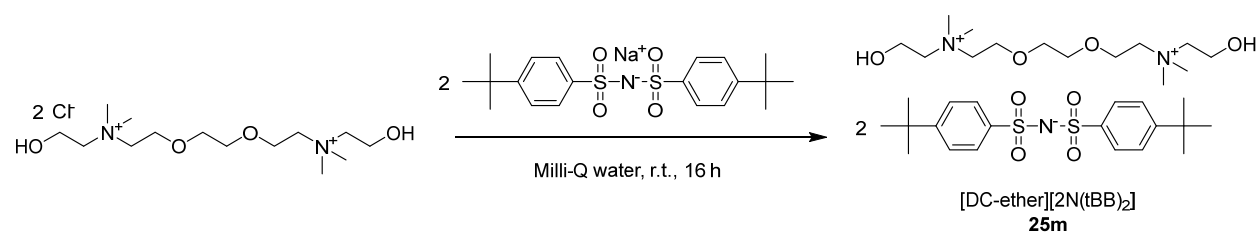
yield. <sup>1</sup>H NMR (400 MHz, Methanol-d<sub>4</sub>) δ 7.58 – 7.51 (m, 4H), 7.55 – 7.45 (m, 4H), 7.35 – 7.27 (m, 4H),

7.11 – 7.04 (m, 4H), 4.01 (dq, *J* = 5.0, 2.5 Hz, 4H), 3.94 (dq, *J* = 7.4, 2.5 Hz, 4H), 3.73 – 3.65 (m, 8H), 3.63

– 3.56 (m, 4H), 3.23 (s, 12H), 2.32 (s, 6H), 1.31 (s, 18H); <sup>13</sup>C NMR (101 MHz, Methanol-d<sub>4</sub>) δ 154.29,

141.13, 140.96, 140.79, 128.34, 126.38, 126.20, 124.71, 69.90, 66.74 – 66.29 (m), 64.79 – 64.47 (m), 64.46,

55.67, 52.12 – 51.58 (m), 47.47, 47.25, 47.04, 34.34, 30.30, 20.13.

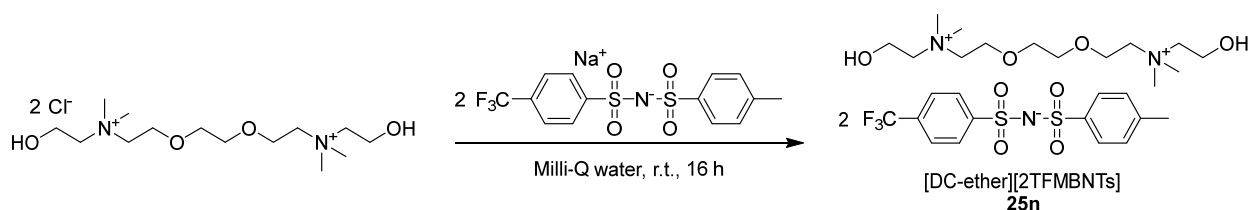


**2,2'-(ethane-1,2-diylbis(oxy))bis(*N*-(2-hydroxyethyl)-*N,N*-dimethylethan-1-aminium) bis((4-(tert-**

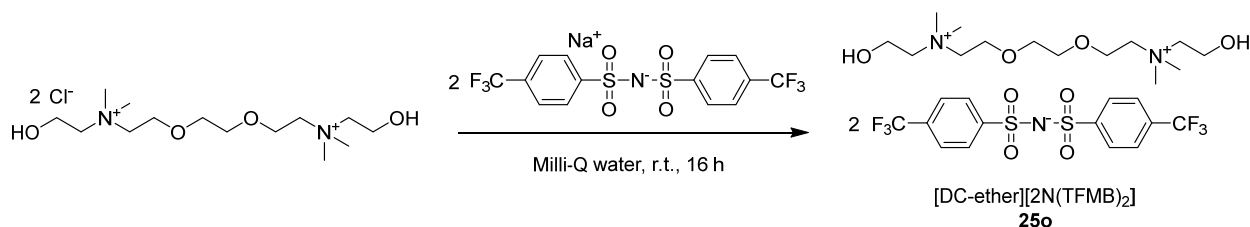
**butyl)phenyl)sulfonyl)azanide (**25m**):** To a 25 mL round bottom was added **4j** ([DC-ether][2Cl]; 0.282 g,

0.772 mmol, 1.0 equiv.), **21f<sub>ii</sub>** ([Na][N(tBB)<sub>2</sub>]; 0.500 g, 1.16 mmol, 1.5 equiv.), and Milli-Q water

(100 mL). The reaction stirred at room temperature for 16 h. The water layer was removed *in vacuo*. The crude compound was then stirred in acetone (15 mL) at room temperature for 16 h. The solid was then filtered, and the filtrate was collected and concentrated *in vacuo*. The product (**25m**) was isolated as a white solid in 91.0% yield.  $^1\text{H}$  NMR (400 MHz, Acetone- $d_6$ )  $\delta$  7.72 – 7.64 (m, 8H), 7.40 – 7.32 (m, 8H), 4.79 (t,  $J = 5.2$  Hz, 2H), 4.11 (s, 4H), 4.04 (t,  $J = 4.7$  Hz, 4H), 3.90 – 3.83 (m, 4H), 3.83 – 3.76 (m, 4H), 3.37 (s, 12H), 1.31 (s, 38H);  $^{13}\text{C}$  NMR (101 MHz, Acetone- $d_6$ )  $\delta$  153.11, 143.41, 126.46, 124.60, 69.99, 66.60, 64.72, 64.61, 56.10, 52.24, 34.46, 30.72.

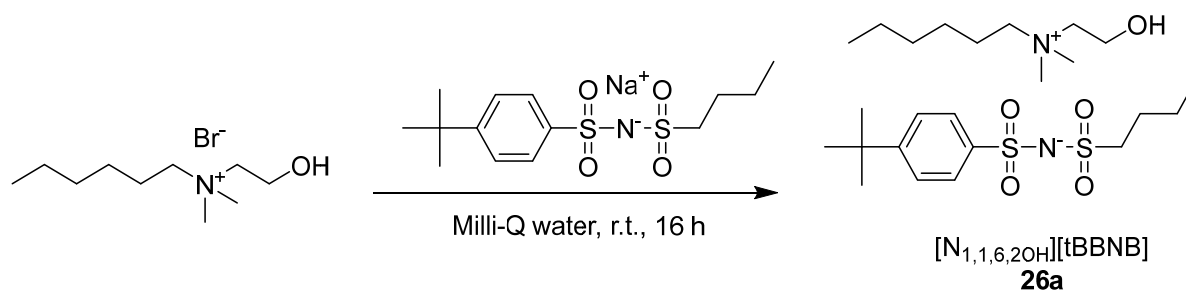


**2,2'-(ethane-1,2-diylbis(oxy))bis(*N*-(2-hydroxyethyl)-*N,N*-dimethylethan-1-aminium) tosyl((4-(trifluoromethyl)phenyl)sulfonyl)azanide (**25n**):** To a 25 mL round bottom was added **4j** ([DC-ether][2Cl]; 0.243 g, 0.664 mmol, 1.0 equiv.), **21g<sub>ii</sub>** ([Na][TFMBNTs]; 0.400 g, 0.997 mmol, 1.5 equiv.), and Milli-Q water (100 mL). The reaction stirred at room temperature for 16 h. The water was removed *in vacuo* and the crude solid was washed with acetone (25 mL) for 16 h at room temperature. The solid was then filtered, and the filtrate was collected, and residual solvent was removed *in vacuo*. The product (**25n**) was isolated as a viscous liquid in 25.2% yield.  $^1\text{H}$  NMR (400 MHz, Acetone- $d_6$ )  $\delta$  7.91 – 7.85 (m, 4H), 7.62 (d,  $J = 8.2$  Hz, 4H), 7.60 – 7.55 (m, 4H), 7.12 – 7.05 (m, 4H), 4.11 (dq,  $J = 5.0, 2.5$  Hz, 4H), 4.06 (dq,  $J = 7.5, 2.4$  Hz, 4H), 3.90 – 3.83 (m, 4H), 3.80 – 3.64 (m, 8H), 3.38 (s, 12H), 2.30 (s, 6H);  $^{13}\text{C}$  NMR (101 MHz, Acetone- $d_6$ )  $\delta$  149.58, 142.69, 140.42, 130.90 (q,  $J = 32.1$  Hz), 128.34, 127.46, 126.69, 124.87 (q,  $J = 3.9$  Hz), 124.16 (q,  $J = 271.8$  Hz), 69.96, 66.63, 64.68, 64.59, 56.00, 52.23 (t,  $J = 3.6$  Hz), 20.38;  $^{19}\text{F}$  NMR (376 MHz, Acetone- $d_6$ )  $\delta$  -62.98.



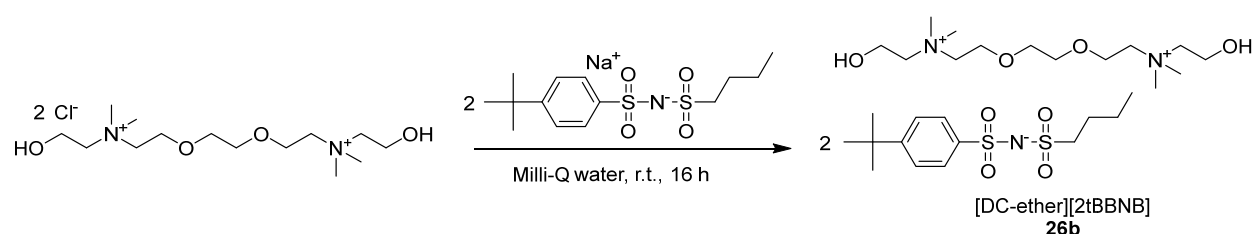
**2,2'-(ethane-1,2-diylbis(oxy))bis(*N*-(2-hydroxyethyl)-*N,N*-dimethylethan-1-aminium) bis((4-(trifluoromethyl)phenyl)sulfonyl)azanide (**25o**):** To a 25 mL round bottom was added **4j** ([DC-ether][2Cl<sup>-</sup>]; 0.267 g, 0.732 mmol, 1.0 equiv.), **21h<sub>ii</sub>** ([Na][N(TFMB)<sub>2</sub>]; 0.500 g, 1.10 mmol, 1.5 equiv.), acetone (15 mL), and Milli-Q water (15 mL). The reaction stirred at room temperature for 16 h. The solvent was removed *in vacuo*. Then, the crude product was then washed with acetone (15 mL) for 1 h at room temperature. The solid was then filtered, and the filtrate was collected, and residual solvent was removed *in vacuo*. The product (**25o**) was isolated as a solid in 30.7% yield. <sup>1</sup>H NMR (400 MHz, Methanol-d<sub>4</sub>) δ 7.84 – 7.78 (m, 8H), 7.62 – 7.56 (m, 8H), 4.04 (dq, *J* = 5.3, 2.6 Hz, 4H), 3.98 (dq, *J* = 5.0, 2.4 Hz, 4H), 3.77 – 3.71 (m, 4H), 3.70 (s, 4H), 3.66 – 3.59 (m, 4H), 3.27 (s, 12H); <sup>13</sup>C NMR (101 MHz, Methanol-d<sub>4</sub>) δ 147.24, 132.28 (q, *J* = 32.8 Hz), 127.16, 125.36 – 124.70 (m), 124.97 (q), 69.89, 66.68 – 66.37 (m), 64.74 – 64.54 (m), 64.45, 55.64, 52.20 – 51.54 (m); <sup>19</sup>F NMR (376 MHz, Methanol-d<sub>4</sub>) δ -64.34.

#### 2.4.21 Synthesis of ILs containing third-generation bis(sulfonyl)azanide anions

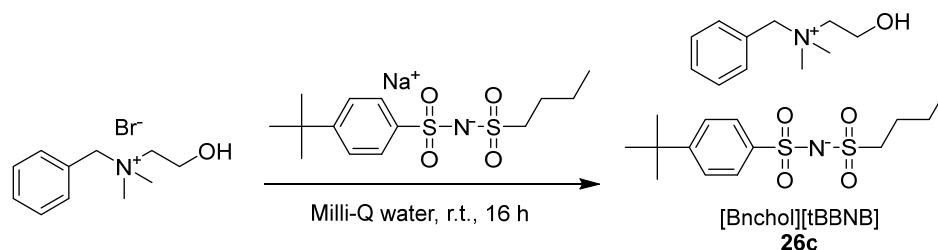


***N*-(2-hydroxyethyl)-*N,N*-dimethylhexan-1-aminium ((4-(tert-butyl)phenyl)sulfonyl)(butylsulfonyl)azanide (**26a**):** To 50 mL round bottom flask was added **2c** ([N<sub>1,1,6,2OH</sub>][Br<sup>-</sup>]; 0.351 g, 1.35 mmol, 1.2 equiv.), **22a<sub>ii</sub>** ([Na][tBBNB]; 0.400 g, 1.13 mmol, 1.0 equiv.), and Milli-Q water (25 mL). The mixture stirred at room temperature for 16 h. The water was removed *in vacuo*. DCM (10 mL) was added to the crude product

and the DCM/IL mixture was washed with Milli-Q water (5x10 mL). The solution was then concentrated *in vacuo* to reveal the product (**26a**) as a viscous liquid in 41.7% yield.  $^1\text{H}$  NMR (400 MHz, Methanol- $d_4$ )  $\delta$  7.89 – 7.81 (m, 2H), 7.57 – 7.49 (m, 2H), 3.98 (dq,  $J = 7.5, 2.6$  Hz, 2H), 3.50 – 3.43 (m, 2H), 3.43 – 3.35 (m, 2H), 3.14 (s, 6H), 3.07 – 2.98 (m, 2H), 1.84 – 1.68 (m, 2H), 1.57 – 1.20 (m, 19H), 0.93 (td,  $J = 7.2, 4.6$  Hz, 6H);  $^{13}\text{C}$  NMR (101 MHz, Methanol- $d_4$ )  $\delta$  154.42, 142.35, 126.21, 124.94, 65.50 – 65.29 (m), 65.16 – 64.95 (m), 55.57, 54.10, 50.85 – 50.67 (m), 34.44, 31.02, 30.26, 25.89, 25.69, 22.20, 22.15, 21.33, 12.95, 12.73.

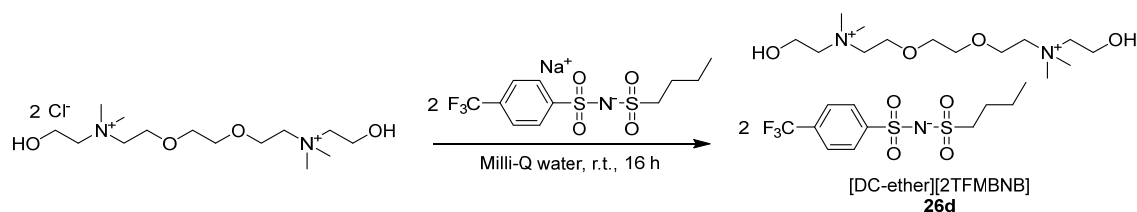


**2,2'-(ethane-1,2-diylbis(oxy))bis(*N*-(2-hydroxyethyl)-*N,N*-dimethylethane-1-aminium) ((4-(tert-butyl)phenyl)sulfonyl)(butylsulfonyl)azanide (**26b**):** To a 50 mL round bottom flask was added **4j** ([DC-ether][2Cl]); 0.274 g, 0.750 mmol, 1.0 equiv.), **22a<sub>ii</sub>** ([Na][tBBNB]); 0.400 g, 1.13 mmol, 1.5 equiv.), and Milli-Q water (25 mL). The reaction stirred at room temperature for 16 h. Then, the water was removed *in vacuo*, and the crude ionic liquid was washed with acetone (25 mL) and filtered. The acetone filtrate was concentrated *in vacuo*. Next, the crude product was dissolved in DCM (15 mL) and washed with Milli-Q water (3x25 mL). The DCM was removed *in vacuo* and residual water was removed using a lyophilizer. The product (**26b**) was isolated as a viscous liquid in 25.6% yield.  $^1\text{H}$  NMR (400 MHz, Methanol- $d_4$ )  $\delta$  7.89 – 7.81 (m, 4H), 7.57 – 7.50 (m, 4H), 4.01 (dq,  $J = 5.2, 2.6$  Hz, 4H), 3.96 (dq,  $J = 7.6, 2.6$  Hz, 4H), 3.70 (d,  $J = 5.7$  Hz, 8H), 3.62 – 3.55 (m, 4H), 3.23 (s, 12H), 3.03 – 2.94 (m, 4H), 1.78 – 1.65 (m, 4H), 1.36 (s, 22H), 0.91 (t,  $J = 7.4$  Hz, 6H);  $^{13}\text{C}$  NMR (101 MHz, Methanol- $d_4$ )  $\delta$  154.52, 142.20, 126.21, 124.97, 69.89, 66.49 (t,  $J = 2.8$  Hz), 64.53 (d,  $J = 3.0$  Hz), 64.43, 55.59, 53.96, 51.94 – 51.49 (m), 34.43, 30.22, 25.86, 21.28, 12.68.



***N*-benzyl-2-hydroxy-*N,N*-dimethylethan-1-aminium ((4-(tert-butyl)phenyl)sulfonyl)(butylsulfonyl)**

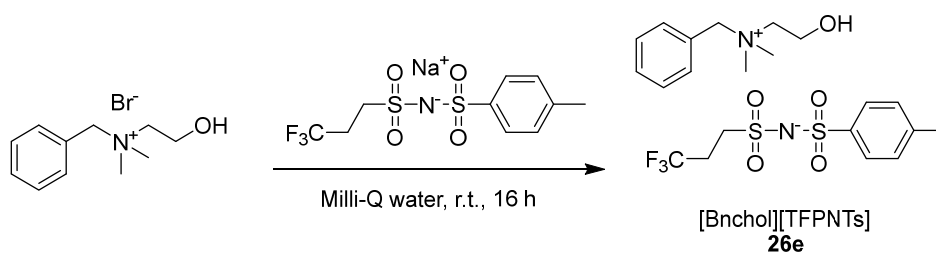
**azanide (26c):** To 50 mL round bottom flask was added **23a** ([Bnchol][Br]) (0.351 g, 1.35 mmol, 1.2 equiv.), **22a<sub>ii</sub>** ([Na][tBBNB]; 0.400 g, 1.13 mmol, 1.0 equiv.), and Milli-Q water (25 mL). The mixture stirred at room temperature for 16 h, where an ionic liquid phase formed at the bottom. The water was removed *in vacuo*, and residual cation was precipitated by adding acetone (20 mL). The solid was filtered out, and the filtrate was collected and concentrated *in vacuo*. Then, DCM (10 mL) was added. The DCM/IL mixture was washed with Milli-Q water (2x10 mL). Finally, the solvents were removed *in vacuo* revealing the product (**26c**) was a viscous liquid in 56.2% yield. <sup>1</sup>H NMR (400 MHz, Methanol-d<sub>4</sub>) δ 7.89 – 7.81 (m, 2H), 7.65 – 7.46 (m, 7H), 4.62 (s, 2H), 4.07 (dq, *J* = 7.6, 2.7 Hz, 2H), 3.53 – 3.46 (m, 2H), 3.10 (s, 6H), 3.07 – 2.99 (m, 2H), 1.80 – 1.68 (m, 2H), 1.43 – 1.33 (m, 2H), 1.33 (s, 9H), 0.91 (t, *J* = 7.4 Hz, 3H); <sup>13</sup>C NMR (101 MHz, Methanol-d<sub>4</sub>) δ 154.45, 142.30, 133.06, 130.44, 128.88, 127.66, 126.21, 124.96, 69.03 – 68.84 (m), 65.43 – 65.22 (m), 55.59, 54.11, 49.88 – 49.68 (m), 34.41, 30.23, 25.89, 21.30, 12.71.



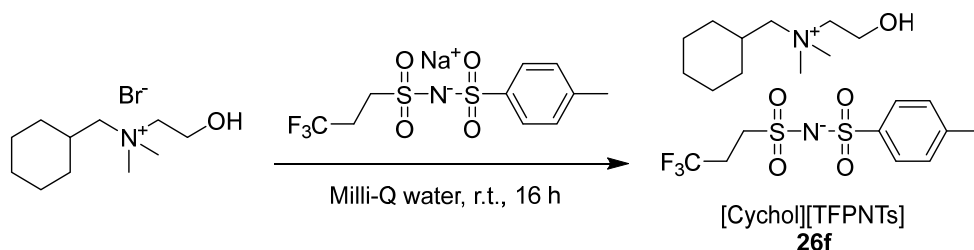
**2,2'-(ethane-1,2-diylbis(oxy))bis(*N*-(2-hydroxyethyl)-*N,N*-dimethylethan-1-aminium) (butylsulfonyl)**

**((4-(trifluoromethyl)phenyl)sulfonyl)azanide (26d):** To a 100 mL round bottom was added **4j** ([DC-ether][2Cl]); 0.199 g, 0.544 mmol, 1.0 equiv.), **22b<sub>ii</sub>** ([Na][TFMBNB]; 0.300 g, 0.817 mmol, 1.5 equiv.), and Milli-Q water (25mL). The reaction stirred at room temperature for 16 h. The water was removed *in vacuo*. Then, the crude solid was washed with DCM (15 mL) for 1 h at room temperature. The solid was

then filtered out, and the filtrate was collected and concentrated *in vacuo*. Lastly, the compound was washed with acetone (1x10 mL) for 1 h at room temperature, and the mixture was filtered, and the filtrate was collected and concentrated *in vacuo*. The product (**26d**) was isolated as a viscous liquid in 45.3% yield.  $^1\text{H}$  NMR (400 MHz, Methanol- $d_4$ )  $\delta$  8.14 – 8.07 (m, 4H), 7.81 (d,  $J = 8.2$  Hz, 4H), 4.01 (dq,  $J = 7.6, 2.7$  Hz, 4H), 3.94 (dq,  $J = 5.2, 2.5$  Hz, 4H), 3.69 (d,  $J = 10.7$  Hz, 8H), 3.62 – 3.55 (m, 4H), 3.23 (s, 12H), 3.14 – 3.05 (m, 4H), 1.82 – 1.69 (m, 4H), 1.43 (h,  $J = 7.4$  Hz, 4H), 0.94 (t,  $J = 7.3$  Hz, 6H);  $^{13}\text{C}$  NMR (101 MHz, Methanol- $d_4$ )  $\delta$  149.19 (d,  $J = 1.5$  Hz), 132.19 (q,  $J = 32.4$  Hz), 127.21, 125.13 (q,  $J = 3.8$  Hz), 127.71 – 119.36 (m), 69.86, 66.56 – 66.36 (m), 64.66 – 64.48 (m), 64.41, 55.58, 54.22, 51.93 – 51.72 (m), 25.88, 21.27, 12.68;  $^{19}\text{F}$  NMR (376 MHz, Methanol- $d_4$ )  $\delta$  -64.14.



***N*-benzyl-2-hydroxy-*N,N*-dimethylethan-1-aminium tosyl((3,3,3-trifluoropropyl)sulfonyl)azanide (26e):** To a 25 mL round bottom flask was added **23a** ([Bnchol][Br]; 265 mg, 1.02 mmol, 1.2 equiv.), **22c<sub>ii</sub>** ([Na][TFPNTs]; 0.300 g, 0.849 mmol, 1.0 equiv.), and Milli-Q water (15 mL). The reaction stirred at room temperature for 16 h. No ionic liquid phase separated so the product was deemed water soluble, and thus, no workup nor characterization was performed.



***N*-(cyclohexylmethyl)-2-hydroxy-*N,N*-dimethylethan-1-aminium tosyl((3,3,3-trifluoropropyl)sulfonyl)azanide (26f):** To a 25 mL round bottom flask was added **23c** ([Cychol][Br]; 271 mg, 1.02 mmol,

1.2 equiv.), **22c<sub>ii</sub>** ([Na][TFPNTs]; 0.300 g, 0.849 mmol, 1.0 equiv.), and Milli-Q water (15 mL). The reaction stirred at room temperature for 16 h. No ionic liquid phase separated so the product was deemed water soluble, and thus, no workup nor characterization was performed.

## 2.5 References

- (1) Earle, M. J. & Seddon, K. R. Ionic liquids. Green solvents for the future. *Pure Appl. Chem.* **72**, 1391–1398 (2000).
- (2) Marsh, K. N., Boxall, J. A. & Lichtenthaler, R. Room temperature ionic liquids and their mixtures - A review. *Fluid Phase Equilib.* **219**, 93–98 (2004).
- (3) Mecerreyes, D. Polymeric ionic liquids: Broadening the properties and applications of polyelectrolytes. *Progress in Polymer Science (Oxford)* vol. 36 1629–1648 (2011).
- (4) Giernoth, R. *Task-specific ionic liquids. Angewandte Chemie - International Edition* vol. 49 2834–2839 (John Wiley & Sons, Ltd, 2010).
- (5) Raut, D. G. *et al.* A morpholinium ionic liquid for cellulose dissolution. *Carbohydr. Polym.* **130**, 18–25 (2015).
- (6) Clark, K. D. *et al.* Extraction of DNA by magnetic ionic liquids: Tunable solvents for rapid and selective DNA analysis. *Anal. Chem.* **87**, 1552–1559 (2015).
- (7) Nakashima, K., Kubota, F., Maruyama, T. & Goto, M. Ionic liquids as a novel solvent for lanthanide extraction. *Anal. Sci.* **19**, 1097–1098 (2003).
- (8) Zheng, D., Wang, X., Zhang, M. & Ju, C. Synergistic Effects Between the Two Choline-Based Ionic Liquids as Lubricant Additives in Glycerol Aqueous Solution. *Tribol. Lett.* **67**, 1–13 (2019).
- (9) Lewandowski, A. & Świdarska-Mocek, A. Ionic liquids as electrolytes for Li-ion batteries—An overview of electrochemical studies. *J. Power Sources* **194**, 601–609 (2009).
- (10) Egorova, K. S., Gordeev, E. G. & Ananikov, V. P. Biological Activity of Ionic Liquids and Their Application in Pharmaceutics and Medicine. *Chem. Rev.* **117**, 7132–7189 (2017).
- (11) Dupont, J., de Souza, R. F. & Suarez, P. A. Z. Ionic Liquid (Molten Salt) Phase Organometallic Catalysis. *Chem. Rev.* **102**, 3667–3692 (2002).
- (12) Lin, I. J. B. & Vasam, C. S. Metal-containing ionic liquids and ionic liquid crystals based on imidazolium moiety. *J. Organomet. Chem.* **690**, 3498–3512 (2005).
- (13) Wang, C. *et al.* Tuning the Basicity of Ionic Liquids for Equimolar CO<sub>2</sub> Capture. *Angew. Chemie* **123**, 5020–5024 (2011).
- (14) Petkovic, M., Seddon, K. R., Rebelo, L. P. N. & Pereira, C. S. Ionic liquids: A pathway to

- environmental acceptability. *Chem. Soc. Rev.* **40**, 1383–1403 (2011).
- (15) Cromie, S. R. T., Del Pópolo, M. G. & Ballone, P. Interaction of room temperature ionic liquid solutions with a cholesterol bilayer. *J. Phys. Chem. B* **113**, 11642–11648 (2009).
- (16) Zhang, Z. X. *et al.* Asymmetrical dicationic ionic liquids based on both imidazolium and aliphatic ammonium as potential electrolyte additives applied to lithium secondary batteries. *Electrochim. Acta* **53**, 4833–4838 (2008).
- (17) Shahkaramipour, N., Adibi, M., Seifkordi, A. A. & Fazli, Y. Separation of CO<sub>2</sub>/CH<sub>4</sub> through alumina-supported geminal ionic liquid membranes. *J. Memb. Sci.* **455**, 229–235 (2014).
- (18) Fang, D., Yang, J. & Jiao, C. Dicationic ionic liquids as environmentally benign catalysts for biodiesel synthesis. *ACS Catal.* **1**, 42–47 (2011).
- (19) Anderson, J. L., Ding, R., Ellern, A. & Armstrong, D. W. Structure and properties of high stability geminal dicationic ionic liquids. *J. Am. Chem. Soc.* **127**, 593–604 (2005).
- (20) Montalbán, M. G., Villora, G. & Licence, P. Ecotoxicity assessment of dicationic versus monocationic ionic liquids as a more environmentally friendly alternative. *Ecotoxicol. Environ. Saf.* **150**, 129–135 (2018).
- (21) Esson, M. M. & Mecozzi, S. Preparation, Characterization, and Formulation Optimization of Ionic-Liquid-in-Water Nanoemulsions toward Systemic Delivery of Amphotericin B. *Mol. Pharm.* **17**, 2221–2226 (2020).
- (22) Weaver, K. D., Kim, H. J., Sun, J., MacFarlane, D. R. & Elliott, G. D. Cyto-toxicity and biocompatibility of a family of choline phosphate ionic liquids designed for pharmaceutical applications. *Green Chem.* **12**, 507–51 (2010).
- (23) Mena, I. F., Diaz, E., Palomar, J., Rodriguez, J. J. & Mohedano, A. F. Cation and anion effect on the biodegradability and toxicity of imidazolium– and choline–based ionic liquids. *Chemosphere* **240**, 124947 (2020).
- (24) Stolte, S. *et al.* Effects of different head groups and functionalised side chains on the aquatic toxicity of ionic liquids. *Green Chem.* **9**, 1170–1179 (2007).
- (25) Chauhan, V. *et al.* Aggregation behavior of non-cytotoxic ester functionalized morpholinium based ionic liquids in aqueous media. *J. Colloid Interface Sci.* **446**, 263–271 (2015).
- (26) Siqueira, L. J. A. & Ribeiro, M. C. C. Alkoxy chain effect on the viscosity of a quaternary ammonium ionic liquid: Molecular dynamics simulations. *J. Phys. Chem. B* **113**, 1074–1079 (2009).
- (27) Oulego, P. *et al.* Relationships between the physical properties and biodegradability and bacteria toxicity of fatty acid-based ionic liquids. *J. Mol. Liq.* **292**, (2019).
- (28) Ibsen, K. N. *et al.* Mechanism of Antibacterial Activity of Choline-Based Ionic Liquids (CAGE).

- ACS Biomater. Sci. Eng.* **4**, 2370–2379 (2018).
- (29) Banerjee, A. *et al.* Ionic liquids for oral insulin delivery. *Proc. Natl. Acad. Sci. U. S. A.* **115**, 7296–7301 (2018).
- (30) Ohno, H. & Fukumoto, K. Amino Acid Ionic Liquids. *Acc. Chem. Res.* **40**, 1122–1129 (2007).
- (31) Kumari, P. & Kashyap, H. K. Sensitivity and Resilience of Phosphatidylcholine and Phosphatidylethanolamine Lipid Membranes against Cholinium Glycinate Biocompatible Ionic Liquid. *J. Phys. Chem. B* **123**, 4550–4561 (2019).
- (32) Kumari, M., Gupta, A., Shobhna & Kashyap, H. K. Molecular Dynamics Evaluation of the Effect of Cholinium Phenylalaninate Biocompatible Ionic Liquid on Biomimetic Membranes. *J. Phys. Chem. B* **124**, 6748–6762 (2020).
- (33) Stoimenovski, J., MacFarlane, D. R., Bica, K. & Rogers, R. D. Crystalline vs. ionic liquid salt forms of active pharmaceutical ingredients: A position paper. *Pharm. Res.* **27**, 521–526 (2010).
- (34) Stefanovic, R., Ludwig, M., Webber, G. B., Atkin, R. & Page, A. J. Nanostructure, hydrogen bonding and rheology in choline chloride deep eutectic solvents as a function of the hydrogen bond donor. *Phys. Chem. Chem. Phys.* **19**, 3297–3306 (2017).
- (35) Ventura, S. P. M. *et al.* Designing ionic liquids: The chemical structure role in the toxicity. *Ecotoxicology* **22**, 1–12 (2013).
- (36) Bonhôte, P., Dias, A. P., Papageorgiou, N., Kalyanasundaram, K. & Grätzel, M. Hydrophobic, Highly Conductive Ambient-Temperature Molten Salts. *Inorg. Chem.* **35**, 1168–1178 (1996).
- (37) Huddleston, J. G. *et al.* Characterization and comparison of hydrophilic and hydrophobic room temperature ionic liquids incorporating the imidazolium cation. *Green Chem.* **3**, 156–164 (2001).
- (38) Singh, O., Singla, P., Aswal, V. K. & Mahajan, R. K. Impact of Aromatic Counter-Ions Charge Delocalization on the Micellization Behavior of Surface-Active Ionic Liquids. *Langmuir* **35**, 14586–14595 (2019).
- (39) Cho, C. W., Pham, T. P. T., Jeon, Y. C. & Yun, Y. S. Influence of anions on the toxic effects of ionic liquids to a phytoplankton *selenastrum capricornutum*. *Green Chem.* **10**, 67–72 (2008).
- (40) Freire, M. G., Santos, L. M. N. B. F., Fernandes, A. M., Coutinho, J. A. P. & Marrucho, I. M. An overview of the mutual solubilities of water-imidazolium-based ionic liquids systems. *Fluid Phase Equilib.* **261**, 449–454 (2007).
- (41) Saito, G., Swanson, J. A. & Lee, K. D. Drug delivery strategy utilizing conjugation via reversible disulfide linkages: Role and site of cellular reducing activities. *Adv. Drug Deliv. Rev.* **55**, 199–215 (2003).
- (42) Carter, E. B. *et al.* Sweet success: Ionic liquids derived from non-nutritive sweeteners. *Chem. Commun.* **4**, 630–631 (2004).

## CHAPTER 3

# Physicochemical and Toxicological Analysis of Hydrophobic Ionic Liquids

---

**Contributions:** Dr. Mark Sacchetti of the Zeeh Pharmaceutical Experimental Station assisted in the measurements for the differential scanning calorimeter, viscometer, and Karl-Fisher titrator. Dr. Thomas Stringfellow of the University of Wisconsin-Madison School of Pharmacy Analytical Instrumentation Center assisted in the quantitative NMR experiments. Professor Michael Taylor and Dylan Sebo provided embryos for the zebrafish toxicity studies.

**This chapter has been published, in part, as a manuscript – Reference:** Padilla, M., Bertz, C., Berdusco, N. & Mecozzi, S. Expanding the Structural Diversity of Hydrophobic Ionic Liquids: Physicochemical Properties and Toxicity of Novel Gemini Ionic Liquids. *Green Chem.* 4375–4385 (2021) doi:10.1039/d1gc00742d.

## Abstract

Ionic liquids (ILs) have emerged as promising new materials for a variety of applications in both industry and academia. This is due to their unique properties, including high chemical and thermal stability, low flammability and vapor pressure, structural diversity, ability to solubilize a wide range of compounds, and high ionic conductivity. Unfortunately, many ILs are toxic, especially to aquatic species. Therefore, while it is important to characterize the physicochemical properties of ILs, it is also essential to evaluate their toxicity profiles. In Chapter 2, several distinct classes of ILs were synthesized, including many novel hydrophobic ILs (HILs). Here, since these compounds have never been characterized, select HILs were assessed for their melting temperature, viscosity, water solubility, and hygroscopicity. These include HILs containing monocholinium and dicholinium cations paired with  $[\text{NTf}_2]$  and first-, second-, and third-generation bis(sulfonyl)azanide anions. Additionally, the HILs are examined for their toxicity in an *in vitro* cellular model and in zebrafish (*Danio rerio*). Throughout these studies, the ILs revealed unique and interesting properties, and many trends were observed that could be used to assist in the development of future HILs.

### 3.1 Introduction

The remarkable properties of ILs allow them to be used in diverse fields such as electronics<sup>1</sup>, formulation science<sup>2</sup>, catalysis<sup>3</sup>, and separations<sup>4</sup>. Libraries of ILs can be developed quickly using relatively simple organic synthesis techniques. Additionally, with the growing interest in IL research in both industry and academia, several companies, including BASF, IoLiTec, and Solaronix, sell ILs in high quantity and quality. Although structural diversity is a core feature of ILs, rationalizing the properties of specific ILs based on structure can be challenging. This is because slight alterations in IL architecture can result in dramatic changes in the physicochemical properties of ILs. This phenomenon is a result of the complex nanostructure inherent in a liquid phase of ions.

Decades of research have revealed that each IL has a unique nanostructure, many of which are heterogenous.<sup>5</sup> Studies on ILs using molecular dynamics have demonstrated that ILs employ a variety of intermolecular interactions, including, but not limited to, hydrogen bonding, London dispersion forces,  $\pi$ -stacking, and dipole-dipole interactions.<sup>6</sup> Furthermore, ILs can form discrete structures as well as aggregates including micelles<sup>7</sup>, ion pairs<sup>8</sup>, globular formations<sup>9</sup>, spongelike networks<sup>10</sup>, and onion-like layers composed of alternating cations and anions<sup>11</sup>. Since many ILs have both lipophilic and polar groups, multiple domains of hydrophobic and hydrophilic assemblies can exist within a single IL.<sup>12</sup> Strikingly, ILs can have dramatic structural changes when coming into contact with different materials.<sup>13</sup>

Although IL nanostructure is not the focus of this chapter, these studies reveal the challenges of predicting IL properties as well as the necessity for undergoing comprehensive physicochemical testing. For HILs, which is the focus of this chapter, there are certain properties that are essential to examine in order to ascertain the applicability of these compounds. For example, many ILs are used in the catalysis of water-sensitive materials, and so it is important to understand the hygroscopicity of the salts to prevent unwanted side-reactions due to the water trapped in the HIL.<sup>14</sup> Assessing hydrophobicity is important also, as several HILs are employed in liquid-liquid extractions of aqueous solutions.<sup>4</sup> Since HILs have a wide range of hydrophobicities, it is important to calculate their water solubilities so that a particular HIL is not completely dissolved by water during the extraction. Other important parameters include viscosity, as less

viscous ILs are easier to handle, and melting points, as ILs with higher melting points cannot be utilized in low temperature applications.

While the unique properties of ILs have facilitated their utilization in different areas, the same properties have earned them a “green” moniker. The designation of ILs as environmentally friendly is based on their negligible vapor pressure and chemical and thermal stability, meaning they will not evaporate into the atmosphere nor readily decompose, unlike many traditional solvents and materials.<sup>15</sup> Unfortunately, the rigorous exploration of ILs has revealed that many are not “green”. Instead, some ILs have been found to be toxic to humans and wildlife – especially aquatic species.<sup>16,17</sup> Also, due to their relative newness and unique structures, the syntheses of ILs can be costly and energy intensive.<sup>18</sup>

IL toxicity can occur in different avenues. The first generation of ILs were not stable in an ambient environment and thus would readily decompose.<sup>19</sup> Current ILs are more stable, but many are hygroscopic and will absorb large amounts of water, which can facilitate degradation into harmful molecules. Additionally, although ILs are designated as thermally stable, degradation can arise when ILs are used at high temperatures, however this is dependent on the specific IL.<sup>20</sup> Lastly, as ILs are often regenerated, recycled, or reused, especially in industrial settings, harmful agents can become trapped in the salt, or reagents can react with the ILs to yield toxic molecules that will then contaminate future applications.<sup>21</sup>

While the unintentional transformation of ILs as well as the capturing of harmful agents can lead to toxicity, most instances of toxicity are from the native ILs themselves. As a result, the past decade has seen a surge in studies on the relationship between IL structure and toxicity. Many structural trends have been observed, where features such as long alkyl chains on the cation and anion have been found to increase toxicity as they can insert themselves into lipid bilayers, disrupting cell integrity.<sup>22-24</sup>

The frequently-used hydrophobic anions, which include bis(trifluoromethanesulfonyl)amide ([NTf<sub>2</sub>]), hexafluorophosphate ([PF<sub>6</sub>]), and tetrafluoroborate ([BF<sub>4</sub>]), are significantly more toxic than halide and carboxylate anions.<sup>25</sup> The [PF<sub>6</sub>] and [BF<sub>4</sub>] anions can hydrolyze to produce fluoride, a toxic compound; although the potency of these ions depends on the corresponding cation, environment, and organism.<sup>26,27</sup> The origin of the [NTf<sub>2</sub>] anion toxicity is less certain, although molecular simulation studies

suggest that the anion can enter lipid bilayers, reassociate with the corresponding cation, and distort lipid packing.<sup>28</sup> As a result of these phenomena, there is a general trend that increasing hydrophobicity increases toxicity.<sup>29</sup> While hydrophilic ILs can be used in many circumstances, some applications require hydrophobic ILs (HILs), such as in liquid-liquid extractions of aqueous media.<sup>4</sup> One limiting factor is that HILs are constrained in their structural diversity, often composed of a tetraalkylammonium or heterocyclic cation with a long alkyl chain, and paired with a [NTf<sub>2</sub>], [PF<sub>6</sub>], or [BF<sub>4</sub>] anion.

Although several classes of ILs were synthesized in Chapter 2, only certain ILs were evaluated in this chapter. This is because many of the ILs were hydrophilic and did not fit the scope of these studies, which focused exclusively on HILs. Additionally, some HILs were too structurally dissimilar from the core ILs studied. The monocholinium and dicholinium ILs containing [NTf<sub>2</sub>] anions and first-generation bis(sulfonyl)azanide anions were the focal point of these studies as they possessed favorable and interesting properties, as the large majority are hydrophobic and liquid at room temperature. The monocholinium and dicholinium ILs incorporating second- and third-generation bis(sulfonyl)azanide anions were also tested in limited capacity to assess different, but related, ILs, and develop structure-property trends.

The selected ILs underwent physicochemical analysis that included measuring melting point, viscosity, water solubility, and hygroscopicity. Additionally, the toxicity of several IL salt precursors and ILs were evaluated using a cellular *in vitro* model and zebrafish (*Danio rerio*). Through these studies, many interesting properties were uncovered. The HILs with [NTf<sub>2</sub>] and first-generation bis(sulfonyl)azanide anions have low melting points compared to the ILs with second- and third-generation bis(sulfonyl)azanide anions, with many having glass transition temperatures. Dicholinium ILs and ILs containing aromatic anions possess high viscosities in contrast to monocholinium and non-aromatic ILs. Unlike the previous parameters, the water solubility and hygroscopicity values are IL-specific and depend on the specific architectures of the individual HILs, rather than their overall subclass. This is true also for the toxicity studies, which revealed a wide range of harmful and benign ILs.

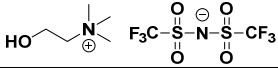
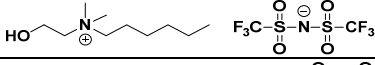
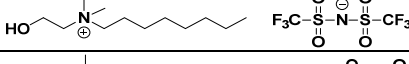
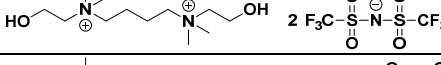
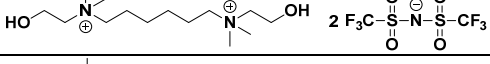
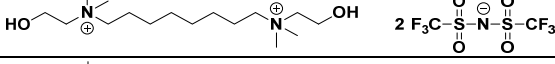
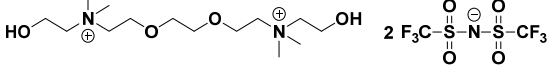
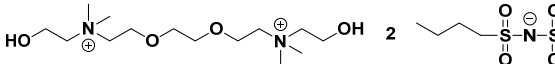
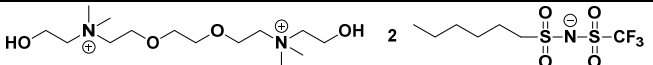
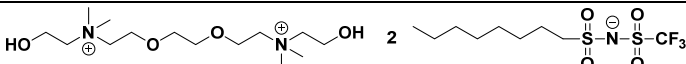
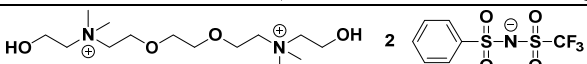
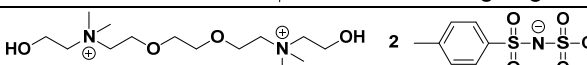
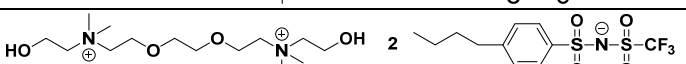
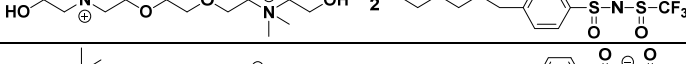
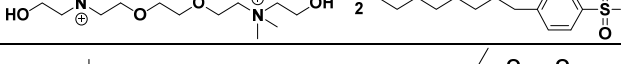
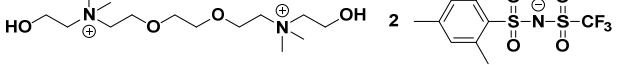
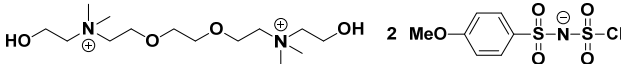
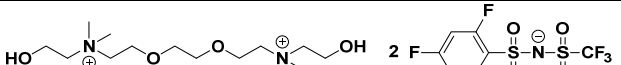
## 3.2 Results and Discussion

### 3.2.1 Differential scanning calorimetry

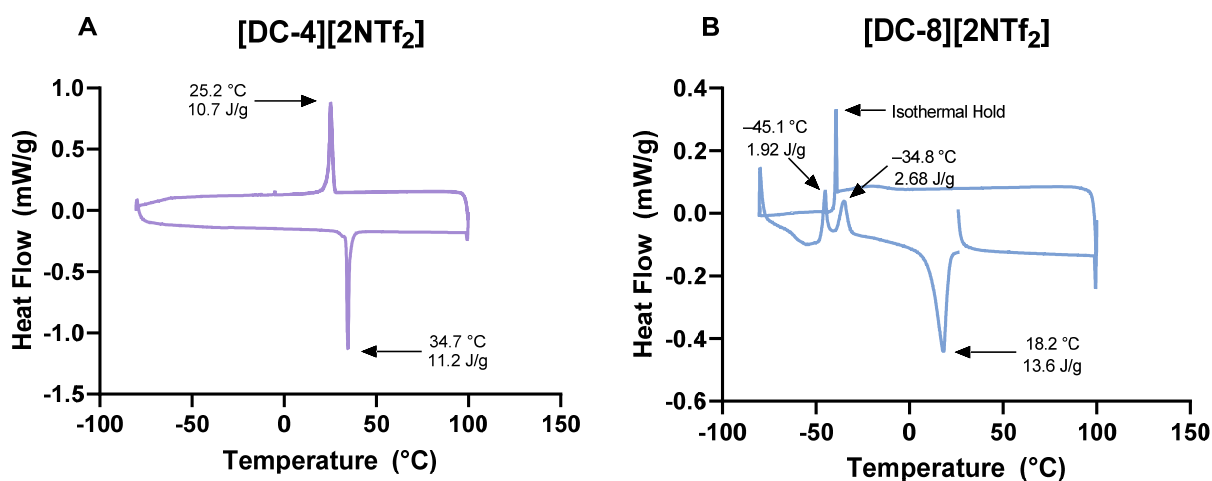
Various ILs were evaluated for physical transformations using differential scanning calorimetry (DSC), which is a technique that measures the amount of heat needed to increase the temperature of a sample compared to a standard. When materials have a phase transition, a sharp endothermic or exothermic peak can be observed on the instrument software. Similarly, many materials, such as ILs, have glass transition temperatures that can be determined using DSC. For each IL, a standard cooling rate of 10 °C/min was used, while the heating rates and isothermal holds were optimized for each compound. DSC conditions and thermograms for each IL can be found in the Appendix.

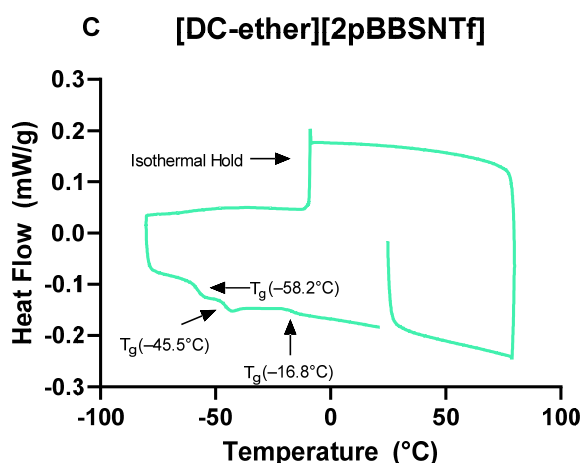
The first class of ILs analyzed were the monocholinium and dicholinium ILs containing either [NTf<sub>2</sub>] anions or the first-generation bis(sulfonyl)azanide ILs (**Table 3.1**). These latter anions had one trifluoromethane group and either an alkyl, aryl, or alkyl aryl substituent on the other end. Out of the twenty ILs investigated, only [DC-4][2NTf<sub>2</sub>] (**13i**) is a solid at room temperature. Interestingly, this IL has a melting point at 34.7 °C and a freezing point at 25.2 °C (**Figure 3.1A**). In general, the twenty ILs have lower melting points than most hydrophilic ILs.<sup>30</sup> ILs with lower melting temperatures are preferred as they can be utilized in more applications. Here, the phenomenon of lower melting temperature is mainly due to the symmetric and asymmetric bis(sulfonyl)azanide anions, as both species are weakly coordinating ions due to the high electron delocalization from the extended  $\pi$ -conjugation system inherent in the molecule as well as the electronegative oxygen and fluorine atoms surrounding the nitrogen atom. Although less significant, the alkyl groups on the quaternary ammonium cations help to delocalize the positive charge, further weakening the coordination potential.

<b>Table 3.1</b> Physical transformation temperatures of monocholinium and dicholinium ILs paired with [NTf <sub>2</sub> ] anions and first-generation bis(sulfonyl)azanide anions. T <sub>g</sub> is the glass transition temperature and T <sub>m</sub> is the melting point. Bold values represent T <sub>m</sub> . <sup>a</sup> [DC-4][2NTf <sub>2</sub> ] has a melting point at 34.7 °C and a separate freezing point at 25.2 °C.			
#	Ionic Liquid	Structure	T <sub>g</sub> and T <sub>m</sub> (°C)

<b>13a</b>	[chol][NTf <sub>2</sub> ]		<b>0.23,</b> 22.7
<b>13b</b>	[N <sub>1,1,4,2OH</sub> ][NTf <sub>2</sub> ]		8.56
<b>13c</b>	[N <sub>1,1,6,2OH</sub> ][NTf <sub>2</sub> ]		
<b>13d</b>	[N <sub>1,1,8,2OH</sub> ][NTf <sub>2</sub> ]		8.70
<b>13i</b>	[DC-4][2NTf <sub>2</sub> ]		<b>34.7,</b> <b>25.2<sup>a</sup></b>
<b>13k</b>	[DC-6][2NTf <sub>2</sub> ]		-62.7
<b>13m</b>	[DC-8][2NTf <sub>2</sub> ]		<b>18.2</b>
<b>13p</b>	[DC-ether][2NTf <sub>2</sub> ]		-65.9, -16.0
<b>18a</b>	[DC-ether][2BSNTf]		8.23
<b>18b</b>	[DC-ether][2HSNTf]		-67.3
<b>18c</b>	[DC-ether][2OSNTf]		-65.7, 18.3
<b>18d</b>	[DC-ether][2PhSNTf]		-58.1, -46.1
<b>18e</b>	[DC-ether][2TsNTf]		-42.6
<b>18f</b>	[DC-ether][2pBBSNTf]		-58.2, -45.5, -16.8
<b>18g</b>	[DC-ether][2pHBSNTf]		-54.6, 17.9
<b>18h</b>	[DC-ether][2pOBSNTf]		-59.8
<b>18i</b>	[DC-ether][2MesSNTf]		-49.3
<b>18j</b>	[DC-ether][2pMBSNTf]		-44.6
<b>18k</b>	[DC-ether][2TFBSNTf]		-41.8
<b>18l</b>	[DC-ether][2PFBSNTf]		-50.1, -41.0, 28.3

Only three ILs, [chol][NTf<sub>2</sub>] (**13a**), [DC-4][2NTf<sub>2</sub>] (**13i**), and [DC-8][2NTf<sub>2</sub>] (**13m**) possess a melting point, with [chol][NTf<sub>2</sub>] (**13a**) having both a melting point and glass transition temperature. [DC-8][2NTf<sub>2</sub>] (**13m**) possesses two unique exothermic peaks at -45.1 °C and -34.8 °C (**Figure 3.1B**). While the identity of these peaks is unclear, they are likely related to molecular reorganizations, possibly liquid crystal-related behavior. Similar peaks were observed for [chol][NTf<sub>2</sub>]. Conversely, the thermogram of [N<sub>1,1,6,2OH</sub>][NTf<sub>2</sub>] (**13c**) contained no notable transformations. The other sixteen ILs revealed only glass transition temperatures, mainly in the range of -40 °C to -60 °C. Some of these ILs contained more than one glass transition temperature, including [DC-ether][2pBBSNTf] (**13f**), which has three distinct glass transition temperatures (**Figure 2.1C**). The ILs containing asymmetric anions have only glass transition temperatures, which are generally at lower temperatures than the ILs with symmetric anions. This supports the idea that less symmetry weakens crystal lattice energy and suppresses the melting temperature.<sup>31</sup> Among the asymmetric anions, there are no obvious correlations between structure and glass transition temperature. Additional DSC runs were performed using temperatures as high as 250 °C; however, no physical transformations were observed above 50 °C, and instead, many ILs began to decompose (data not shown).



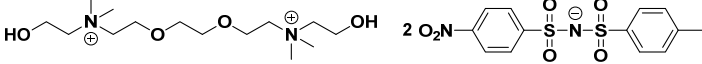
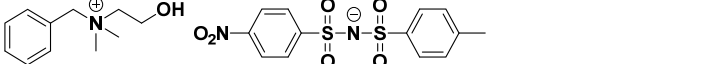
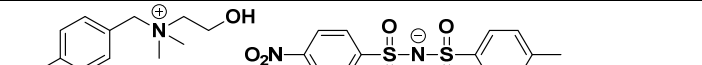
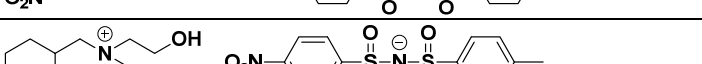
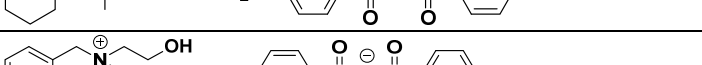
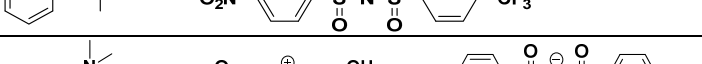
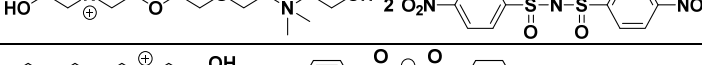
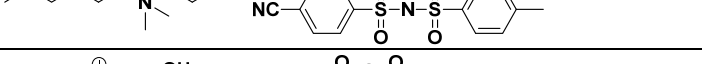
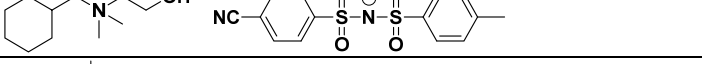
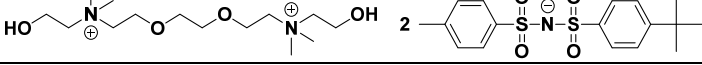
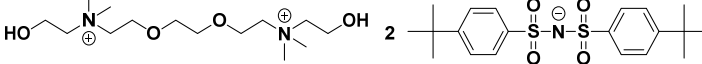
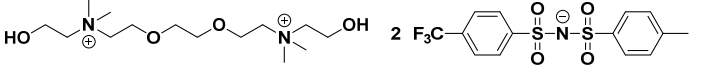
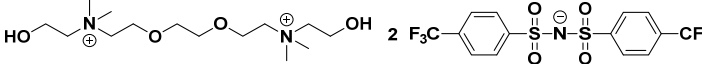
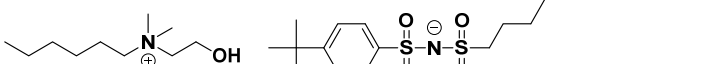
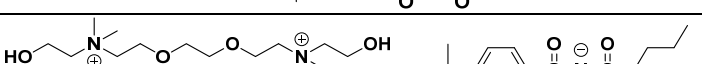


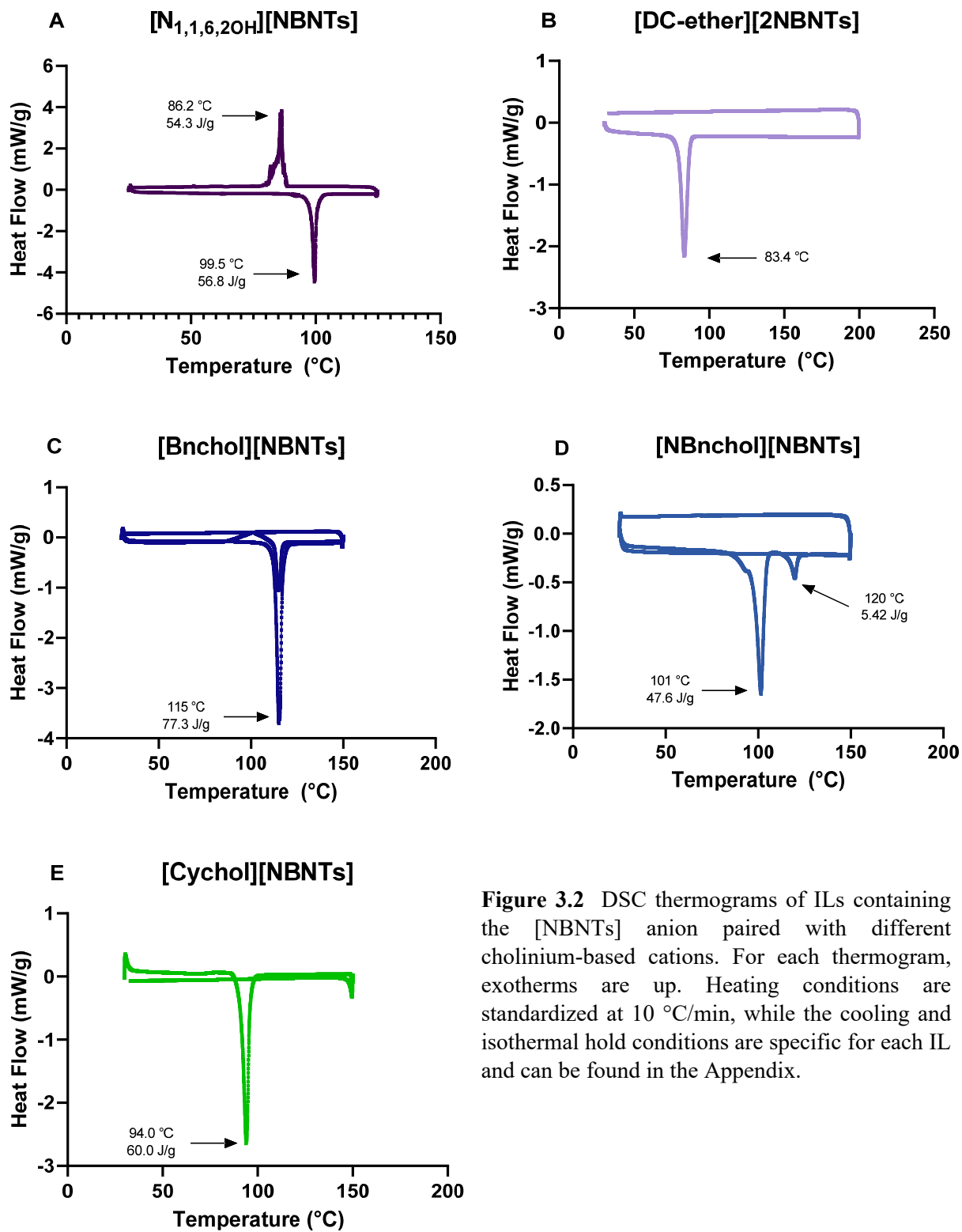
**Figure 3.1** DSC thermograms for (A) [DC-4][2NTf<sub>2</sub>], (B) [DC-8][2NTf<sub>2</sub>], and (C) [DC-ether][2pBBSNTf]. For each thermogram, exotherms are up. Heating conditions are standardized at 10 °C/min, while the cooling and isothermal hold conditions are specific for each IL and can be found in the Appendix.

The next set of compounds analyzed via DSC were the ILs containing [DC-ether] and monocholinium cations paired with second- and third-generation bis(sulfonyl)azanide anions (**Table 3.2**). The first set of these ILs utilized different cations paired with the [NBNTs] anion (**Figure 3.2**). Interestingly, [Cychol][NBNTs] (**25e**) has the lowest melting temperature at 60.0 °C, whereas the other compounds have melting temperatures between 80 °C and 115 °C. However, in a separate set of ILs that utilized the [CBNTs] anion, the results were different. Here, [Cychol][CBNTs] (**25j**) has a melting temperature at 87.2 °C, whereas [N<sub>1,1,6,2OH</sub>][CBNTs] (**25h**) has a melting temperature at 87.4 °C and a separate freezing temperature of 60.0 °C. This indicates that the cations alone cannot be used to reliably predict the phase transition temperatures. Similar to [N<sub>1,1,6,2OH</sub>][CBNTs] (**25h**), [N<sub>1,1,6,2OH</sub>][NBNTs] (**25a**) also has separate melting and freezing points at 99.5 °C and 86.2 °C, respectively.

**Table 3.2** Physical transformation temperatures of monocholinium and dicholinium ILs paired with second- and third-generation bis(sulfonyl)azanide anions.  $T_g$  is the glass transition temperature and  $T_m$  is the melting point. Bold values represent  $T_m$ . <sup>a</sup> [N<sub>1,1,6,2OH</sub>][NBNTs] has a melting point at 99.5 °C and a separate freezing point at 86.2 °C. <sup>b</sup> [DC-ether][2N(NB)<sub>2</sub>] has a melting point at 162 °C and a separate freezing point at 132 °C. <sup>c</sup> [N<sub>1,1,6,2OH</sub>][CBNTs] has a melting point at 87.4 °C and a separate freezing point at 60.0 °C.

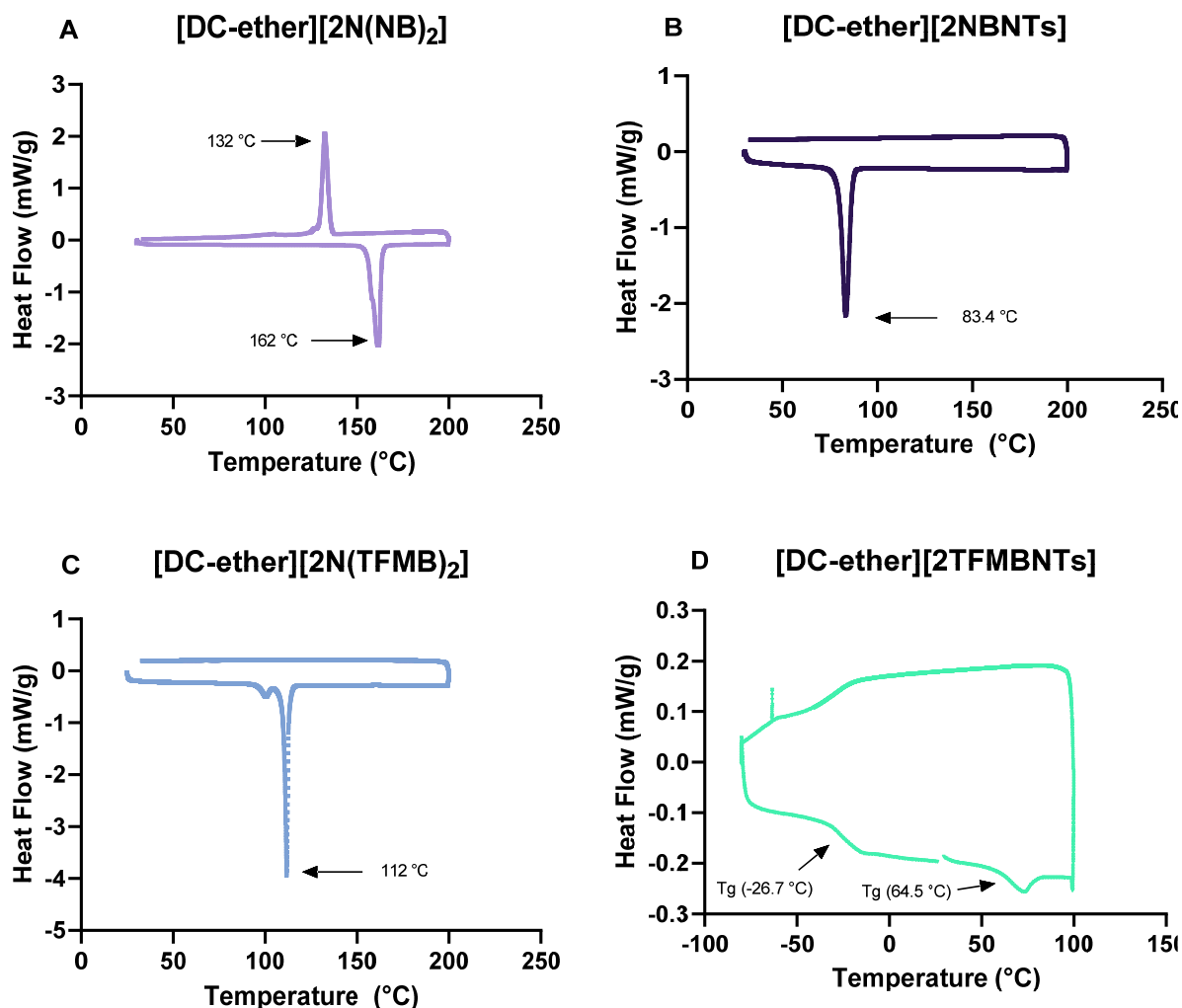
#	Ionic Liquid	Structure	$T_g$ and $T_m$ (°C)
<b>25a</b>	[N <sub>1,1,6,2OH</sub> ][NBNTs]		<b>86.2, 99.5<sup>a</sup></b>

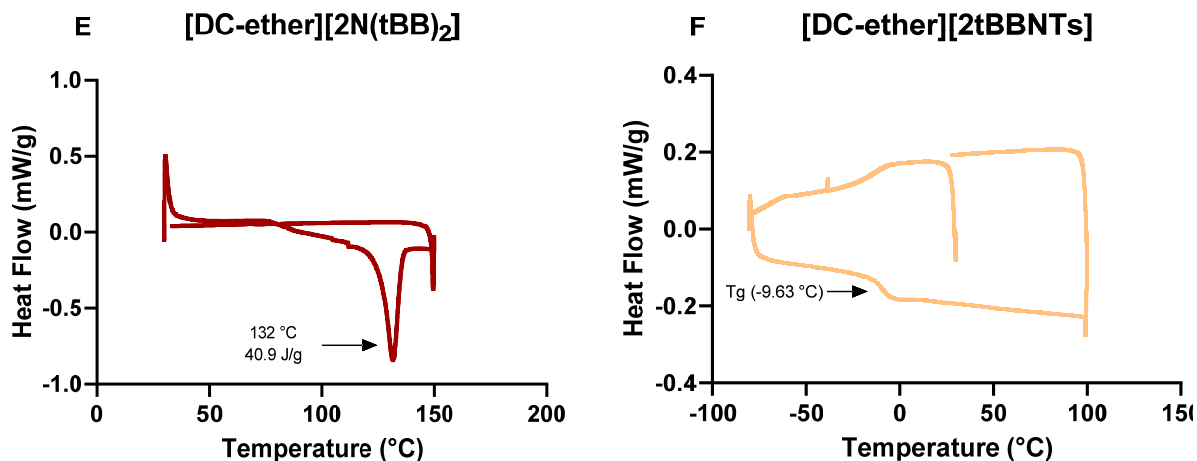
25b	[DC-ether] [2NBNTs]		83.4
25c	[Bnchol] [NBNTs]		115
25d	[NBnchol] [NBNTs]		101
25e	[Cychol] [NBNTs]		60.0
25f	[Bnchol] [NBNTFMB]		117, 121
25g	[DC-ether] [2N(NB) <sub>2</sub> ]		132, 162 <sup>b</sup>
25h	[N <sub>1,1,6,2OH</sub> ] [CBNTs]		60.0, 87.4 <sup>c</sup>
25j	[Cychol] [CBNTs]		87.2
25l	[DC-ether] [2tBBNTs]		-9.63
25m	[DC-ether] [2N(tBB) <sub>2</sub> ]		132
25n	[DC-ether] [2TFMBNTs]		-26.7, 64.5
25o	[DC-ether] [2N(TFMB) <sub>2</sub> ]		112
26a	[N <sub>1,1,6,2OH</sub> ] [tBBNB]		-53.7
26b	[DC-ether] [2tBBNB]		-28.5
26c	[Bnchol] [tBBNB]		-17.9



**Figure 3.2** DSC thermograms of ILs containing the [NBNTs] anion paired with different cholinium-based cations. For each thermogram, exotherms are up. Heating conditions are standardized at 10 °C/min, while the cooling and isothermal hold conditions are specific for each IL and can be found in the Appendix.

As described above, symmetric compounds increase the phase transition temperature, and this was observed for [DC-ether][2(NB)<sub>2</sub>] (**25g**), [DC-ether][2N(tBB)<sub>2</sub>] (**25m**), and [DC-ether][2N(TFMB)<sub>2</sub>] (**25o**), which have melting temperatures much higher than the ILs containing asymmetric versions of these anions (**Figure 3.3**). Lastly, ILs containing third-generation anions did not have defined melting and freezing points, and instead only have glass transition temperatures. This is similar to the [DC-ether] ILs containing first generation bis(sulfonyl)azanides anions (**18a–18l**), which do not have noticeable phase transition temperatures and only have glass transition temperatures. This could be due to the presence of the alkyl chains and the absence of a second aromatic group on the anion.





**Figure 3.3** DSC thermograms of [DC-ether] ILs containing symmetric and asymmetric second-generation bis(sulfonyl)azanide anions. For each thermogram, exotherms are up. Heating conditions are standardized at 10 °C/min, while the cooling and isothermal hold conditions are specific for each IL and can be found in the Appendix.

### 3.2.2 Viscosity

Viscosity is an important characteristic to examine in IL research as small structural differences can result in substantial changes in viscosity. The ideal IL viscosity depends on the application, although less viscous ILs are often preferred as they are easier to handle. The viscosity of ILs are primarily determined by hydrogen bonding and Van der Waals interactions, but depending on the structure of the IL, other intermolecular interactions can be important.<sup>32</sup> The viscosity of monocholinium and dicholinium ILs containing [NTf<sub>2</sub>] anions or first-generation bis(sulfonyl)azanide anions was measured at 25 °C, with the exception of [DC-4][2NTf<sub>2</sub>] (**13i**), which has a melting temperature of 35 °C and could not be determined using the instrument (**Table 3.3**). A wide range of viscosities was observed among the different subgroups of the ILs. For example, the dicholinium ILs are 5- to 10-fold more viscous than the monocholinium ILs.

#	Ionic Liquid	Structure	Viscosity (cP)
13a	[chol][NTf <sub>2</sub> ]		185.5
13b	[N <sub>1,1,4,2OH</sub> ][NTf <sub>2</sub> ]		156.2
13c	[N <sub>1,1,6,2OH</sub> ][NTf <sub>2</sub> ]		211.4
13d	[N <sub>1,1,8,2OH</sub> ][NTf <sub>2</sub> ]		252.9
13i	[DC-4][2NTf <sub>2</sub> ]		solid
13k	[DC-6][2NTf <sub>2</sub> ]		3,111
13m	[DC-8][2NTf <sub>2</sub> ]		3,223
13p	[DC-ether][2NTf <sub>2</sub> ]		1,345
18a	[DC-ether][2BSNTf]		8,854
18b	[DC-ether][2HSNTf]		8,311
18c	[DC-ether][2OSNTf]		10,580
18d	[DC-ether][2PhSNTf]		20,060
18e	[DC-ether][2TsNTf]		47,470
18f	[DC-ether][2pBBSNTf]		7,733
18g	[DC-ether][2pHBSNTf]		21,020
18h	[DC-ether][2pOBSNTf]		48,590
18i	[DC-ether][2MesSNTf]		>172,000
18j	[DC-ether][2pMBSNTf]		82,030
18k	[DC-ether][2TFBSNTf]		68,880
18l	[DC-ether][2PFBSNTf]		59,120

While the origin of the increase in viscosity is unclear, it is likely that the presence of the two alcohol groups on the dicholinium cation facilitates more hydrogen bonding interactions, increasing viscosity. Among the dicholinium cations, [DC-ether][2NTf<sub>2</sub>] (**13p**) was found to be less viscous than [DC-8][2NTf<sub>2</sub>] (**13m**), 1,345 cP vs. 3,223 cP, despite the former that has oxygen atoms in the octyl chain that can function as hydrogen bond acceptors. Instead, the oxygen atoms of the alkoxy chain distort intermolecular packing of alkyl chains, resulting in a decrease in viscosity.<sup>33,34</sup> Interestingly, [DC-ether][2NTf<sub>2</sub>] (**13p**) is 10- to 100-fold less viscous than the ILs containing aryl asymmetric anions. This could be a result of  $\pi$ -stacking interactions increasing viscosity; however, there are no known studies that analyze the viscosity of aryl-containing ILs.

Among the functionalized aryl ILs, there is a trend that benzene substitution increases viscosity. In particular, the viscosity of [DC-ether][2MesSNTf] (**18i**) (>172,000 cP) is beyond the upper limit of detection of the instrument. The one exception is [DC-ether][2pBBSNTf] (**18f**) (7,733 cP), which has a viscosity much lower than [DC-ether][2PhSNTf] (**18d**) (20,060 cP). This result is likely due to the presence of the alkyl chain that disrupts the hydrogen bonding network, lowering the viscosity. However, this phenomenon is restricted to short alkyl chains, as longer alkyl chains resulted in increased viscosity compared to the parent IL. Additionally, as the alkyl chain was extended, the viscosity increased, a feature that is well-documented in the IL literature.<sup>32</sup> These latter results are due to the larger number of Van der Waals interactions that increase viscosity dramatically. It should be noted that a methyl group itself is not long enough to disrupt the hydrogen bonding network and can increase viscosity in certain cases. For example, [chol][NTf<sub>2</sub>] (**13a**) (185.5 cP) has a higher viscosity than [N<sub>1,1,4,2OH</sub>][NTf<sub>2</sub>] (**13b**) (156.2 cP), while [DC-ether][2TsNTf] (**18e**) (47,470 cP) has a higher viscosity than both [DC-ether][2pBBSNTf] (**18f**) and [DC-ether][2pHBSNTf] (**18g**; 21,020 cP).

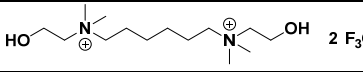
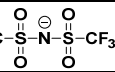
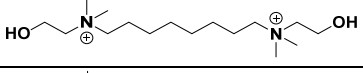
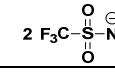
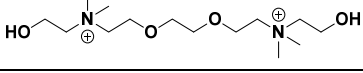
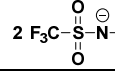
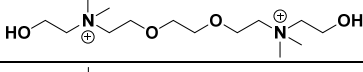
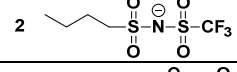
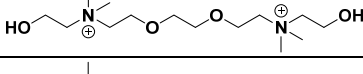
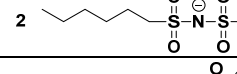
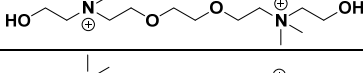
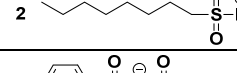
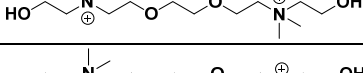
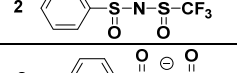
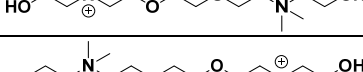
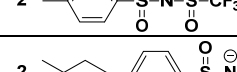
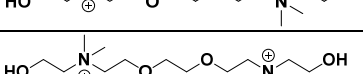
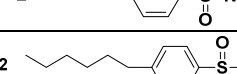
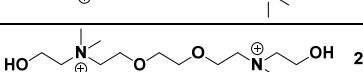
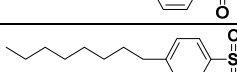
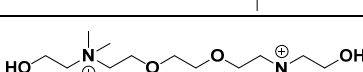
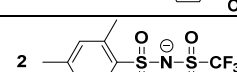
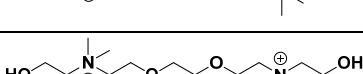
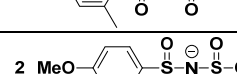
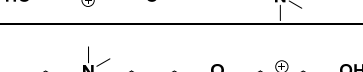
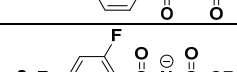
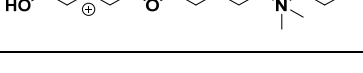
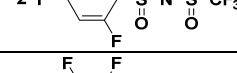
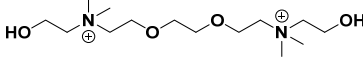
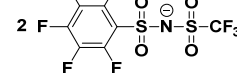
For ILs with second-generation bis(sulfonyl)azanide anions that are liquid at room temperature, the viscosities were too high to calculate. Likely, the presence of two aryl groups increases the number of  $\pi$ -stacking interactions, making these ILs much more viscous.

### 3.2.3 Water solubility

The hydrophobicity of an IL depends on its electron delocalization and lipophilicity. Although the hydrophobicity of the anion is often what determines the water solubility of the IL, the cation can also play a significant role.<sup>35</sup> Typically, HILs have a lipophilic cation paired with a weakly coordinating anion such as [NTf<sub>2</sub>]. These anions have limited hydrogen bonding with water due to their substantial electron delocalization.<sup>35</sup>

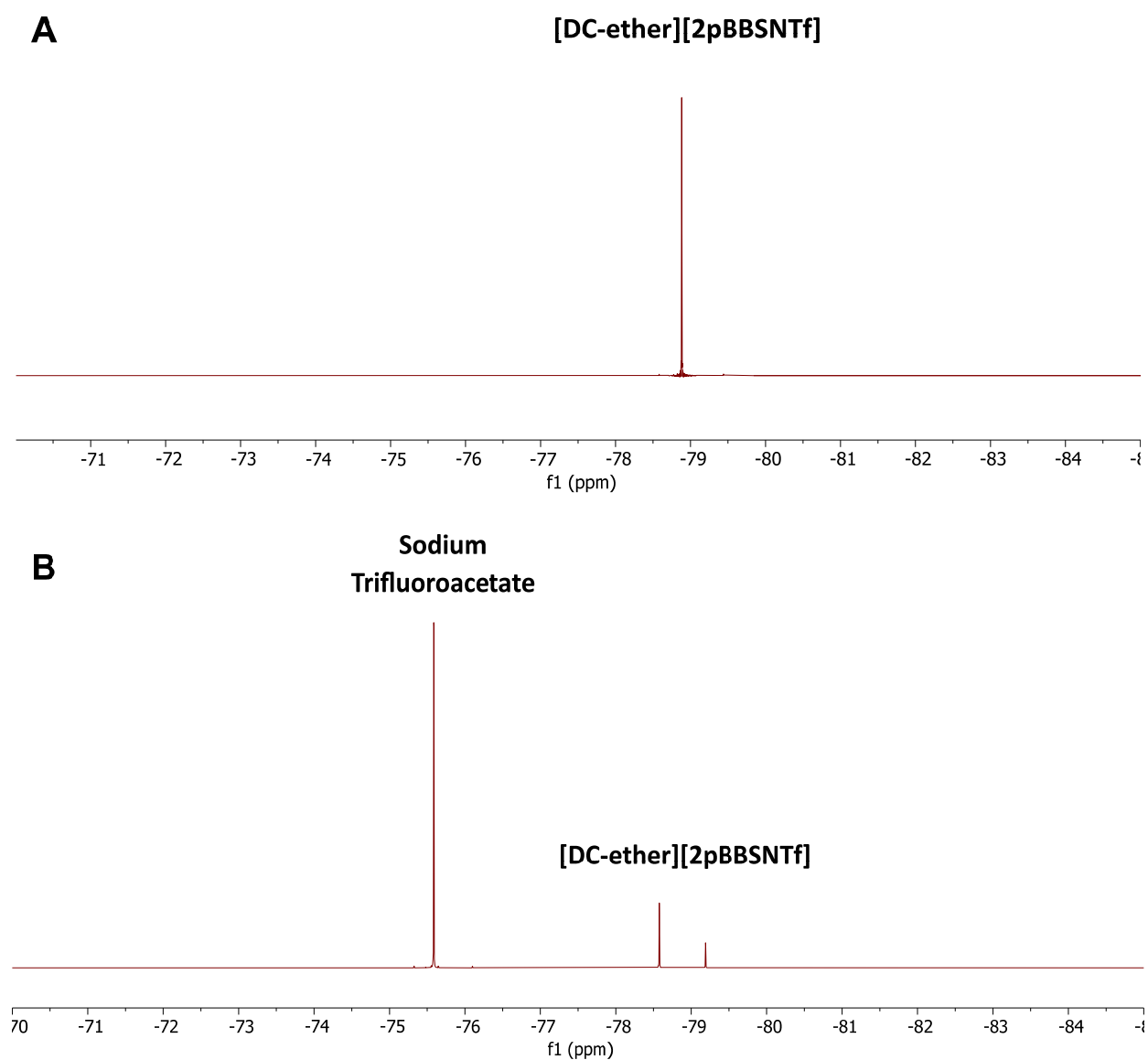
In the first set of studies, the water solubility of each monocholinium and dicholinium ILs containing [NTf<sub>2</sub>] anions or first generation bis(sulfonyl)azanide anions was evaluated using quantitative <sup>19</sup>F NMR, where sodium trifluoroacetate (NaTFA) was employed as the standard (**Table 3.4**). To ensure a sufficient relaxation time was used during the NMR experiments, the *T*<sub>1</sub> values of NaTFA and each IL were calculated using an inverse recovery experiment (**Table A.1**). Since the largest *T*<sub>1</sub> value was 3 s, a universal recycle delay time, *D*<sub>1</sub>, of 30 s was deemed sufficient to allow for proper relaxation in each experiment. The singlet from the trifluoromethane group of each IL was compared to the trifluoromethane peak of NaTFA. Due to the different chemical environments of the IL and standard, the two trifluoromethane moieties have chemical shifts that were far enough apart to allow for accurate integration. The quantitative NMR (qNMR) spectra for each IL can be found in the Appendix.

<b>Table 3.4</b> Water solubility values of monocholinium and dicholinium ILs containing [NTf <sub>2</sub> ] anions and first-generation bis(sulfonyl)azanide anions.			
#	Ionic Liquid	Structure	Water Solubility (mM)
<b>13a</b>	[chol][NTf <sub>2</sub> ]		314
<b>13b</b>	[N <sub>1,1,4,2OH</sub> ][NTf <sub>2</sub> ]		34.6
<b>13c</b>	[N <sub>1,1,6,2OH</sub> ][NTf <sub>2</sub> ]		16.3
<b>13d</b>	[N <sub>1,1,8,2OH</sub> ][NTf <sub>2</sub> ]		4.98
<b>13i</b>	[DC-4][2NTf <sub>2</sub> ]		29.1

<b>13k</b>	[DC-6][2NTf <sub>2</sub> ]	 2 	17.0
<b>13m</b>	[DC-8][2NTf <sub>2</sub> ]	 2 	9.49
<b>13p</b>	[DC-ether][2NTf <sub>2</sub> ]	 2 	23.7
<b>18a</b>	[DC-ether][2BSNTf]	 2 	water soluble
<b>18b</b>	[DC-ether][2HSNTf]	 2 	29.8
<b>18c</b>	[DC-ether][2OSNTf]	 2 	5.89
<b>18d</b>	[DC-ether][2PhSNTf]	 2 	51.2
<b>18e</b>	[DC-ether][2TsNTf]	 2 	20.5
<b>18f</b>	[DC-ether][2pBBSNTf]	 2 	2.99
<b>18g</b>	[DC-ether][2pHBSNTf]	 2 	0.525
<b>18h</b>	[DC-ether][2pOBSNTf]	 2 	0.118
<b>18i</b>	[DC-ether][2MesSNTf]	 2 	7.75
<b>18j</b>	[DC-ether][2pMBSNTf]	 2 	27.3
<b>18k</b>	[DC-ether][2TFBSNTf]	 2 	18.7
<b>18l</b>	[DC-ether][2PFBSNTf]	 2 	8.93

Throughout the qNMR experiments, there was a tendency for the ILs to aggregate in D<sub>2</sub>O, resulting in the formation of peaks that were not present in the NMRs in deuterated organic solvents. While most of these peaks composed <1% of the integration area, a few ILs have larger peaks, such as [DC-ether][2pBBSNTf] (**18f**), which formed two distinct peaks (**Figure 3.4**). The ILs with aryl-alkyl anion all formed two peaks, likely due to the formation of micelles. The formation of aggregates and nanostructures of ILs in aqueous and other media is well-known, with NMR being one of the main techniques to study them.<sup>36-38</sup> Out of the twenty ILs in the study, only [DC-ether][2BSNTf] (**18a**) is water soluble. Interestingly,

the water solubility of [DC-ether][2HSNTf] (**18b**; 29.8 mM) is close to [DC-ether][2NTf<sub>2</sub>] (**13p**; 23.7 mM), meaning, by extending the alkyl chain of the anion by only two methylene units, the hydrophobicity of the IL dramatically increases.



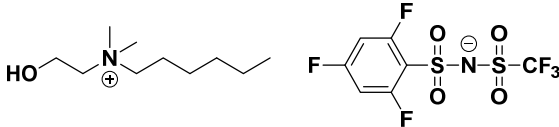
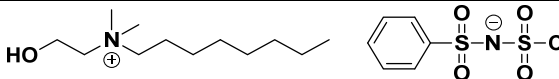
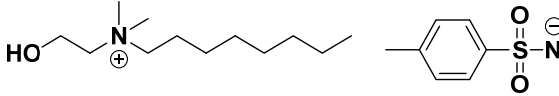
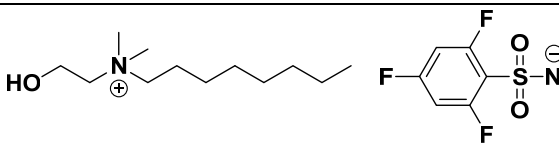
**Figure 3.4** (A) <sup>19</sup>F NMR spectrum of [DC-ether][2pBBSNTf] in acetone-d<sub>6</sub>. (B) Quantitative <sup>19</sup>F-NMR spectrum of [DC-ether][2pBBSNTf] in D<sub>2</sub>O with sodium trifluoroacetate used as the standard.

Within all subgroups, water solubility decreased with increasing alkyl chain length. These results support previous research that demonstrates that the hydrophobicity of a trifluoromethane group can be mimicked by a sufficiently long alkyl chain<sup>39</sup>, and that longer alkyl chains increase hydrophobicity<sup>35</sup>. Interestingly, [DC-ether][2PhSNTf] (**18d**; 51.2 mM) has a water solubility much higher than [DC-ether][2NTf<sub>2</sub>] (**13p**); however, each of the ILs with substituted aromatic moieties have water solubilities comparable or lower than [DC-ether][2NTf<sub>2</sub>] (**13p**). These data suggest that the electron delocalization capacity of a trifluoromethane moiety can be replicated or enhanced by using a substituted aromatic group, but not a benzene group. The hydrophobicity can be further reduced by adding multiple substituents to the benzene ring, as observed with [DC-ether][2MesSNTf] (**18i**; 7.75 mM), [DC-ether][2TFBSNTf] (**18k**; 18.7 mM), and [DC-ether][2PFBSNTf] (**18l**; 8.93 mM). [DC-ether][2pOBSNTf] (**18h**; 0.118 mM) has the lowest water solubility, being 200-fold less water soluble than [DC-ether][2NTf<sub>2</sub>] (**13p**). This indicates that a combination of a long alkyl chain and delocalizing aromatic group can significantly increase hydrophobicity.

In comparing ILs with different cations, [chol][NTf<sub>2</sub>] (**13a**; 314 mM) has the highest water solubility out of all the ILs in the first study. By increasing the alkyl chain length of only one of the methyl groups of [chol][NTf<sub>2</sub>] (**13a**) to a butyl group, as in [N<sub>1,1,4,2OH</sub>][NTf<sub>2</sub>] (**13b**; 34.6 mM), the water solubility decreases by 10-fold. The same decrease in water solubility was observed for [DC-4][2NTf<sub>2</sub>] (**13i**; 29.1 mM), which contains a dicholinium cation with a butyl linker. Among the dicholinium and cholinium cations with the same alkyl chain length, there are only minor differences in the water solubilities. However, despite having the same linker length, the water solubility of [DC-ether][2NTf<sub>2</sub>] (**13p**) is higher than [DC-8][2NTf<sub>2</sub>] (**13m**; 9.49 mM). This is due to the presence of oxygen atoms in the [DC-ether] cation that are polar and can function as hydrogen bond acceptors.

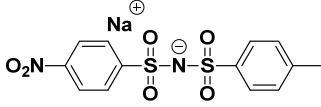
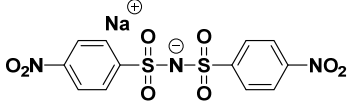
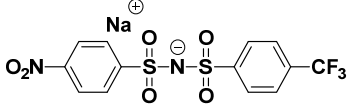
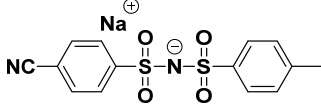
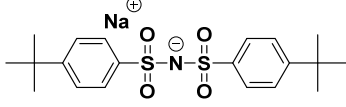
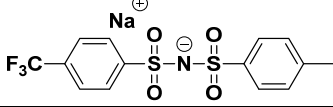
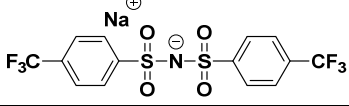
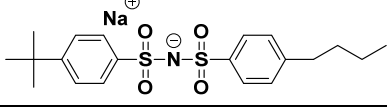
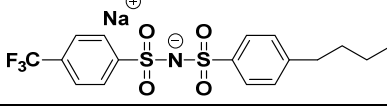
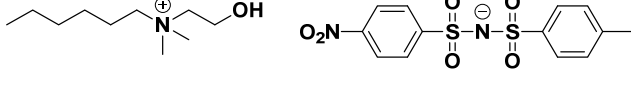
In a separate set of studies, four monocholinium ILs with first-generation bis(sulfonyl)azanide anions were examined (**Table 3.5**). Interestingly, the water solubility of these ILs showed a strong dependence on the cation. For example, while [DC-ether][2PhSNTf] (**18d**; 51.2 mM) is relatively water soluble, [N<sub>1,1,8,2OH</sub>][PhSNTf] (**19e**; 6.82 mM) is significantly less water soluble, likely due to the

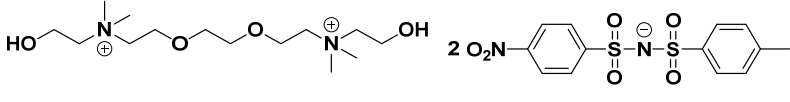
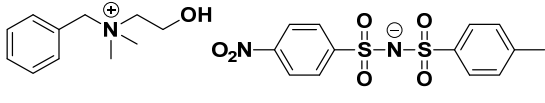
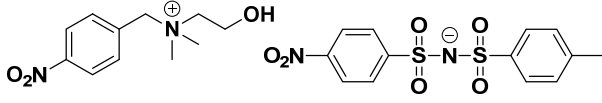
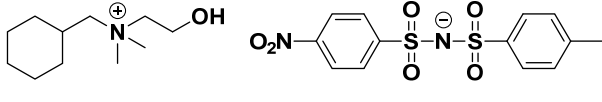
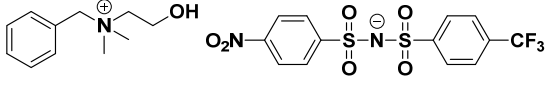
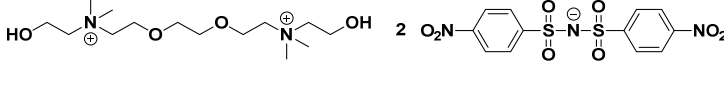
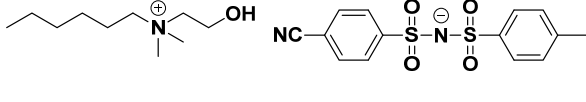
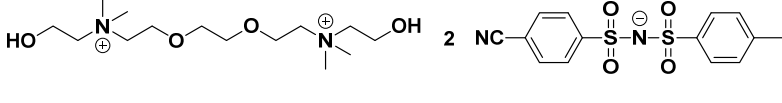
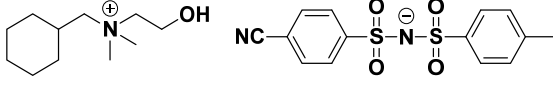
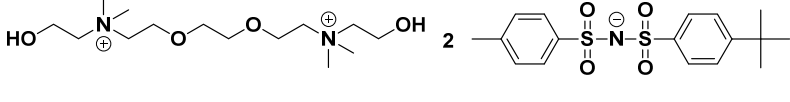
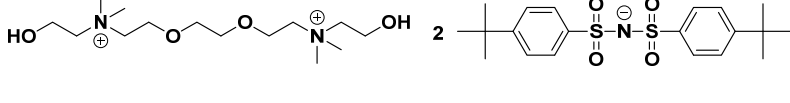
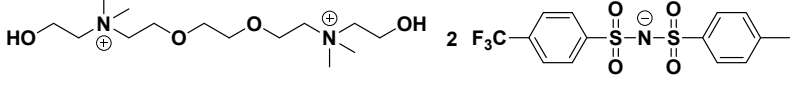
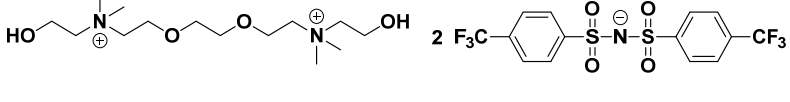
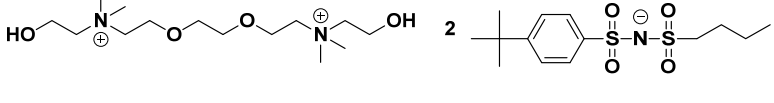
hydrophobic octyl chain. This was also observed in  $[N_{1,1,6,2OH}][TFBNTs]$  (**19c**; 13.7 mM) and  $[N_{1,1,8,2OH}][TFBSNTf]$  (**19g**; 5.03 mM), which were both more hydrophobic than  $[DC-ether][2TFBSNTf]$  (**18k**; 18.7 mM). Due to the presence of two positively charged cholinium groups as well as an alkoxy linker, the  $[DC-ether]$  cation is more hydrophilic than the alkyl cholinium cations.

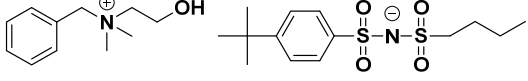
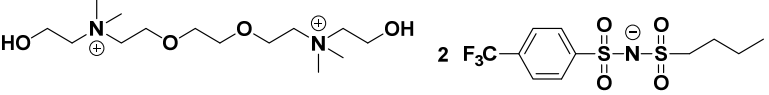
<b>Table 3.5</b> Water solubility of alkyl monocholinium ILs with first-generation bis(sulfonyl)azanide anions.			
#	Ionic Liquid	Structure	Water Solubility (mM)
<b>19c</b>	$[N_{1,1,6,2OH}][TFBSNTf]$		13.7
<b>19e</b>	$[N_{1,1,8,2OH}][PhSNTf]$		6.82
<b>19f</b>	$[N_{1,1,8,2OH}][TsSNTf]$		4.54
<b>19g</b>	$[N_{1,1,8,2OH}][TFBSNTf]$		5.03

The ILs with second- and third-generation bis(sulfonyl)azanide anions were evaluated for water solubility. Unlike the previous anions, some of the anion salts are hydrophobic, and thus their water solubilities were measured as well. Since many of these compounds do not contain fluorine atoms,  $^1H$  NMR was utilized, where either 1,4-dioxanes or sodium acetate were used as the standards. For the qNMR studies with  $^1H$  NMR, a  $D_1$  time of 60 s was chosen as individual  $T_1$  values were not calculated for these compounds. The water solubility of the anion salts and ILs (**Table 3.6**) revealed that the hydrophobicity of the salt precursor may not correlate with the corresponding IL water solubility. For example  $[Na][N(NB)_2]$  (**21b<sub>ii</sub>**) has a water solubility of 74.5 mM, whereas  $[DC-ether][2N(NB)_2]$  (**25g**) has water solubility of 0.631

mM. It is likely that the IL forms an extremely hydrophobic nanostructure than cannot be formed by the anion alone. Out of the anions assessed,  $[\text{Na}][\text{N}(\text{NB})_2]$  (**21b<sub>ii</sub>**) was the only one that displayed this property.

<b>Table 3.6</b> Water solubility of second- and third-generation bis(sulfonyl)azanide anions and ILs with cholinium-based cations.			
#	Salts and Ionic Liquids	Structure	Water Solubility (mM)
<b>21a<sub>ii</sub></b>	$[\text{Na}][\text{NBNTs}]$		18.4
<b>21b<sub>ii</sub></b>	$[\text{Na}][\text{N}(\text{NB})_2]$		74.5
<b>21c<sub>ii</sub></b>	$[\text{Na}][\text{NBNTFMB}]$		11.7
<b>21d<sub>ii</sub></b>	$[\text{Na}][\text{CBNTs}]$		45.2
<b>21e<sub>ii</sub></b>	$[\text{Na}][\text{tBBNTs}]$		Water soluble
<b>21f<sub>ii</sub></b>	$[\text{Na}][\text{N}(\text{tBB})_2]$		8.46
<b>21g<sub>ii</sub></b>	$[\text{Na}][\text{TFMBNTs}]$		Water soluble
<b>21h<sub>ii</sub></b>	$[\text{Na}][\text{N}(\text{TFMB})_2]$		4.03
<b>22a<sub>ii</sub></b>	$[\text{Na}][\text{tBBNB}]$		Water soluble
<b>22b<sub>ii</sub></b>	$[\text{Na}][\text{TFMBNB}]$		Water soluble
<b>25a</b>	$[\text{N}_{1,1,6,2\text{OH}}][\text{NBNTs}]$		6.93

25b	[DC-ether] [2NBNTs]		11.2
25c	[Bnchol] [NBNTs]		4.43
25d	[NBnchol] [NBNTs]		2.46
25e	[Cychol] [NBNTs]		12.0
25f	[Bnchol] [NBNTFMB]		2.52
25g	[DC-ether] [2N(NB) <sub>2</sub> ]		0.631
25h	[N <sub>1,1,6,2</sub> OH] [CBNTs]		21.1
25i	[DC-ether] [2CBNTs]		35.7
25j	[Cychol] [CBNTs]		24.1
25l	[DC-ether] [2tBBNTs]		4.88
25m	[DC-ether] [2N(tBB) <sub>2</sub> ]		0.954
25n	[DC-ether] [2TFMBNTs]		9.71
25o	[DC-ether] [2N(TFMB) <sub>2</sub> ]		1.11
26b	[DC-ether] [2tBBNB]		80.7

<b>26c</b>	[Bnchol] [tBBNB]		26.9
<b>26d</b>	[DC-ether] [2TFMBNB]		48.3

To evaluate the impact of the cation on water solubility, [DC-ether][2Cl] (**4j**) and a series of monocholinium cations were paired with [Na][NBNTs] (**21a<sub>ii</sub>**), which itself is relatively hydrophobic, with a water solubility of 18.4 mM. Overall, the resulting ILs are more hydrophobic than [Na][NBNTs] (**21a<sub>ii</sub>**), with [DC-ether][2NBNTs] (**25b**; 11.2 mM) and [Cychol][NBNTs] (**25e**; 12.0 mM) being the most water soluble out of the group, while [NBnchol][NBNTs] (**25d**; 2.46 mM) was the least water soluble. For [NBnchol][NBNTs] (**25d**), the presence of the 4-nitrobenzene ring can delocalize electron density, allowing for a more hydrophobic IL. The high hydrophilicity of [DC-ether] has been previously discussed, and here, the cation consistently forms ILs with higher water solubilities than with ILs containing other cations. Intriguingly, when pairing different cations with [Na][CBNTs] (**21d<sub>ii</sub>**; 45.2 mM), [Cychol][CBNTs] (**25j**; 24.1 mM) has a water solubility closer to [N<sub>1,1,6,20H</sub>][CBNTs] (**25h**; 21.1 mM) than [DC-ether][2CBNTs] (**25i**; 35.7 mM). These results underscore the notion that the hydrophobicity of a specific IL may not correlate with the hydrophobicities of the individual ions.

Among ILs containing different anions and the same cation, certain trends emerged. The second-generation anion salts containing electron-withdrawing groups revealed some hydrophobicity, except for [Na][TFMBNTs] (**21g<sub>ii</sub>**), which is water soluble. The methyl on the tosyl group is electron-donating and thus hinders the delocalization of the negative charge. This likely explains why the asymmetric anion salt was hydrophilic, while the corresponding symmetric anion salt, [Na][N(TFMB)<sub>2</sub>] (**21h<sub>ii</sub>**; 4.03 mM), was very hydrophobic. Although the toluene group resulted in lower hydrophobicity, the 4-(tertbutyl)benzene group significantly increased hydrophobicity, as in the case of [Na][N(tBB)<sub>2</sub>] (**21f<sub>ii</sub>**; 8.46 mM). Resembling [Na][TFMBNTs] (**21g<sub>ii</sub>**), [Na][tBBNTs] (**21e<sub>ii</sub>**) was water soluble. The symmetric salts led to ILs with low

water solubilities, including [DC-ether][2N(tBB)<sub>2</sub>] (**25m**; 0.954 mM) and [DC-ether][2N(TFMB)<sub>2</sub>] (**25o**; 1.11 mM).

The third-generation anion salts were all water soluble because the butyl chain does not delocalize electron density as greatly as aryl moieties. When paired with the hydrophilic cation [DC-ether][2Cl] (**4j**), the compounds, [DC-ether][2tBBNB] (**26b**; 80.7 mM) and [DC-ether][2TFMBNB] (**26d**; 48.3 mM), were among the ILs with the highest water solubilities. Although, when paired with a more hydrophobic cation, such as in the case of [Bnchol][tBBNB] (**26c**; 26.9 mM), the water solubility was greatly reduced. This latter result, as previously described, reveals that the water solubility of an IL can be decreased by increasing the hydrophobicity of only one of the ions.

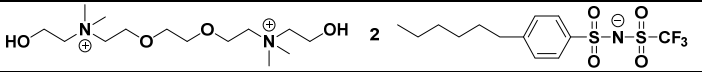
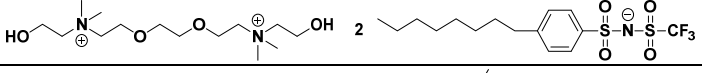
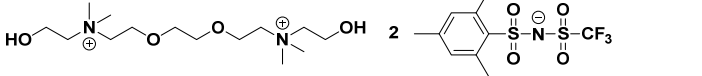
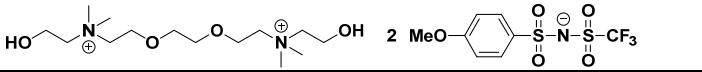
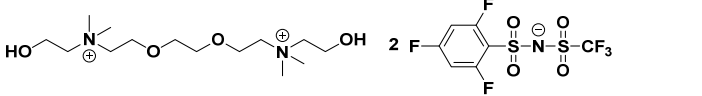
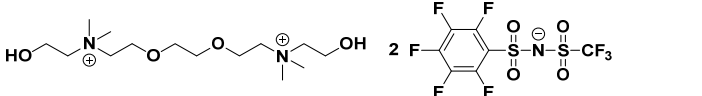
### 3.2.4 Hygroscopicity

While the water solubility determines the amount of IL that is dissolved in water, it is important to consider the amount of water that can absorb into the IL. When water is introduced into an IL, properties such as viscosity and melting temperature are altered.<sup>38</sup> The presence of water can be detrimental depending on the intended application of the IL. For example, when ILs are used as solvents or catalysts for chemical synthesis, water impurities can lead to unwanted side reactions.

The concentration of water in the monocholinium and dicholinium ILs containing [NTf<sub>2</sub>] anions and 1<sup>st</sup> generation bis(sulfonyl)azanide anions was evaluated in two different scenarios, each measured by coulometric Karl Fisher titration (**Table 3.7**). In the first study, the ILs were saturated by mixing with excess water. In the second study, the ILs were placed in a vacuum oven set to 80 °C for 16 h. For the first study, the percent mass fraction of water (W<sub>H<sub>2</sub>O</sub>,%) in the ILs ranged from 2.5 to 17%. Apart from [DC-ether][2TFBSNTf] (**18k**) and [DC-ether][2PFBSNTf] (**18l**), the ILs with asymmetric anions absorbed more water than the ILs containing the [NTf<sub>2</sub>] anion. Previous research has shown that ILs with the [NTf<sub>2</sub>] anion absorb less water than ILs containing other hydrophobic anions, such as [BF<sub>4</sub>] and [PF<sub>6</sub>].<sup>40</sup> [DC-ether][2HSNTf] (**18b**; 17.0%) and [DC-ether][2OSNTf] (**18c**; 17.1%) have the largest mass fraction of water, indicating that the presence of an aromatic group actually decreases water absorption, but not as

significantly as a trifluoromethane group. Intriguingly, there is no direct relationship between hydrophobicity and hygroscopicity for these ILs, indicating that each parameter is a result of distinct intermolecular interactions between the ILs and water. Still, there is a general trend that the hygroscopicity is larger than the water solubility, meaning when the IL is mixed with excess water, the concentration of water in the IL layer is larger than the concentration of IL in the water layer. This feature has been observed with other HILs.<sup>41</sup>

#	Ionic Liquid	Structure	Hygroscopicity (W <sub>H2O</sub> ,%), sat.
13a	[chol][NTf <sub>2</sub> ]		7.95 ± 0.35
13b	[N <sub>1,1,4,2OH</sub> ][NTf <sub>2</sub> ]		3.51 ± 0.14
13c	[N <sub>1,1,6,2OH</sub> ][NTf <sub>2</sub> ]		2.92 ± 0.13
13d	[N <sub>1,1,8,2OH</sub> ][NTf <sub>2</sub> ]		2.52 ± 0.19
13i	[DC-4][2NTf <sub>2</sub> ]		5.63 ± 0.12
13k	[DC-6][2NTf <sub>2</sub> ]		7.69 ± 0.35
13m	[DC-8][2NTf <sub>2</sub> ]		3.88 ± 0.20
13p	[DC-ether][2NTf <sub>2</sub> ]		5.83 ± 0.88
18a	[DC-ether][2BSNTf]		water soluble
18b	[DC-ether][2HSNTf]		17.0 ± 0.8
18c	[DC-ether][2OSNTf]		17.1 ± 0.7
18d	[DC-ether][2PhSNTf]		10.6 ± 0.3
18e	[DC-ether][2TsNTf]		12.2 ± 0.2
18f	[DC-ether][2pBBSNTf]		10.9 ± 0.8

<b>18g</b>	[DC-ether] [2pHBSNTf]		10.1 ± 0.2
<b>18h</b>	[DC-ether] [2pOBSNTf]		12.5 ± 1.2
<b>18i</b>	[DC-ether] [2MesSNTf]		10.7 ± 0.6
<b>18j</b>	[DC-ether] [2pMBSNTf]		13.5 ± 0.4
<b>18k</b>	[DC-ether] [2TFBSNTf]		7.69 ± 0.26
<b>18l</b>	[DC-ether] [2PFBSNTf]		5.15 ± 0.55

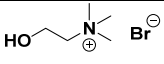
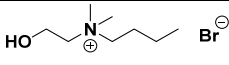
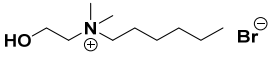
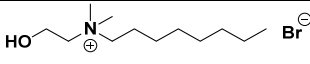
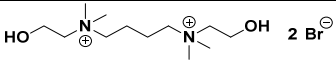
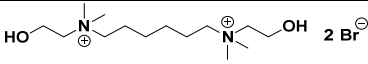
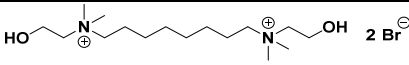
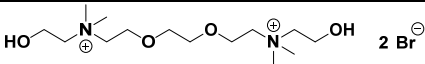
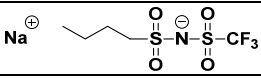
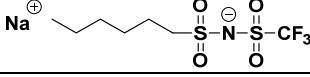
In the second study, the percent mass fraction of water for all twenty ILs in the study was below 0.1%, with many being below the limit of detection for the instrument (**Table A.2**). These results indicate that most of the water can be easily removed from these HILs, although completely removing all traces of water may require special procedures.

### 3.2.5 *In vitro* toxicity

The tunability of ILs allows for the facile synthesis of diverse libraries of compounds; however, ILs are not typically evaluated for toxicity. Assessing and understanding the harmfulness of ILs is an essential part of translating these substances into usable technologies. When conducting *in vivo* and *in vitro* toxicity experiments for HILs, the individual cations and anions should be evaluated as IL toxicity is often based on the most toxic ion, which cannot be known when testing only the IL. The HIL itself needs to be assessed too, as the toxicity values are often different from the salt precursors. While many experiments use saturated aquatic organism media or cell media solutions of the HIL, this strategy is not recommended unless the solubility of the HIL is known for the specific media being used. The water solubility of HILs can greatly increase or decrease in aquatic organism media or cell media compared to pure water, so great care must be taken to ensure accuracy. An alternative strategy is to weigh a known quantity of the HIL, dissolve it in a specified volume of media, and then calculate the concentration. This latter method was

used for the following *in vitro* and zebrafish toxicity experiments, and a detailed description can be found in sections 3.4.6 and 3.4.7.

Since the toxicity of ILs is often due to their ability to disrupt lipid bilayers, *in vitro* cellular assays are an ideal starting place to analyze IL cytotoxicity. First, alkyl cholinium, dicholinium, and first-generation bis(sulfonyl)azanide anion salt precursors and corresponding ILs were examined in 4T1-Luc mouse breast cancer cells (**Table 3.8**). Each compound was incubated in 4T1-Luc cells for 24 h at varying concentrations, and the cytotoxicity was evaluated using a CellTiter-Blue assay. A time of 24 h was chosen to minimize the replication of 4T1-Luc cells, as ILs can affect cell viability and cell proliferation in different manners.<sup>42</sup>

<b>Table 3.8</b> LC50 values for alkyl cholinium, dicholinium, and first-generation bis(sulfonyl)azanide salt precursors and corresponding ILs in 4T1-Luc mouse breast cancer cells. The substances were incubated in cells for 24 h. The values in the parentheses represent 95% confidence intervals. <sup>a</sup> These salts precipitated at higher concentrations, and thus LC50 values could not be calculated.			
#	Salts and Ionic Liquids	Structure	4T1-Luc LC50 (mM)
1	[chol][Br]		74.7 (70.4–79.4)
2a	[N <sub>1,1,4,2OH</sub> ][Br]		28.6 (25.5–32.0)
2c	[N <sub>1,1,6,2OH</sub> ][Br]		10.7 (9.14–12.7)
2d	[N <sub>1,1,8,2OH</sub> ][Br]		1.12 (0.971–1.31)
4c	[DC-4][2Br]		98.4 (91.7–105)
4e	[DC-6][2Br]		40.8 (36.9–44.9)
4g	[DC-8][2Br]		59.2 (53.5–65.5)
4j	[DC-ether][2Cl]		89.8 (78.3–102)
17d	[Na][BSNTf]		13.4 (11.5–15.6)
17e	[Na][HSNTf]		1.32 (1.11–1.57)

17f	[Na][OSNTf]		0.104 (0.0993–0.109)
17g	[Na][PhSNTf]		4.53 (4.01–5.11)
17h	[Na][TsSNTf]		2.84 (2.37–3.45)
17j	[Na][pBBSNTf]		0.442 (0.416–0.468)
17k	[Na][pHBSNTf]		>0.200 <sup>a</sup>
17lii	[Na][pOBSNTf]		>0.100 <sup>a</sup>
17m	[Na][MesSNTf]		0.792 (0.710–0.888)
17n	[Na][pMBSNTf]		3.87 (3.04–4.92)
17o	[Na][TFBSNTf]		4.14 (3.55–4.85)
17p	[Na][PFBSNTf]		0.379 (0.332–0.432)
	[Li][NTf <sub>2</sub> ]		2.16 (1.90–2.48)
13a	[chol][NTf <sub>2</sub> ]		3.42 (2.89–4.01)
13b	[N <sub>1,1,4,2OH</sub> ][NTf <sub>2</sub> ]		1.99 (1.72–2.37)
13c	[N <sub>1,1,6,2OH</sub> ][NTf <sub>2</sub> ]		3.28 (2.43–4.96)
13d	[N <sub>1,1,8,2OH</sub> ][NTf <sub>2</sub> ]		4.80 (3.75–6.52)
13i	[DC-4][2NTf <sub>2</sub> ]		1.95 (1.64–2.42)
13k	[DC-6][2NTf <sub>2</sub> ]		1.97 (1.32–3.91)
13m	[DC-8][2NTf <sub>2</sub> ]		1.79 (1.24–3.21)
13p	[DC-ether][2NTf <sub>2</sub> ]		1.45 (1.19–1.86)
18a	[DC-ether][2BSNTf]		11.7 (10.2–13.9)
18b	[DC-ether][2HSNTf]		6.10 (5.23–7.38)

<b>18c</b>	[DC-ether] [2OSNTf]		2	0.199 (0.184–0.215)
<b>18d</b>	[DC-ether] [2PhSNTf]		2	3.22 (2.87–3.62)
<b>18e</b>	[DC-ether] [2TsNTf]		2	1.37 (1.08–2.27)
<b>18f</b>	[DC-ether] [2pBBSNTf]		2	0.115 (0.110–0.121)
<b>18g</b>	[DC-ether] [2pHBSNTf]		2	0.126 (0.117–0.136)
<b>18h</b>	[DC-ether] [2pOBSNTf]		2	0.0337 (0.0320–0.0354)
<b>18i</b>	[DC-ether] [2MesSNTf]		2	0.458 (0.391–0.545)
<b>18j</b>	[DC-ether] [2pMBSNTf]		2	2.21 (1.92–2.63)
<b>18k</b>	[DC-ether] [2TFBSNTf]		2	1.33 (1.24–1.44)
<b>18l</b>	[DC-ether] [2PFBSNTf]		2	0.236 (0.197–0.293)
	[N <sub>1,8,8,8</sub> ] [NTf <sub>2</sub> ]			0.00650 (0.00561–0.00744)

The individual cations largely showed low toxicity, with LC<sub>50</sub> values above 10 mM. This supports the notion that choline-derived cations are less toxic than tetraalkylammonium and heterocyclic cations. The one exception was [N<sub>1,1,8,2OH</sub>][Br] (**2d**), which due to the long alkyl chain, has an LC<sub>50</sub> of 1.12 mM. Gratifyingly, the [DC-8][2Br] (**4g**) cation has a significantly higher LC<sub>50</sub> value of 59.2 mM, highlighting that long alkyl chains that are capped at both ends with charged groups appear to have reduced toxicity. This effect is most likely due to the difficulty of the dication to insert efficiently into a cell membrane. While the other cations and anions exhibited higher toxicity with increasing alkyl chain length, the dicholinium cations did not. The [Na][pOBSNTf] (**17l**) and [Na][pHBSNTf] (**17k**) salts precipitated over the course of 24 h at concentrations higher than 0.1 and 0.2 mM, respectively. For these two salts, the same phenomenon was observed in different cell media. It is likely that the cells consume certain salts and

proteins that are essential for solubilizing these hydrophobic anions, resulting in their precipitation over time. As a result, their LC50 values could not be calculated.

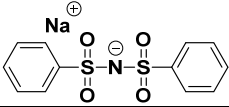
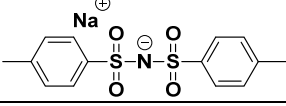
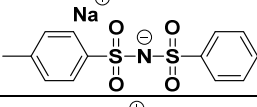
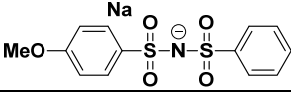
The other anions exhibited a range of toxicities that are both above and below the LC50 value of the control salt, [Li][NTf<sub>2</sub>] (2.16 mM). Among the anions containing aryl moieties, [Na][PFBSNTf] (**17p**; 0.379 mM) is the most toxic, likely due to the reactivity of the pentafluorophenyl group. Only [Na][BSNTf] (**17d**; 13.4 mM) has an LC50 value that was significantly higher than [Li][NTf<sub>2</sub>], indicating that for cellular studies, only modest decreases in toxicity can be obtained when replacing a trifluoromethane group with another hydrophobic moiety.

The aryl anions [Na][PhSNTf] (**17g**; 4.53 mM), [Na][TsNTf] (**17h**; 2.84 mM), [Na][pMBSNTf] (**17n**; 3.87 mM), and [Na][TFBSNTf] (**17o**; 4.14 mM) have LC50 values slightly higher than [Li][NTf<sub>2</sub>]. Although aromaticity increases toxicity for cations<sup>43</sup>, incorporating an aromatic group does not seem to affect the toxicity of the anions, rather it is the substituents on the benzene ring that can increase toxicity. It should be noted that most HILs are composed of aromatic cations that use a nitrogen-containing ring, whereas these anions do not. It is possible that the presence of the nitrogen can contribute to the toxicity, although further studies are needed to validate this idea.

For the ILs, the LC50 values were slightly lower but closely resembled the LC50 values of the corresponding anion salts, apart from [DC-ether][2pOBSNTf] (**18h**; 0.0337 mM), which has an LC50 value much lower than [Na][pOBSNTf] (**17li**). The [DC-ether] ILs have Gemini cations, meaning they have two anions, which could explain the slight increase in toxicity compared to the corresponding salt precursors. The commercially available [N<sub>1,8,8,8</sub>][NTf<sub>2</sub>] was used as a negative control for the toxicity studies. Due to the presence of the three octyl chains, the toxicity of [N<sub>1,8,8,8</sub>][NTf<sub>2</sub>] (0.00650 mM) is extremely high, being 1,000-fold more toxic than [N<sub>1,1,8,2OH</sub>][NTf<sub>2</sub>] (**13d**; 4.80 mM), which has only one octyl chain. Conversely, the least toxic IL is the hydrophilic [DC-ether][2BSNTf] (**18a**; 11.7 mM), underscoring that hydrophobicity correlates to cytotoxicity. Previous toxicology research on different cell lines using HILs containing the [NTf<sub>2</sub>] anion supports these studies, where if the anion is more toxic than the cation, then the LC50 ranges

from 1–5 mM.<sup>29,44</sup> However, HILs containing cations with long alkyl chains are more toxic than the [NTF<sub>2</sub>] anion and have LC50 values in the sub-millimolar range.

The next set of compounds studied were second- and third-generation bis(sulfonyl)azanide anions and ILs as well as the cyclic monocholinium cations and ILs (**Table 3.9**). Similar to the first study, the toxicity of the anions depended on the substituents on the aryl ring. The least toxic compounds contained the 4-methoxyphenyl moiety, which was less toxic than the phenyl version – [Na][N(MB)<sub>2</sub>] (**20f<sub>ii</sub>**; 38.2 mM) compared to [Na][NPh<sub>2</sub>] (**20a<sub>ii</sub>**; 24.5 mM). Akin to the first generation bis(sulfonyl)azanide anions, adding a methyl to the benzene ring increased toxicity. The different electron-withdrawing groups revealed strikingly different LC50 values. For example, [Na][CBNTs] (**21c<sub>ii</sub>**; 22.9 mM) and [Na][NBNTs] (**21a<sub>ii</sub>**; 67% viability at saturation) were much less toxic than [Na][TFMBNTs] (**21g<sub>ii</sub>**; 2.80 mM) as well as the anions with 4-(tertbutyl)benzene groups, such as [Na][tBBNTs] (**21e<sub>ii</sub>**; 0.668 mM). Intriguingly, [Na][N(NB)<sub>2</sub>] (**21b<sub>ii</sub>**), which has a water solubility of 74.5 mM, is much less soluble in cell media. As a result, the exact LC50 value could not be calculated for the anion salt and corresponding IL. This was also the case for compounds with the [NBNTs] ion.

<b>Table 3.9</b> LC50 values for second- and third-generation IL salt precursors and ILs in 4T1-Luc mouse breast cancer cells. The substances were incubated in 4T1 cells for 24 h. The values in the parentheses represent 95% confidence intervals. <sup>a</sup> The hydrophobicity of these compounds prevented exact LC50 values from being calculated.			
#	Salts and Ionic Liquids	Structure	4T1-Luc LC50 (mM)
<b>20a<sub>ii</sub></b>	[Na][NPh <sub>2</sub> ]		24.5 (19.8–31.2)
<b>20b<sub>ii</sub></b>	[Na][NTs <sub>2</sub> ]		4.04 (3.17–5.09)
<b>20c<sub>ii</sub></b>	[Na][PhNTs]		14.6 (10.9–19.3)
<b>20d<sub>ii</sub></b>	[Na][MBNPh]		28.1 (21.8–39.8)

20eii	[Na][MBNTs]		19.6 (18.0–21.2)
20fii	[Na][N(MB) <sub>2</sub> ]		38.2 (35.7–41.2)
21a <sub>ii</sub>	[Na][NBNTs]		67% viability <sup>a</sup>
21b <sub>ii</sub>	[Na][N(NB) <sub>2</sub> ]		>4.89 mM <sup>a</sup>
21c <sub>ii</sub>	[Na][NBNTFMB]		2.58 (2.05–3.62)
21d <sub>ii</sub>	[Na][CBNTs]		22.9 (20.1–27.9)
21e <sub>ii</sub>	[Na][tBBNTs]		0.668 (0.621–0.717)
21f <sub>ii</sub>	[Na][N(tBB) <sub>2</sub> ]		0.233 (0.190–0.280)
21g <sub>ii</sub>	[Na][TFMBNTs]		2.80 (2.28–3.83)
21h <sub>ii</sub>	[Na][N(TFMB) <sub>2</sub> ]		1.19 (1.14–1.25)
22a <sub>ii</sub>	[Na][tBBNB]		3.28 (3.17–3.40)
22b <sub>ii</sub>	[Na][TFMBNB]		24.5 (16.8–43.7)
22c <sub>ii</sub>	[Na][TFPNTs]		23.5 (21.7–25.6)
23a	[Bnchol][Br]		22.3 (20.7–24.0)
23b	[NBnchol][Br]		2.52 (2.41–2.63)
23c	[Cychol][Br]		7.83 (6.56–9.23)

25a	[N <sub>1,1,6,2OH</sub> ] [NBNTs]		1.86 (1.61–2.18)
25b	[DC-ether] [2NBNTs]		82% viability <sup>a</sup>
25c	[Bnchol] [NBNTs]		6.18 (3.32–17.1)
25d	[NBnchol] [NBNTs]		1.72 (1.53–2.00)
25e	[Cychol] [NBNTs]		4.78 (3.80–5.91)
25f	[Bnchol] [NBNTFMB]		1.02 (0.932–1.13)
25g	[DC-ether] [2N(NB) <sub>2</sub> ]		66% viability <sup>a</sup>
25i	[DC-ether] [2CBNTs]		13.4 (9.69–30.0)
25j	[Cychol] [CBNTs]		6.17 (4.99–8.27)
25l	[DC-ether] [2tBBNTs]		0.401 (0.372–0.433)
25m	[DC-ether] [2N(tBB) <sub>2</sub> ]		0.119 (0.115–0.124)
25n	[DC-ether] [2TFMBNTs]		0.891 (0.847–0.934)
25o	[DC-ether] [2N(TFMB) <sub>2</sub> ]		0.354 (0.333–0.377)
26a	[N <sub>1,1,6,2OH</sub> ] [tBBNB]		1.93 (1.83–2.03)
26b	[DC-ether] [2tBBNB]		1.24 (1.15–1.33)
26c	[Bnchol] [tBBNB]		2.24 (1.93–2.57)
26d	[DC-ether] [2TFMBNB]		1.93 (1.73–2.13)

The third-generation bis(sulfonyl)azanide anions have improved LC<sub>50</sub> values as one of the aryl groups was replaced with a less toxic butyl chain. While the first-generation anion [Na][TsNTf] (**17h**) has an LC<sub>50</sub> value of 2.84 mM, the anion [Na][TFPNTs] (**22c<sub>ii</sub>**) has an LC<sub>50</sub> value of 23.5 mM. This highlights a curious result, in that trifluoromethane groups that are extended by an alkyl chain are less toxic; however,

trifluoromethane groups on aryl rings do not result in a decrease in toxicity. More studies are needed to probe this phenomenon.

For the new cyclic cations (**23a–23c**), there were surprising toxicity results. [Bnchol][Br] (**23a**; 22.3 mM) is less toxic than [Cychol][Br] (**23c**; 7.83 mM), despite the former has a benzene ring while the latter incorporates a cyclohexane ring. Additionally, [N<sub>1,1,6,2OH</sub>][Br] (**2c**; 10.7 mmol), which possesses a linear hexyl chain, is also less toxic than [Cychol][Br] (**23c**). [NBnchol][Br] (**23b**) has the highest toxicity of the cations with an LC<sub>50</sub> value of 2.52 mM, likely due to the nitro group; however, the presence of a nitro group on the anions did not significantly increase toxicity. Still, these cations are significantly more toxic than the [DC-ether][2Cl] (**4j**; 89.8 mM), indicating that the dicholinium architecture is more biocompatible than the substituted monocholinium cations.

### 3.2.6 Zebrafish developmental toxicity

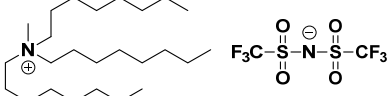
To ascertain the full profile of IL toxicity, different biological models need to be utilized. One of the most well-studied models are zebrafish (*Danio rerio*). While being excellent markers for aquatic toxicity, zebrafish are easy to handle, have a fast spawn rate, and have translucent eggs. The latter point is important for analyzing developmental toxicity. Zebrafish offer a more realistic model over cell monolayers as the former have functioning organs and physiological systems. Additionally, zebrafish and humans have related genomes with many orthologous genes.<sup>45</sup>

The LC<sub>50</sub> values for the alkyl cholinium, dicholinium, and first-generation bis(sulfonyl)azanide anion salt precursors and corresponding ILs were calculated using a zebrafish development study, in a similar fashion to the cellular studies (**Table 3.10**). Here, fertilized embryos were incubated in Instant Ocean egg water that contained various concentrations of the compounds. Developmental malformations were observed over a 72 h period. Longer incubation periods were not chosen as zebrafish begin to swallow after 72 h. By restricting swallowing, the developmental malformations and mortality become solely due to the compounds absorbing through the skin and gills, allowing for easier analysis. The LC<sub>50</sub> for each compound was calculated at the end of the 72 h period.

**Table 3.10** LC50 values for alkyl cholinium, dicholinium, and first-generation bis(sulfonyl)azanide salt precursors and corresponding ILs in zebrafish. The substances were incubated with zebrafish embryos for 72 h. The values in the parentheses represent 95% confidence intervals.

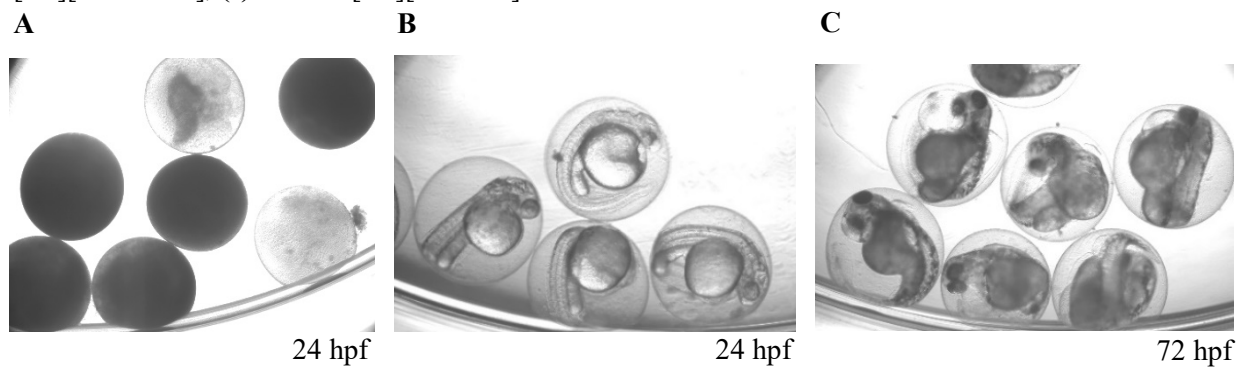
#	Salts and Ionic Liquids	Structure	4T1-Luc LC50 (mM)
1	[chol][Br]		124 (123–126)
2a	[N <sub>1,1,4,2OH</sub> ][Br]		95.2 (88.9–102)
2c	[N <sub>1,1,6,2OH</sub> ][Br]		32.0 (27.6–38.1)
2d	[N <sub>1,1,8,2OH</sub> ][Br]		11.3 (10.3–13.1)
4c	[DC-4][2Br]		60.9 (54.6–66.6)
4e	[DC-6][2Br]		45.4 (44.1–46.4)
4g	[DC-8][2Br]		39.2 (29.8–48.6)
4j	[DC-ether][2Cl]		76.2 (69.0–82.8)
17d	[Na][BSNTf]		5.18 (2.98–5.76)
17e	[Na][HSNTf]		0.596 (0.428–0.821)
17f	[Na][OSNTf]		0.300 (0.261–0.337)
17g	[Na][PhSNTf]		18.3 (17.5–19.1)
17h	[Na][TsNTf]		6.84 (4.67–9.71)
17j	[Na][pBBSNTf]		1.19 (0.808–1.82)
17k	[Na][pHBSNTf]		0.210 (0.206–0.216)
17lii	[Na][pOBSNTf]		0.0159 (0.00997–0.0241)
17m	[Na][MesSNTf]		3.10 (2.26–4.71)
17n	[Na][pMBSNTf]		8.98 (7.99–10.1)
17o	[Na][TFBSNTf]		7.40 (6.39–8.22)

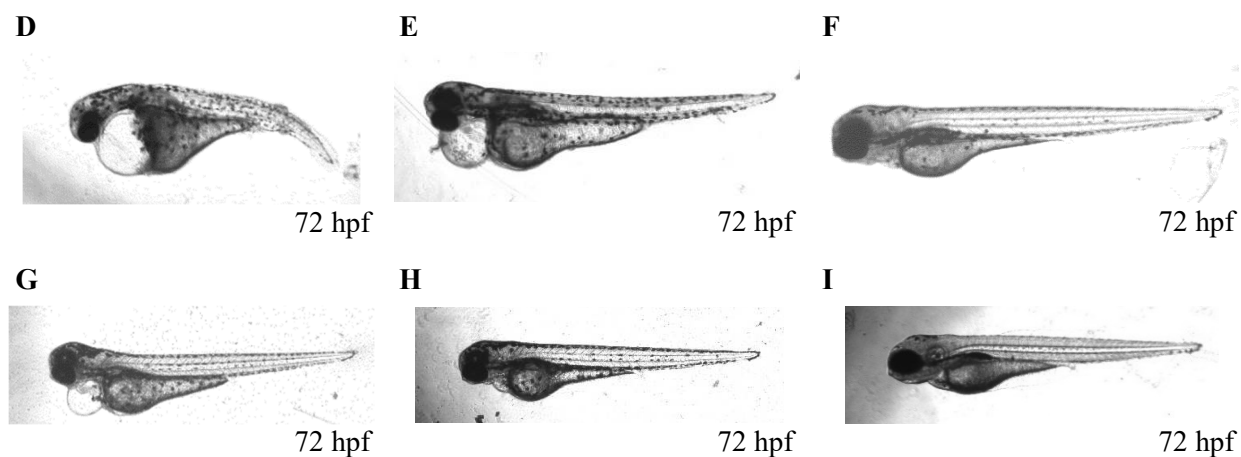
17p	[Na] [PFBSNTf]		0.237 (0.225–0.246)
	[Li][NTf <sub>2</sub> ]		0.745 (0.576–0.919)
13a	[chol][NTf <sub>2</sub> ]		0.483 (0.439–0.531)
13b	[N <sub>1,1,4,2OH</sub> ][NTf <sub>2</sub> ]		0.463 (0.339–0.568)
13c	[N <sub>1,1,6,2OH</sub> ][NTf <sub>2</sub> ]		0.831 (0.736–0.935)
13d	[N <sub>1,1,8,2OH</sub> ][NTf <sub>2</sub> ]		0.558 (0.554–0.563)
13i	[DC-4] [2NTf <sub>2</sub> ]		0.458 (0.378–0.560)
13k	[DC-6] [2NTf <sub>2</sub> ]		0.429 (0.423–0.436)
13m	[DC-8] [2NTf <sub>2</sub> ]		0.329 (0.319–0.339)
13p	[DC-ether] [2NTf <sub>2</sub> ]		0.344 (0.235–0.455)
18a	[DC-ether] [2BSNTf]		1.29 (0.835–1.91)
18b	[DC-ether] [2HSNTf]		0.828 (0.433–1.44)
18c	[DC-ether] [2OSNTf]		0.268 (0.222–0.334)
18d	[DC-ether] [2PhSNTf]		16.8 (15.9–17.7)
18e	[DC-ether] [2TsNTf]		9.94 (9.25–10.6)
18f	[DC-ether] [2pBBSNTf]		0.822 (0.684–0.962)
18g	[DC-ether] [2pHBSNTf]		0.111 (0.0316–0.201)
18h	[DC-ether] [2pOBSNTf]		0.00959 (0.00847–0.0109)
18i	[DC-ether] [2MesSNTf]		3.16 (3.04–3.29)
18j	[DC-ether] [2pMBSNTf]		5.65 (5.41–5.92)
18k	[DC-ether] [2TFBSNTf]		2.94 (2.91–2.98)
18l	[DC-ether] [2PFBSNTf]		0.0737 (0.0409–0.143)

	$[N_{1,8,8,8}]$ $[NTf_2]$		0.00234 (0.00230– 0.00239)
--	------------------------------	---	----------------------------------

The zebrafish LC50 values for the ILs and IL salt precursors are akin to those of the 4T1-Luc cells, being within a 10-fold difference; however, the ILs have a larger discrepancy than the precursor salts. Increases in alkyl chain length for both the cations and anions resulted in higher toxicity, which is consistent with the 4T1-Luc studies reported in section 2.2.5 and zebrafish studies for other ILs.<sup>46</sup> In examining the IL precursor salts, the alkyl cholinium cations have significantly lower toxicity than either the alkyl anions or aryl-alkyl anions. These anions, especially the ones with octyl chains, were able to penetrate the chorion and induce death within 24 h, as indicated by the rapid fungal growth in most of the eggs (**Figure 3.5A,B**). Conversely,  $[N_{1,1,8,20H}][Br]$  (**2d**; 11.3 mM) has low toxicity, despite containing an octyl chain.  $[N_{1,8,8,8}][NTf_2]$  (0.00234 mM) was used as a negative control and was the most toxic IL evaluated in this study, supporting the idea that a greater number of long chains correlates with higher toxicity. The dicholinium salts revealed tremendous biocompatibility regardless of alkyl chain length. Although comparisons to other dications would be useful, to our knowledge, there are no other examples of zebrafish toxicity experiments with dicationic species.

**Figure 3.5** Representative images of zebrafish exposed to (A) 0.083 mM  $[Na][pOBSNTf]$  (black color represents post-mortem fungal growth), (B) egg water, (C) 1.4 mM  $[Li][NTf_2]$ , (D) 0.96 mM  $[Li][NTf_2]$ , (E) 0.43 mM  $[Li][NTf_2]$ , (F) egg water, (G) 4.3 mM  $[Na][TsNTf]$ , (H) 6.7 mM  $[Na][TFBSNTf]$ , (I) 11 mM  $[Na][PhSNTf]$ .





The [Li][NTf<sub>2</sub>] (0.745 mM) salt has increased toxicity in zebrafish compared to the 4T1-Luc cells, which resulted in an increase in toxicity for all ILs that contain the [NTf<sub>2</sub>] anion. Each of these ILs have strikingly similar mortality profiles at high concentrations, where the zebrafish embryos developed relatively normally for 24–48 h but could not hatch, and thus died in their eggs (**Figure 3.5C**). At lower concentrations, the zebrafish had noticeable enlargements of the yolk sac as well as pericardial edema (**Figure 3.5D–F**). Previous studies using ILs with the [NTf<sub>2</sub>] anion have shown similar LC50 values of 200–500  $\mu$ M in zebrafish despite having different cations<sup>29,46</sup> and have indicated that the anion causes abnormal heart rates and liver damage in zebrafish<sup>47</sup>. Interestingly, the aryl ILs, apart from [DC-ether][2PFBSNTf] (**18I**; 0.0737 mM) and the aryl-alkyl ILs, have higher LC50 values and less severe developmental malformations at elevated compound concentrations, with the most common malformations being pericardial edema and curved spines (**Figure 3.5G–I**).

### 3.3 Conclusion

In this chapter, a diverse array of novel HILs were analyzed for their physiochemical properties and toxicities. Physical transformation temperatures, viscosity, water solubility, and hygroscopicity were evaluated as they are important characteristics of HILs. Often, ILs need to possess specific features depending on the application. This could include HILs with low viscosities, low hygroscopicity values, or

low water solubility values. Still, many reported ILs, especially HILs, are not properly characterized, and thus they may not be used for different purposes, as their properties are unknown. By performing and reporting the properties of ILs, others can utilize these ILs rather than undergoing the arduous task of designing and synthesizing the exact IL needed for their applications.

In comparing ILs with  $[\text{NTf}_2]$  and other bis(sulfonyl)azanide anions, several interesting results were revealed. Symmetry and the presence of aromatic moieties on the anions greatly increases the melting temperature of the corresponding ILs. While the ILs with  $[\text{NTf}_2]$  anions were liquid at room temperature, the ILs with first-generation bis(sulfonyl)azanide anions, which are all asymmetric, exhibit lower temperature physical transformations. Conversely, ILs with symmetric second-generation bis(sulfonyl)azanides are all solid at room temperature. Aromaticity also greatly increased viscosity, as demonstrated by ILs containing anions with two aromatic groups, whose viscosities were so large that they could not be measured. The influence of the aryl group on water solubility was dependent on the functionalization of the benzene ring. Aryl groups containing electron-withdrawing groups and alkyl chains, including tertbutyl groups, significantly increased hydrophobicity compared to aryl groups with electron-donating moieties. It is likely that groups with delocalized negative charge and lipophilic features lower water solubility. However, it is unclear how electron-donating groups influence hydrophobicity compared to electron-withdrawing groups when applied to the cations with aromatic rings; although, this will be investigated in future experiments with new ILs.

Dicholinium-based ILs composed of  $[\text{NTf}_2]$  anions have higher viscosities than the monocholinium counterparts; however, when paired with the synthesized bis(sulfonyl)azanide anions, the monocholinium- and dicholinium-based ILs have similarly high viscosities. Interestingly, the dicholinium and monocholinium ILs with identical alkyl chain lengths have similar water solubility values when paired with the same anion. Meanwhile, due to the alkoxy linker,  $[\text{DC-ether}]$  ILs have high water solubility values than  $[\text{DC-8}]$  ILs. Curiously, water solubility did not correlate with hygroscopicity. Here, ILs with  $[\text{NTf}_2]$  anions are much less hygroscopic than most of the ILs with asymmetric anions, especially anions with only alkyl chains on one end.

The toxicity analyses of the ILs revealed both known trends and unreported trends. Increasing alkyl chain strongly correlated with higher mortality in both cells and zebrafish, which is a recognized phenomenon. Gratifyingly, the dicholinium cations, which have the alkyl groups tethered, demonstrated tremendous biocompatibility compared to their monocholinium counterparts. For the anions, the presence of an aromatic group had unexpected toxicity results. While compounds with [NTf<sub>2</sub>] anions facilitated severe morphological disfigurements and mortality in zebrafish, the first-generation bis(sulfonyl)azanide anions did not result in improper embryo development, and instead, the toxicity corresponded to the individual substituents. Functional groups on the aromatic ring such as cyano, nitro, and methoxy show good tolerability, whereas structures such as tertbutyl, trifluoromethane, and methyl demonstrate increased toxicity. More studies are needed to further understand the rationale behind the disparities in the toxicity of different aryl groups.

The physicochemical and toxicological studies underscore the complex relationship between structure and properties. A substantial number of ILs with diverse architectures need to be evaluated to establish these correlations. However, experimental studies themselves do not reveal the underlying mechanisms that govern the specific properties of ILs. Computational analyses are needed to probe how IL nanostructure affects IL characteristics. Still, the results from this chapter provide a stepping-stone for the rigorous analysis of IL properties and toxicities. Future studies will involve characterizing new ILs with closely related structures as well as performing additional experiments such as thermal gravimetric analysis, neutron scattering, and critical micelle concentration studies, as these studies could aid in the understanding of IL structure-property relationships.

## **3.4 Experimental**

### *3.4.1 Materials*

Fetal bovine serum and penicillin-streptomycin were purchased from Thermo Fisher Scientific (Waltham, MA). High Glucose Dulbecco's Modified Eagles Medium was purchased from Cytiva (Marlborough, MA). CellTiter-Blue reagent was purchased from Promega (Madison, WI). Hydranal –

Coulomat AG was purchased from Honeywell (Charlotte, NC). Solvents and all other reagents were purchased from Sigma-Aldrich (Milwaukee, WI).

#### 3.4.2 Differential scanning calorimetry

Thermograms were recorded using a DSC Q2000 differential scanning calorimeter (TA Instruments, New Castle, DE). The heating rate was 10 °C/min. The cooling rate and isothermal holds were optimized for each compound as described below. For all thermograms, exothermic peaks are up. The thermograms were analyzed using Universal Analysis Software (TA Instruments). Glass transition temperatures were selected at the midpoint of the curve. Prism 9.0.0 (GraphPad Software, La Jolla, CA) was used to redisplay the graphs.

#### 3.4.3 Viscosity

Viscosity was measured using a Brookfield DV1 Viscometer (Brookfield Engineering, Middleboro, MA) equipped with a CP-51 spindle and attached to a PolyScience Digital Temperature Controller (Niles, IL). The temperature was set to 25 °C for each IL. Prior to measuring, all ILs were placed in a vacuum oven set to 80 °C and were dried for at least 16 h. In each experiment, 0.5 mL of IL was added to the viscometer chamber where the ILs equilibrated for at least 3 min. The spindle speed was adjusted to the highest setting before reaching the upper limit of detection.

#### 3.4.4 Quantitative NMR spectroscopy

Prior to the quantitative study, the  $T_1$  values of each IL and sodium trifluoroacetate (NaTFA) were determined using a Varian UI 500 MHz spectrometer equipped with a Nalorac Quad Nucleus DD probe (qn6121, 5 mm). The  $T_1$  values were calculated to ensure that a proper recycle delay,  $D_1$ , value was chosen during the quantitative studies such that the signals fully relaxed between pulses. An inversion recovery experiment was acquired with 18 independent quadratically spaced variable ( $\tau$ ) values covering a range of five times the estimated  $T_1$  value. The following parameters were employed for the acquisition of the  $T_1$  spectra: 500 MHz; spectra width, 3 ppm; number of points, 100,000; number of transients, 16; relaxation

delay, 3–6 s. See **Table 3.4** for the specific relaxation delay parameters used for each  $T_1$  experiment. Prior to performing the inversion—recovery  $T_1$  measurements, the  $^{19}\text{F}$   $90^\circ$  pulse width was calibrated independently for each sample system. The processing included a line broadening of 1 Hz. Based on the calculated  $T_1$  values, a common  $D_1$  time of 30 s was deemed sufficient and was used for the quantitative studies.

Sample preparation for each IL was as follows: 0.25 mL of IL and 1.0 mL of deuterium oxide were pipetted into a 1.8 mL Eppendorf tube. The mixture rotated for 16 h. Afterwards, the sample was centrifuged at 13,300 rpm for 10 min to separate the water and IL layers. From the upper layer of the Eppendorf tube, 735  $\mu\text{L}$  of deuterium oxide was transferred via a pipette to an NMR tube. The NMR tube was then spiked with 15  $\mu\text{L}$  of a previously prepared sodium trifluoroacetate, sodium acetate, or 1,4-dioxane solution. Each of these compounds were used as standards and were prepared in deuterium oxide at various concentrations depending on the assumed water solubility of the IL.

The quantitative NMR experiments were performed using a Bruker Avance III HD 400 MHz NMR spectrometer. The following parameters were employed for the acquisition of the  $^{19}\text{F}$  NMR spectra: 400 MHz; spectral width, 15 ppm; O1P,  $-77.5$  ppm; relaxation delay, 30 s; number of transients, 64. The integration of the internal standard trifluoromethane peak was compared to the integration of the IL trifluoromethane peak. The following equation was used to determine the IL water solubility:

$$[\text{IL}] = [\text{NaTFA}] * \frac{\text{Integration of IL}}{\text{Integration of NaTFA}} * \frac{\text{\# of trifluoromethane fluorine atoms in IL}}{3}$$

For  $^1\text{H}$  NMR experiments, the following parameters were used: 400 MHz; spectral width, 10 ppm; O1P, 4.5 ppm; relaxation delay, 60 s; number of transients, 32. The integration of the internal standard sodium acetate or 1,4-dioxane peak was compared to the integration of an IL peak of similar peak height that did not overlap with neighboring peaks. The following equation was used to determine the IL water solubility when sodium acetate was used as the standard:

$$[\text{IL}] = [\text{NaOAc}] * \frac{\text{Integration of IL}}{\text{Integration of NaOAc}} * \frac{\text{\# of hydrogen atoms of the integrated peak of the IL}}{3}$$

The following equation was used to determine the IL water solubility when 1,4-dioxanes was used as the standard:

$$[\text{IL}] = [\text{Dioxanes}] * \frac{\text{Integration of IL}}{\text{Integration of dioxanes}} * \frac{\text{\# of hydrogen atoms of the integrated peak of the IL}}{8}$$

#### 3.4.5 Hygroscopicity

Two separate sets of experiments were performed to analyze the hygroscopicity of the ILs. In the first set of experiments, 200 mg of the ILs and 1 mL of Millipore Milli-Q water was added to 1.8 mL Eppendorf tubes. The samples rotated for 16 h to ensure complete saturation. Afterwards, the Eppendorf tubes were centrifuged at 13,300 rpm for 10 min to ensure the IL and water layers were completely separated. The top water layers were carefully removed, and approximately 10 mg of the ILs were weighed into 6 mL glass vials and crimped. Water content was analyzed using an 831 KF Coulometer attached to an 860 KF Thermoprep vacuum oven (Metrohm, Herisau, Switzerland). The oven was set to 130 °C, and water content was analyzed via coulometric Karl Fisher titration, using Hydranal – Coulomat AG as the analyte. All ILs were analyzed in triplicate. In the second set of experiments, the ILs were placed in an 80 °C vacuum oven for 16 h before water content was measured. The same procedure as described above was used to determine water content. The oven method was used as the ionic properties of the ILs prevented direct injection in the Karl Fisher chamber. There was no significant increase in water content when the Thermoprep vacuum oven was set above 130 °C, and instead, many of the ILs began to decompose.

#### 3.4.6 In Vitro Toxicity

Different concentrations of the IL salt precursors and ILs were prepared in High Glucose Dulbecco's Modified Eagle Media, containing 10% fetal bovine serum and 5% penicillin-streptomycin (DMEM+). Since the solubility of the ILs in DMEM+ was unknown, the solutions were prepared by first weighing 10 mg of IL into 15 mL conical tubes. As a starting point, 5 mL of DMEM+ was added to each tube. The ILs were dissolved using a bath sonicator set to 50 °C. The tubes were centrifuged at 4,000 rpm for 2 min to check if the ILs were completely dissolved. If there was residual IL, more DMEM+ was added to the conical tubes, and the ILs were dissolved as described above. This process continued until the ILs

were completely dissolved. Afterwards, the ILs were serially diluted in DMEM+ to obtain the desired set of concentrations. Separately, 4T1-Luc mouse breast cancer cells were plated onto 96-well plates at a concentration of 4,000 cells/well. The cells were incubated overnight in a 37 °C/5% CO<sub>2</sub> chamber. Afterwards, the cell media was replaced with the DMEM+ mixtures containing the IL salt precursors and the ILs. Six replicates were used for each concentration and at least four different concentrations were used for each compound. The cells were incubated for 24 h. Cell viability was analyzed using a CellTiter-Blue assay by following the manufacturer's instructions. LC50 values and 95% confidence intervals were calculated by non-linear least squares analyses using Prism 9.0.0 (GraphPad Software, La Jolla, CA).

### 3.4.7 Zebrafish developmental toxicity

An embryo–larval zebrafish (*Danio rerio*) model was used to evaluate the toxicity of the IL salt precursors and ILs. AB and TL zebrafish strains were obtained from Dr. Michael Taylor at the University of Wisconsin-Madison School of Pharmacy, where the fish were cultured until sexual maturation. Zebrafish were maintained in a light/dark cycle of 14:10 h at 28.5 °C in egg water (0.03% Instant Ocean, Blacksburg, VA). The adult fish were fed *Artemia nauplii* twice daily. Embryos were obtained from adult fish with a ratio of 1:2 for female to male. Breeding groups were placed in separate spawning aquariums, equipped with a mesh bottom to prevent the eggs from being cannibalized. Crossing was induced in the morning. After 1 h, eggs free of macroscopically discernible symptoms of infection and disease were collected, rinsed with egg water, and transferred into Petri dishes until chemical exposure. The embryo–larval toxicity assay was subsequently conducted. Zebrafish embryos were added to 24-well plates at 8 embryos/well. Each well was filled with 2 mL of egg water.

The IL salt precursors and the ILs were dissolved at various concentrations in egg water. Since the solubility of the ILs in egg water was unknown, the solutions were prepared by first weighing 10 mg of IL into 15 mL conical tubes. As a starting point, 5 mL of egg water was added to each tube. The ILs were dissolved via bath sonication at 50 °C. The tubes were centrifuged at 4,000 rpm for 2 min to check if the ILs were completely dissolved. If there was residual IL, more egg water was added to the conical tubes,

and the IL solubilization process was repeated as described above. This procedure continued until the ILs were completely dissolved. Afterwards, the ILs were serially diluted in egg water to obtain the desired set of concentrations. The embryos were treated with the compound solutions. Two replicates were used for each concentration and at least eight different concentrations were used for each compound. The plates were covered and incubated at 28.5 °C in a light/dark cycle of 14:10 throughout the 72 hpf exposure period. The observations of zebrafish development were made directly in the well using a StereoZoom 4 stereomicroscope (Diagnostic Instruments Inc., Sterling Heights, MI) every 24 h. Embryos and larvae were considered dead when no heartbeat was observed. The number of hatched embryos and a cumulative mortality tally were recorded every 24 h, until the final time of 72 h was reached. Images were obtained using a Nikon Eclipse TE300 inverted fluorescence phase contrast microscope (Melville, NY) using SPOT Software 4.7.0 (Diagnostic Instruments Inc., Sterling Heights, MI). LC50 values and 95% confidence intervals were calculated by non-linear least squares analyses using Prism 9.0.0 (GraphPad Software, La Jolla, CA). There was no difference in the toxicity results between the AB and TL zebrafish strains.

### 3.5 References

- (1) Appetecchi, G. B., Scaccia, S., Tizzani, C., Alessandrini, F. & Passerini, S. Synthesis of Hydrophobic Ionic Liquids for Electrochemical Applications. *J. Electrochem. Soc.* **153**, A1685 (2006).
- (2) Zakrewsky, M. & Mitragotri, S. Therapeutic RNAi robed with ionic liquid moieties as a simple, scalable prodrug platform for treating skin disease. *J. Control. Release* **242**, 80–88 (2016).
- (3) Fang, D., Yang, J. & Jiao, C. Dicationic ionic liquids as environmentally benign catalysts for biodiesel synthesis. *ACS Catal.* **1**, 42–47 (2011).
- (4) Tomé, L. I. N. *et al.* Tryptophan extraction using hydrophobic ionic liquids. *Sep. Purif. Technol.* **72**, 167–173 (2010).
- (5) Canongia Lopes, J. N. A. J. N. A. & Pádua, A. A. H. A. H. Nanostructural organization in ionic liquids. *J. Phys. Chem. B* **110**, 3330–3335 (2006).
- (6) Hayes, R., Warr, G. G. & Atkin, R. Structure and Nanostructure in Ionic Liquids. *Chem. Rev.* **115**, 6357–6426 (2015).
- (7) Jiang, W., Wang, Y. & Voth, G. A. Molecular dynamics simulation of nanostructural organization

- in ionic liquid/water mixtures. *J. Phys. Chem. B* **111**, 4812–4818 (2007).
- (8) Marekha, B. A., Kalugin, O. N. & Idrissi, A. Non-covalent interactions in ionic liquid ion pairs and ion pair dimers: a quantum chemical calculation analysis. *Phys. Chem. Chem. Phys.* **17**, 16846–16857 (2015).
  - (9) Kapoor, U. & Shah, J. K. Globular, Sponge-like to Layer-like Morphological Transition in 1-n-Alkyl-3-methylimidazolium Octylsulfate Ionic Liquid Homologous Series. *J. Phys. Chem. B* **122**, 213–228 (2018).
  - (10) Hayes, R., Imberti, S., Warr, G. G. & Atkin, R. Effect of Cation Alkyl Chain Length and Anion Type on Protic Ionic Liquid Nanostructure. *J. Phys. Chem. C* **118**, 13998–14008 (2014).
  - (11) Zhou, H. *et al.* Nanoscale perturbations of room temperature ionic liquid structure at charged and uncharged interfaces. *ACS Nano* **6**, 9818–9827 (2012).
  - (12) Ji, Y., Shi, R., Wang, Y. & Saielli, G. Effect of the chain length on the structure of ionic liquids: From spatial heterogeneity to ionic liquid crystals. *J. Phys. Chem. B* **117**, 1104–1109 (2013).
  - (13) Sha, M., Wu, G., Dou, Q., Tang, Z. & Fang, H. Double-layer formation of [Bmim][PF<sub>6</sub>] Ionic liquid triggered by surface negative charge. *Langmuir* **26**, 12667–12672 (2010).
  - (14) Sureshkumar, M. & Lee, C. K. Biocatalytic reactions in hydrophobic ionic liquids. *Journal of Molecular Catalysis B: Enzymatic* vol. 60 1–12 (2009).
  - (15) Rogers, R. D., Seddon, K. R. & Volkov, S. *Green Industrial Applications of Ionic Liquids. Green Industrial Applications of Ionic Liquids* (Kluwer Academic Publishers, 2002). doi:10.1007/978-94-010-0127-4\_25.
  - (16) Petkovic, M., Seddon, K. R., Rebelo, L. P. N. & Pereira, C. S. Ionic liquids: A pathway to environmental acceptability. *Chem. Soc. Rev.* **40**, 1383–1403 (2011).
  - (17) Zhao, D., Liao, Y. & Zhang, Z. D. Toxicity of ionic liquids. *Clean - Soil, Air, Water* **35**, 42–48 (2007).
  - (18) Konda, N. M. *et al.* Understanding cost drivers and economic potential of two variants of ionic liquid pretreatment for cellulosic biofuel production. *Biotechnol. Biofuels* **7**, 1–11 (2014).
  - (19) Wilkes, J. S., Levitsky, J. A., Wilson, R. A. & Hussey, C. L. Dialkylimidazolium Chloroaluminate Melts: A New Class of Room-Temperature Ionic Liquids for Electrochemistry, Spectroscopy, and Synthesis. *Inorg. Chem.* **21**, 1263–1264 (1982).
  - (20) Wooster, T. J., Johanson, K. M., Fraser, K. J., MacFarlane, D. R. & Scott, J. L. Thermal degradation of cyano containing ionic liquids. *Green Chem.* **8**, 691–69 (2006).
  - (21) Mai, N. L., Ahn, K. & Koo, Y. M. Methods for recovery of ionic liquids - A review. *Process Biochemistry* vol. 49 872–881 (2014).
  - (22) Pretti, C. *et al.* Acute toxicity and biodegradability of N-alkyl-N-methylmorpholinium and N-

- alkyl-DABCO based ionic liquids. *Ecotoxicol. Environ. Saf.* **74**, 748–753 (2011).
- (23) Galluzzi, M., Schulte, C., Milani, P. & Podestà, A. Imidazolium-Based Ionic Liquids Affect Morphology and Rigidity of Living Cells: An Atomic Force Microscopy Study. *Langmuir* **34**, 12452–12462 (2018).
- (24) Weaver, K. D., Kim, H. J., Sun, J., MacFarlane, D. R. & Elliott, G. D. Cyto-toxicity and biocompatibility of a family of choline phosphate ionic liquids designed for pharmaceutical applications. *Green Chem.* **12**, 507–51 (2010).
- (25) Stolte, S. *et al.* Effects of different head groups and functionalised side chains on the aquatic toxicity of ionic liquids. *Green Chem.* **9**, 1170–1179 (2007).
- (26) Lee, S. M., Chang, W. J., Choi, A. R. & Koo, Y. M. Influence of ionic liquids on the growth of *Escherichia coli*. *Korean J. Chem. Eng.* **22**, 687–690 (2005).
- (27) Cho, C. W., Pham, T. P. T., Jeon, Y. C. & Yun, Y. S. Influence of anions on the toxic effects of ionic liquids to a phytoplankton *Selenastrum capricornutum*. *Green Chem.* **10**, 67–72 (2008).
- (28) Yoo, B., Shah, J. K., Zhu, Y. & Maginn, E. J. Amphiphilic interactions of ionic liquids with lipid biomembranes: A molecular simulation study. *Soft Matter* **10**, 8641–8651 (2014).
- (29) Steudte, S., Stepnowski, P., Cho, C. W., Thöming, J. & Stolte, S. (Eco)toxicity of fluoro-organic and cyano-based ionic liquid anions. *Chem. Commun.* **48**, 9382–9384 (2012).
- (30) Trohalaki, S., Pachter, R., Drake, G. W. & Hawkins, T. Quantitative structure-property relationships for melting points and densities of ionic liquids. *Energy and Fuels* **19**, 279–284 (2005).
- (31) Ding, Y. S., Zha, M., Zhang, J. & Wang, S. S. Synthesis, characterization and properties of geminal imidazolium ionic liquids. *Colloids Surfaces A Physicochem. Eng. Asp.* **298**, 201–205 (2007).
- (32) Bonhôte, P., Dias, A. P., Papageorgiou, N., Kalyanasundaram, K. & Grätzel, M. Hydrophobic, Highly Conductive Ambient-Temperature Molten Salts. *Inorg. Chem.* **35**, 1168–1178 (1996).
- (33) Zhou, Z. Bin, Matsumoto, H. & Tatsumi, K. Low-melting, low-viscous, hydrophobic ionic liquids: 1-Alkyl(alkyl ether)-3-methylimidazolium perfluoroalkyltrifluoroborate. *Chem. - A Eur. J.* **10**, 6581–6591 (2004).
- (34) Siqueira, L. J. A. & Ribeiro, M. C. C. Alkoxy chain effect on the viscosity of a quaternary ammonium ionic liquid: Molecular dynamics simulations. *J. Phys. Chem. B* **113**, 1074–1079 (2009).
- (35) Freire, M. G. *et al.* Mutual Solubilities of Water and Hydrophobic Ionic Liquids. *J. Phys. Chem. B* **111**, 13082–13089 (2007).
- (36) Singh, T. & Kumar, A. Aggregation behavior of ionic liquids in aqueous solutions: Effect of alkyl

- chain length, cations, and anions. *J. Phys. Chem. B* **111**, 7843–7851 (2007).
- (37) Zhao, Y., Gao, S., Wang, J. & Tang, J. Aggregation of ionic liquids [C<sub>n</sub>mim]Br (n = 4, 6, 8, 10, 12) in D<sub>2</sub>O: A NMR study. *J. Phys. Chem. B* **112**, 2031–2039 (2008).
- (38) Cade, E. A., Petenuci III, J. & Hoffmann, M. M. Aggregation Behavior of Several Ionic Liquids in Molecular Solvents of Low Polarity — Indication of a Bimodal Distribution. *ChemPhysChem* **17**, 520–529 (2016).
- (39) Porada, J. H., Mansueto, M., Laschat, S. & Stubenrauch, C. Microemulsions with hydrophobic ionic liquids: Influence of the structure of the anion. *J. Mol. Liq.* **227**, 202–209 (2017).
- (40) Maiti, A., Kumar, A. & Rogers, R. D. Water-clustering in hygroscopic ionic liquids - An implicit solvent analysis. *Phys. Chem. Chem. Phys.* **14**, 5139–5146 (2012).
- (41) Chaumont, A., Schurhammer, R. & Wipff, G. Aqueous interfaces with hydrophobic room-temperature ionic liquids: A molecular dynamics study. *J. Phys. Chem. B* **109**, 18964–18973 (2005).
- (42) Wang, P. *et al.* Cytotoxicity, genotoxicity, oxidative stress, and apoptosis in HepG2 cells induced by the imidazole ionic liquid 1-dodecyl-3-methylimidazolium chloride. *Environ. Toxicol.* **35**, 665–672 (2020).
- (43) Ventura, S. P. M. *et al.* Designing ionic liquids: The chemical structure role in the toxicity. *Ecotoxicology* **22**, 1–12 (2013).
- (44) Kumar, R. A. *et al.* In vitro cytotoxicities of ionic liquids: Effect of cation rings, functional groups, and anions. *Environ. Toxicol.* **24**, 388–395 (2009).
- (45) Yang, L. *et al.* Zebrafish embryos as models for embryotoxic and teratological effects of chemicals. *Reprod. Toxicol.* **28**, 245–253 (2009).
- (46) Pretti, C. *et al.* Acute toxicity of ionic liquids for three freshwater organisms: *Pseudokirchneriella subcapitata*, *Daphnia magna* and *Danio rerio*. *Ecotoxicol. Environ. Saf.* **72**, 1170–1176 (2009).
- (47) Pandey, A., Ekka, M. K., Ranjan, S., Maiti, S. & Sachidanandan, C. Teratogenic, cardiotoxic and hepatotoxic properties of related ionic liquids reveal the biological importance of anionic components. *RSC Adv.* **7**, 22927–22935 (2017).

## CHAPTER 4

### Ionic Liquids as Components for Drug Delivery Vehicles

---

**Contributions:** Nick Ruark assisted in the formulation of the nanoemulsions containing [DC-5][2NTf<sub>2</sub>]. Colin Bertz and Nicole Berdusco assisted in the formulation of nanoemulsions with ILs composed of first-generation bis(sulfonyl)azanide anions. Dr. Montira Tangsangasakri assisted with the mice injections. Professor Michael Taylor provided instruction and embryos for the zebrafish toxicity studies.

## Abstract

Ionic liquids (ILs) possess a unique trait in that they can be tuned to solubilize different classes of molecules that range from hydrophilic to hydrophobic. This property has been leveraged in pharmaceutical applications, where ILs are used as excipients in formulations to assist in dissolving drugs with low solubility in biological media. In a more niche approach, ILs have been successfully employed in nanotechnology applications to create IL-based drug delivery vehicles. Compared to traditional formulations, drug delivery vehicles have improved properties, including target specificity and enhanced drug protection. In this chapter, hydrophobic ILs (HILs) are explored as materials for nanoparticles, mainly, nanoemulsions. The stability, toxicity, and properties of these nanoparticles were examined.

The studies revealed that stability is an essential component for forming biocompatible formulations. When paired with poloxamers, the ILs could form stable and small nanoparticles; however, these solutions produced toxic effects in both zebrafish and mice, likely due to their instability in the bloodstream. Traditional nanoemulsions incorporating ILs required the use of medium chain triglycerides (MCT) as a cosolvent to prevent immediate phase separation. Only ILs with enhanced lipophilicity and large ratios of MCT could form small, safe, and long-lasting nanoemulsions.

## 4.1 Introduction

Drug formulation remains an indispensable field for the translation of new therapies, as many therapeutics are insoluble in water, unstable in physiological media, and produce harmful side effects. While formulations can be composed of a variety of different molecules, each one serving a distinct purpose, only a few classes of compounds contribute to the solubilization of drugs. These classes typically are limited to lipids, polyethylene glycol (PEG), and pegylated lipids.<sup>1</sup> The lack of diverse ingredients is due to the difficulty in finding biocompatible materials. This can be a problem as many drugs require intravenous administration, which prevents the use of free-floating oils that can be needed to solubilize hydrophobic therapeutics. The latter obstacle can be overcome by employing nanotechnology to design nanoparticles capable of delivering drugs.<sup>2</sup> Vehicles such as liposomes<sup>3</sup>, nanoemulsions<sup>4</sup>, micelles<sup>5</sup>, and lipid nanoparticles<sup>6</sup> utilize different complex molecules and polymers to form structures that encapsulate and protect therapeutics. Nanoparticles are designed to be suspended in aqueous solutions and thus they are safe to inject due to their nanometer size.

While the outer shell of most drug delivery vehicles can be composed of a wide-range of unique polymers, surfactants, and other molecules, the media inside the nanoparticle that dissolves the drug is still limited to aqueous buffers and different classes of lipids or lipid-like compounds. Drug delivery vehicles, including micelles, nanoemulsions, and lipid nanoparticles rely on hydrophobic and lipophilic alkyl groups to solubilize therapeutics, while liposomes and other similar vehicles utilize a water core. Therefore, drugs, such as amphotericin B, which are neither solely hydrophilic nor lipophilic can be exceptionally troublesome to encapsulate and formulate.<sup>7</sup> As a result, many drugs that have high potency are unable to reach clinical trials as they cannot be safely and effectively formulated.

The dearth of solubilization materials has led to the exploration of ILs as solvents or cosolvents for pharmaceutical applications. In the past two decades, ILs have emerged that can solubilize a wide range of structurally disparate small molecule therapeutics like paclitaxel<sup>8</sup>, itraconazole<sup>9</sup>, and acyclovir<sup>10</sup>, and even biotherapeutics such as siRNA<sup>11</sup> and insulin<sup>12</sup>. The astonishing solubilization properties are due to the array of intermolecular interactions that ILs can participate in. Additionally, libraries of ILs can be readily

synthesized, where each liquid has a slightly different structure, yet possesses a unique dissolution profile. Therefore, it is only a matter of finding the right IL for the desired drug.

Due to liquid nature of ILs, the compounds have been almost exclusively employed in emulsion systems. As discussed in greater detail in section 5.1, emulsions are kinetically stable colloidal dispersions composed of a continuous liquid phase. The solution typically involves two phases, often oil and aqueous, that form particles stabilized by an appropriate surfactant. Oil-in-water (o/w) emulsions have oil droplets dispersed in an aqueous solution, whereas water-in-oil (w/o) emulsions have aqueous droplets in a larger oil solution. Since the ILs themselves can be hydrophilic, hydrophobic, and even fluorophilic<sup>13</sup>, a variety of unique emulsion formats have been fashioned. This includes IL-in-oil (IL/o)<sup>10</sup>, oil-in-IL (o/IL)<sup>14</sup>, IL-in-water (IL/w)<sup>15</sup>, and water-in-IL (w/IL)<sup>16</sup> emulsions, although IL/o and IL/w are mainly used for therapeutic applications. For example, the Mecozzi group recently explored a IL/w nanoemulsion system for the delivery of amphotericin B.<sup>15</sup> Here, the ILs [DC-7][2NTf<sub>2</sub>] (**13l**) and [chol][hex] (**5a**) were used to solubilize amphotericin B at a high concentration and were employed as the hydrophobic phase of the nanoemulsion, which was formulated using distearoyl-rac-glycerol-PEG2K (DSG-PEG<sub>2000</sub>) as the surfactant and MCT as a cosolvent. In a minimum inhibitory concentration (MIC) assay using *Candida albicans*, the IL nanoemulsion performed as potently as the FDA-approved formulation Fungizone® but was significantly less toxic when the two were compared in a hemolysis study.

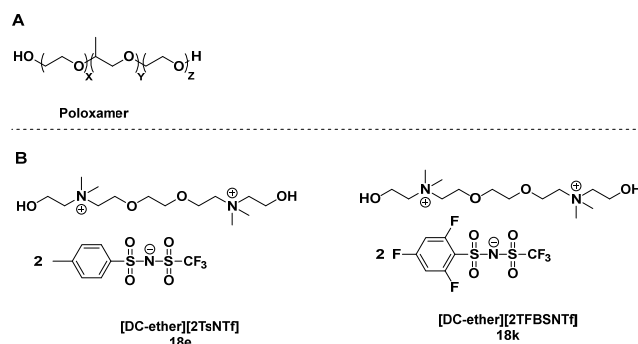
In this chapter, various HILs from Chapter 2 are used to create formulations. In the first set of studies, poloxamers were employed to create micelle-like or nanoemulsion-like particles with the ILs [DC-ether][2TsNTf] (**18e**) and [DC-ether][2TFBSNTf] (**18k**). Although the formulations could encapsulate a high volume of IL, they were ultimately found to be toxic in zebrafish and mice. Nanoemulsion systems were then explored using DSG-PEG<sub>2000</sub> as the primary surfactant. Several monocholinium and dicholinium ILs were tested, and it was revealed that the lack of IL lipophilicity required the use of MCT as a cosolvent to form stable nanoemulsions. However, although initially stable, severe toxicity was observed when intravenously injecting the nanoparticles into mice, likely due to phase separation of the nanoemulsions in the bloodstream. ILs with long alkyl chains, such as [DC-ether][2pOBSNTf] (**18h**), formed long-lasting

nanoemulsions when used with high ratios of MCT, and did not induce toxic side-effects when injected intravenously in mice.

## 4.2 Results and Discussion

### 4.2.1 Poloxamer-based IL nanoparticles

Previous research has demonstrated that poloxamers, also known as Pluronic<sup>®</sup>, can form stable micelle-like or emulsion-like formulations with ILs.<sup>17</sup> Poloxamers are nonionic triblock copolymers, composed of an internal hydrophobic polypropylene oxide (PPO) chain tethered in between two hydrophilic polyethylene oxide (PEO) chains (**Figure 4.1A**). They have a long history as biocompatible components in drug delivery systems<sup>18</sup>, and as such, formulations containing poloxamers and HILs were explored.



**Figure 4.1** (A) Structure of poloxamers. (B) Structure of [DC-ether][2TsNTf] and [DC-ether][2TFBSNTf].

Four poloxamers were chosen based on their availability as well as their different hydrophobic and hydrophilic chain lengths. Each formulation was prepared by dissolving an appropriate amount of poloxamer in saline using bath sonication, adding the corresponding IL, and vigorously shaking and vortexing until a homogenous solution formed. The HILs [DC-ether][2TsNTf] (**18e**) and [DC-ether][2TFBNSTf] (**18k**) were employed for the poloxamer studies (**Figure 4.1B**).

The first poloxamer tried was P123, which has an average molecular weight of 5,800 g/mol and contains approximately twenty PEO units on each chain and an average of seventy internal PPO units, making for a more hydrophobic polymer. Various [DC-ether][2TFBNSTf] (**18k**) and saline ratios as well as P123 concentrations were assessed (**Table 4.1**). Interestingly, the different concentration ranges and P123 concentrations resulted in similar sized micelles of around  $11 \pm 5$  nm. Note, unless otherwise specified, the sizes are intensity weighted. This included IL and saline ratios of 1:8.8–1:30 as well as P123 concentrations of 13.1–46.5 mM. Note, all ratios presented in this chapter are v/v. The IL-containing

particles represent only a small fraction of the total particle population, as the large majority are micelles composed of only the poloxamer. Here, sizes are reported using an intensity-weighted function, as the IL-containing micelles or micelle-like nanoparticles are generally larger and thus have higher intensity. When a volume-weighted function is employed, only smaller non-IL poloxamer micelles are observed.

<b>Table 4.1</b> List of components for each IL formulation containing P123. Size distribution is intensity weighted. Formulations were prepared by dissolving the polymer in saline via bath sonication, adding the IL, and vigorously shaking and vortexing until a homogeneous solution formed.					
#	[DC-ether] [2TFBSNTf]	P123 (mM)	Saline (mL)	Additional Components	Particle Size Distribution (nm)
1	0.100	13.3	2.5	None	14.6 ± 6.1
2	0.114	40.2	1.0	None	11
3	0.500	30.0	6.0	None	11.4 ± 5.0
4	0.400	25.2	6.0	None	11
5	0.200	46.5	2.0	None	11.9 ± 3.1
6	0.100	13.1	3.0	None	11
7	0.114	28.6	2.0	BGG (0.255 mg)	8.32 ± 1.09 (70%); 276 ± 24 (30%)
8	0.114	28.6	2.0	BSA (0.228 mg)	10.0 ± 2.6 (97%); 130 ± 23 (3%)

Although the P123-only micelles have a smaller size of  $7.2 \pm 2.8$  nm, it is still unclear whether the IL droplets are in the particle core. Since no separate IL layer was found in the formulations, even after centrifuging, IL droplets are either encapsulated in the micelle-like particles or dissolved in the polymer solution. As such, two separate trials were conducted that involved dissolving either bovine serum albumin (BSA) or bovine gamma globulin (BGG) in [DC-ether][2TFBSNTf] (**18k**). These proteins can be solubilized in the ILs and will remain dissolved even when washed with water (data not shown). Therefore, since the proteins are hydrophilic, they will not be encapsulated in the poloxamer-only micelles, meaning if there is a significant increase in micelle size, it must indicate that the IL, containing the large proteins, is encapsulated in the nanoparticle. The formulation containing the IL and BSA revealed particle sizes of 97%  $10 \pm 2$  nm and 3%  $130 \pm 23$  nm, while the solution of IL and BGG had particle sizes of 70%  $8.3 \pm 1.1$  nm and 30%  $276 \pm 24$  nm. While most of the micelles for each formulation are mainly poloxamer or poloxamer

with some IL, there are particles present with much larger sizes, indicating that the poloxamers encapsulate the ILs containing the proteins. Still, the identity of the larger particles is unclear as micelles typically have sizes less than 100 nm. More studies are needed to further understand these formulations in terms of their particle structure.

The next poloxamer examined was L35, which is a smaller copolymer with an average molecular weight of 1,900 g/mol, where 50% of the units are PEO. The solutions were formulated with [DC-ether][2TsNTf] (**18e**) at a 1:10 IL and saline ratio with different concentrations of L35 (**Table 4.2**). Low concentrations of L35 resulted in larger particles, as observed with the formulation composed of 41 mM L35 that had a particle size of  $1770 \pm 282$  nm. L35 concentrations of 76 mM and 343 mM resulted in size distributions of 79%  $256 \pm 239$  and 21%  $4.1 \pm 1.0$  and 100%  $179 \pm 51$  nm, respectively. It is likely that the small size of L35 means the IL requires more polymer to stabilize. Still, similar to the formulations with P123, the identity of the larger particles remains unclear.

<b>Table 4.2</b> List of components for each IL formulation containing L35, F68, or F127. Size distribution is intensity weighted. Formulations were prepared by dissolving the polymer in saline via bath sonication, adding the IL, and vigorously shaking and vortexing until a homogeneous solution formed.				
#	IL (mL)	Poloxamer (mM)	Saline (mL)	Particle Size Distribution (nm)
1	[DC-ether][2TsNTf] (0.1)	L35 (41.4)	1.00	$1770 \pm 282$
2	[DC-ether][2TsNTf] (0.1)	L35 (76.4)	1.00	$256 \pm 128$ (79%); $4.14 \pm 1.04$ (21%)
3	[DC-ether][2TsNTf] (0.1)	L35 (343)	1.00	$179 \pm 51$
4	[DC-ether][2TsNTf] (0.1)	F68 (5.93)	2.00	$463 \pm 83$
5	[DC-ether][2TFBSNTf] (0.1)	F68 (5.53)	2.00	$1680 \pm 303$
6	[DC-ether][2TsNTf] (0.1)	F127 (7.41)	2.00	$859 \pm 203$ (72%); $13.0 \pm 2.4$ (28%)
7	[DC-ether][2TFBSNTf] (0.1)	F127 (2.98)	2.75	$1750 \pm 477$

In the following studies, the poloxamers F68 and F127, which have average molecular weights of 8,350 and 12,500 g/mol, respectively, were formulated with [DC-ether][2TFBSNTf] (**18k**) and [DC-ether][2TsNTf] (**18e**) (**Table 4.2**). The sizes of the corresponding particles formed with [DC-ether][2TFBNSTf] (**18k**) were approximately 1,700 nm, regardless of the poloxamer. However, the particle sizes decreased to roughly 600 nm for the F68 and F127 formulations with [DC-ether][2TsNTf] (**18e**). Interestingly, there seems to be a larger dependence on the IL structure than the poloxamer type, at least for F68 and F127. Since both polymers are composed of mainly PEO units, rather than PPO units, it is likely that the degree of hydrophobicity and hydrophilicity is more important than the size of the poloxamers. This was also revealed for P123 and L35, which have lower amounts of PEO units.

Due to the success of P123 and L35, new formulations were created that used both poloxamers to see if a synergistic stabilization affect could be observed (**Table 4.3**). Here, the two poloxamers were paired with [DC-ether][2TsNTf] (**18e**) at IL and saline ratios that spanned 1:10 to 1:15. Additionally, different concentrations of P123 and L35 were tested. While the ratio of IL and saline did not significantly affect the particle size, at least for this range, the concentrations of P123 and L35 had a larger impact. When the concentration of P123 was above 6 mM or when the concentration of L35 was higher than 40 mM, the particles had average sizes greater than 40 nm. When the formulations had concentrations of P123 and L35 both below those respective values, the particle size dropped to approximately 20 nm. The particles are likely not nanoemulsions due to their small size, so it is possible that excess poloxamer is associating with the ILs to form larger cores, although this hypothesis would need to be validated with further studies.

In the next experiment, high pressure microfluidized was employed as an alternative formulation method. In microfluidization, air tanks push a piston that circulates a crude suspension through an interaction chamber to induce micronization. The chamber splits the solution into two paths which then collide at high energy to reduce the size of the particles. Here, an optimized formulation incorporating a 1:16 ratio of IL and saline with 4.7 mM P123 and 27 mM L35 was evaluated. The solution was first vigorously shaken and vortexed, and then was circulated through a microfluidizer at 6,000 psi for one minute. After passing through a 100 nm filter, the size distribution was 95%  $19 \pm 7$  nm and 5%  $3.2 \pm 0.6$

nm, meaning the size was not significantly different from the formulations produced without microfluidization. The latter results support the hypothesis that the particles are not nanoemulsions and are likely micelle-like structures or some type of aggregate, as higher energy formulations methods typically decrease particle size for nanoemulsions.

<b>Table 4.3</b> List of components for each IL formulation containing P123 and L35. Size distribution is intensity weighted. Formulations were prepared by dissolving the polymer in saline via bath sonication, adding the IL, and vigorously shaking and vortexing until a homogeneous solution formed. <sup>a</sup> This formulation was also passed through a microfluidizer at 6,000 psi for 1 min.				
#	[DC-ether] [2TsNTf] (mL)	Poloxamer (mM)	Saline (mL)	Particle Size Distribution (nm)
1	0.20	P123 (23.2); L35 (40.7)	3.0	30.5 ± 11.0 (63%); 8.12 ± 2.73 (38%)
2	0.15	P123 (7.18); L35 (34)	2.0	24.6 ± 10.2 (89%); 4.93 ± 1.25 (11%)
3	0.30	P123 (4.72); L35 (34)	3.0	19.5 ± 10.6
4	0.20	P123 (12.9); L35 (62.1)	3.0	49.2 ± 17.2 (89%); 4.67 ± 0.96 (11%)
5	0.10	P123 (6.71); L35 (64.5)	1.5	45.8 ± 18.6 (89%); 4.60 ± 1.04 (11%)
6	0.10	P123 (16.8); L35 (60.6)	1.5	41.4 ± 12.4 (87%); 4.32 ± 0.70 (13%)
7	0.10	P123 (2.75); L35 (66.0)	1.5	43.7 ± 14.4 (83%); 3.55 ± 0.60 (17%)
8 <sup>a</sup>	1.0	P123 (4.66); L35 (26.8)	16	19.8 ± 7.2 (95%); 3.25 ± 0.62 (5%)

#### 4.2.2 Toxicity of poloxamer-based IL nanoparticles

To evaluate whether the nanoparticles composed of poloxamers and ILs are viable for therapeutic applications, select formulations were injected into ICR mice. In the first study, the [DC-ether][2TFBSNTf] solution with 40.2 mM P123 (**Table 4.1, 2**) was diluted 2X in saline and injected intravenously through the tail vein. The 0.1 mL injection resulted in immediate pain in the mouse. Upon injecting a separate mouse with 0.1 mL of the 4X diluted solution, no adverse effects were observed. Next, a different [DC-ether][2TFBSNTf] solution composed of 46.5 mM P123 (**Table 4.1, 5**) was injected into two ICR mice at

a volume of 0.1 mL and dilutions of 2X and 4X. Unfortunately, both injections resulted in the mice dying, likely due to the higher concentration of IL in the formulation.

The next set of experiments involved the P123-L35 formulations which were able to encapsulate larger amounts of IL. The P123-L35-[DC-ether][2TsNTf] solution that formed the smallest particle size without microfluidization (**Table 4.3, 3**) was injected into ICR mice. A 0.1 mL injection of the formulation at 4X dilution prompted a mild reaction that lasted five minutes, whereas a 0.1 mL injection at 2X dilution induced a severe reaction for fifteen minutes, where the latter mouse became lethargic and was breathing heavily. The second formulation examined was the P123-L35-[DC-ether][2TsNTf] solution created via microfluidization (**Table 4.3, 8**). A neat 0.1 mL intravenous injection resulted in the death of an ICR mouse. These results suggest that the formulations do not properly stabilize the IL or that the particles aggregate when they enter the harsh environment of the bloodstream.

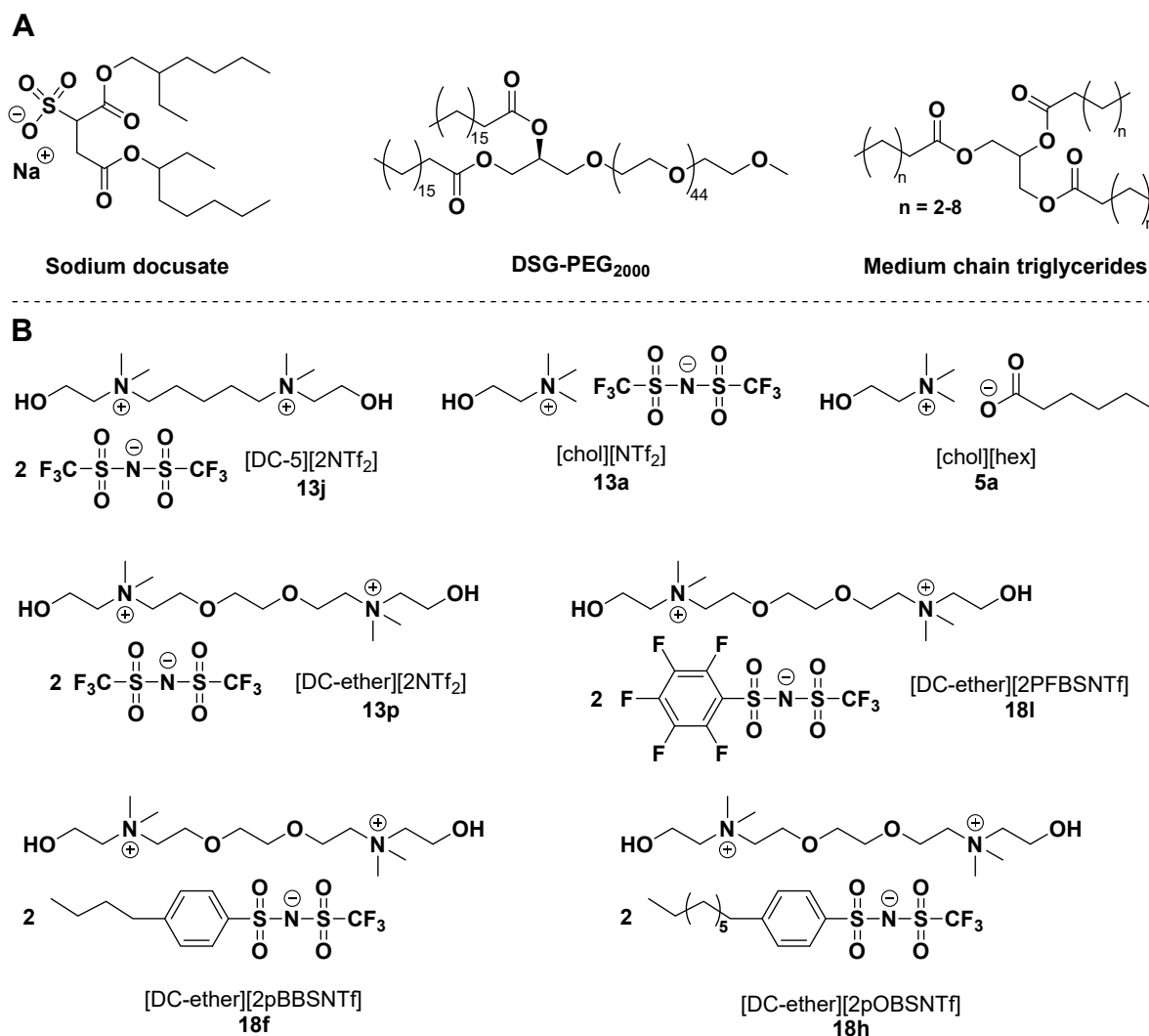
To further probe the toxicity of these formulations, a zebrafish developmental study was performed. As described in section 3.2.6, zebrafish are an optimal model for evaluating toxicity due to their fast respawn time, translucent eggs, and genetic homology to humans. Three formulations were produced which contained P123, L35, or P123 and L35. Separately, P123 and P123-L35 solutions were formulated with [DC-ether][2TFBSNTf] (**13k**) and [DC-ether][2TsNTf] (**13e**), respectively. A list of the components for the five formulations can be found in **Table 4.4**. Zebrafish embryos were incubated in 10X and 100X dilutions of each formulation. After adding the formulations, the chorion immediately became deformed, regardless of the composition and concentration of the solutions. Additionally, the 10X diluted formulations displayed immense toxicity, with the exception of the L35-only solution. The embryo disfiguration is a result of the surfactant-like nature of the polymers as surfactants can partially dissolve and penetrate the chorion. Overall, the poloxamers, with the exception of L35, were toxic even without the ILs. While L35 is the most biocompatible poloxamer, the polymer cannot sufficiently encapsulate ILs on its own. As a result of the toxicity and unclear nanoparticle structures, the poloxamers were not tested further as drug delivery components.

**Table 4.4** List of components for each IL formulation used in the zebrafish toxicity studies. Formulations were prepared by dissolving the polymer in saline via bath sonication, adding the IL (if used), and vigorously shaking and vortexing until a homogeneous solution formed. Particle size was not measured.

#	IL (mL)	Poloxamer (mM)	Saline (mL)
1	[DC-ether][2TBSNTf] (0.250)	P123 (26.3)	2.8
2	None	P123 (28.3)	2.8
3	[DC-ether][2TsNTf] (0.250)	P123 (5.56); L35 (42.7)	1.8
4	None	P123 (6.23); L35 (47.9)	1.8
5	None	L35 (49.7)	1.8

#### 4.2.3 Nanoemulsions incorporating [DC-5][2NTf<sub>2</sub>] and docusate

Owing to the toxicity of the poloxamer solutions, a strategy involving more traditional nanoemulsions was tried. The HIL [DC-5][2NTf<sub>2</sub>] (**13j**) was chosen as a model HIL due to its facile synthesis (see section 2.2.6) and its unique Gemini structure. See **Figure 4.2** for the structures of the surfactants, cosolvents, and ILs used in the following sections. Initially, [DC-5][2NTf<sub>2</sub>] (**4j**) was formulated into a nanoemulsion using sodium docusate, which is an FDA-approved drug that is commonly used as a laxative. The drug is also used as an emulsifier due to its lipophilic and charged structure, and thus was deemed as an appropriate surfactant initially. The nanoemulsions were formulated by three cycles of high-speed homogenization for five minutes and bath sonication for five minutes and then were passed through a 450 nm filter. In the first trial, [DC-5][2NTf<sub>2</sub>] (**13j**) was mixed with saline containing 50 mM sodium docusate in a 1:11 ratio. The resulting nanoemulsion showed a medium size of  $504 \pm 332$  nm but quickly phase separated. Next, MCT was employed as a cosolvent to help stabilize the nanoemulsion. MCT was chosen as it is an FDA-approved oil and has been successfully employed by the Mecozzi group as a cosolvent for long-lasting nanoemulsions containing fluorophilic media for theranostic purposes.<sup>4</sup> Here, a 1:1 ratio of [DC-5][2NTf<sub>2</sub>] (**13j**) and MCT was combined with a 50 mM docusate solution in saline in the same 1:11 ratio of hydrophobic and saline phases. After formulation, the resulting nanoemulsion possessed an initial size of  $436 \pm 289$  nm and maintained homogeneity over the course of several days.



**Figure 4.2 (A)** Structures of sodium docusate, DSG-PEG<sub>2000</sub>, and medium chain triglycerides. **(B)** Structures of the ILs used throughout the nanoemulsion studies.

#### 4.2.4 Nanoemulsions incorporating [DC-5][2NTf<sub>2</sub>] and DSG-PEG<sub>2000</sub>

As the laxative properties of sodium docusate were ultimately undesirable, the neutral pegylated lipid, DSG-PEG<sub>2000</sub>, was utilized as a surfactant to form nanoemulsions (**Table 4.5**). DSG-PEG<sub>2000</sub> is used ubiquitously as a polymer for a variety of nanoparticles and is heavily employed in the Mecozzi lab to stabilize nanoemulsions.<sup>15,19,20</sup> A nanoemulsion composed of [DC-5][2NTf<sub>2</sub>] (**13j**) and 5 mM DSG-PEG<sub>2000</sub> saline solution in a 1:16 ratio resulted in an unstable formulation with an initial size of  $1650 \pm 1330$  that quickly phase separated. However, when formulated with a 1:1 ratio of [DC-5][2NTf<sub>2</sub>] (**13j**) and MCT, the

resulting nanoemulsion had long-term stability, with an initial size of  $220 \pm 91$  nm and a size of  $203 \pm 88$  after ninety days. As a control, a nanoemulsion was prepared without any IL, using a 1:16 ratio of MCT and 5 mM DSG-PEG<sub>2000</sub> solution, and formed similarly stable particles with an initial size of  $217 \pm 81$  nm.

**Table 4.5** List of components for the formulations containing [DC-5][2NTf<sub>2</sub>] and DSG-PEG<sub>2000</sub>. Size distribution is intensity weighted. Formulations were prepared by dissolving the polymer in saline via bath sonication, adding the IL, and undergoing three cycles of homogenization at 21,500 rpm for 5 min followed by bath sonication for 5 min, and then passed through a 450 nm filter – unless otherwise specified.

#	[DC-5][2NTf <sub>2</sub> ] (mL)	MCT (mL)	DSG-PEG <sub>2000</sub> (mM)	Saline (mL)	Additional component or formulation strategy	Initial Particle Size (nm)
1	0.125	None	5.0	2.0	None	$1650 \pm 1330$
2	0.0625	0.0625	5.0	2.0	None	$220 \pm 91$
3	None	0.125	5.0	2.0	None	$217 \pm 81$
4	0.0320	0.0320	5.0	1.0	None	$207 \pm 99$
5	0.0625	0.0625	10	2.0	None	$174 \pm 87$
6	0.125	None	10	2.0	None	Phase separated
7	0.0625	None	10	2.0	None	Phase separated
8	0.0313	None	10	2.0	None	Phase separated
9	0.125	0.125	10	2.0	None	$285 \pm 158$
10	0.250	0.250	10	2.0	None	$1230 \pm 811$
11	0.0625	0.0625	10	2.0	TAMRA dye	$171 \pm 89$
12	0.0625	0.0625	10	2.0	Three cycles of 10 min for each step	$188 \pm 78$
13	0.0313	0.0313	10	1.0	Homogenization then probe sonication	$170 \pm 87$
14	0.0313	0.0313	10	1.0	Probe sonication then homogenization	$183 \pm 81$
15	0.0313	0.0313	10	1.0	200 nm filter	$140 \pm 69$
16	0.0313	0.0313	15	1.0	200 nm filter	$120 \pm 62$
17	0.0313	0.0313	20	1.0	200 nm filter	$101 \pm 54$
18	0.0313	0.0313	10	1.0	None	$165 \pm 85$
19	0.0217	0.0421	10	1.0	None	$164 \pm 81$
20	0.0158	0.0474	10	1.0	None	$215 \pm 95$
21	0.0127	0.0506	10	1.0	None	$208 \pm 85$
22	0.0316	0.0474	10	1.0	None	$183 \pm 86$
23	0.0316	0.0632	10	1.0	None	Phase separated
24	0.0250	0.150	10	1.0	None	$240 \pm 132$

25	0.237	0.710	10	17	Microfluidized at 5,000 psi for 1 min	174 ± 13
----	-------	-------	----	----	--	----------

As the addition of MCT greatly assisted in stabilizing the nanoemulsions, a series of formulations were produced that incorporated [DC-5][2NTf<sub>2</sub>] (**13j**), DSG-PEG<sub>2000</sub>, and MCT in various ratios and formulation conditions. When decreasing the total formulation volume from 2.125 mL to 1.062 mL but maintaining the same 1:1:32 ratio of IL, MCT, and saline, the particle size was not altered significantly. When the formulation included 10 mM DSG-PEG<sub>2000</sub>, the particle size slightly decreased to 174 ± 87 nm. The latter formulation had only a marginal increase in size after two months, but at around ninety days, the size ballooned to 1210 ± 395 nm. A trend emerged where higher concentrations of DSG-PEG<sub>2000</sub> decreased the initial particle size. However, utilizing 10 mM DSG-PEG<sub>2000</sub> could not stabilize nanoemulsions composed of [DC-5][2NTf<sub>2</sub>] (**13j**) with no MCT, as the formulations immediately phase separated. This included formulations composed of 1:16, 1:18, and 1:32 ratios of IL and saline. When the MCT and IL volumes were doubled and prepared in a 10 mM DSG-PEG<sub>2000</sub> saline solution in a 1:1:16 ratio, the particle size increased to 285 ± 158 nm. A 1:1:8 ratio prompted an extreme decrease in stability and a substantial increase in size to 1230 ± 811 nm.

To ensure that [DC-5][2NTf<sub>2</sub>] is encapsulated in the particles, the IL was mixed with a pink TAMRA dye that was not soluble in either the saline solution or MCT. When formulated in an IL, MCT, and 10 mM DSG-PEG<sub>2000</sub> saline solution ratio of 1:1:32, the nanoemulsion showed a homogenous pink solution, where no pink precipitant was observed upon centrifugation. Additionally, the formulation had a consistent particle size of 171 ± 89 nm. It is unclear how the MCT and IL are encapsulated in the nanoemulsion, especially as the two liquids do not form a single phase when mixed. There are several instances of nanoemulsions that contain a Janus core, where two immiscible components are encapsulated in a single particle; however, more studies would be needed to verify this structure.<sup>21</sup>

Increasing the formulation time to three cycles of ten minutes of homogenization followed by ten minutes of bath sonication resulted in no significant decrease in particle size. Upon employing probe sonication

instead of bath sonication, the resulting nanoemulsion had a comparable size of  $170 \pm 87$  nm; however, a large amount of foam was created that complicated the formulation procedure. When probe sonication was utilized before homogenization, the foam decreased, but the particle size increased slightly to  $183 \pm 81$  nm. As probe sonicators are known to damage cargo, especially biomolecules, the technique was not pursued further, and bath sonication was used instead.

In the previous formulations, the nanoemulsions were passed through a 450 nm filter, which excluded only large particles. When a 200 nm filter was employed, the average particle size decreased dramatically to  $140 \pm 69$  nm compared to formulations that were passed through a 450 nm filter, due to the exclusion of medium-sized nanoparticles. Nanoemulsions that utilized 15 and 20 mM DSG-PEG<sub>2000</sub> resulted in smaller particles of  $120 \pm 62$  nm and  $101 \pm 54$  nm, respectively. Unfortunately, the smaller filter size resulted in nanoemulsions that were substantially diluted. Since this strategy would result in the loss of a significant amount of encapsulated drug, a 450 nm filter was used for the remainder of the studies.

In the next set of studies, a series of nanoemulsions with different MCT and IL ratios as well as various total hydrophobic phase and saline ratios were prepared. For each of these cases, a 10 mM DSG-PEG saline solution was mixed with the IL and MCT. These nanoemulsions were formulated using the standard three cycles of homogenization at 21,500 rpm for five minutes and bath sonication for five minutes, followed by passing the solution through a 450 nm filter. The first five nanoemulsions used a 1:16 ratio of hydrophobic phase and saline. A control nanoemulsion consisting of 1:1 [DC-5][2NTf<sub>2</sub>] (**13j**) and MCT had a size of  $165 \pm 85$  nm. When adjusted to 1:2, 1:3, and 1:4 ratios of the IL and MCT, the particle sizes became  $164 \pm 81$ ,  $215 \pm 95$ ,  $208 \pm 85$  nm, respectively. Formulations utilizing larger volumes of the total hydrophobic phase gradually became more unstable, especially when a significant volume of IL was incorporated. For example, when using a 2:3 ratio of IL and MCT as well as a 1:13 ratio of hydrophobic phase and saline, the particles had a size of  $183 \pm 86$  nm, which is similar to the control. However, a formulation composed of [DC-5][2NTf<sub>2</sub>] (**13j**) and MCT at a ratio of 1:2 and a hydrophobic phase and saline ratio of 1:11 phase separated immediately. Interestingly, using a 1:6 ratio of IL and MCT and an

overall 1:5 ratio of hydrophobic phase and saline, produced a nanoemulsion with a modest size of  $240 \pm 132$  nm.

The final study utilized microfluidization. Here, a solution of [DC-5][2NTf<sub>2</sub>] (**13j**) and MCT in a 1:3 ratio was homogenized for one minute in a 10 mM DSG-PEG<sub>2000</sub> solution with an overall 1:17 ratio of hydrophobic phase and saline. The crude nanoemulsion circulated through a microfluidizer at 5,000 psi for one minute and then passed through a 450 nm filter. The microfluidized nanoemulsion had an initial size of  $174 \pm 13$  nm and held a consistent size over the course of 83 days, although phase separation eventually transpired.

#### 4.2.5 Nanoemulsions incorporating monocholinium and [DC-ether] ILs

The next series of nanoemulsions were formulated with ILs containing monocholinium and [DC-ether] cations (**Table 4.6**). In the first set of experiments, [chol][NTf<sub>2</sub>] (**13a**) was formulated without MCT in 10 mM DSG-PEG<sub>2000</sub> saline solutions. Unfortunately, at IL and saline ratios of 1:3.3 and 1:18, the nanoemulsions immediately phase separated. When a 1:1 ratio of [chol]NTf<sub>2</sub>] (**13a**) and [DC-5][2NTf<sub>2</sub>] (**13j**) was employed with an overall IL and saline ratio of 1:3.3, phase separation also occurred. However, when a 1:1:1 ratio of [chol]NTf<sub>2</sub>] (**13a**), [DC-5][2NTf<sub>2</sub>] (**13j**), and MCT were used, a stable nanoemulsion, albeit a larger one, formed with a particle size of  $539 \pm 259$  nm. When [chol][hex] (**5a**) was chosen as the IL and formulated in a 1:6 IL and MCT ratio, and an overall 1:5 hydrophobic phase and saline ratio, a nanoemulsion with a small size of  $215 \pm 108$  nm formed. Intriguingly, when the same nanoemulsion was produced without [chol][hex] (**5a**), an equivalent size of  $213 \pm 102$  nm was observed. Although [chol][hex] (**5a**) has increased lipophilicity compared to [chol][NTf<sub>2</sub>] (**13a**) and [DC-5][2NTf<sub>2</sub>] (**13j**), the IL is water soluble and is likely not in the hydrophobic core of the nanoemulsion.

<p><b>Table 4.6</b> List of components for formulations containing monocholinium and [DC-ether] ILs as well as DSG-PEG<sub>2000</sub>. Size distribution is intensity weighted. Formulations were prepared by dissolving the polymer in saline via bath sonication, adding the IL, and undergoing three cycles of homogenization at 21,500 rpm for 5 min followed by bath sonication for 5 min, and then passed through a 450 nm filter – unless otherwise specified.</p>
---

#	IL (mL)	MCT (mL)	DSG-PEG <sub>2000</sub> (mM)	Saline (mL)	Other formulation strategy	Initial Particle Size (nm)
1	[chol][NTf <sub>2</sub> ] (0.0555)	None	10	1.0	None	Phase separated
2	[chol][NTf <sub>2</sub> ] (0.300)	None	10	1.0	None	Phase separated
3	[chol][NTf <sub>2</sub> ] (0.150); [DC-5][2NTf <sub>2</sub> ] (0.150)	None	10	1.0	None	Phase separated
4	[chol][NTf <sub>2</sub> ] (0.111); [DC-5][2NTf <sub>2</sub> ] (0.111)	0.111	10	1.0	None	539 ± 259
5	[chol][hex] (0.0250)	0.150	10	1.0	None	215 ± 108
6	None	0.150	10	1.0	None	213 ± 102
7	[DC-ether][2NTf <sub>2</sub> ] (0.0211)	0.0423	10	1.0	None	179 ± 89
8	[DC-ether][2NTf <sub>2</sub> ] (0.0158)	0.0474	10	1.0	None	196 ± 99
9	[DC-ether][2NTf <sub>2</sub> ] (0.0316)	0.0632	10	1.0	None	191 ± 90
10	[DC-ether][2NTf <sub>2</sub> ] (0.0432)	0.0216	10	1.0	None	Phase separated
11	[DC-ether][2NTf <sub>2</sub> ] (0.666)	1.33	10	16	Microfluidized at 5,000 psi for 1 min	146 ± 32
12	[DC-ether][2NTf <sub>2</sub> ] (1.00)	None	10	17	Microfluidized at 5,000 psi for 1 min	942 ± 549
13	[DC-ether][2PFBSNTf] (0.500)	1.50	20	16	Microfluidized at 5,000 psi for 1 min	138 ± 51

Next, [DC-ether][2NTf<sub>2</sub>] (**13p**) was chosen as the IL has lower viscosity, which has been shown to decrease nanoemulsion size due to easier droplet separation.<sup>22</sup> Nanoemulsions composed of 1:2 and 1:3 IL and MCT ratios in an overall 1:17 ratio of hydrophobic phase and saline produced particles with similar sizes of 179 ± 89 and 196 ± 99 nm. A comparable size of 191 ± 90 nm was observed for a nanoemulsion containing a 1:13 ratio of hydrophobic phase and saline, with a 1:2 ratio of IL and MCT. Intriguingly, when a 2:1 ratio of IL and MCT was used with an overall hydrophobic phase and saline ratio of 1:17, the particle size decreased to 137 ± 75; although, this nanoemulsion quickly phase separated.

When a nanoemulsion with [DC-ether][2NTf<sub>2</sub>] (**13p**) was microfluidized at a 1:2 IL and MCT ratio and a 1:8 hydrophobic phase and saline ratio, a small nanoemulsion was formed that had an initial size of 146 ± 32 nm. Unfortunately, some IL precipitated after a few days. When a similar formulation was

produced without MCT, the resulting nanoemulsion had a substantial size of  $942 \pm 549$  nm and phase separated within 48 h. The last nanoemulsion of this set involved [DC-ether][2PFBSNTf] (**18i**), which was microfluidized in a 1:3 IL and MCT ratio and a 1:8 hydrophobic phase and saline ratio. Smaller nanoparticles were formed with an initial size of  $138 \pm 51$  nm. This nanoemulsion used 20 mM DSG-PEG<sub>2000</sub>, which likely explains the smaller size; however, similar to the other formulations, a small volume of IL precipitated after only 48 h.

#### *4.2.6 Nanoemulsions incorporating ILs containing first-generation bis(sulfonyl)azanide anions with alkyl-aryl substituents*

The lack of stability of the previous nanoemulsions revealed that the hydrophobic core may have high surface tension. This due to the ILs, which lack lipophilicity and are unable to engage in intermolecular interactions with MCT. To test this hypothesis, nanoemulsions were formulated with MCT that contained ILs with lipophilic alkyl chains. The first of these nanoemulsions employed [DC-ether][2pBBSNTf] (**18f**), an IL with a butyl chain. The nanoemulsion was prepared using a 1:3 ratio of IL and MCT as well as a 1:5.3 ratio of hydrophobic phase and saline, using 10 mM DSG-PEG<sub>2000</sub>. The resulting formulation had a sizeable initial particle diameter of  $450 \pm 290$  nm. Due to the larger size, a series of formulations containing [DC-ether][2pOBSNTf] (**18h**) were produced (**Table 4.7**). This IL has a long octyl chain that is significantly more lipophilic. The surfactant-like structure of [DC-ether][2pOBSNTf] (**18h**) prompted investigations as to whether the IL could form micelle-like structures in a saline solution. Upon homogenizing the IL and saline in a 1:10 ratio, the solution immediately phase separated. However, when mixing the IL with a 10 mM DSG-PEG<sub>2000</sub> saline solution in the same ratio, the micelle-like nanoparticles formed with an initial particle size distribution of 53%  $10.5 \pm 5.0$  nm and 47%  $3.21 \pm 0.75$  nm. As a control, the particle size of a solution of 10 mM DSG-PEG<sub>2000</sub> without IL, resulted in micelles with a size of  $15.0 \pm 4.6$  nm. To evaluate whether the IL could solubilize a drug and be formulated in the DSG-PEG<sub>2000</sub> micelle system, paclitaxel was used as a model. Although [DC-ether][2pOBSNTf] (**18h**) can dissolve paclitaxel at a concentration of approximately 20 mg/mL (data not shown), the drug was dissolved at 10 mg/mL in the IL. The IL-paclitaxel solution was mixed with a 10 mM DSG-PEG<sub>2000</sub> solution in a 1:10 ratio and homogenized at 30,000 rpm

for two minutes. Intriguingly, the IL phase separated. When a formulation was homogenized using a 1:20 ratio of IL-paclitaxel and saline, phase separation occurred again. These results reveal that a certain nanostructure is needed to encapsulate paclitaxel, but the IL-DSG-PEG<sub>2000</sub> particles adopt a different architecture.

<b>Table 4.7</b> List of components for formulations containing [DC-ether][2pOBSNTf]. Size distribution is intensity weighted. Formulations were prepared by homogenizing the components at 30,000 rpm for 2 min. PTX represents paclitaxel.						
#	[DC-ether][2pOBSNTf] (mL)	MCT (mL)	DSG-PEG <sub>2000</sub> (mM)	Saline (mL)	Additional component	Initial Particle Size (nm)
1	0.20	None	None	2	None	Phase separated
2	0.20	None	10	2	None	10.5 ± 5.0 (53%); 3.21 ± 0.75 (47%)
3	None	None	10	2	None	15.0 ± 4.6
4	0.20	None	10	2	PTX (2 mg)	Phase separated
5	0.10	None	10	2	PTX (2 mg)	Phase separated
6	0.25	1.00	10	7	None	1130 ± 628
7	0.055	0.110	20	1	None	206 ± 108
8	0.055	0.165	20	1	None	314 ± 176
9	0.027	0.110	20	1	None	186 ± 80

Due to the inability of [DC-ether][2pOBSNTf] (**18h**) to form micelle-like solutions after dissolving a drug, such as paclitaxel, the nanoemulsion strategy was revisited. The first nanoemulsion of this series involved a 1:4 ratio of IL and MCT with a total ratio of 1:5.6 organic phase and saline using 10 mM DSG-PEG<sub>2000</sub>. Note, this and the following nanoemulsions did not incorporate paclitaxel. Upon homogenizing at 30,000 rpm for two minutes, the resulting nanoemulsion had a particle size of 1130 ± 628 nm. Due to the enormous particle size, a new formulation was produced that utilized a 1:2 ratio of [DC-ether][2pOBSNTf] (**18h**) and MCT as well as a 1:5.5 ratio of organic phase and saline. The nanoemulsion formed smaller particles of 206 ± 108 nm. When a larger amount of MCT was used in a similar formulation, the initial particle sized increased to 314 ± 176 nm and particulates were observed that settled to the bottom of the solution. This third formulation had a 1:3 ratio of IL and MCT and a 1:4.1 ratio of organic phase and saline, and likely had an oil phase that was too large despite the saline solution containing 20 mM DSG-PEG<sub>2000</sub>.

As an alternative strategy, the final nanoemulsion employed a wider IL and MCT ratio of 1:4 as well as less overall hydrophobic phase compared to saline (1:6.8). The resulting nanoemulsion had a smaller particle size of  $186 \pm 80$  nm and was stable for several months. The significant increase in stability is likely due to favorable interactions between MCT and [DC-ether][2pOBSNTf] (**18h**) due to the long alkyl chain of the latter IL.

#### 4.2.7 Toxicity of IL nanoemulsions

As in the case of the poloxamer-based IL nanoparticles, the IL-containing nanoemulsions were evaluated for toxicity by injecting select formulations into mice. In the first study, a nanoemulsion was prepared that incorporated a 1:3 ratio of [DC-ether][2TsNTf] (**13e**) and MCT as well as a 4:14 ratio of hydrophobic phase and saline. A 10 mM DSG-PEG<sub>2000</sub> solution was used as the polymer. The nanoemulsion was prepared by homogenizing at 21,500 rpm for one minute and then circulating the crude formulation through a microfluidizer at 5,000 psi for one minute. The resulting formulation was passed through a 450 nm filter and had an initial particle size of  $164 \pm 50$  nm. The nanoemulsion was diluted 3X and 5X, and 0.2 mL of each diluted formulation was injected into ICR mice via the tail vein. No side effects were observed for either diluted nanoemulsion. However, upon injecting the formulation at 1.5X dilution on the following day, the ICR mouse immediately died. It was later observed that some of the IL had precipitated out of the nanoemulsion only 24 h after preparation.

A second nanoemulsion was prepared as described above, except a concentration of 20 mM DSG-PEG<sub>2000</sub> was employed. The initial particle size decreased to  $127 \pm 46$  nm and no IL precipitated over the course of 48 h. Injections of 0.1 mL and 0.2 mL of the nanoemulsion at 3X dilution into ICR mice did not induce death; however, the 0.2 mL injection resulted in the mouse experiencing pain for fifteen minutes, as observed by the mouse's hunched posture and squinted eyes. Upon injecting a separate ICR mouse with 0.2 mL of the nanoemulsion at 1.5X dilution, the mouse experienced pain over the course of thirty minutes. The combined studies highlight that the stability of the nanoemulsion is essential, as phase separation, regardless of how small, can induce rapid death upon intravenous injection. Still, the second experiment

revealed that the IL-based nanoemulsions have inherent toxicity, even when diluted. The root of the toxicity is unclear, but it is likely a result of nanoemulsions phase separating upon entering the harsh bloodstream environment.

To assess whether the toxicity is due to the neat IL or dissolved IL, [DC-ether][2PFBSNTf] (**18l**) was mixed well with saline via vortexing and sonication. The layers were separated by centrifugation, and 0.1 mL of the saline layer was injected intravenously into an ICR mouse through the tail vein. Gratifyingly, no adverse effects were observed, indicating that the neat IL is responsible for the toxicity. In the previous experiments, when the nanoparticles phase separated in the bloodstream, IL droplets are released that likely caused embolisms, inducing rapid death in the mice.

Next, the nanoemulsions containing [DC-ether][2pOBSNTf] (**18h**) were examined for toxicity. The nanoemulsions containing ratios of IL and MCT between 1:1 and 1:3 produced obvious discomfort and pain when 0.2 mL were injected neat into BALB/C mice. These effects occurred regardless of the ratio of hydrophobic phase and saline. However, the nanoemulsion composed of a 1:4 ratio of [DC-ether][2pOBSNTf] (**18h**) and MCT with a 1:6.8 ratio of hydrophobic phase and saline did not generate side effects when 0.2 mL were injected neat into two different BALB/C mice. These results demonstrate that the stability of the nanoemulsion is essential for limiting toxicity upon intravenous injection. While not a true correlation of bloodstream stability, the latter nanoemulsion was stable for the longest period of time in storage conditions (4 °C).

### 4.3 Conclusion

This chapter explored formulations involving new HILs. In the first set of experiments, two ILs, [DC-ether][2TsNTf] (**18e**) and [DC-ether][2TFBSNTf] (**18k**), were formulated with poloxamers of various lengths and hydrophobicities. It was determined that longer and more hydrophobic poloxamers can form more stable nanoparticles that encapsulate higher volumes of IL. In particular, a mixture of P123 and L35 resulted in particles that are approximately 19 nm in diameter that are stable in storage conditions for months. These poloxamer formulations were produced by simply shaking and vortexing a mixture of a

saline solution of poloxamer and the corresponding IL. When more rigorous formulation methods were employed, such as microfluidization, the particle size did not decrease, suggesting that these particles may be micelles. Dissolving BSA and BGG into the IL and undergoing the standard formulation process resulted in a particle size increase. This result implies that the IL is not dissolved in the poloxamer solution, but rather, is a component of the nanoparticle; although, more studies are needed to verify the structure of the nanoparticles. Unfortunately, the high concentrations of poloxamer needed to encapsulate the IL resulted in very toxic formulations that induced side effects and mortality in mice and zebrafish.

A more traditional nanoemulsion approach was tested in the next series of studies. It was determined that the ILs need a cosolvent to form stable nanoemulsions. As such, MCT, an FDA-approved oil, was added in the majority of formulations. The necessity of using MCT as a cosolvent is likely due to the polymer, DSG-PEG<sub>2000</sub>, which was used throughout the studies. The polymer is composed of PEG and lipid segments, and so it is possible that the IL cannot properly interact with the hydrophobic portion due to the lack of lipophilicity; however, adding MCT helps to increase the overall lipophilicity of the combined hydrophobic phase. Stability was further increased by adding a higher concentration of DSG-PEG<sub>2000</sub>. Toxicity was observed when formulations containing ILs with no lipophilicity were injected into mice. As with the poloxamer studies, it is likely that the particles are phase separating under the harsh conditions of the bloodstream, resulting in IL droplets inducing embolisms. Fortunately, when [DC-ether][2pOBSNTf] (**18h**) was utilized and higher ratios of MCT were added, the resulting nanoemulsions were stable for several months and prompted no observable toxicity when injected intravenously into mice.

The cumulative results reveal a complex picture in that traditional nanoparticles may not offer a facile path for the formulation of HILs, which is why the literature is dominated by formulations with hydrophilic ILs. This is because drug delivery vehicles such as micelles and nanoemulsions rely on the separation of a lipid phase and an aqueous phase. Since HILs are unique in that they are a hydrophobic ionic phase, traditional polymers and surfactants may not interact sufficiently to stabilize them. Some success was had with [DC-ether][2pOBSNTf] (**18h**) as a few injections of formulations with the IL did not reveal obvious side effects in mice. However, the zebrafish studies in Chapter 3 (section 3.2.6) highlighted

that ILs with long alkyl chains, including [DC-ether][2pOBSNTf] (**18h**), are tremendously toxic. To form more stable and biocompatible formulations, the HIL architecture may need to be redesigned to incorporate more lipophilicity, perhaps by adding short alkyl chains. Moreover, new polymers and surfactants that do not rely on PEG and lipid blocks are needed. Still, the ability of ILs to dissolve a wide array of drugs means that IL formulations have the potential to revolutionize the field of drug delivery, and thus, more research is needed in this emerging area.

## 4.4 Experimental

### 4.4.1 Materials

Normal saline (AirLife sterile 0.9% sodium chloride for irrigation USP) was obtained from the University of Wisconsin Hospital Pharmacy. Paclitaxel was purchased from LC Laboratories (Woburn, MA). Distearoyl-rac-glycerol-PEG2K was purchased from Avanti Polar Lipids, Inc (Alabaster, AL). Medium chain triglycerides (Neobee M-5) were purchased from Spectrum Chemical MFG Corp. (New Brunswick, NJ). Solvents and all other reagents were purchased from Sigma-Aldrich Co. (Milwaukee, WI).

### 4.4.2 Formulation of poloxamer-based IL nanoparticles

To a 13 mL centrifuge tube was added the corresponding poloxamer and saline. The polymer was dissolved via bath sonication at room temperature. Then, the representative IL was added, and the mixture was shaken and vortexed vigorously until a homogeneous solution formed. Depending on the particle size, certain formulations were passed through a sterile 25 mm, 100 nm cellulose filter (Thermo Fisher Scientific Inc., Waltham, MA) into a new 13 mL centrifuge tube if size permitted. All formulations were stored at 4 °C.

### 4.4.3 Dynamic light scattering of poloxamer-based IL nanoparticles

Particle size was measured by dynamic light scattering (DLS) with a Zetasizer Nano-ZS (Malvern Instruments Ltd., UK) at 25 °C with a 173° detection angle. The nanoparticle solutions were diluted in a polystyrene cuvette with Millipore Milli-Q water to a concentration of approximately 0.1 mg/mL of

poloxamer. Light scattering measurements were performed in triplicate. The number of scans of each run was determined automatically by the instrument. The data were reported as intensity-weighted average diameters.

#### *4.4.4 Formulation of IL-containing nanoemulsions without microfluidization*

To a 13 mL centrifuge tube was added DSG-PEG<sub>2000</sub> and saline at various amounts and volumes, respectively. The polymer was dissolved via bath sonication at room temperature. Then, MCT and the corresponding IL were added. The mixture underwent three cycles of homogenization at 21,500 rpm for 5 min and bath sonication at room temperature for 5 min. The resulting solution was passed through either a 200 nm or 450 nm sterile 25 mm cellulose filter (Thermo Fisher Scientific Inc., Waltham, MA) into a new 13 mL centrifuge tube if size permitted. In certain cases, bath sonication was replaced with probe sonication, in which the solutions were placed on ice and sonicated using a Q500 probe sonicator (QSonica, Newtown, CT) for 1 min at power setting 5, with 10 s intervals at 20% amplitude. The formulations containing [DC-ether][2pOBSNTf] (**18i**) were prepared by homogenization at 30,000 rpm for 2 min and were passed through a sterile 25 mm, 450 nm cellulose filter if size permitted. All formulations were stored at 4 °C.

#### *4.4.5 Formulation of nanoparticles using microfluidization*

In the case of the poloxamer nanoparticles, P123 (500 mg) and L35 (944 mg) were dissolved in a 50 mL falcon tube containing sterile, normal saline (16 mL; 0.9% w/w sodium chloride) by bath sonication at room temperature. Then, [DC-ether][2TsNTf] (**18e**) (1.0 mL) was added and the solution was mixed with a high-speed homogenizer (200 Homogenizer, VWR International, Radnor, PA) for 1 min at 21,500 rpm and passed through a sterile 25 mm, 450 nm cellulose acetate filter if size permitted. Then, the crude emulsions were further mixed using a microfluidizer (model M-110S, Microfluidics Corp., Newton, MA) for 1 min at 6,000 psi with a cooling bath kept at 0 °C. The final emulsions were passed through a sterile 25 mm, 450 nm cellulose filter if size permitted and stored at 4 °C.

For the IL-containing nanoemulsions, DSG-PEG<sub>2000</sub> solutions (10–20 mM) were prepared in sterile, normal saline (0.9% w/w sodium chloride) and sonicated at room temperature until fully dissolved. The polymer

solutions were combined with MCT and the corresponding IL. The prepared solutions were mixed with a high-speed homogenizer for 1 min at 21,500 rpm and passed through a sterile 25 mm, 450 nm cellulose acetate filter if size permitted. Then, the crude emulsions were further mixed using a microfluidizer for 1 min at 5,000 psi with a cooling bath kept at 0 °C. The final emulsions were passed through a sterile 25 mm, 450 nm cellulose filter if size permitted and stored at 4 °C. Prior to the formulation steps, all instrumentation was precleaned with 100% ethanol, 70% ethanol, 100% methanol, 70% methanol, and Millipore Milli-Q water

#### *4.4.6 Dynamic light scattering of IL-containing nanoemulsions*

The nanoemulsions were diluted to obtain an intensity factor of ~500 by diluting the nanoemulsion with Millipore Milli-Q water. Dynamic light scattering was performed on a NICOMP 380ZLS (Particle Sizing Systems, Santa Barbara, CA). Each particle size analysis was run for 5 min at room temperature in a polystyrene cuvette and repeated three times. The data was analyzed using Gaussian analysis and reported as intensity weighted average diameters.

#### *4.4.7 Evaluation of nanoparticle toxicity in mice*

All animal experiments were approved by the Institutional Animal Care and Use Committee (IACUC) at the University of Wisconsin-Madison. ICR and BALB/C mice were injected in the tail vein with neat formulations or formulations diluted in sterile, normal saline (0.9% w/w sodium chloride). Immediately after injecting the formulation, mouse activity was monitored closely. Signs of pain and discomfort were recorded and timestamped. Mice were deemed fully recovered after 15 min had passed from the most recent display of pain or discomfort.

#### *4.4.8 Zebrafish developmental toxicity*

An embryo–larval zebrafish (*Danio rerio*) model was used to evaluate the toxicity of the IL salt precursors and ILs. Zebrafish (TL strain) were obtained from Dr. Michael Taylor at the University of Wisconsin-Madison School of Pharmacy, where the fish were cultured until sexual maturation. Zebrafish were maintained in a light/dark cycle of 14:10 h at 28.5 °C in egg water (0.03% Instant Ocean, Blacksburg,

VA). The adult fish were fed *Artemia nauplii* twice daily. Embryos were obtained from adult fish with a ratio of 1:2 for female to male. Breeding groups were placed in separate spawning aquariums, equipped with a mesh bottom to prevent the eggs from being cannibalized. Crossing was induced in the morning. After 1 h, eggs free of macroscopically discernible symptoms of infection and disease were collected, rinsed with egg water, and transferred into Petri dishes until chemical exposure. The embryo–larval toxicity assay was subsequently conducted. Zebrafish embryos were added to 24-well plates at 8 embryos/well. Each well was filled with 2 mL of egg water.

The embryos were treated with the poloxamer formulations at 10X and 100X dilutions in egg water. Two replicates were used for each dilution. Additional wells containing zebrafish embryos were incubated with only egg water, which served as controls. The plates were covered and incubated at 28.5 °C in a light/dark cycle of 14:10 throughout the 72 hpf exposure period. The observations of zebrafish development were made directly in the well using a stereomicroscope (Nikon SMZ18, Melville, NY) every 24 h. Embryos and larvae were considered dead when no heartbeat was observed.

#### 4.5 References

- (1) Pouton, C. W. & Porter, C. J. H. Formulation of lipid-based delivery systems for oral administration: Materials, methods and strategies. *Adv. Drug Deliv. Rev.* **60**, 625–637 (2008).
- (2) Bobo, D., Robinson, K. J., Islam, J., Thurecht, K. J. & Corrie, S. R. Nanoparticle-Based Medicines: A Review of FDA-Approved Materials and Clinical Trials to Date. *Pharm. Res.* **33**, 2373–2387 (2016).
- (3) Chen, Z. *et al.* Targeted Delivery of CRISPR/Cas9-Mediated Cancer Gene Therapy via Liposome-Templated Hydrogel Nanoparticles. *Adv. Funct. Mater.* **27**, 1703036 (2017).
- (4) Barres, A. R., Wimmer, M. R. & Mecozi, S. Multicompartment Theranostic Nanoemulsions Stabilized by a Triphilic Semifluorinated Block Copolymer. *Mol. Pharm.* **14**, 3916–3926 (2017).
- (5) Decato, S., Bemis, T., Madsen, E. & Mecozi, S. Synthesis and characterization of perfluoro-tert-butyl semifluorinated amphiphilic polymers and their potential application in hydrophobic drug delivery. *Polym. Chem.* **5**, 6461–6471 (2014).
- (6) Aldayel, A. M. *et al.* Lipid nanoparticles with minimum burst release of TNF- $\alpha$  siRNA show strong activity against rheumatoid arthritis unresponsive to methotrexate. *J. Control. Release* **283**,

- 280–289 (2018).
- (7) Hamill, R. J. Amphotericin B formulations: A comparative review of efficacy and toxicity. *Drugs* **73**, 919–934 (2013).
  - (8) Chowdhury, M. R. *et al.* Ionic-Liquid-Based Paclitaxel Preparation: A New Potential Formulation for Cancer Treatment. *Mol. Pharm.* **15**, 2484–2488 (2018).
  - (9) Williams, H. D. *et al.* Ionic liquids provide unique opportunities for oral drug delivery: Structure optimization and in vivo evidence of utility. *Chem. Commun.* **50**, 1688–1690 (2014).
  - (10) Moniruzzaman, M., Tamura, M., Tahara, Y., Kamiya, N. & Goto, M. Ionic liquid-in-oil microemulsion as a potential carrier of sparingly soluble drug: Characterization and cytotoxicity evaluation. *Int. J. Pharm.* **400**, 243–250 (2010).
  - (11) Zakrewsky, M. & Mitragotri, S. Therapeutic RNAi robed with ionic liquid moieties as a simple, scalable prodrug platform for treating skin disease. *J. Control. Release* **242**, 80–88 (2016).
  - (12) Vaidya, A. & Mitragotri, S. Ionic liquid-mediated delivery of insulin to buccal mucosa. *J. Control. Release* **327**, 26–34 (2020).
  - (13) Tsurumaki, A. & Ohno, H. Dissolution of oligo(tetrafluoroethylene) and preparation of poly(tetrafluoroethylene)-based composites by using fluorinated ionic liquids. *Chem. Commun.* **54**, 409–412 (2018).
  - (14) Tao, L. *et al.* Heterogeneous hydroformylation of long-chain alkenes in IL-in-oil Pickering emulsion. *Green Chem.* **20**, 188–196 (2018).
  - (15) Esson, M. M. & Mecozzi, S. Preparation, Characterization, and Formulation Optimization of Ionic-Liquid-in-Water Nanoemulsions toward Systemic Delivery of Amphotericin B. *Mol. Pharm.* **17**, 2221–2226 (2020).
  - (16) Demirkurt, B., Cakan-Akdogan, G. & Akdogan, Y. Preparation of albumin nanoparticles in water-in-ionic liquid microemulsions. *J. Mol. Liq.* **295**, 111713 (2019).
  - (17) Zheng, L. *et al.* Effect of ionic liquids on the aggregation behavior of PEO-PPO-PEO block copolymers in aqueous solution. *J. Phys. Chem. B* **111**, 1327–1333 (2007).
  - (18) Pitto-Barry, A. & Barry, N. P. E. Pluronic® block-copolymers in medicine: From chemical and biological versatility to rationalisation and clinical advances. *Polym. Chem.* **5**, 3291–3297 (2014).
  - (19) Ying, B. & Campbell, R. B. Delivery of kinesin spindle protein targeting siRNA in solid lipid nanoparticles to cellular models of tumor vasculature. *Biochem. Biophys. Res. Commun.* **446**, 441–447 (2014).
  - (20) Shobaki, N., Sato, Y., Suzuki, Y., Okabe, N. & Harashima, H. Manipulating the function of tumor-associated macrophages by siRNA-loaded lipid nanoparticles for cancer immunotherapy. *J. Control. Release* **325**, 235–248 (2020).

- (21) Wei, D., Ge, L., Lu, S., Li, J. & Guo, R. Janus Particles Templated by Janus Emulsions and Application as a Pickering Emulsifier. *Langmuir* **33**, 5819–5828 (2017).
- (22) Qian, C. & McClements, D. J. Formation of nanoemulsions stabilized by model food-grade emulsifiers using high-pressure homogenization: Factors affecting particle size. *Food Hydrocoll.* **25**, 1000–1008 (2011).

## CHAPTER 5

### MCT Nanoemulsions for the Efficient Delivery of siRNA

---

**Contributions:** The Wisconsin Center for NanoBioSystems provided instruction for the nanoparticle tracking analysis studies. Dr. Montira Tangsangaksri and Chih-Chun Chang assisted in the *in vivo* murine tumor model work. Dr. Jin Liu provided support for the RT-qPCR experiments. The University of Wisconsin Carbone Cancer Center Experimental Animal Pathology Lab prepared H&E stains. Paige Arneson and Dr. Paul Marker obtained images of the H&E slides.

**This chapter has been submitted, in part, as a manuscript – Reference:** Padilla, M. S., Tangsangaksri, M., Chang, C. C., & Mecozzi, S. MCT Nanoemulsions for the Efficient Delivery of siRNA. *Submitted*.

## Abstract

Numerous diseases are rooted in the unnatural abundance of proteins, and while the symptoms can be treated with traditional drugs; ultimately, curing these diseases involves targeting proteins directly, which requires specialized therapeutics. While small molecule agents have found some success in targeting certain protein classes, many proteins are “undruggable” due to their structural architecture. In the past two decades, nucleic acid treatments, especially siRNA therapies, have emerged as viable tools against undruggable proteins usually by targeting protein transcription or translation. Unfortunately, direct injections of siRNA, and most nucleic acids, results in rapid degradation and immune activation. siRNA efficacy can be greatly enhanced by encapsulating the biomolecule into a drug delivery vehicle.

In this chapter, an oil-in-water (o/w) nanoemulsion is used to deliver siRNA targeting Twist1, a protein that contributes to tumor metastasis in a variety of cancers. The FDA-approved oil, medium chain triglycerides (MCT), is used as the hydrophobic phase for the nanoemulsion. The siRNA is paired with dioleoyl-3-trimethylammonium-propane (DOTAP) to form a hydrophobic salt that is soluble at high concentrations in MCT. The resulting MCT/siRNA-DOTAP solution is formulated into a nanoemulsion with an average particle size of 140 nm. The nanoemulsion displays long term stability over the course of 195 days. In an in vivo murine tumor model, the nanoemulsion facilitates a 46% decrease in Twist1 mRNA after 48 h.

## 5.1 Introduction

Overexpressed proteins are contributors to and accelerators of many types of cancers. This includes proteins such as human epidermal growth factor receptor 2 (HER2)<sup>1</sup>, polo-like kinase 1 (PLK1)<sup>2</sup>, and Ras<sup>3</sup>. For decades, researchers have explored methods to downregulate protein expression as an avenue to treat cancer. The prototypical therapeutics are small molecule agents, which bind to proteins to stop their function. While this method has produced FDA-approved chemotherapeutics, this approach is limited to proteins where such a binding site is available, which has been theorized to be only 10–15% of all proteins.<sup>4</sup> Recently, biotherapeutics have emerged as a more versatile platform. Biological molecules such as enzymes and nucleic acids can inhibit protein function by targeting the corresponding gene(s), transcription, translation, or the protein itself, greatly broadening the number of oncoproteins that can be targeted.<sup>5</sup>

A major class of biological drugs is small interfering RNAs (siRNAs). siRNA drugs fall under the domain RNA interference (RNAi) therapies, which utilize short RNA sequences to target mRNA and prevent protein translation. The canonical siRNA is a double-stranded RNA composed of nineteen nucleotides with two nucleotide overhangs on each strand. Once inside a cell, protein silencing is facilitated by the RNA-induced silencing complex (RISC), a ribonucleoprotein complex that uses the siRNA to locate and cleave mRNA. Since the sequence of the siRNA, not the structure, is what determines which mRNA is targeted, any protein that is constructed via translation can theoretically be silenced.<sup>6</sup>

While siRNA technology held great promise at the onset of discovery, it was decades before the technology received its first FDA-approval. As of now, there are only two FDA-approved siRNA drugs: GIVLAARIR<sup>®</sup> (givosiran)<sup>7</sup> and ONPATTRO<sup>®</sup> (patisiran)<sup>8</sup> from Alnylam Pharmaceuticals, Inc., although notably, neither drug treats cancer. The delay in siRNA approval is largely a result of the inability to effectively deliver the nucleic acid.<sup>9</sup> siRNA, like other biomolecules, cannot cross cell membranes unaided, and is susceptible to immune recognition and enzymatic degradation. As a result, much of the research on siRNA has been in chemically modifying the nucleic acids and developing nanocarriers, both to enhance delivery and overall efficacy.

Several types of drug delivery systems have been developed to deliver siRNA, such as polymeric micelles<sup>10</sup>, solid lipid nanoparticles (SLNs)<sup>11</sup>, cationic liposomes<sup>12</sup>, viral vectors<sup>13</sup>, and gold nanoparticles<sup>14</sup>. Despite the diversity among drug carriers, nanoemulsions remain relatively underutilized. Nanoemulsions are kinetically stable particles in the 100–400 nm range that are formulated by using high energy methods to mix two immiscible liquids and an appropriate surfactant. Nanoemulsions are advantageous over other nanoparticles as they can be composed of simple and non-toxic components, have high stability, and contain a large oil droplet core, the latter allows for the loading of a high hydrophobic payload.<sup>15</sup>

The major blockade in adapting nanoemulsions for the delivery of siRNA is the inability of the hydrophobic core to dissolve the hydrophilic nucleic acids. One method to overcome this has been to employ cationic surfactants that forms a complex with the siRNA on the surface of the nanoemulsion.<sup>16</sup> Unfortunately, these cationic nanoemulsions are well-known for their toxicity.<sup>17</sup> An alternative strategy to encapsulate siRNA in lipid cores is to utilize hydrophobic ion pairing (HIP). In HIP, the counterions of the siRNA are replaced with a hydrophobic cations in a 1:1 charge ratio, transforming the siRNA into a hydrophobic salt.<sup>18</sup> Since the siRNA is electrostatically bound to hydrophobic molecules, the structure of the siRNA remains unaffected. HIP of siRNA has been a successful technique for SLNs, although this methodology has not been applied to nanoemulsions.<sup>19</sup>

Here, we present a proof-of-concept nanoemulsion for the delivery of siRNA targeting the Twist1 protein (siRNA<sub>Twist1</sub>). Twist1 is a transcription factor that promotes the epithelial-to-mesenchymal transition (EMT) of cells in a variety of cancers including breast cancer, lung cancer, and neuroblastoma.<sup>20</sup> The EMT pathway, which is a natural biological process that occurs during embryo development, can result in cancerous cells escaping a tumor and inducing metastasis. Here, we pair siRNA<sub>Twist1</sub> with the cationic lipid dioleoyl-3-trimethylammonium-propane (DOTAP) to form a hydrophobic salt. The nanoemulsion is prepared using medium chain triglycerides (MCT) as the oil phase. Our previous studies have indicated that using MCT results in low toxic and highly stable nanoemulsions.<sup>21</sup> Additionally, the siRNA-DOTAP complex is found to have low water solubility and high solubility in MCT. The drug-containing oil is formulated into a nanoemulsion using distearoyl-rac-glycerol-PEG2K (DSG-PEG<sub>2000</sub>) as the surfactant.

The resulting nanoemulsion displays remarkable long-term stability, low toxicity, and gene knockdown *in vivo*.

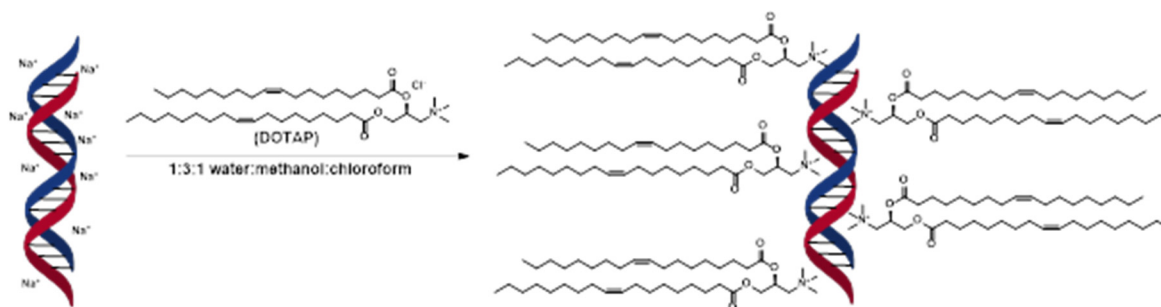
## 5.2 Results

### 5.2.1 Hydrophobic ion pairing

The HIP reaction was performed using a modified lipid extraction protocol (**Scheme 5.1**).<sup>22</sup> The siRNA and DOTAP were combined in a weight ratio of 1:2.5, which corresponds to a 1:1 ratio of the negatively charged phosphate groups of the siRNA and positively charged DOTAP molecules. A mixture of water, methanol, and chloroform in a volume ratio of 1:3:1 was used as the reaction medium. The corresponding mixture became turbid immediately upon adding the reagents but over several hours developed into a clear solution, which indicated the completion of the reaction. After adding chloroform and water to phase separate the mixture, the siRNA-DOTAP complex was isolated from the unpaired siRNA that remained in the water layer. The pairing efficiency was measured by analyzing the residual siRNA in the water layer, using a Quant-iT OliGreen ssDNA assay kit and calculated by the following equation:

$$\text{Pairing Efficiency} = \frac{\text{siRNA}_{\text{total,mg}} - \text{siRNA}_{\text{water,mg}}}{\text{siRNA}_{\text{total,mg}}} \times 100\%$$

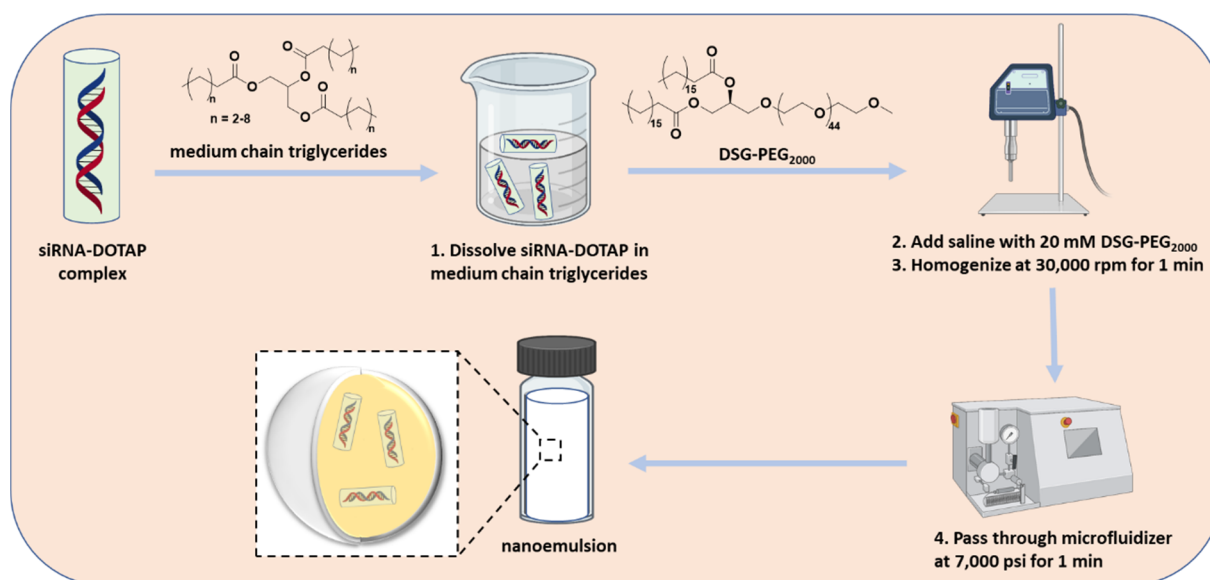
An average pairing efficiency of 99% was observed, indicating that the HIP technique converted almost all the siRNA into a hydrophobic salt.



**Scheme 5.1** Hydrophobic ion pairing of DOTAP and siRNA.

### 5.2.2 Nanoemulsion preparation

The formulation was prepared as an oil-in-water (o/w) nanoemulsion using MCT derived from coconut oil as the hydrophobic phase (**Scheme 5.2**). The siRNA-DOTAP complex was found to be soluble in MCT at concentrations as high as 28 mg/mL, corresponding to 8 mg/mL of siRNA in MCT. Three nanoemulsions were formulated that contained siRNA<sub>Twist1</sub>-DOTAP (NE<sub>Twist1</sub>), scramble siRNA-DOTAP (NE<sub>scramble</sub>), or no siRNA-DOTAP (NE<sub>empty</sub>). The nanoemulsions were prepared in saline using 20 mM distearoyl-rac-glycerol-PEG2K (DSG-PEG<sub>2000</sub>), and were formulated by high-speed homogenization at 30,000 rpm for 1 min followed by high-pressure microfluidization at 7,000 psi for 1 min. The resulting nanoemulsions were milky-white homogeneous solutions.

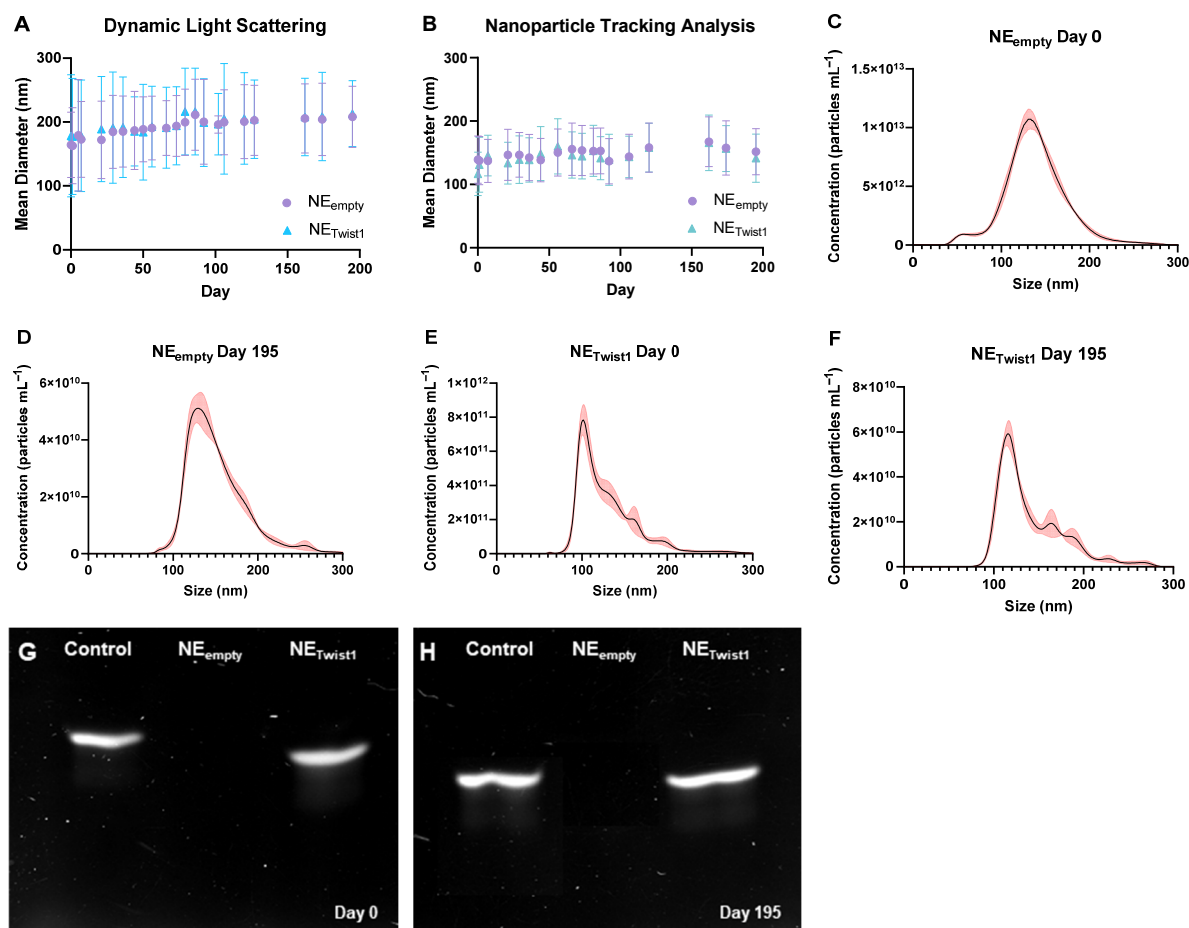


**Scheme 5.2** Formulation methodology for the nanoemulsions containing siRNA-DOTAP complexes. Created with BioRender.com.

### 5.2.3 Nanoemulsion characterization

Particle size was measured by dynamic light scattering (DLS) and nanoparticle tracking analysis (NTA). NE<sub>empty</sub> and NE<sub>Twist1</sub> had similar initial sizes of  $164 \pm 51$  nm and  $178 \pm 95$  nm for DLS, respectively, and  $139 \pm 37$  nm and  $131 \pm 43$  nm for NTA, respectively (**Figure 5.1A,B**). The DLS and NTA measurements for NE<sub>scramble</sub> were consistent with NE<sub>Twist1</sub> and can be found in the Appendix. NTA revealed

a small number of particles between 200–300 nm (**Figure 5.1C–F**), which likely explains the larger sizes calculated via DLS, as small concentrations of larger particles can bias DLS data. The concentration of the nanoemulsions was calculated via NTA to be  $10^{12}$ – $10^{13}$  particles/mL for all formulations. Over the course of 195 days in storage at 4 °C, the nanoparticle size for NE<sub>empty</sub> and NE<sub>Twist1</sub> grew to  $208 \pm 48$  nm and  $213 \pm 52$  nm for DLS, respectively, and  $152 \pm 43$  nm and  $141 \pm 36$  nm for NTA, respectively.



**Figure 5.1** Change in particle size over time as measured by (A) DLS and (B) NTA. Error bars represent standard deviation. (C–F) Concentration of nanoparticles as a function of size measured by NTA. Error bars are the red overlay and represent SEM. Urea-PAGE images of NE<sub>Twist1</sub> siRNA integrity on (G) day 0 and (H) day 195. The control is Twist1 siRNA.

The integrity of the siRNA within the nanoparticles of NE<sub>Twist1</sub> was evaluated by urea-PAGE (**Figure 5.1G,H**). There were no signs of degradation immediately after the formulation process or after 195 days in storage at 4 °C.

#### 5.2.4 Encapsulation efficiency and release

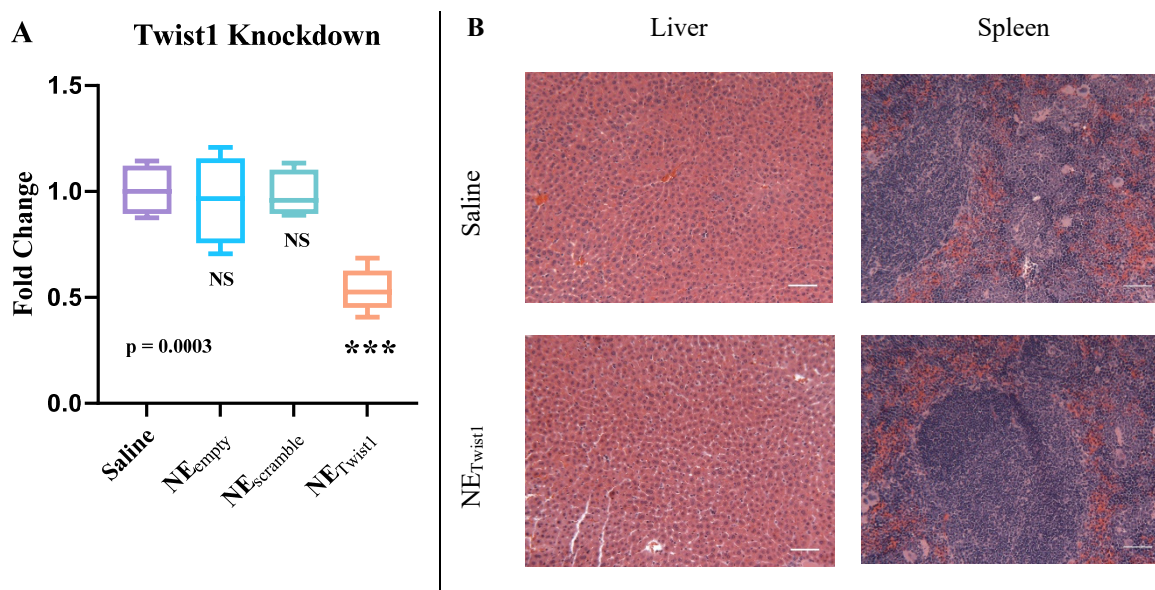
Encapsulation efficiency (EE) was determined by using scramble siRNA harboring a Cy5 dye (siRNA<sub>scramble,Cy5</sub>). This siRNA was paired with DOTAP and formulated into a nanoemulsion (NE<sub>scramble,Cy5</sub>) as described above. After preparation, NE<sub>scramble,Cy5</sub> was centrifuged in a 100 kDa molecular weight cut off (MWCO) spin column. The fluorescence of the filtrate was compared to the fluorescence of the residual nanoemulsion, and the corresponding siRNA masses were evaluated using a standard curve. EE was calculated by the following equation:

$$EE = \frac{\text{siRNA}_{\text{unfiltered},\mu\text{g}}}{\text{siRNA}_{\text{unfiltered},\mu\text{g}} + \text{siRNA}_{\text{filtered},\mu\text{g}}} \times 100\%$$

EE was determined to be 85%. After 60 days at 4 °C, the encapsulation efficiency of NE<sub>scramble,Cy5</sub> was recalculated for the neat nanoemulsion, and it was revealed that no siRNA had been released during this period.

#### 5.2.5 In vivo gene knockdown and histology

Four groups of six mice were inoculated on the right flank with 4T1-Luc cells and the tumors were allowed to grow until they reached a size of 100 mm<sup>3</sup>. At timepoints 0 and 24 h, the mice received a 200 μL intravenous injection of either saline, NE<sub>empty</sub>, NE<sub>scramble</sub>, or NE<sub>Twist1</sub>, where NE<sub>scramble</sub> and NE<sub>Twist1</sub> had siRNA concentrations of 6.2 mg/kg/injection. At 48 h, the mice were sacrificed, and gene knockdown was evaluated via RT-qPCR (**Figure 5.2A**). The RT-qPCR study revealed an average of 46% knockdown of Twist1 mRNA in the NE<sub>Twist1</sub> group. Additionally, H&E stains of the livers and spleens of the NE<sub>Twist1</sub> group revealed no observable toxicity (**Figure 5.2B**).



**Figure 5.2 (A)** Relative knockdown of Twist1 mRNA, ascertained via RT-qPCR using GAPDH as the housekeeping gene. Bars represent minimum and maximum values (n=6), one-way ANOVA, \*\*\* $p = 0.0003$ . **(B)** Representative images of hematoxylin and eosin stains of mice livers and spleens from the saline and NE<sub>Twist1</sub> groups. Scale bars represent 64  $\mu\text{m}$ .

### 5.3 Discussion

Nanoemulsions offer a unique platform for drug delivery due to their simple components and facile preparation. DOTAP was chosen as the hydrophobic ion as it has been successfully employed in SLNs to create hydrophobic siRNA salts.<sup>18</sup> DOTAP can exhibit toxicity at high concentrations due to the formation of a positively charged surface on the corresponding particles.<sup>17</sup> Here, the DOTAP is formulated at a low concentration and is electrostatically bound to the siRNA that is encapsulated in the nanoemulsion. By mixing the siRNA and DOTAP at a 1:1 charge ratio, almost all the siRNA was paired and made hydrophobic. Previous studies have indicated that this ratio results in near quantitative yield for the corresponding hydrophobic salt.<sup>19</sup>

For the oil phase, MCT was utilized as it is a non-toxic FDA-approved oil that is frequently found in food, cosmetics, and other drug formulations.<sup>23</sup> The large solubility of the siRNA in MCT is due to DOTAP, which envelops the nucleic acid in a highly lipophilic layer of alkyl chains. No siRNA precipitated after the complex was dissolved in MCT, indicating that the oil does not disrupt the siRNA-DOTAP complex. The surfactant, DSG-PEG<sub>2000</sub>, is also FDA-approved and is utilized ubiquitously to make stable

nanoparticles, including for the delivery of nucleic acids.<sup>24</sup> Ionic surfactants were not chosen due to their toxicity as well as their potential to disturb the siRNA-DOTAP complexes.

Remarkably, the formulation was prepared by only one 1 min of homogenization and 1 min of microfluidization and resulted in the formation of sub-200 nm particles. This demonstrates the ease at which nanoemulsions can be produced. Additionally, the nanoemulsions satisfy the FDA requirement that states that parenteral emulsions must have particles sizes below 500 nm to prevent the possibilities of capillary embolism.<sup>25</sup> However, although the initial particle size is an important parameter, nanoemulsions are thermodynamically unstable, so it is essential to monitor their size as they age. Gratifyingly, the particles had only slight increases in size over a prolonged period, which demonstrates the promising stability of these nanoemulsions.

Both DLS and NTA were employed to determine particle size. While DLS is a more tradition method for calculating particle size, NTA is unique in that it analyzes individual particles, meaning these measurements are not biased by large particles, which is the case for DLS.<sup>26</sup> As shown in **Figure 5.1C–F**, NE<sub>empty</sub> has a Gaussian distribution of particle sizes, whereas NE<sub>Twist1</sub> has more than one distinct maximum. This is likely due to the nanoparticles encapsulating a variable number of siRNA-DOTAP complexes with certain numbers of encapsulated complexes being more favorable than others, which would correspond to the different maxima in the size distributions.

The high encapsulation efficiency demonstrates that the siRNA-DOTAP complex does not become separated during the formulation process, indicating that both components remain solubilized in the MCT droplets. Furthermore, due to the large oil core of nanoemulsions, more siRNA-DOTAP complexes can be encapsulated into a single particle compared to other drug delivery systems. This is especially important as the siRNA itself is sizeable at 7.5 nm in length and 2.5 nm in width.<sup>27</sup> Along with favorable EE, the siRNA had long-term stability in the nanoemulsions in 4 °C storage conditions. It is likely that the DOTAP cations as well as the MCT offer protection from nucleic acid hydrolysis. This is an important consideration as many RNA technologies must be stored at –80 °C or they rapidly degrade.

The efficacy of the formulations could not be evaluated using *in vitro* cell experiments due to the density of the nanoemulsions. Since MCT is less dense than water and occupies most of the volume of the nanoemulsion, only a minute fraction of nanoparticles will be internalized by cell monolayers, which settle at the bottom of petri dishes. As such, the efficacy of the nanoemulsion was assessed only *in vivo*. Through two IV injections, a significant reduction in Twist1 expression was observed, underscoring the potency of this formulation. The promising *in vivo* data was facilitated by the large 6.2 mg/kg siRNA injections that were enabled by the high solubility of the siRNA-DOTAP complex in MCT as well as the large oil droplet core. Additionally, no liver nor spleen toxicity was observed during the study, supporting the claims that the nanoemulsion components are safe. Together, these results demonstrate that the formulation can safely and effectively deliver siRNA *in vivo*, underscoring the potential of nanoemulsion-based systems for delivering hydrophilic biological therapeutics.

#### 5.4 Conclusion

The delivery of siRNA is hindered by the many physiological barriers that prevent foreign nucleic acids from reaching inside the cell. Here, a nanoemulsion was adapted as a novel siRNA delivery vehicle. To leverage the large oil core of nanoemulsions, the hydrophilic siRNA was paired with DOTAP to form a hydrophobic siRNA complex that is soluble at high concentrations in lipophilic media. MCT was chosen as the oil due to its low toxicity and ubiquity in other medical and consumer applications. The MCT/siRNA-DOTAP mixture was formulated into a nanoemulsion using DSG-PEG<sub>2000</sub> as the surfactant. The nanoparticles had an initial size of ~135 nm, which grew to only ~145 nm after half a year in storage conditions. In a murine tumor model, the nanoemulsion loaded with siRNA<sub>Twist1</sub> demonstrated 46% gene knockdown during a 48 h period. No liver or spleen toxicity was observed during the experiment. Collectively, this study shows that nanoemulsions can be used for the efficient delivery of nucleic acids in a safe and controlled manner.

## 5.5 Experimental

### 5.5.1 Materials

Normal saline (AirLife sterile 0.9% sodium chloride for irrigation USP) was purchased from the University of Wisconsin Hospital Pharmacy. 1,2-dioleoyl-3-trimethylammonium-propane (chloride salt) and distearoyl-rac-glycerol-PEG2K were purchased from Avanti Polar Lipids, Inc (Alabaster, AL). Medium chain triglycerides (Neobee M-5) were purchased from Spectrum Chemical MFG Corp. (New Brunswick, NJ). siRNA was purchased from Dharmacon (Lafayette, CO). Penicillin-streptomycin solution and phosphate buffered saline were purchased from Corning Inc. (Manassas, VA). Fetal bovine serum, RNase-free water, TaqMan RNA-to-Ct kit, GAPDH TaqMan assay, Twist1 Taqman assay, SYBR-Safe DNA gel stain, and Quant-iT OliGreen ssDNA assay were purchased from Thermo Fisher Scientific Inc. (Waltham, MA). The SequaGel UreaGel 19:1 denaturing gel system was purchased from National Diagnostics (Charlotte, NC). Solvents and all other reagents were purchased from Sigma-Aldrich Co. (Milwaukee, WI).

siRNA<sub>Twist1</sub> Sense: 5'-GCU-GAG-CAA-GAU-UCA-GAC-CdTdT-3'

siRNA<sub>Twist1</sub> Antisense: 5'-P-GGU-CUG-AAU-CUU-GCU-CAG-CdTdT-3'

siRNA<sub>scramble</sub> Sense: 5'-GGU-AGA-CCA-GAC-CGU-UAC-AdTdT-3'

siRNA<sub>scramble</sub> Antisense: 5'-P-UGU-AAC-GGU-CUG-GUC-UAC-CdTdT-3'

siRNA<sub>scramble,Cy5</sub> Sense: 5'-Cy5-GGU-AGA-CCA-GAC-CGU-UAC-AdTdT-3'

siRNA<sub>scramble,Cy5</sub> Antisense: 5'-P-UGU-AAC-GGU-CUG-GUC-UAC-CdTdT-3'

### 5.5.2 Hydrophobic ion pairing

siRNA and DOTAP-Cl were mixed in a 1:2.5 ratio w/w in a solution of RNase-free water, methanol, and chloroform in a 1:3:1 ratio v/v/v. The solution stirred for 7 h at room temperature, turning from a turbid solution to clear. Then, the solution underwent phase separation by adding equal volume amounts of chloroform and RNase-free water. The layers separated, and the water layer was extracted with chloroform (3x8 mL). The organic layers were combined and washed with RNase-free water (3x10 mL).

The mixture was concentrated *in vacuo* to produce a yellow and white solid mixture, or a blue solid mixture in the case of the siRNA<sub>scramble,Cy5</sub>. The residual siRNA in the water layers were combined, lyophilized, and saved for further analysis. The solid was then dissolved in a 1:1 chloroform and MCT mixture v/v. The solution was mixed well, and the chloroform was removed *in vacuo*. The MCT/DOTAP-siRNA solution was kept under high vacuum until the preparation of the nanoemulsion.

### 5.5.3 Pairing efficiency

Pairing efficiency was measured using a Quant-iT OliGreen ssDNA assay according to the manufacturer's instructions. The lyophilized free siRNA from the water layer of the hydrophobic ion pairing step was resuspended in 1X Tris EDTA (TE) buffer. siRNA<sub>Twist1</sub> was used to generate the standard curve.

### 5.5.4 Nanoemulsion preparation

DSG-PEG<sub>2000</sub> solution (20 mM) was prepared in sterile, normal saline (0.9% w/w sodium chloride) and sonicated at room temperature until fully dissolved. The polymer solution was combined with neat MCT or MCT containing the corresponding siRNA-DOTAP complex in a 13:4 ratio v/v. Prior to the formulation steps, all instrumentation was precleaned with 100% ethanol, 70% ethanol, 100% methanol, 70% methanol, and Millipore Milli-Q water. The prepared solutions were homogenized with a high-speed homogenizer (200 Homogenizer, VWR International, Radnor, PA) for 1 min at 30,000 rpm and passed through a sterile 25 mm, 0.45  $\mu$ m cellulose acetate filter (Thermo Fisher Scientific Inc., Waltham, MA). Then, the crude emulsions were further mixed using a microfluidizer (model M-110S, Microfluidics Corp., Newton, MA) for 1 min at 7,000 psi with a cooling bath kept at 0 °C. The final emulsions were passed through a sterile 25 mm, 0.45  $\mu$ m cellulose filter and stored at 4 °C.

### 5.5.5 siRNA integrity

NE<sub>Twist1</sub> was evaluated for siRNA integrity immediately after formulation and after 195 days in storage at 4 °C. The nanoemulsion was mixed with a solution of dilute bromophenol blue in 7 M urea in a

1:5 ratio v/v. The samples were run on a 15% urea-polyacrylamide gel using the SequaGel UreaGel 19:1 denaturing gel system for 60 min at 200 V.  $NE_{\text{empty}}$  and free  $siRNA_{\text{scramble,Cy5}}$  were used as a negative control and positive control, respectively. The gels were stained with dilute SYBR-Safe DNA gel stain for 10 min before being visualized by a Bio-Rad ChemiDoc MP Imaging System (Hercules, CA).

#### *5.5.6 Dynamic light scattering*

The nanoemulsions were diluted to obtain an intensity factor of  $\sim 500$  by diluting the nanoemulsion 600-fold in Millipore Milli-Q water. Dynamic light scattering was performed on a NICOMP 380ZLS (Particle Sizing Systems, Santa Barbara, CA). Each particle size analysis was run for 5 min at room temperature in a polystyrene cuvette and repeated three times. The data was analyzed using Gaussian analysis and reported as intensity weighted average diameters.

#### *5.5.7 Nanoparticle tracking analysis*

The nanoemulsions were diluted 10,000-fold in Millipore Milli-Q water such that  $\sim 80$  particles were always tracked. Size distribution was measured using a Nanosight NS300 equipped with a 488 nm laser, and analyzed using Nanosight NTA 3.3 software (Malvern Instruments, UK). For each run, five videos of 60 s were recorded at camera level 9 and syringe pump speed of 50. Runs were analyzed at 25 frames/sec using a detection threshold of 3. The instrument was washed with Millipore Milli-Q water before and after each run.

#### *5.5.8 Encapsulation efficiency*

Immediately after formulation and after 60 days in storage at 4 °C,  $NE_{\text{scramble,Cy5}}$  was diluted 10X in RNase-free water and filtered through a 0.5 mL Amicon 100 kDa MWCO spin column at 14,000 rpm for 30 min. The spin column was then inverted and centrifuged at 4,000 rpm for 2 min in a new centrifuge tube to obtain the unfiltered components, which were then diluted to the same volume as the filtered components with RNase-free water. Fluorescence was analyzed by a Synergy H1 microplate reader (Biotek, Winooski, VT) using 630 nm as the emission wavelength and 690 nm as the excitation wavelength. A calibration curve was used to convert to the fluorescence into mass. Free  $siRNA_{\text{scramble,Cy5}}$  was filtered through the 100 kDa

MWCO spin column using the same conditions to evaluate the average amount of siRNA that can be filtered. This was used to adjust the  $\text{siRNA}_{\text{filtered}}$  and  $\text{siRNA}_{\text{unfiltered}}$  values.

#### 5.5.9 *In vivo gene knockdown*

All animal experiments were approved by the Institutional Animal Care and Use Committee (IACUC) at the University of Wisconsin-Madison. BALB/C female mice of age 6–8 weeks (Jackson Laboratories) were inoculated subcutaneously in the right flank with  $1 \times 10^6$  4T1-Luc cells. After tumors grew to 100  $\text{mm}^3$ , the mice were randomly divided into four groups of six mice. The mice were injected intravenously (0.2 mL) at 0 and 24 h with the following treatment: saline,  $\text{NE}_{\text{empty}}$ ,  $\text{NE}_{\text{scramble}}$  (6.2 mg/kg/injection of siRNA), and  $\text{NE}_{\text{Twist1}}$  (6.2 mg/kg/injection of siRNA). After 48 h, the mice were euthanized, and the tumors were extracted. The tumors were washed with 1X phosphate buffered saline (PBS) and the total RNA was extracted and purified using a GeneJet RNA purification kit (Thermo Fisher Scientific), where the tumors were homogenized for 30 sec at 20,000 rpm in lysis buffer using a high-speed homogenizer (Homogenizer 150, Fischer, Waltham, MA). mRNA concentration and purity were assessed by analyzing the absorbance at 260 nm and the  $A_{260}/A_{280}$  ratio respectively, using a Synergy H1 microplate reader (Biotek, Winooski, VT) equipped with a 16-sample Take3 micro-volume plate. All total RNA had a  $A_{260}/A_{280}$  value of greater than 2.0. Relative gene expression of the Twist1 gene was compared to the GAPDH (housekeeping) gene using a TaqMan 1-step RNA-to-Ct kit, and Twist1 and GAPDH TaqMan assays, according to manufacturer's protocol, and measured on a QuantStudio 7 Flex Real-Time PCR System (Thermo Fisher Scientific, Waltham, MA). Spleen and livers from the saline and  $\text{NE}_{\text{Twist1}}$  groups were dissected after euthanizing the mice. The organs were sectioned and stained by H&E. Images of the slides were obtained using a Leica DMLB fluorescence microscope (Wetzlar, Germany).

#### 5.5.10 *Statistical analysis*

Statistical analysis was performed using Prism (GraphPad Software 9.0.1, San Diego, CA). Gene knockdown significance was analyzed by one-way ANOVA followed by a post-analysis Tukey test.

## 5.6 References

- (1) Yarden, Y. Biology of HER2 and Its Importance in Breast Cancer. *Oncology* **61**, 1–13 (2001).
- (2) Liu, Z., Sun, Q. & Wang, X. PLK1, A Potential Target for Cancer Therapy. *Transl. Oncol.* **10**, 22–32 (2017).
- (3) Prior, I. A., Lewis, P. D. & Mattos, C. A comprehensive survey of ras mutations in cancer. *Cancer Research* vol. 72 2457–2467 (2012).
- (4) Verdine, G. L. & Walensky, L. D. The challenge of drugging undruggable targets in cancer: Lessons learned from targeting BCL-2 family members. *Clinical Cancer Research* vol. 13 7264–7270 (2007).
- (5) Lazo, J. S. & Sharlow, E. R. Drugging Undruggable Molecular Cancer Targets. *Annu. Rev. Pharmacol. Toxicol.* **56**, 23–40 (2016).
- (6) Pai, S. I. *et al.* Prospects of RNA interference therapy for cancer. *Gene Ther.* **13**, 464–477 (2006).
- (7) Thapar, M., Rudnick, S. & Bonkovsky, H. L. Givosiran, a novel treatment for acute hepatic porphyrias. *Expert Rev. Precis. Med. Drug Dev.* **6**, 9–18 (2021).
- (8) Akinc, A. *et al.* The Onpatro story and the clinical translation of nanomedicines containing nucleic acid-based drugs. *Nature Nanotechnology* vol. 14 1084–1087 (2019).
- (9) Dowdy, S. F. Overcoming cellular barriers for RNA therapeutics. *Nat. Biotechnol.* **35**, 222–229 (2017).
- (10) Matsumoto, S. *et al.* Environment-responsive block copolymer micelles with a disulfide cross-linked core for enhanced siRNA delivery. *Biomacromolecules* **10**, 119–127 (2009).
- (11) Aldayel, A. M. *et al.* Lipid nanoparticles with minimum burst release of TNF- $\alpha$  siRNA show strong activity against rheumatoid arthritis unresponsive to methotrexate. *J. Control. Release* **283**, 280–289 (2018).
- (12) Tagami, T. *et al.* Anti-angiogenic therapy via cationic liposome-mediated systemic siRNA delivery. *Int. J. Pharm.* **422**, 280–289 (2012).
- (13) Tomar, R. S., Matta, H. & Chaudhary, P. M. Use of adeno-associated viral vector for delivery of small interfering RNA. *Oncogene* **22**, 5712–5715 (2003).
- (14) Song, W. J., Du, J. Z., Sun, T. M., Zhang, P. Z. & Wang, J. Gold nanoparticles capped with polyethyleneimine for enhanced siRNA delivery. *Small* **6**, 239–246 (2010).
- (15) Singh, Y. *et al.* Nanoemulsion: Concepts, development and applications in drug delivery. *Journal of Controlled Release* vol. 252 28–49 (2017).
- (16) Li, Z. *et al.* Perfluorocarbon Nanoemulsions for Combined Pulmonary siRNA Treatment of Lung Metastatic Osteosarcoma. *Adv. Ther.* **2**, 1900039 (2019).
- (17) Lv, H., Zhang, S., Wang, B., Cui, S. & Yan, J. Toxicity of cationic lipids and cationic polymers in

- gene delivery. *J. Control. Release* **114**, 100–109 (2006).
- (18) Xue, H. Y. & Wong, H. L. Tailoring nanostructured solid-lipid carriers for time-controlled intracellular siRNA kinetics to sustain RNAi-mediated chemosensitization. *Biomaterials* **32**, 2662–2672 (2011).
- (19) Lobovkina, T. *et al.* In vivo sustained release of siRNA from solid lipid nanoparticles. *ACS Nano* **5**, 9977–9983 (2011).
- (20) Khan, M. A. *et al.* Thymoquinone inhibits cancer metastasis by downregulating TWIST1 expression to reduce epithelial to mesenchymal transition. *Oncotarget* **6**, 19580–19591 (2015).
- (21) Barres, A. R., Wimmer, M. R. & Mecozzi, S. Multicompartment Theranostic Nanoemulsions Stabilized by a Triphilic Semifluorinated Block Copolymer. *Mol. Pharm.* **14**, 3916–3926 (2017).
- (22) Bligh, E. G. & Dyer, W. J. A rapid method of total lipid extraction and purification. *Can. J. Biochem. Physiol.* **37**, 911–917 (1959).
- (23) Traul, K. A., Driedger, A., Ingle, D. L. & Nakhasi, D. Review of the toxicologic properties of medium-chain triglycerides. *Food Chem. Toxicol.* **38**, 79–98 (2000).
- (24) Choi, J. S., MacKay, J. A. & Szoka, F. C. Low-pH-Sensitive PEG-Stabilized Plasmid–Lipid Nanoparticles: Preparation and Characterization. *Bioconjug. Chem.* **14**, 420–429 (2003).
- (25) Driscoll, D. F. Lipid injectable emulsions: Pharmacopeial and safety issues. *Pharmaceutical research* vol. 23 1959–1969 (2006).
- (26) Filipe, V., Hawe, A. & Jiskoot, W. Critical evaluation of Nanoparticle Tracking Analysis (NTA) by NanoSight for the measurement of nanoparticles and protein aggregates. *Pharm. Res.* **27**, 796–810 (2010).
- (27) Schroeder, A., Levins, C. G., Cortez, C., Langer, R. & Anderson, D. G. Lipid-based nanotherapeutics for siRNA delivery. *J. Intern. Med.* **267**, 9–21 (2010).

## **CHAPTER 6**

### Conclusions



## 6.1 Primary Findings and Conclusions

The research presented in this thesis represents innovative approaches to nanoemulsion-mediated drug delivery. The majority of this thesis work is based on the need for new hydrophobic materials that can dissolve a larger number of therapeutics and be formulated into a nanoemulsion. Ionic liquids (ILs), especially room temperature hydrophobic ILs (HILs), presented a unique option due to their ability to dissolve a wide range of drugs at high concentrations. Since this research is still in its infancy in the Mecozzi lab, a significant amount of work went into synthesizing and characterizing novel HILs. New HILs were needed as traditional HILs were found to have characteristics unsuitable for intravenous nanoemulsion delivery, such as high toxicity, water solubility, and viscosity. The anions and cations were functionalized with distinct molecular architectures and the corresponding ILs were evaluated for specific properties and toxicities. This tunability is a unique trait for ILs, and as such, dozens of IL or IL-like compounds were synthesized. Although most of these compounds did not fit the strict criteria to become a component of a nanoemulsion due to one or more unfavorable characteristics, some ILs showcased enormous potential. During the formulation experiments, certain HILs were chosen and were prepared with poloxamers. Although these formulations resulted in sub-50 nm particles, large concentrations of poloxamers were needed, which created a toxic formulation as assessed in zebrafish and mice. When prepared as nanoemulsions, it was revealed that medium chain triglycerides (MCT) oil was required as a cosolvent as it enhanced the lipophilicity of the hydrophobic droplet. A few promising nanoemulsions were produced that utilized lipophilic HILs, which resulted in extremely stable particles with small particle sizes of approximately 200 nm.

In a smaller, but significant project, an MCT-only nanoemulsion was formulated that was capable of delivering small interfering RNA (siRNA), a therapeutic nucleic acid. The hydrophilicity of the siRNA was overcome by pairing it with a cationic lipid, allowing the complex to be solubilized at a high concentration in MCT. The nanoemulsion displayed a small size and remarkable stability and was able to facilitate gene knockdown in an *in vivo* murine tumor model.

### 6.1.1 Synthesis and characterization of cholinium-based HILs

Chapters 2 and 3 describe the design, synthesis, and application of new HILs. Many traditional HILs are toxic due to their cations, which are typically composed of long alkyl chains and heteroaromatic headgroups. As an alternative strategy, cholinium, a biologically-essential nutrient, was chosen. Although long alkyl chains were needed to increase hydrophobicity, a Gemini architecture was employed that tethered the alkyl chains in between two cholinium moieties. This structure was found to induce less toxicity than monocholinium species with long alkyl chains in both mammalian cells and zebrafish. The anion proved to be more difficult, and as such, the majority of the first chapter is dedicated to the synthesis of diverse anions. Initially, the dicholinium cations were paired with bis(trifluoromethanesulfonyl)amide ([NTf<sub>2</sub>]), which is a non-coordinating anion that is commonly used in the synthesis of HILs. While the [NTf<sub>2</sub>] formed HILs with low melting points and acceptable viscosities and water solubilities, the anions caused severe morphological defects in zebrafish at sub-millimolar concentrations, despite having a modest toxicity profile in mammalian cells.

As a result, a series of anions were synthesized that utilized the bis(sulfonyl)azanide core but attached different groups onto one or more of the sulfonyl moieties. The first-generation anions have a trifluoromethane group, similar to [NTf<sub>2</sub>], and either an alkyl, aryl, or alkyl-aryl functionalization attached to the bis(sulfonyl)azanide core. When paired with [DC-ether], a dicholinium cation with an alkoxy linker, the resulting ILs displayed a wide variety of physiochemical properties and toxicities. The ILs with alkyl-aryl anions had tremendous *in vitro* and *in vivo* toxicity, while aryl groups such as 2,4,6-trifluorobenzene, 4-methoxybenzene, and tosyl resulted in more favorable LC50 values. However, the aryl-alkyl groups, especially [pOBSNTf], which contains an octyl group, created HILs with low micromolar water solubility. The HILs with first-generation anions also had much higher viscosities than HILs with [NTf<sub>2</sub>] anions.

The second-generation anions removed the trifluoromethane group completely and had aryl moieties on either end of the sulfonyl groups instead. It was discovered that aryl compounds with electron donating groups such as methoxy and methyl resulted in ILs that were water soluble. When these groups were replaced with electron withdrawing functionalities like cyano, nitro, and trifluoromethane, as well as

a hydrophobic tertbutyl group, the water solubility of the corresponding ILs significantly decreased. Unfortunately, these ILs were generally solid at room temperature regardless of the choice of cation. The toxicities of these latter anions varied, as nitro and cyano groups resulted in anions with higher LC50 values in mammalian cells, whereas trifluoromethane and tertbutyl caused higher toxicities. As a result of the unpredictability of the bis(arylsulfonyl)azanide anions, a third generation was started. Although only a few structures have been synthesized, the anions contain an aryl moiety and a short alkyl or alkyl-like chain. The ILs with third-generation anions have much lower melting temperatures at the cost of higher water solubilities. Since only a few anions and ILs have been produced, more work needs to be performed to fully understand this class of compounds.

### *6.1.2 IL formulations*

Two distinct strategies were employed to construct formulations containing ILs, as described in Chapter 4. In the first set of attempts, poloxamers were utilized as they are a triblock polymer that contains alternating polyethylene oxide (PEO) and polypropylene oxide (PPO) units that can interact with ILs and form particles. These formulations were composed of a HILs, one or more poloxamers, and saline. It was found that poloxamers that are longer and have higher proportions of PPO were better able to form small and stable formulations. Although the exact structure of the nanoparticles is unknown, they have sizes of less than 30 nm and likely contain a HIL droplet, as demonstrated by studies involving the successful encapsulation of bovine serum albumin and bovine gamma globulin. Unfortunately, the poloxamer-HIL formulations were toxic in both zebrafish and mice, where in the latter, several mice died after intravenous tail vein injections, probably due to phase separation or aggregation of the particles.

The poloxamer formulations were abandoned due to the toxicity results and a more traditional nanoemulsion approach was tried. Here, the ILs were mixed with DSG-PEG<sub>2000</sub>, a neutral pegylated lipid, using a variety of high energy methods. It was quickly realized that the lack of lipophilicity in the HILs necessitated the use of a cosolvent, as particles composed of only DSG-PEG<sub>2000</sub>, saline, and a HIL quickly phase separated. When MCT was added, the particles were more stable. Increasing the amount of MCT

relative to the HIL resulted in more stable nanoemulsions; however, increasing the overall hydrophobic phase volume while maintaining the same saline volume produced less stable particles. Still, the nanoemulsions encapsulating MCT and a HIL produced severe toxicity in mice upon tail vein injections, likely due to the phase separation of the nanoemulsion. Fortunately, when [DC-ether][2pOBSNTf] was employed as the HIL, the resulting formulation induced no visual toxicity in mice. This is due to the long lipophilic octyl chain that can interact more strongly with MCT.

### *6.1.3 Delivery of hydrophobic siRNA using MCT-containing nanoemulsions*

In Chapter 5, a more traditional nanoemulsion formulation was developed that was able to deliver siRNA. As MCT was used as the hydrophobic phase of the nanoemulsion, only lipophilic therapeutics could be dissolved and thus delivered. Since siRNA represents an exciting new class of drugs, the therapeutic was optimized for nanoemulsion-mediated delivery. The hydrophilicity of siRNA was overcome by pairing the nucleic acid with dioleoyl-3-trimethylammonium propane (DOTAP), which is a lipophilic cation. A hydrophobic ion pairing procedure was adopted from an older lipid extraction method and resulted in 99% of the siRNA becoming complexed to DOTAP. This resulting complex is insoluble in water but extremely soluble in MCT. The corresponding emulsion was prepared using high speed homogenization and high pressure microfluidization to produce stable particles with a hydrodynamic diameter of ~135 nm, as evaluated by nanoparticle tracking analysis.

Encapsulation efficiency was calculated using a fluorescent siRNA, and it was revealed that 85% of the siRNA stayed in the nanoemulsion. Gratifyingly, the particles are stable for over two-hundred days in 4 °C storage conditions, only increasing in size by ~10 nm. Additionally, the siRNA showed no signs of degradation during this time period, despite the tendency of siRNA to decompose in these conditions. In an *in vivo* study, the nanoemulsion facilitated gene knockdown in a murine tumor model of Twist1, an oncoprotein involved in tumor metastasis. Upon inspecting the mice for toxicity, no liver or spleen damage was observed.

## 6.2 Final Remarks

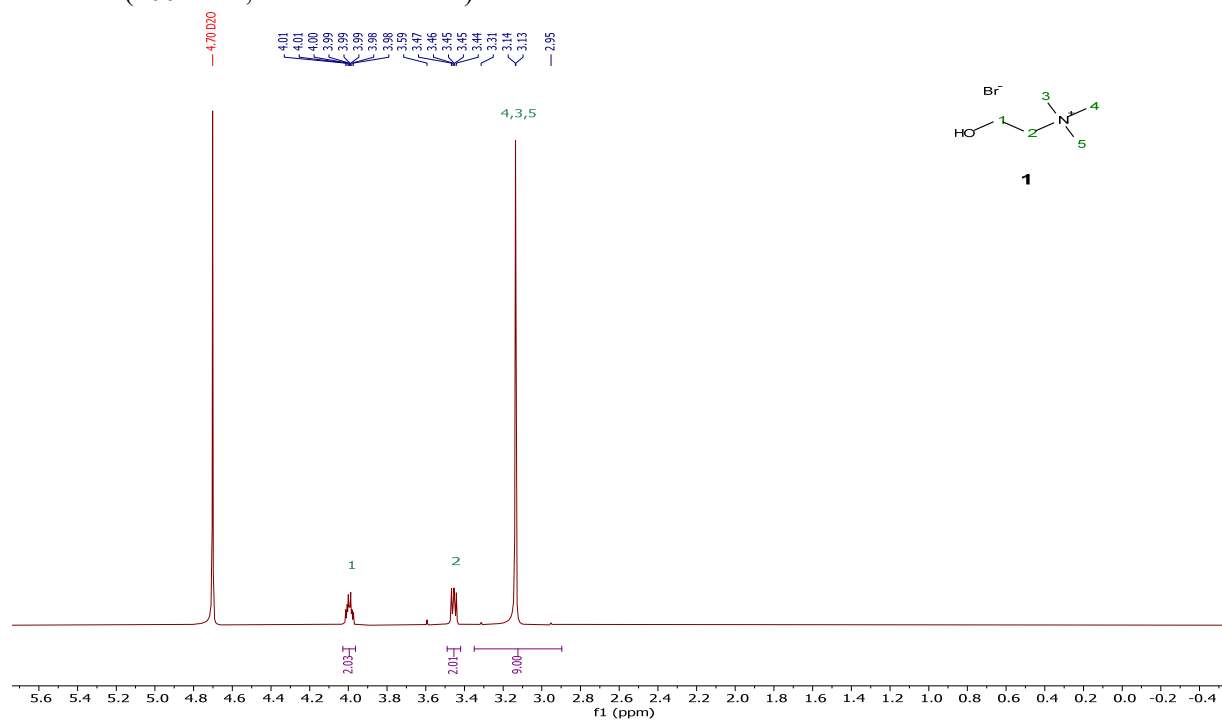
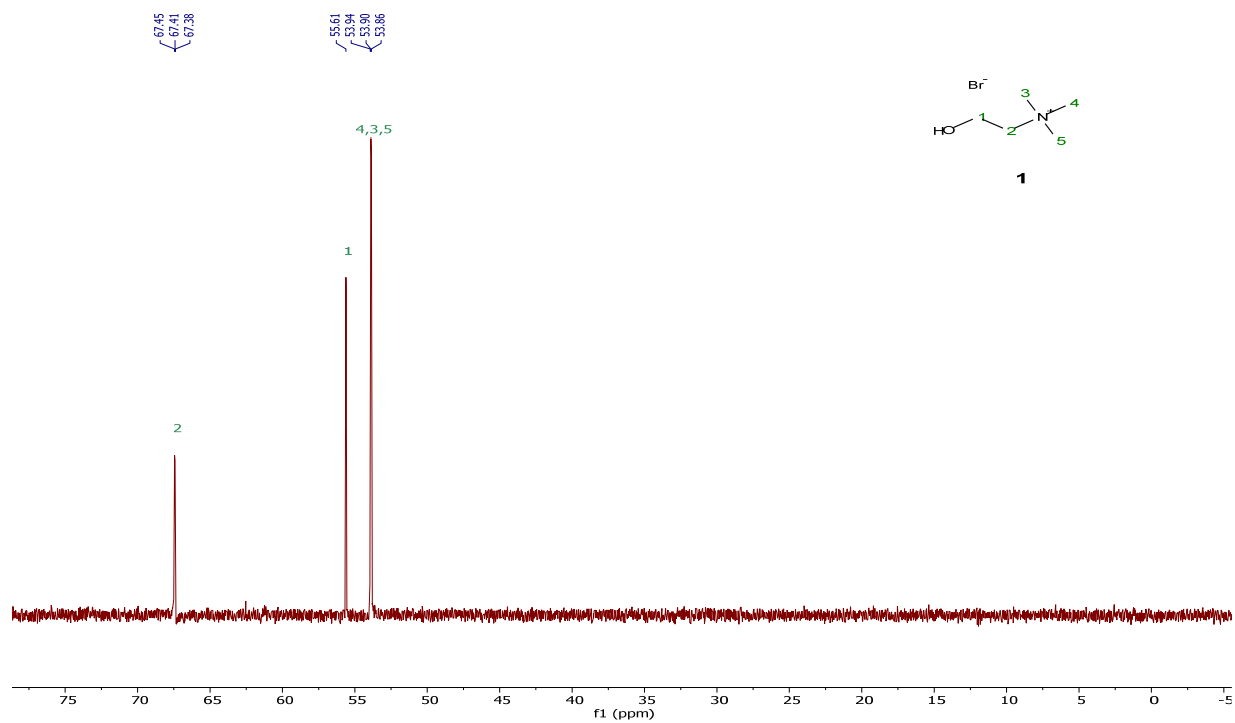
The development and application of HILs in the Mecozzi lab began only a few years ago but has since blossomed into an exciting project with the potential to be applied to different research fields. Due to the newness of the project, much of the work has been on the synthesis and characterization of novel cations and anions that can form low toxic HILs with favorable physicochemical properties. Still, there is room to develop the next-generation of HILs. From the results in Chapter 2 and 3, the aryl groups seem to significantly increase melting temperature and viscosity, regardless of the functionalization. Future HILs should incorporate other moieties, such as short alkyl chains with electron withdrawing groups. Additionally, although the cholinium-based cations have an excellent toxicity profile, the dicholinium species may be too hydrophilic to be employed. Cholinium cations with medium length alkyl chains, show enhanced hydrophobicity and have low toxicity relative to longer alkyl chains. Additionally, branching alkyl chains may offer a solution to decrease water solubility and maintain a favorable toxicity profile.

While new classes of HILs have been developed, they have not been successfully applied to produce nanoemulsions capable of delivering therapeutics in a safe and effective manner. This is likely due to the lack of lipophilicity present in the current anions and cations, which makes the liquid incompatible with lipophilic polymers such as DSG-PEG<sub>2000</sub>. As a result, a large amount of the hydrophobic droplet needs to be composed of MCT to help stabilize the particles. There are two viable solutions for this problem: either the polymer is changed so that it has an aqueous block and a block compatible with HILs, or the HILs themselves need to become more lipophilic. For the latter case, the aforementioned strategies may be offer solutions to this problem.

Lastly, the project involving the delivery of hydrophobic siRNA was successful *in vivo*, although there is still room to study and optimize the formulation. The drug release in saline and *in vivo* is an unknown, yet essential, parameter that can be solved through the clever utilization of fluorescent siRNA. Additionally, the formulation procedure and composition can be altered to create smaller and more stable particles. In terms of the drug choice, the hydrophobic ion pairing strategy can likely be applied to other nucleic acid drugs like plasmids and mRNA.

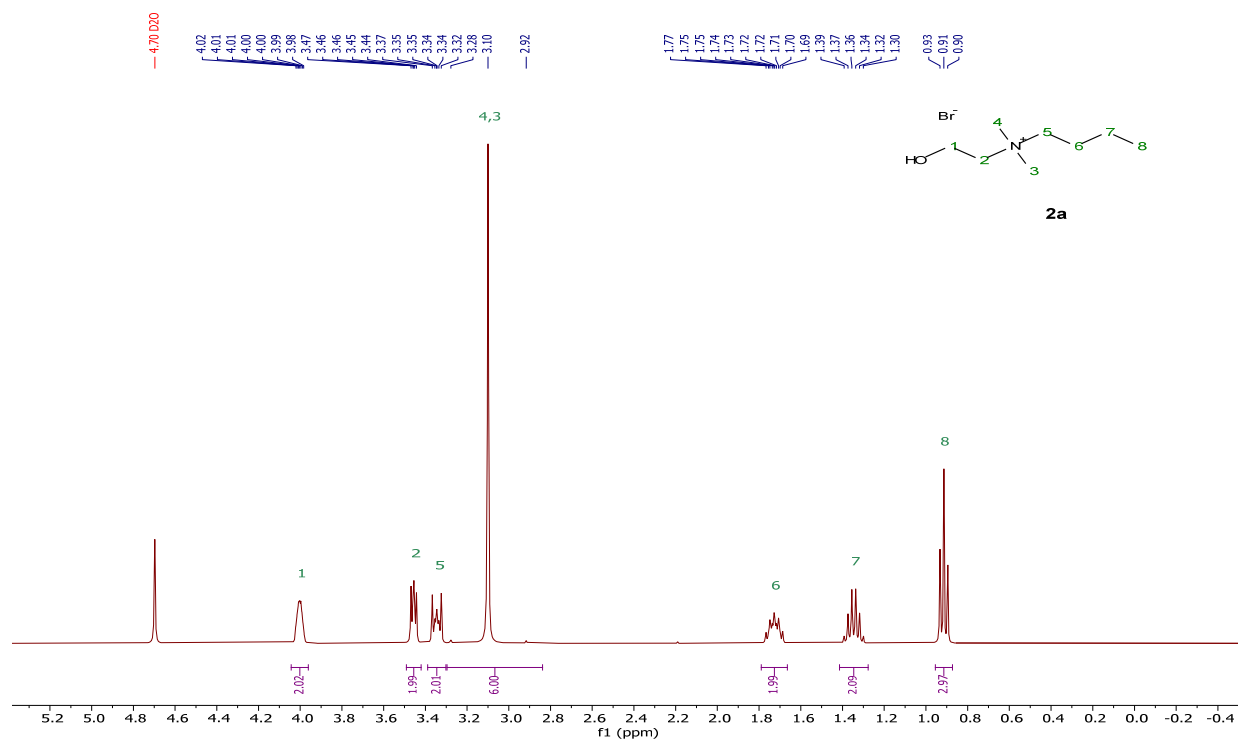
## **APPENDIX**

## A.1 Nuclear Magnetic Resonance Spectra for Synthesis

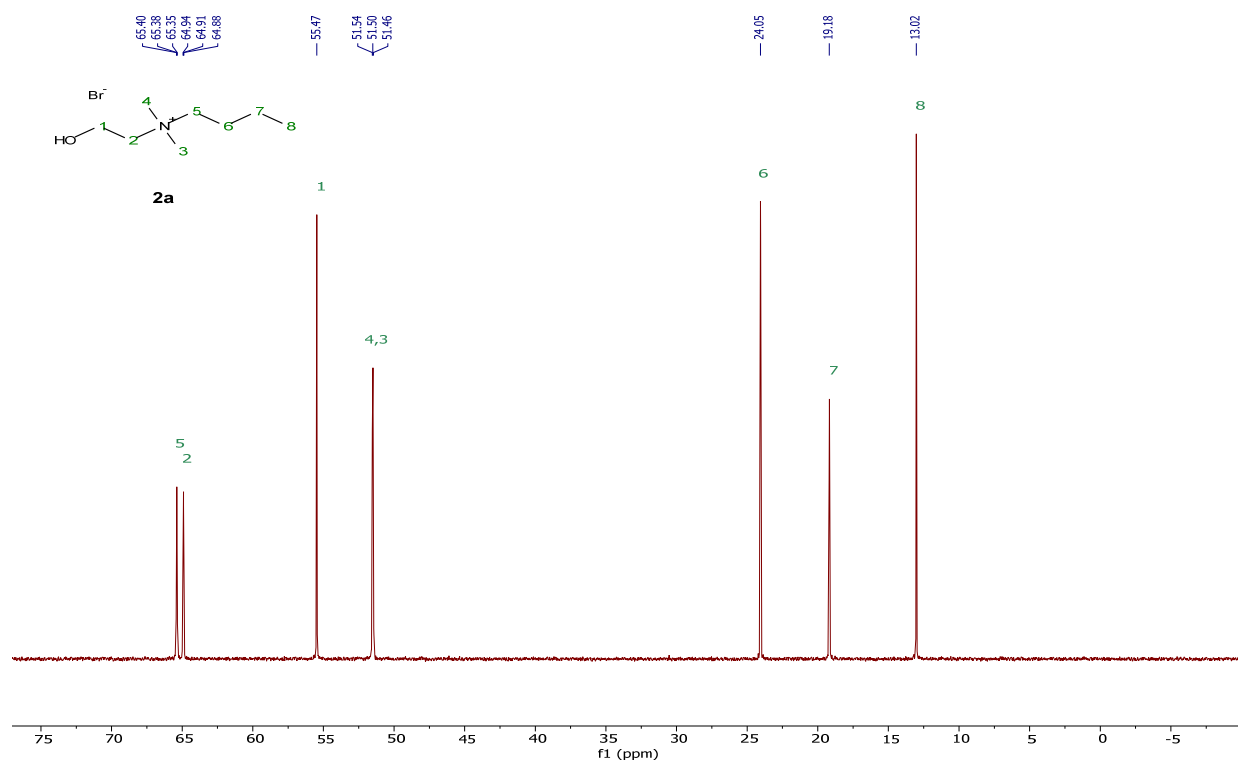
[chol][Br], **1** $^1\text{H}$  NMR (400 MHz, Deuterium Oxide) $^{13}\text{C}\{^1\text{H}\}$  NMR (101 MHz, Deuterium Oxide)

$[N_{1,1,4,2OH}][Br^-]$ , **2a**

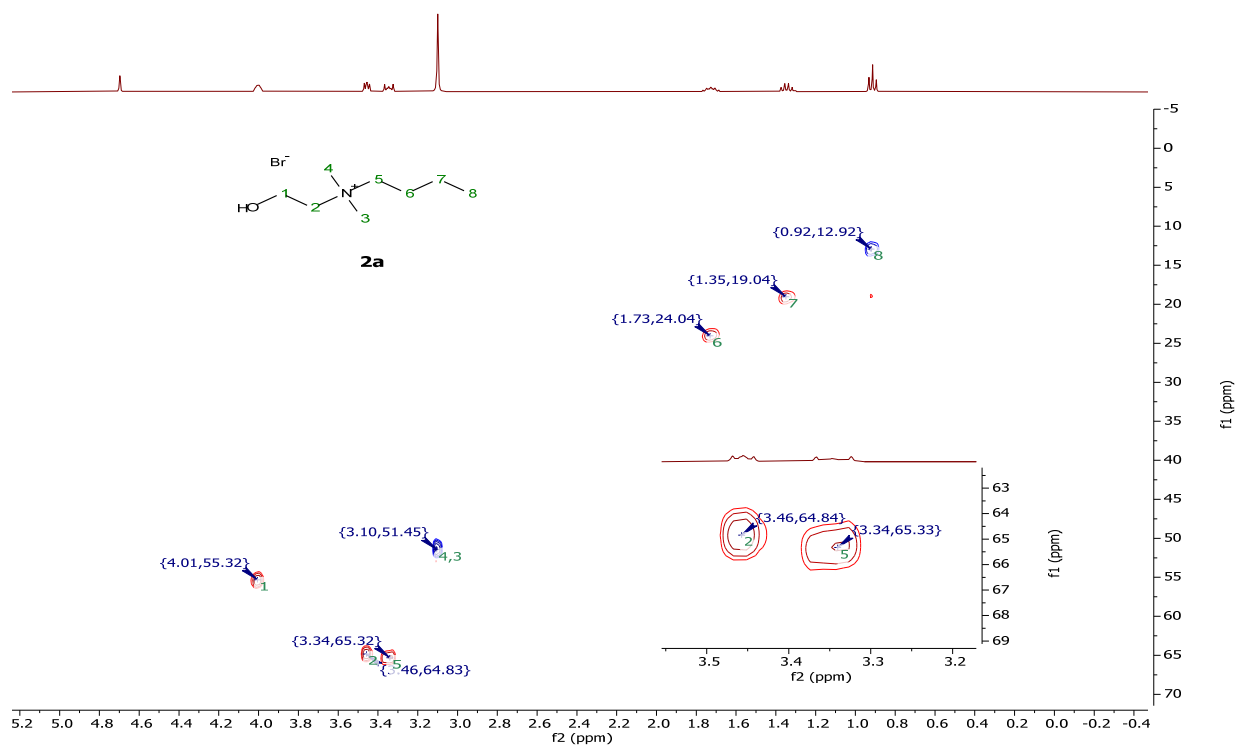
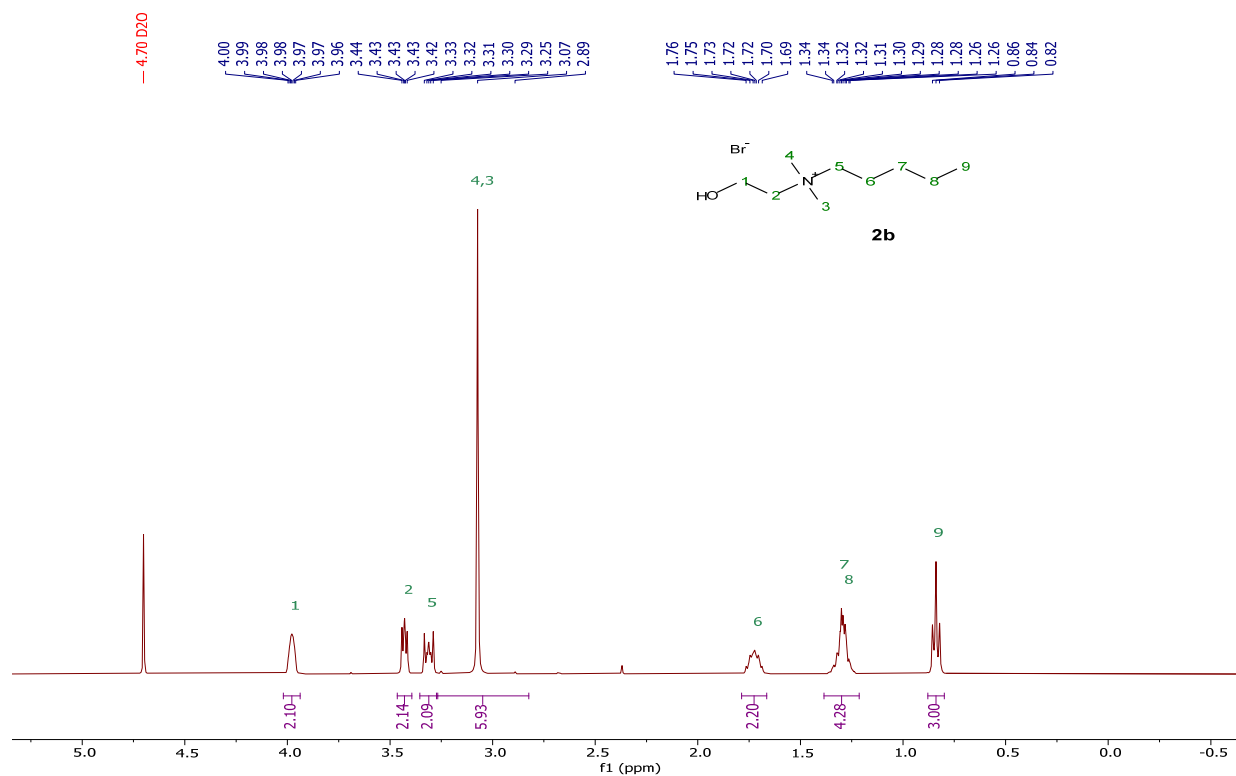
$^1H$  NMR (400 MHz, Deuterium Oxide)

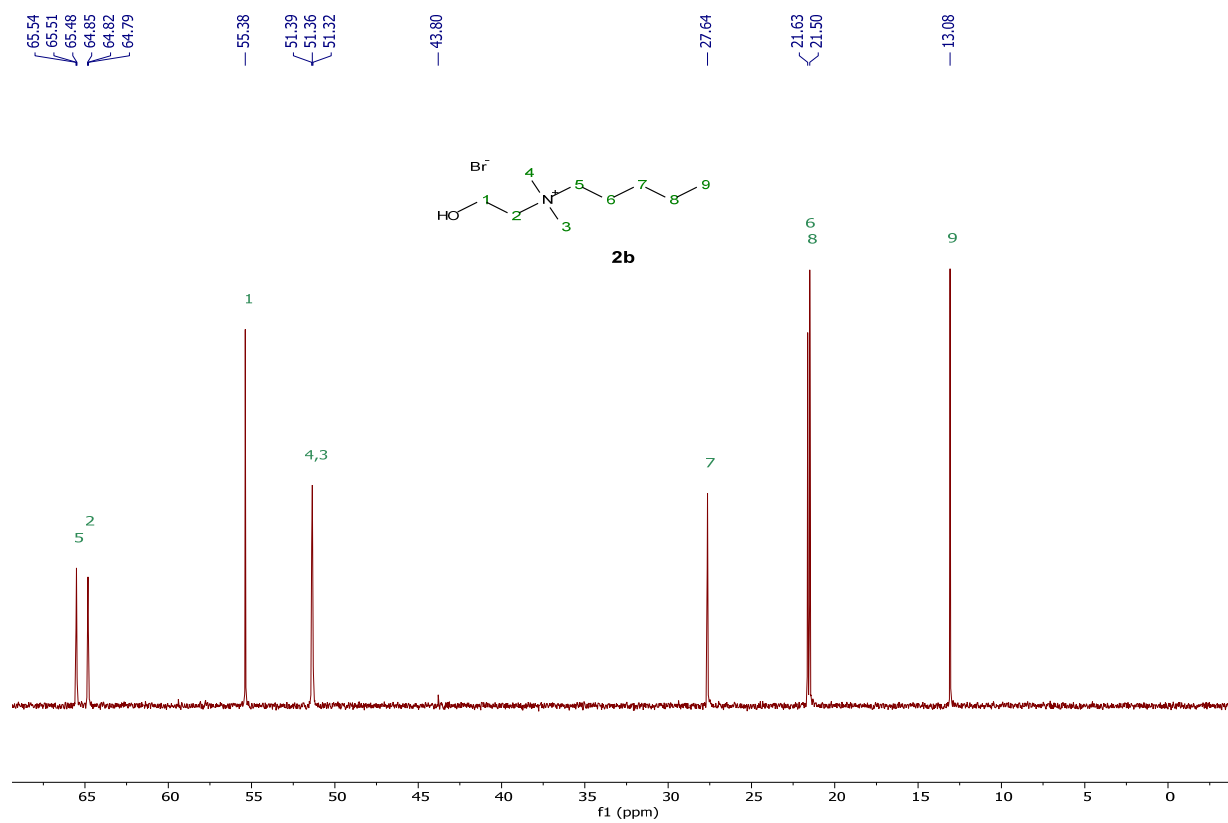
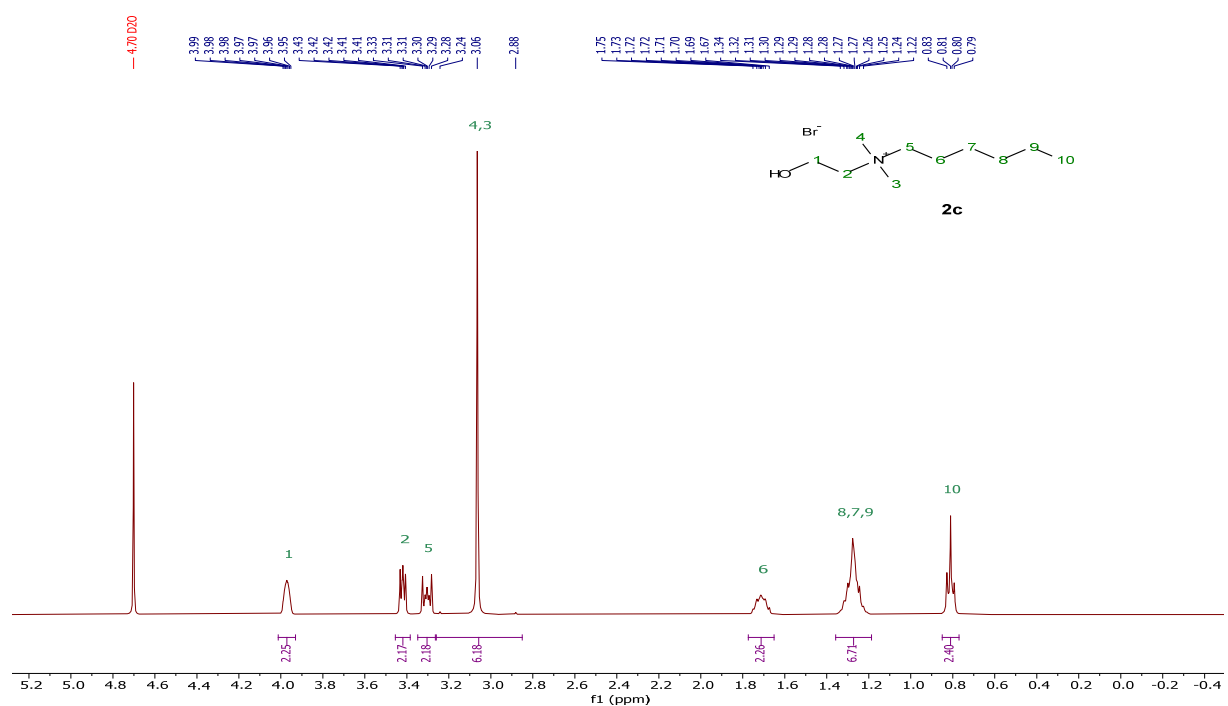


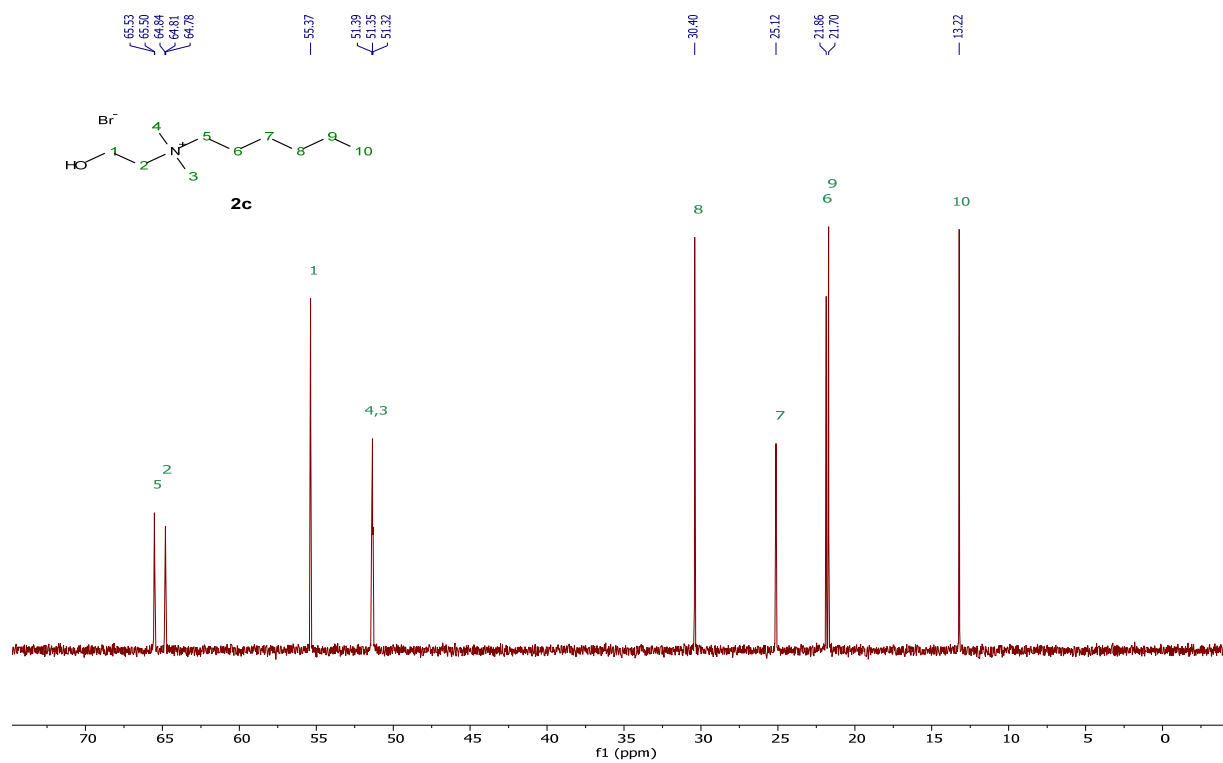
$^{13}C\{^1H\}$  NMR (101 MHz, Deuterium Oxide)



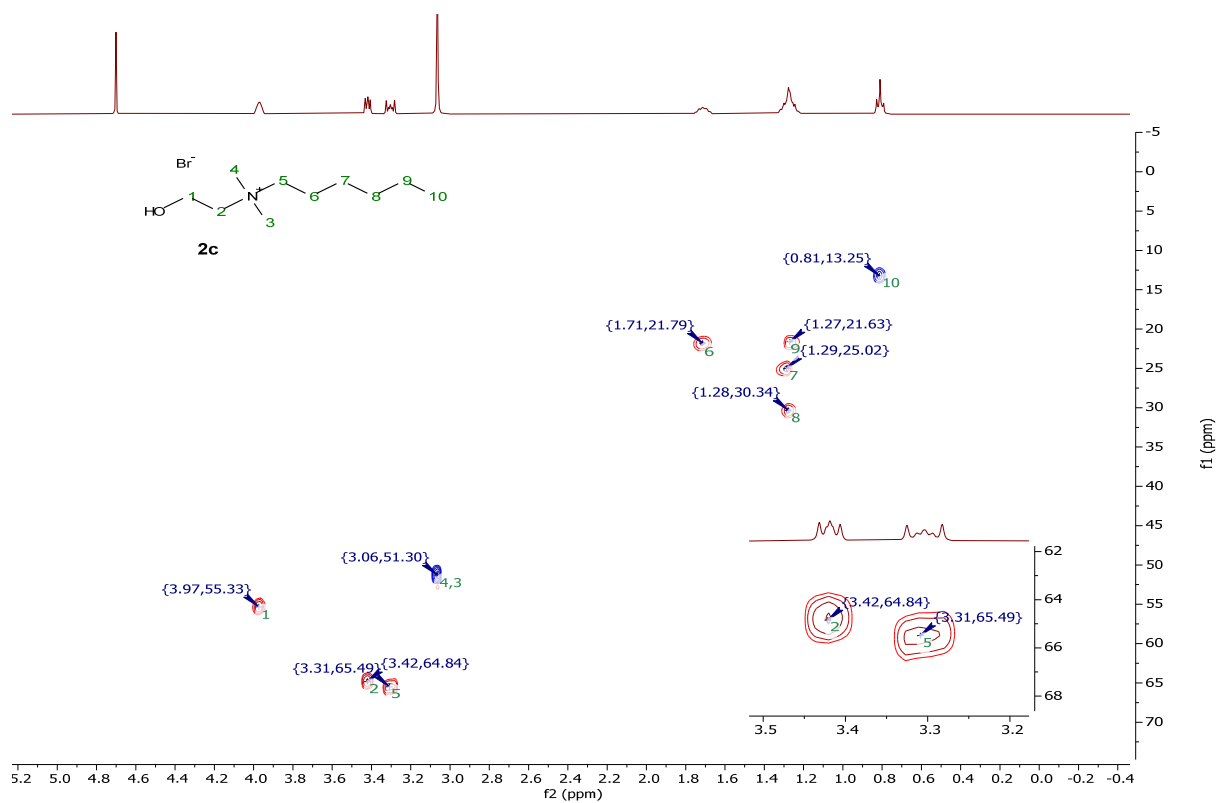
## HSQC (Deuterium Oxide)

 $[\text{N}_{1,1,5,2\text{OH}}][\text{Br}]$ , **2b** $^1\text{H}$  NMR (400 MHz, Deuterium Oxide)

$^{13}\text{C}\{^1\text{H}\}$  NMR (101 MHz, Deuterium Oxide) $[\text{N}_{1,1,6,2\text{OH}}][\text{Br}]$ , **2c** $^1\text{H}$  NMR (400 MHz, Deuterium Oxide)

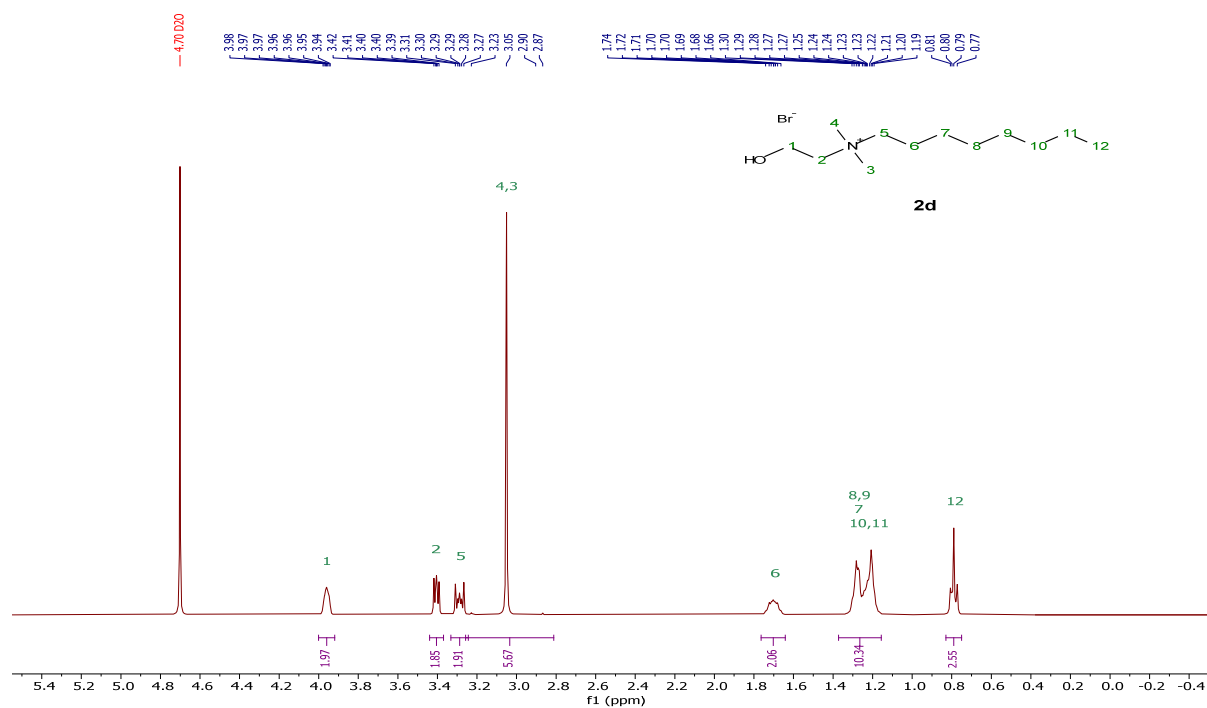
$^{13}\text{C}\{^1\text{H}\}$  NMR (101 MHz, Deuterium Oxide)

## HSQC (Deuterium Oxide)

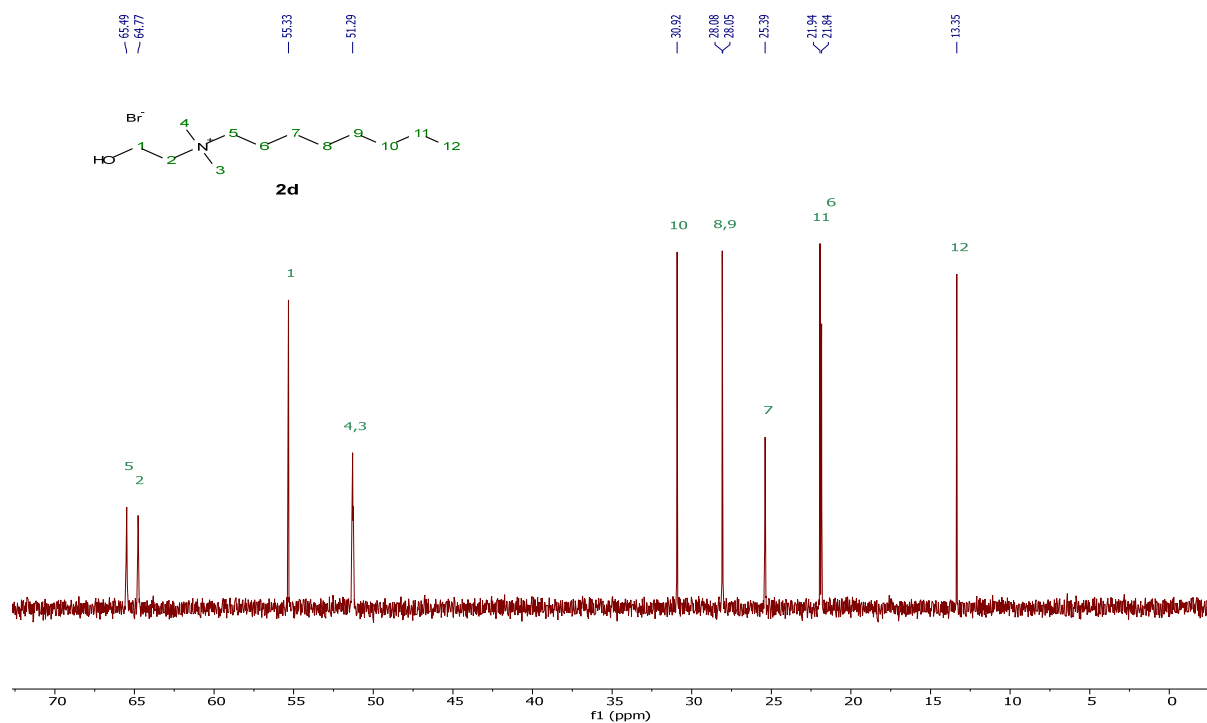


[N<sub>1,1,8,2OH</sub>][Br<sup>-</sup>], **2d**

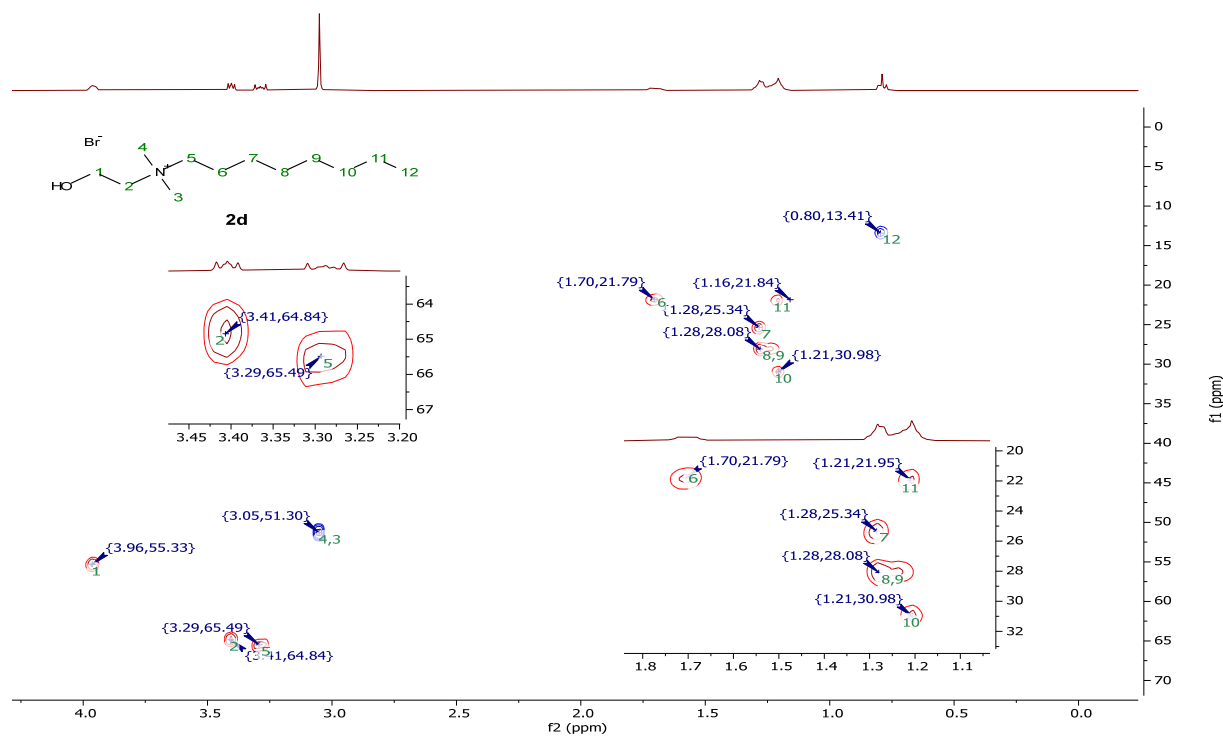
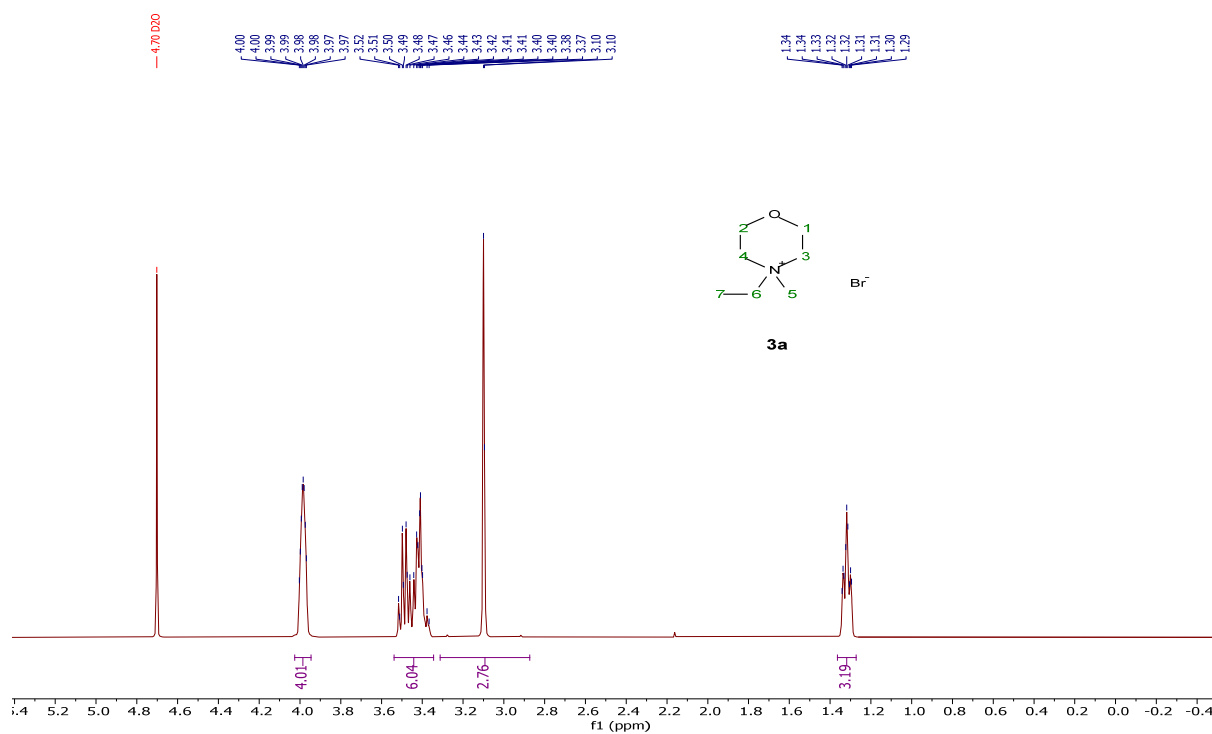
<sup>1</sup>H NMR (400 MHz, Deuterium Oxide)



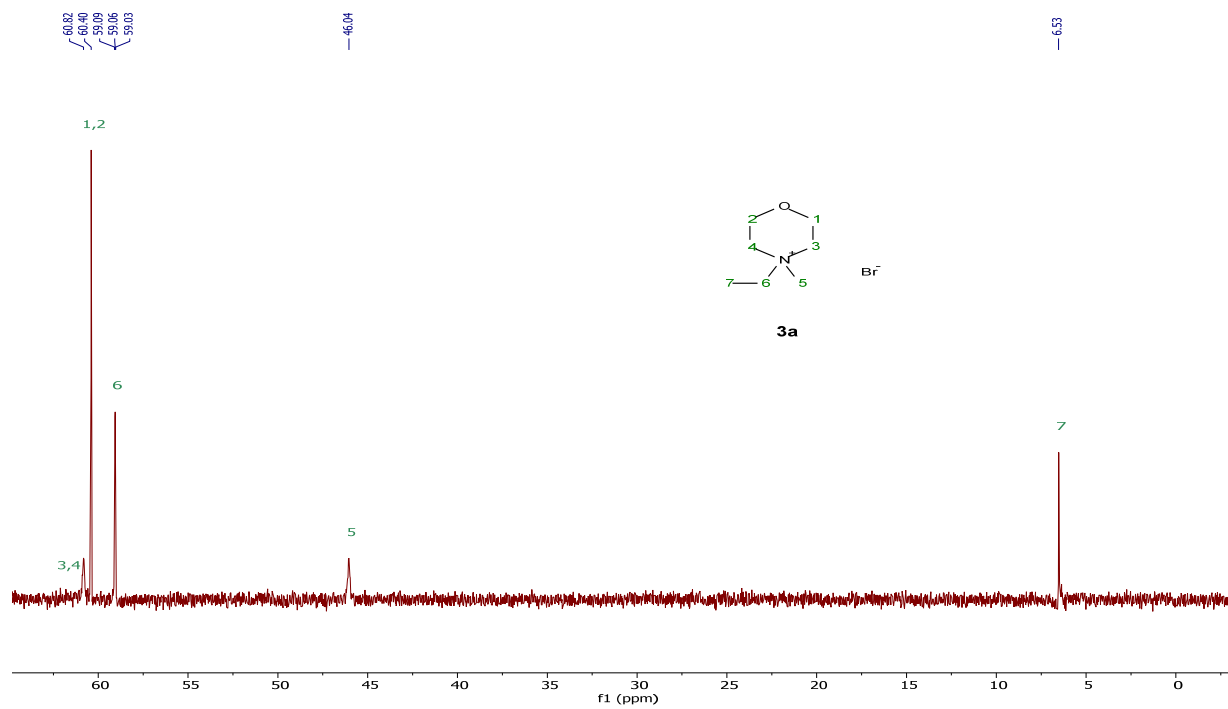
<sup>13</sup>C {<sup>1</sup>H} NMR (101 MHz, Deuterium Oxide)



## HSQC (Deuterium Oxide)

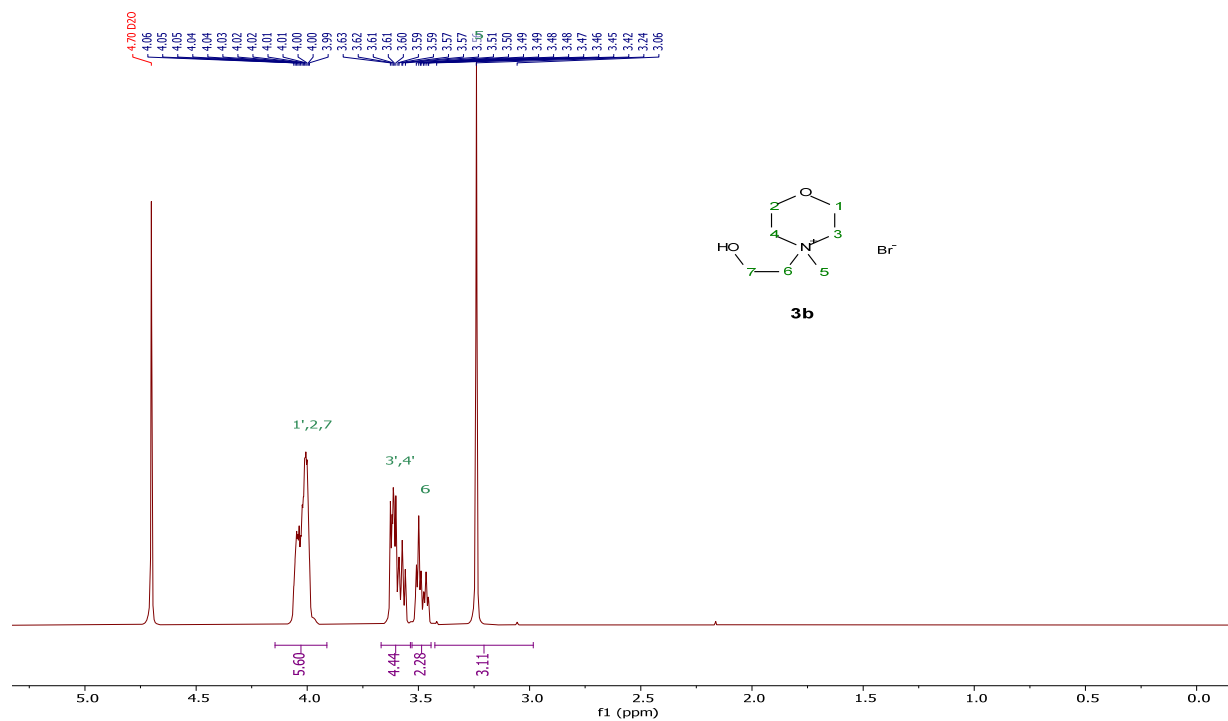
[morph<sub>1,2</sub>][Br], **3a**<sup>1</sup>H NMR (400 MHz, Deuterium Oxide)

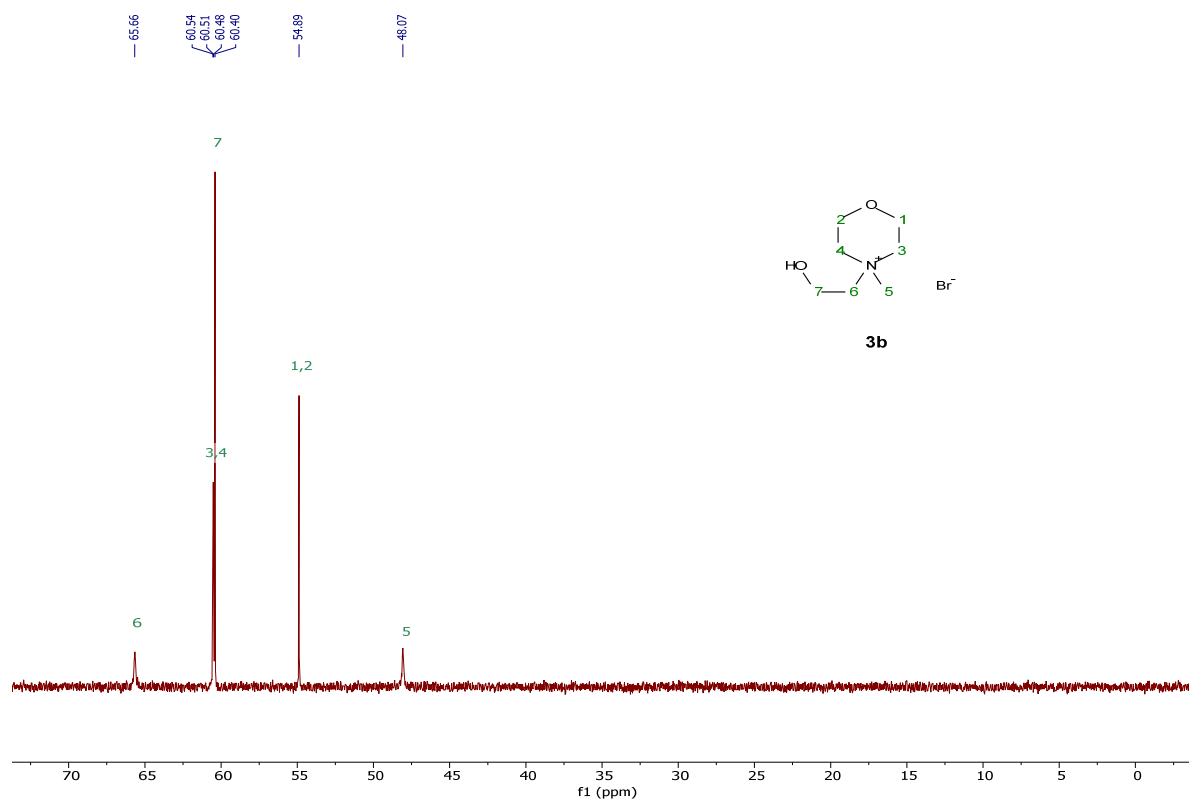
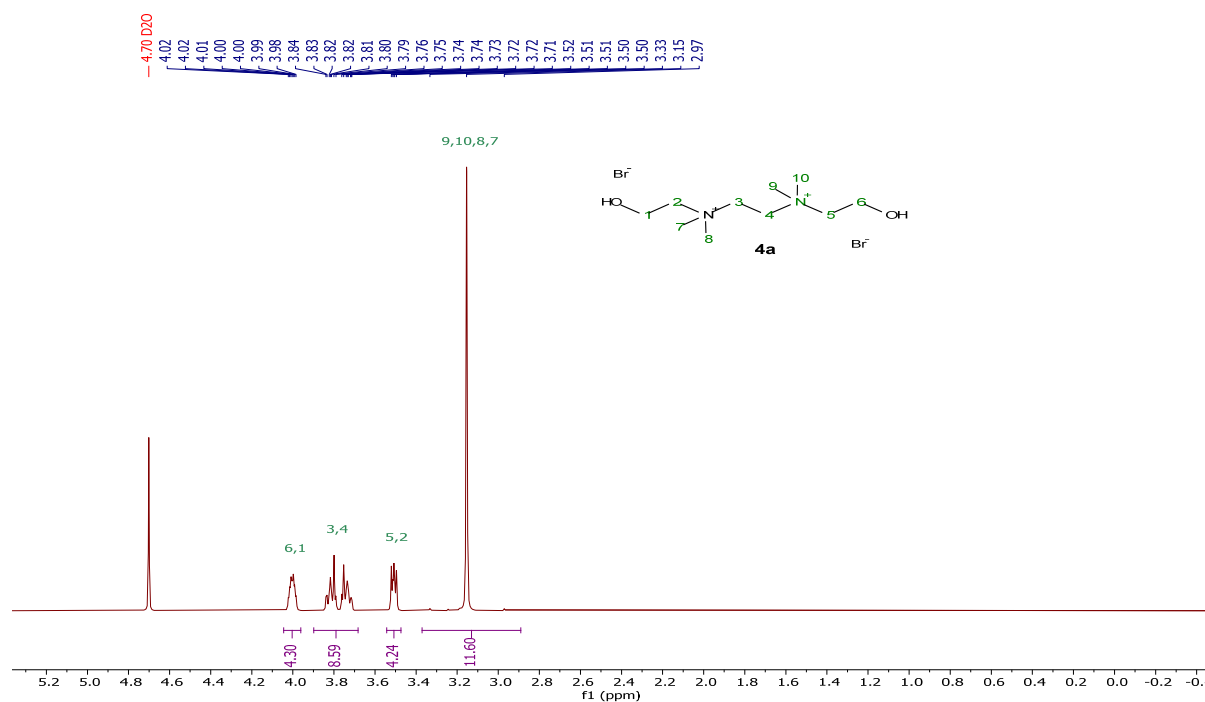
$^{13}\text{C}\{^1\text{H}\}$  NMR (101 MHz, Deuterium Oxide)

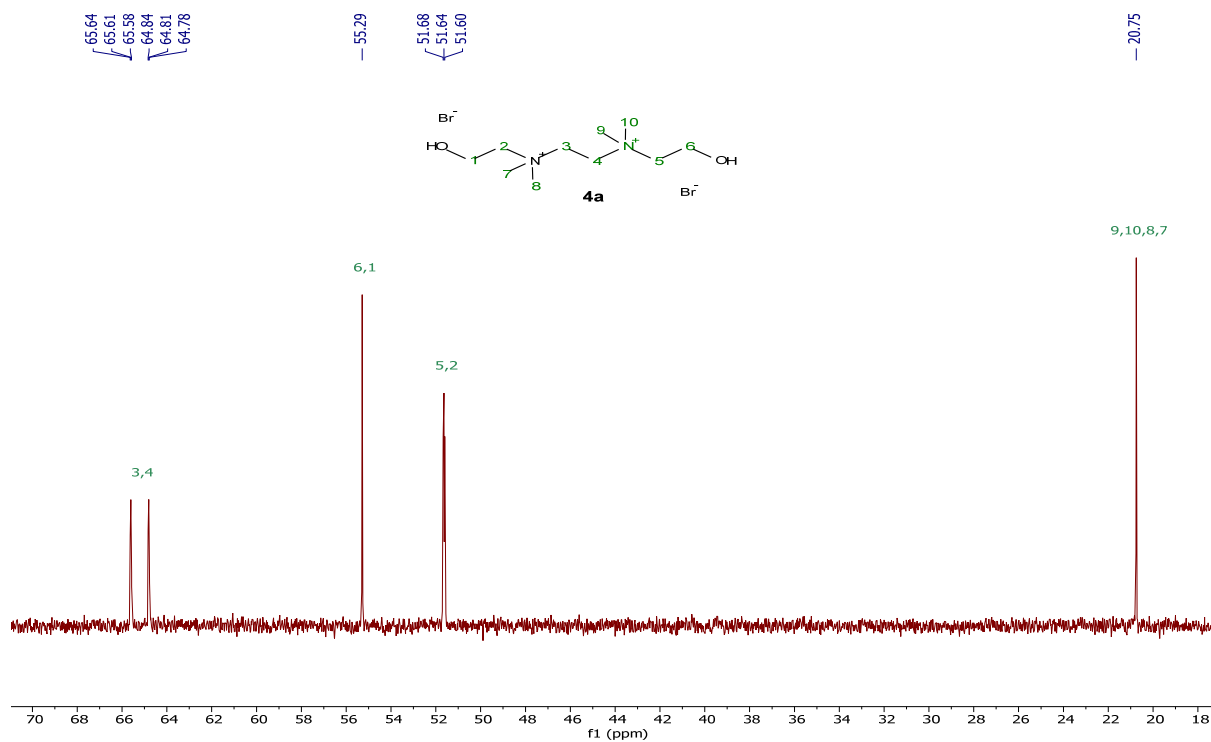
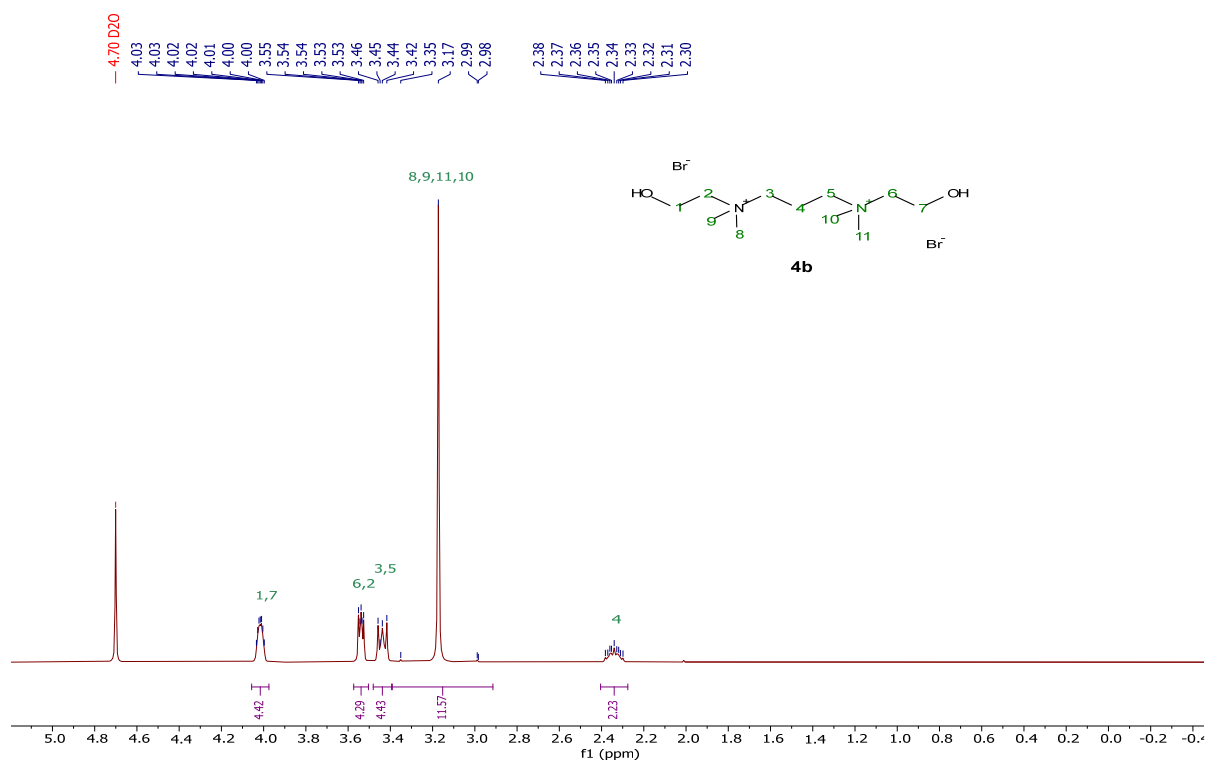


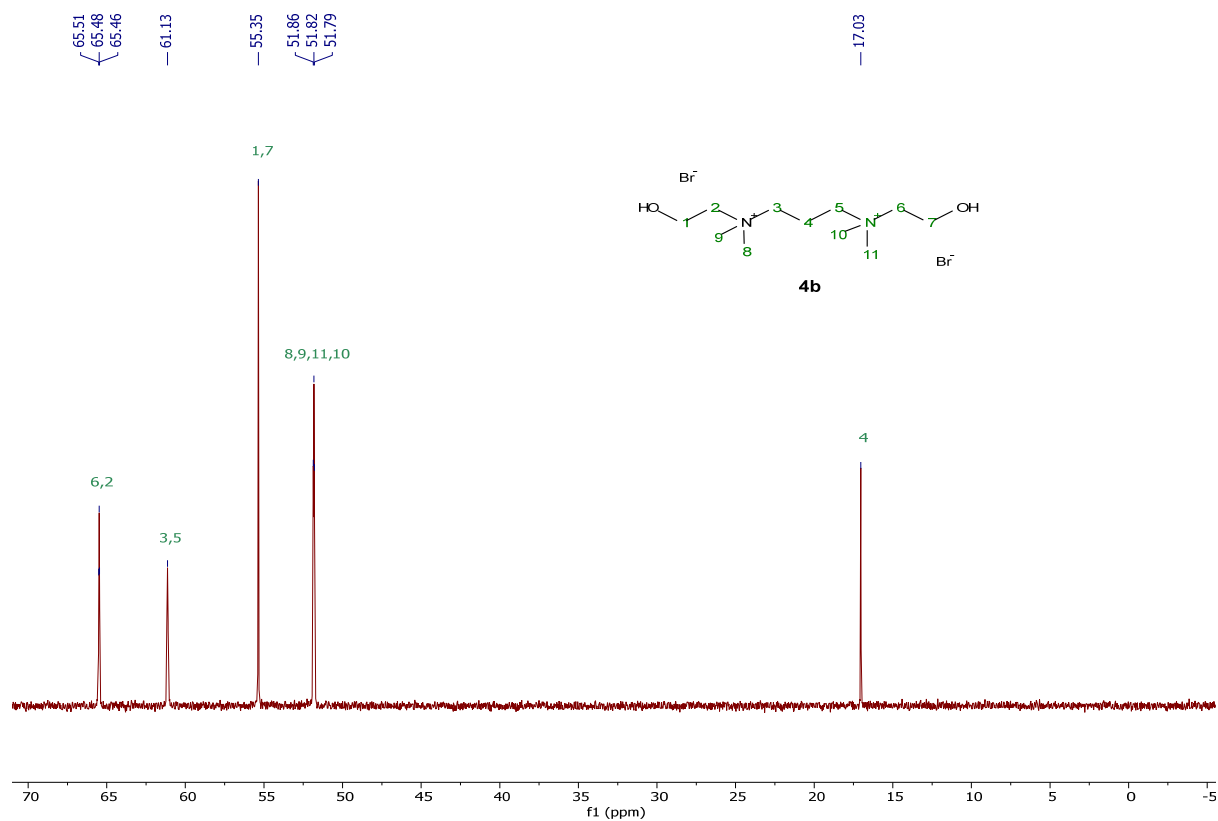
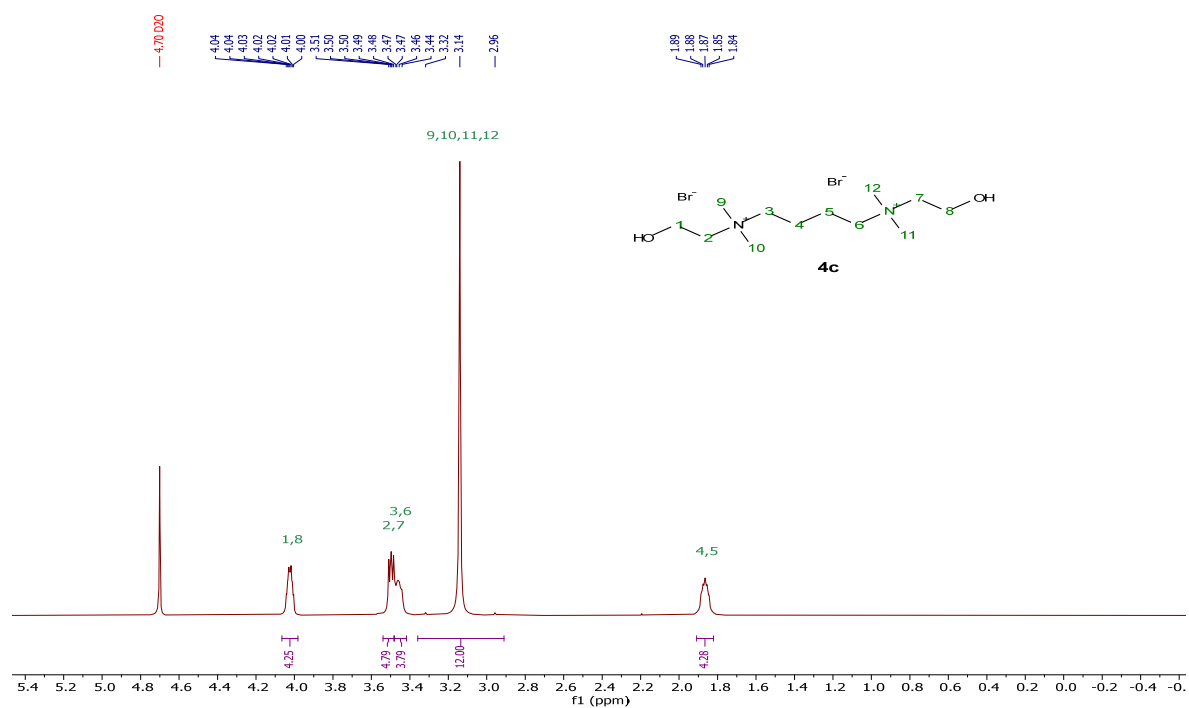
[morph<sub>1,2OH</sub>][Br], **3b**

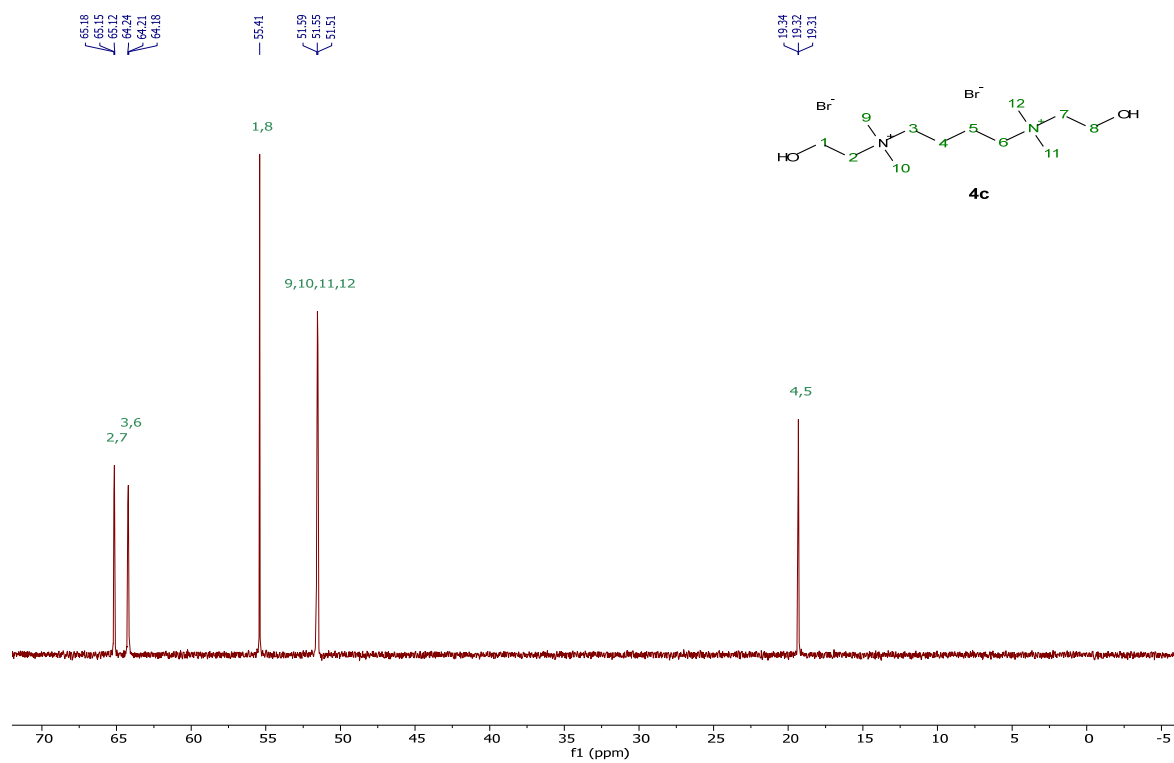
$^1\text{H}$  NMR (400 MHz, Deuterium Oxide)



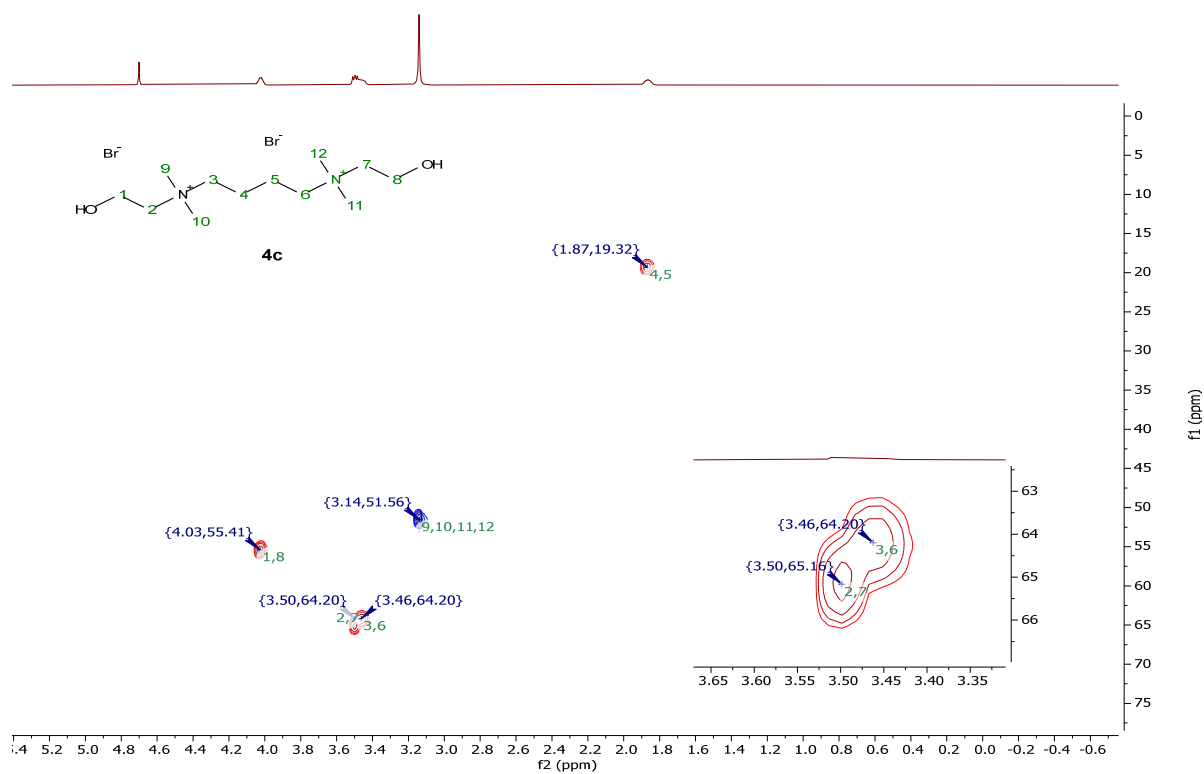
$^{13}\text{C}\{^1\text{H}\}$  NMR (101 MHz, Deuterium Oxide)[DC-2][2Br], **4a** $^1\text{H}$  NMR (400 MHz, Deuterium Oxide)

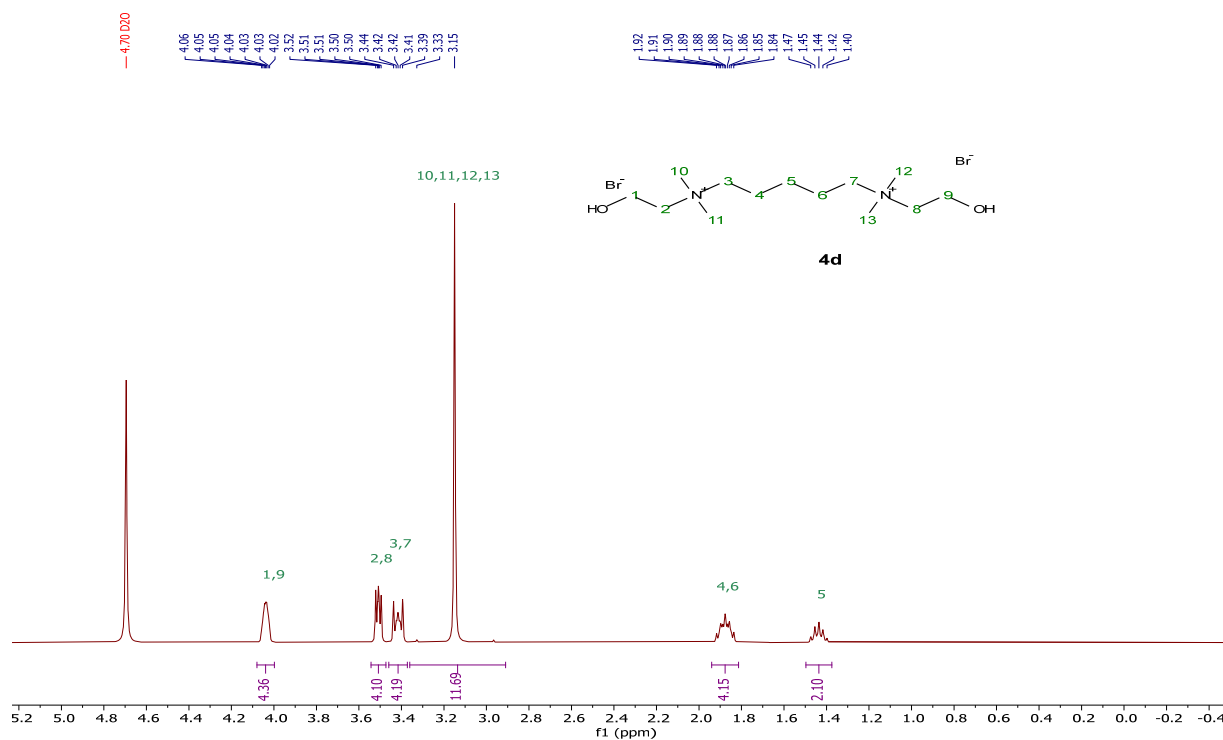
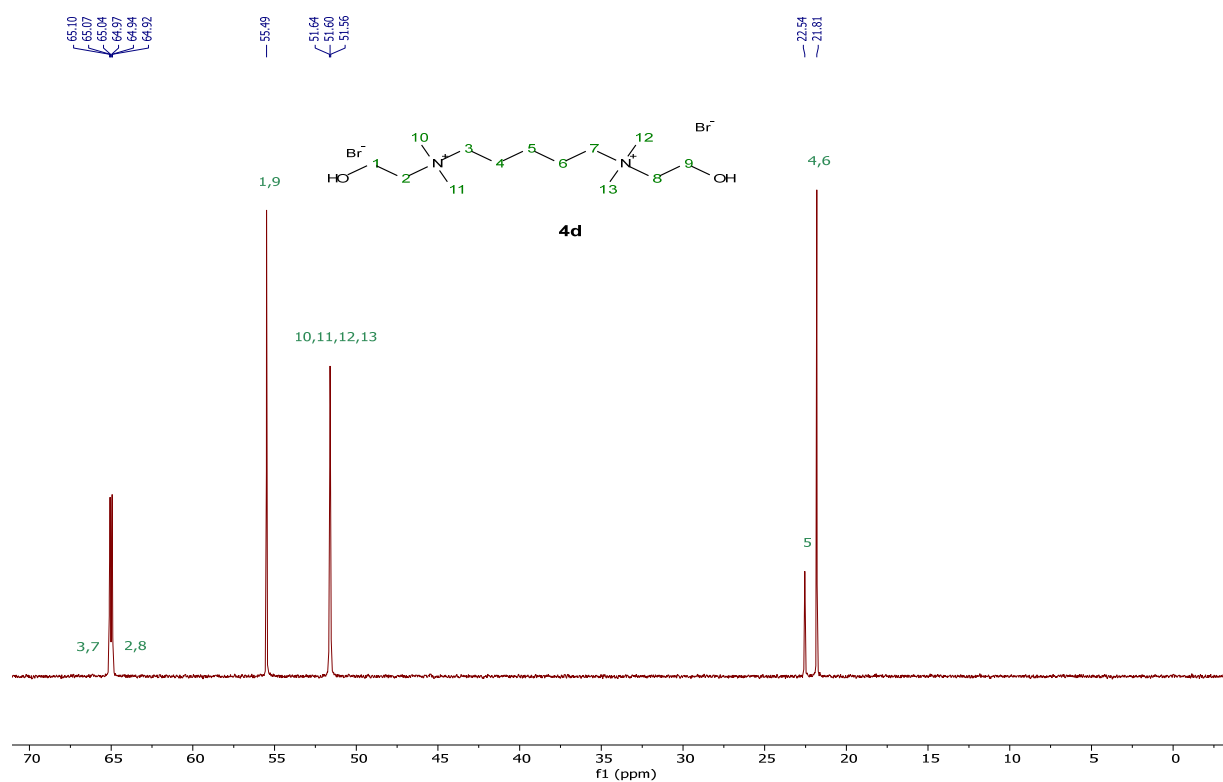
$^{13}\text{C}\{^1\text{H}\}$  NMR (101 MHz, Deuterium Oxide)[DC-3][2Br], **4b** $^1\text{H}$  NMR (400 MHz, Deuterium Oxide)

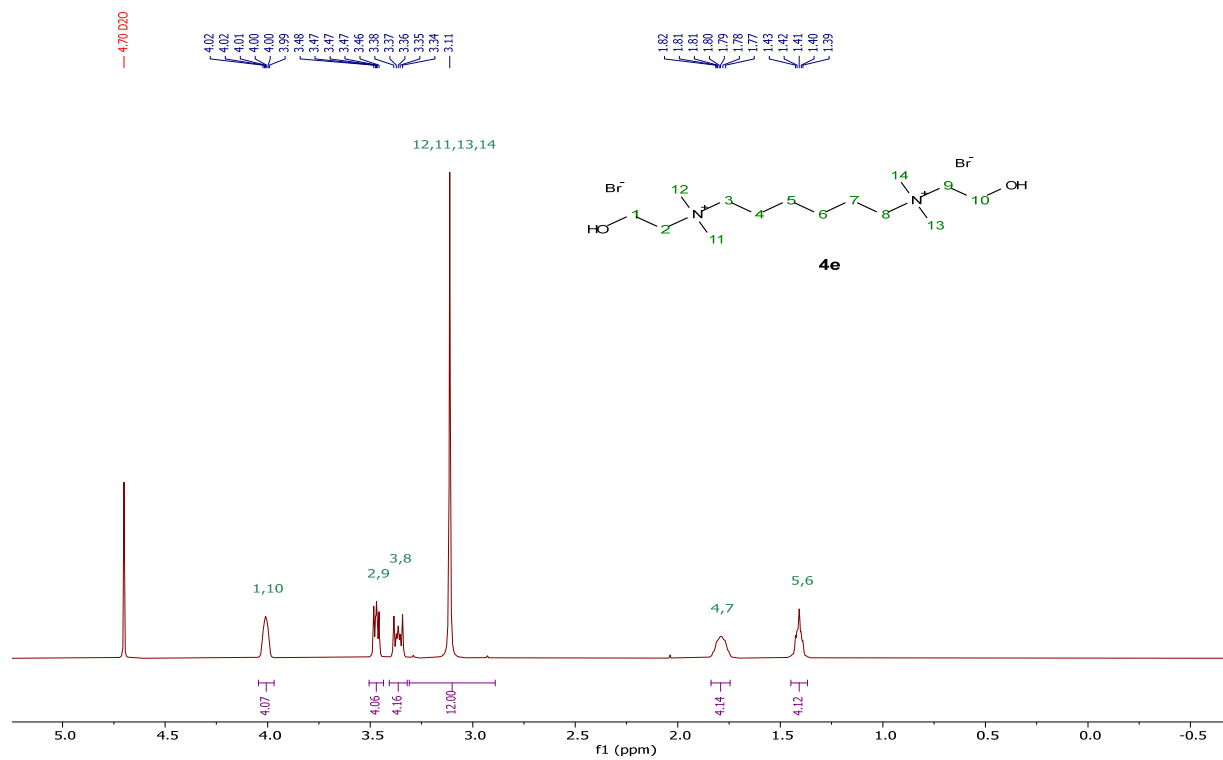
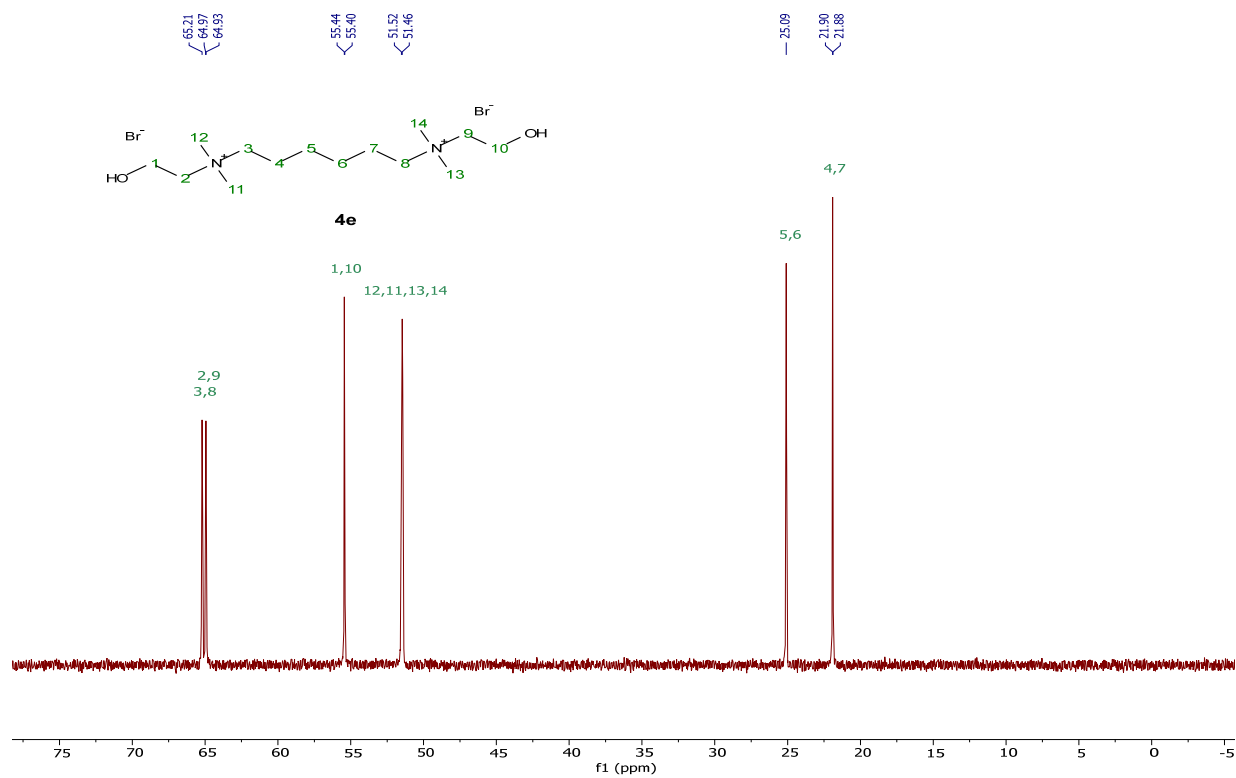
$^{13}\text{C}\{^1\text{H}\}$  NMR (101 MHz, Deuterium Oxide)[DC-4][2Br], **4c** $^1\text{H}$  NMR (400 MHz, Deuterium Oxide)

$^{13}\text{C}\{^1\text{H}\}$  NMR (101 MHz, Deuterium Oxide)

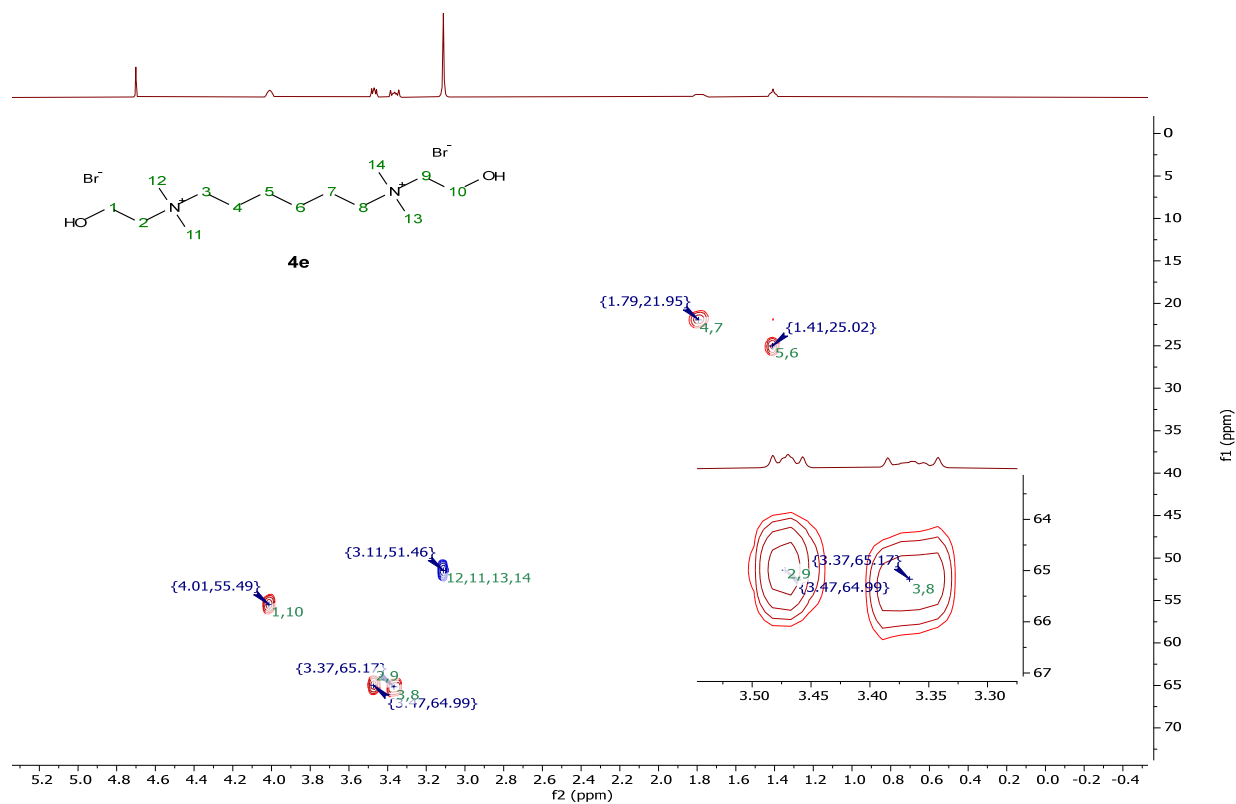
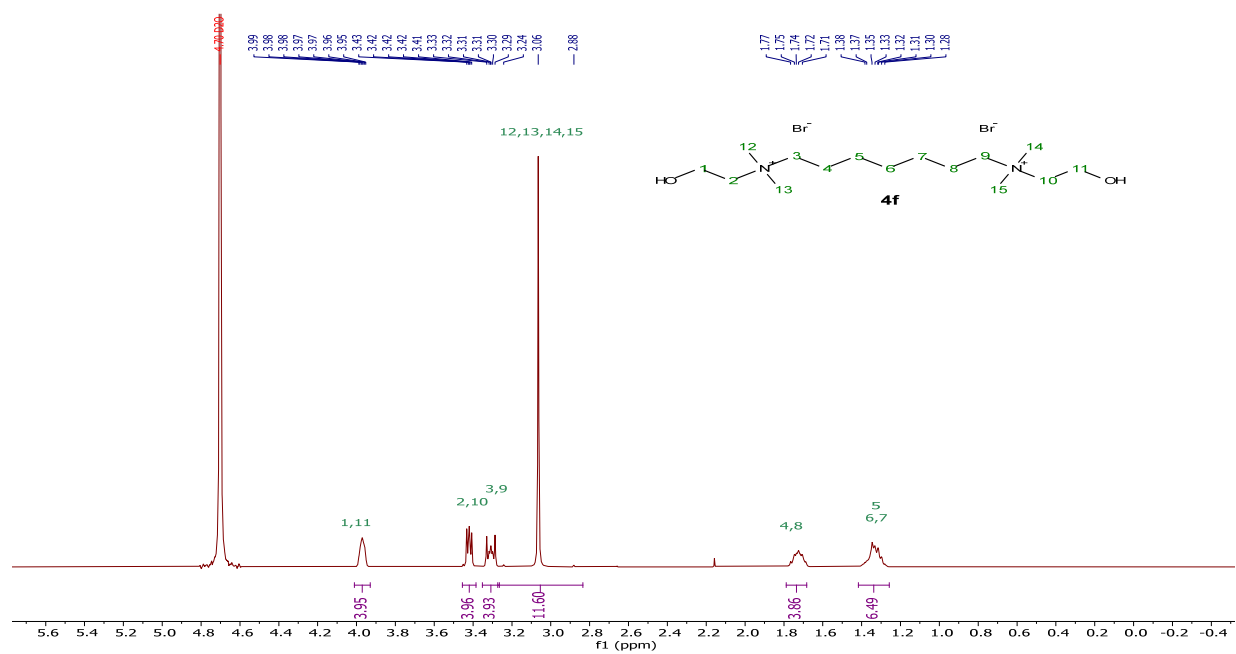
## HSQC (Deuterium Oxide)



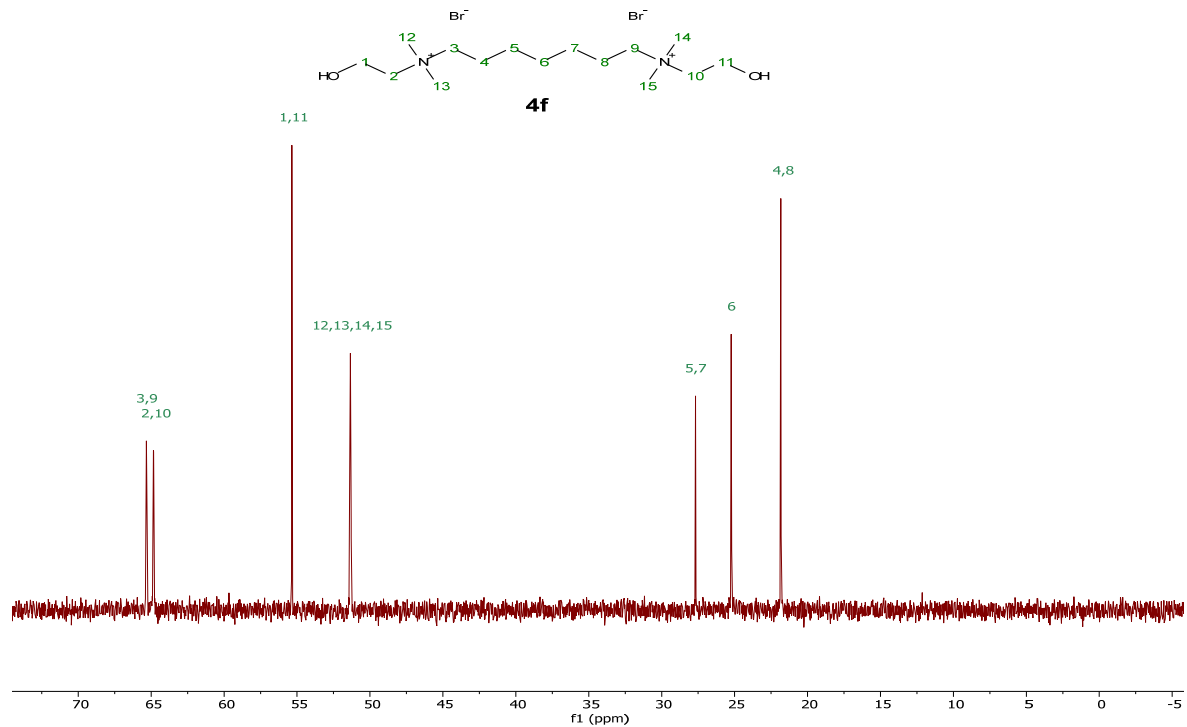
[DC-5][2Br], **4d** $^1\text{H}$  NMR (400 MHz, Deuterium Oxide) $^{13}\text{C}\{^1\text{H}\}$  NMR (101 MHz, Deuterium Oxide)

[DC-6][2Br], **4e** $^1\text{H}$  NMR (400 MHz, Deuterium Oxide) $^{13}\text{C}\{^1\text{H}\}$  NMR (101 MHz, Deuterium Oxide)

## HSQC (Deuterium Oxide)

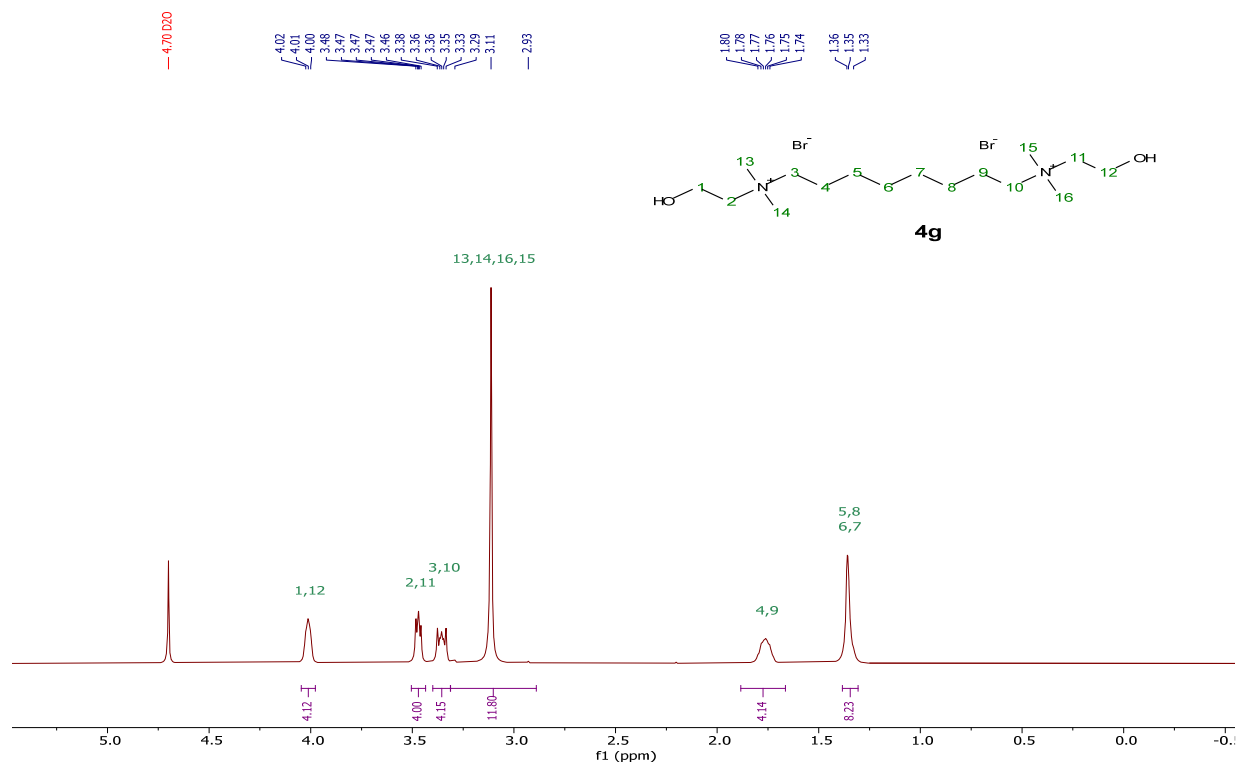
[DC-7][2Br], **4f** $^1\text{H}$  NMR (400 MHz, Deuterium Oxide)

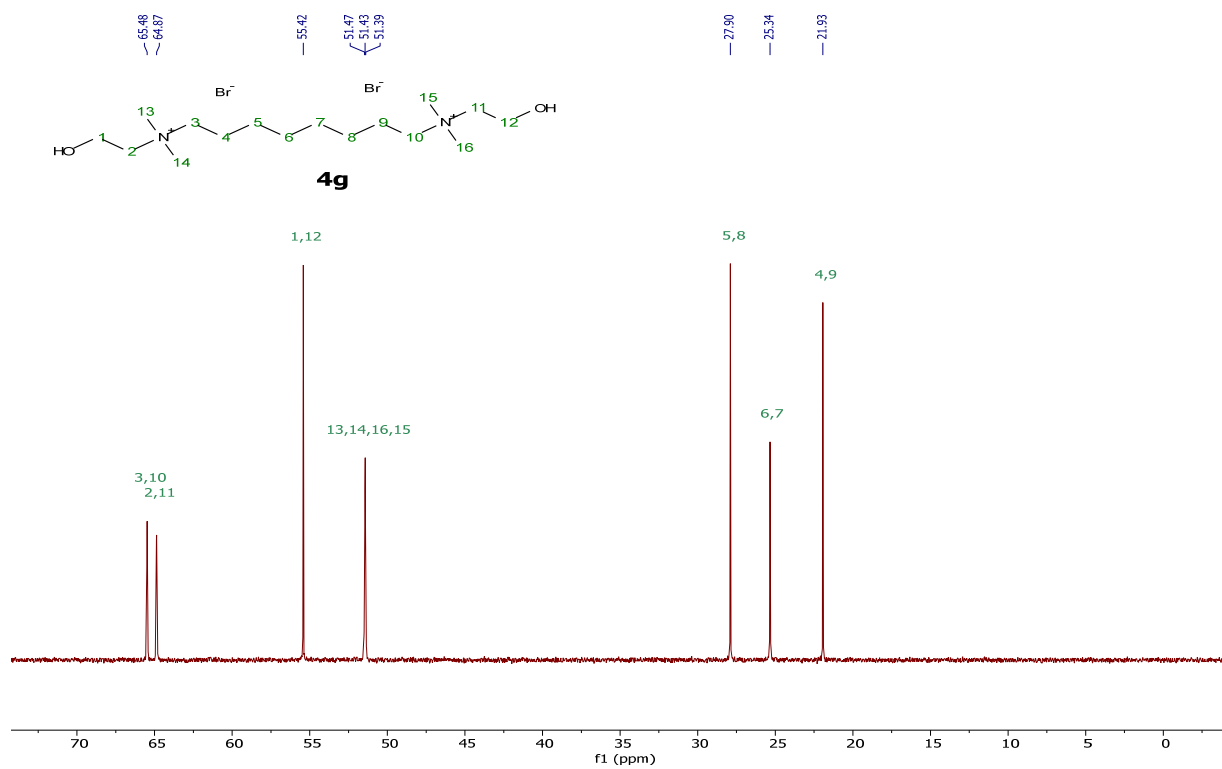
$^{13}\text{C}\{^1\text{H}\}$  NMR (101 MHz, Deuterium Oxide)



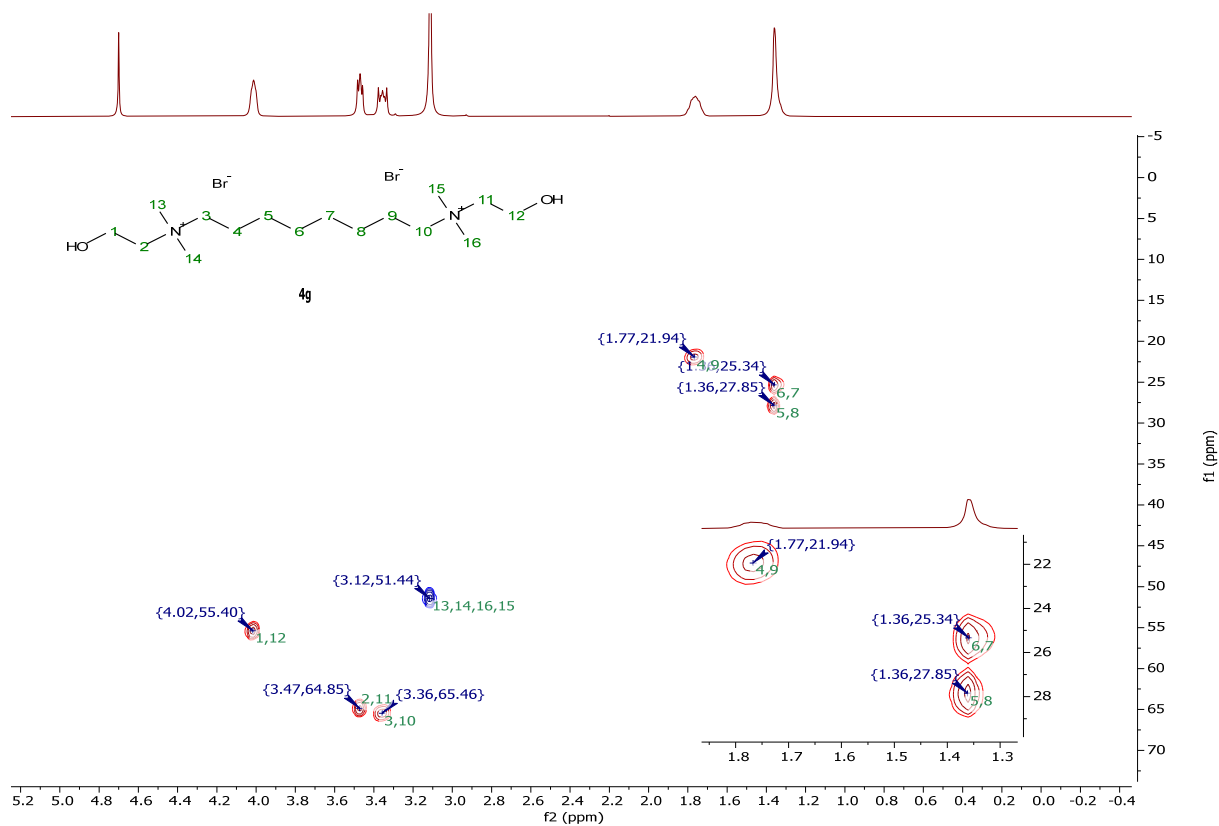
[DC-8][2Br], **4g**

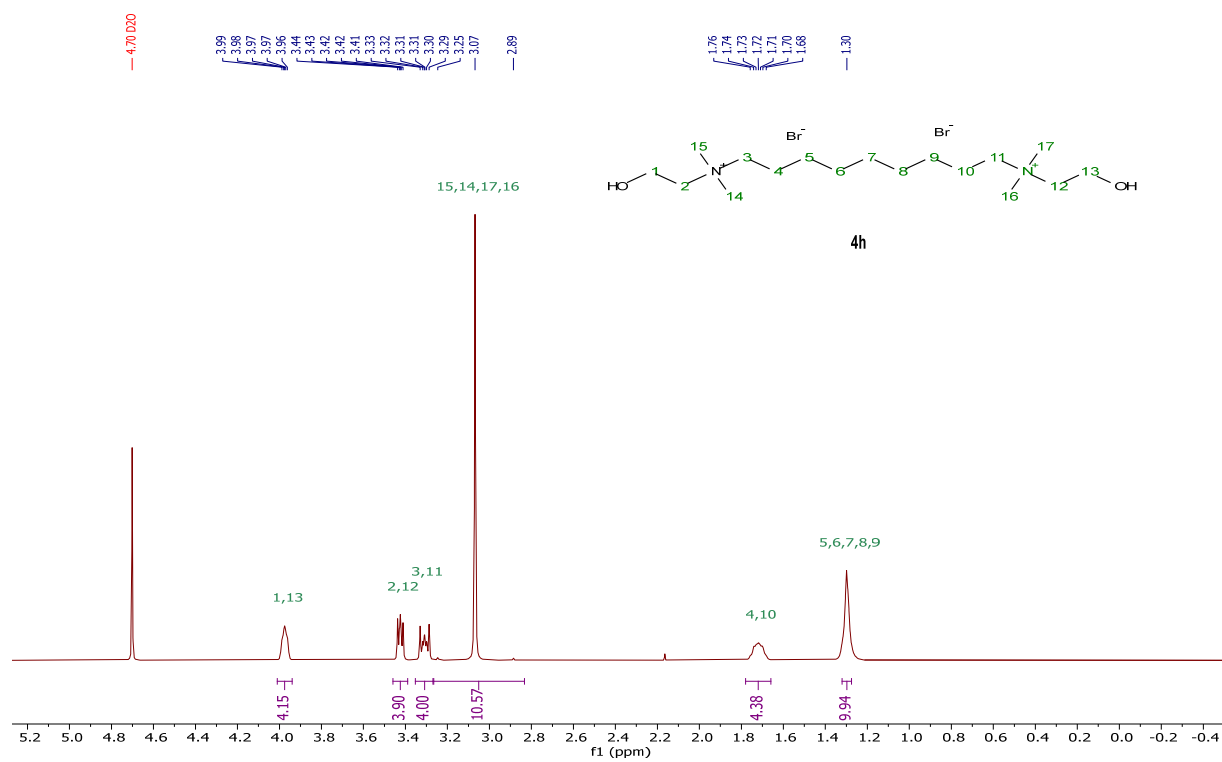
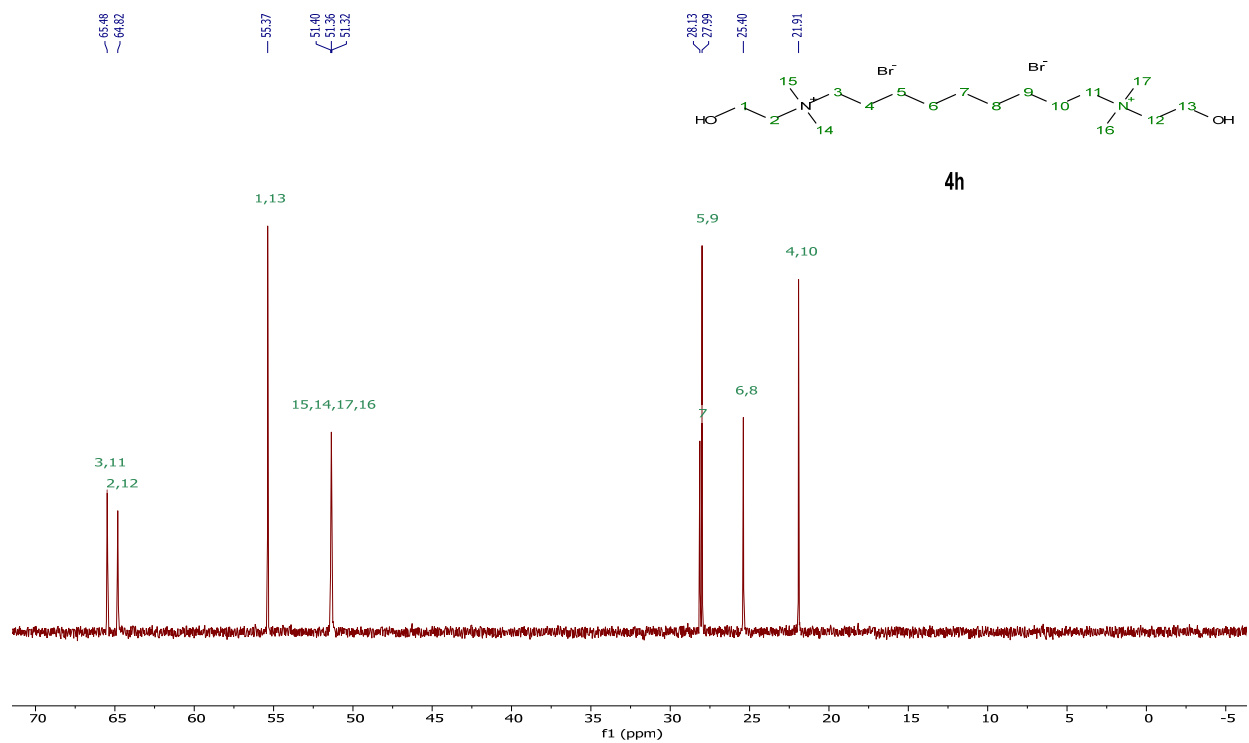
$^1\text{H}$  NMR (400 MHz, Deuterium Oxide)

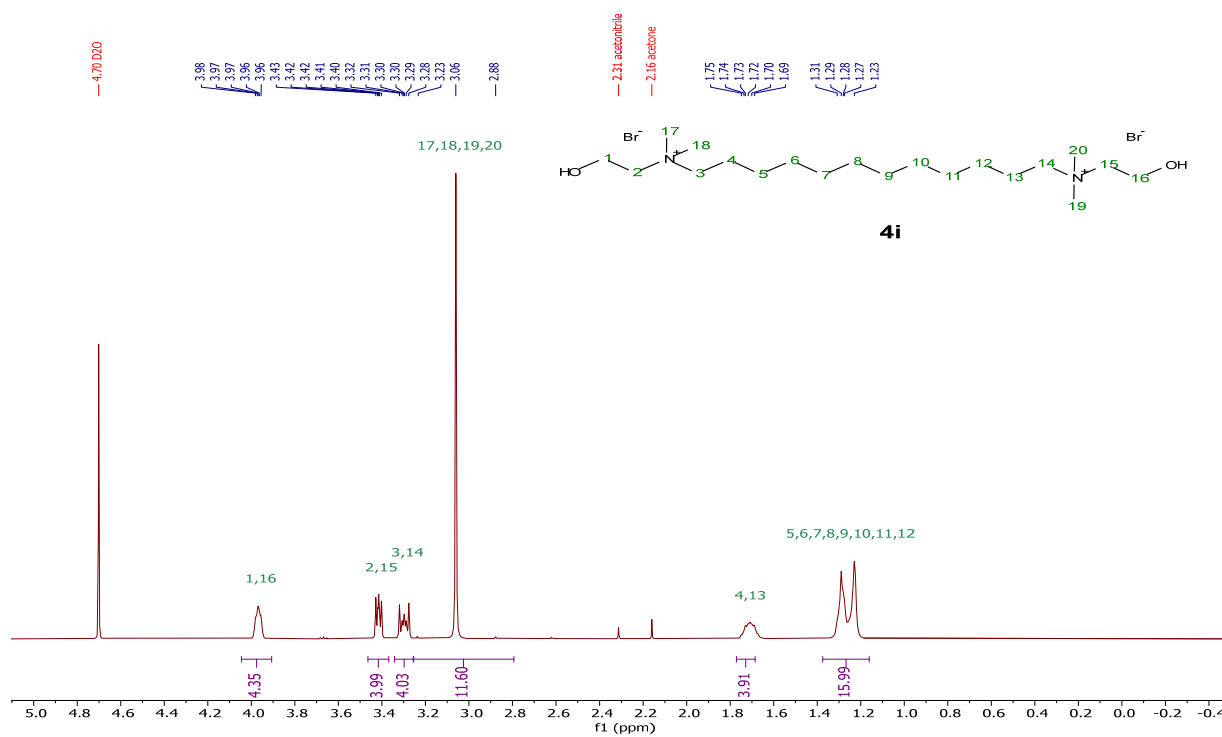
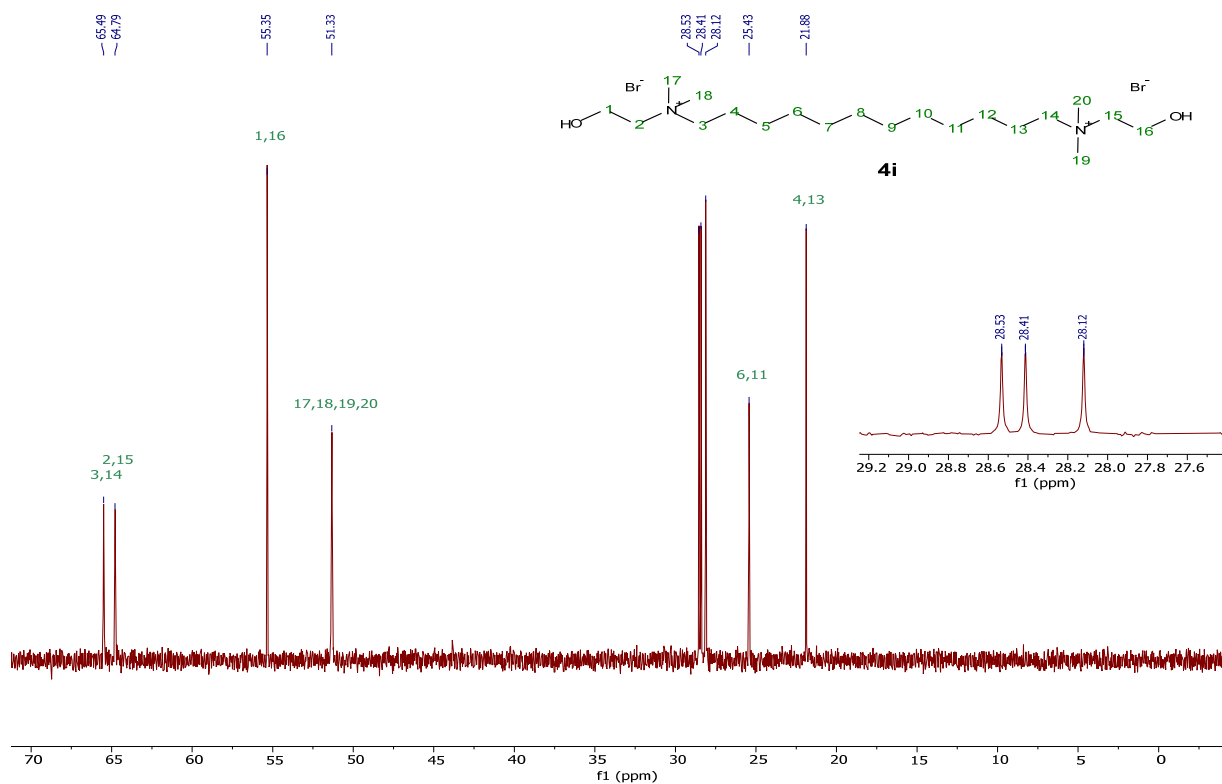


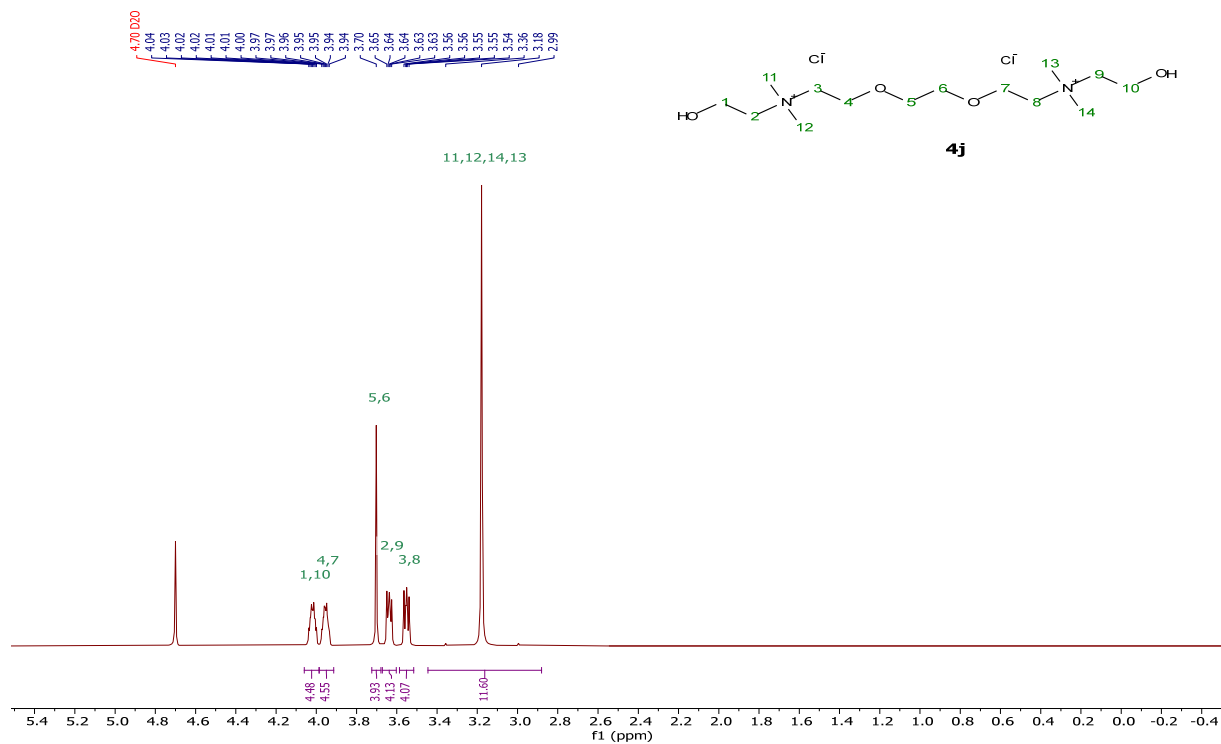
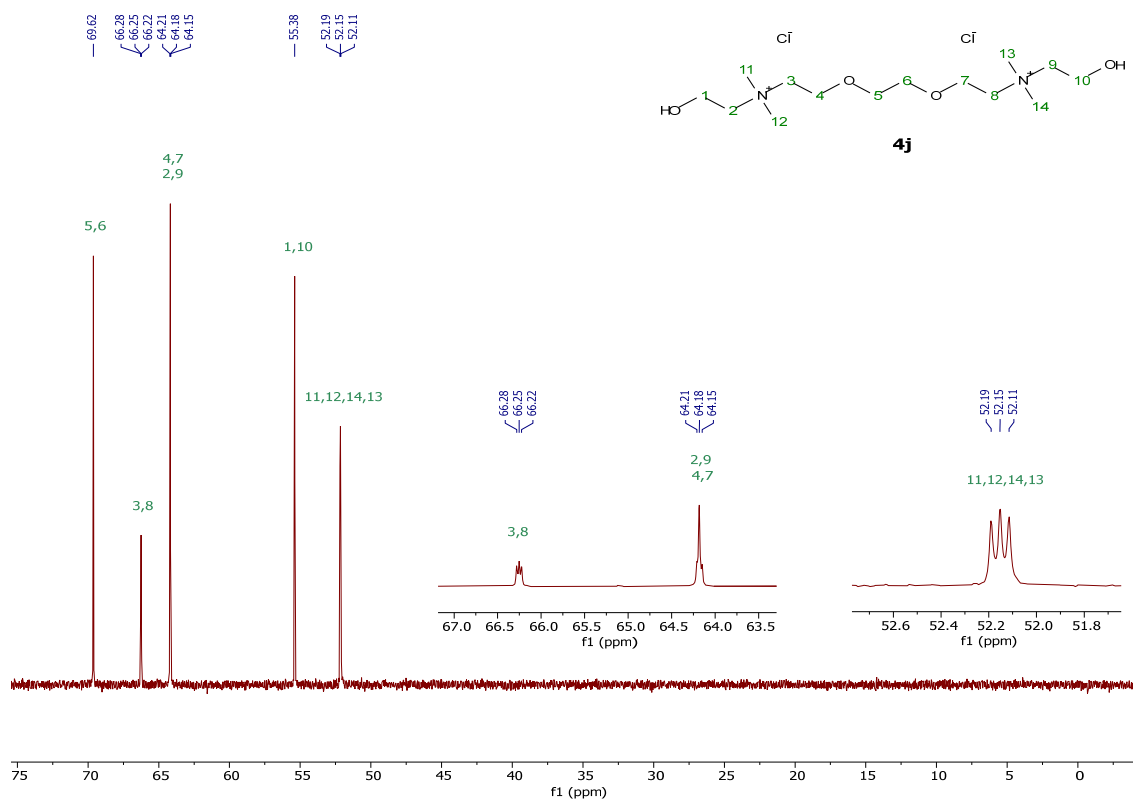
$^{13}\text{C}\{^1\text{H}\}$  NMR (101 MHz, Deuterium Oxide)

## HSQC (Deuterium Oxide)

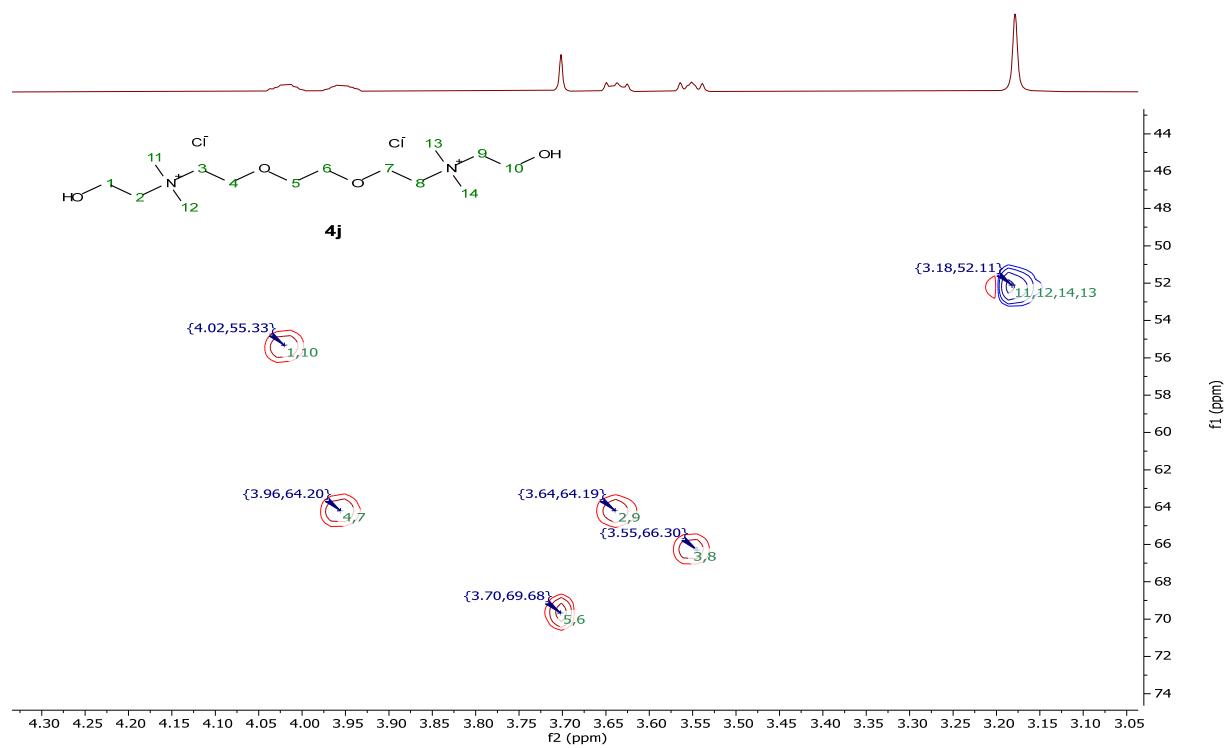
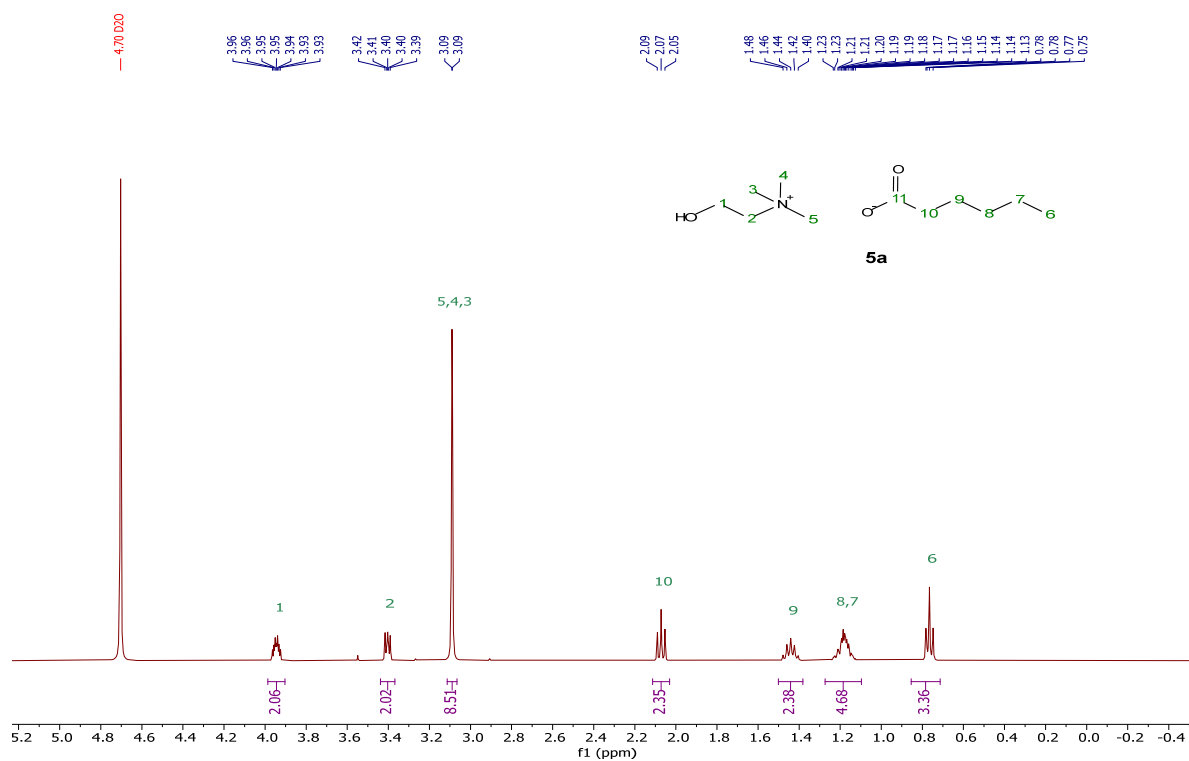


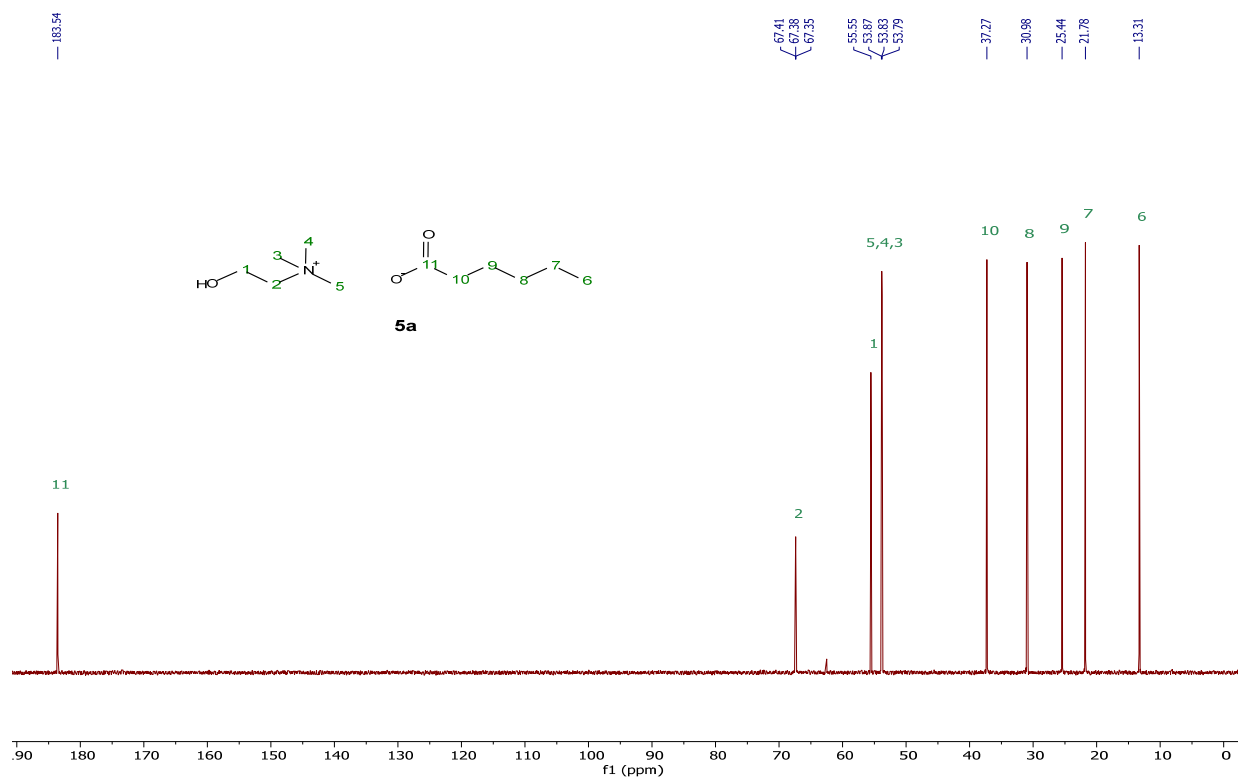
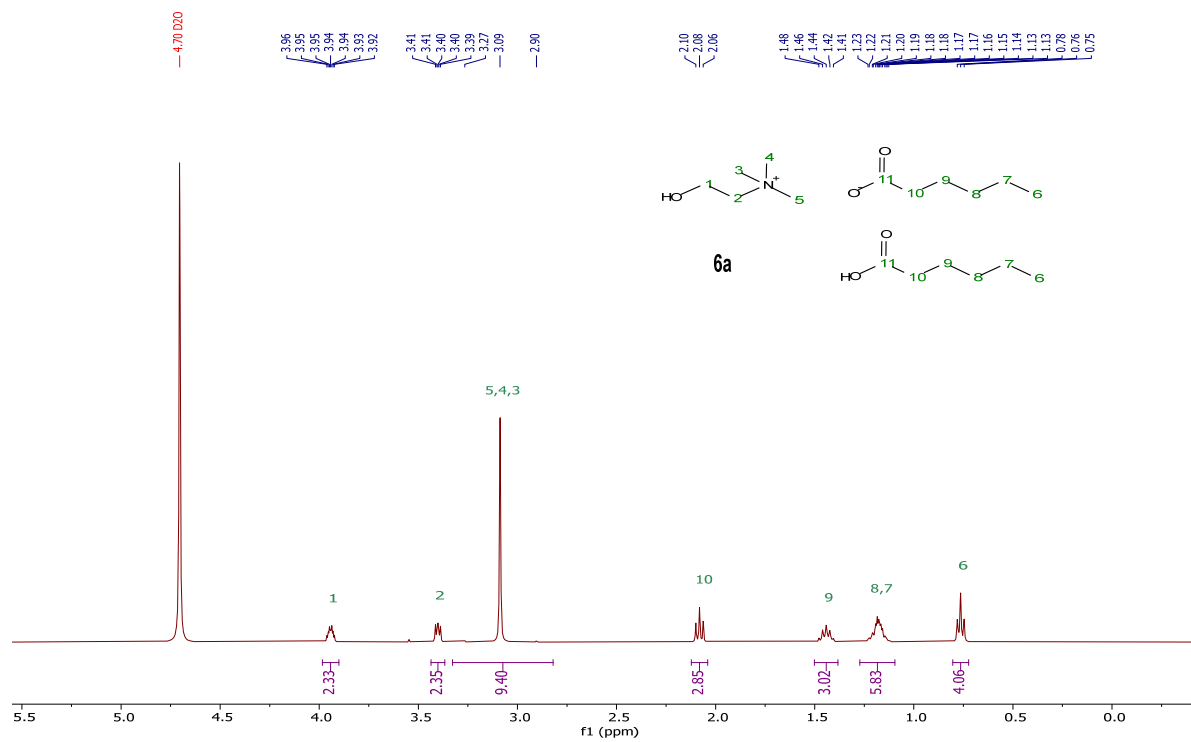
[DC-9][2Br], **4h** $^1\text{H}$  NMR (400 MHz, Deuterium Oxide) $^{13}\text{C}\{^1\text{H}\}$  NMR (101 MHz, Deuterium Oxide)

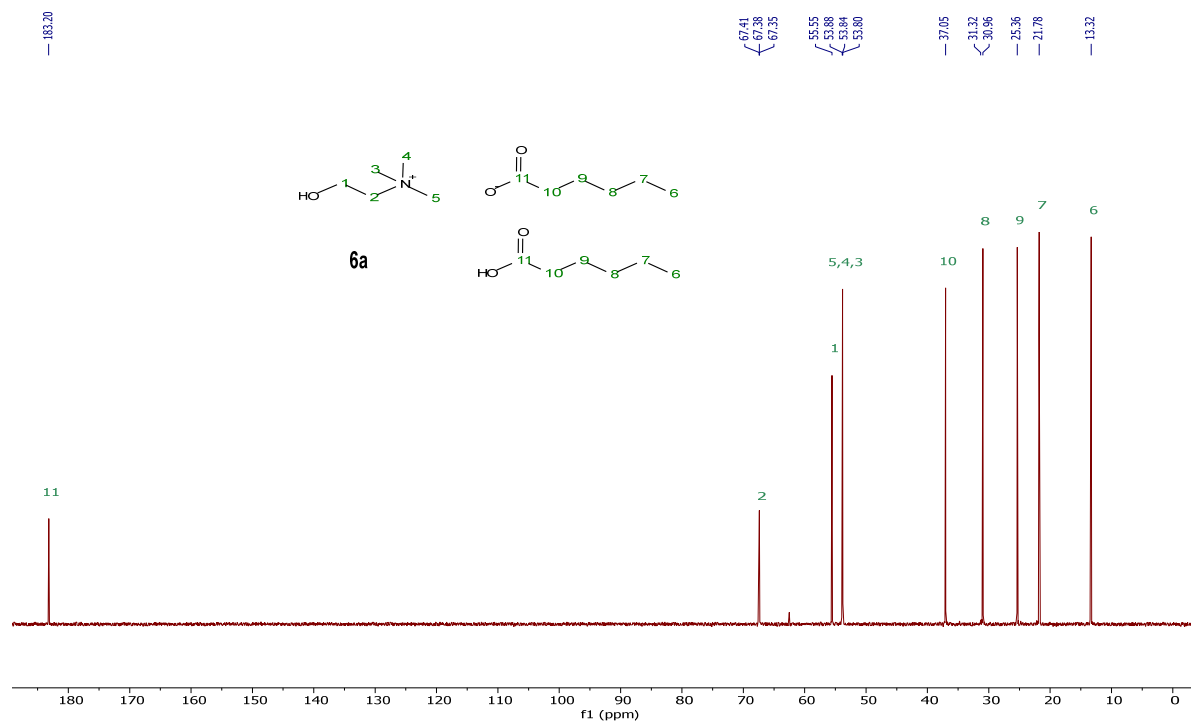
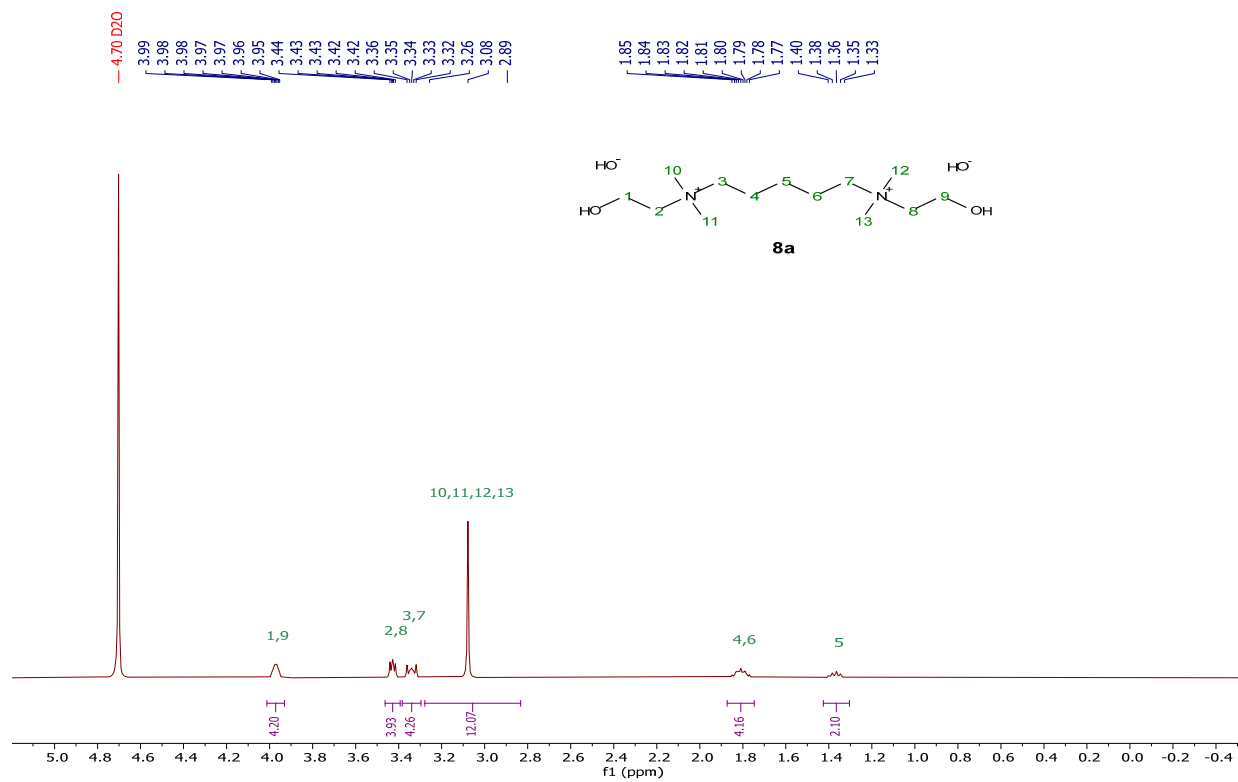
[DC-12][2Br], **4i** $^1\text{H}$  NMR (400 MHz, Deuterium Oxide) $^{13}\text{C}\{^1\text{H}\}$  NMR (101 MHz, Deuterium Oxide)

[DC-ether][2Cl], **4j** $^1\text{H}$  NMR (400 MHz, Deuterium Oxide) $^{13}\text{C}\{^1\text{H}\}$  NMR (101 MHz, Deuterium Oxide)

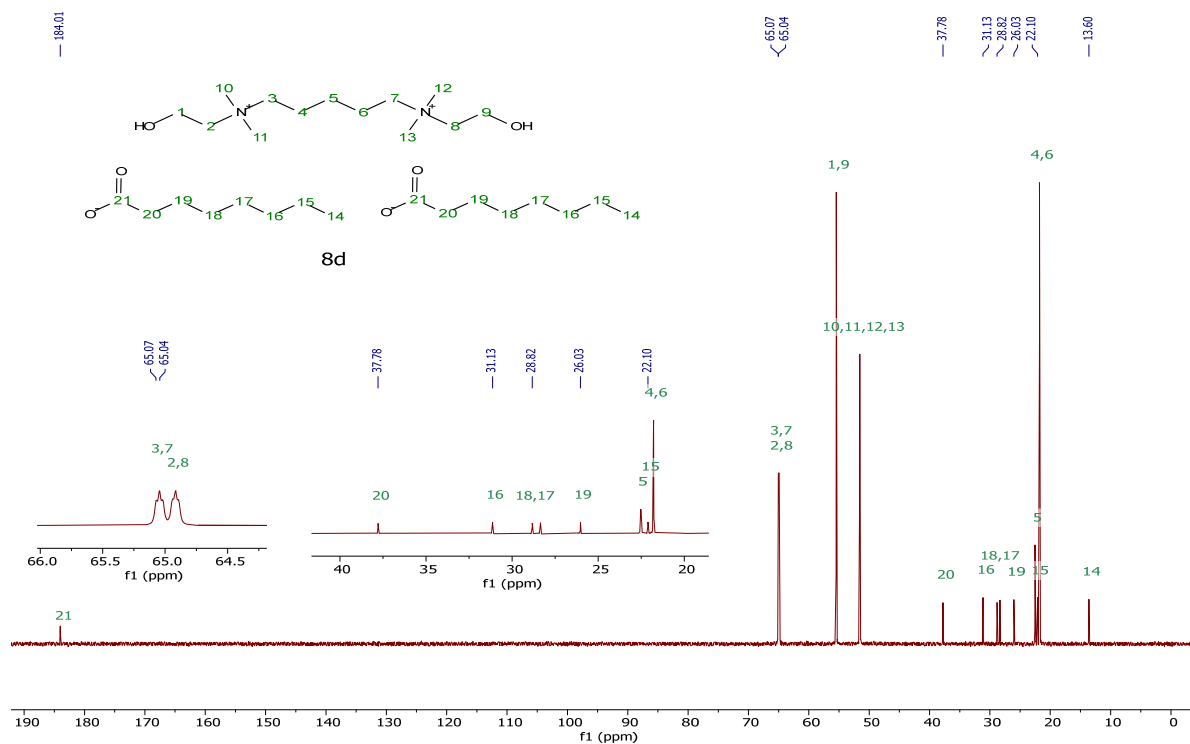
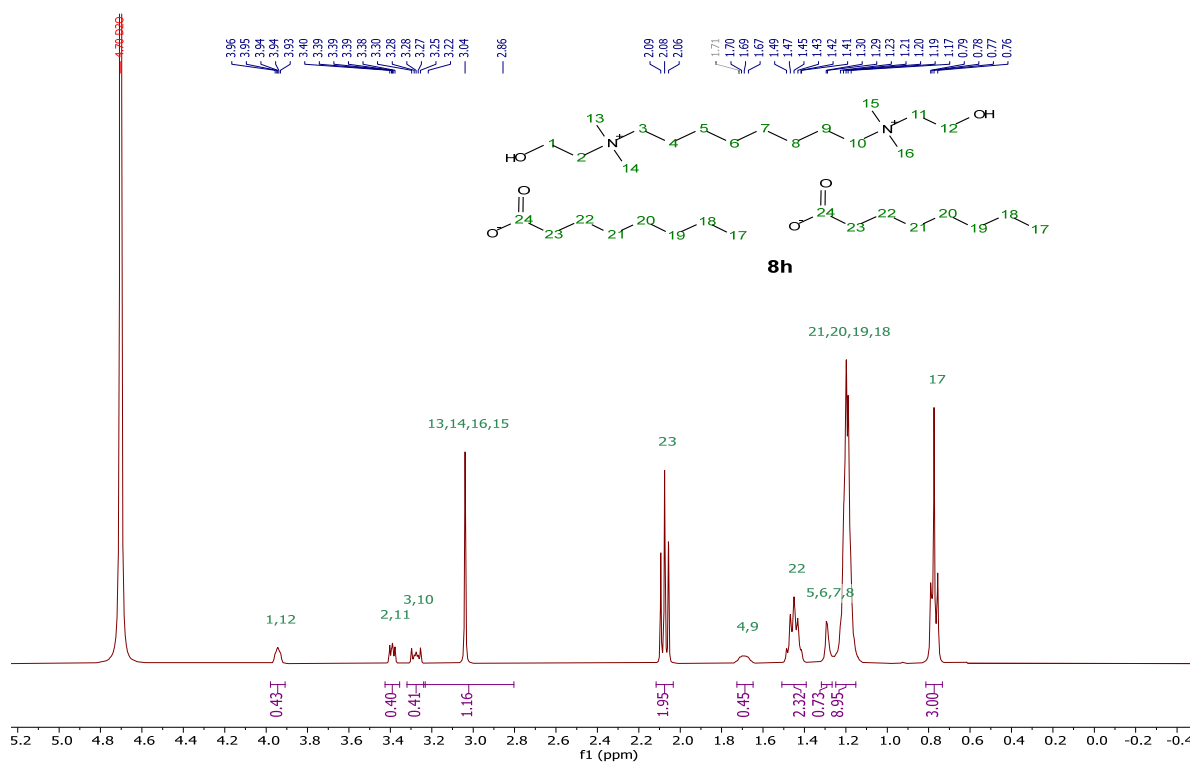
## HSQC (Deuterium Oxide)

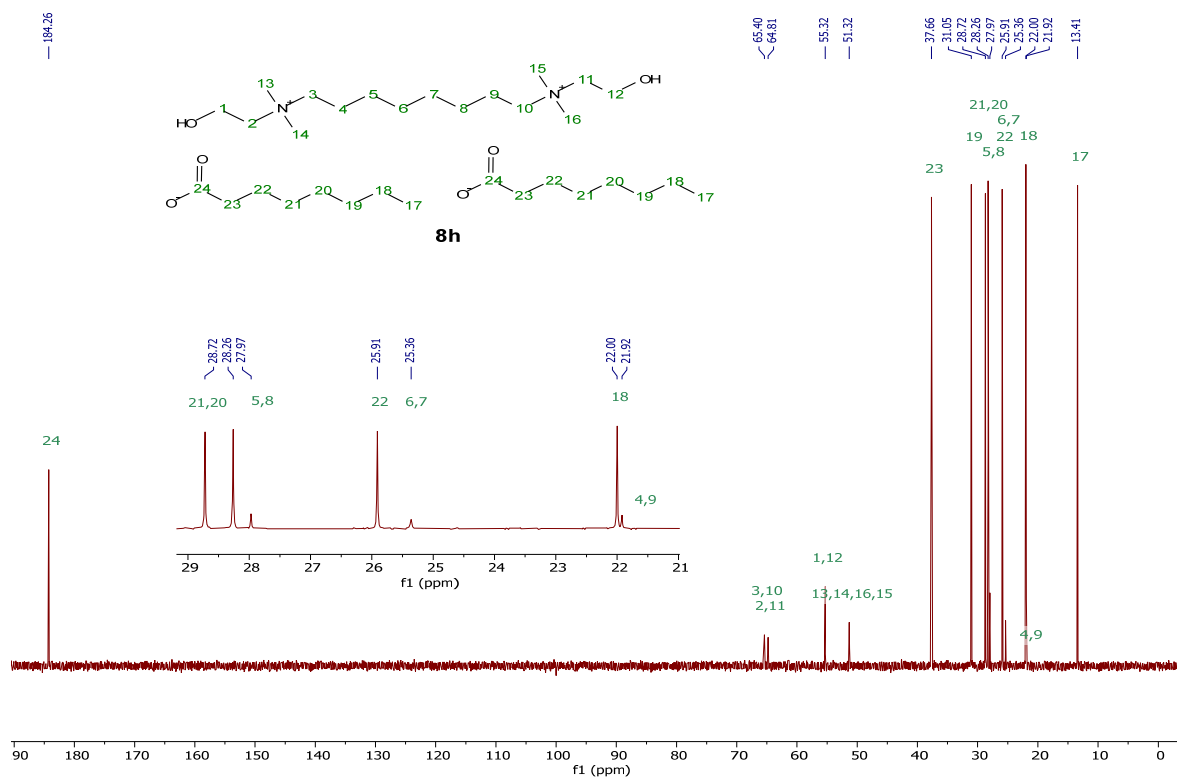
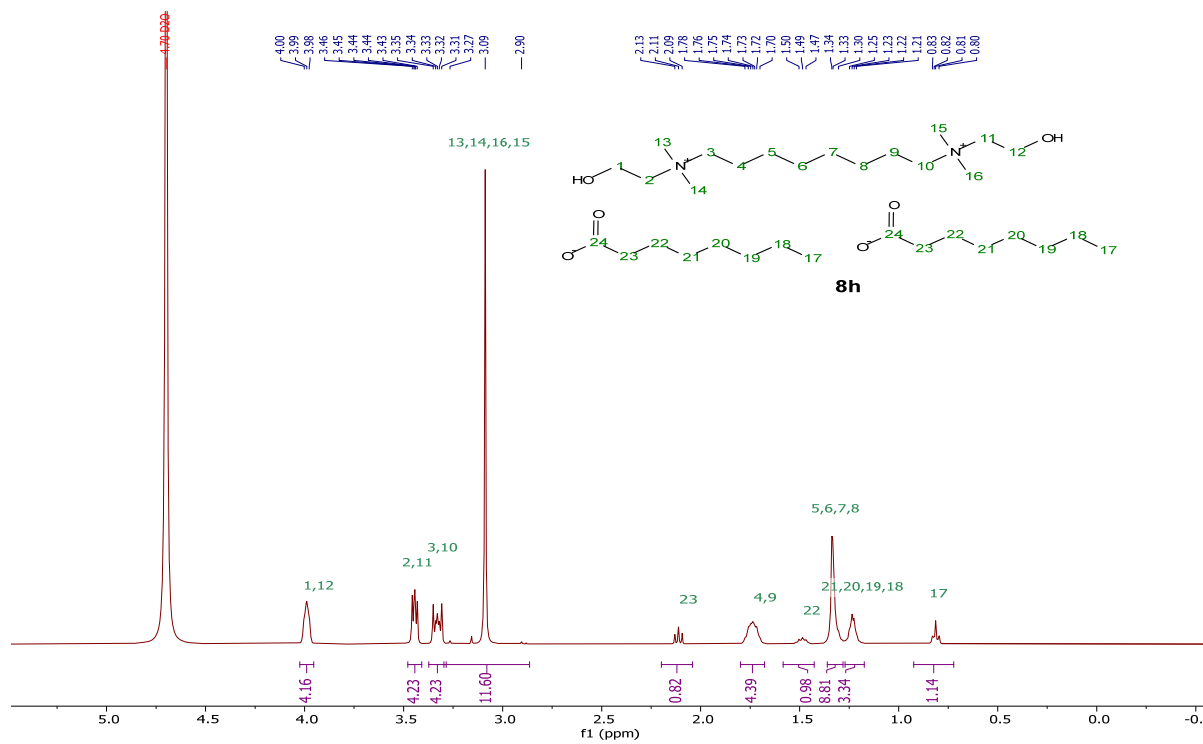
[chol][hex], **5a** $^1\text{H}$  NMR (400 MHz, Deuterium Oxide)

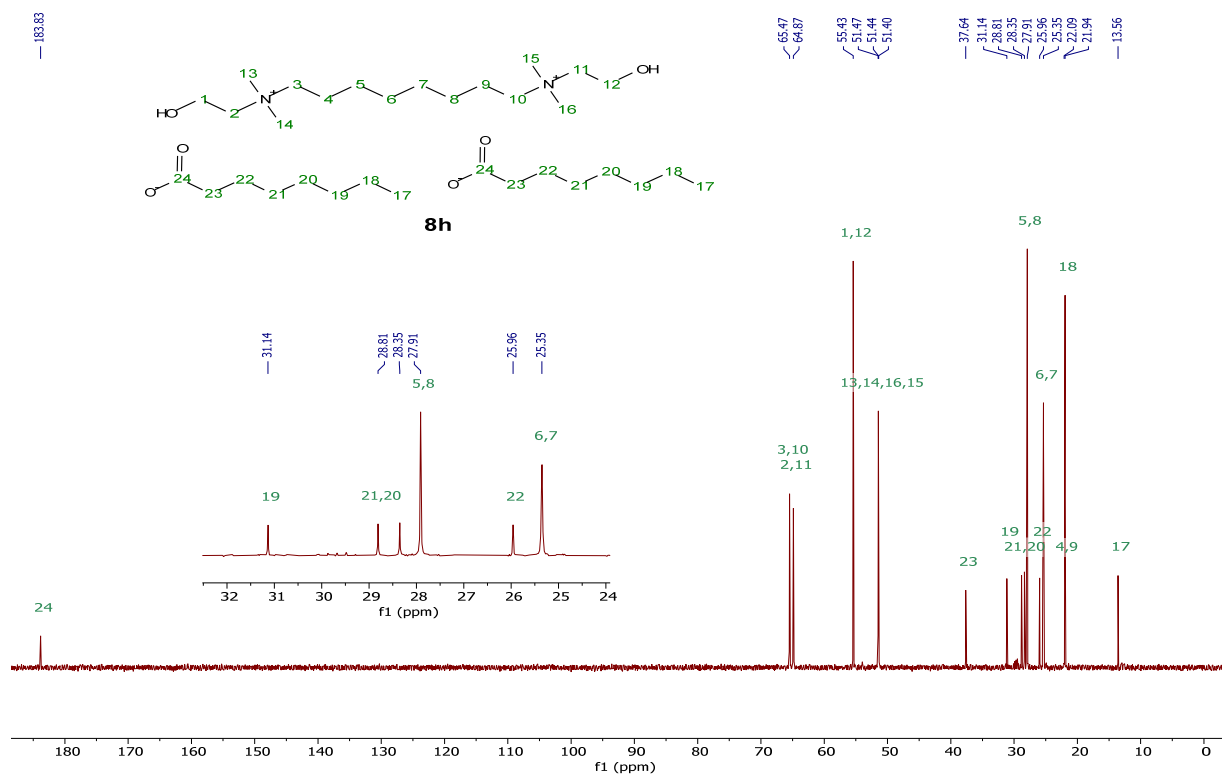
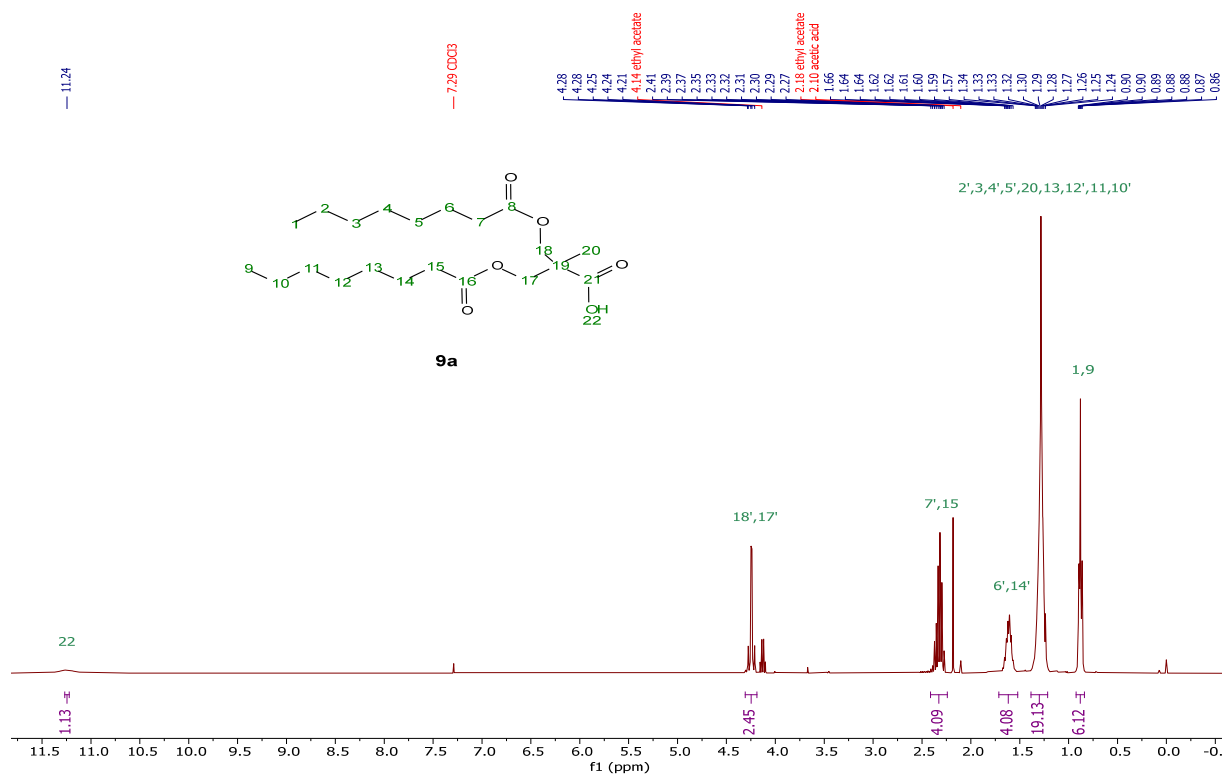
$^{13}\text{C}\{^1\text{H}\}$  NMR (101 MHz, Deuterium Oxide)[chol][hex] hex DES, **6a** $^1\text{H}$  NMR (400 MHz, Deuterium Oxide)

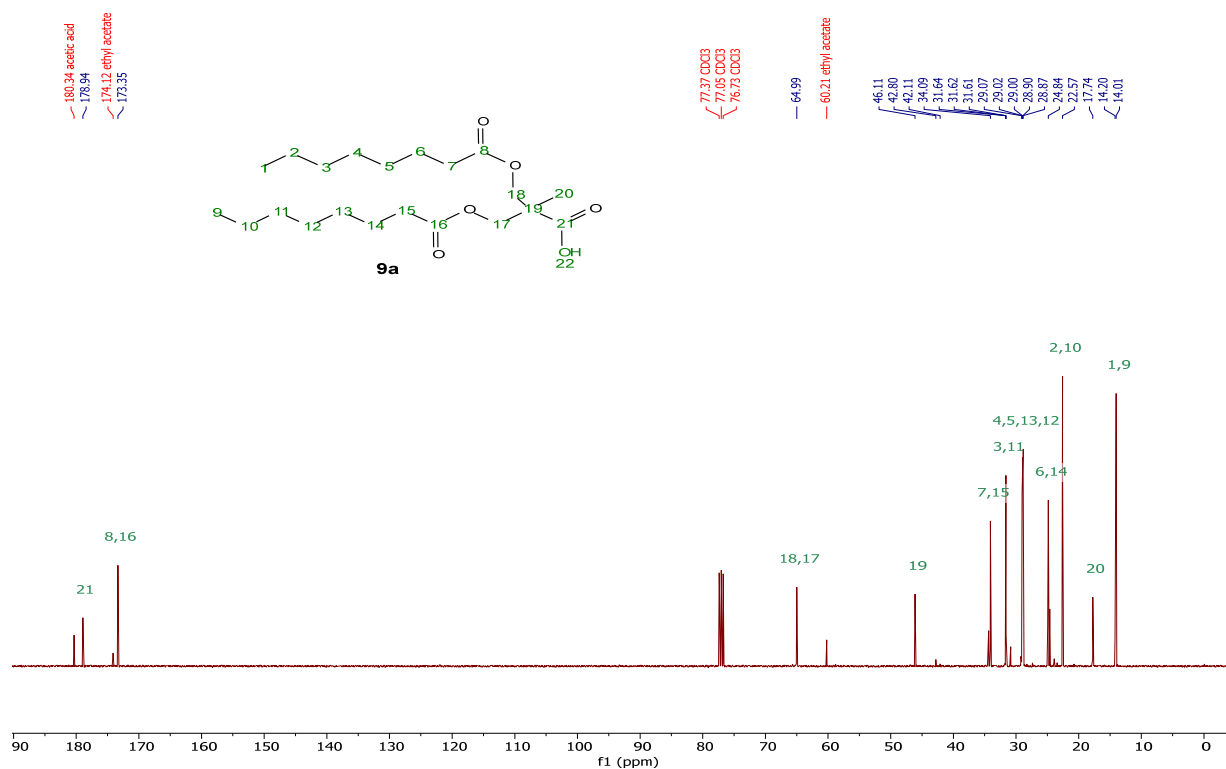
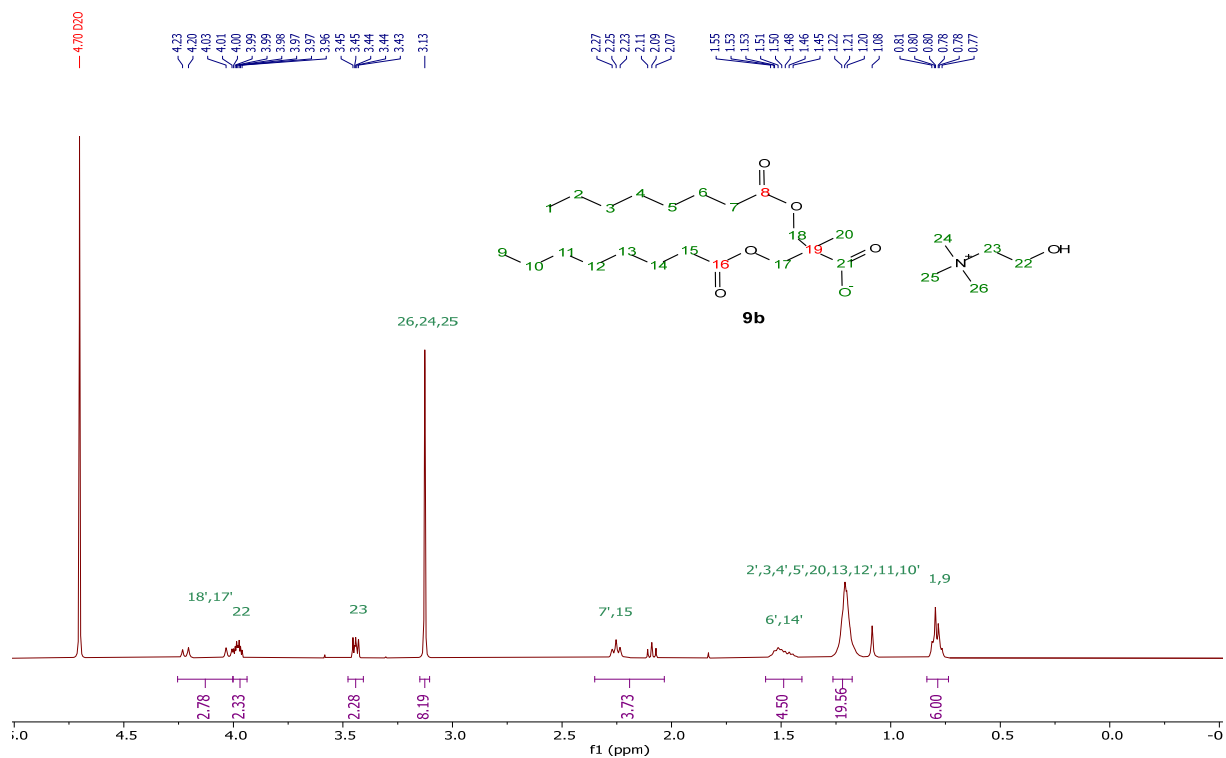
$^{13}\text{C}\{^1\text{H}\}$  NMR (101 MHz, Deuterium Oxide)[DC-5][2OH], **8a** $^1\text{H}$  NMR (400 MHz, Deuterium Oxide)

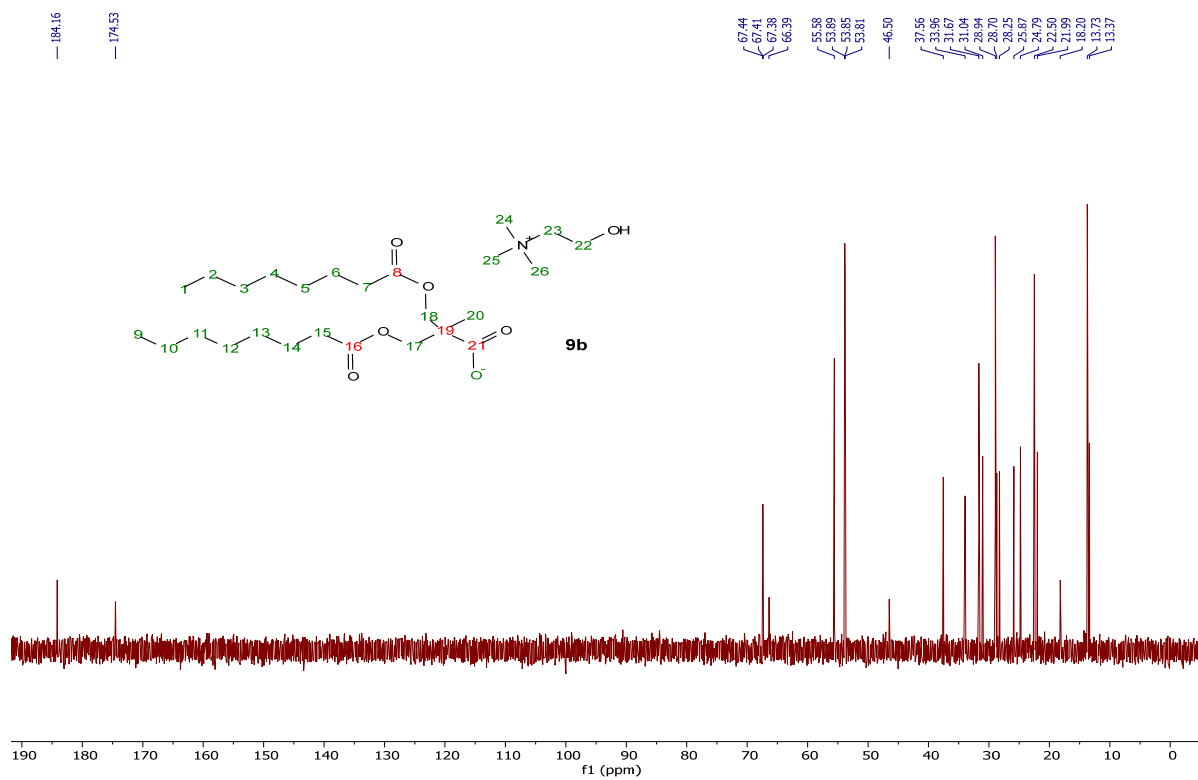


$^{13}\text{C}\{^1\text{H}\}$  NMR (101 MHz, Deuterium Oxide)[DC-8][2oct], **8h**; Precipitant: $^1\text{H}$  NMR (400 MHz, Deuterium Oxide)

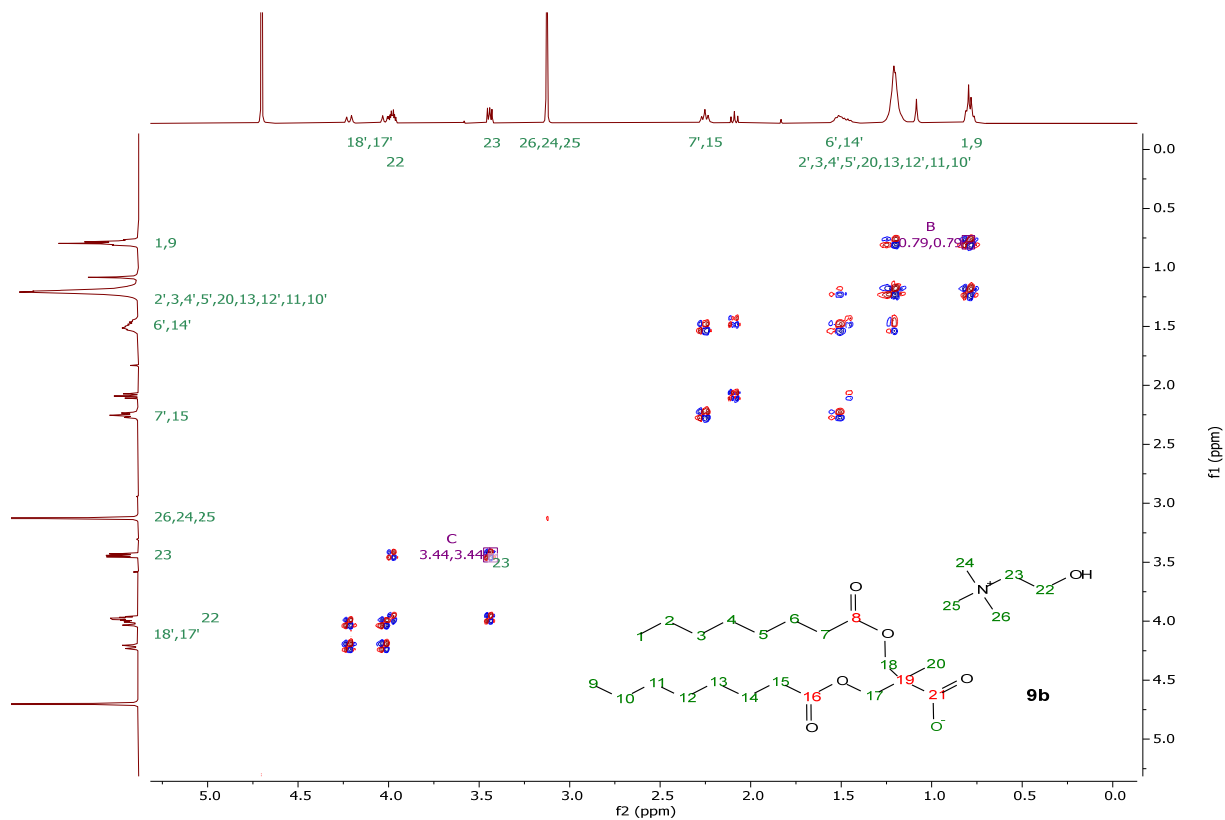
$^{13}\text{C}\{^1\text{H}\}$  NMR (101 MHz, Deuterium Oxide)[DC-8][2oct], **8h**; Filtrate: $^1\text{H}$  NMR (400 MHz, Deuterium Oxide)

$^{13}\text{C}\{^1\text{H}\}$  NMR (101 MHz, Deuterium Oxide)**9a** $^1\text{H}$  NMR (400 MHz, Chloroform-d)

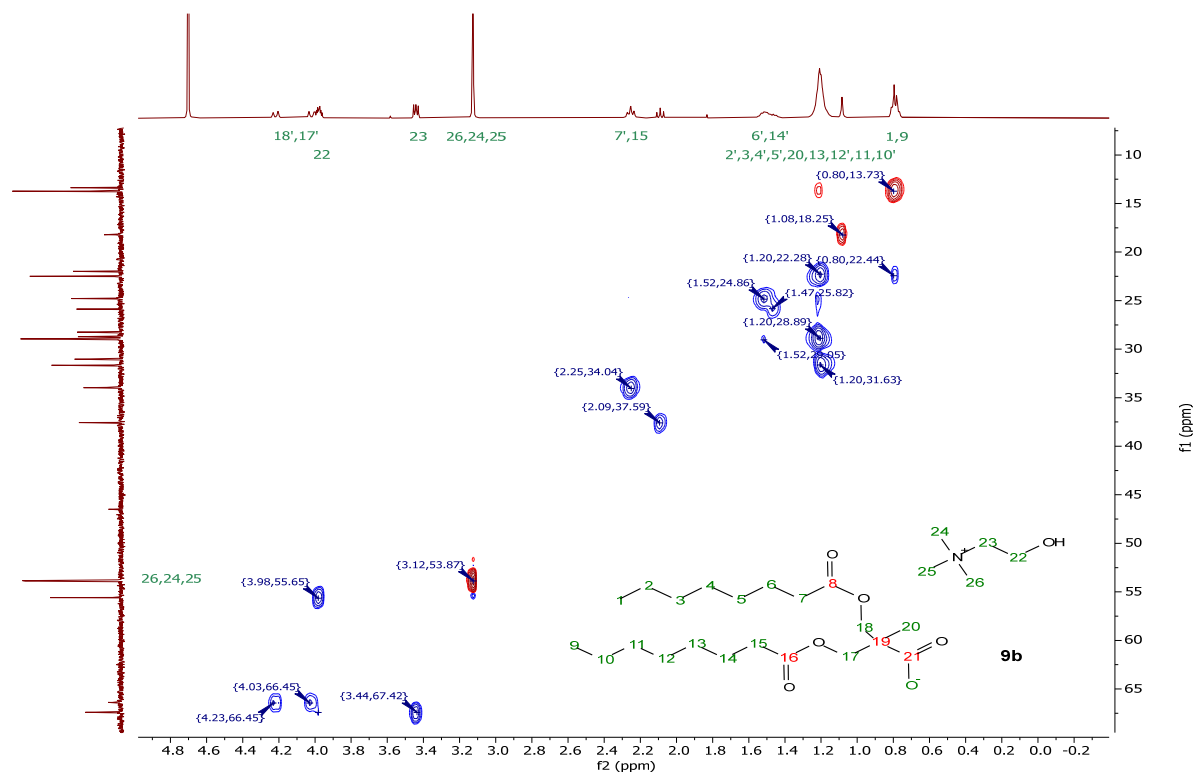
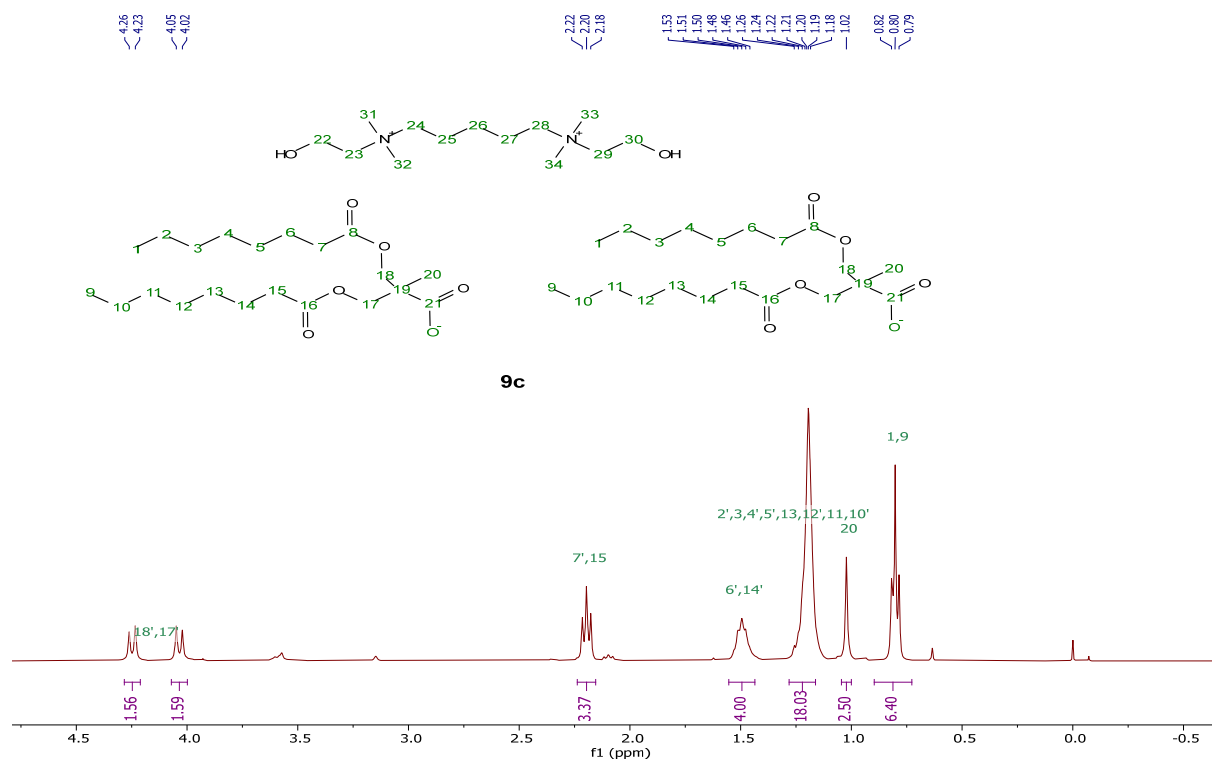
$^{13}\text{C}\{^1\text{H}\}$  NMR (101 MHz, Chloroform-d)[chol][DOP], **9b** $^1\text{H}$  NMR (400 MHz, Deuterium Oxide)

$^{13}\text{C}\{^1\text{H}\}$  NMR (101 MHz, Deuterium Oxide)

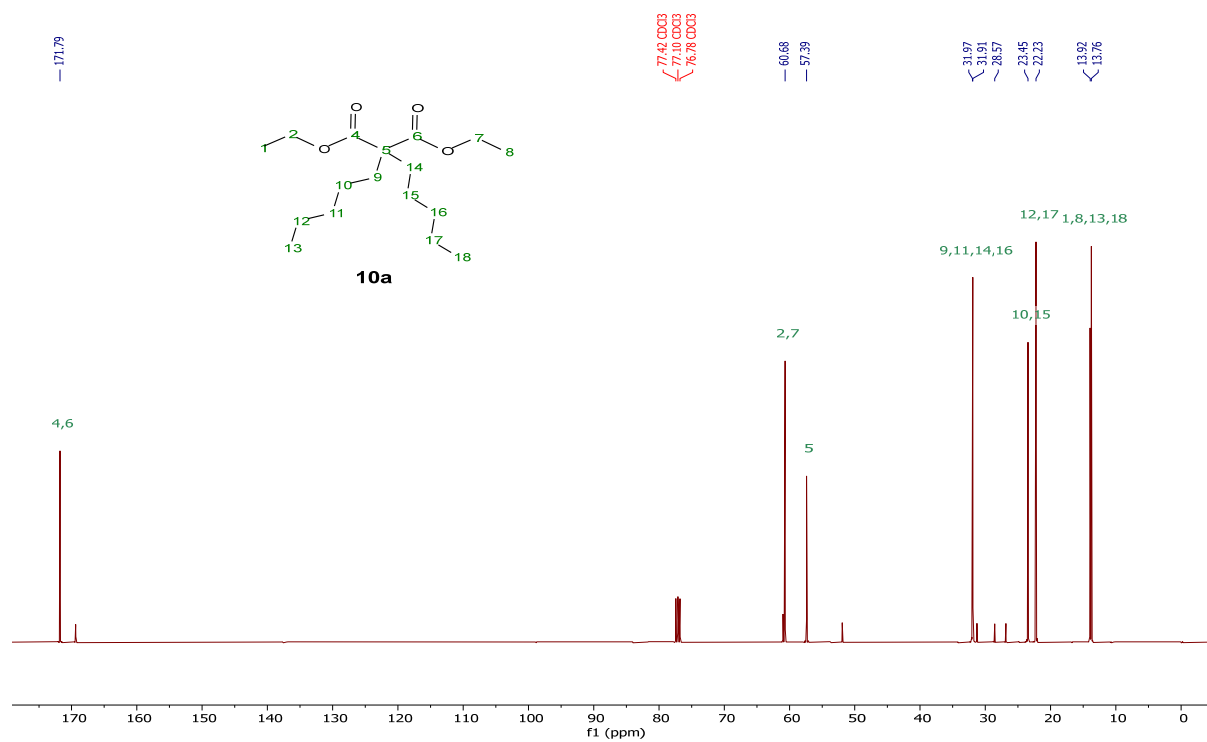
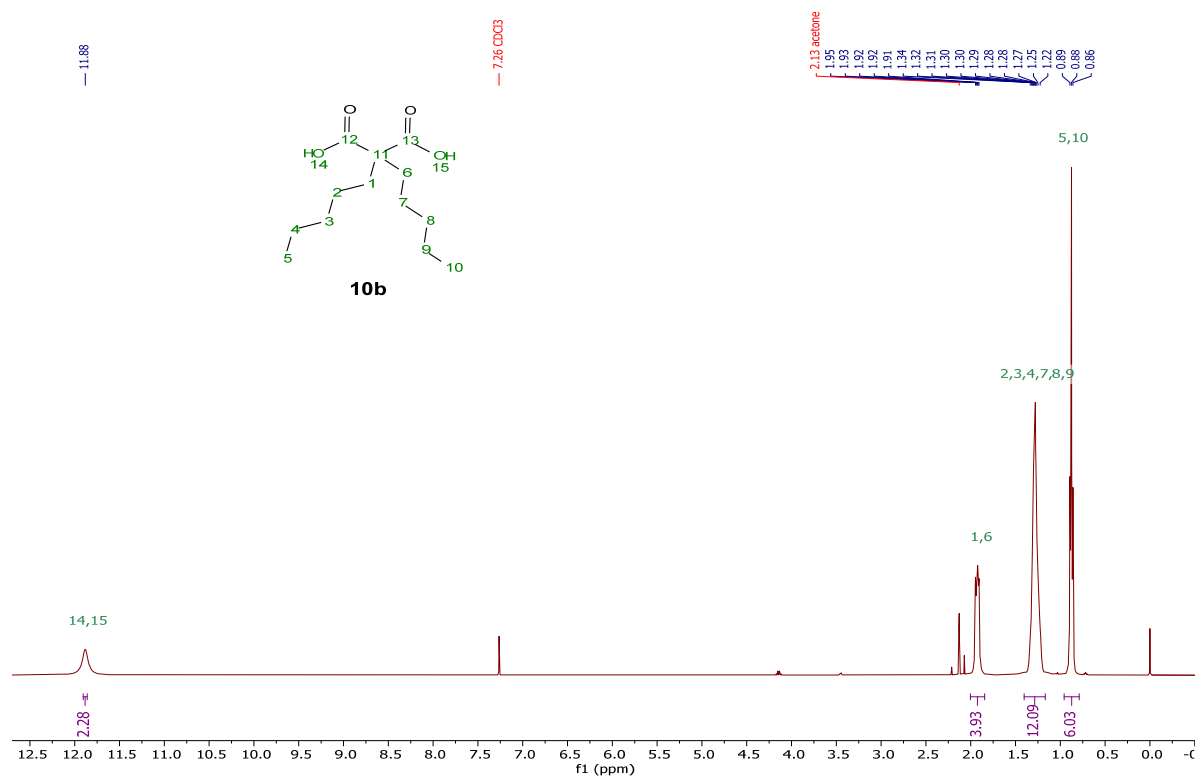
## COSY (Deuterium Oxide)

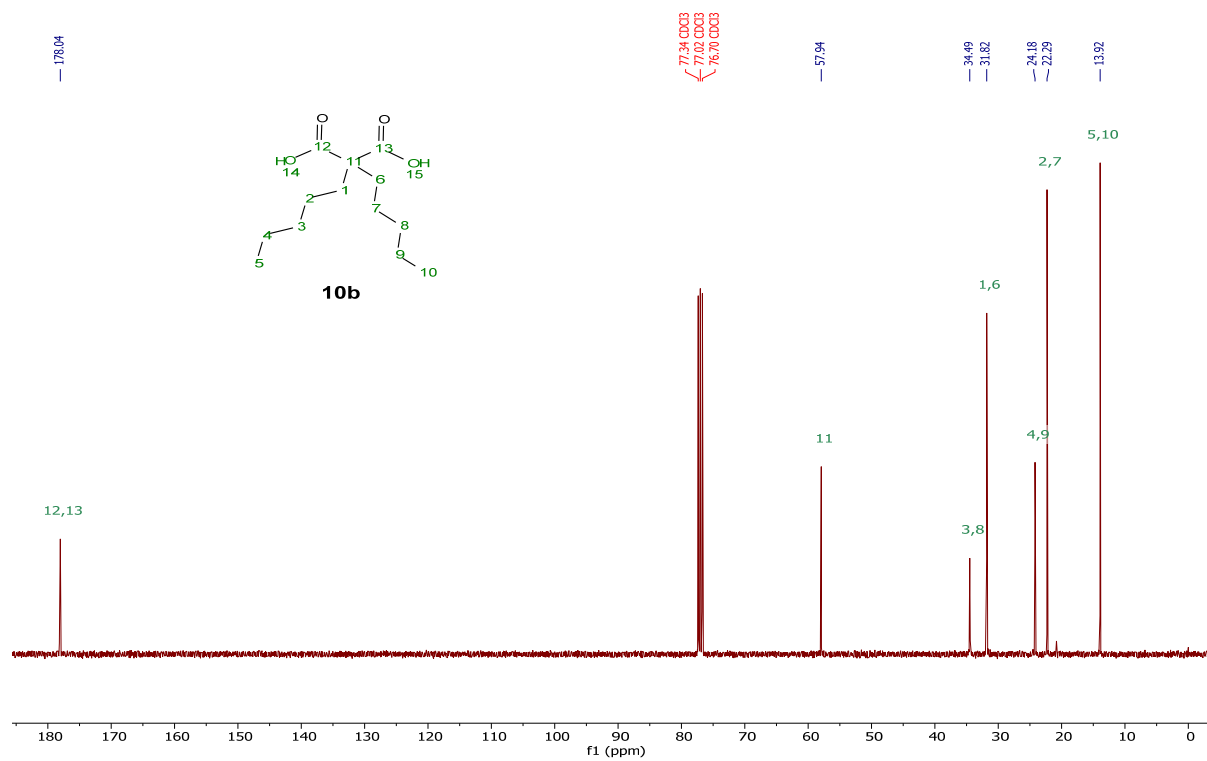
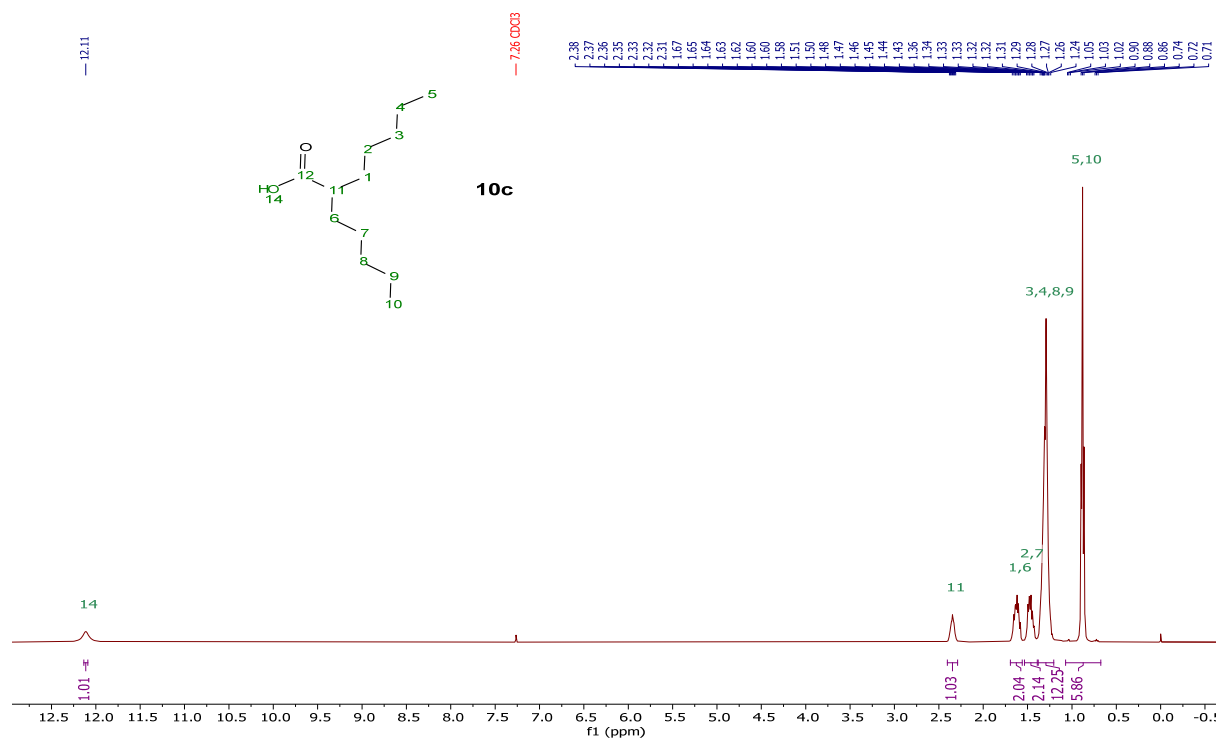


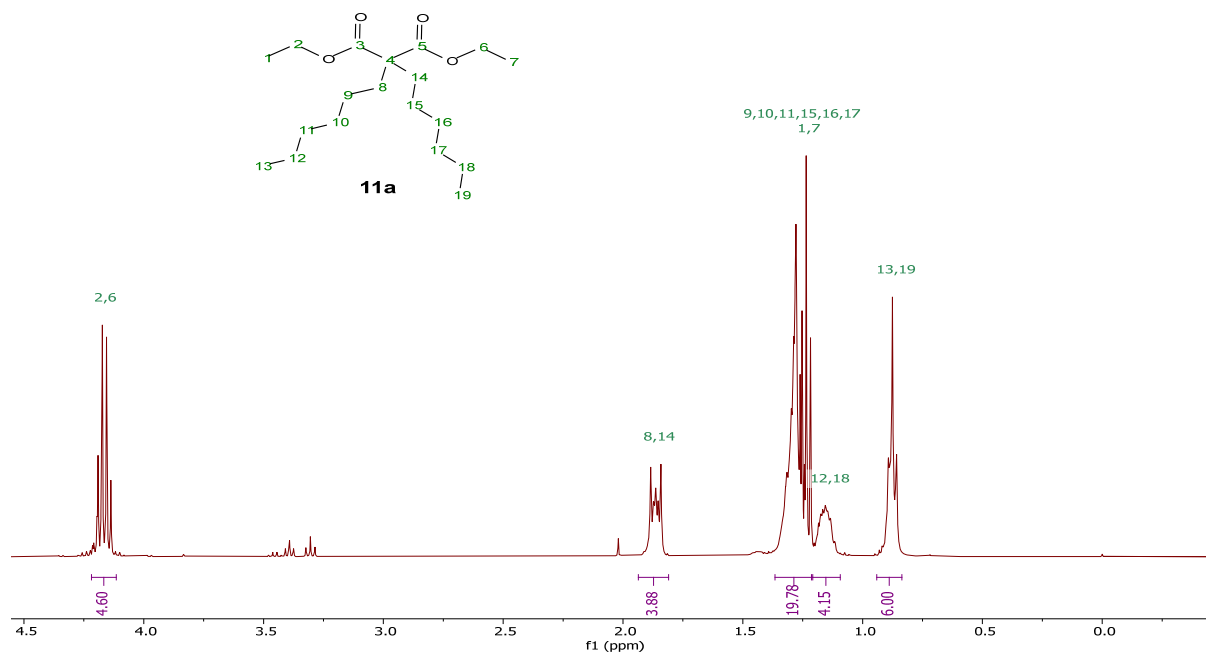
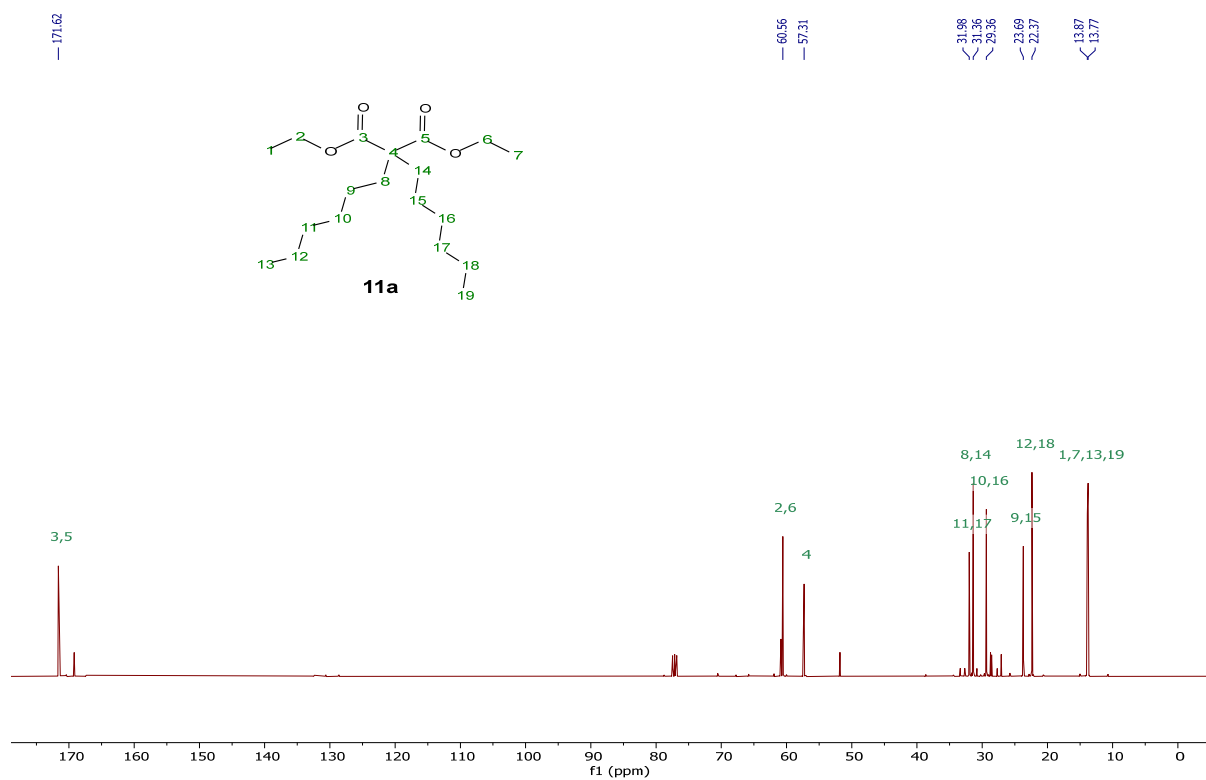
## HSQC (Deuterium Oxide)

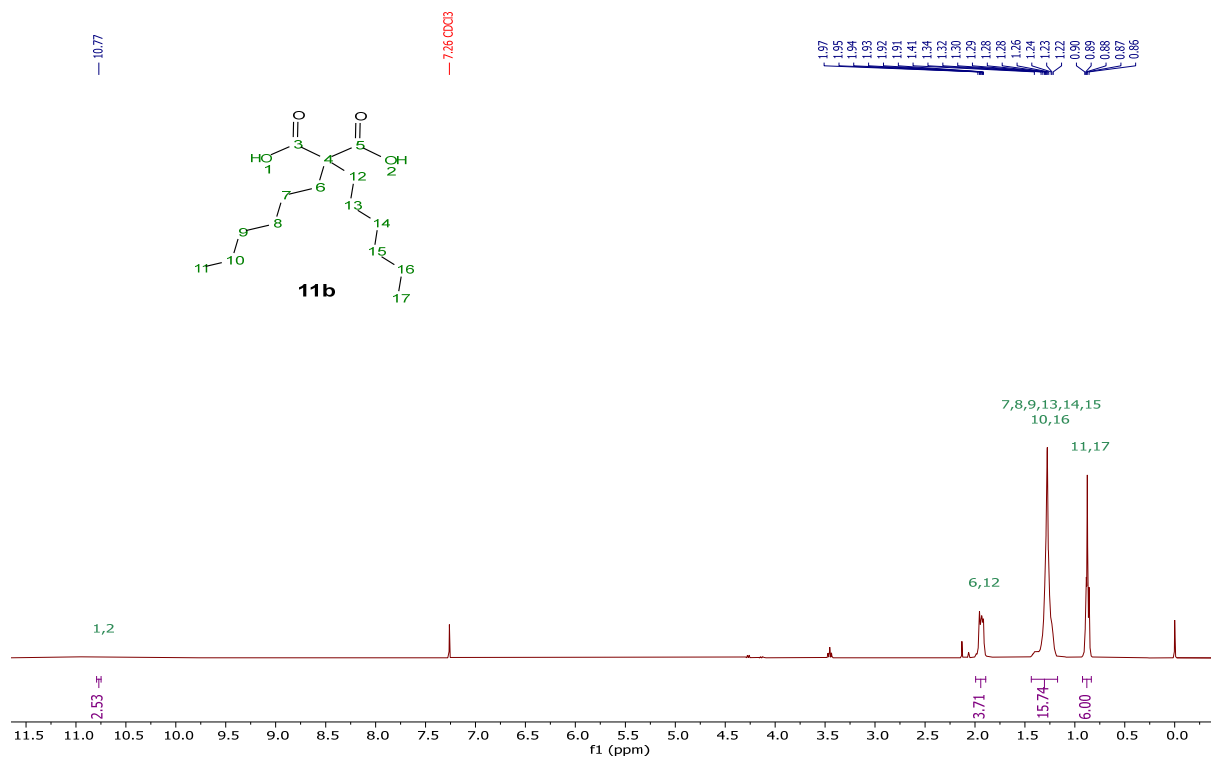
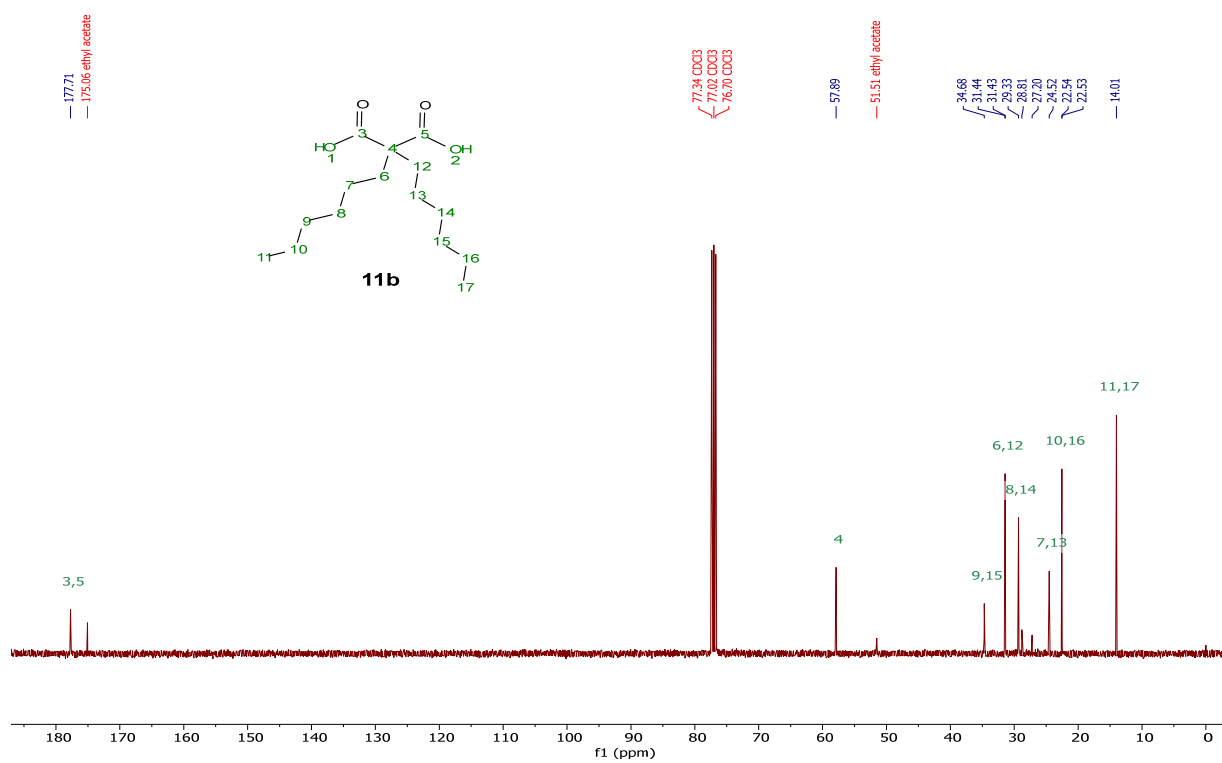
[DC-5][2DOP], **9c**<sup>1</sup>H NMR (400 MHz, Chloroform-d)

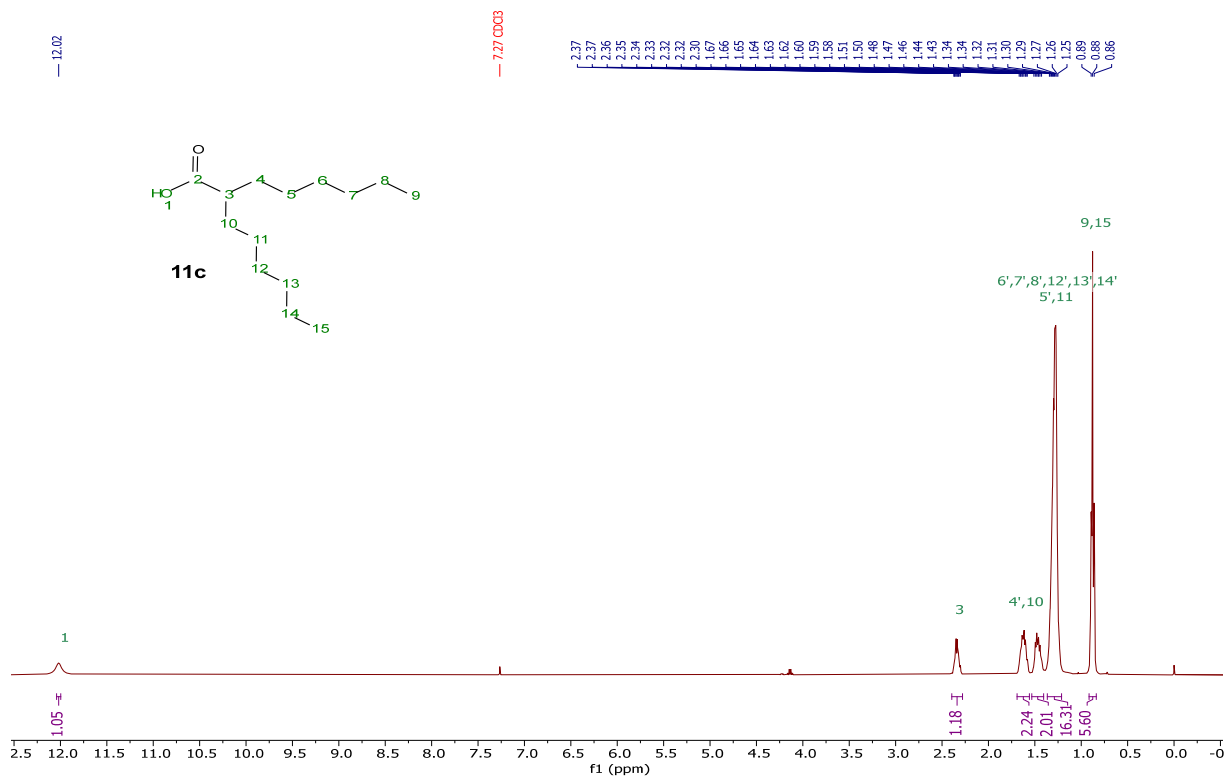
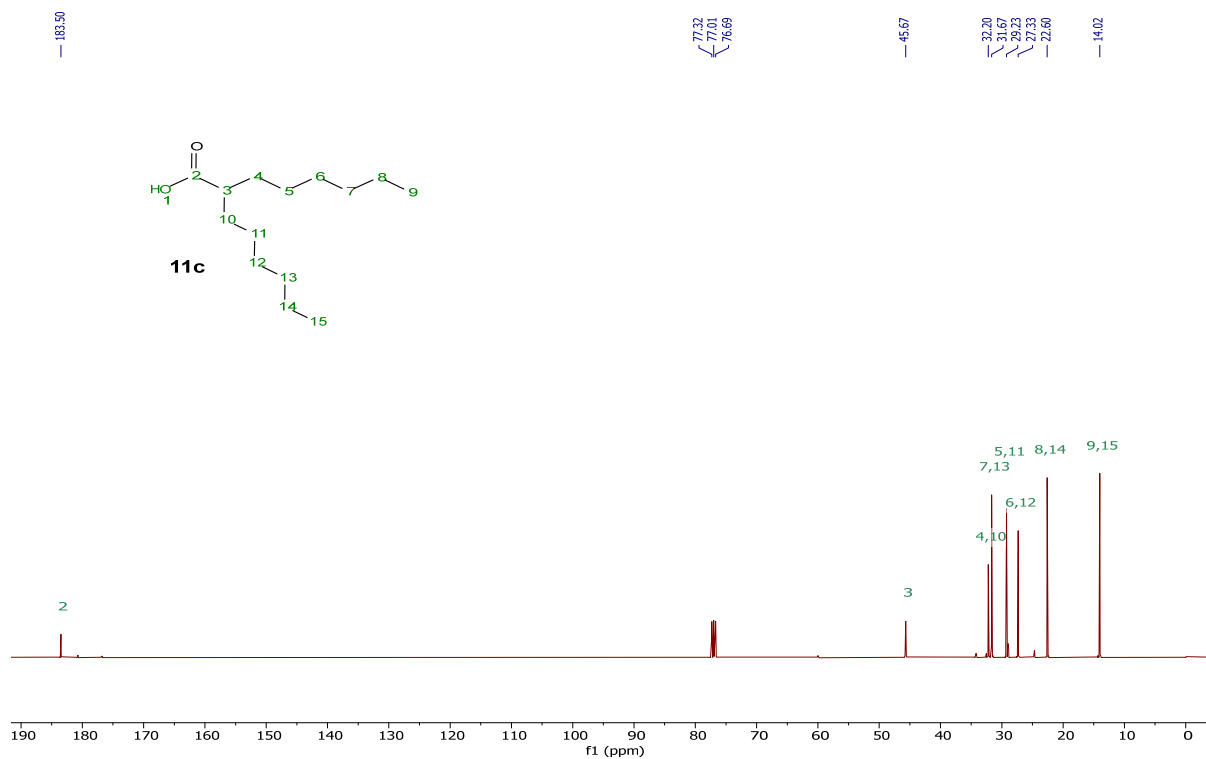


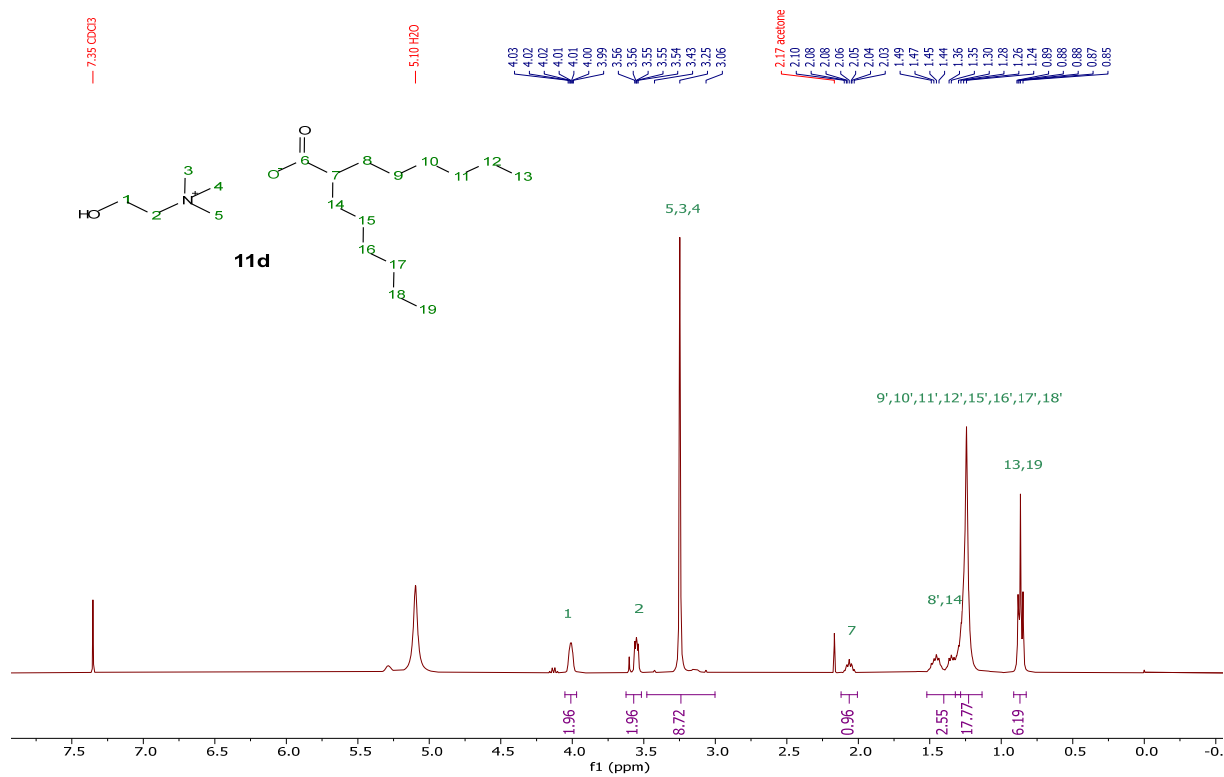
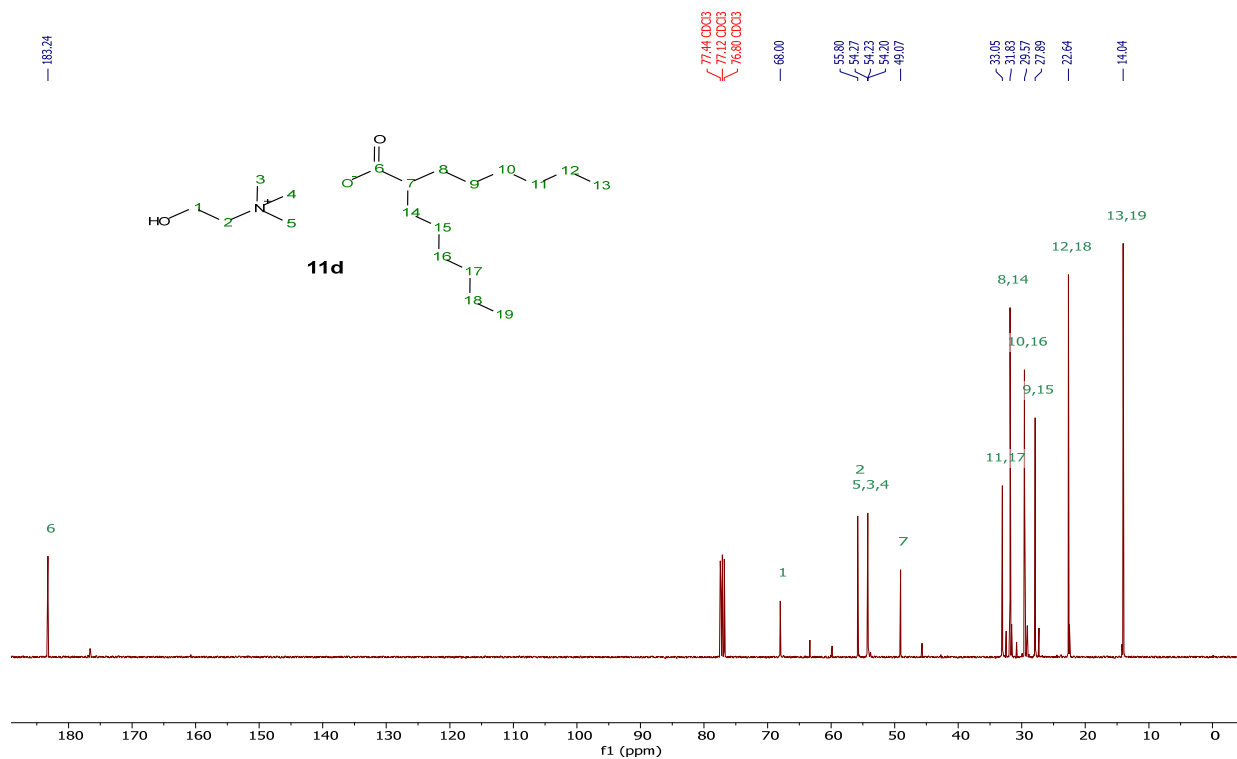
$^{13}\text{C}\{^1\text{H}\}$  NMR (101 MHz, Chloroform-d)**10b** $^1\text{H}$  NMR (400 MHz, Chloroform-d)

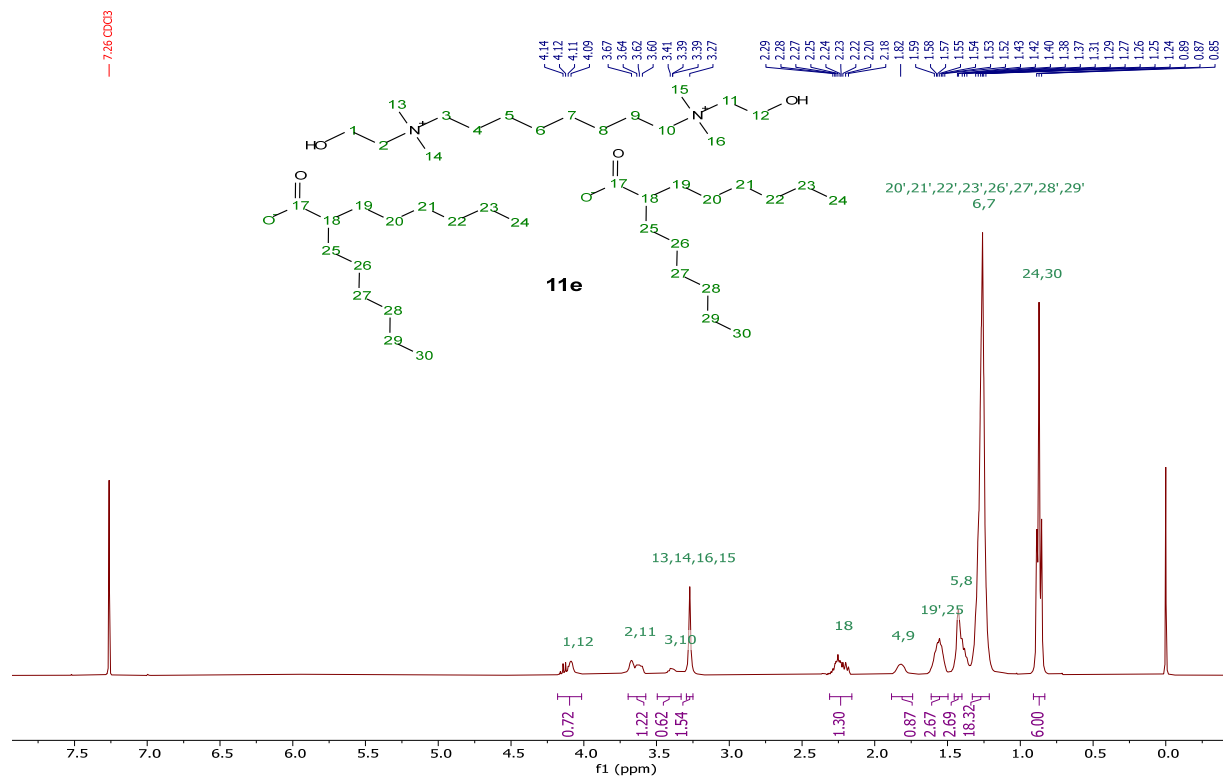
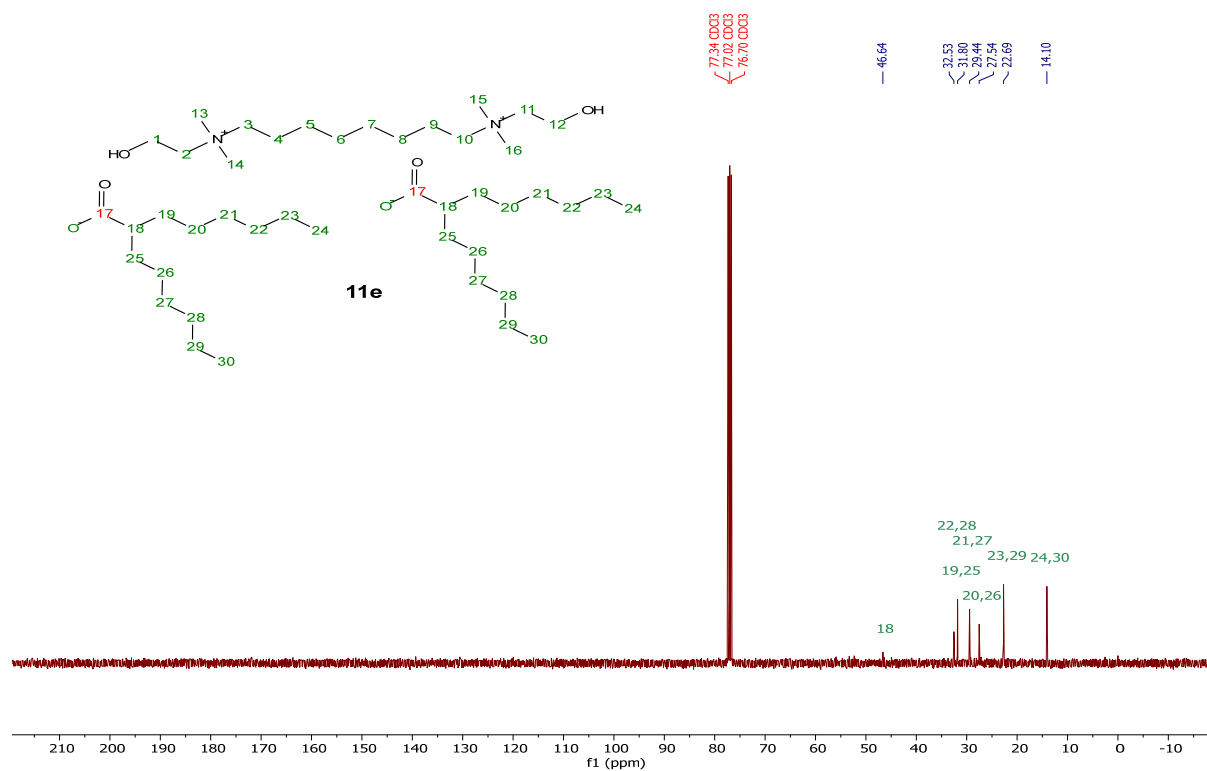
$^{13}\text{C}\{^1\text{H}\}$  NMR (101 MHz, Chloroform-d)**10c** $^1\text{H}$  NMR (400 MHz, Chloroform-d)

**11a** $^1\text{H}$  NMR (400 MHz, Chloroform-d) $^{13}\text{C}\{^1\text{H}\}$  NMR (101 MHz, Chloroform-d)

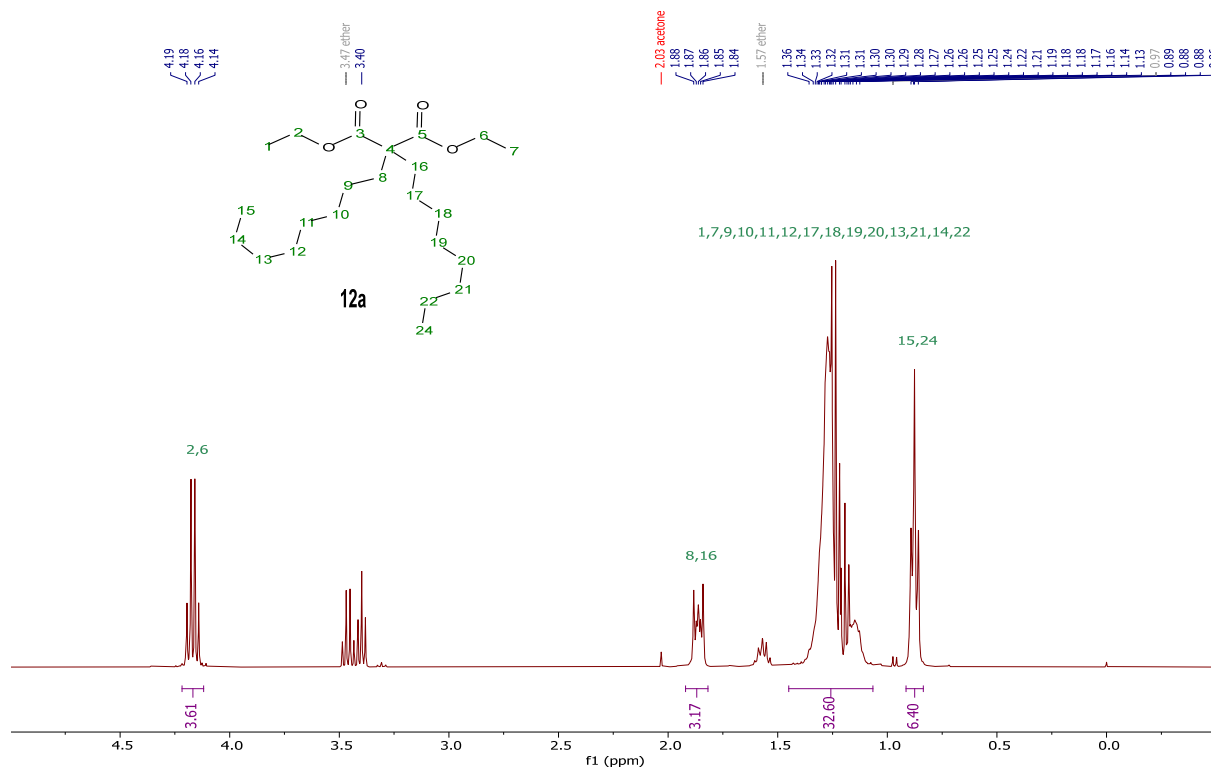
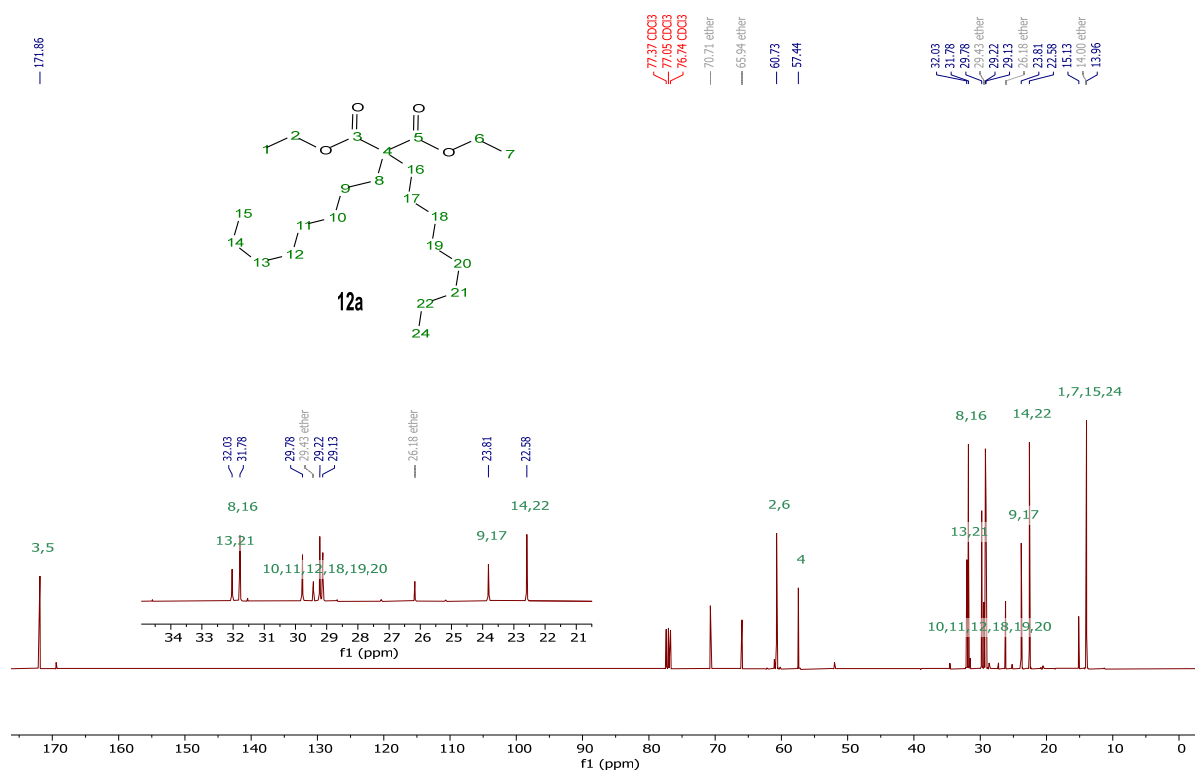
**11b** $^1\text{H}$  NMR (400 MHz, Chloroform-d) $^{13}\text{C}\{^1\text{H}\}$  NMR (101 MHz, Chloroform-d)

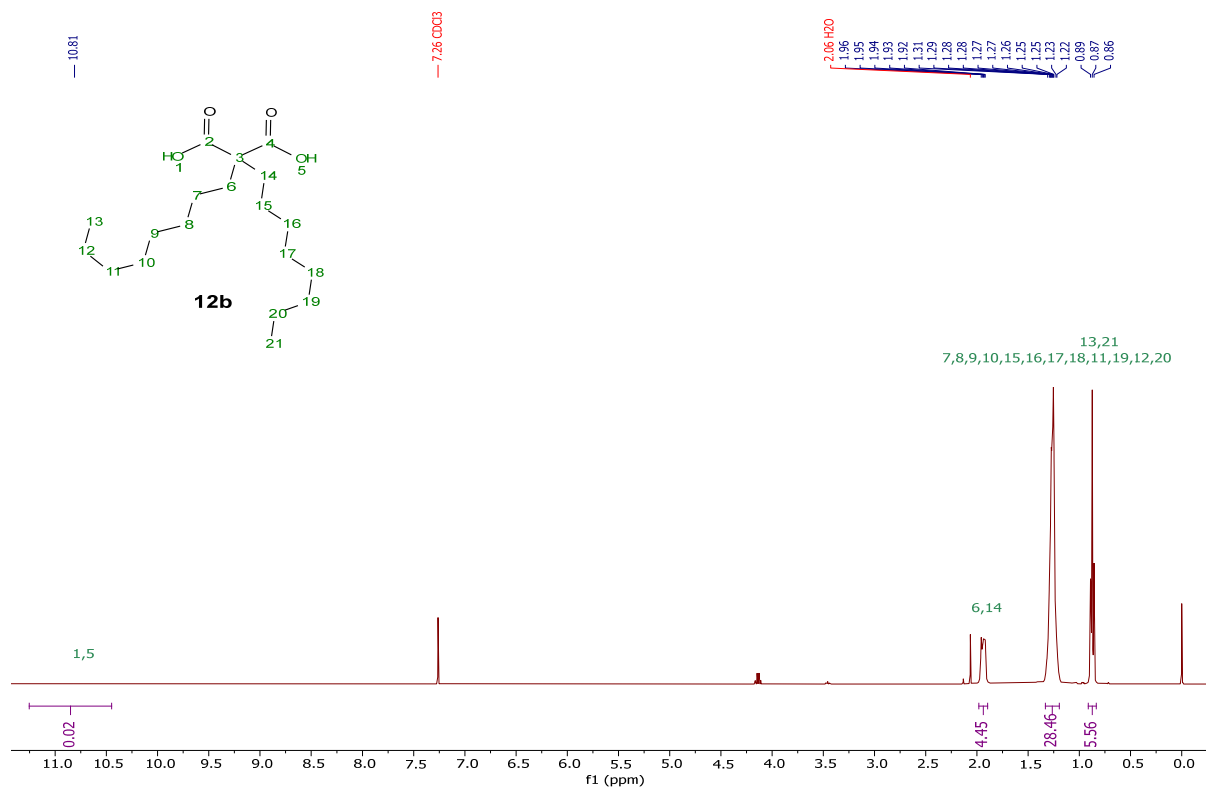
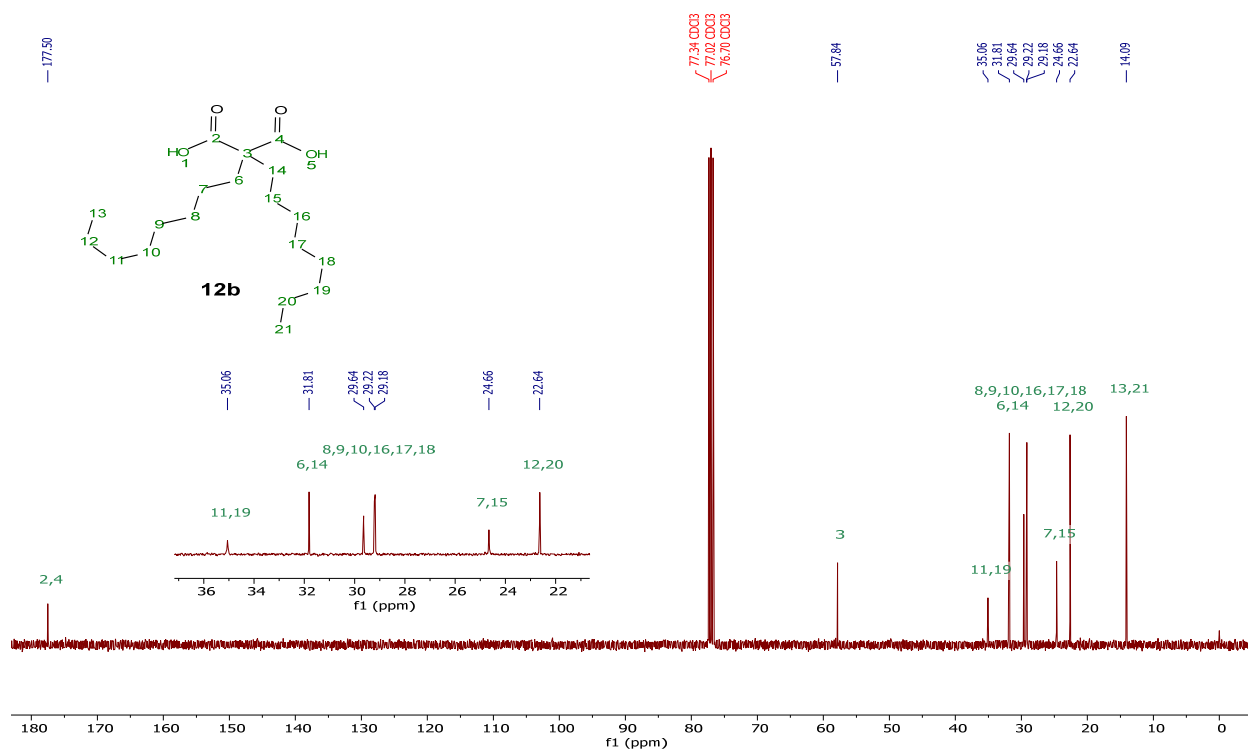
**11c** $^1\text{H}$  NMR (400 MHz, Chloroform-d) $^{13}\text{C}\{^1\text{H}\}$  NMR (101 MHz, Chloroform-d)

[chol][hoct], **11d** $^1\text{H}$  NMR (400 MHz, Chloroform-d) $^{13}\text{C}\{^1\text{H}\}$  NMR (101 MHz, Chloroform-d)

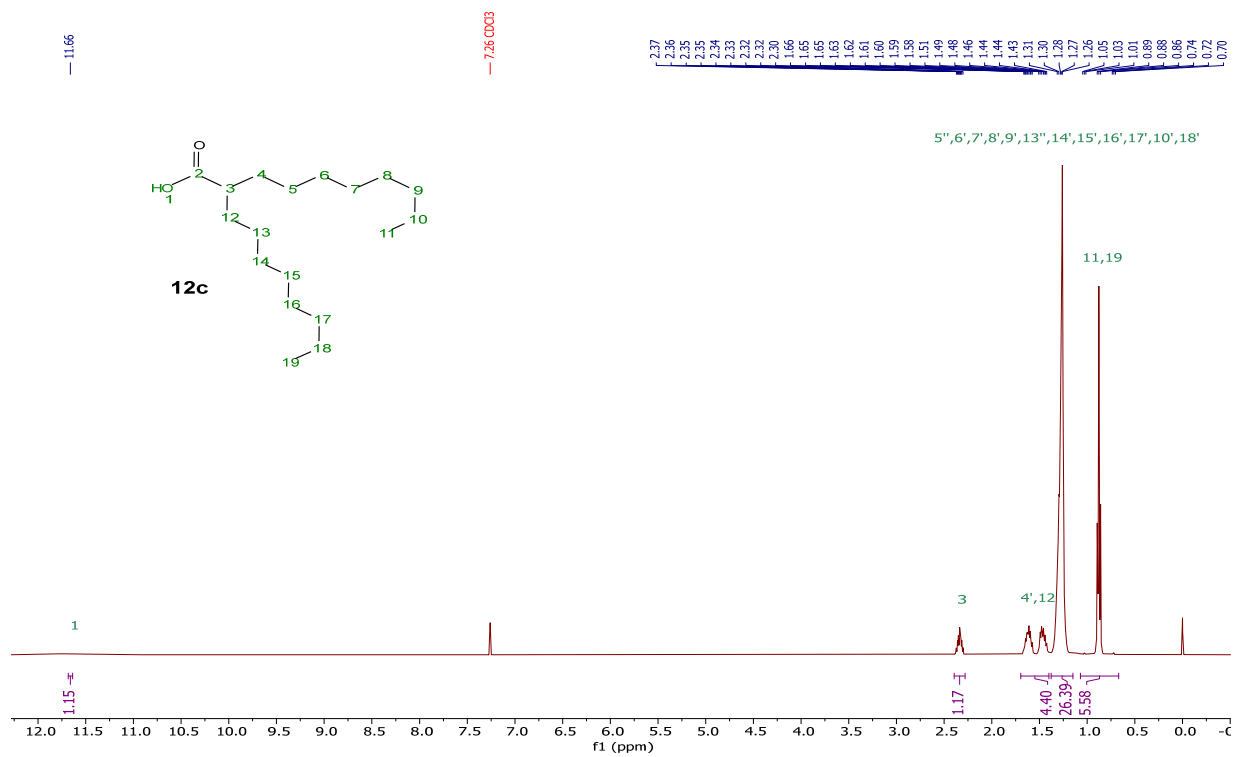
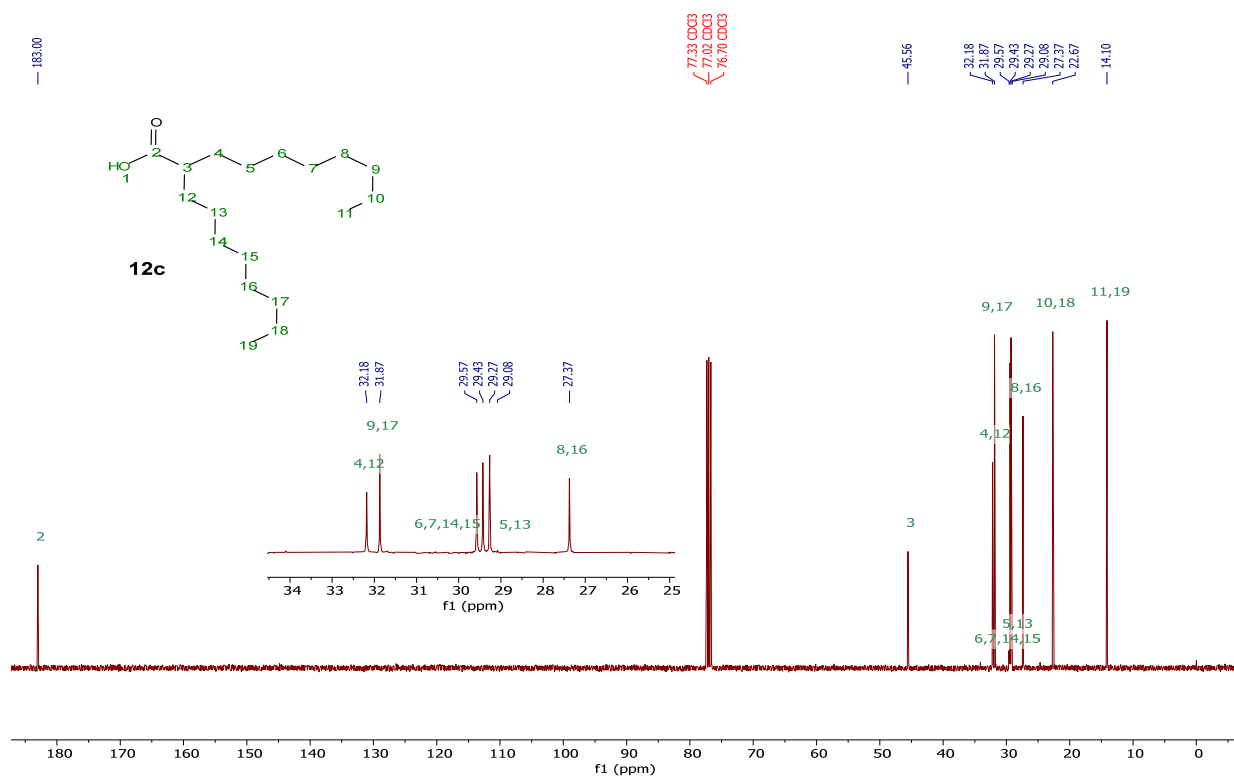
[DC-8][2hoct], **11e** $^1\text{H}$  NMR (400 MHz, Chloroform-d) $^{13}\text{C}\{^1\text{H}\}$  NMR (101 MHz, Chloroform-d)

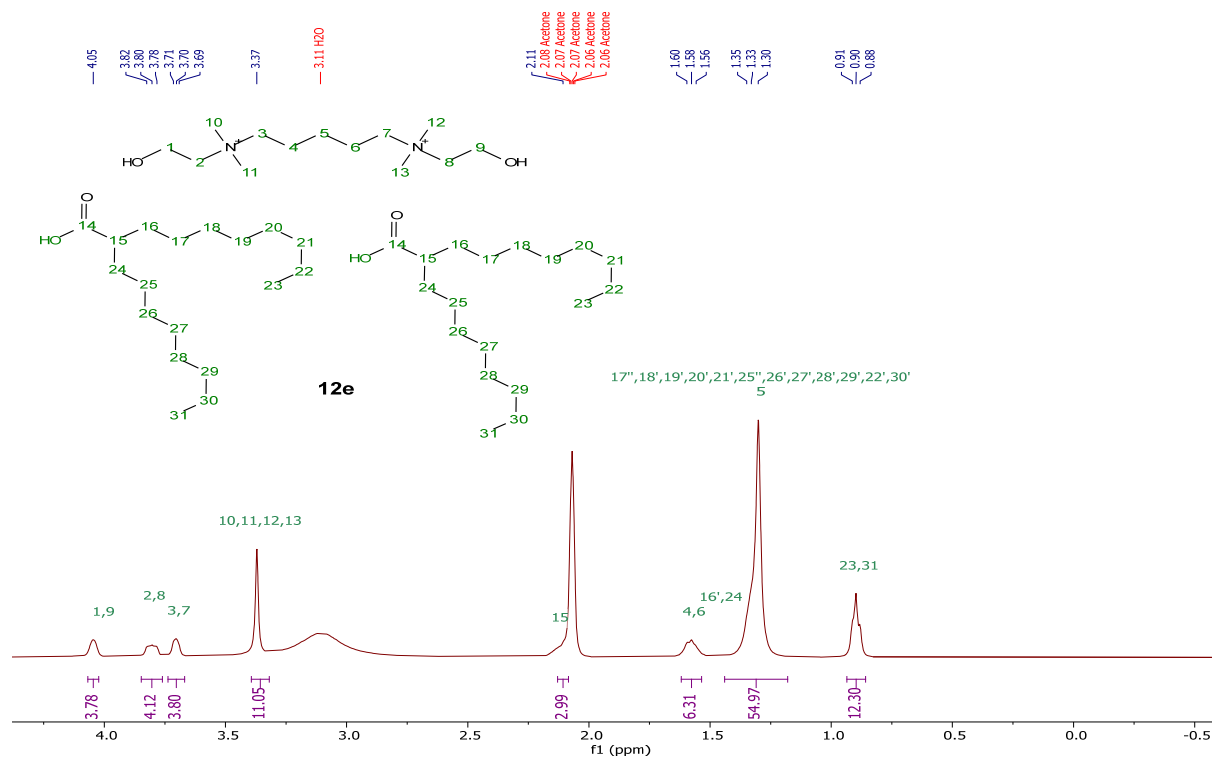
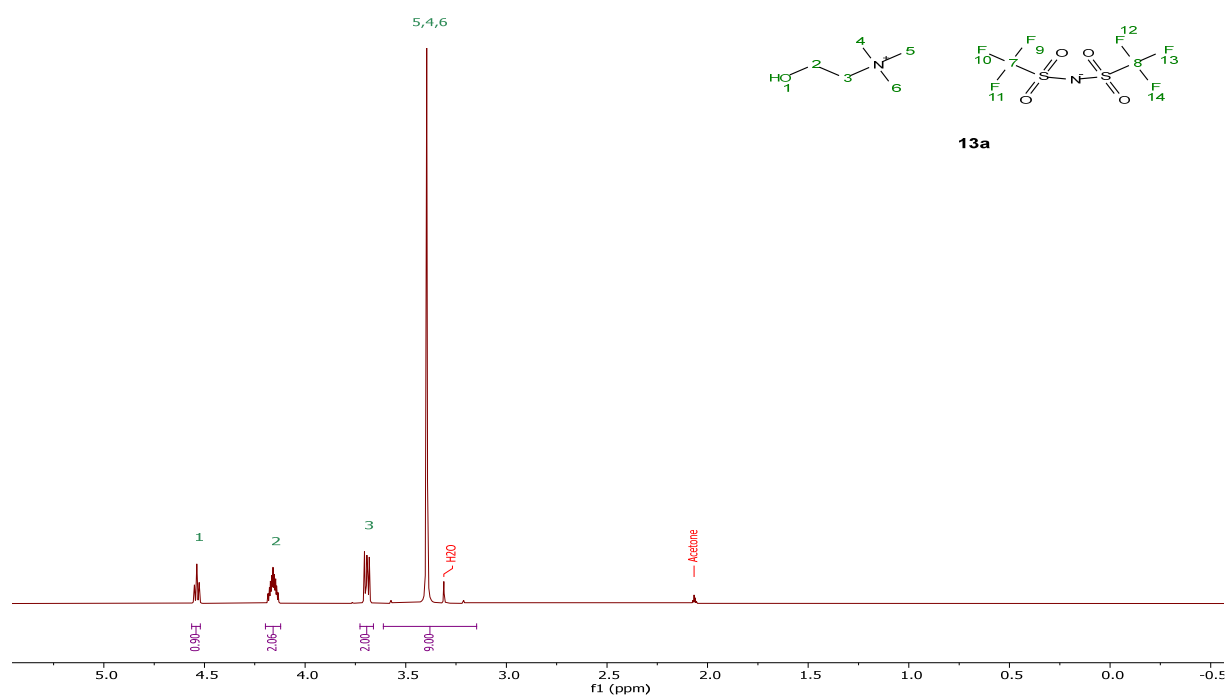
## 12a

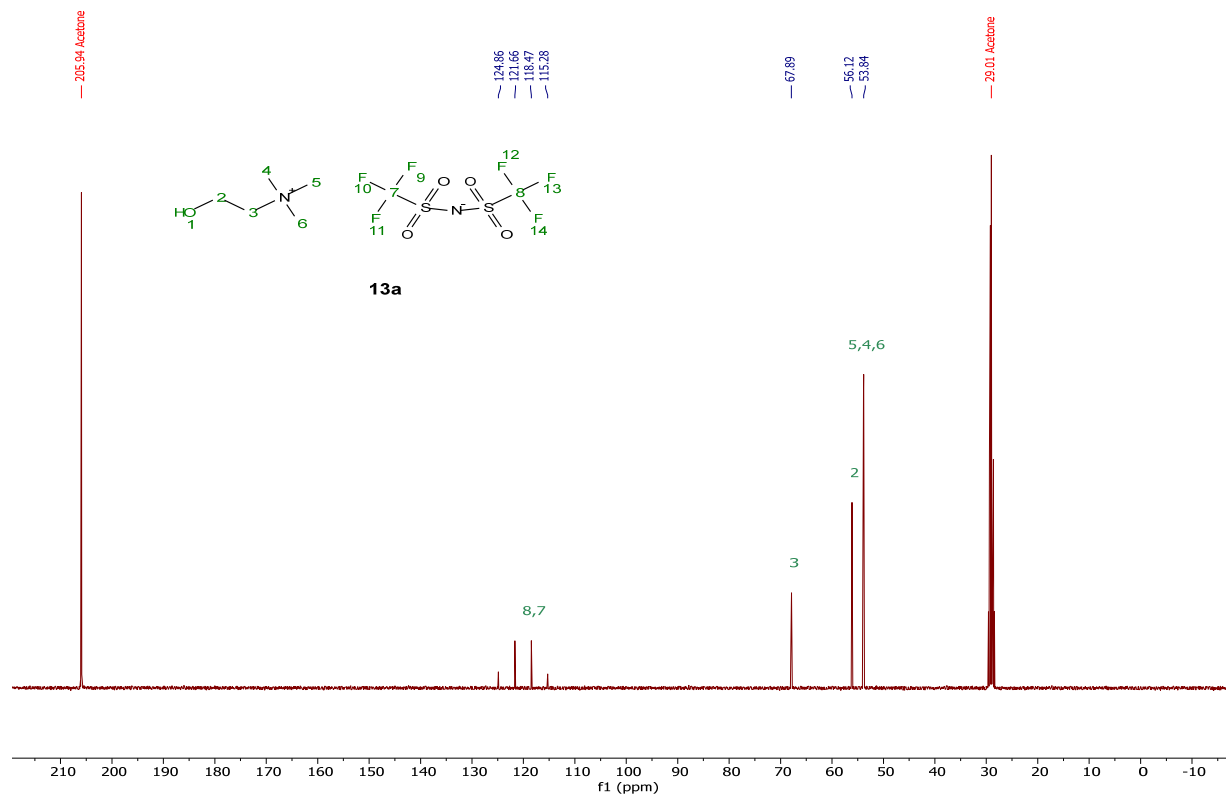
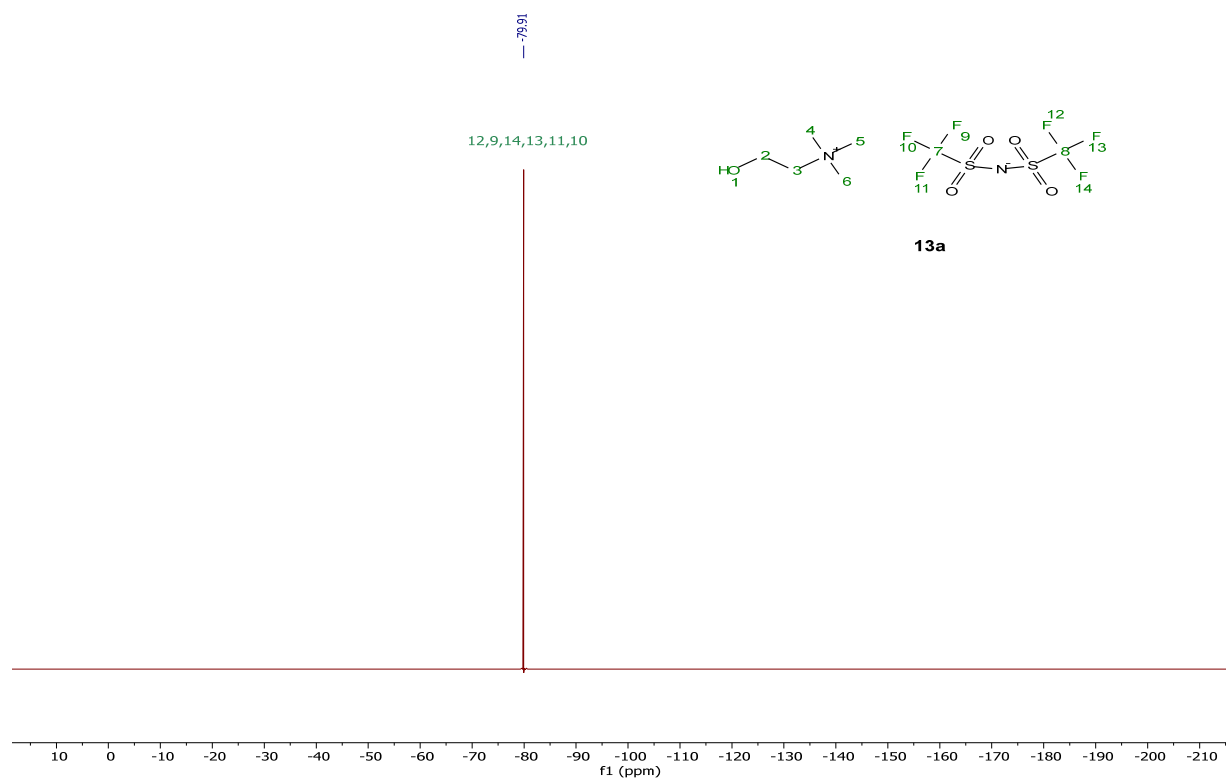
 $^1\text{H}$  NMR (400 MHz, Chloroform-d) $^{13}\text{C}\{^1\text{H}\}$  NMR (101 MHz, Chloroform-d)

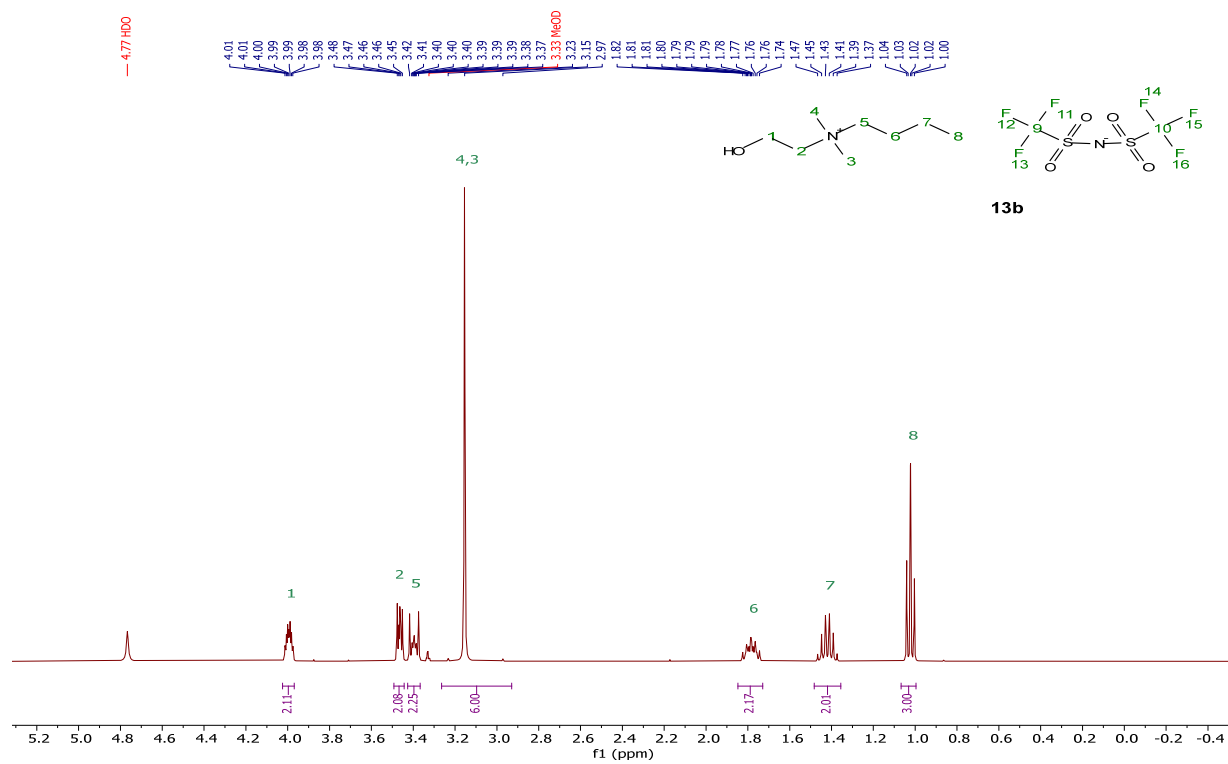
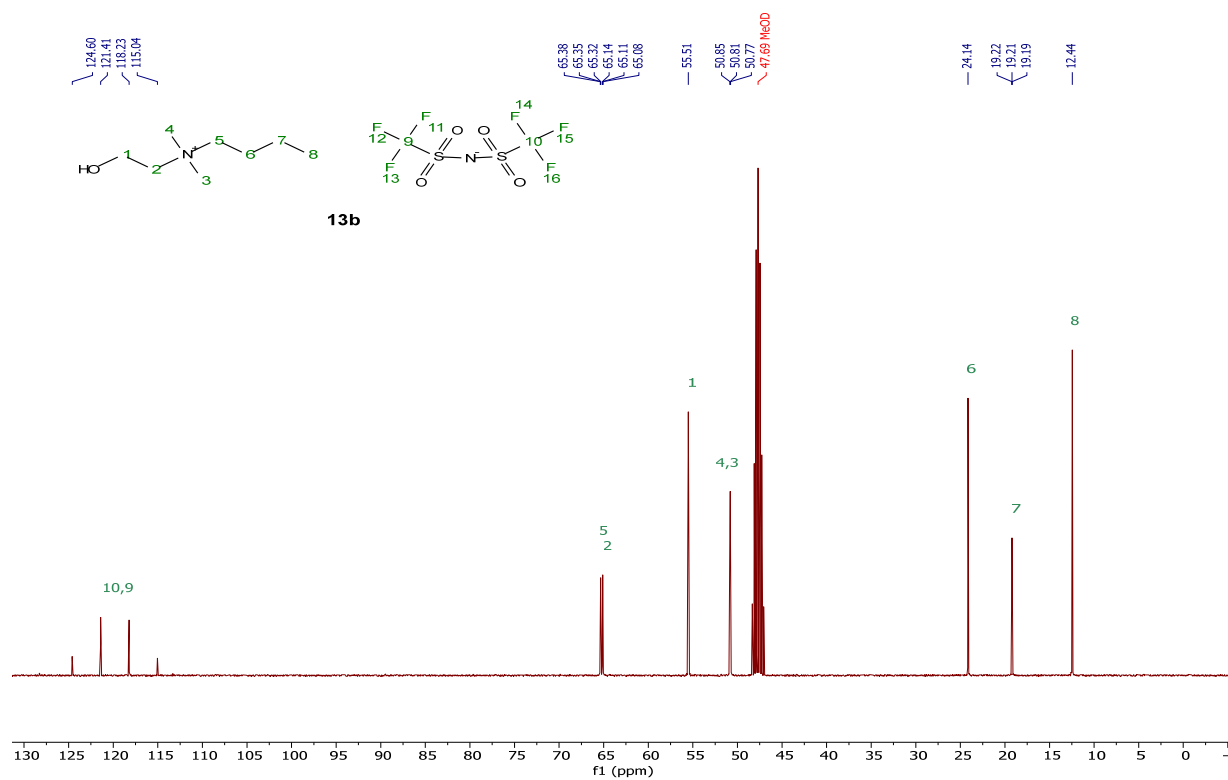
**12b** $^1\text{H}$  NMR (400 MHz, Chloroform-d) $^{13}\text{C}\{^1\text{H}\}$  NMR (101 MHz, Chloroform-d)

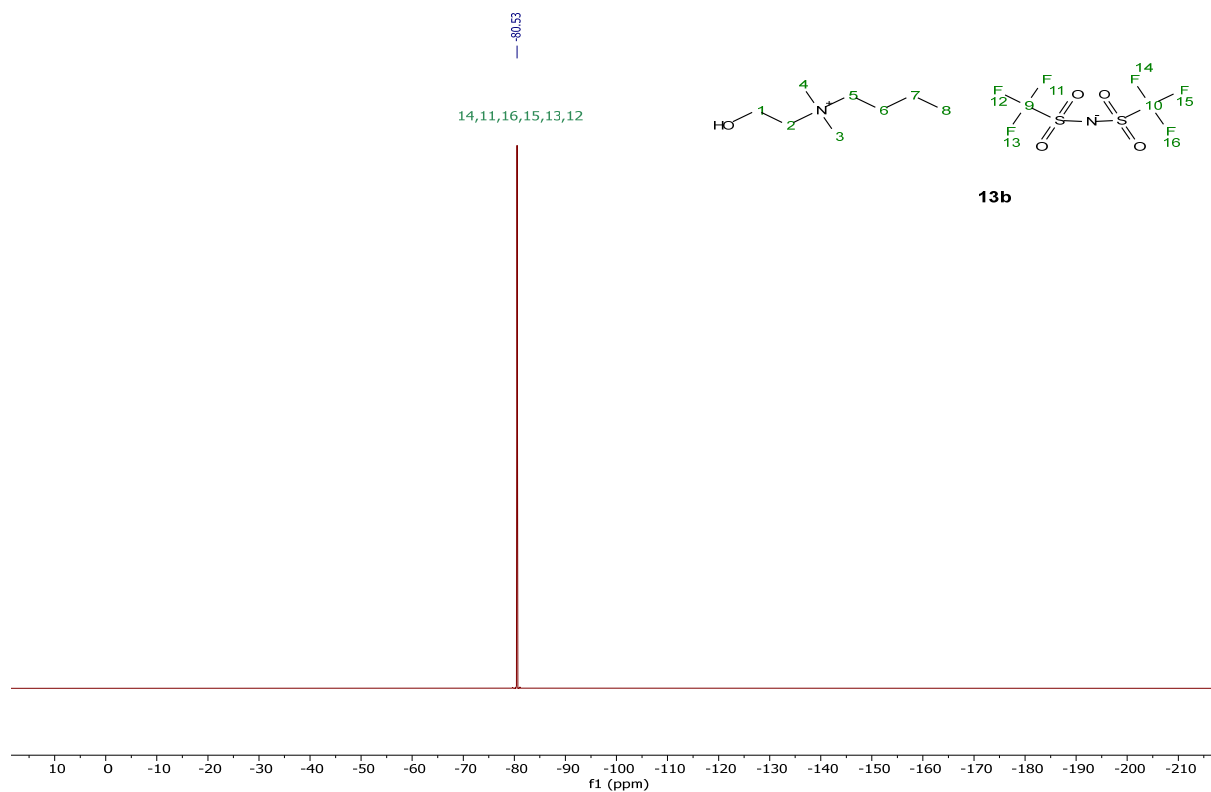
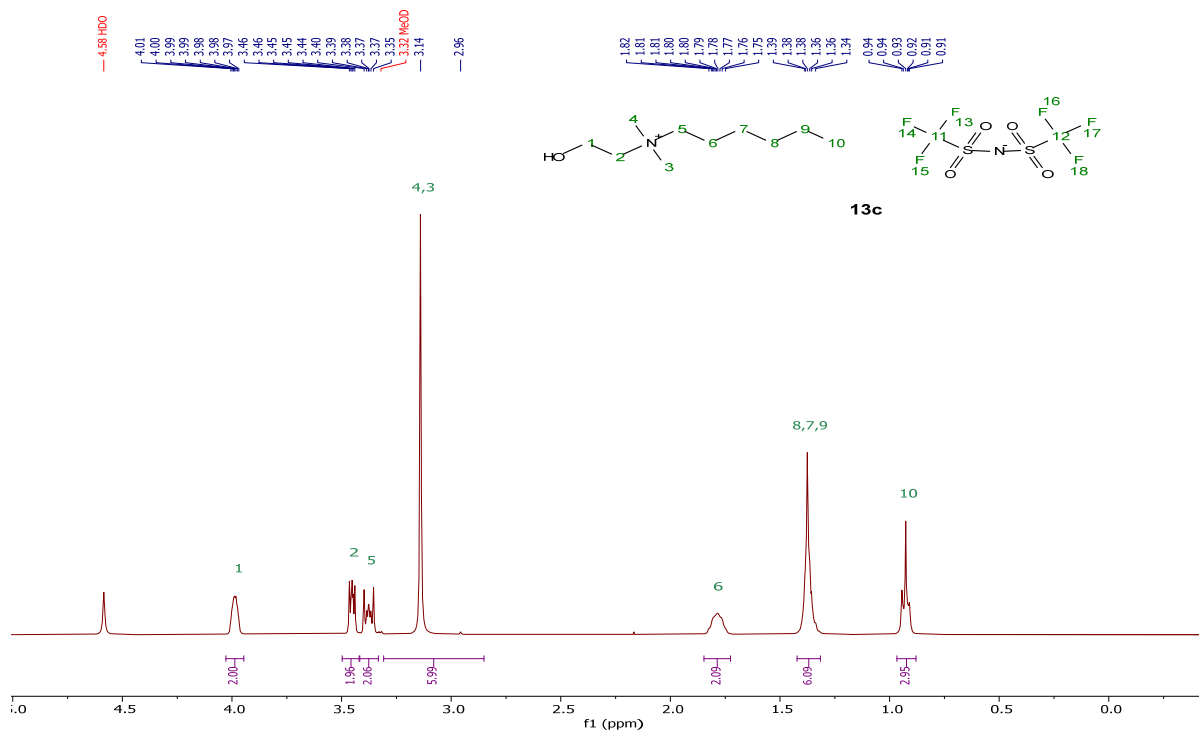
## 12c

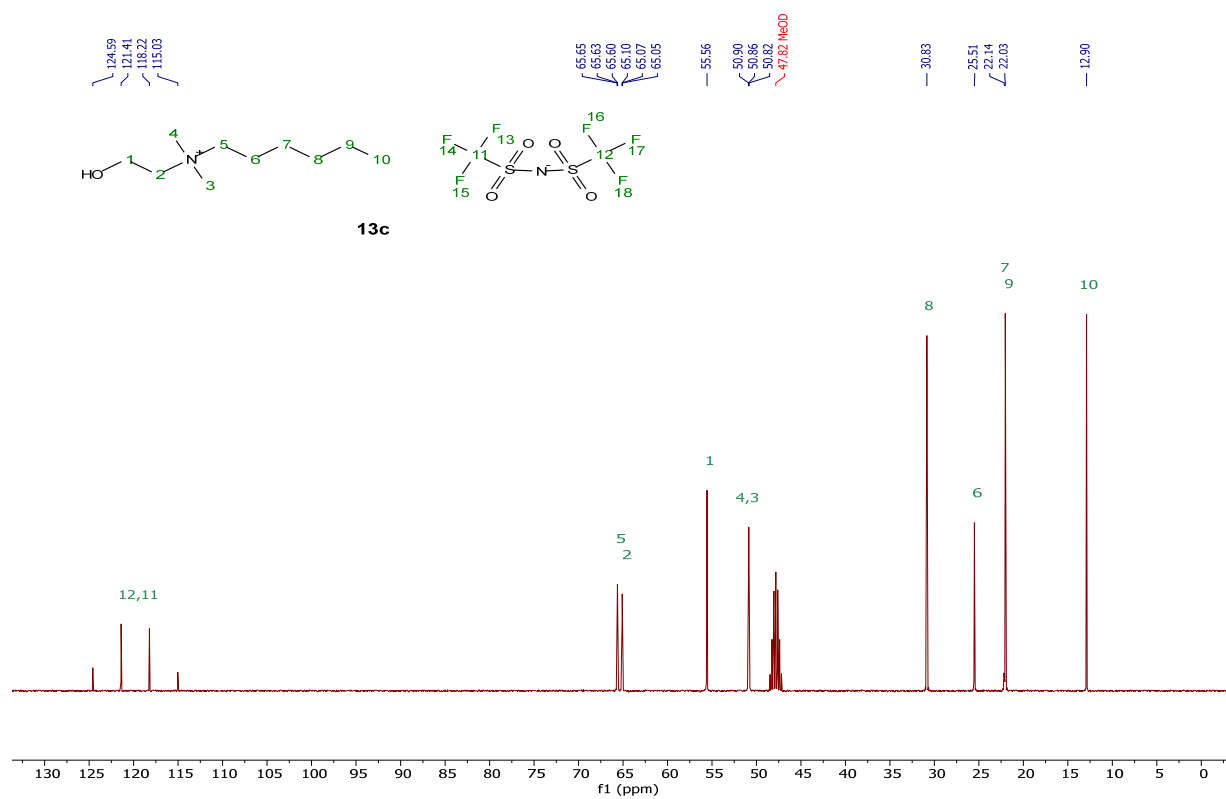
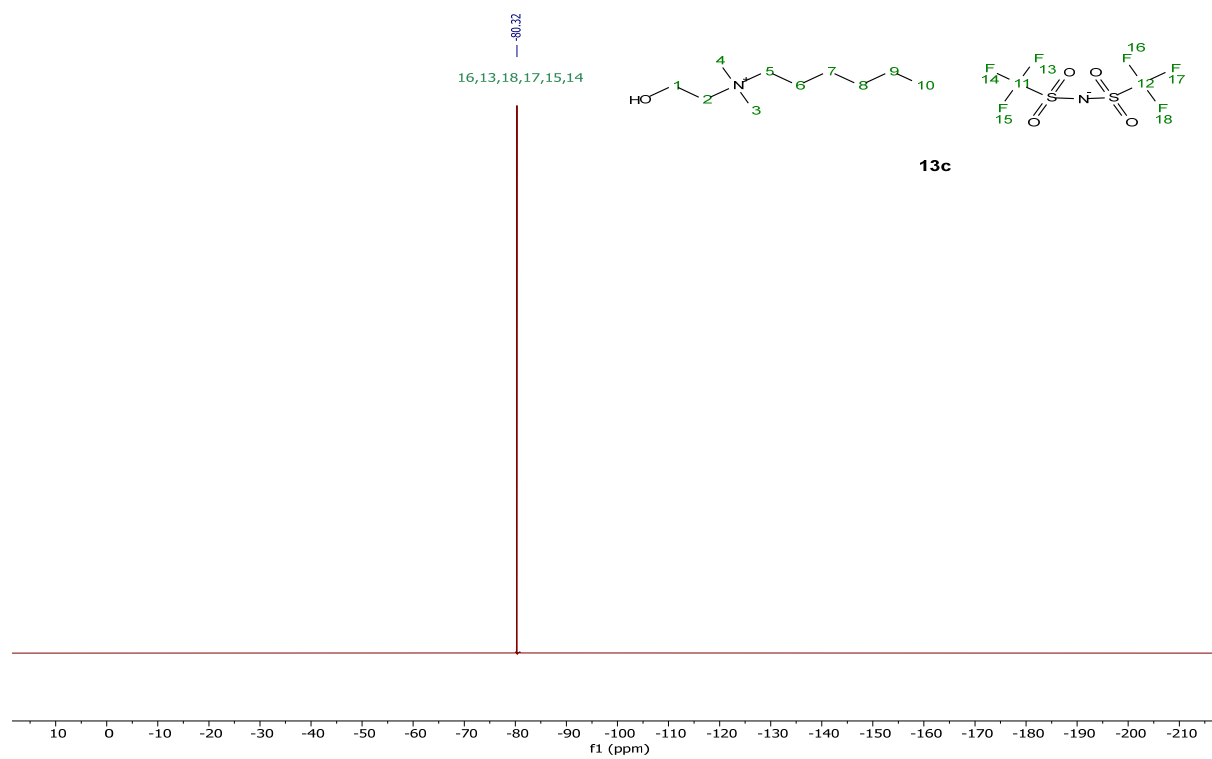
 $^1\text{H}$  NMR (400 MHz, Chloroform-d) $^{13}\text{C}\{^1\text{H}\}$  NMR (101 MHz, Chloroform-d)

[DC-5][2odec], **12e** $^1\text{H}$  NMR (400 MHz, Acetone- $d_6$ )[chol][NTf<sub>2</sub>], **13a** $^1\text{H}$  NMR (400 MHz, Acetone- $d_6$ )

$^{13}\text{C}\{^1\text{H}\}$  NMR (101 MHz, Acetone- $d_6$ ) $^{19}\text{F}$  NMR (376 MHz, Acetone- $d_6$ )

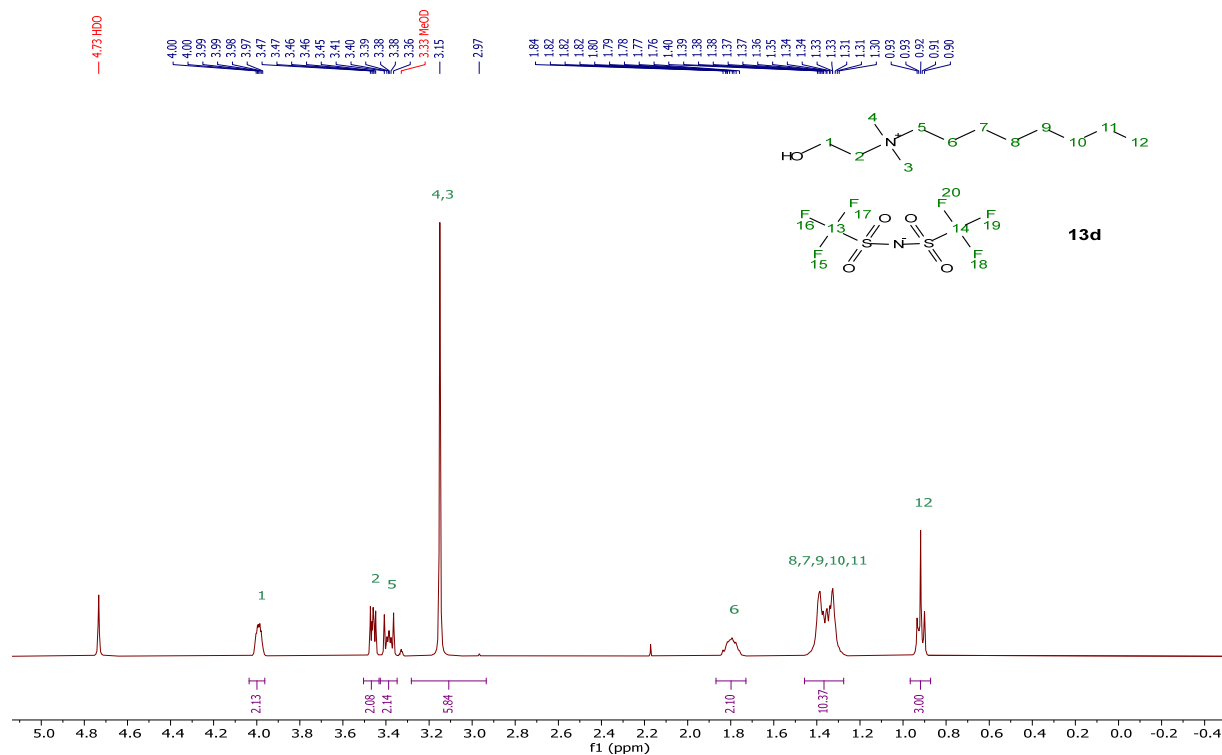
[N<sub>1,1,4,2OH</sub>][NTf<sub>2</sub>], **13b**<sup>1</sup>H NMR (400 MHz, Methanol-d<sub>4</sub>)<sup>13</sup>C{<sup>1</sup>H} NMR (101 MHz, Methanol-d<sub>4</sub>)

$^{19}\text{F}$  NMR (376 MHz, Methanol- $d_4$ ) $[\text{N}_{1,1,6,2\text{OH}}][\text{NTf}_2]$ , **13c** $^1\text{H}$  NMR (400 MHz, Methanol- $d_4$ )

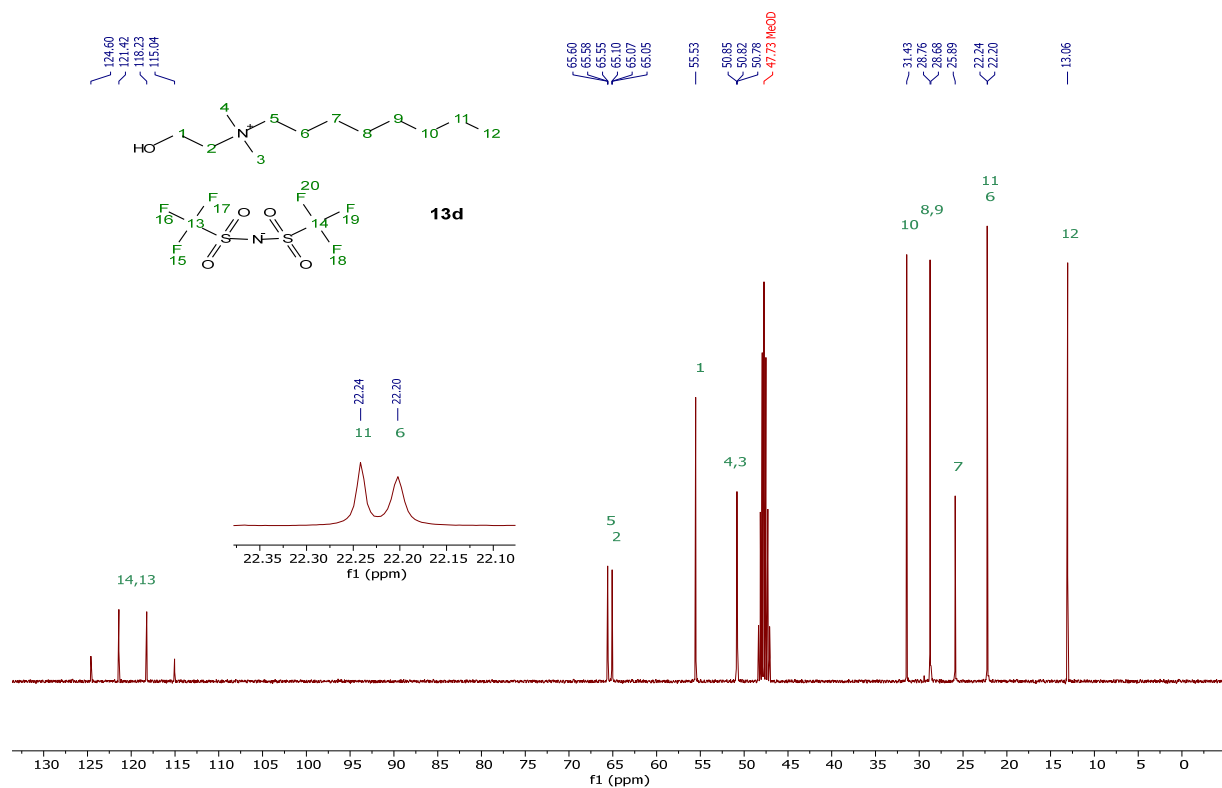
$^{13}\text{C}\{^1\text{H}\}$  NMR (101 MHz, Methanol-d<sub>4</sub>) $^{19}\text{F}$  NMR (376 MHz, Methanol-d<sub>4</sub>)

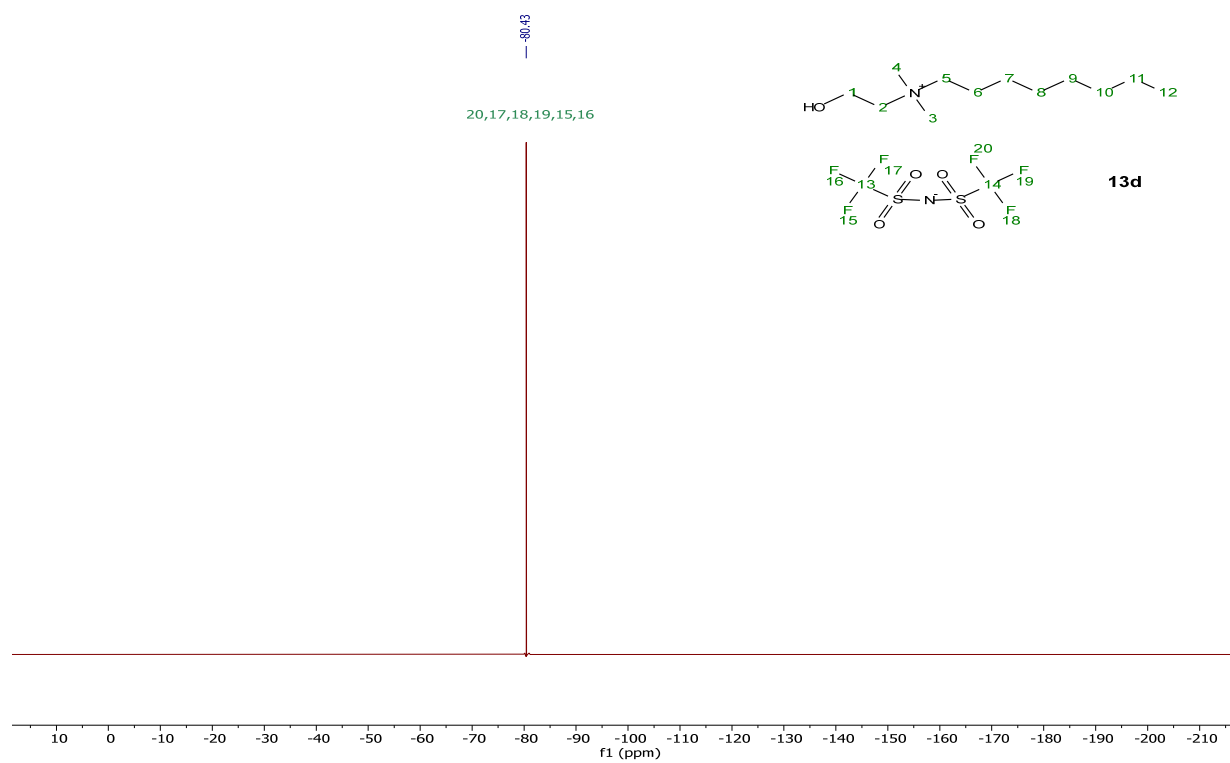
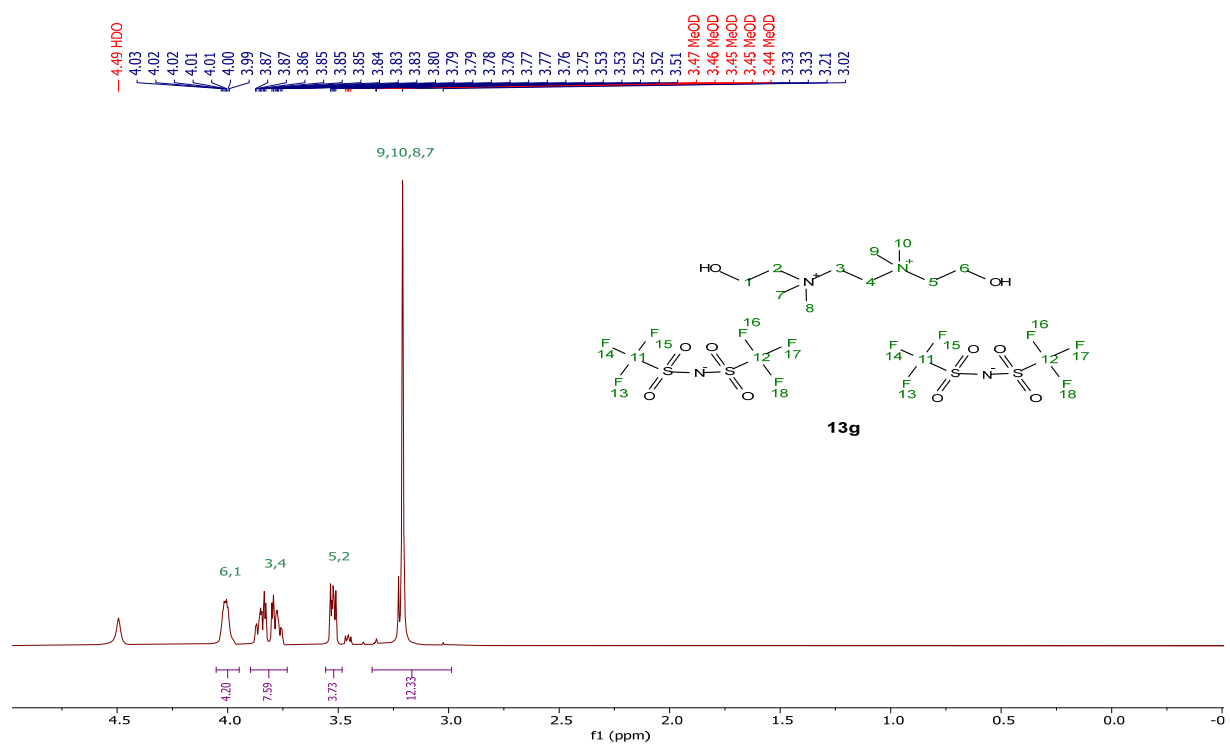
$[N_{1,1,8,2OH}][NTf_2]$ , **13d**

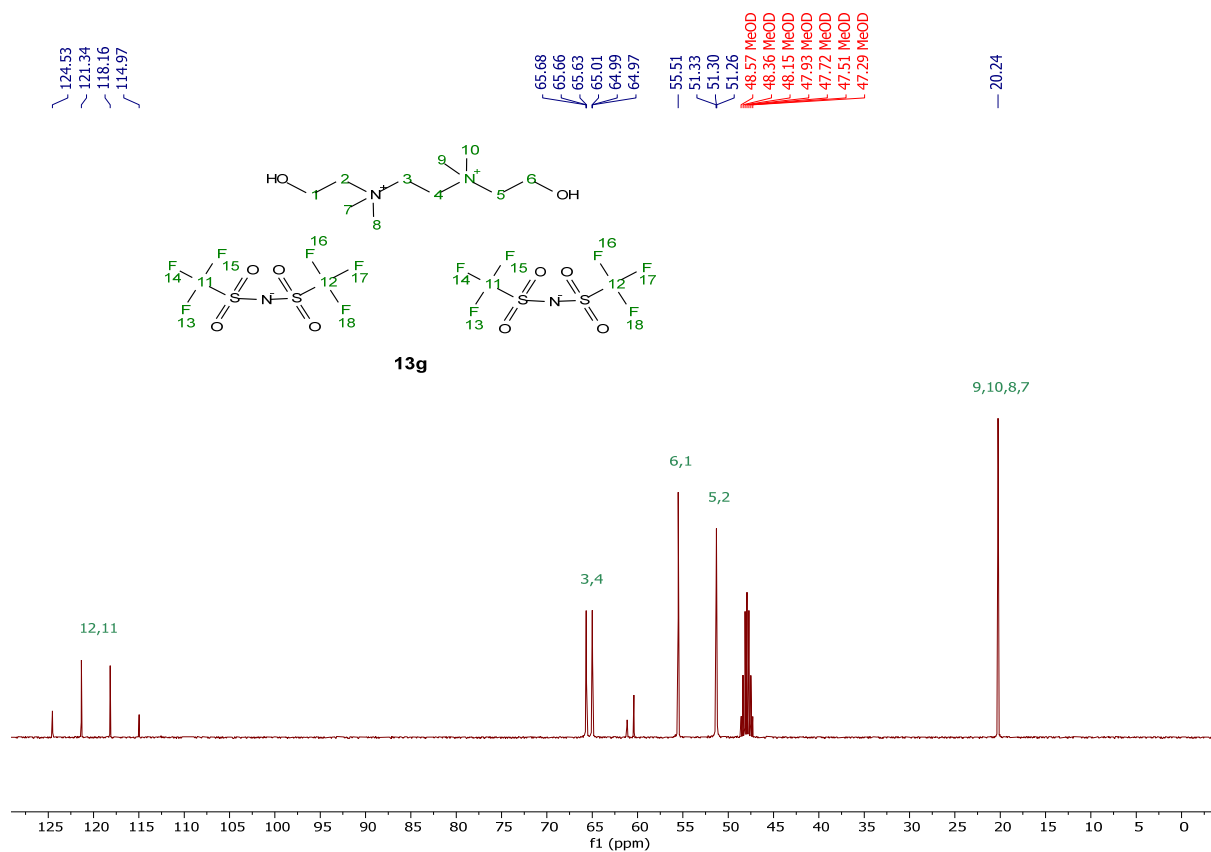
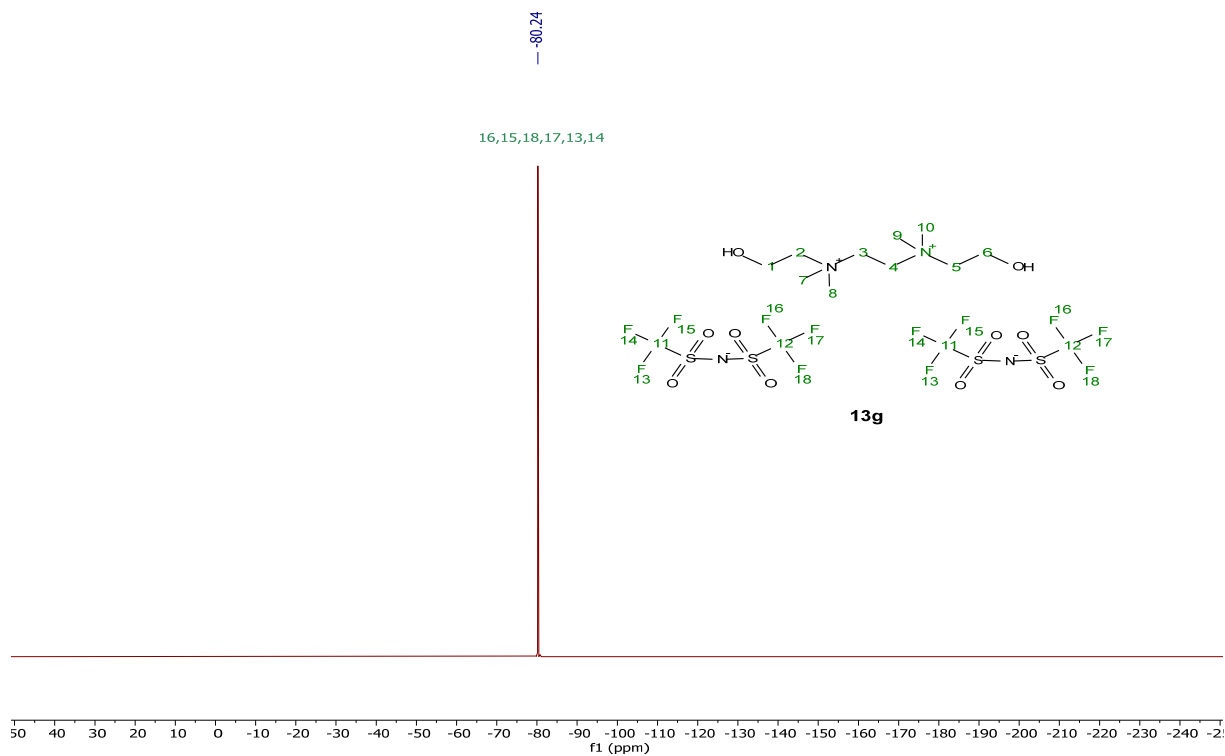
$^1H$  NMR (400 MHz, Methanol-d<sub>4</sub>)

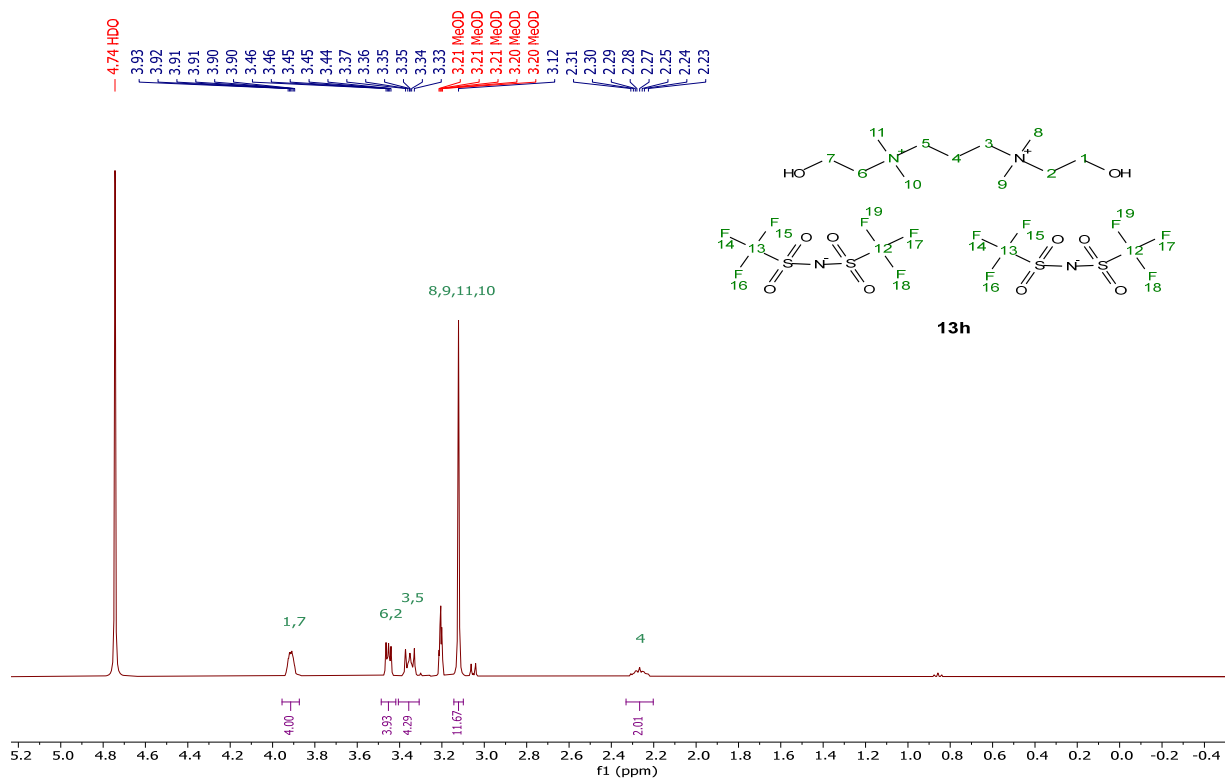
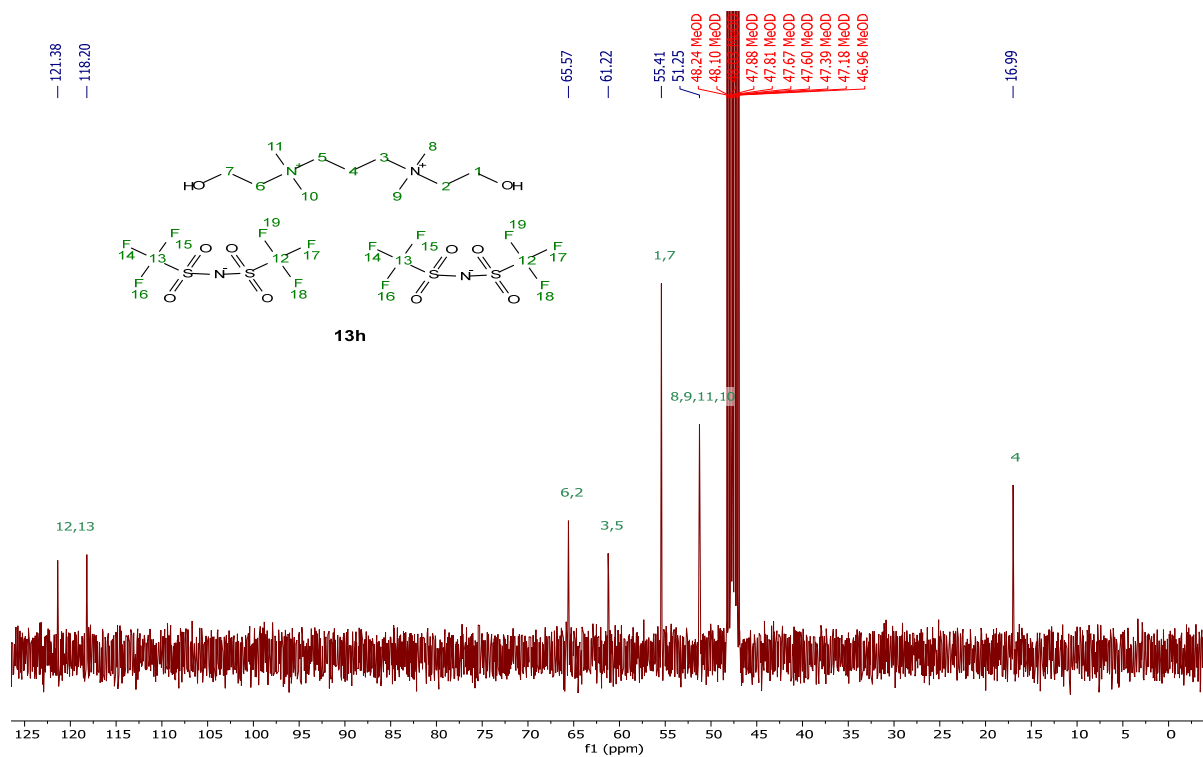


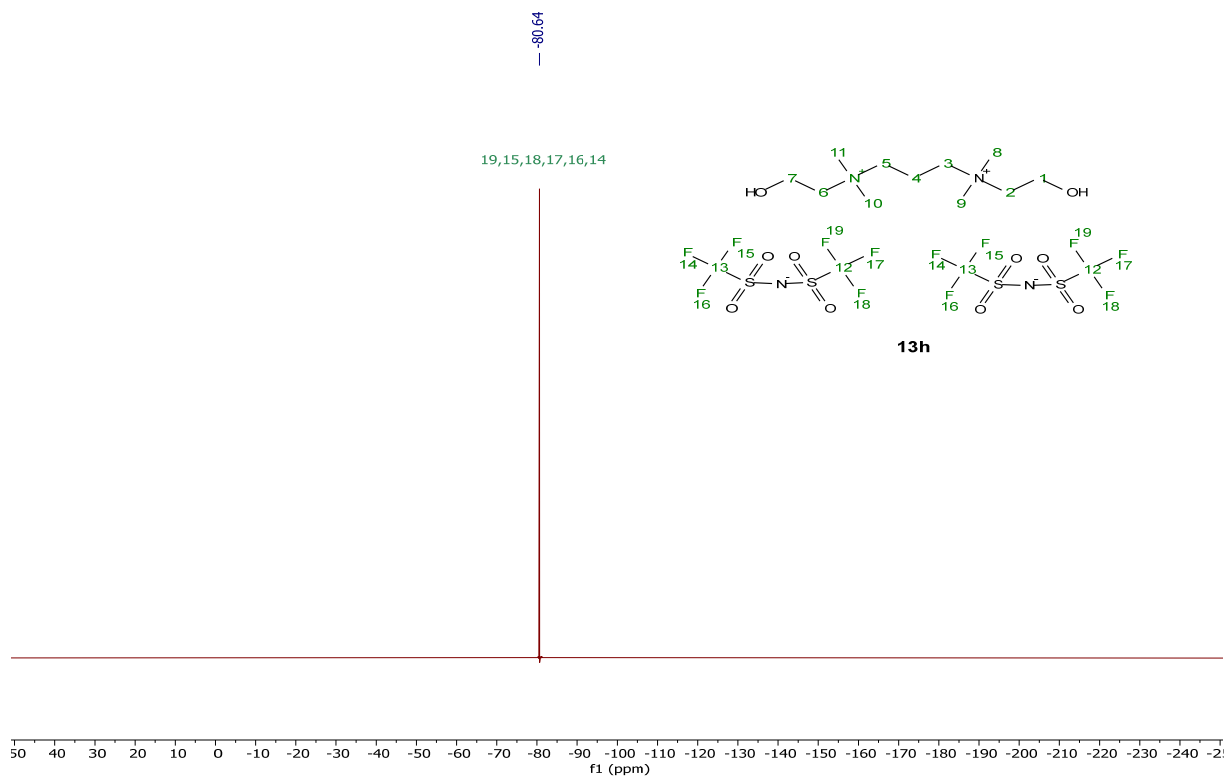
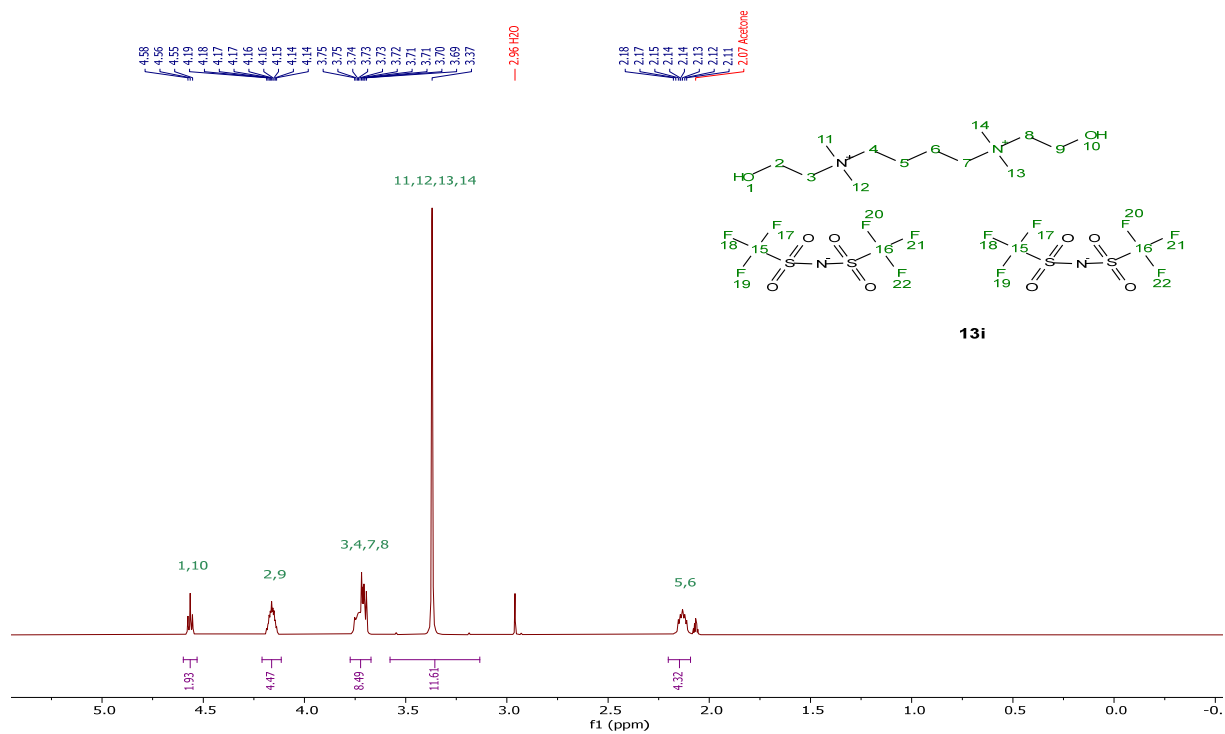
$^{13}C\{^1H\}$  NMR (101 MHz, Methanol-d<sub>4</sub>)

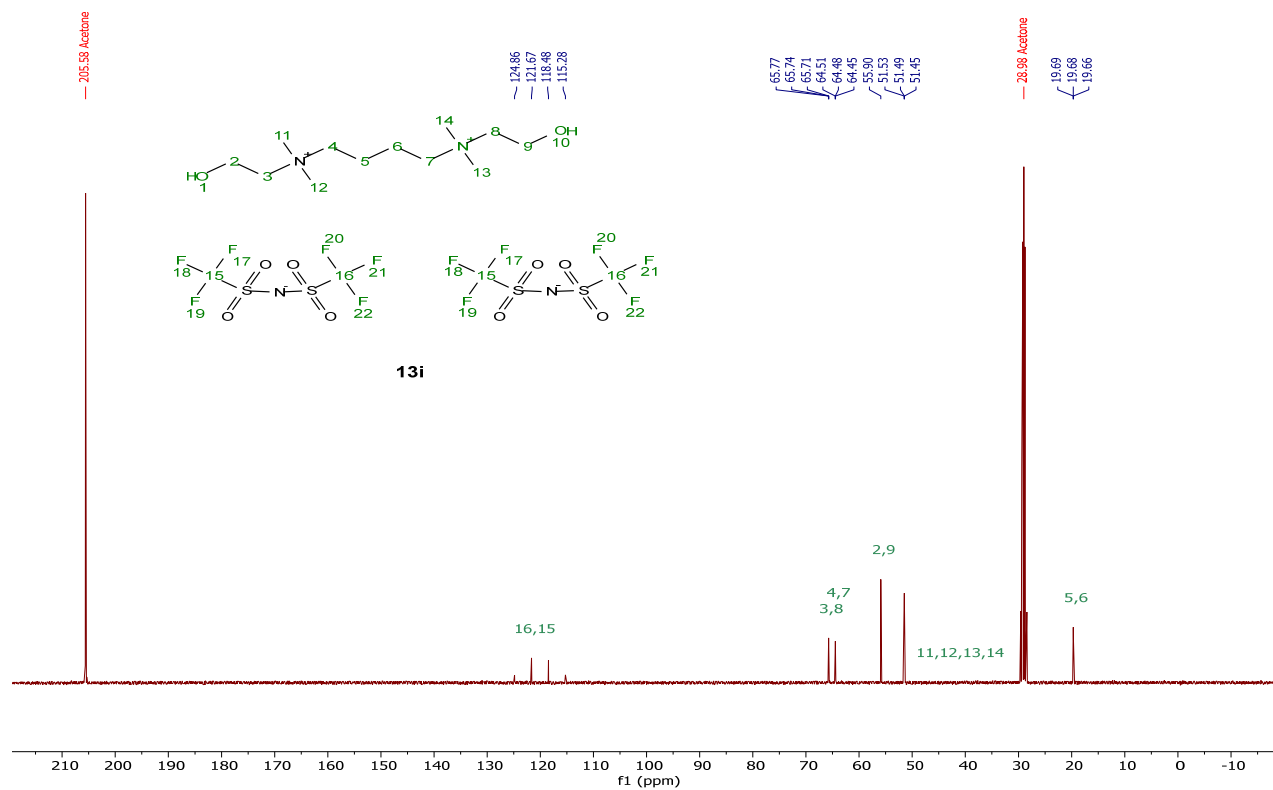
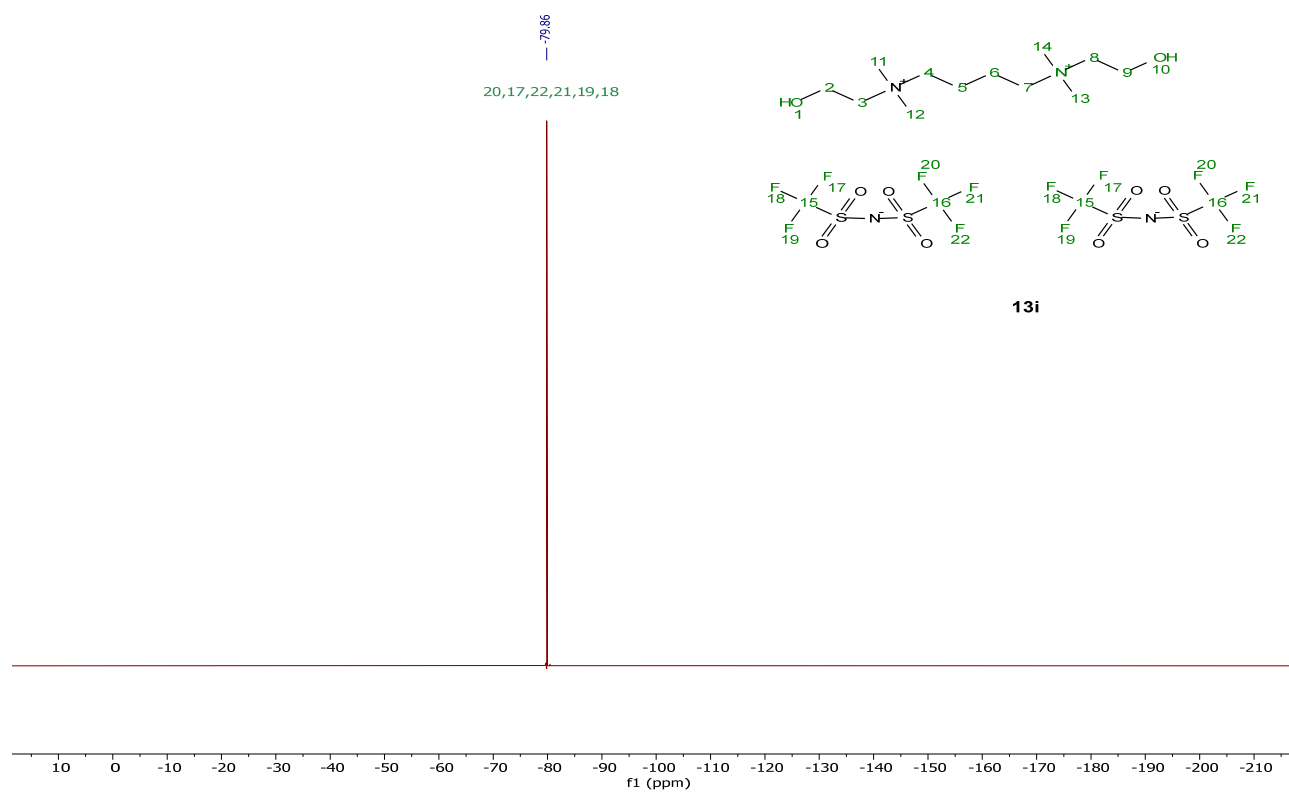


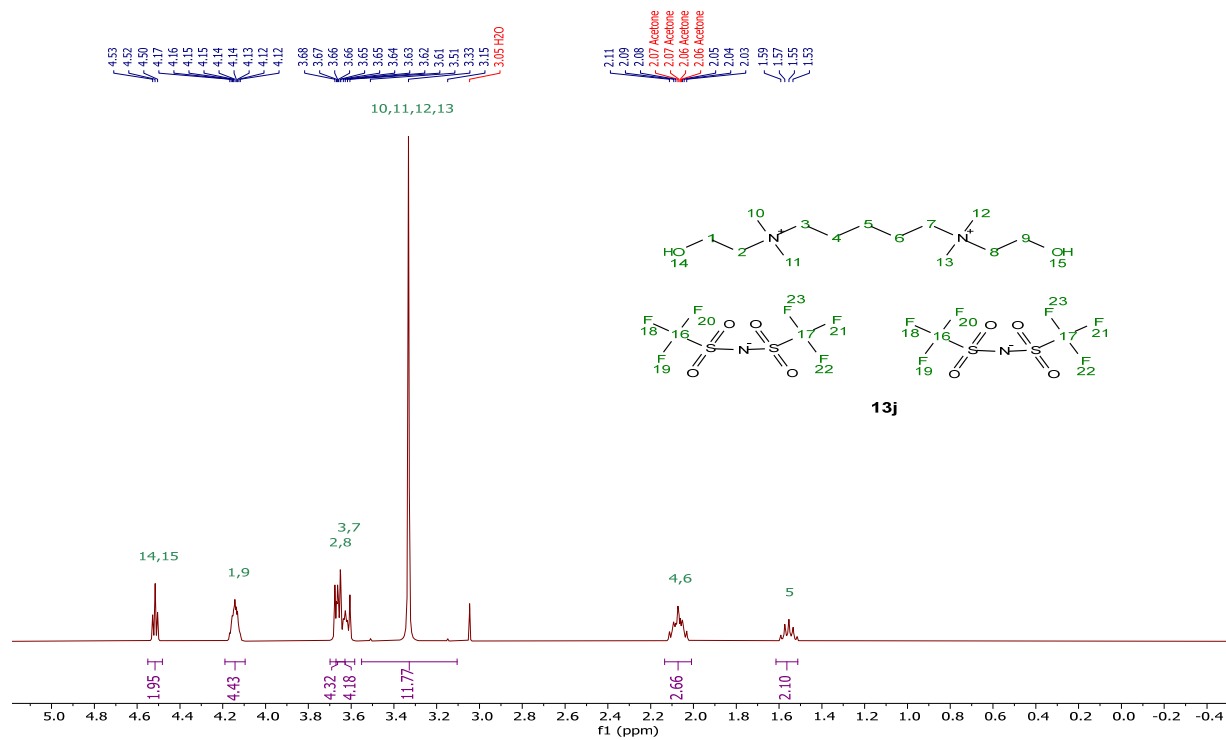
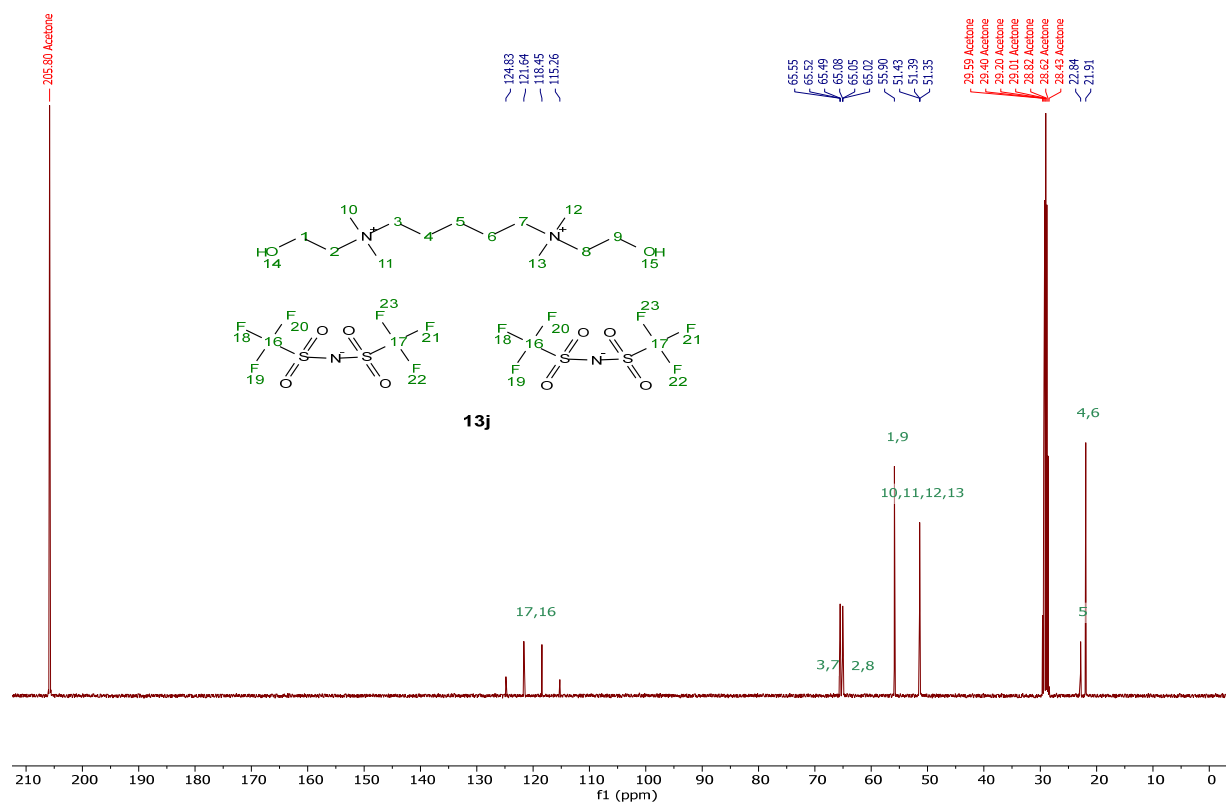
$^{19}\text{F}$  NMR (376 MHz, Methanol- $d_4$ )[DC-2][2NTf<sub>2</sub>], **13g** $^1\text{H}$  NMR (400 MHz, Methanol- $d_4$ )

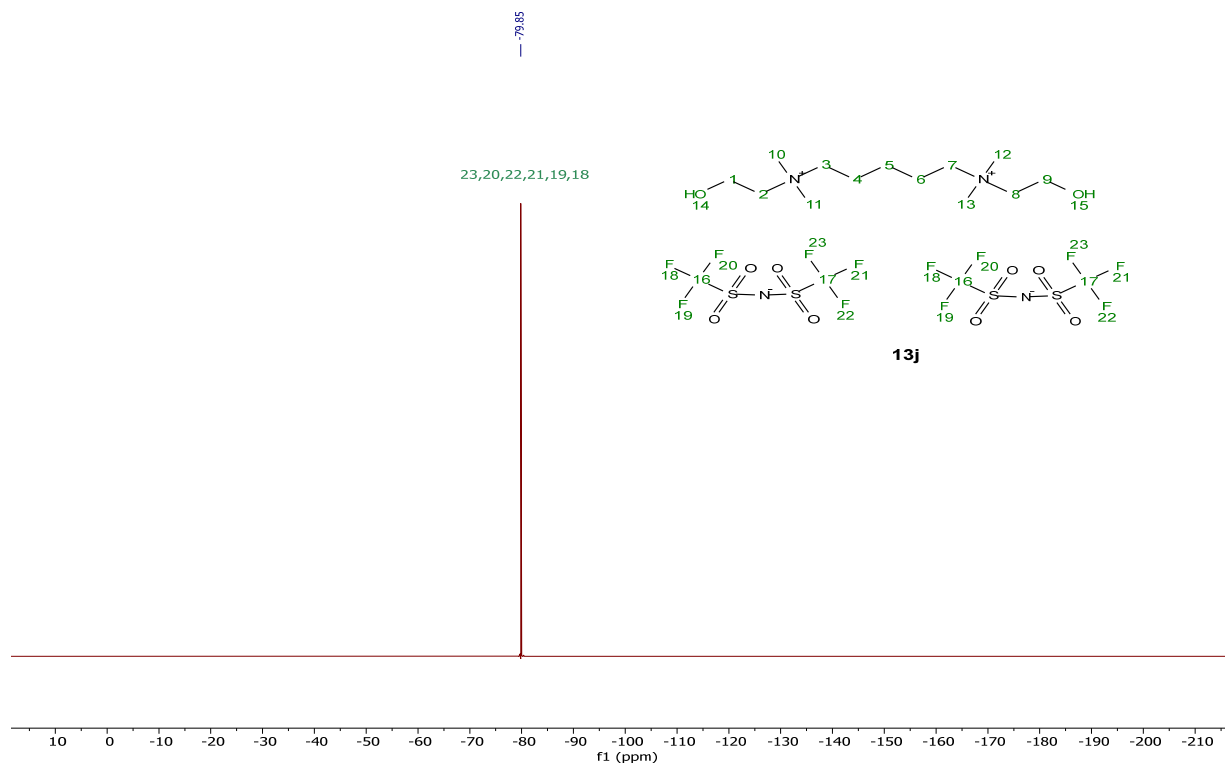
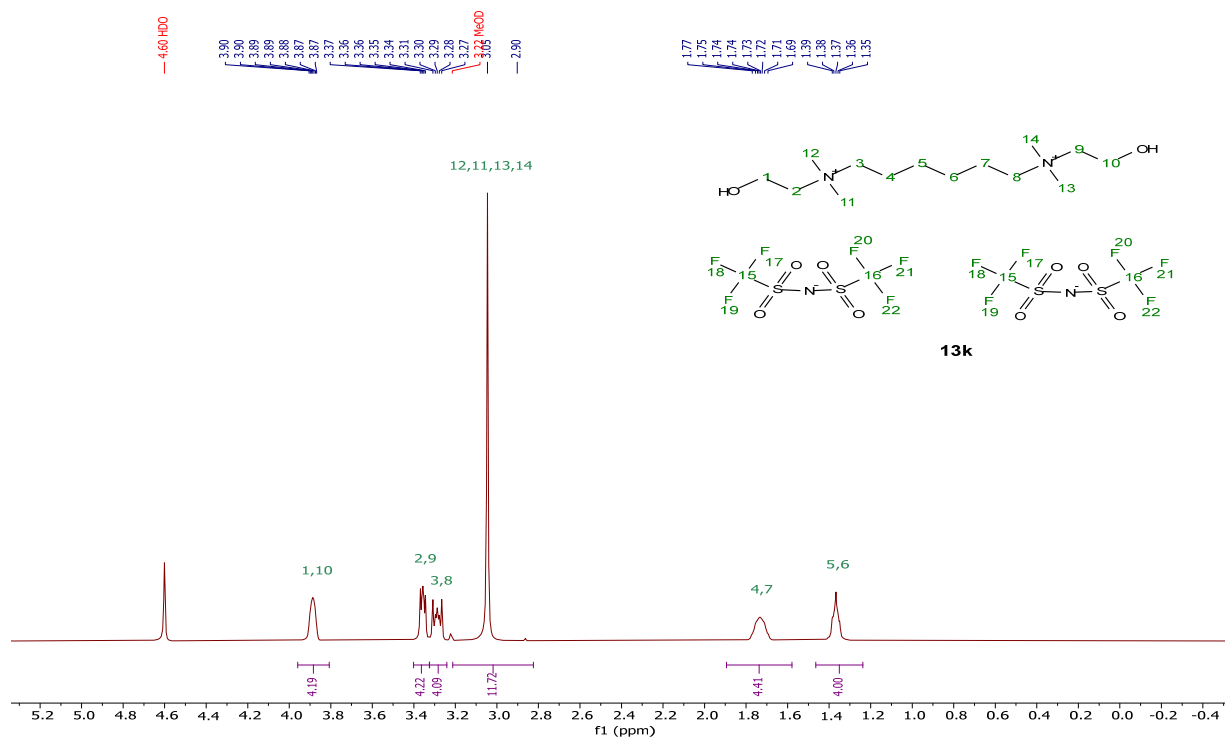
$^{13}\text{C}\{^1\text{H}\}$  NMR (101 MHz, Methanol-d<sub>4</sub>) $^{19}\text{F}$  NMR (376 MHz, Methanol-d<sub>4</sub>)

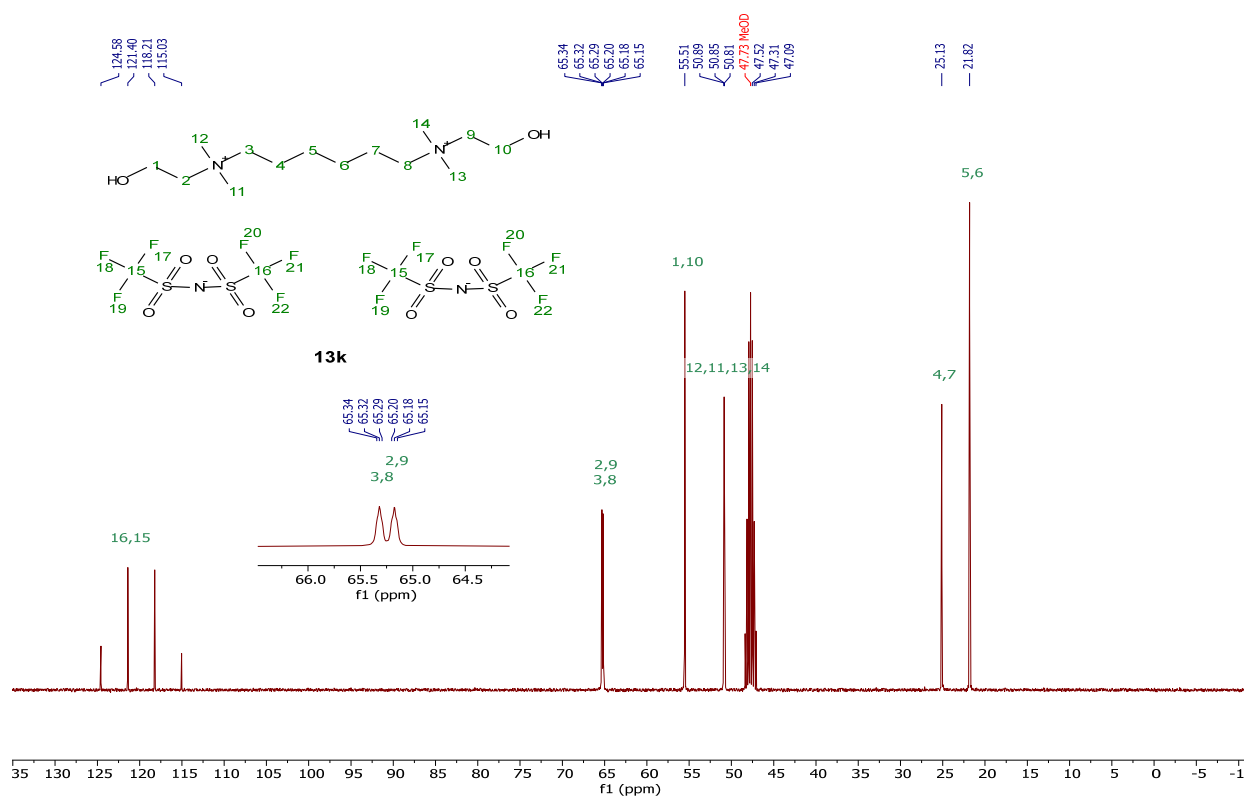
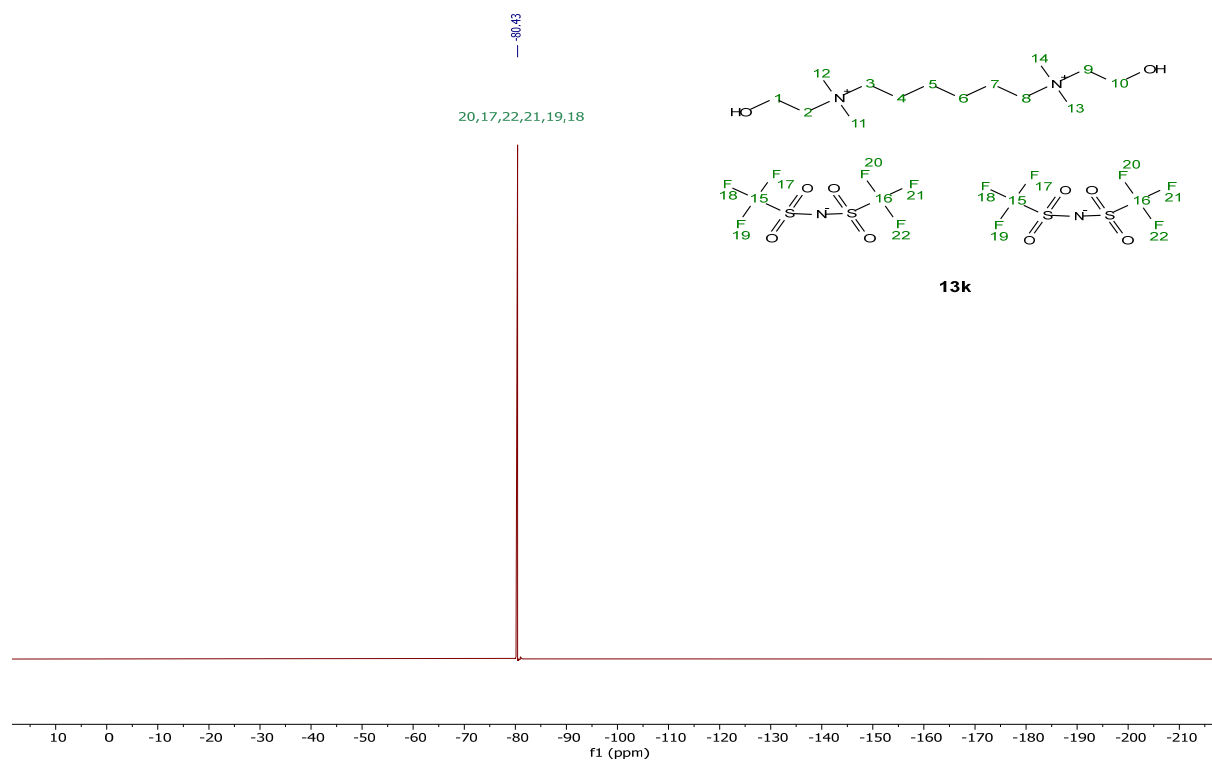
[DC-3][2NTf<sub>2</sub>], **13h**<sup>1</sup>H NMR (400 MHz, Methanol-d<sub>4</sub>)<sup>13</sup>C{<sup>1</sup>H} NMR (101 MHz, Methanol-d<sub>4</sub>)

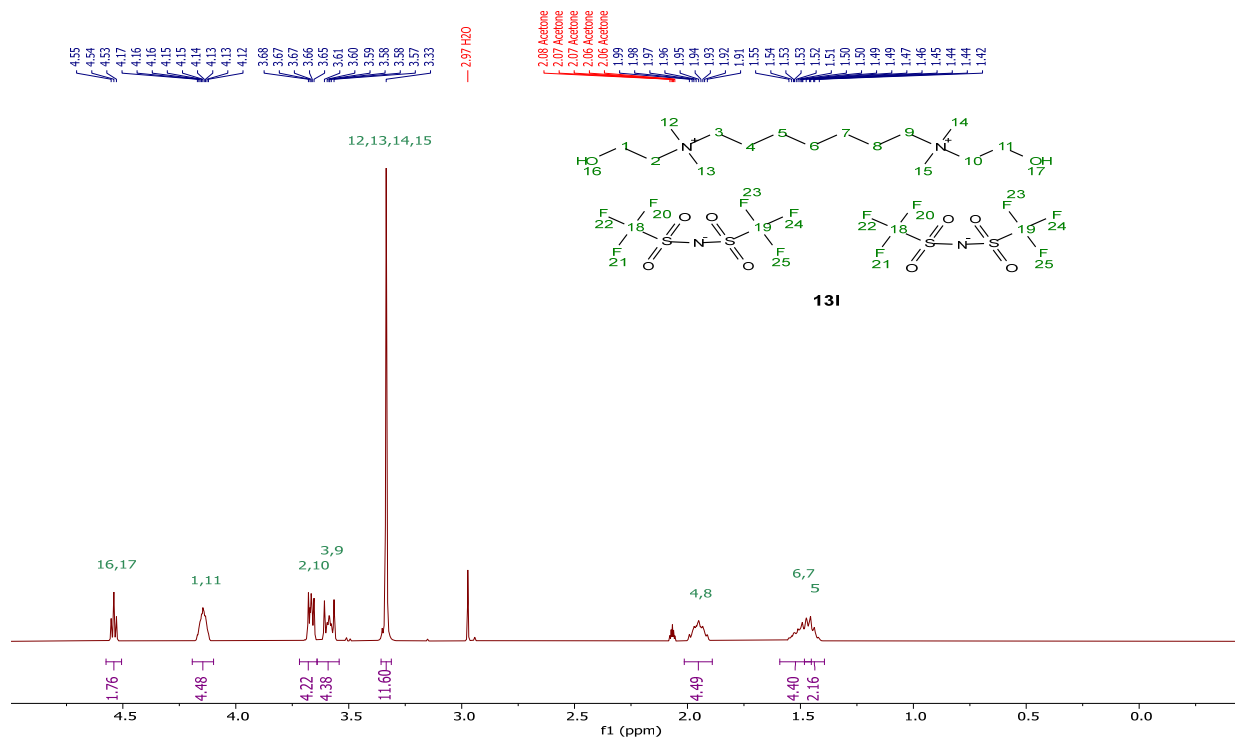
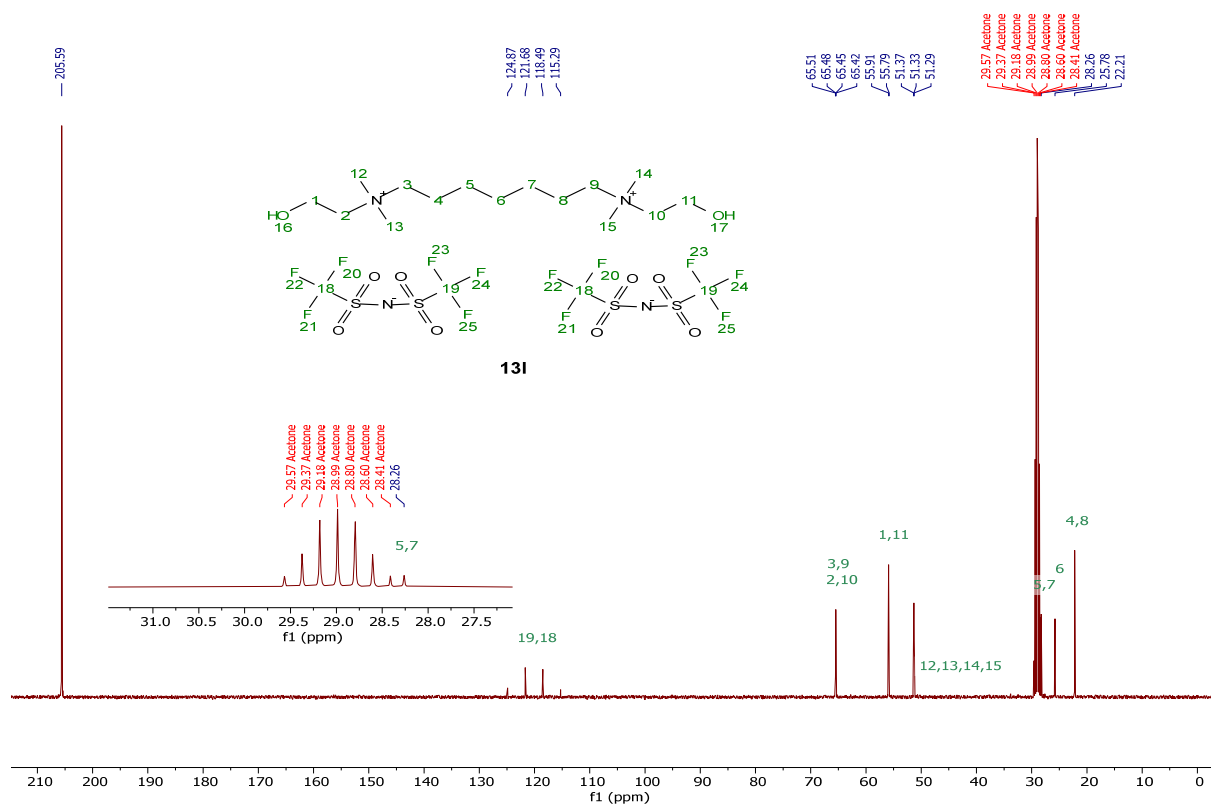
$^{19}\text{F}$  NMR (376 MHz, Methanol- $d_4$ )[DC-4][2NTf<sub>2</sub>], **13i** $^1\text{H}$  NMR (400 MHz, Acetone- $d_6$ )

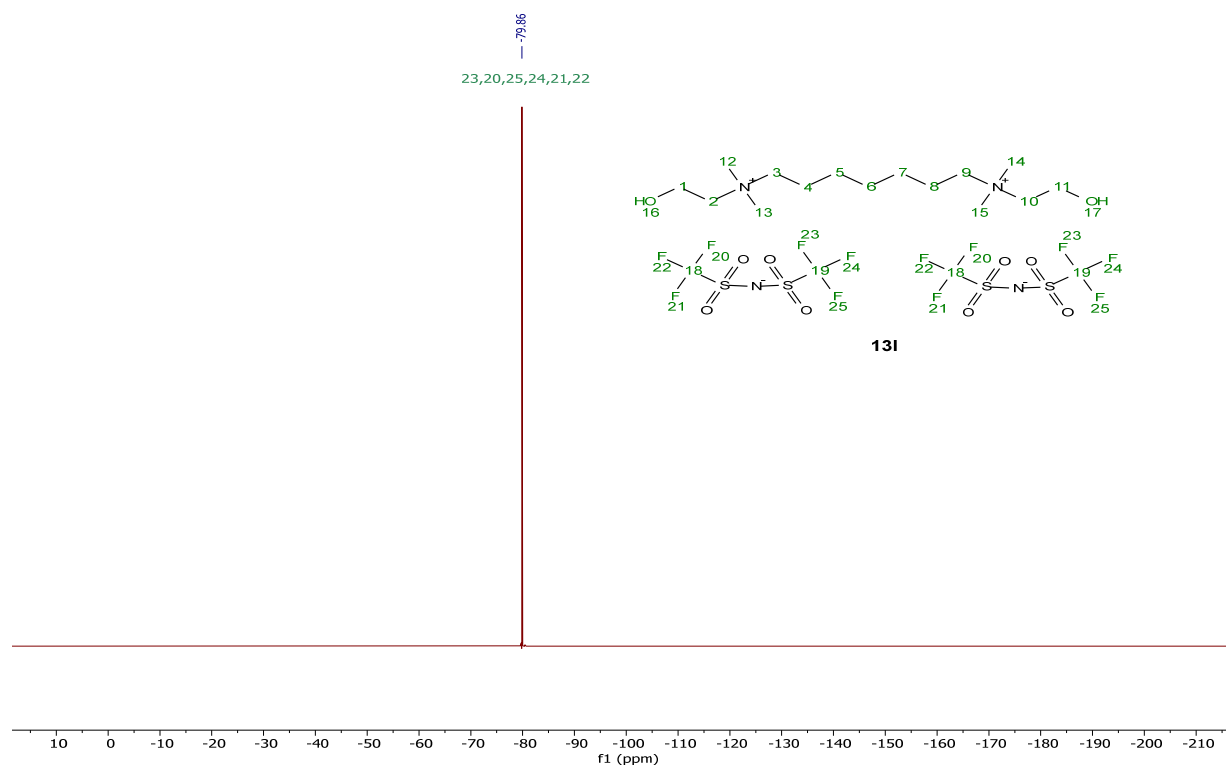
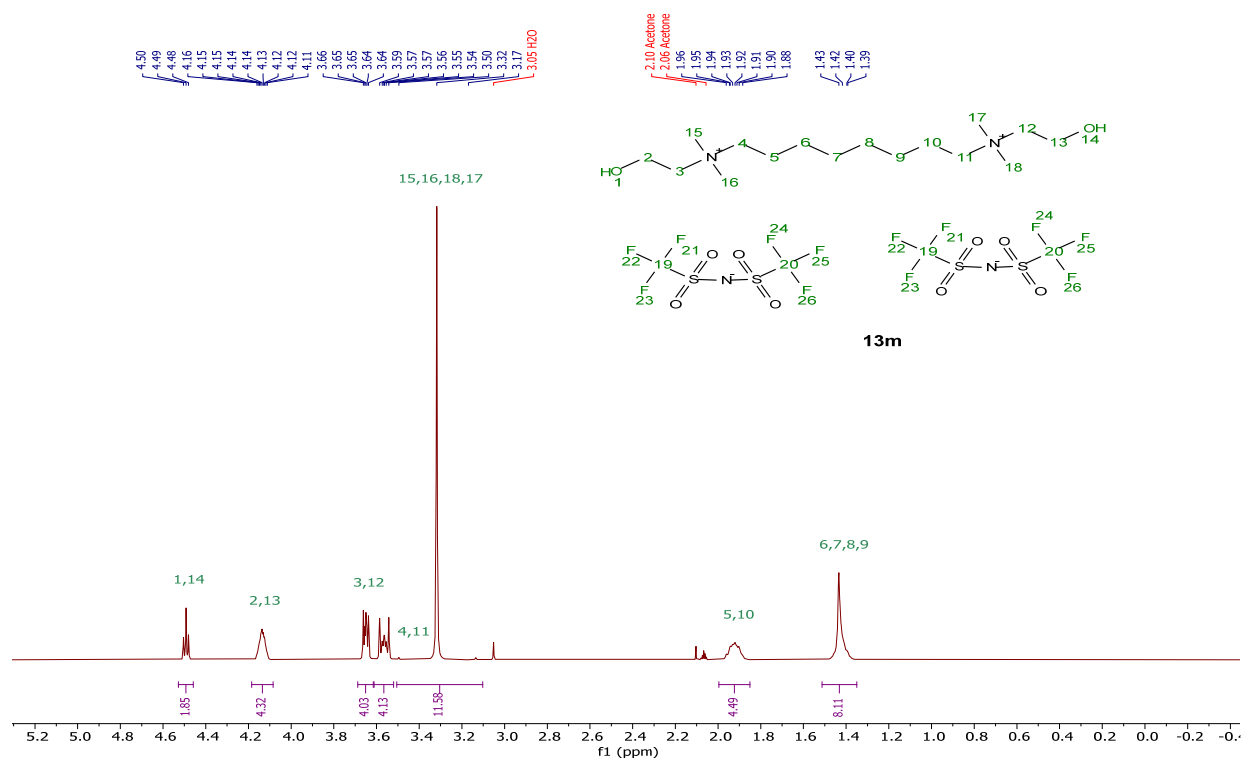
$^{13}\text{C}\{^1\text{H}\}$  NMR (101 MHz, Acetone- $d_6$ ) $^{19}\text{F}$  NMR (376 MHz, Acetone- $d_6$ )

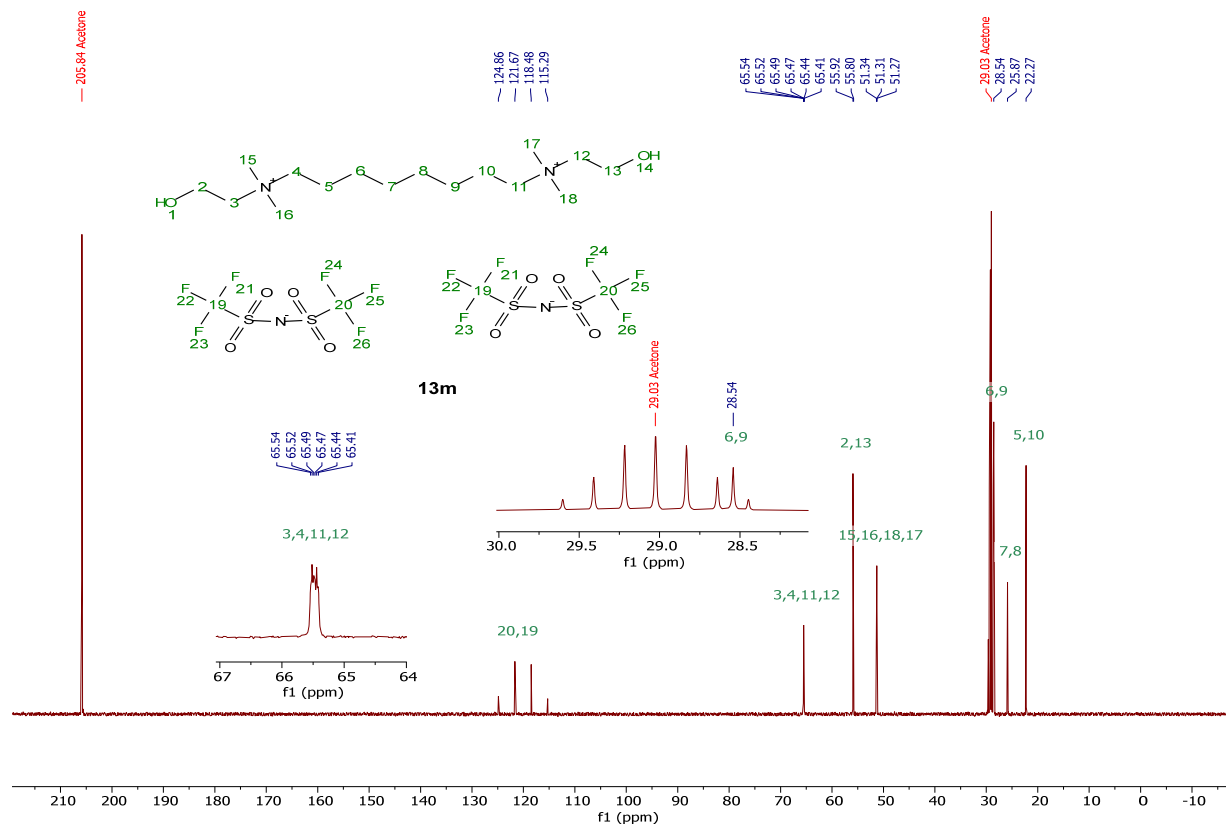
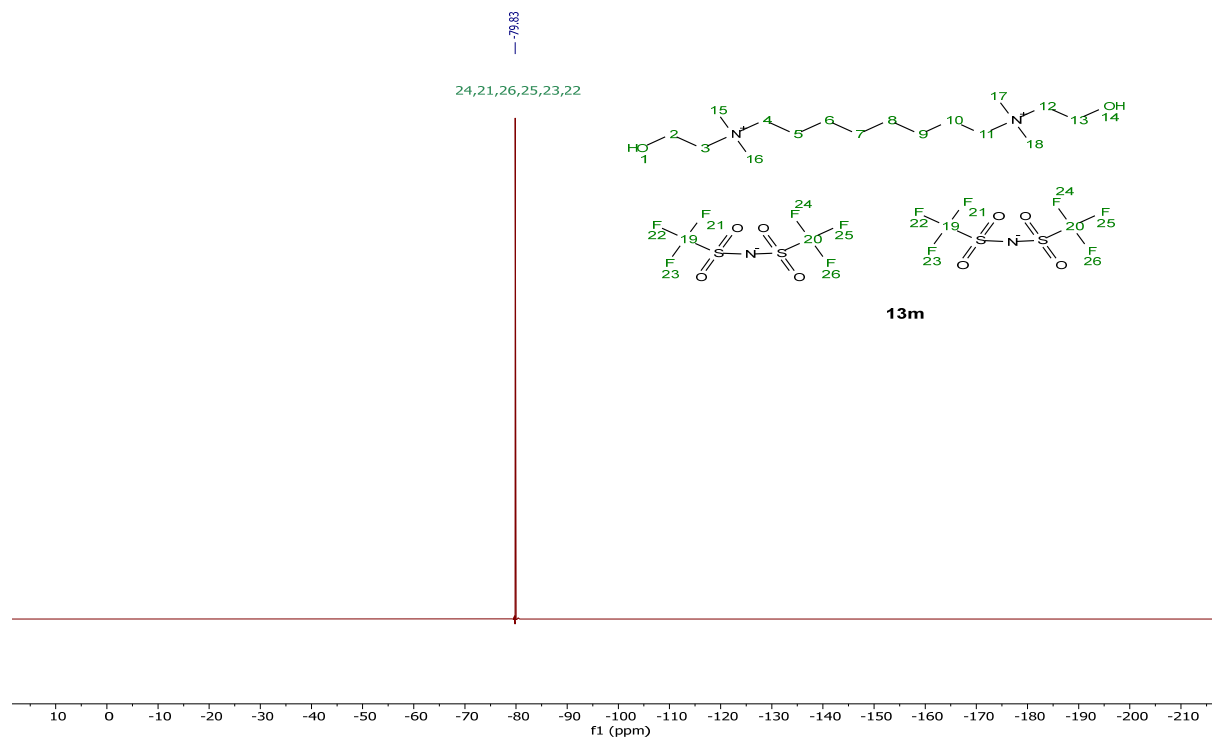
[DC-5][2NTf<sub>2</sub>], **13j**<sup>1</sup>H NMR (400 MHz, Acetone-d<sub>6</sub>)<sup>13</sup>C {<sup>1</sup>H} NMR (101 MHz, Acetone-d<sub>6</sub>)

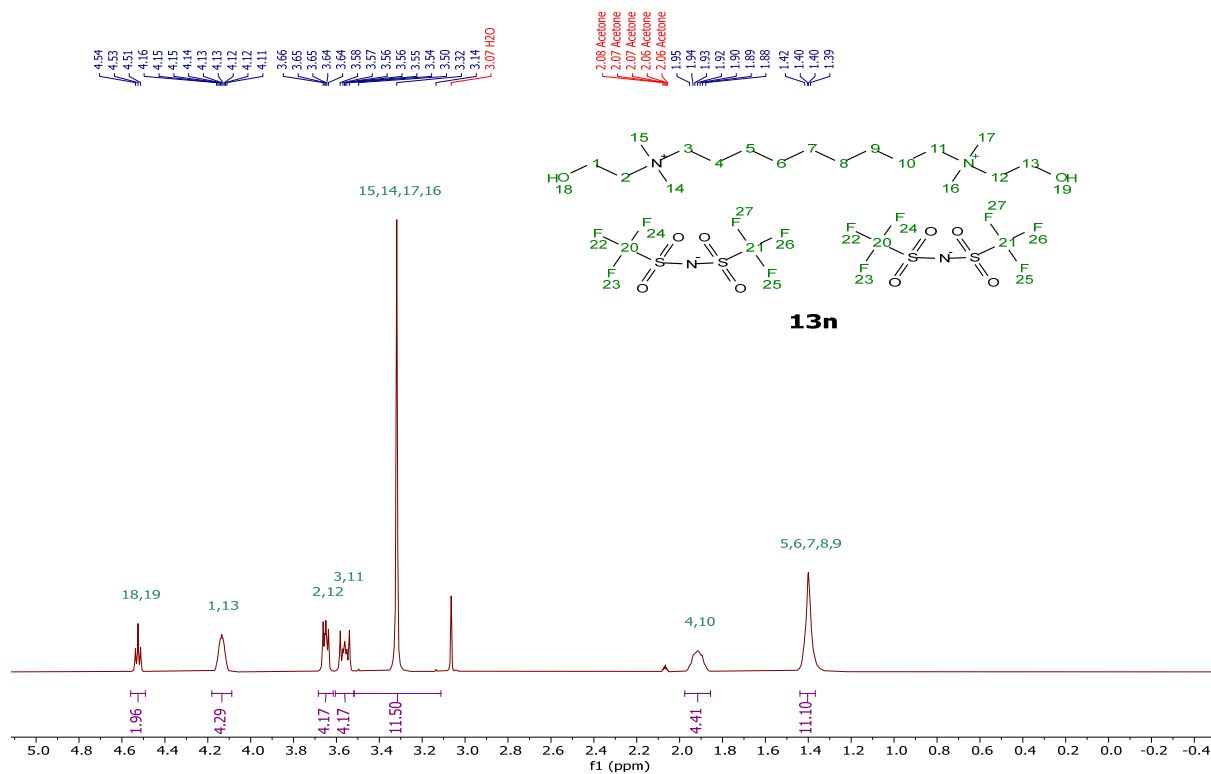
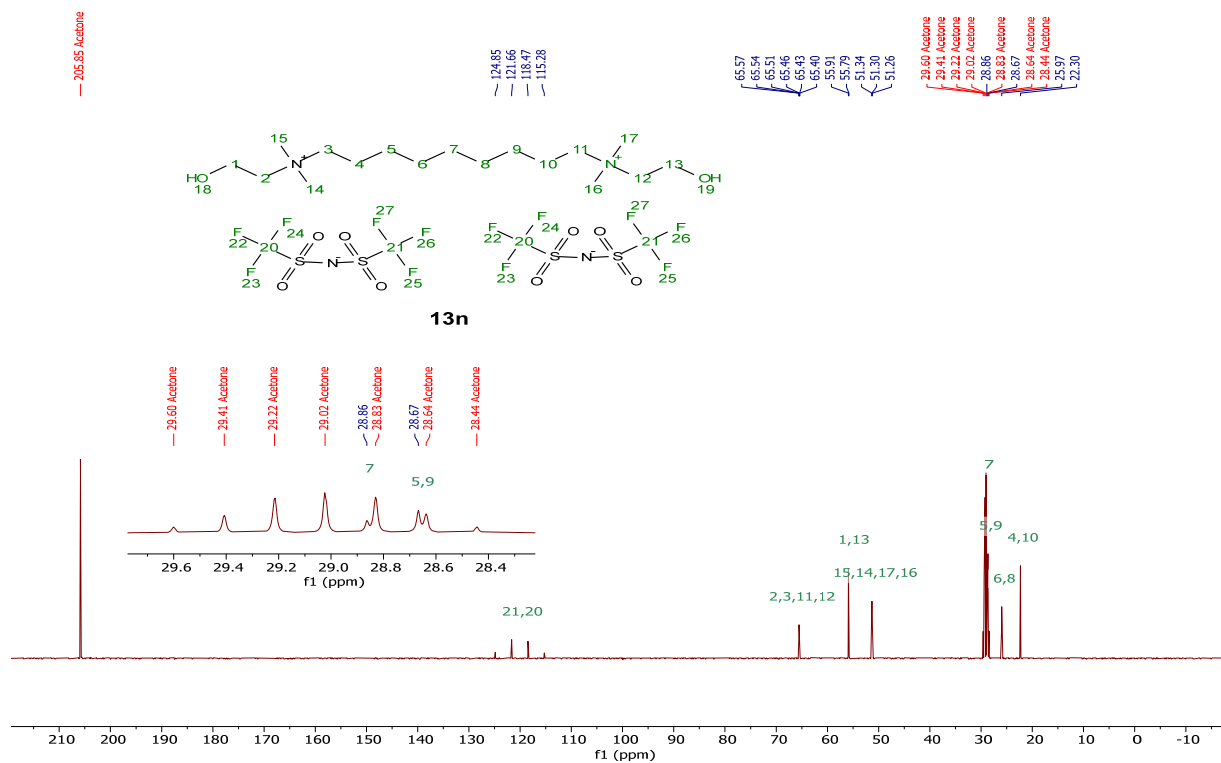
$^{19}\text{F}$  NMR (376 MHz, Acetone- $d_6$ )[DC-6][2NTf<sub>2</sub>], **13k** $^1\text{H}$  NMR (400 MHz, Methanol- $d_4$ )

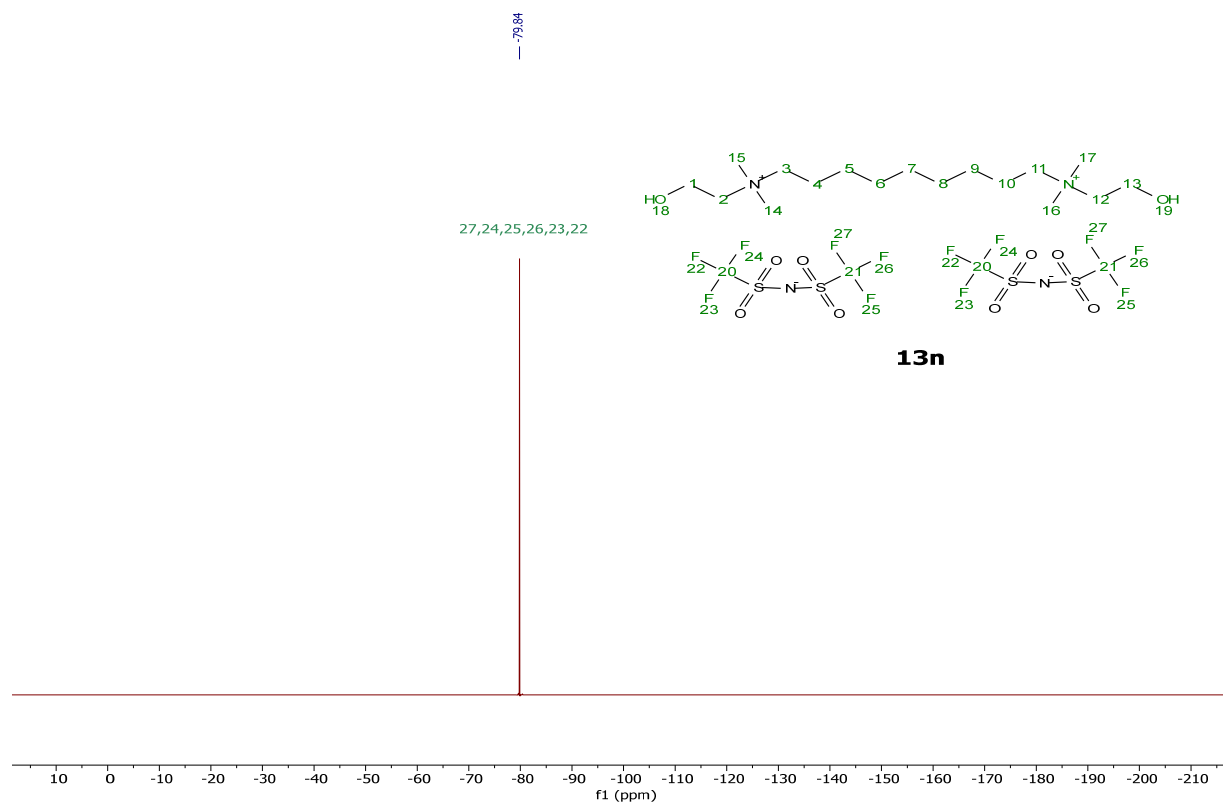
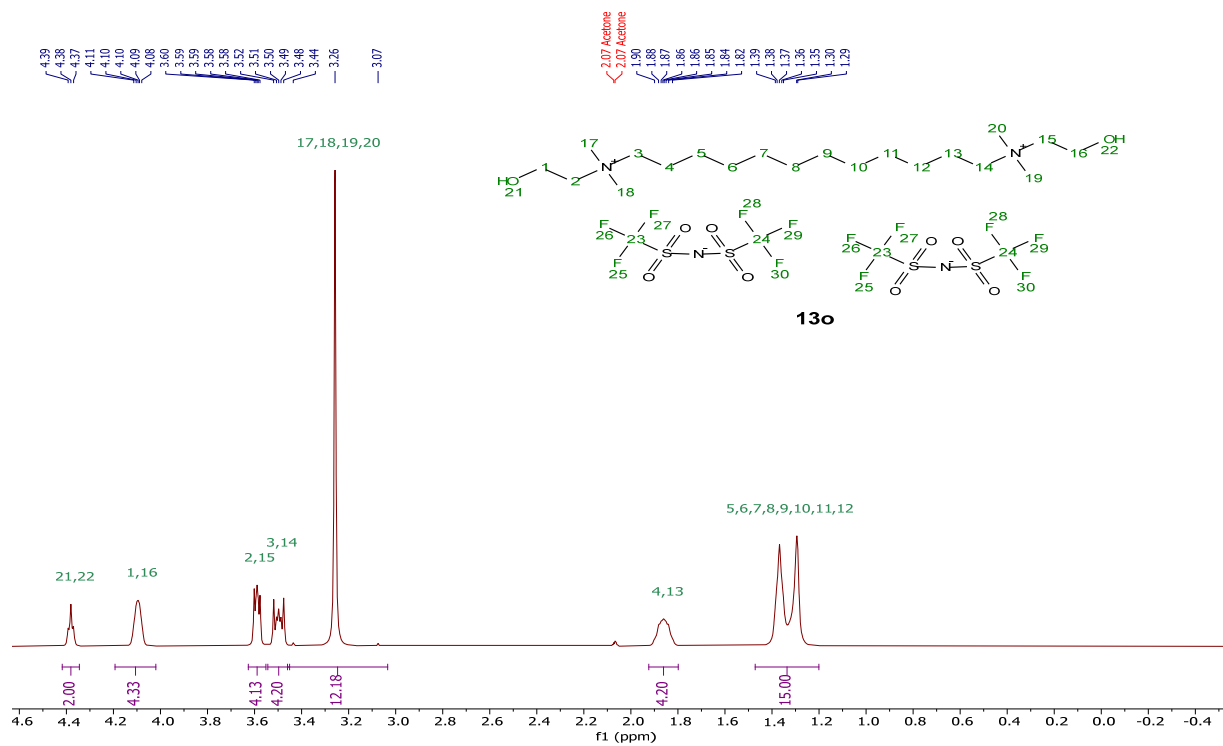
$^{13}\text{C}\{^1\text{H}\}$  NMR (101 MHz, Methanol-d<sub>4</sub>) $^{19}\text{F}$  NMR (376 MHz, Methanol-d<sub>4</sub>)

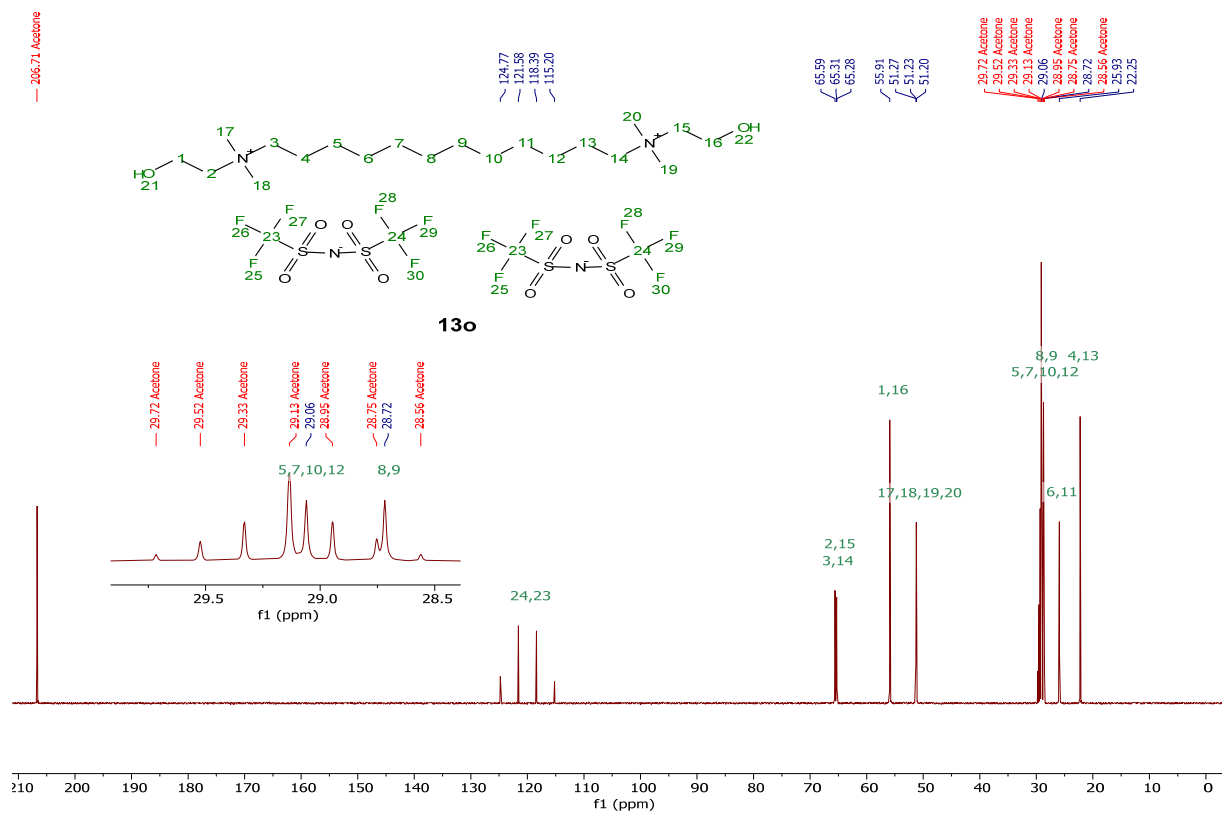
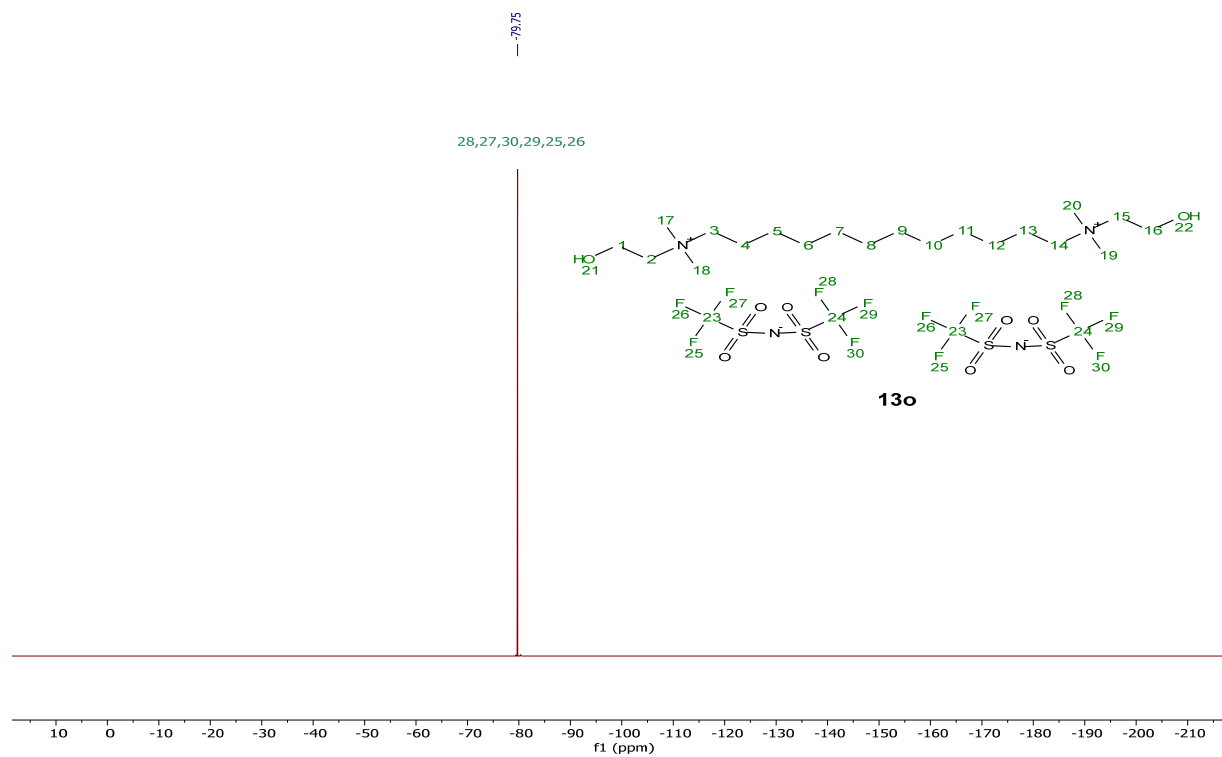
[DC-7][2NTf<sub>2</sub>], **131**<sup>1</sup>H NMR (400 MHz, Acetone-d<sub>6</sub>)<sup>13</sup>C{<sup>1</sup>H} NMR (101 MHz, Acetone-d<sub>6</sub>)

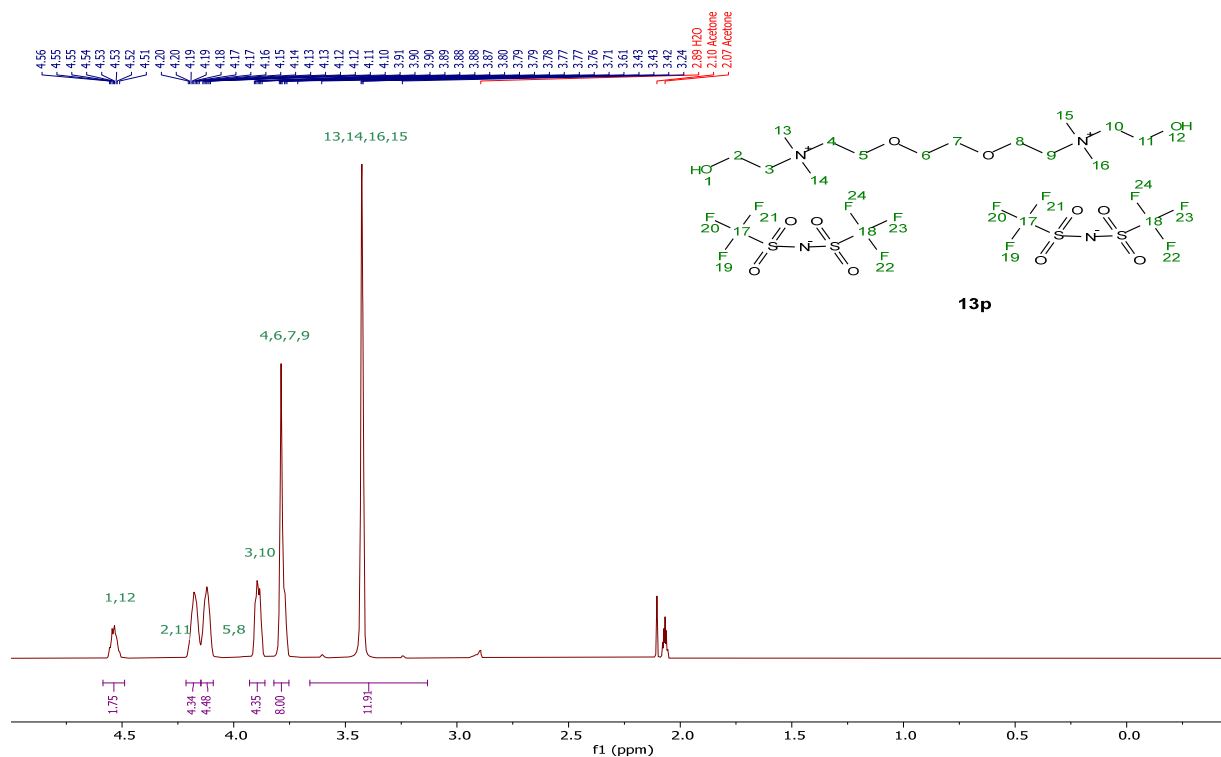
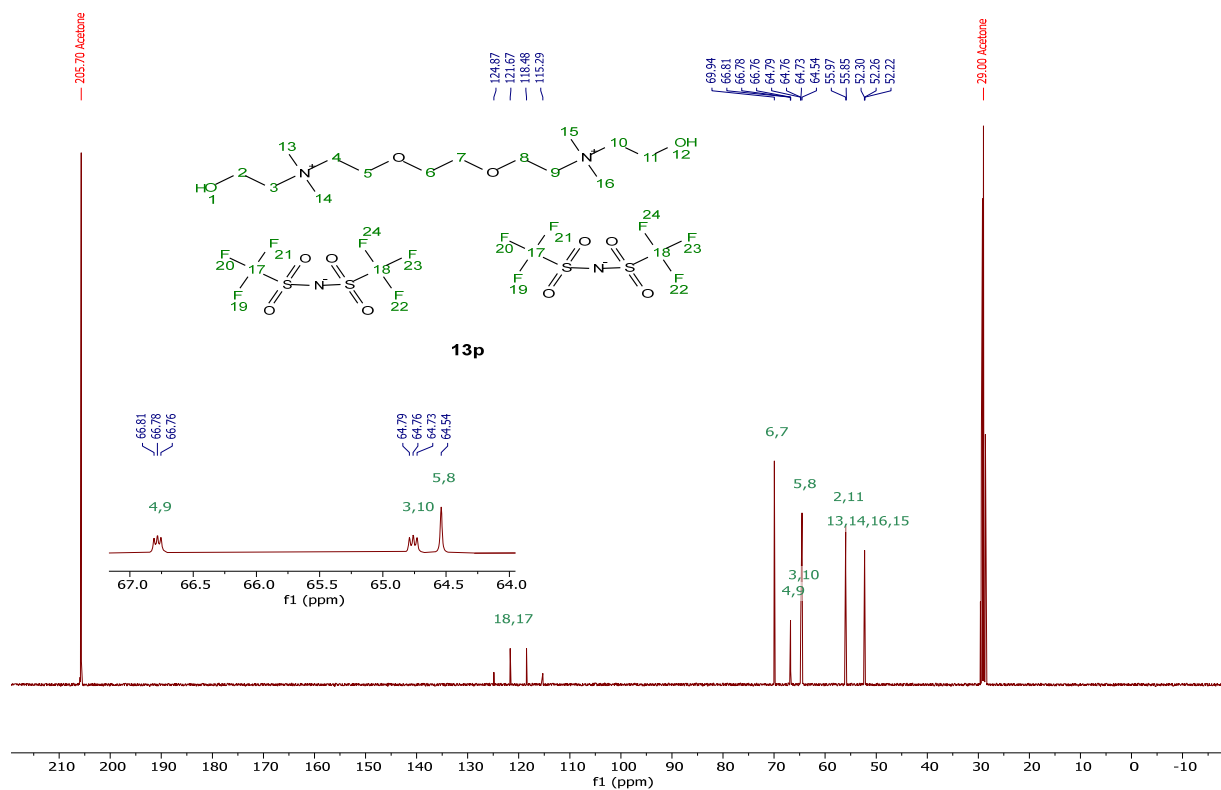
$^{19}\text{F}$  NMR (376 MHz, Acetone- $d_6$ )[DC-8][2NTf<sub>2</sub>], **13m** $^1\text{H}$  NMR (400 MHz, Acetone- $d_6$ )

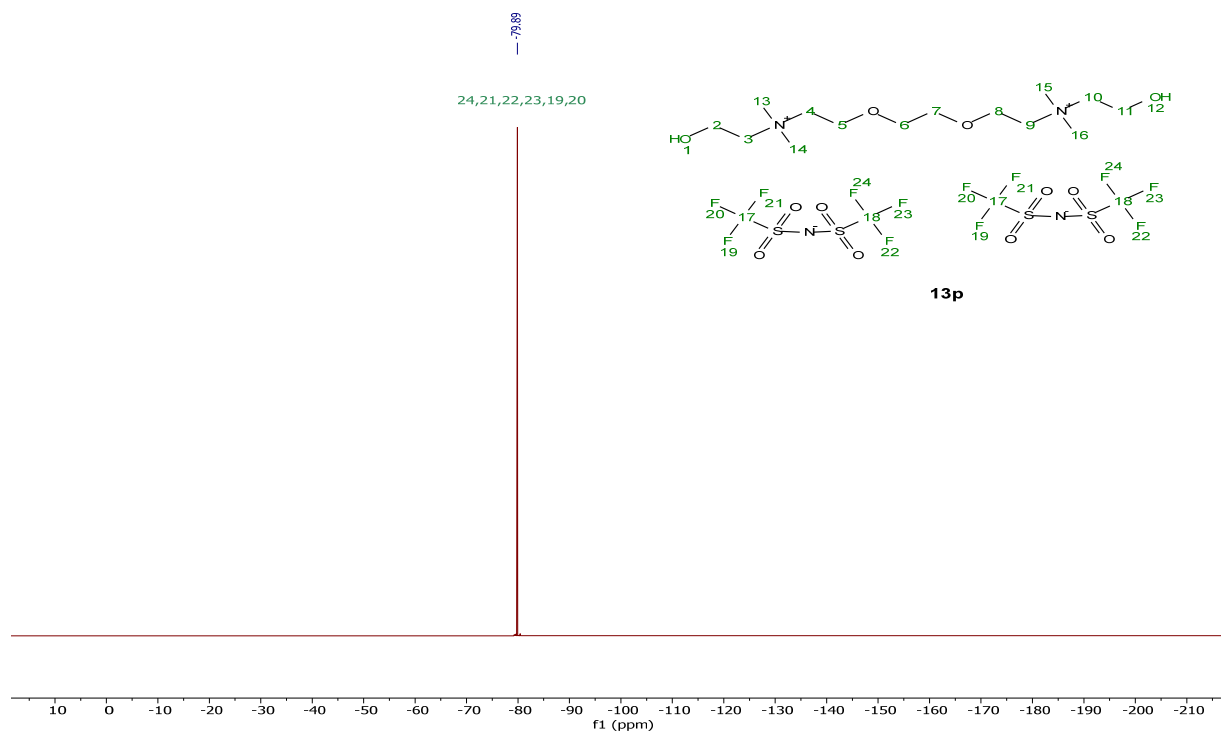
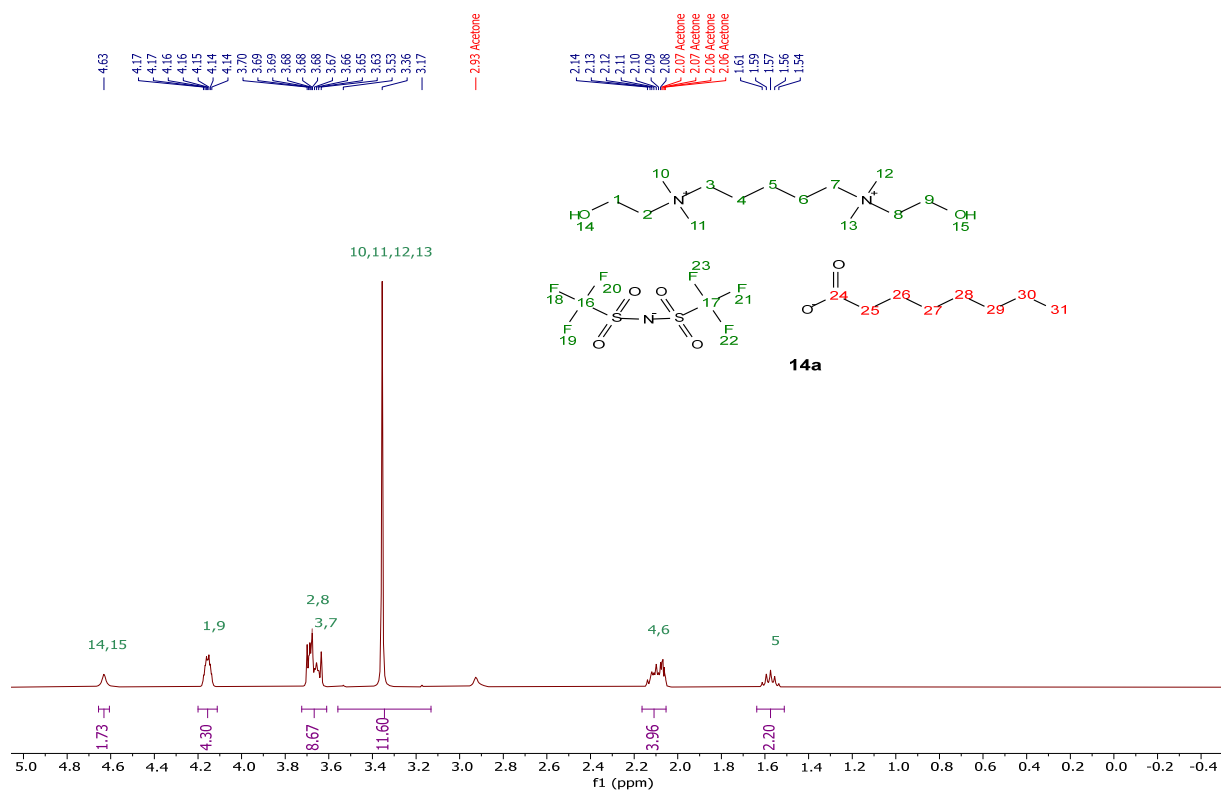
$^{13}\text{C}\{^1\text{H}\}$  NMR (101 MHz, Acetone-d<sub>6</sub>) $^{19}\text{F}$  NMR (376 MHz, Acetone-d<sub>6</sub>)

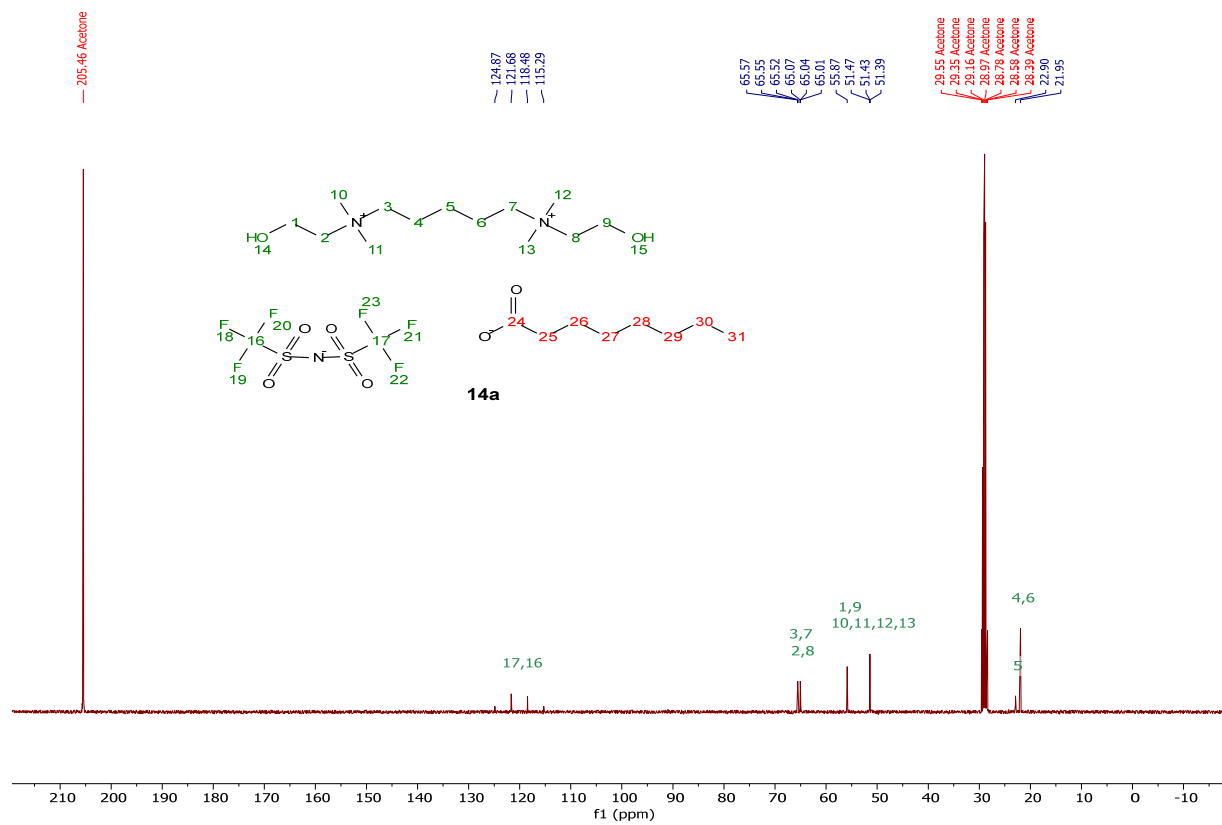
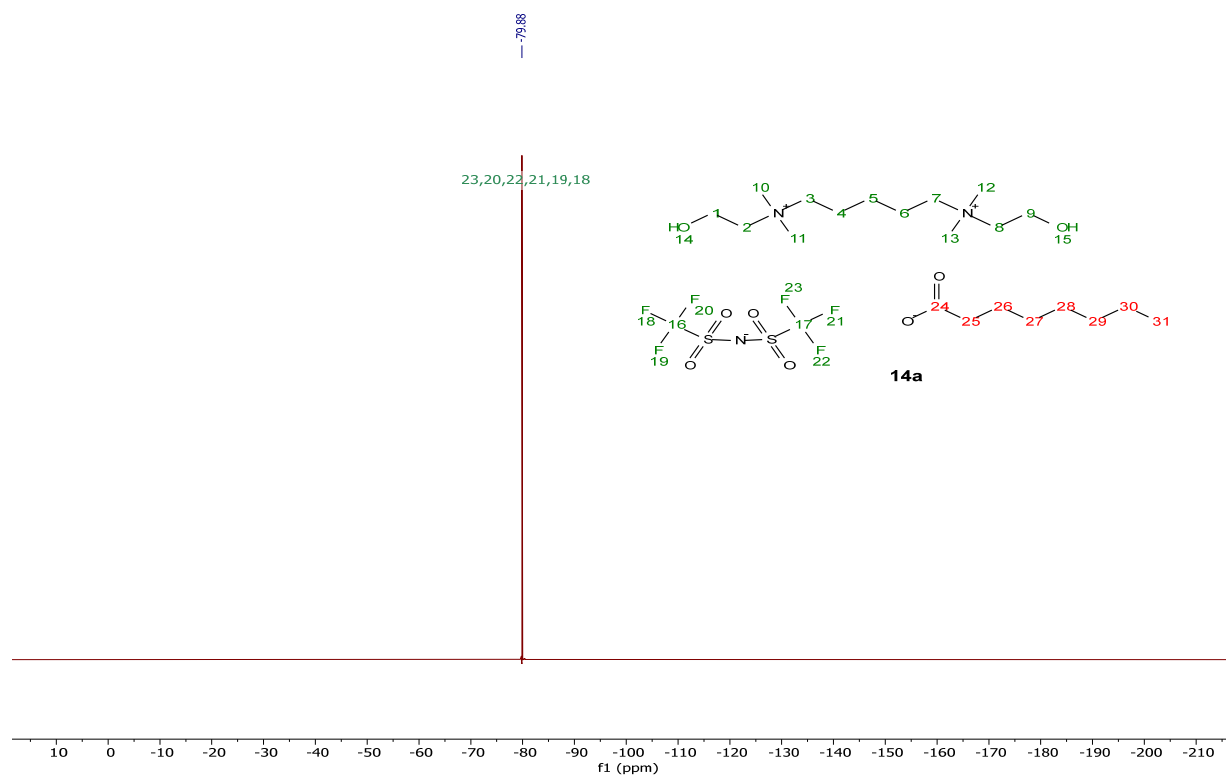
[DC-9][2NTf<sub>2</sub>], **13n**<sup>1</sup>H NMR (400 MHz, Acetone-d<sub>6</sub>)<sup>13</sup>C{<sup>1</sup>H} NMR (101 MHz, Acetone-d<sub>6</sub>)

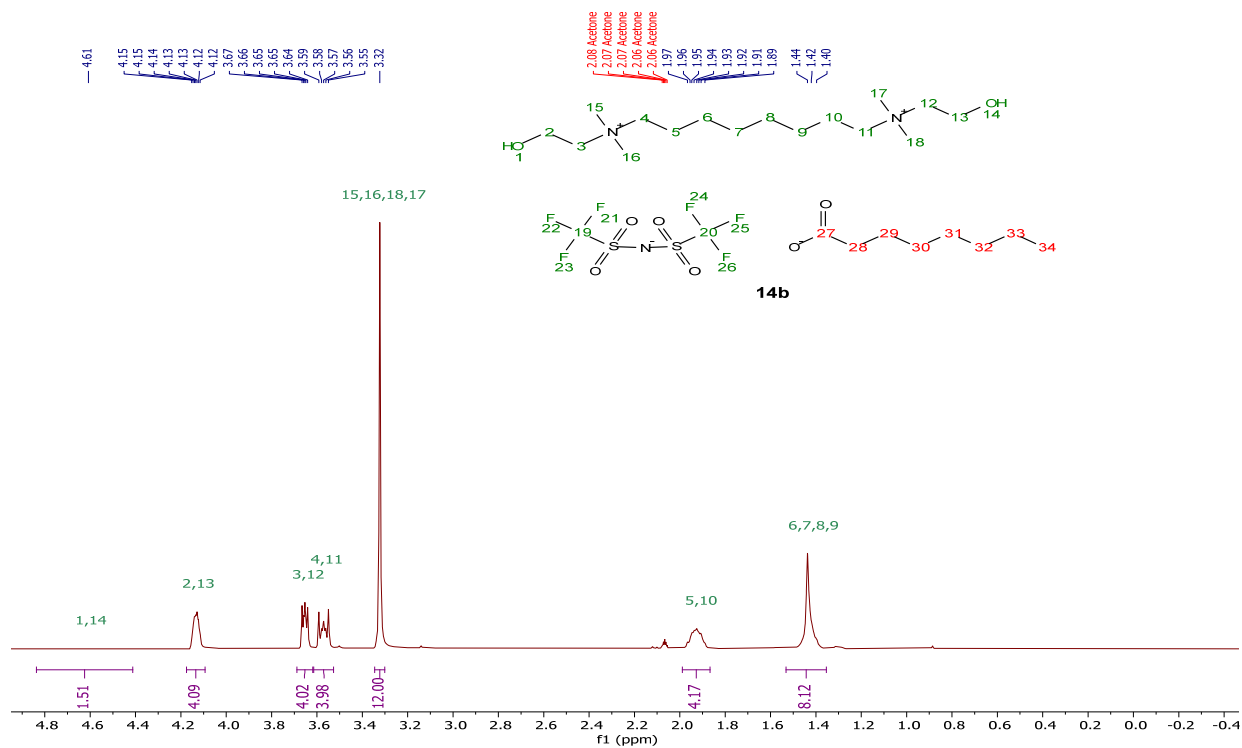
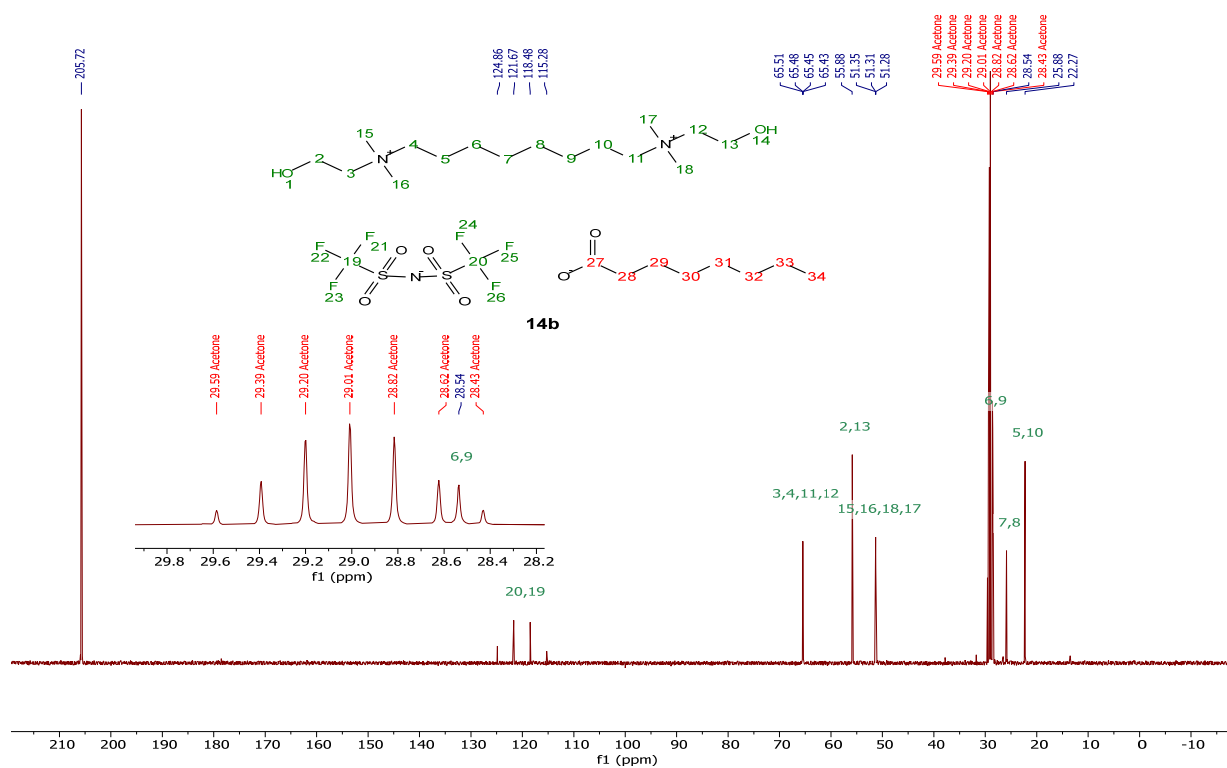
$^{19}\text{F}$  NMR (376 MHz, Acetone- $d_6$ )[DC-12][2NTf<sub>2</sub>], **13o** $^1\text{H}$  NMR (400 MHz, Acetone- $d_6$ )

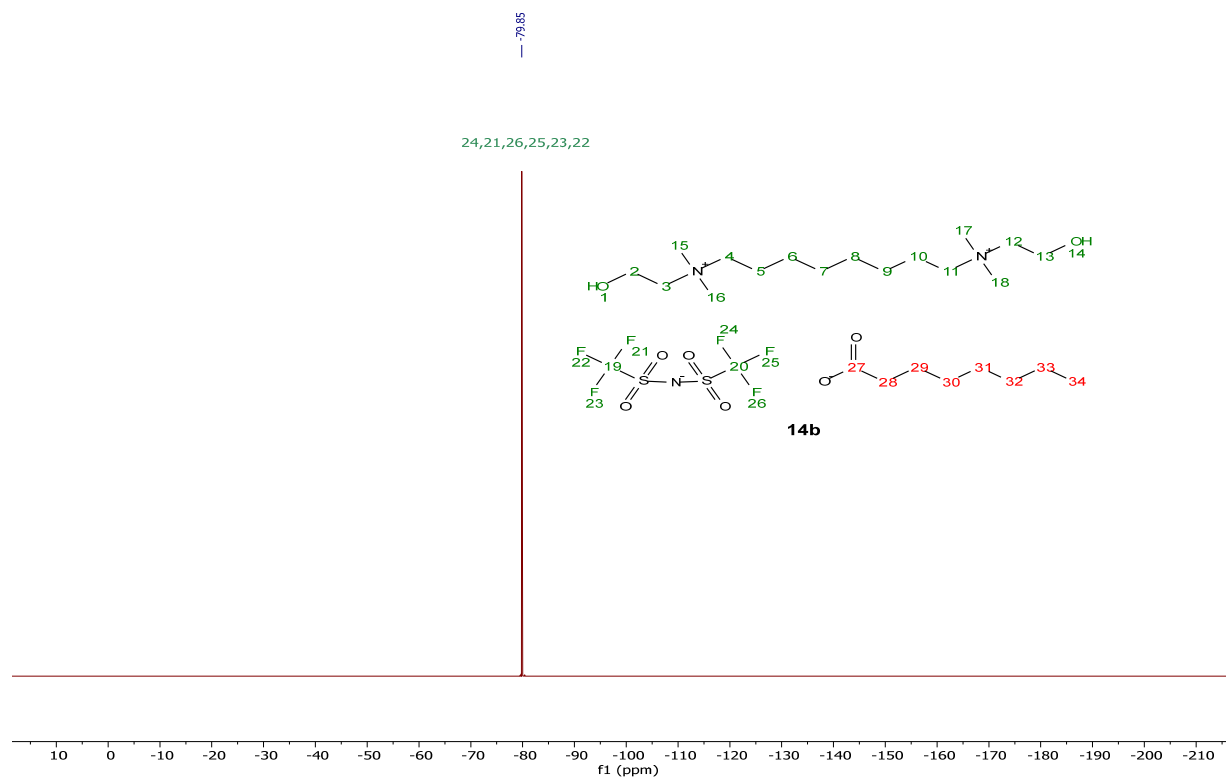
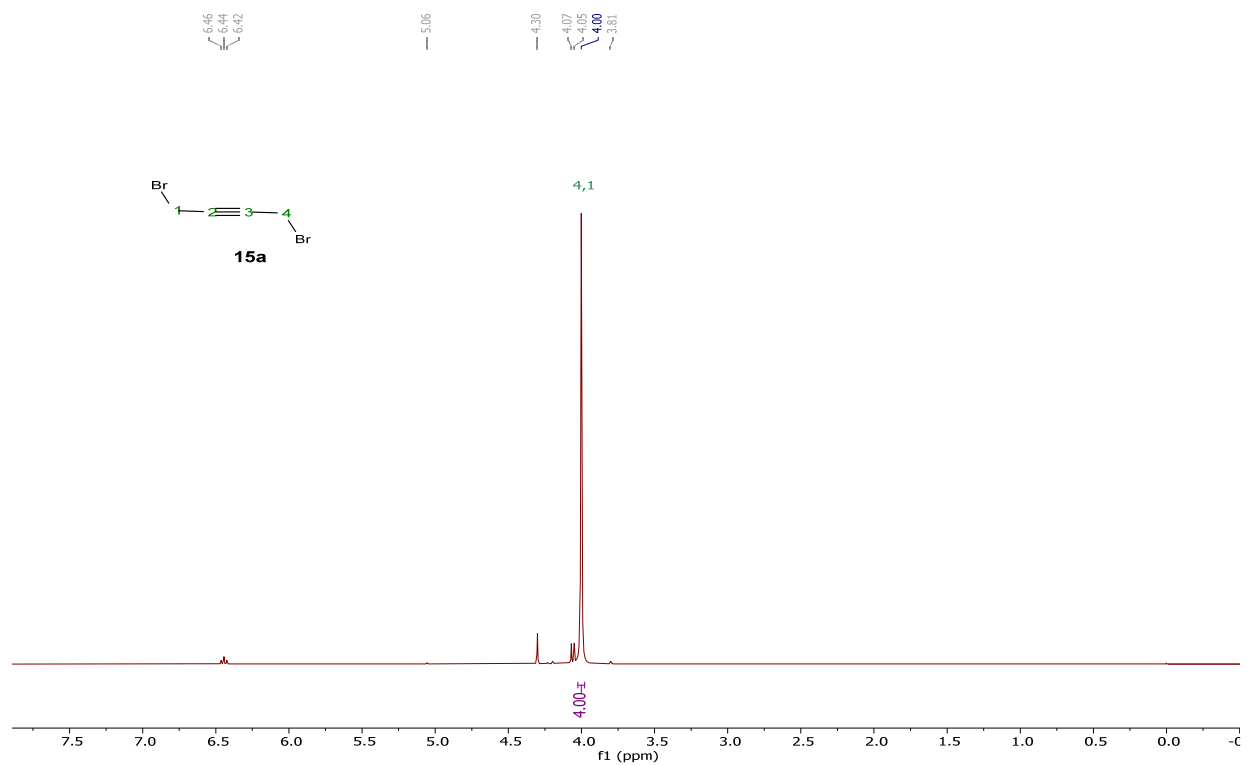
$^{13}\text{C}\{^1\text{H}\}$  NMR (101 MHz, Acetone-d<sub>6</sub>) $^{19}\text{F}$  NMR (376 MHz, Acetone-d<sub>6</sub>)

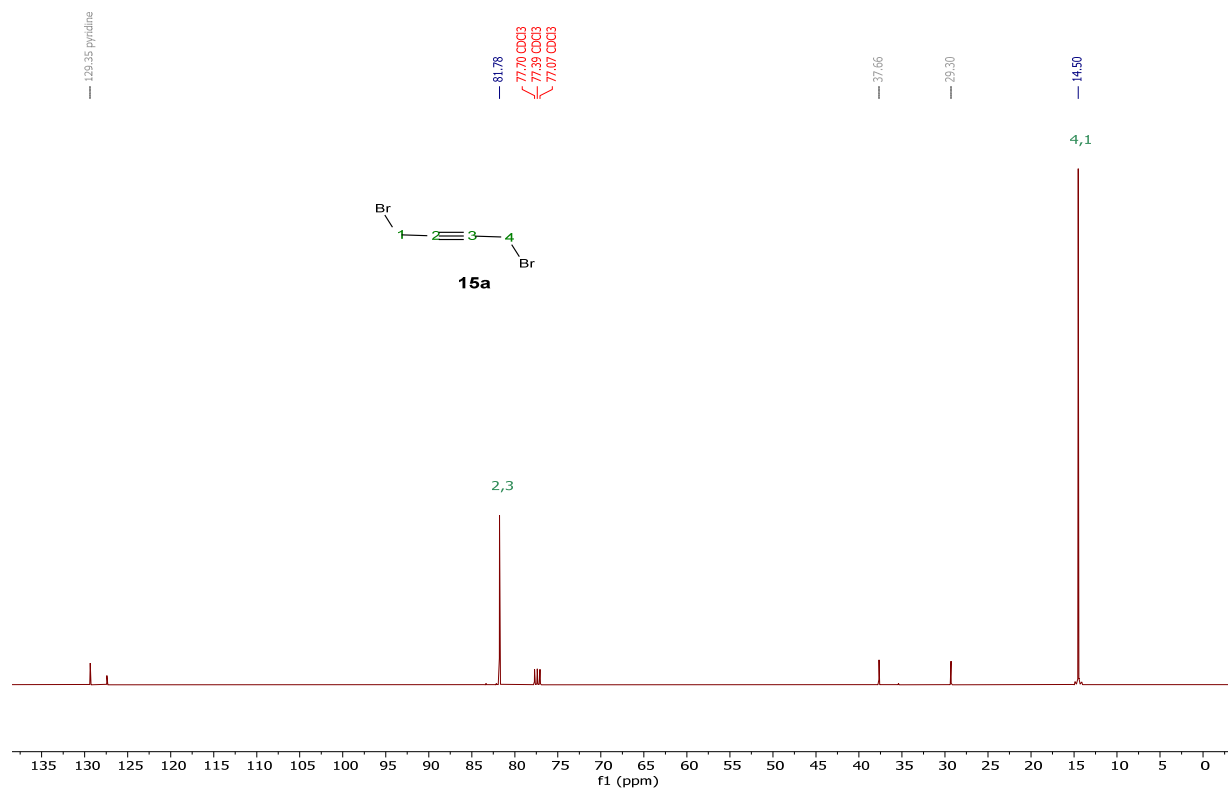
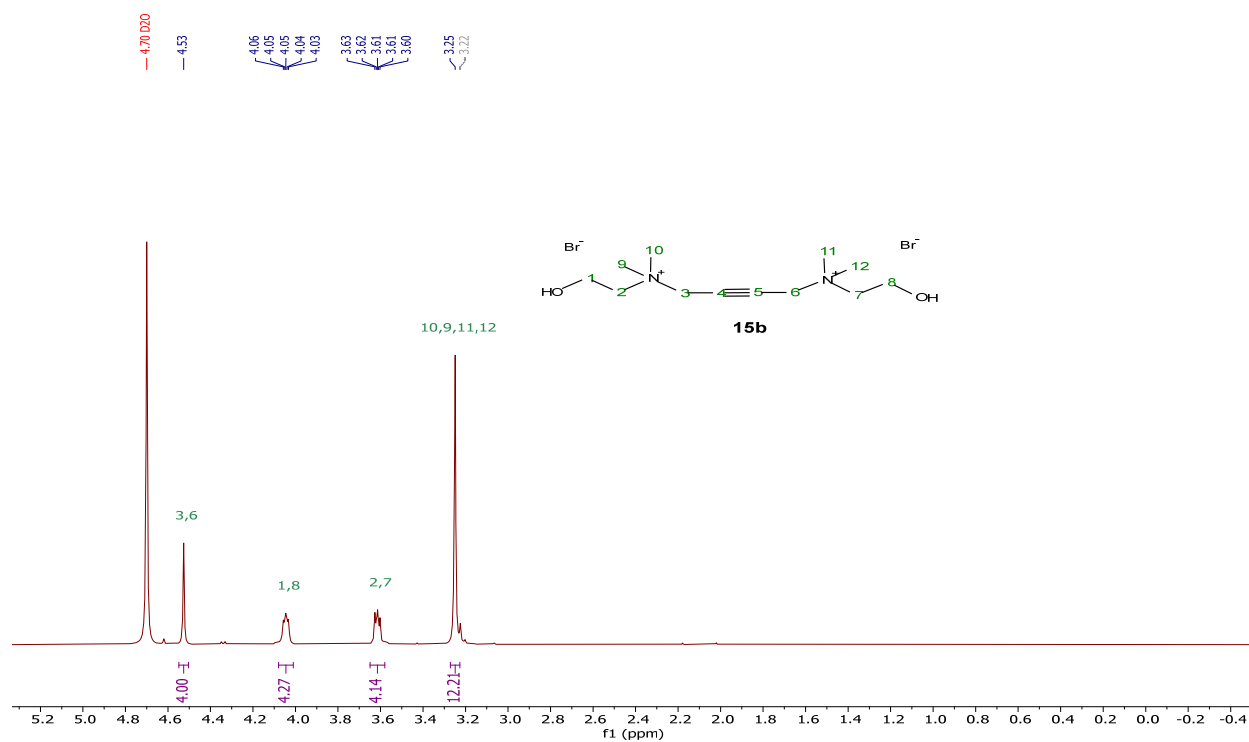
[DC-ether][2NTf<sub>2</sub>], **13p**<sup>1</sup>H NMR (400 MHz, Acetone-d<sub>6</sub>)<sup>13</sup>C{<sup>1</sup>H} NMR (101 MHz, Acetone-d<sub>6</sub>)

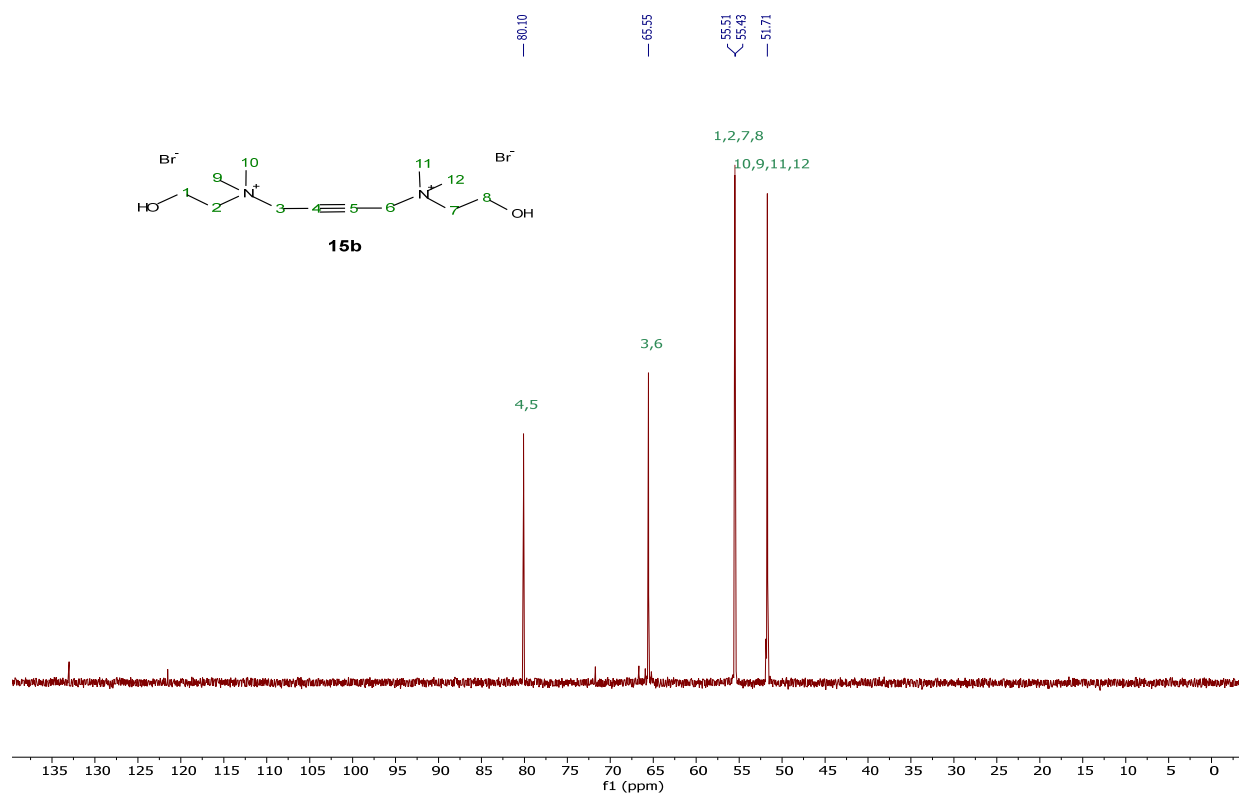
$^{19}\text{F}$  NMR (376 MHz, Acetone- $d_6$ )[DC-5][NTf<sub>2</sub>][oct], **14a** $^1\text{H}$  NMR (400 MHz, Acetone- $d_6$ )

$^{13}\text{C}\{^1\text{H}\}$  NMR (101 MHz, Acetone- $d_6$ ) $^{19}\text{F}$  NMR (376 MHz, Acetone- $d_6$ )

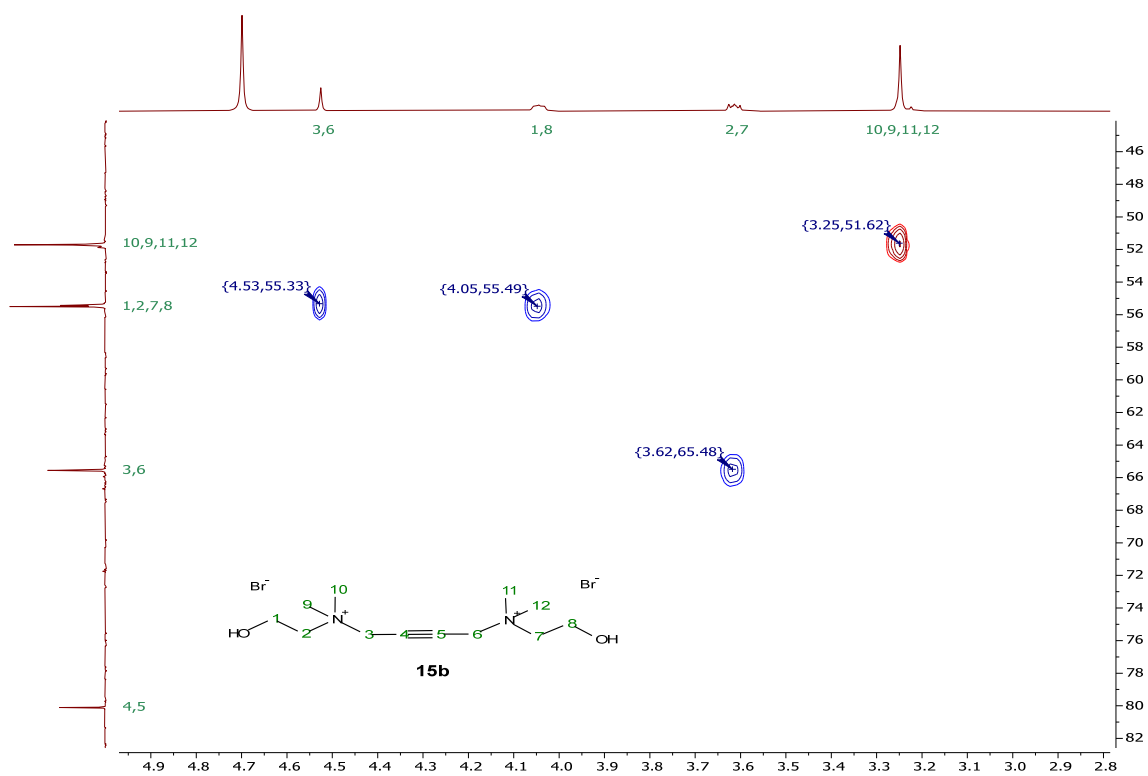
[DC-8][NTf<sub>2</sub>][oct], **14b**<sup>1</sup>H NMR (400 MHz, Acetone-d<sub>6</sub>)<sup>13</sup>C{<sup>1</sup>H} NMR (101 MHz, Acetone-d<sub>6</sub>)

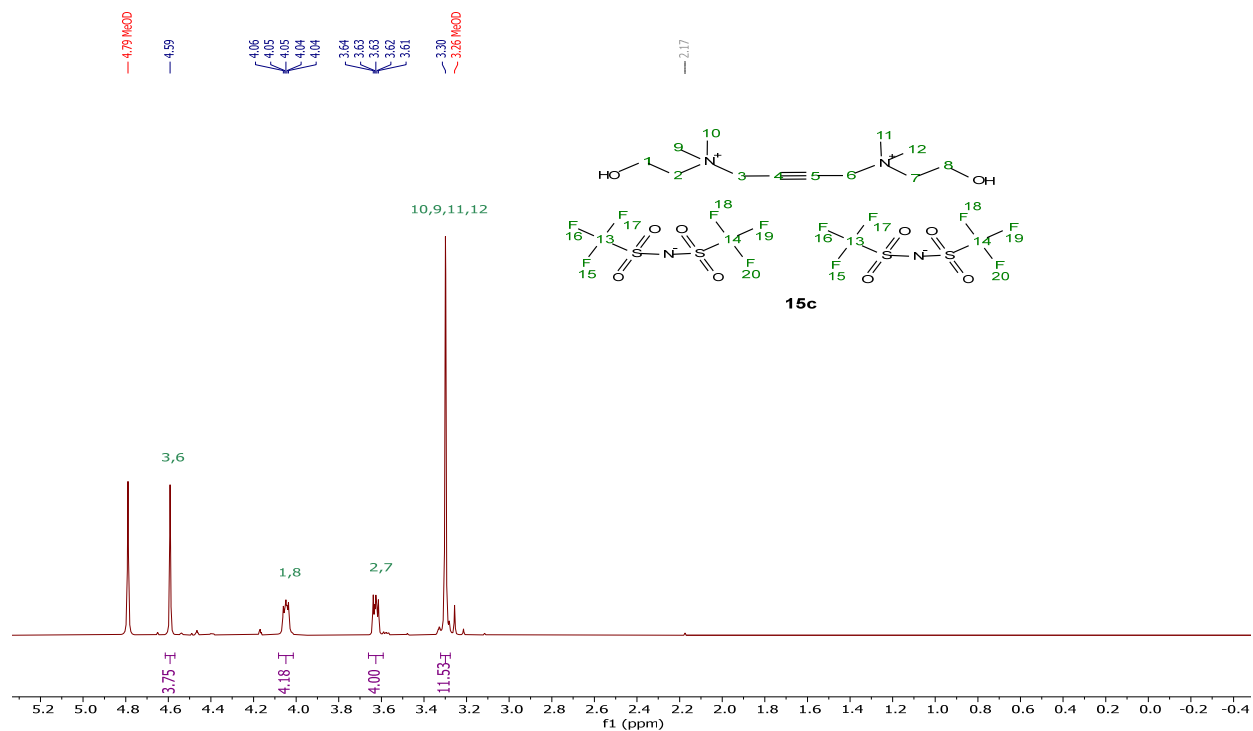
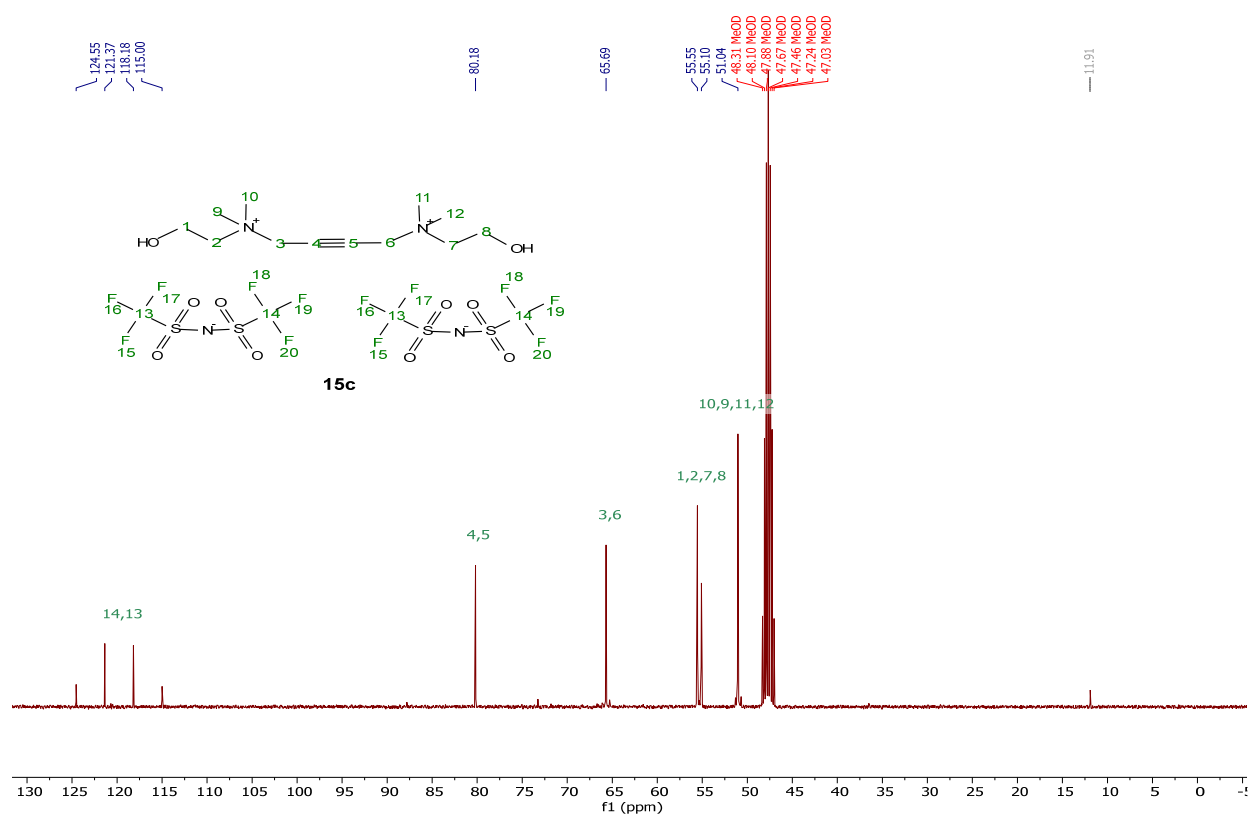
$^{19}\text{F}$  NMR (376 MHz, Acetone- $d_6$ )**15a** $^1\text{H}$  NMR (400 MHz, Chloroform- $d$ )

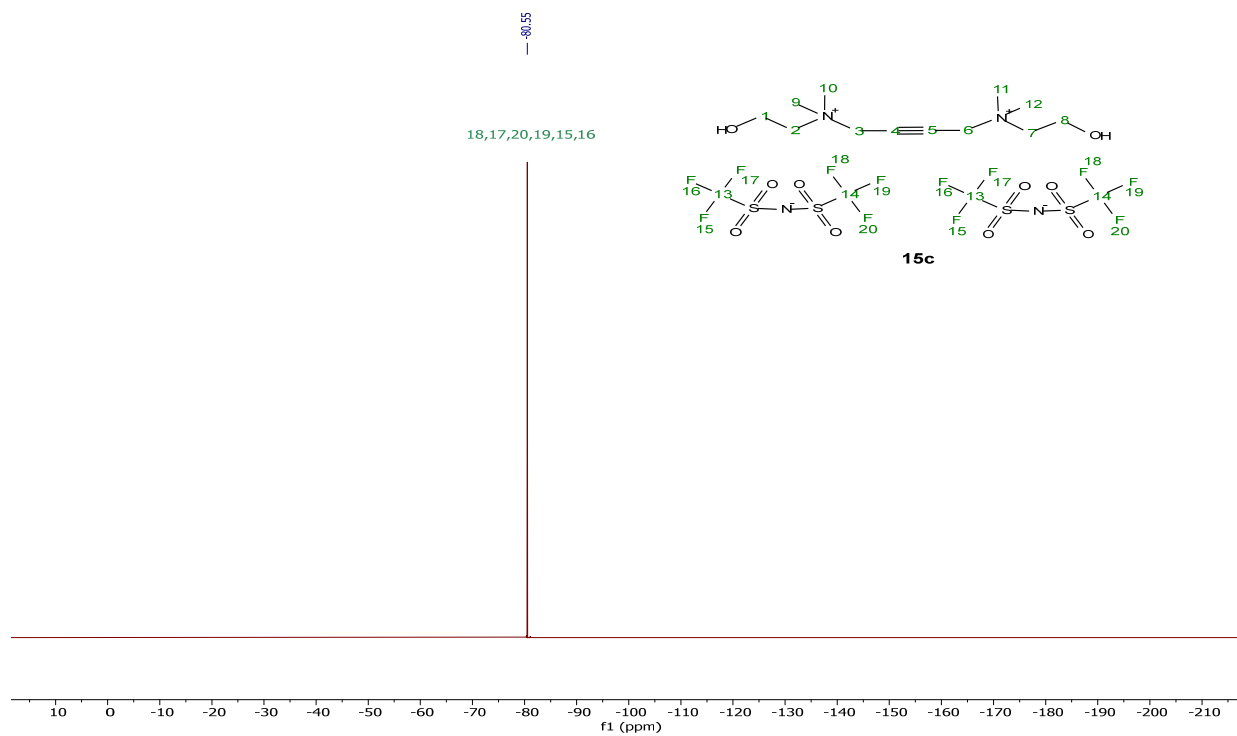
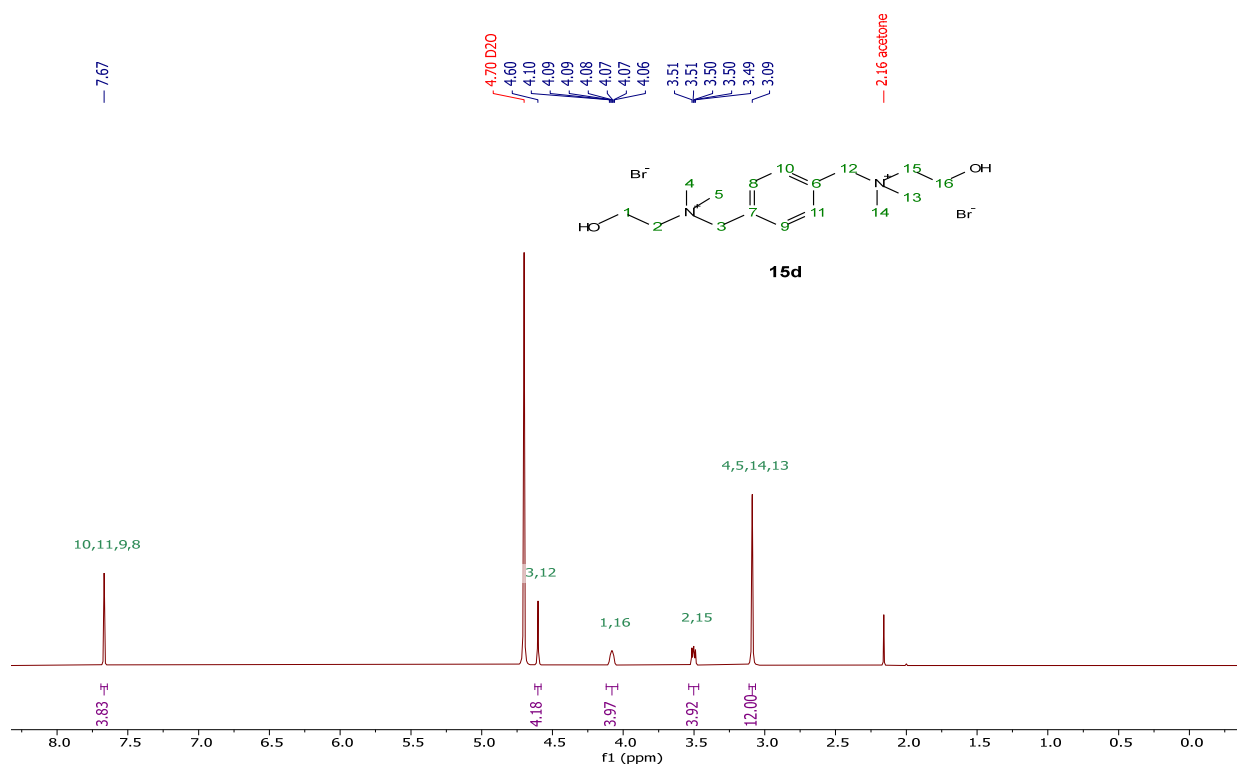
$^{13}\text{C}\{^1\text{H}\}$  NMR (101 MHz, Chloroform-d)[DC-yne][2Br], **15b** $^1\text{H}$  NMR (400 MHz, Deuterium Oxide)

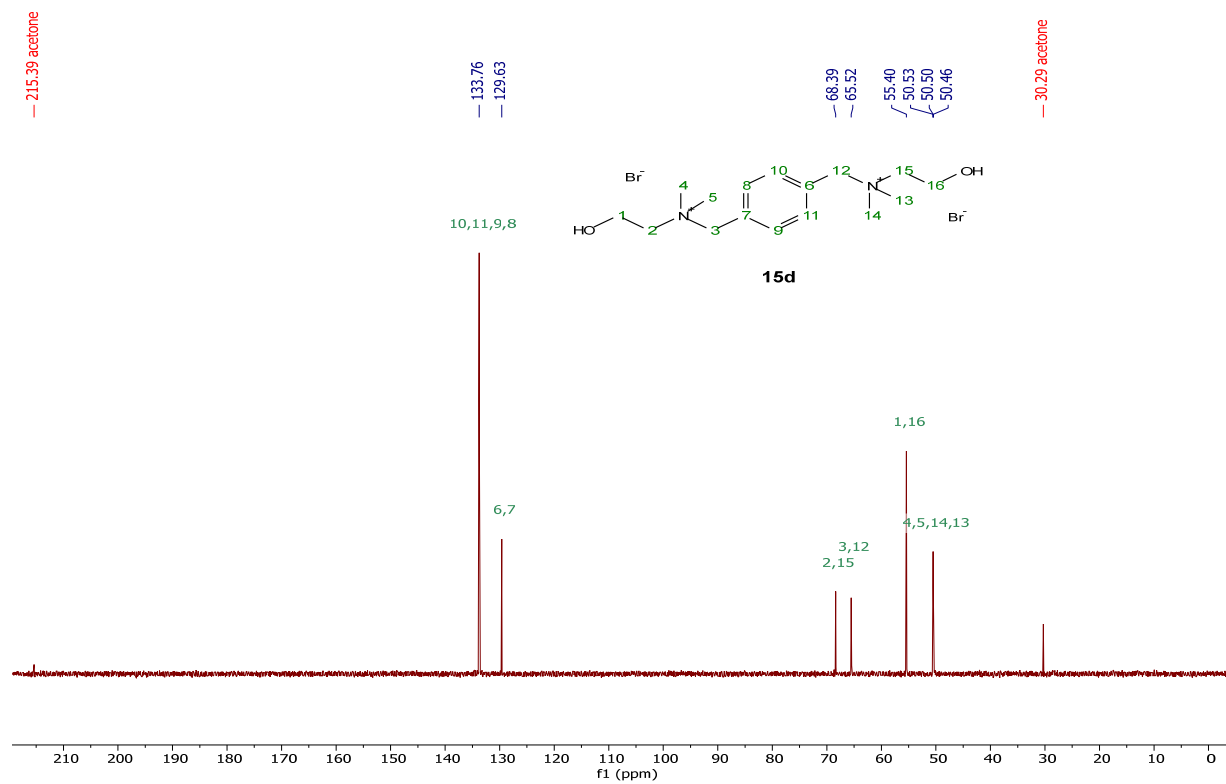
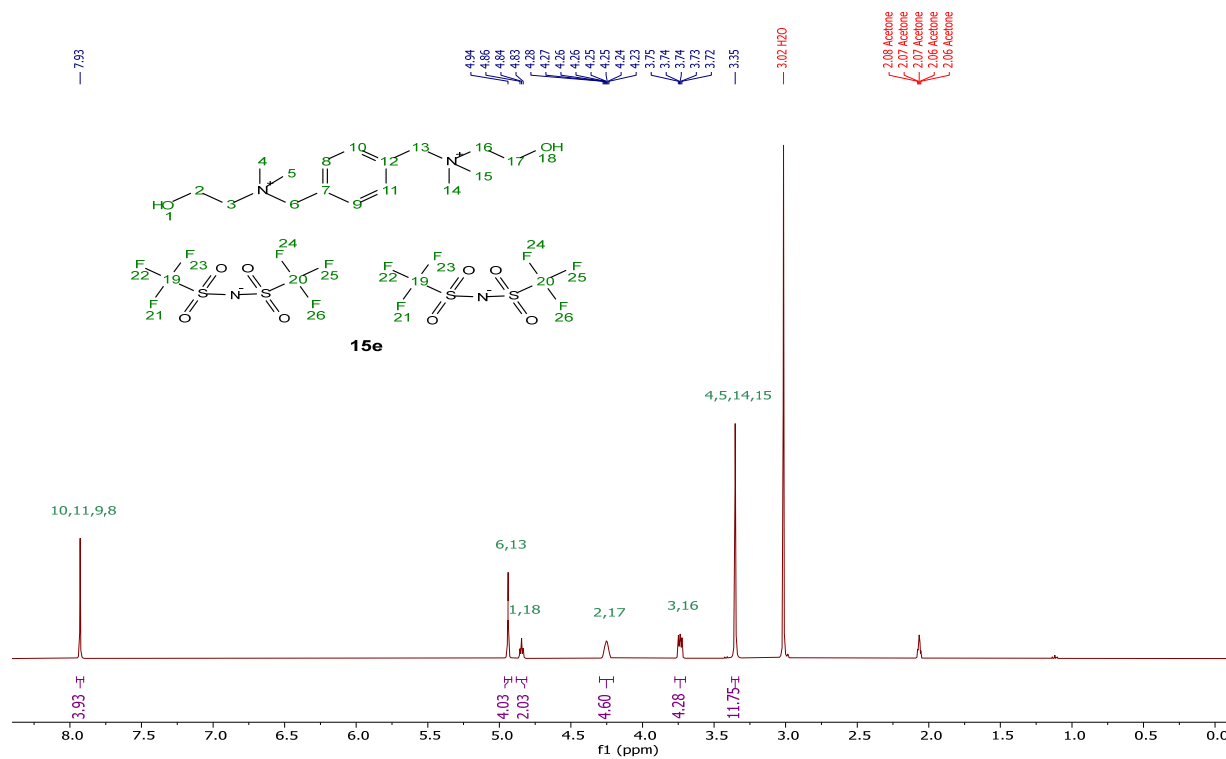
$^{13}\text{C}\{^1\text{H}\}$  NMR (101 MHz, Deuterium Oxide)

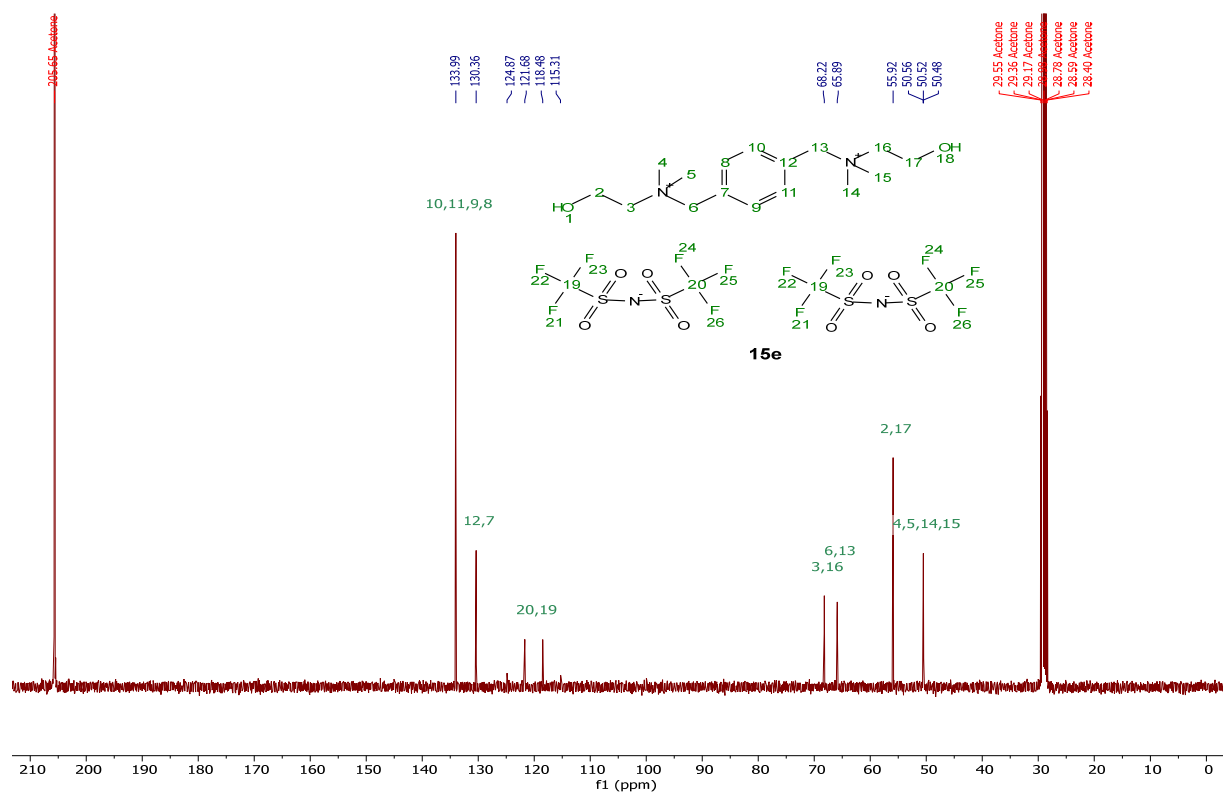
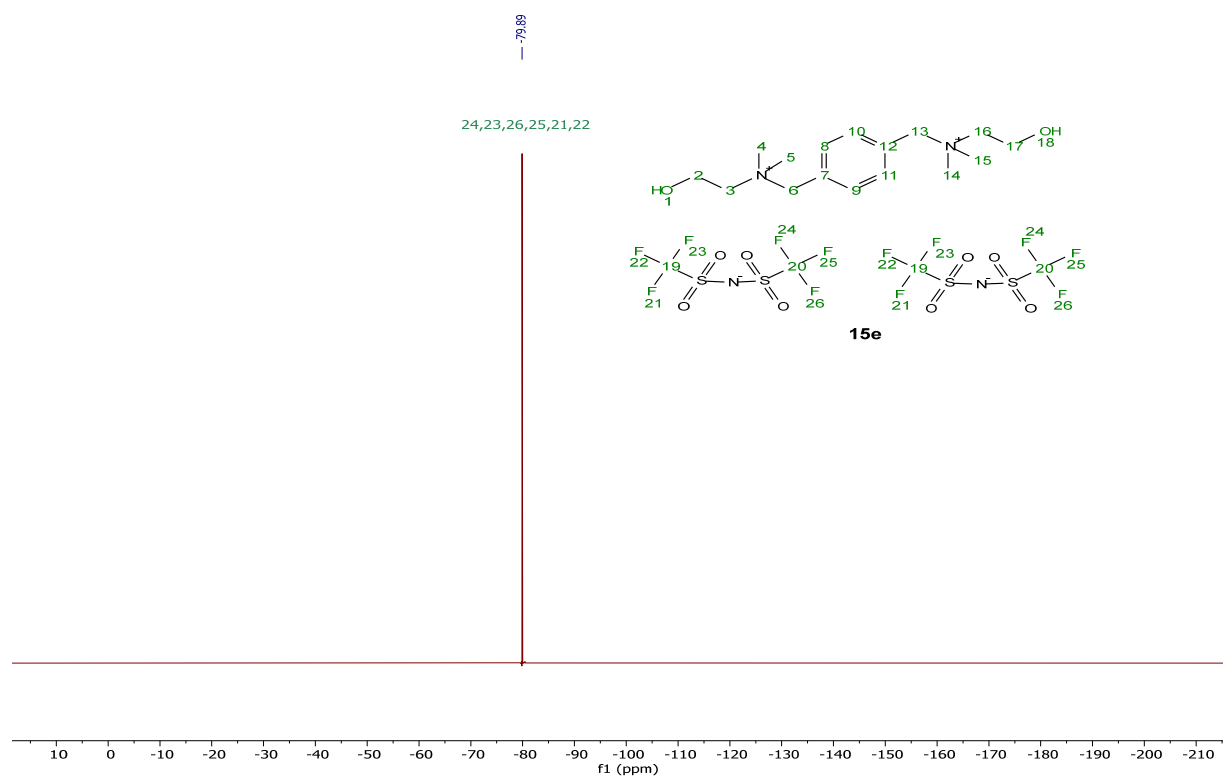
## HSQC (Deuterium Oxide)

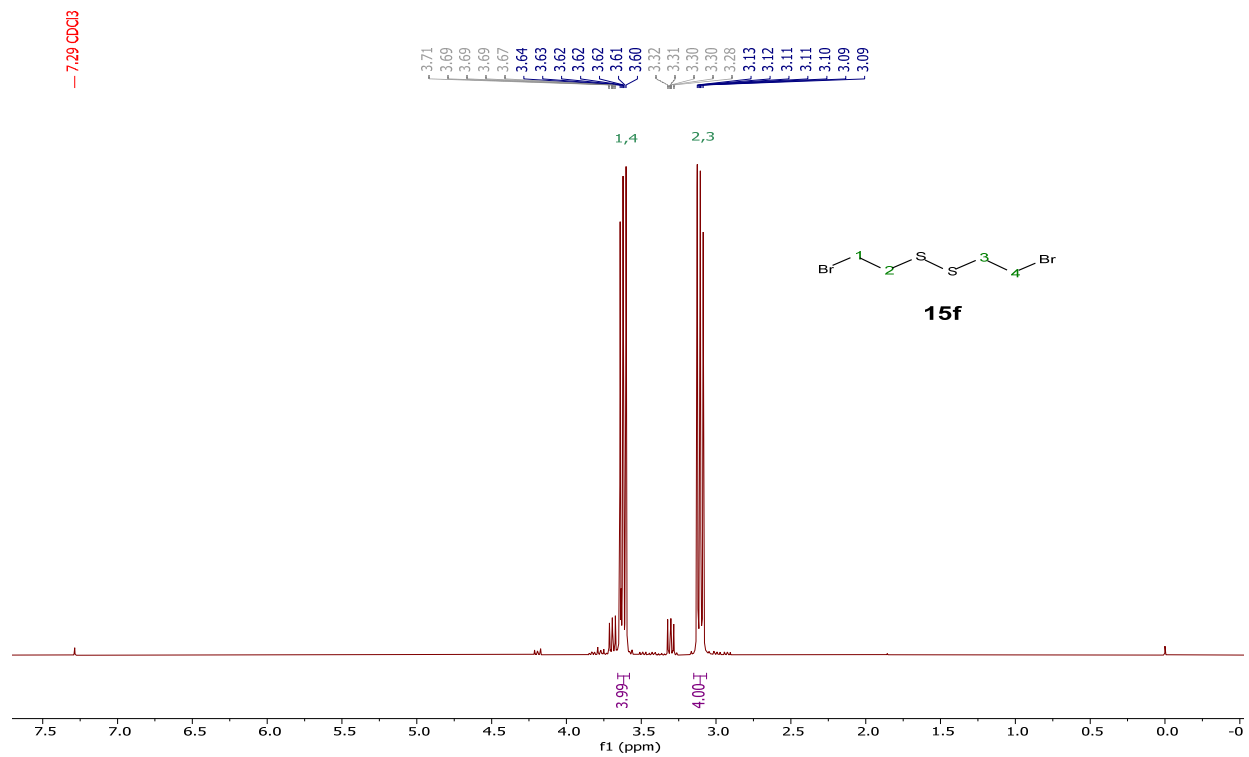
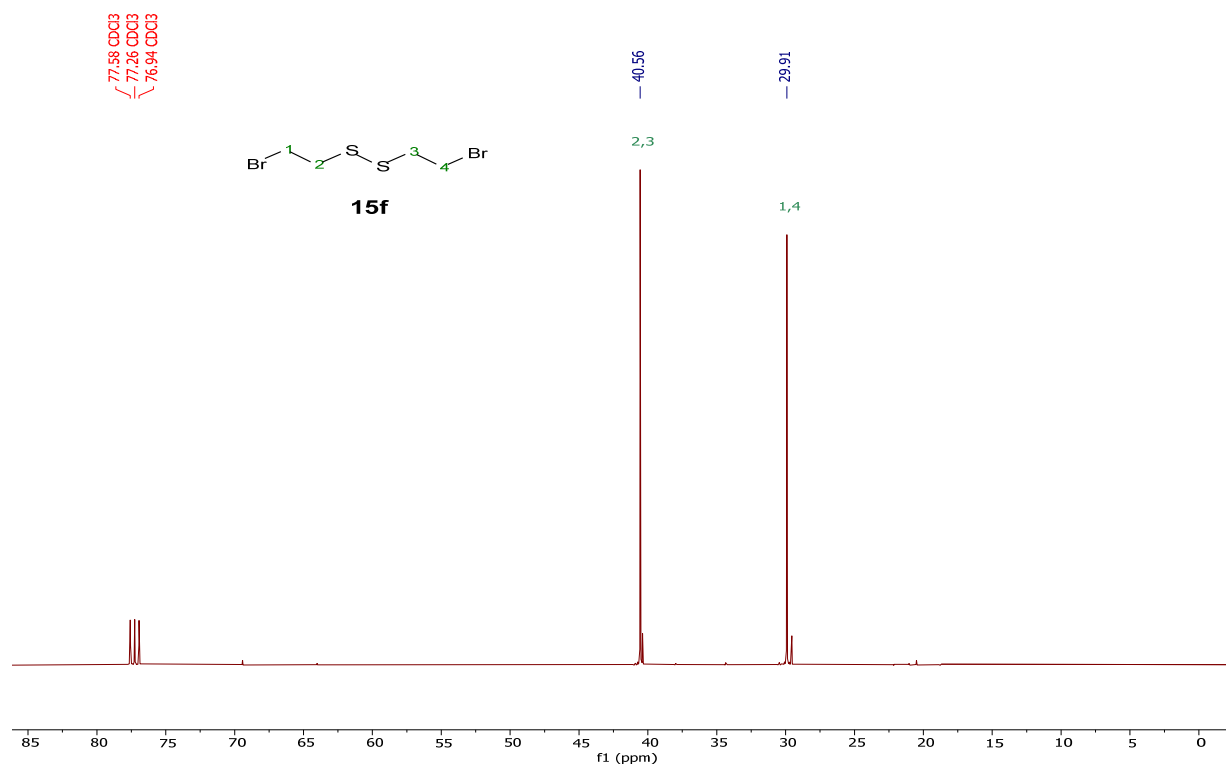


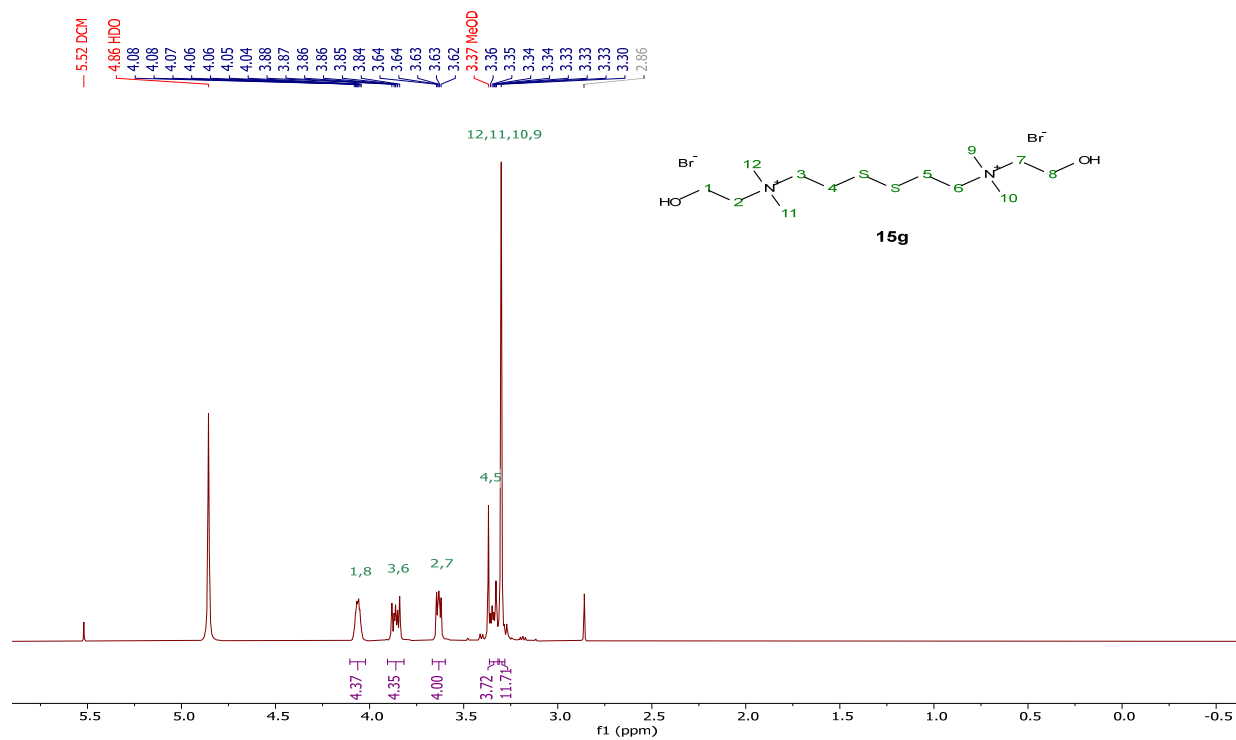
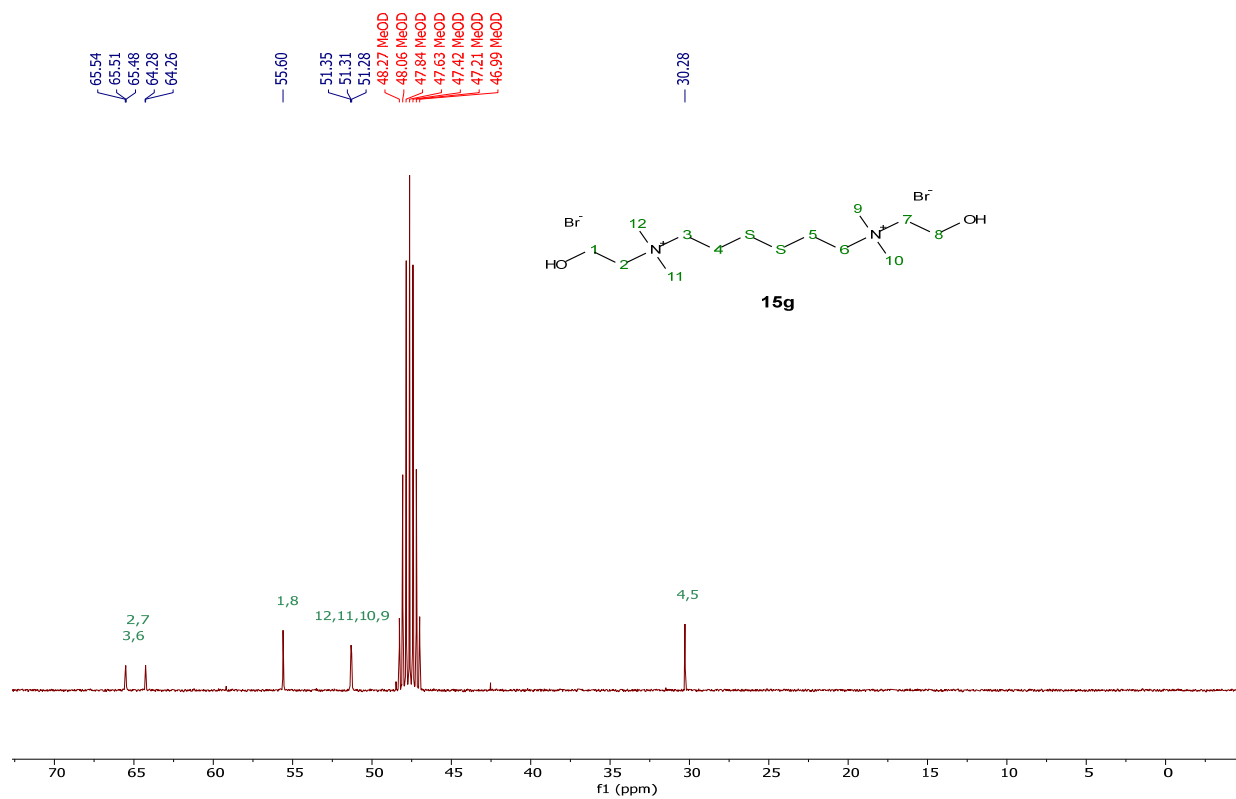
[DC-yne][2NTf<sub>2</sub>], **15c**<sup>1</sup>H NMR (400 MHz, Methanol-d<sub>4</sub>)<sup>13</sup>C{<sup>1</sup>H} NMR (101 MHz, Methanol-d<sub>4</sub>)

$^{19}\text{F}$  NMR (376 MHz, Methanol- $d_4$ )[DC-Ar][2Br], **15d** $^1\text{H}$  NMR (400 MHz, Deuterium Oxide)

$^{13}\text{C}\{^1\text{H}\}$  NMR (101 MHz, Acetone- $d_6$ )[DC-Ar][2NTf $_2$ ], **15e** $^1\text{H}$  NMR (400 MHz, Acetone- $d_6$ )

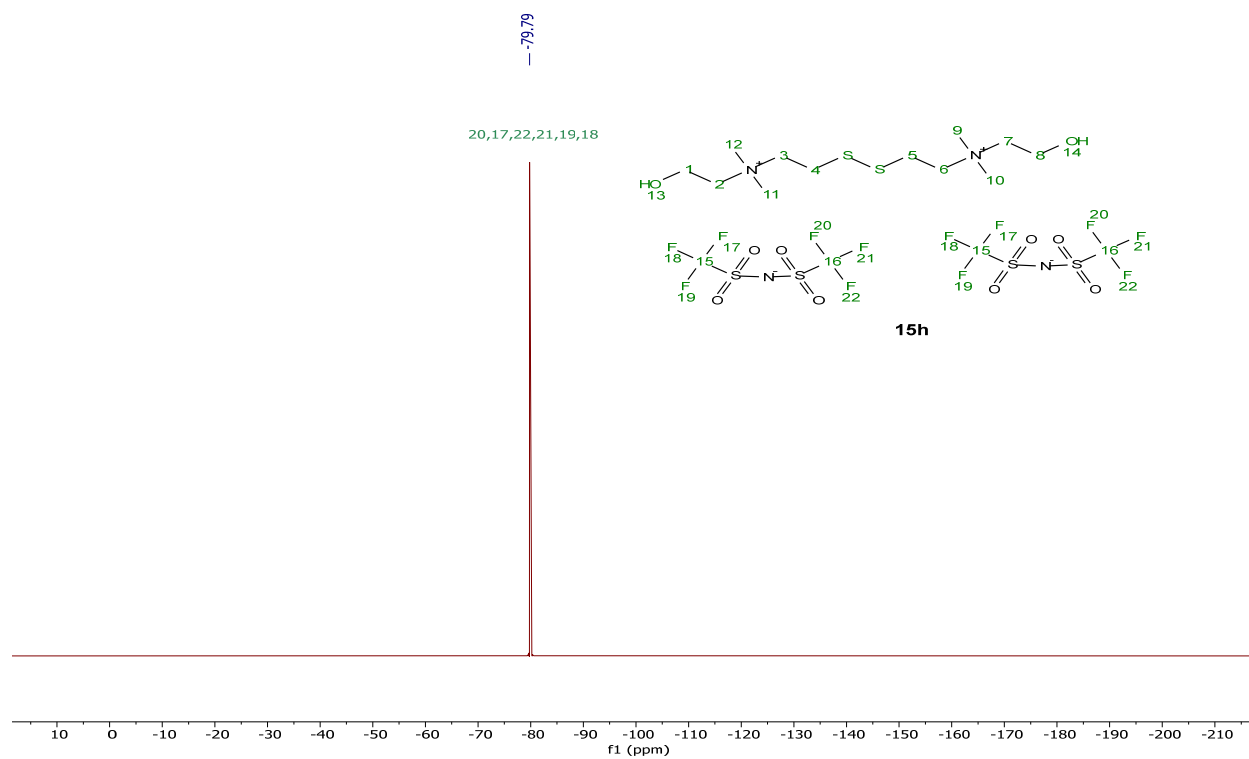
$^{13}\text{C}\{^1\text{H}\}$  NMR (101 MHz, Acetone- $d_6$ ) $^{19}\text{F}$  NMR (376 MHz, Acetone- $d_6$ )

**15f** $^1\text{H}$  NMR (400 MHz, Chloroform-d) $^{13}\text{C}\{^1\text{H}\}$  NMR (101 MHz, Chloroform-d)

[DC-SS][Br], **15g** $^1\text{H}$  NMR (400 MHz, Methanol-d<sub>4</sub>) $^{13}\text{C}\{^1\text{H}\}$  NMR (101 MHz, Methanol-d<sub>4</sub>)

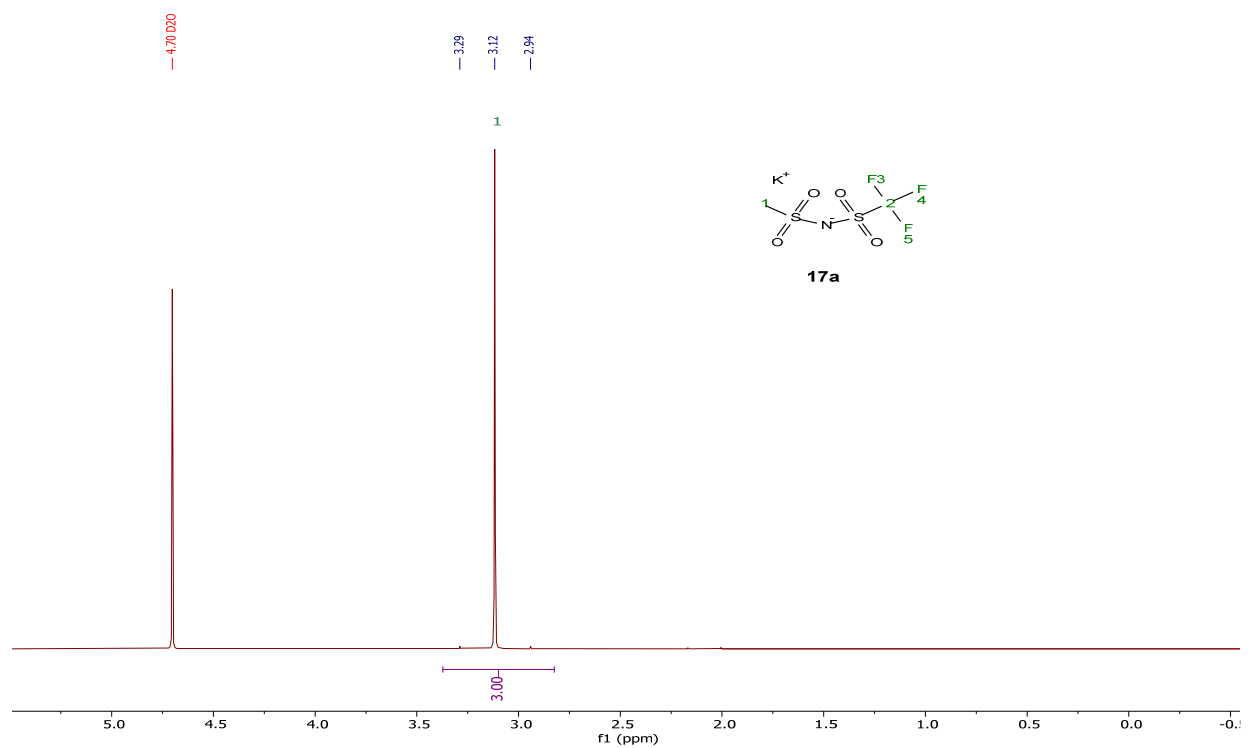


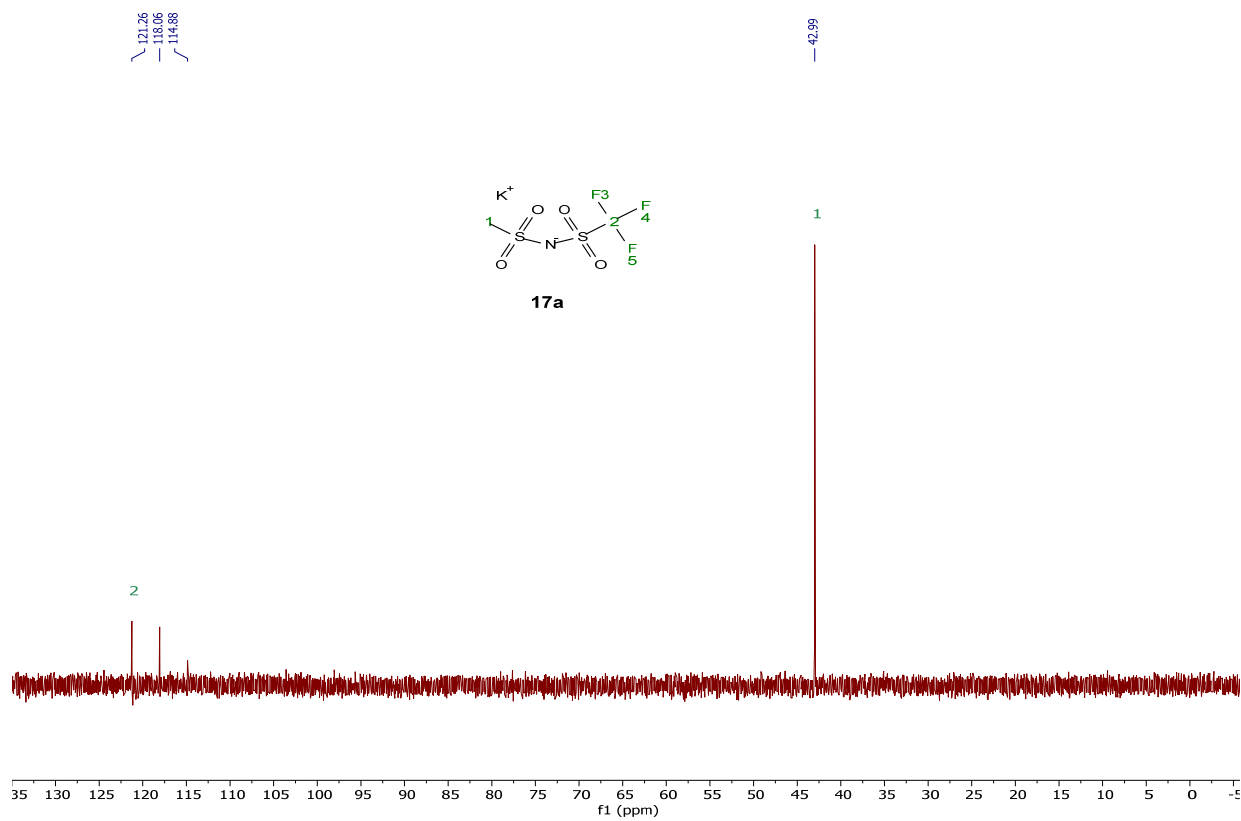
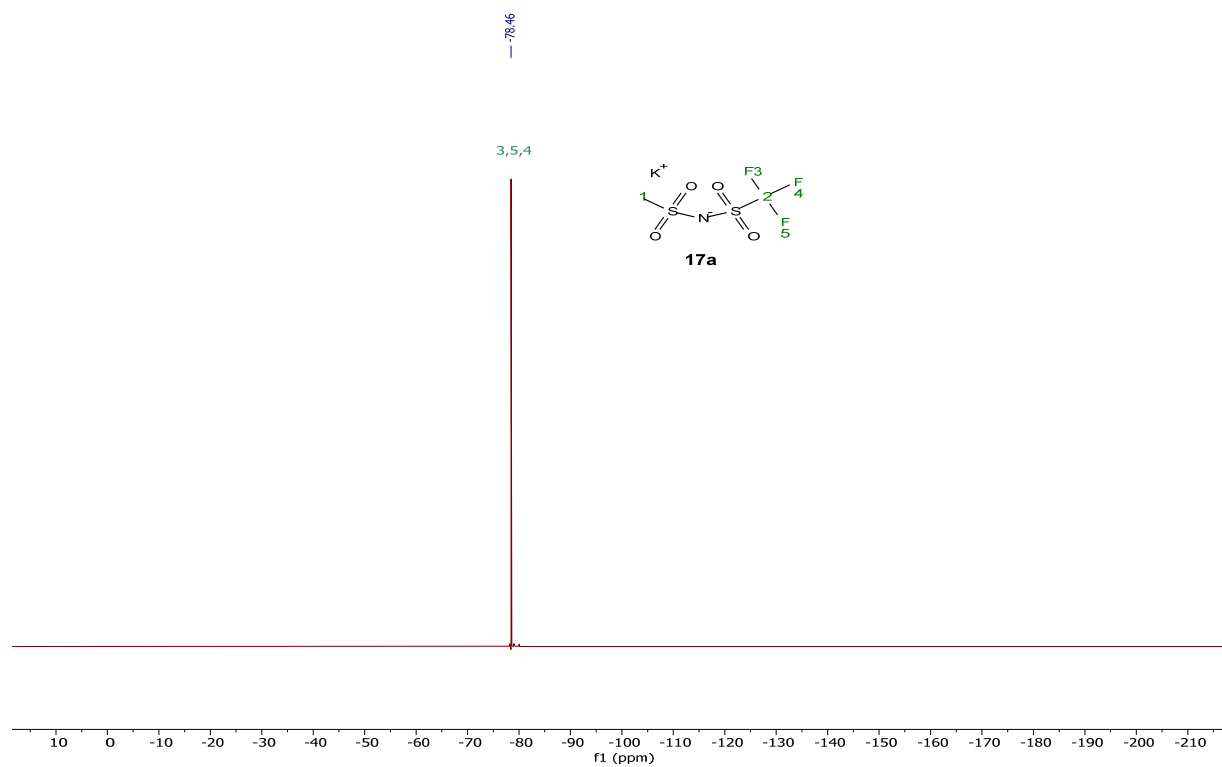
$^{19}\text{F}$  NMR (376 MHz, Acetone- $d_6$ )

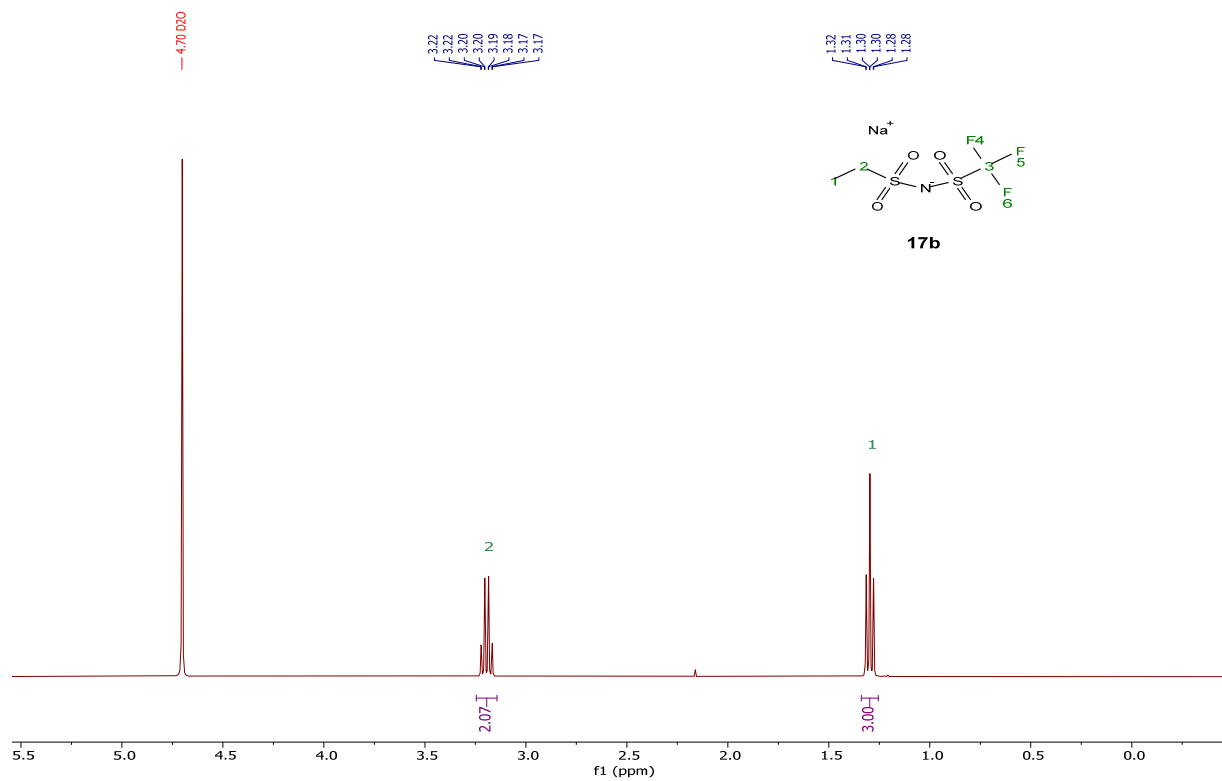
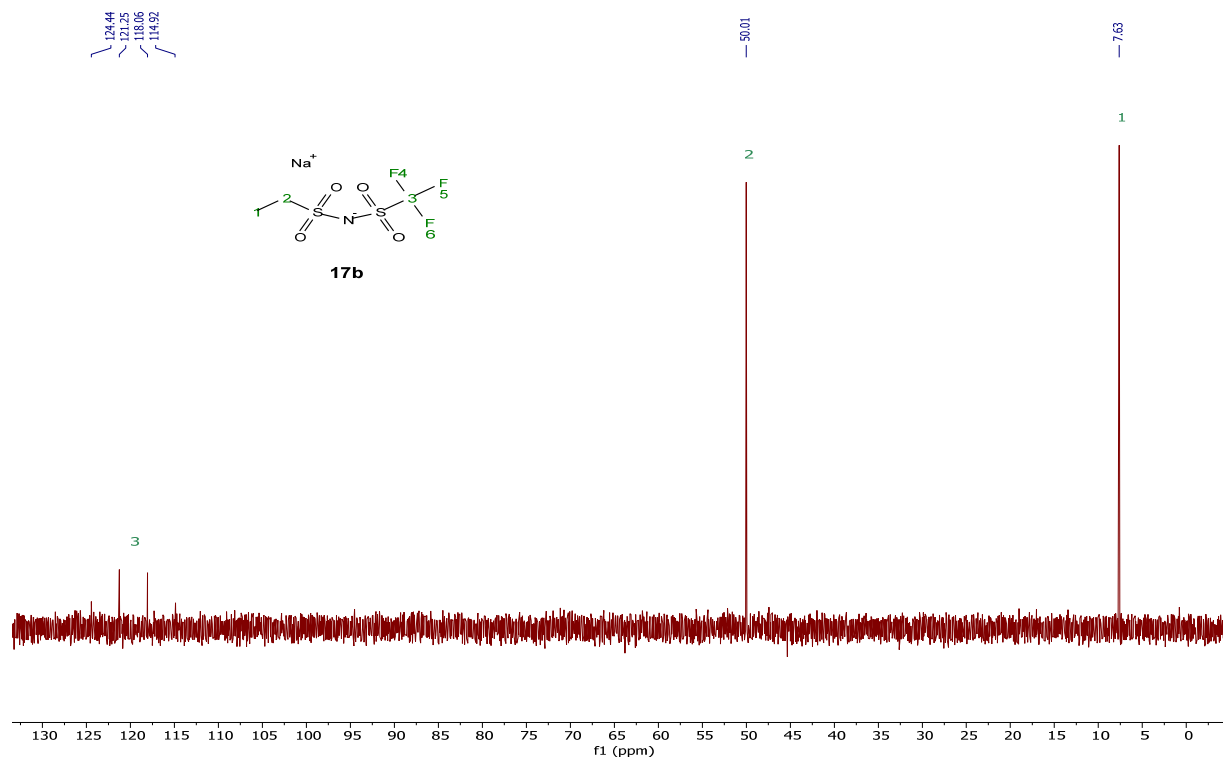


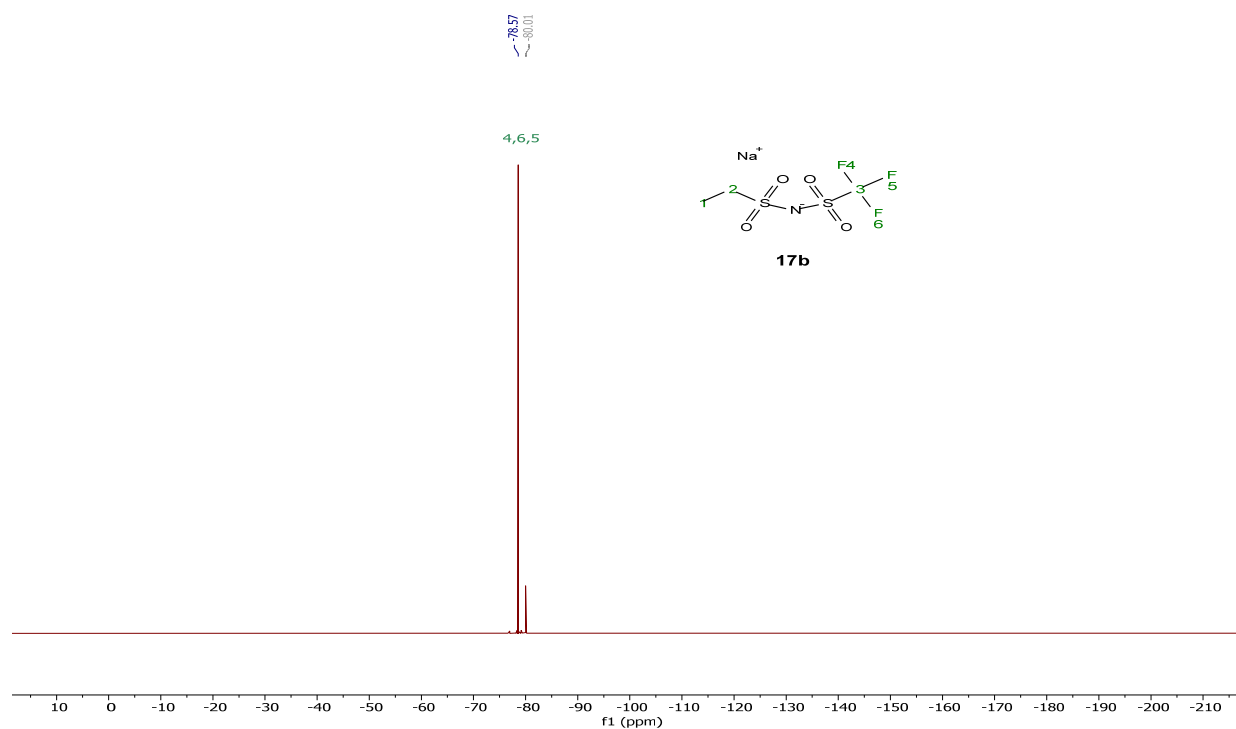
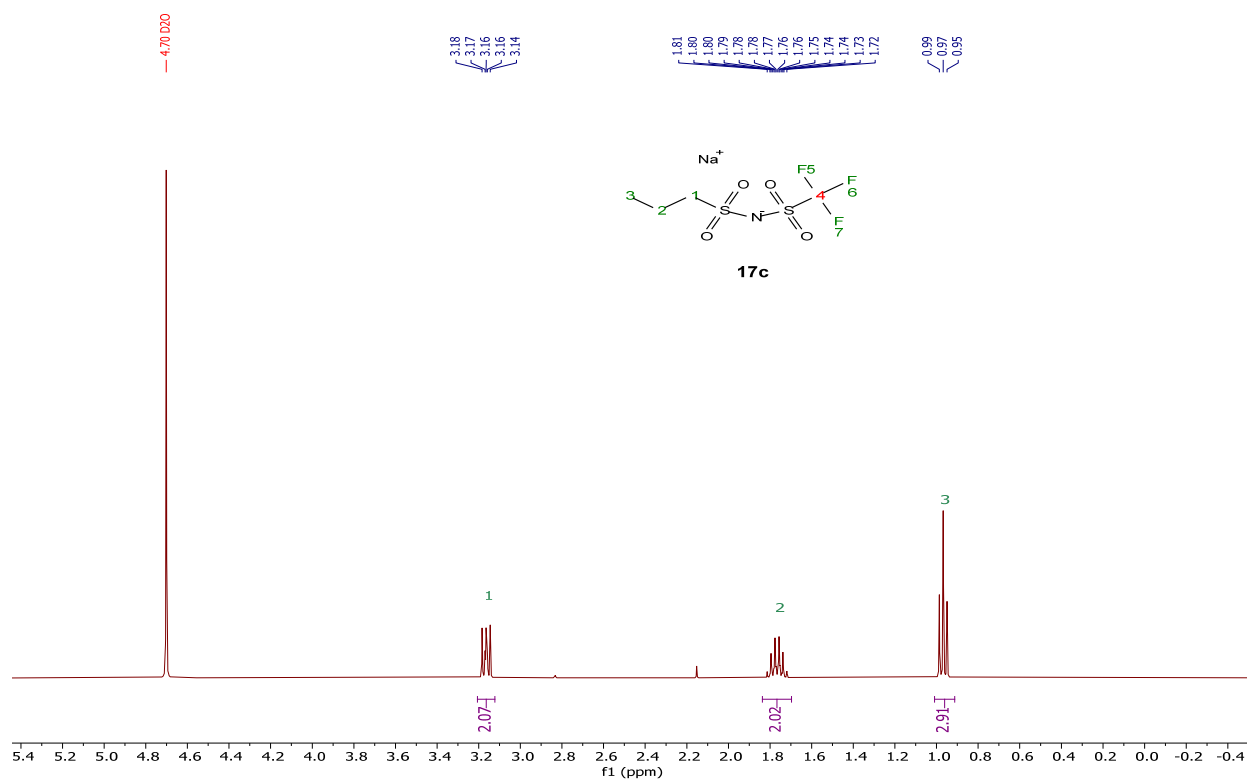
[K][MsNTf], **17a**

$^1\text{H}$  NMR (400 MHz, Deuterium Oxide)

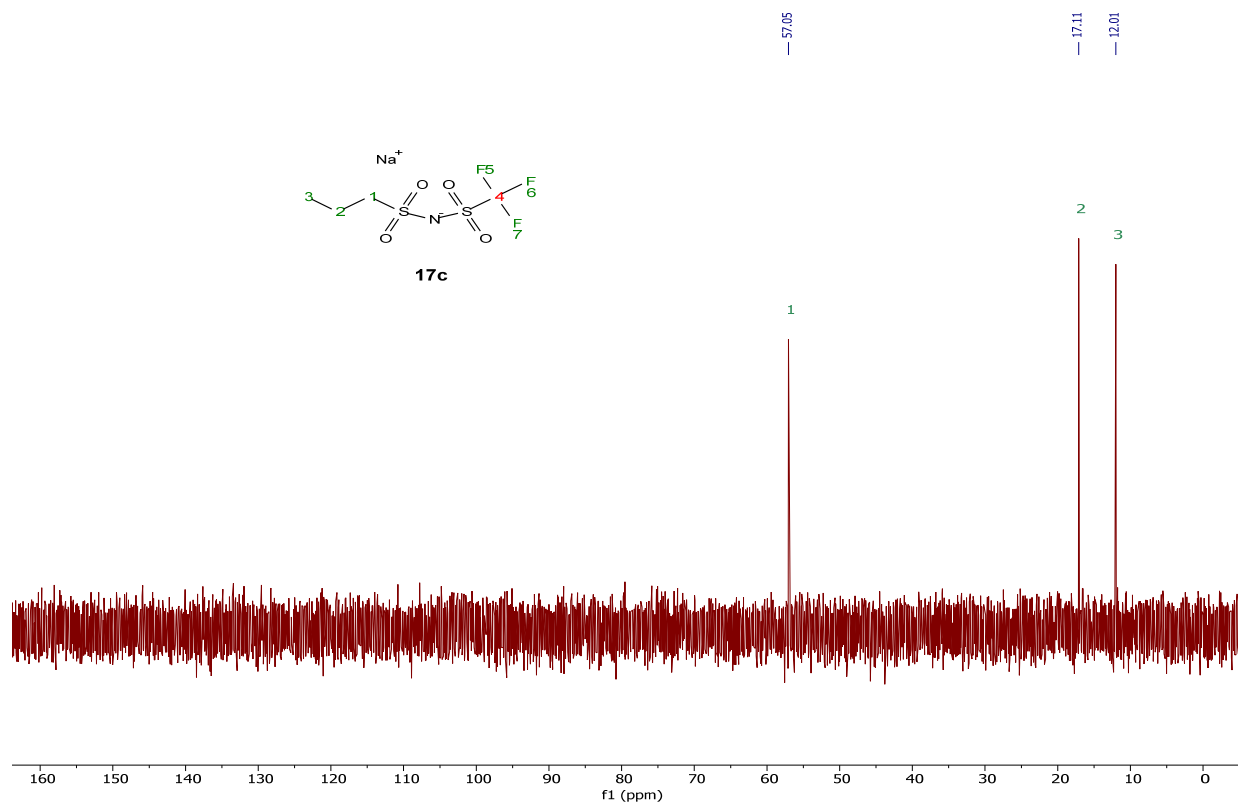


$^{13}\text{C}\{^1\text{H}\}$  NMR (101 MHz, Deuterium Oxide) $^{19}\text{F}$  NMR (376 MHz, Deuterium Oxide)

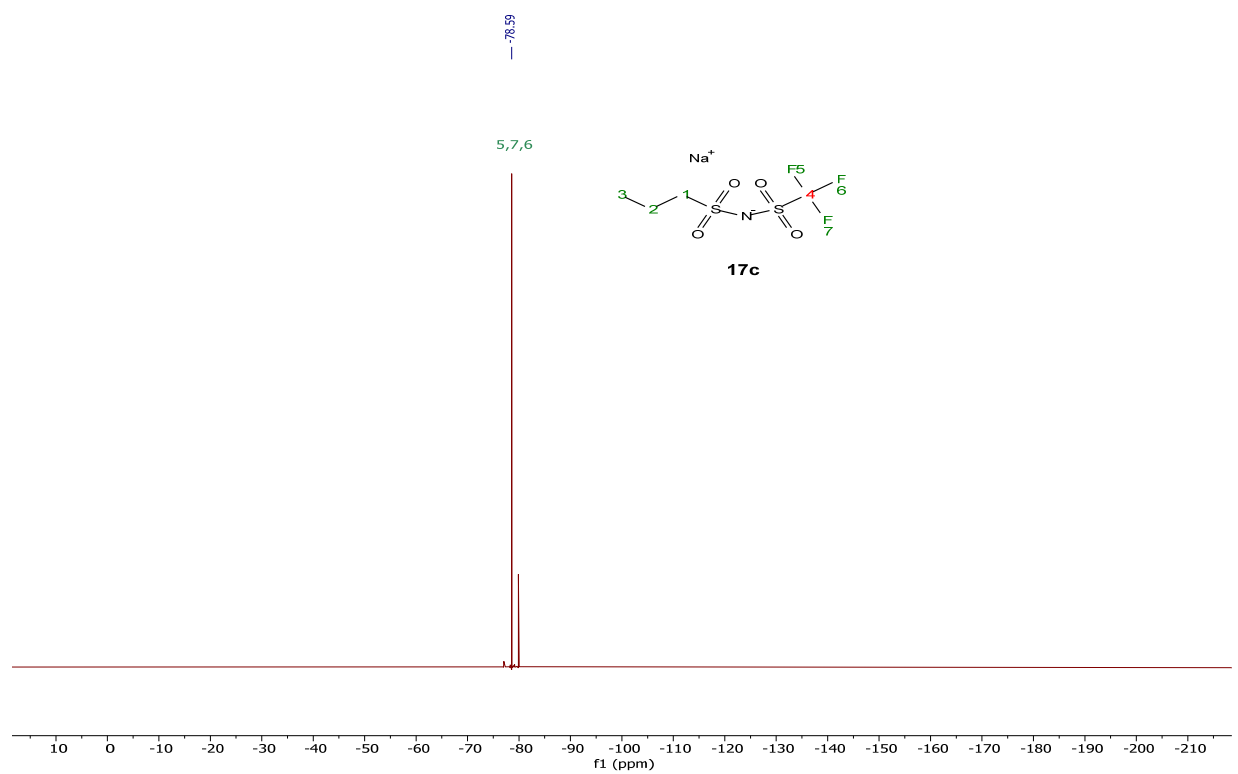
**[Na][EtSNTf], 17b**<sup>1</sup>H NMR (400 MHz, Deuterium Oxide)<sup>13</sup>C{<sup>1</sup>H} NMR (101 MHz, Deuterium Oxide)

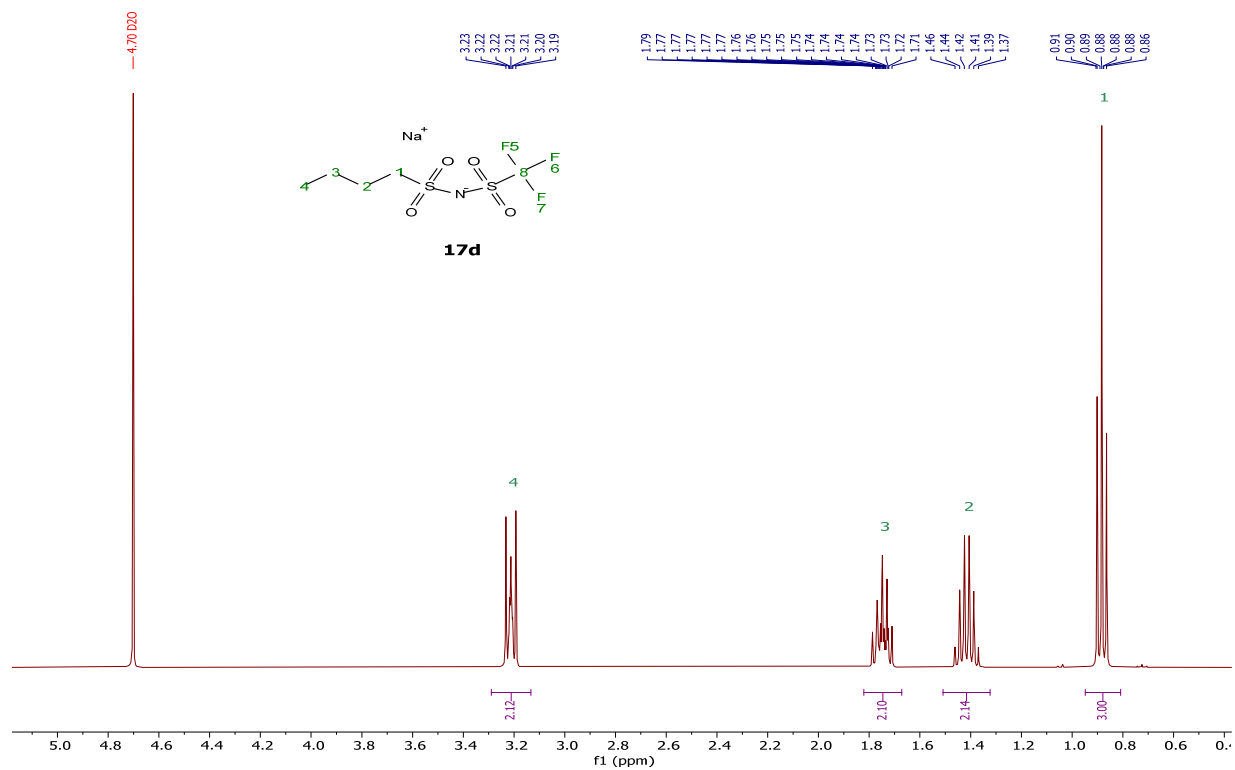
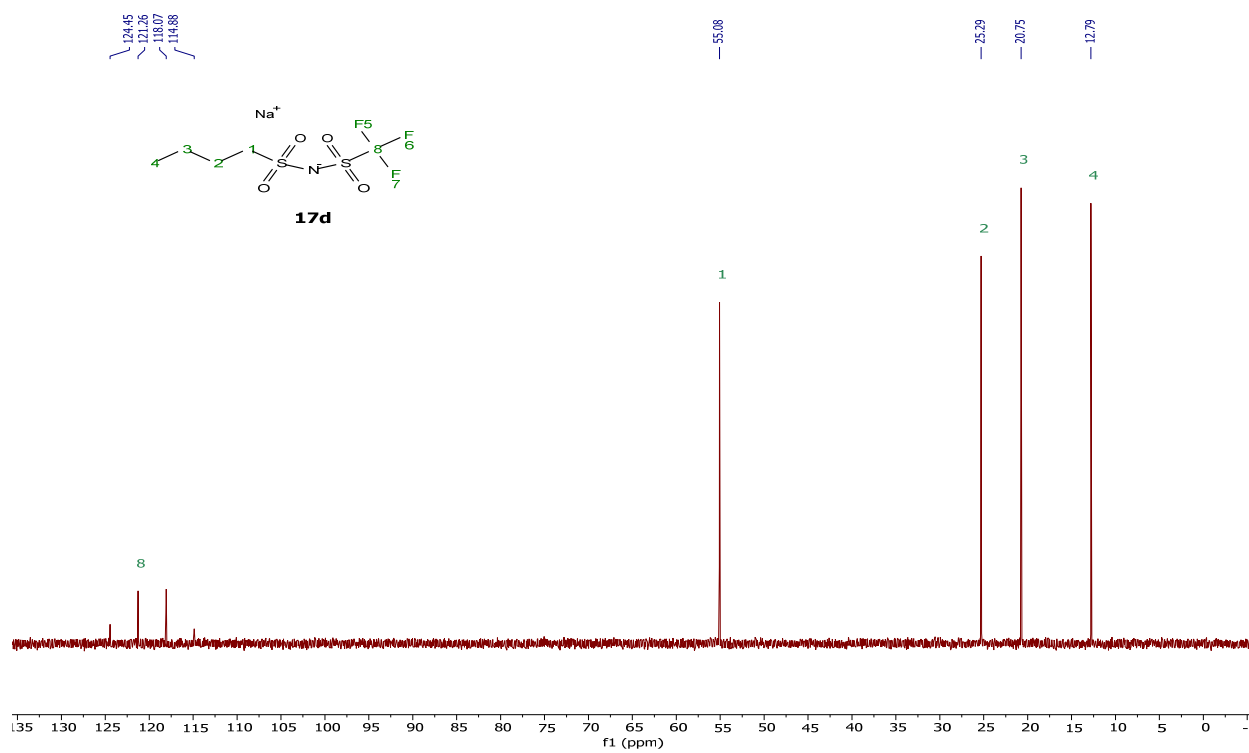
$^{19}\text{F}$  NMR (376 MHz, Deuterium Oxide)[Na][PrSNTf], **17c** $^1\text{H}$  NMR (400 MHz, Deuterium Oxide)

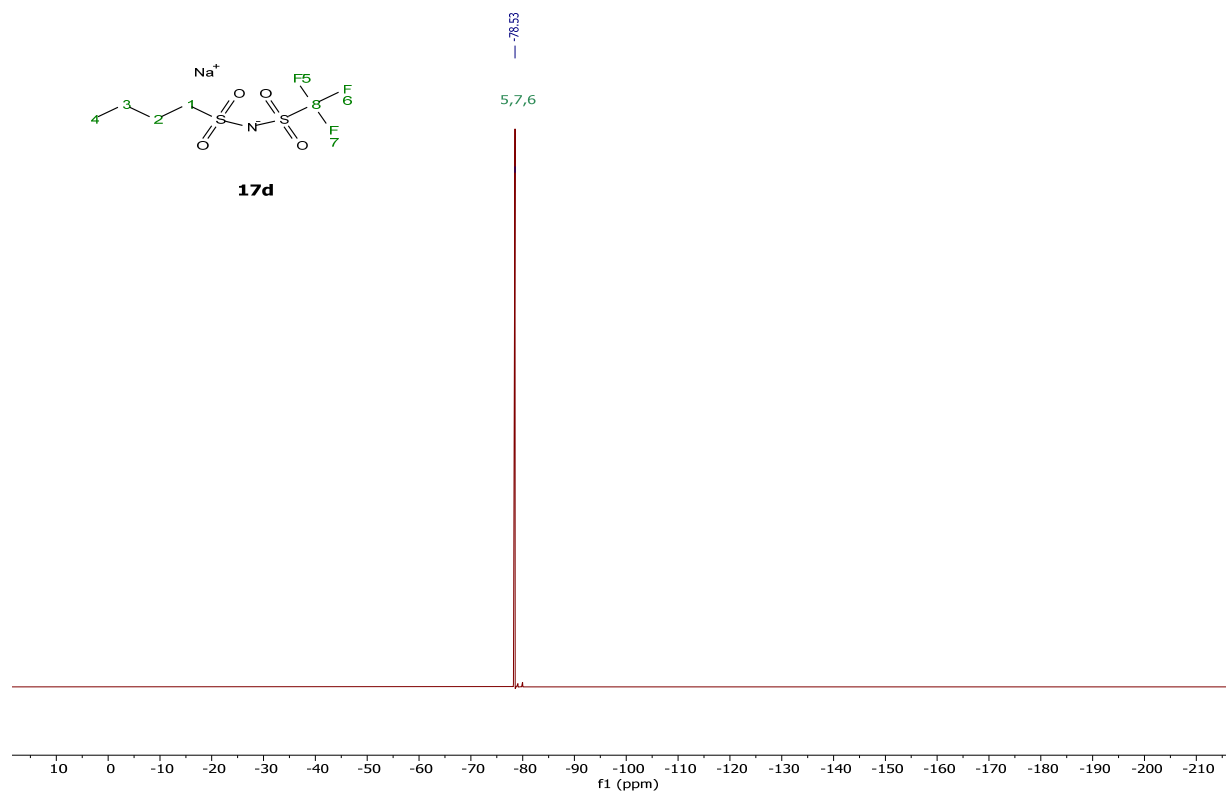
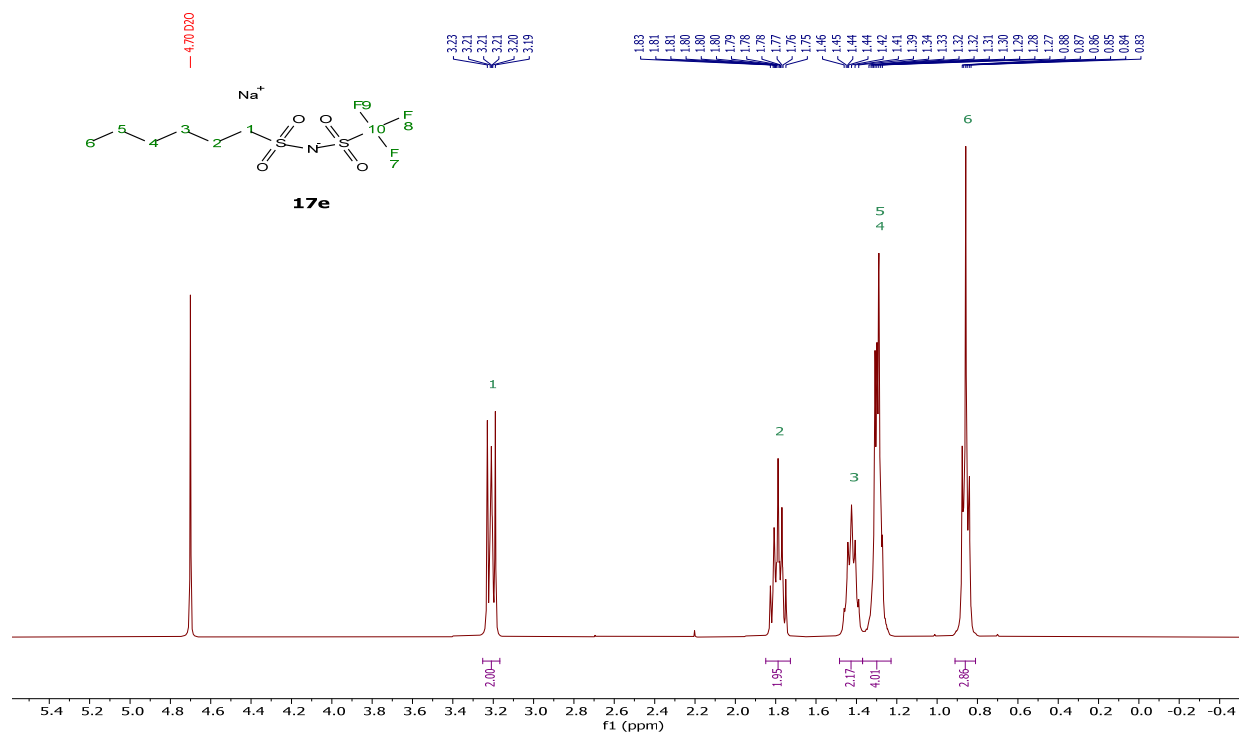
$^{13}\text{C}\{^1\text{H}\}$  NMR (101 MHz, Deuterium Oxide)

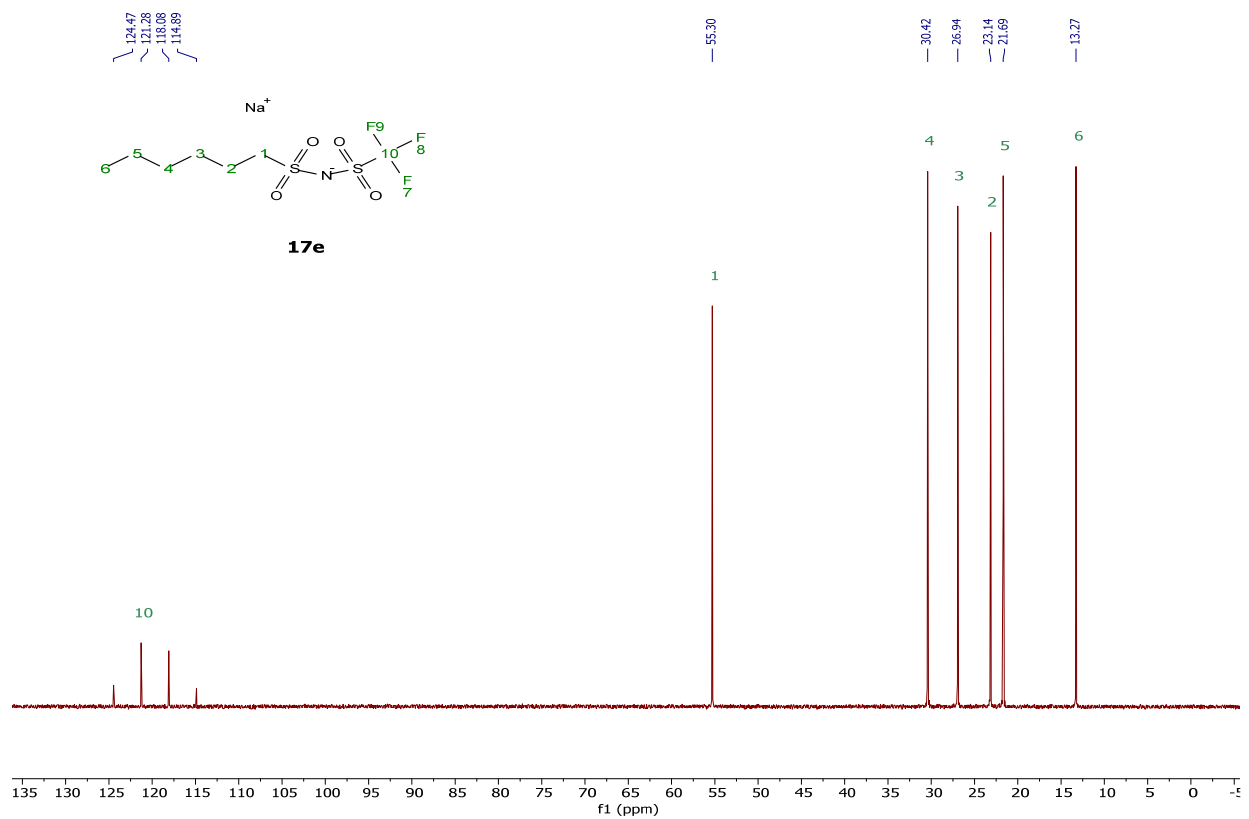


$^{19}\text{F}$  NMR (376 MHz, Deuterium Oxide)

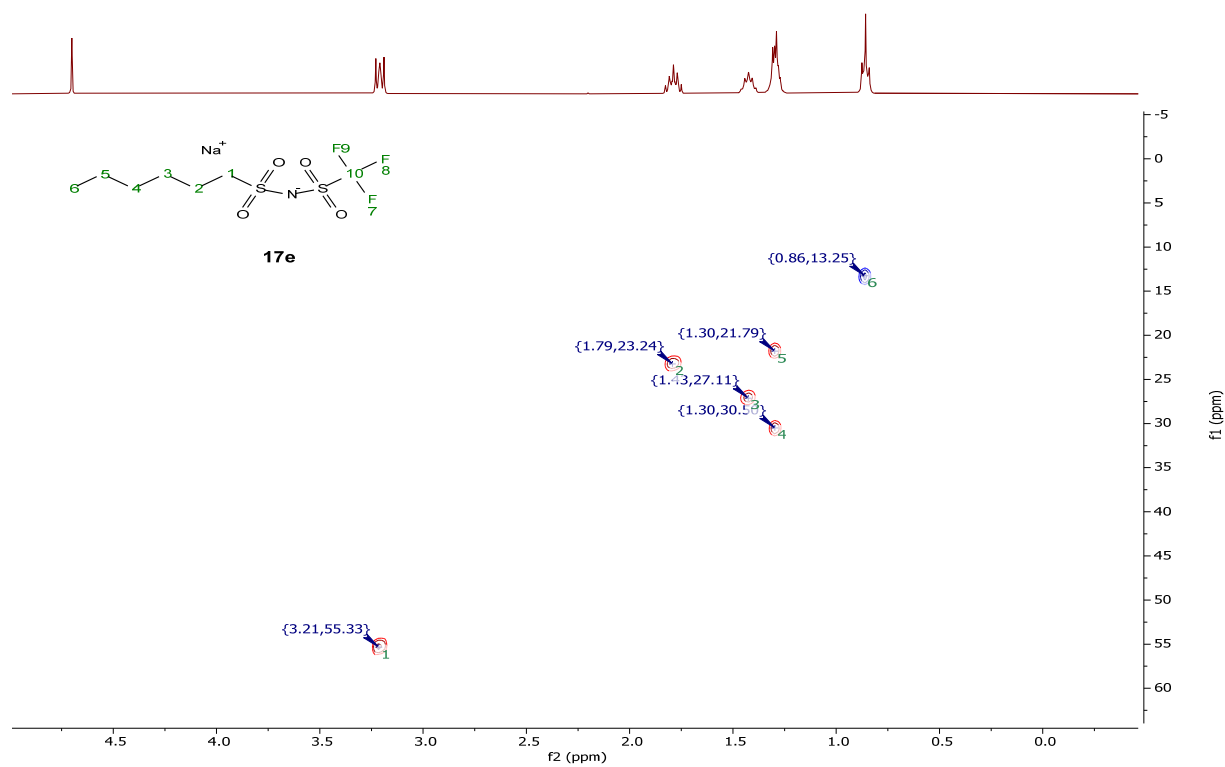


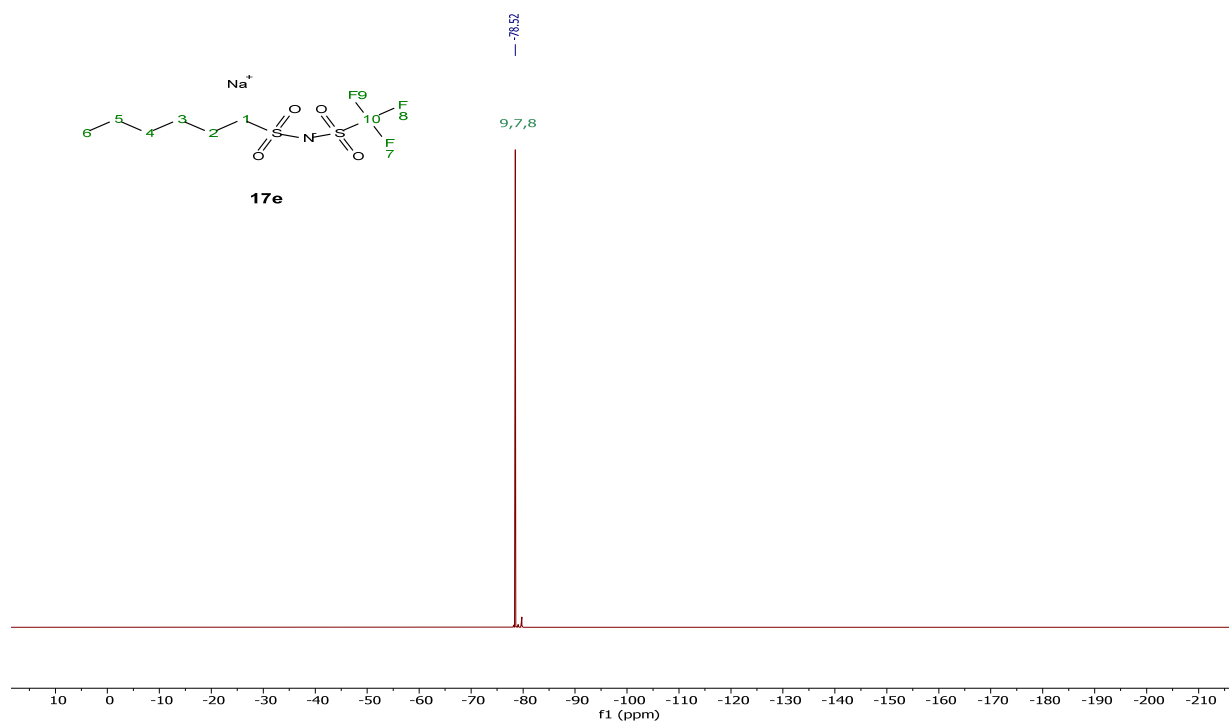
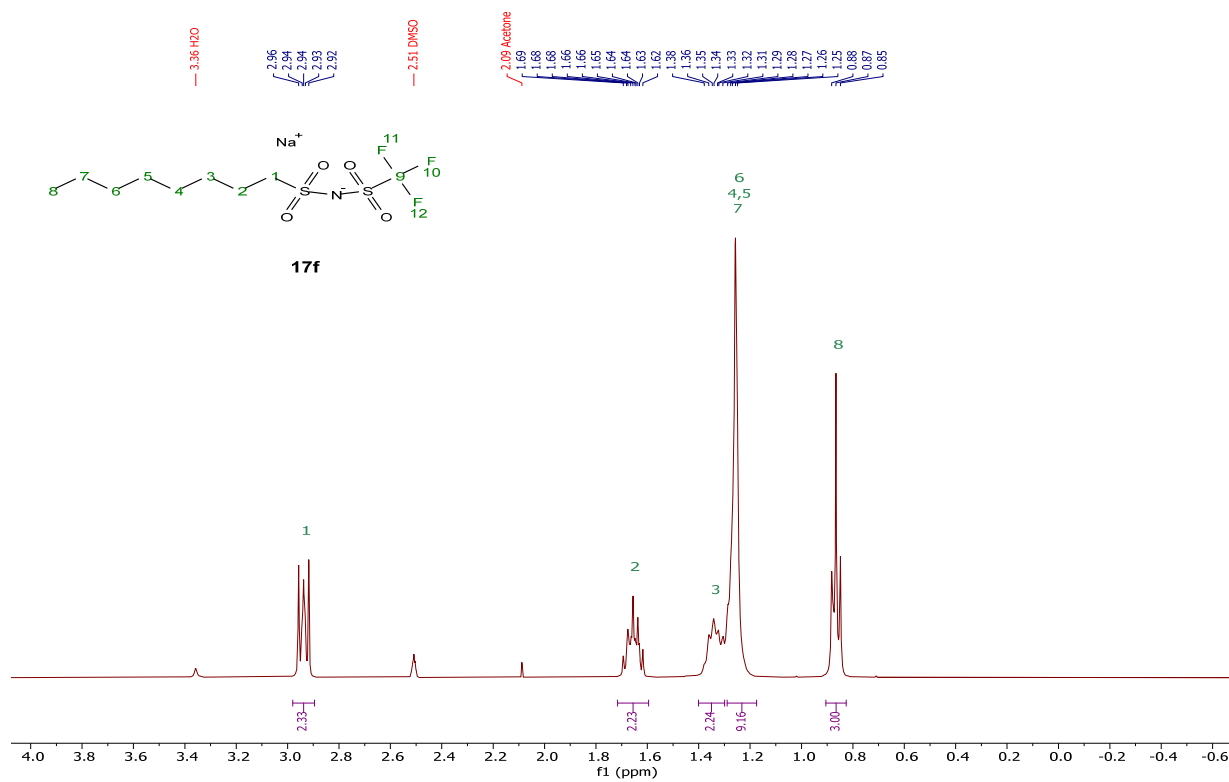
[Na][BSNTf], **17d** $^1\text{H}$  NMR (400 MHz, Deuterium Oxide) $^{13}\text{C}\{^1\text{H}\}$  NMR (101 MHz, Deuterium Oxide)

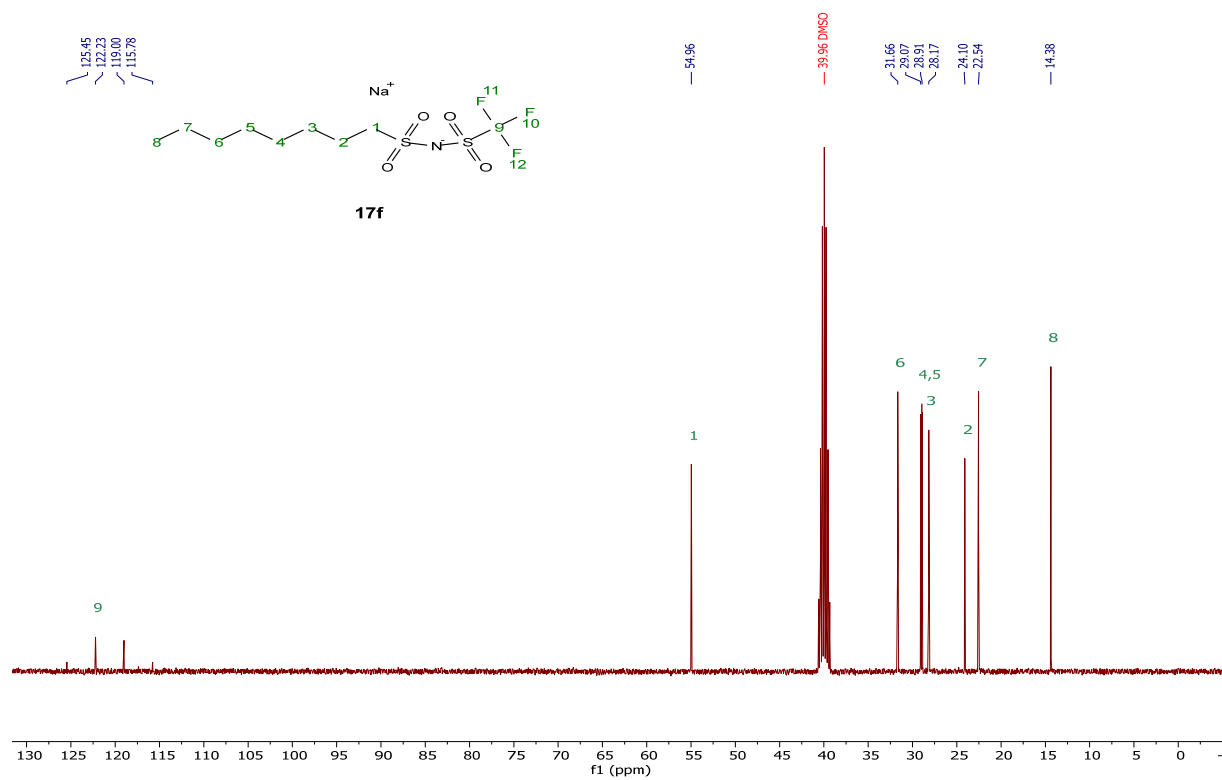
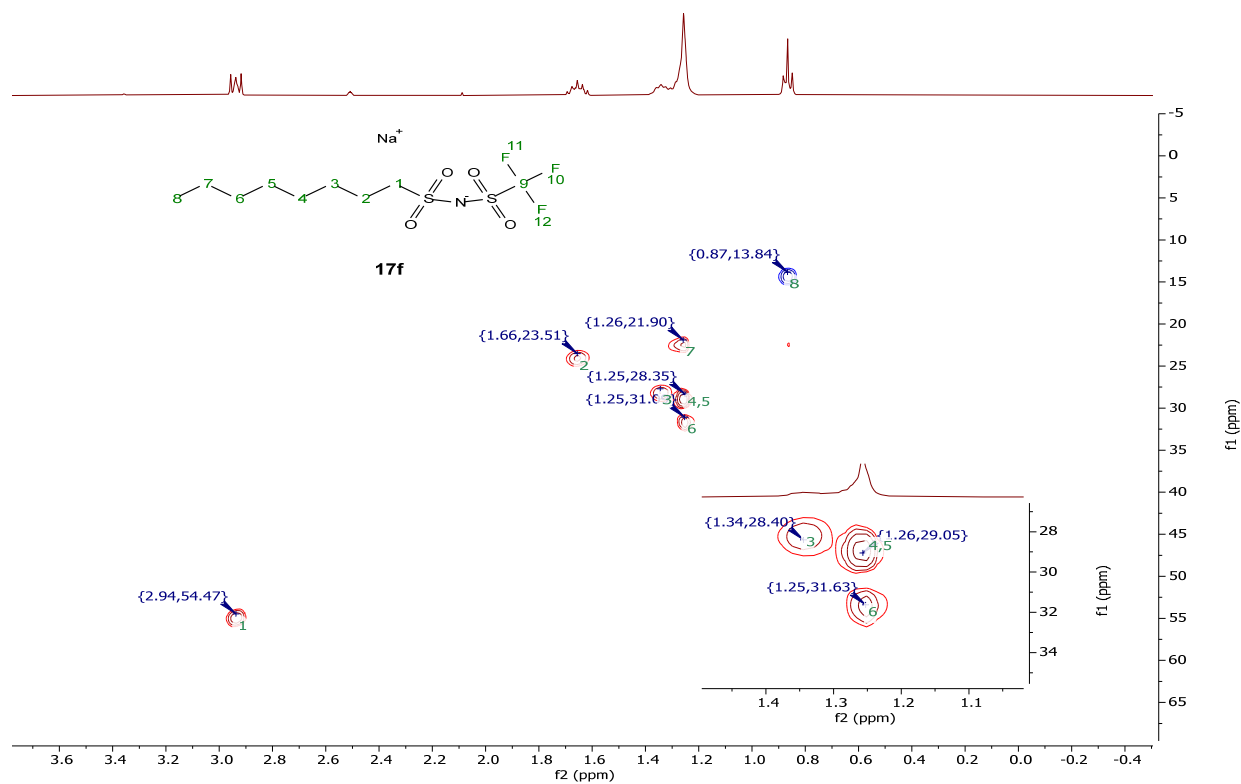
$^{19}\text{F}$  NMR (376 MHz, Deuterium Oxide)[Na][HSNTf], **17e** $^1\text{H}$  NMR (400 MHz, Deuterium Oxide)

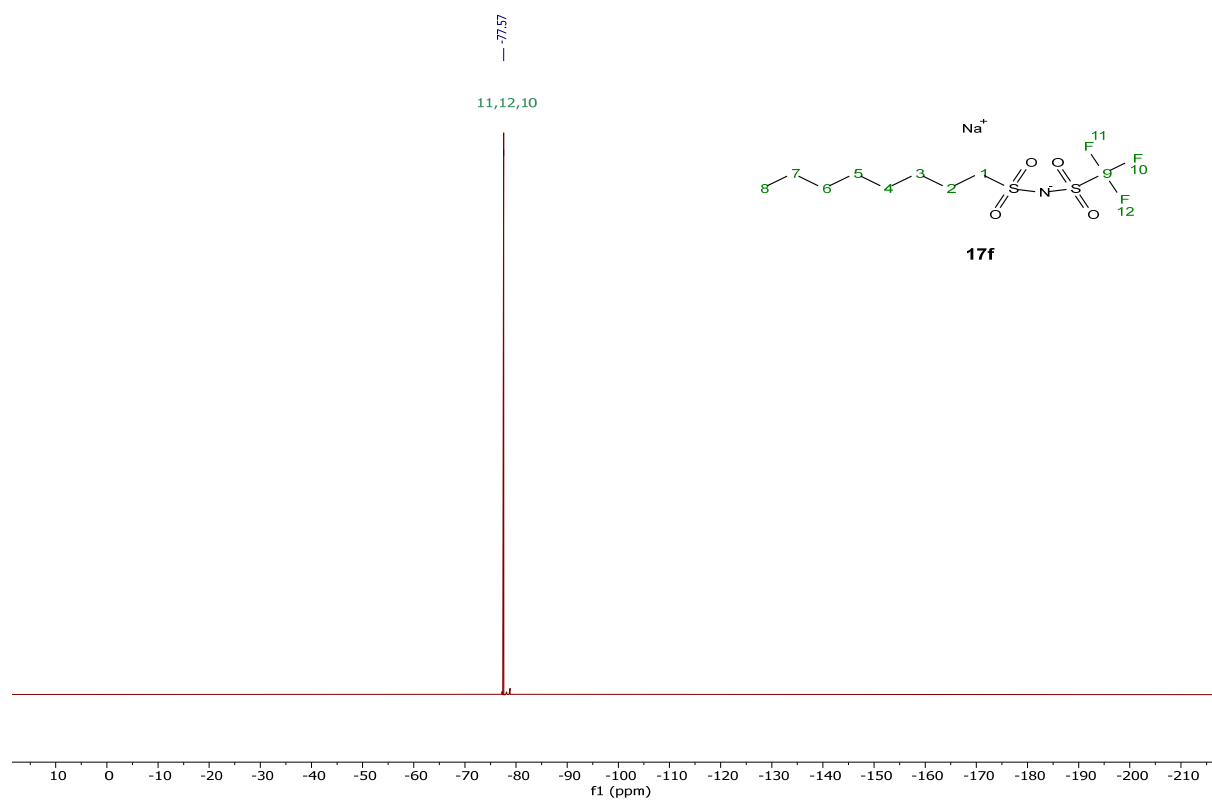
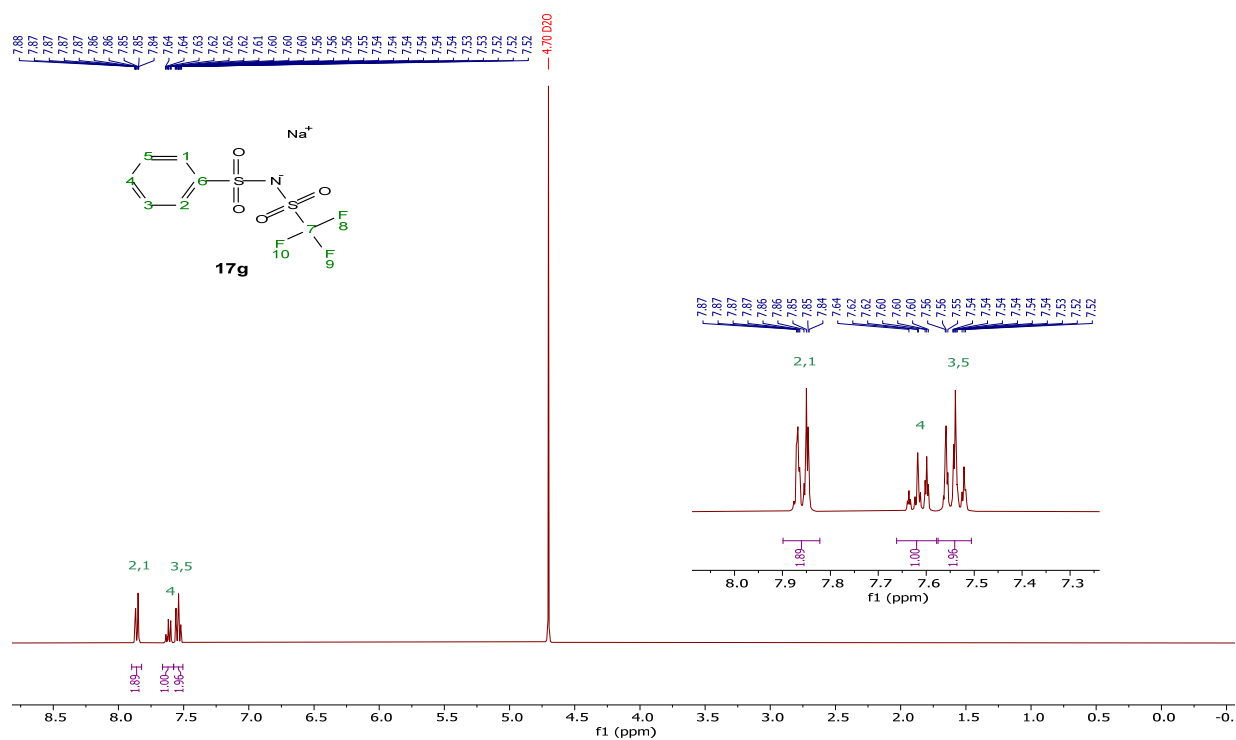
$^{13}\text{C}\{^1\text{H}\}$  NMR (101 MHz, Deuterium Oxide)

## HSQC (Deuterium Oxide)



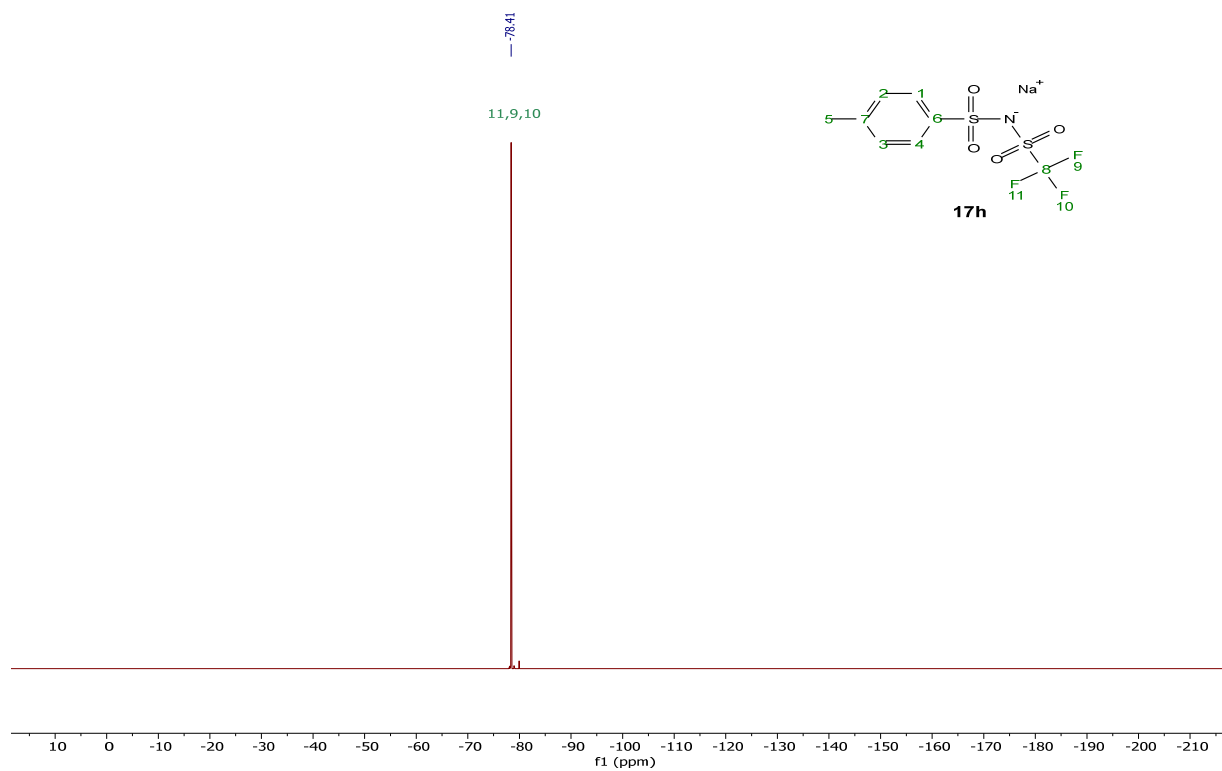
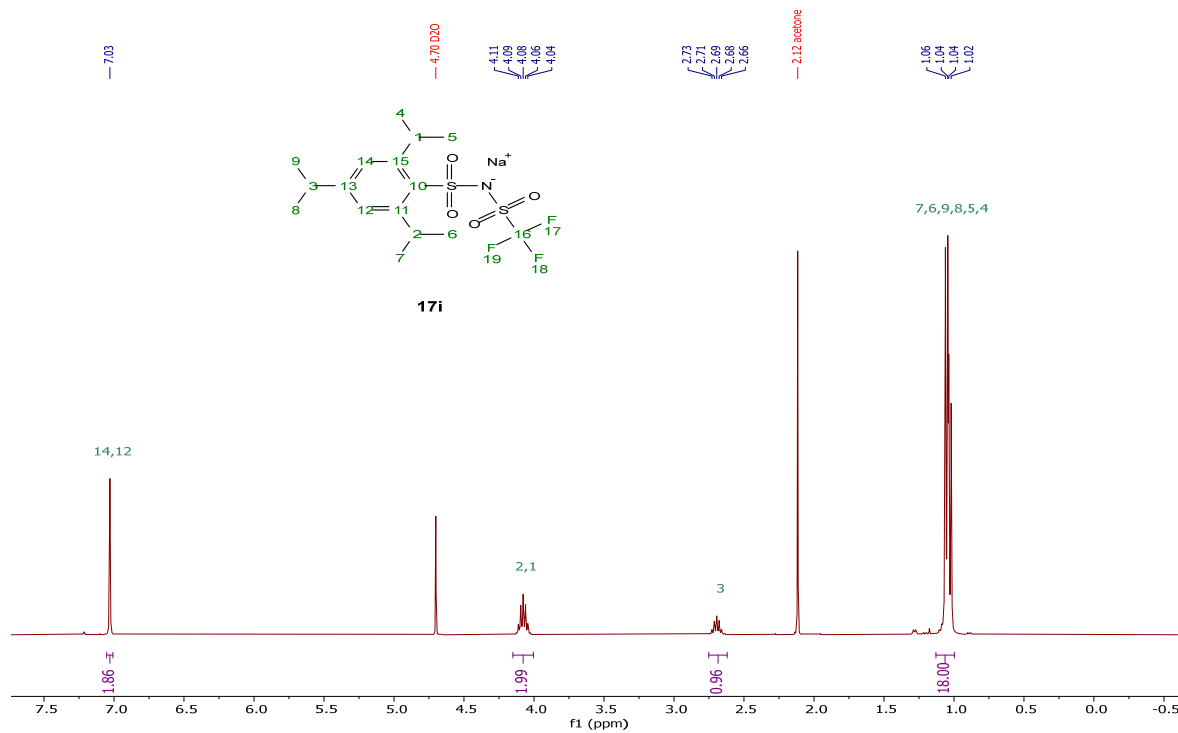
$^{19}\text{F}$  NMR (376 MHz, Deuterium Oxide)[Na][OSNTf], **17f** $^1\text{H}$  NMR (400 MHz, DMSO- $d_6$ )

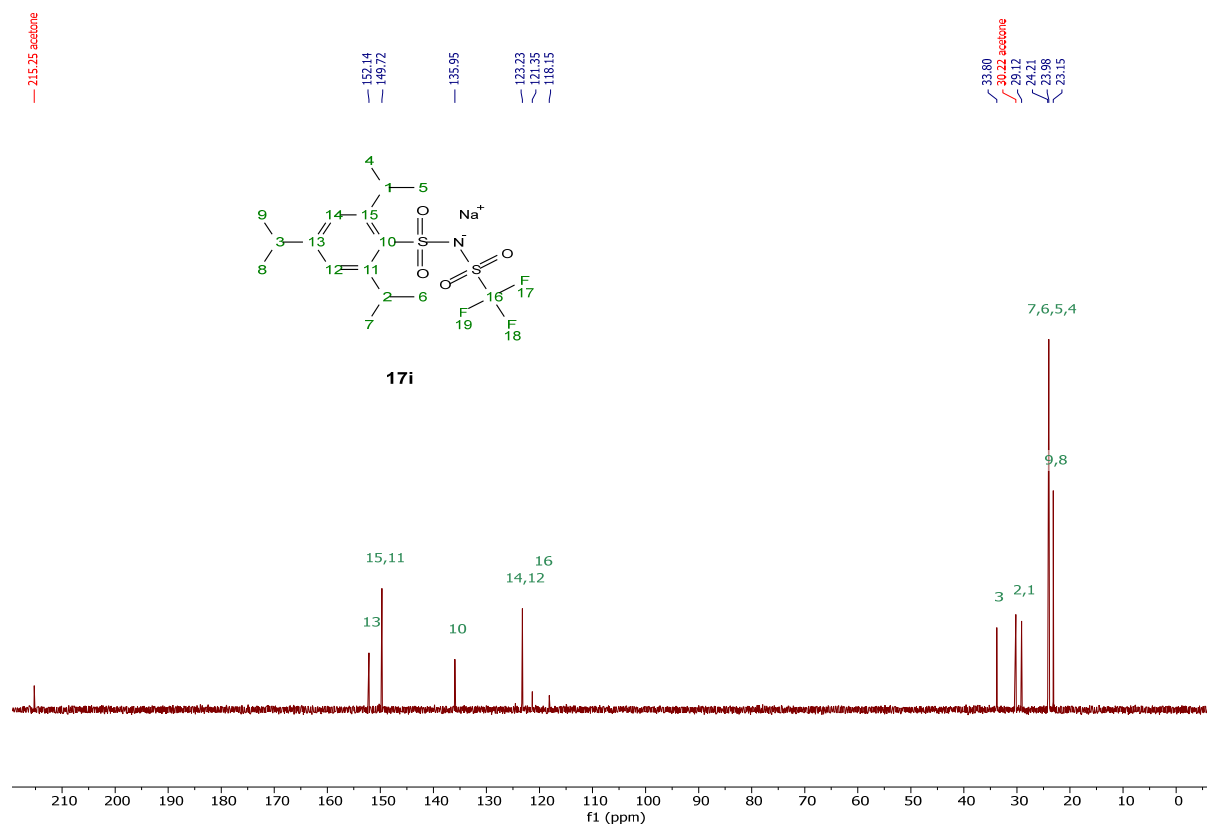
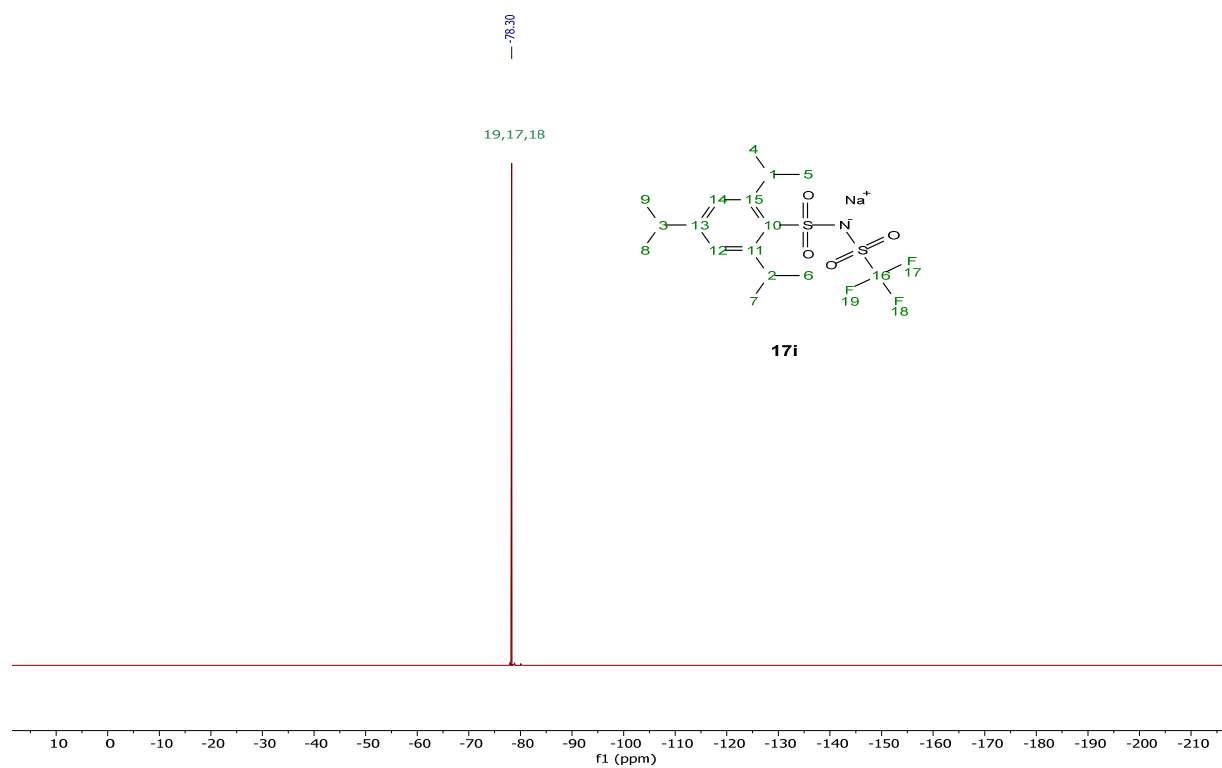
$^{13}\text{C}\{^1\text{H}\}$  NMR (101 MHz, DMSO-d<sub>6</sub>)

 HSQC (DMSO-d<sub>6</sub>)


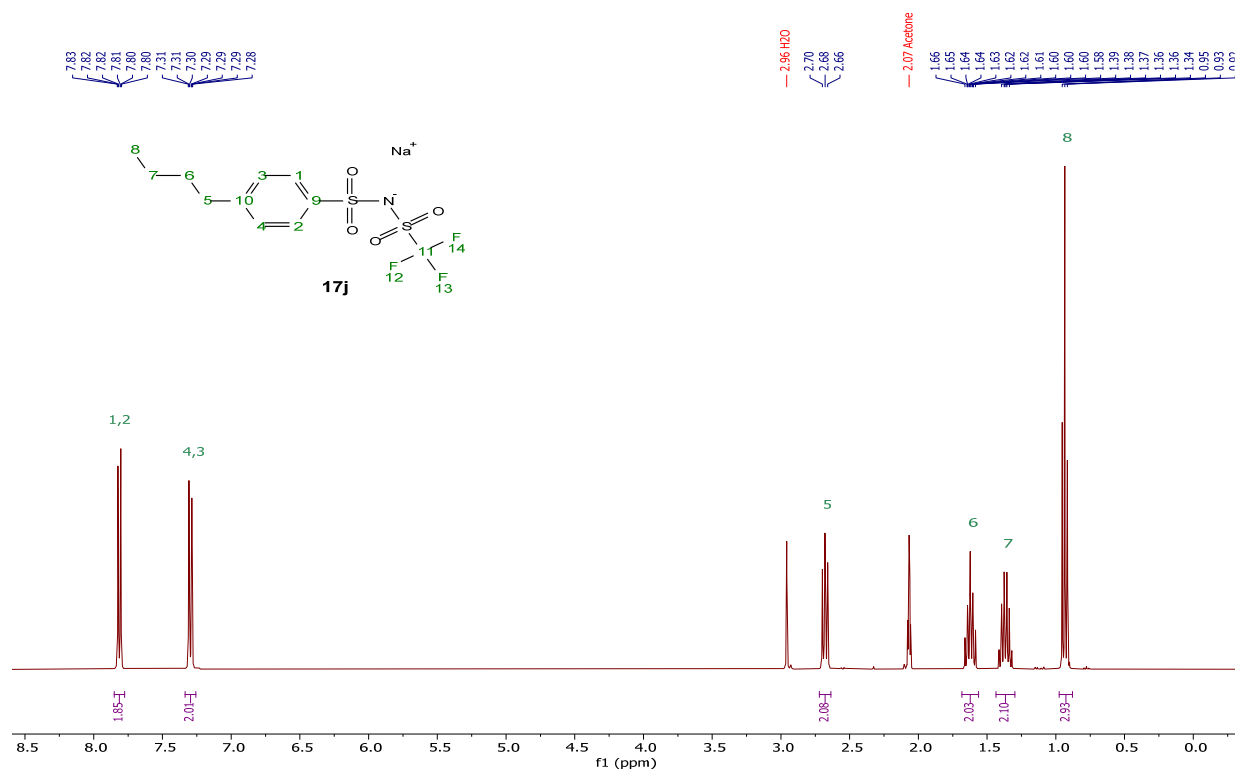
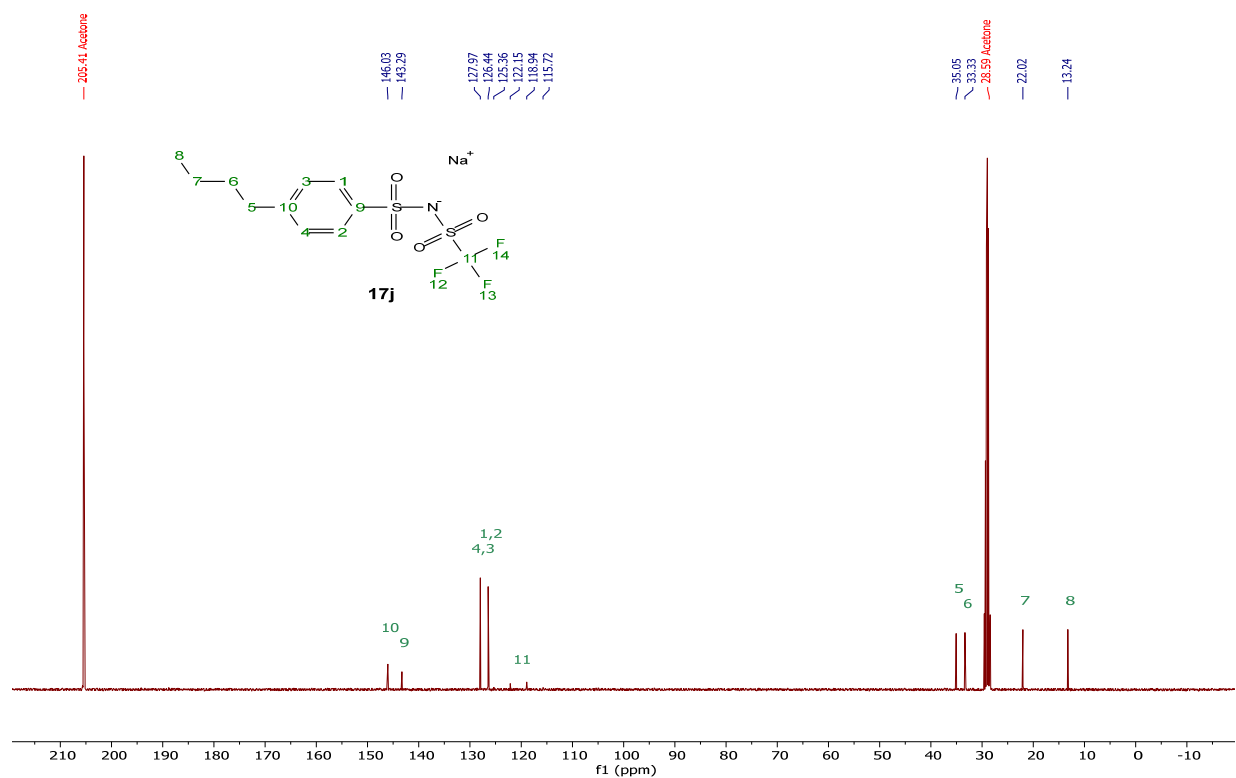
$^{19}\text{F}$  NMR (376 MHz, DMSO- $d_6$ )[Na][PhSNTf], **17g** $^1\text{H}$  NMR (400 MHz, Deuterium Oxide)

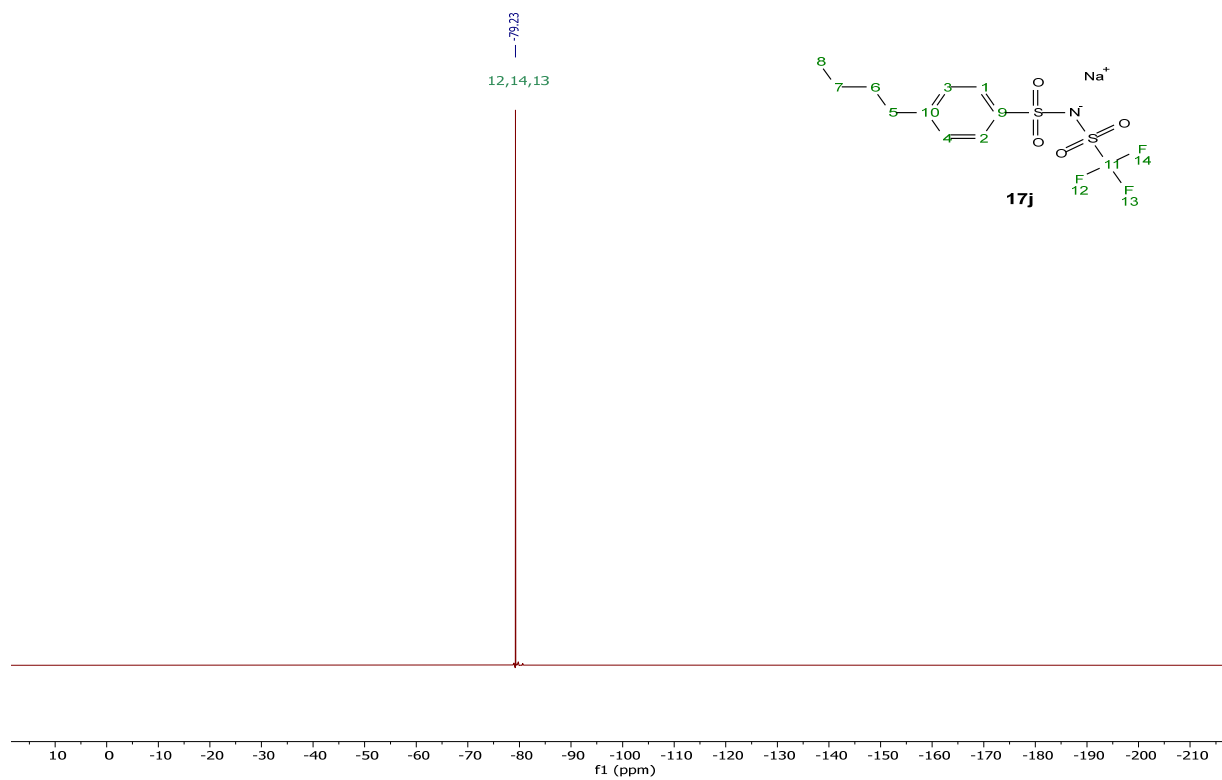
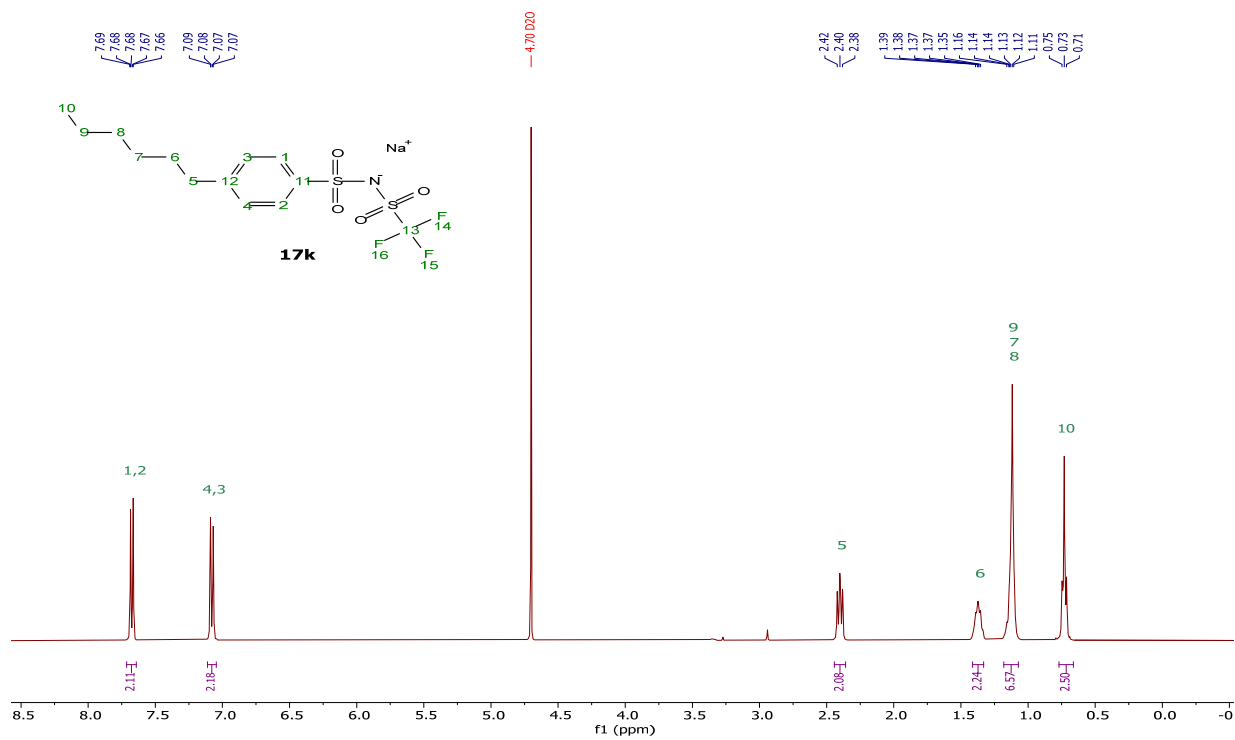


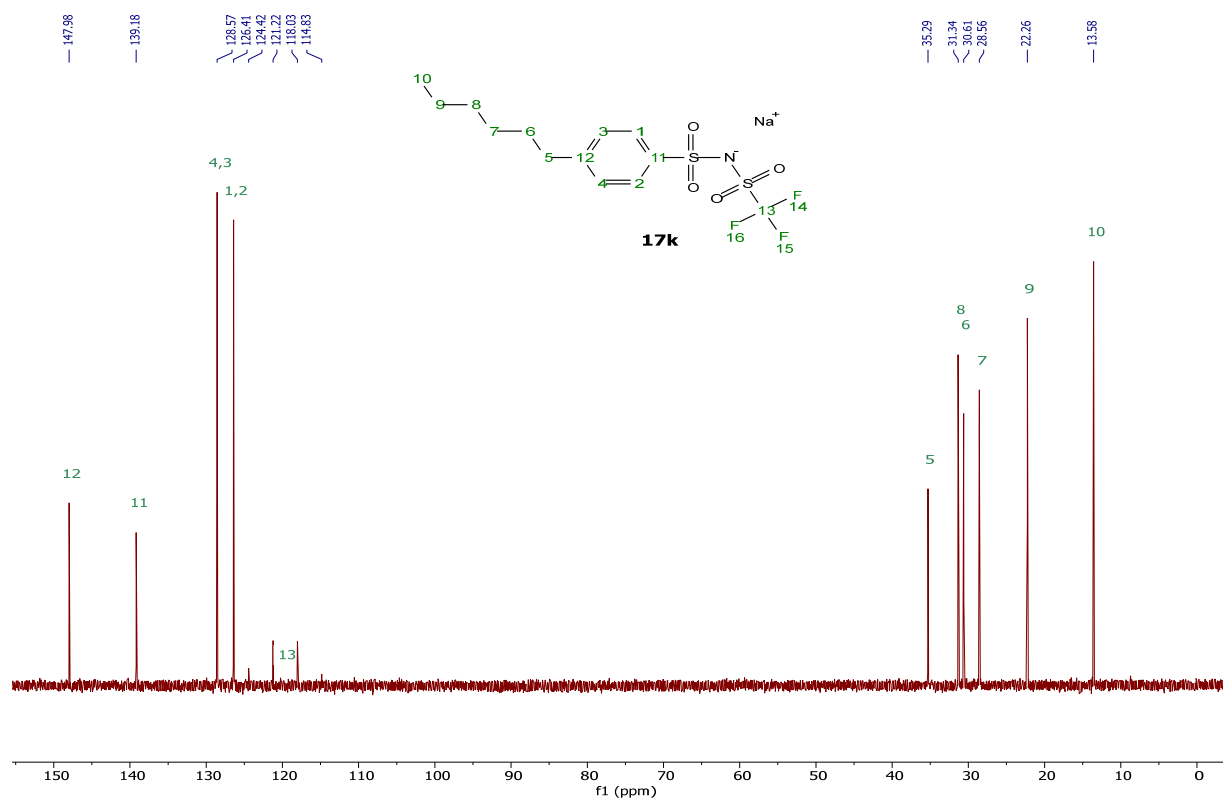


$^{19}\text{F}$  NMR (376 MHz, Deuterium Oxide)[Na][TIBSNTf], **17i** $^1\text{H}$  NMR (400 MHz, Deuterium Oxide)

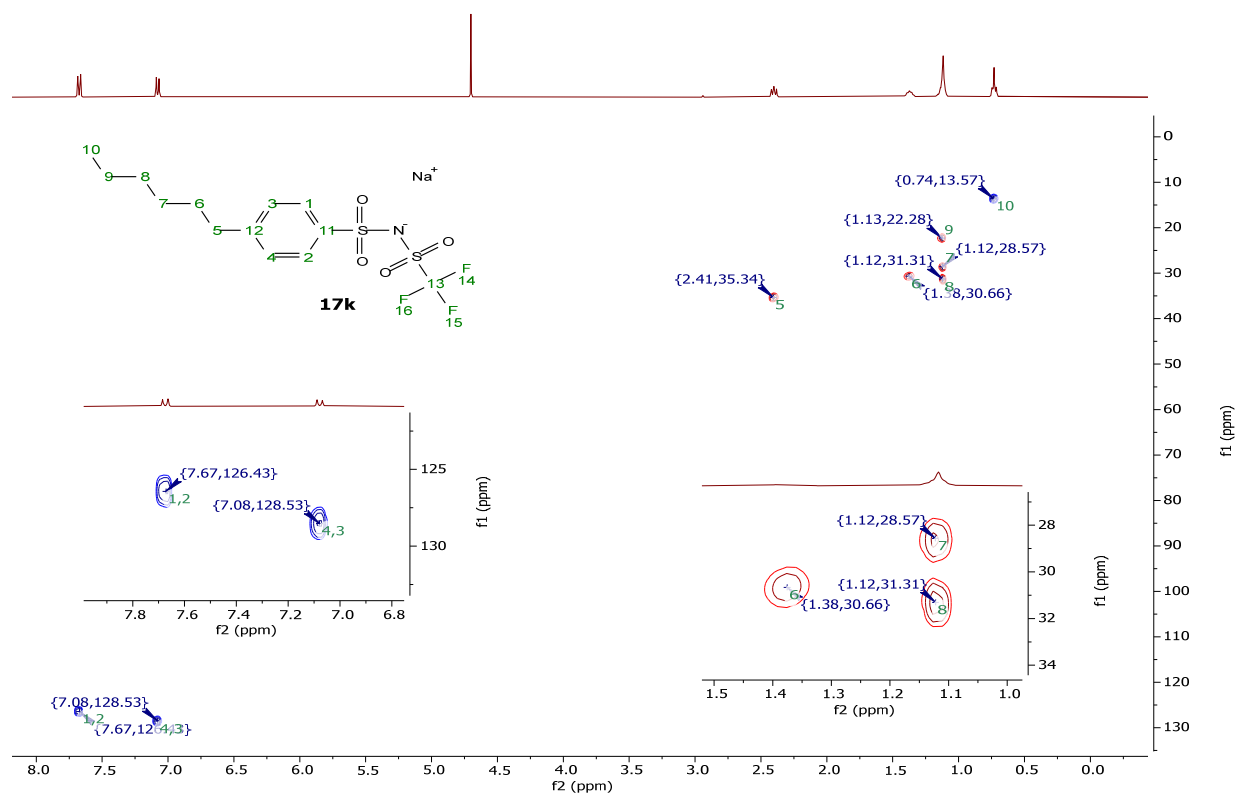
$^{13}\text{C}\{^1\text{H}\}$  NMR (101 MHz, Deuterium Oxide) $^{19}\text{F}$  NMR (376 MHz, Deuterium Oxide)

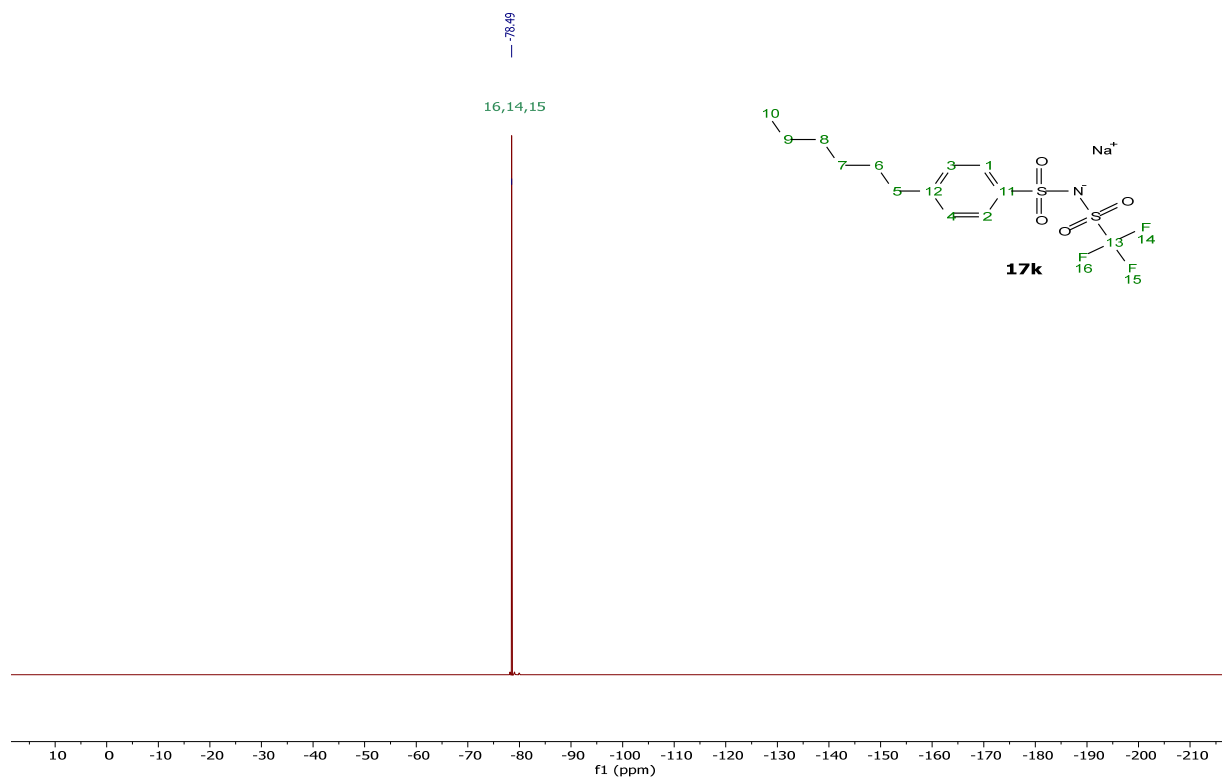
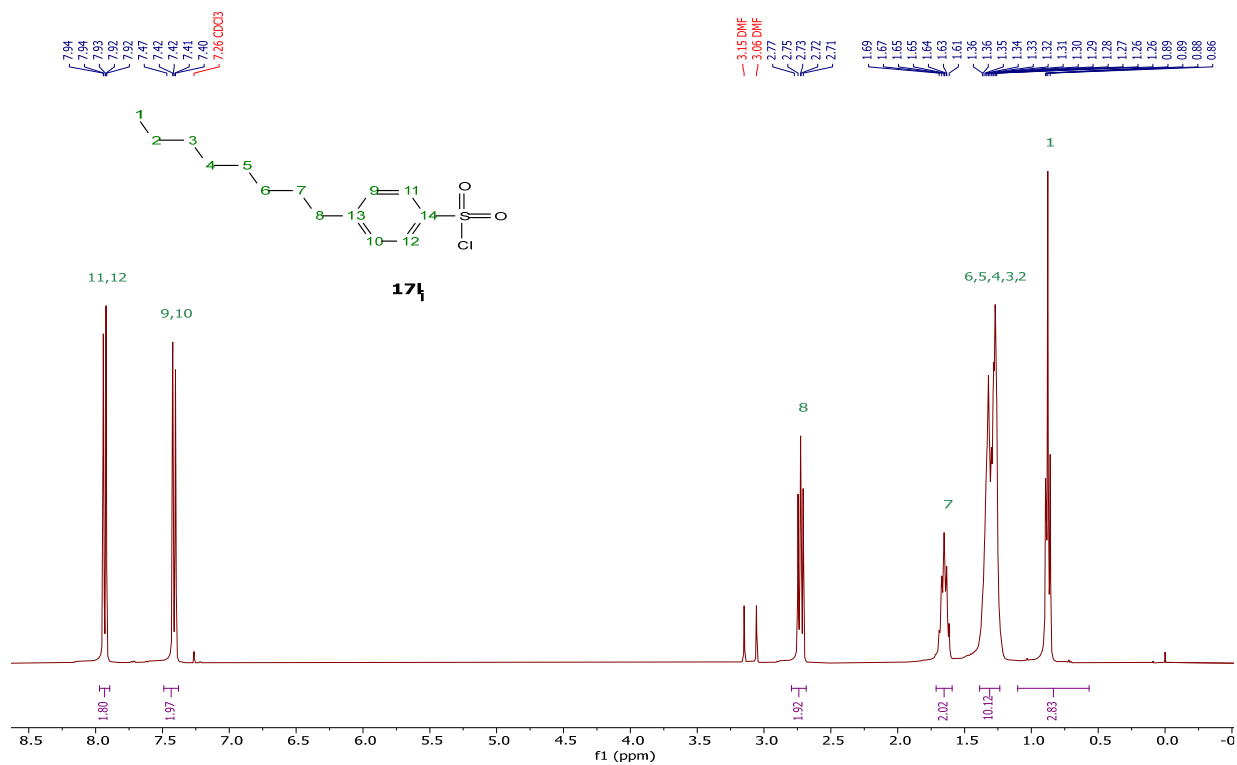
[Na][pBBSNTf], **17j** $^1\text{H}$  NMR (400 MHz, Acetone- $d_6$ ) $^{13}\text{C}\{^1\text{H}\}$  NMR (101 MHz, Acetone- $d_6$ )

$^{19}\text{F}$  NMR (376 MHz, Acetone- $d_6$ )[Na][pHBSNTf], **17k** $^1\text{H}$  NMR (400 MHz, Deuterium Oxide)

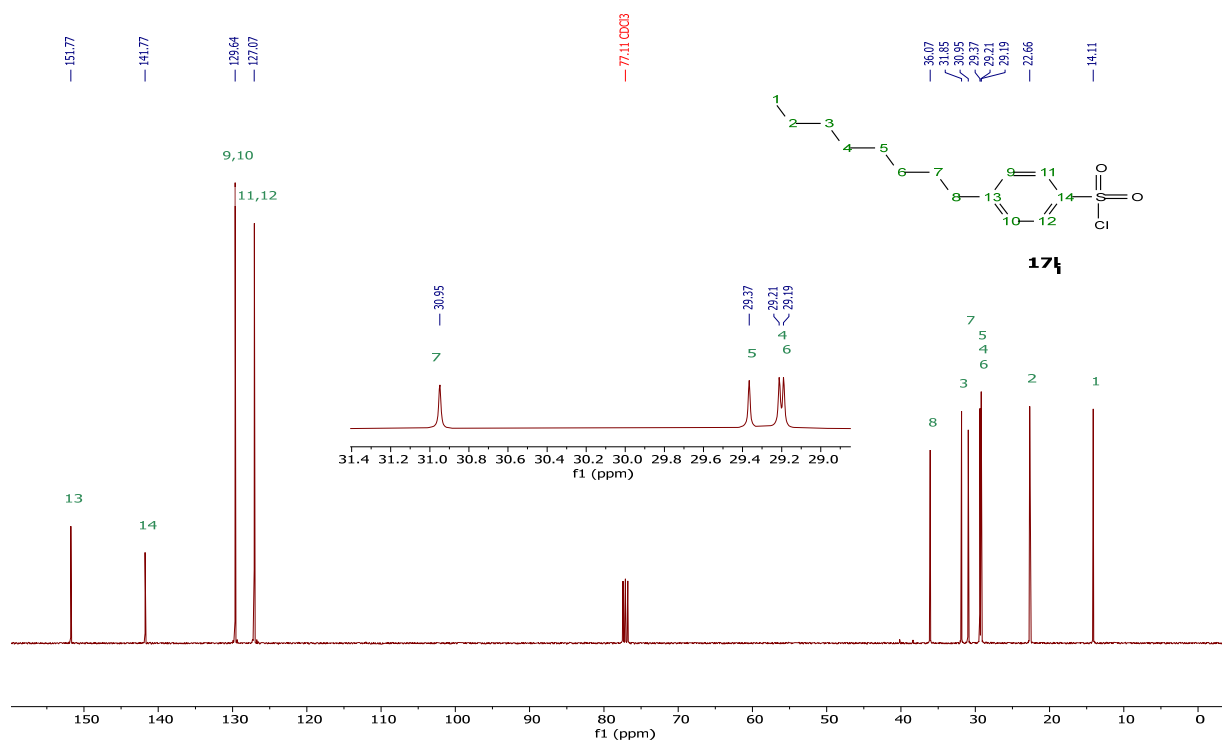
$^{13}\text{C}\{^1\text{H}\}$  NMR (101 MHz, Deuterium Oxide)

## HSQC (Deuterium Oxide)



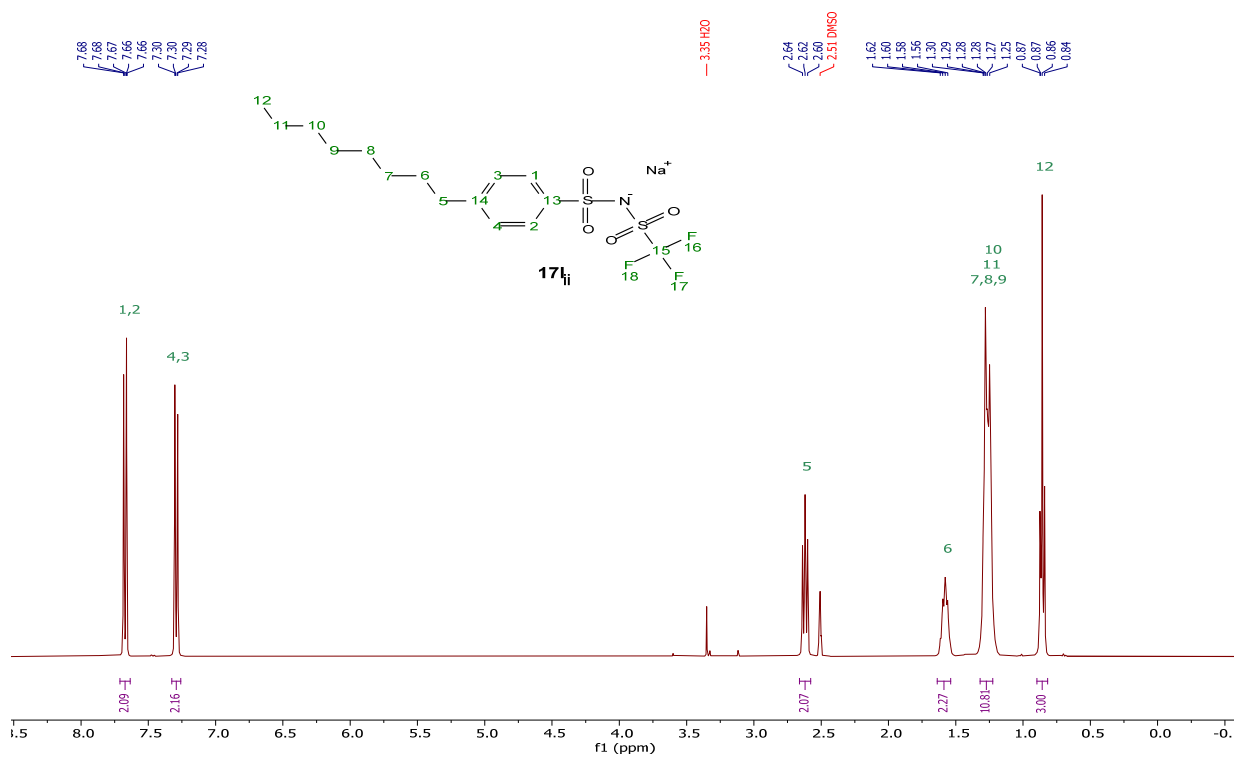
$^{19}\text{F}$  NMR (376 MHz, Deuterium Oxide)**17i** $^1\text{H}$  NMR (400 MHz, Chloroform-d)

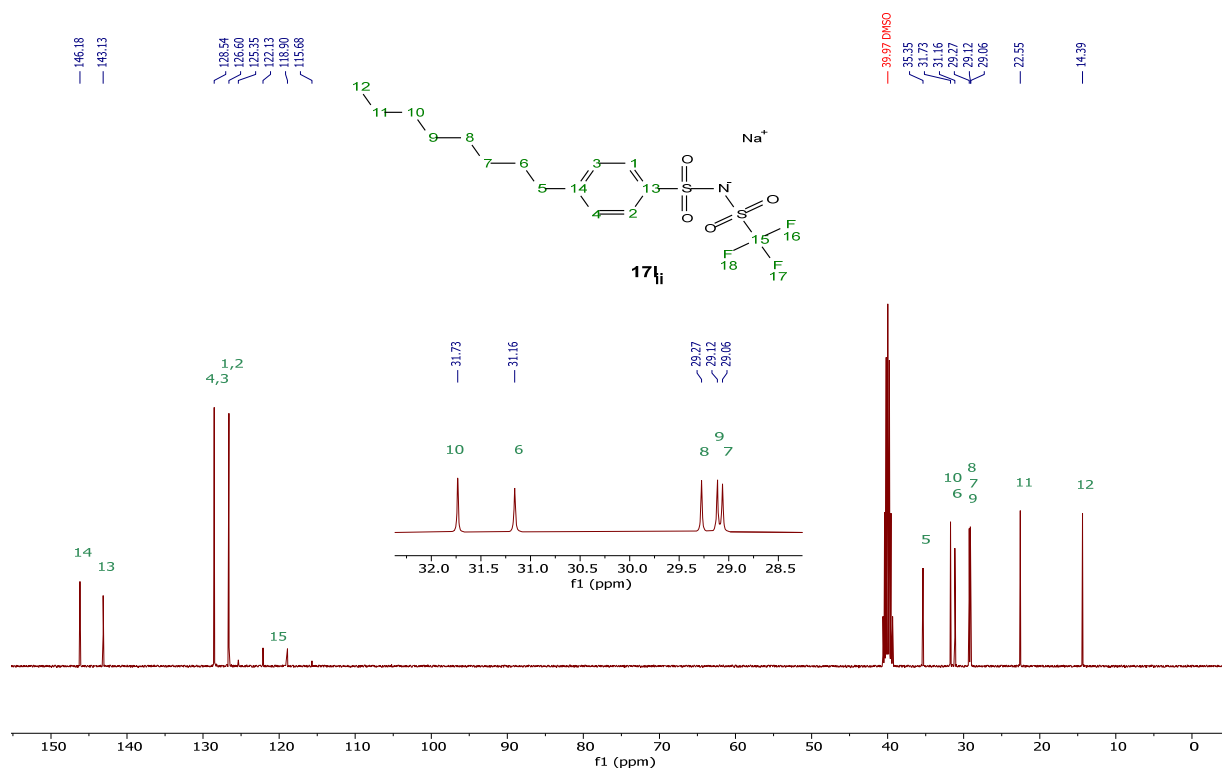
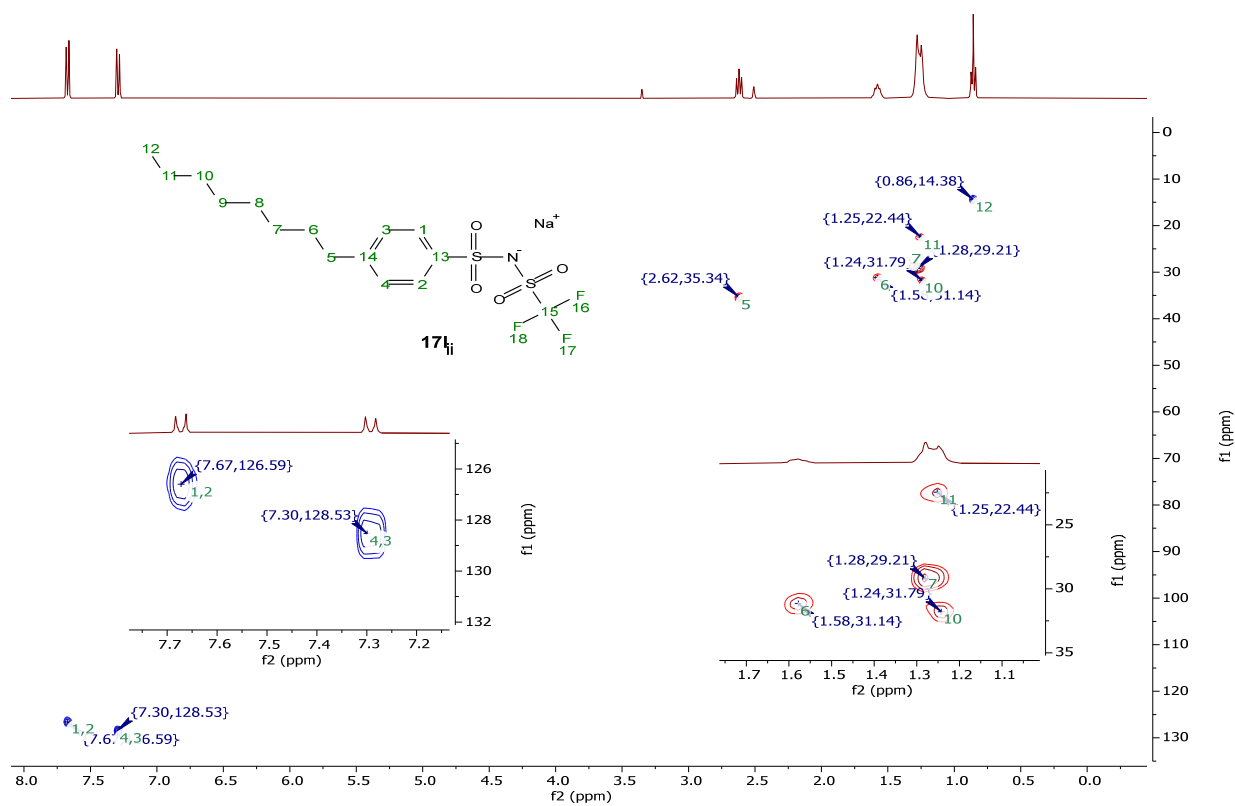
$^{13}\text{C}\{^1\text{H}\}$  NMR (101 MHz, Chloroform-d)

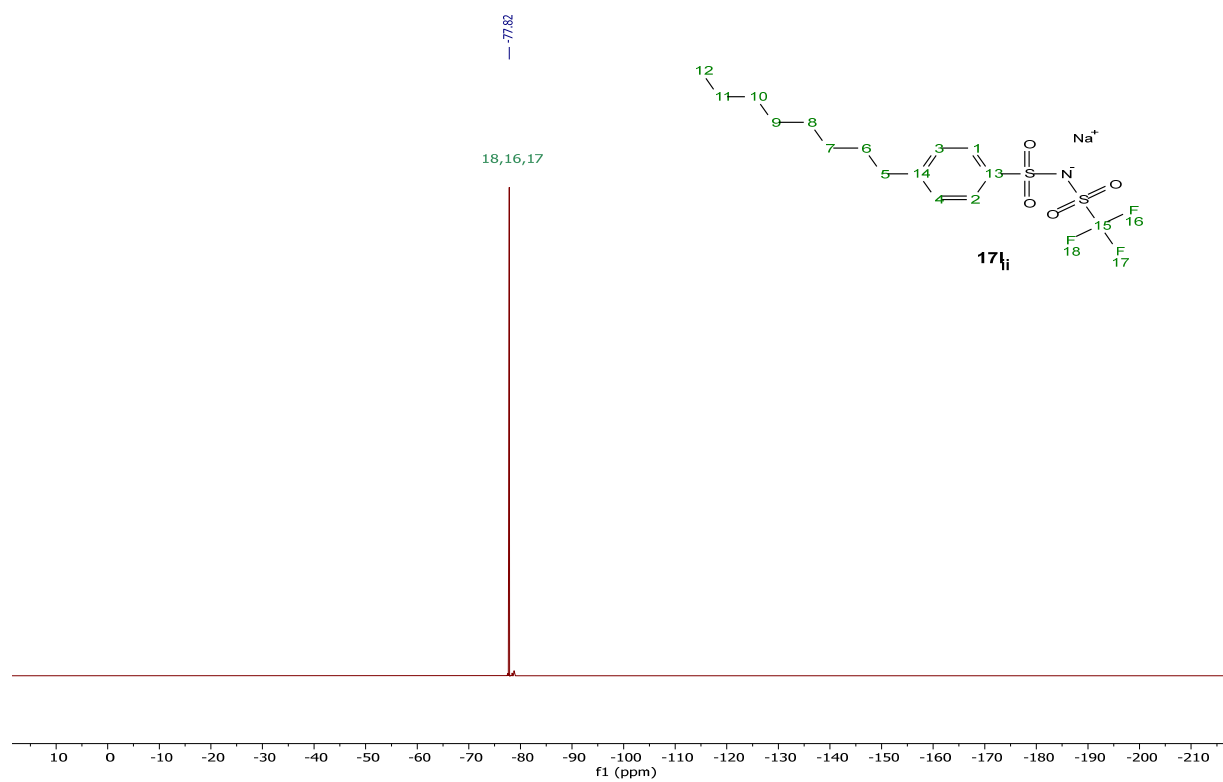
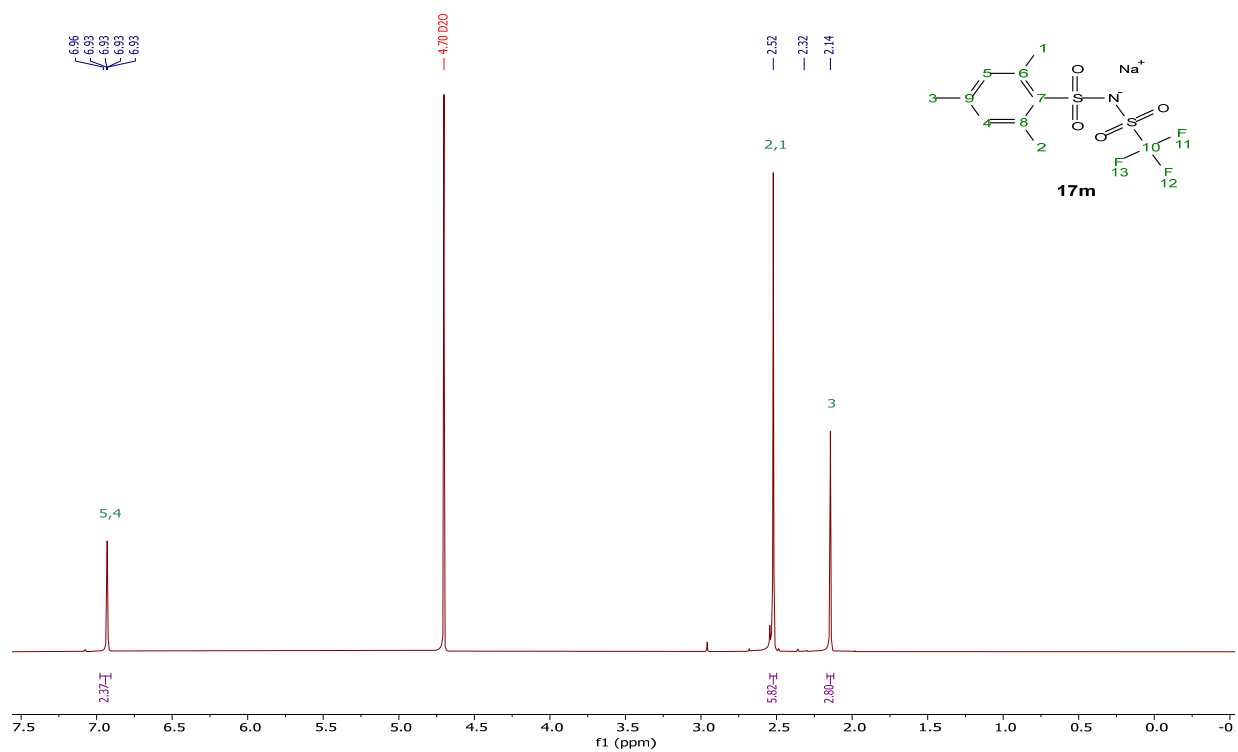


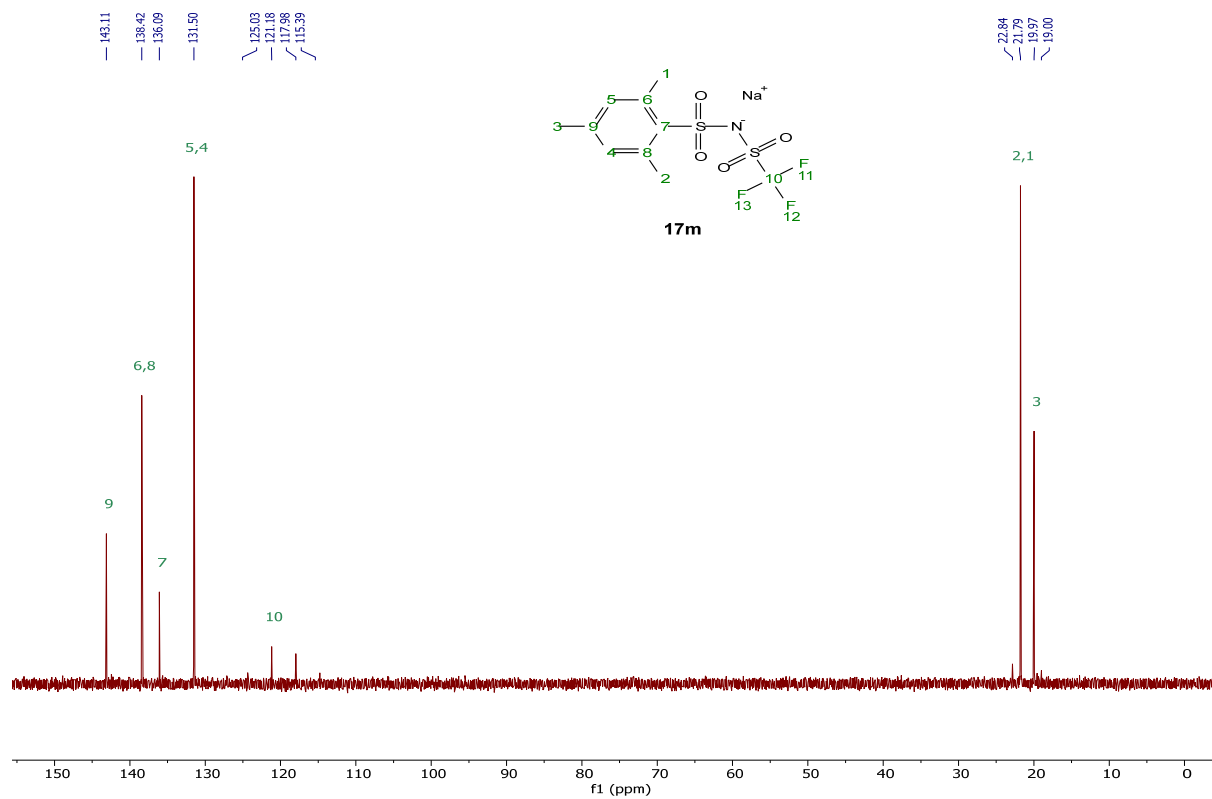
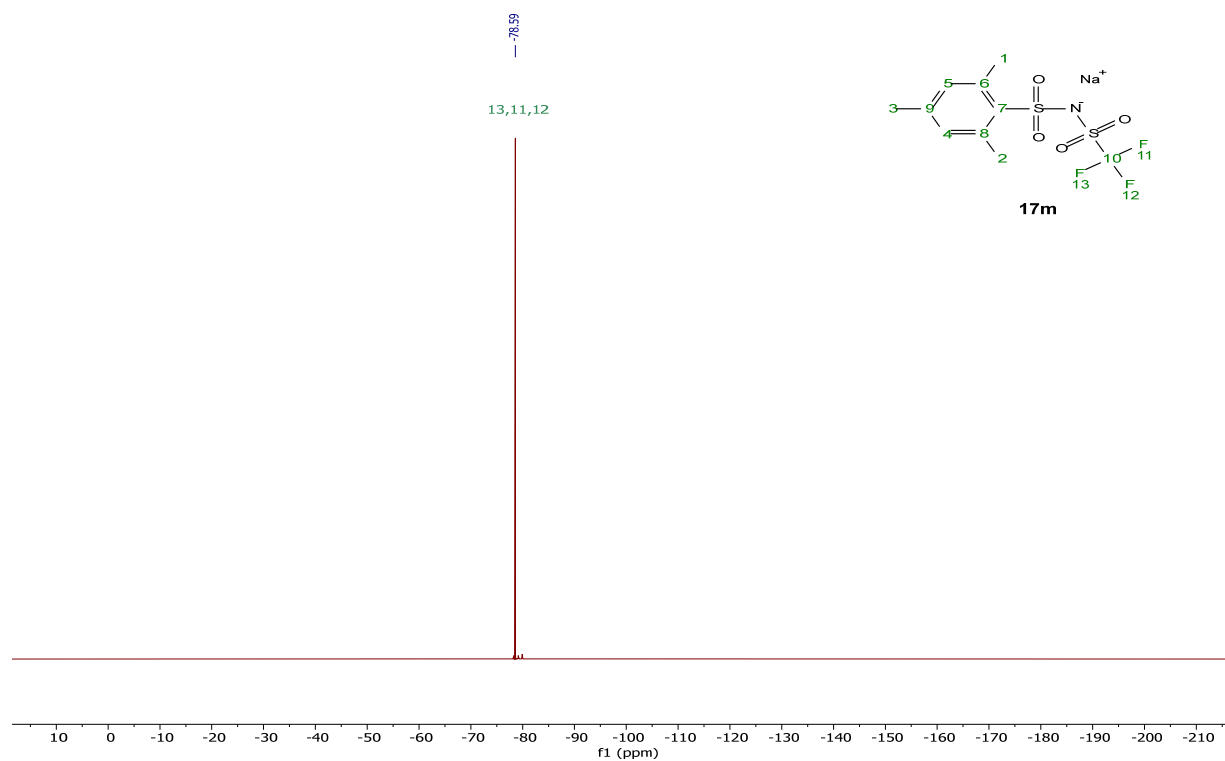
[Na][pOBSNTf], **17ii**

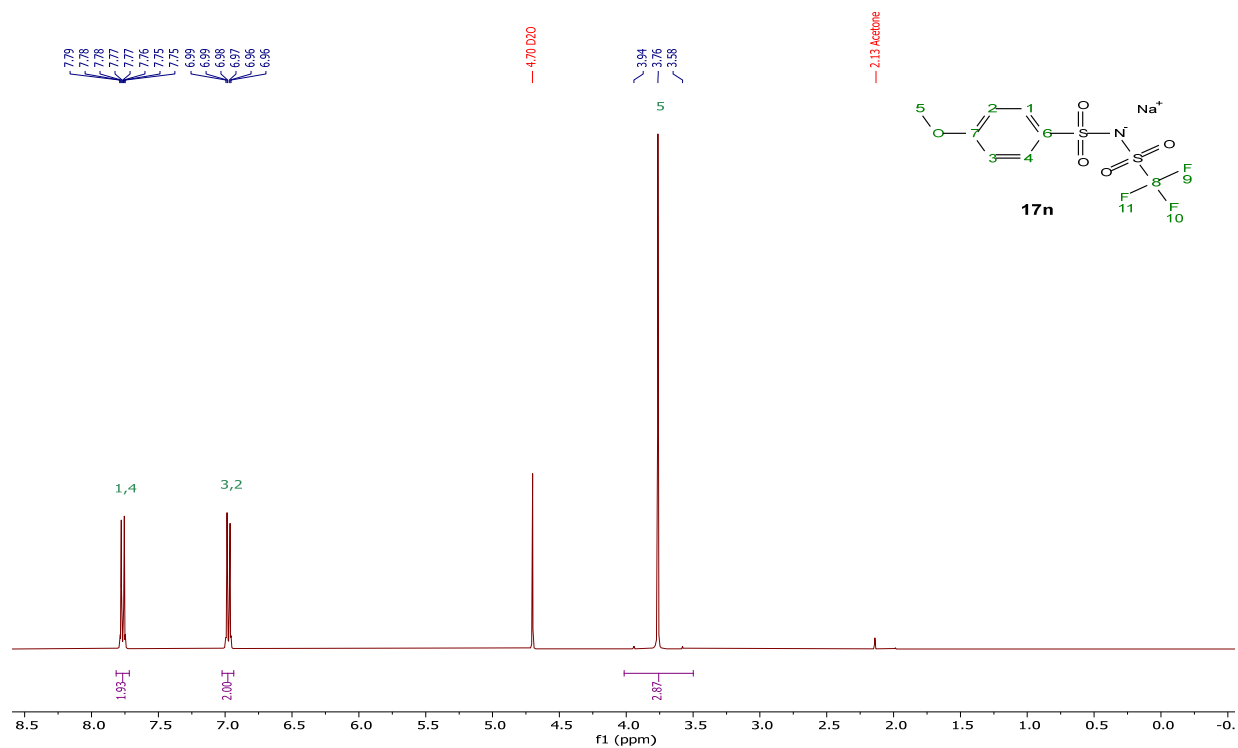
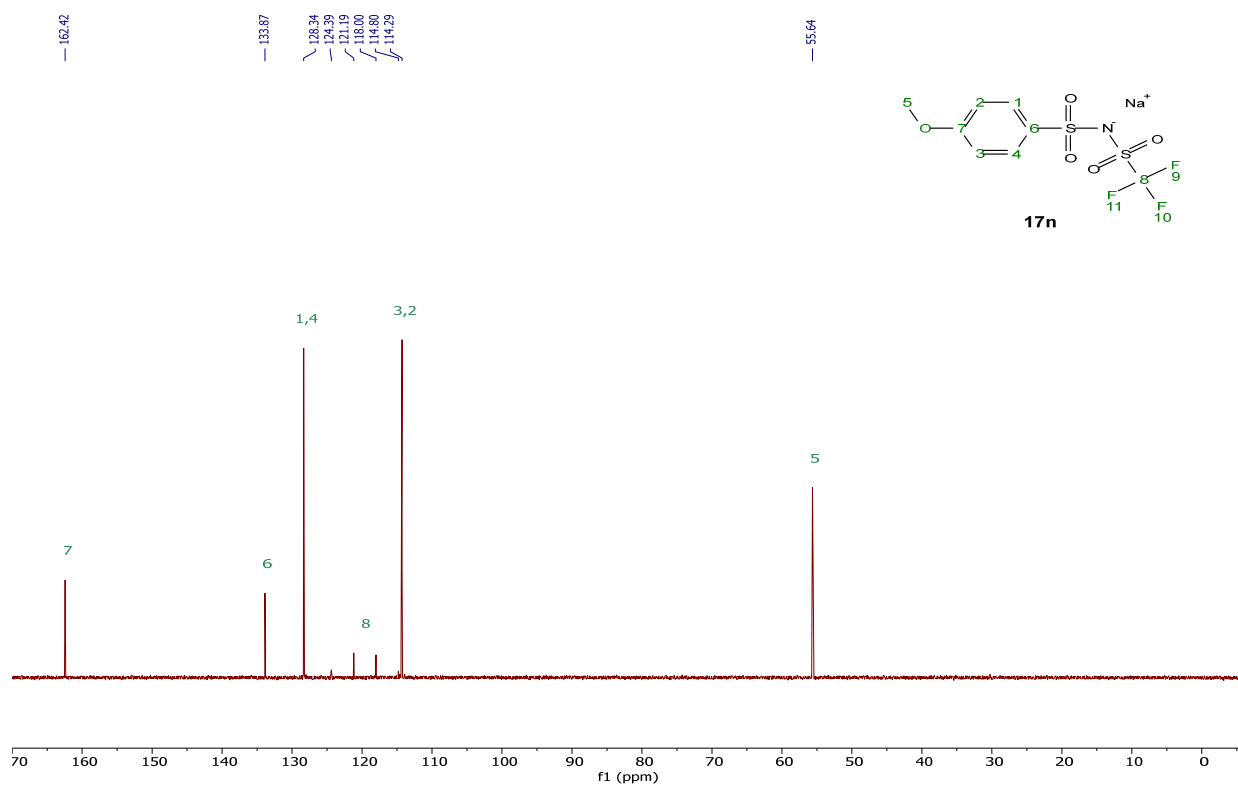
$^1\text{H}$  NMR (400 MHz, DMSO-d<sub>6</sub>)

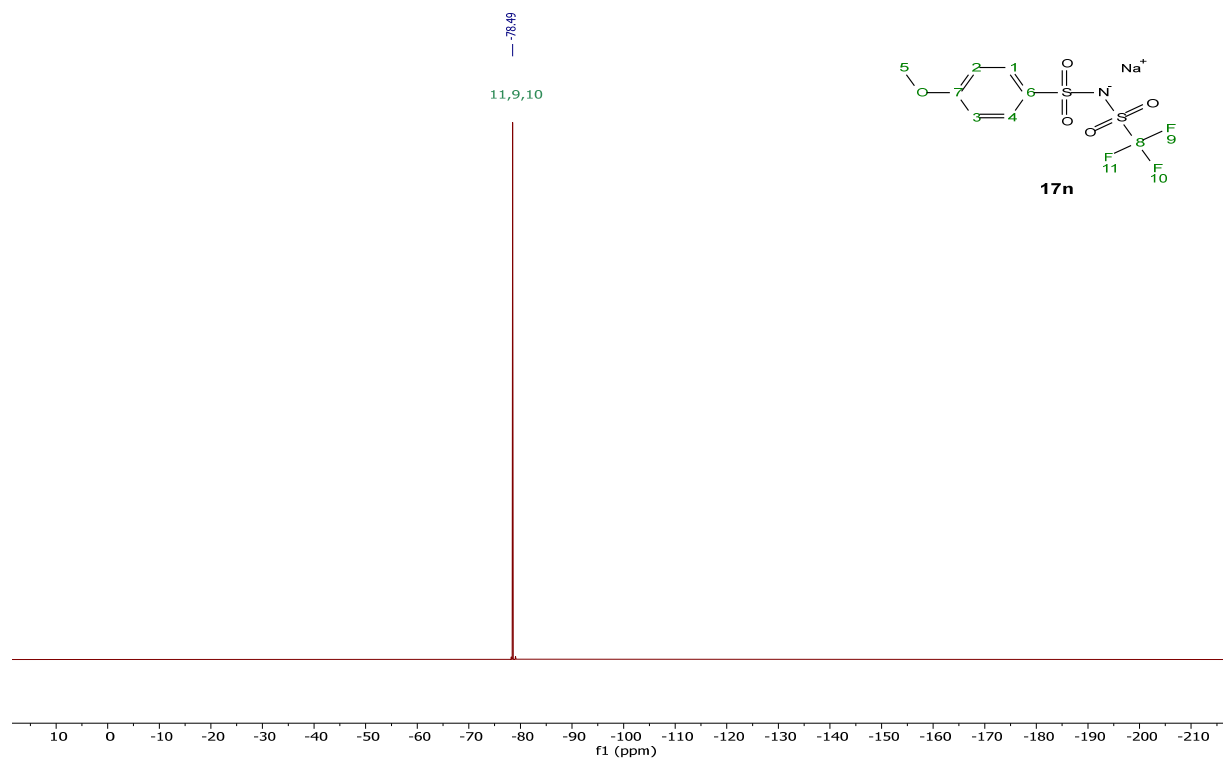
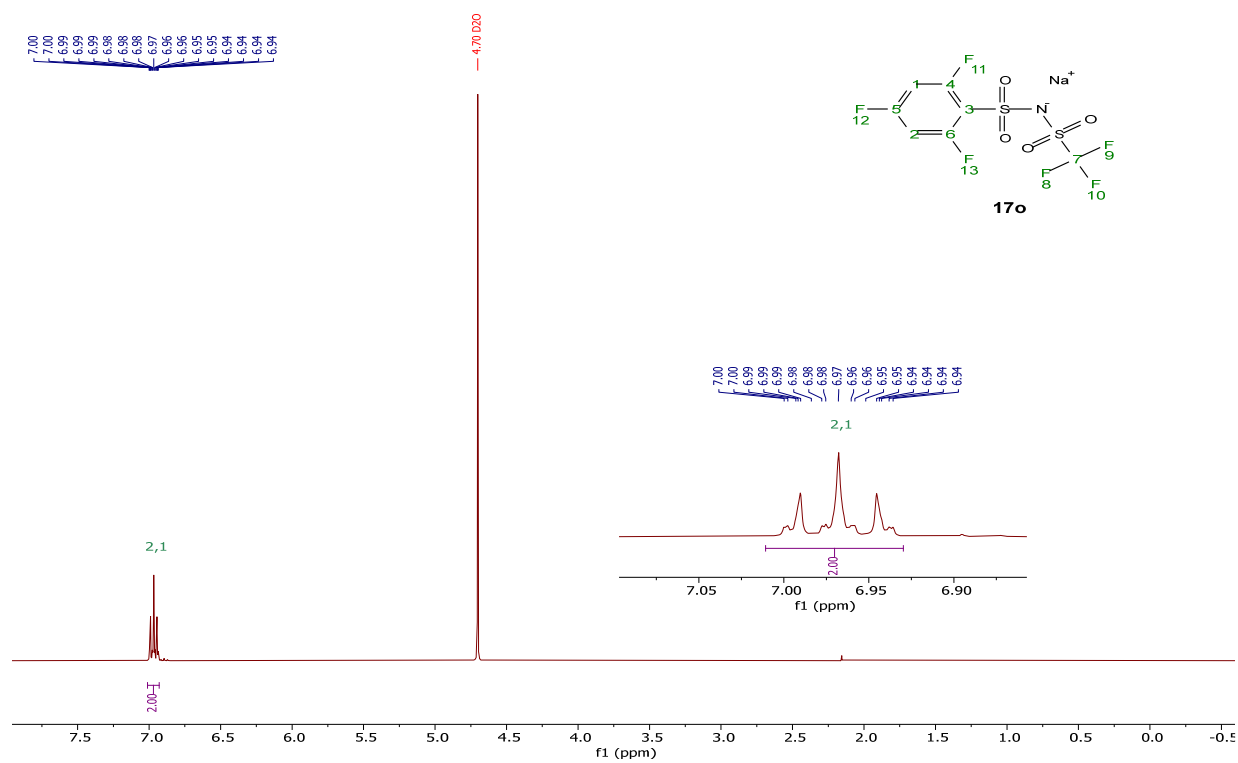


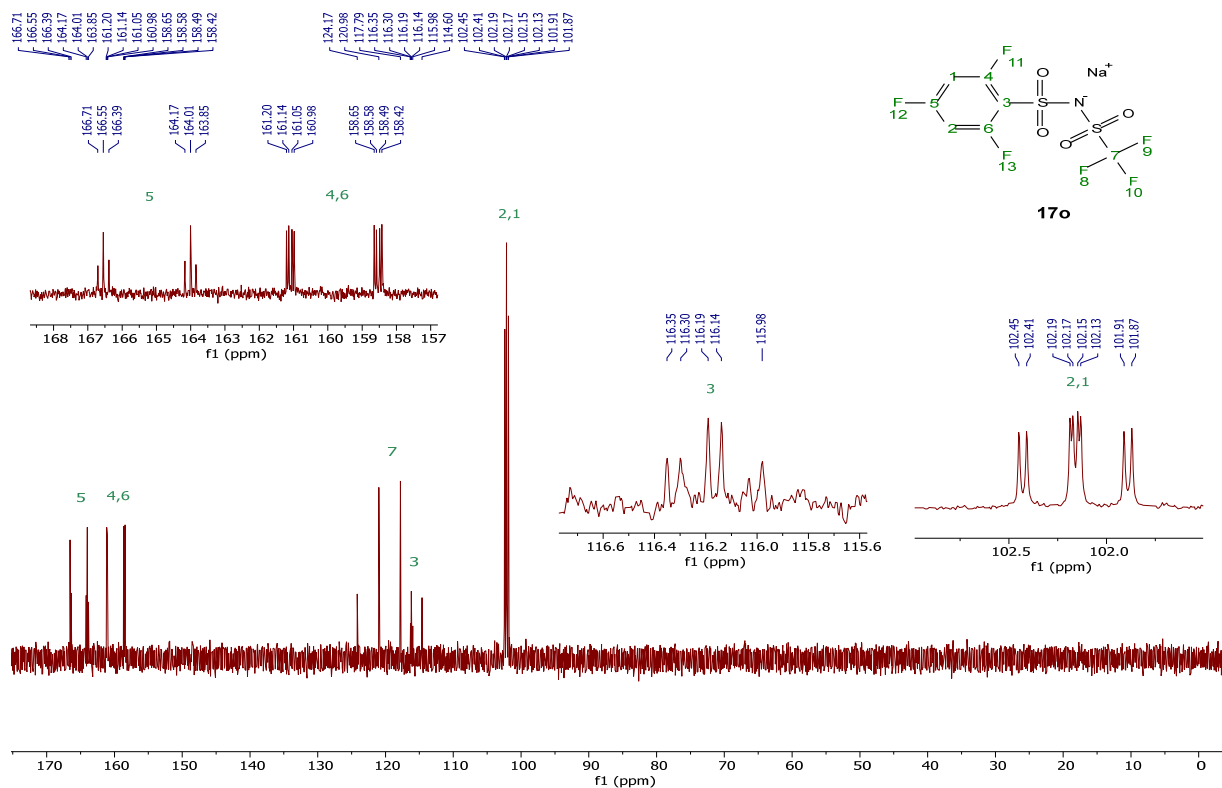
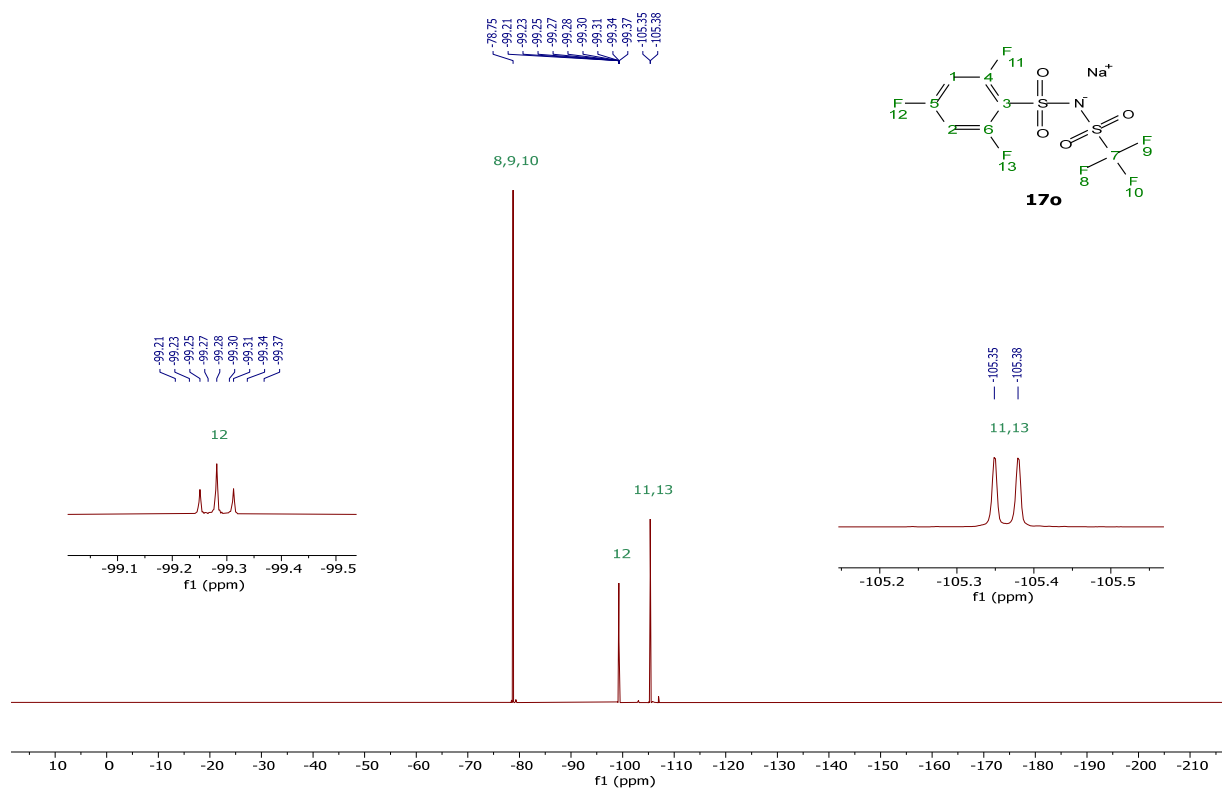
$^{13}\text{C}\{^1\text{H}\}$  NMR (101 MHz, DMSO-d<sub>6</sub>)HSQC (DMSO-d<sub>6</sub>)

$^{19}\text{F}$  NMR (376 MHz, DMSO- $d_6$ )[Na][MesSNTf], **17m** $^1\text{H}$  NMR (400 MHz, Deuterium Oxide)

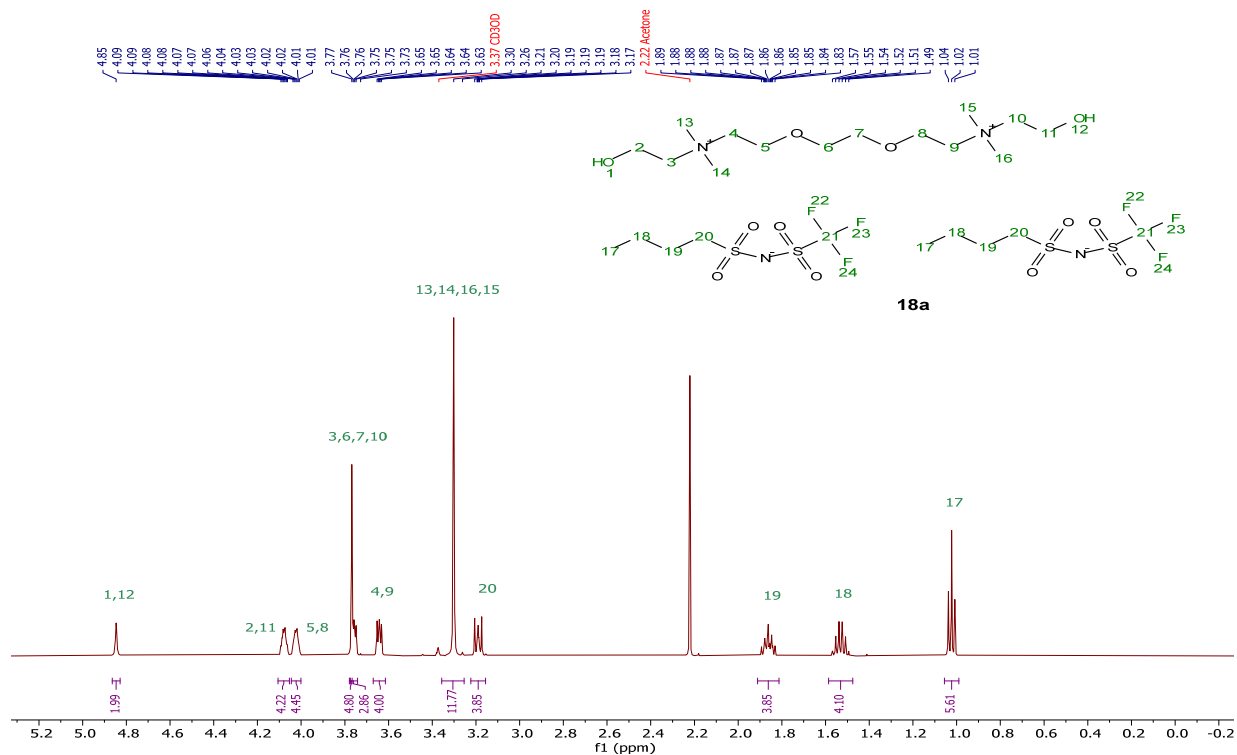
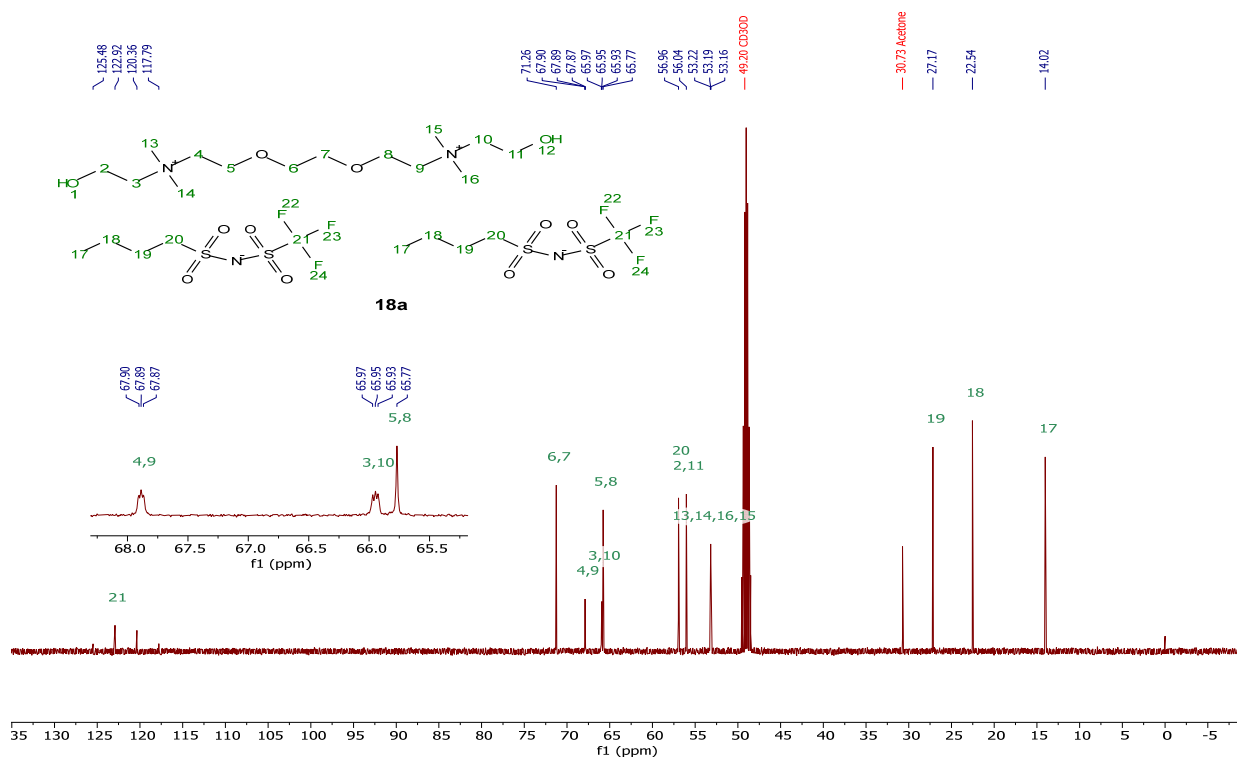
$^{13}\text{C}\{^1\text{H}\}$  NMR (101 MHz, Deuterium Oxide) $^{19}\text{F}$  NMR (376 MHz, Deuterium Oxide)

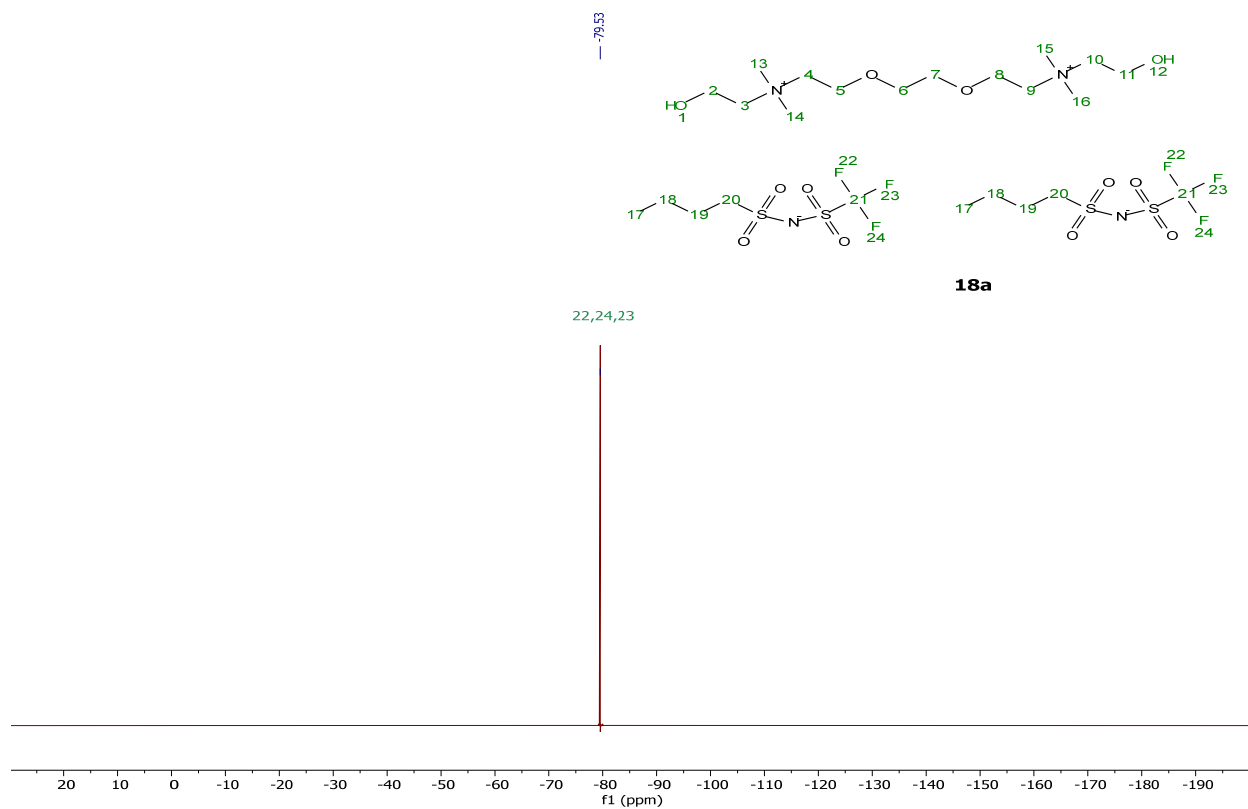
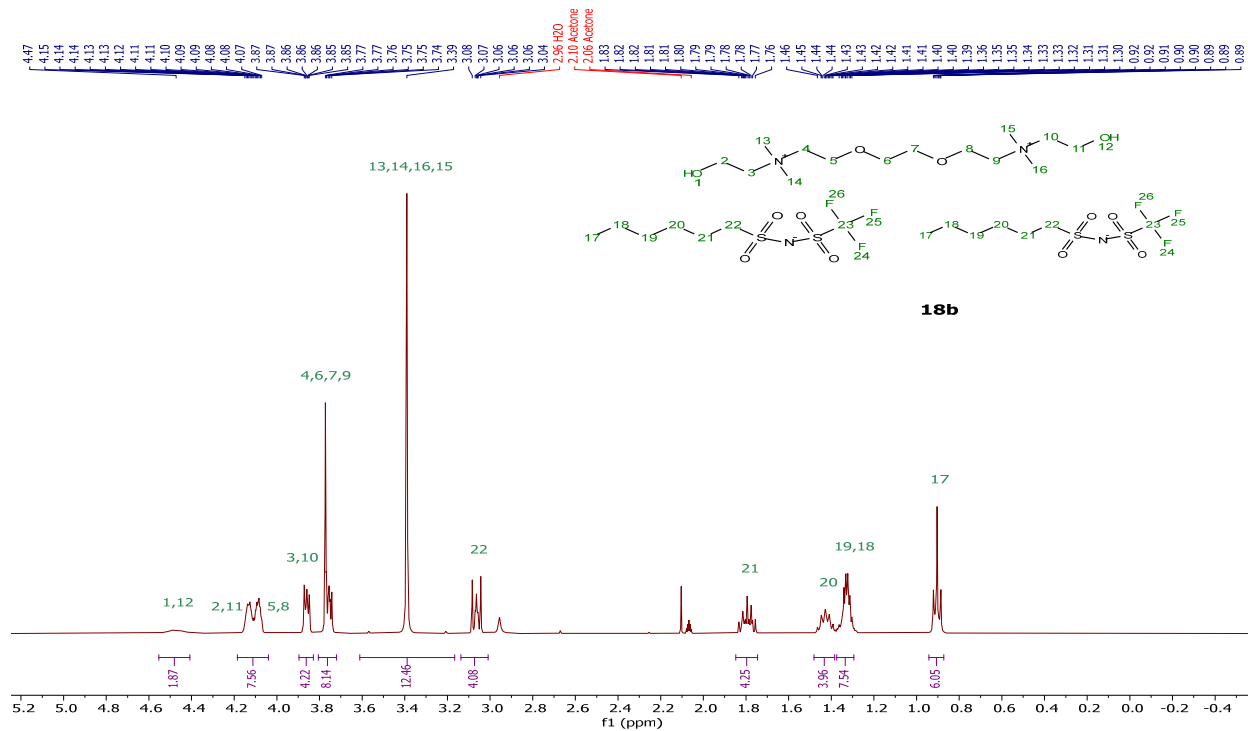
[Na][pMBSNTf], **17n** $^1\text{H}$  NMR (400 MHz, Deuterium Oxide) $^{13}\text{C}\{^1\text{H}\}$  NMR (101 MHz, Deuterium Oxide)

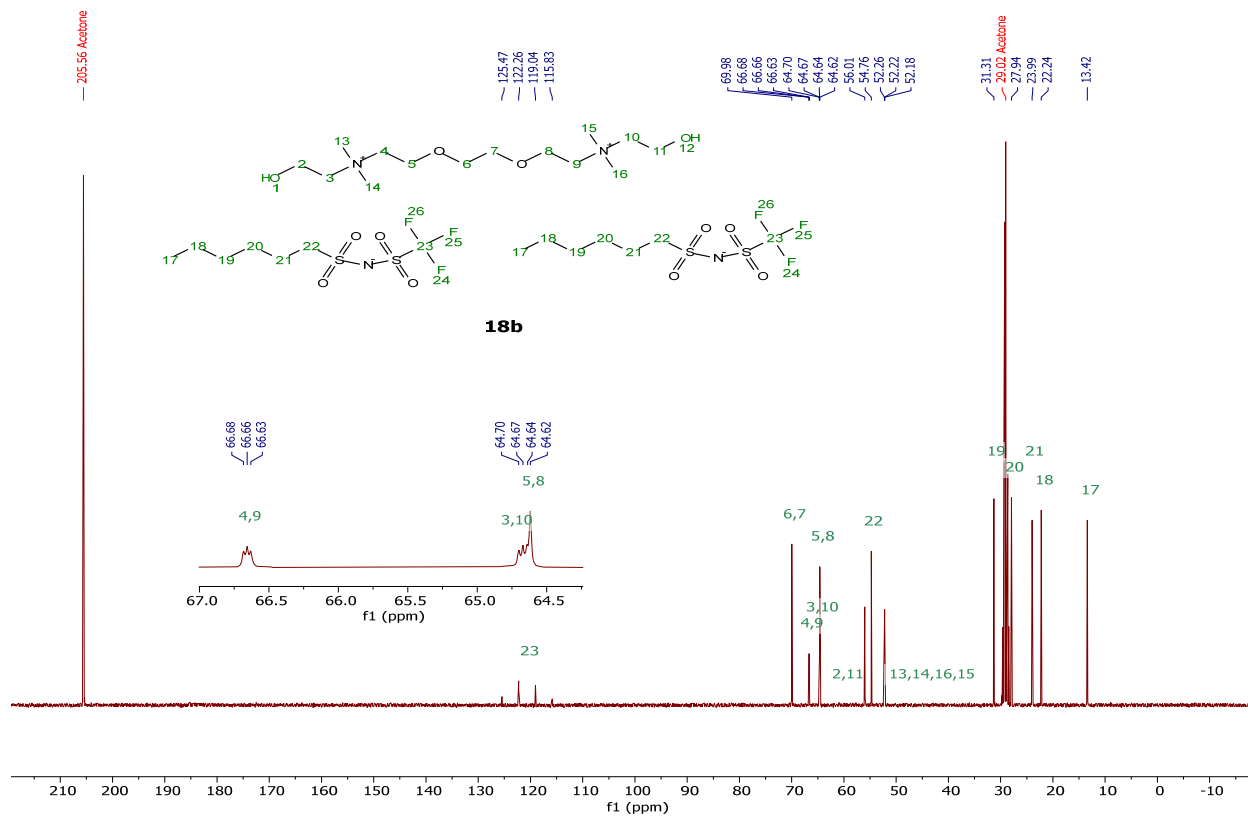
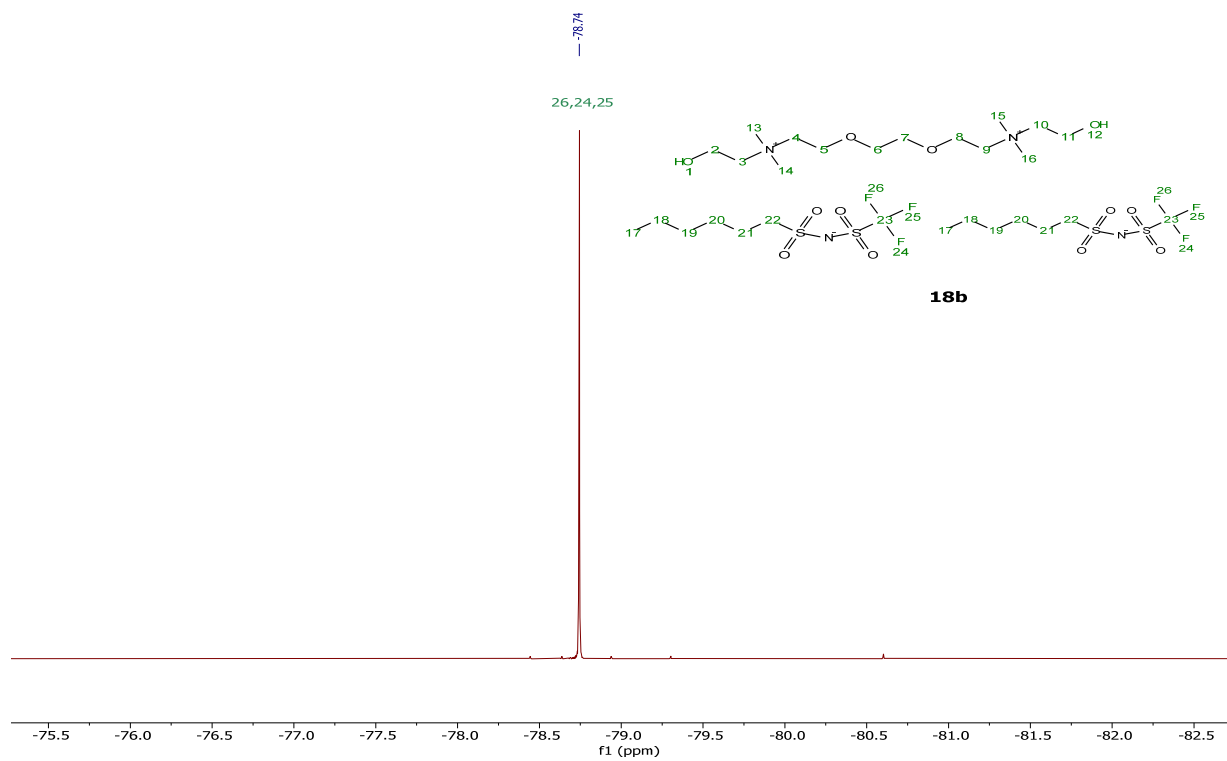
$^{19}\text{F}$  NMR (376 MHz, Deuterium Oxide)[Na][TFBSNTf], **17o** $^1\text{H}$  NMR (400 MHz, Deuterium Oxide)

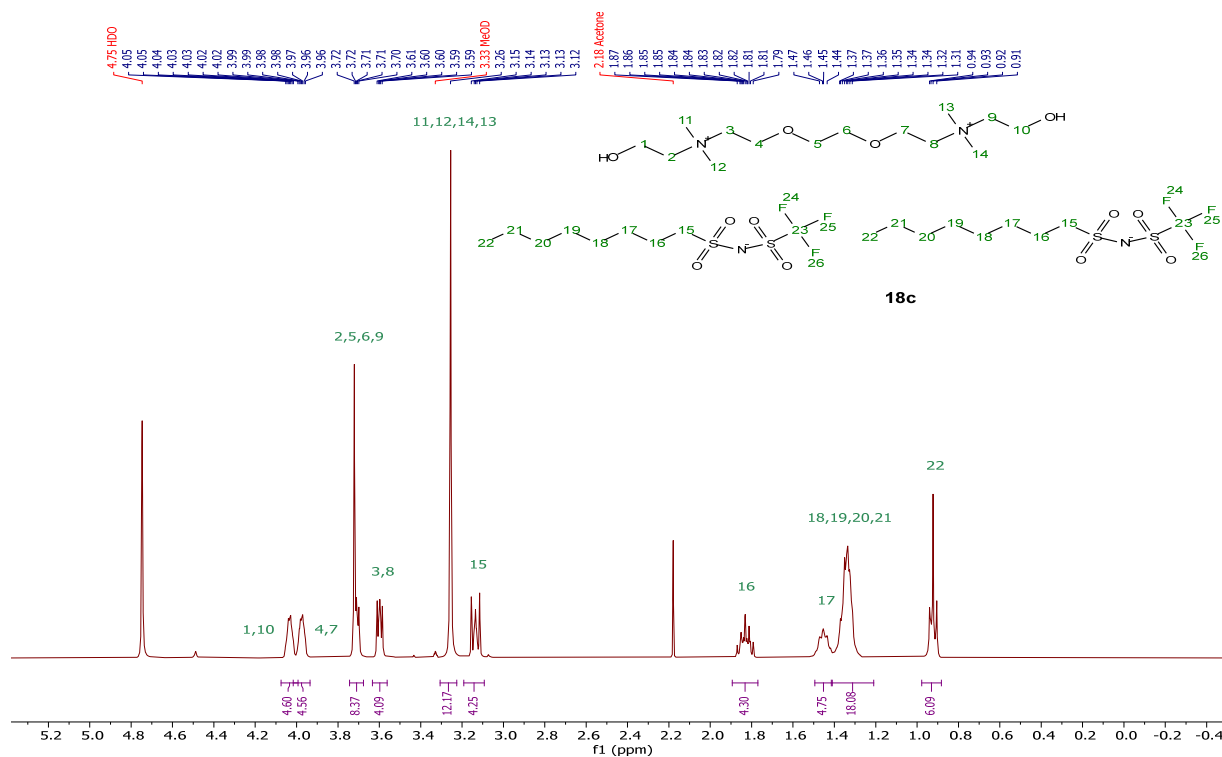
$^{13}\text{C}\{^1\text{H}\}$  NMR (101 MHz, Deuterium Oxide) $^{19}\text{F}$  NMR (376 MHz, Deuterium Oxide)

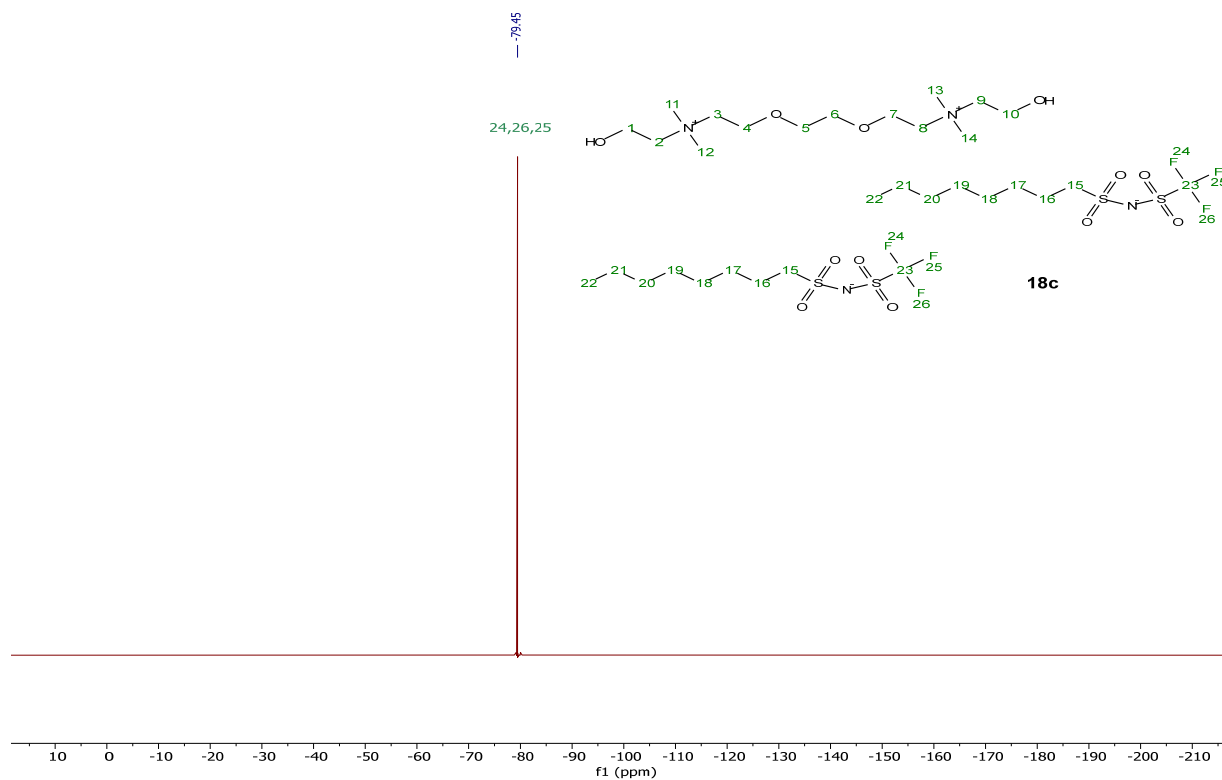
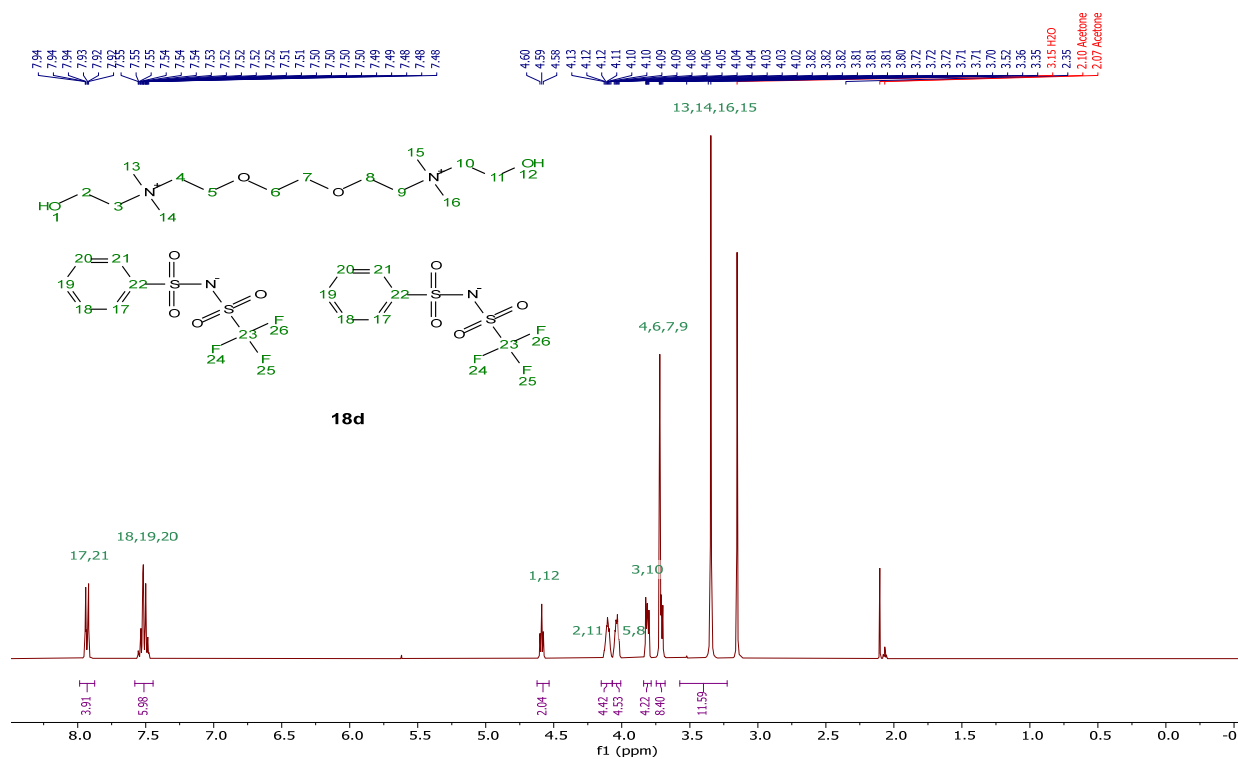


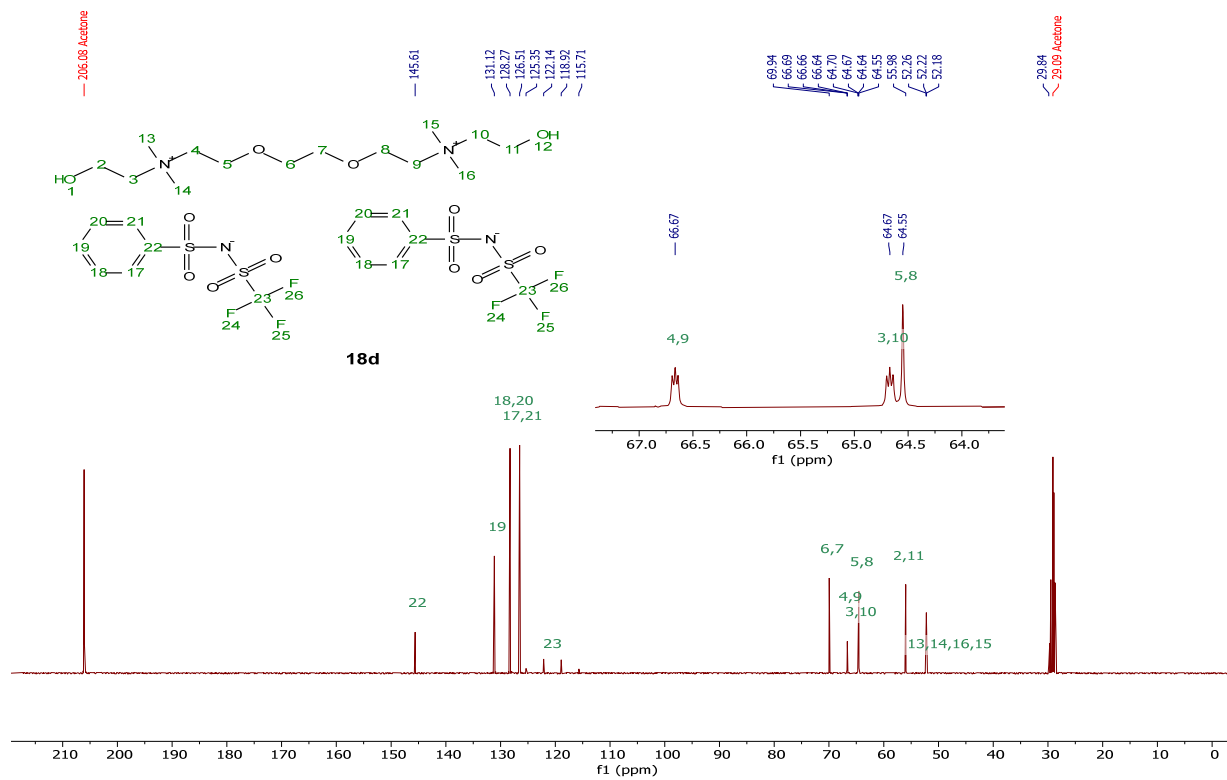
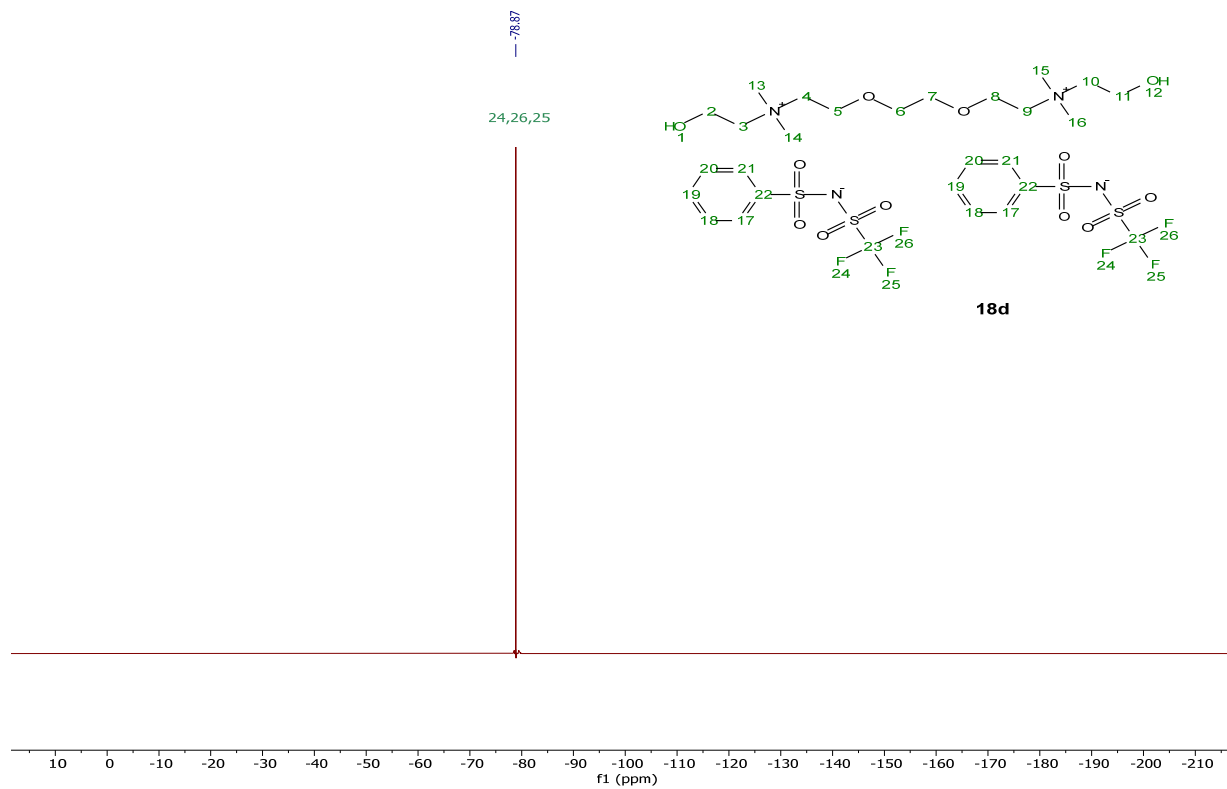
[DC-ether][2BSNTf], **18a** $^1\text{H}$  NMR (500 MHz, Acetone- $d_6$ ) $^{13}\text{C}\{^1\text{H}\}$  NMR (126 MHz, Acetone- $d_6$ )

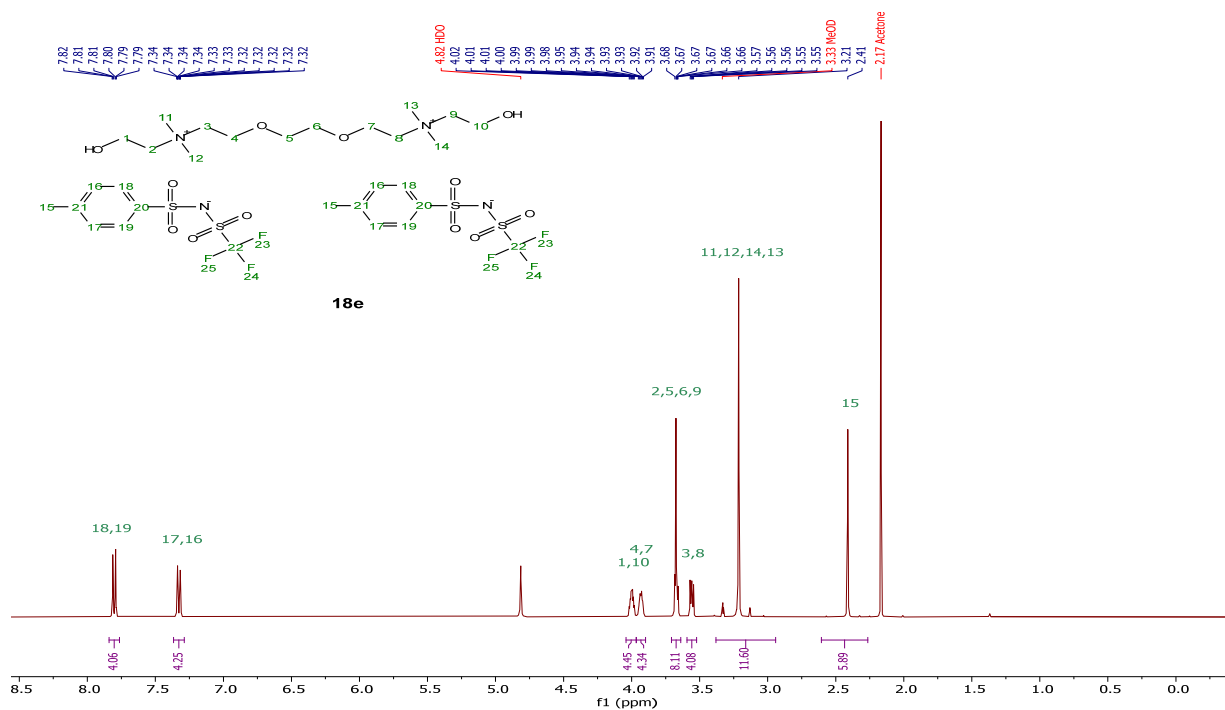
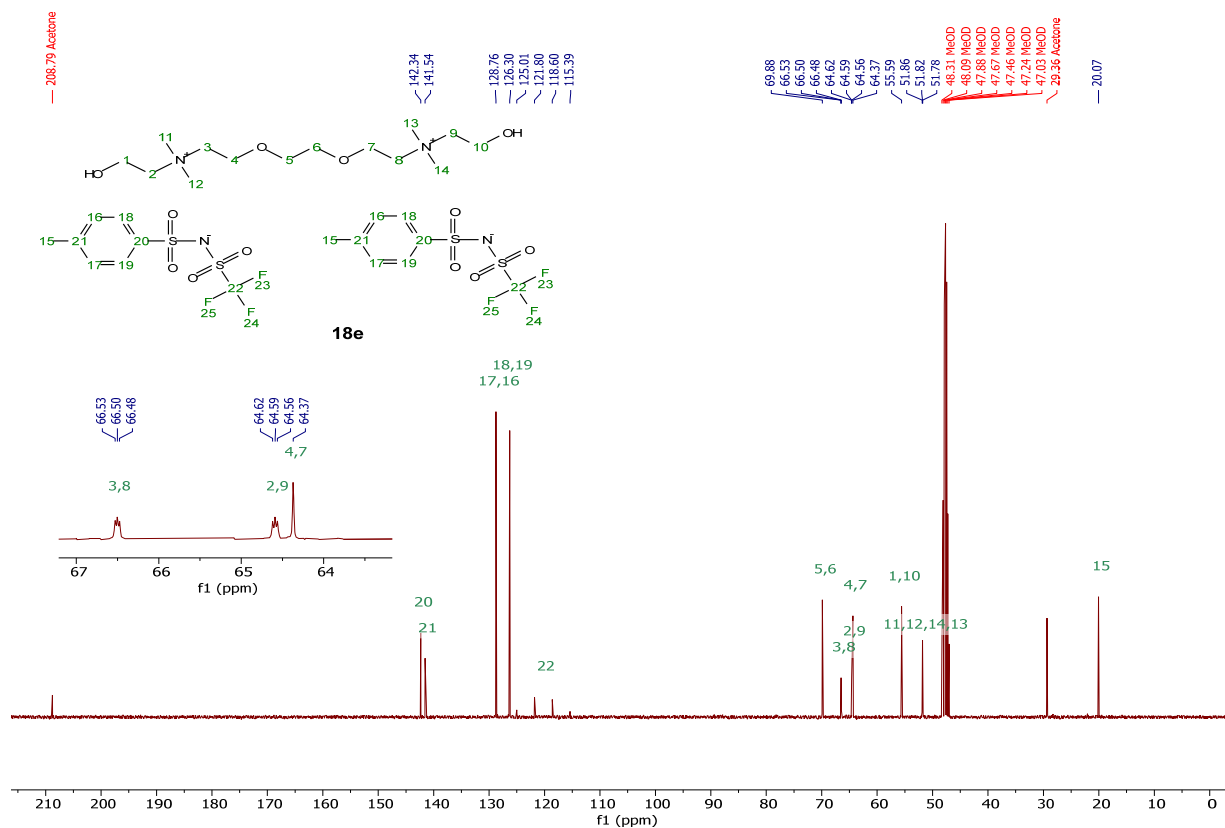
$^{19}\text{F}$  NMR (470 MHz, Acetone- $d_6$ )[DC-ether][2HSNTf], **18b** $^1\text{H}$  NMR (400 MHz, Acetone- $d_6$ )

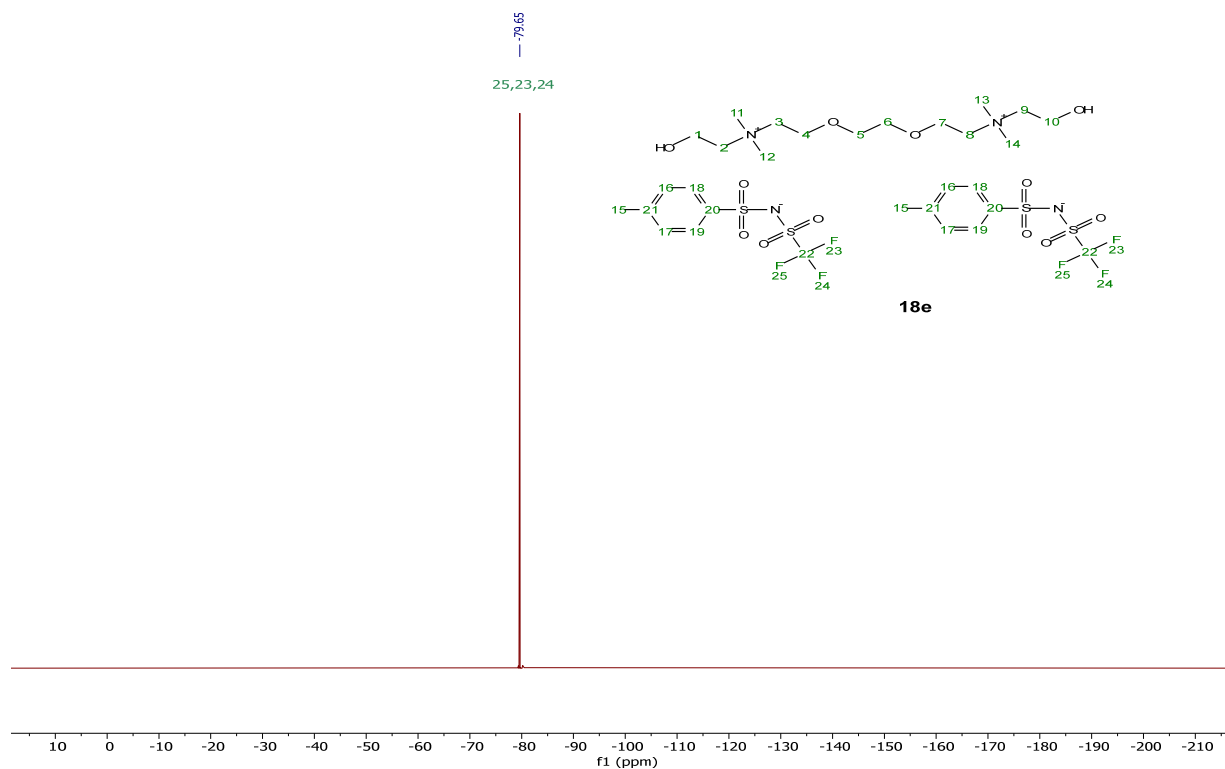
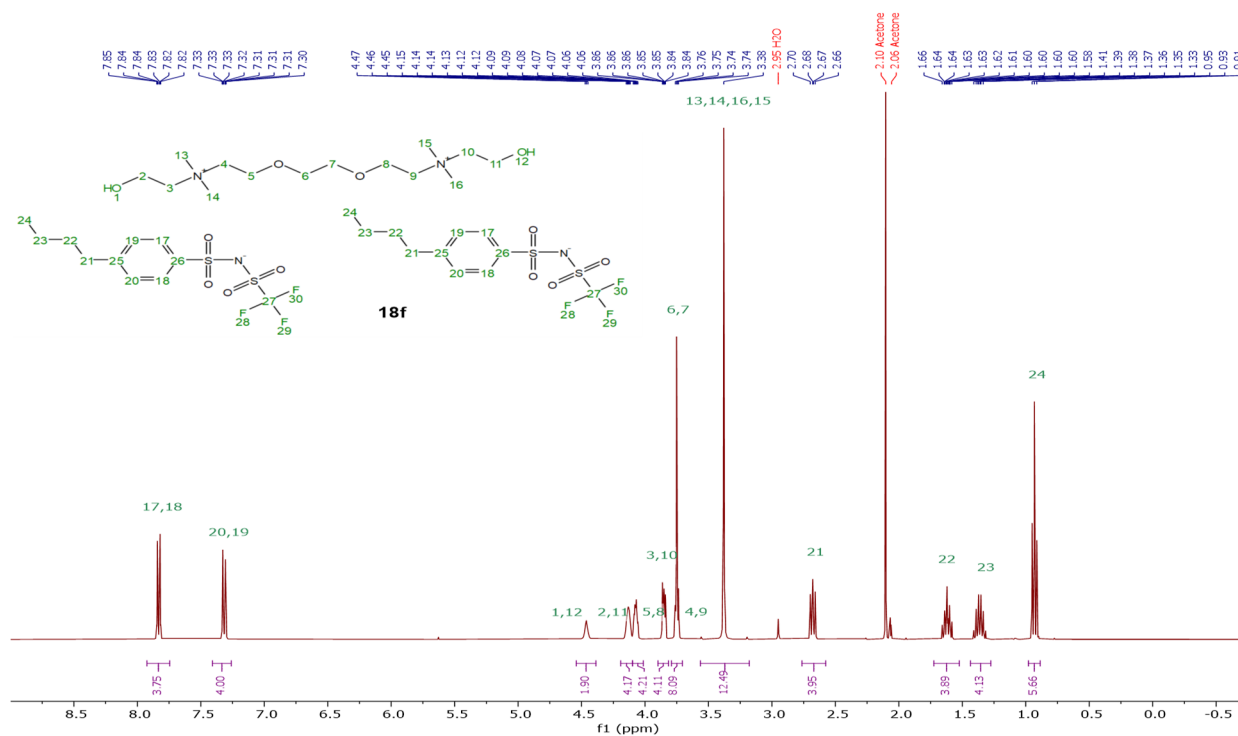
$^{13}\text{C}\{^1\text{H}\}$  NMR (101 MHz, Acetone- $d_6$ ) $^{19}\text{F}$  NMR (376 MHz, Acetone- $d_6$ )

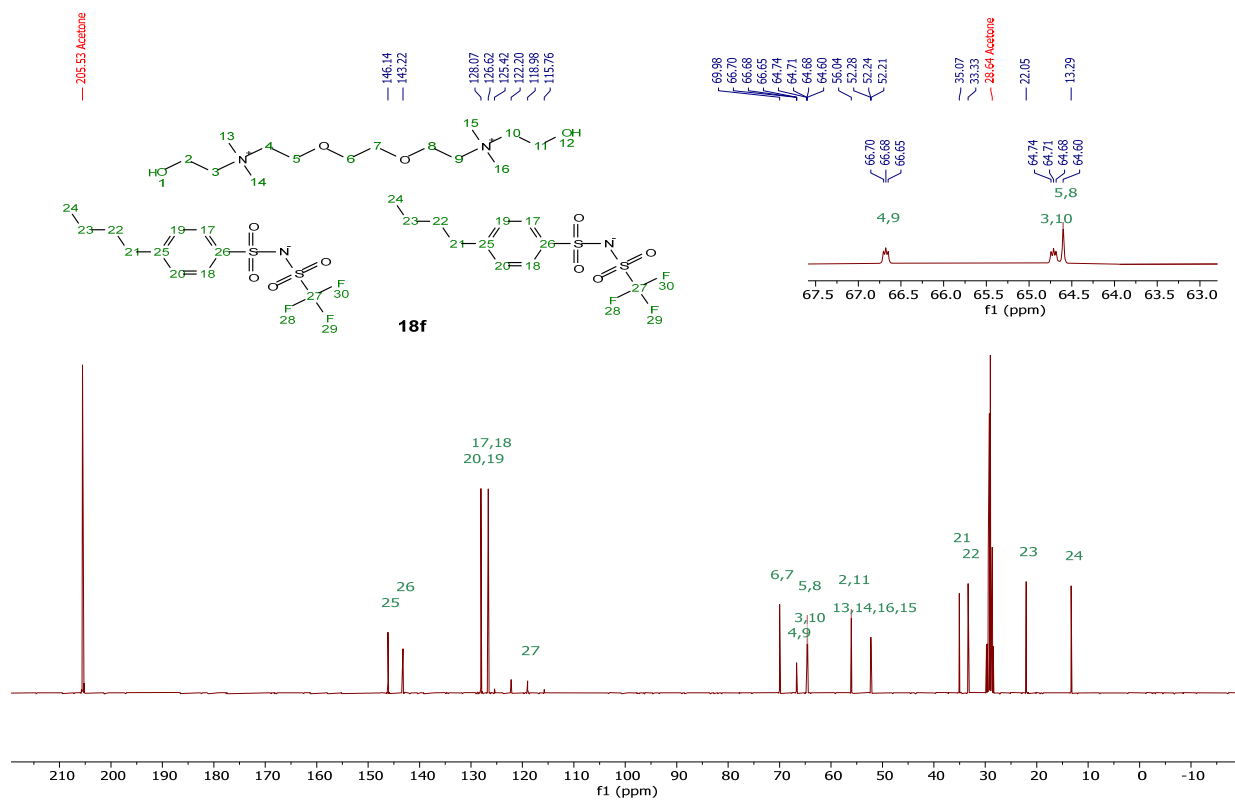
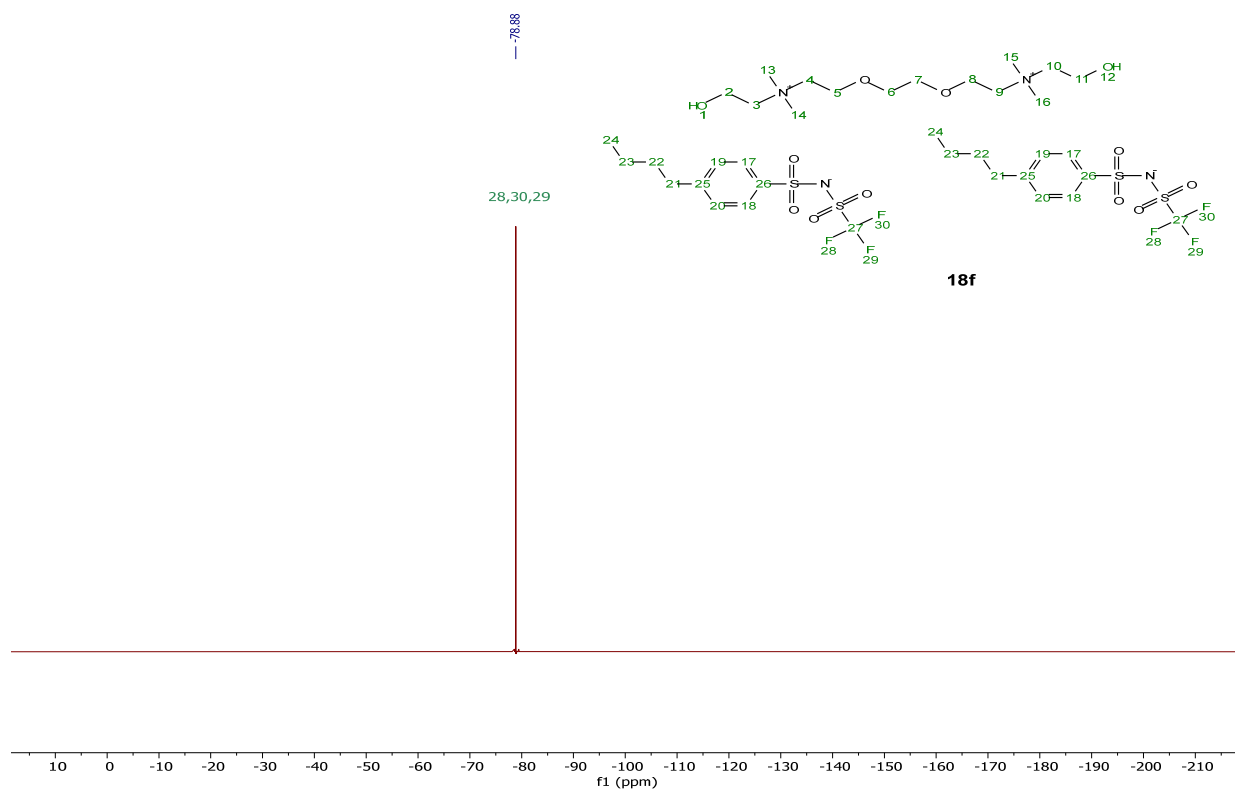
[DC-ether][2OSNTf], **18c** $^1\text{H}$  NMR (400 MHz, Methanol- $d_4$ )

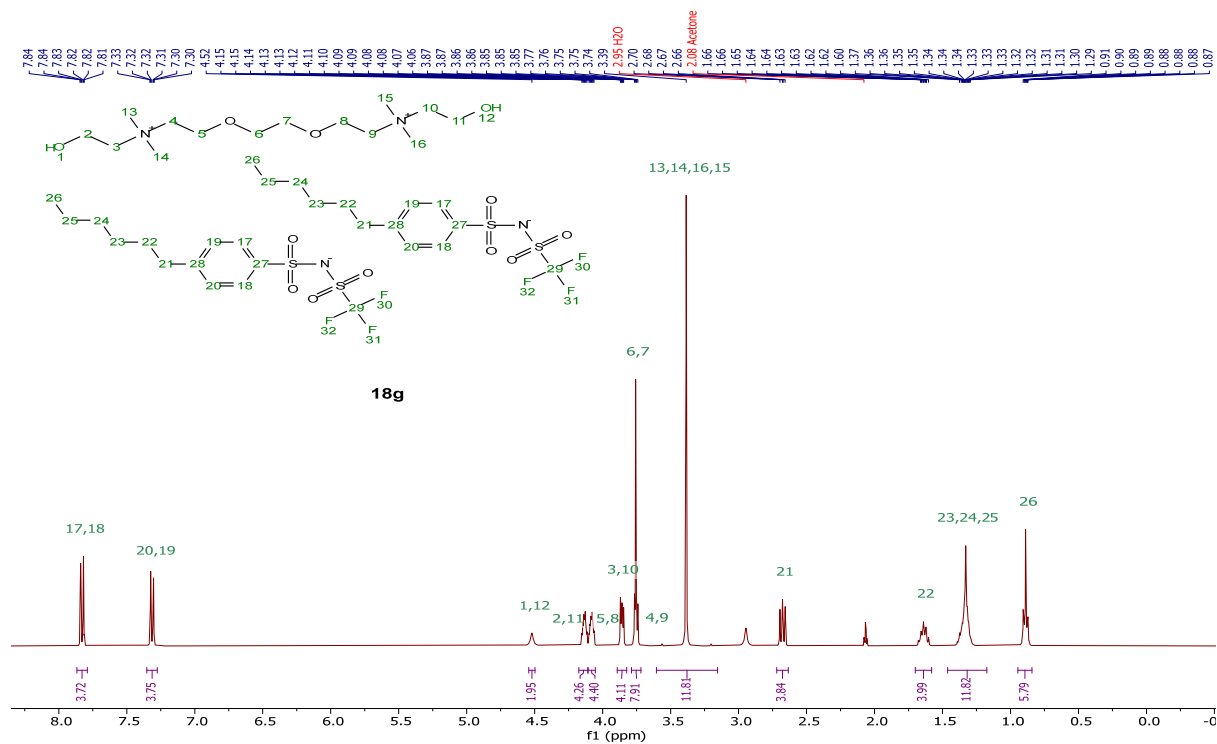
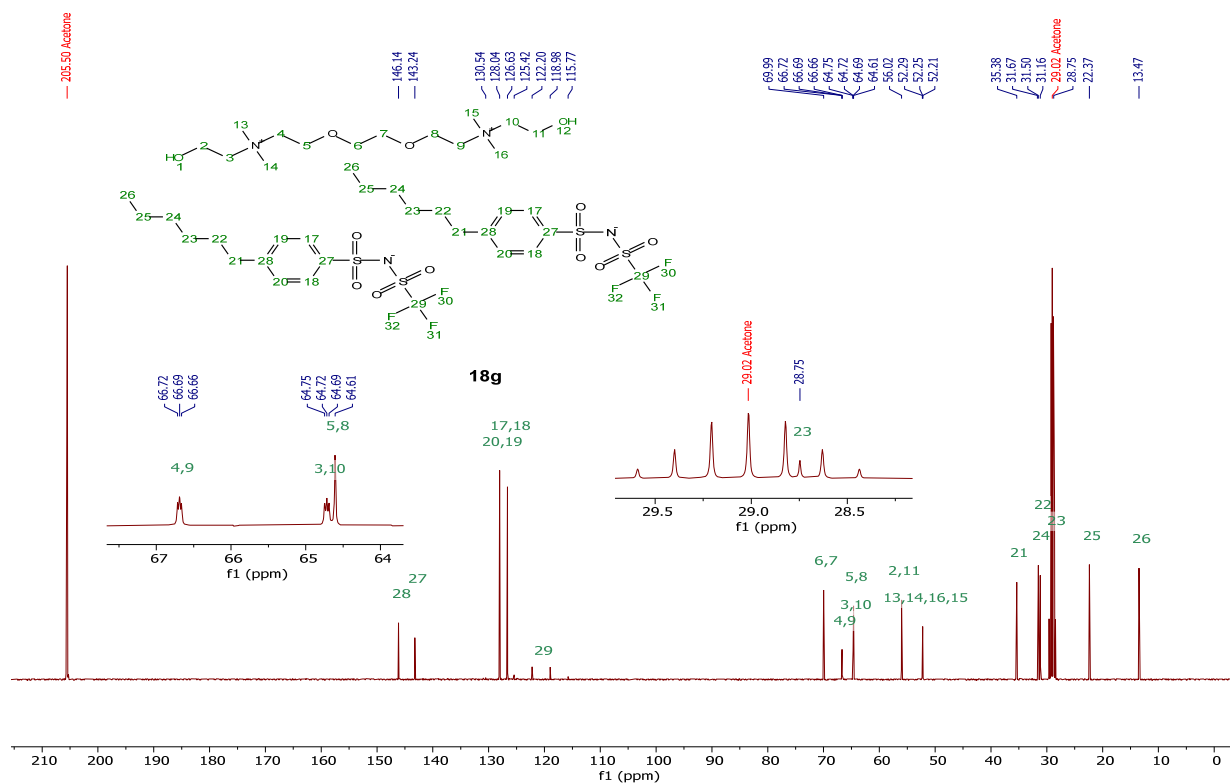
$^{19}\text{F}$  NMR (376 MHz, Acetone- $d_6$ )[DC-ether][2PhSNTf], **18d** $^1\text{H}$  NMR (400 MHz, Acetone- $d_6$ )

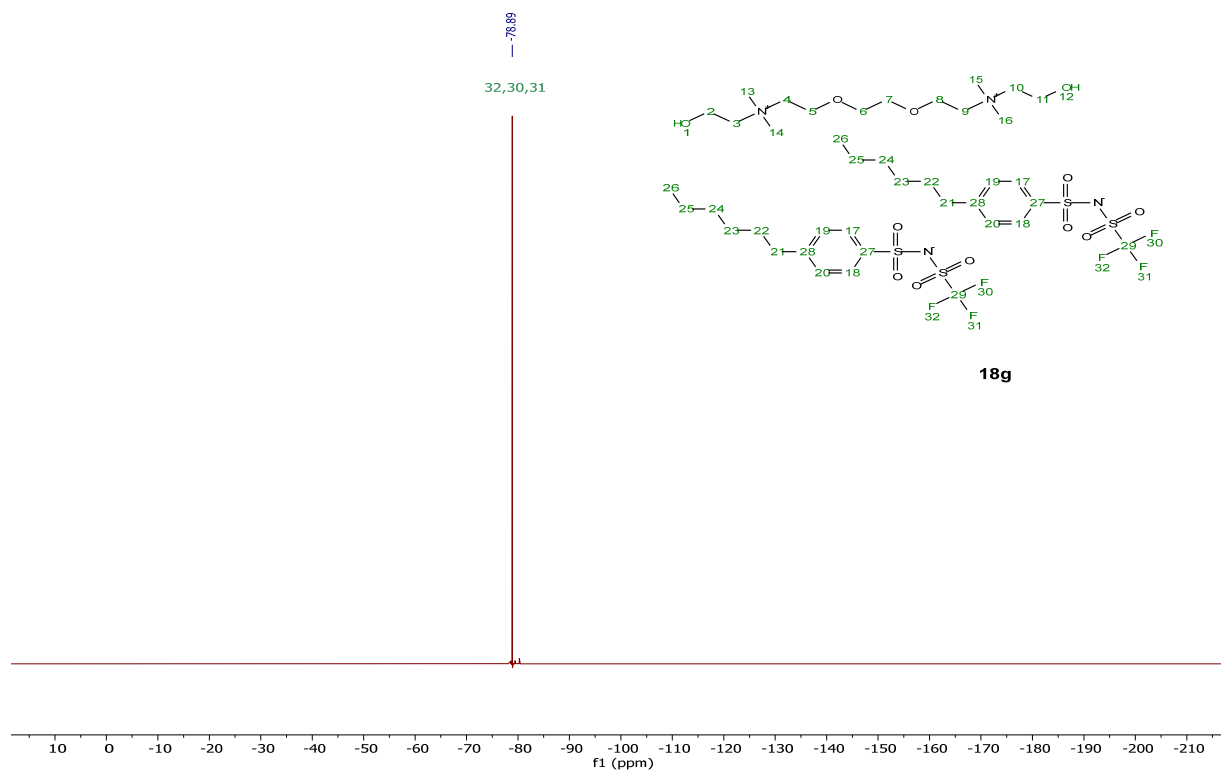
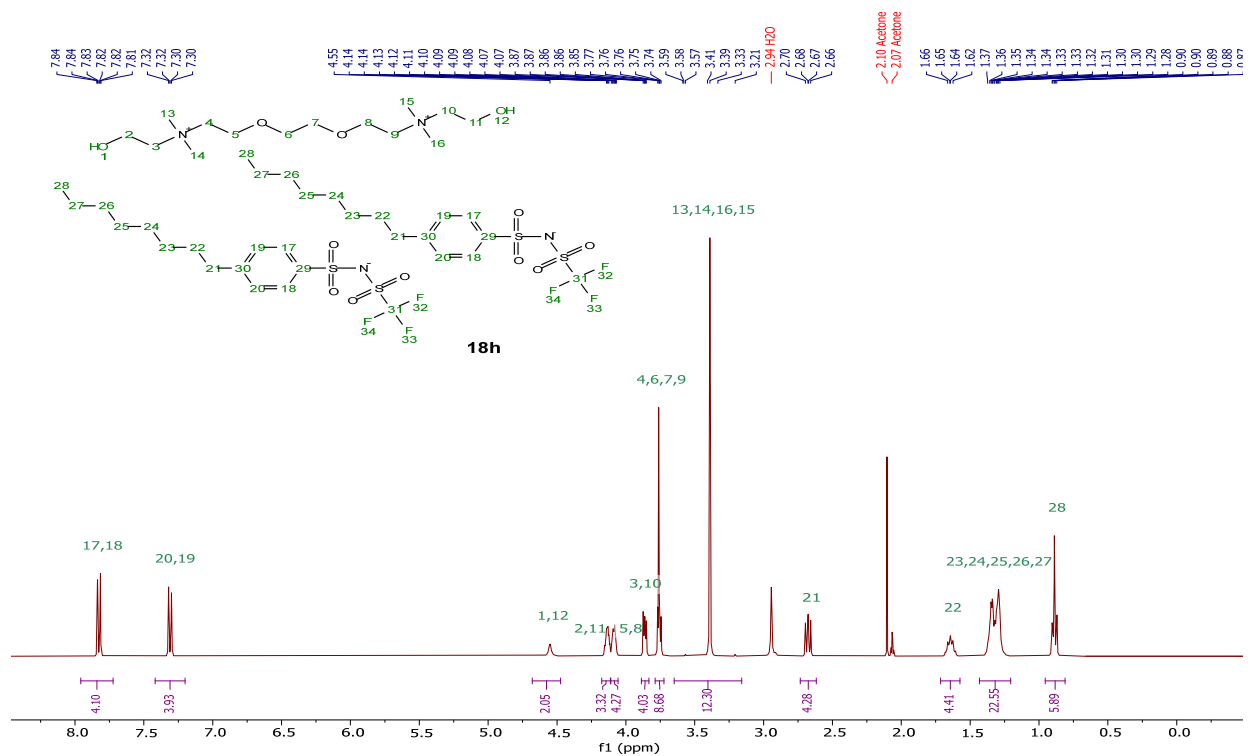
$^{13}\text{C}\{^1\text{H}\}$  NMR (101 MHz, Acetone-d<sub>6</sub>) $^{19}\text{F}$  NMR (376 MHz, Acetone-d<sub>6</sub>)

[DC-ether][2TsNTf], **18e** $^1\text{H}$  NMR (400 MHz, Methanol- $d_4$ ) $^{13}\text{C}\{^1\text{H}\}$  NMR (101 MHz, Methanol- $d_4$ )

$^{19}\text{F}$  NMR (376 MHz, Methanol- $d_4$ )[DC-ether][2pBBSNTf], **18f** $^1\text{H}$  NMR (400 MHz, Acetone- $d_6$ )

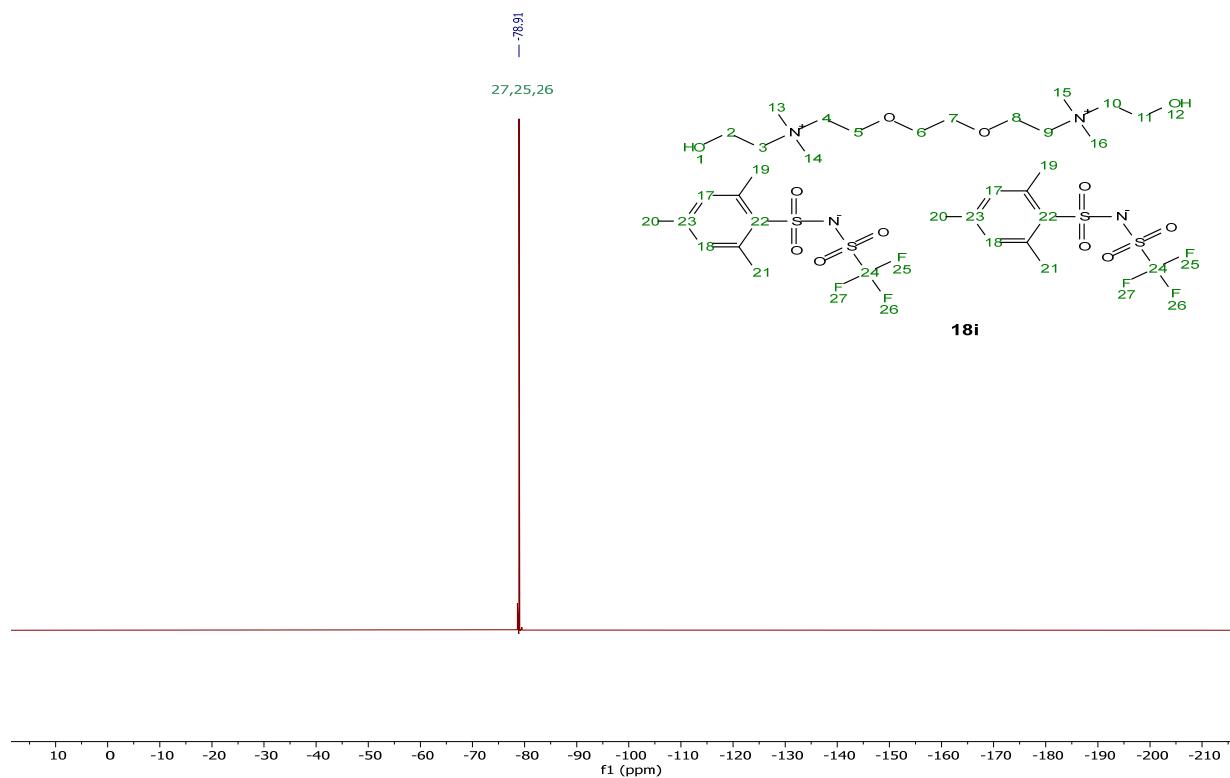
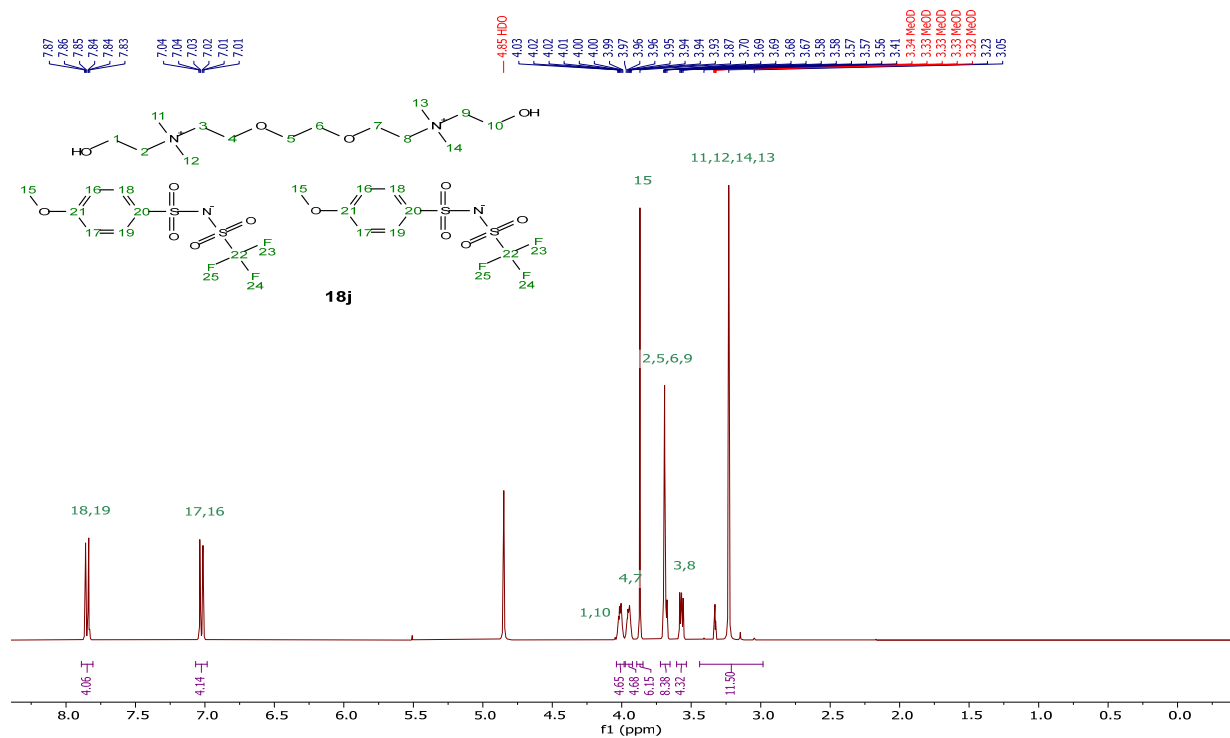
$^{13}\text{C}\{^1\text{H}\}$  NMR (101 MHz, Acetone- $d_6$ ) $^{19}\text{F}$  NMR (376 MHz, Acetone- $d_6$ )

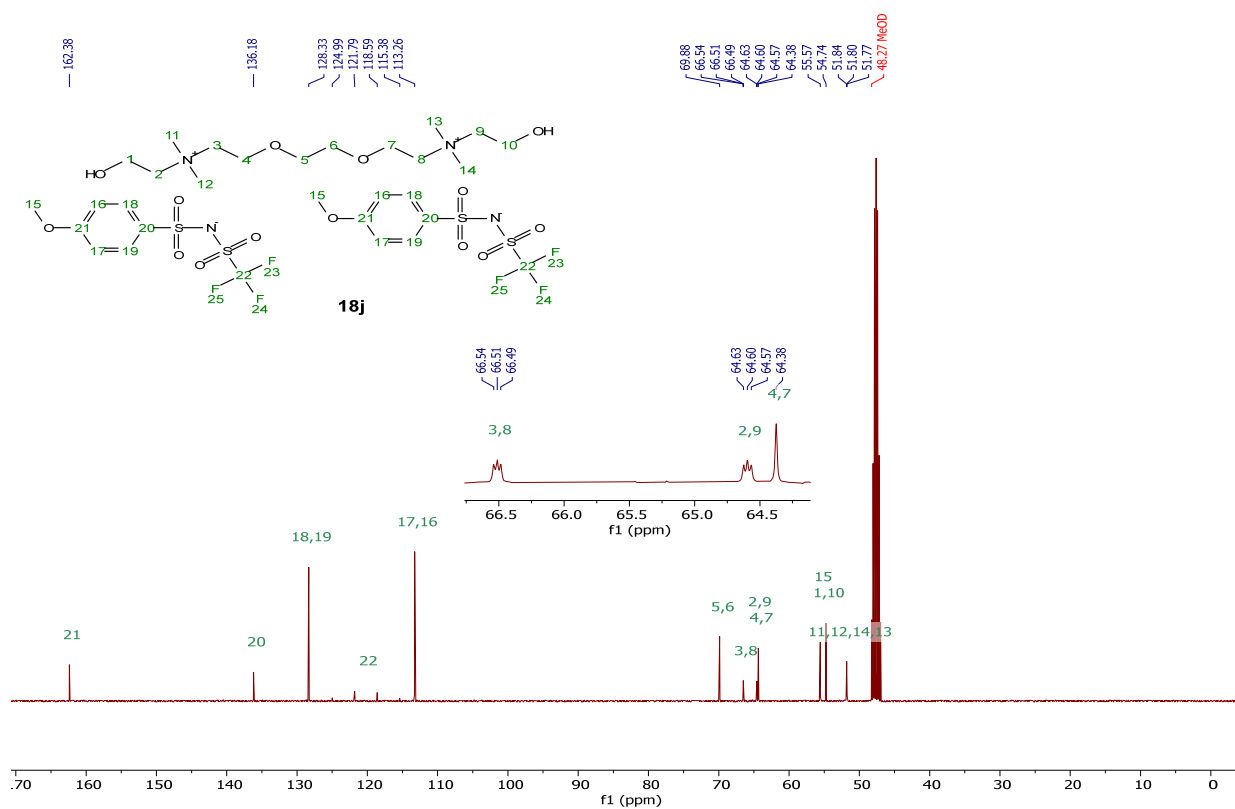
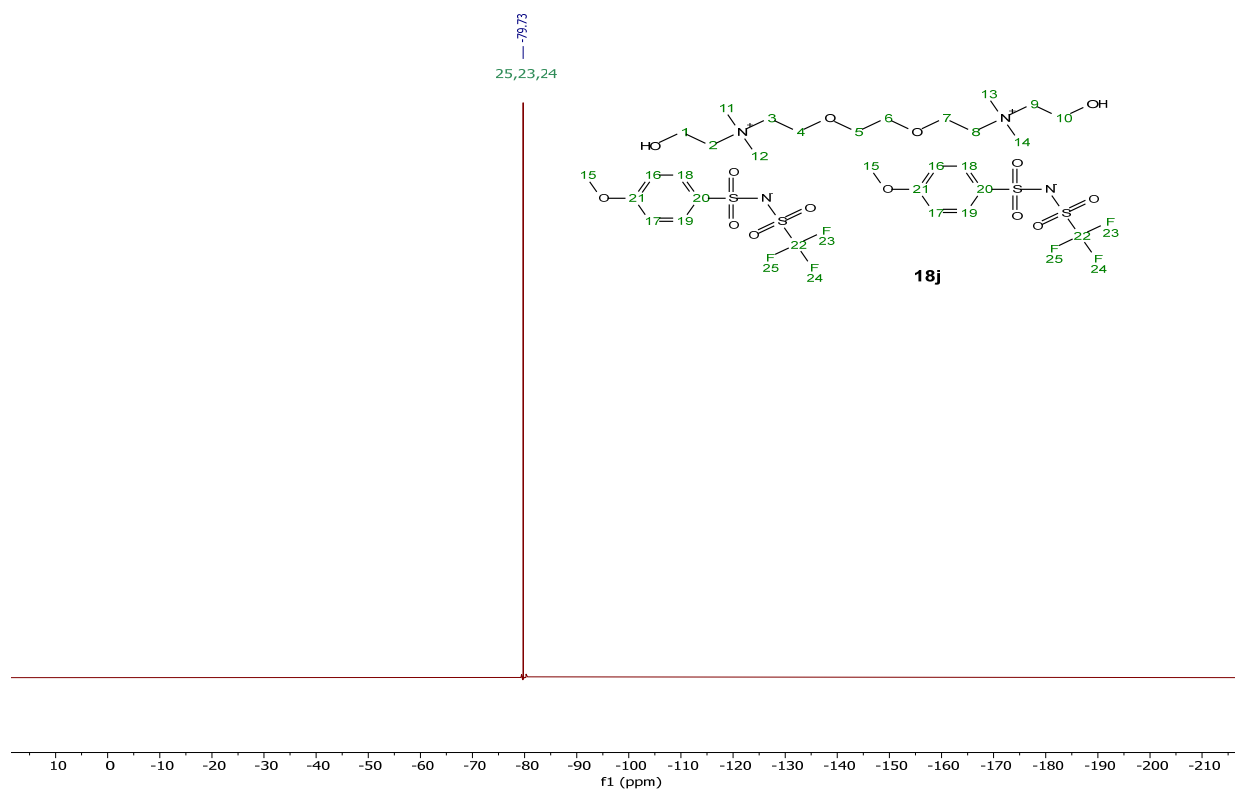
[DC-ether][2pHBSNTf], **18g** $^1\text{H}$  NMR (400 MHz, Acetone-d<sub>6</sub>) $^{13}\text{C}\{^1\text{H}\}$  NMR (101 MHz, Acetone-d<sub>6</sub>)

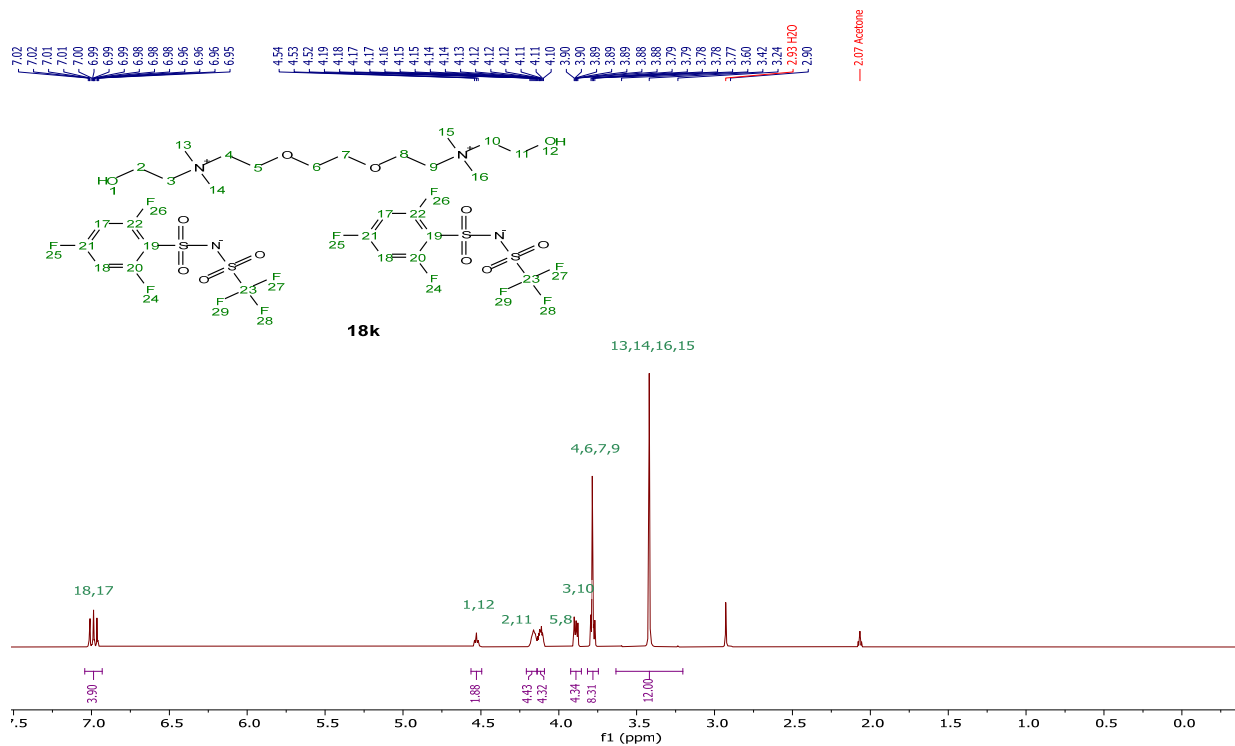
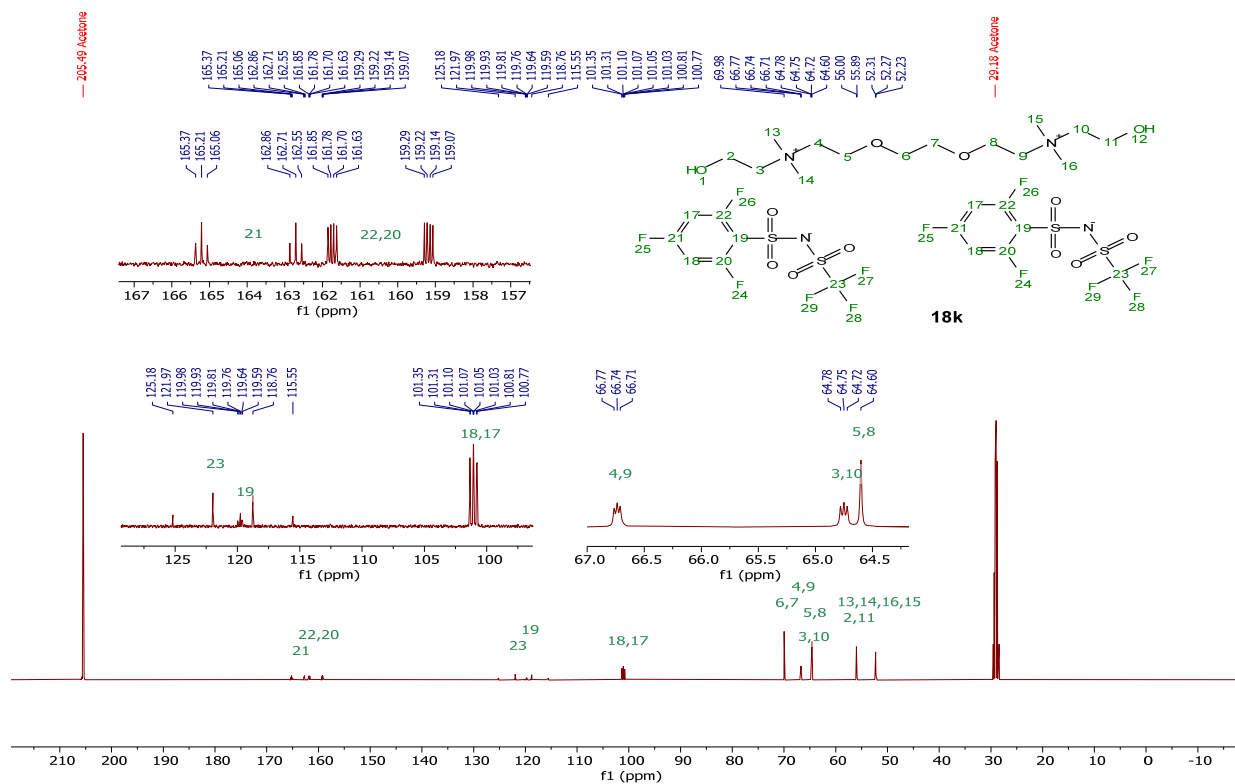
$^{19}\text{F}$  NMR (376 MHz, Acetone- $d_6$ )[DC-ether][2pOBSNTf], **18h** $^1\text{H}$  NMR (400 MHz, Acetone- $d_6$ )

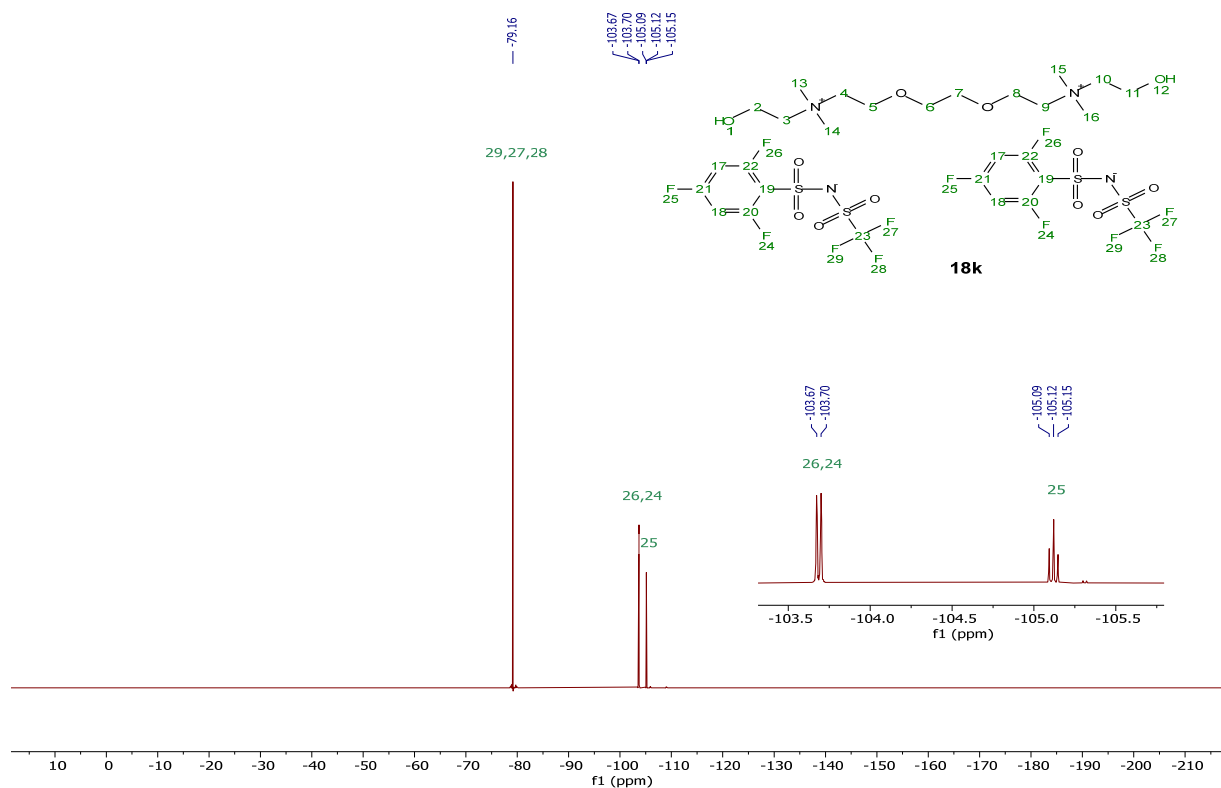
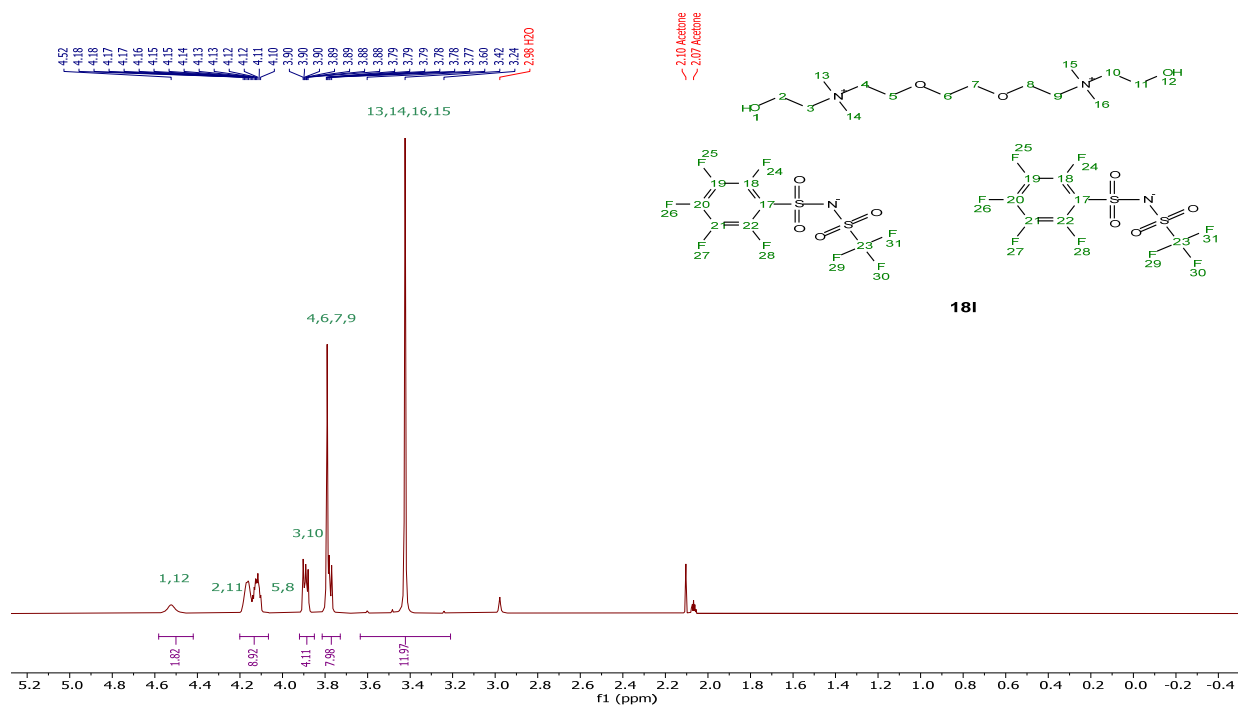


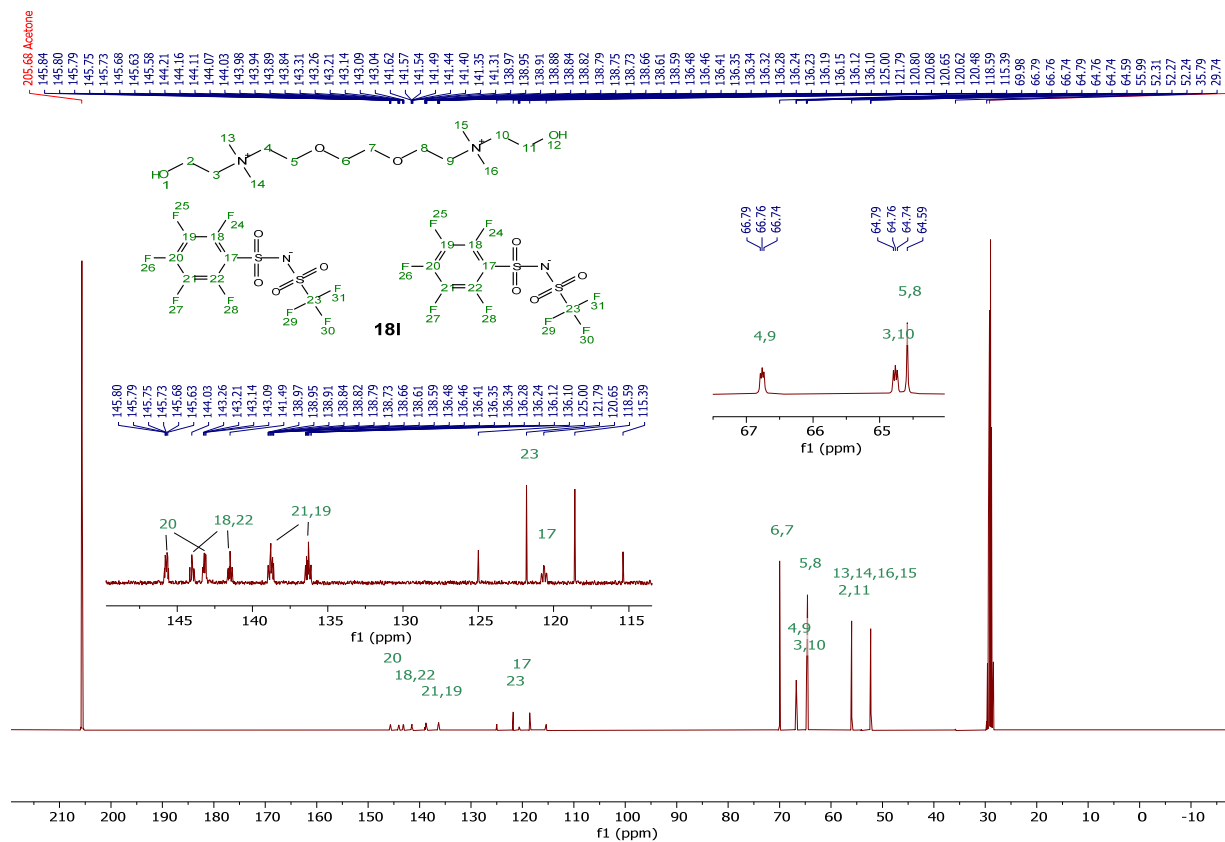
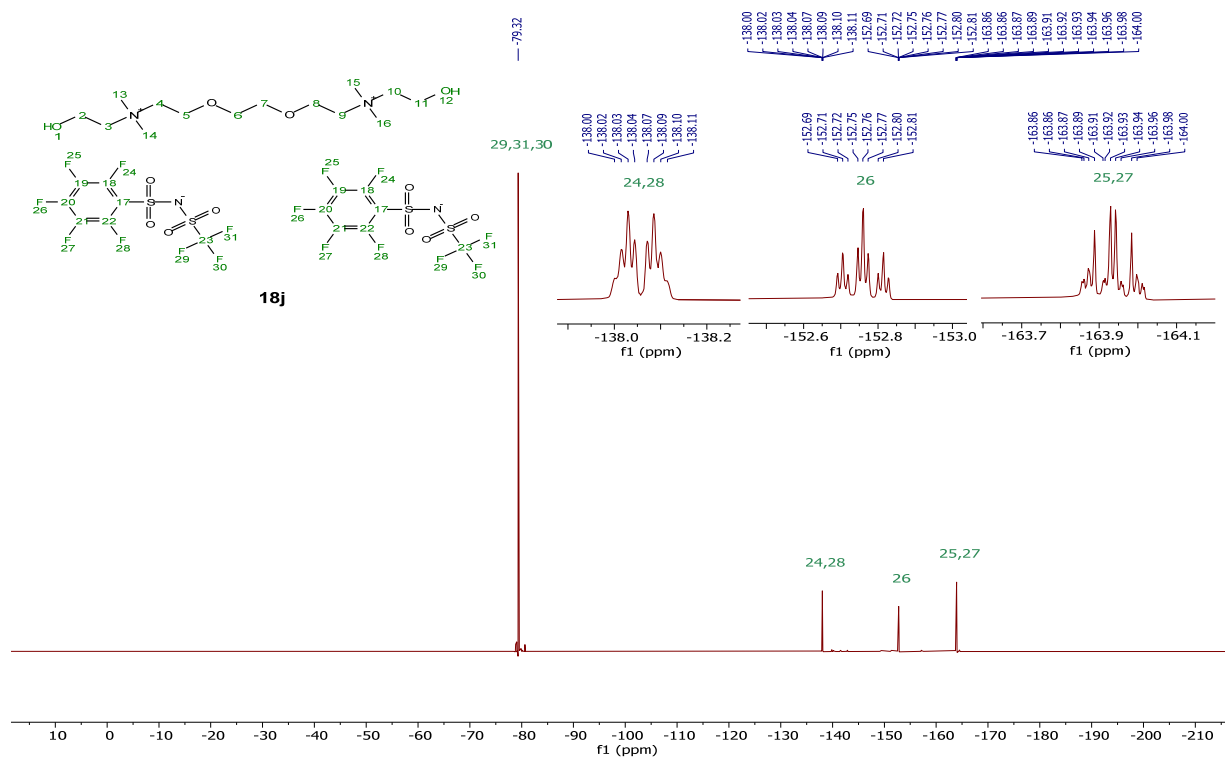


$^{19}\text{F}$  NMR (376 MHz, Acetone- $d_6$ )[DC-ether][2pMBSNTf], **18j** $^1\text{H}$  NMR (400 MHz, Methanol- $d_4$ )

$^{13}\text{C}\{^1\text{H}\}$  NMR (101 MHz, Acetone- $d_6$ ) $^{19}\text{F}$  NMR (376 MHz, Methanol- $d_4$ )

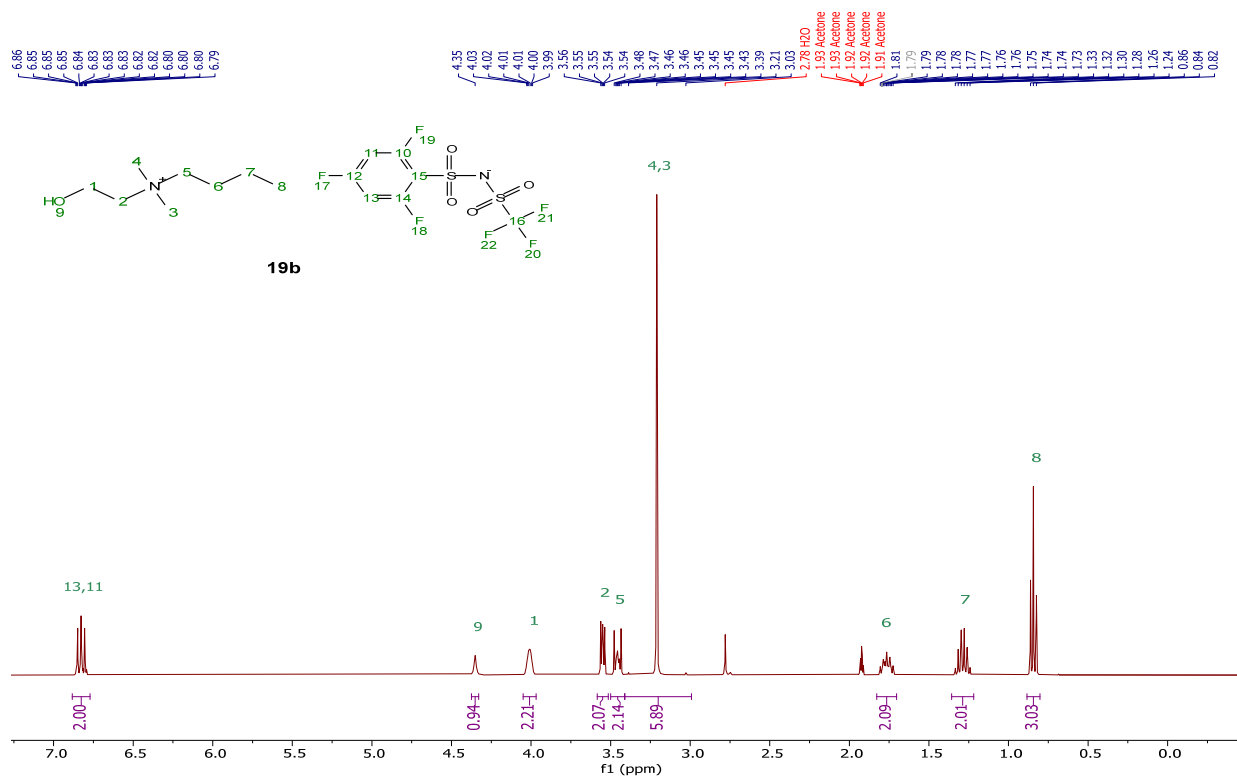
[DC-ether][2TFBSNTf], **18k** $^1\text{H}$  NMR (400 MHz, Acetone- $d_6$ ) $^{13}\text{C}\{^1\text{H}\}$  NMR (101 MHz, Acetone- $d_6$ )

$^{19}\text{F}$  NMR (376 MHz, Acetone- $d_6$ )[DC-ether][2PFBSNTf], **18l** $^1\text{H}$  NMR (400 MHz, Acetone- $d_6$ )

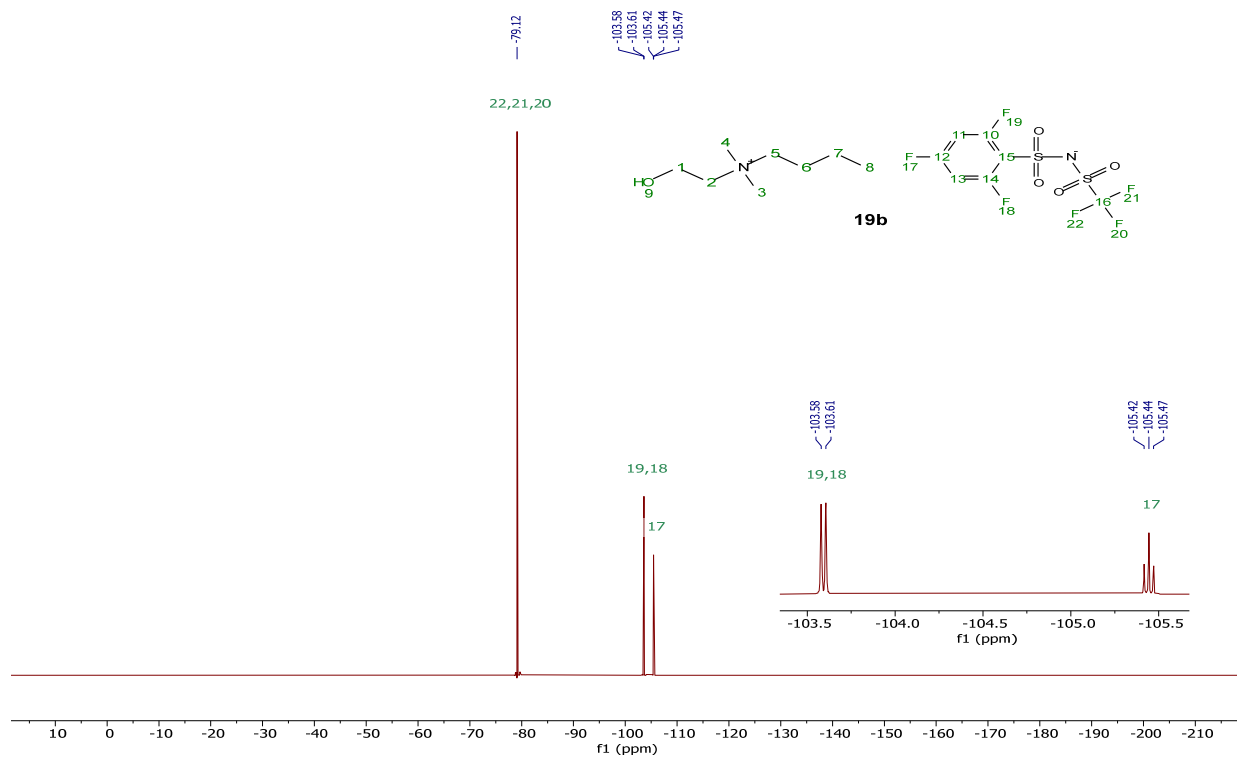
$^{13}\text{C}\{^1\text{H}\}$  NMR (101 MHz, Acetone- $d_6$ ) $^{19}\text{F}$  NMR (376 MHz, Acetone- $d_6$ )

$[N_{1,1,4,2OH}][TFBSNTf]$ , **19b**

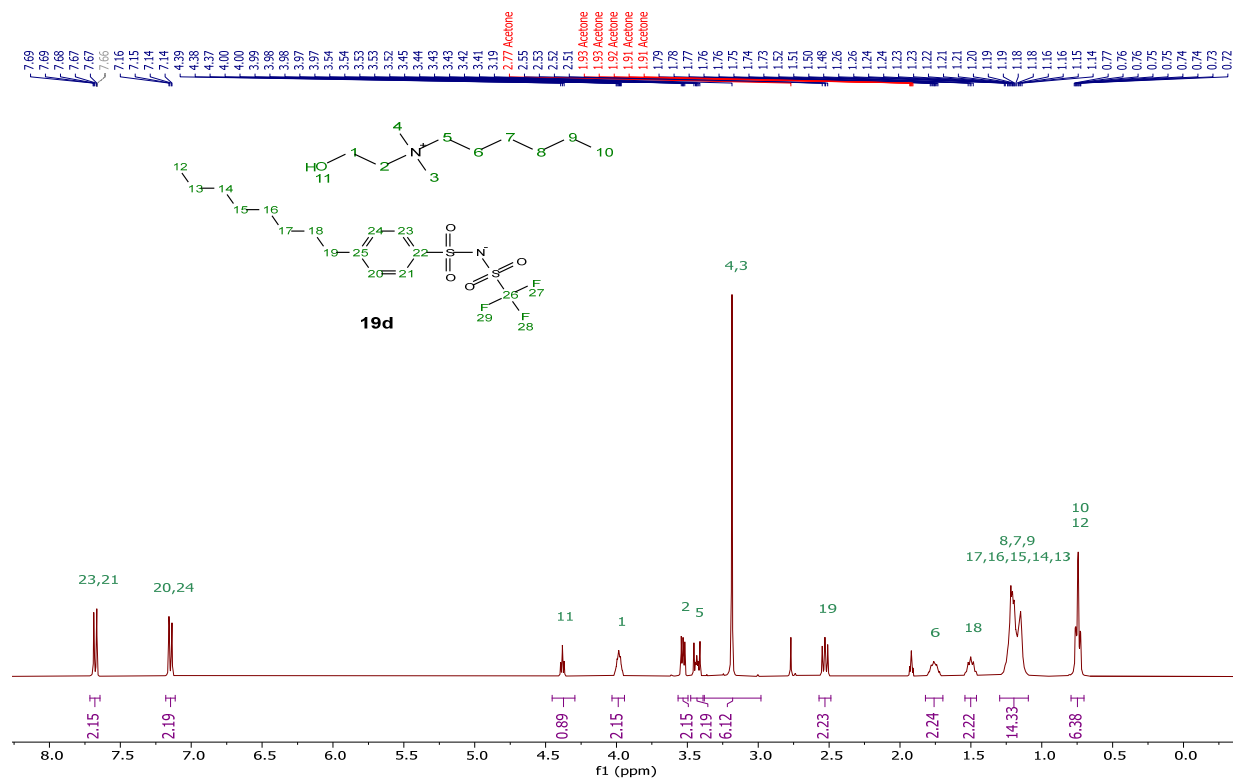
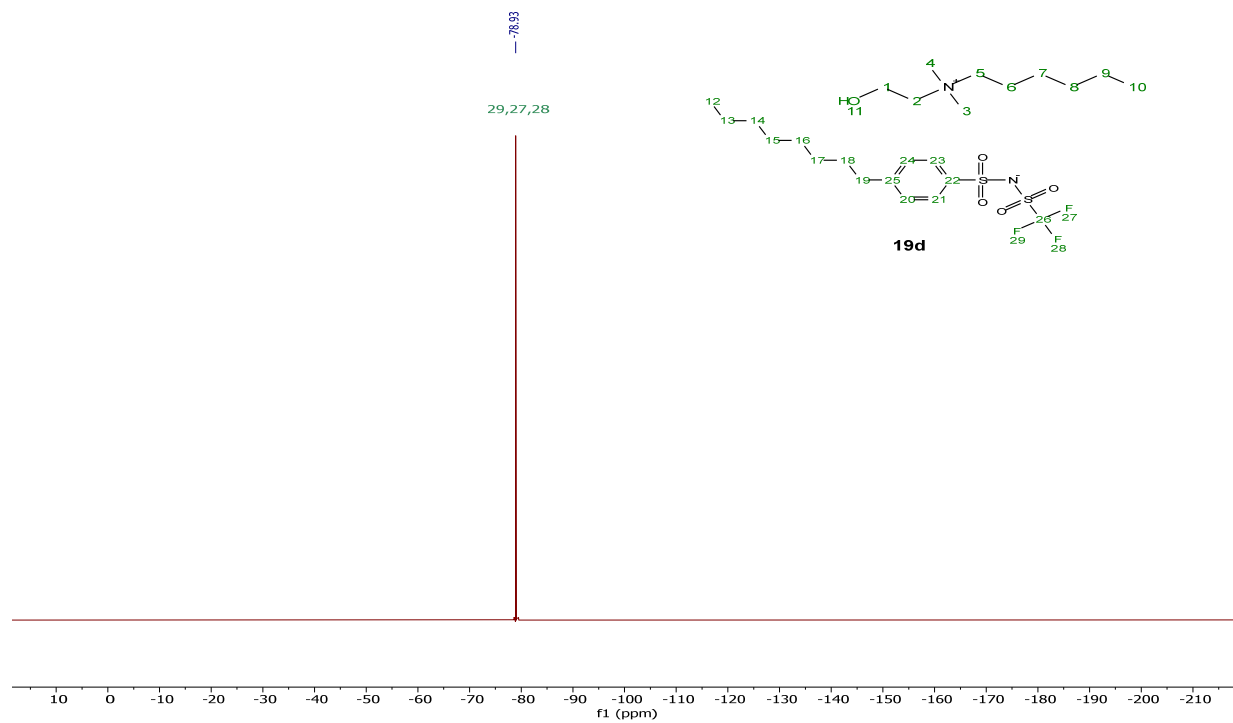
$^1H$  NMR (400 MHz, Acetone- $d_6$ )

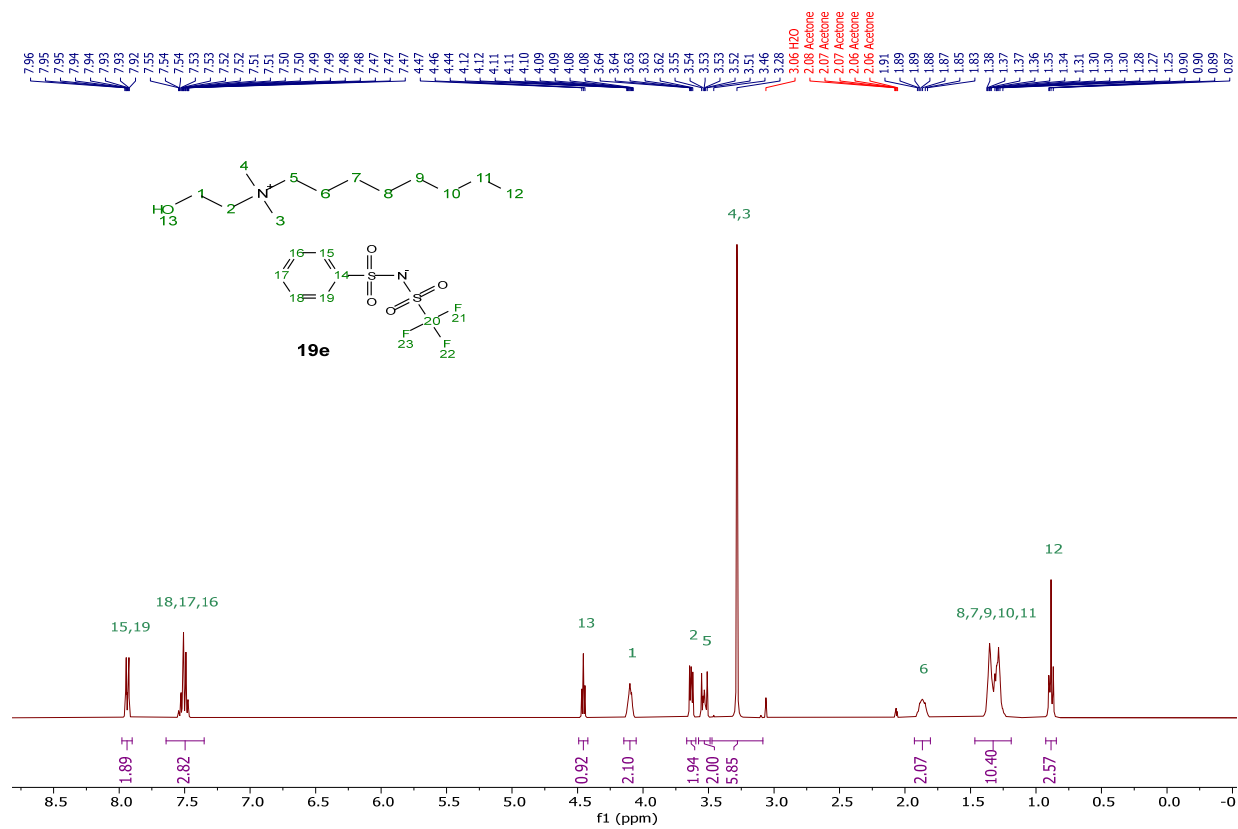
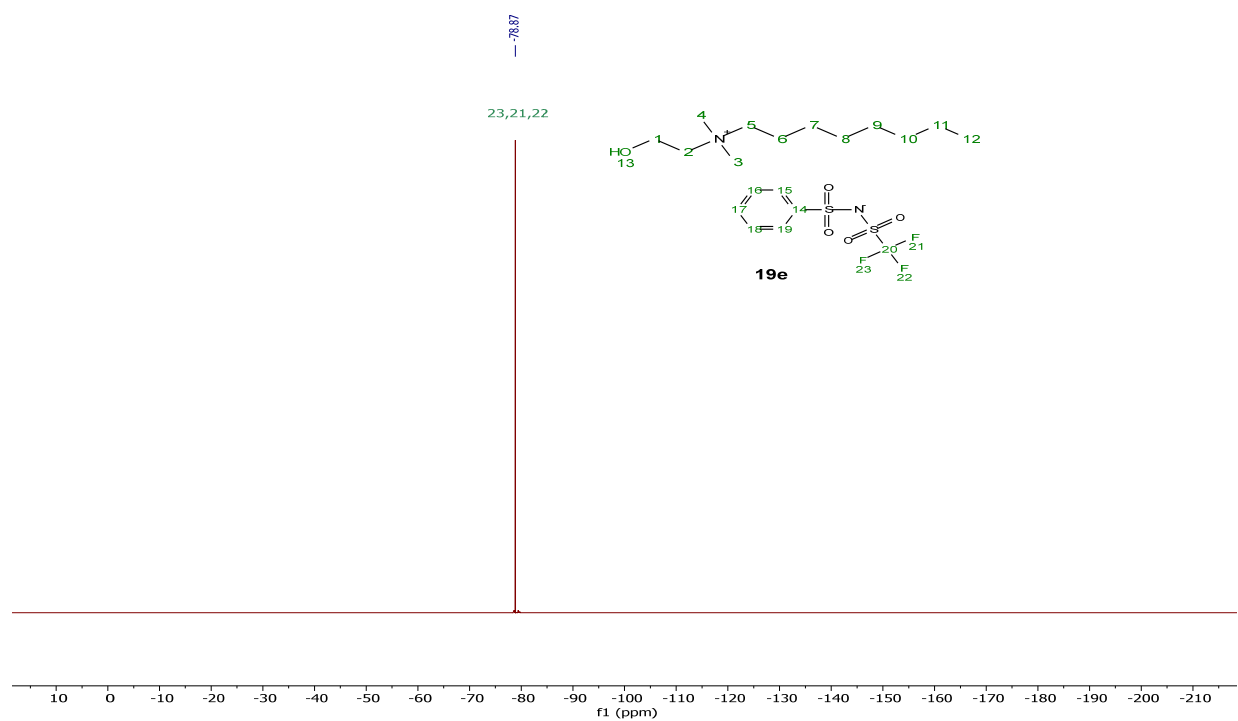


$^{19}F$  NMR (376 MHz, Acetone- $d_6$ )



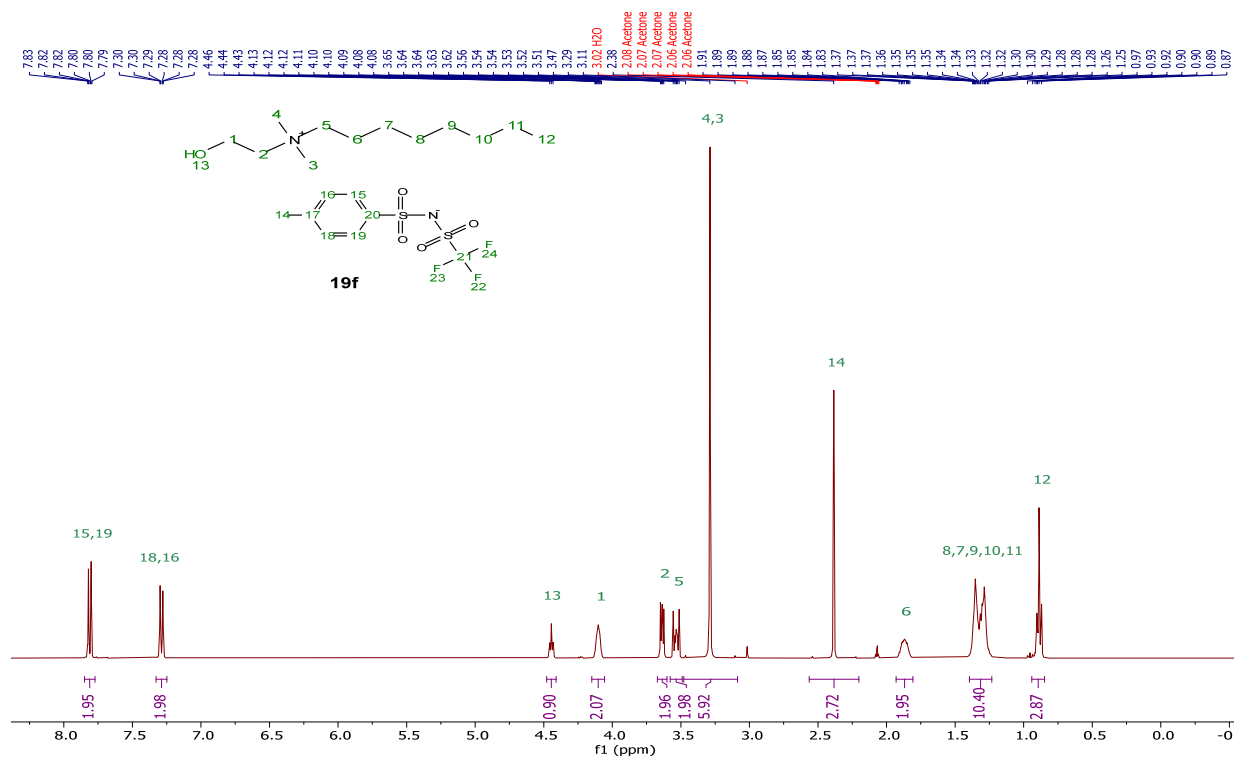


[N<sub>1,1,6,2OH</sub>][pOBSNTf], **19d**<sup>1</sup>H NMR (400 MHz, Acetone-d<sub>6</sub>)<sup>19</sup>F NMR (376 MHz, Acetone-d<sub>6</sub>)

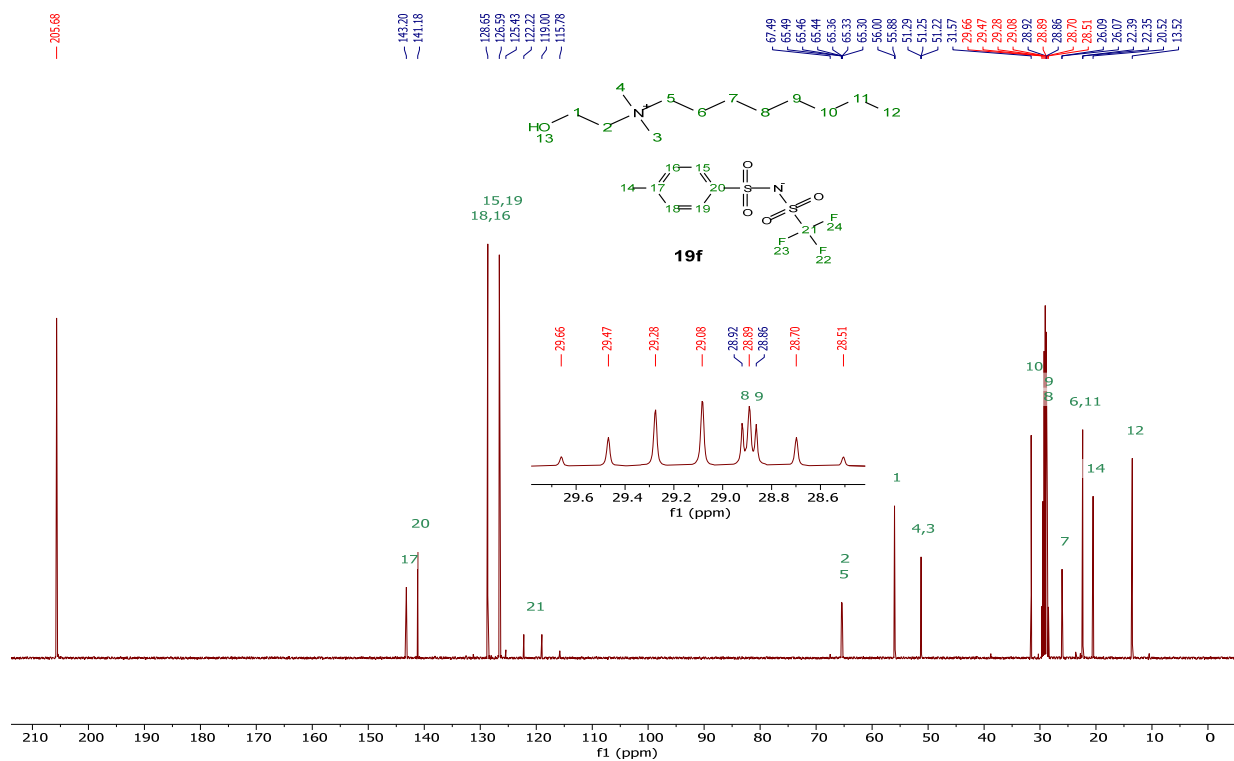
[N<sub>1,1,8,2OH</sub>][pOBSNTf], **19e**<sup>1</sup>H NMR (400 MHz, Acetone-d<sub>6</sub>)<sup>19</sup>F NMR (376 MHz, Acetone-d<sub>6</sub>)

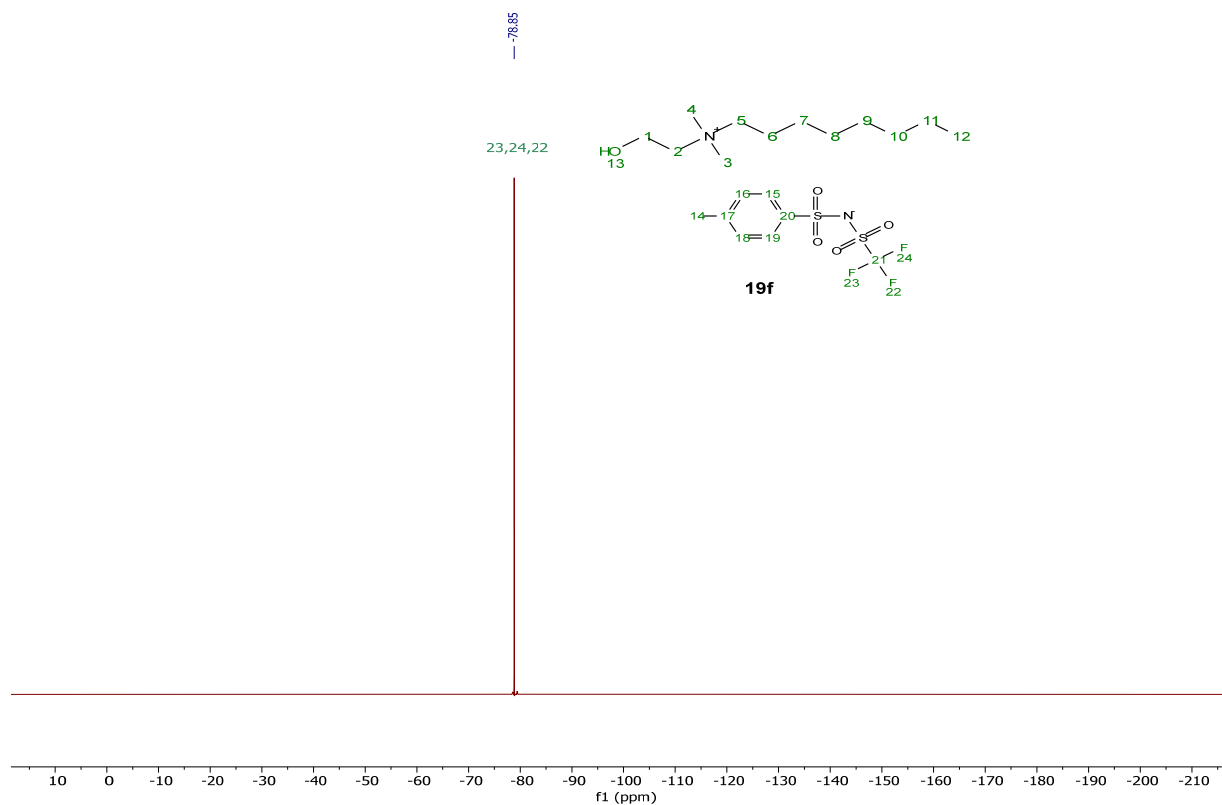
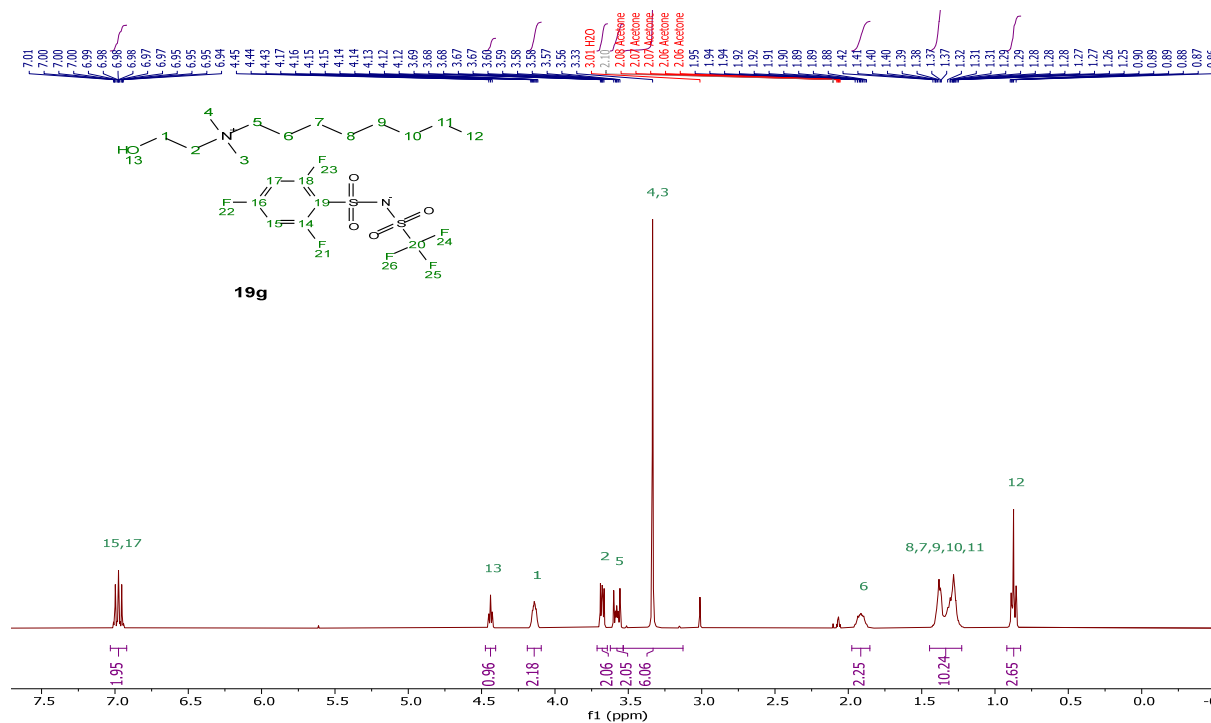
[N<sub>1,1,8,2OH</sub>][TsNTf], **19f**

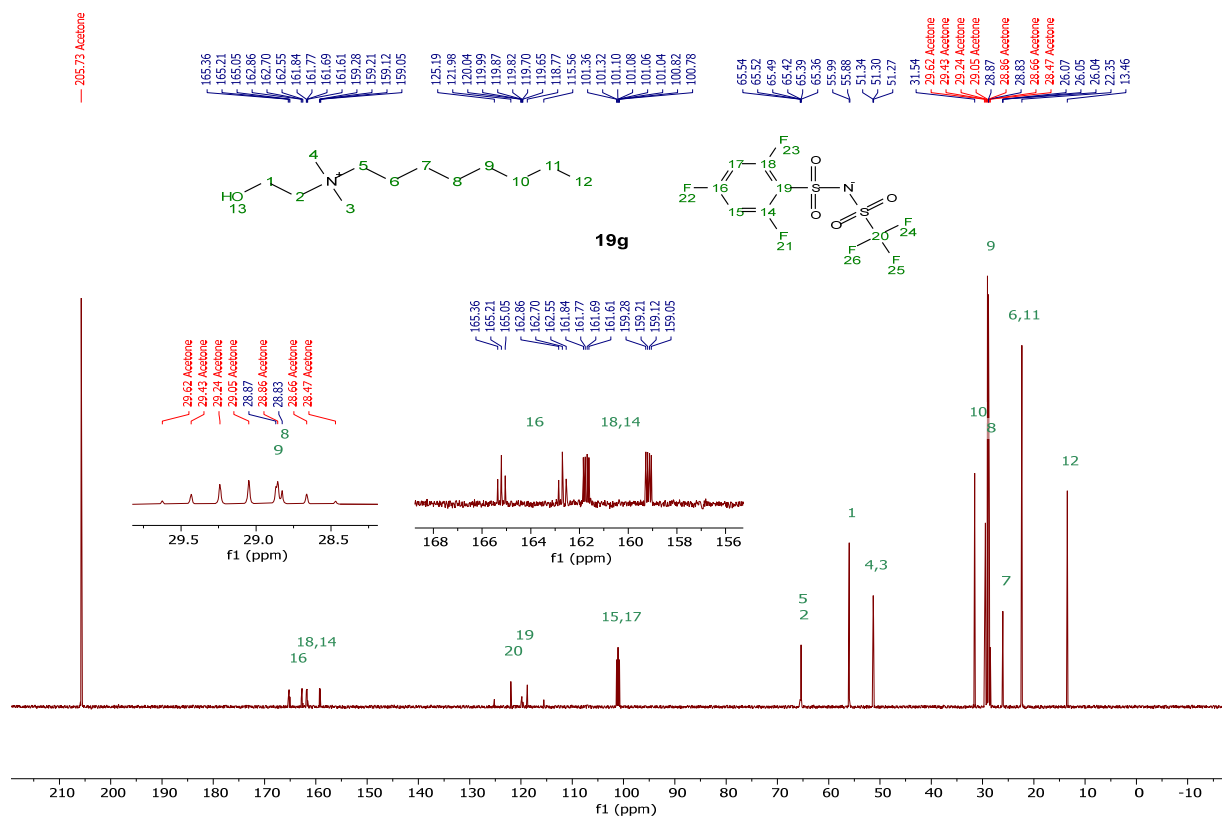
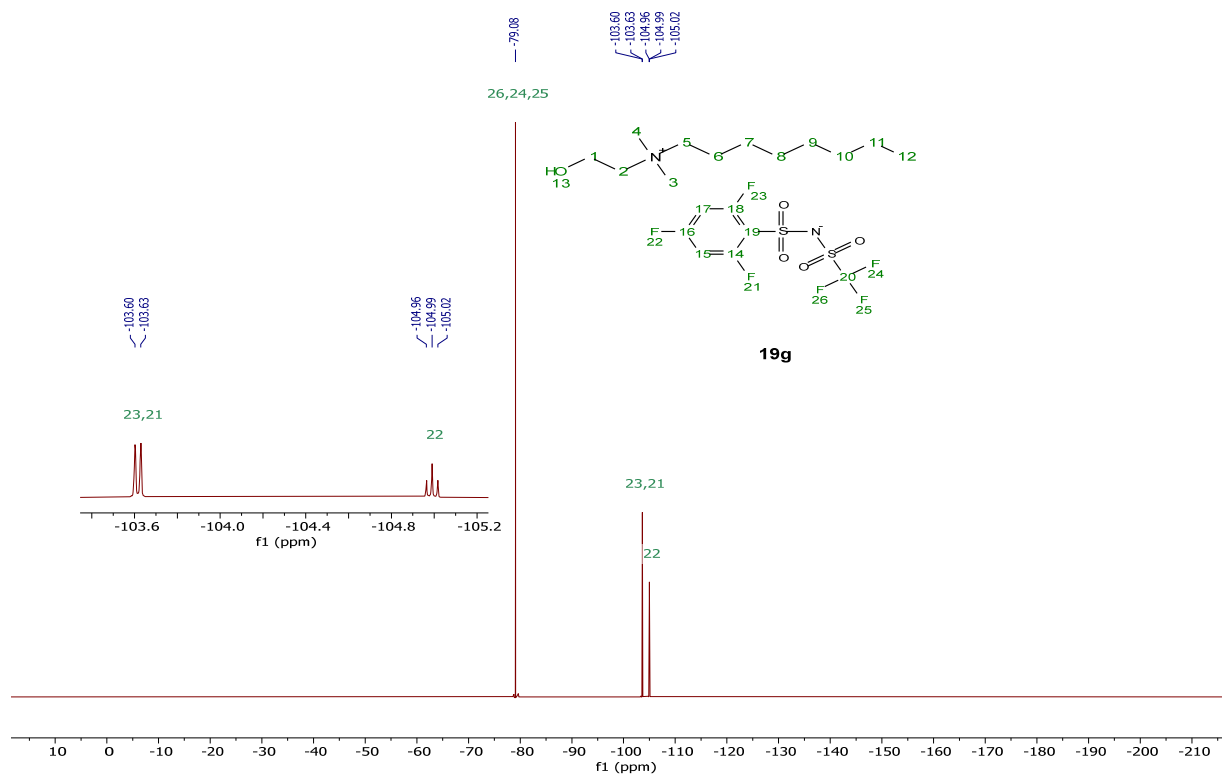
<sup>1</sup>H NMR (400 MHz, Acetone-d<sub>6</sub>)

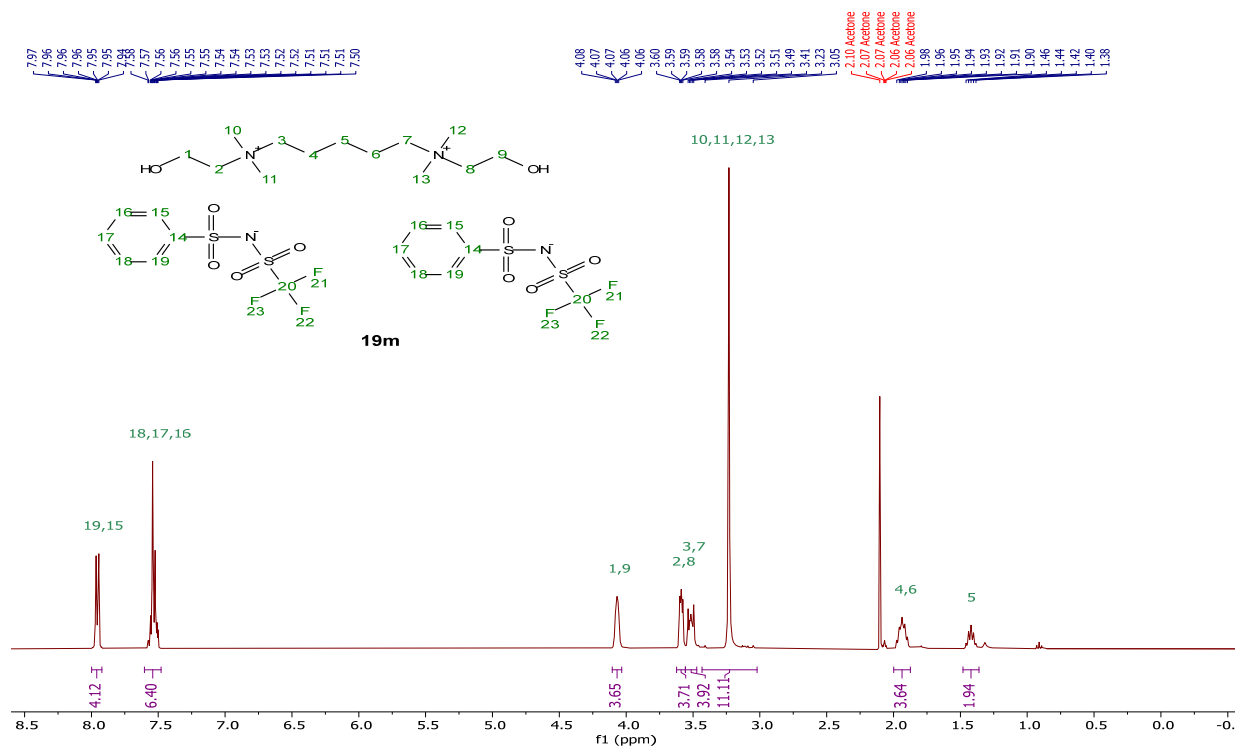
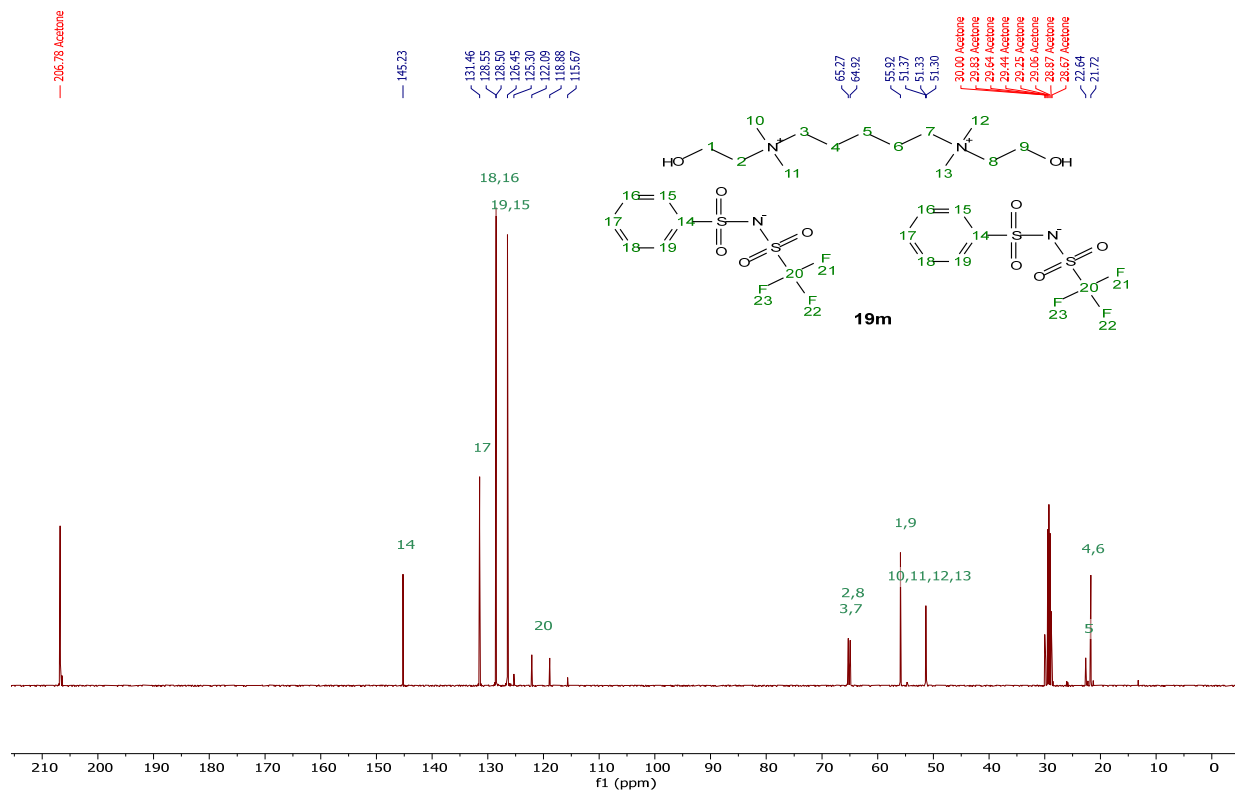


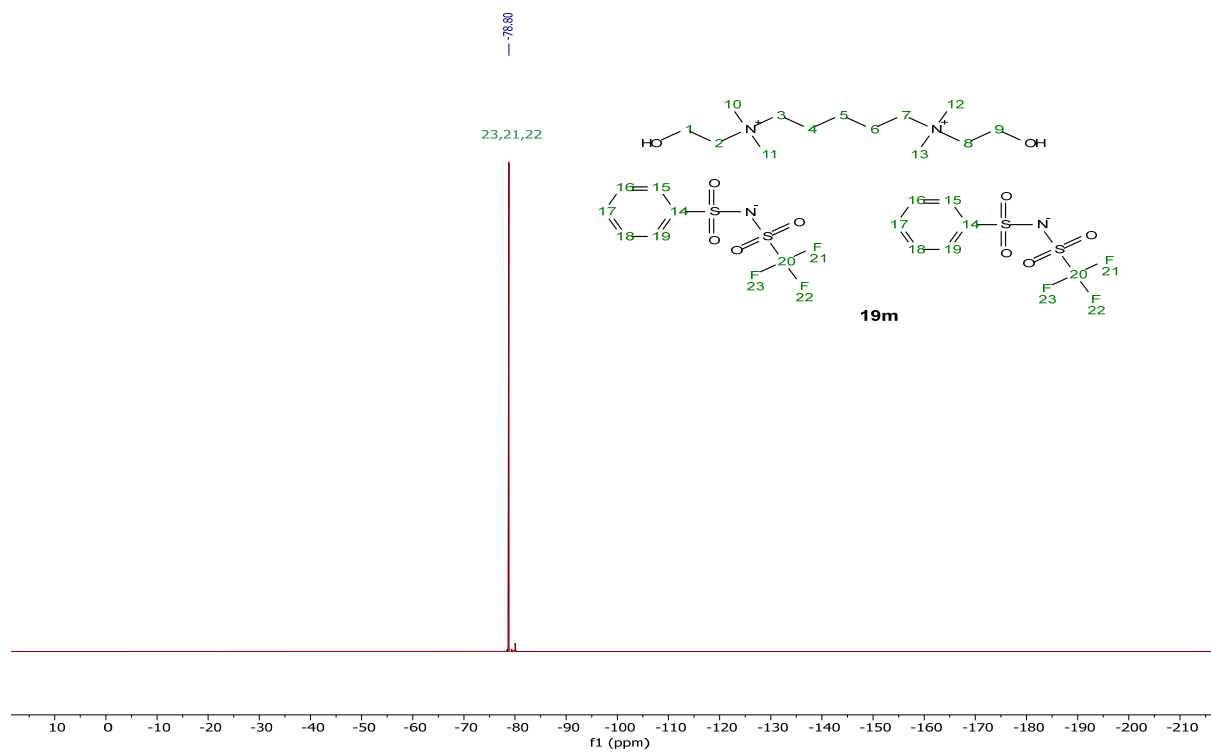
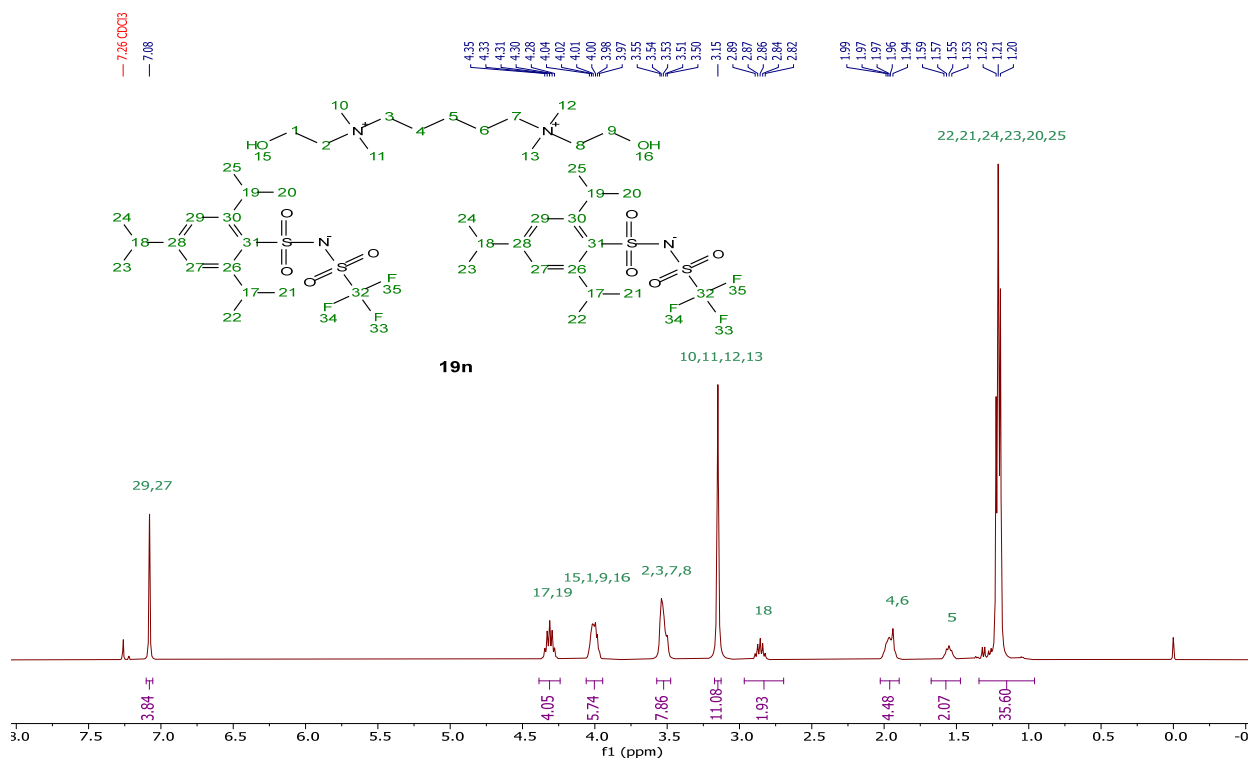
<sup>13</sup>C{<sup>1</sup>H} NMR (101 MHz, Acetone-d<sub>6</sub>)

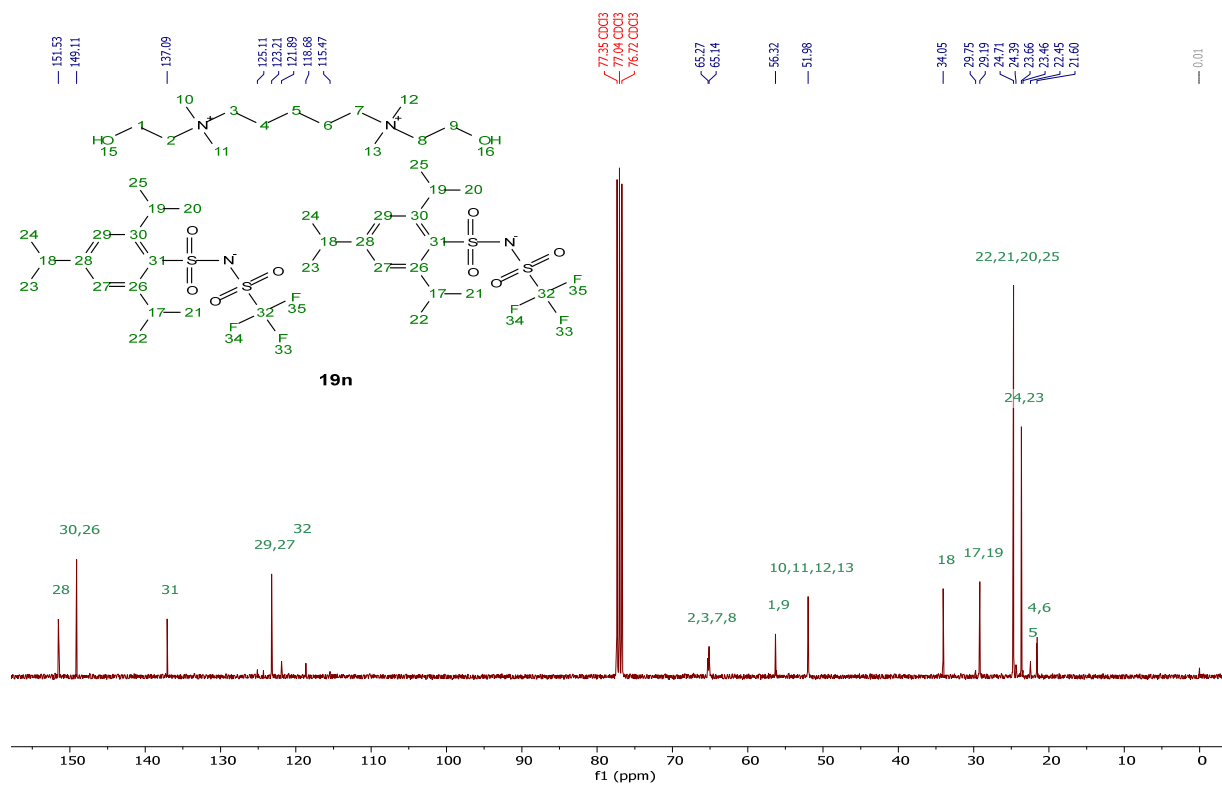
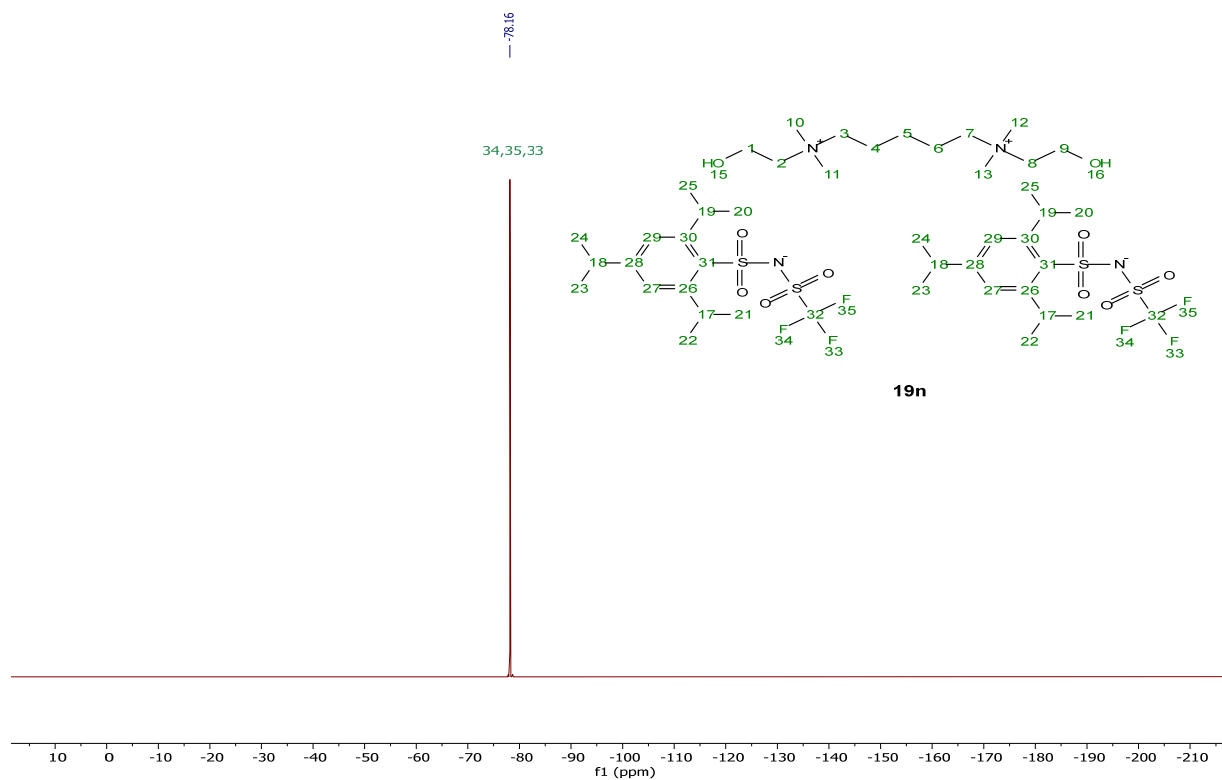


$^{19}\text{F}$  NMR (376 MHz, Acetone- $d_6$ )[ $\text{N}_{1,1,8,2\text{OH}}$ ][TFBSNTf], **19g** $^1\text{H}$  NMR (400 MHz, Acetone- $d_6$ )

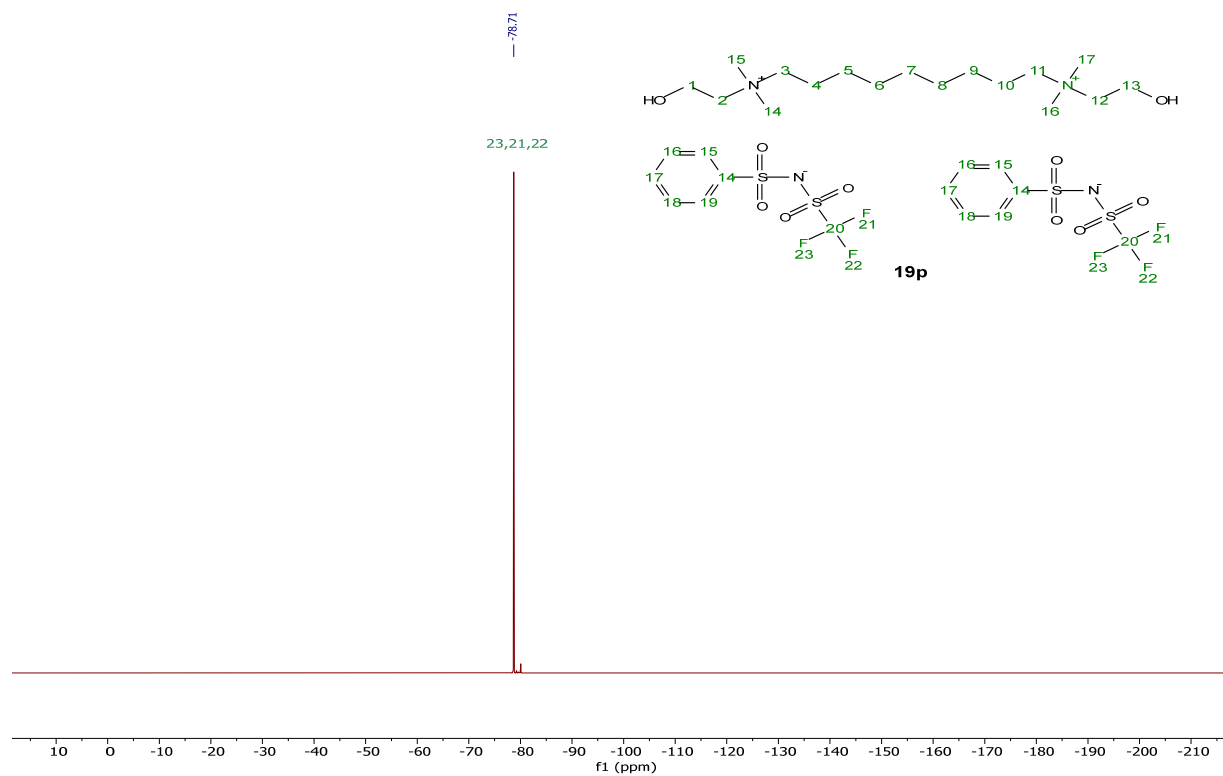
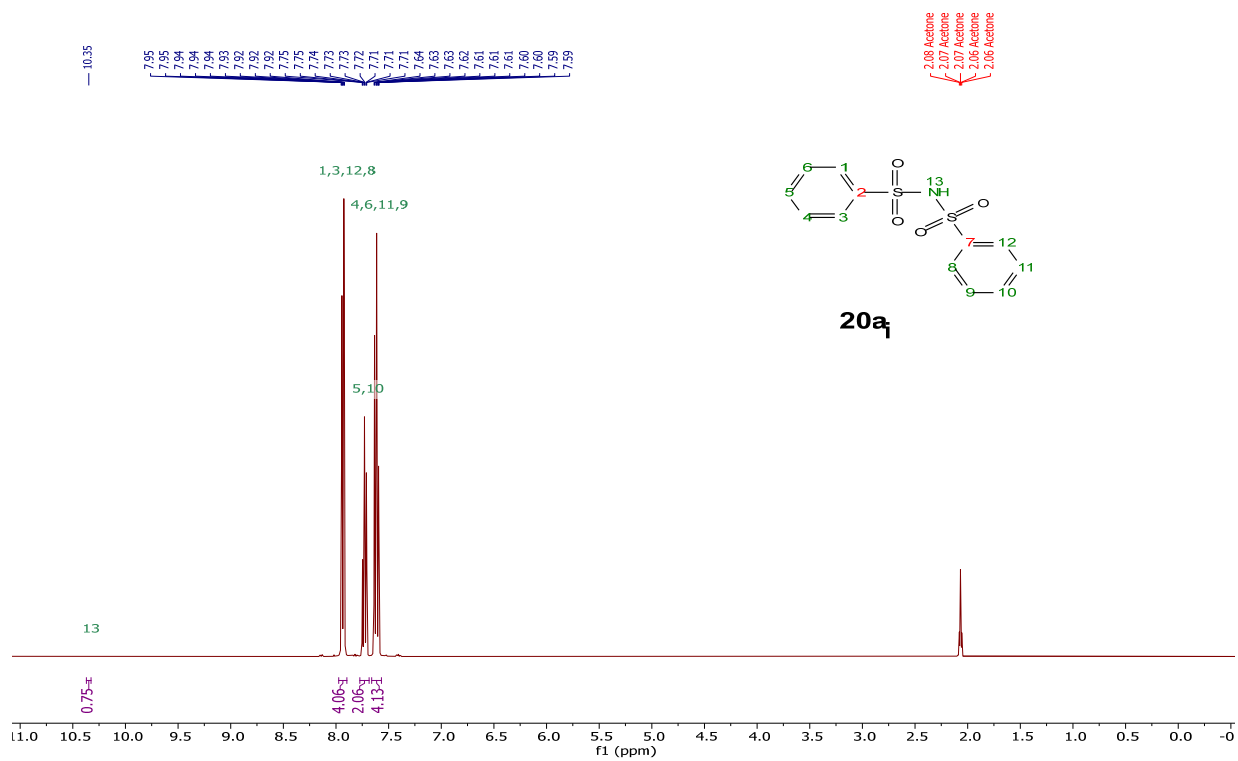
$^{13}\text{C}\{^1\text{H}\}$  NMR (101 MHz, Acetone-d<sub>6</sub>) $^{19}\text{F}$  NMR (376 MHz, Acetone-d<sub>6</sub>)

[DC-5][2PhSNTf], **19m** $^1\text{H}$  NMR (400 MHz, Acetone- $d_6$ ) $^{13}\text{C}\{^1\text{H}\}$  NMR (101 MHz, Acetone- $d_6$ )

$^{19}\text{F}$  NMR (376 MHz, Acetone- $d_6$ )[DC-5][2TIPSNTf], **19n** $^1\text{H}$  NMR (400 MHz, Chloroform- $d$ )

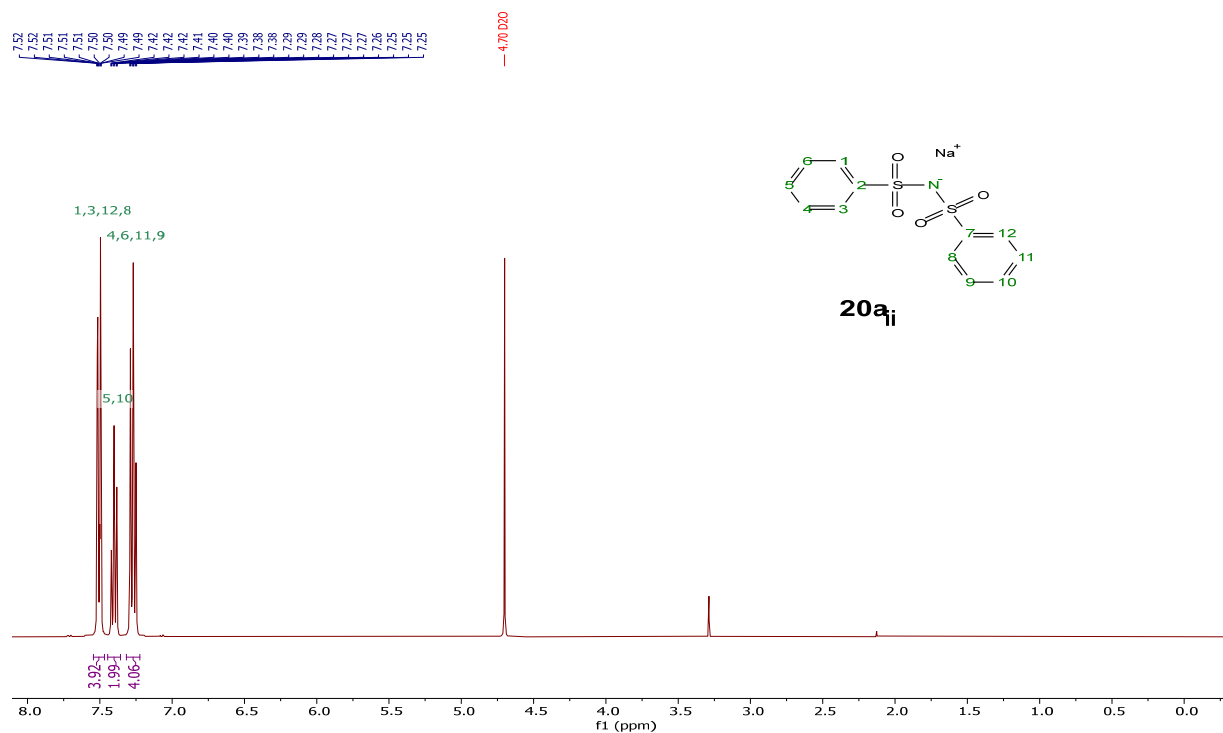
$^{13}\text{C}\{^1\text{H}\}$  NMR (101 MHz, Chloroform-d) $^{19}\text{F}$  NMR (376 MHz, Chloroform-d)



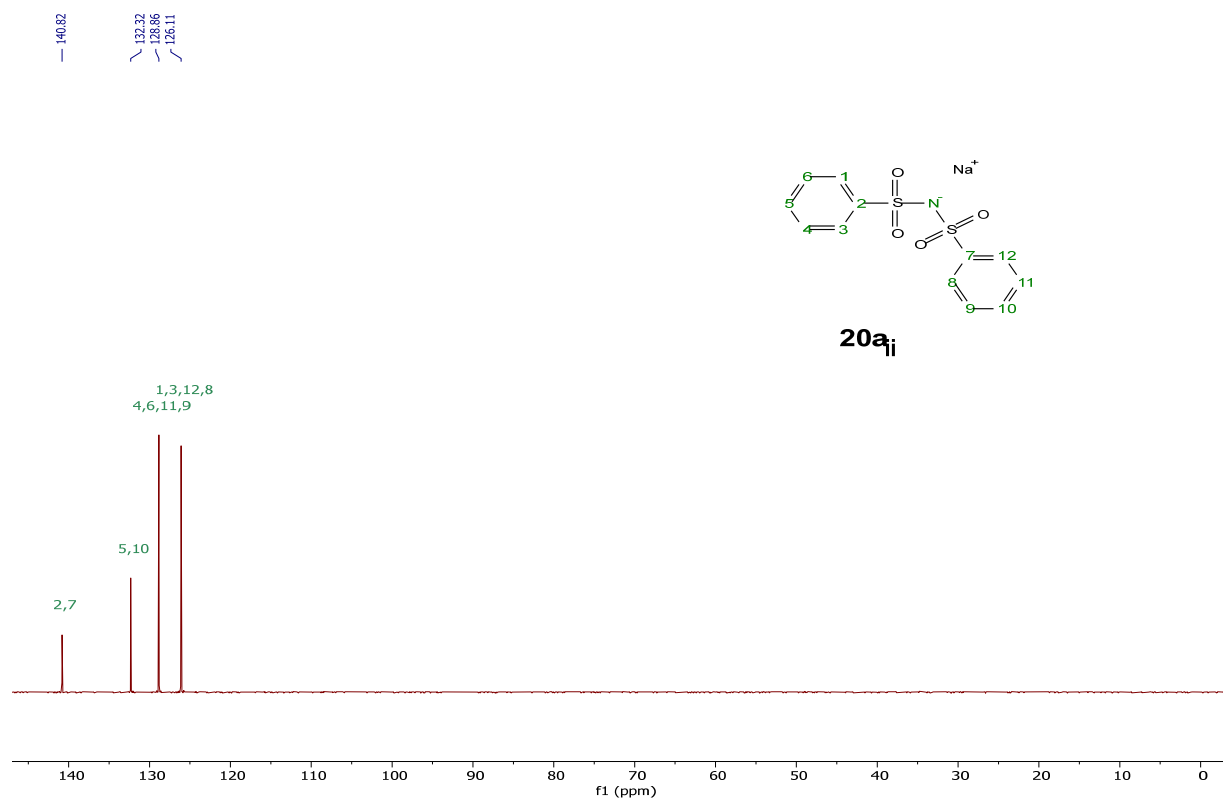
$^{19}\text{F}$  NMR (376 MHz, Acetone- $d_6$ )**20a<sub>i</sub>** $^1\text{H}$  NMR (400 MHz, Acetone- $d_6$ )

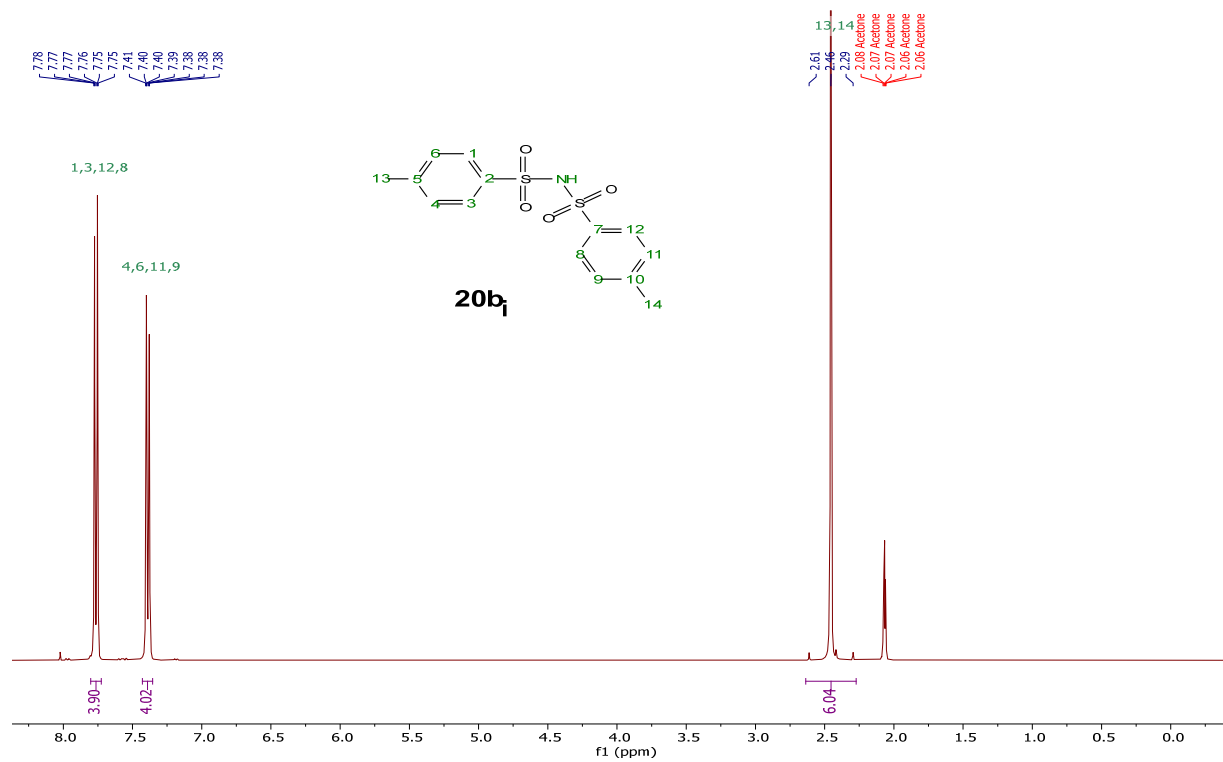
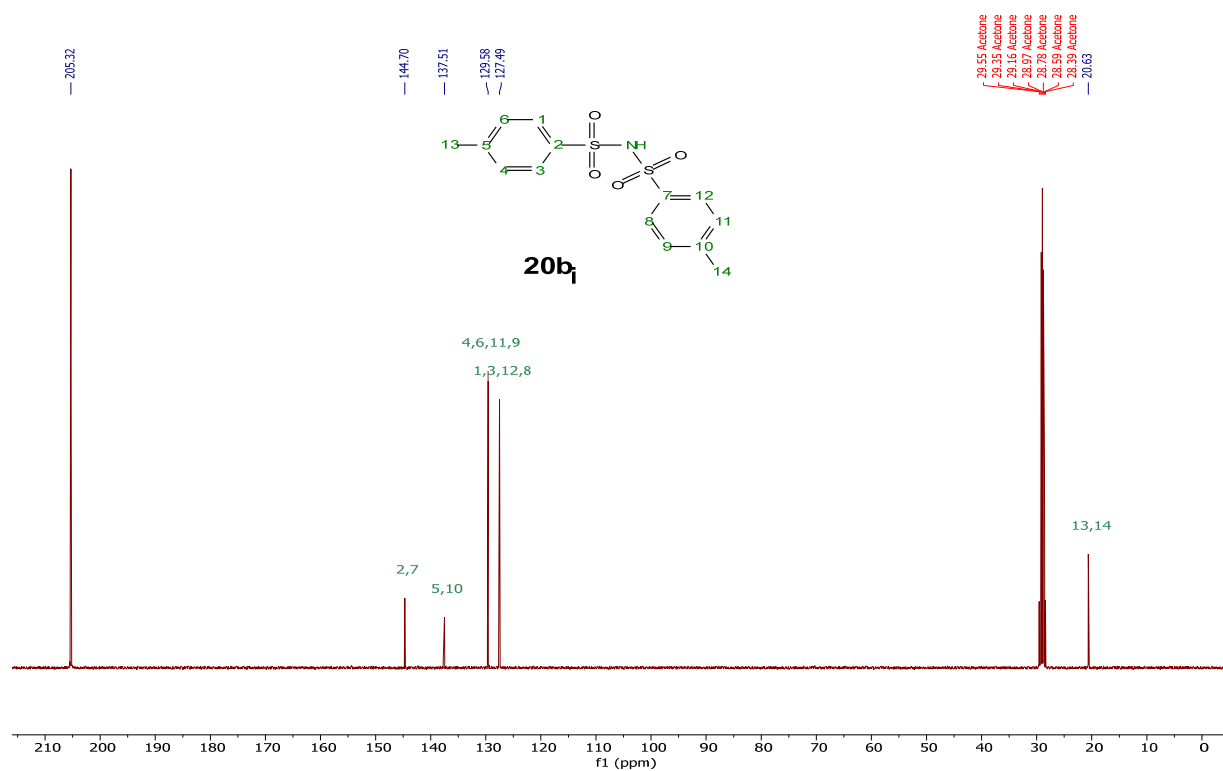
[Na][NPh<sub>2</sub>], **20a<sub>ii</sub>**

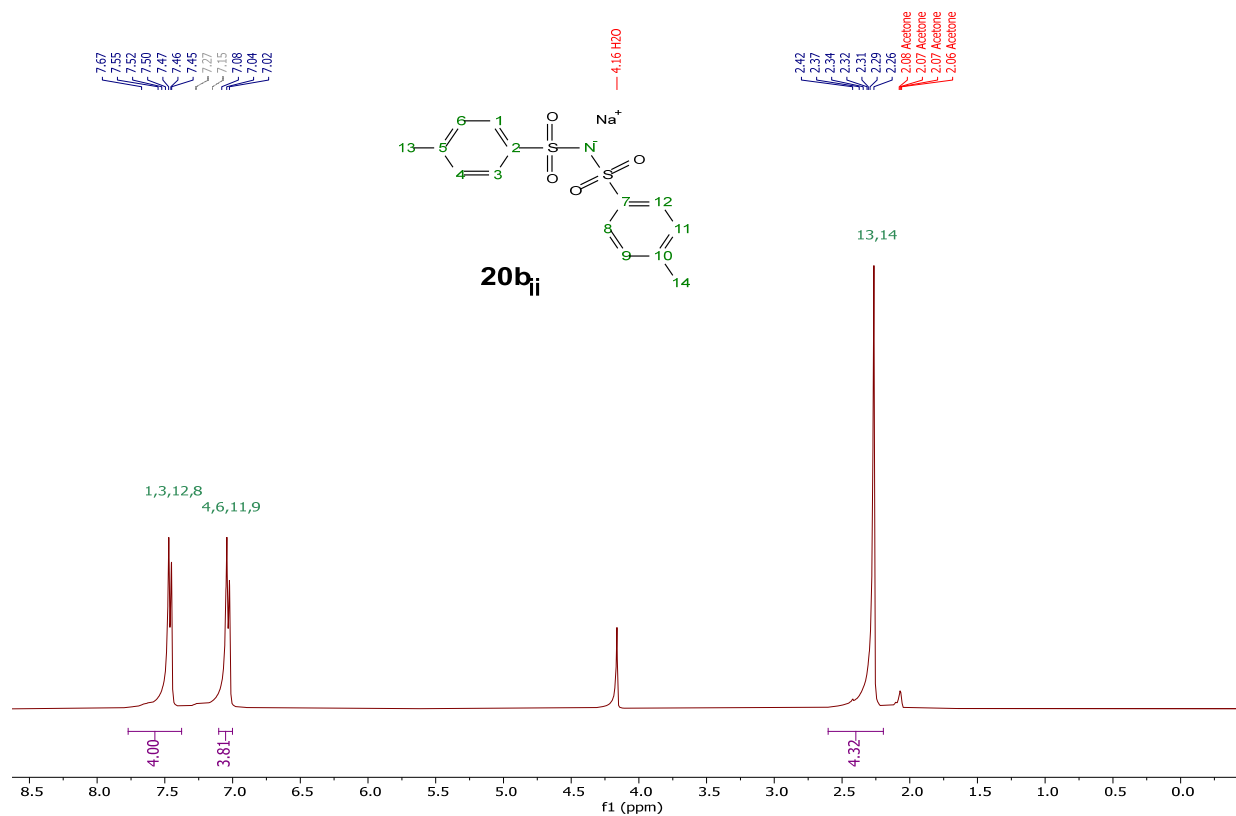
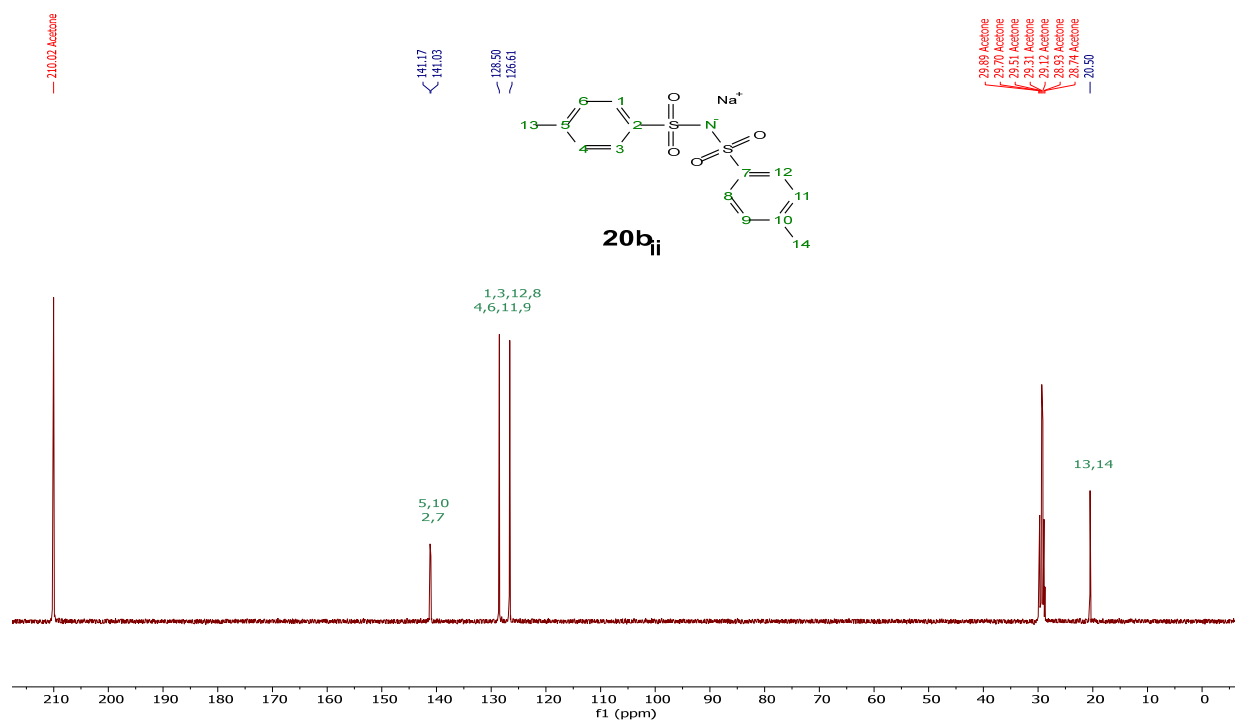
<sup>1</sup>H NMR (400 MHz, Deuterium Oxide)

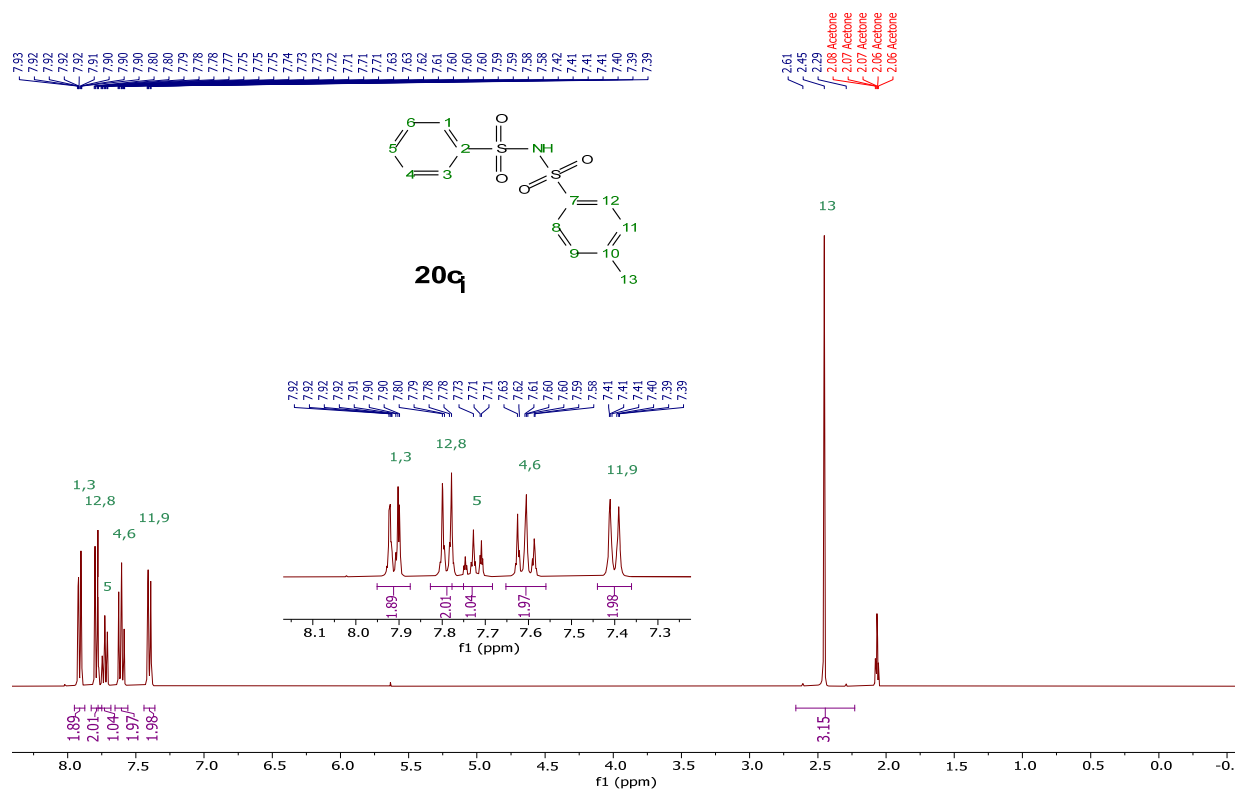
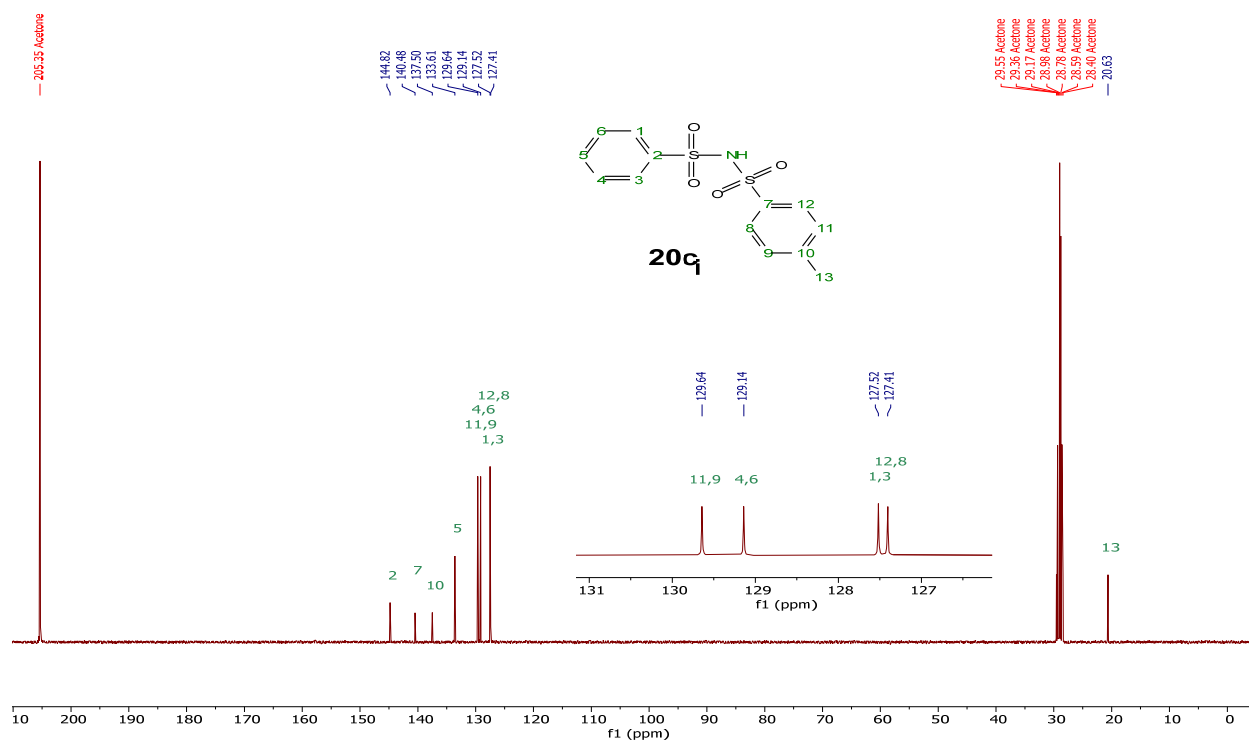


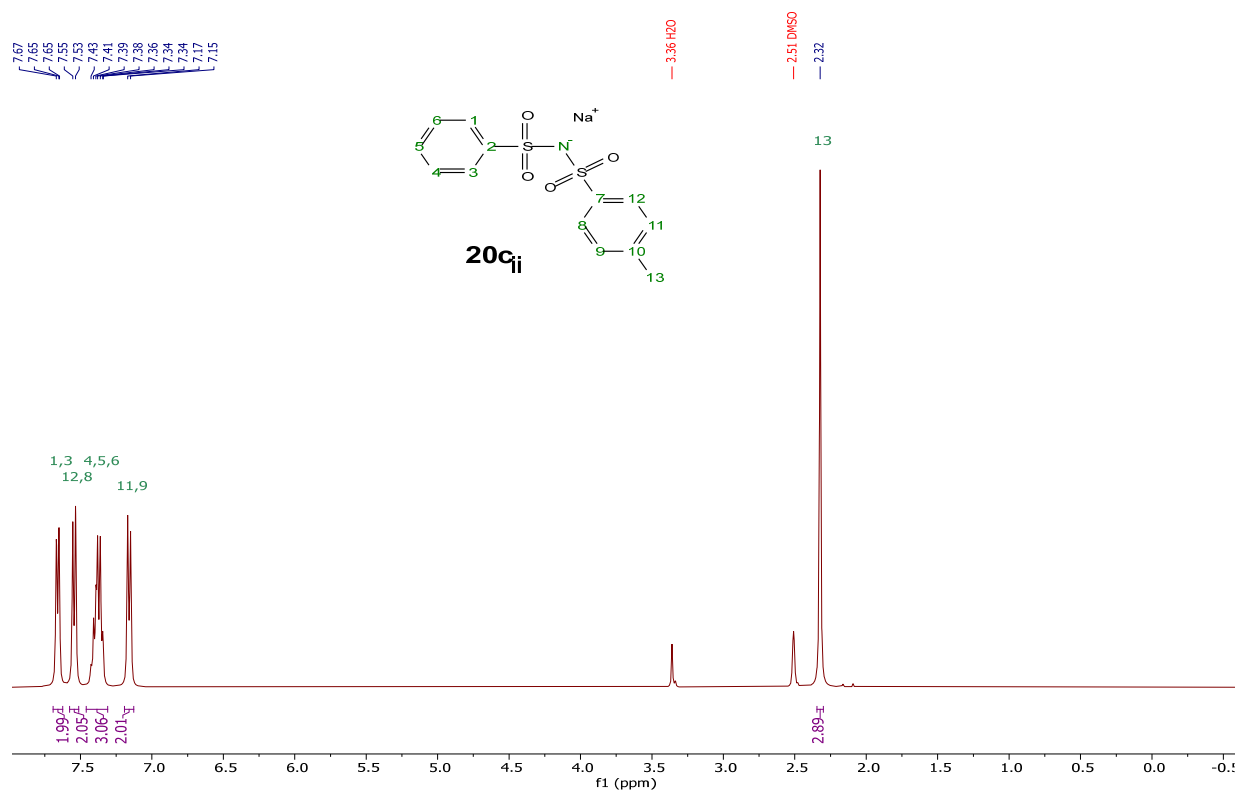
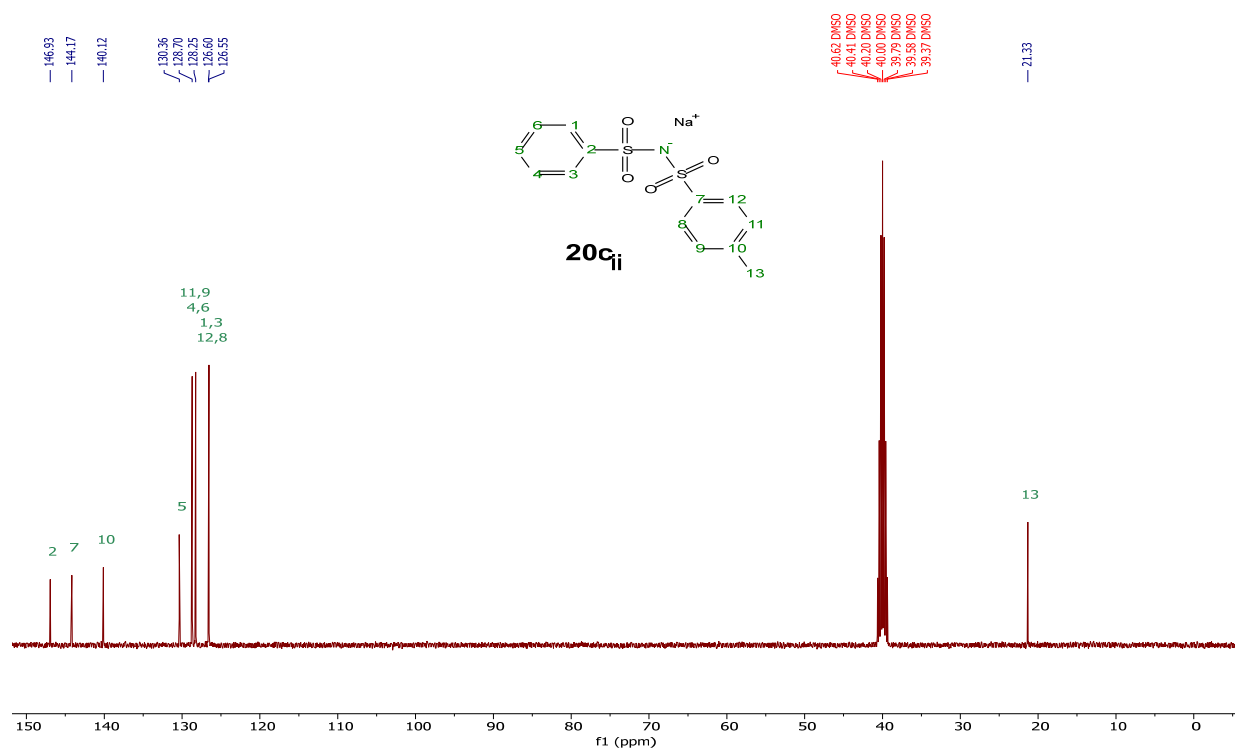
<sup>13</sup>C{<sup>1</sup>H} NMR (101 MHz, Deuterium Oxide)



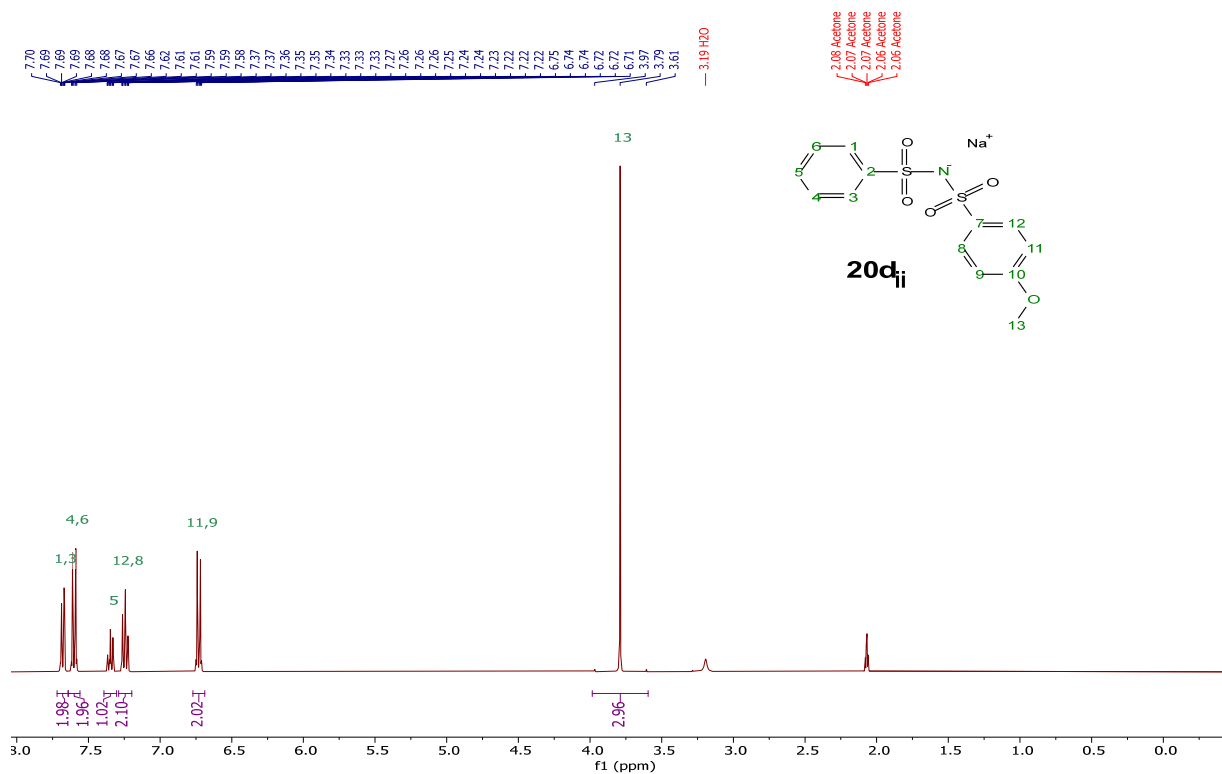
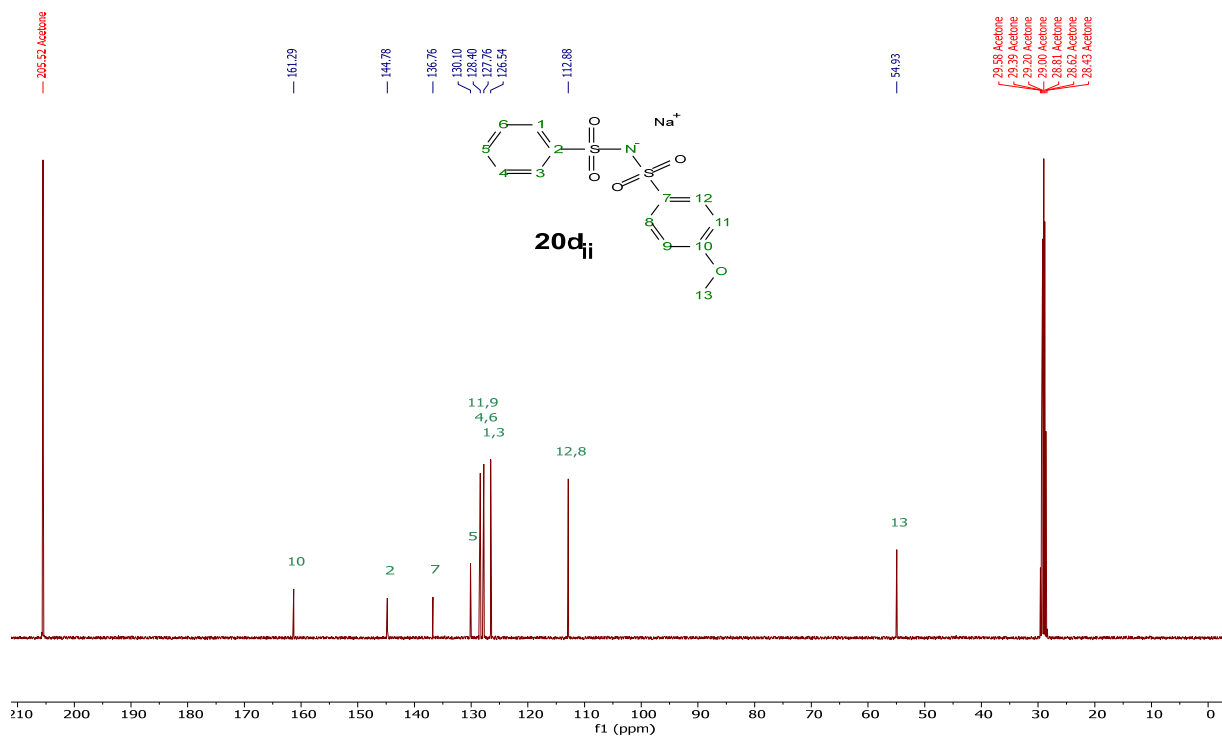
**20b<sub>i</sub>**<sup>1</sup>H NMR (400 MHz, Acetone-d<sub>6</sub>)<sup>13</sup>C{<sup>1</sup>H} NMR (101 MHz, Acetone-d<sub>6</sub>)

[Na][NTs<sub>2</sub>], **20b<sub>ii</sub>**<sup>1</sup>H NMR (400 MHz, Acetone-d<sub>6</sub>)<sup>13</sup>C{<sup>1</sup>H} NMR (101 MHz, Acetone-d<sub>6</sub>)

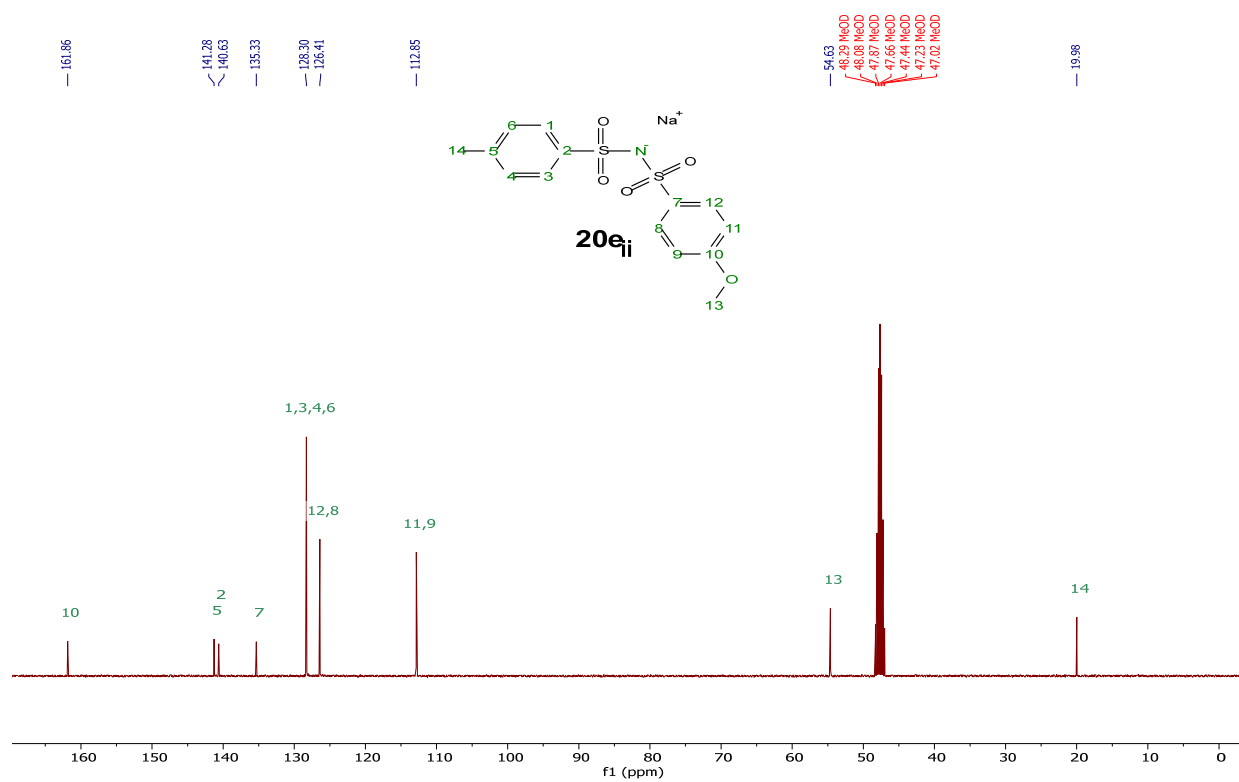
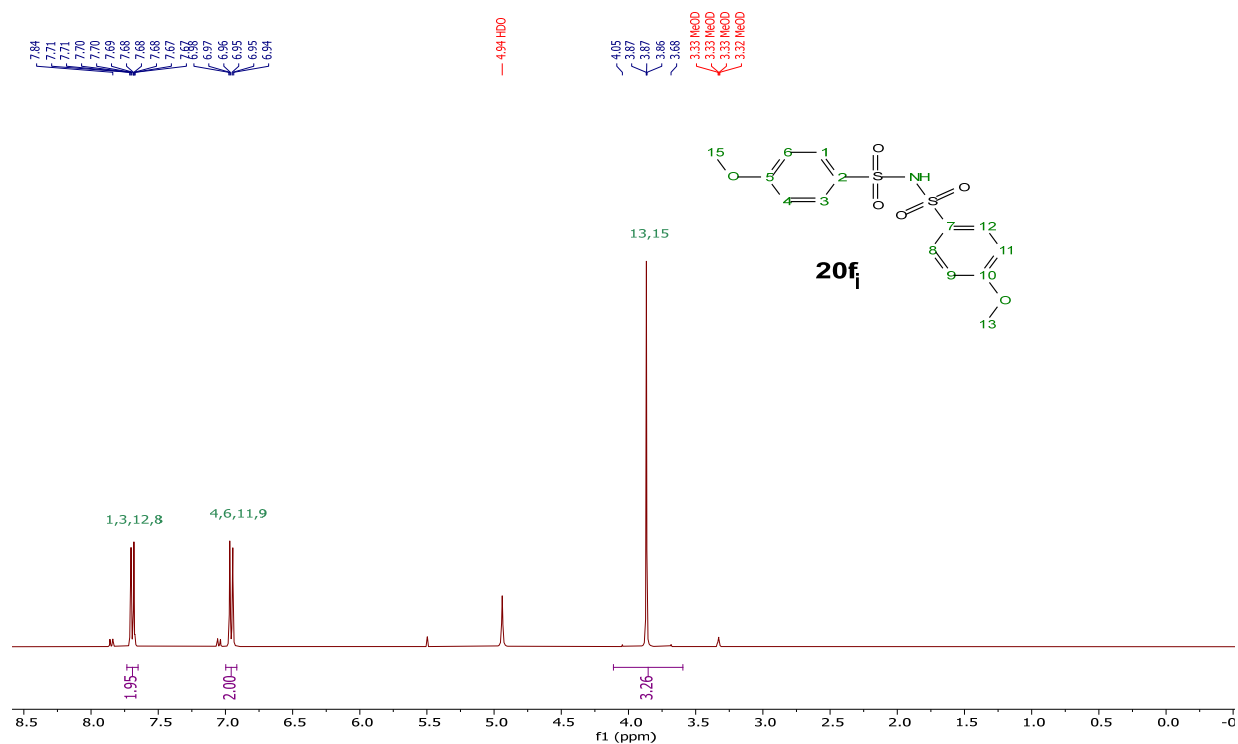
**20c<sub>i</sub>**<sup>1</sup>H NMR (400 MHz, Acetone-d<sub>6</sub>)<sup>13</sup>C {<sup>1</sup>H} NMR (101 MHz, Acetone-d<sub>6</sub>)

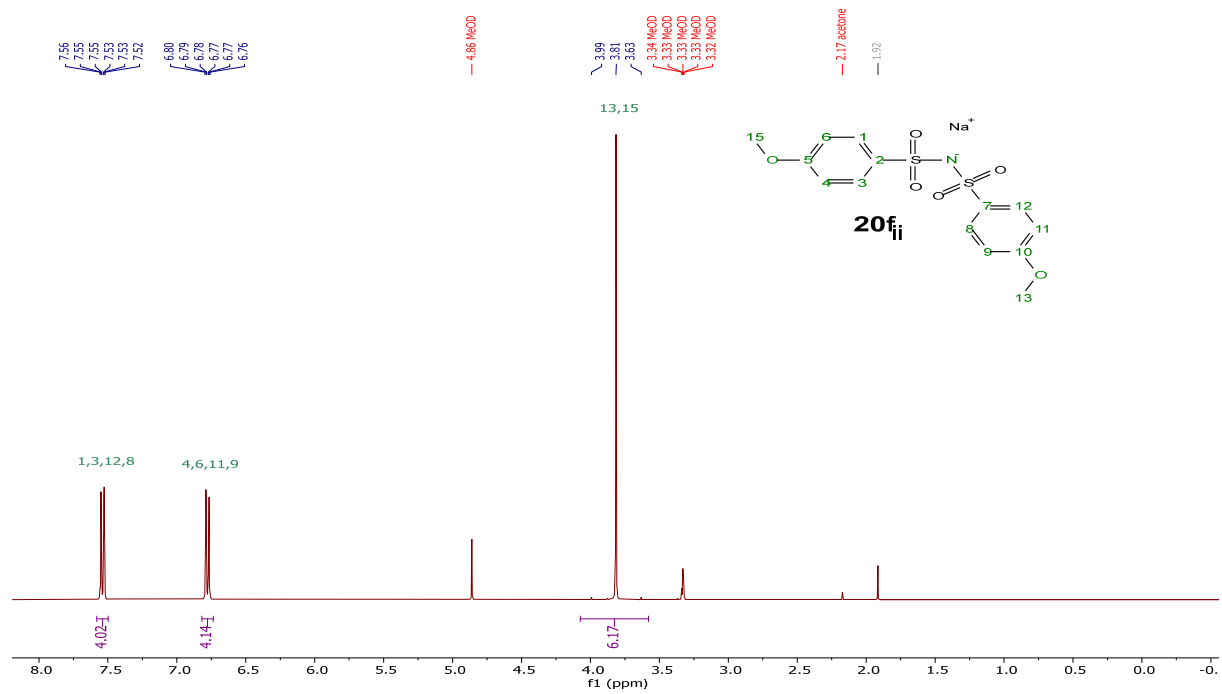
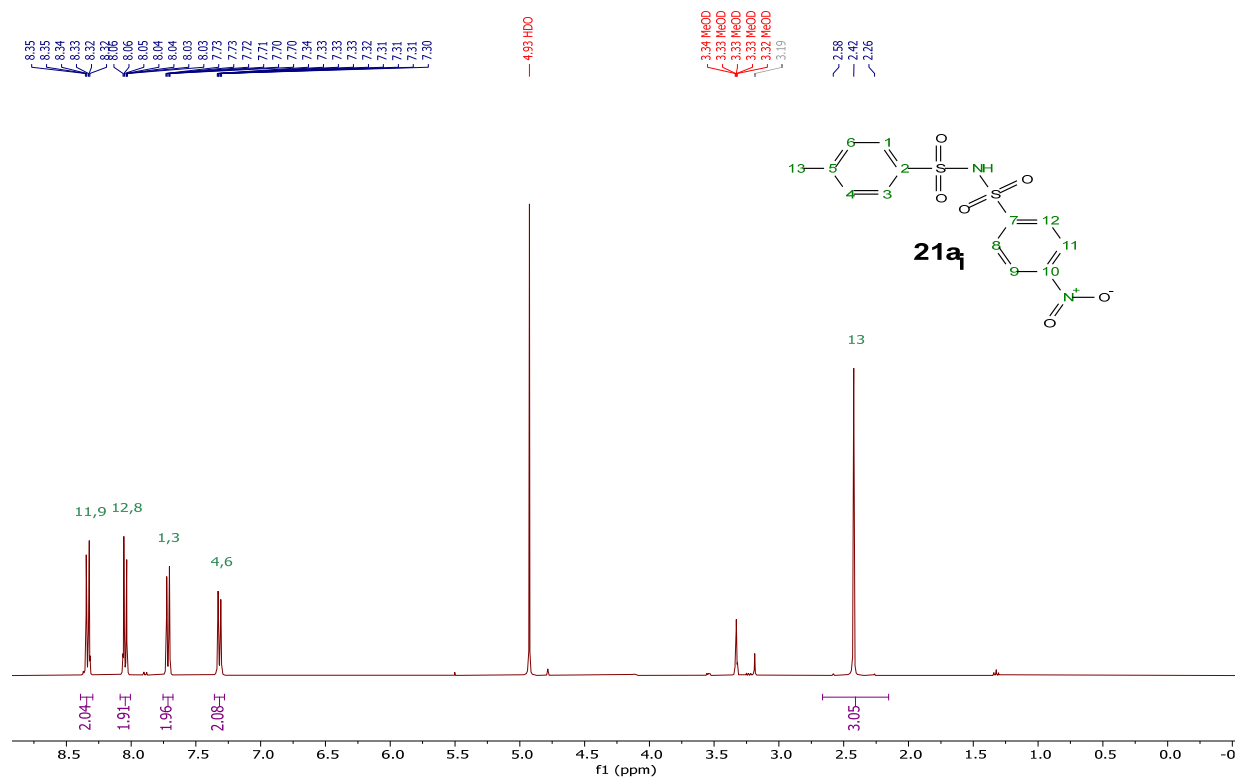
[Na][PhNTs], **20c<sub>ii</sub>**<sup>1</sup>H NMR (400 MHz, Acetone-d<sub>6</sub>)<sup>13</sup>C{<sup>1</sup>H} NMR (101 MHz, Acetone-d<sub>6</sub>)

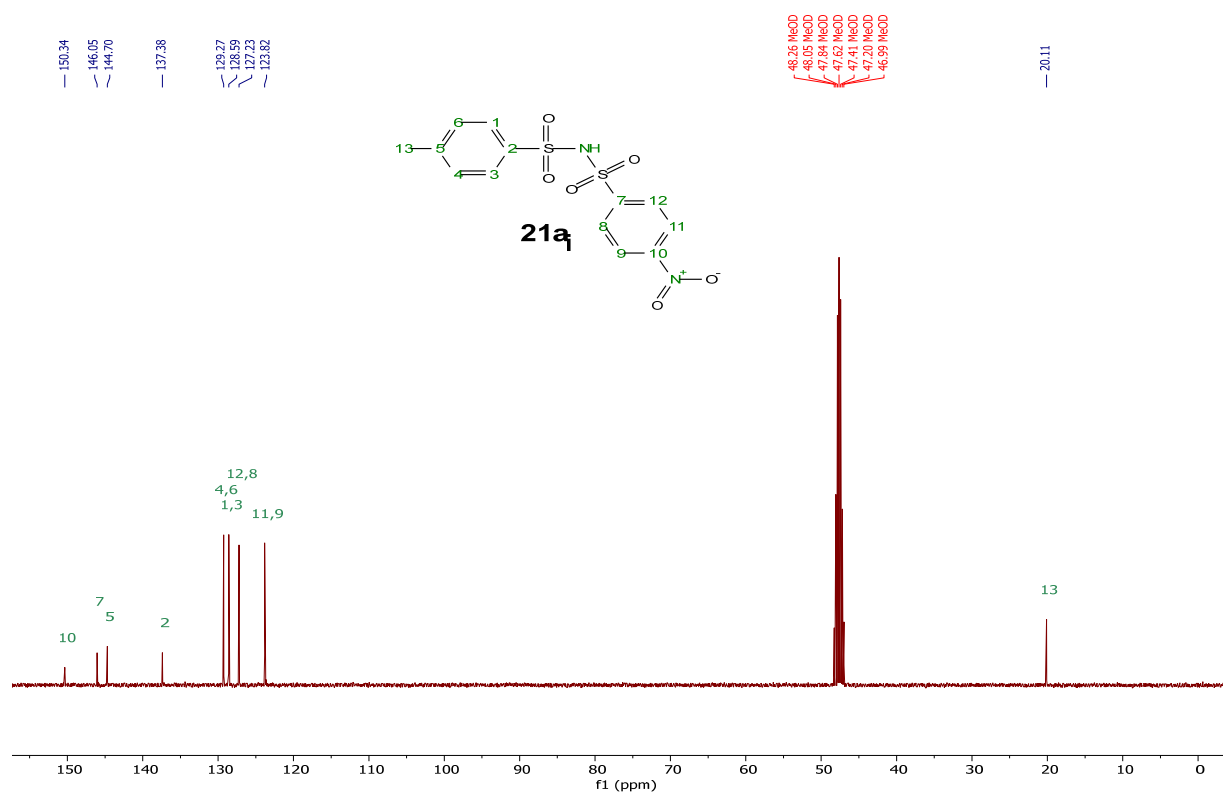
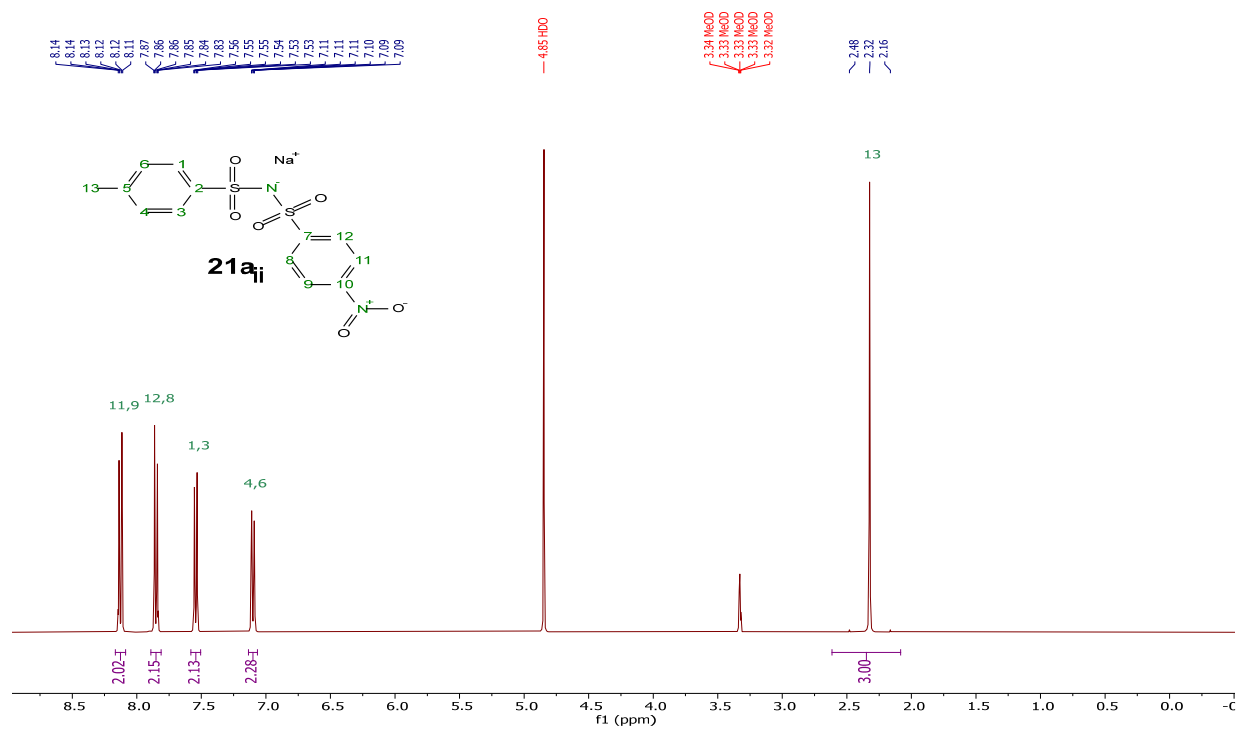


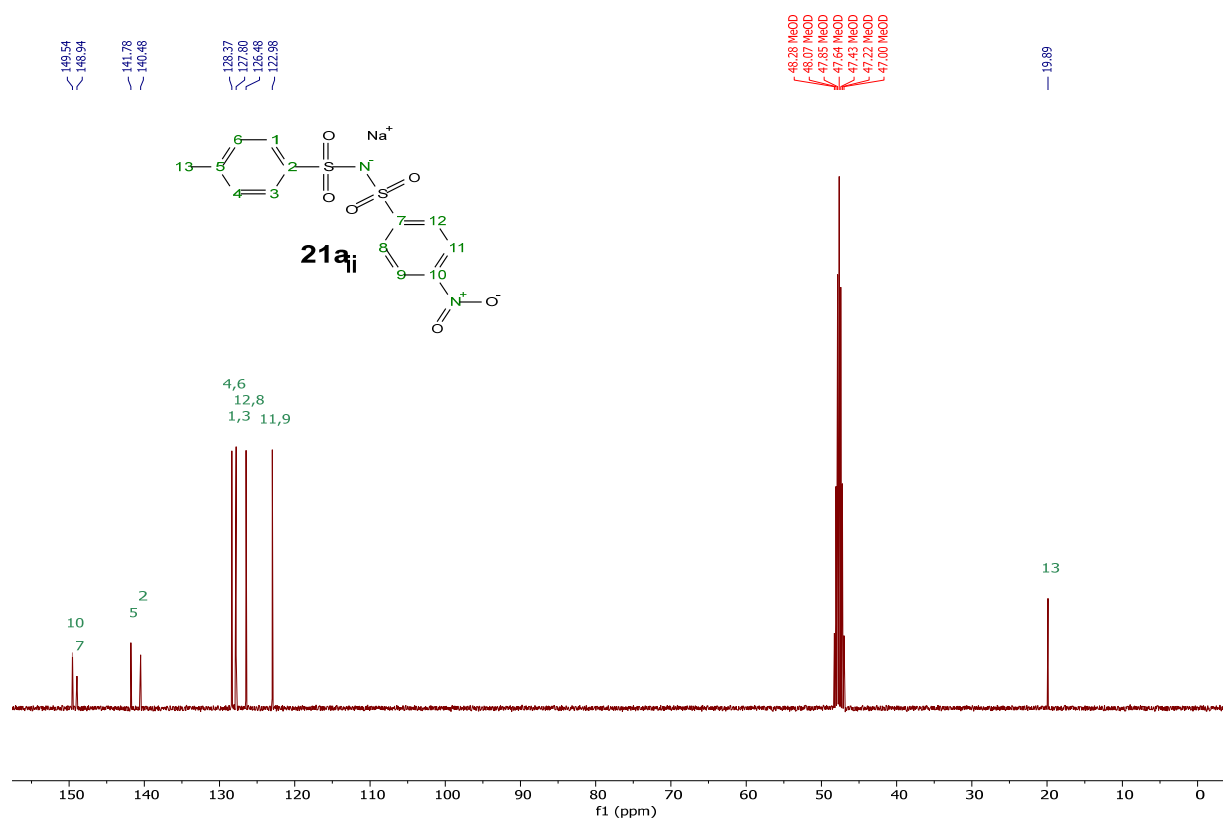
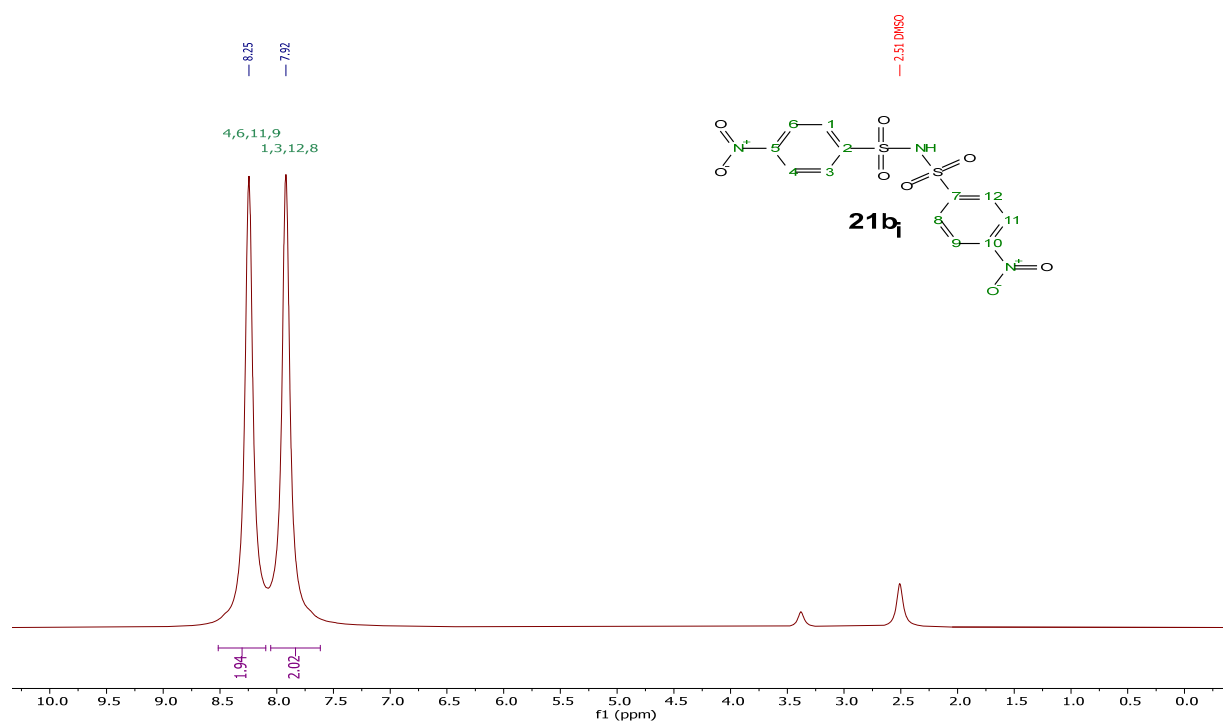
[Na][MBNPh], **20d<sub>ii</sub>**<sup>1</sup>H NMR (400 MHz, Acetone-d<sub>6</sub>)<sup>13</sup>C{<sup>1</sup>H} NMR (101 MHz, Acetone-d<sub>6</sub>)



$^{13}\text{C}\{^1\text{H}\}$  NMR (101 MHz, Methanol-d<sub>4</sub>)**20f<sub>i</sub>** $^1\text{H}$  NMR (400 MHz, Methanol-d<sub>4</sub>)

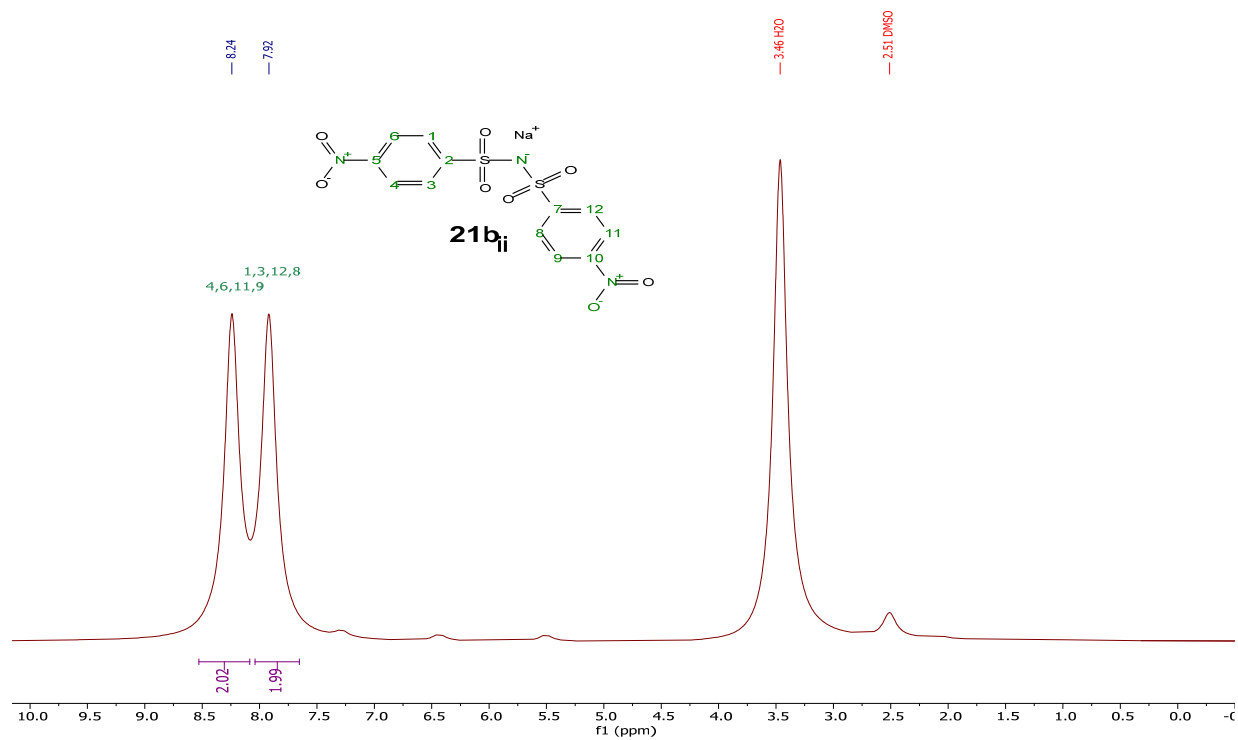
[Na][N(MB)<sub>2</sub>], **20f<sub>ii</sub>**<sup>1</sup>H NMR (400 MHz, Methanol-d<sub>4</sub>)**21a<sub>i</sub>**<sup>1</sup>H NMR (400 MHz, Methanol-d<sub>4</sub>)

$^{13}\text{C}\{^1\text{H}\}$  NMR (101 MHz, Methanol-d<sub>4</sub>)[Na][NBNTs], **21a<sub>ii</sub>** $^1\text{H}$  NMR (400 MHz, Methanol-d<sub>4</sub>)

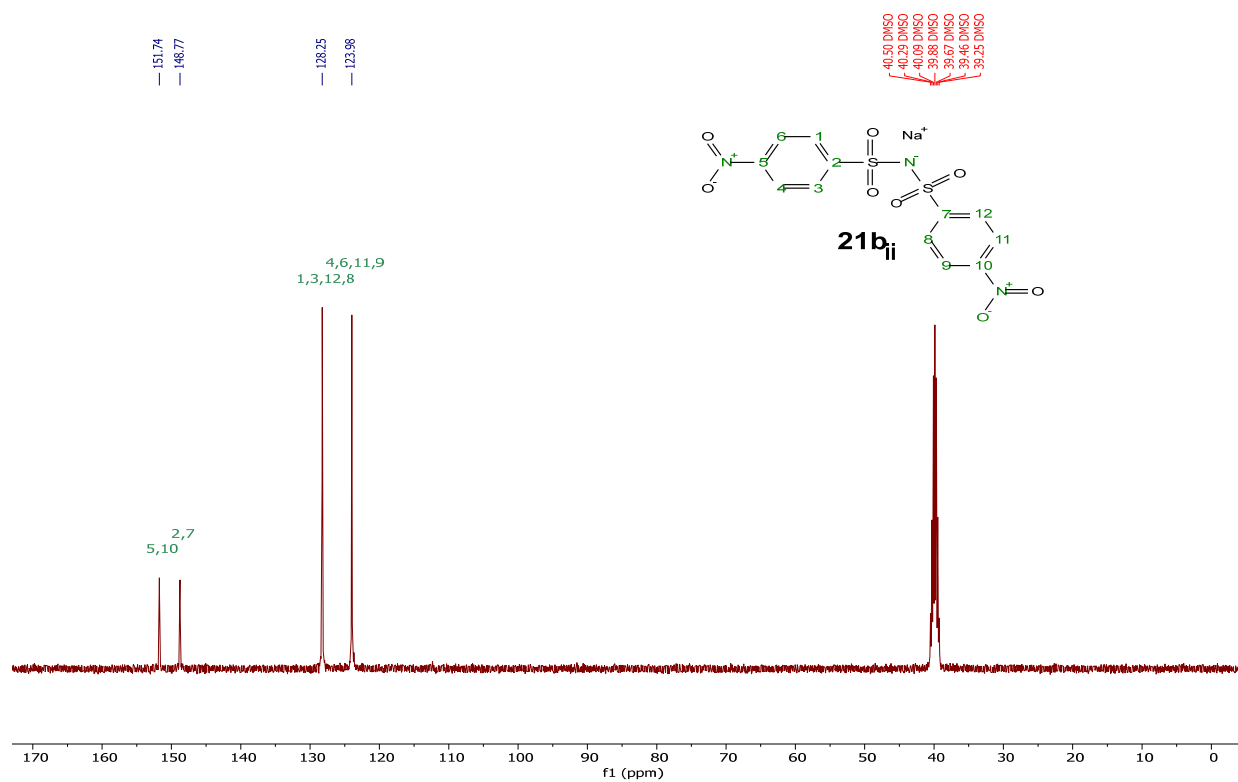
$^{13}\text{C}\{^1\text{H}\}$  NMR (101 MHz, Methanol-d<sub>4</sub>)**21b<sub>i</sub>** $^1\text{H}$  NMR (400 MHz, DMSO-d<sub>6</sub>)

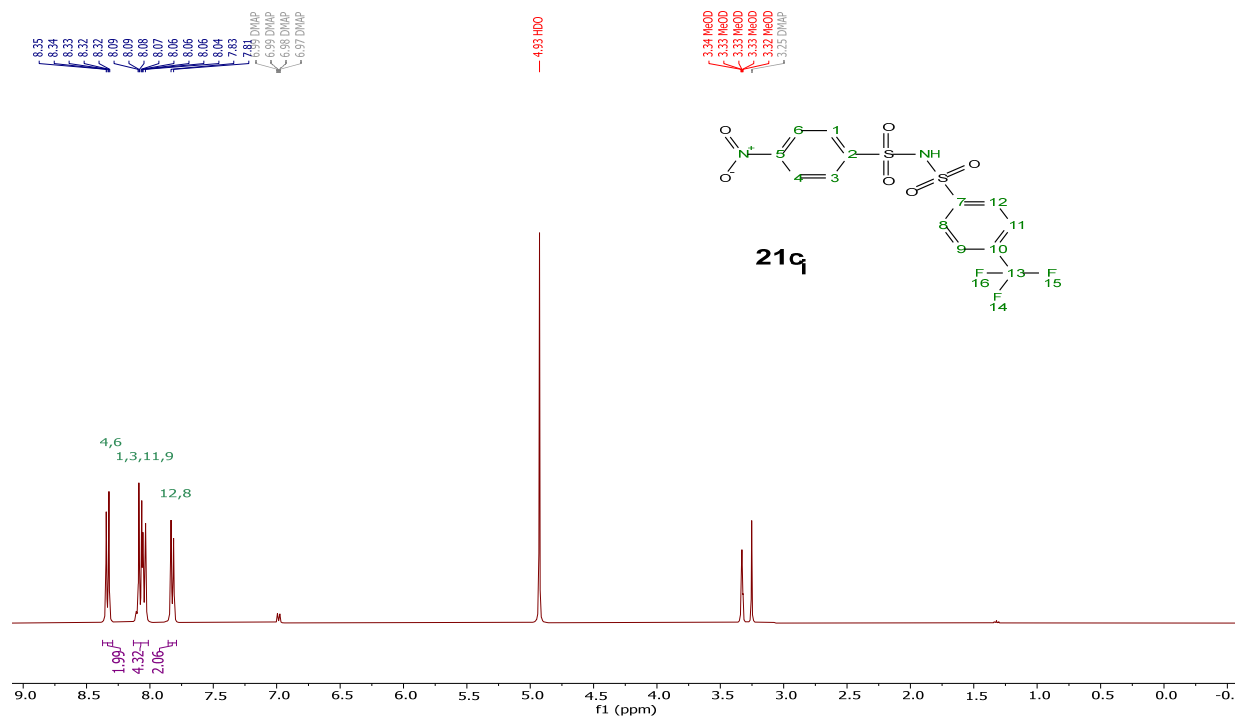
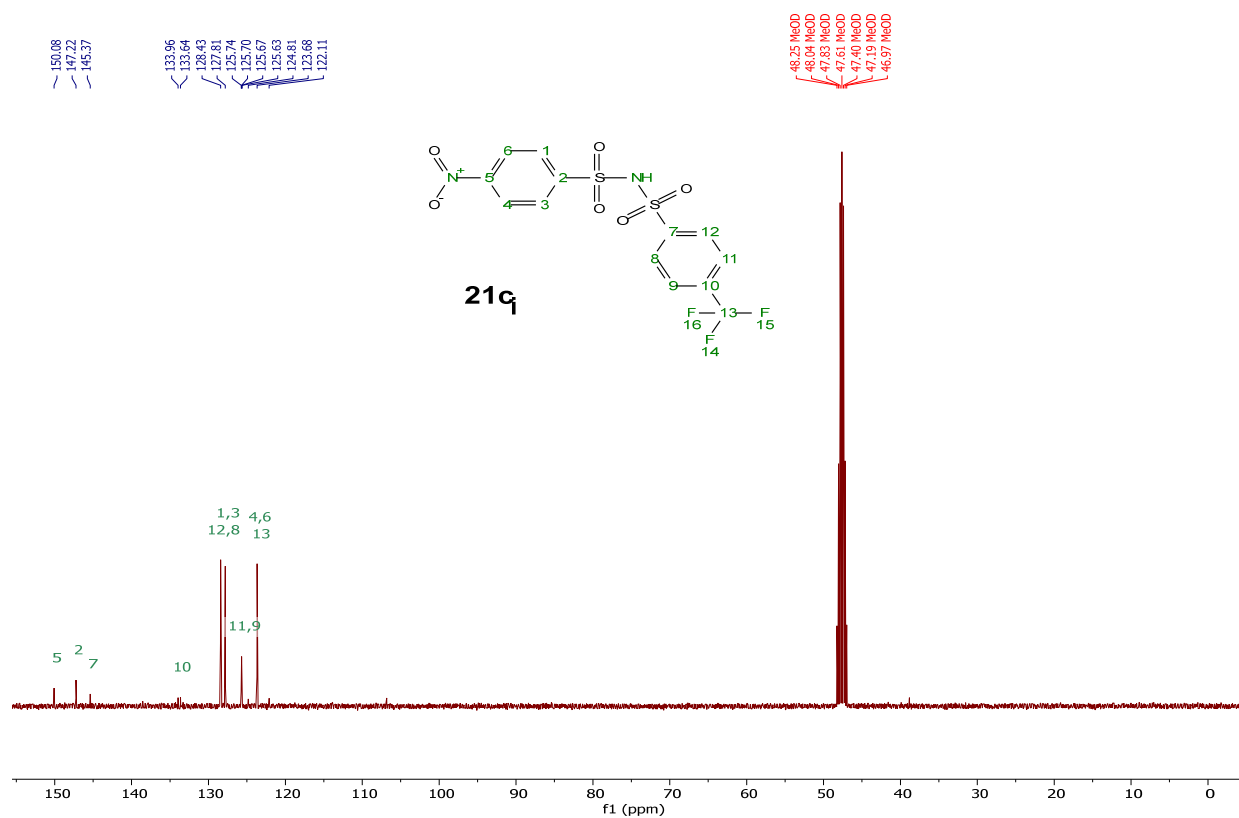
[Na][N(NB)<sub>2</sub>], **21b<sub>ii</sub>**

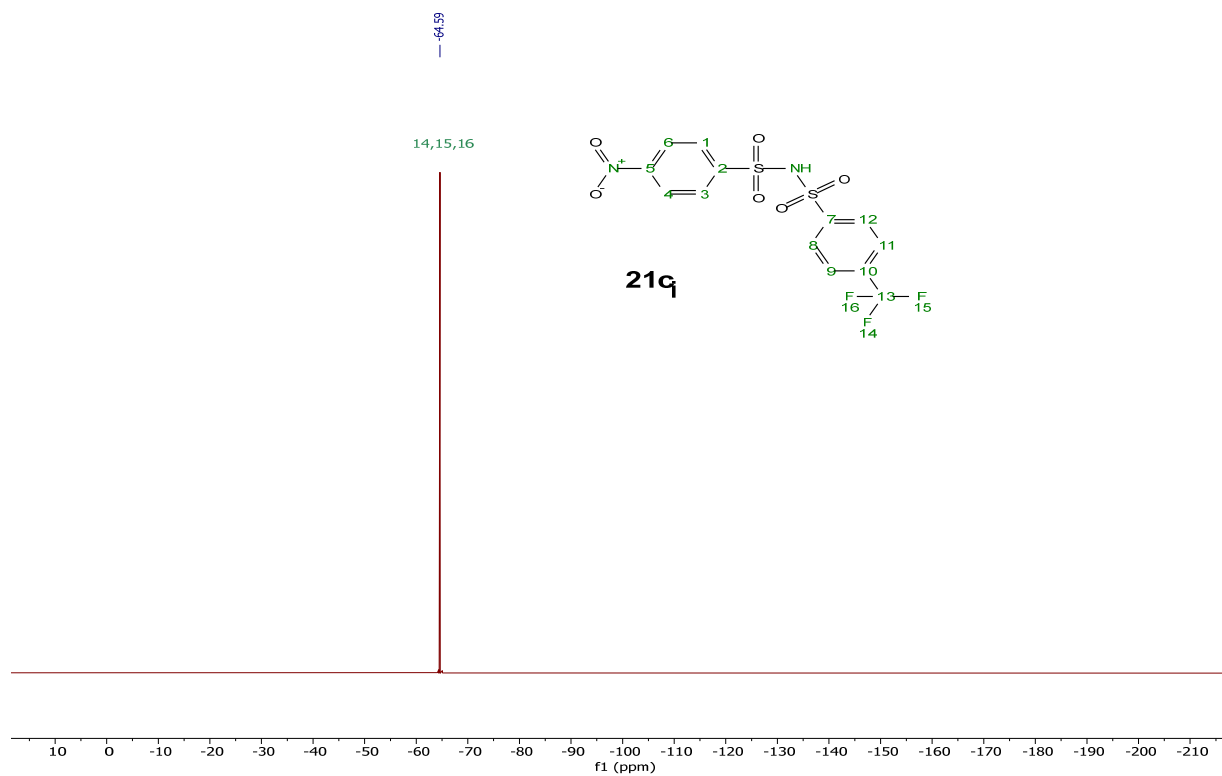
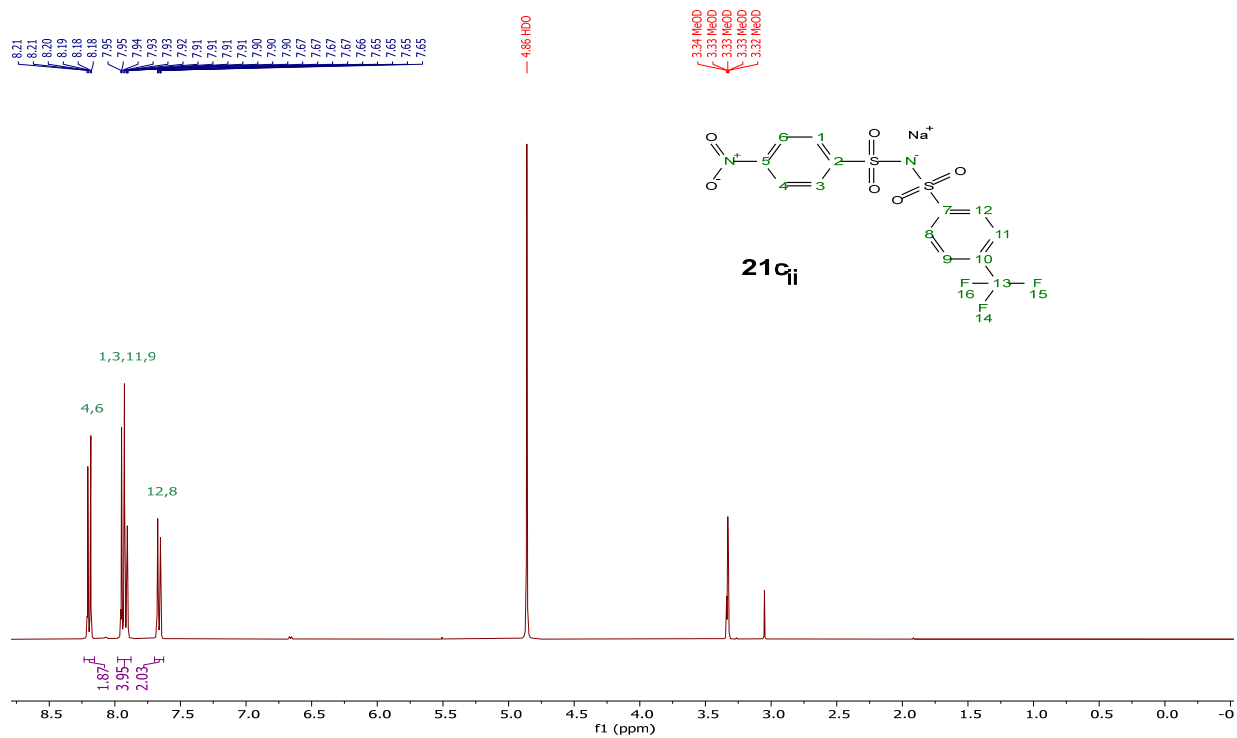
<sup>1</sup>H NMR (400 MHz, DMSO-d<sub>6</sub>)

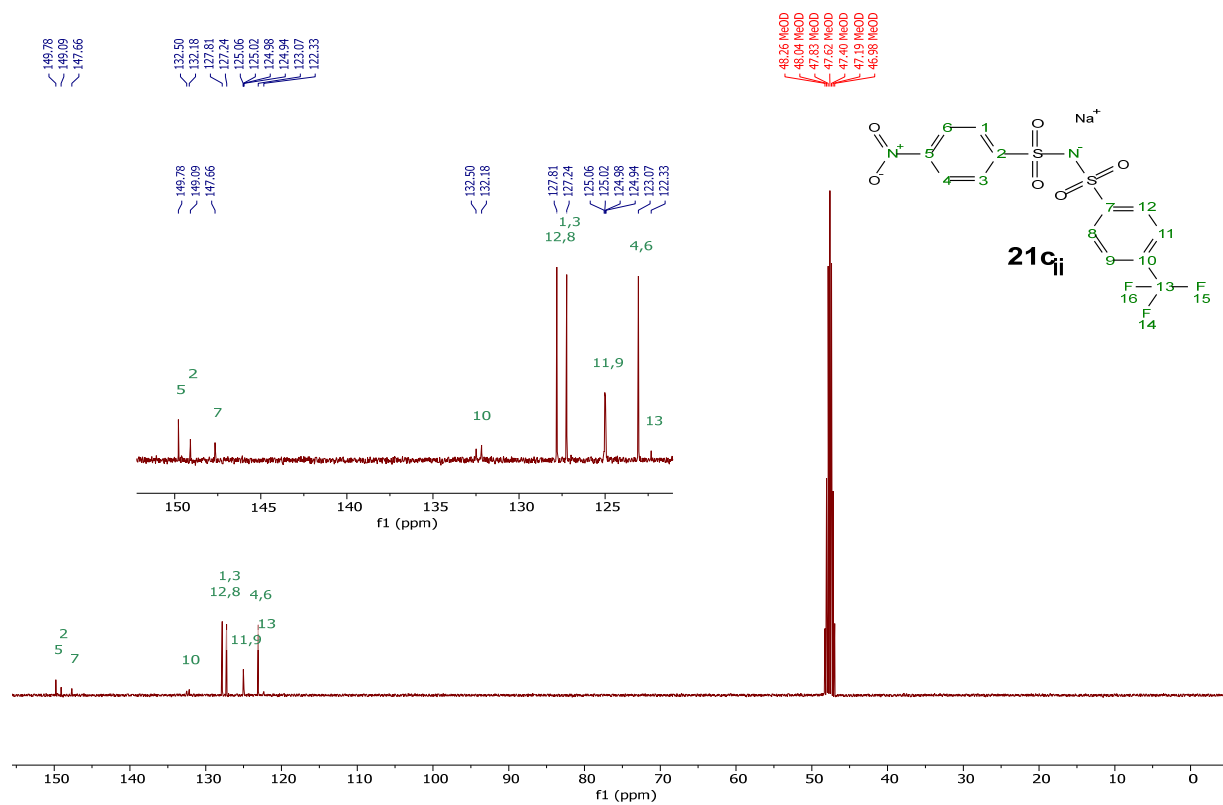
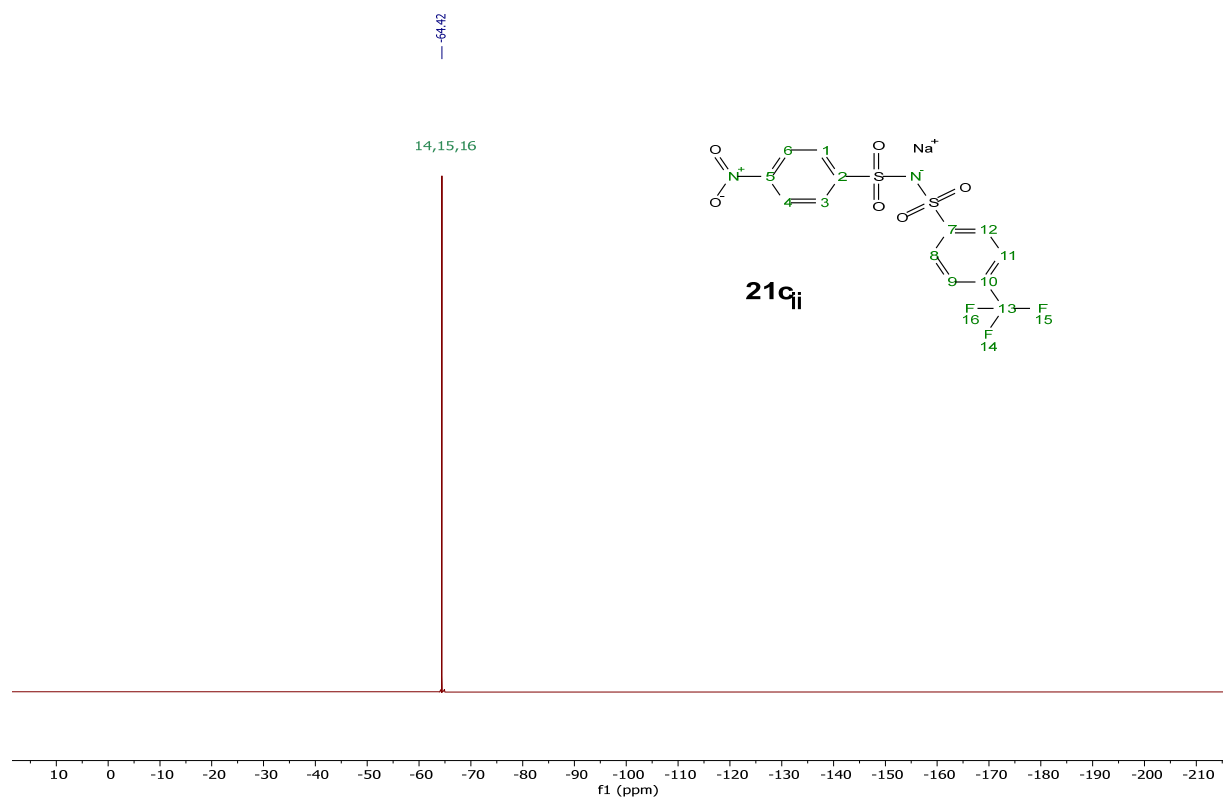


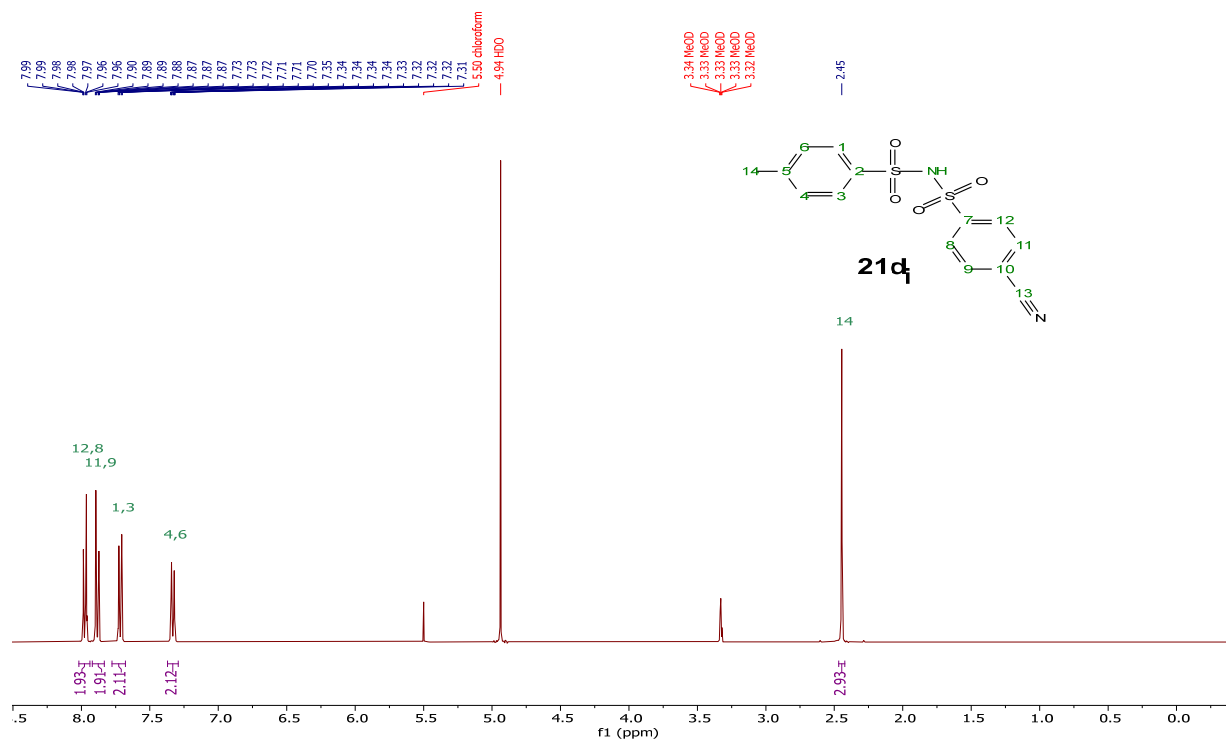
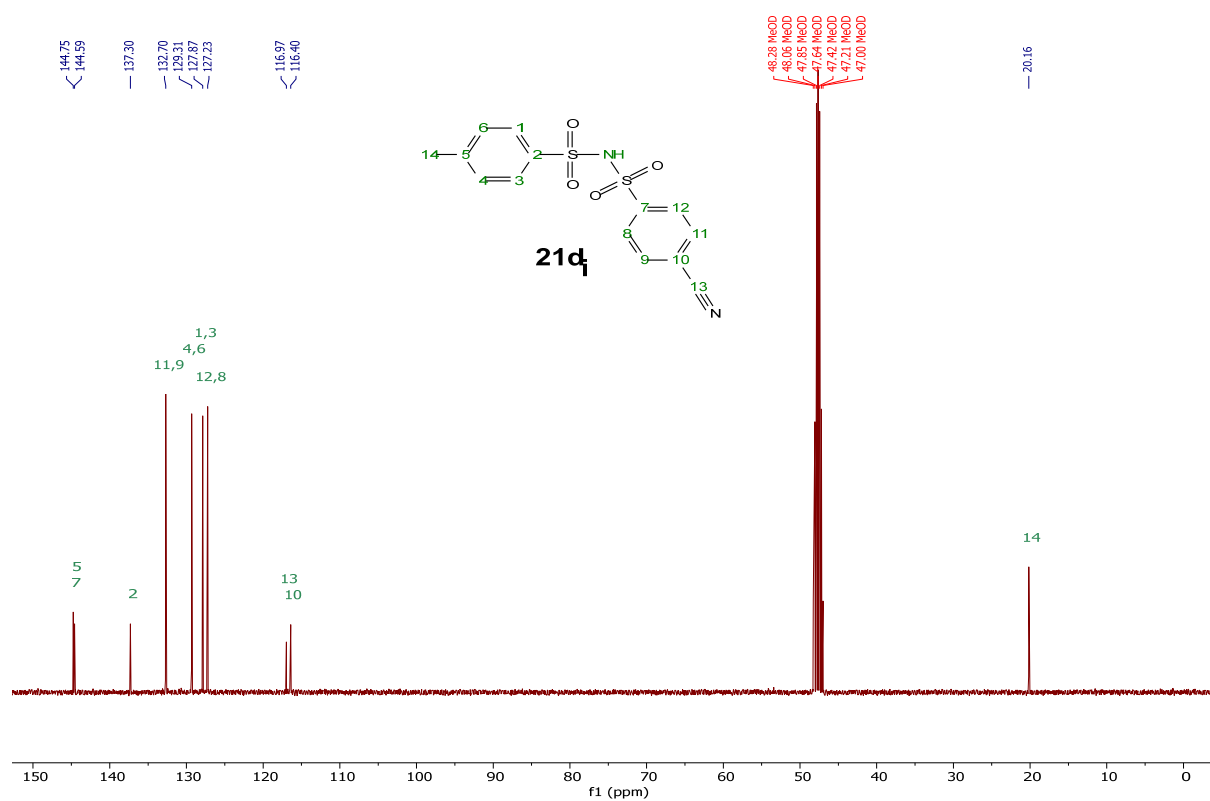
<sup>13</sup>C {<sup>1</sup>H} NMR (101 MHz, DMSO-d<sub>6</sub>)

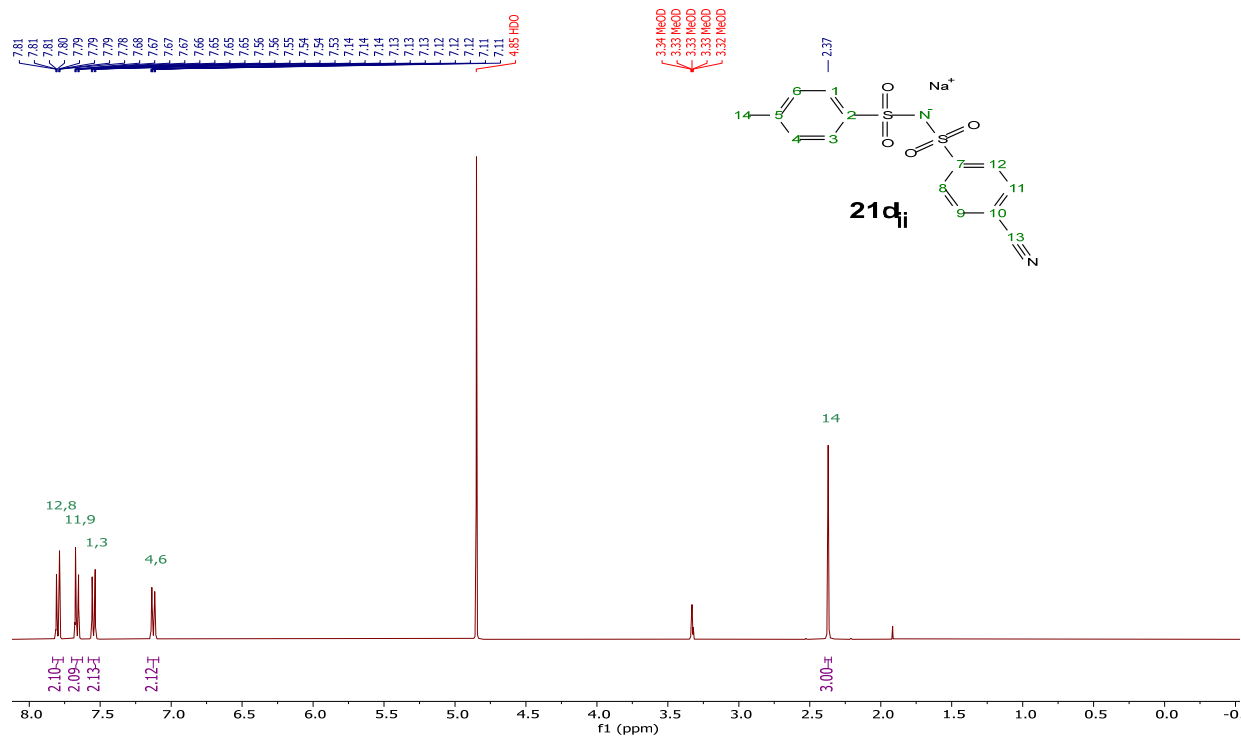
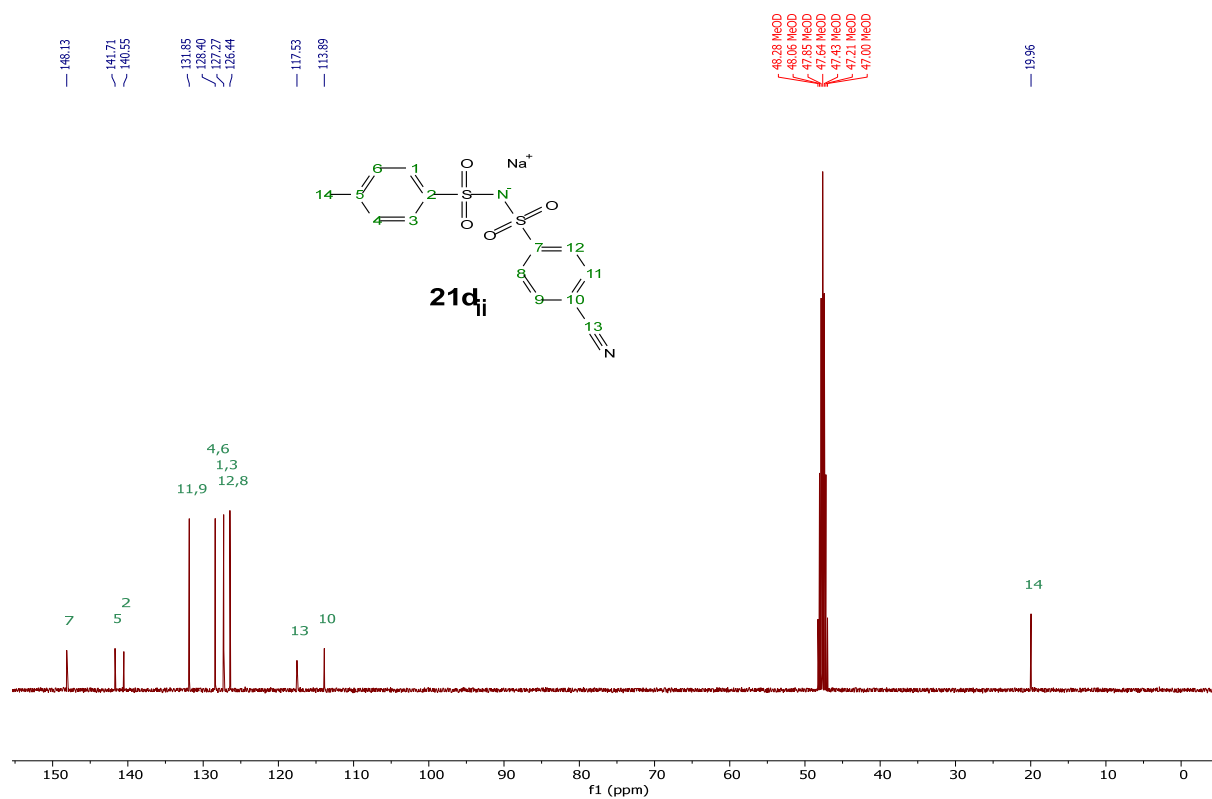


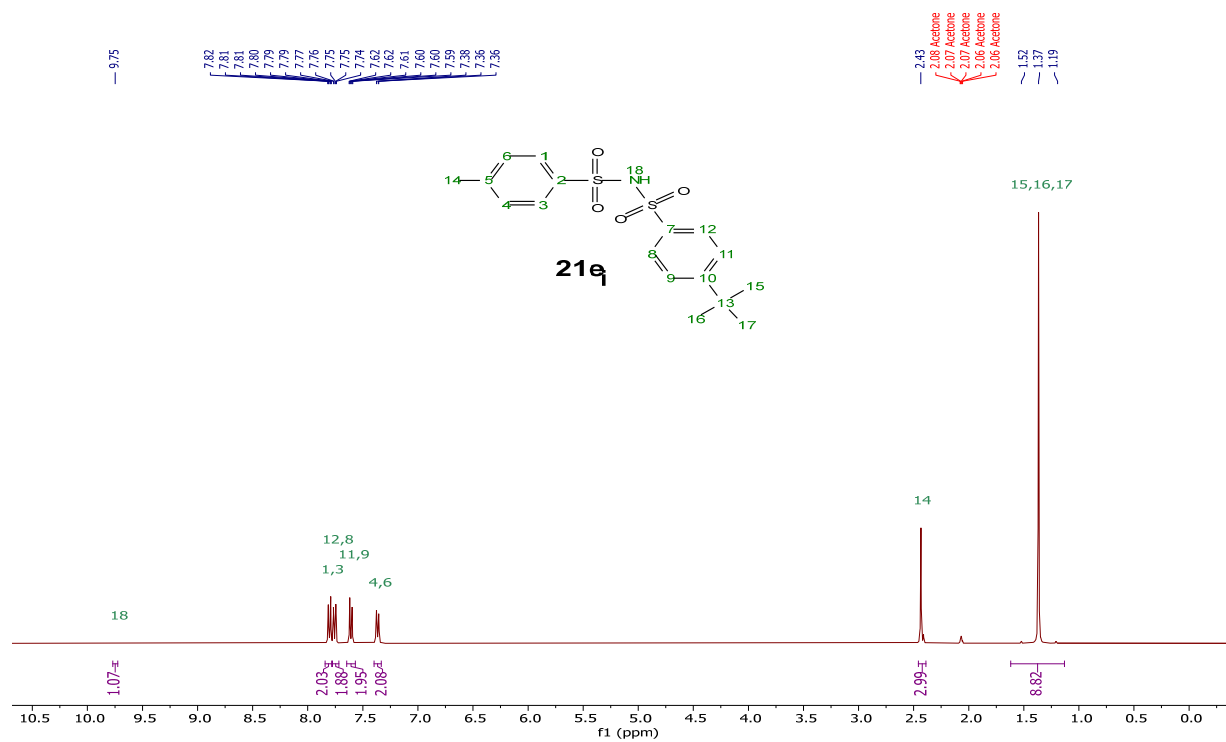
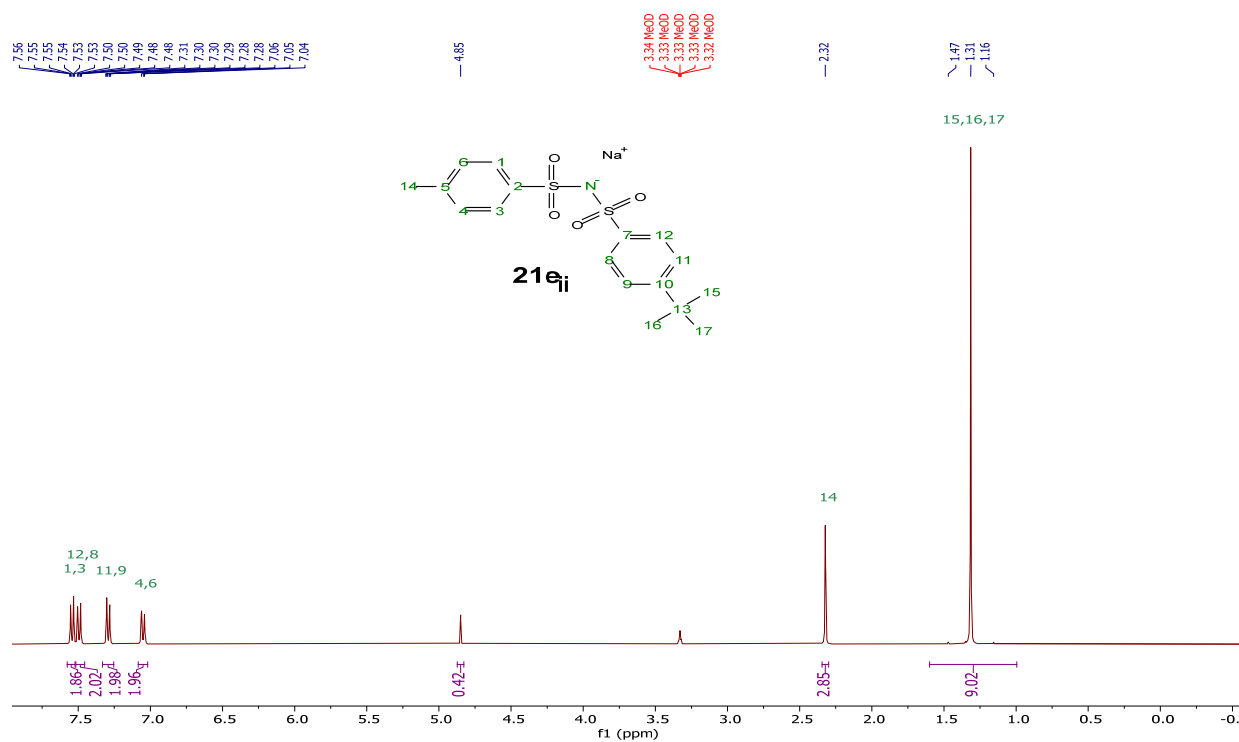
**21c<sub>i</sub>**<sup>1</sup>H NMR (400 MHz, Methanol-d<sub>4</sub>)<sup>13</sup>C{<sup>1</sup>H} NMR (101 MHz, Methanol-d<sub>4</sub>)

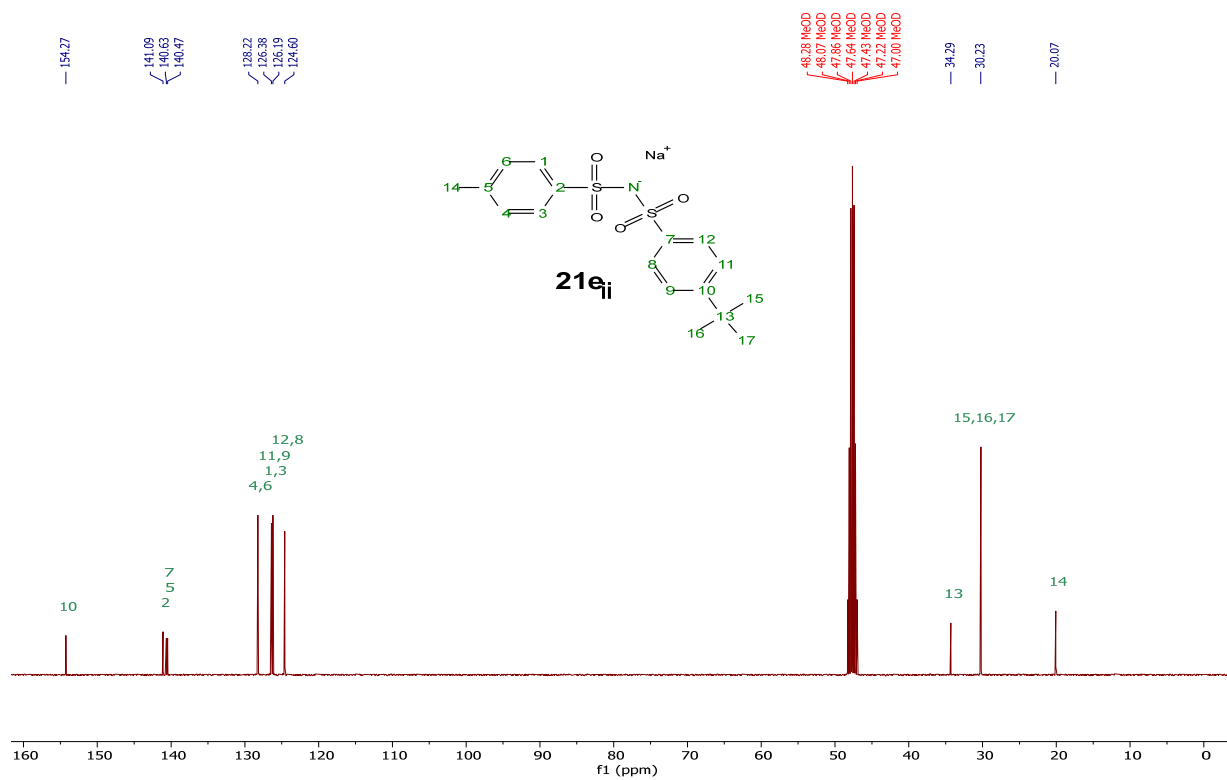
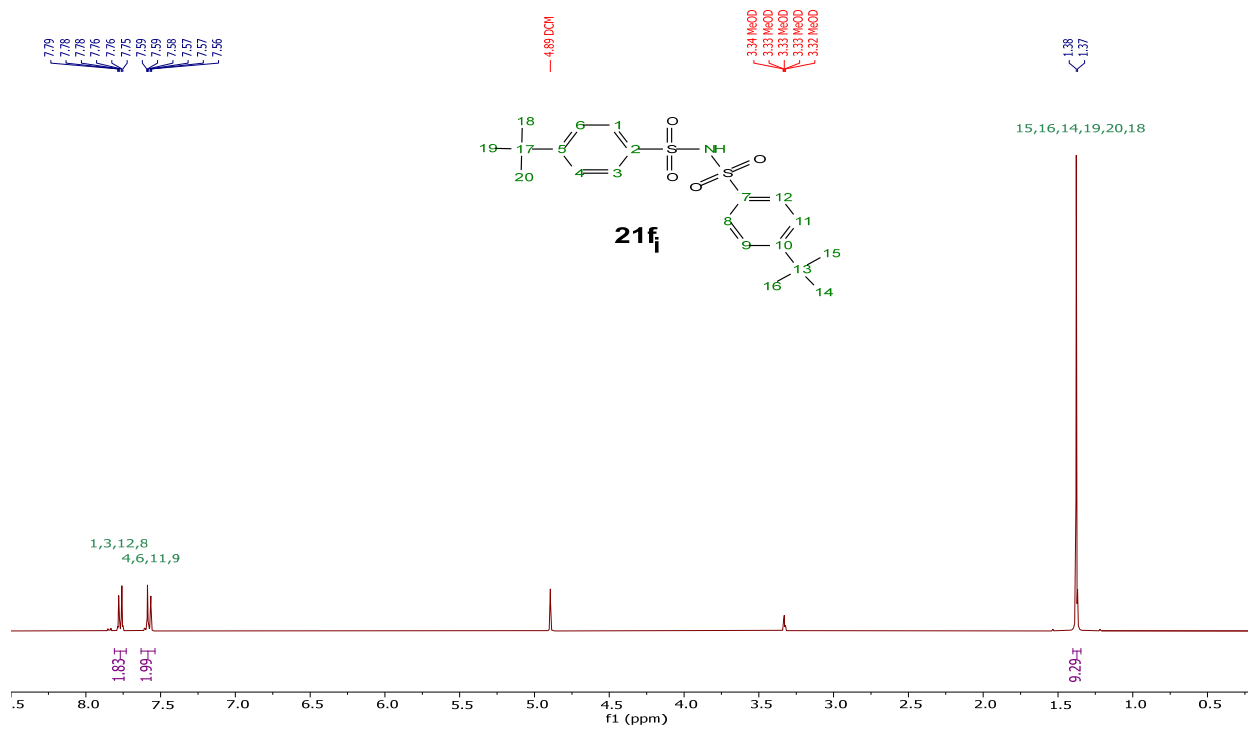
$^{19}\text{F}$  NMR (376 MHz, Methanol- $d_4$ )[Na][NBNTFMB], **21c<sub>ii</sub>** $^1\text{H}$  NMR (400 MHz, Methanol- $d_4$ )

$^{13}\text{C}\{^1\text{H}\}$  NMR (101 MHz, Methanol-d<sub>4</sub>) $^{19}\text{F}$  NMR (376 MHz, Methanol-d<sub>4</sub>)

**21d<sub>i</sub>**<sup>1</sup>H NMR (400 MHz, Methanol-d<sub>4</sub>)<sup>13</sup>C {<sup>1</sup>H} NMR (101 MHz, Methanol-d<sub>4</sub>)

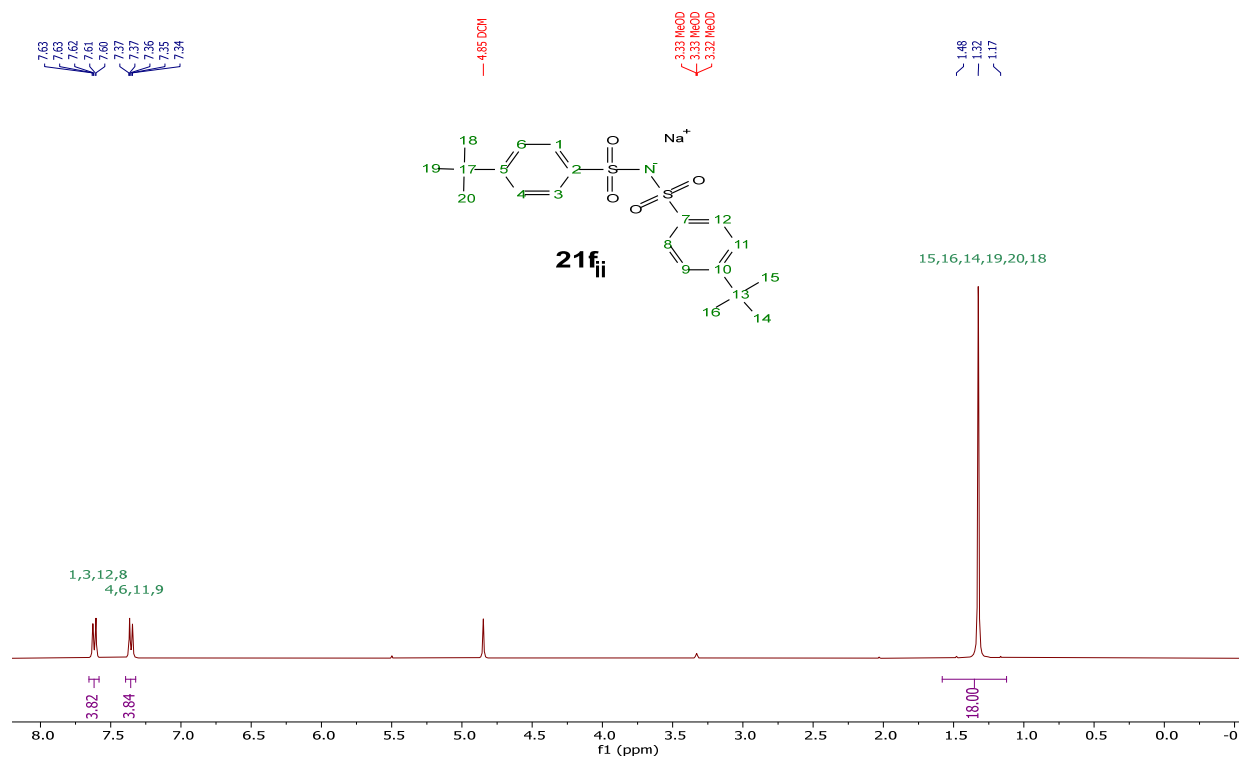
[Na][CBNTs], **21d<sub>ii</sub>**<sup>1</sup>H NMR (400 MHz, Methanol-d<sub>4</sub>)<sup>13</sup>C{<sup>1</sup>H} NMR (101 MHz, Methanol-d<sub>4</sub>)

**21e<sub>i</sub>**<sup>1</sup>H NMR (400 MHz, Acetone-d<sub>6</sub>)**[Na][tBBNTs], 21e<sub>ii</sub>**<sup>1</sup>H NMR (400 MHz, Methanol-d<sub>4</sub>)

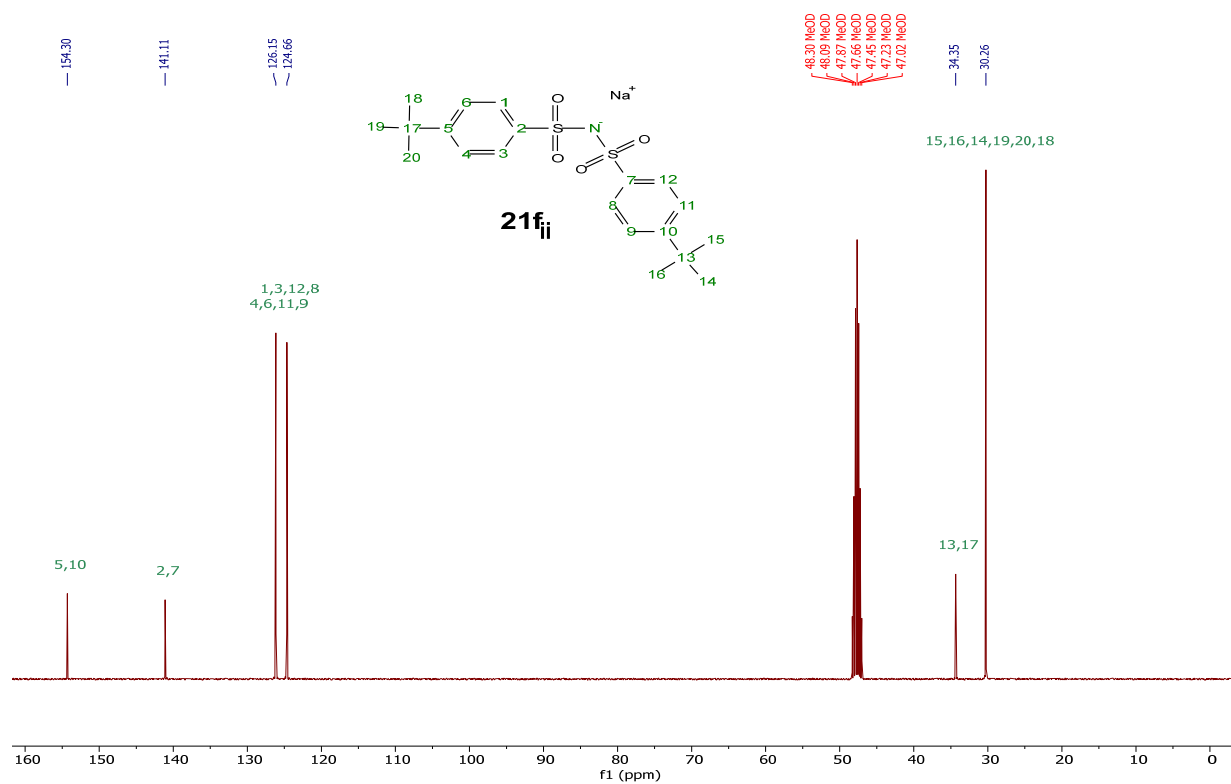
$^{13}\text{C}\{^1\text{H}\}$  NMR (101 MHz, Methanol-d<sub>4</sub>)**21f<sub>i</sub>** $^1\text{H}$  NMR (400 MHz, Methanol-d<sub>4</sub>)

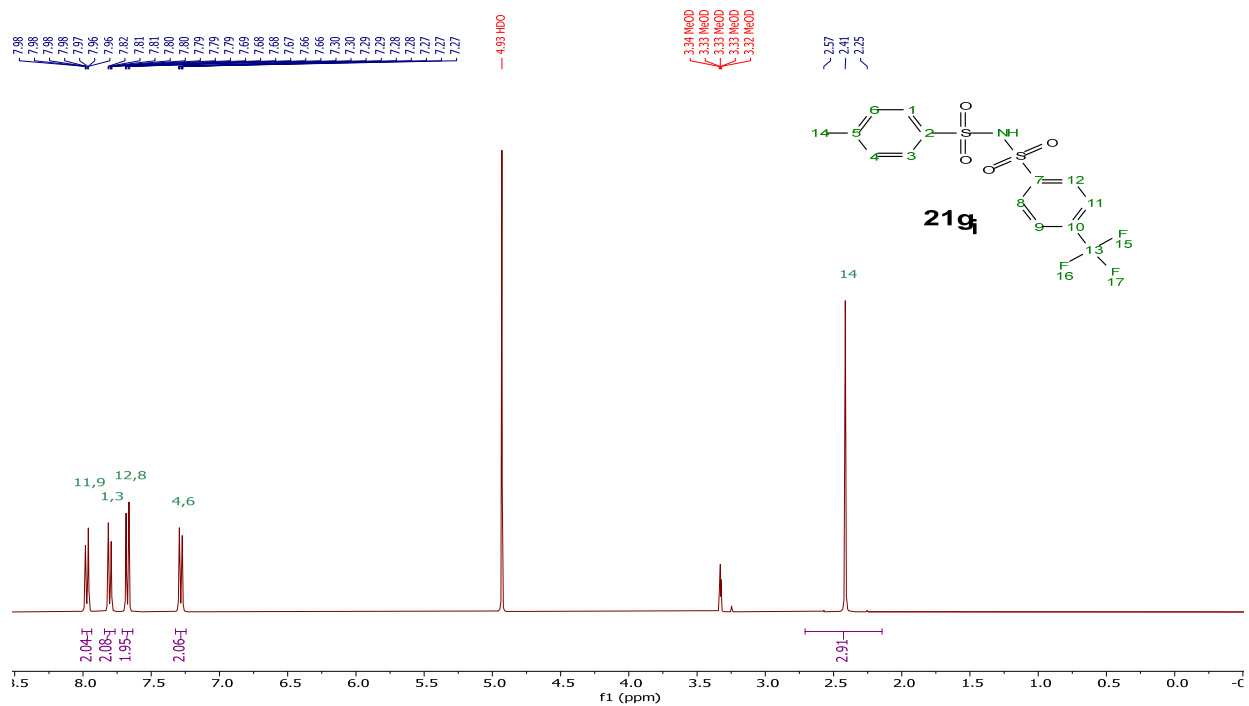
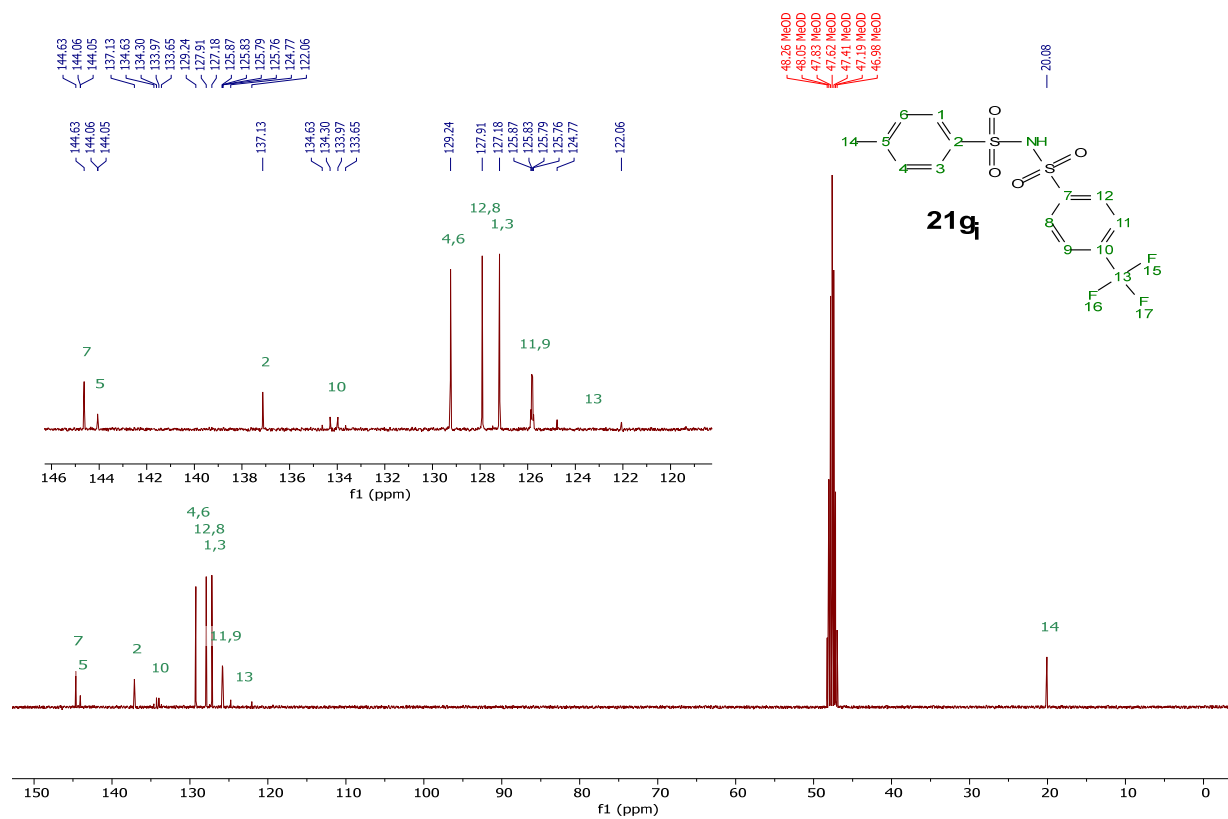
[Na][N(tBB)<sub>2</sub>], **21f<sub>ii</sub>**

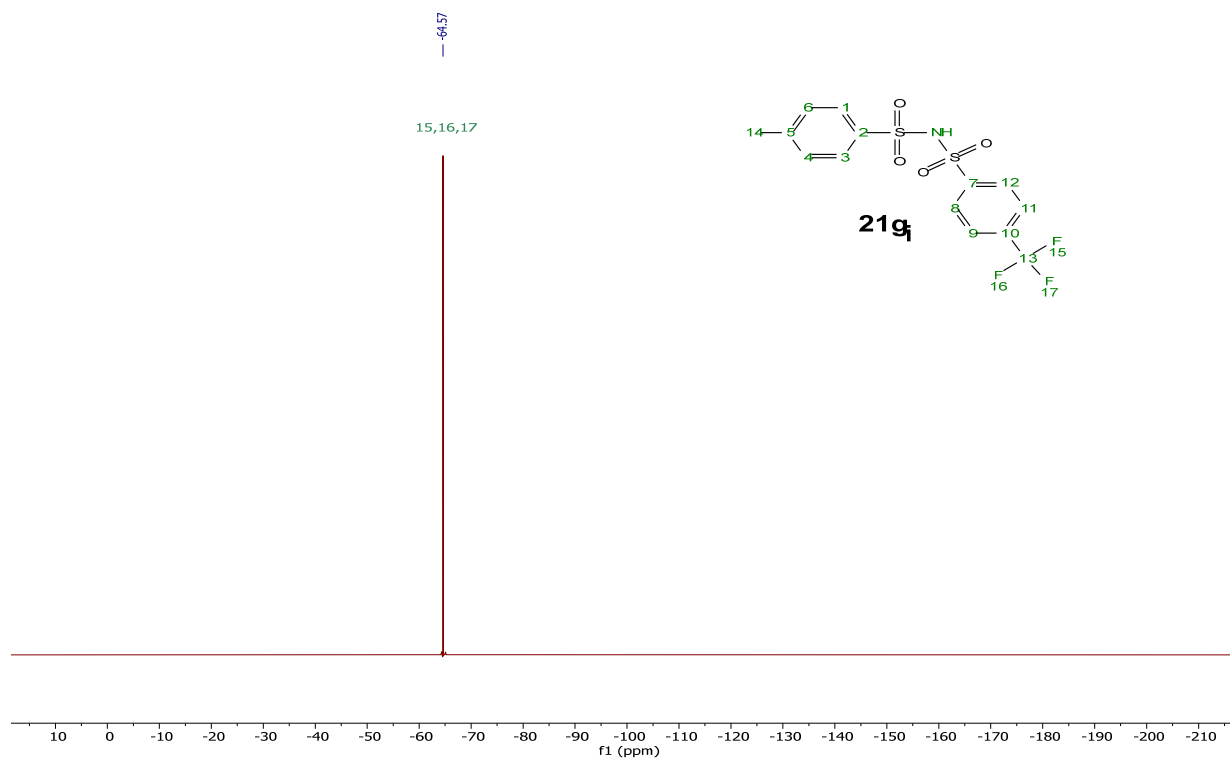
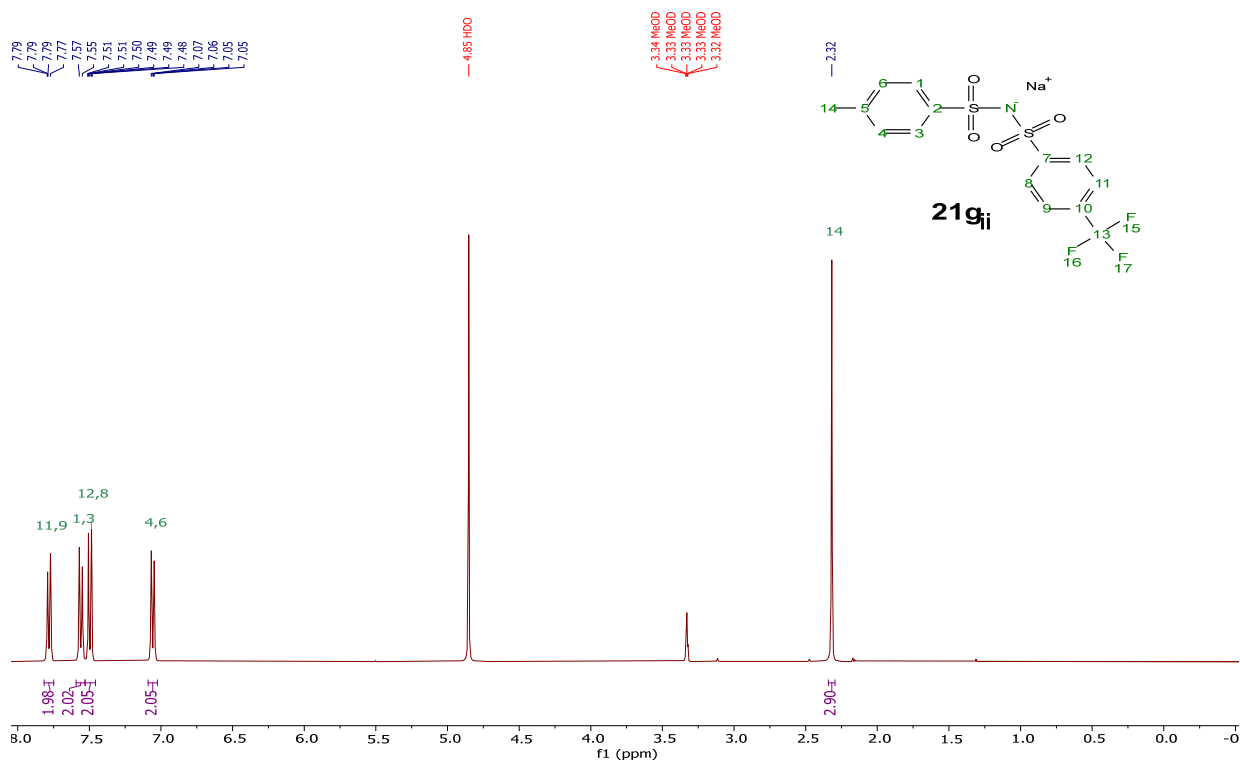
<sup>1</sup>H NMR (400 MHz, Methanol-d<sub>4</sub>)

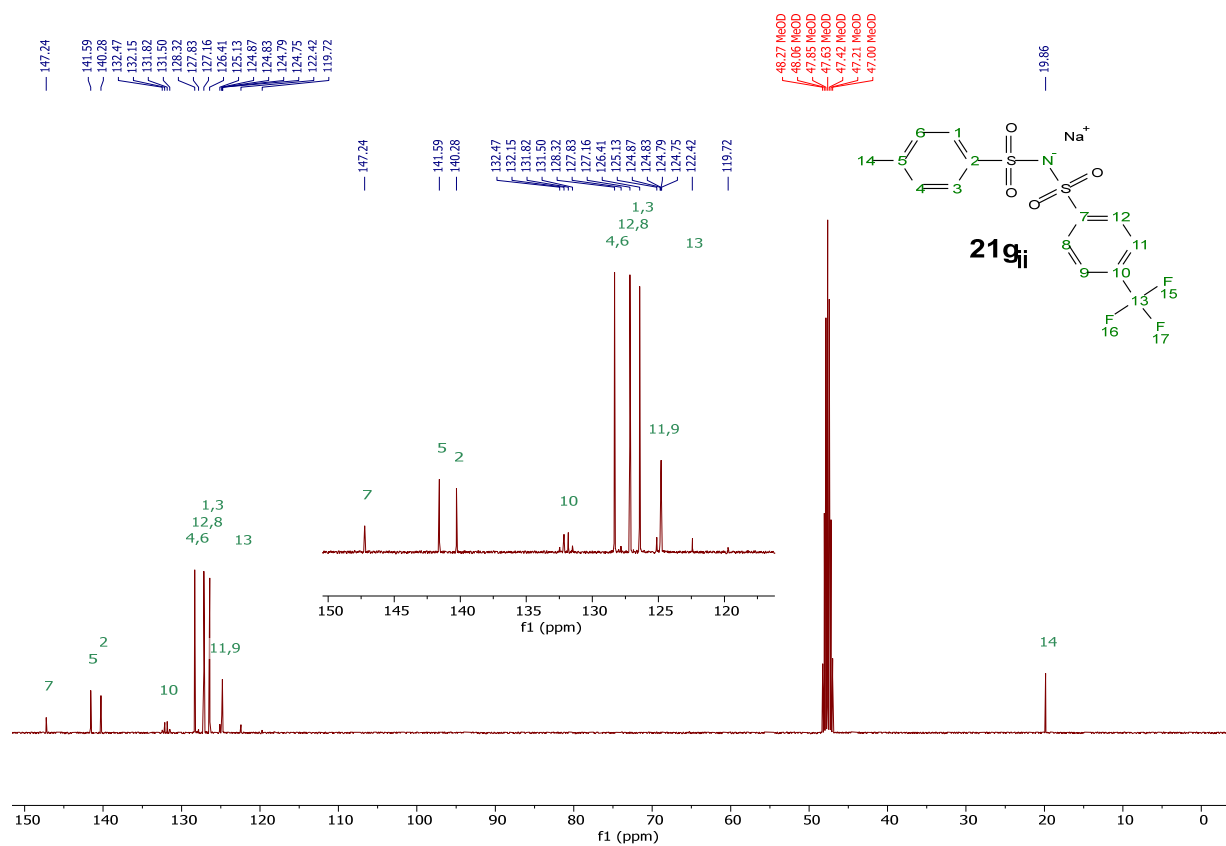
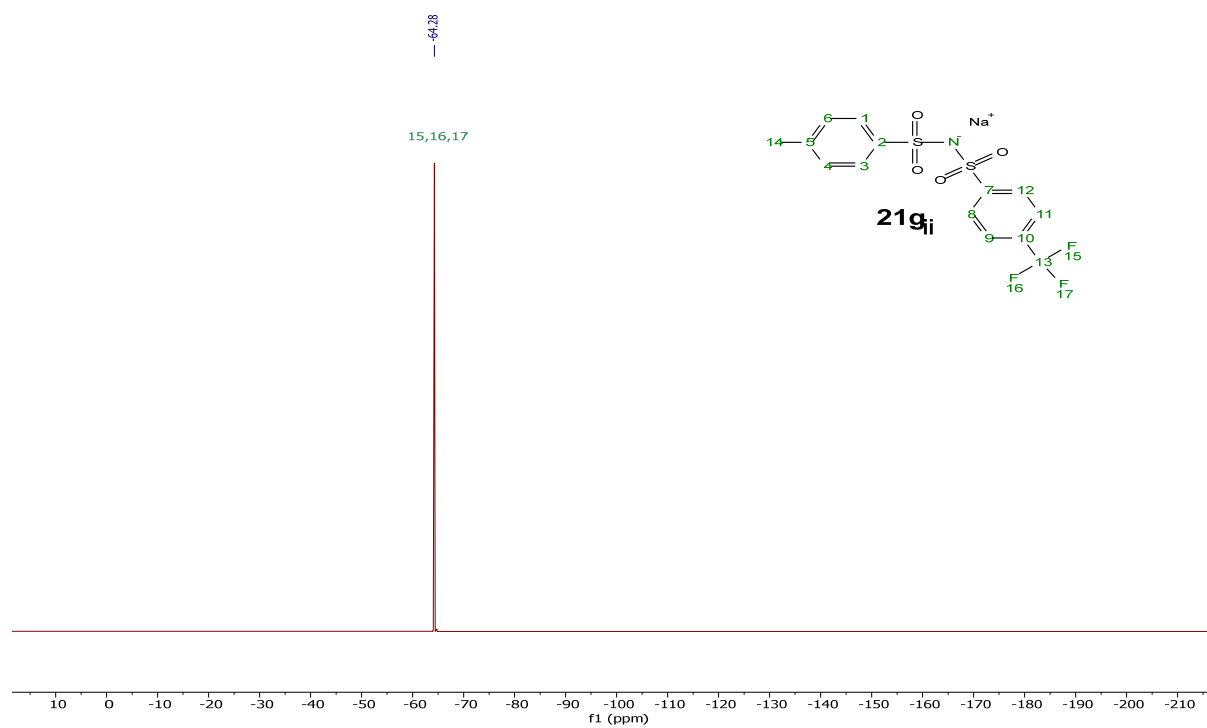


<sup>13</sup>C{<sup>1</sup>H} NMR (101 MHz, Methanol-d<sub>4</sub>)

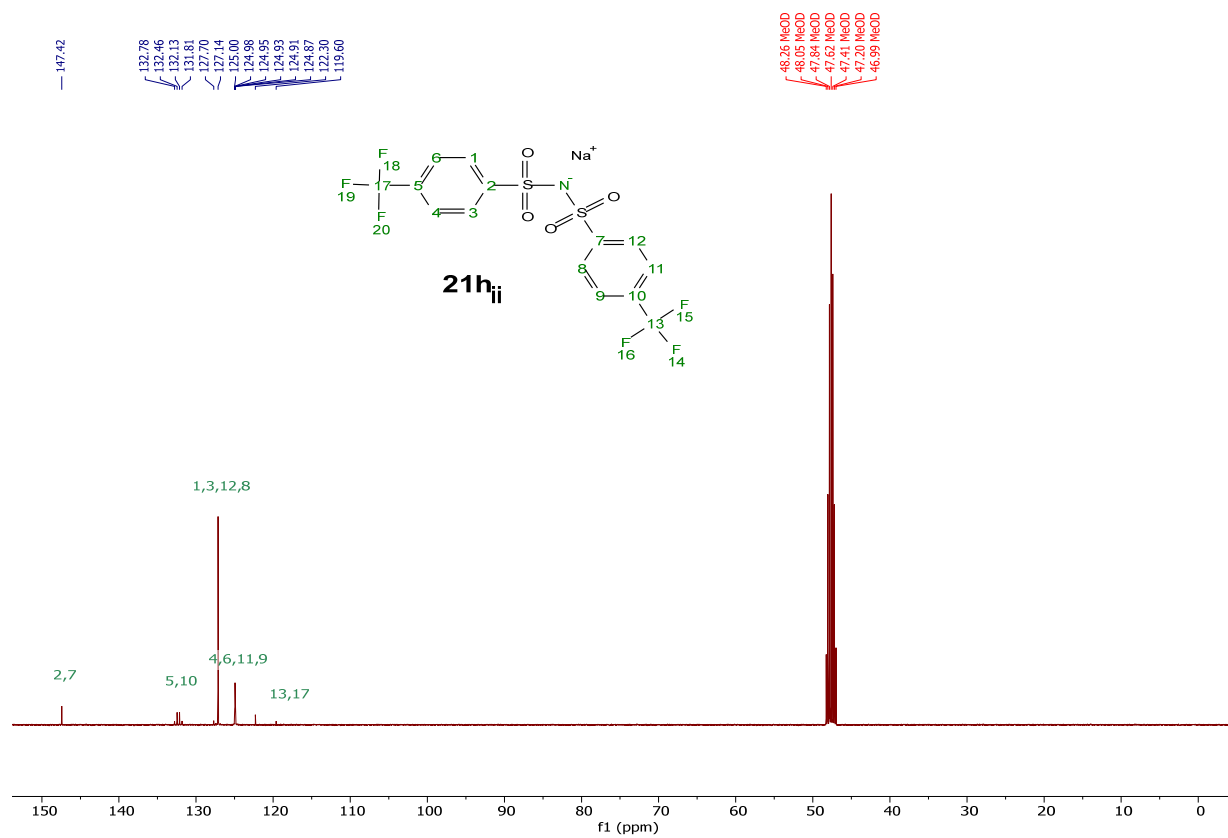
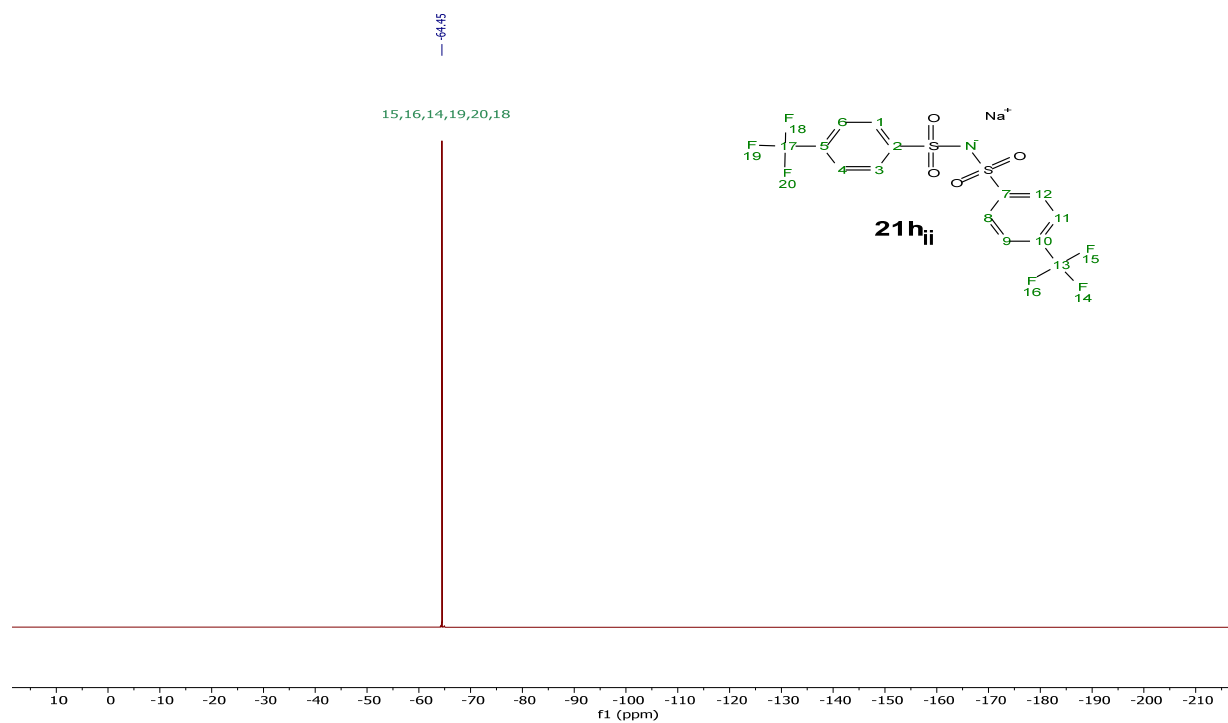


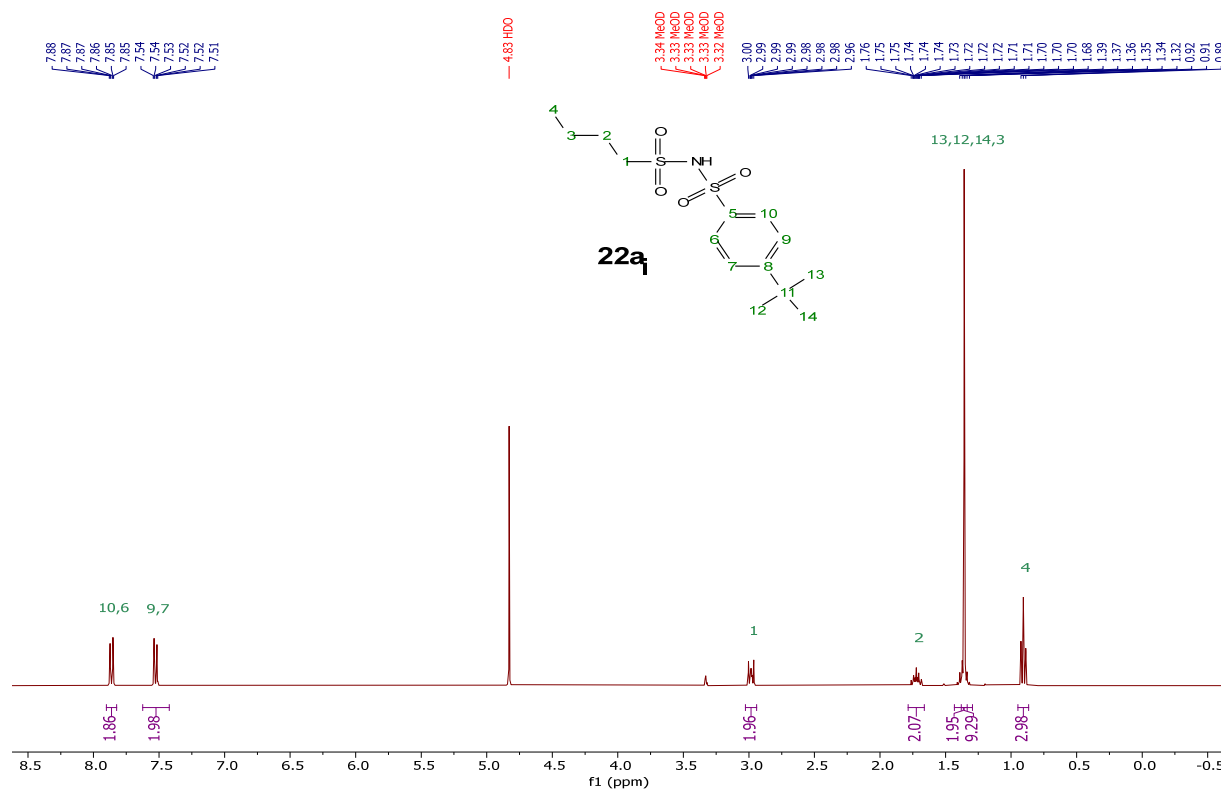
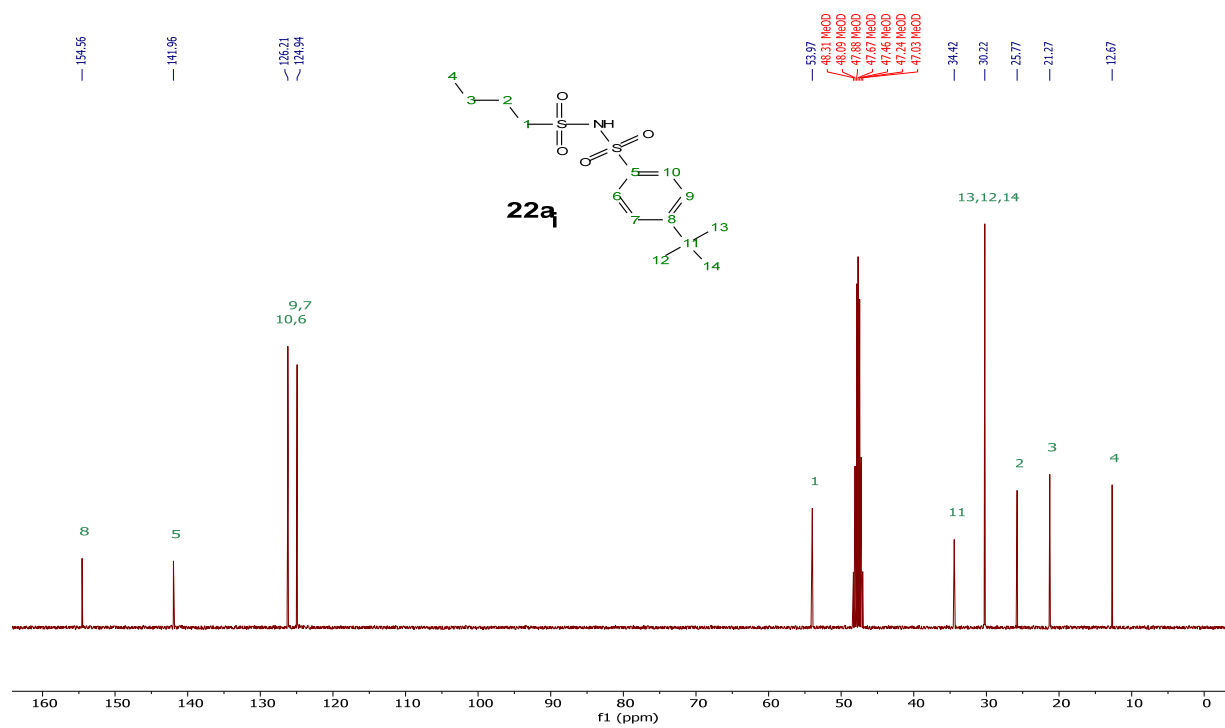
**21g** $^1\text{H}$  NMR (400 MHz, Methanol- $d_4$ ) $^{13}\text{C}\{^1\text{H}\}$  NMR (101 MHz, Methanol- $d_4$ )

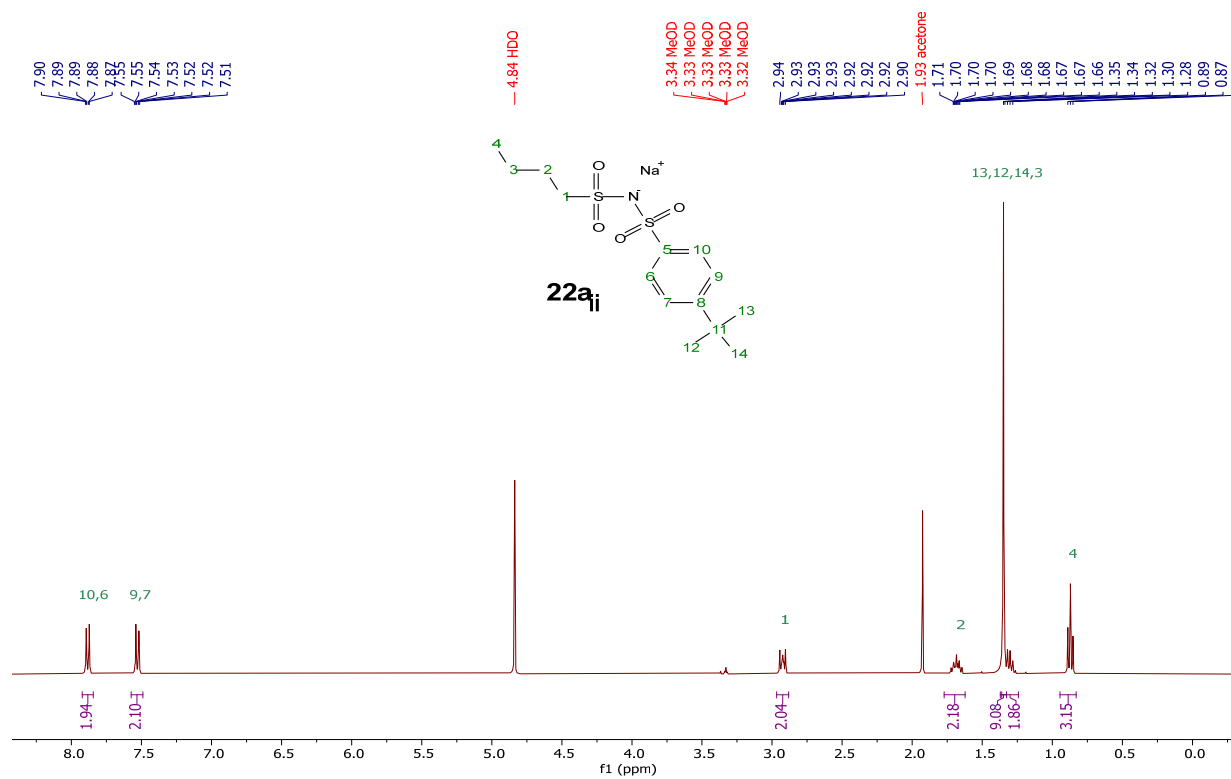
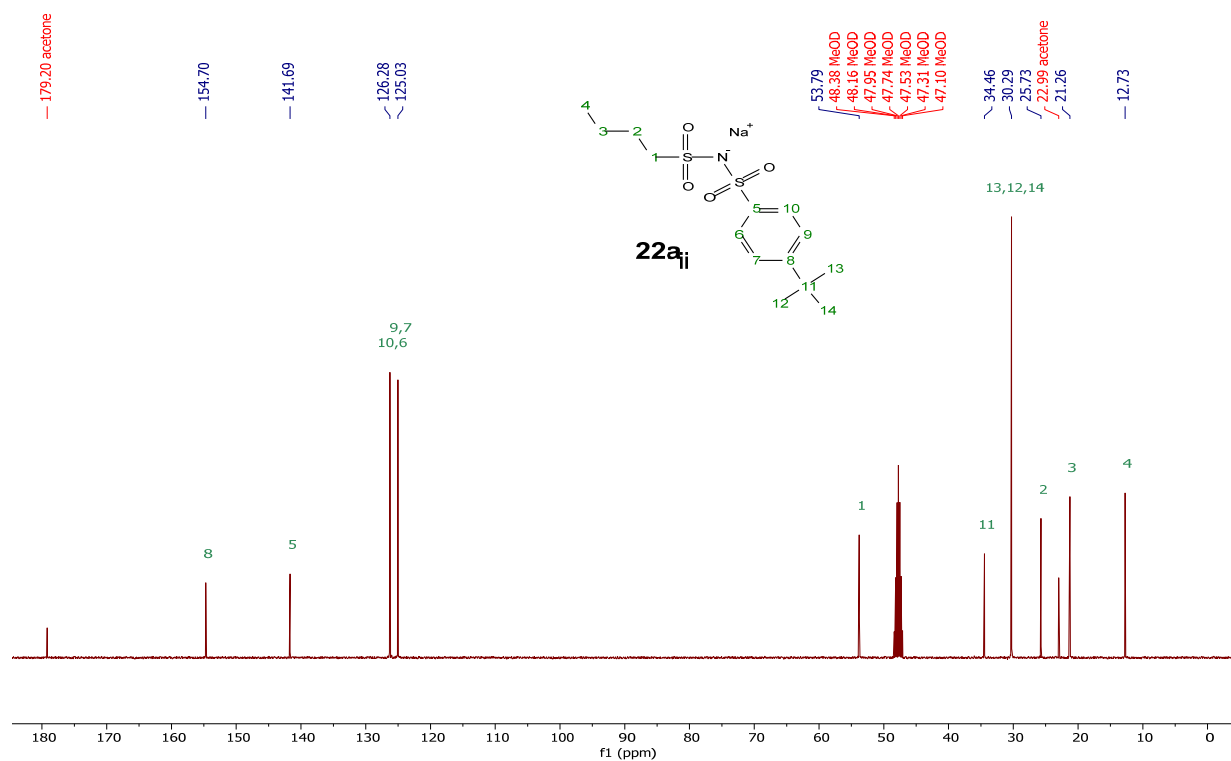
$^{19}\text{F}$  NMR (376 MHz, Methanol- $d_4$ )[Na][TFMBNTs], **21gii** $^1\text{H}$  NMR (400 MHz, Methanol- $d_4$ )

$^{13}\text{C}\{^1\text{H}\}$  NMR (101 MHz, Methanol-d<sub>4</sub>) $^{19}\text{F}$  NMR (376 MHz, Methanol-d<sub>4</sub>)

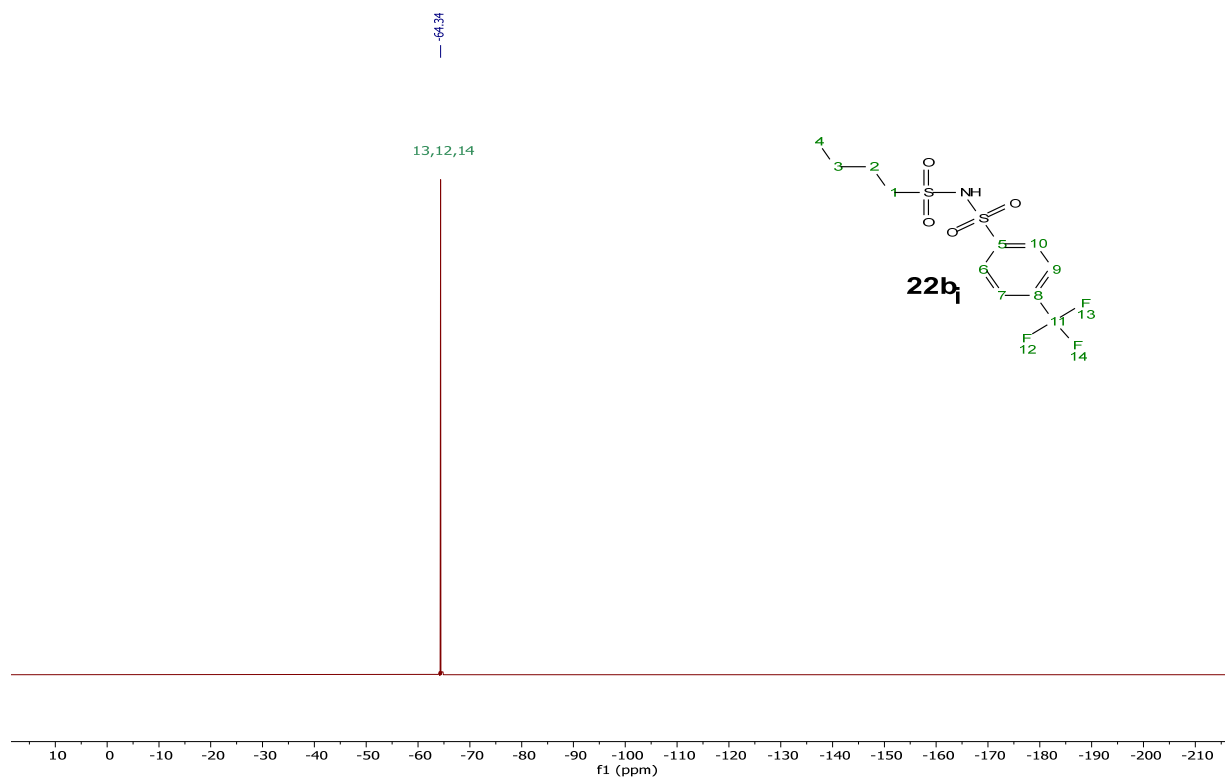
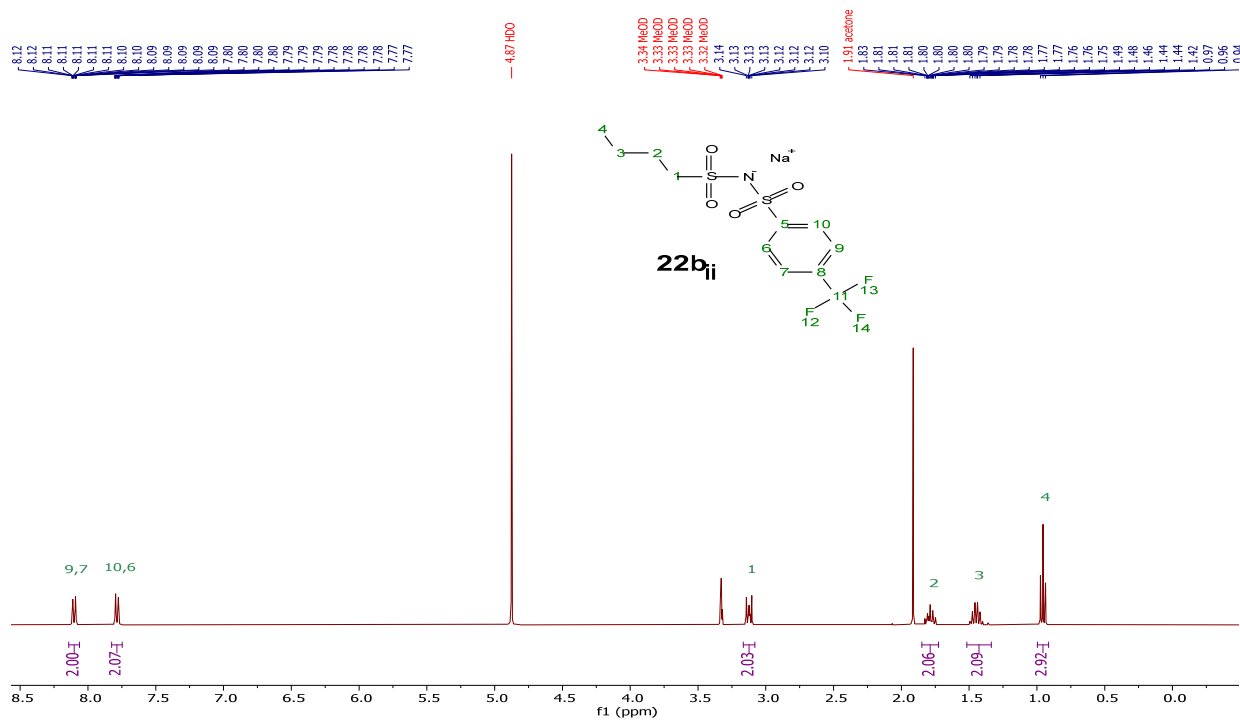


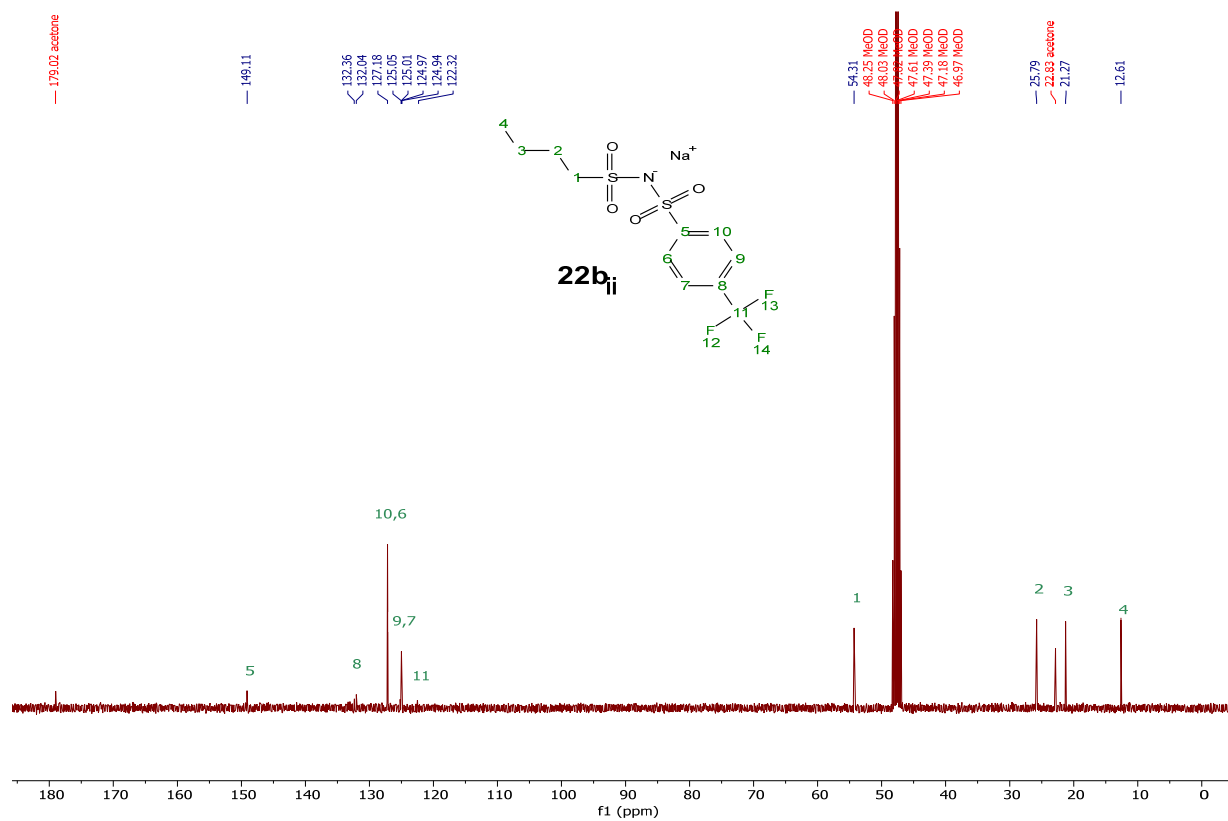
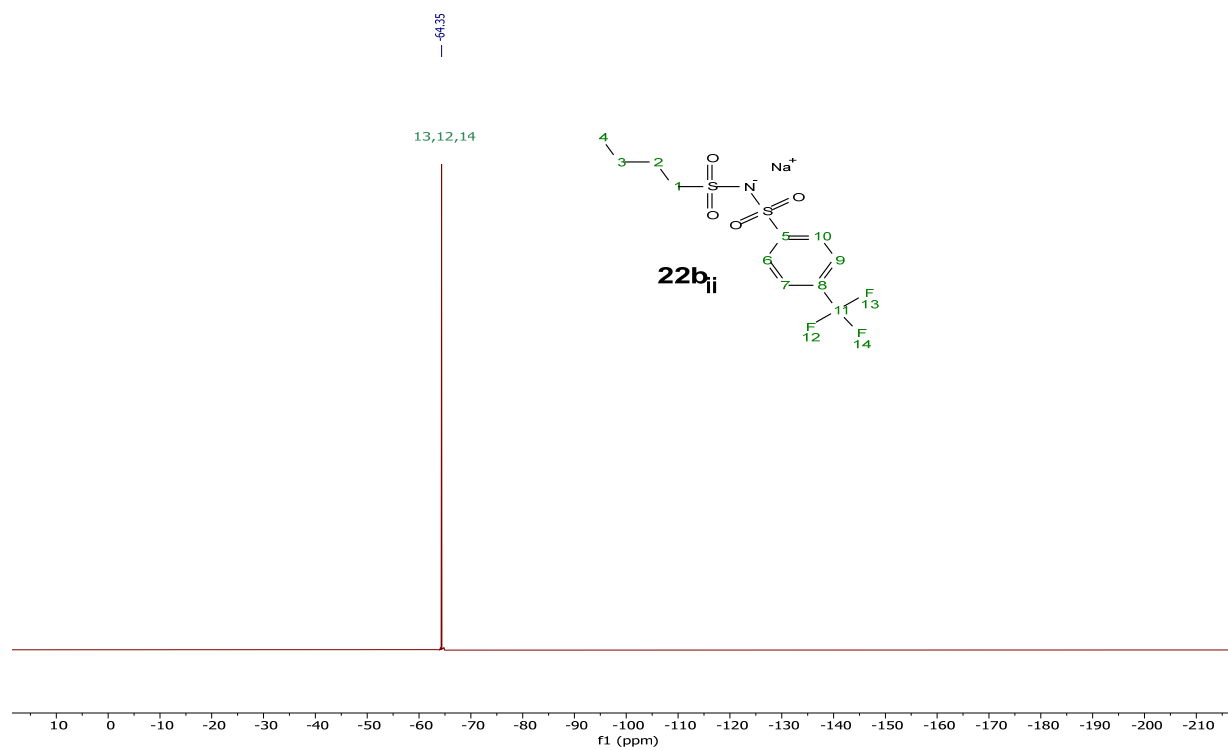
$^{13}\text{C}\{^1\text{H}\}$  NMR (101 MHz, Methanol-d<sub>4</sub>) $^{19}\text{F}$  NMR (376 MHz, Methanol-d<sub>4</sub>)

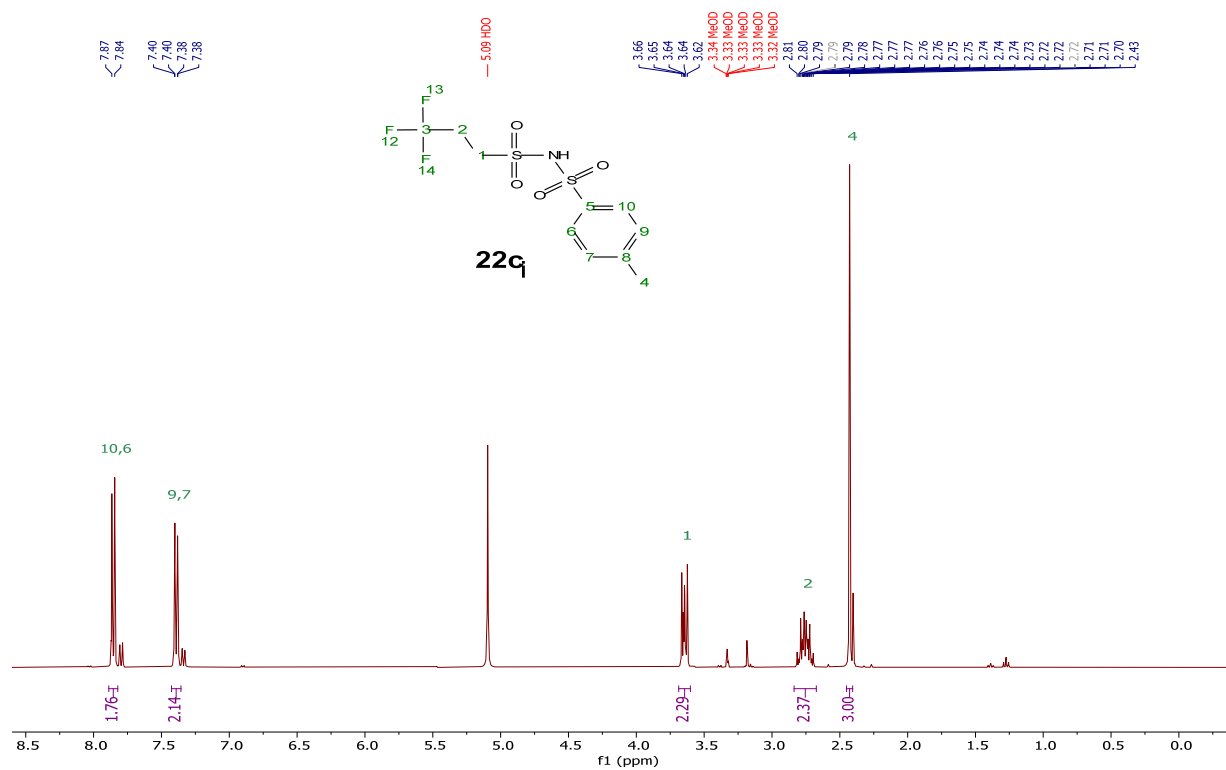
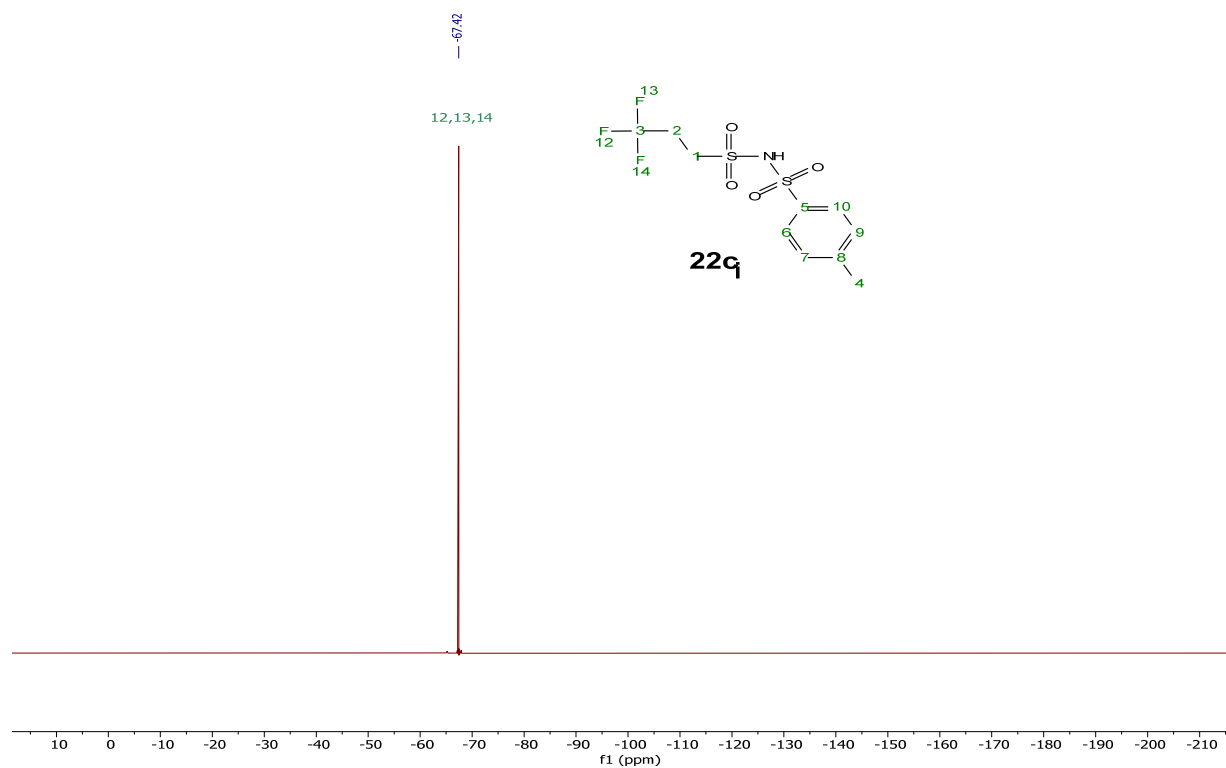
**22a<sub>i</sub>**<sup>1</sup>H NMR (400 MHz, Methanol-d<sub>4</sub>)<sup>13</sup>C{<sup>1</sup>H} NMR (101 MHz, Methanol-d<sub>4</sub>)

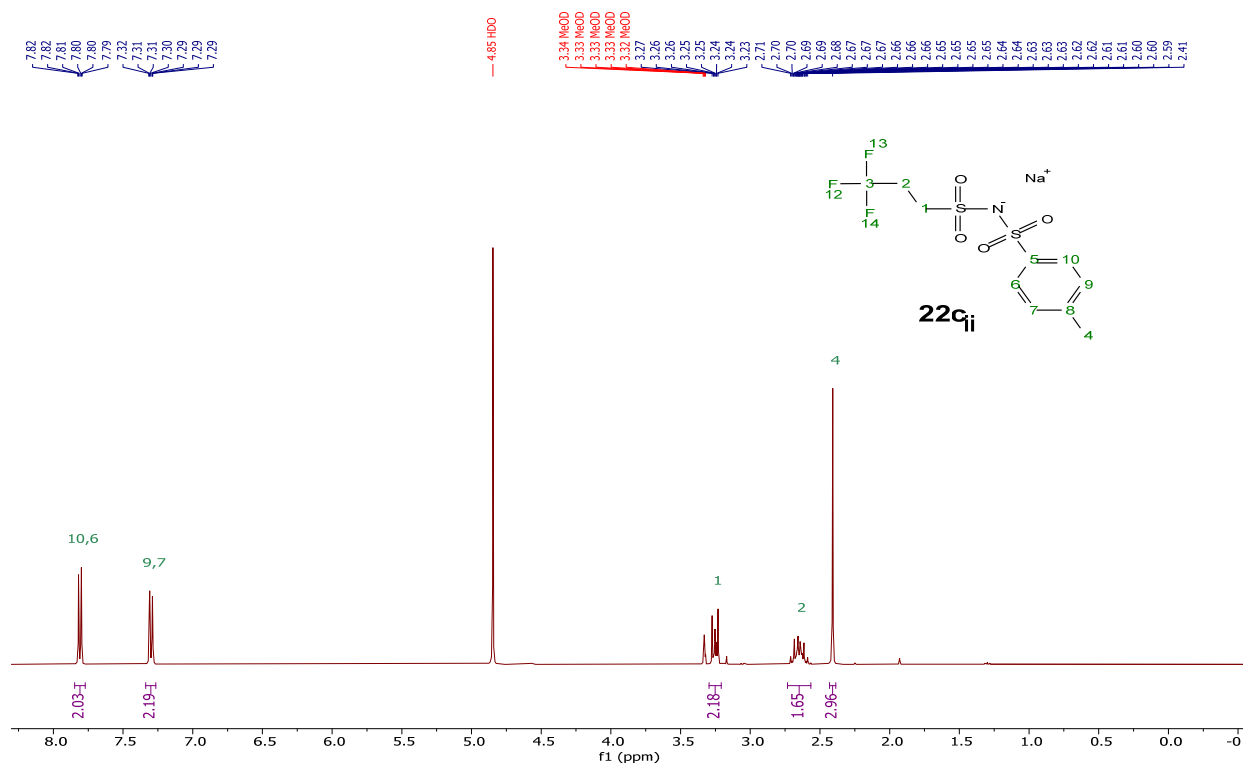
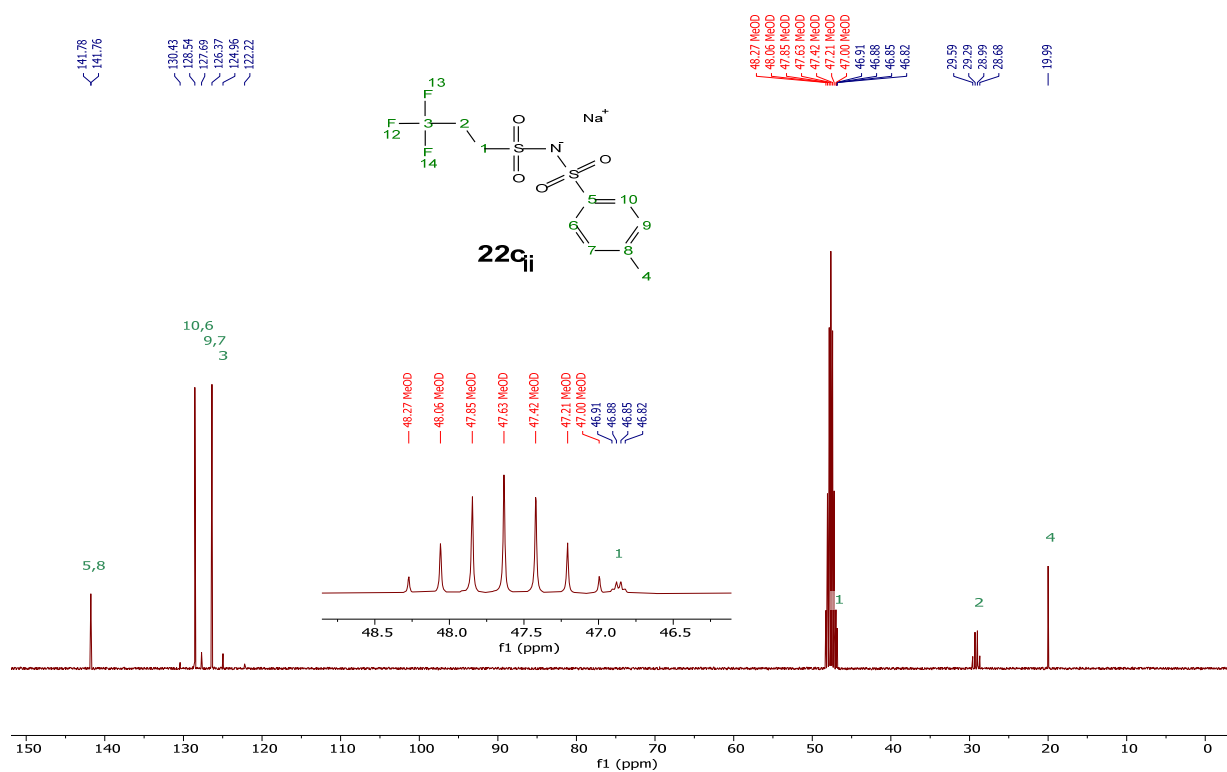
[Na][tBBNB], **22a<sub>ii</sub>**<sup>1</sup>H NMR (400 MHz, Methanol-d<sub>4</sub>)<sup>13</sup>C{<sup>1</sup>H} NMR (101 MHz, Methanol-d<sub>4</sub>)

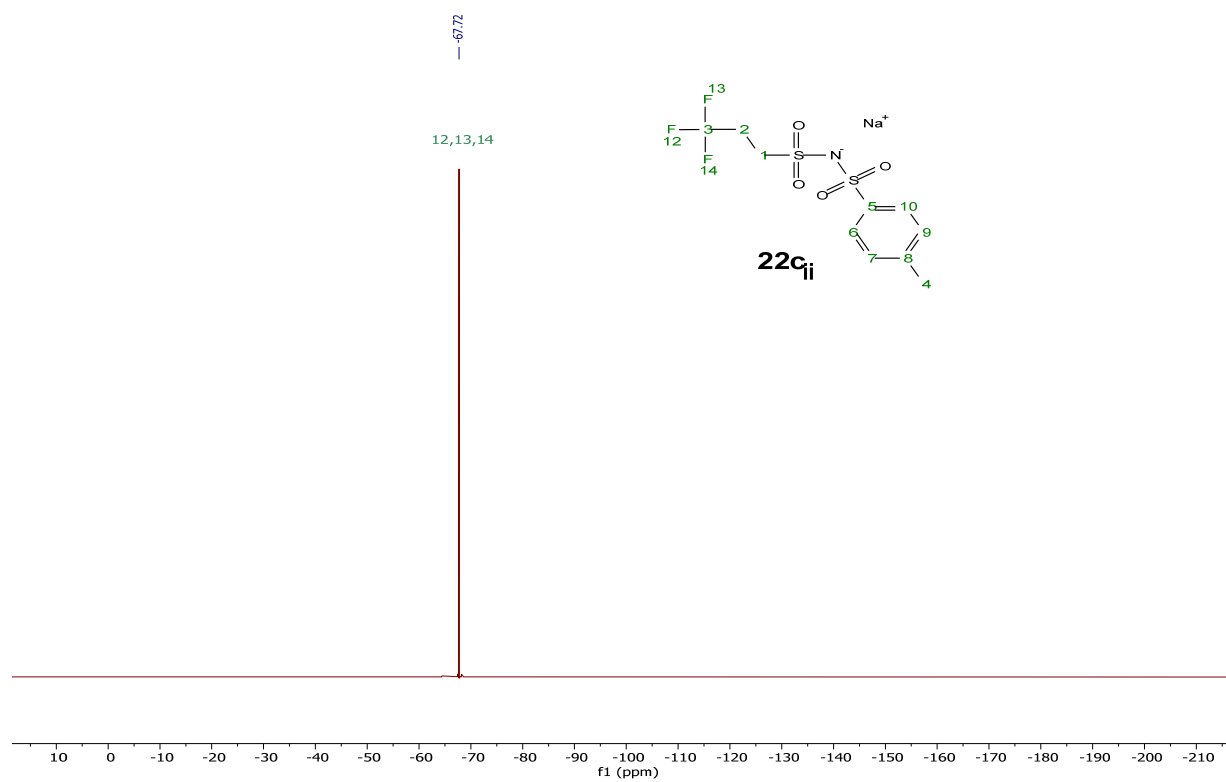
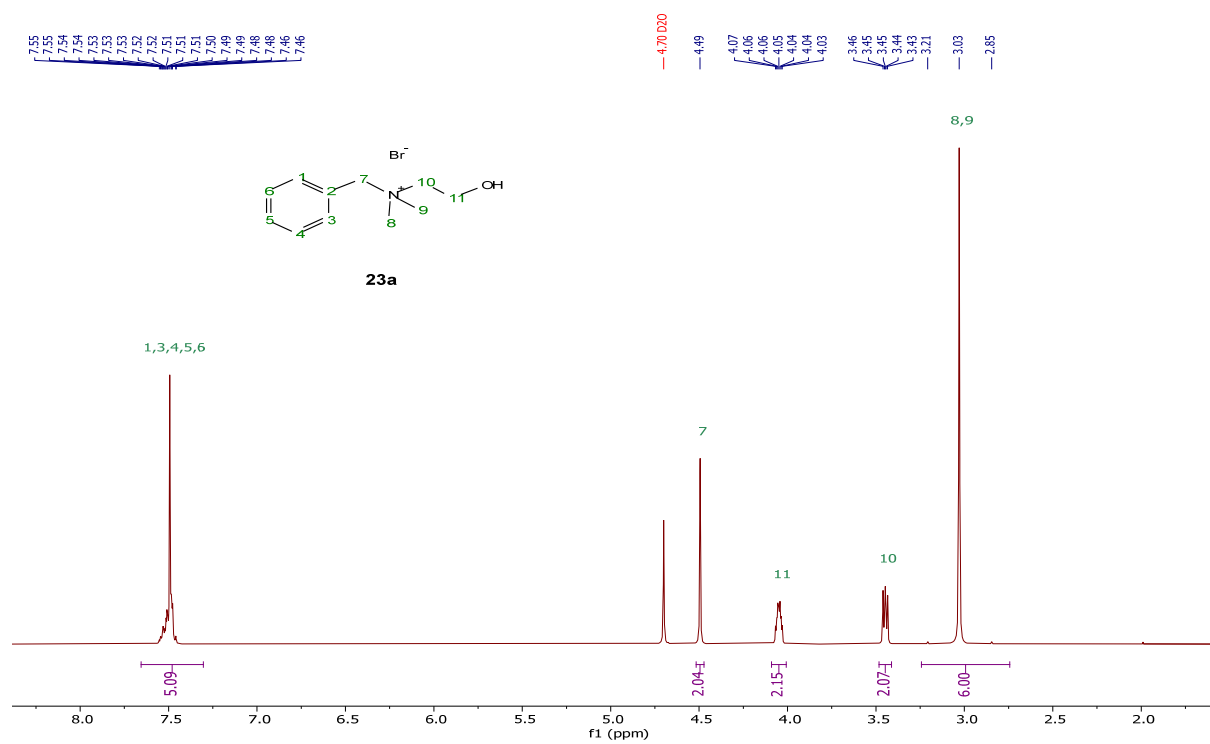


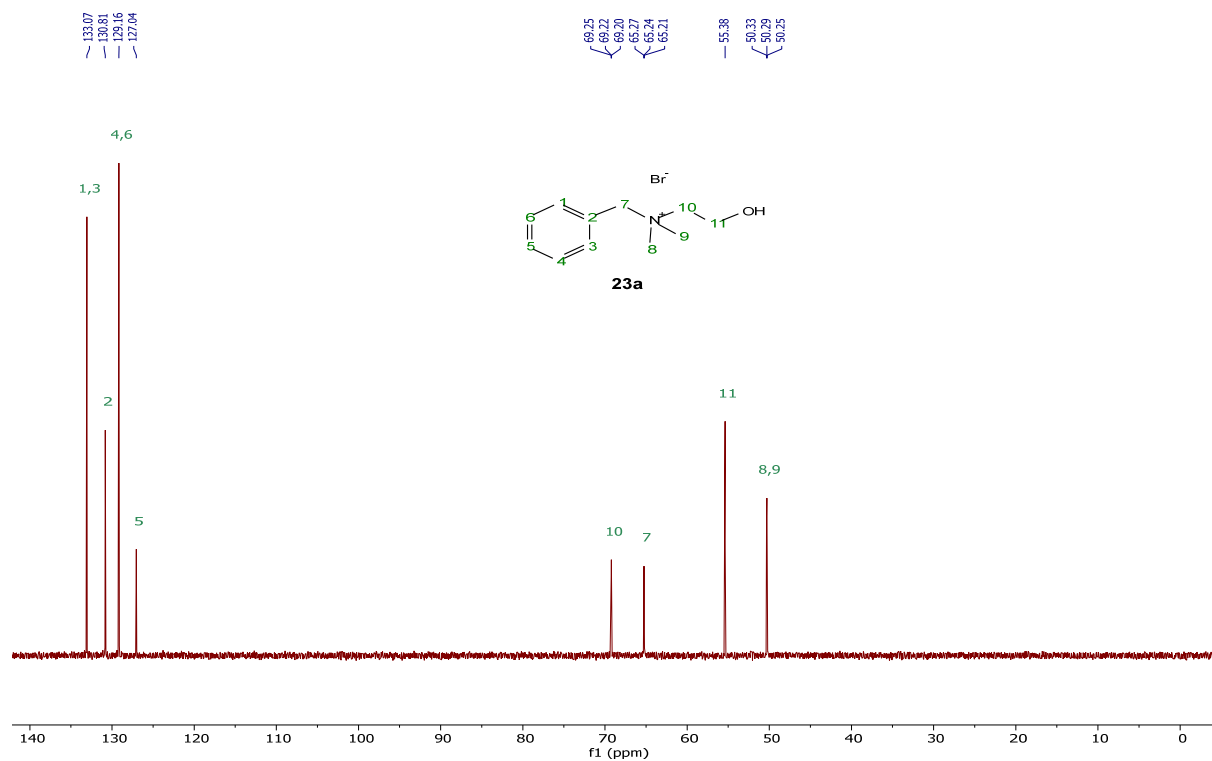
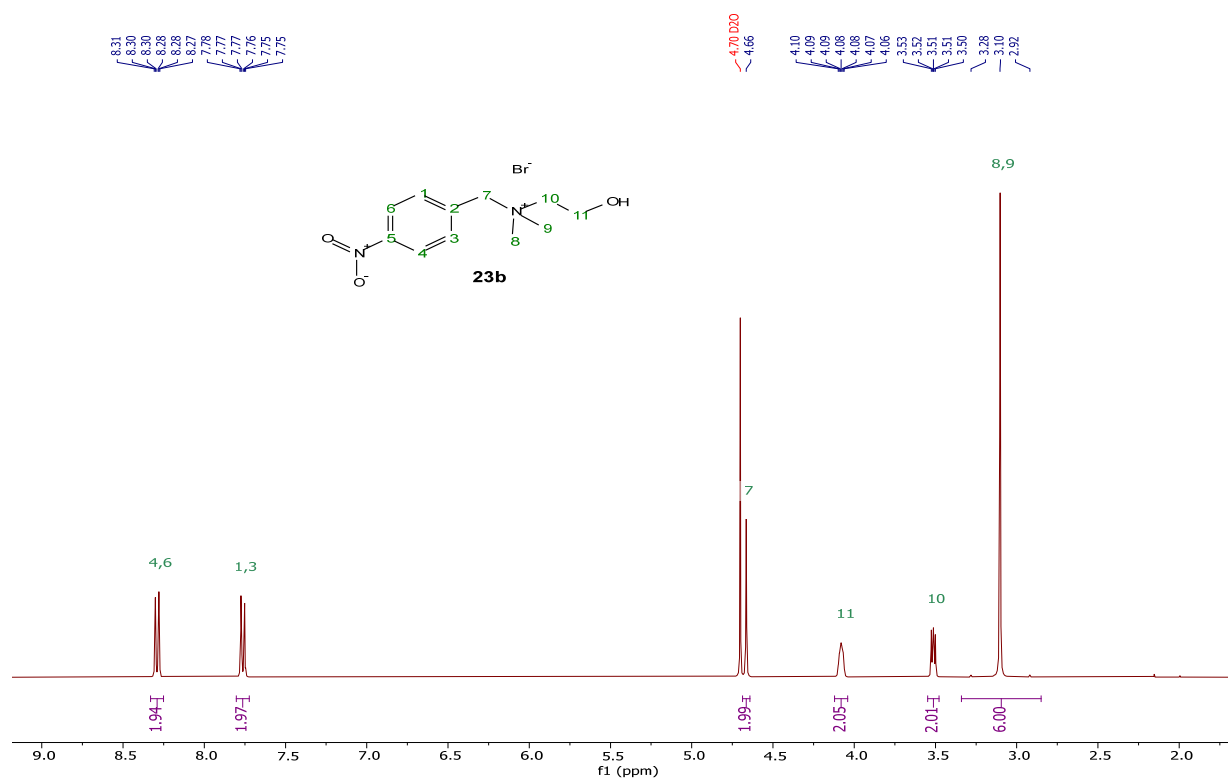
$^{19}\text{F}$  NMR (376 MHz, Methanol- $d_4$ )[Na][TFMBNB], **22b<sub>ii</sub>** $^1\text{H}$  NMR (400 MHz, Methanol- $d_4$ )

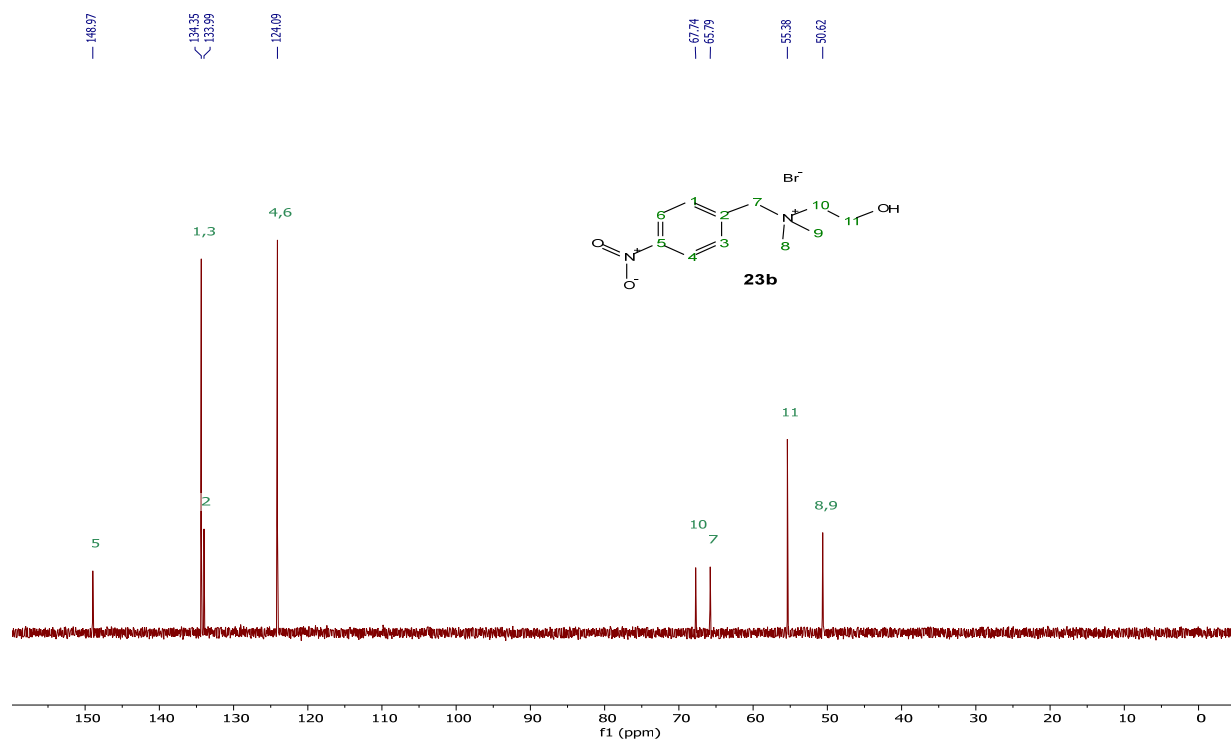
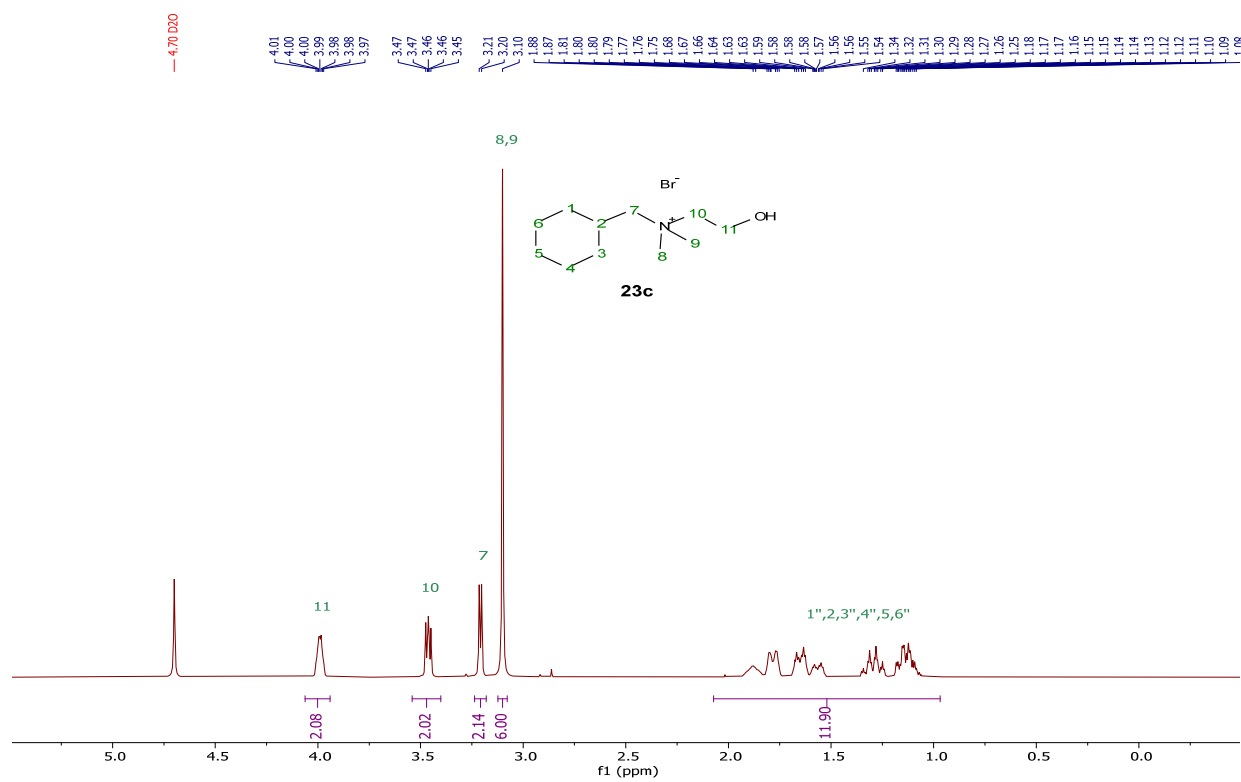
$^{13}\text{C}\{^1\text{H}\}$  NMR (101 MHz, Methanol-d<sub>4</sub>) $^{19}\text{F}$  NMR (376 MHz, Methanol-d<sub>4</sub>)

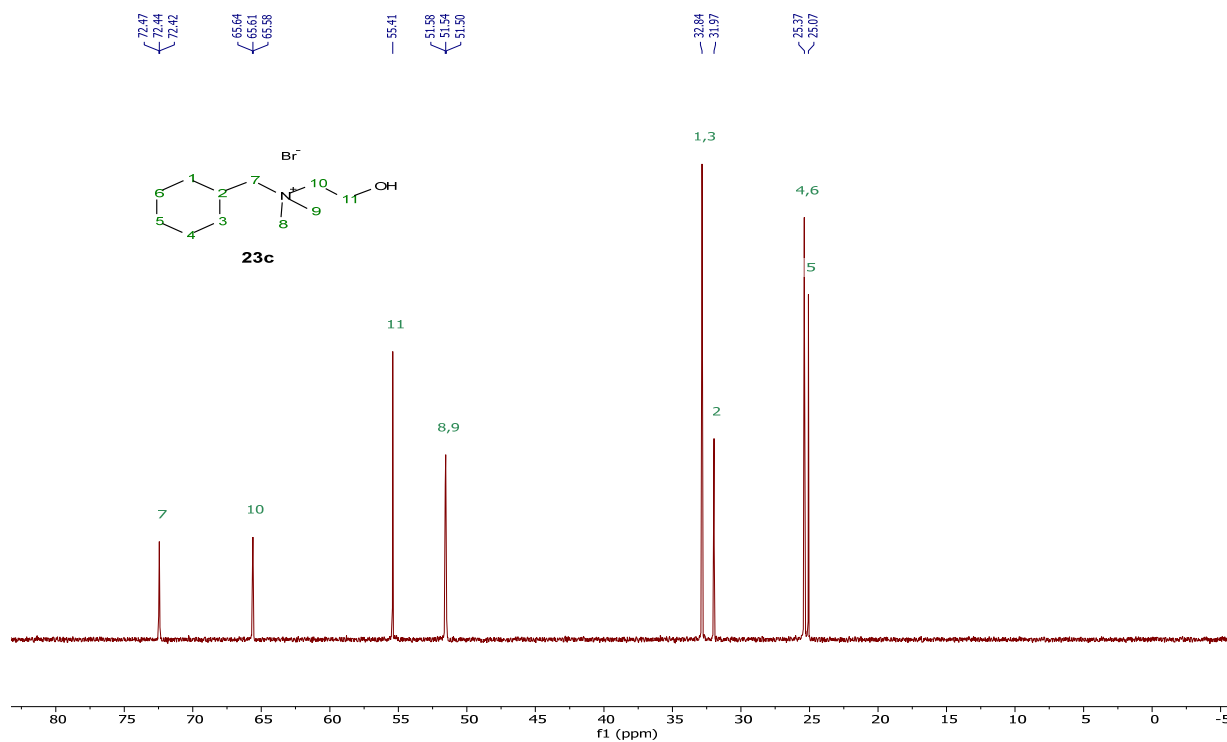
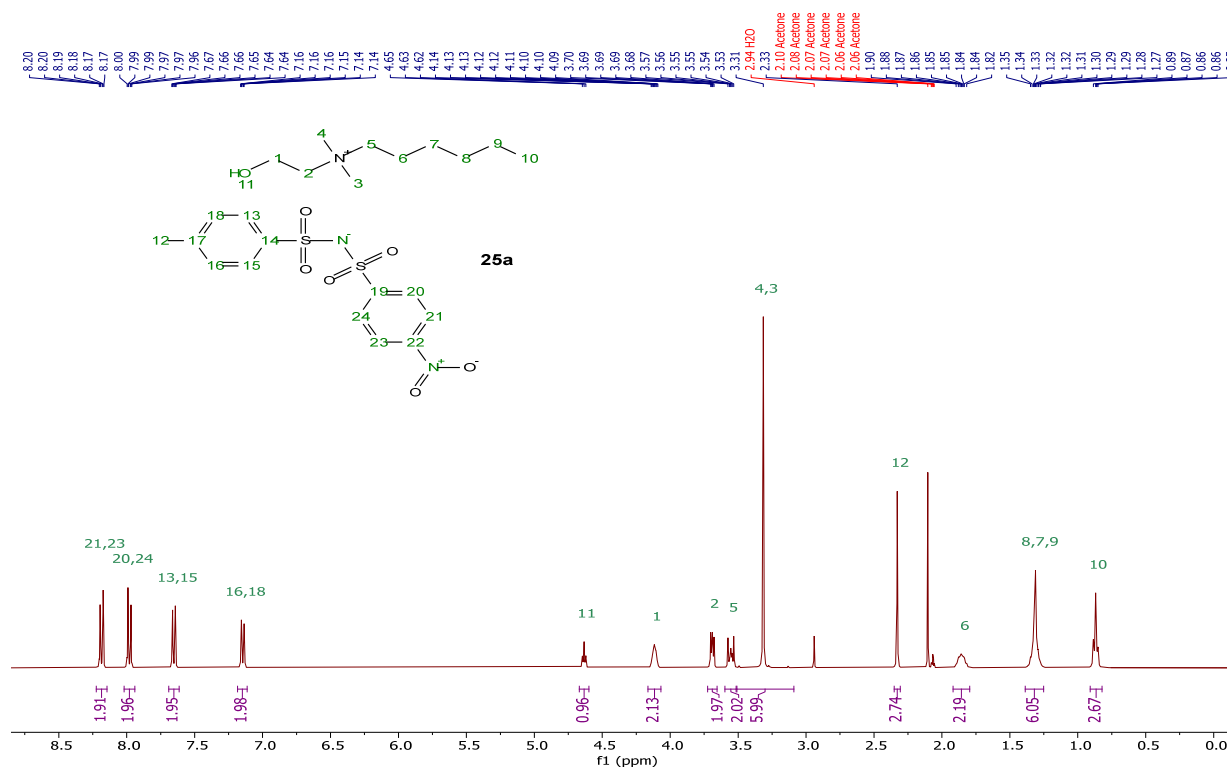
**22c<sub>i</sub>**<sup>1</sup>H NMR (400 MHz, Methanol-d<sub>4</sub>)<sup>19</sup>F NMR (376 MHz, Methanol-d<sub>4</sub>)

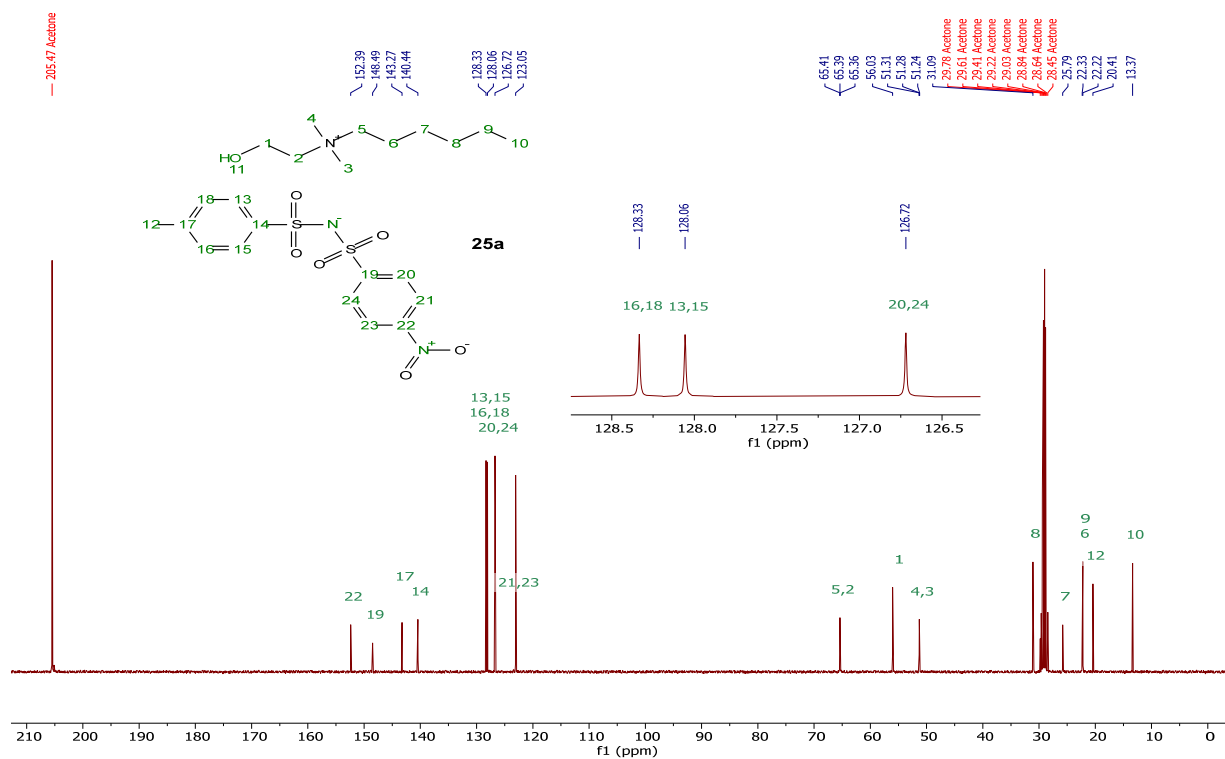
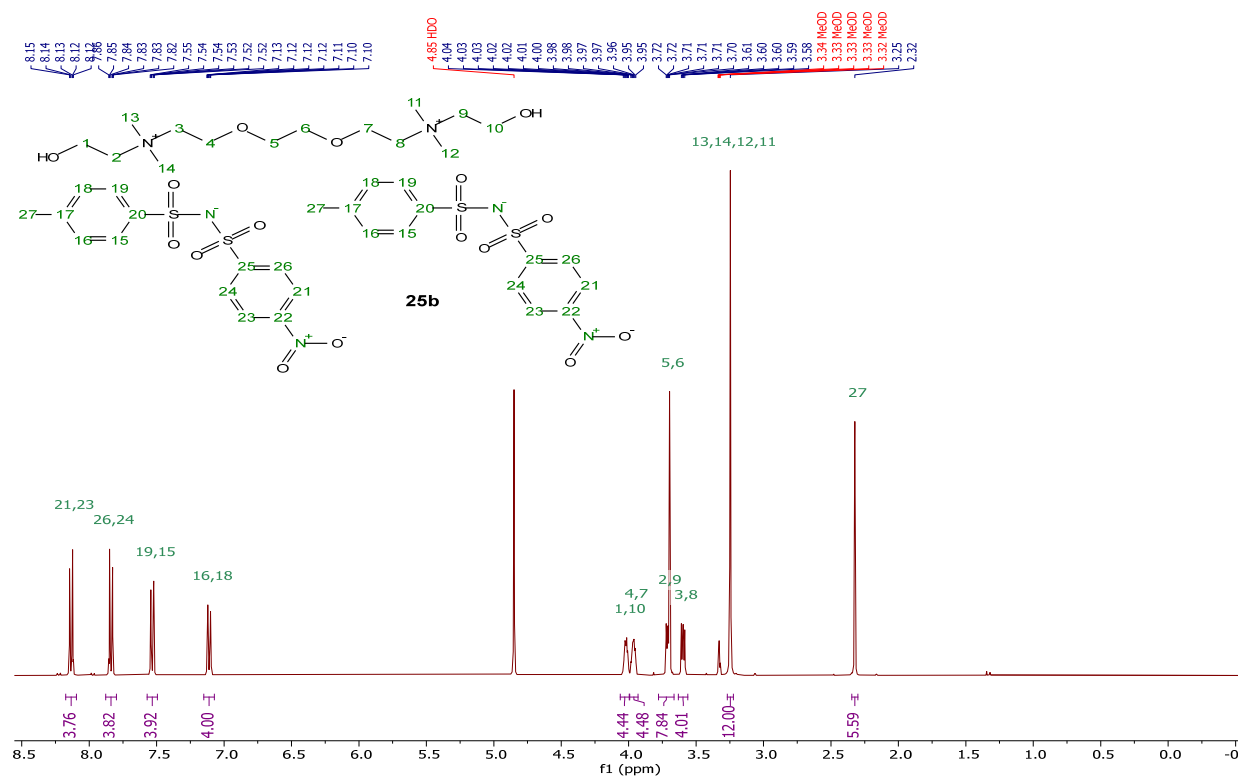
[Na][TFPNTs], **22c<sub>ii</sub>**<sup>1</sup>H NMR (400 MHz, Methanol-d<sub>4</sub>)<sup>13</sup>C{<sup>1</sup>H} NMR (101 MHz, Methanol-d<sub>4</sub>)

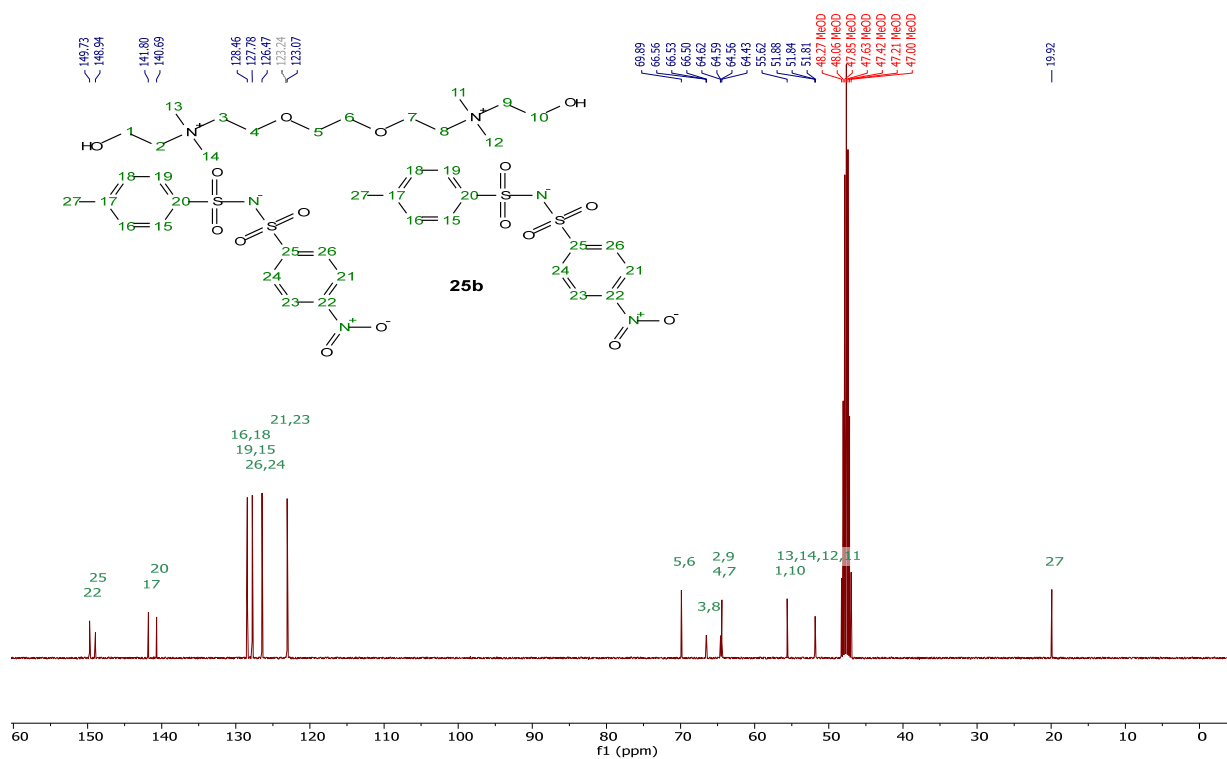
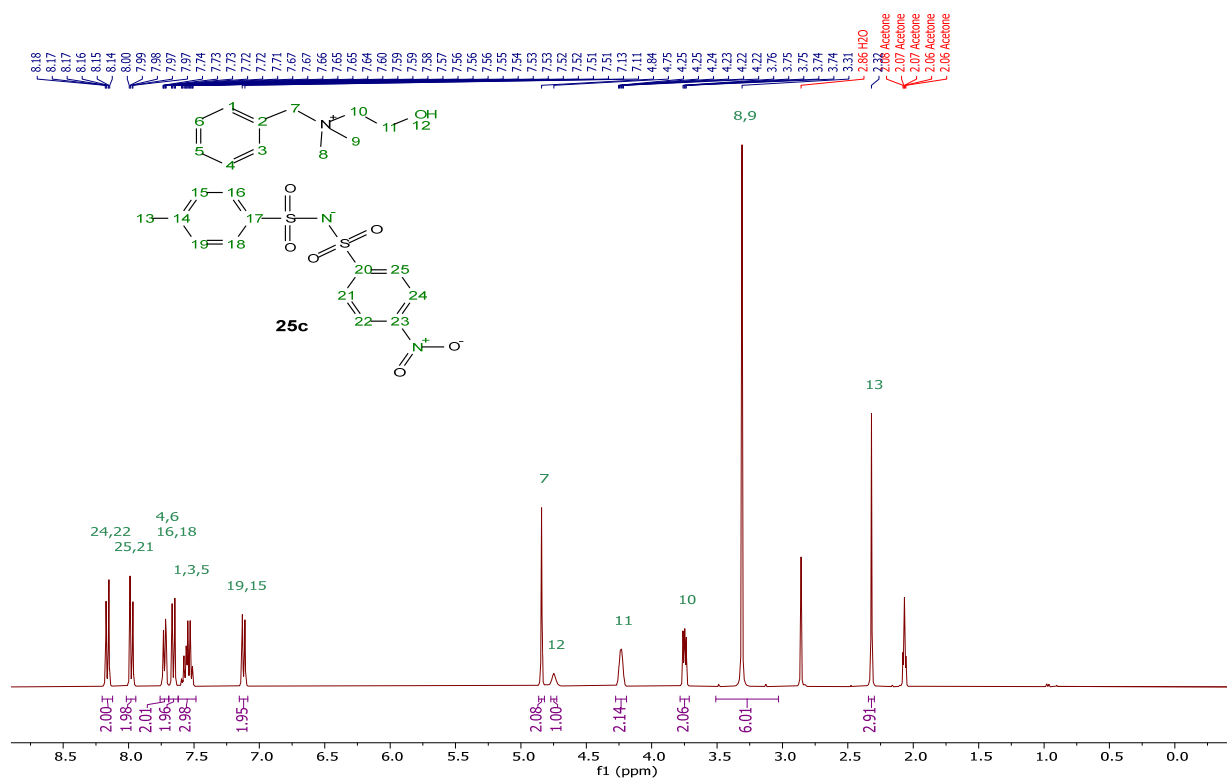
$^{19}\text{F}$  NMR (376 MHz, Methanol- $d_4$ )[Bnchol][Br], **23a** $^1\text{H}$  NMR (400 MHz, Deuterium Oxide)

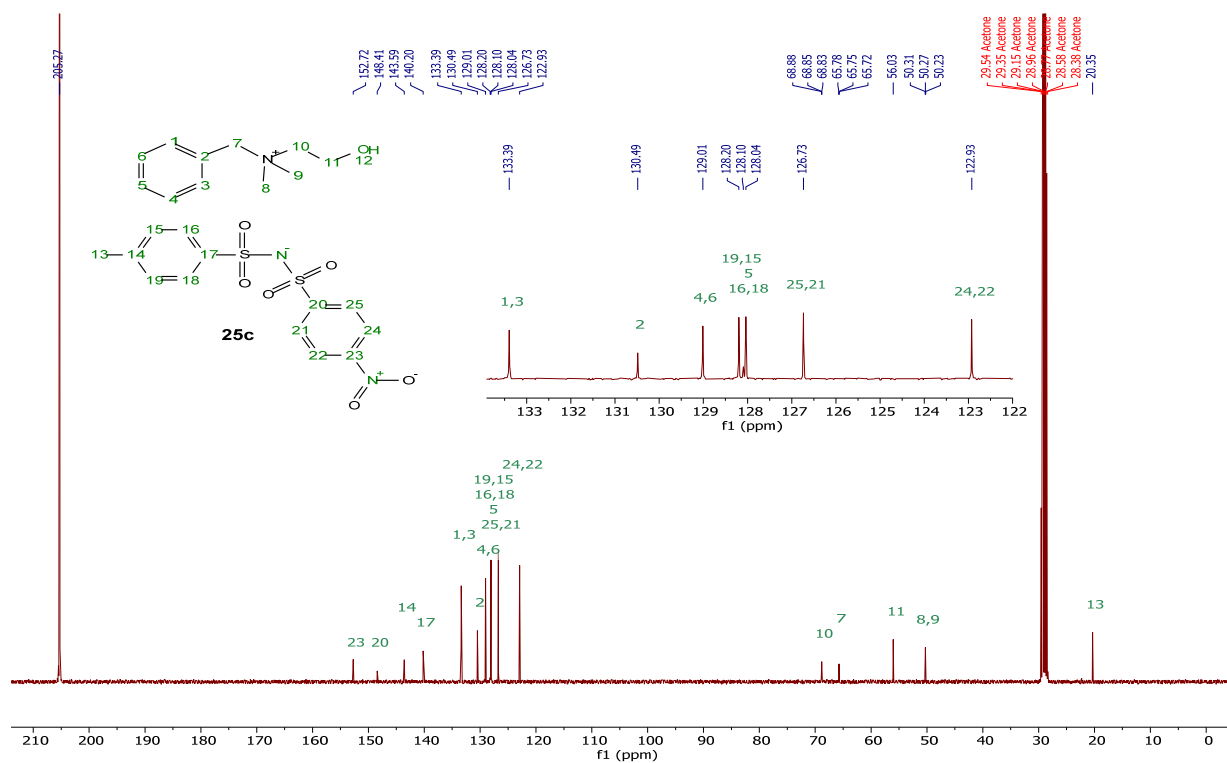
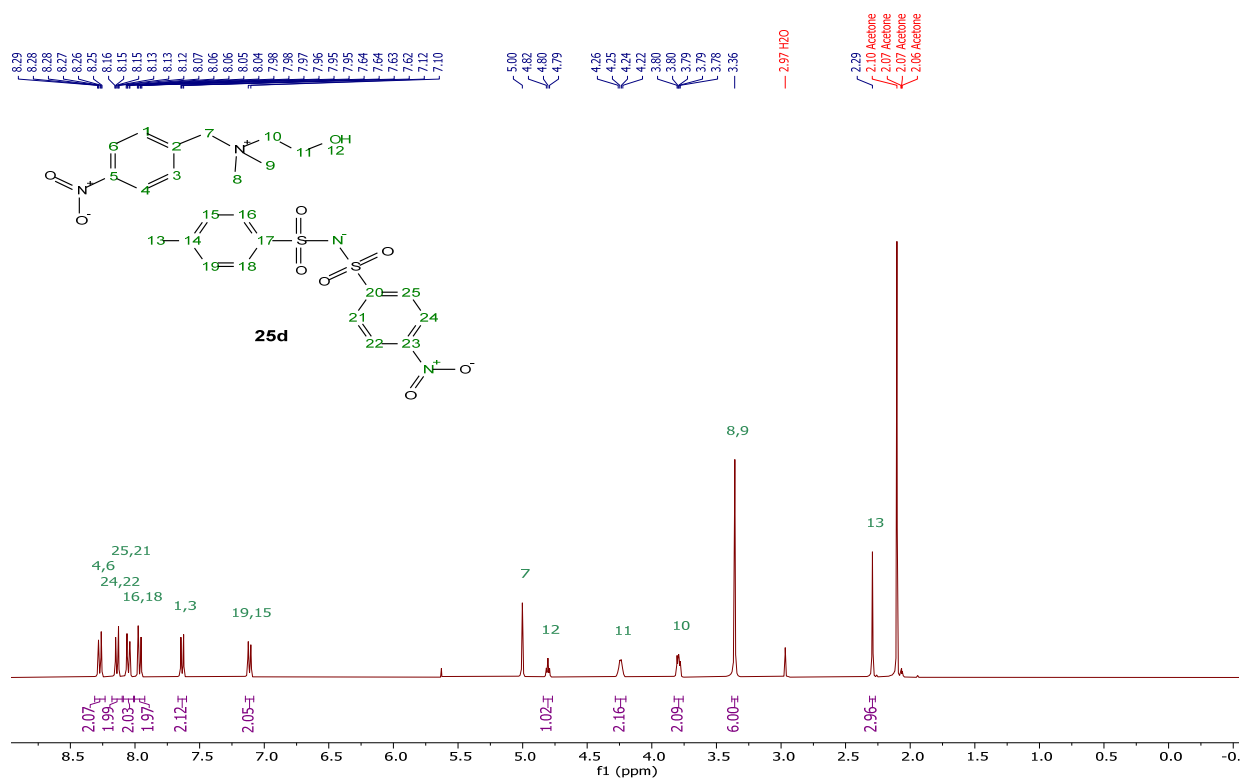
$^{13}\text{C}\{^1\text{H}\}$  NMR (101 MHz, Deuterium Oxide)[NBnchol][Br], **23b** $^1\text{H}$  NMR (400 MHz, Deuterium Oxide)

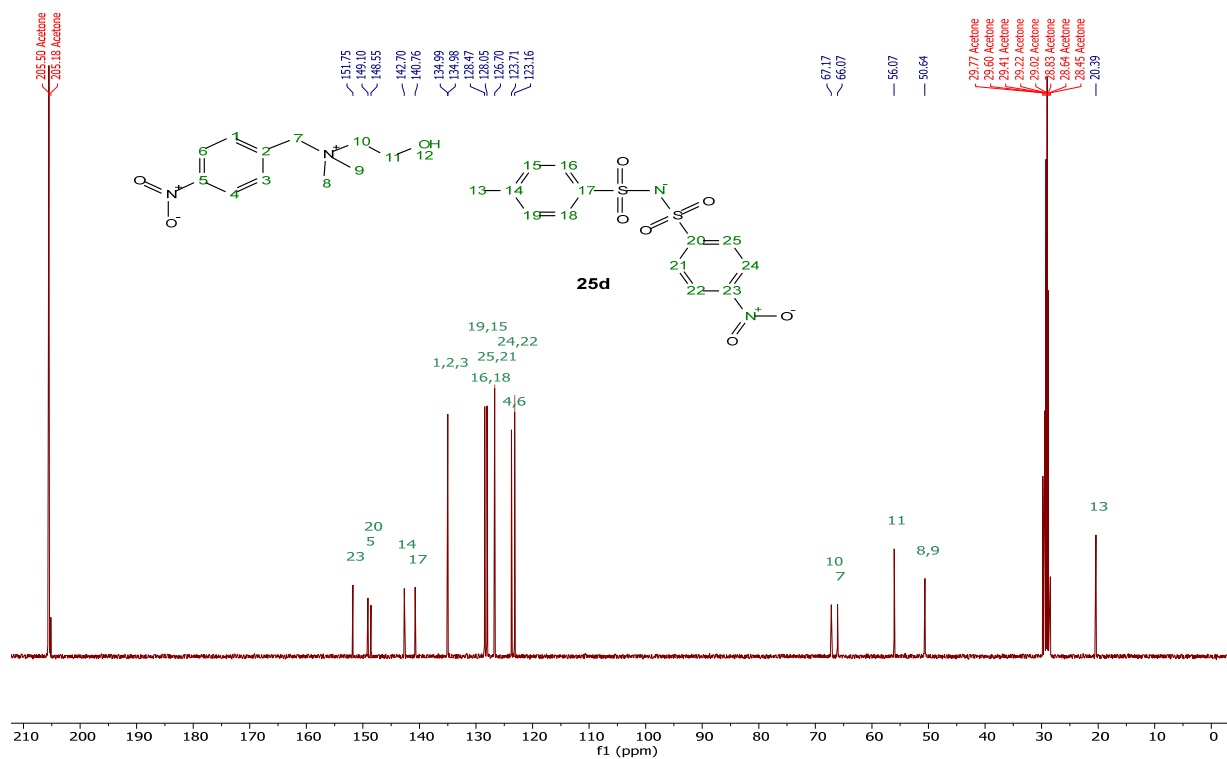
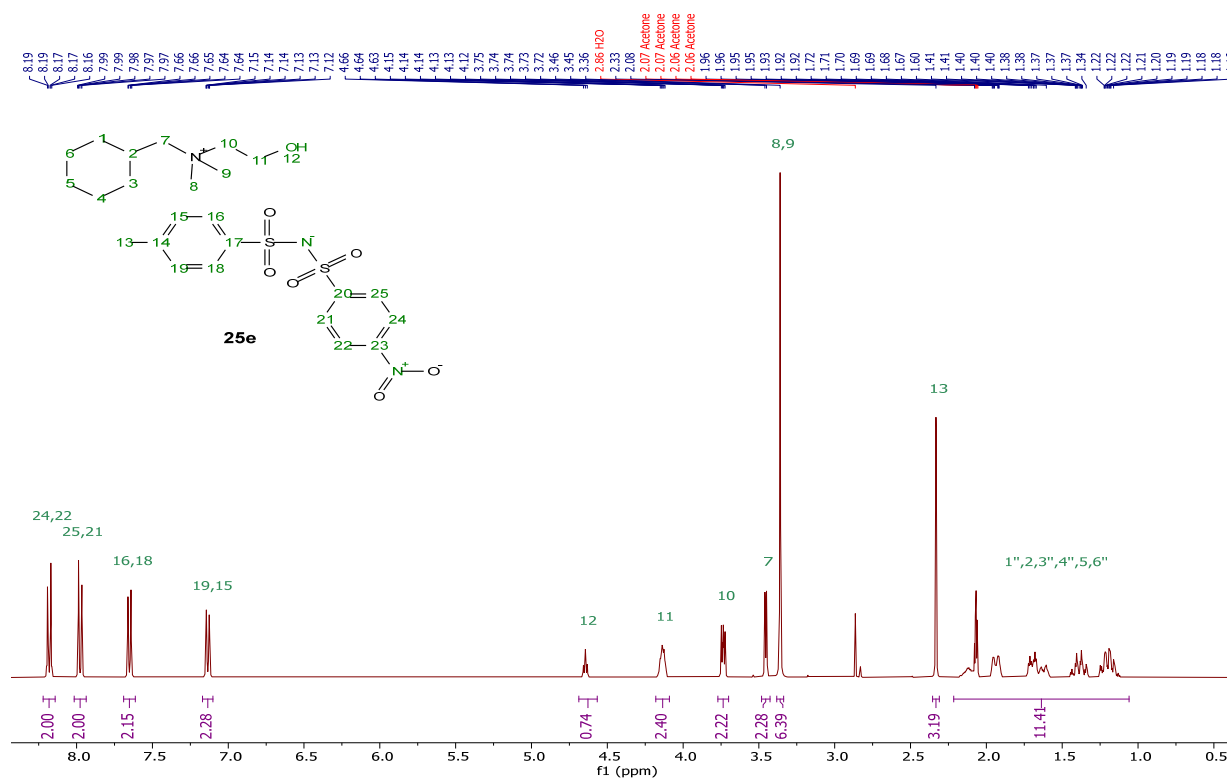
$^{13}\text{C}\{^1\text{H}\}$  NMR (101 MHz, Deuterium Oxide)[Cychol][Br], **23c** $^1\text{H}$  NMR (400 MHz, Deuterium Oxide)

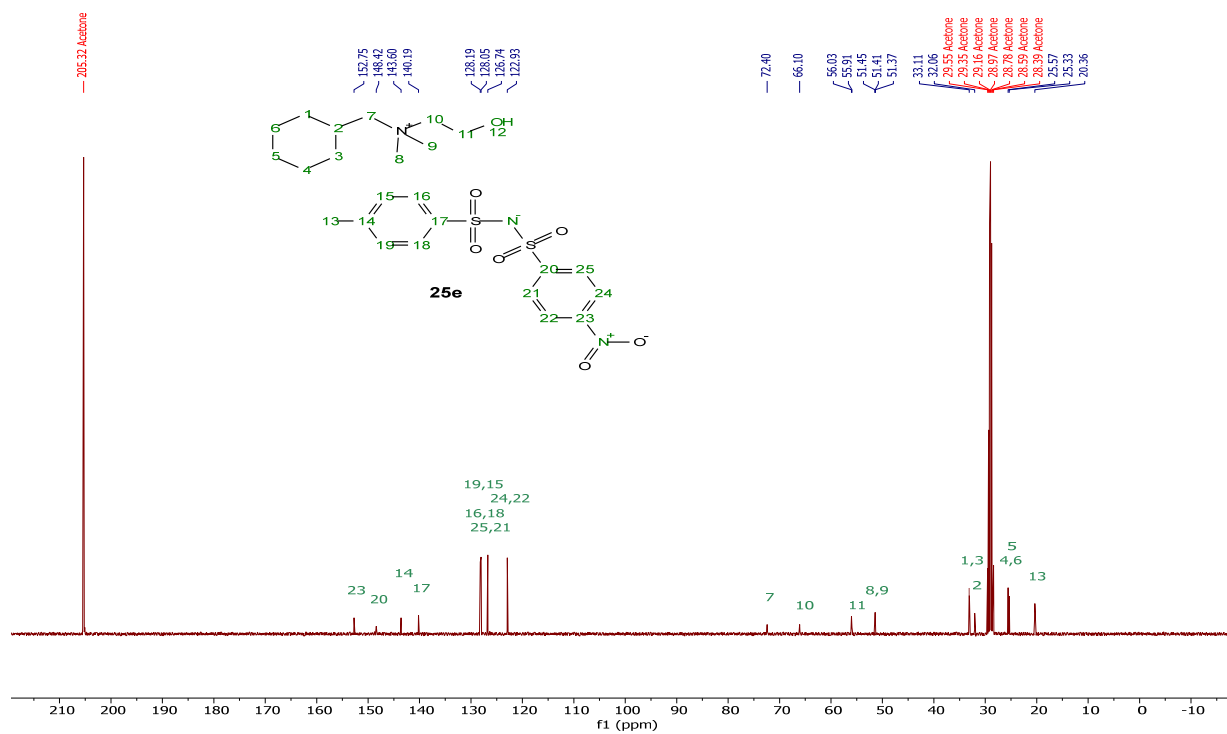
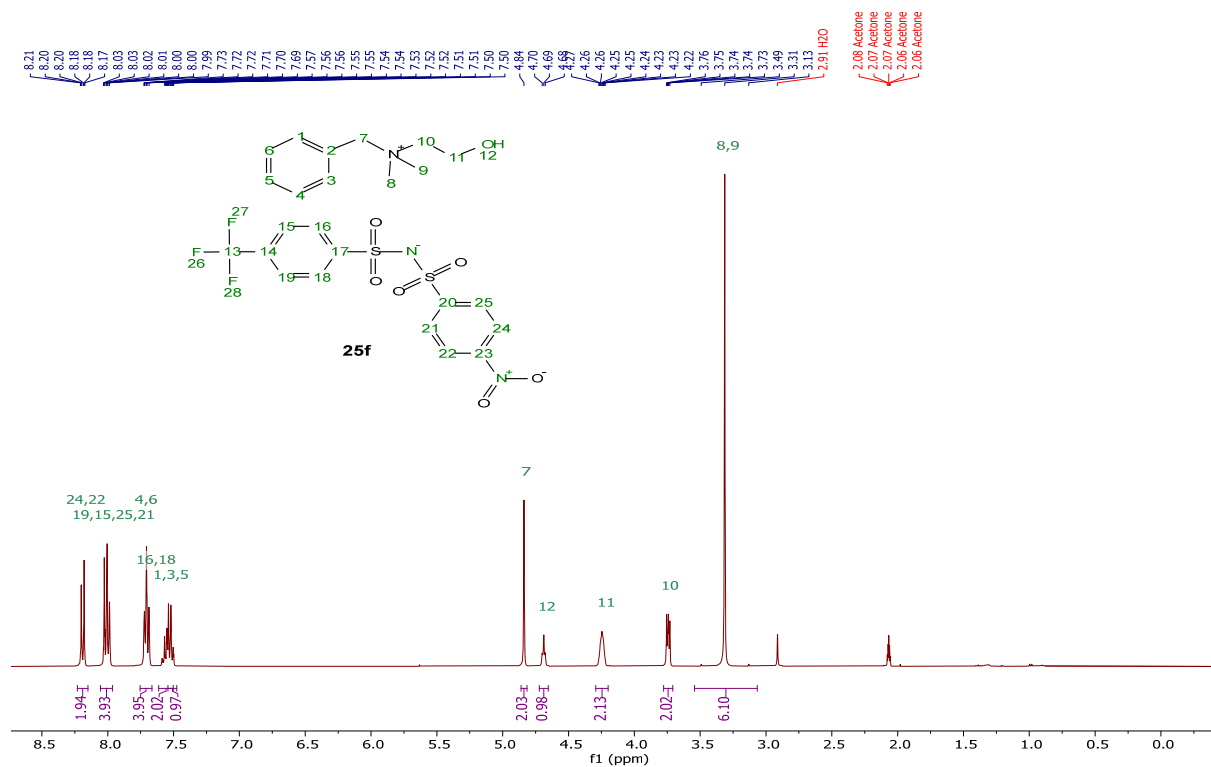
$^{13}\text{C}\{^1\text{H}\}$  NMR (101 MHz, Deuterium Oxide) $[\text{N}_{1,1,6,2\text{OH}}][\text{NBNTs}]$ , **25a** $^1\text{H}$  NMR (400 MHz, Acetone- $d_6$ )

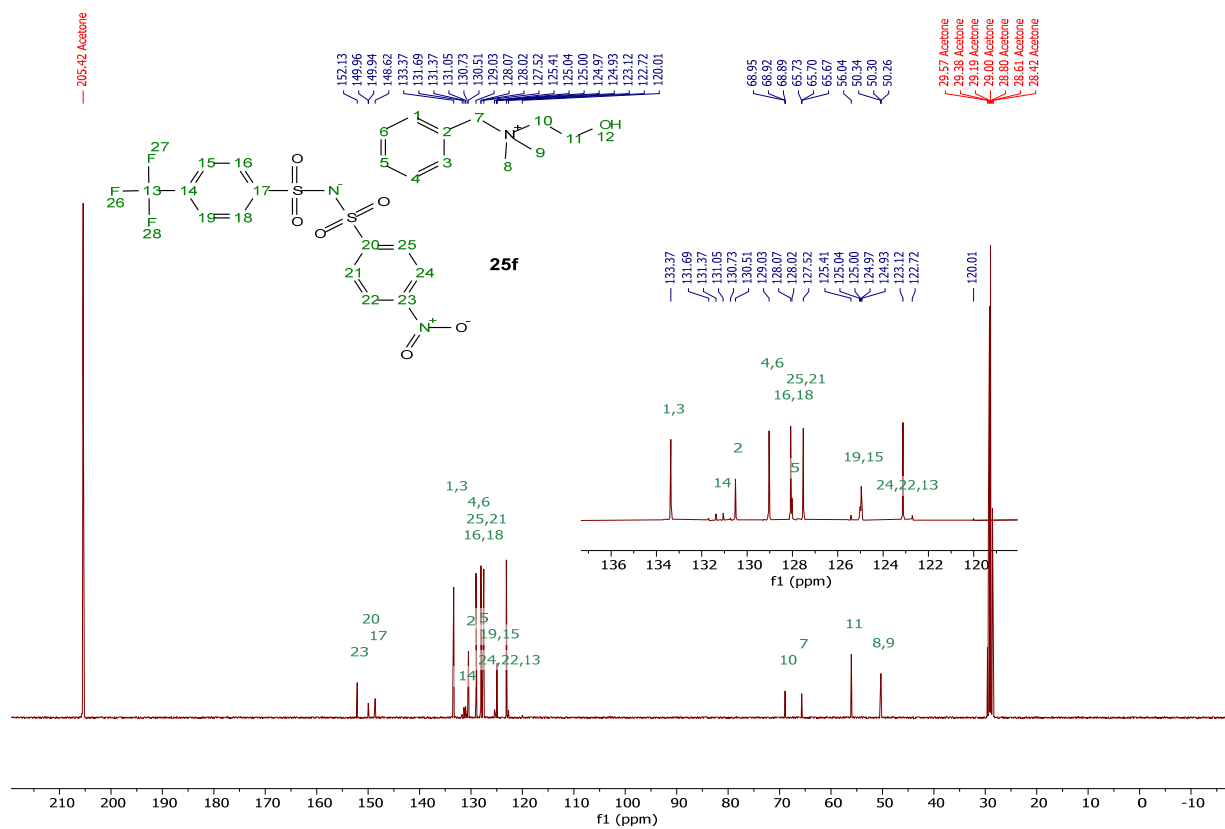
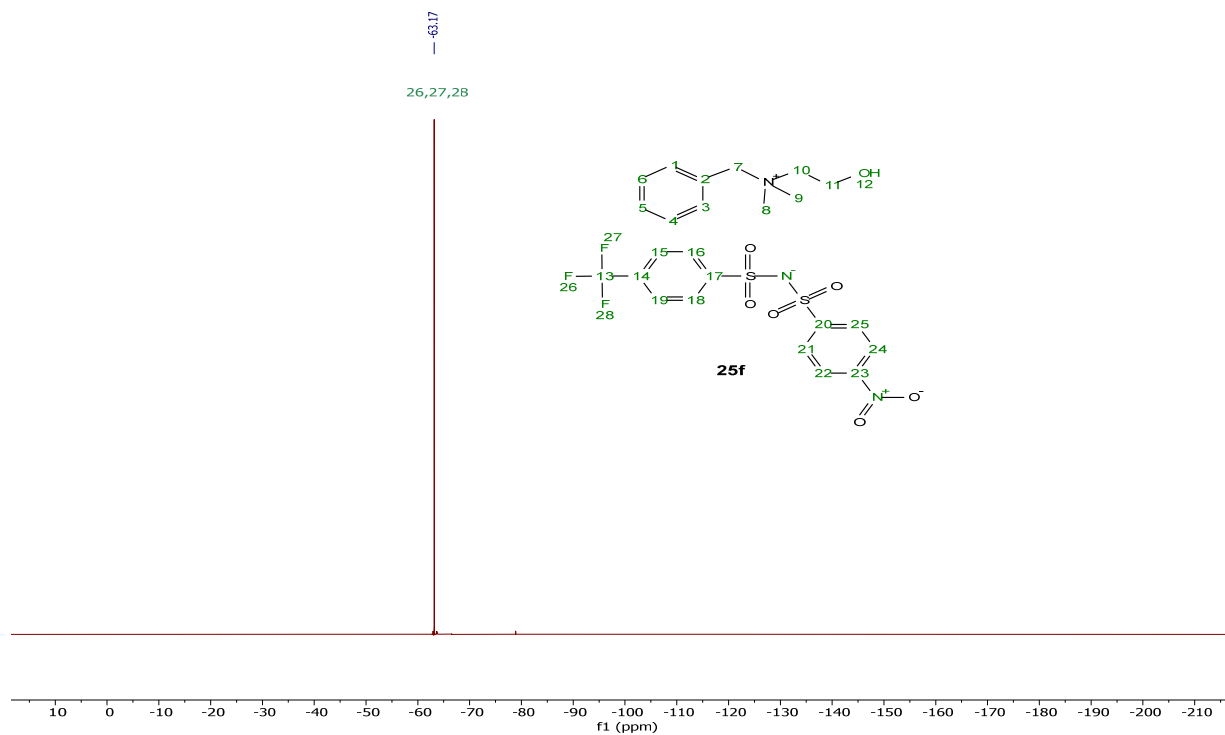
$^{13}\text{C}\{^1\text{H}\}$  NMR (101 MHz, Acetone- $d_6$ )[DC-ether][2NBNTs], **25b** $^1\text{H}$  NMR (400 MHz, Methanol- $d_6$ )

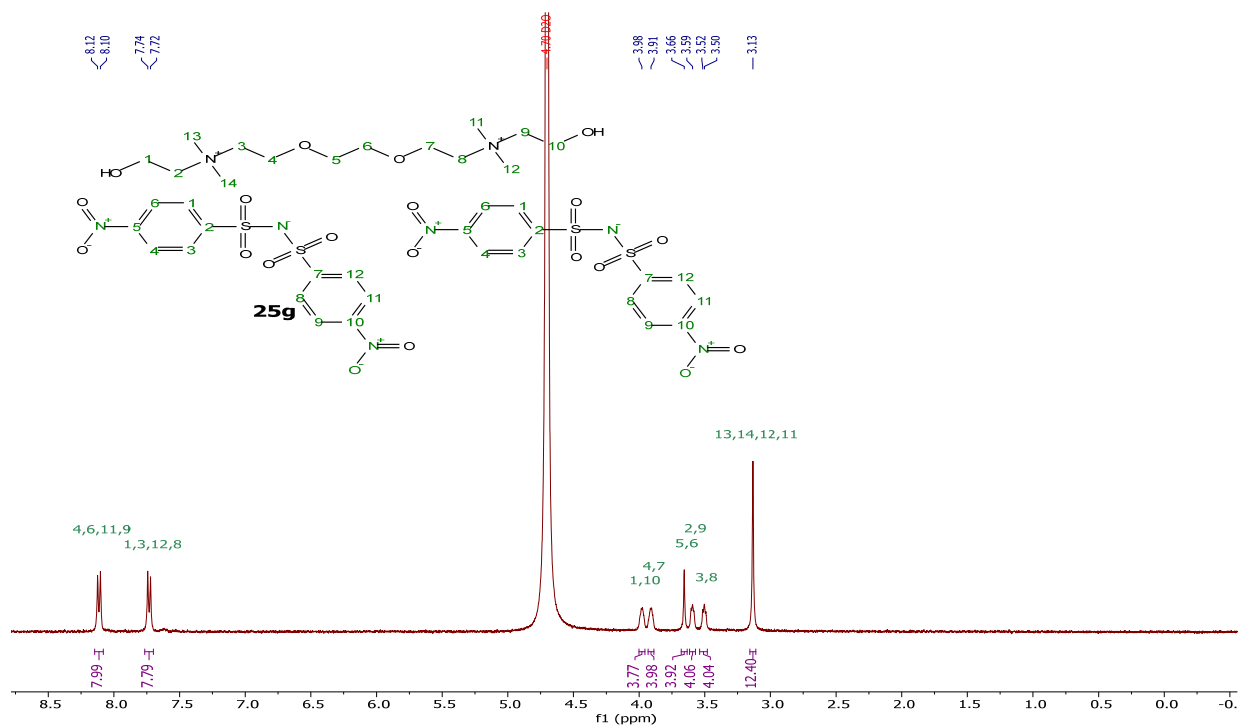
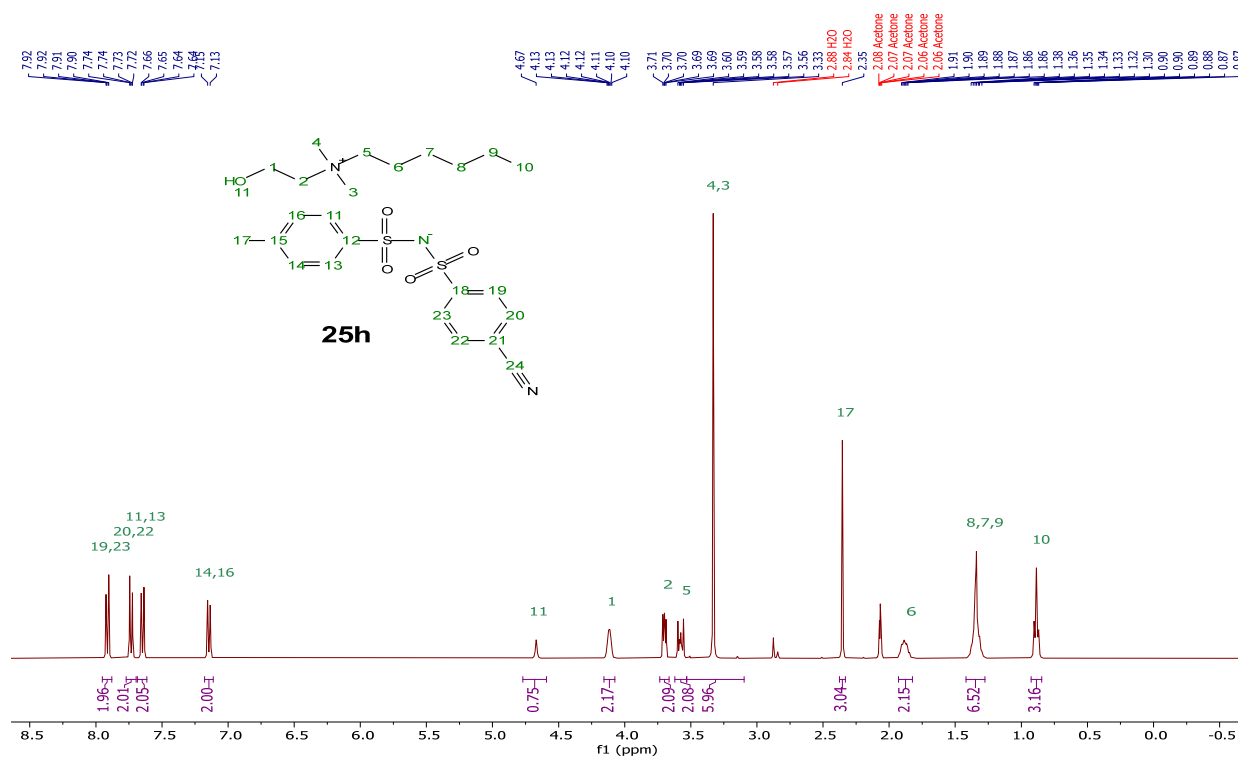
$^{13}\text{C}\{^1\text{H}\}$  NMR (101 MHz, Methanol- $d_4$ )[Bnchol][NBNTs], **25c** $^1\text{H}$  NMR (400 MHz, Acetone- $d_6$ )

$^{13}\text{C}\{^1\text{H}\}$  NMR (101 MHz, Acetone- $d_6$ )[NBnchol][NBNTs], **25d** $^1\text{H}$  NMR (400 MHz, Acetone- $d_6$ )

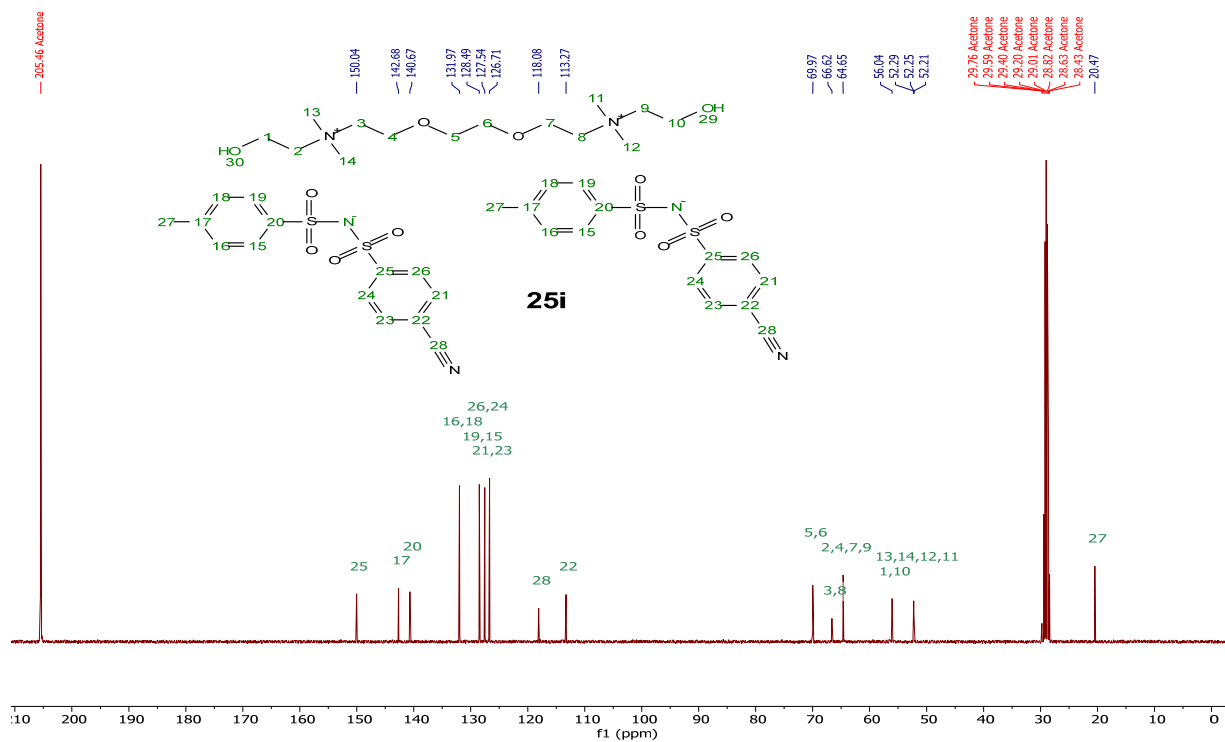
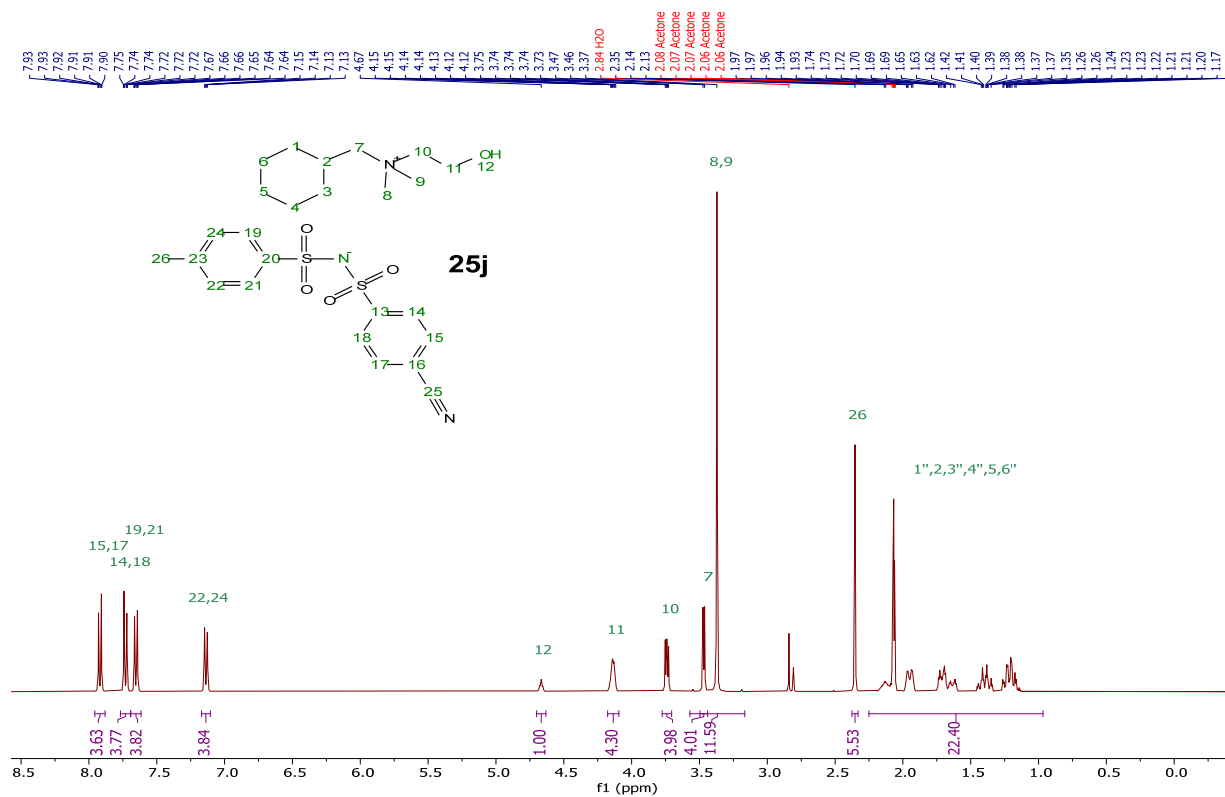
$^{13}\text{C}\{^1\text{H}\}$  NMR (101 MHz, Acetone- $d_6$ )[Cychol][NBNTs], **25e** $^1\text{H}$  NMR (400 MHz, Acetone- $d_6$ )

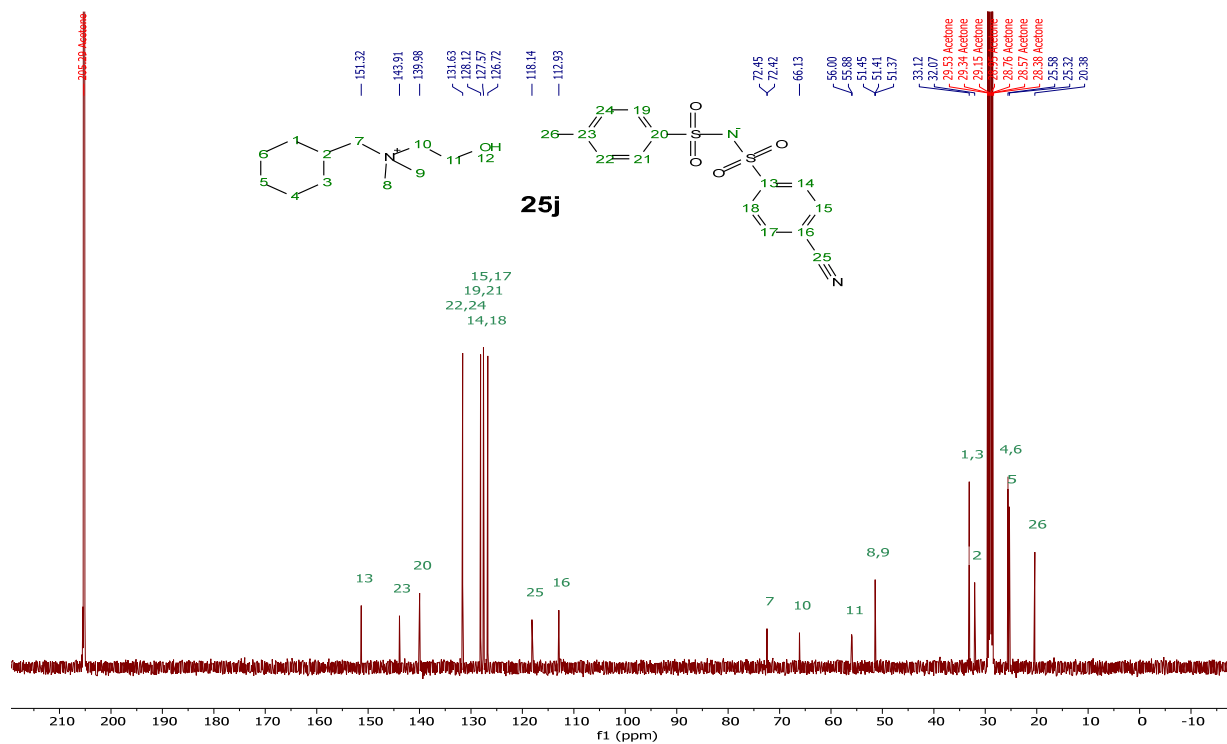
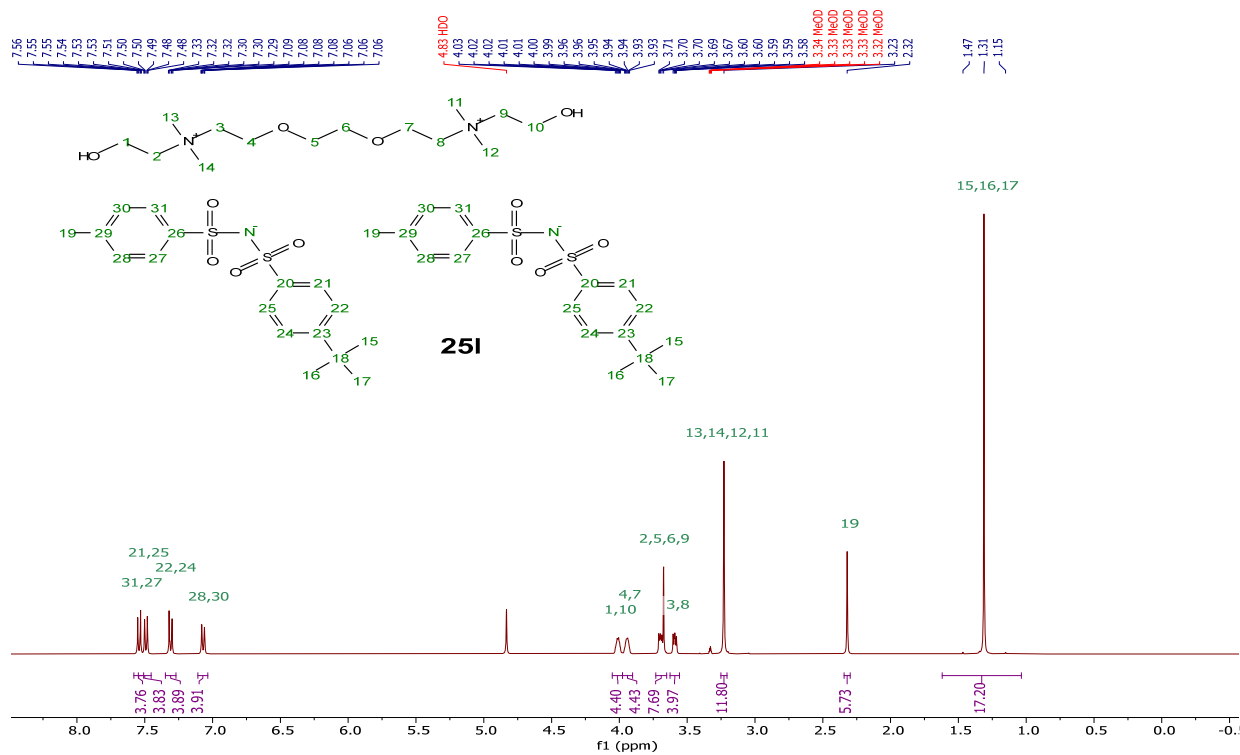
$^{13}\text{C}\{^1\text{H}\}$  NMR (101 MHz, Acetone- $d_6$ )[Bnchol][NBNTFMB], **25f** $^1\text{H}$  NMR (400 MHz, Acetone- $d_6$ )

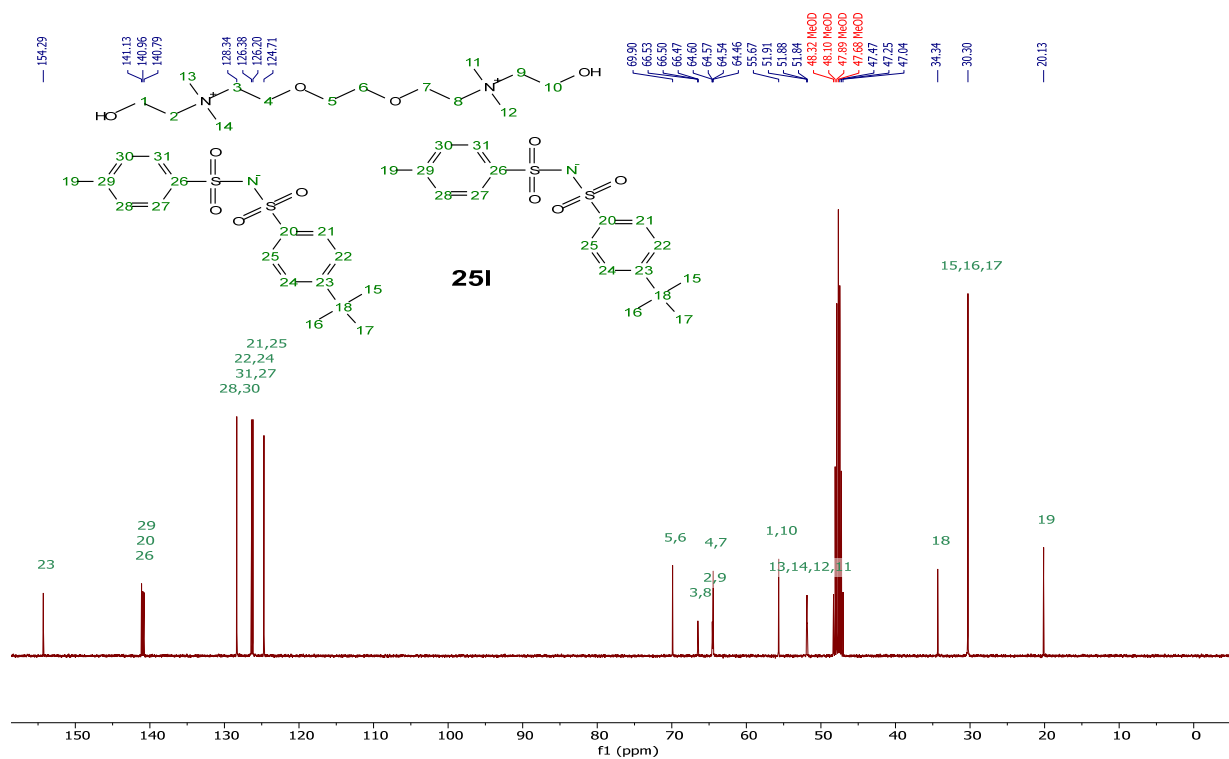
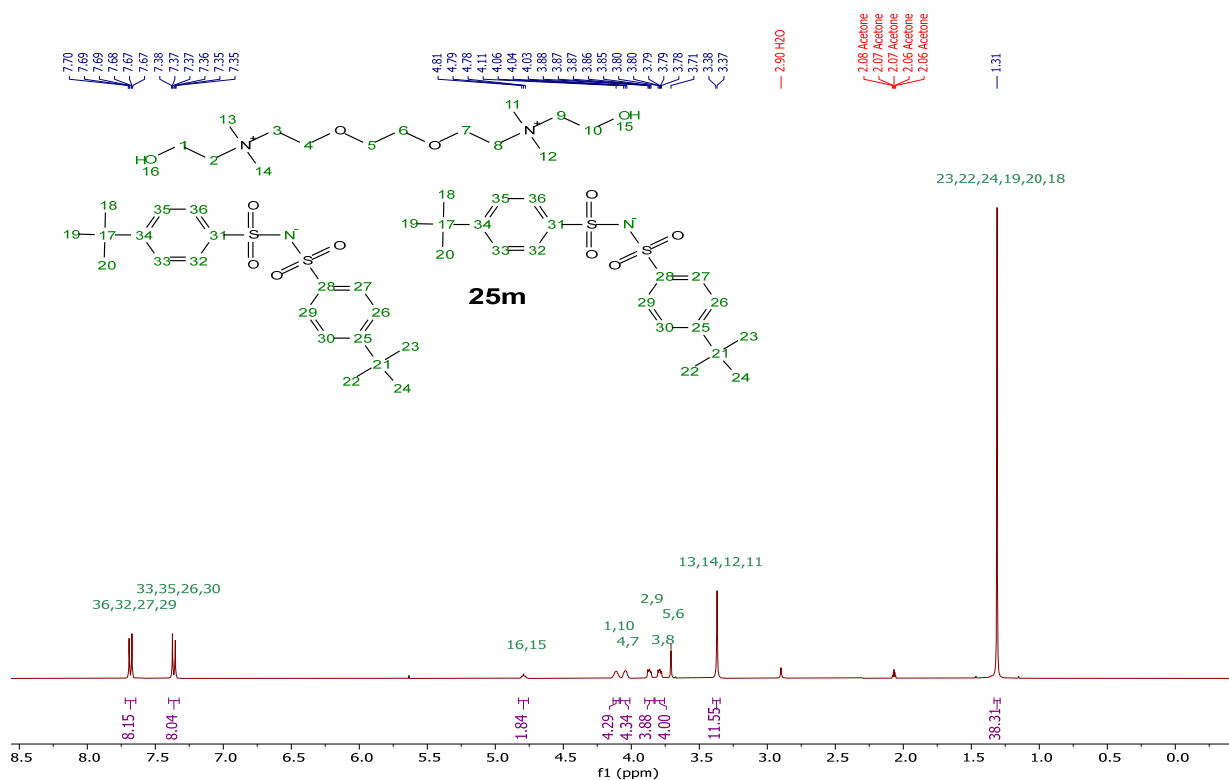
$^{13}\text{C}\{^1\text{H}\}$  NMR (101 MHz, Acetone- $d_6$ ) $^{19}\text{F}$  NMR (376 MHz, Acetone- $d_6$ )

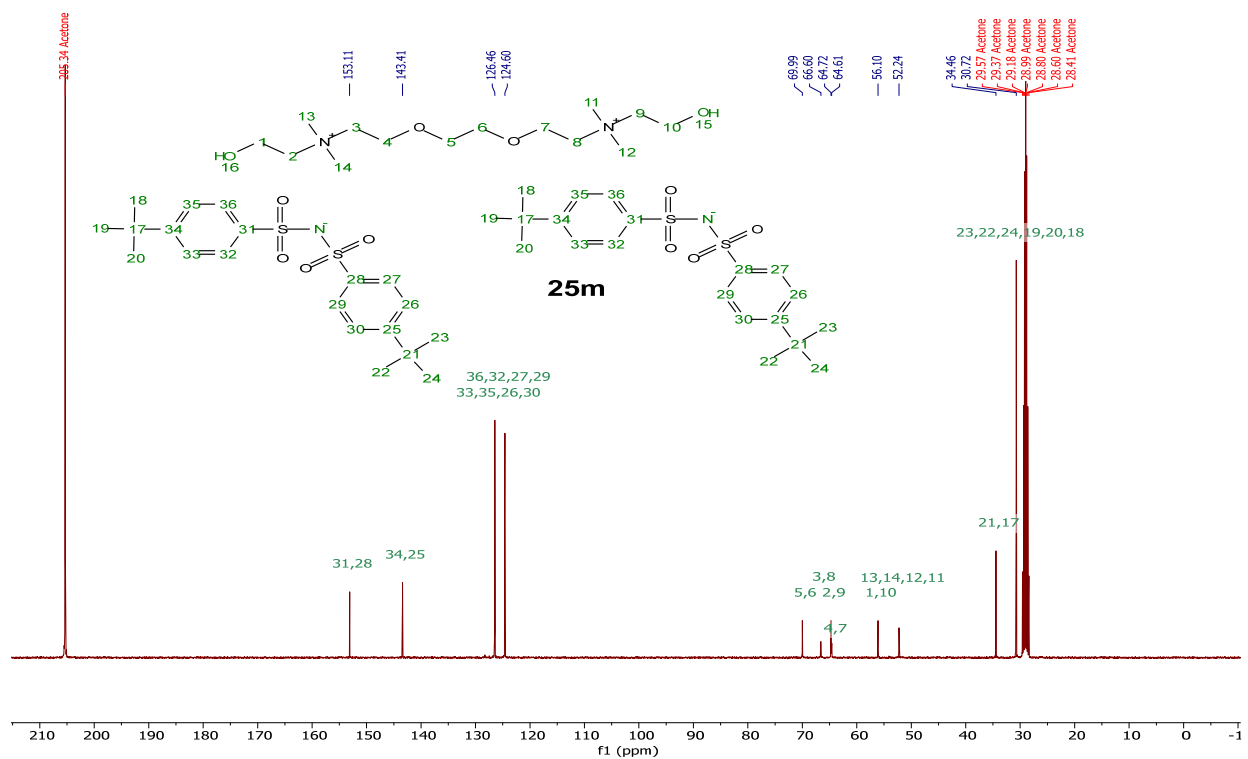
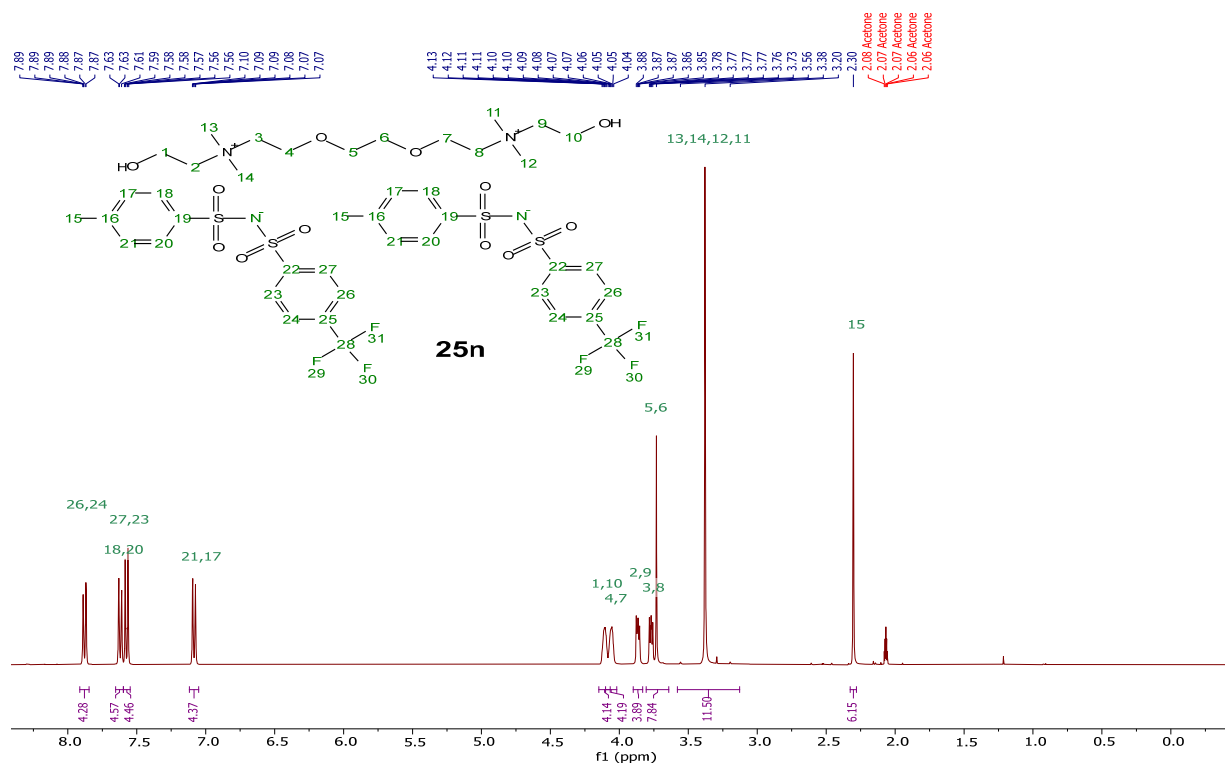
[DC-ether][2N(NB<sub>2</sub>)], **25g**<sup>1</sup>H NMR (400 MHz, Deuterium Oxide)[N<sub>1,1,6,2OH</sub>][CBNTs], **25h**<sup>1</sup>H NMR (400 MHz, Acetone-d<sub>6</sub>)

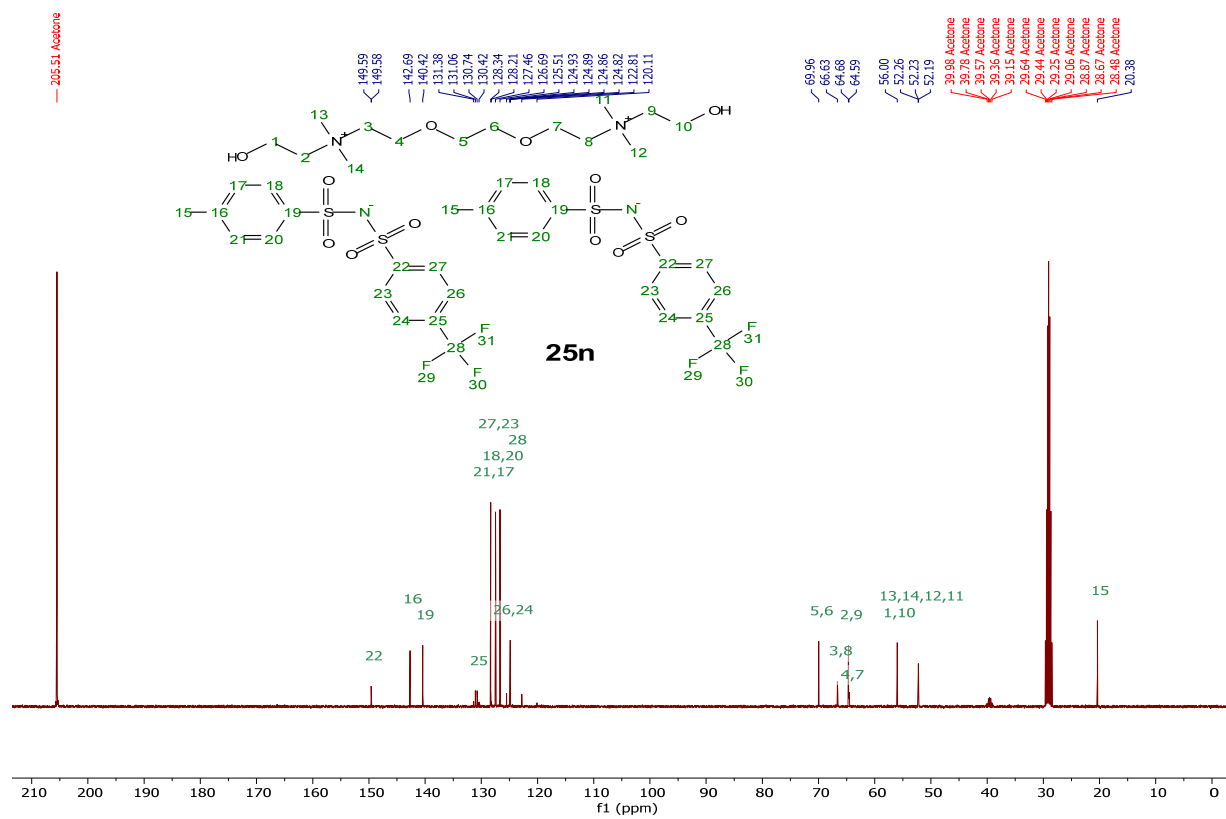
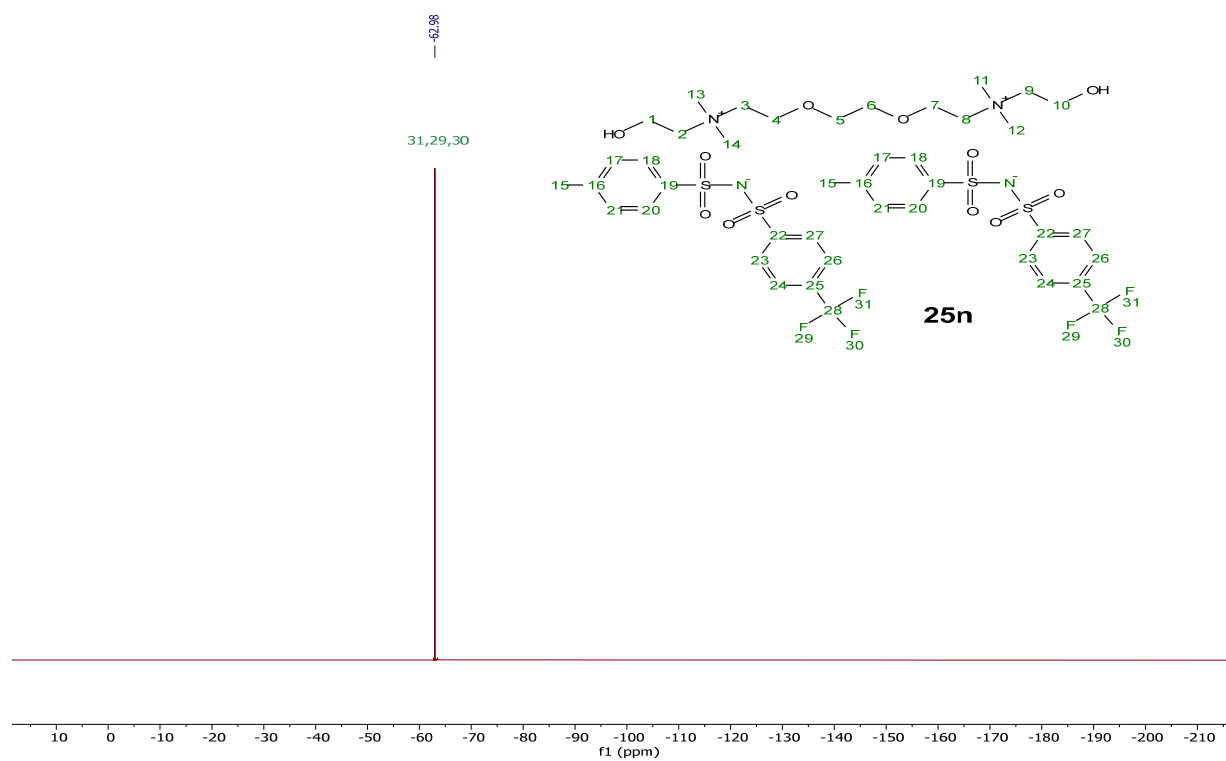


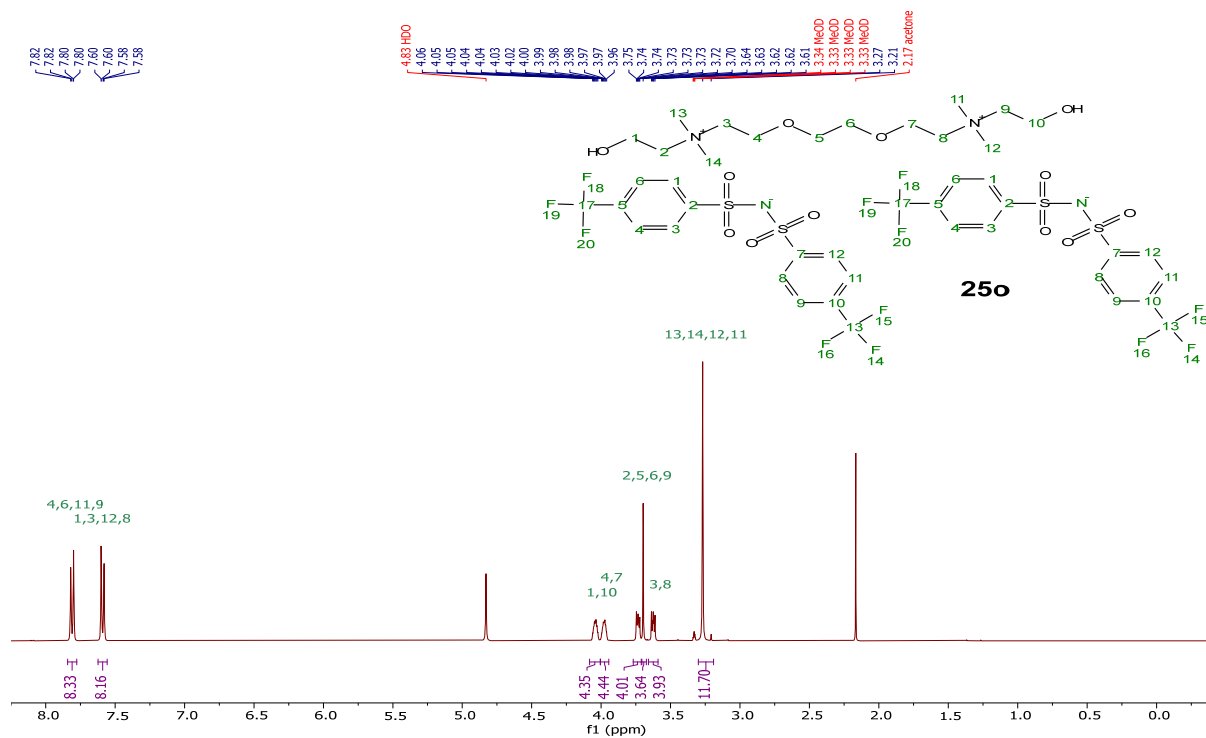
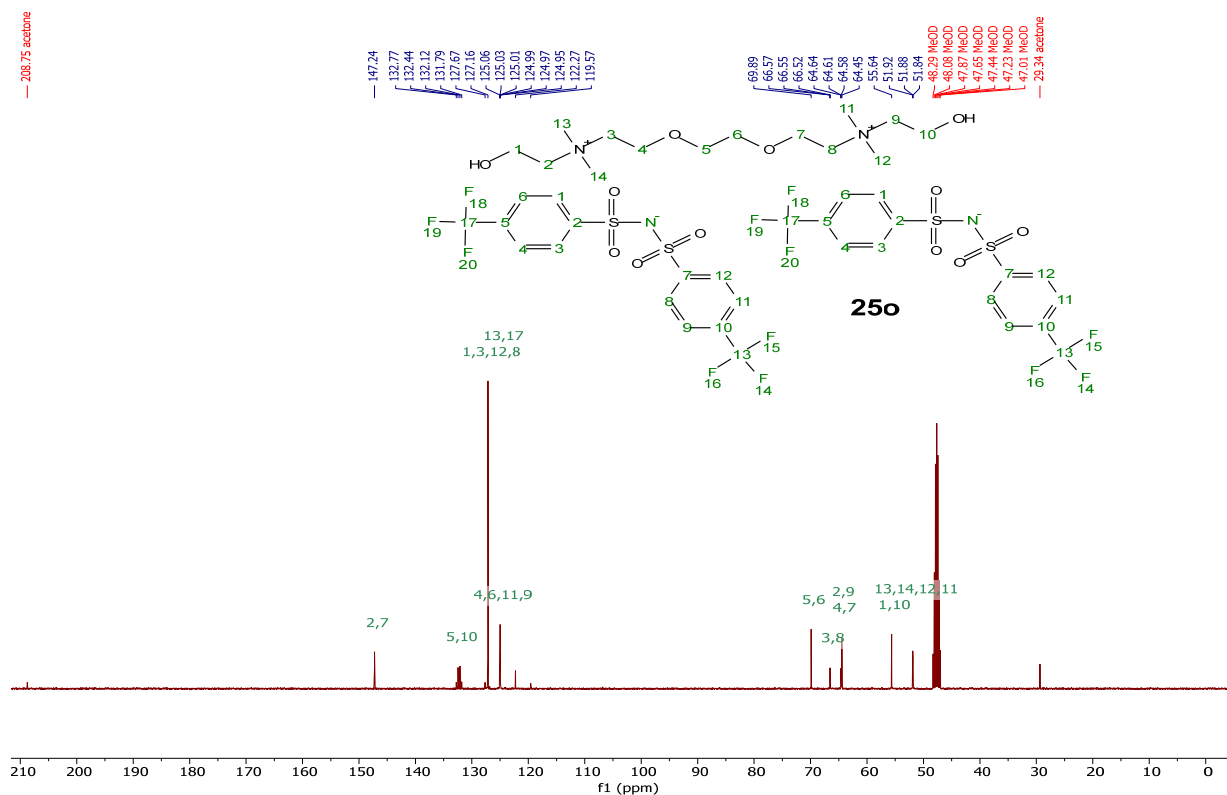
$^{13}\text{C}\{^1\text{H}\}$  NMR (101 MHz, Acetone- $d_6$ )[Cychol][CBNTs], **25j** $^1\text{H}$  NMR (400 MHz, Acetone- $d_6$ )

$^{13}\text{C}\{^1\text{H}\}$  NMR (101 MHz, Acetone- $d_6$ )[DC-ether][2tBBNTs], **25i** $^1\text{H}$  NMR (400 MHz, Methanol- $d_4$ )

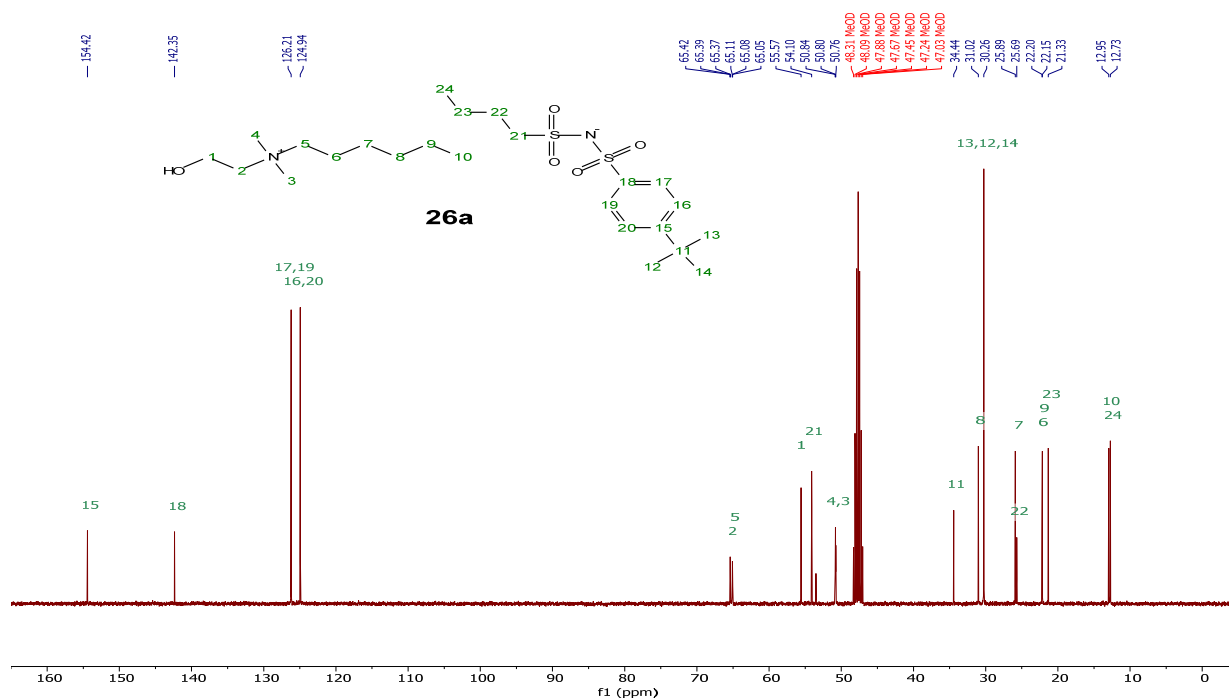
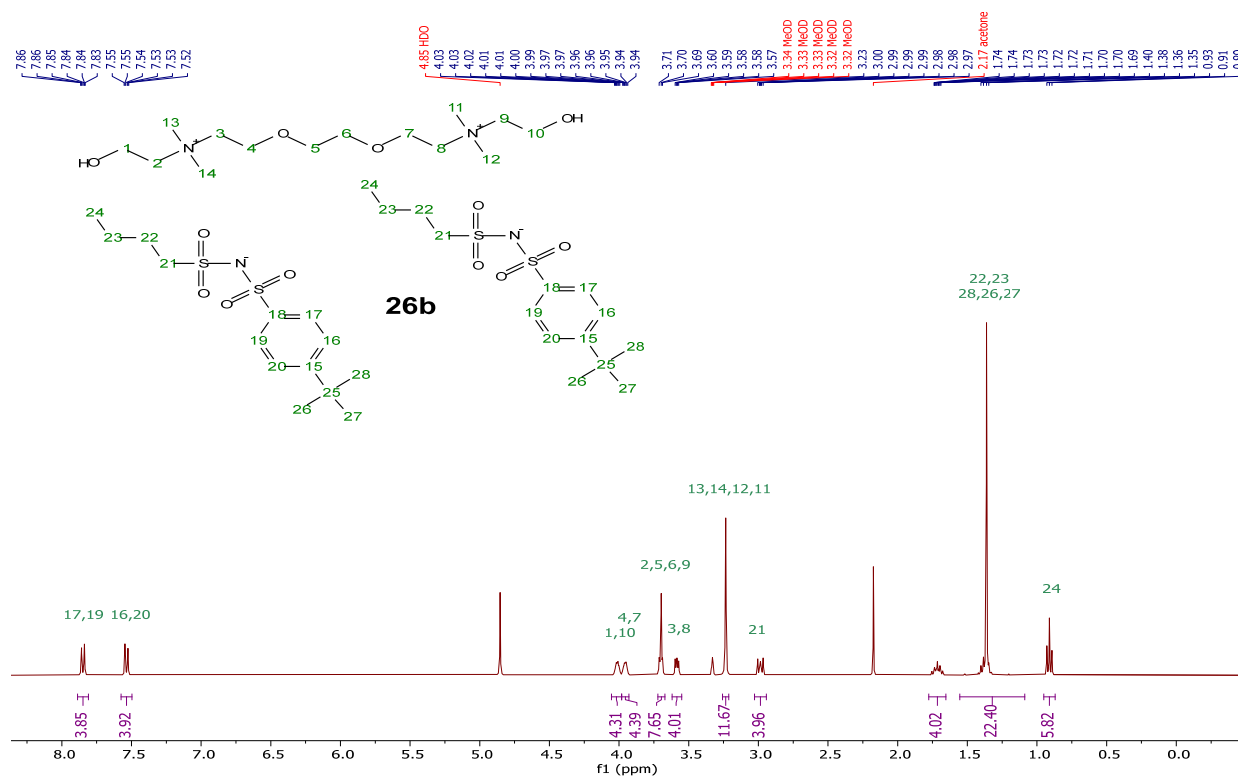
$^{13}\text{C}\{^1\text{H}\}$  NMR (101 MHz, Methanol- $d_4$ )[DC-ether][2N(tBB) $_2$ ], **25m** $^1\text{H}$  NMR (400 MHz, Acetone- $d_6$ )

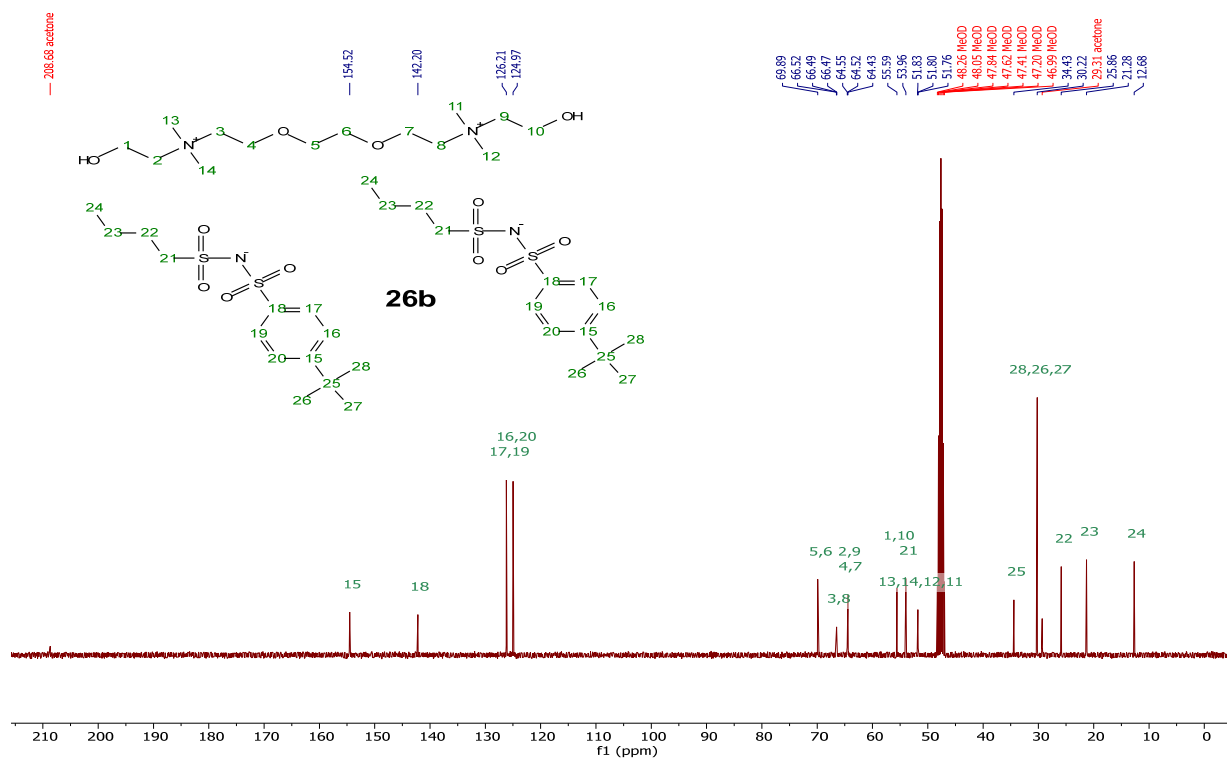
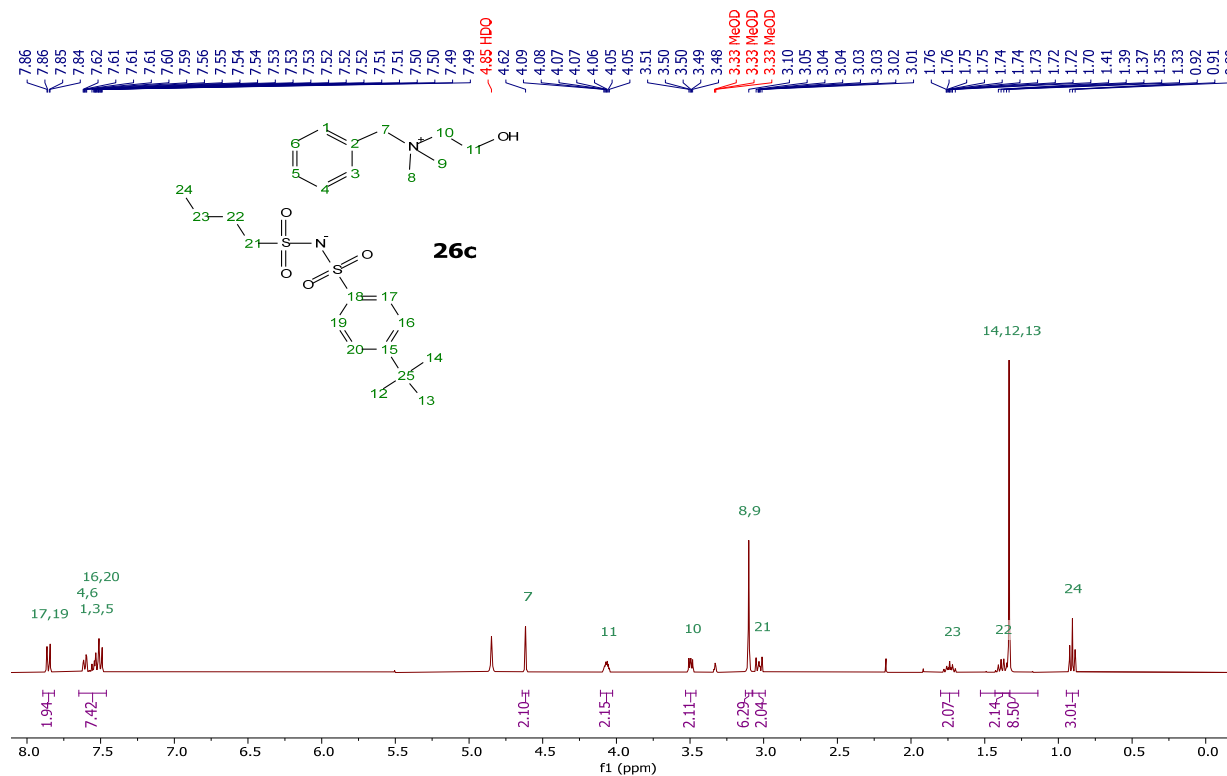
$^{13}\text{C}\{^1\text{H}\}$  NMR (101 MHz, Acetone- $d_6$ )[DC-ether][2TFMBNTs], **25n** $^1\text{H}$  NMR (400 MHz, Acetone- $d_6$ )

$^{13}\text{C}\{^1\text{H}\}$  NMR (101 MHz, Acetone- $d_6$ ) $^{19}\text{F}$  NMR (376 MHz, Acetone- $d_6$ )

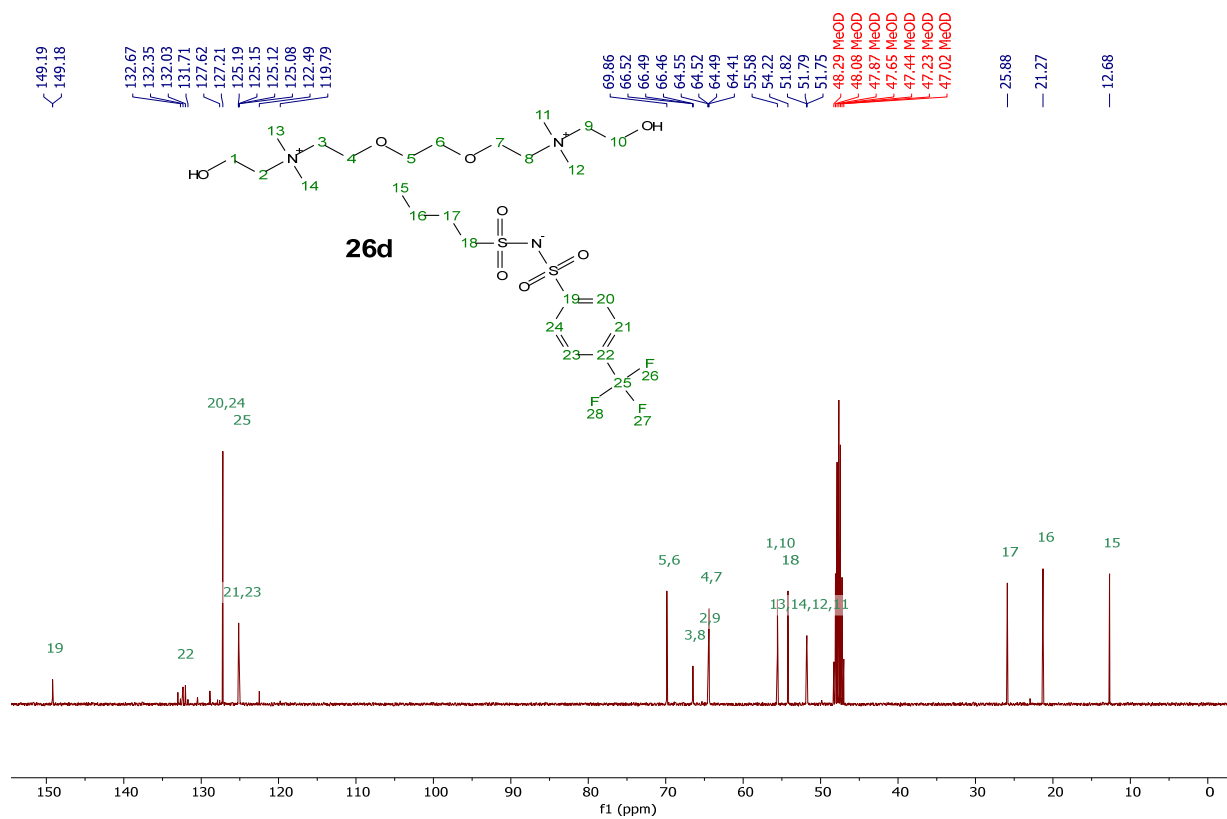
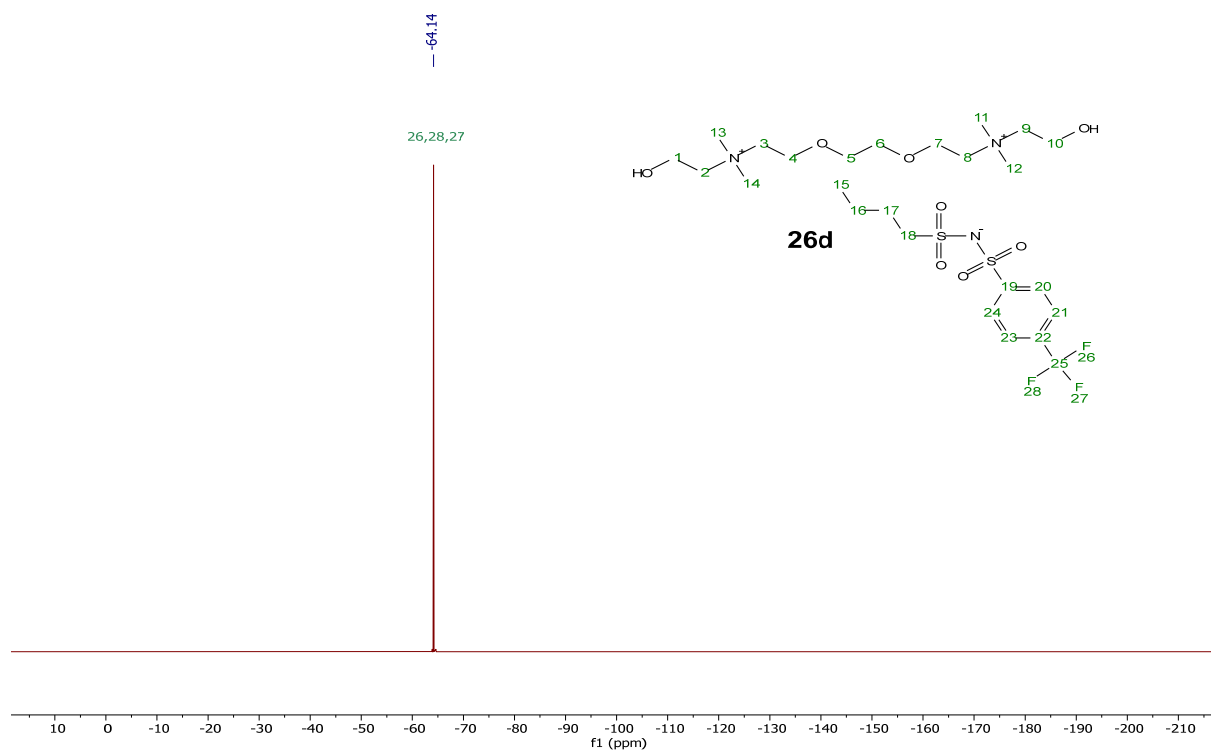
[DC-ether][2N(TFMB)<sub>2</sub>], **25o**<sup>1</sup>H NMR (400 MHz, Methanol-d<sub>4</sub>)<sup>13</sup>C {<sup>1</sup>H} NMR (101 MHz, Methanol-d<sub>4</sub>)



$^{13}\text{C}\{^1\text{H}\}$  NMR (101 MHz, Methanol-d<sub>4</sub>)[DC-ether][2tBBNB], **26b** $^1\text{H}$  NMR (400 MHz, Methanol-d<sub>4</sub>)

$^{13}\text{C}\{^1\text{H}\}$  NMR (101 MHz, Methanol- $d_4$ )[Bnchol][tBBNB], **26c** $^1\text{H}$  NMR (400 MHz, Methanol- $d_4$ )

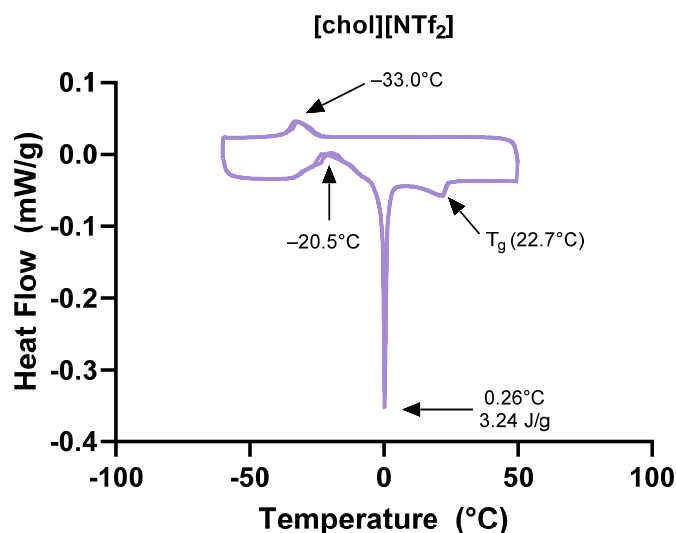


$^{13}\text{C}\{^1\text{H}\}$  NMR (101 MHz, Methanol-d<sub>4</sub>) $^{19}\text{F}$  NMR (376 MHz, Methanol-d<sub>4</sub>)

## A.2 Differential Scanning Calorimetry Thermograms

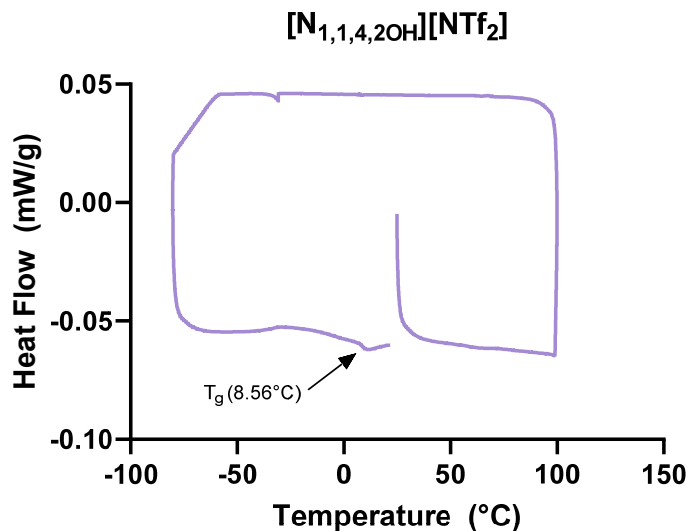
[chol][NTf<sub>2</sub>], **13a**

1: Equilibrate at 50.00 °C; 2: Ramp 10.00 °C/min to -60.00 °C; 3: Isothermal for 10.00 min; 4: Mark end of cycle 0; 5: Ramp 10.00 °C/min to 50.00 °C; 6: Isothermal for 1.00 min; 7: Mark end of cycle 1; 8: Ramp 10.00 °C/min to -60.00 °C; 9: Isothermal for 10.00 min; 10: Mark end of cycle 2; 11: Ramp 10.00 °C/min to 50.00 °C



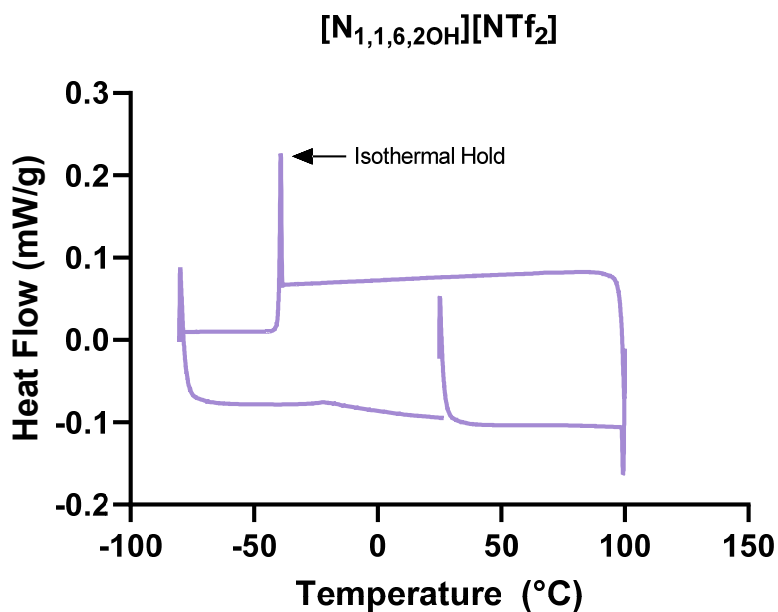
[N<sub>1,1,4,2OH</sub>][NTf<sub>2</sub>], **13b**

1: Equilibrate at 25.00 °C; 2: Ramp 10.00 °C/min to 100.00 °C; 3: Isothermal for 10.00 min; 4: Mark end of cycle 0; 5: Ramp 10.00 °C/min to -80.00 °C; 6: Isothermal for 10.00 min; 7: Mark end of cycle 1; 8: Ramp 10.00 °C/min to 25.00 °C



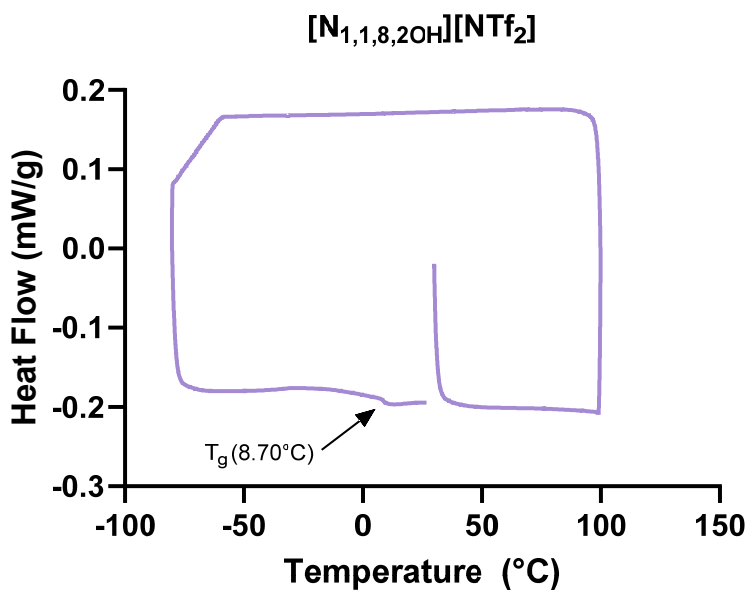
$[N_{1,1,6,2OH}][NTf_2]$ , **13c**

1: Equilibrate at 25.00 °C; 2: Ramp 10.00 °C/min to 100.00 °C; 3: Isothermal for 10.00 min; 4: Mark end of cycle 0; 5: Ramp 10.00 °C/min to -40.00 °C; 6: Ramp 2.00 °C/min to -80.00 °C; 7: Isothermal for 20.00 min; 8: Mark end of cycle 1; 9: Ramp 10.00 °C/min to 30.00 °C



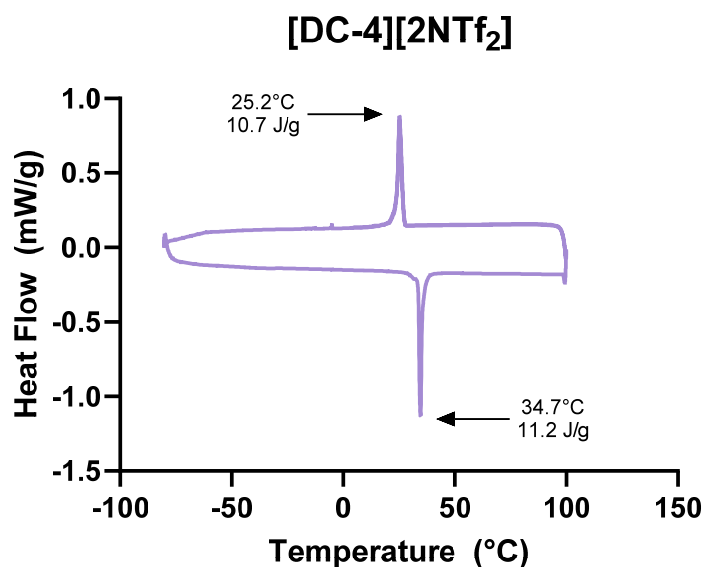
$[N_{1,1,8,2OH}][NTf_2]$ , **13d**

1: Equilibrate at 30.00 °C; 2: Ramp 10.00 °C/min to 100.00 °C; 3: Isothermal for 10.00 min; 4: Mark end of cycle 0; 5: Ramp 10.00 °C/min to -80.00 °C; 6: Isothermal for 10.00 min; 7: Mark end of cycle 1; 8: Ramp 10.00 °C/min to 30.00 °C

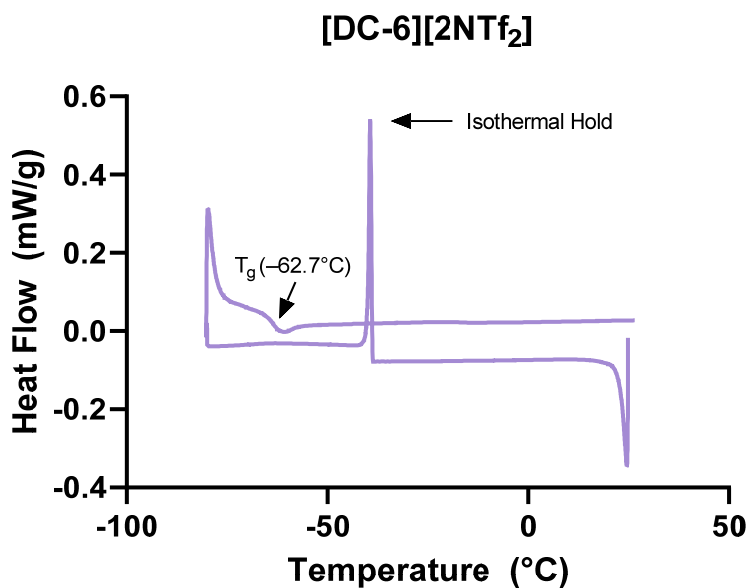


**[DC-4][2NTf<sub>2</sub>], 13i**

1: Equilibrate at 30.00 °C; 2: Ramp 10.00 °C/min to 100.00 °C; 3: Isothermal for 15.00 min; 4: Mark end of cycle 0; 5: Ramp 10.00 °C/min to -80.00 °C; 6: Isothermal for 20.00 min; 7: Mark end of cycle 1; 8: Ramp 10.00 °C/min to 100.00 °C; 9: Isothermal for 1.00 min; 10: Mark end of cycle 2; 11: Ramp 10.00 °C/min to 0.00 °C

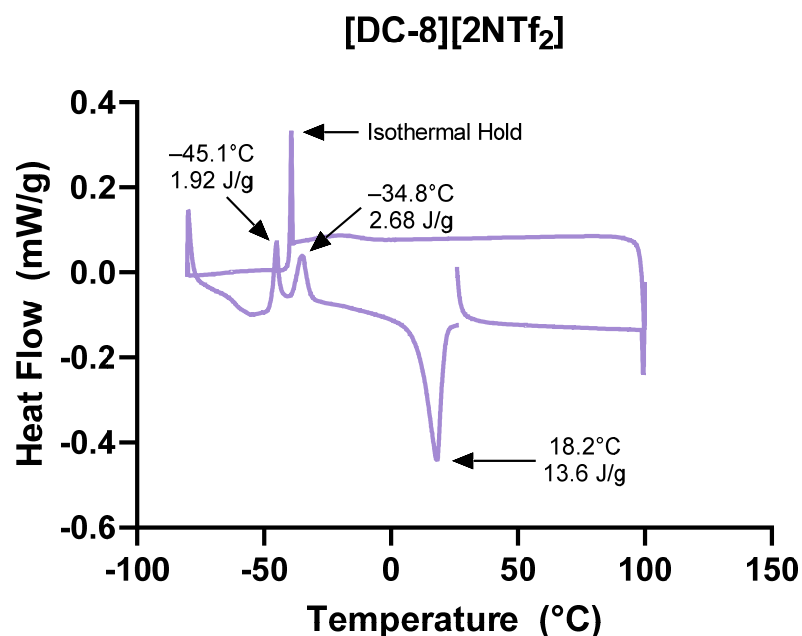
**[DC-6][2NTf<sub>2</sub>], 13k**

1: Equilibrate at 25.00 °C; 2: Mark end of cycle 0; 3: Ramp 10.00 °C/min to -40.00 °C; 4: Ramp 2.00 °C/min to -80.00 °C; 5: Isothermal for 30.00 min; 6: Mark end of cycle 1; 7: Ramp 10.00 °C/min to 30.00 °C

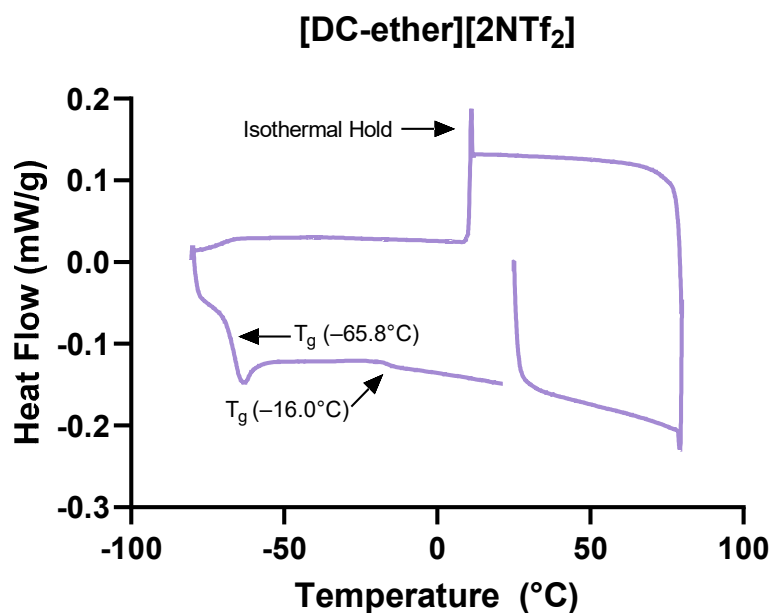


**[DC-8][2NTf<sub>2</sub>], 13m**

1: Equilibrate at 25.00 °C; 2: Ramp 10.00 °C/min to 100.00 °C; 3: Isothermal for 10.00 min; 4: Mark end of cycle 0; 5: Ramp 10.00 °C/min to -40.00 °C; 6: Ramp 2.00 °C/min to -80.00 °C; 7: Isothermal for 10.00 min; 8: Mark end of cycle 1; 9: Ramp 10.00 °C/min to 30.00 °C

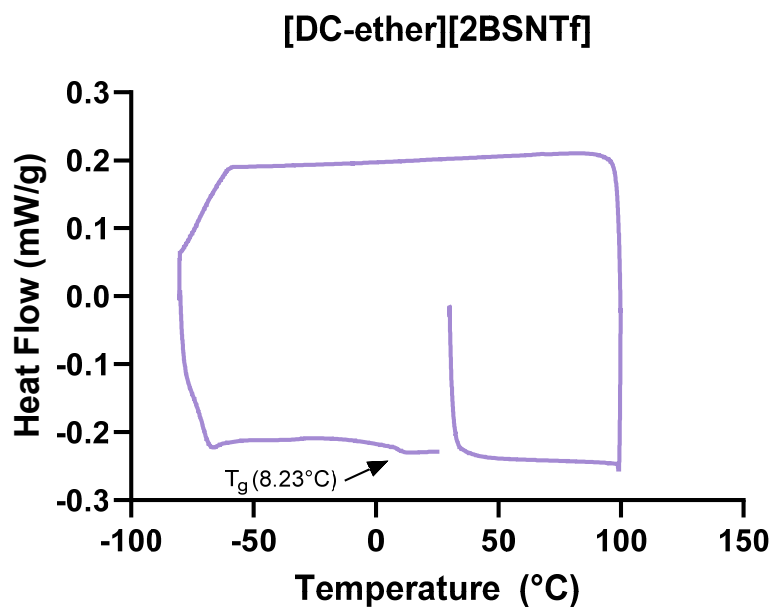
**[DC-ether][2NTf<sub>2</sub>], 13p**

1: Equilibrate at 25.00 °C; 2: Ramp 10.00 °C/min to 80.00 °C; 3: Isothermal for 20.00 min; 4: Mark end of cycle 0; 5: Ramp 10.00 °C/min to 10.00 °C; 6: Ramp 2.00 °C/min to -80.00 °C; 7: Isothermal for 30.00 min; 8: Mark end of cycle 1; 9: Ramp 10.00 °C/min to 25.00 °C

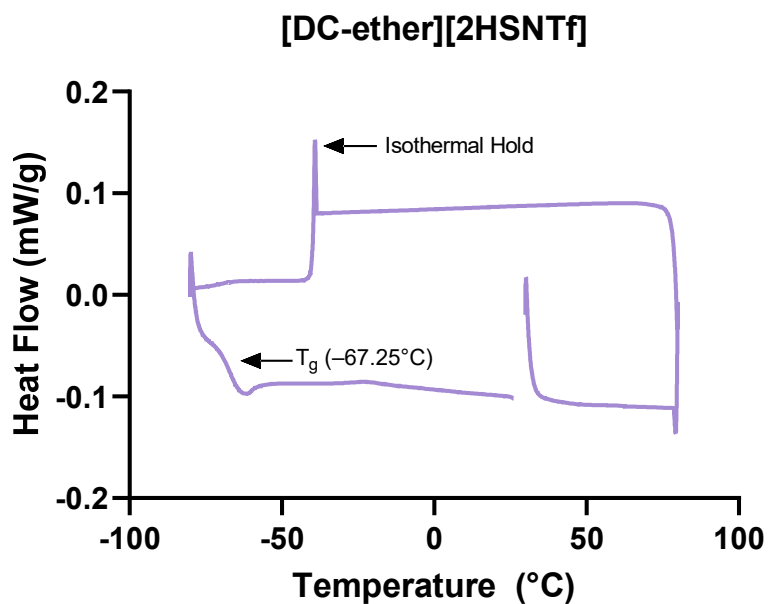


**[DC-ether][2BSNTf], 18a**

1: Equilibrate at 30.00 °C; 2: Ramp 10.00 °C/min to 100.00 °C; 3: Isothermal for 10.00 min; 4: Mark end of cycle 0; 5: Ramp 10.00 °C/min to -80.00 °C; 6: Isothermal for 10.00 min; 7: Mark end of cycle 1; 8: Ramp 10.00 °C/min to 30.00 °C

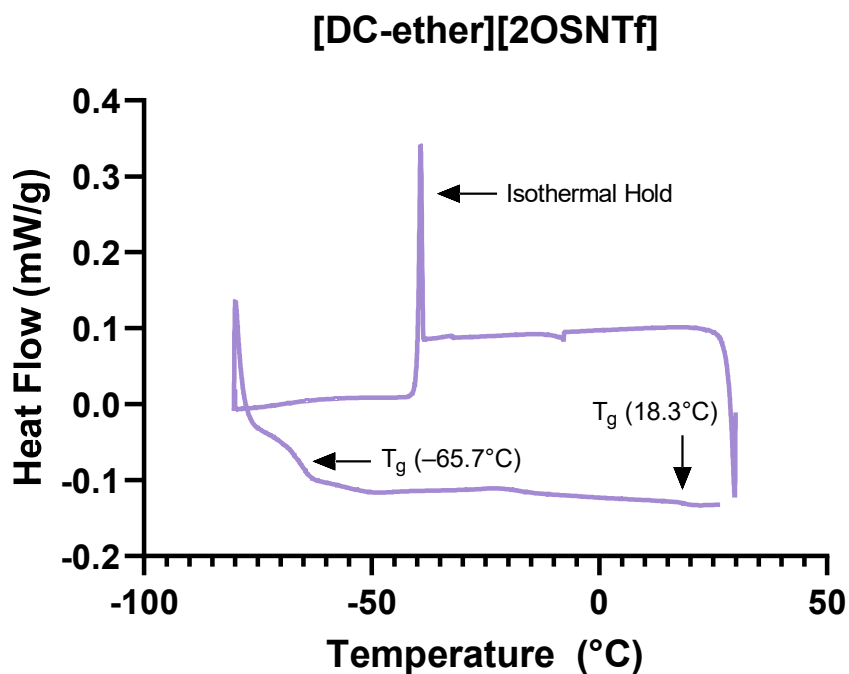
**[DC-ether][2HSNTf], 18b**

1: Equilibrate at 30.00 °C; 2: Ramp 10.00 °C/min to 80.00 °C; 3: Isothermal for 15.00 min; 4: Mark end of cycle 0; 5: Ramp 10.00 °C/min to -40.00 °C; 6: Ramp 2.00 °C/min to -80.00 °C; 7: Isothermal for 20.00 min; 8: Mark end of cycle 1; 9: Ramp 10.00 °C/min to 30.00 °C



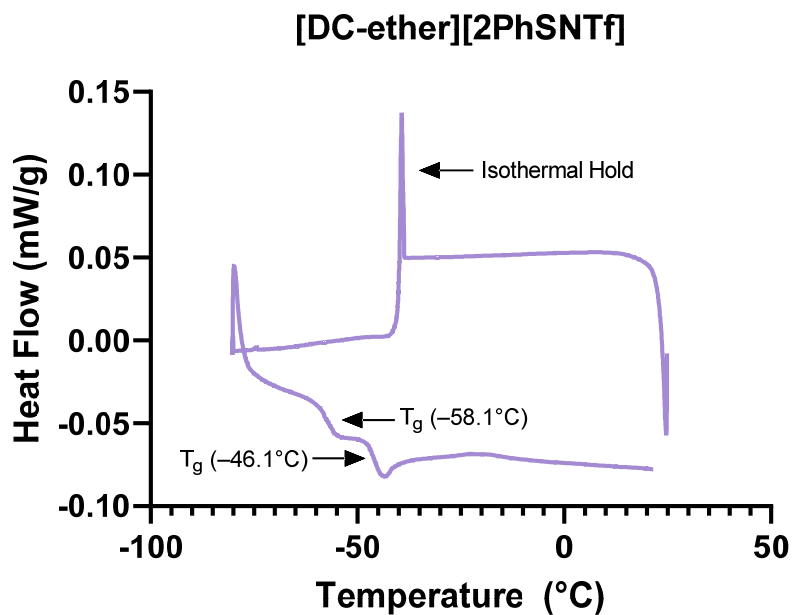
[DC-ether][2OSNTf], 18c

1: Equilibrate at 30.00 °C; 2: Ramp 10.00 °C/min to -40.00 °C; 3: Ramp 2.00 °C/min to -80.00 °C; 4: Isothermal for 10.00 min; 5: Mark end of cycle 0; 6: Ramp 10.00 °C/min to 30.00 °C



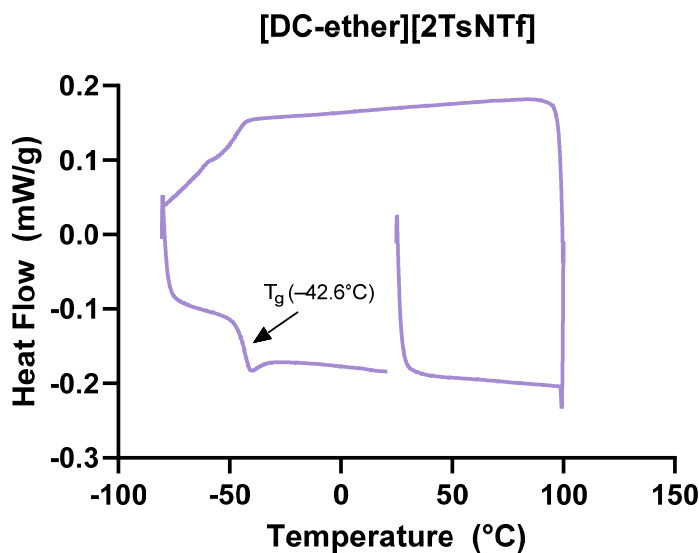
[DC-ether][2PhSNTf], 18d

1: Equilibrate at 25.00 °C; 2: Ramp 10.00 °C/min to 40.00 °C; 3: Mark end of cycle 0; 4: Ramp 2.00 °C/min to -80.00 °C; 5: Isothermal for 10.00 min; 6: Mark end of cycle 1; 7: Ramp 10.00 °C/min to 25.00 °C



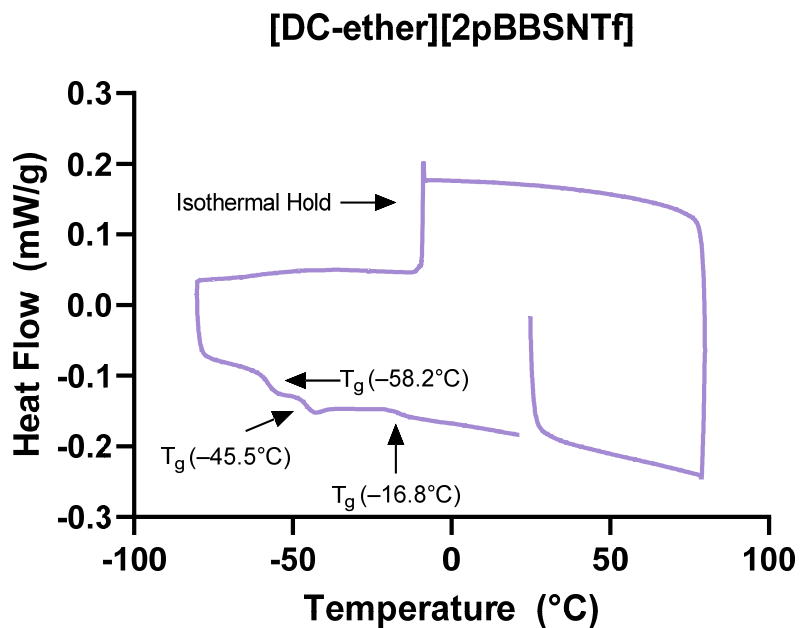
## [DC-ether][2TsNTf], 18e

1: Equilibrate at 25.00 °C; 2: Ramp 10.00 °C/min to 100.00 °C; 3: Isothermal for 10.00 min; 4: Mark end of cycle 0; 5: Ramp 10.00 °C/min to -80.00 °C; 6: Isothermal for 10.00 min; 7: Mark end of cycle 1; 8: Ramp 10.00 °C/min to 25.00 °C



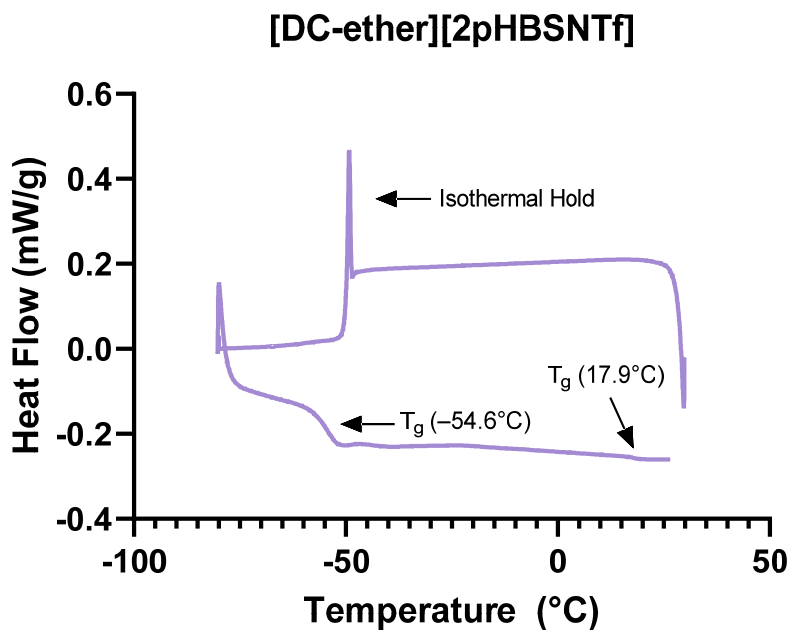
## [DC-ether][2pBBSNTf], 18f

1: Equilibrate at 25.00 °C; 2: Ramp 10.00 °C/min to 80.00 °C; 3: Isothermal for 1.00 min; 4: Mark end of cycle 0; 5: Ramp 10.00 °C/min to -10.00 °C; 6: Ramp 2.00 °C/min to -80.00 °C; 7: Isothermal for 30.00 min; 8: Mark end of cycle 1; 9: Ramp 10.00 °C/min to 25.00 °C



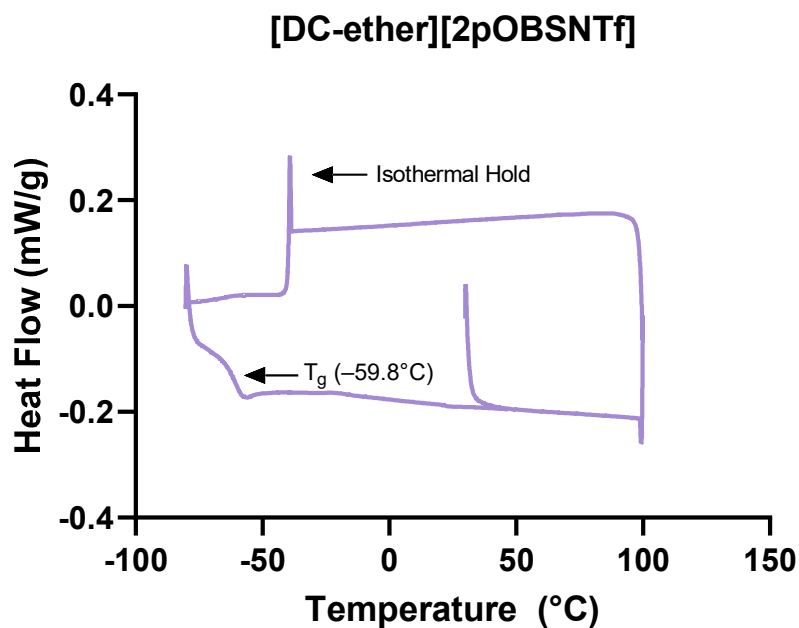
[DC-ether][2pHBSNTf], 18g

1: Equilibrate at 30.00 °C; 2: Ramp 10.00 °C/min to -50.00 °C; 3: Ramp 2.00 °C/min to -80.00 °C; 4: Isothermal for 10.00 min; 5: Mark end of cycle 0; 6: Ramp 10.00 °C/min to 30.00 °C



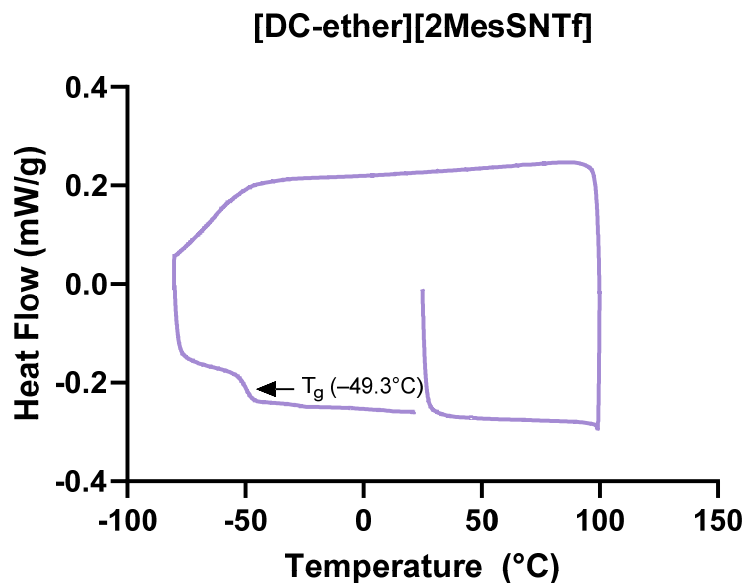
[DC-ether][2pOBSNTf], 18h

1: Equilibrate at 30.00 °C; 2: Ramp 10.00 °C/min to 100.00 °C; 3: Isothermal for 10.00 min; 4: Mark end of cycle 0; 5: Ramp 10.00 °C/min to -40.00 °C; 6: Ramp 2.00 °C/min to -80.00 °C; 7: Isothermal for 20.00 min; 8: Mark end of cycle 1; 9: Ramp 10.00 °C/min to 50.00 °C



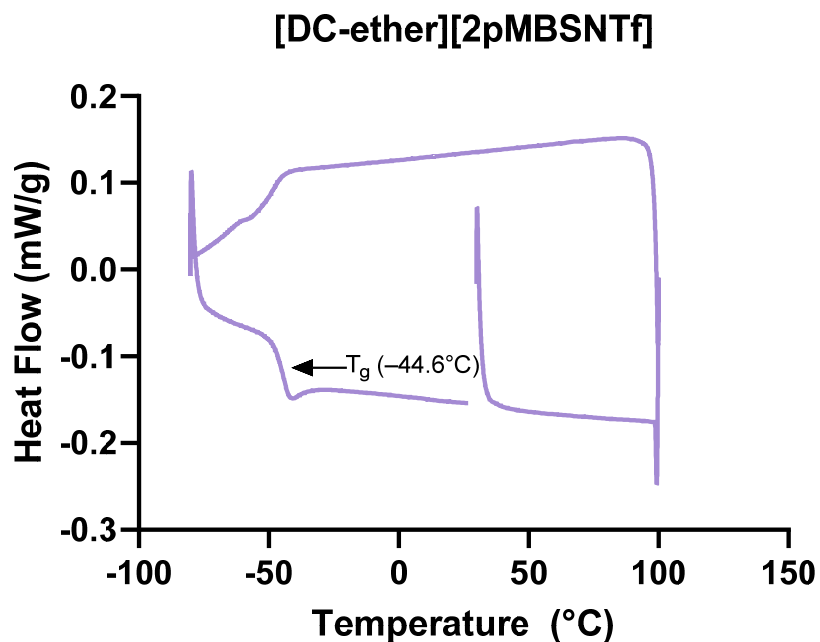
[DC-ether][2MesSNTf], **18i**

1: Equilibrate at 25.00 °C; 2: Ramp 10.00 °C/min to 100.00 °C; 3: Isothermal for 10.00 min; 4: Mark end of cycle 0; 5: Ramp 10.00 °C/min to -80.00 °C; 6: Isothermal for 10.00 min; 7: Mark end of cycle 1; 8: Ramp 10.00 °C/min to 25.00 °C



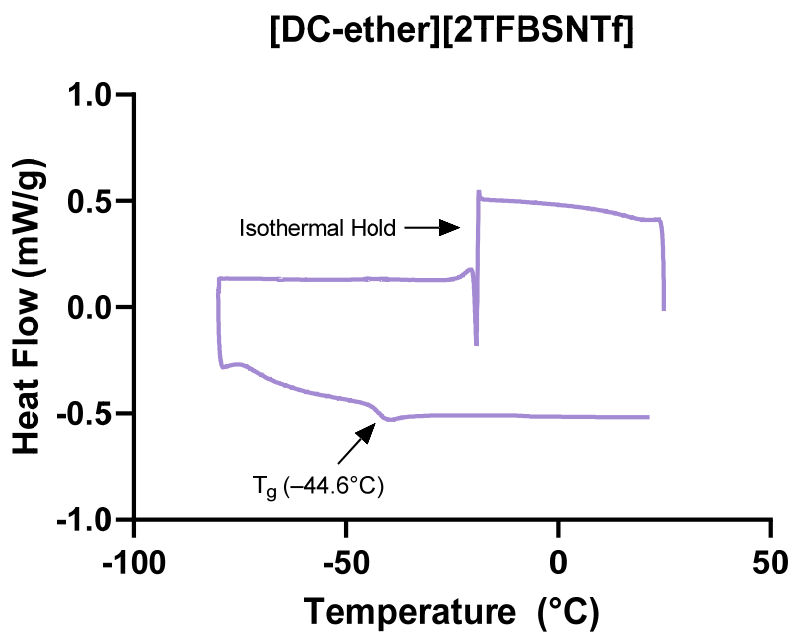
[DC-ether][2pMBSNTf], **18j**

1: Equilibrate at 30.00 °C; 2: Ramp 10.00 °C/min to 100.00 °C; 3: Isothermal for 10.00 min; 4: Mark end of cycle 0; 5: Ramp 10.00 °C/min to -80.00 °C; 6: Isothermal for 10.00 min; 7: Mark end of cycle 1; 8: Ramp 10.00 °C/min to 30.00 °C



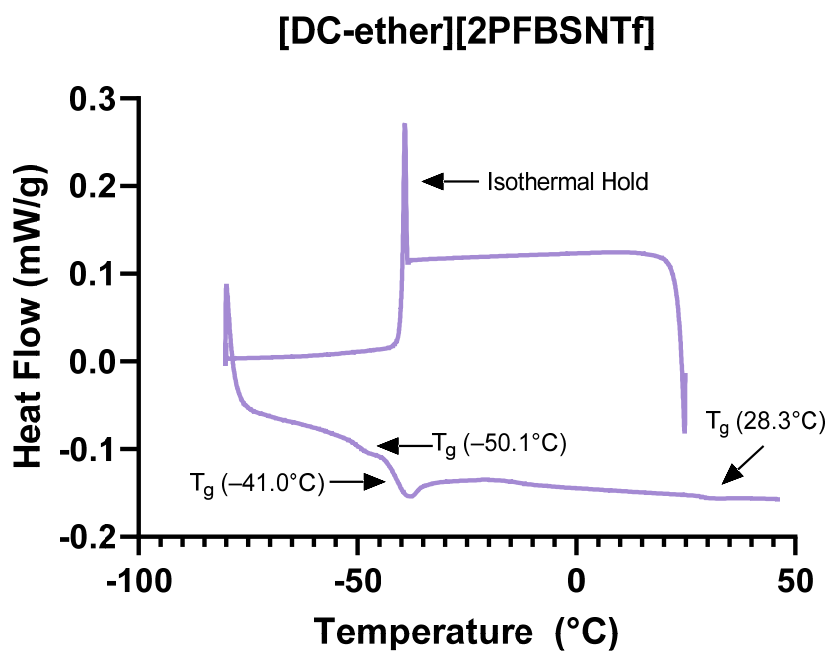
[DC-ether][2TFBSNTf], 18k

1: Equilibrate at 25.00 °C; 2: Ramp 10.00 °C/min to -20.00 °C; 3: Ramp 2.00 °C/min to -80.00 °C; 4: Isothermal for 30.00 min; 5: Mark end of cycle 1; 6: Ramp 10.00 °C/min to 25.00 °C



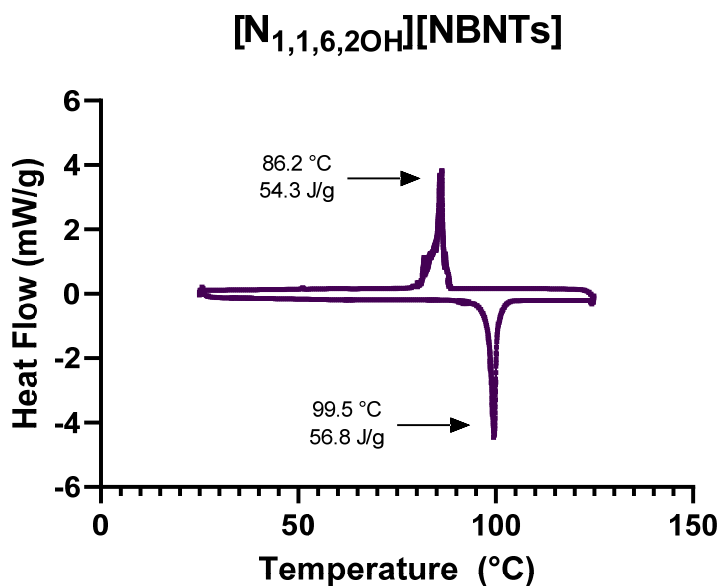
[DC-ether][PFBSNTf], 18l

1: Equilibrate at 25.00 °C; 2: Ramp 10.00 °C/min to -40.00 °C; 3: Ramp 2.00 °C/min to -80.00 °C; 4: Isothermal for 10.00 min; 5: Mark end of cycle 1; 6: Ramp 10.00 °C/min to 50.00 °C

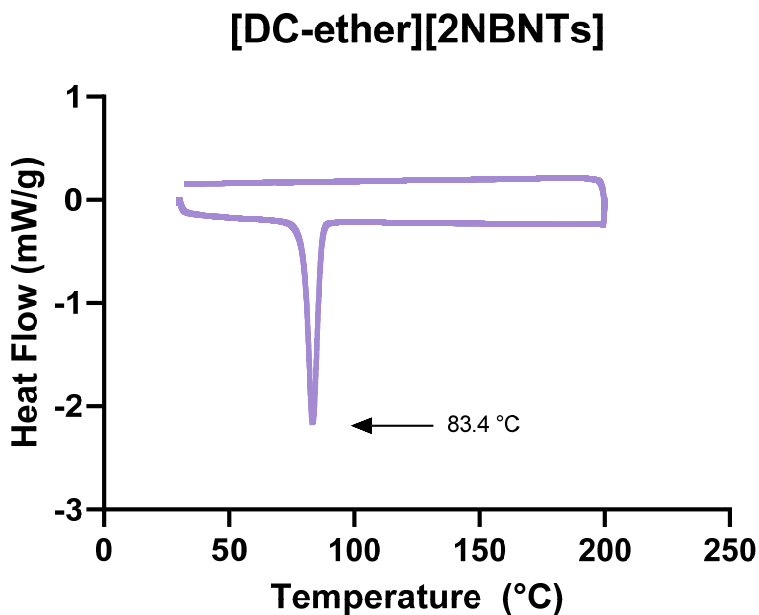


**[N<sub>1,1,6,2OH</sub>][NBNTs], 25a**

1: Equilibrate at 25.00 °C; 2: Ramp 10.00 °C/min to 125.00 °C; 3: Isothermal for 2.00 min; 4: Mark end of cycle 0; 5: Ramp 10.00 °C/min to 25.00 °C; 6: Isothermal for 2.00 min; 7: Mark end of cycle 1; 8: Ramp 10.00 °C/min to 125.00 °C; 9: Isothermal for 2.00 min; 10: Mark end of cycle 2; 11: Ramp 10.00 °C/min to 25.00 °C

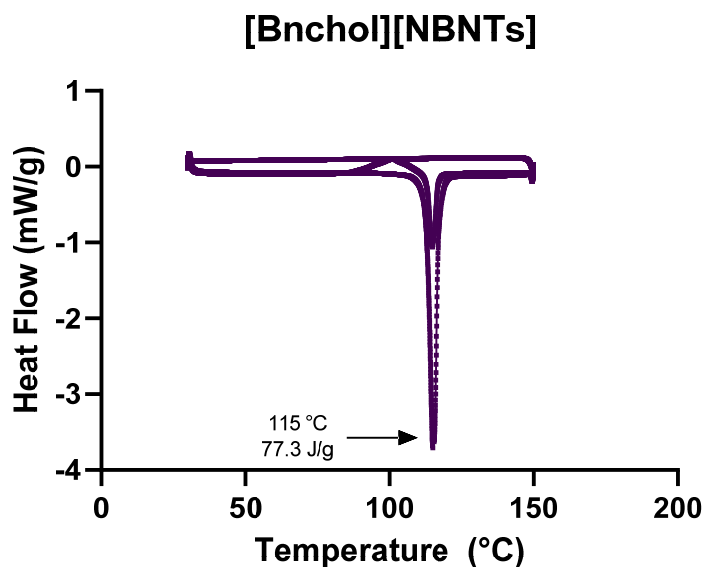
**[DC-ether][2NBNTs], 25b**

1: Equilibrate at 30.00 °C; 2: Ramp 10.00 °C/min to 200.00 °C; 3: Isothermal for 2.00 min; 4: Ramp 10.00 °C/min to 30.00 °C

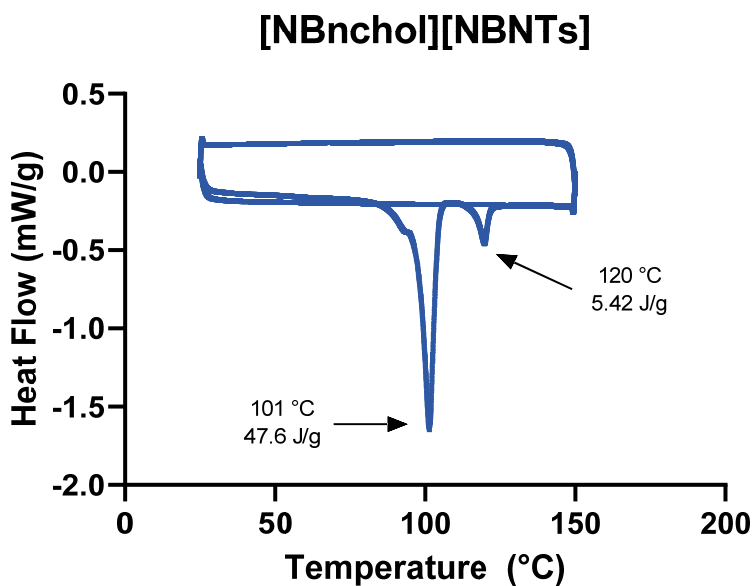


**[Bnchol][NBNTs], 25c**

1: Equilibrate at 30.00 °C; 2: Ramp 10.00 °C/min to 150.00 °C; 3: Isothermal for 2.00 min; 4: Mark end of cycle 0; 5: Ramp 10.00 °C/min to 30.00 °C; 6: Isothermal for 2.00 min; 7: Mark end of cycle 1; 8: Ramp 10.00 °C/min to 150.00 °C; 9: Isothermal for 2.00 min; 10: Mark end of cycle 2; 11: Ramp 10.00 °C/min to 30.00 °C

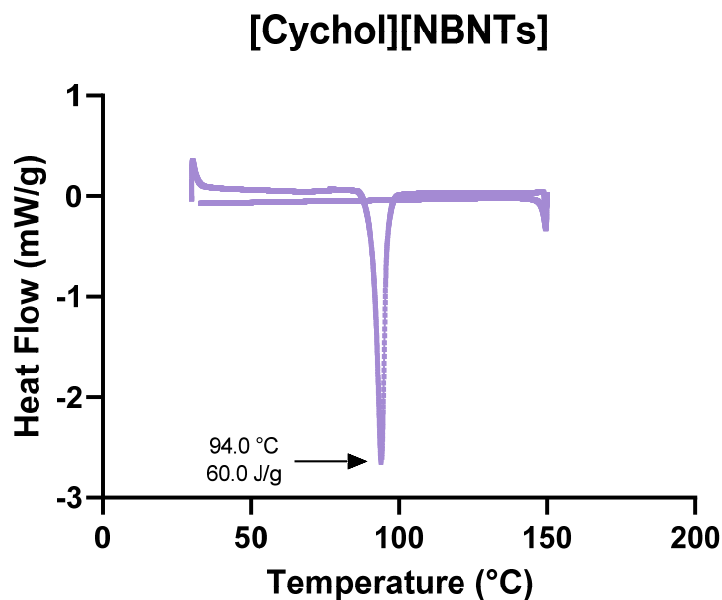
**[NBnchol][NBNTs], 25d**

1: Equilibrate at 25.00 °C; 2: Ramp 10.00 °C/min to 150.00 °C; 3: Isothermal for 2.00 min; 4: Mark end of cycle 0; 5: Ramp 10.00 °C/min to 25.00 °C; 6: Isothermal for 2.00 min; 7: Mark end of cycle 1; 8: Ramp 10.00 °C/min to 150.00 °C; 9: Isothermal for 2.00 min; 10: Mark end of cycle 2; 11: Ramp 10.00 °C/min to 25.00 °C

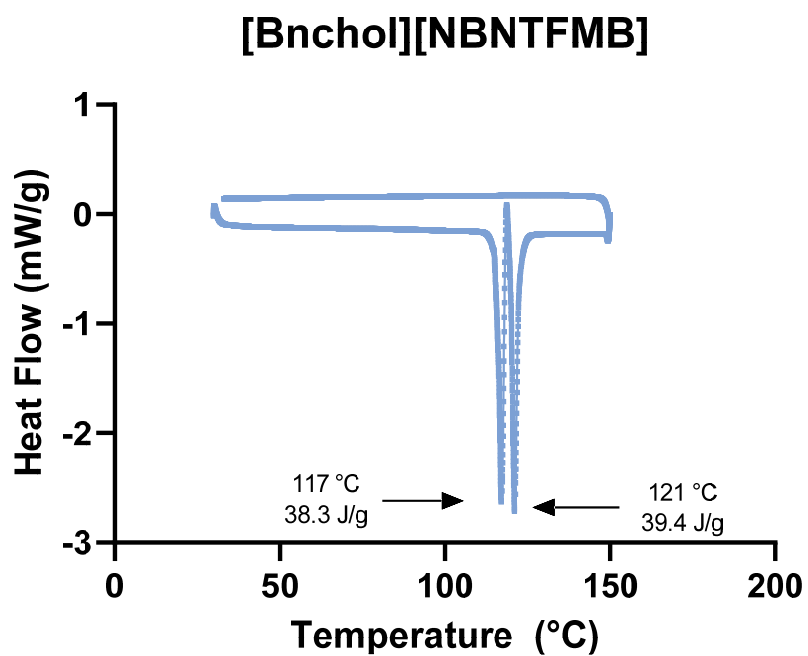


**[Cychol][NBNTs], 25e**

1: Equilibrate at 30.00 °C; 2: Ramp 10.00 °C/min to 150.00 °C; 3: Isothermal for 2.00 min; 4: Mark end of cycle 0; 5: Ramp 10.00 °C/min to 30.00 °C

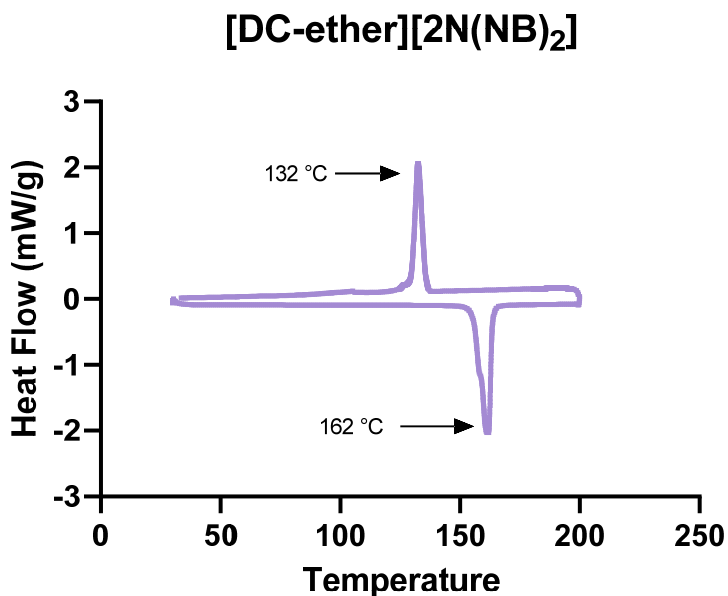
**[Bnchol][NBNTFMB], 25f**

1: Equilibrate at 30.00 °C; 2: Ramp 10.00 °C/min to 150.00 °C; 3: Isothermal for 2.00 min; 4: Ramp 10.00 °C/min to 30.00 °C



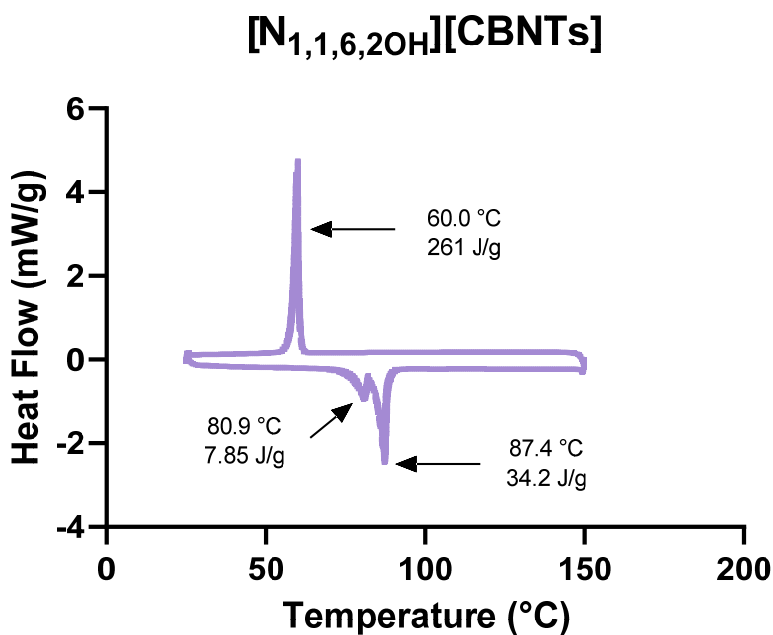
[DC-ether][2N(NB)<sub>2</sub>], 25g

1: Equilibrate at 30.00 °C; 2: Ramp 10.00 °C/min to 200.00 °C; 3: Isothermal for 2.00 min; 4: Ramp 10.00 °C/min to 30.00 °C



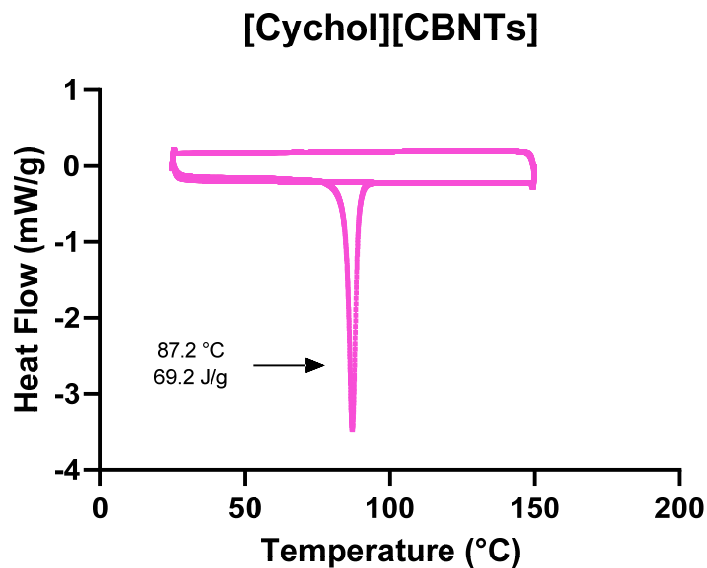
[N<sub>1,1,6,2OH</sub>][CBNTS], 25h

1: Equilibrate at 25.00 °C; 2: Ramp 10.00 °C/min to 150.00 °C; 3: Isothermal for 2.00 min; 4: Ramp 10.00 °C/min to 25.00 °C; 5: Isothermal for 2.00 min; 6: Ramp 10.00 °C/min to 150.00 °C; 7: Isothermal for 2.00 min; 8: Ramp 10.00 °C/min to 25.00 °C

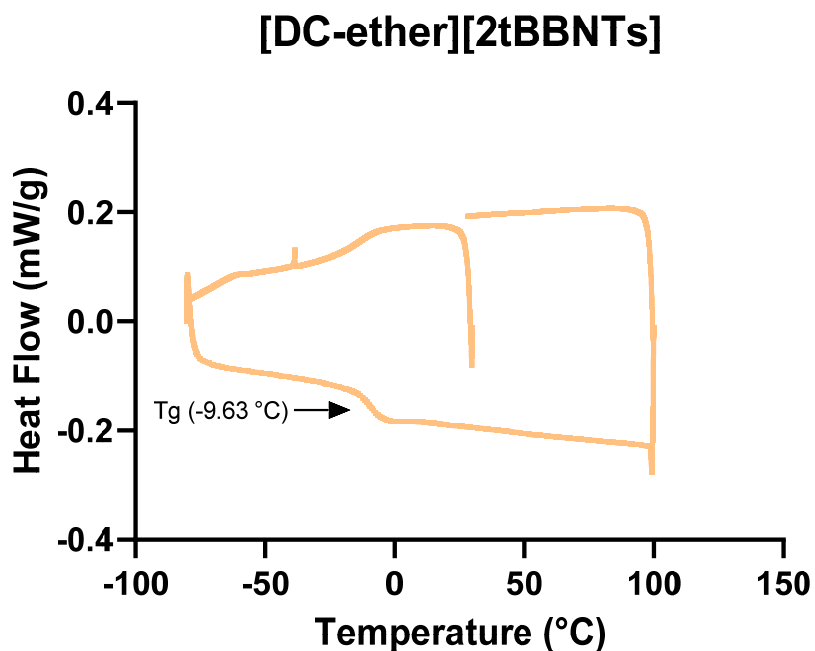


**[Cychol][CBNTs], 25j**

1: Equilibrate at 25.00 °C; 2: Ramp 10.00 °C/min to 150.00 °C; 3: Isothermal for 2.00 min; 4: Ramp 10.00 °C/min to 25.00 °C; 5: Isothermal for 2.00 min; 6: Ramp 10.00 °C/min to 150.00 °C; 7: Isothermal for 2.00 min; 8: Ramp 10.00 °C/min to 25.00 °C

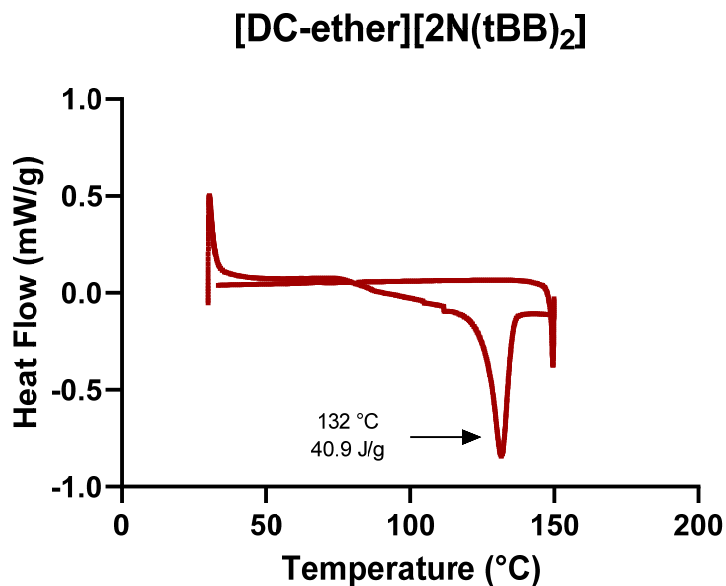
**[DC-ether][2tBBNTs], 25I**

1: Equilibrate at 30.00 °C; 2: Ramp 10.00 °C/min to -80.00 °C; 3: Mark end of cycle 0; 4: Isothermal for 2.00 min; 5: Ramp 10.00 °C/min to 100.00 °C; 6: Isothermal for 2.00 min; 7: Mark end of cycle 1; 8: Ramp 10.00 °C/min to 25.00 °C



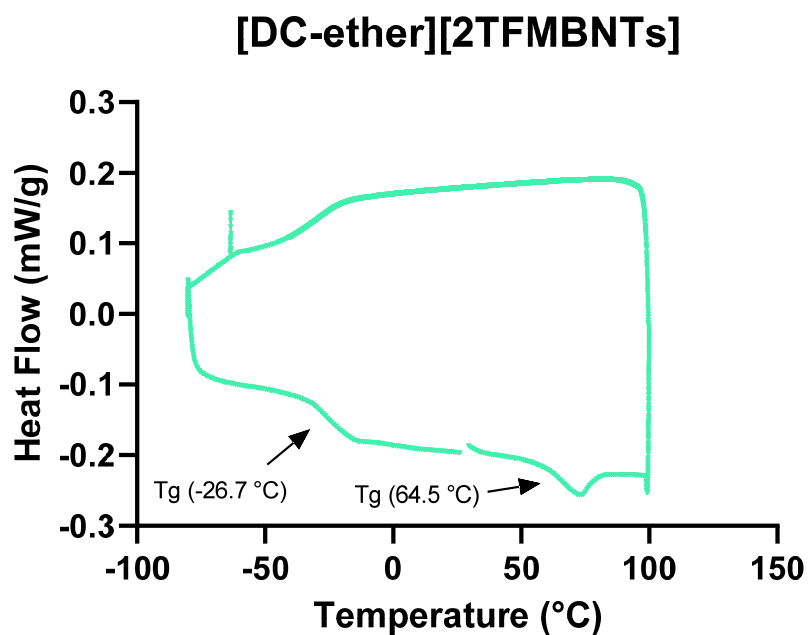
[DC-ether][2N(tBB)<sub>2</sub>], 25m

1: Equilibrate at 30.00 °C; 2: Ramp 10.00 °C/min to 150.00 °C; 3: Isothermal for 2.00 min; 4: Mark end of cycle 0; 5: Ramp 10.00 °C/min to 30.00 °C



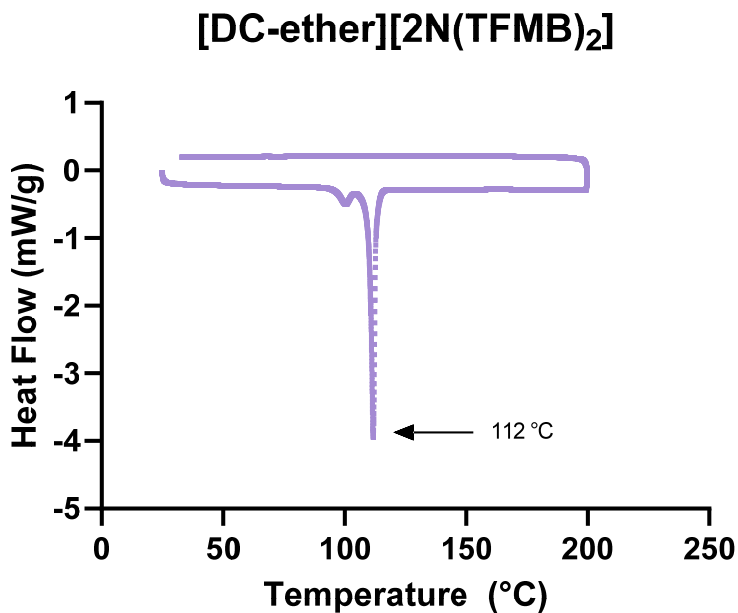
[DC-ether][2TFMBNTs], 25n

1: Equilibrate at 25.00 °C; 2: Ramp 10.00 °C/min to 100.00 °C; 3: Isothermal for 2.00 min; 4: Mark end of cycle 0; 5: Ramp 10.00 °C/min to -80.00 °C; 6: Isothermal for 2.00 min; 7: Mark end of cycle 1; 8: Ramp 10.00 °C/min to 30.00 °C

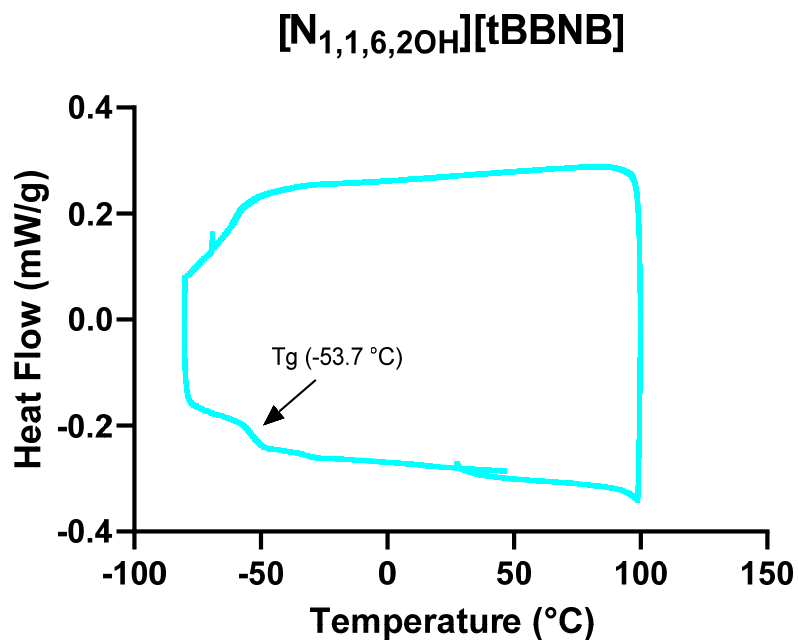


**[DC-ether][2N(TFMB)<sub>2</sub>], 25o**

1: Equilibrate at 25.00 °C; 2: Ramp 10.00 °C/min to 200.00 °C; 3: Isothermal for 2.00 min; 4: Ramp 10.00 °C/min to 30.00 °C

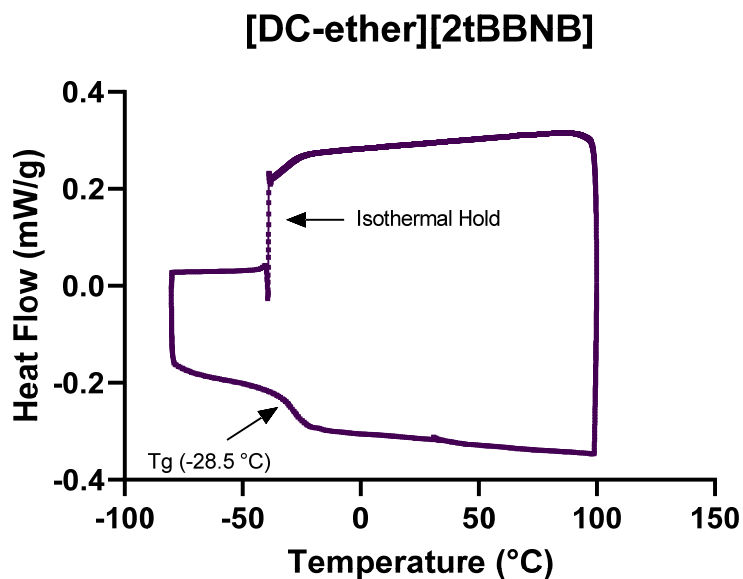
**[N<sub>1,1,6,2OH</sub>][tBBNB], 26a**

1: Equilibrate at 25.00 °C; 2: Ramp 10.00 °C/min to 100.00 °C; 3: Isothermal for 2.00 min; 4: Mark end of cycle 0; 5: Ramp 10.00 °C/min to -80.00 °C; 6: Isothermal for 2.00 min; 7: Mark end of cycle 1; 8: Ramp 10.00 °C/min to 50.00 °C

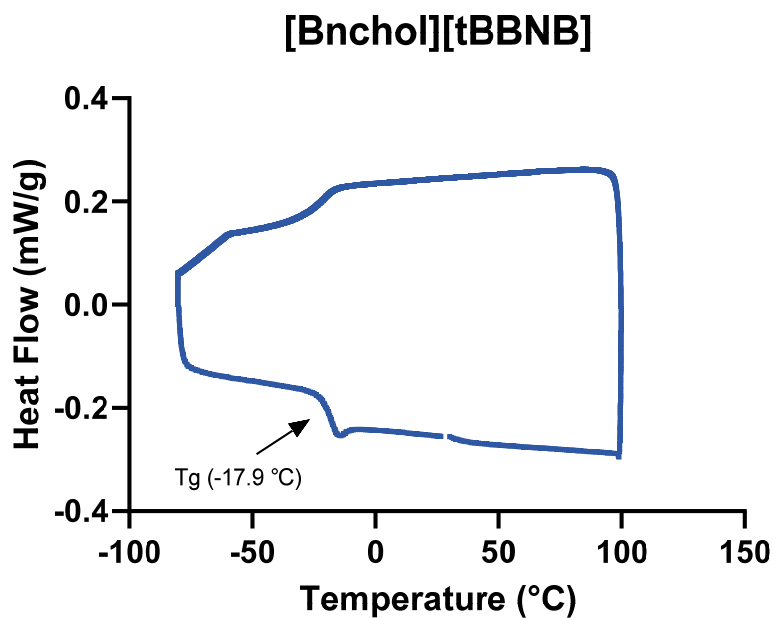


**[DC-ether][2tBBNB], 26b**

1: Equilibrate at 25.00 °C; 2: Ramp 10.00 °C/min to 100.00 °C; 3: Isothermal for 2.00 min; 4: Mark end of cycle 0; 5: Ramp 10.00 °C/min to -40.00 °C; 6: Ramp 2.00 °C/min to -80.00 °C; 7: Isothermal for 10.00 min; 8: Mark end of cycle 1; 9: Ramp 10.00 °C/min to 40.00 °C

**[Bnchol][tBBNB], 26c**

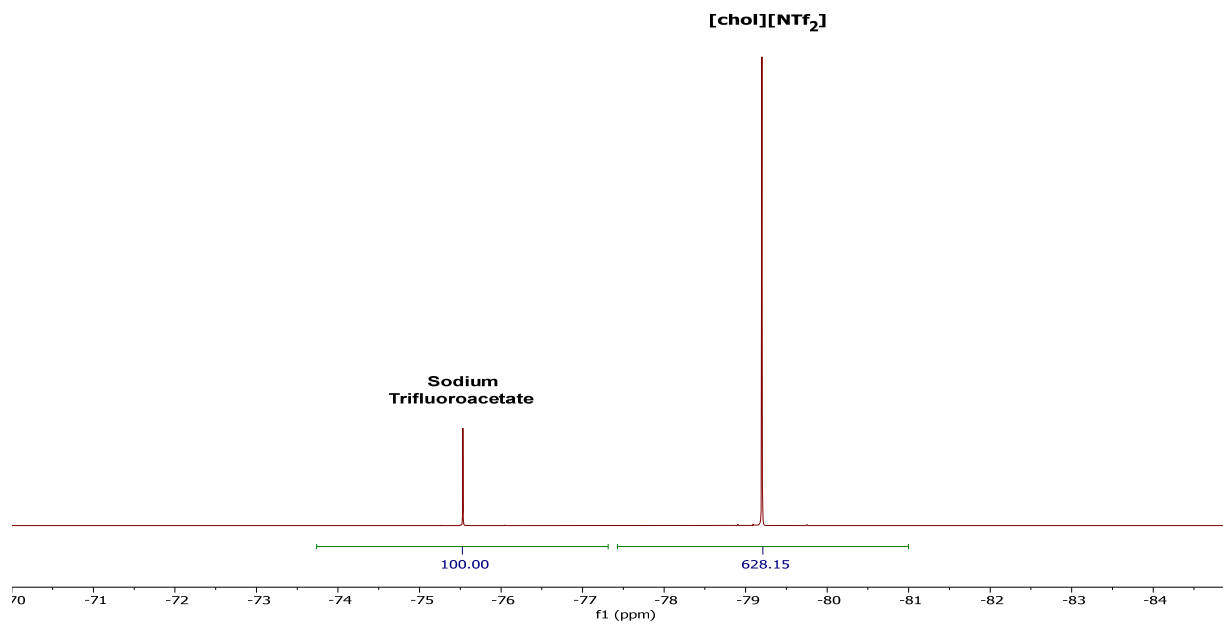
1: Equilibrate at 25.00 °C; 2: Ramp 10.00 °C/min to 100.00 °C; 3: Isothermal for 2.00 min; 4: Mark end of cycle 0; 5: Ramp 10.00 °C/min to -80.00 °C; 6: Isothermal for 2.00 min; 7: Mark end of cycle 1; 8: Ramp 10.00 °C/min to 30.00 °C



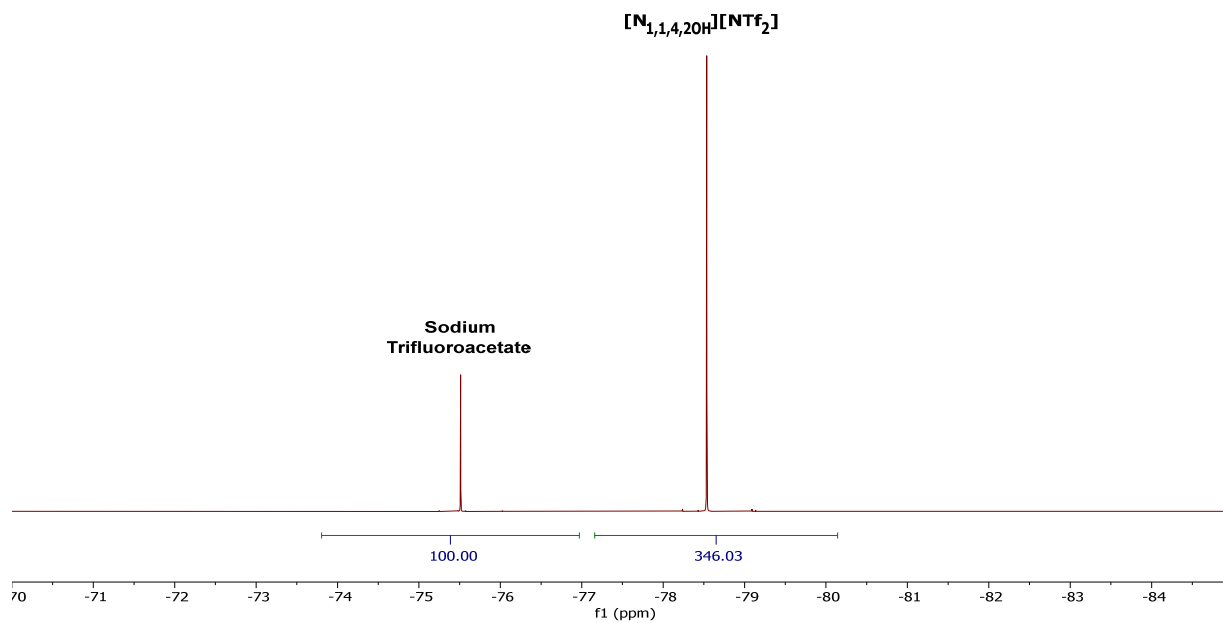
### A.3 Quantitative $^{19}\text{F}$ NMR Parameters and Spectra for Water Solubility Studies

<b>Table A.1</b> Recycle delay ( $D_1$ ) parameters used for the inversion recovery experiments for each monocholinium and dicholinium IL composed of $[\text{NTf}_2]$ and first-generation bis(sulfonyl)azanide anions, and corresponding $T_1$ values.			
#	Ionic Liquid	$D_1$ (s)	$T_1$ (s)
<b>13a</b>	$[\text{chol}][\text{NTf}_2]$	6	$2.02 \pm 0.02$
<b>13b</b>	$[\text{N}_{1,1,4,2\text{OH}}][\text{NTf}_2]$	10	$2.94 \pm 0.04$
<b>13c</b>	$[\text{N}_{1,1,6,2\text{OH}}][\text{NTf}_2]$	6	$2.96 \pm 0.02$
<b>13d</b>	$[\text{N}_{1,1,8,2\text{OH}}][\text{NTf}_2]$	6	$2.90 \pm 0.02$
<b>13i</b>	$[\text{DC-4}][2\text{NTf}_2]$	16	$2.88 \pm 0.02$
<b>13k</b>	$[\text{DC-6}][2\text{NTf}_2]$	8	$2.97 \pm 0.06$
<b>13m</b>	$[\text{DC-8}][2\text{NTf}_2]$	8	$2.91 \pm 0.02$
<b>13p</b>	$[\text{DC-ether}][2\text{NTf}_2]$	10	$2.86 \pm 0.03$
<b>18a</b>	$[\text{DC-ether}][2\text{BSNTf}]$	8	$1.78 \pm 0.01$
<b>18b</b>	$[\text{DC-ether}][2\text{HSNTf}]$	8	$1.80 \pm 0.01$
<b>18c</b>	$[\text{DC-ether}][2\text{OSNTf}]$	3	$2.02 \pm 0.02$
<b>18d</b>	$[\text{DC-ether}][2\text{PhSNTf}]$	10	$1.85 \pm 0.02$
<b>18e</b>	$[\text{DC-ether}][2\text{TsSNTf}]$	6	$1.63 \pm 0.03$
<b>18f</b>	$[\text{DC-ether}][2\text{pBBSNTf}]$	6	$1.86 \pm 0.02$
<b>18g</b>	$[\text{DC-ether}][2\text{pHBSNTf}]$	8	$1.78 \pm 0.16$
<b>18h</b>	$[\text{DC-ether}][2\text{pOBSNTf}]$	8	$1.50 \pm 0.01$
<b>18i</b>	$[\text{DC-ether}][2\text{MesSNTf}]$	8	$1.76 \pm 0.01$
<b>18j</b>	$[\text{DC-ether}][2\text{pMBSNTf}]$	10	$1.87 \pm 0.01$
<b>18k</b>	$[\text{DC-ether}][2\text{TFBSNTf}]$	8	$1.87 \pm 0.01$
<b>18l</b>	$[\text{DC-ether}][2\text{PFBSNTf}]$	6	$3.04 \pm 0.06$

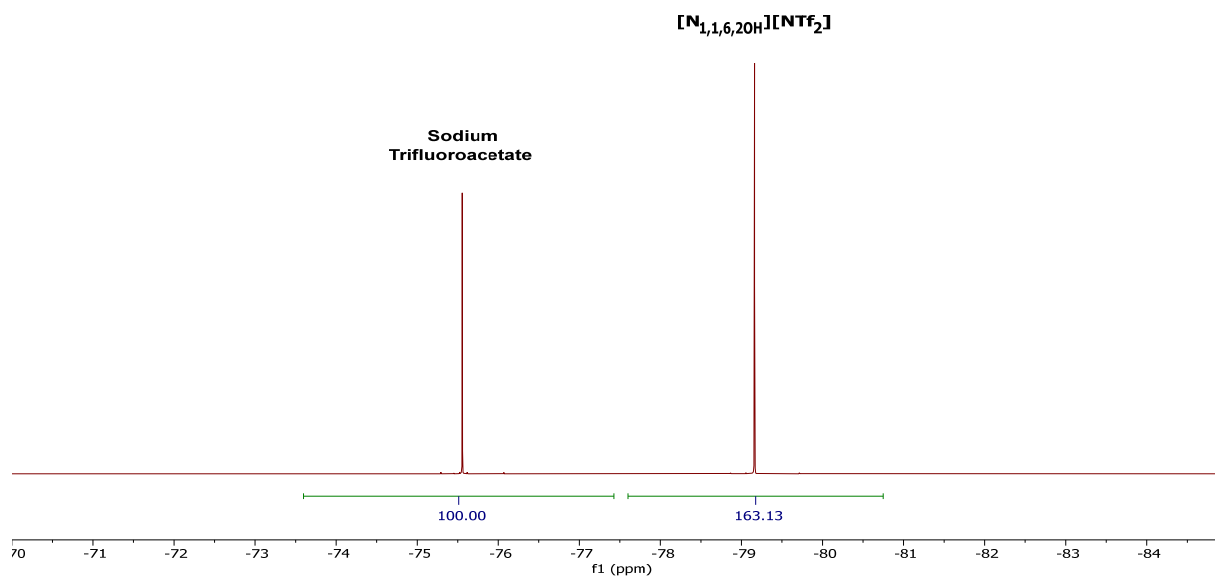
[chol][NTf<sub>2</sub>], **13a**



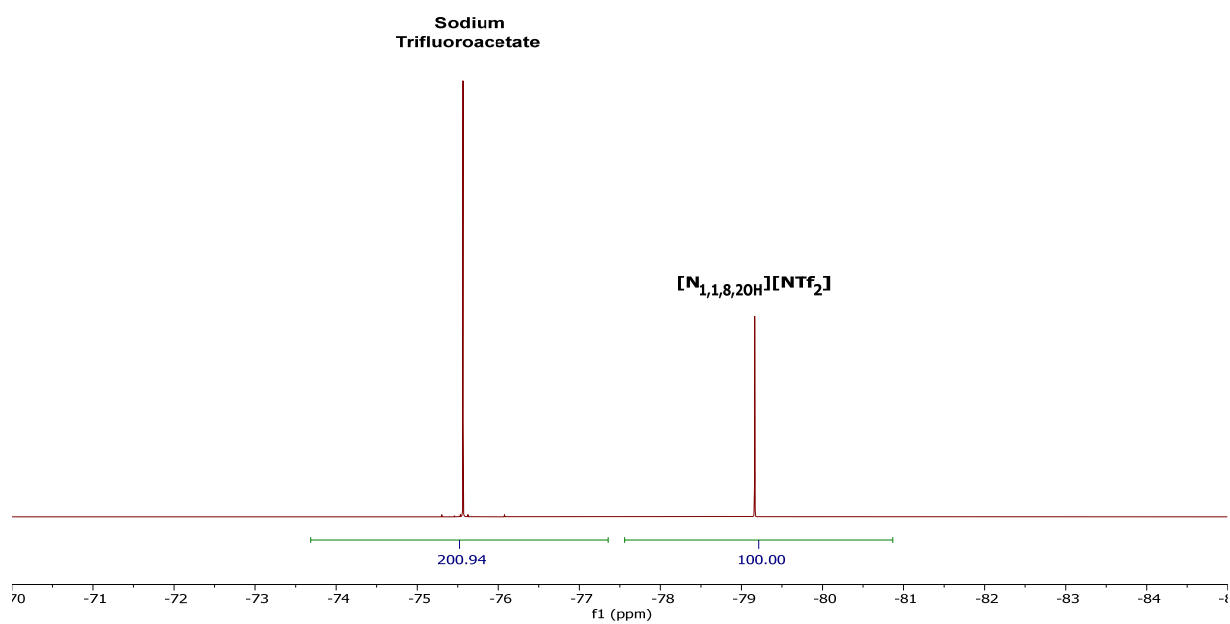
[N<sub>1,1,4,2OH</sub>][NTf<sub>2</sub>], **13b**



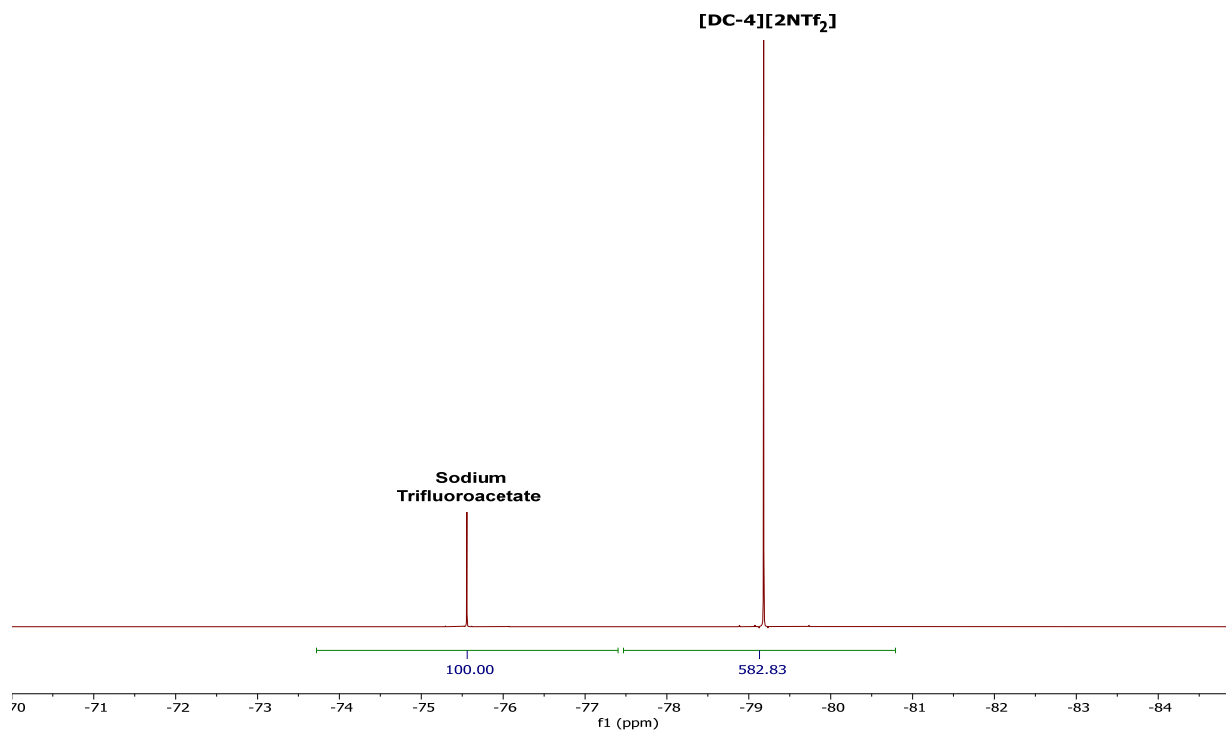
$[N_{1,1,6,2OH}][NTf_2]$ , **13c**



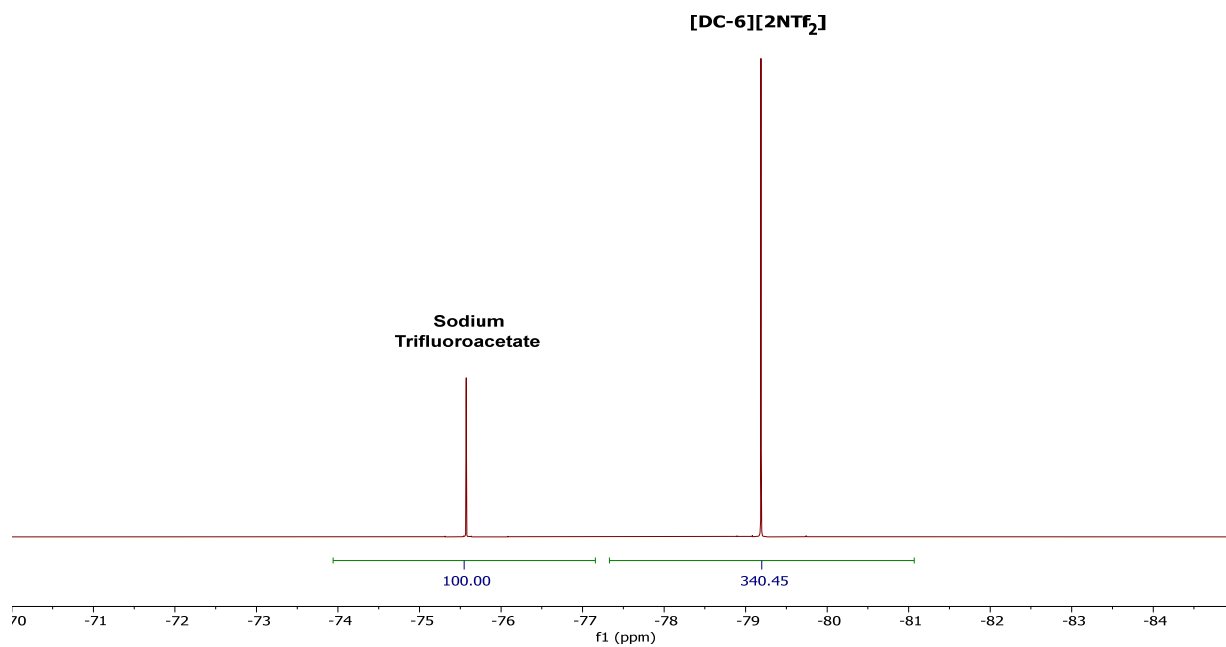
$[N_{1,1,8,2OH}][NTf_2]$ , **13d**



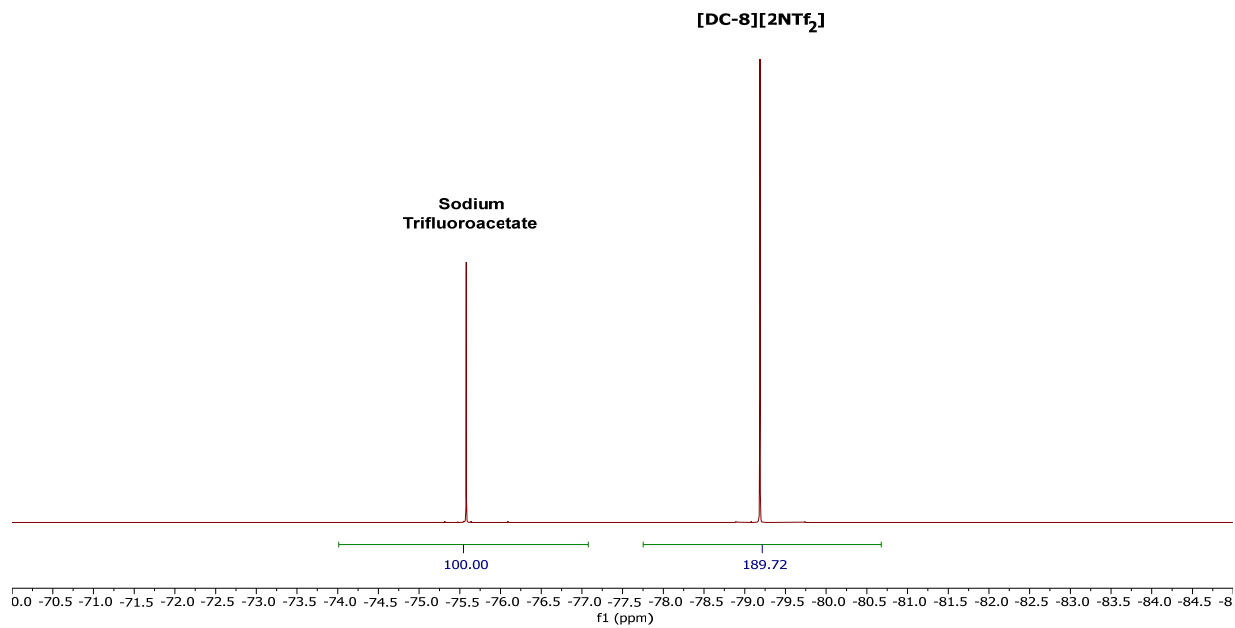
[DC-4][2NTf<sub>2</sub>], **13i**



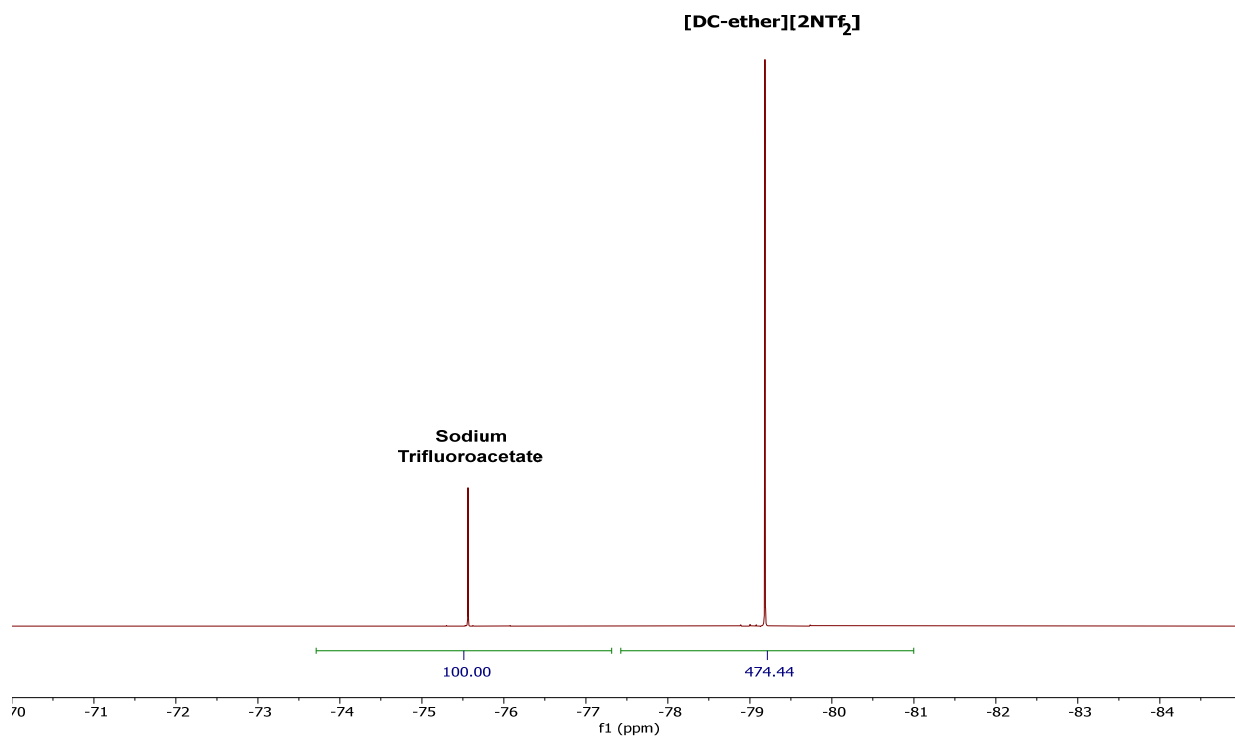
[DC-6][2NTf<sub>2</sub>], **13k**



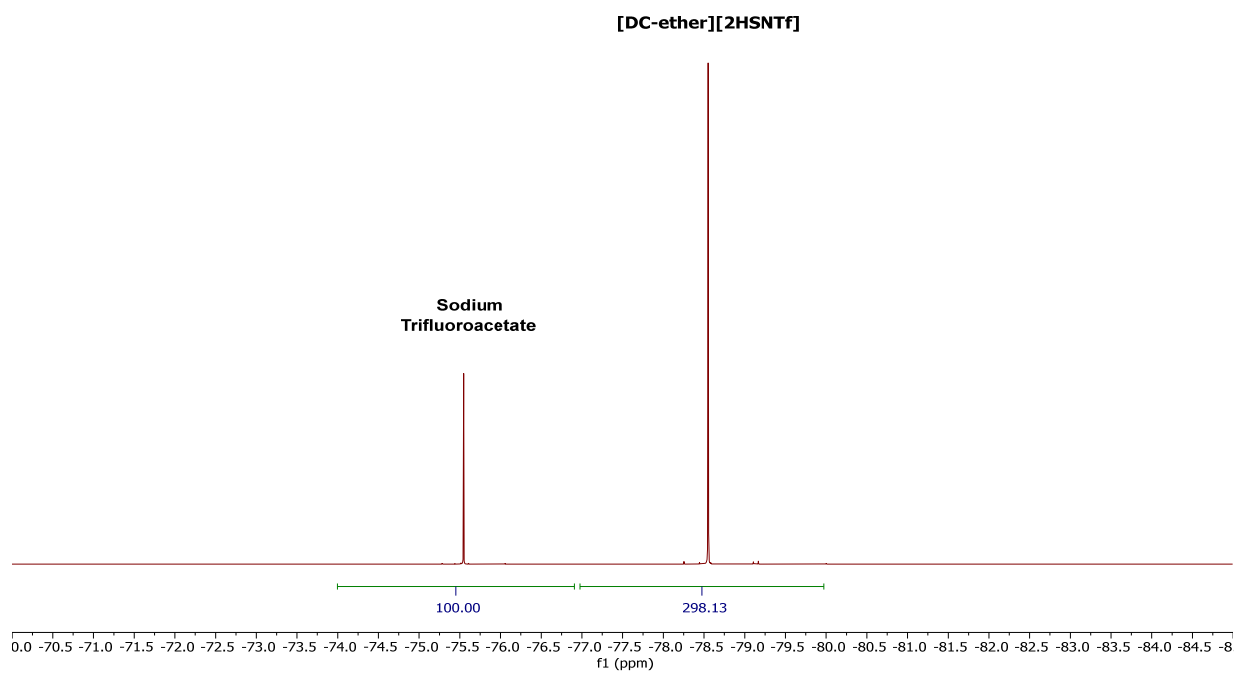
[DC-8][2NTf<sub>2</sub>], **13m**



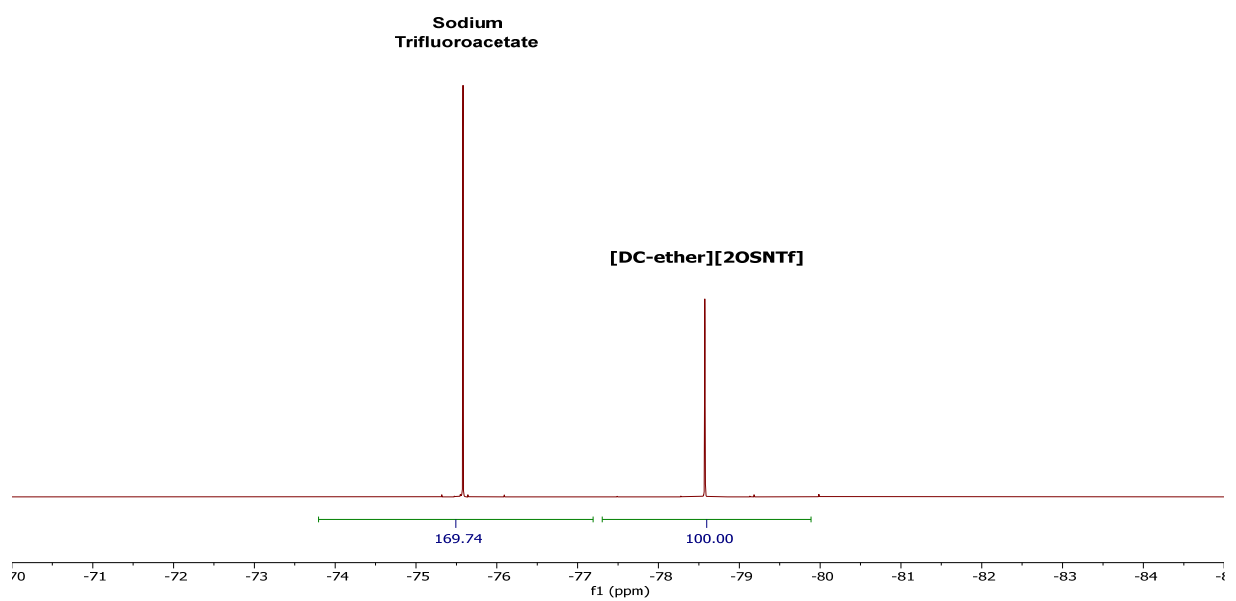
[DC-ether][2NTf<sub>2</sub>], **13p**



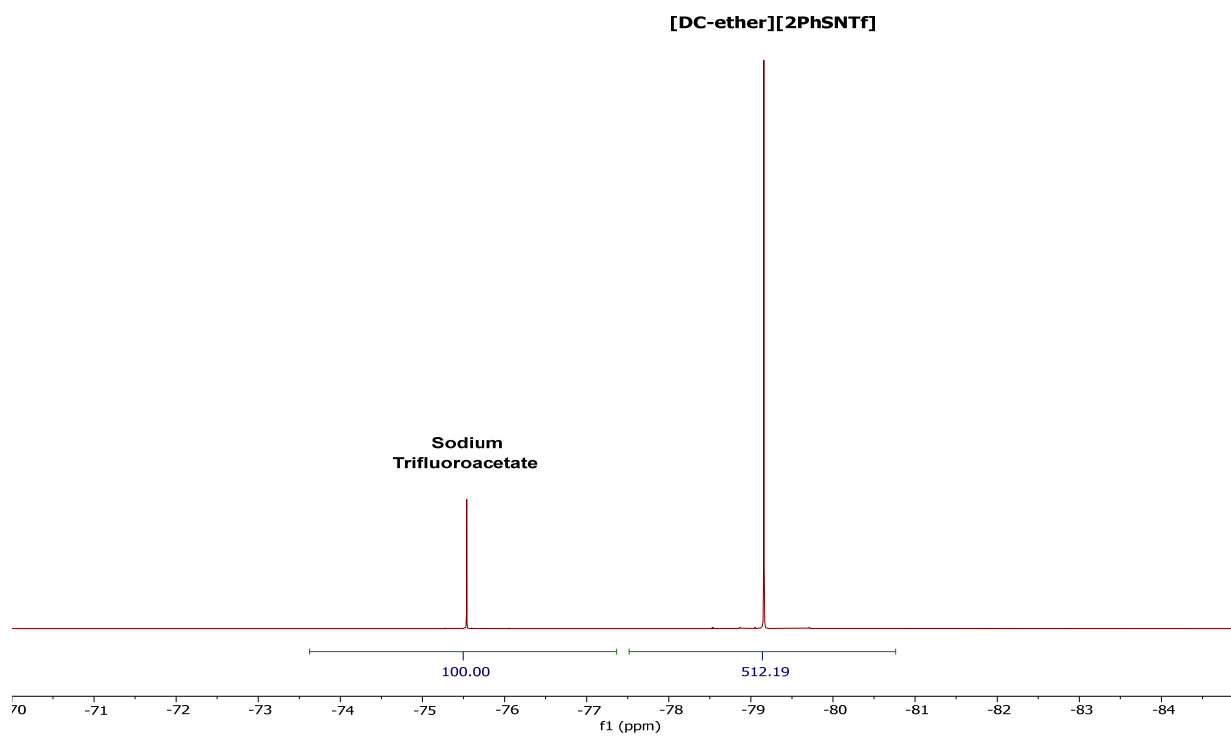
[DC-ether][2HSNTf], **18b**



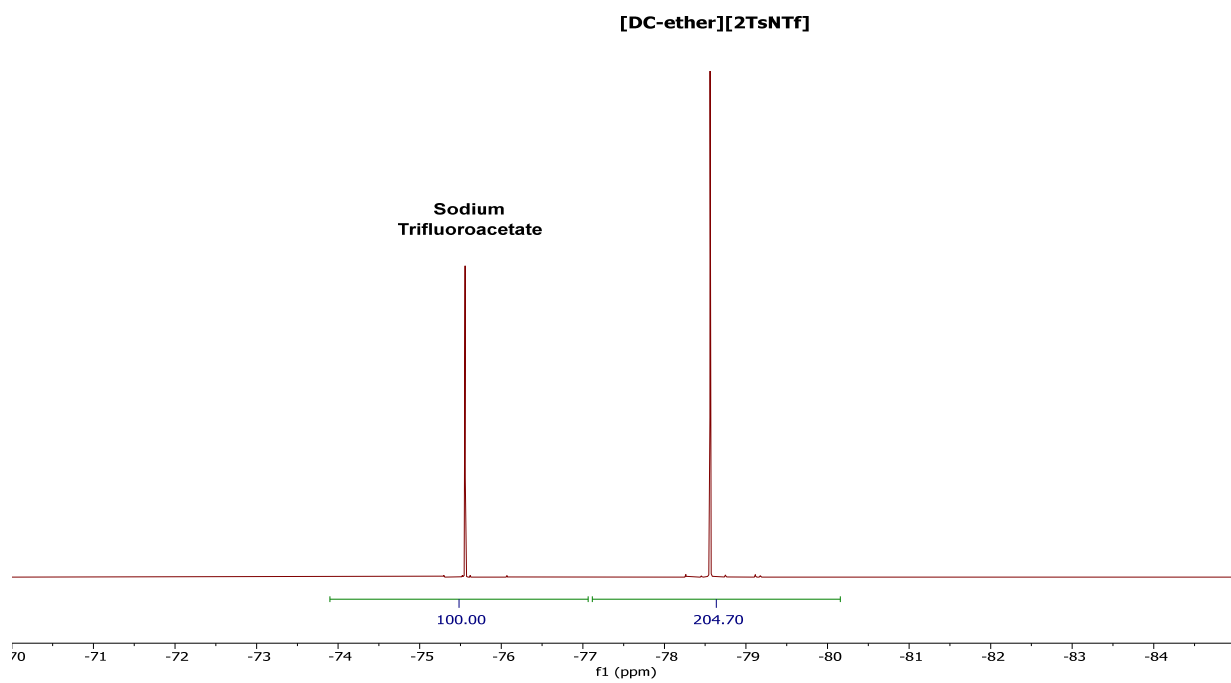
[DC-ether][2OSNTf], **18c**



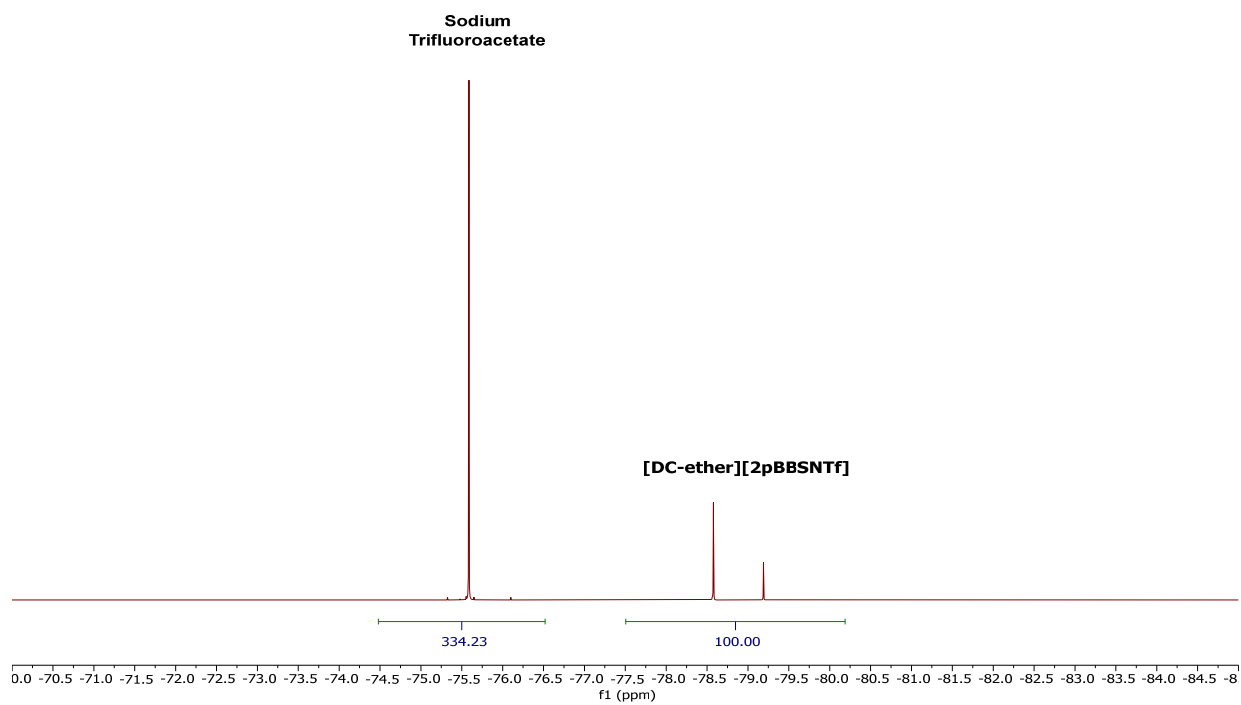
[DC-ether][2PhSNTf], **18d**



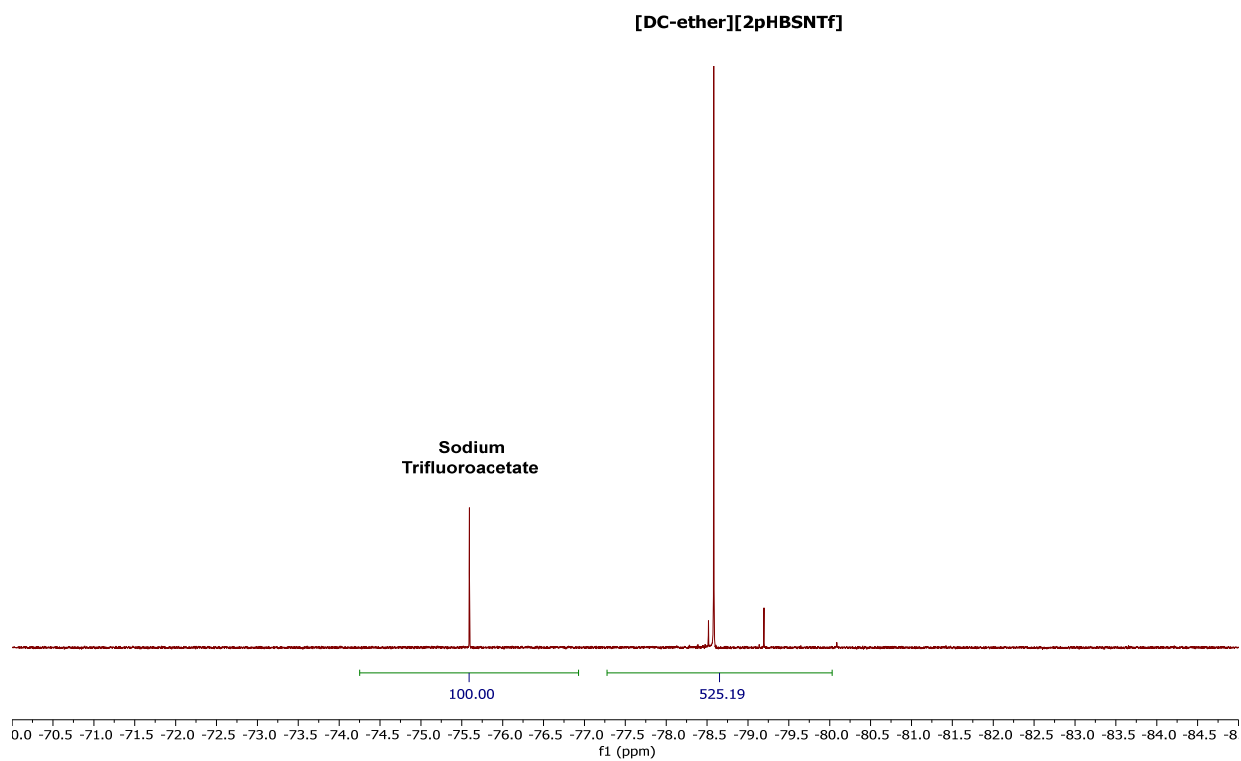
[DC-ether][2TsNTf], **18e**

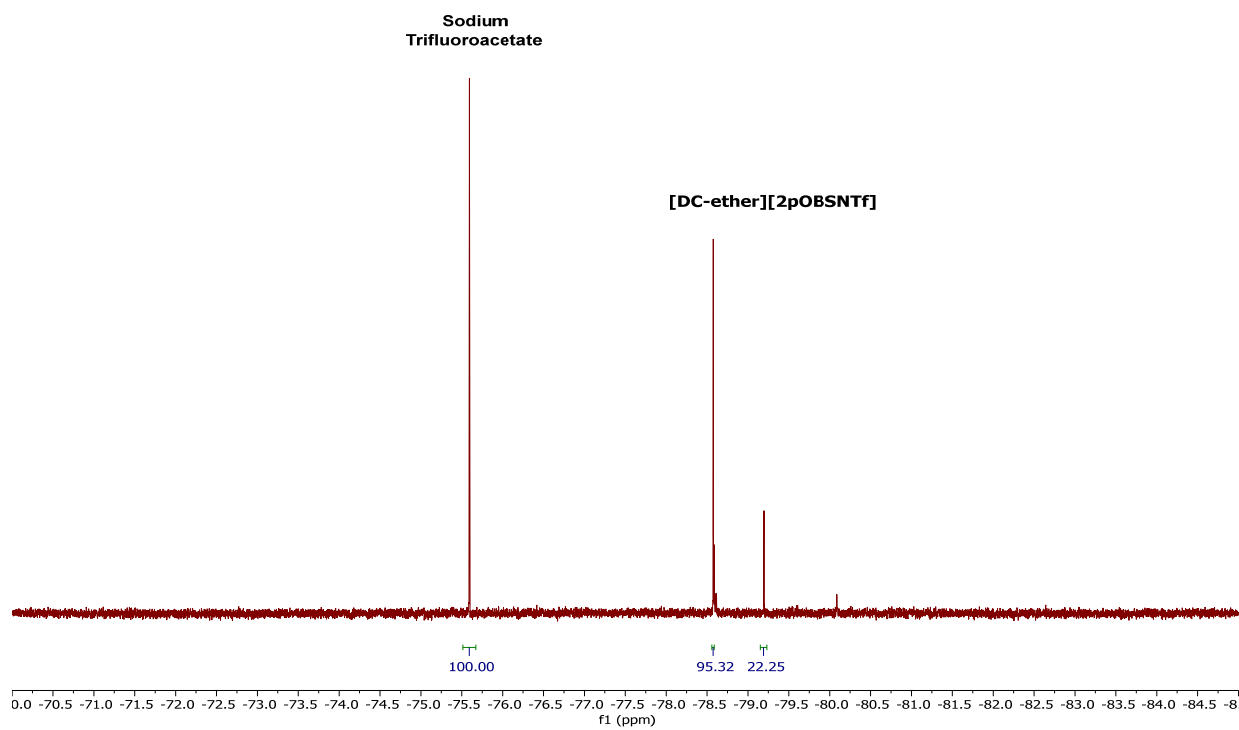
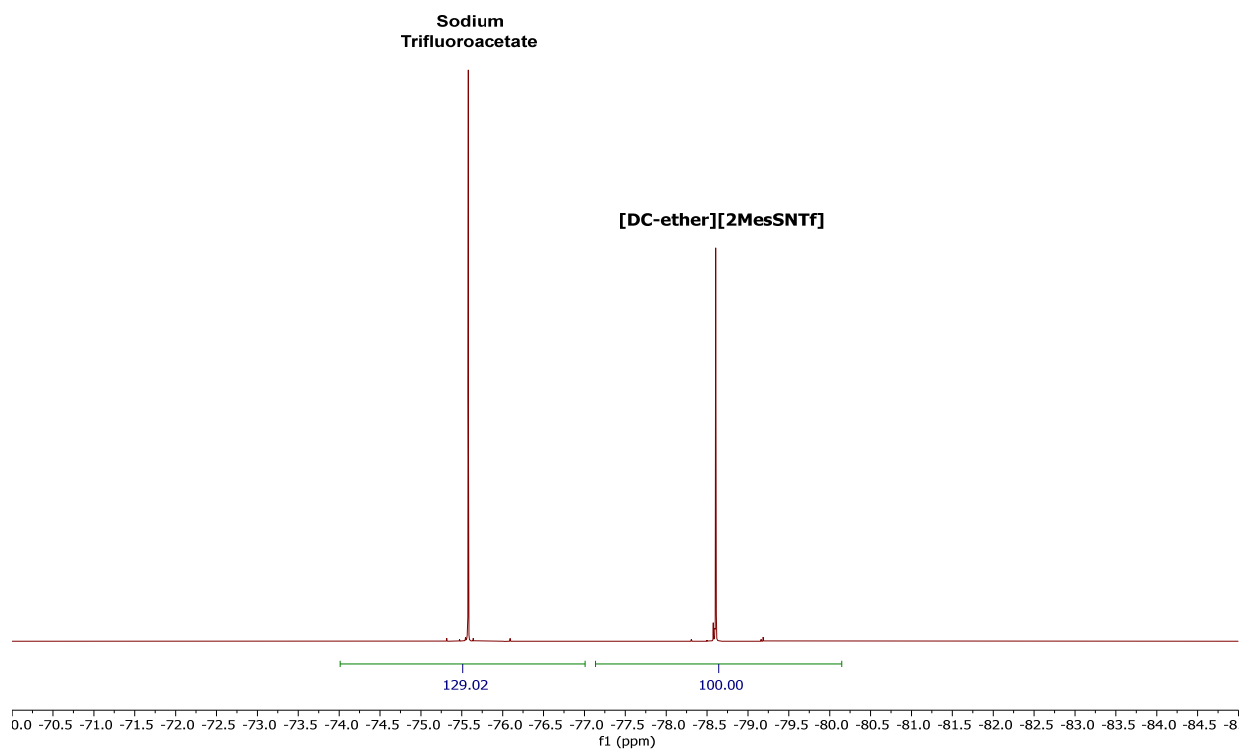


[DC-ether][2pBBSNTf], **18f**

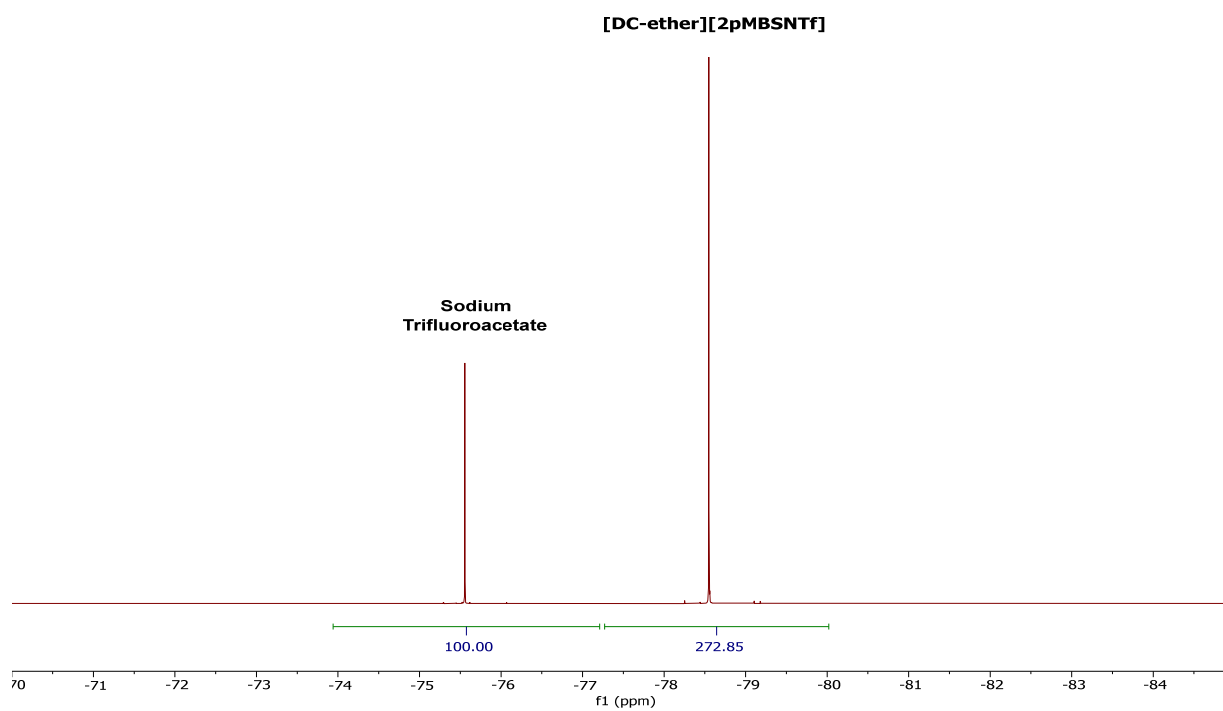


[DC-ether][2pHBSNTf], **18g**

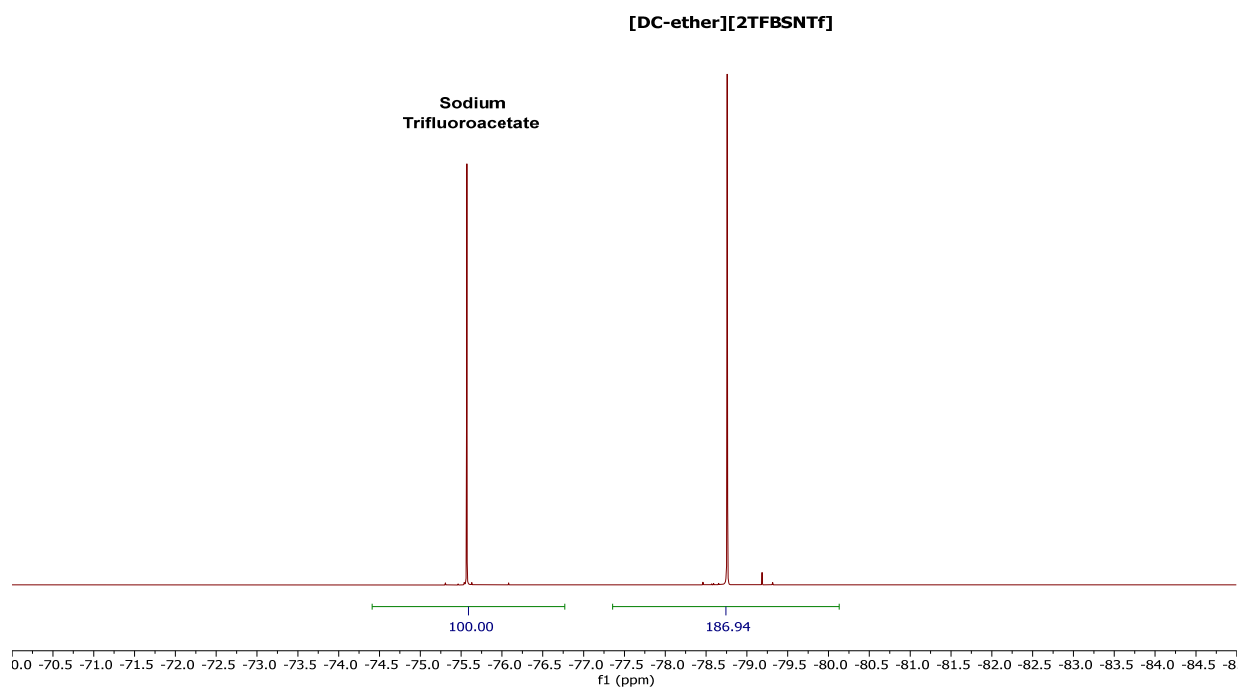


**[DC-ether][2pOBSNTf], 18h****[DC-ether][2MesSNTf], 18i**

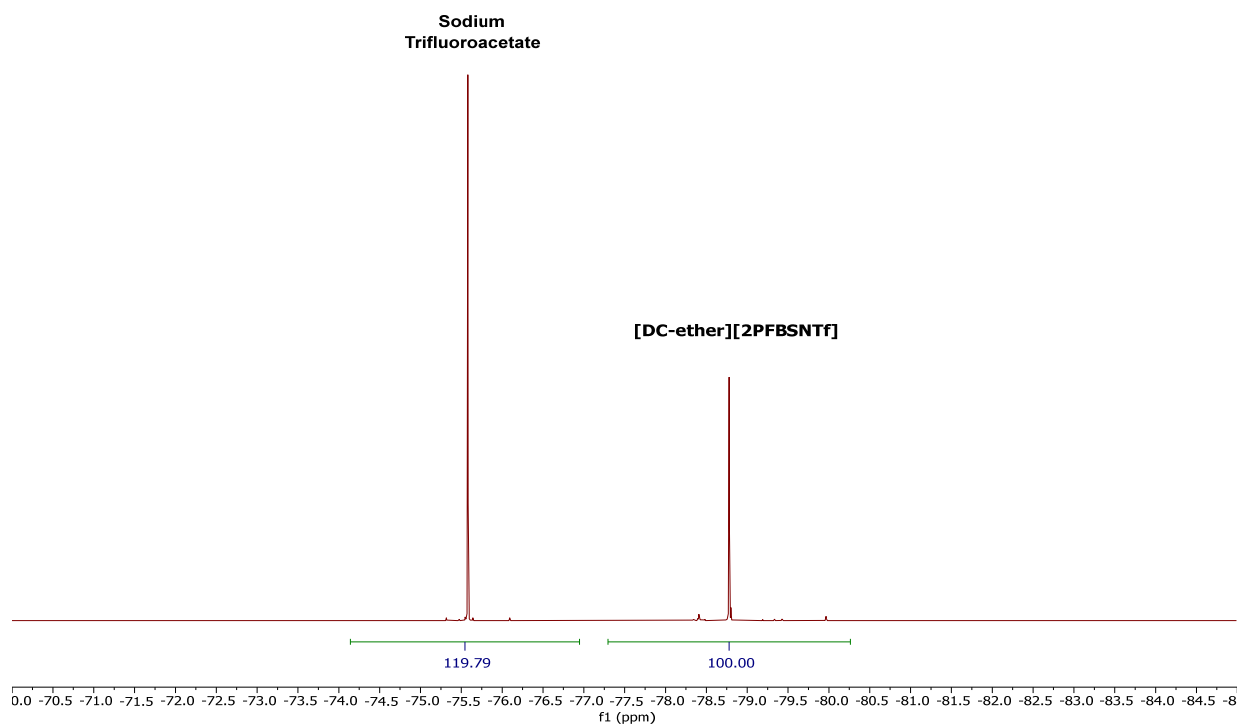
[DC-ether][2pMBSNTf], **18j**



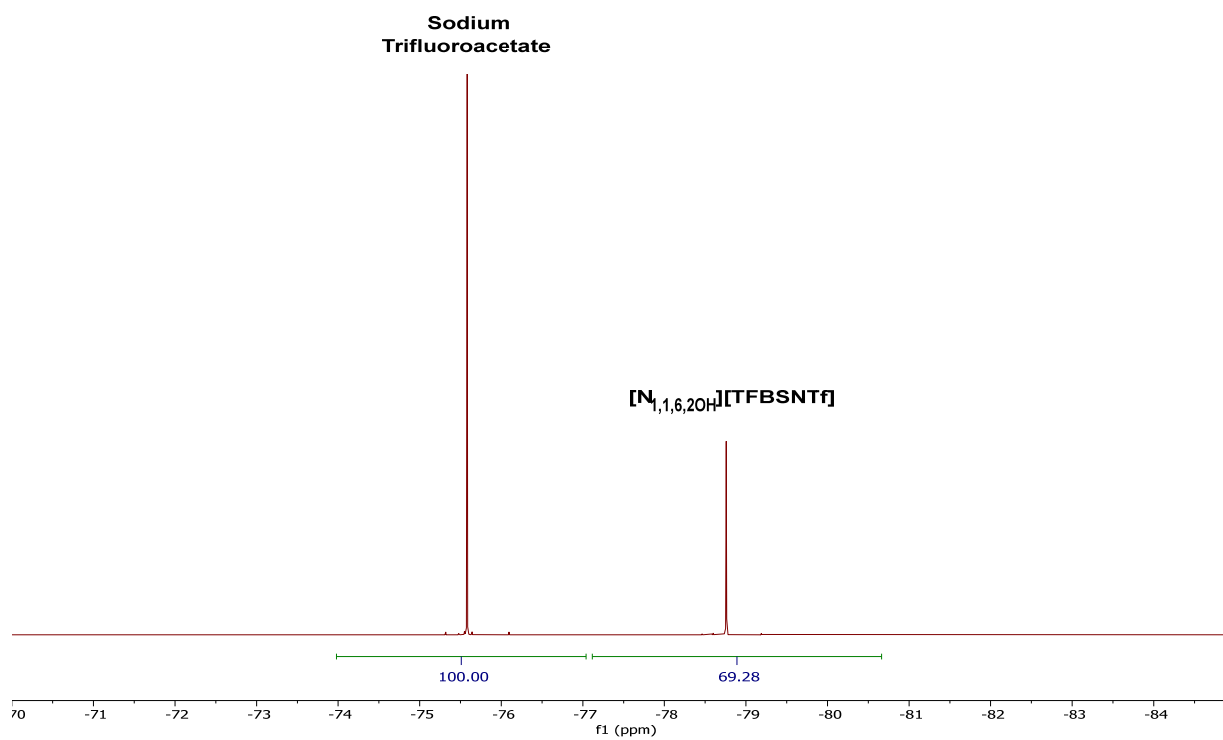
[DC-ether][2TFBSNTf], **18k**



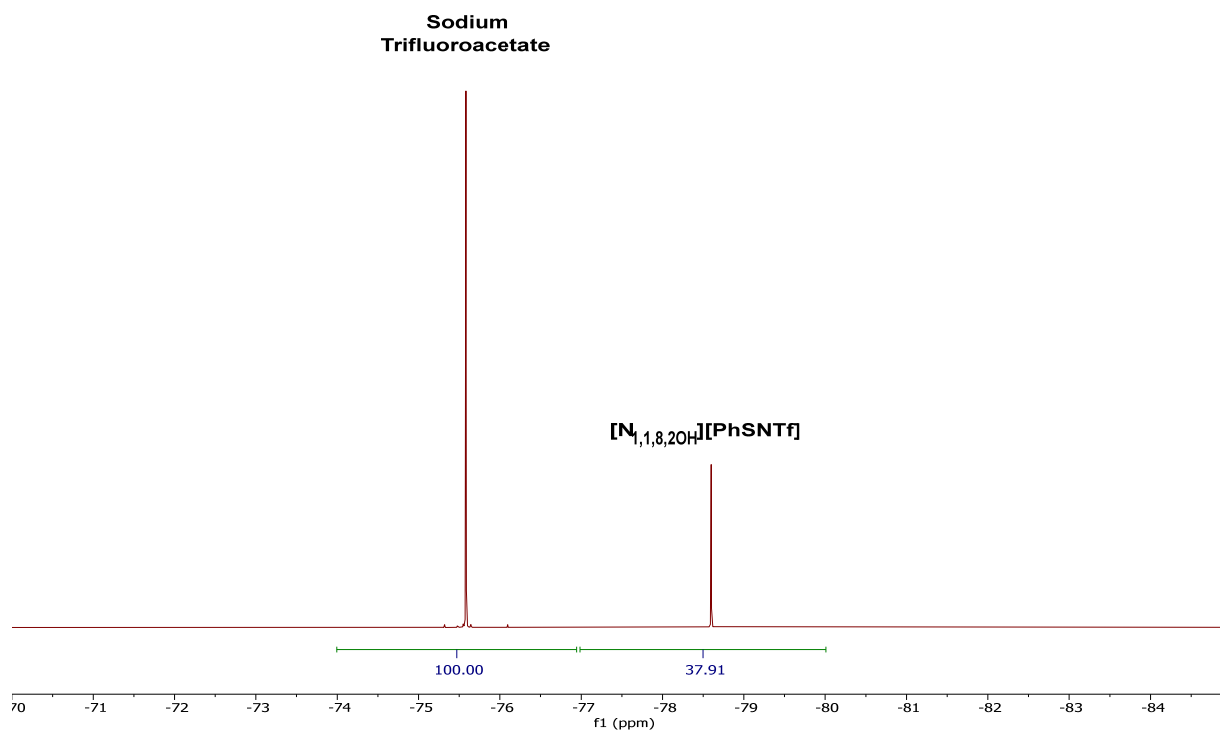
[DC-ether][2PFBSNTf], **18I**



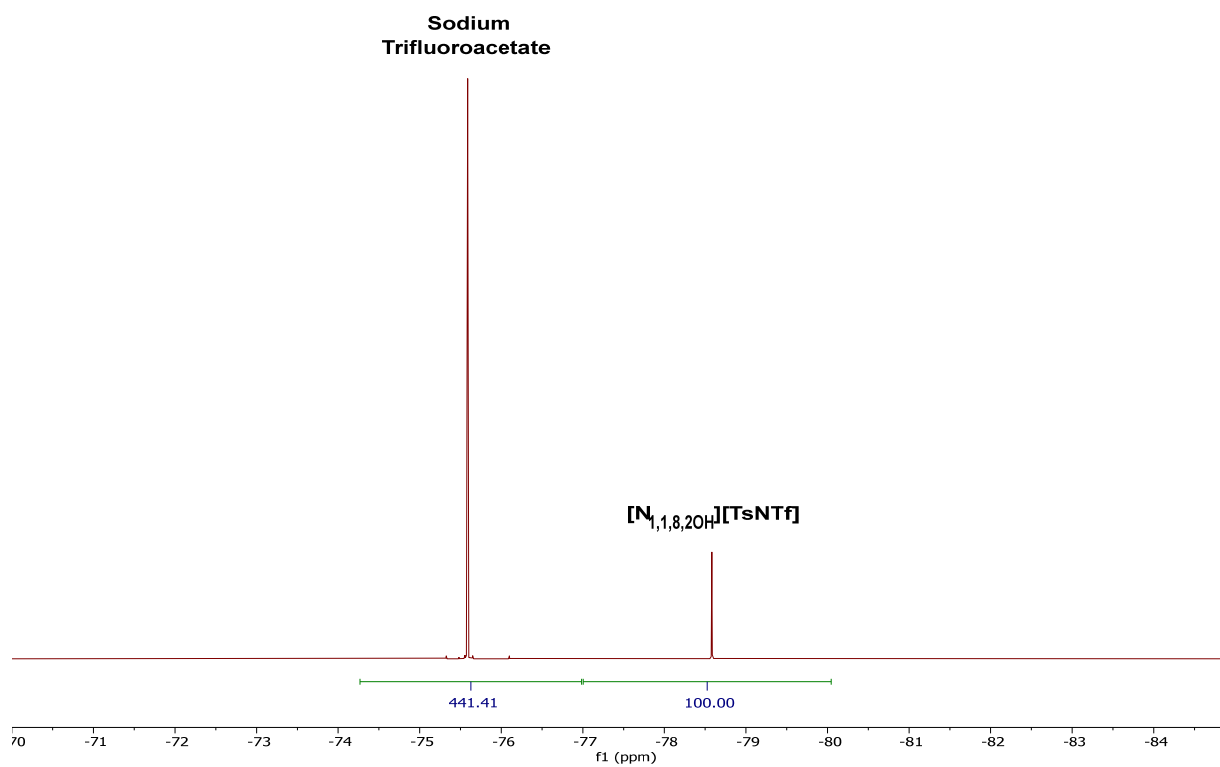
[N<sub>1,1,6,2OH</sub>][TFBSNTf], **19c**



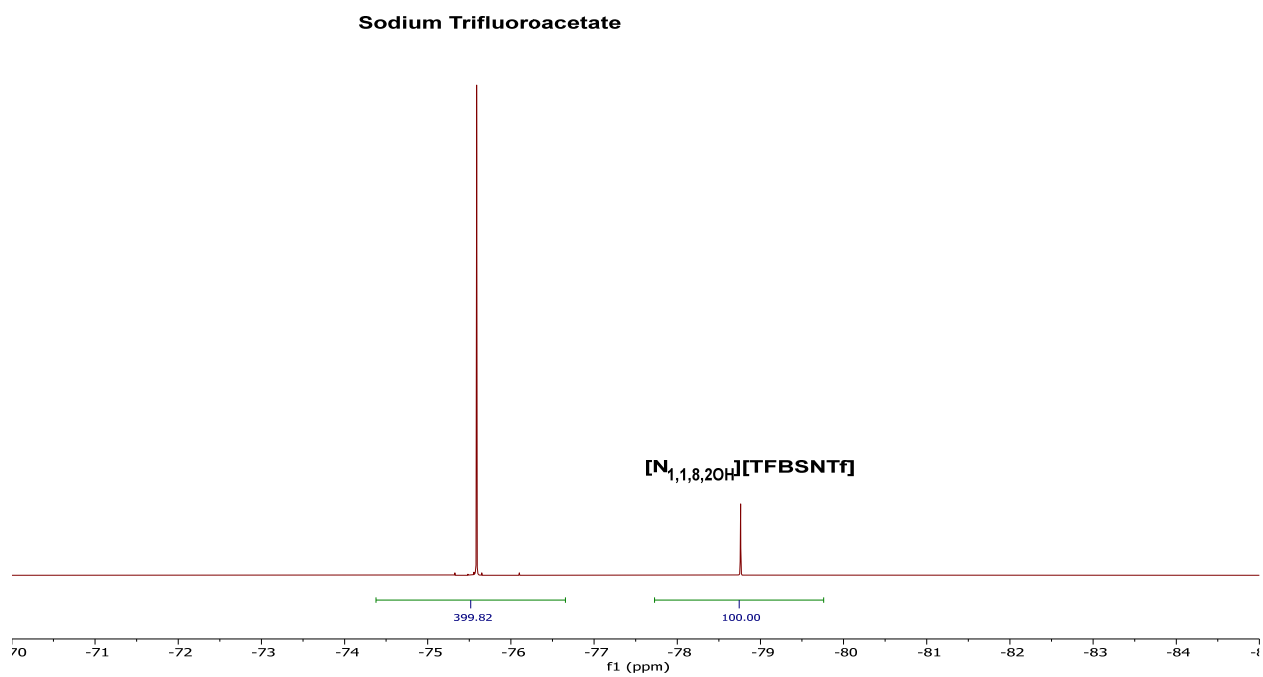
$[N_{1,1,8,2OH}][PhSNTf]$ , **19e**



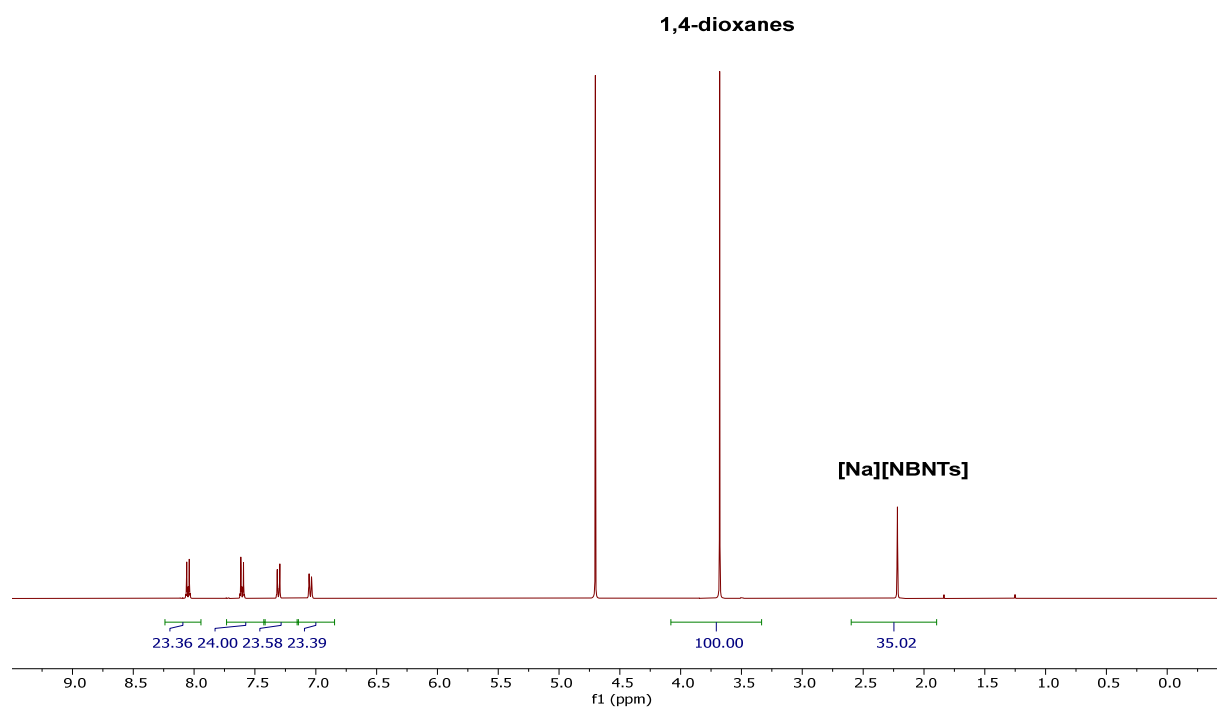
$[N_{1,1,8,2OH}][TsSNTf]$ , **19f**



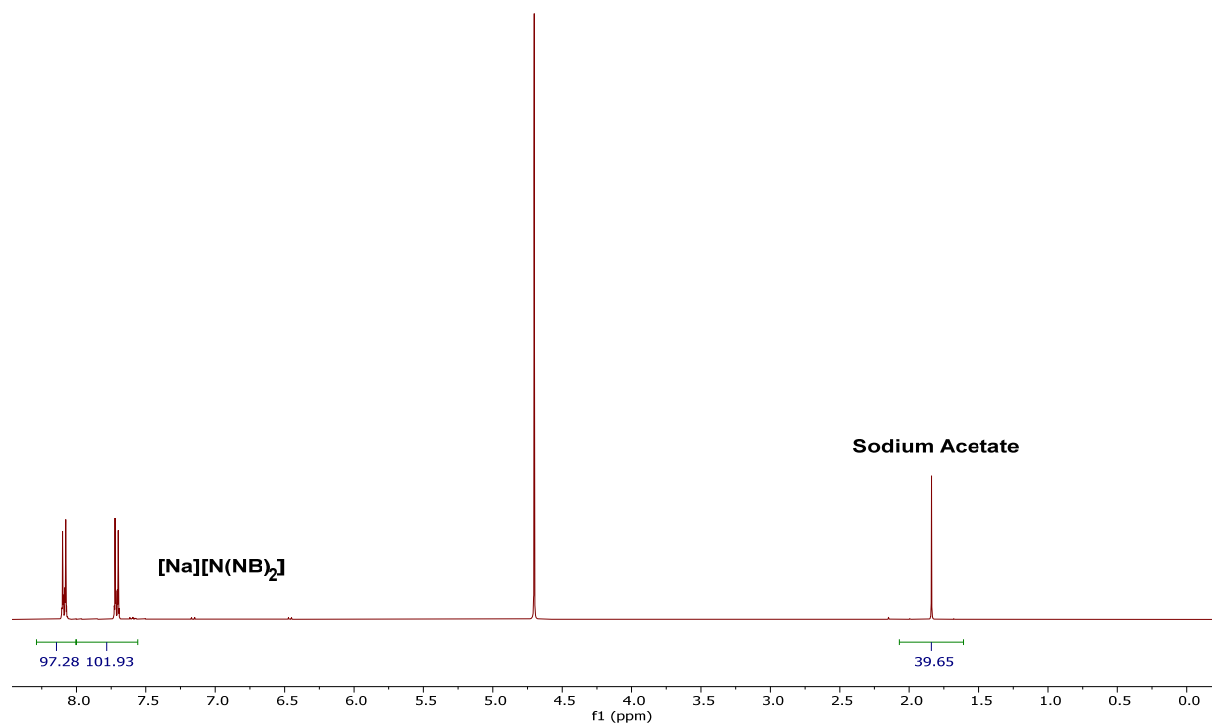
[N<sub>1,1,8,2OH</sub>][TFBSNTf], **19g**



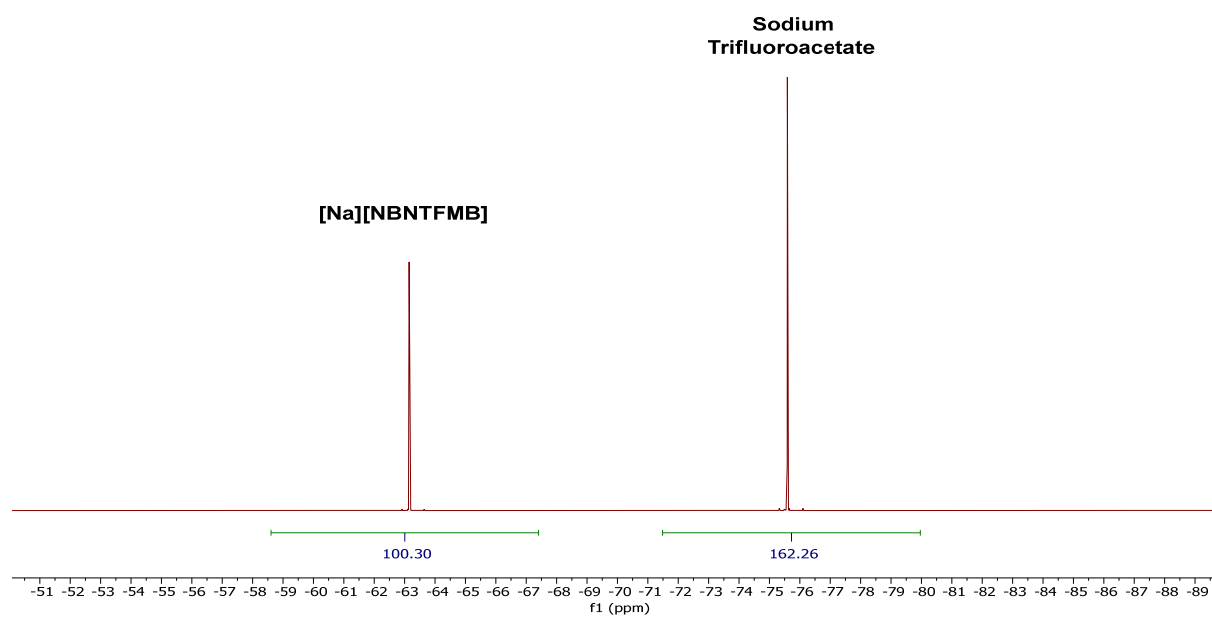
[Na][NBNTs], **21a<sub>ii</sub>**

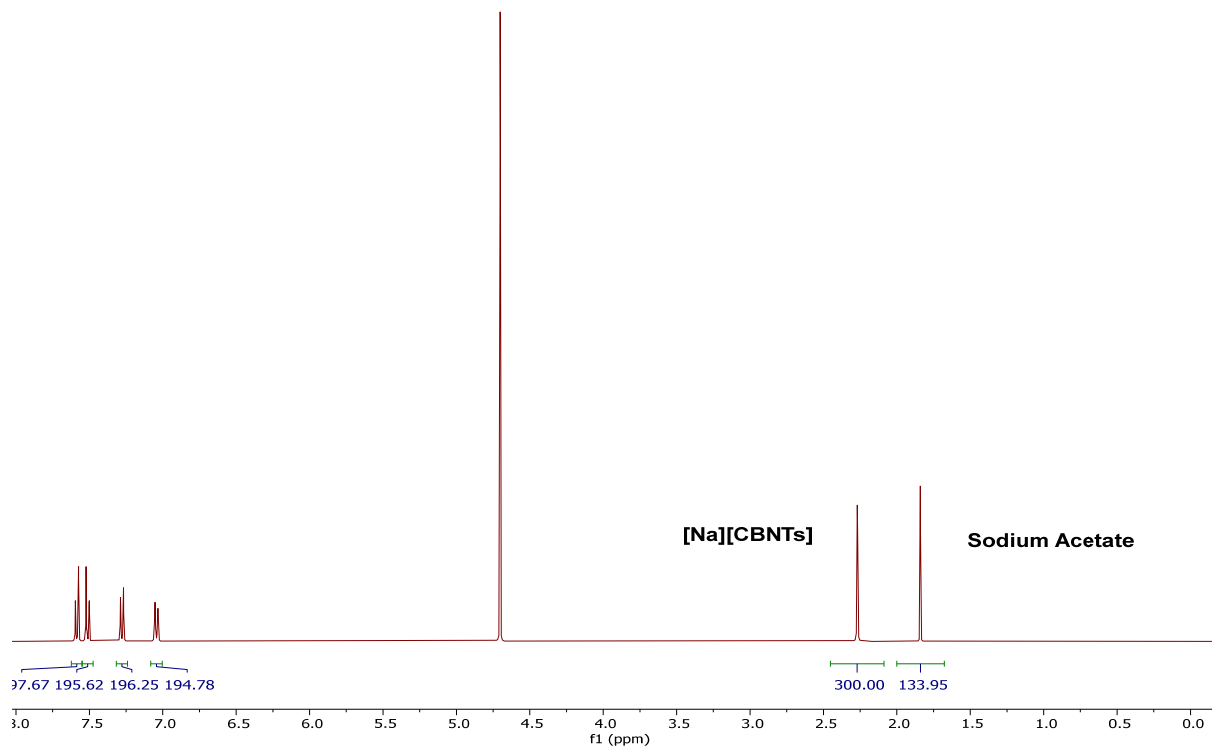
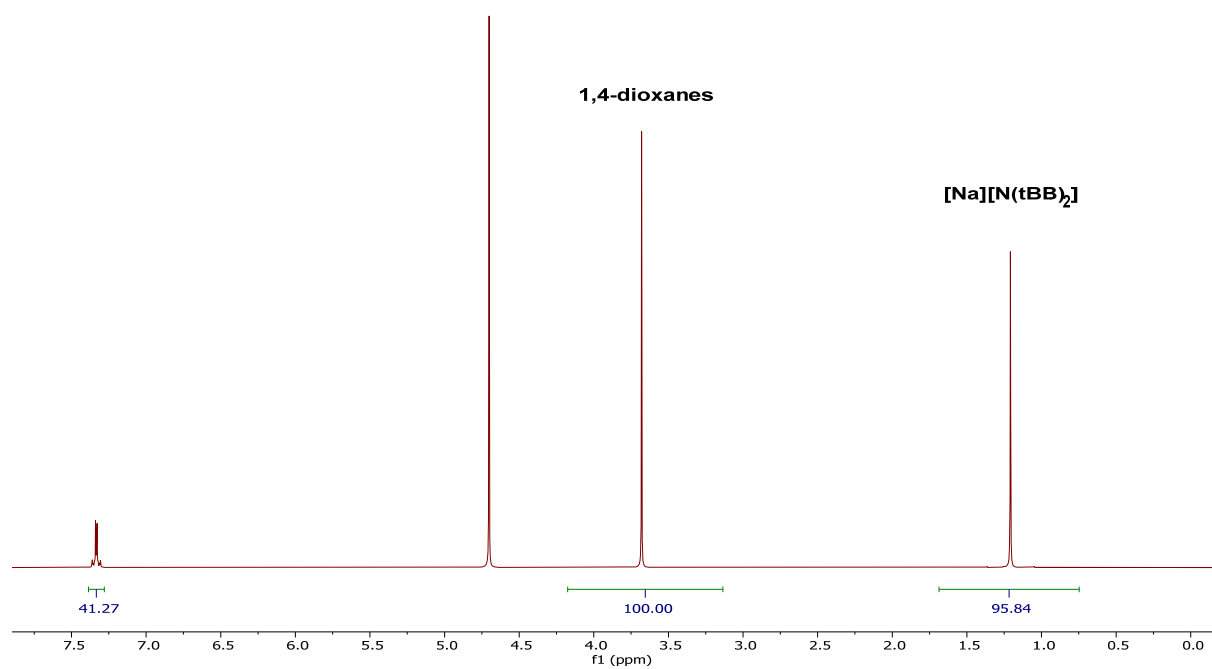


[Na][N(NB)<sub>2</sub>], **21bii**

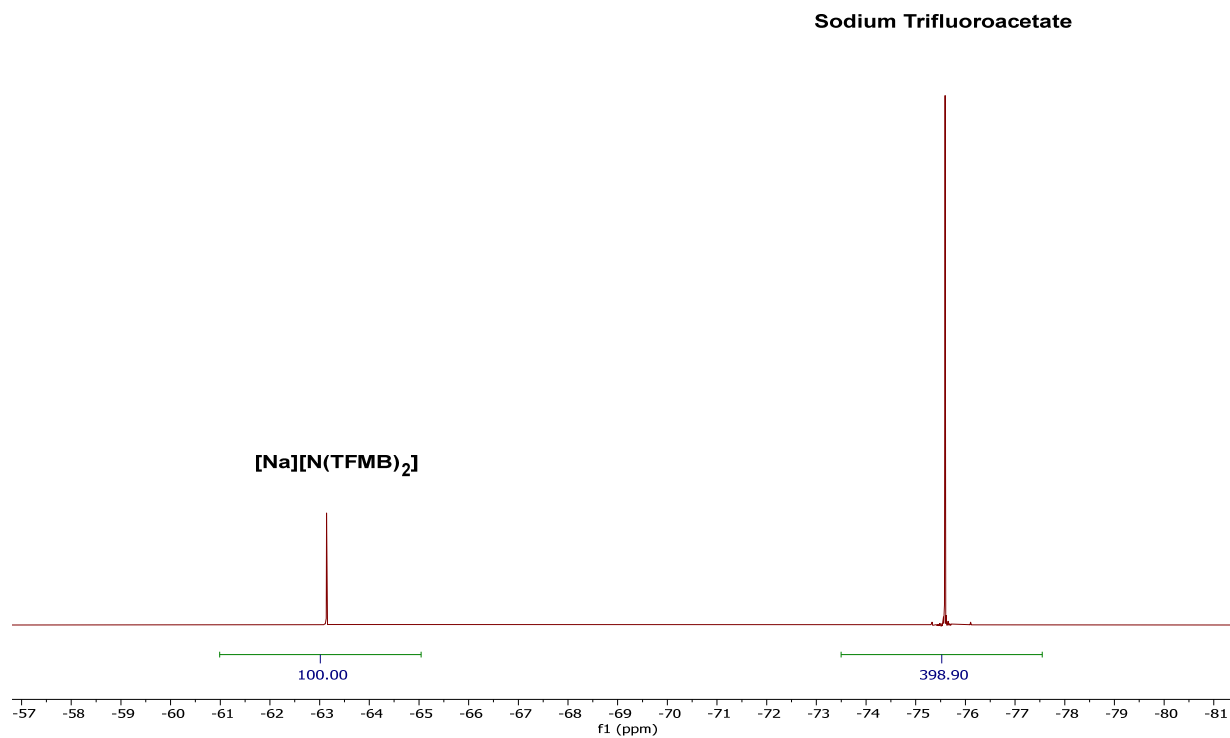


[Na][NBNTFMB], **21cii**

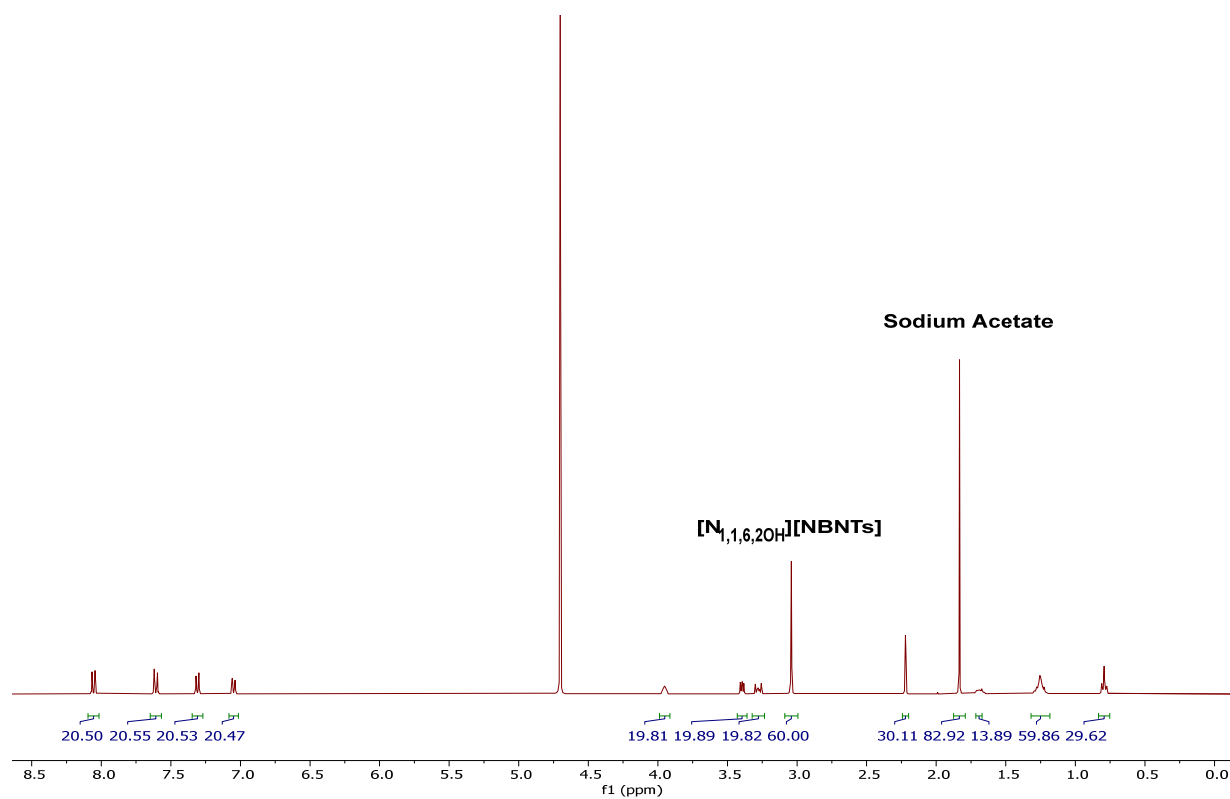


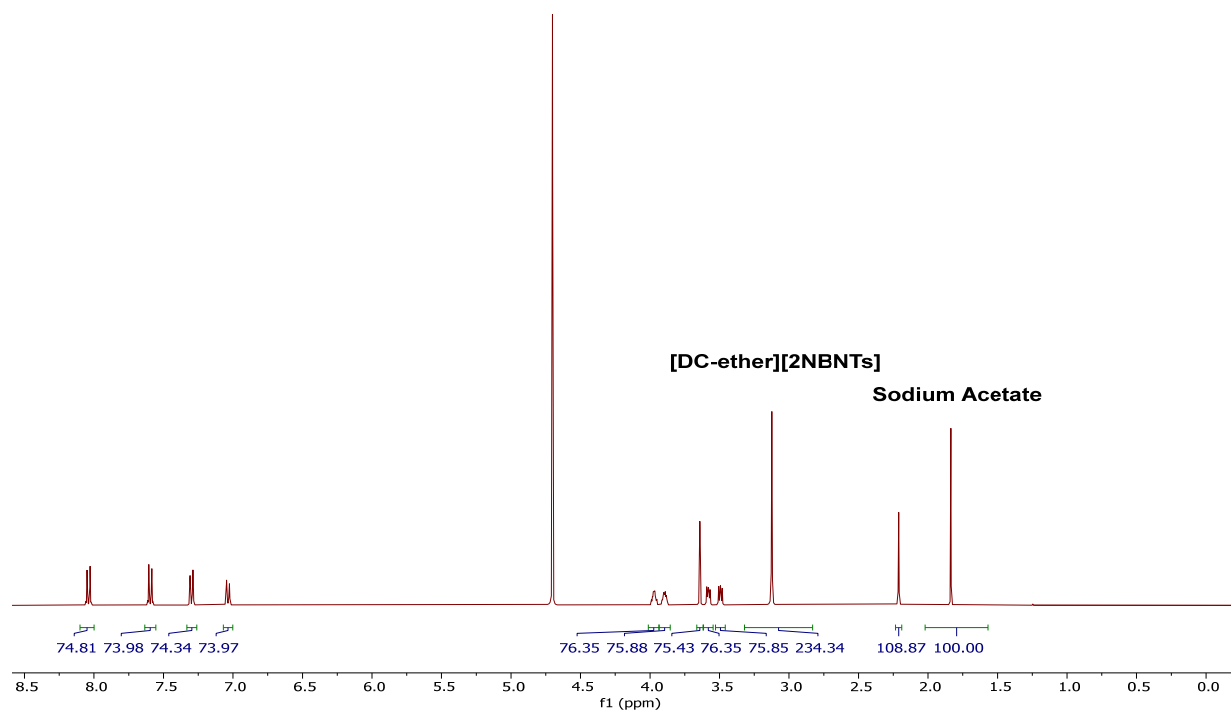
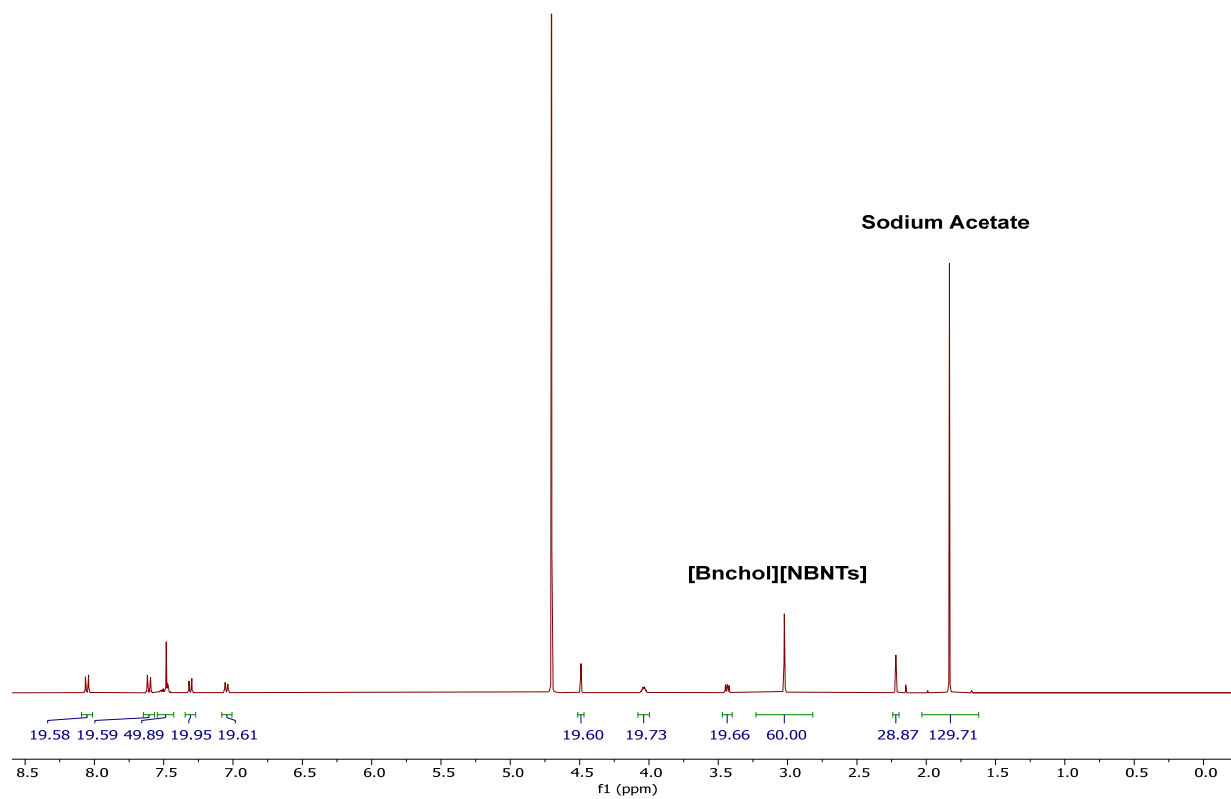
$[\text{Na}][\text{CBNTs}]$ , **21d<sub>ii</sub>** $[\text{Na}][\text{N}(\text{tBB})_2]$ , **21f<sub>ii</sub>**

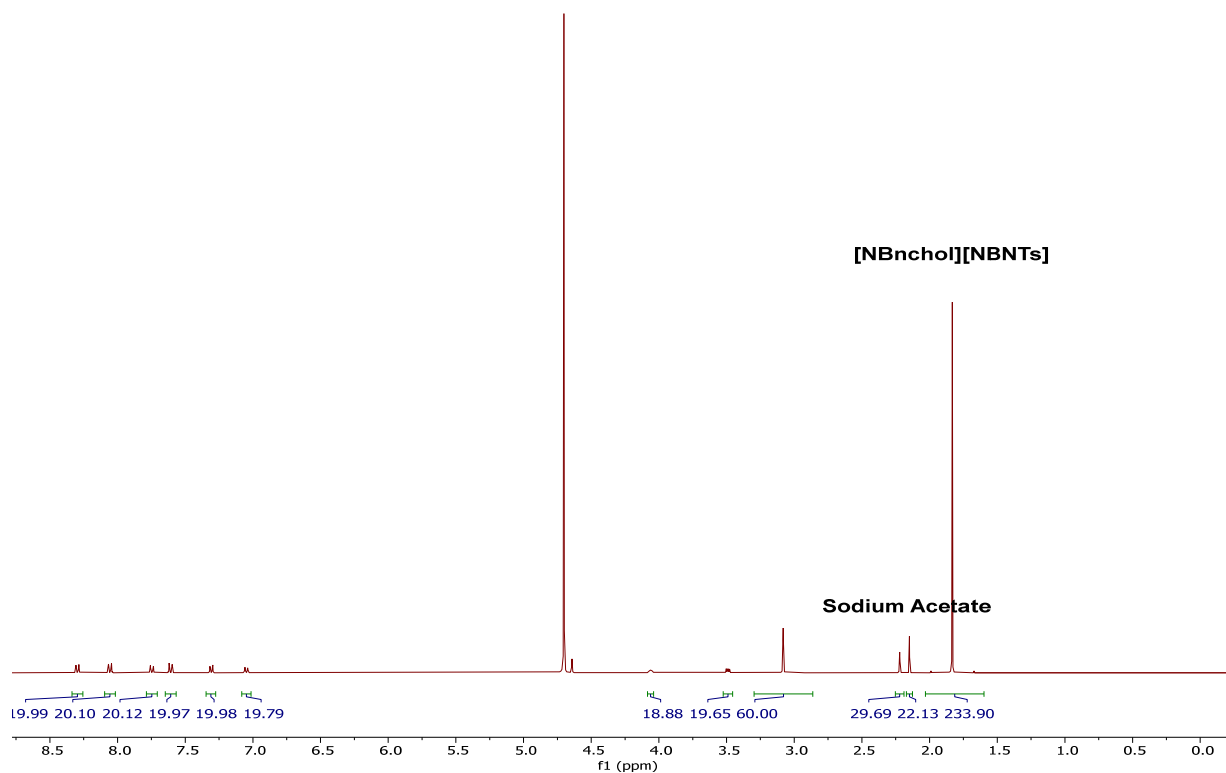
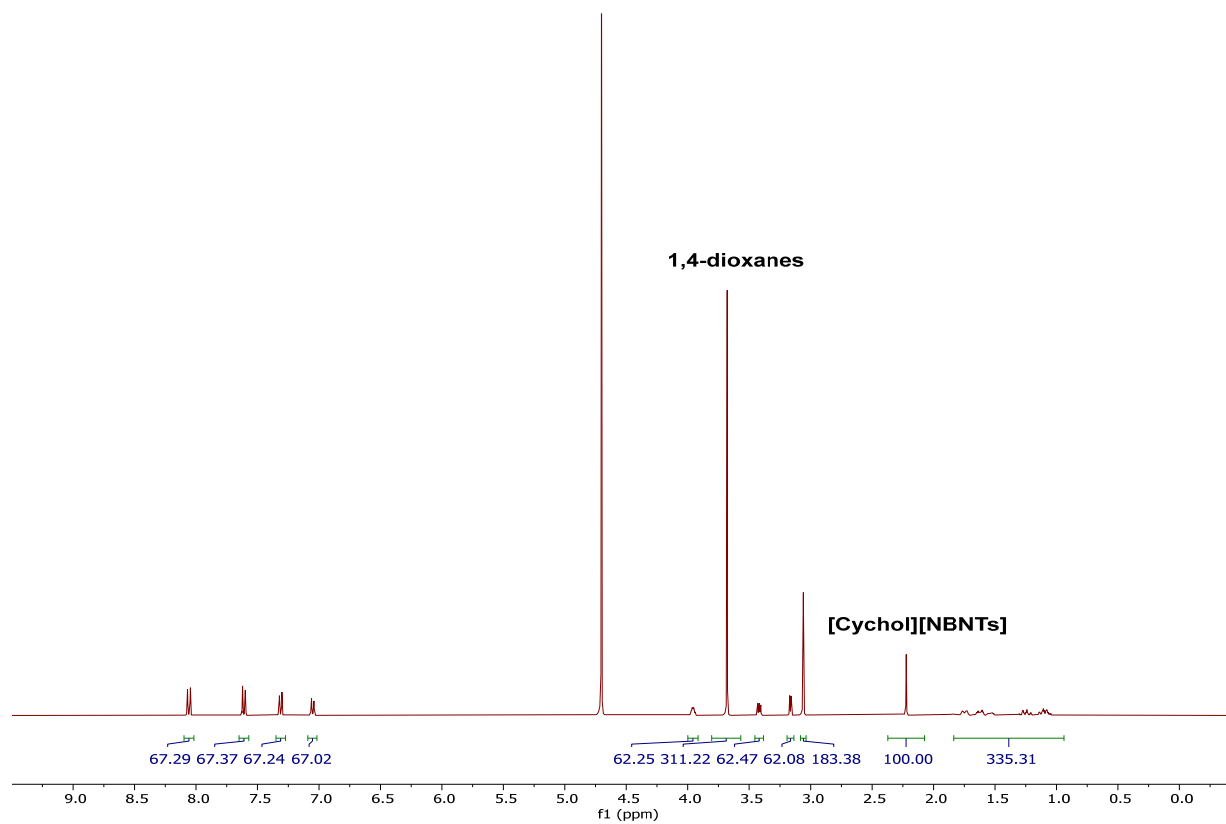
[Na][N(TFMB)<sub>2</sub>], **21hii**



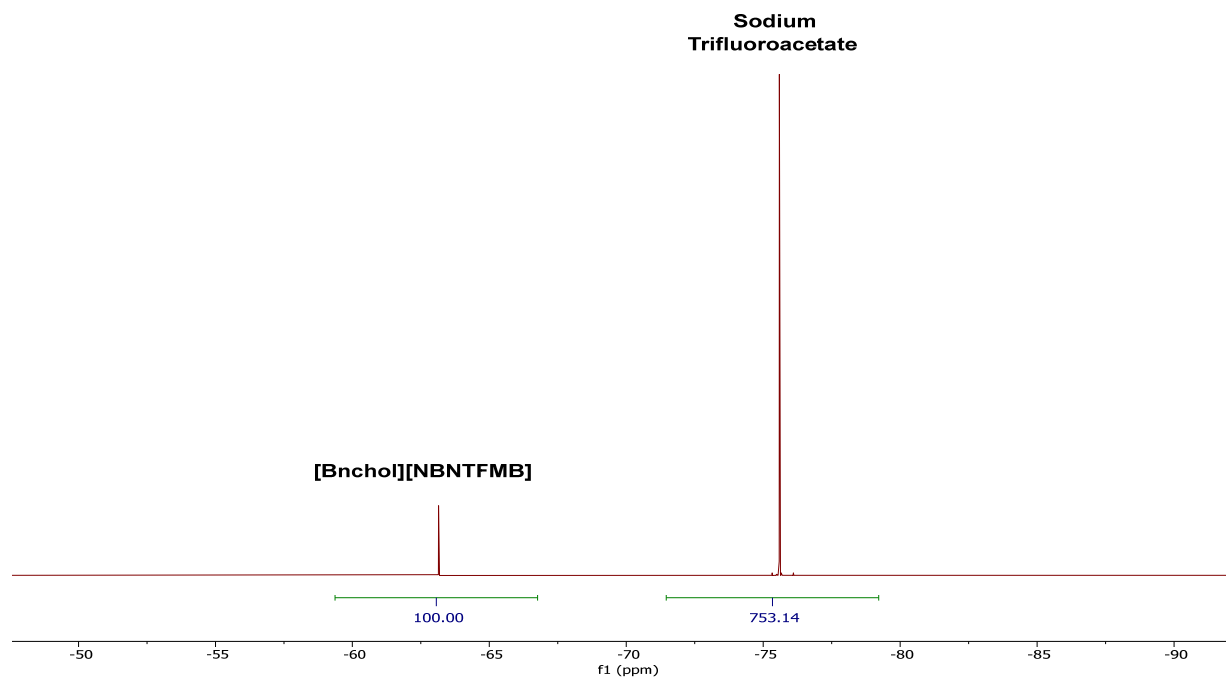
[N<sub>1,1,6,2OH</sub>][NBNTs], **25a**



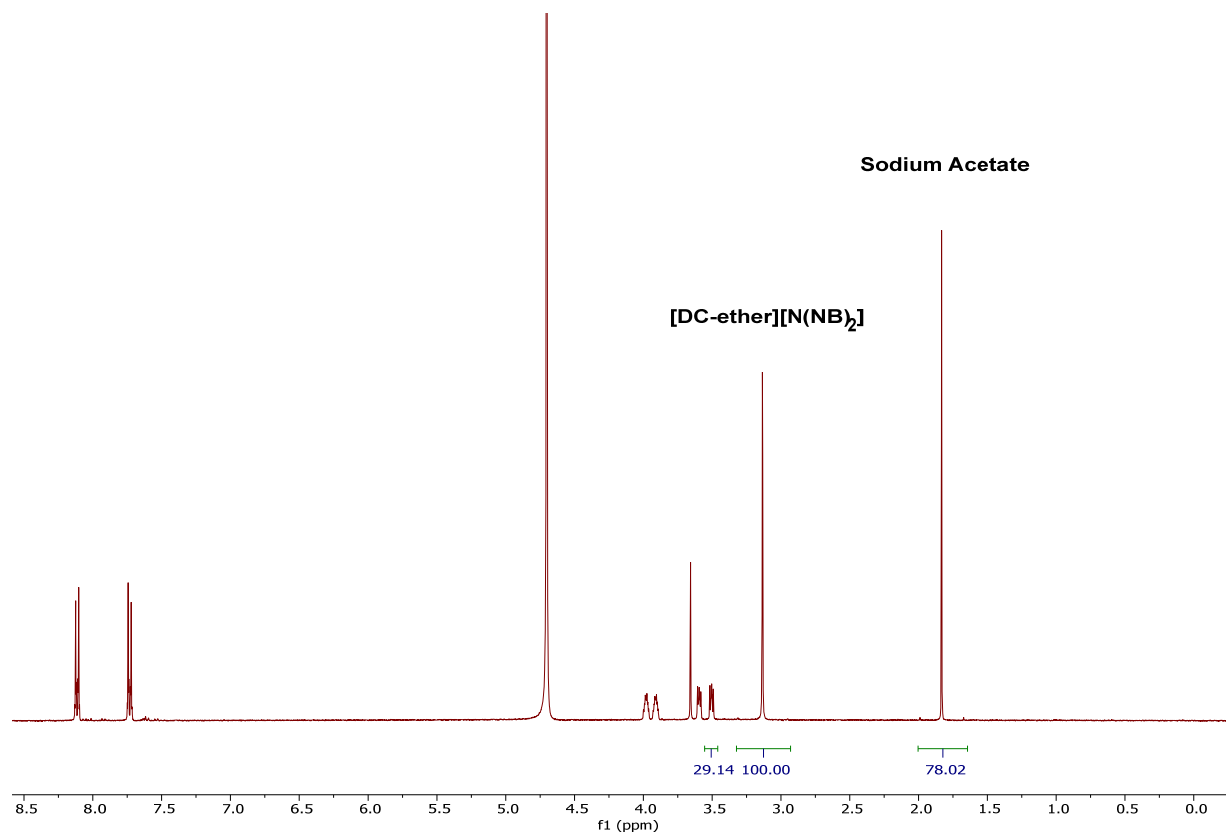
**[DC-ether][2NBNTs], 25b****[Bnchol][NBNTs], 25c**

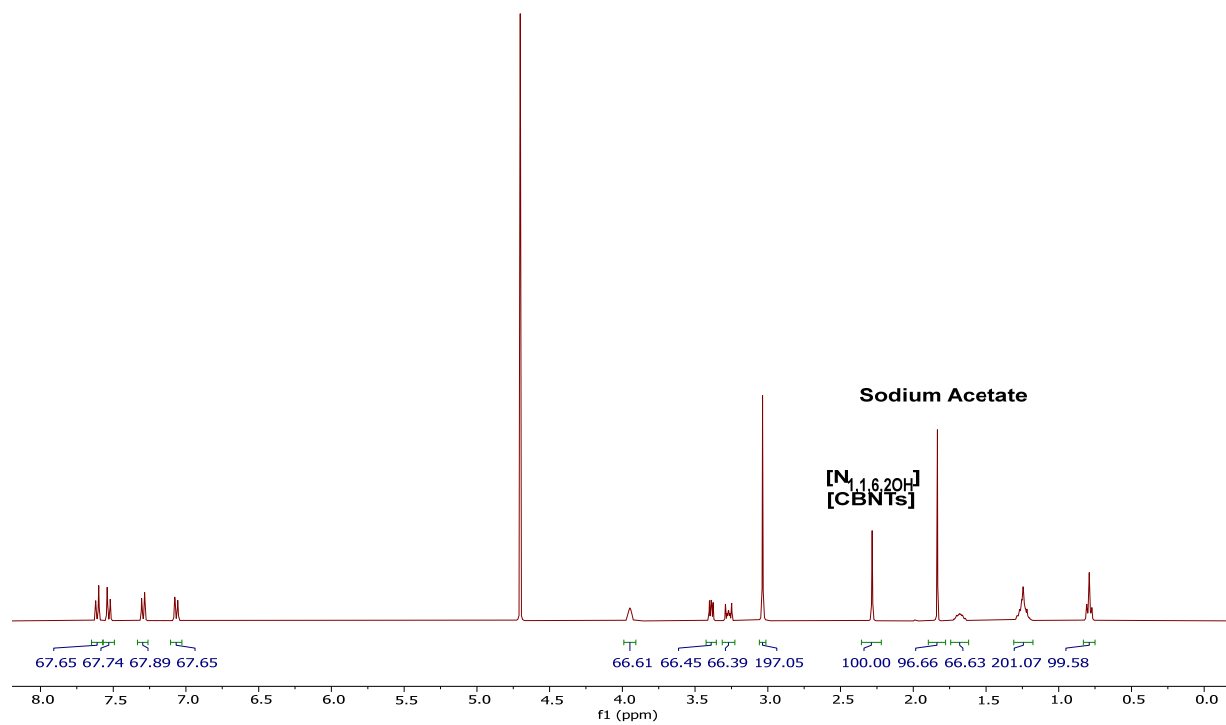
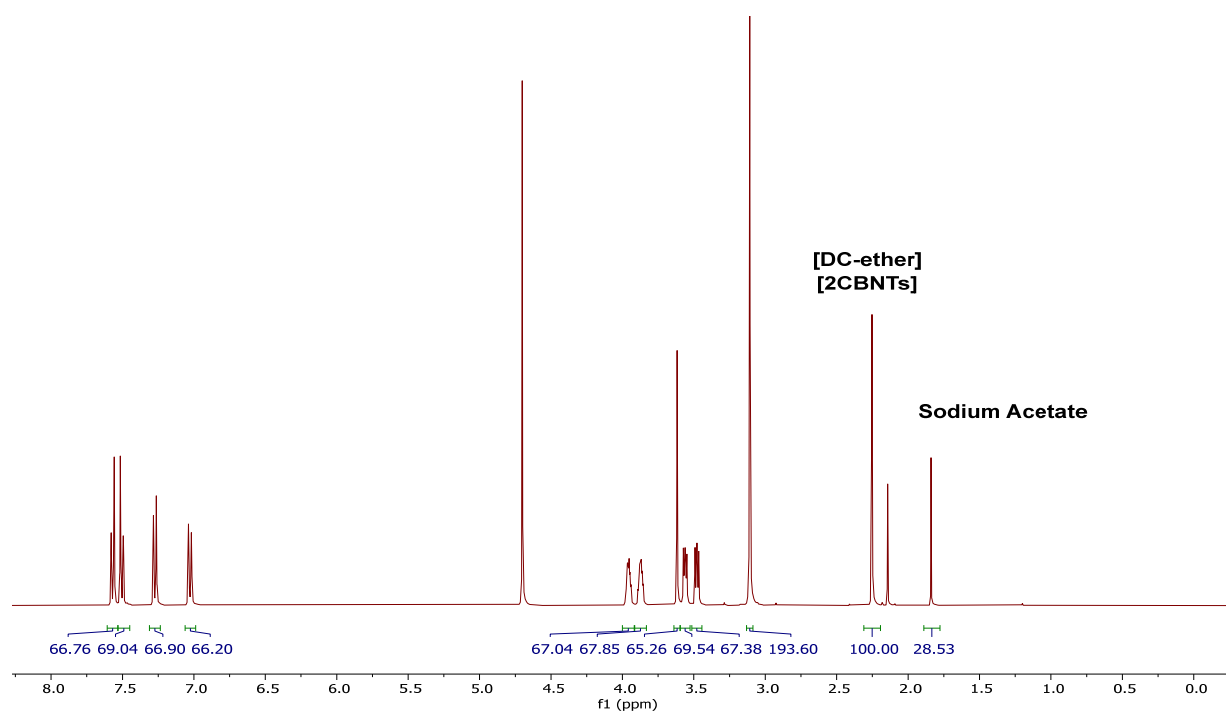
**[NBnchol][NBNTs], 25d****[Cychol][NBNTs], 25e**

[Bnchol][NBNTFMB], **25f**

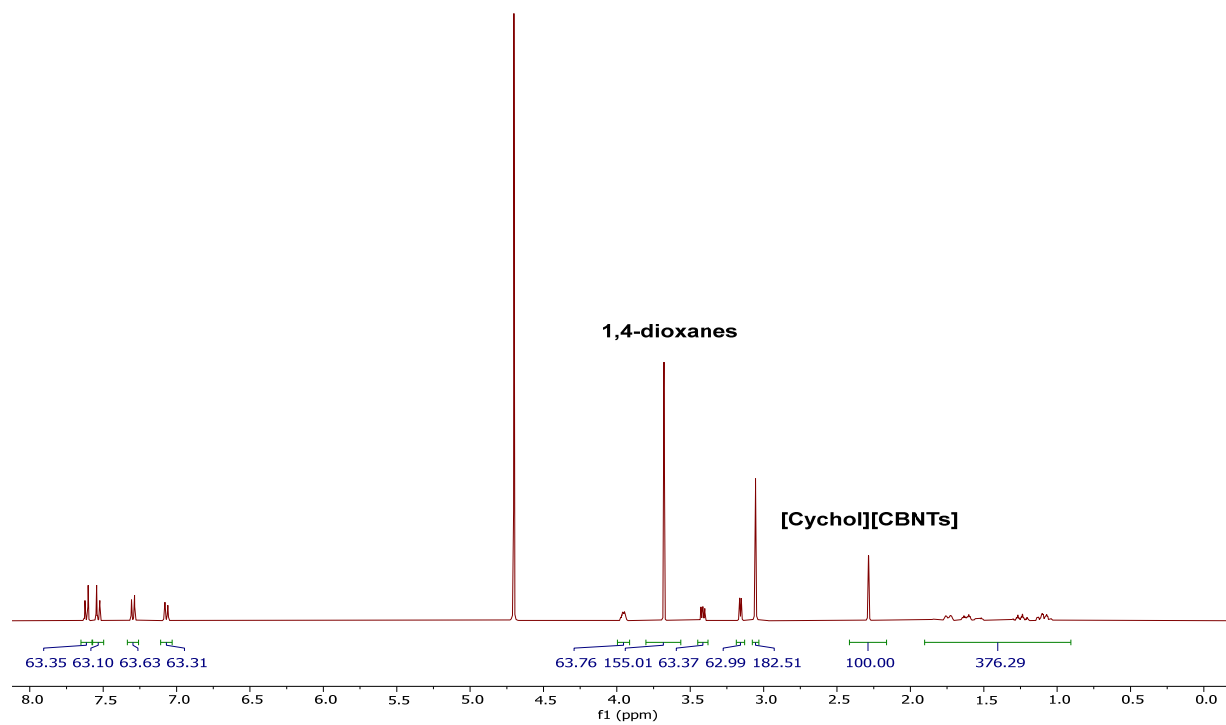


[DC-ether][2N(NB)<sub>2</sub>], **25g**

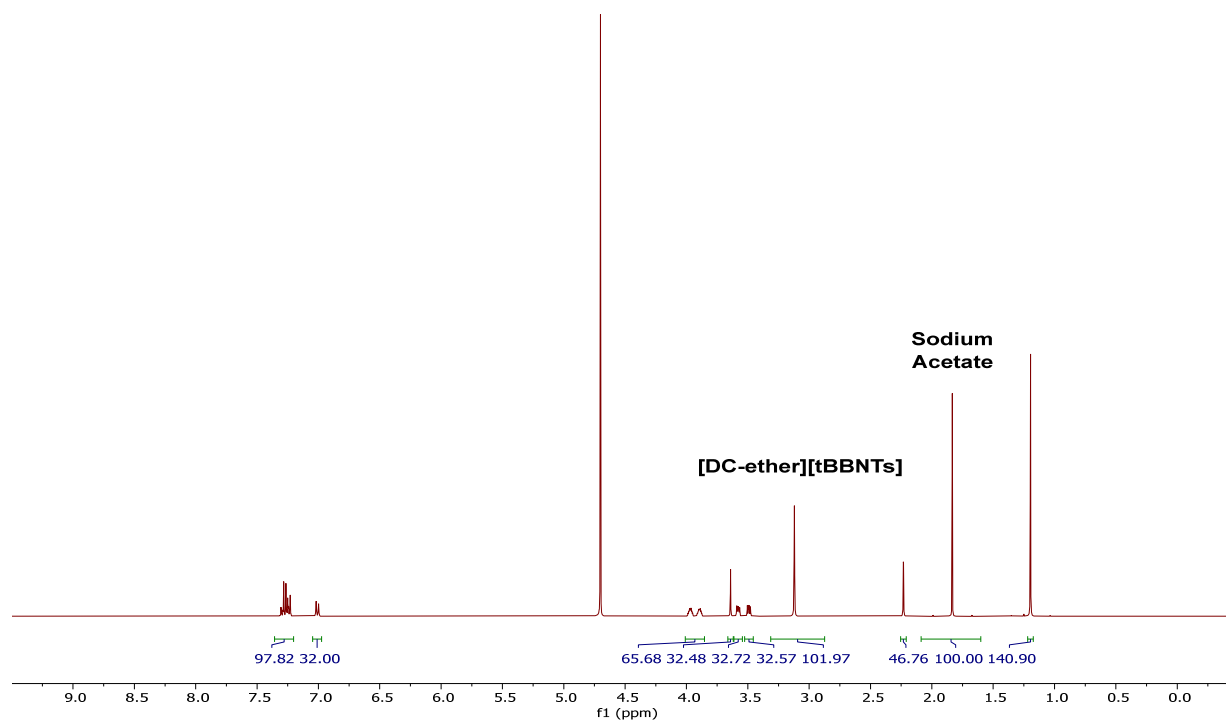


$[N_{1,1,6,2OH}][CBNTs]$ , **25h** $[DC-ether][2CBNTs]$ , **25i**

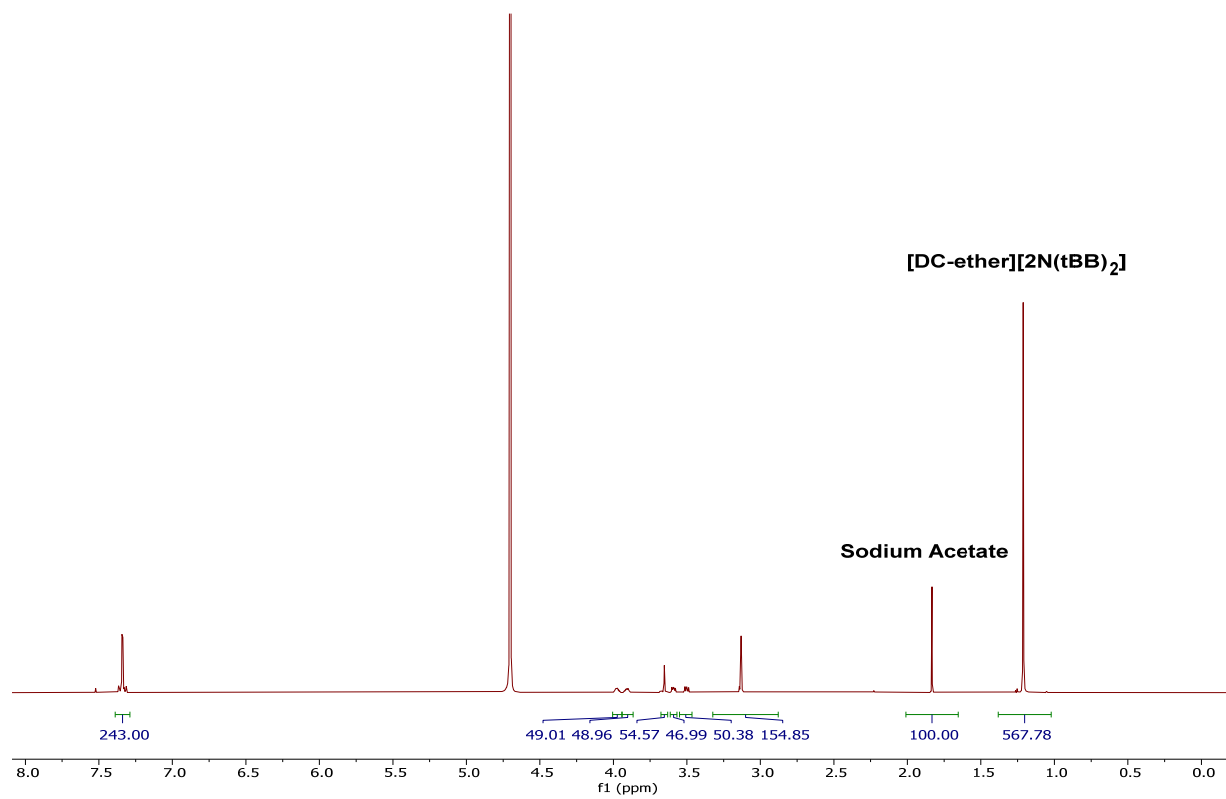
## [Cychol][CBNTs], 25j



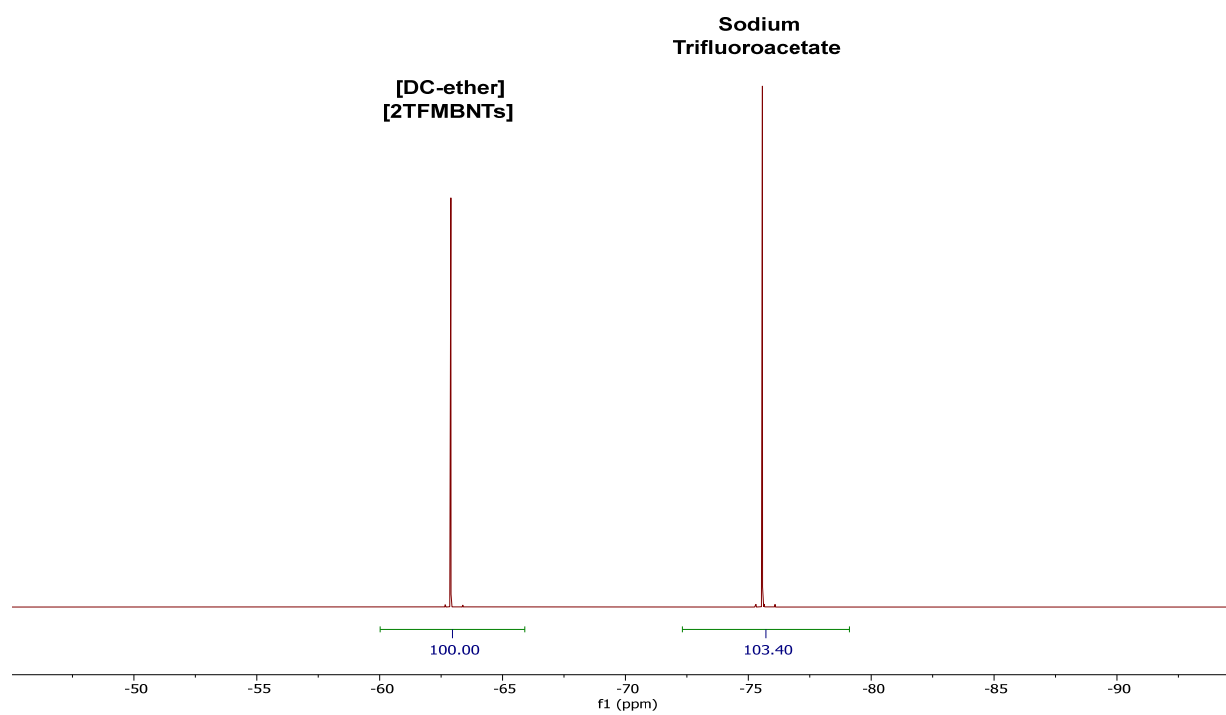
## [DC-ether][2tBBNTs], 25l



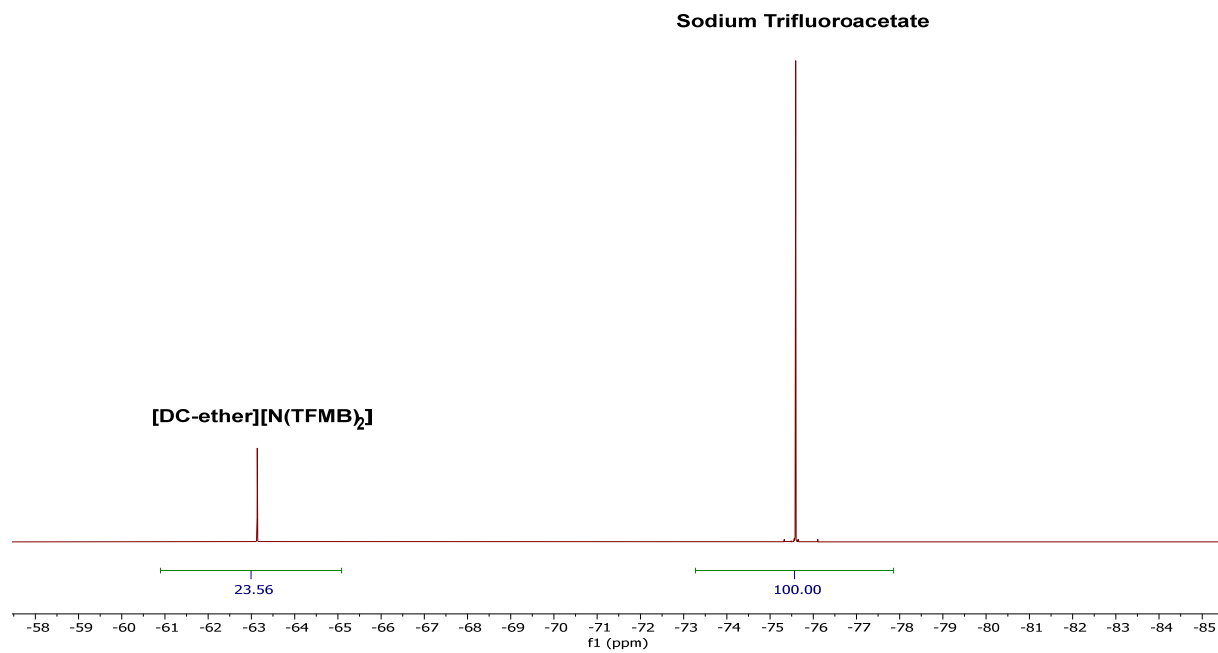
[DC-ether][2N(tBB)<sub>2</sub>], 25m



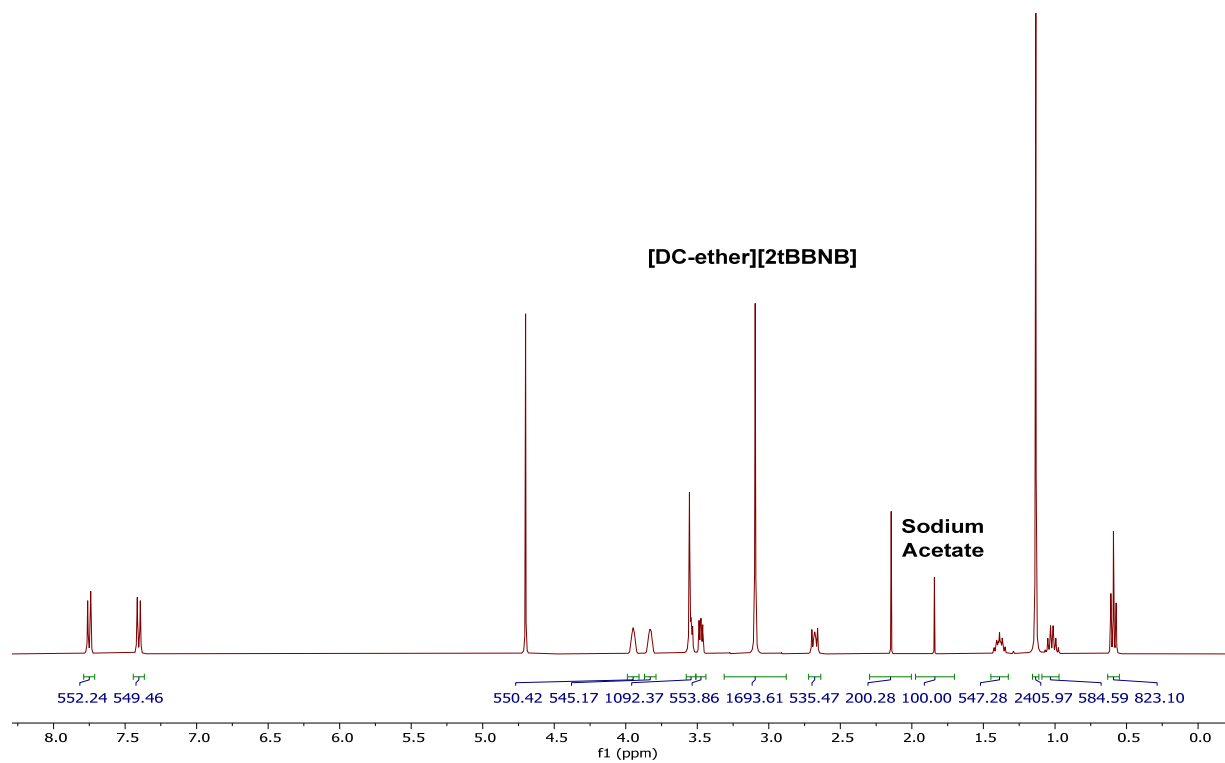
[DC-ether][2TFMBNTs], 25n



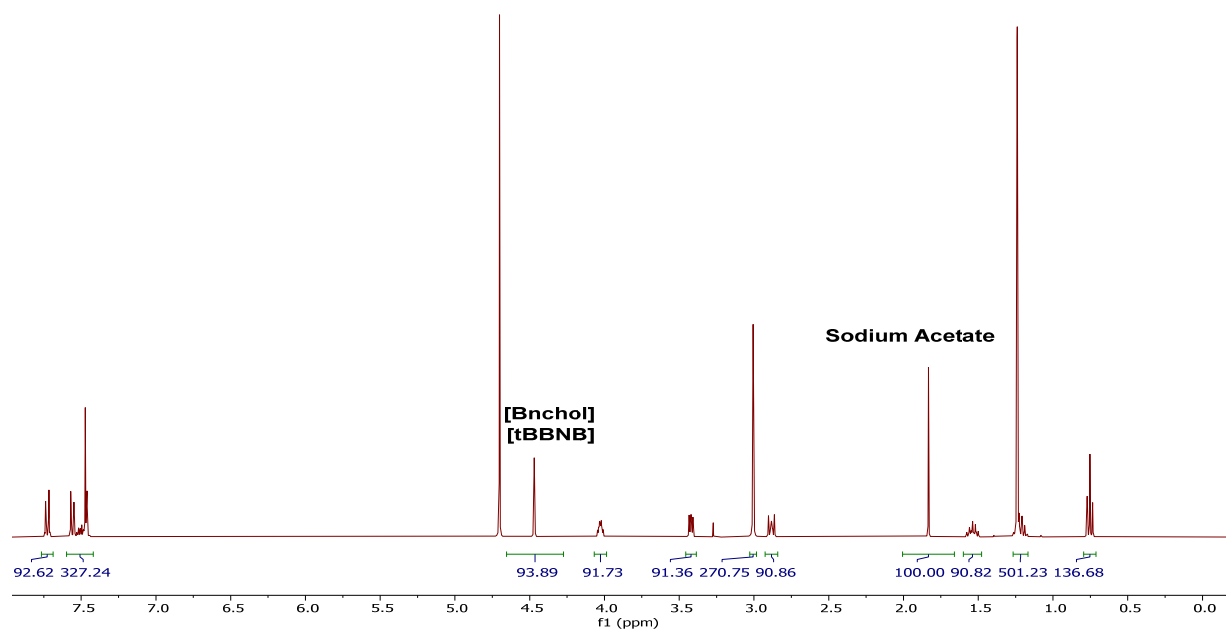
[DC-ether][2N(TFMB)<sub>2</sub>], **25o**



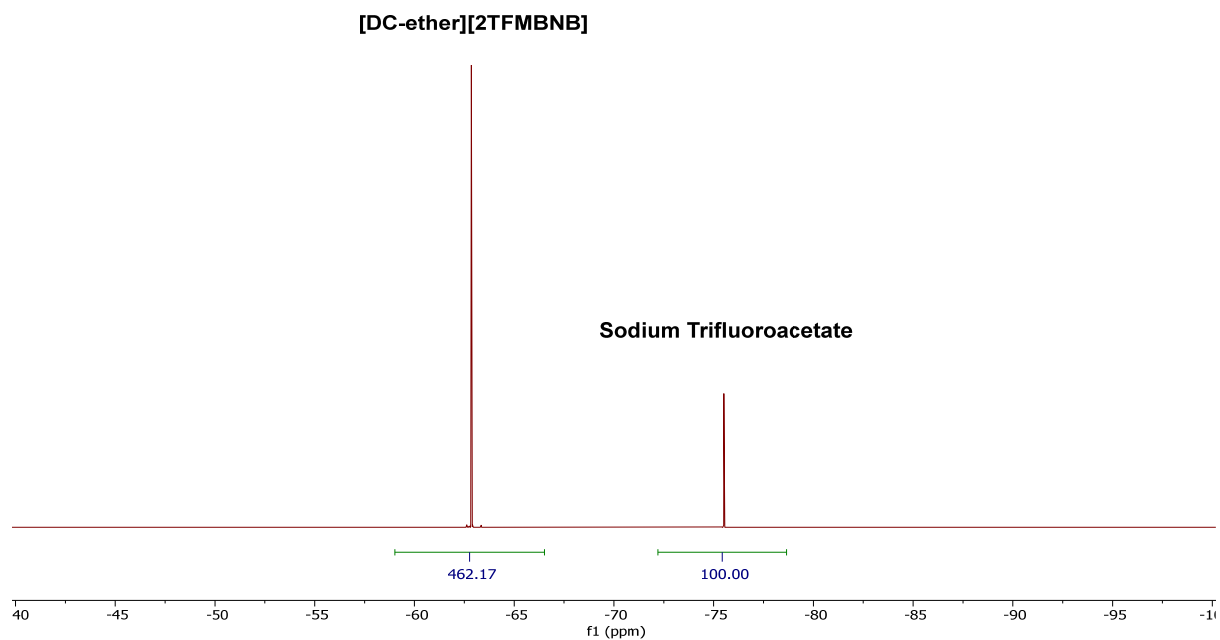
[DC-ether][2tBBNB], **26b**



[Bnchol][tBBNB], **26c**



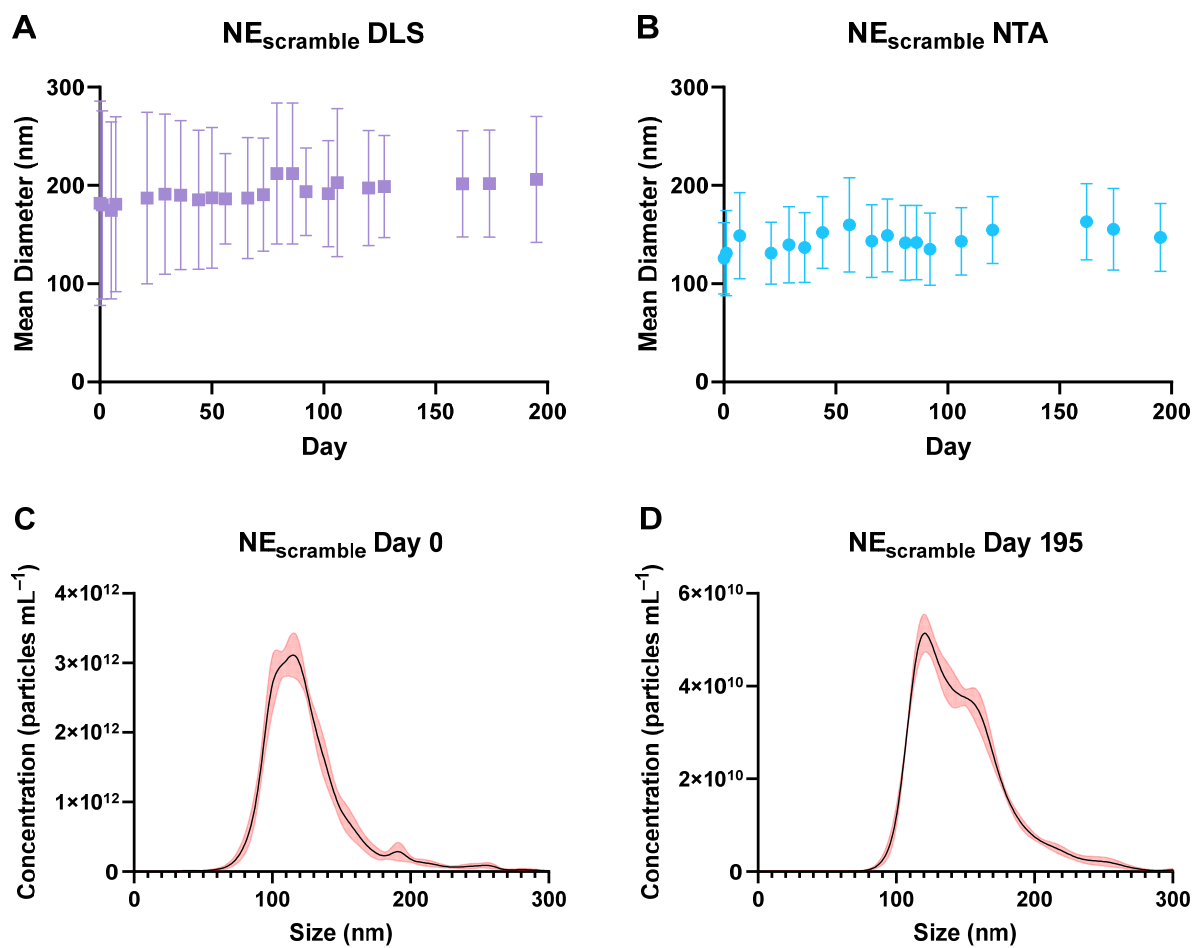
[DC-ether][2TFMBNB], **26d**



#### A.4 Hygroscopicity of Dried Cholinium-based Ionic liquids containing [NTf<sub>2</sub>] and first-generation bis(sulfonyl)azanide anions

<b>Table A.2</b> Hygroscopicity of cholinium and dicholinium ILs composed of [NTf <sub>2</sub> ] anions and first-generation bis(sulfonyl)azanide anions after drying in an 80 °C vacuum oven for 16 h. Values represent percent mass fraction.		
#	Ionic Liquid	Hygroscopicity (W <sub>H2O</sub> ,%), dry
<b>13a</b>	[chol][NTf <sub>2</sub> ]	0.092 ± 0.013
<b>13b</b>	[N <sub>1,1,4,2OH</sub> ][NTf <sub>2</sub> ]	0.056 ± 0.015
<b>13c</b>	[N <sub>1,1,6,2OH</sub> ][NTf <sub>2</sub> ]	0.021 ± 0.007
<b>13d</b>	[N <sub>1,1,8,2OH</sub> ][NTf <sub>2</sub> ]	0.041 ± 0.002
<b>13i</b>	[DC-4][2NTf <sub>2</sub> ]	Too low to detect
<b>13k</b>	[DC-6][2NTf <sub>2</sub> ]	Too low to detect
<b>13m</b>	[DC-8][2NTf <sub>2</sub> ]	Too low to detect
<b>13p</b>	[DC-ether][2NTf <sub>2</sub> ]	0.035 ± 0.012
<b>18a</b>	[DC-ether][2BSNTf]	0.042 ± 0.022
<b>18b</b>	[DC-ether][2HSNTf]	Too low to detect
<b>18c</b>	[DC-ether][2OSNTf]	0.046 ± 0.002
<b>18d</b>	[DC-ether][2PhSNTf]	0.021 ± 0.009
<b>18e</b>	[DC-ether][2TsNTf]	Too low to detect
<b>18f</b>	[DC-ether][2pBBSNTf]	0.014 ± 0.004
<b>18g</b>	[DC-ether][2pHBSNTf]	0.074 ± 0.023
<b>18h</b>	[DC-ether][2pOBSNTf]	Too low to detect
<b>18i</b>	[DC-ether][2MesSNTf]	Too low to detect
<b>18j</b>	[DC-ether][2pMBSNTf]	Too low to detect
<b>18k</b>	[DC-ether][2TFBSNTf]	Too low to detect
<b>18l</b>	[DC-ether][2PFBSNTf]	0.029 ± 0.007

### A.5 Particle Size Analysis of NE<sub>scramble</sub>



**Figure A.1** Change in particle size over time for NE<sub>scramble</sub> as measured by (A) dynamic light scattering and (B) nanoparticle tracking analysis. Error bars represent standard deviation. (C–D) Concentration of nanoparticles as a function of size. Error bars represent SEM.